Advanced Gas Storage Concepts:
Technologies for the Future

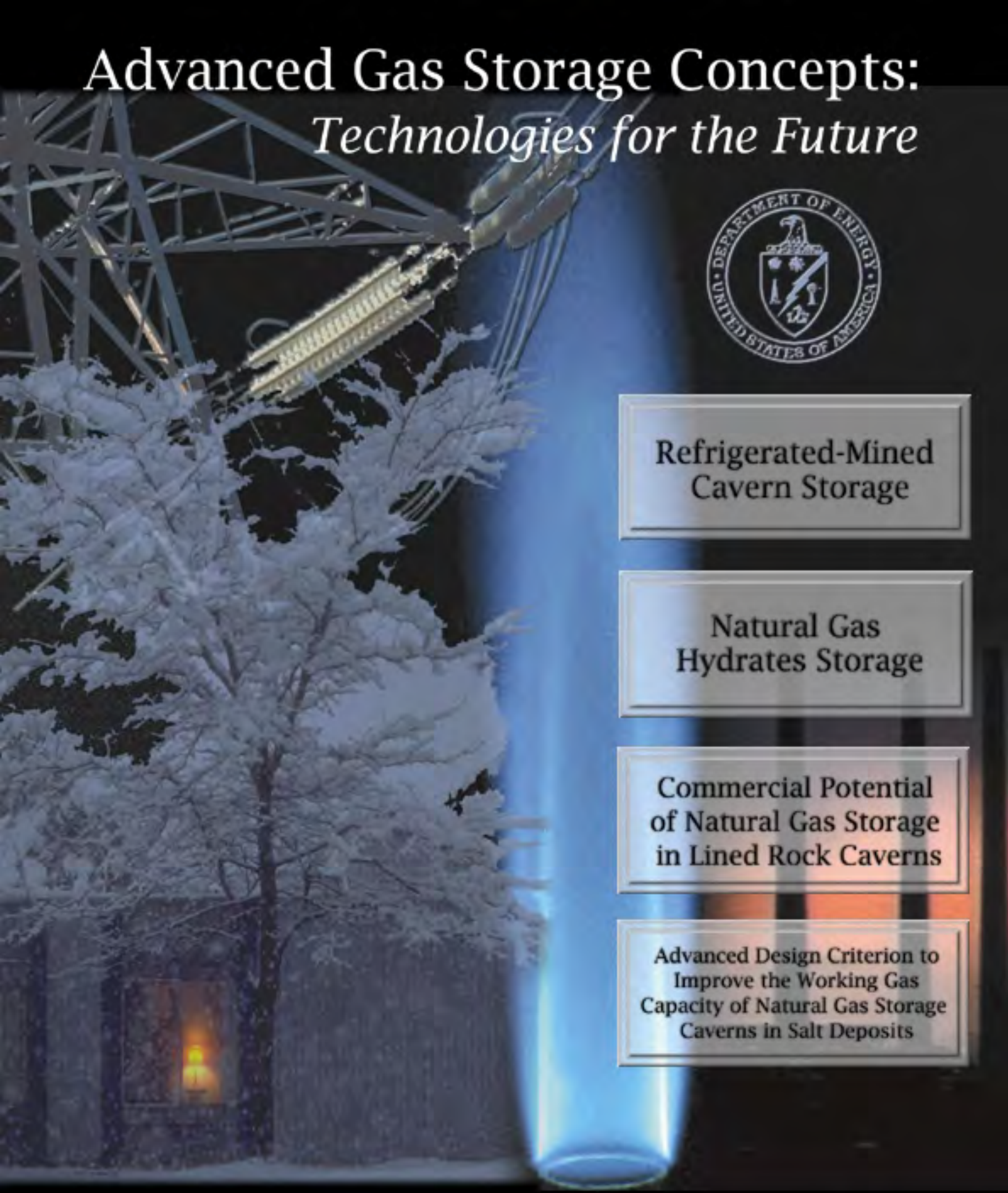

Refrigerated-Mined Cavern Storage

Natural Gas Hydrates Storage

Commercial Potential of Natural Gas Storage in Lined Rock Caverns

Advanced Design Criterion to Improve the Working Gas Capacity of Natural Gas Storage Caverns in Salt Deposits

February 1, 2000

Disclaimer

ADVANCED UNDERGROUND GAS STORAGE CONCEPTS REFRIGERATED-MINED CAVERN STORAGE Final Report DOE Contract Number DE-AC26-97FT34349 *Submitted by:* PB-KBB INC. 11757 Katy Freeway, Suite 600 Houston, TX 77079 September 1998	**CHILLED GAS STORAGE IN MINED CAVERNS WORKSHOPS** November 3, 1998 - Houston, Texas November 5, 1998 - Pittsburgh, Pennsylvania

ADVANCED UNDERGROUND GAS STORAGE CONCEPTS
REFRIGERATED-MINED CAVERN STORAGE

FINAL REPORT

DOE CONTRACT NUMBER DE-AC26-97FT34349

SUBMITTED BY:
PB-KBB INC.
11757 KATY FREEWAY, SUITE 600
HOUSTON, TX 77079

SEPTEMBER 1998

Disclaimer

ADVANCED UNDERGROUND GAS STORAGE CONCEPTS
REFRIGERATED-MINED CAVERN STORAGE
FINAL DRAFT REPORT

ABSTRACT

Limited demand and high cost has prevented the construction of hard rock caverns in this country for a number of years. The storage of natural gas in mined caverns may prove technically feasible if the geology of the targeted market area is suitable; and economically feasible if the cost and convenience of service is competitive with alternative available storage methods for peak supply requirements. It is believed that mined cavern storage can provide the advantages of high delivery rates and multiple fill-withdrawal cycles in areas where salt cavern storage is not possible. In this research project, PB-KBB merged advanced mining technologies and gas refrigeration techniques to develop conceptual designs and cost estimates to demonstrate the commercialization potential of the storage of refrigerated natural gas in hard rock caverns. Five regions of the U.S.A. were studied for underground storage development and PB-KBB reviewed the literature to determine if the geology of these regions was suitable for siting hard rock storage caverns. Area gas market conditions in these regions were also studied to determine the need for such storage. Based on an analysis of many factors, a possible site was determined to be in Howard and Montgomery Counties, Maryland. The area has compatible geology and a gas industry infrastructure for the nearby market populous of Baltimore and Washington D.C..

As Gas temperature is lowered, the compressibility of the gas reaches an optimum value. The compressibility of the gas, and the resultant gas density, is a function of temperature and pressure. This relationship can be used to commercial advantage by reducing the size of a storage cavern for a given working volume of natural gas. This study looks at this relationship and and the potential for commercialization of the process in a storage application. A conceptual process design, and cavern design were developed for various operating conditions. Potential site locations were considered and a typical plant layout was developed. In addition a geomechanical review of the proposed cavern design was performed, evaluating the stability of the mine rooms and shafts, and the effects of the refrigerated gas temperatures on the stability of the cavern.

Capital and operating cost estimates were also developed for the various temperature cases considered. The cost estimates developed were used to perform a comparative market analysis of this type of gas storage system to other systems that are commercially used in the region of the study.

User Note:

The following Table of Contents, List of Tables, and List of Figures are provided with text links to the associated section, table or figure. By clicking on the appropriate text the cursor will move to the appropriate document page.

TABLE OF CONTENTS

LIST OF TABLES

LIST OF FIGURES

LIST OF FIGURES (Continued.)

LIST OF CONCEPTUAL DRAWINGS
(IN APPENDICES)

861-GG-001	Electrical Symbol Diagram
861-GG-002	Piping & Instrument Symbol Diagram
861-GG-003	List of Drawings
861-GP-001	General Facility Layout
861-GP-002	General Equipment Layout
861-AC-001	Office/Control Building Elevation
861-AC-002	Office/Control Building Plan
861-ED-001	One Line Drawing - Conceptual Design (1 of 3)
861-ED-002	One Line Drawing - Conceptual Design (2 of 3)
861-ED-003	One Line Drawing - Conceptual Design (3 of 3)
861-LB-004	Two Shaft Mine Showing Development and Benching Headings
861-LB-005	Shaft Outfitting During Construction
861-LB-006	Mine General Arrangement
861-LB-007	General Cavern Layout - 2,500' Depth
861-LB-008	General Cavern Layout - 3,000' Depth
861-LB-009	Gas Distribution System in Mine - 3,000 ft Depth
861-LB-010	Section ‘A-A’ 3000' Depth
861-MD-001	Process Flow Diagram
861-MD-002	Meter Skid
861-MD-003	Gas Compression System
861-MD-004	Molecular Sieve Dehydrator
861-MD-005	Regeneration Gas System
861-MD-006	Refrigeration System
861-MD-007	Storage Cavern and Heater
861-MP-001	Compressor Building Plan & Elevation

ADVANCED UNDERGROUND GAS STORAGE CONCEPTS
REFRIGERATED-MINED CAVERN STORAGE
FINAL DRAFT REPORT

EXECUTIVE SUMMARY

Over the past 40 years, cavern storage of LPG's, petrochemicals, such as ethylene and propylene, and other petroleum products has increased dramatically. In 1991, the Gas Processors Association (GPA) lists the total U.S. underground storage capacity for LPG's and related products of approximately 519 million barrels (82.5 million cubic meters) in 1,122 separate caverns. Of this total, 70 are hard rock caverns and the remaining 1,052 are caverns in salt deposits. However, along the eastern seaboard of the U.S. and the Pacific northwest, salt deposits are not available and therefore, storage in hard rocks is required.

Limited demand and high cost has prevented the construction of hard rock caverns in this country for a number of years. The storage of natural gas in mined caverns may prove technically feasible if the geology of the targeted market area is suitable; and economically feasible if the cost and convenience of service is competitive with alternative available storage methods for peak supply requirements. Competing methods include LNG facilities and remote underground storage combined with pipeline transportation to the area.

It is believed that mined cavern storage can provide the advantages of high delivery rates and multiple fill-withdrawal cycles in areas where salt cavern storage is not possible. In this research project, PB-KBB merged advanced mining technologies and gas refrigeration techniques to develop conceptual designs and cost estimates to demonstrate the commercialization potential of the storage of refrigerated natural gas in hard rock caverns.

DOE has identified five regions, that have not had favorable geological conditions for underground storage development: New England, Mid-Atlantic (NY/NJ), South Atlantic (DL/MD/VA), South Atlantic (NC/SC/GA), and the Pacific Northwest (WA/OR). PB-KBB reviewed published literature and in-house databases of the geology of these regions to determine suitability of hard rock formations for siting storage caverns, and gas market area storage needs of these regions.

Many factors were analyzed in the selection of possible storage sites. These included available gas transmission pipelines, proximity to metropolitan areas, accessible power and water, proximity to environmentally sensitive areas, rock types, potential disposal sites for excavated material, and a sufficient water table for the storage formation. Based on this analysis, suitable geology for a possible site was found in Howard and Montgomery Counties, Maryland. Areas in this region have sufficient extent, are isotropic in nature, and are of high quality with excellent mechanical and physical properties for mined storage caverns. This area is also near commercial gas transmission lines that serve both Baltimore and Washington D.C.

Based upon the general site selection, the design parameters for the storage facility were developed. The

compressibility of natural gas, and the resultant gas density, is a function of temperature and pressure. At a given temperature, the compressibility of gas reaches an optimum value as shown in Figure 4-1. This relationship can be used to commercial advantage by reducing the size of a storage cavern for a given working volume of natural gas. As the temperature is lowered, the gas density increases, allowing more gas storage in a given size of cavern. The decreased cavern costs for the lower temperatures, requires an investment in refrigeration equipment, and will have recurring refrigeration energy and maintenance costs. Although the mass of stored gas is greatest for any given pressure at the minimum operating temperature, the amount of heat influx into the cavern is greater at lower temperatures requiring more refrigeration. Temperatures of +20°F, 0°F and -20°F were considered in the analysis. The minimum temperature, -20°F, was selected since commonly available carbon steel piping materials may be specified at the design conditions.

The final site design for this study consists of a mined cavern of approximately 37 million cubic feet at a depth of 3000 feet for gas stored at a temperature of -20 °F and a maximum pressure of 1250 psig. This would provide a working storage gas volume of five billion standard cubic feet. The surface site for the process facilities requires approximately four acres, with additional two to three acres necessary for the mine shafts and mining operation. Drawing 861-GP-001 shows a typical facility layout. A conceptual process design was developed that includes process equipment for gas measurement, compression, dehydration, refrigeration, and withdrawal gas heating. Equipment was sized for receipt and delivery rates of 250 million standard cubic feet per day, which provides a 20 day fill or withdrawal cycle for the five billion standard cubic feet of working gas storage.

The conceptual design of the mined cavern was prepared to demonstrate that a facility can be feasibly constructed, without the requirement for unique or unproven construction techniques, and to provide a basis for the cost estimate and construction schedule. The actual construction of such a facility will require a comprehensive geotechnical feasibility study performed at the site to determine subsurface geologic conditions as a prerequisite for a detailed design. Conventional state-of-the-art mining techniques were assumed for the conceptual design and are detailed in the report body. Consideration was given to optimum shaft and room sizes for the assumed formation and depth to assure mine stability. In addition a geomechanical review of the proposed cavern design was performed by RESPEC, evaluating the stability of the mine rooms and shafts, and the effects of the refrigerated gas temperatures on the stability of the cavern. The results of the study suggest the thermal effects do not have a large impact on the stability of the properties of the granite. Section 9 of the report discusses the health and safety aspects of the process design and the cavern, with attention given to emergency conditions and protective devices and procedures.

A rough order of magnitude cost estimate was developed for the facility for the optimum case considered. The cost summary is shown in Table 10-8. The facility is estimated to cost $178 million or approximately $35.60 per thousand standard cubic feet of gas stored. This is based on five billion standard cubic feed of working gas. The mining costs were estimated to be $20 per barrel of mined space developed. The

annual operating costs depend upon local labor rates and energy costs, however a range of costs are presented in Tables 10-9 and 10-10 based on anticipated energy usage and plant labor requirements. Table 10-11 presents a summary of the major operating costs for the facility, based on energy costs of $2.50 per million BTUs.

The cost estimates developed were used to perform a comparative market analysis of this type of gas storage system to other systems that are commercially used in the region of the study. Table 12-1 lists the unit capital costs for several existing storage projects of various designs for comparison to this study.

Capital costs of the Refrigerated Mined Cavern (RMC) project are substantially higher than the comparison group, however some differences in systems should be noted. The RMC project provides multiple high capacity peaking cycles per year as compared to the single cycle of some of the existing systems, particularly LNG. The ability to cycle several times per year allows the costs to be spread over a larger volume of gas , reducing unit costs of service. Table 12-2 summarizes rates for a series of LNG and salt storage projects, compared to a 15-year levelized rate for the RMC project.

Section 1
INTRODUCTION

The service that a natural gas cavern can provide is the modern equivalent of the old gas holder operations. Recent trends in market and natural gas delivery terms, encountered by gas distribution companies today, suggest that cavern storage of natural gas merits close examination.

The high-energy prices and resultant conservation (lower thermostat setting, better insulation, etc.) have resulted in new patterns in consumption of natural gas. Although consumption per household, as a result of conservation, has fallen, several distribution companies have experienced that, on extra cold days, the conservation ethic disappears and additional gas is used which results in very high peak-day send outs.

Thus, many distribution companies that have maintained their annual space-heating load over the past few years (by adding more customers to compensate for conservation) are experiencing disproportionately high needle peaking requirements. Cavern storage of natural gas provides singular sendout characteristics which suit such requirements, without the environmental, code compliance and gas compatibility problems, or feedstock supply and price uncertainty encountered by LNG or propane/air.

Over the past 40 years, cavern storage of LPG's, petrochemicals, such as ethylene and propylene, and other petroleum products has increased dramatically. In 1991, the Gas Processors Association (GPA) lists the total U.S. underground storage capacity for LPG's and related products of approximately 519 million barrels (82.5 million cubic meters) in 1,122 separate caverns. Of this total, 70 are hard rock caverns and the remaining 1,052 are caverns in salt deposits. However, along the eastern seaboard of the U.S. and the Pacific northwest, salt deposits are not available and therefore, storage in hard rocks is required.

Because of the limited demand and high cost, hard rock caverns have not been built in this country for a number of years. The storage of natural gas in mined caverns will be successful if it can be proven to be technically feasible given the geology of the targeted market area; and economically feasible if the cost of service can be justified based on needs of the market and the flexibility of operation to meet peak needs, that cavern storage can provide, compared to alternative storage methods if available. The latter would include LNG facilities that are being installed or investigated in many areas, and remote underground storage combined with pipeline transportation to the area.

LNG facilities are particularly costly and only provide for a single storage cycle per year, whereas cavern storage can be cycled a number of times depending on design criteria. The large number of salt cavern projects both in the producing and market areas in recent years have proven the desirability and cost effectiveness of such high delivery, multiple cycle capability. It is believed that mined cavern storage can provide these same advantages in those areas where the development of salt cavern storage is not possible. Since the last hard rock caverns were constructed, advanced mining techniques and modern rock mechanics technology have been introduced and perfected that have the potential to reduce the cost of constructing

hard rock storage caverns. Also, the technology and equipment used to refrigerate natural gas is proven, and in a storage application, can significantly reduce the physical volume of space required to store a given quantity of gas. For example, refrigerating the gas to -40°F would reduce the required space by 50%, a significant potential savings in mining costs.

In this research project, PB-KBB merged advanced mining technologies and gas refrigeration techniques to develop conceptual designs and cost estimates to demonstrate the commercial potential of storage of refrigerated natural gas in hard rock caverns. The storage of refrigerated natural gas in hard rock mined caverns will be successful if:

- It can be demonstrated that the capabilities available fit the hourly, daily, weekly and seasonal gas load variations for both conventional gas markets and electric-generated plant markets.
- Costs of service for single- and multi-cycle storage with mined caverns are favorable compared to out-of-region storage/pipeline and LNG alternatives.

For this project, an in-house literature search was conducted to target regions which may require underground storage, but may not have either large salt deposits or suitable brine disposal facilities. The Gas Research Institute 1994 Topical Report entitled “Future Seasonal Natural Gas Loads and Gas Delivery Capacity Requirements in the Lower-48 United States” provided an indication of the combined peaking and market area gas storage needs by 2010 in areas primarily along the eastern seaboard of the U.S. and the Pacific Northwest, areas which have rock formations in which mined cavern storage can be installed near the point of use. The areas reviewed included New England, Mid-Atlantic (NY/NJ), South Atlantic (DL/MD/VA), South Atlantic (NC/SC/GA) and the Pacific Northwest. However, since 1994 there has been significant asset development activity in most of the regions which would temper or alter the conclusions of the 1994 study. Based on the review of the geological literature and the potential for storage, this project targeted the DL/MD/VA region for further study.

Section 2

LITERATURE SEARCH FOR SELECTING TARGET AREAS

DOE has identified five regions, based on the Gas Research Institute 1994 Topical Report entitled "Future Seasonal Natural Gas Loads and Gas Delivery Capacity Requirements in the Lower-48 United States," that do not have favorable geological conditions for underground storage development. These regions are:

New England

Mid-Atlantic (NY/NJ)

South Atlantic (DL/MD/VA)

South Atlantic (NC/SC/GA)

Pacific Northwest (WA/OR)

Published literature and in-house databases relating to the geology of these regions were reviewed for the purpose of determining suitability of hard rocks for siting storage caverns, which could provide combined peaking and market area gas storage needs of these regions. Furthermore, since 1994 there has been significant asset development activity in most of the regions that might temper or alter the conclusions of the 1994 study. Therefore, in-house databases developed since 1994 were reviewed to update each region's capacity situation.

The purpose of this study was to select one target area for the research study relating to refrigerated-mined cavern storage.

General Requirements for Storage Sites

The following are some of the general requirements for storage sites:

- Proximity to transportation systems, such as pipeline, that are to be used for bringing in or shipping out the stored gas to minimize the extent of new pipelines construction. This is of particular importance in areas where approval of new pipeline rights of way is often difficult to obtain.
- More advantageously, and especially for meeting the peaking needs, the storage space would be created near a marketing area, such as a metropolitan area or a strategically located point from which thickly populated areas may be served. Market centers, with their access to multiple pipeline interconnections and supplies, provide a natural platform for gas trading, risk management and opportunity for arbitrage. Storage in Market Center is a multi-purpose resource, such as to support short-term gas loans, gas balancing, and peaking services ("Natural Gas 1996 - Issues and Trends," Energy Information Administration, Dec. 1996).

- Adequate electric power and water supply should be available for storage
- Construction site should be easily accessible
- Congested areas should be avoided, especially environmentally sensitive areas (i.e., natural, state, and local parks, monuments, reservoirs, etc., and areas zoned “residential”)
- Suitability of rock for storage - All rock types must be tested locally for site suitability

    (a) The cavern host rock should be as impervious and free of fractures as possible to minimize leakage.

    (b) The rock should be strong enough requiring little or no artificial support of the cavern roof for the given dimensions. Stronger the rock type, the larger the size of the cavern that can be constructed.

    (c) The rock should be uniform and should have little or no jointing, faults and other discontinuities such as shear zone. This impacts the strength of the rock, leakage potential and the dimensions of the underground openings.

    (d) For economic reasons, the rock should be easy to excavate for the shafts and underground caverns.

    (e) The rocks through which the shaft will pass should not be incompetent or be heavy water-bearing, since water control in shaft sinking would require stabilization techniques such as grouting, or freezing, which are expensive.

    (f) Shale and siltstone have been most favorable types of sedimentary rocks because they are impervious, and relatively easy to excavate. However, these rocks require extensive artificial supports, such as roof bolts.

    (g) Igneous and metamorphic rocks are also impervious, could form tight caverns and are strong enough to have self-supporting roofs of the caverns. Large size caverns can be constructed in these types of rocks.

- Availability of space nearby for disposal of the excavated material.
- Sufficient water table to maintain a positive hydrostatic head at the pressures used for storage.

<u>New England Region</u>

The following information is taken from a paper by Oswald Farquhar of the University of Massachusetts (“Favorable Bedrock Formations for Deep, Man-made Caverns in New England (USA)” - Rockstore 77).

The principal rocks of New England belong to four time sequences - Precambrian, late Precambrian to Middle Ordovician, Silurian through Middle Devonian, and Late Paleozoic.

Farquhar considers about 90 formations as suitable for caverns; however, further data is still required to confirm site location. He considers half a dozen rock types as potentially favorable, viz., granite, gabbro, gneiss, massive schists, diorite and amphibolite. Granitic rocks are the most common, with uniaxial compressive strength varying from 1000 to 2500 kg/cm^2. They comprise about one-quarter of the whole region, one or more favorable units being located closest to most industrial and population centers where peak power need exists.

C. W. Wolfe of Boston University ("Underground Storage of Liquid Petroleum Hydrocarbons in the United States," Research and Coordinating Committee, Interstate Oil Compact Commission) believes that only the northeastern part of Massachusetts around Boston, containing the Cambridge formation is suitable for cavern location. The formations consist of Devonian or carboniferous siltstones, conglomerate tillite, lavas and tuffs.

Lloyd J. French of the State Development Commission of Connecticut believes that lack of suitable geological maps make it virtually impossible to locate and evaluate suitable structures.

The 1994 GRI study forecasted a new peaking market area storage need of 269 MMCFD and neew annual delivery or pipeline capacity needs of 1,130 MMCFD by the year 2010. Since the time of that study, approximately 978 MMCFD of pipeline expansion projects have been announced into the region, reducing the total net requirement to approximately 421 MMCFD. These include 90 MMCFD of expansion at DOMAC LNG, 510 MMCFD of new pipeline capacity in the form of the Maritimes and Northeast project, 200 MMCFD of Iroquois pipeline expansion, and 178 MMCFD of Portland Natural Gas Transmission capacity.

New market area, refrigerated hard rock peaking storage capacity into New England would compete with expansion LNG and opportunities to expand new and existing pipeline paths planned for the region. Assuming that the proposed projects detailed above are placed into service, the 2010 net requirement for new deliverability is reduced to a total of 421 MMCFD. Moreover, any incremental need is likely to require more pipeline capacity relative to peaking capacity, given the relatively low overall percentage of peaking/market area storage need to pipeline need as identified in the GRI study.

Mid-Atlantic (NY/NJ)

New York

Storage in salt beds already exists, or is either undergoing construction, or is planned. Two projects are in operation.

Much of east central and western New York is underlain by shale beds, which could be suitable for mined

storage. The Middle Devonian Hamilton shale beds are fine-grained, medium gray to black and calcareous in varying degrees and contain several limestone beds. The Tully limestone over most of the area is a uniform, thick bed of dense limestone, which would form a suitable roof for a mined shale cavity.

The following description for locating caverns in hard rock are taken from W. Lynn Kreidler, Senior Petroleum Geologist of New York State Science Service, report to Research and Coordinating Committee of Interstate Oil Compact Commission.

New York State has two main areas of hard rocks in which storage caverns are possible. One of the areas is the Adirondack Mountains or northeastern New York. The other area is the "Hudson Highlands." This is a section in southeastern New York, which takes in parts of Duchess, Putnam, Rockland, Orange and Westchester counties. The "Hudson Highlands" of Precambiran gneiss which extend from New England southward into New Jersey, and intersect the Hudson River in the area of West Point, NY. Other areas of outcrop of the Precambiran gneiss are along the east side of the Hudson River in Westchester County and extend to the south into Bronx County.

A mined storage cavity in the gneiss would be expensive compared to salt caverns, but the factor of nearness of these rocks to the metropolitan consumer area would serve to counterbalance the construction costs. The cavern must be sealed to prevent leakage through cracks or fissure caused by minor faulting or shearing.

New Jersey

New Jersey has hundreds of steel tanks storing hydrocarbons all along the navigable waters of the Delaware and Arthur kills. This type of storage on the ground surface is expensive and is unsafe, and thus, there would be a greater need for large, economic and safe underground storage in the area.

The following information on probable rock deposit for potential storage site is taken from the report of Meredith Johnson, State Geologist of New Jersey to the Interstate Oil Compact Commission.

Limestone is a relatively strong rock, and a cavern located in this rock will require little or no roof support, provided the cavern is located in an area not heavily faulted. For the Metropolitan New York area, the nearest limestone is at Peapack, some 25 miles from Newark. The Phillipsburg-Easton area is also underlain by limestone.

Some caverns have been constructed in shale. However, control measures must be undertaken in order to prevent sloughing of the shale around the opening. Much of the metropolitan area surrounding Paterson, passaic, Newark, Elizabeth and New Brunswick is underlain by Triassic shale and sandstone. Triassic sandstones are not very porous, their permeability being due to the fracture systems, which traverse them, just as with shale. Structurally sandstones are stronger than shales.

Part of the Martinsburg argillaceous rock has been metamorphosed to slate. It is stronger than shale and

a cavern, excavated in this material, would require little support. The slatey portion of the Martinsburg is found within two beds of rock extending northeastward form Delaware and Slateford on the Delaware River.

Granite rocks are very strong and a cavern excavated in this type of rock will stay open for a very long time and would require very little, if any artificial support. However, these rocks have been subjected to regional stresses, which have developed a number of crisscross fractures. Regions of heavy fracturing and faulting must be avoided for storage caverns. Many sites in the Highlands could be suitable where the unweathered crystalline rock of this type is relatively impermeable.

At Trenton there is a gabbro rock which is dense, impervious and very strong. A storage cavern in it will not require any support. Much more widespread in their occurrence are the dikes and sills of diabase, and flows of basalt, – all of Triassic age – which are found near Lambertville, on the Delaware, and in many a hill and ridge between the Delaware and the Hudson. The largest of these is the palisades – Rock Hill Sill which could provide the storage needs of the Bergen Hill – New York area. The full thickness of the Palisades sill is 900 to 1000 ft.

The 1994 GRI study forecasted a new peaking/market area storage need of approximately 1.4 BCFD and a new pipeline capacity need of approximately 1.1 BDFC by 2010. However, since that time, this region has been the focus of the majority of new asset development activity in the U.S. At present, there are at least four new pipeline capacity projects planned for the region, including Market Link (Independence, Niagara Expansion) at BCFD, Spectrum/Exclsior at 500 MMCFD, Eastern Express at 500 MMCFD, and Millenium Pipeline at 650 MMCFD. The net effect of these 2.65 BCFD of projects is to effectively reduce the regional need to zero, or slightly negative as depicted in Table 2-2.

While it is unlikely that all of these projects will be successfully developed, their presence and sheer magnitude of number tends to place even more pressure on any new market area storage proposals that might come forward for the region.

South Atlantic (DL/MD/VA)

Delaware

Not much information is available regarding the rock type suitable for cavern location. John H. Groot, State Geologist, has recommended further investigation by core test hole drilling and pressure testing, especially in the Cockeyville marble.

Maryland

The following geological information is taken from the publication entitled “Preliminary Design Study of Underground Pumped Hydro and Compressed-Air Energy Storage in Hard Rock,” Volume 5, EM-1589, Vol. 5, Research Project 1081-1 DOE/ET 5047-5. (See Figure 2-1)

The State is divided into five distinct physiographic provinces ranging from east to west, these being the Coastal Plain, Piedmont, Blue Ridge, Valley and Ridge and Appalachian Plateau.

The Coast Plain consists of porous and water-bearing sedimentary rocks, and is not considered to be a viable site because of difficulty of interpretation beneath the thick coastal sediments. Similarly, the Valley and Ridge and Appalachian Plateau are not satisfactory because they are sedimentary rocks, have low compressive strength, have high permeability, are folded and faulted.

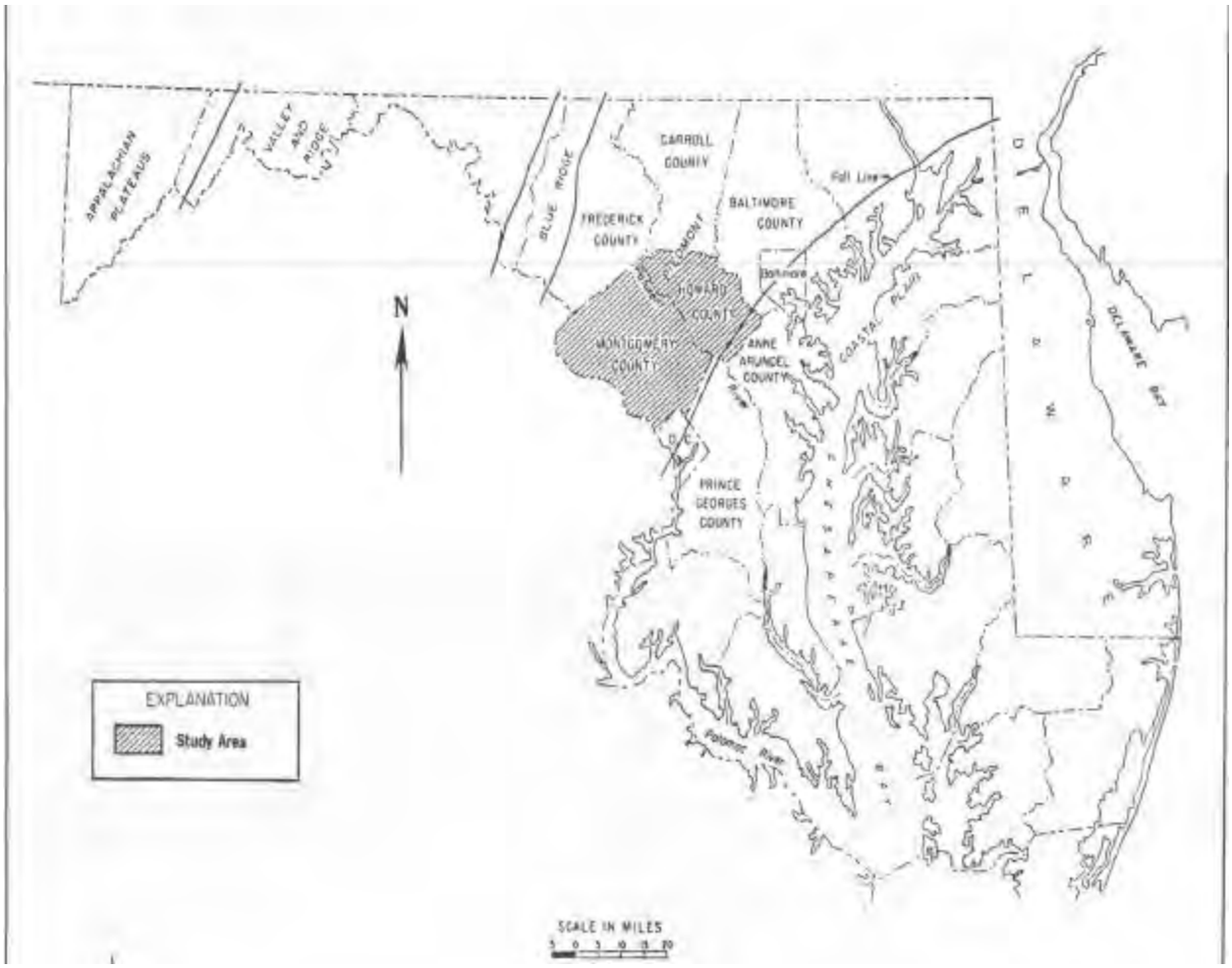

FIGURE 2-1. Physiographic Map of Maryland

The Piedmont extends westward from the Coastal Plain to the Blue Ridge, a distance of approximately 40 miles. The stratigraphic sequence of the Maryland Piedmont ranges from the crystalline rocks of Precambrian basement to Triassic sedimentary rocks. The Precambrian basement rocks of the Baltimore Gneiss complex are overlain by the metamorphic rocks of the Glenarm series, a series of late Precambrian schists, gneisses, marbles, etc. These rocks are in turn intruded by a series of Paleozoic age igneous intrusive ranging from granites to basalt.

The Blue Ridge Province extends from the Catocin Mountains on the east to South Mountain on the west. Structurally, the Blue Ridge is a predominant uplifted anticline. Its core consists of granodiorite and biotite granite gneisses.

The more favorable rock types that fall within the desirable ranges of physical and mechanical characteristics are the younger intact granites and high-grade metamorphic rocks such as gabbros, granodiorites and gneisses. Many of these rocks are massive, isotropic in nature and are of high quality with excellent mechanical and physical properties for sustaining large underground openings.

The seismicity of Maryland was found to be extremely low. There are no known active faults within the area.

Peaking Needs of Delaware/Maryland/Virginia

The 1994 GRI study forecasted a need for 450 MMCFD of new peaking/market area storage capacity and 803 MMCFD of new pipeline capacity by 2010.

While there are no relatively modest pipeline expansions for the area on the books by Columbia Gas Transmission and CNG totaling 272 MMCFD, there appears to be little or no efforts underway to develop new peaking/market area storage capacity in the region. However, it is important to remember the possibility that an overbuilt downstream market, such as New York/New Jersey would be able to offer a number of peaking services to upstream markets via displacement. This would tend to de-emphasize the need for new peaking storage into this region in favor of new pipeline capacity needed to meet the annual delivery capacity requirement.

New market area and peaking storage would tend to compete with services from new pipelines downstream offered back to the region via displacement. Once these projects are built into the New York and New Jersey region to meet annual or baseload needs, the incremental cost of redelivering the services back upstream are very low.

Virginia

Very little information is available on the suitable rock type for storage cavern location.

South Atlantic (NC/SC/GA)

North Carolina

The Piedmont and Mountain Provinces of North Carolina are underlain with igneous and metamorphosed rocks. However, the suitability of any rock type for cavern location has not been determined due to the lack of field investigations.

South Carolina

No features in the State have been identified as suitable for storage caverns.

Georgia

Storage caverns could be located in the crystalline formations, such as Stone Mountain, near Atlanta. However, more detailed information is lacking.

Peaking Needs of North Carolina/South Carolina/Georgia

The 1994 GRI study predicted a peaking market area storage need of approximately 1.2 BCFD and new annual delivery capacity needs of approximately 700 MMCFD.

Two significant LNG projects, Pine Needle and Etowah, have been announced for the region along with a number of relatively small expansions/additions to the Transco delivery system. Pipe Needle, located in North Carolina, represents an incremental 400 MMCFD of vaporization capacity, Etowah, a recently announced project proposed for Polk County, Georgia would have a design capability of 450 MMCFD. The three Transco expansions collectively account for 347 MMCFD of incremental capacity. The net effect is to reduce the overall capacity need of the region as outlined in the GRI study to about 681 MMCFD. It is important to note however that new LNG projects can often encounter high levels of resistance both with respect to permitting and customer acceptance and this should be accounted for making an assessment of the likelihood of success of such proposals. Overall, this area appears to offer significant promise for a new peaking/market area storage facility.

Pacific Northwest (WA/OR)

Washington

Storage caverns could be located in the granitic rock areas close to the transportation facilities. These areas are north of Spokane. However, not much information is available on faults, fissure or cracks in these rocks. Shale is another possibility with the western part of the state.

Oregon

No information is available on the suitability of any rock for storage cavern locations.

Peaking Needs of Washington/Oregon/Idaho

The GRI study called for 401 MMCFD of new market area/peaking storage capacity and 366 MMCFD of new

pipeline capacity by 2010.

Various expansion projects have been announced that could largely satisfy the needs of this region. Northwest Pipeline is planning an expansion of its system through the Columbia River Gorge to serve needs west of the Cascades (approximately 250 MMCFD). Expansions are also proposed for Jackson Prairie and Mist Storage (WA and OR, respectively) totaling 294 MMCFD. Finally, an LNG project sized at 250 MMCFD vaporization capacity is proposed for the Sumas, WA area. This project would compete with the Northwest Pipeline expansion project and/or the 215 MMCFD BC Gas Southern Crossing project proposed for southern British Columbia. The total deliverability of these projects, excluding Southern Crossing, is 694 MMCFD, reducing the net need for new capacity to approximately 70 MMCFD.

CONCLUSIONS

Based on the 1994 Report of Gas Records Institute (Table 2-1) it would appear that the most desirable region for further study should be the Mid-Atlantic (NY/NJ) area which has the highest peaking needs of the five regions. On the basis of that study and the geological information, the optimum site should be the West Point area in New York which is close to the Columbia Gas and the Algonquin Transmission Lines, serving many metropolitan areas.

The 1994 GRI study takes a comprehensive look at need for pipeline capacity and peaking/market area storage by region through the year 2010. Since its publication in 1994, a number of new proposals for expanding existing facilities and/or building new facilities have come forward.

The New York/New Jersey market is the most competition laden in terms of new proposals. New England shows a need for capacity, but this is likely to be dominated by a need for pipeline or year-round capacity relative to peaking capacity. Several new proposals for the Pacific Northwest region reduce the net need significantly. Either South Atlantic region would appear to be a good candidate for new projects, as evidenced by the recent announcement and development of two new LNG proposals for the NC/SC/GA area (Table 2-2).

For the South Atlantic (DL/MD/VA) region, the Piedmont rocks of Maryland are the most suitable rock types for location of a storage cavern. Ellicott City Granodiorites have sufficient extent, are isotropic in nature, are of high quality with excellent mechanical and physical properties for storage caverns. The Ellicott City area is close to the Transcontinental Gas Pipeline, Columbia Gas Transmission Lines, Fredrick Gas Col. Line, Washington Gas and Light CO., and the CNG Transmission. It will serve both Baltimore and Washington D.C. area. This site is therefore recommended for further study for the location of a refrigerated mined gas storage cavern.

Table 2-1
Summary of 2010 Peaking and Market Area Gas Storage Requirements of Selected Regions of the US (1994)

Region	Peaking/Market Area Storage Needs (MMCF/day)
New England	269
Mid Atlantic (NY/NJ)	1,352
South Atlantic (DL/MD/VA)	450
South Atlantic (NC/SC/GA)	1,190
Pacific Northwest (WA/OR)	401

Source: GRI Topical Report – Future Seasonal Natural Gas Loads and Gas Delivery Capacity Requirements in the Lower 48 United States (1/94)

Table 2-2
1994 Edition of the Baseline Projection

	New Peaking/Market Area Storage Needs, 2010 (1) (MMCFD)	New Annual Delivery Capacity Needs, 2010 (MMCFD)	Planned or Completed Pipeline & Expansion Projects, 1994-1997 (2) (MMCFD)	Net Requirement (MMCFD)
New England (ME/VT/NH/MA/CT/RI)	269	1,130	978	421
Mid Atlantic (NY/NJ)	1,412	1,158	2,650	(80)
South Atlantic (DL/MD/VA)	450	803	272	981
South Atlantic (NC/SC/GA)	1,190	688	11,197	681
Pacific Northwest (WA/OR/ID)	401	366	695	73

Note: (1) Assumed “high bound” on peak shaving
(2) DOE/EIA Natural Gas 1996 Issues and Trends (December, 1995) and in-house data.

Section 3

SELECTED PROCESS AND CAVERN DESIGN PARAMETERS

The process design parameters selected for this study are as follows:

Maximum gas pressures:	1,080 - 1,250 psi
Minimum gas pressures:	250 psig and 100 psig
Operating temperatures:	-20°F, 0°F and +20°F
Cavern depth:	2,500 - 3,000 feet
Operating pressure gradient:	0.433 psi/ft
Working gas volume:	5 Billion Standard Cubic Feet (BSCF)
Gas withdrawal rate:	250 Million Standard Cubic Feet per Day (MMSCFD)
Gas injection rate:	250 MMscfd
Incoming gas temperature:	50°F to 80°F
Dehydration:	Water content reduction from 7 lbm/MMscf to < 1 lbm/MMscf prior to chilling (TEG or Mole Sieve-type)
Production casing diameter:	20 inch OD (0.500" wall)

The design parameters were selected based on cavern operating experience as well as an understanding of the limitations of the geology with respect to cavern depth. Industry experience with mining operations in hard rock would suggest limiting the cavern depth to approximately 2,500 - 3,000 feet. The maximum operating pressure of the cavern is determined by specifying a maximum pressure gradient equal to 95 percent of the hydrostatic head of water, 0.433 psi/ft.

Generally, crack or fissures occur naturally in rock. Water is usually found in these cracks or fissures. Natural gas stored underground may be prevented from leaking from a hard rock cavern via the cracks or fissures by storing the gas at no more than a 0.433 psi/ft gradient which is equal to a pressure of approximately 1,250 psig for the cavern at the selected depth of 3,000 feet below ground.

A higher maximum cavern pressure would reduce the required cavern size for a given mass of stored gas. In theory, increasing the cavern depth would allow for a higher gas storage pressure, allowing for a smaller cavern; however, the cost of cavern construction at a depth deeper than 3,000 feet would likely be prohibitive. Another means for increasing the mass of stored gas, without increasing the storage pressure, is lowering the gas temperature and maintaining the lower temperature in the cavern. The lower temperature results in a more favorable gas compressibility, i.e., the gas is more efficiently packed.

Three temperatures were considered in the analysis: +20°F, 0°F and -20°F. The minimum temperature, -20°F, was selected since most commonly-available carbon steel piping materials may be safely subjected

to the required maximum operating pressure and external stresses. At lower temperatures, special metallurgy may be required. At any given pressure in the operating pressure range of the cavern, the mass of gas contained is greatest at the lowest of the three operating temperatures.

Although the mass of stored gas is greatest for any given pressure at the minimum operating temperature, the amount of heat influx into the cavern is greater at lower temperatures than at higher temperatures. Maintaining a -20°F cavern temperature will require more refrigeration than at +20°F; therefore, there is an economic trade-off. A larger, unrefrigerated cavern will have higher construction costs than a smaller, refrigerated cavern. A refrigerated cavern will require refrigeration equipment and will have recurring refrigeration energy and maintenance costs.

Two minimum, or "cushion gas" pressures were considered: 100 psig and 250 psig. Maintaining a minimum cushion of gas in the cavern may reduce the influx of subsurface water via cracks and fissures in the surrounding rock. A higher cushion gas pressure may also eliminate the need for recompressing the gas as it is withdrawn. Also, a higher minimum gas pressure results in a higher minimum gas density and greater storage well deliverability. Since the storage well must deliver 250 MMSCFD, a higher minimum gas pressure will ensure adequate well deliverability as the cavern pressure approaches a minimum.

A lower minimum cavern pressure results in a smaller cavern size requirement for a given mass of working gas. "Working gas" is defined as the useable volume of stored gas or the total stored gas volume, minus the "cushion gas". A lower minimum cavern pressure means less cushion gas and a lower overall "total" gas volume (total gas volume = working gas volume + cushion gas volume), for a given working gas volume. Both the lower and higher minimum cavern pressures will likely result in required gas recompression. Typical transmission pipelines operate at pressures greater than 250 psig. Since compressors must be used for gas injection into the cavern, the same compressors may be used for gas recompression requirements during withdrawal.

A gas injection rate of 250 MMscfd was selected, based on a 5 BSCF working gas volume and a 20-day cavern fill rate. The 20-day cavern fill rate is common throughout the gas storage industry. A 250 MMscfd cavern withdrawal rate was selected. The fill and withdrawal rates are maximums and will be used for determining compressor and refrigeration equipment sizing among other things. The temperature of the incoming gas is assumed as ranging from 60 to 80°F which is the commonly-found temperature range of gas after being transported long distances via underground pipelines.

Due to the low temperatures anticipated during storage operations, the gas obtained from the gas transmission pipelines may contain too much water. Pipeline industry standards require a water content of not more than 7 lbm/MMscf of gas. This water content is acceptable as long as the gas temperature remains above 40 to 50°F. However, since the gas may be cooled to as low as minus 20°F, additional dehydration will be required prior to refrigerating the incoming gas.

Upon withdrawal from the cavern, the water content of the gas is expected to be sufficiently low as to not require dehydration.

The production casing diameter (OD) is assumed to be 20 inches. This diameter should prove sufficiently large so as not to result in excessive pressure losses, with a minimum cavern pressure of 250 psig at a maximum temperature of 20°F.

CAVERN DESIGN PARAMETERS

I. Number and Type of Shafts

Shaft size and the required number of shafts will be determined based on the hoisting rates to complete the cavern as quickly as possible and provide adequate ventilation. The major constraint would be how fast the broken material from the cavern can be hoisted to the shafts.

II. Shaft Depth

Shaft depths of 2,000, 2,500 and 3,000 ft will be considered with the design for the purpose of cost optimization. The hydrostatic pressure at 3,000 ft depth will be about 1300 psi. The lithostatic pressure at this depth will be approximately 3000 psi. The shaft lining will be designed for these loads.

III. Shaft Location

The shafts will be located within a shaft pillar, approximately in the middle of the cavern.

IV. Cavern Size

The cavern will be sized to contain 5 billion SCF of working gas volume a 777 MMSCF of cushion gas at 250 psig and -20°F. At a temperature of -20°F and a minimum gas pressure of 250 psig, the total cavern volume will be approximately 37 million cubic feet.

V. Ventilation

A ventilation current of 300,000 cfm will be provided for the health and safety of the personnel. Initially, a mine fan with tubing will provide the air. The rooms should be connected by cross-cuts to reduce frictional losses in tubing.

VI. Ground Control

The need for ground control measures will be determined in a rock mechanics study of the strata. Need for rock-bolt pattern will be studied and an optimum design proposed. The need for shotcrete around the cavern for gas storage purposes will also be investigated in the rock mechanics study.

VII. Disposal of Excavated Material

Surface design will include a pit to dispose of excavated material from the shafts and cavern, until removed from the site.

VIII. Suitable Rock Types

(a) The cavern host rock should be as impervious and free of fractures as possible to minimize leakage.

(b) The rock should be strong enough requiring little or no artificial support of the cavern roof for the given dimensions. Stronger the rock type, the larger the size of the cavern that can be constructed.

(c) The rock should be uniform and should have little or no jointing, faults and other discontinuities such as shear zone. This impacts the strength of the rock, leakage potential and the dimensions of the underground openings.

(d) For economic reasons, the rock should be easy to excavate for the shafts and underground caverns.

(e) The rocks through which the shaft will pass should not be incompetent or be heavy, water-bearing, since water control in shaft sinking would require stabilization techniques such as grouting, or freezing, which are expensive.

Section 4
CHILLING COMPRESSED NATURAL GAS TO MINIMIZE STORAGE SPACE

BASIC PRINCIPLE

The compressibility factor of natural gas, and the resultant gas density, is a function of temperature and pressure. When the temperature of natural gas is decreased form normal ambient temperatures, the compressibility factor decreases and the density of the gas increases. At a given temperature, as gas pressure increases, the compressibility factor reaches a minimum value, and then increases with additional pressure. This is shown in Figure 4-1. Figure 4-2 shows the relationship of gas volume to cavern pressure at various storage temperatures, for a fixed cavern special volume. These relationships of volume, temperature, pressure and compressibility are based on the General Gas Law and Charles/Boyles Law:

General Gas Law

$$PV = ZNRT$$
$$D = 1 / V = P / ZNRT$$

Where:

P = pressure of the gas in Psia
V = volume of gas in cubic feet
Z = gas compressibility factor
R = universal gas constant, 10.73 for all gases with the above units
T = temperature of the gas in absolute (460 + °F)
D = gas density in lbs. / cubic feet

Charles Law

$$P_{sc}\ V_{sc} / T_{sc}\ Z_{sc} = P_{cavern}\ V_{cavern} / T_{cavern}\ Z_{cavern}$$

Where:

P_{sc} = pressure at standard conditions, psia

P_{cavern} = pressure in the cavern, psia

V_{sc} = volume, cubic feet at standard conditions

V_{cavern} = volume of the cavern in cubic feet

Z_{cavern} = the gas compressibility factor in the cavern at cavern pressure

Z_{sc} = the gas compressibility factor at standard conditions

T_{sc} = temperature, absolute, (460 + °F) at standard conditions

T_{cavern} = temperature, absolute in the cavern

Rearranging terms to solve for the amount of natural gas in cubic feet at standard conditions, (14.73 psi, and

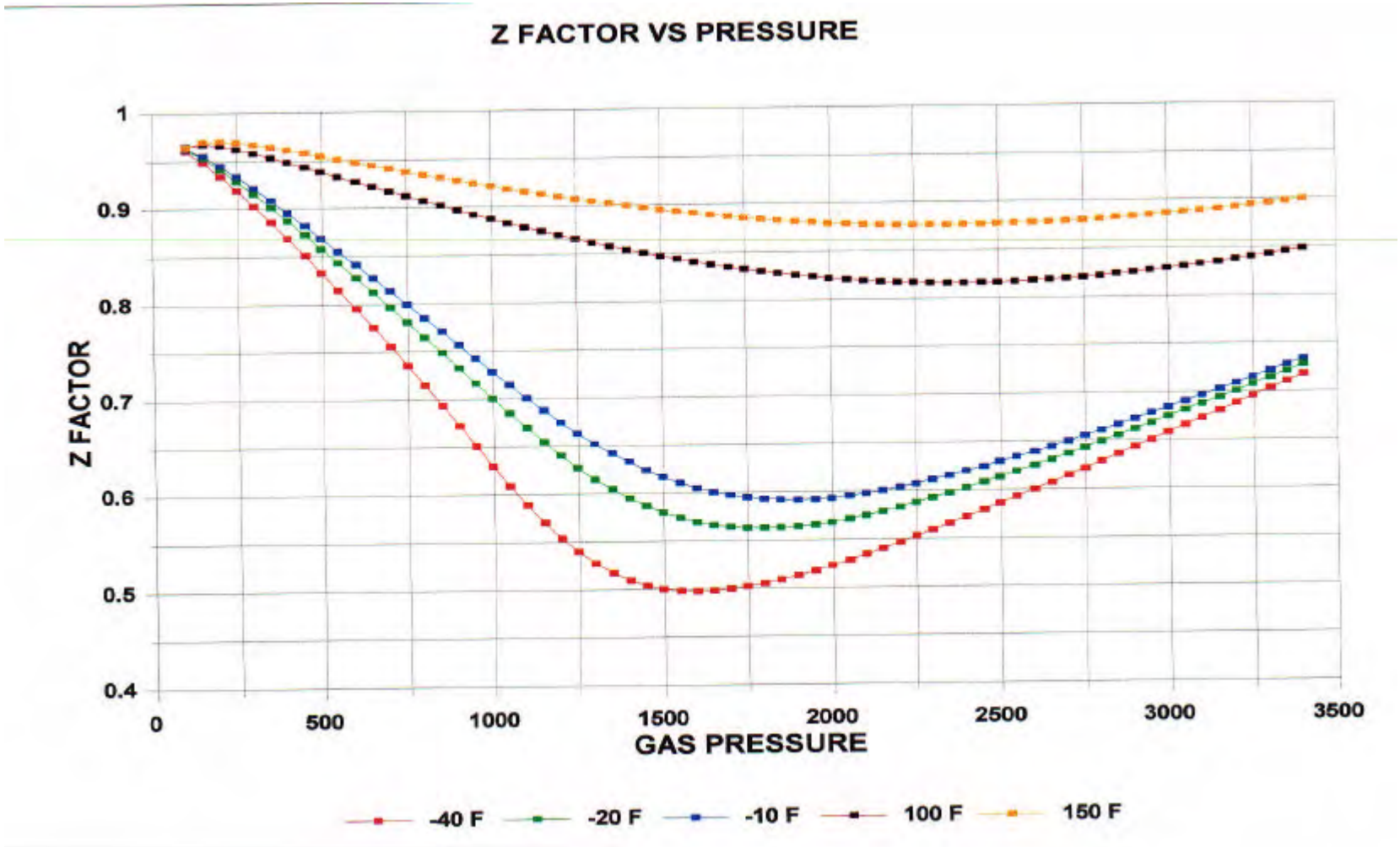

Figure 4-1 Graph of Z Factor Vs Pressure

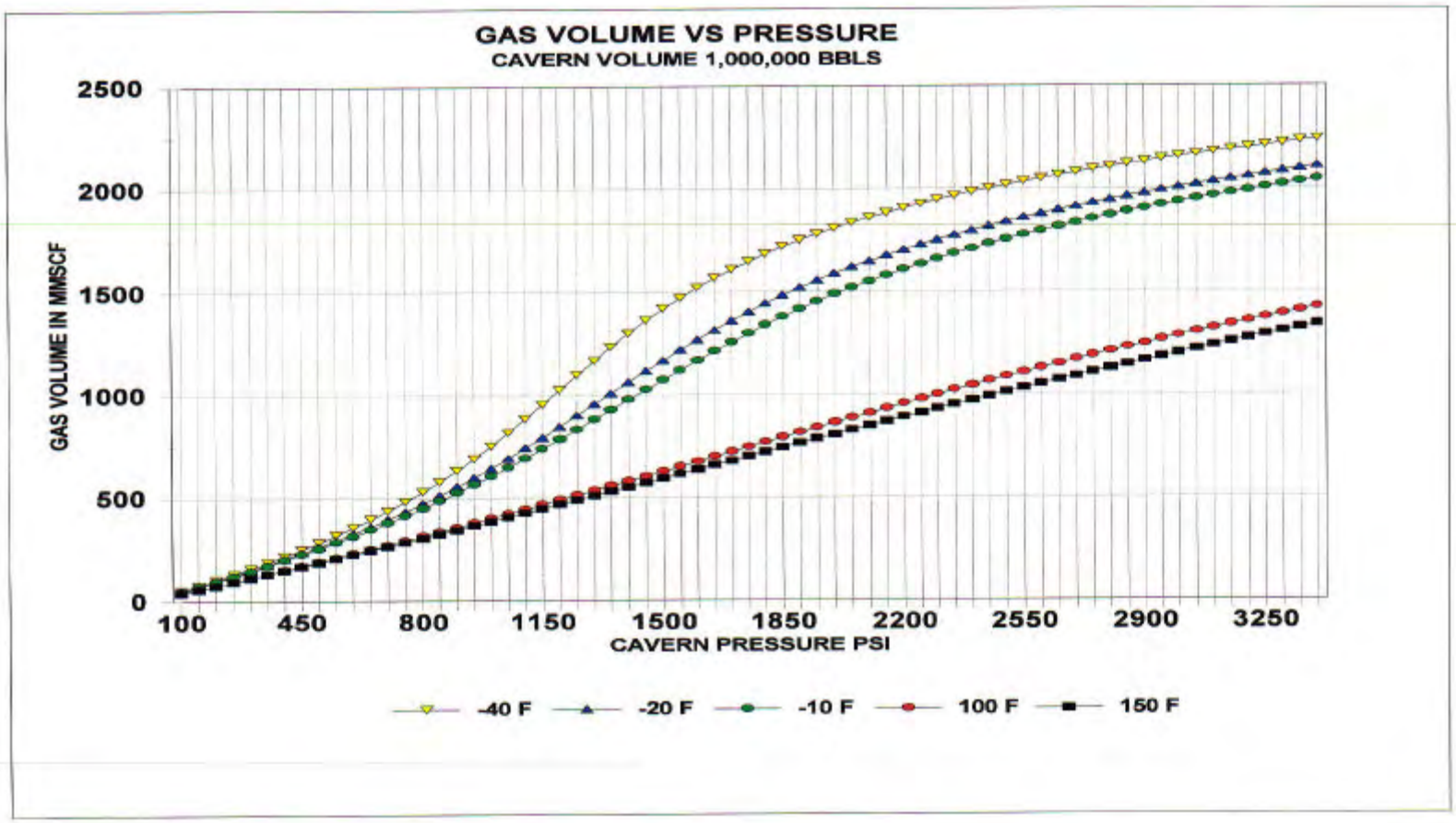

Figure 4-2 Graph of Gas Volume Vs Pressure

60°F).

$$V_{sc} = (P_{cavern}\ V_{cavern} / T_{cavern}\ Z_{cavern}) * Z_{sc}\ T_{sc} / P_{sc})$$

Referring to the above equation for V_{sc} cubic feet of gas stored, the amount of natural gas that can be stored in a given space increases as the temperature and compressibility factor decreases. Or, to store a given amount of gas, at a given pressure, the space (cavern volume) required decreases as the temperature and compressibility decreases.

Assuming that the cavern gas temperature is 100°F, the cavern volume is 1,000,000 barrels, and the pressure in the cavern is 1,500 psia, the volume of gas at standard conditions is as follows:

V_{sc} = (1,500 psia * 1,000 bbl * 5.6146 ft^3/bbl * 1.0 * 520) / (560 * 0.84 * 14.73)
= 632,038.3 cubic feet

Based upon the above sample calculations, the amount of gas that can be stored in a 1,000,000-barrel cavern at -20°F is 1,165,010.95 / 632,038.3 or 1.843 times as much as can be stored at 100°F, or the cavern volume could be reduced to 1,000,000 bbl / 1.843 = 542,593.6 bbl to store 632,038.3 cubic feet of gas.

Based upon these preliminary calculations, we evaluated the costs of developing a facility for the storage of chilled compressed natural gas utilizing conventional gas processing and refrigeration equipment along with a conventionally mined storage cavern in a hard rock formation.

Section 5

PROCESS CONCEPTUAL DESIGN

Efficient storage of gas in underground caverns requires process equipment which properly conditions the gas beforehand. (See Process Flow Drawing 861-MD-001.) The gas, to be stored, will likely be drawn from a large natural gas transmission line (trunkline) at a pressure, which may be too low for efficient storage in an underground cavern. The trunkline pressure may vary from 400 to 600 psig during the heating season to as high as 1,300 psig during the summer months. The storage cavern requires gas from 650 psig to 1,250 psig, depending upon the depth of the cavern, (from 1500 to 3,000 feet).

In the case of a cavern mined in rock, such as that being considered in this study, the maximum operating pressure is based on cavern depths of 1,500, 2,000, 2,500 and 3,000 feet. Therefore, the maximum cavern pressures are limited to 650, 866, 1,083 and 1,250 psig, based on the hydrostatic head of water at the respective depths.

Since the gas in the trunkline may be at a pressure as low as 400 psig, the gas will have to be compressed in order to fill the cavern. The gas compression will be achieved by at least one, and likely several, gas compressors operating in parallel. The compressors may be driven by electric motors, gas turbines, or piston engines.

PROCESS DESCRIPTION

Measurement

The process begins by drawing pipeline-quality natural gas from one or more natural gas transmission lines, which may border the facility. The gas is first measured with custody transfer-type orifice meters, which are completely automated and can transmit measurement data via telephone, microwave system and satellite. The meter skid consists of four 12-inch meter tubes along with a climate-controlled instrument building. The skid is self-contained and requires a minimal amount of human intervention. Gas flow to the meter skid is controlled by a switching valve skid, which directs gas flow, depending on whether gas is being injected into the cavern or withdrawn.

Compression

Since the incoming gas is expected to be at pressures as low as 400 to 600 psig, the gas must be compressed in order to be stored in the cavern at 1,250 psig.In this particular study, two Solar Turbines (Caterpillar) C406 centrifugal compressors, each driven by Mars 90 gas turbines, were used for a total horsepower capability of over 20,000 HP. The maximum requirements occur during injection into the cavern depending upon the depth of the cavern. The maximum horsepower requirement during injection ranges from approximately 4,500 for the 1,500-foot depth cavern, to 17,000 HP for the 3,000-foot depth cavern. To compress 250 MMscfd from 350 psig to the 1125 psig required for storage will require 16,900 HP.

These compressors will also be used during cavern withdrawal whenever the cavern pressure is lower than the delivery pressure at one or more transmission pipeline connections. A maximum flow rate of 250 MMscfd will occur during gas withdrawal from the cavern. At this flow rate, approximately 15,000 HP (maximum) of recompression would be required, assuming a 250 psig minimum cavern pressure (225 psig at the compressor suction) and a 600 psig maximum transmission pipeline pressure (650 psig compressor discharge pressure).

Each compressor/turbine unit is fully automated and is fueled with pipeline-quality natural gas. The units are housed in a sound-deadened, insulated building.

Before entering each of the two compressors, the incoming gas passes through two vertical separators, which scrub the gas of any liquids. The gas compressors are designed to compress gas and cannot tolerate any liquids.

Once the gas stream is compressed, it is cooled by fin-fan air coolers. At the higher pressures, liquids, such as water and heavy hydrocarbons, may condense. These liquids can harm the molecular sieve material used for drying the gas stream, prior to being chilled; therefore, two vertical separators are placed downstream of the compressor aftercooler.

Dehydration

The gas taken from transmission pipelines is conditioned for typical pipeline operating conditions; however, the gas is not likely to be sufficiently conditioned for cold storage operations. In general, pipeline-quality natural gas contains too much water for the expected storage temperature of minus (-) 20^{o}F or lower. Too high of a water content in the gas may result in the formation of methane hydrates, a hybrid crystalline structure of water and methane molecules. The methane hydrates ("hydrates") are stable at high pressures (500-1000 psig and higher) and temperatures from about 60^{o}F and below.

Prevention of methane hydrate formation is achieved by removing a quantity of water sufficient for the anticipated storage temperature. The proposed method for water removal prior to storage in the mine is by physical absorption of the water using molecular sieve desiccant. Molecular sieve is an engineered aluminum oxide (alumina) pellet, which efficiently attracts and holds on to water molecules. Water-laden gas passes through a pressure vessel containing a bed of molecular sieve pellets. The gas emerges with almost no water and can be refrigerated without the chance of forming hydrates.

The maximum water content of "pipeline quality" natural gas is 7 pounds (lb_m) per million standard cubic feet (MMSCF) of gas. The water content must be reduced to less than 1 lb_m per MMSCF before the gas can be refrigerated. This reduction of water content is easily achieved using molecular sieve dehydration. The mole sieve dehydrator consists of two identical, skid-mounted pressure vessels, which are vertically oriented. Two vessels, i.e., beds are used since, while one bed is absorbing water, the second bed is being regenerated.

When the first bed is completely water-laden, as determined by a hygrometer, it is automatically switched off line and regenerated. The second bed is switched on line, allowing for continuous water absorption.

Bed regeneration is carried out by taking a side stream of dehydrated gas and heating it to 550°F in a small, direct-fired heater. Since each of the two beds must be regenerated with a stream of heated natural gas (+550°F), the pressure vessels containing the molecular sieve material (beds) are covered with high temperature insulation. The hot gas heats the molecular sieve material, resulting in water being driven out of the desiccant and carried away by the hot gas stream.

Once the hot gas exits a bed, it is cooled by a small air cooler (not shown), resulting in water condensation. The condensed water drops out in a small separator (Dwg. 861-MD-005) and the gas is routed to the suction of the inlet compressors.

Refrigeration

Once the gas is sufficiently dehydrated, it must be cooled for the purpose of achieving greater storage efficiency when compared to conventional, ambient temperature storage. In the case of a cavern, 1,500 to 3,000 feet below ground level, the ambient (cavern) temperature may be 80 to 100°F or higher. The quantity of gas stored at –20°F is 77 percent greater than at 100°F, for a given storage pressure of 1,250 psig, and a constant cavern volume. Therefore, chilling the gas prior to storage will allow for 5 Bscf of working gas storage in a 37 million cubic foot cavern. If the gas is not chilled, the same 5 Bscf of gas would require a cavern volume of 66 million cubic feet.

The gas will be chilled to approximately –20°F before entering the cavern. The chiller will use refrigerant-grade propane as a refrigerant. The propane refrigerant is capable of chilling the gas to as low as -35°F. If a -40°F storage temperature is desired, a different type of refrigeration system and refrigerant (propylene) must be used. In addition, consideration will have to be made for the metallurgy of the equipment handling the lower temperature.

The refrigeration system may be powered by electric motors or gas turbines. In this study, gas turbine drivers are assumed. The refrigeration system is a compression-expansion type system, consisting of a three stage evaporative cooling system. Each evaporator or “chiller” is a kettle-type shell-and-tube heat exchanger, with the gas stream passing through tubes immersed in boiling liquid propane in the shell of each heat exchanger. Each chiller operates at a different pressure - high, medium and low pressures. The high-pressure chiller is the warmest of the three chillers, while the low-pressure chiller is the coldest. Cooling the incoming gas in three steps results in greater energy efficiency when compared with a single-stage (one low-pressure chiller) refrigeration system.

The boiled propane is compressed by a three-stage, gas turbine-driven (4,500 HP Solar Centaur 40 – one per 1,300 ton unit) centrifugal compressor. It is then condensed in a fin-fan (air) cooler before being reduced in pressure in each of the three evaporators. A total of 40.7 MMBtu/hr of refrigeration will be required (three

1,300 ton units are specified), assuming a 250 MMscfd gas flow rate, a 120°F incoming gas temperature (compressor discharge) and a –20°F storage temperature.

After being chilled, the incoming gas stream will enter the cavern through a 20-inch vertical riser placed in one of the cavern access shafts. The riser will carry the gas to an underground distribution header, installed along one end of the cavern. The chilled gas will exit the header, flowing across to the opposite end of the cavern to an identically configured header ("return header"). The gas then enters the return header and flows through piping along the cavern floor back to a second 20-inch vertical riser ("return riser"). The return riser will share the same cavern access shaft as the riser used for gas injection.

The purpose of the underground distribution and return headers, as well as their placement in the cavern, is for allowing even and thorough distribution of cold gas throughout the cavern. Contact of the cavern surfaces ("rock") with cold gas will chill the cavern and will aid in freezing any naturally occurring water within the pores of the rock. Also, as the rock is chilled, the influx of heat from the surrounding formation is reduced. Over time, a certain thickness of formation surrounding the cavern is chilled until thermal equilibrium is established.

Initially, as chilled gas is injected into the cavern, the gas will be warmed by the rock surrounding the cavern. The gas will, therefore, have to be recooled and then reinjected. During and after the cavern is completely filled with gas, the gas in the cavern will have to be recycled through the chiller in order to maintain the required –20°F (or lower) cavern operating temperature. Also, the recycled gas stream may require dehydration initially before being rechilled, since water may be present in the cavern and could be picked up by the gas.

After the first year of storage operations, the cooling load required to maintain the cavern at -20°F is estimated to be about 10 million Btu/hr. The cooling rate will decline with time, and after 10 years, the estimated cooling load is reduced to about 3.7 million Btu/hr. The cavern will experience beneficial cooling during gas withdrawal periods due to the expansion of the gas upon withdrawal. This is estimated to be about 15.2 million Btu/hr after 1 year of storage operations, and 13.8 million Btu/hr after 10 years of storage operations. Depending upon the frequency of the injection/ withdrawal cycles, much of the cavern cooling load will be provided by the gas expansion during the withdrawal periods. During injection and static operations, maintenance cooling will be provided by circulation through the refrigeration system.

Gas circulation is achieved through the use of a low-pressure boost centrifugal compressor, located on one of the three refrigeration skids. The recirculation compressor will be powered by the same turbine powering the main refrigeration compressor. Once the cavern is full, gas will be withdrawn via one underground header, compressed by the recirculation compressor, chilled and then reinjected into the cavern through the second underground header.

Gas Heating

When the gas is withdrawn, it may require heating. A 60°F gas temperature is ideal since this is an industry-standard temperature used for measurement as well as a typical pipeline operating temperature.

Heating of the gas upon withdrawal is achieved, using a direct-fired, forced draft convection heater. The heat input to warm 250 MMscfd from –20°F to +60°F requires using a 33.1 MMBtu/hr (gross heat input) heater. After the gas is heated it is either, metered and then transferred to the trunkline or it is first recompressed then metered. Since recompression heats the gas, the amount of added heat required from the heater is reduced or not required at all. The amount of recompression depends on the cavern pressure and the trunkline pressure, as well as gas flow rate (250 MMscfd is the design withdrawal flow rate).

Emergency Shutdown System (ESD)

Emergency shutdown will be manually activated at strategically located ESD activation stations. One ESD valve is located on the inlet/discharge pipeline at the facility fence line and two ESD valves are located on each of the two vertical risers, emerging from the cavern.

FACILITY LAYOUT

The facility plot will consist of an area somewhat larger than the border formed from the projection of outer dimension of the cavern. The area occupied by the 3,000-foot depth cavern is approximately 1,000 feet by 1,200 feet (27.5 acres). The area occupied by the shallower caverns will be greater. The area required for the surface facility is 4 to 7 acres. The layout Dwg. 861-GP-001 is an example layout, taking advantage of the ample land area required for the cavern. Since natural gas and refrigerant propane are being handled by mechanical equipment, leakage of these hydrocarbons can occur. Wider spacing between equipment areas may allow for greater safety.

The spacing and location of equipment will be determined on the basis of code requirements and the direction of the prevailing wind. The code requirements specifically address equipment spacing, e.g., a combustion sources, such the regeneration gas heater or flare vent stack, must be 150 feet or more from an area where the potential for hydrocarbon leakage exists.

Section 6
SITE GEOLOGY

An initial brief screening of five areas of the U.S. where additional natural gas storage appears most needed resulted in the selection of the South Atlantic area, comprised of Delaware, Maryland and Virginia as the preferred target area for this research study. The next step was to review the large selected three-state target area to identify a populous area which might benefit most if an economically viable natural gas storage facility could be developed nearby. The Washington, D.C. to Baltimore, Maryland area was selected as the focus for the refrigerated cavern study because of its population density and significant requirement for dependable year-round natural gas supply, plus the indicated coexistence of favorable rock for cavern construction and major cross-country gas supply pipelines. The area of prime interest identified in this study lies within Howard and Montgomery Counties, Maryland, just northwest of the corridor between the two cities (see Figure 6-1).

The scope of work in this study allowed only a broad geological screening effort to identify an area near major gas pipelines with one or more rock types potentially favorable for cavern construction. It was not the intent of this investigation to select a specific rock formation or site for an actual cavern feasibility study. The geological investigation consisted of a preliminary literature search and review. Time and budgetary constraints did not permit a field inspection visit to the area of interest.

Howard and Montgomery Counties lie within the Piedmont physiographic province (see Figure 6-1). The Piedmont Province is a belt of sedimentary, metamorphic and igneous rocks which extends from Alabama northeastward through Maryland to Pennsylvania. The age of formations in the study area spans the geologic time scale from Precambrian, represented by the basement Baltimore Gneiss, up through Quaternary sediments. Nomenclature of formations has evolved over several decades of geologic study. Figure 6-2 is a useful geologic map of the two counties of interest taken from Bulletin 14, the 1954 Maryland Department of Geology, Mines and Water Resources publication, The Water Resources of Howard and Montgomery Counties, which draws upon earlier maps of 1940 and 1953. At that time, the ages of several formations were uncertain. Figure 6-3 is a stratigraphic column for Howard County found in Maryland Geological Survey Bulletin 38, a 1995 publication titled, Water Resources of Howard County, Maryland. Note that in the newer publication some nomenclature has changed and all formations have been assigned to age categories.

The preferred rocks for deep storage cavern construction are high strength, low permeability, crystalline igneous and metamorphic rocks. An abundant representation of such rocks appears to exist in the two counties of interest. A roughly triangular prospective natural gas storage cavern area with a 25-mile southwest-northeast length and a 12-mile wide base, all within 6 miles of a major natural gas pipeline has been identified as the logical area for siting a refrigerated storage cavern.

Of particular value to the selection of the prospective storage cavern area in this refrigerated cavern research exercise were the documented results of a major study of the potential for underground Pumped Hydro and Compressed Air Energy Storage (CAES) in the Washington D.C. to Baltimore area conducted by the Potomac Electric Power Company (PEPCO) and Acres American Inc. under the sponsorship of the U.S. Department of Energy (DOE) and the Electric Power Research Institute (EPRI),during the period 1977 - 1982.

The PEPCO study progressed through a thorough formal screening process, identifying rock formations of probable favorability for cavern mining and ruling out sensitive areas based on environmental and socio-economic factors. That investigation resulted in the identification of seven favorable rock formations for cavern construction, the following five of which are indicated on Figure 6-1 to exist within the prospective cavern area selected for this study:

- Sykesville Boulder Gneiss
- Ellicott City Granodiorite
- Norbeck Quartz Diorite
- Kensington Quartz Diorite
- Guilford Quartz Monzonite

The following descriptions of these favorable formations were provided in PEPCO reports:

Sykesville Boulder Gneiss

Thick bedded to massive, pebble and boulder bearing, arenaceous to pelitic, metamorphic rock. Typically a garnet-oligoclase-mica-quartz gneiss; locally an intensely foliated gneiss or schist.

Ellicott City Granodiorite

Ranges from biotite granodiorite along margin of body to quartz monzonite in core.

Norbeck Quartz Diorite

Ranges from weakly foliated quartz diorite to strongly gneissic and schistose rock with recrystallized texture.

Kensington Quartz Diorite

Moderately to strongly deformed; igneous texture generally destroyed. Ranges from quartz diorite to granodiorite. Comprises thin concordant sheets or wedges along plunging crest of Baltimore anticlinorium.

Guilford Quartz Monzonite

Biotite-muscovite-quartz monzonite; occurs as discontinuous lenticular bodies.

The Sykesville Boulder Gneiss Formation was selected as the prime rock candidate in the PEPCO study and a site near Sunshine in Montgomery County, underlain by that formation, was selected for testing by deep core drilling. One hole was core drilled to a hole length of 3274 feet (to a vertical depth of 2526 feet) in the Sykesville Formation and hydrologically tested (see location on Figure 6-1). It was concluded that geotechnical conditions at the location of the deep core hole are quite favorable for cavern construction.

All five of the above described formations should be considered as potential candidates for a refrigerated natural gas storage cavern. The Sykesville Boulder Gneiss occupies the largest areal extent within the selected prospective refrigerated cavern area, much of it is away from heavily urbanized zones, and it has already been proven favorable at one location. Therefore, based on currently available information, the Sykesville is considered to be the leading rock type candidate for a gas cavern.

GEOTECHNICAL ASSUMPTIONS FOR CAVERN DESIGN

Detailed design of access shafts and underground workings of a hard rock natural gas storage cavern requires a detailed knowledge of the sequence and types of overburden and rocks to be penetrated plus a knowledge of pertinent engineering properties, degree and orientation of fracturing, and stress conditions of the rocks to be excavated. In an actual construction project this information is accumulated in the geotechnical feasibility study which includes the drilling and testing of several core holes.

The current research project is focused on the prospective natural gas storage cavern area identified in Howard and Montgomery Counties, Maryland but no specific site has been selected and no feasibility study has been performed. Therefore, it was necessary to develop a list of geotechnical assumptions which form the basis for the conceptual cavern design exercise. Table 6-1 lists assumed generic properties and conditions chosen to be representative of a typical, structurally good quality, crystalline igneous or metamorphic rock in the area of interest. These geotechnical assumptions were derived partly from results of the deep PEPCO core hole and partly from data acquired in actual projects in similar rock elsewhere. The surprisingly cool temperature of 73°F at 2500 feet depth was measured in the PEPCO core hole.

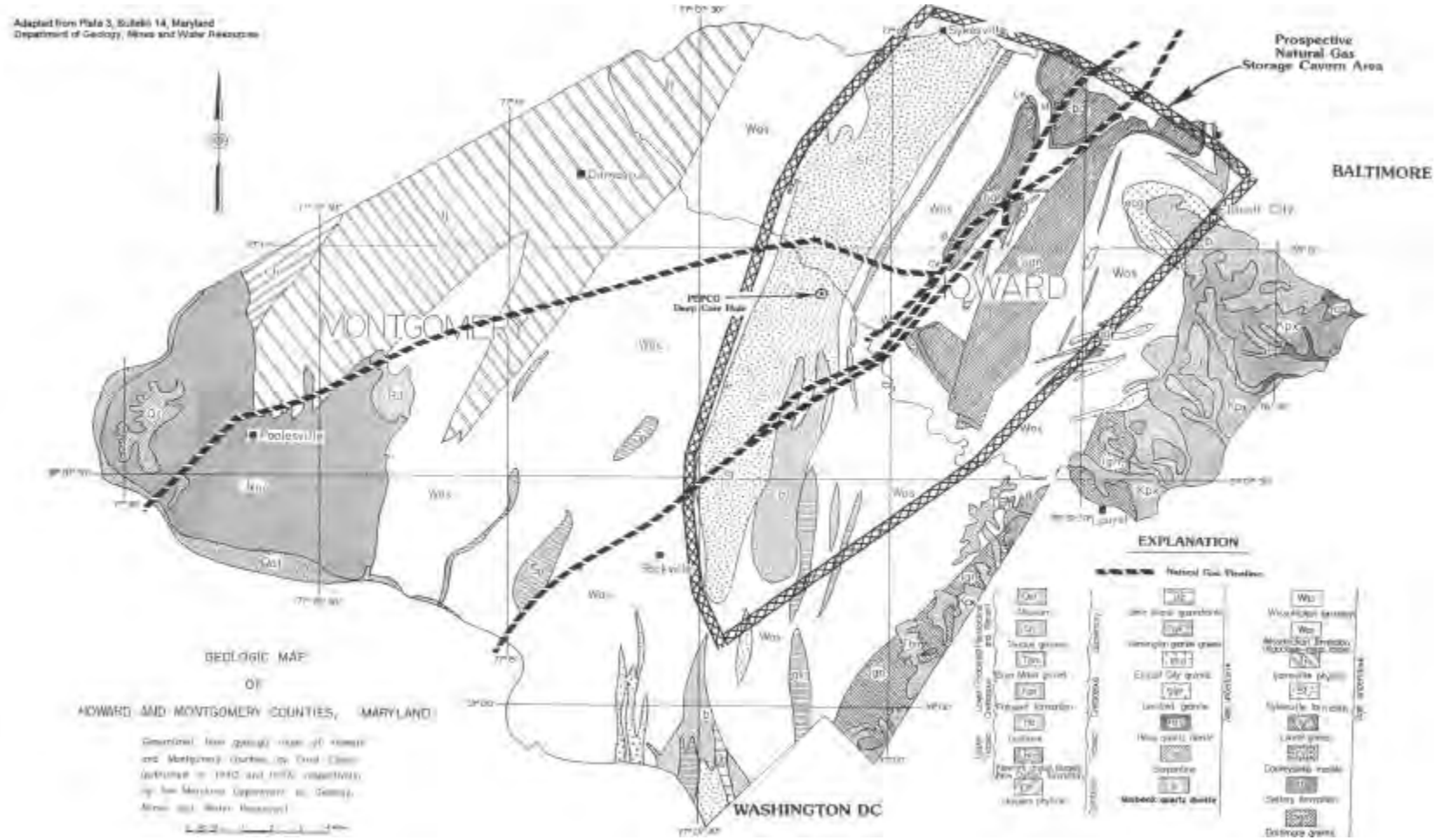

Figure 6-1 - Prospective Natural Gas Storage Cavern Area

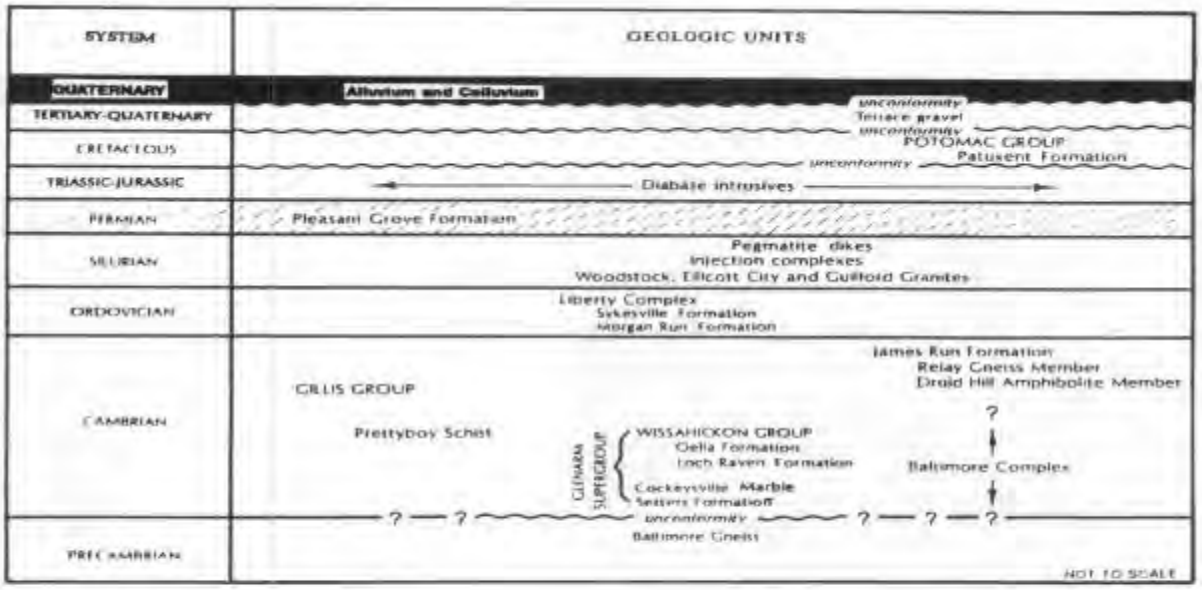

Source: Maryland Geological Survey Bulletin 38, Water Resources of Howard County, Maryland 1995.

Note: The Pleasant Grove Formation was not deposited during Permian time, but rather includes older rock units that have been deformed by shearing and emplacement that probably occurred during Permian time.

Figure 6-2 Stratigraphic Column of Howard County, Maryland

Table 6-1

Geotechnical Assumptions for Conceptual Design of

Refrigerated Natural Gas Storage Cavern

1. Geological Column

0 - 50'	Overburden
50 - 150'	Weathered crystalline rock (igneous or metamorphic)
150 - 3000'	Unweathered crystalline rock (igneous or metamorphic)

2. Rock Properties and Hydrologic Conditions

Unconfined Compressive Strength: . . 2,000 - 20,000 psi (average 10,000 psi)
Tensile Strength: . . . . . 700 psi
Young's Modulus . . . . . .7,500,000 psi
Poisson's Ratio: 0.27
Bulk Density: . . . . . .2.80 g/cc
Porosity: 1%
Hydraulic Conductivity (K): . . . . . 10^{-7} cm/sec at 3000-ft. depth
Temperature at 2500' Depth: . . . . . 73°F
Temperature Gradient: . . . . . .0.64°F/100 feet
Water Table: . . . . . ± 30 feet below surface (in gentle hilly terrain); Near surface (in valley bottoms)

Average RQD index value: . . . . . 85 at 3000-ft. depth

Section 7
CAVERN CONCEPTUAL DESIGN

A conceptual design was prepared for this study to demonstrate that a facility can be feasibly constructed, without the requirement for unique or unproven construction techniques, and to provide a basis for a rough order of magnitude cost estimate and construction schedule.

For the actual construction of such a facility, it is necessary that a comprehensive geotechnical feasibility study be performed at the site to determine subsurface geologic conditions as a prerequisite for a detailed design. This geotechnical feasibility study would consist in part of drilling three or more core holes to a depth of 150'-200' deeper than the cavern floor for the investigation of rock properties and in-situ stress conditions. All of the rock properties, which are a part of the assumptions in this report, would need to be determined. In addition, the nature and orientation of all discontinuities such as joints, foliation and faults must be determined by detailed core logging.

Shaft Sizes

Shafts are the main arteries for the underground operations. They provide ventilating air, passage for hoisting of men and material, and various utilities such as electricity, water, and compressed air.

Shaft sinking entails the major cost of the underground cavern development. The cost is proportional to the size of the shaft, especially for the drilled shaft. Conventionally sunk shafts, however, must have adequate room for the miners to operate economically without getting into each others way. A minimum diameter is about 12' for a conventionally sunk shaft.

For ventilation purposes, two distinct passageways are required: one for the incoming fresh air, and the other for the outgoing contaminated air. The fresh air is needed by the miners, the operating equipment and for removal of dust-laden particles of broken rock. Mine Safety and Health Administration (MSHA) normally requires two shafts in the operating mines for this purpose. One shaft serves as the air intake shaft, and the other as the air return shaft. The second shaft also serves as a second means of egress from the mine in an emergency. However, MSHA has approved, in the past, a single, divided shaft for developmental purposes. One half of the shaft is used for the air intake and the other half as return. Emergency egress may be provided by a torpedo hoist.

Since the shaft-sinking cost is the major cost item, a single, partitioned shaft was considered for this facility. However, this necessitates smaller skips to operate in one half of the shaft. The return trip for a fully loaded skip, from a depth of 2500 ft was calculated to be about 15 minutes. Considering that 4.1 million tons of broken rock would need to be hoisted to the surface from the underground, an inordinately long cavern

development time would be required (six to seven years). For economic hoisting and development schedule, two larger skips would be required in a balanced mode -- one being loaded underground, while the other is being unloaded at the surface. Therefore, a single shaft concept for the facility will be unworkable.

Shaft size is determined by a variety of parameters including the size of hoisting equipment to be installed and the size of the equipment to be lowered into the underground workings to complete the excavations. An additional parameter is the quantity of ventilation air required to provide a safe environment for the underground workers during construction. The excavation equipment will most likely include two-boom electric-hydraulic drill jumbos, eight- to ten-cubic-yard front end loaders and forty- to fifty-ton haul trucks. Equipment of this size is required for efficient construction of the caverns. In order to accommodate these requirements, a shaft of 18- to 20-feet in diameter is recommended.

All of the material excavated from the caverns will be hoisted from the shaft bottom by means of a large double-drum mine hoist and skips that automatically load and unload. It is necessary to crush the material so that all of the material would be smaller than about twelve inches so that it can be easily loaded into the skips. This would be done through the use of a large jaw crusher installed at the shaft bottom. The crushing equipment will include a dump hopper of sufficient size so that the haul trucks can dump directly into the hopper with additional rehandling of the waste material. Once on surface, the waste rock would be hauled to a storage site or, depending on the ownership of the material, it could be further crushed and sold as aggregate.

Shaft Construction

Shafts are constructed by three primary methods: conventional drill and blast techniques, blind hole drilling and raise boring. An additional method, “V-moling”, is available, although used only infrequently. The three drilling methods are more mechanized than the conventional method, and do not require workers to be in the working are of the excavation.

Conventional drill and blast construction is the most commonly used for shaft excavation. This method is successfully employed in virtually any size or shape of shaft and is limited in depth only by the length of hoisting ropes being manufactured and the size of joisting equipment available. It is flexible and can be adapted to suit any type of ground conditions that may be encountered. The excavations can be constructed to a very accurate vertical tolerance, a condition that is required where hoisting equipment is to be installed. Blind hole drilling is limited to holes of 16 feet in diameter and 2000 feet in depth. Depth and diameter are limited by size of drilling equipment available. This method is better suited to softer rock formations. It cannot always be used in geologic settings where there are alluvial deposits containing boulders. Accurate vertical alignment cannot be assured.

Raise boring is similar to blind hole drilling except that the cutting tool is placed at the bottom of the excavation and attached to a drill string set into a previously-drilled pilot hole. This method can be used for excavations up to 20 feet diameter and 2500 feet deep; the depth of excavation is limited by the size of equipment available. Shafts can be raised in any rock formation that does not require immediate support for the excavation. In order to use this construction technique, there must be access to the shaft bottom prior to drilling the pilot hole. Correct vertical alignment of the shaft can be assured, although this assurance can be difficult and expensive. Unless great care is exercised in drilling the pilot hole, the hole can deviate from vertical by 5- to 10 percent. Even one percent deviation is unacceptable for shafts intended to be equipped with high-speed hoisting equipment.

V-moling a shaft is similar to blind drilling in that the cutting tool starts excavation at the top and proceeds downward. This method is limited to shafts of 28 feet diameter. It requires that a raise-bored pilot hole be completed prior to starting the main shaft excavation. Access to the bottom of the shaft is required prior to drilling the pilot raise.

Of these principal methods, the best suited for primary access to the caverns is conventional drilling and blasting. The service shaft can be excavated by use of raise boring, however, extra care will be required in drilling the pilot hole because this shaft will be equipped with hoisting equipment and a true vertical shaft is required.

The first step in shaft construction is mobilization and site preparation. Mobilization will consist of off-site and on-site activities. Off-site activities will include preparation of equipment, relocating personnel to the site, initial engineering and design activities, setup of job cost system and long-lead item ordering and tracking. On-site mobilization will include setup of offices, dryhouse, sanitary facilities, placing temporary utilities, set up the shop, surface equipment and warehouse. It will also include grading and drainage, building access roads and storage areas. At this time the contractor will also set up the shaft sinking equipment which will include the hoisting equipment, head frame and muck handling equipment. It is estimated that the contractor will require approximately 3000 kVA electrical service.

Shaft sinking will begin with construction of the shaft collar, the initial reach of the shaft through the overburden and into competent rock. Depending upon the nature and depth of overburden, the collar will be excavated using a clamshell or backhoe, and supported with ring beams and timber lagging or liner plate and ring beams. The initial twenty feet of excavation is usually completed with a backhoe and is sufficiently large to accommodate a prefabricated ring beam and lagging support cylinder. The inside diameter of this structure will be two feet larger than the finished diameter of the shaft. After the support structure is in place, it will be backfilled with compacted fill and the shaft bottom leveled and prepared for placing the first twenty feet of shaft concrete. Reinforcing steel is placed as required. A concrete slab is placed around the shaft collar at grade and footings for the head frame are installed. The footings may be either driven or drilled

piles or spread footings depending on soil conditions and head frame loading.

The shaft collar is then completed to competent rock using equipment that is appropriate for the material to be excavated. It may include clamshell, a small excavator or overshot mucking machine loading material into a sinking bucket. The material is hoisted to surface using a crane then dumped. As the excavation advances, liner plate and ring beams or ring beams and timber lagging are installed for temporary support of the excavation. Depending upon soil loading conditions, the inside diameter of the temporary support is nominally two feet larger in diameter than the finished shaft. This activity is continued until the collar reaches competent rock.

The excavation is continued into rock for approximately twenty feet, and the rock excavation is enlarged to form a bearing haunch that provides support for the collar concrete. The concrete forms are lowered into the shaft and the haunch is placed. Shaft lining concrete is then placed upward to join the collar lining that was initially placed. Reinforcing steel is placed as required by final design.

While the shaft collar is under construction, the remainder of the shaft sinking plant is installed. This includes setting the mine hoist, work deck winches and form winches, and preparation of the shaft head-frame. The Galloway (work stage) is assembled and made ready for installation and a concrete batch plant is set up if needed. When all activity in the shaft collar is complete, the head frame and hoisting equipment are erected and made ready for shaft construction.

The shaft sinking operation consists of a normal drill-blast-muck cycle, excavating approximately ten-foot-long blast rounds. Drilling will be done with a shaft drill jumbo and mucking by Eimco 630 or Cryderman shaft mucker loading five-cubic yard (CY) sinking buckets for hoisting to the surface. Spot bolting with wire mesh installed concurrently with sinking is assumed to provide safe working conditions. Every twenty feet, the excavation cycle will be interrupted and a twenty foot long section of shaft concrete lining installed. The curb ring will be lowered from the previous pour and suspended from twelve hanging rods. After aligning and securing the curb ring, the forms will be stripped from the previous pour and lowered in sections, realigned and secured. The twenty foot section will then be concreted up to the previous pour. Concrete will be delivered using the hoist and concrete buckets or slick line. Separate form winches will be provided for handling the curb ring and shaft forms. The cycle will be interrupted for installation of the water rings at the appropriate elevations and construction of the crusher level station.

Development from the shaft into the mining level will be started using hand-held jack-leg drills and a skid-steer loader. This equipment will be used to excavate an area of sufficient size to accommodate a mining jumbo and loading equipment. At this time, only the top heading of the excavation will be completed. After the equipment has been assembled, development will continue with the excavation of the crusher station. In addition to the crushing station development, a drift to the service shaft area will be excavated.

Temporary lifting eyes will be located in the crown of the crusher area to assist with assembly of the crusher and hopper. A monorail hoist to service the crusher will be installed at that time as well. Ground support will most likely consist of rock bolts and welded wire mesh.

Mining on the storage cavern level will continue until the access to the service shaft has been completed and supported with rock bolts. After the initial excavation to the service shaft is complete, all of the crushing and material handling equipment for the crusher will be brought into the cavern and stored. The mining equipment used for initial development will then be removed from the cavern and the large production mining equipment brought into the cavern and assembled. The shaft will then be continued to its final depth and the cutouts for the skip loading equipment will be excavated and lined with twelve inches of plain concrete.

The shaft sinking equipment will then be removed and utility installation will begin. Shaft piping includes one six-inch dewatering line, one six-inch compressed air line, one 1-1/2 inch fuel line, and one 2-inch water supply line. Shaft cables include a high voltage power line, leaky feeder communications line, dial telephone cable, fiber-optic cabling and control cabling. All shaft cable and pipes will be suspended in the shaft on steel brackets bolted to the lining with epoxy anchor bolts. The cables will be installed from the top of the shaft and proceed downward. Cable reels are placed on the Galloway which is then slowly lowered. As the deck moves downward, the cables are spooled off the reels and secured to the cable hangers. Following completion of cable installation, the Galloway will be returned to the surface and the shaft set up for steel installation.

Steel installation is also conducted from the top of the shaft progressing downward. Control of the steel location is by the use of plumb lines positioned at known distances from the steel sets. The first set is accurately placed in the shaft collar and secured to the concrete. A set of shaft guides is then positioned in the shaft and secured to the collar steel set, the deck is lowered and the second set is brought to the deck. Templates will be used to accurately locate drill holes used to secure the buntons seats to the concrete. The bunton seats are loosely secured to the concrete and the buntons are placed and aligned to the plumb lines. The shaft guides are then bolted to the buntons and all bolts are tightened with an impact wrench. When all bolts are tight and steel alignment is correct, another set of bunton steel is brought into the shaft and the cycle repeated. This activity will continue until the steel has reached the crusher level.

Construction of the underground crushing station will commence when the shaft equipping sequence reaches the cavern level. This work will begin with the installation of the skip loading equipment so that the shaft steel can be installed simultaneously with that equipment. Electrical and mechanical installation of the crushing equipment will follow shortly thereafter with all activities in the crusher, and skip loading station being undertaken concurrently. At the completion of these activities, the crushing and skip-loading equipment will be tested, commissioned and put in service. Excavation of the remaining work on the storage

cavern level will begin. Fan and fire door bulkheads will be installed, and the ventilation system installed, a dewatering sump completed and an underground equipment service area established.

Service Shaft Construction

Once the production shaft has reached the storage cavern level, an access tunnel must be driven to the service shaft location in preparation for raise boring of the service shaft facility. The access drift will be sized to facilitate the movement of the raise bore head to the site. The service shaft site must be of sufficient dimension to allow ease of material handling required by raise boring activities. Sizing of the material handling equipment is dependent upon the haulage distance to the production shaft as well as the size of the raise bore opening.
It is assumed that the finished dimensions of the raise bored shaft will be approximately 2500 vertical feet in length and ten feet in diameter. When the underground raise bore station is completed, access area for the raise boring equipment will be completed on the surface. This includes the foundation for the raise bore and drilling of the pilot hole. The pilot hole must be drilled to very strict vertical tolerances as it will be the control for vertical alignment of the bored shaft.

After agreement that the pilot hole is within tolerance for verticality, the rise bore head is transported to the underground site and assembled to the size and configuration for the opening to be constructed. Rods are then connected to the cutter head and raising is begun. Material from the remaining process falls to the developed underground area, and is removed to the production shaft for hoisting to the surface for disposal. Material generated by raise boring can be classified as minus six inch rock.

After reaming the shaft to the surface has been completed, the raise boring equipment is demobilized from the site and the unitized concrete lining equipment is mobilized to the surface location. Concrete lining is performed from the surface collar downward in 20 foot lifts. When lining the service shaft has been completed, the lining equipment is removed and shaft furnishings are installed in much the same manner as in the production shaft.

Storage Cavern

Cavern Orientation

The orientation of the main storage cavern with regard to the geologic conditions is extremely important. This can only be done with information obtained from a site specific geotechnical feasibility study. The decision is largely based on the avoidance of undesirable conditions and must of necessity involve compromises. Ideally, the long axis of the main caverns should be parallel to the direction of the principal horizontal in situ stress and perpendicular to the most significant discontinuities such as fractures, joints, and faults. Obviously, perpendicularity to all negative discontinuities cannot be achieved in an actual situation, so the choice of orientation becomes a best compromise based on experience as to what conditions present

the greatest problems to both the cavern stability and air tightness of the operating facility.

Cavern Design and Construction

The cavern volume for a 2500-ft deep facility will be approximately 47 MMCF (for 5 billion cu. ft of working gas, at -20°F and compressed to 1083 psi). However, if the gas is compressed to 1250 psig (for 3,000-ft deep cavern), the space requirement will be less. This is discussed in some detail in the "Optimization" Section. For economic reasons, the cavern sizes should be as large as possible. For an opening size of 80' x 80', a total length of 7,234 lineal feet of cavern space is required. In order to reduce the haulage distance and to reduce the real estate cost of surface property, it is more convenient to break down into 7 tunnels, approximately 1033' long. However, if the shaft is located centrally to further reduce the hauling distance, seven tunnels, approximately 500' on each side of the shaft, are needed. Cross-cuts will be needed every 200' for ventilation purpose. These cross-cuts provide further storage space.

Large storage caverns, highway tunnels and other underground structures where the top of the excavation is higher than about thirty feet are commonly constructed using the "top heading and bench" method of excavation. This process is employed because mining equipment is not able to access the entire working face of the excavation. The excavation will be completed by mining the upper portion of the opening with one or more smaller openings sized to suit the equipment available.

In this cavern, the top heading would be mined with a heading approximately twenty-seven feet wide and thirty feet high driven down the center of the excavation. When the central heading has advanced approximately eighty feet, one of the remaining sides would be started and would remain that distance behind the first. As the headings advance an additional eighty feet, the remaining side is excavated again remaining an approximate distance of eighty feet behind. Roof support is installed and maintained to the working faces. When all of the top headings have been excavated, the remaining bench is excavated in either one or two lifts. In this cavern, it may be advantageous to mine the bench in two lifts rather than one because of the volume of muck generated. Blasted rock will be delivered to the hoisting shaft in haul trucks then transferred to the shaft material handling system.

The storage cavern could also be created by use of one or more tunnel-boring machines (TBM). These machines are commonly used for construction of circular tunnels ranging in diameter from 6- to 40 feet and are successfully used in virtually all rock types. In situations where the excavation must be immediately support, temporary support is erected within the tail shield of the machine. Ground support may consist of ring beams and lagging, liner plate and ring beams or pre-cast concrete tunnel liner. Excavated material is transported away from the machine in rail cars or on conveyor belts. It would not require crushing prior to being hoisted.

The largest available TBM will excavate an opening of approximately 1250 square feet. In order to create 47 million cubic feet of storage, 37,500 feet of tunnel would be required. The proposed 80- x 80-foot caverns done by drilling and blasting require only 7500 feet of excavation. In addition, the production shaft required

to support this TBM operation would need to be at least 30 feet in diameter. While it is technically possible to construct this shaft, it would be much more expensive than the shaft required to support the drill-blast cavern construction. Using the TBM method is not recommended.

The major pieces of equipment used for construction of the caverns would include two boom electric-hydraulic drill jumbos, Cat 990 or equivalent front end loaders and 40-ton haul truck, similar to a Cat 769 haul truck. Support equipment would include a roof bolting jumbo, shotcrete machine, mechanic's trucks, lubrication trucks and an explosives truck. All equipment will have the necessary safety equipment for operating in an underground environment.

Ventilation air would be supplied through the service shaft which would have the main fan installed at the surface and operating on intake. The intake air would be routed through the service shaft because that shaft would be used as the primary entrance to the caverns for personnel. With the spread of underground equipment, the ventilation air required would be approximately 300,000 cubic feet per minute. Air flow in the cavern would be controlled by using ventilation stoppings, air regulators and doors. These features would be dismantled after the cavern excavation is completed.

The material transfer system would be comprised of the bump hopper and hydraulic rock breaker, a jaw crusher and scalping grizzly, skip loading surge hopper, skip loading flasks and much skips an hoist. Jaw crushers are the most efficient and economical equipment to reduce the size of blasted rock to a size that can be easily loaded into the muck skips. The grizzly would be installed under the dump hopper to allow undersized material to bypass the crusher, increasing the capacity of the crusher and improving the efficiency of the crushing plant. Oversize material will pass through the crusher. Any material that is too large to enter the crusher will be broken with the hydraulic rock breaker.

Undersized and crushed rock will be transferred to the skip loader surge bin with a conveyor belt mounted beneath the crusher. The surge bin will be monitored with load cells or photoelectric sensors so that the crushing plant will automatically stop to prevent overfilling the hopper. Material flows by gravity from the hopper to the skip loading flasks; flow control is through the use of guillotine gates that are automatically controlled by load cells in the skip flasks. When an empty skip arrives at the skip loader, the skip flask is opened and muck is loaded into the skip. If the flask is not full, the guillotine gate at the surge hopper would open and allow muck to fill the flask. When the skip flask is empty, the discharge gate is closed and a signal sent that enables hoist operation.

After all of the cavern excavation is completed, the mining equipment would be disassembled and removed. This would include removal of the muck skips, crusher, and skip loading equipment. Any temporary fixtures, such as ventilation bulkheads and the equipment repair facility would be dismantled as well. This hoisting equipment would remain in place to provide access while the gas storage equipment was being installed. The hoisting equipment could remain in place to provide access to the caverns for inspection and maintenance, or decommissioned and removed from the site.

General arrangement of the system is shown in Drawing 861-LB-006. Shaft outfitting is shown in Drawing 861-LB-005. Cavern layout for a 2500' deep facility is shown in Drawing 861-LB-007. Cavern layout for 3000' deep facility is shown in Drawing 861-LB-008.

Roof Control

For stability, the roof of the opening will be arched, avoiding sharp corners with the walls of the opening. Pattern bolting may be needed for the protection of the workers. For this purpose, 8' long bolts will be fully grouted into the roof. All lose rock will be brought down by a rigid boom scaler (Gradall). In the benched area, lose rock in the roof will be hand scaled with the help of a Cherry Picker.

Ventilation

Initially, ventilation will be with a fan and tubing providing air at the working face. Once connection has been made between the two shafts, a fan delivering about 300,000 cfm will be installed at the surface in the man and material shaft. Brattice will be used to convey air to the working area. Floor mounted cyclone fans will circulate the air at the face to remove any noxious fumes.

Shaft Seals

Once the cavern construction, gas injection and delivery system, and the gas recirculation system are complete, shafts will be sealed to contain the gas under pressure. The seal will consist of massive concrete structure (30-35' thick) keyed 5' into the sides of the shaft walls to resist the uplift pressure of 1100 to 1250 psi gas.

Cavern Inerting System

The normal air in the cavern atmosphere will contain about 21 percent oxygen, by volume, which may result in an explosion from an ignition of the gas mixed with air. The cavern, therefore, must be inerted. In order to inert the cavern, a partial vacuum should be applied and then repressurizing the cavern with inert gas. The inert gas could be obtained from liquid nitrogen, liquid carbon dioxide or exhaust gas from a fuel oil burner. Nitrogen and carbon dioxide are not available in large quantities and have high costs. Therefore, exhaust gas, which can be produced by a fuel oil burning gas generator, should be used.

The system would consist of a vacuum pump, five inert gas generators complete with pumps, cooling towers, and fuel supply system.

The first step in the inerting process would be to reduce the pressure in the mine from 14.7 psia to 7.0 psia. This pressure is well below that required to prevent combustion. After evacuation, five inert gas generators, producing 10,000 scfm of exhaust gas will fill the cavern. Each exhaust gas generator would be equipped with a combustor and a quenching water system complete with a separate cooling tower and circulation pump to cool the discharge gases to 110°F. An oxygen analyzer would be used to monitor the discharge of each inert gas generator for the presence of oxygen.

Gas Distribution System in the Cavern

After being chilled, the incoming gas stream will enter the cavern through a vertical riser placed in one of the cavern access shafts. The riser will carry the gas to an underground distribution header, installed along one end of the cavern. The chilled gas will exit the header, flowing across the opposite end of the cavern to an identically configured header (“return header”). The gas then enters the return header and flows through piping along the cavern floor back to a second vertical riser (“return riser”). The return rise may share the same cavern access shaft as the riser used for gas injection.

The purpose of the underground distribution and return headers, as well as their placement in the cavern, is for allowing even and thorough distribution of cold gas throughout the cavern. Contact of the cavern surfaces ("rock") with cold gas will chill the cavern and will aid in freezing any naturally occurring water within the pores of the rock. Also, as the rock is chilled, the influx of heat from the surrounding formation is reduced. Over time, a certain thickness of formation surrounding the cavern is chilled until thermal equilibrium is established.

Construction Equipment

The following construction equipment will be required for the gas storage cavern:

- Double-Drum with Clutch Hoist for Production Shaft
- Single Divided Drum Hoist for Men and Material Shaft
- One Work Stage
- Two 20-ton Skips
- Mancage
- Two Double (or Triple) Boom Electrohydraulic Jumbo Drills
- One Vertical Drill
- ANFO Loading and Blasting Rig
- Two Front-End Loaders (Cat 990 or equivalent)
- Two 40-ton Trucks
- One Roof Bolter
- One Rigid Boom Scaler (Gradall)
- One 80' high Cherry Picker for Handscaling
- Jaw Crusher
- Conveyors and Hoppers
- Power Distribution System
- Compressor and Compressed Air Distribution System
- Dewatering Pump
- Construction Fan with Tubing for Shaft Sinking
- Lubrication Truck
- 300,000 cfm Fan for Cavern Ventilation
- One 5-Stage Centrifugal Compressor (900 HP) for Evacuating Air
- Five Inert Gas Generators (120,000 scfh/unit) with Cooling Towers

CONCLUSIONS

1) The most practical method of cavern construction is conventional drilling and blasting one or more top headings then benching the balance of the excavation. Hydraulic drilling equipment, front end loaders and haul rucks should be used.

2) The minimum shaft diameter required to support this construction is 18-20 feet. Any smaller shaft diameter would not allow easy access for the mining equipment.

3) Material mined to create the caverns would need to be crushed prior to hoisting.

4) The smallest service shaft would be a 10-foot-finished-diameter raise bored shaft. The service shaft would be used for the ventilation air supply.

5) The production hoisting equipment would be used to assist with installing the gas storage equipment and piping.

Section 8

GEOMECHANICAL REVIEW OF PROPOSED CAVERN DESIGN FOR STORAGE OF REFRIGERATED NATURAL GAS

8.1 INTRODUCTION

This study has resulted in a preliminary design of the cavern and access shafts for storage of refrigerated natural gas in a mined storage chamber. The project has identified a potential location for the refrigerated gas storage cavern in the Ellicott City granodiorite in Maryland for further study.

The access shafts will have diameters of 18 feet and 10 feet from the surface to a depth of about 3,000 feet. The shafts will be used initially for access during construction of the cavern and then as entryways for the pipelines carrying the gas into and out of storage. The life expectancy of the shafts must equal the life expectancy of the storage facility.

The preliminary design for the underground facility is for a room-and-pillar mined cavern located at about 3,000-foot depth. The cavern will be comprised of a set of rooms, each 80 feet high by 80 feet wide. The rooms will be spaced on 280-foot by 230-foot centers. The center of the cavern will be dominated by a shaft pillar of 200 feet by 380 feet. The shaft pillar will contain the two access shafts that will be used for development of the cavern, and later, delivery of stored gas. The immediate rooms around the shaft facility will not be benched and will be about 25 feet high.

This chapter evaluates the preliminary mine design in order to determine:

Stability of the 80-foot-wide rooms.

Maximum stable span of the rooms.

Required pillar thickness for the studied room spans.

Stability of the shaft and need for lining.

Effect of the refrigerated gas temperatures on the stability of the facility.

Assumed rock properties were used in the evaluation of the mined chambers. The study utilized both analytical approaches and finite element modeling to determine the stability of the openings. Published reports of empirical studies for support of the openings were used to recommend initial support methods for the refrigerated gas storage cavern.

8.2 TECHNICAL APPROACH

8.2.1 Potential Storage Site Properties

The site properties for the refrigerated gas cavern are provided in Tables 8-1, 8-2, and 8-3.

Table 8-1. Geological Column

Depth	Material
0-50 feet	Overburden
50-150 feet	Weathered crystalline rock
150-3,000 feet	Unweathered crystalline rock

Table 8-2. Properties of Unweathered Crystalline Rock

Property	Value
Unconfined compressive strength	2,000-20,000 psi; Average = 10,000 psi
Tensile strength	700 psi
Young s modulus	7,500,000 psi
Poisson s ratio	0.27
Bulk density	2.80 g/cc
Porosity	1%
Temperature at 3,000-foot depth	73 ^{o}F
Average RQD index value	85 at 3,000-foot depth
Water table	Within 30 feet of surface
Hydraulic conductivity	10^{-7} cm/sec at 3,000-foot depth

Table 8-3. Gas Operating Conditions

Property	Value
Gas storage pressure, maximum	1,370 psi
Gas storage pressure, minimum	250 psi
Refrigerated gas temperature	-20 ^{o}F

To determine the effect of the refrigerated gas temperatures on the strength of the granite, thermal properties of granite were obtained from literature sources. The sources include Carslaw and Jaeger [1959] and Kuriyagawa et al. [1977]. The thermal properties are given in Table 8-4.

Table 8-4. Thermal Properties of Granite

Property	Value
Coefficient of thermal expansion	3.75×10^{-6}
Specific heat	880 J/kg-K
Thermal conductivity	2.51 W/m-K

To apply the analytical and empirical methods to the evaluation of the design of the refrigerated gas storage cavern, several additional assumptions were made. These assumptions are:

1. There are two joint sets present at the site.
2. Neither joint set is horizontal.
3. Water inflow (free water in the joints) will be less than 10 gallons per minute (gpm).

8.2.2 In Situ Stresses

The in situ stress state (magnitude of the horizontal and vertical stresses as well as the orientation of the horizontal stresses) affects the size of openings that can safely be constructed underground and the orientation of the openings that will enhance their stability. Regions subjected to tectonic forces may have maximum stresses that are greatly in excess of the stresses imposed by the vertical load of the rock. Generally, the axis of underground openings should be oriented between 15^o and 30^o of the major principal stress [Selmer-Olsen and Broch, 1977].

A review of the literature [Lindner and Halpern, 1978; Zoback and Zoback, 1980; University of Karlsruhe, 1998] on in situ stress magnitude and orientation indicates that the horizontal in situ stress in the region of the proposed storage site is anisotropic. Based on data from Maryland and adjacent portions of Pennsylvania and Virginia, the maximum horizontal stress varies from about 1.08 to 3.16 times the minimum horizontal stress with an average of 2.18. The minimum horizontal stress varies from about 0.9 to 1.4 times the vertical stress with an average of about 1.06. The assumptions for this study are that the maximum stress is equal to twice the minimum horizontal stress, and the minimum horizontal stress is equal to the vertical stress.

The orientation of the major principal stress varies from N 35^o W to N 85^o E. The average orientation of the maximum horizontal stress is N 69^o E.

8.2.3 Room Size and Stability

The evaluation of the proposed mined openings drew upon work from Bieniawski [1976], Barton et al. [1974; 1994], Hoek [1979] and Hoek and Brown [1980]. These papers present analytical formulas and empirical methods to evaluate the stability of underground openings. The empirical methods are based on case histories of existing tunnels and caverns.

Barton et al. [1974] developed a method to describe the competency of rock that is widely used by the Norwegian Geological Institute to describe rock conditions for underground construction. This system of classification is called the Q-system. The Q -system uses:

$$Q = \left(\mathrm{RQD}/J_n\right) \times \left(J_r/J_a\right) \times \left(J_w/\mathrm{SRF}\right) \tag{8-1}$$

where:

RQD = rock quality determination
J_n = number of joint sets
J_a = degree of alteration or clay filling along the joints
J_r = roughness of the joint surfaces
J_w = estimate of potential water inflow
SRF = estimate of rock loading.

Tables to apply numerical values to descriptions of the joint and rock properties are provided by Barton et al. [1974].

From this estimate of competency, Barton et al. [1974] prepared guidelines for the type and amount of support that may be required to support mined openings for long-term use. The development of the Q -system was largely based on experiences in developing underground structures in the Scandinavian countries. Barton [1976] describes successful application of the Q -system in the design of a powerhouse structure. Barton et al. [1994] discusses the application of the Q -system to the design and construction of an underground ice hockey stadium in Norway.

Barton et al. [1974] also developed empirical relationships between rock quality, Q, and roof and wall support pressures. For roof support pressure when there are less than three sets of joints in the rock, the relationship was found to be:

$$P_{roof} = \left(2.0 \times J_n^{1/2} \times Q^{-1/3}\right) / \left(3 \times J_r\right) \tag{8-2}$$

where P_{roof} is the permanent roof support in kg/cm^2.

The wall support pressure is determined using the same equation, but the value of Q is altered. The value of Q is increased to reflect the "more favorable position of excavation walls as opposed to roofs" [Barton et al., 1974]. For $0.1 < Q < 10$, the equation-derived Q should be adjusted to $2.5Q$ for use in estimating wall support pressure, and for a calculated $Q > 10$, Q should be adjusted to $5Q$.

Barton et al. [1974] developed 38 categories of support based on an analysis of about 200 case histories. They looked at the relationship between Q, excavation dimensions, and the support actually used in the case studies. They then developed a table of recommended support methods with numerous subcategories based on dimensions, number of joint sets, support pressure value, and RQD. The support categories were compacted and the support requirements were simplified in Barton et al. [1994] based on continuing study of new underground facilities.

Bieniawski [1976] also developed a similar classification system using somewhat different factors to describe the rock mass:

1. Uniaxial compressive strength
2. Drill core quality or RQD
3. Joint spacing
4. Joint condition
5. Groundwater conditions
6. Joint orientation.

From these parameters, Bieniawski developed a rock quality, Q. The numerical value of Q is derived by summing ratings associated with the various classification parameters. Bieniawski then converted his Q into an RMR (rock mass rating) value for evaluation and analysis according to Equation 8-3.

$$RMR = 9 \times \ln(Q) + 44 \tag{8-3}$$

He drew upon the rock quality relationships along with case histories to estimate the standup time (period of stability) for ranges of unsupported cavern span. Bieniawski provides guidance for the type of support required for long-term stability of relatively shallow, narrow (approximately 10 meters) openings of the type used for vehicular tunnels.

Hoek [1979] proposed a preliminary method to evaluate sites for waste repositories. If this evaluation was favorable, it would then need to be verified by a detailed site investigation. Hoek looked at:

1. Structural conditions, strength, and deformation characteristics of the rock.
2. In situ state of stress.
3. Shape, size, and location in relationship to each other of the excavations.
4. Groundwater conditions.

5. Thermal loading induced by the waste.

Hoek also provided a chart to equate rock quality, stress ratio, and stability methods required to maintain an opening.

8.2.4 Pillar Size

Hoek and Brown [1980] provide methods to determine the stresses in pillars as well the effect of varying the height-to-width ratio of the pillar. The stress on a rectangular pillar is:

$$\sigma_p = \gamma z \left(1 + w_o / w_p\right)\left(1 + l_o / l_p\right) \tag{8-4}$$

where:

σ_p = stress on the pillar
γ = unit weight of the overburden
z = depth to the excavation
w_o = room width
w_p = pillar width
l_o = room width adjacent to the long side of the pillar
l_p = pillar length.

Hoek and Brown [1980] provide a methodology to evaluate the impact of shape (varying the width/height ratio) on the strength of the pillar. The method requires an assessment of the rock quality, the pillar width/height ratio, and the uniaxial compressive strength of the rock. Most of this work relies upon experience with pillars in coal mines.

The rock quality and width/height ratio are used to obtain a ratio between the average pillar strength and the uniaxial compressive strength of the rock. The uniaxial compressive strength of the rock is multiplied by this ratio to derive the average pillar strength. The average pillar strength can then be used to determine the factor of safety for the pillar:

$$\text{Factor of safety} = \sigma_{1s.av} / \sigma_p \tag{8-5}$$

where:

$\sigma_{1s.av}$ = average pllar strength
σ_p = stress on the pillar.

8.2.5 Shaft Stability

In general, the requirement to support shafts is based upon both the functions and environmental conditions of the shaft. The functions of the shaft relate to the expected life of the shaft; its size, shape, and depth; and its intended use. The environmental conditions relate to the in situ stresses, geology, and hydrology of the location. The structural requirements for a shaft are dictated by the physical and mechanical properties of the in situ rock, hydrology, temperature, and tectonic conditions [Ostrowski, 1972]. Shaft support systems serve to reinforce weak or broken rock, withstand active lateral stresses,

limit water inflow, facilitate installation of hoisting equipment, or reduce ventilation requirements. A shaft with a very limited life for personnel or rock movement would not utilize shaft lining for these two purposes.

Based on the geologic setting (Table 8-1) and the rock properties (Table 8-2), the requirement for internal support of the shafts was evaluated. Works by Ostrowski [1972], Abel et al. [1979], and Richards and Abel [1981] were used to evaluate the stresses acting on the shafts and the need for support in the shafts.

The stresses acting on a circular shaft based on Mohr-Coulomb criteria are [Abel et al., 1979]:

$$\sigma_r = \sigma_H \left(1 - \left(r^2 / (r + l)^2\right)\right) \tag{8-6}$$

$$\sigma_t = \sigma_H \left(1 + \left(r^2 / (r + l)^2\right)\right) \tag{8-7}$$

where:

σ_r = radial stress acting on the shaft

σ_t = tangential stress acting on the shaft

σ_H = in situ horizontal stress

r = radius of the shaft

l = extent of the disturbed rock zone from the shaft wall.

Failure of the rock occurs at a stress level equal to:

$$\sigma_f = \sigma_o + (l \times \tan\beta) \tag{8-8}$$

where:

σ_f = tangential stress at failure

$\tan\beta = (1 + \sin\phi)/(1 - \sin\phi)$

ϕ = angle of internal friction of the rock

σ_o = estimated rock mass strength.

Abel et al. [1979] use an iterative process to solve Equations 8-6, 8-7, and 8-8 for l, the horizontal thickness of the disturbed rock zone (DRZ) around the shaft.

The analytical results from Abel et al. [1979] were verified by finite element modeling using **SPECTROM-32** [Callahan et al., 1989]. The **SPECTROM-32** modeling used the anisotropic stresses expected to be present in the host rock.

8.2.6 Thermal Effects of Refrigerated Gas on Rock Strength

Thermally induced stresses and strains will occur when storing chilled natural gas in an underground mine because of the changes in temperature of the host rock. The effects of these thermally induced

stresses on the stability of the storage mine were evaluated using finite element simulations of the mine. **SPECTROM-41** [Svalstad, 1989] is a finite element heat transfer analysis program and was used to predict temperature as a function of time in the granite surrounding the storage mine. This temperature information, in conjunction with the coefficient of thermal expansion of the granite, was used in the thermomechanical finite element program **SPECTROM-32** to determine the effects of temperature changes on mine stability.

The geometry of the natural gas storage mine was approximated with an axisymmetric model. The axisymmetric model conserved the actual volume of the mine, which is represented as three concentric rings at a depth of 914 meters (3,000 feet), as shown in Figure 8-1. The finite element model of the mine is shown in Figure 8-2. It contains 7,433 nodes and 2,412 eight-noded elements. The model extends from the ground surface to a depth of 1,800 meters and has an outside radius of 2,500 meters. The great extents of the boundaries were chosen so that the modeled mine would not be influenced by the boundaries.

The entire model was assumed to be granite. The material properties used to model the granite and evaluate its stability are listed in Tables 8-2 and 8-4. The actual in situ stress state, which is known to be anisotropic, cannot be represented with axisymmetric models, and was therefore, modeled as being isotropic and equal to the weight of the overburden. This results in an isotropic stress of 0.0275 MPa/meter of depth based on granite's density of 2,800 kg/m^3. The in situ stress at the depth of the mine is about 25.1 MPa. The assumed initial in situ temperature of the granite as a function of depth is described by the following equation:

$$T = 10.3 + 0.0164 \times D \tag{8-9}$$

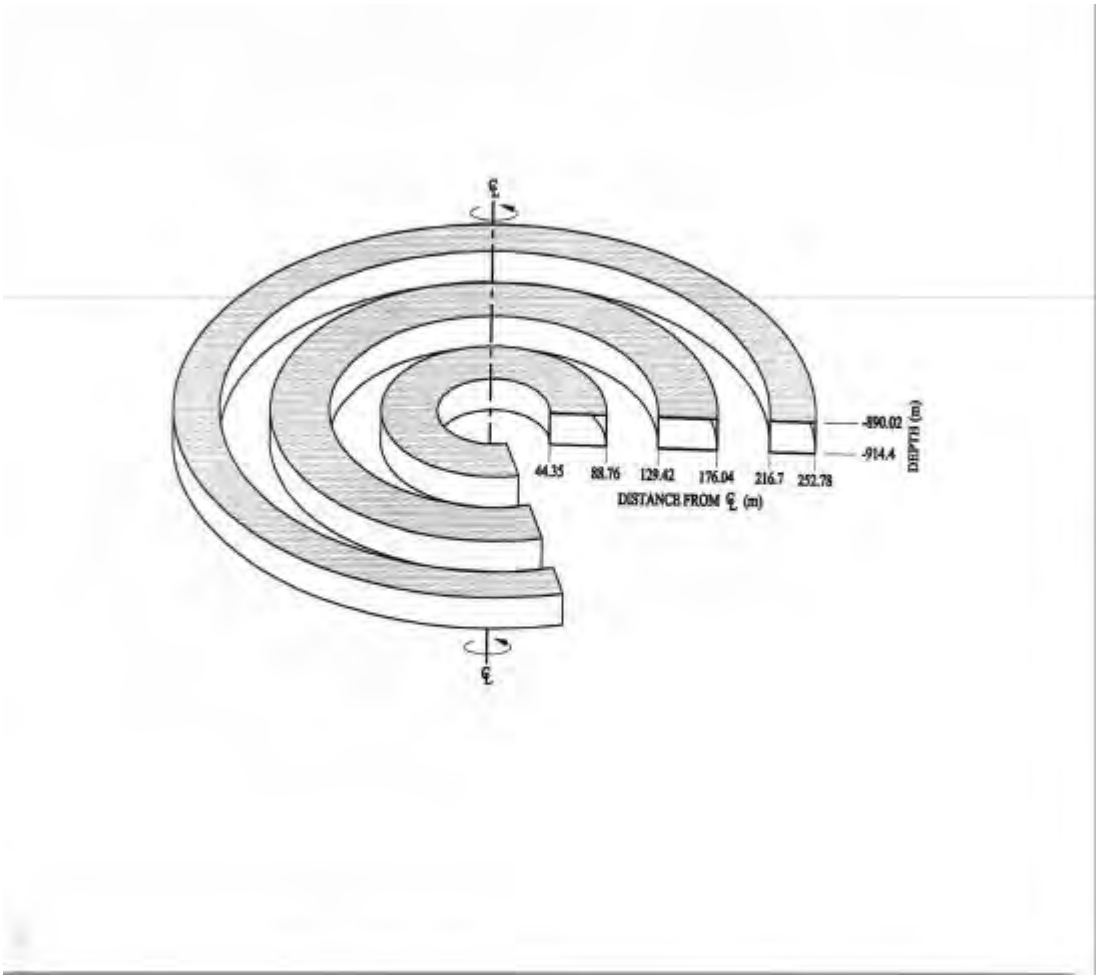

Figure 8-1. Schematic of Axisymmetric Model of Storage Mine.

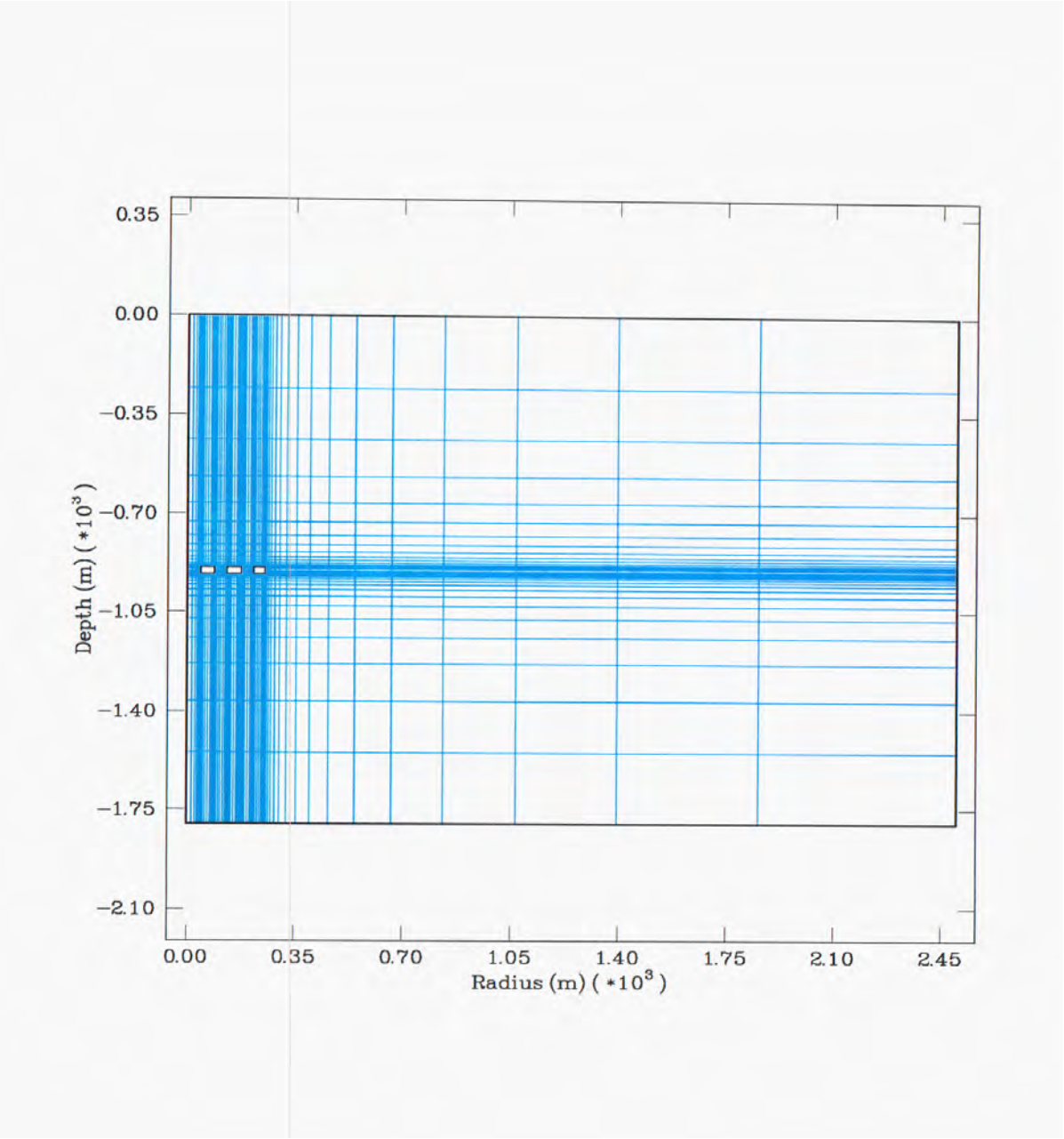

Figure 8-2. Finite Element Mesh of Storage Mine

where the temperature is in degrees centigrade and *D* is the depth in meters. The initial temperature of the granite at the mine level is about 25°C. The gas pressure in the mine and the temperature of the gas were represented in the model by specifying normal tractions and fixed temperatures along the mine surfaces. The planned gas storage temperature in the mine is –28.9°C (–20°F). The planned minimum and maximum gas pressures are 2.1 MPa (300 psi) and 9.1 (1320 psi), respectively.

In an attempt to conservatively evaluate the thermal effects on mine stability, finite element simulations were made of two worst-case scenarios. The two scenarios are: (1) maintaining the minimum gas pressure for a long term of 5 years and (2) during gas withdrawal.

8.3 DESIGN EVALUATION

8.3.1 Room Width

The first step in evaluating the stability of the proposed rooms was to quantify the competency of the rock. Using Barton et al. [1974] as a guide, the following values were used from the rock properties in Table 8-2 and from tables provided in Barton et al. [1974]:

- RQD = 85
- J_n = 4 for two joint sets
- J_r = 2 for smooth, undulating joints
- J_a = 2 for slightly altered joint surfaces
- J_w = 0.66 for medium water inflow
- SRF = 1.0 for high stress and tight structure.

The values chosen to describe the joints, water inflow potential, and zones of weakness in the rock are conservative. However, the chosen descriptions and corresponding numerical values are not at the extreme side of the possible ranges. From these values, Q of the rock mass was calculated (from Equation 8-1) to be 14.0. As seen in Figure 8-3, rooms excavated in this quality of rock would have to be less than about 33 feet in width to stand for an extended time without support. Bieniawski [1976] estimates that this quality rock would support a room width of about 23 feet without support.

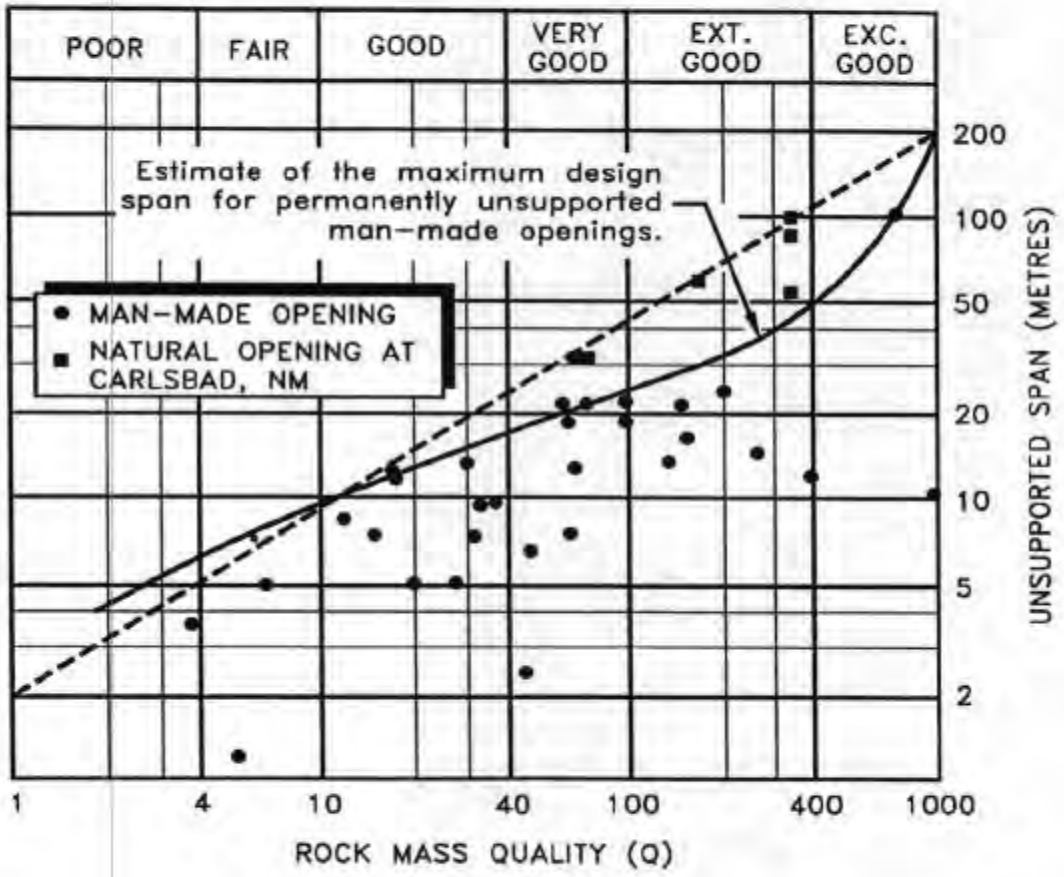

Figure 8-3. Estimate of Maximum Design Span for Permanently Unsupported Man-Made Openings

Using these values of rock quality, wall support pressure, and the proposed room dimensions, recommendations for support were obtained from Barton et al. [1994]. The basic categories of support for the walls and the roof were obtained from Figure 8-4. (This figure is updated and the reinforcement categories are simplified from that in the Barton et al. [1974] report.) ESR listed in Figure 8-4 is the Excavation Support Ratio from Barton et al. [1974]. ESR is an empirical value to reflect the required longevity and safety of the mined openings. For this study, an ESR value of 1.3 was used. This value is recommended for storage rooms, water treatment plants, minor vehicular tunnels, etc. This data placed the walls in support category 2 and the roof in support category 4.

For wall support, the recommended rock support is spot bolting as needed. The recommended roof support is for systematic bolting with tensioned, grouted bolts on 4.5–6-foot (1.5–2-meter) centers, and unreinforced shotcrete 0.2–0.4 inch (4–10 centimeter) thick. Rock bolt length will depend upon the spacing and orientation of rock joints but will be a minimum of 8 feet (2.5 meters).

Bieniawski [1976] does not provide data for recommended support for caverns that are over 10 meters in width. However, for *33-foot- (10-meter-) wide tunnels* in this quality of rock, the recommendation is for 10-foot- (3-meter-) long bolts placed locally in the crown spaced on 8-foot (2.5-meter) centers with wire mesh as needed with the addition of 2 inches (50 millimeters) of shotcrete as needed.

Figure 8-5 shows that Hoek [1979] interprets the work of Barton and Bieniawski to say that light support would probably be required for the quality of rock and location of the proposed refrigerated gas storage cavern.

8.3.2 Maximum Width

Based on the work by Barton et al. [1974], a *supported* room span of up to 130 feet (40 meters) can be easily developed in the Ellicott granodiorite. The support requirements to maintain such rooms are uncertain but *will not be less* than that for the 80-foot-wide rooms. However, complexes of rooms of this width and at 3,000-foot depth have not been routinely constructed.

A 65-meter (215-foot) chamber has been constructed in Norway for an ice hockey rink [Barton et al., 1994]. This chamber is at a depth of about 25 meters (82 feet) in gneiss with an average Q value of about 9. The span is supported with rock bolts and shotcrete. Note that this is a single chamber, not a mined room and pillar complex.

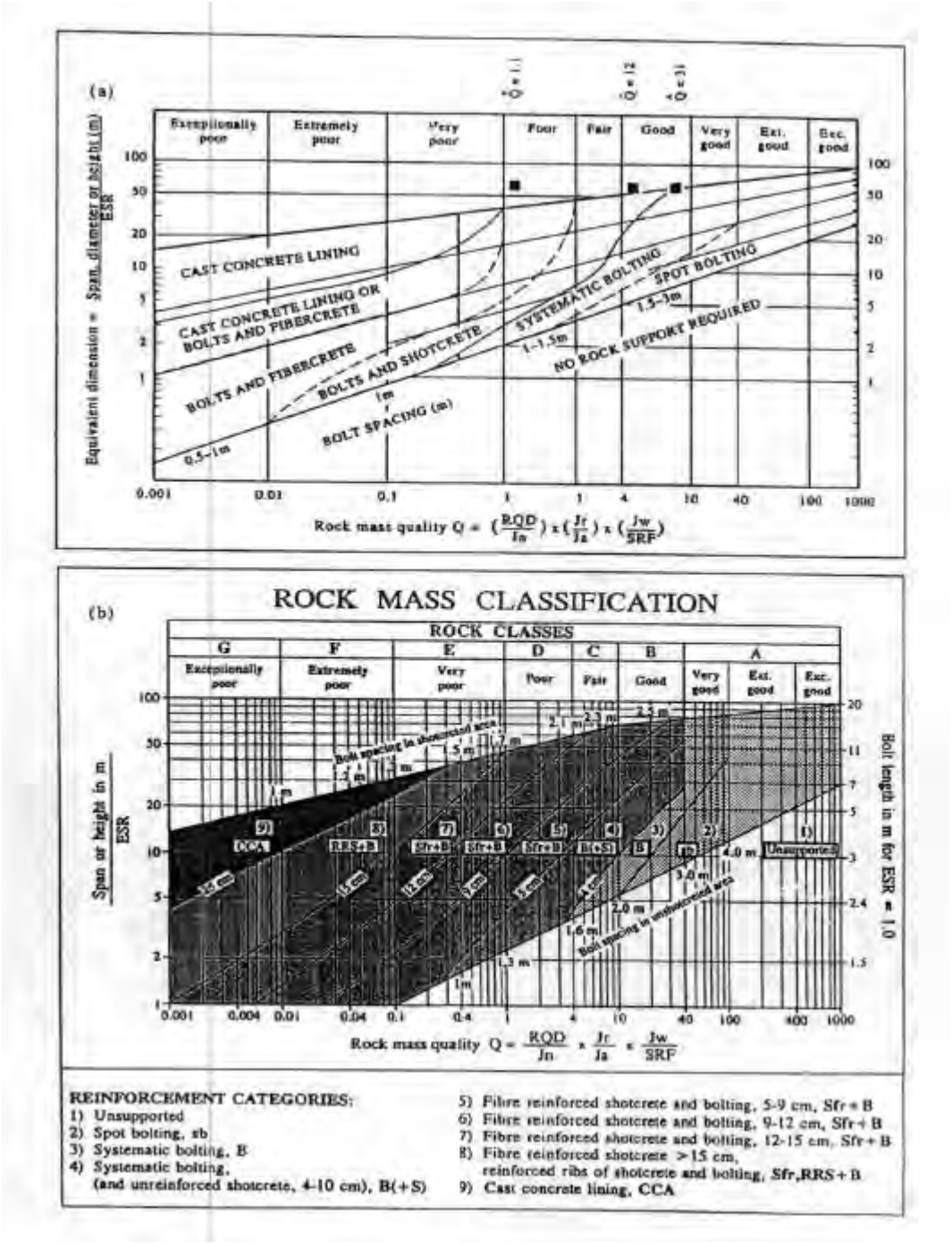

Figure 8-4. Tunnel Support Chart for Categories of Support (After Barton et al. [1994]).

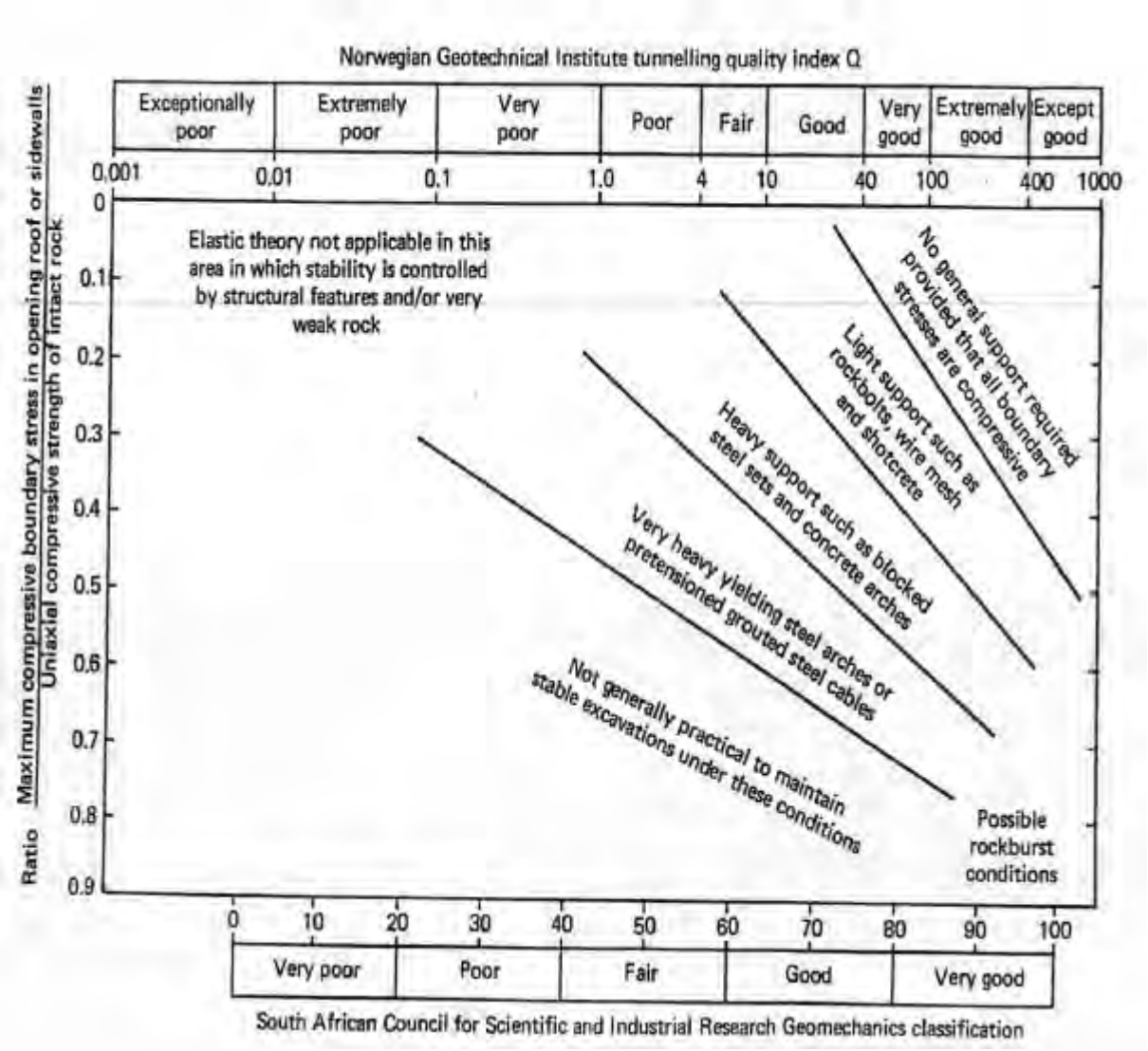

Figure 8-5. Underground Excavation Stability as a Function of Induced Stresses and Rock Mass Quality

8.3.3 Pillar Width

As presently designed, the total vertical stress on the pillars is about 7,800 psi as calculated from Equation 8-4. With a compressive strength of the rock of 10,000 psi, the factor of safety of the pillar is 1.28.

The strength of a pillar is also influenced by its shape. In this case, the pillars are relatively short for their horizontal cross-sectional size. From Figure 8-6, the average pillar strength to uniaxial compressive strength ratio for a pillar with a width-to-height ratio of 1.875 (150 feet/ 80 feet) and in very good quality rock is about 1.45. The average pillar strength is then about 14,500 psi (10,000 psi $\times$ 1.45). *The safety factor is then 1.86 (from Equation 8-5), taking into account the pillar shape.*

8.3.4 Shaft Stability — Analytical Approach

For the analytical approach to estimating the stability of the shaft, the horizontal stresses were assumed to act isotropically on the shaft. The effective in situ stress at the base of the shaft was conservatively estimated to be 9,090 psi from:

$$\sigma_\theta = 3\sigma_{H\,max} - \sigma_{H\,min} \qquad (8\text{-}10)$$

where:

σ_θ = the near-field tangential stress

$\sigma_{H\,max}$ = the maximum horizontal stress of 7,260 psi

$\sigma_{H\,min}$ = the minimum horizontal stress of 3,630 psi.

The rock mass strength was estimated to equal the average unconfined compressive strength of the rock, 10,000 psi, because this value is a conservatively low value for granitic masses. (Granites typically have an unconfined compressive strength in excess of 30,000 psi.) The angle of internal friction of the rock was estimated as 50^o (from Lama and Vutukuri [1978]). The resulting stresses, from Equations 8-6 through 8-8, acting at the transition from “failed” rock (the plastic zone) to “intact” rock (the elastic zone) near the shafts are shown in Table 8-5 and Figures 8-7 and 8-8.

As seen in Figures 8-7 and 8-8, there is a small zone, marked DRZ, immediately adjacent to the shaft wall that is overstressed. This overstressed rock may cause some spalling that may require minor support.

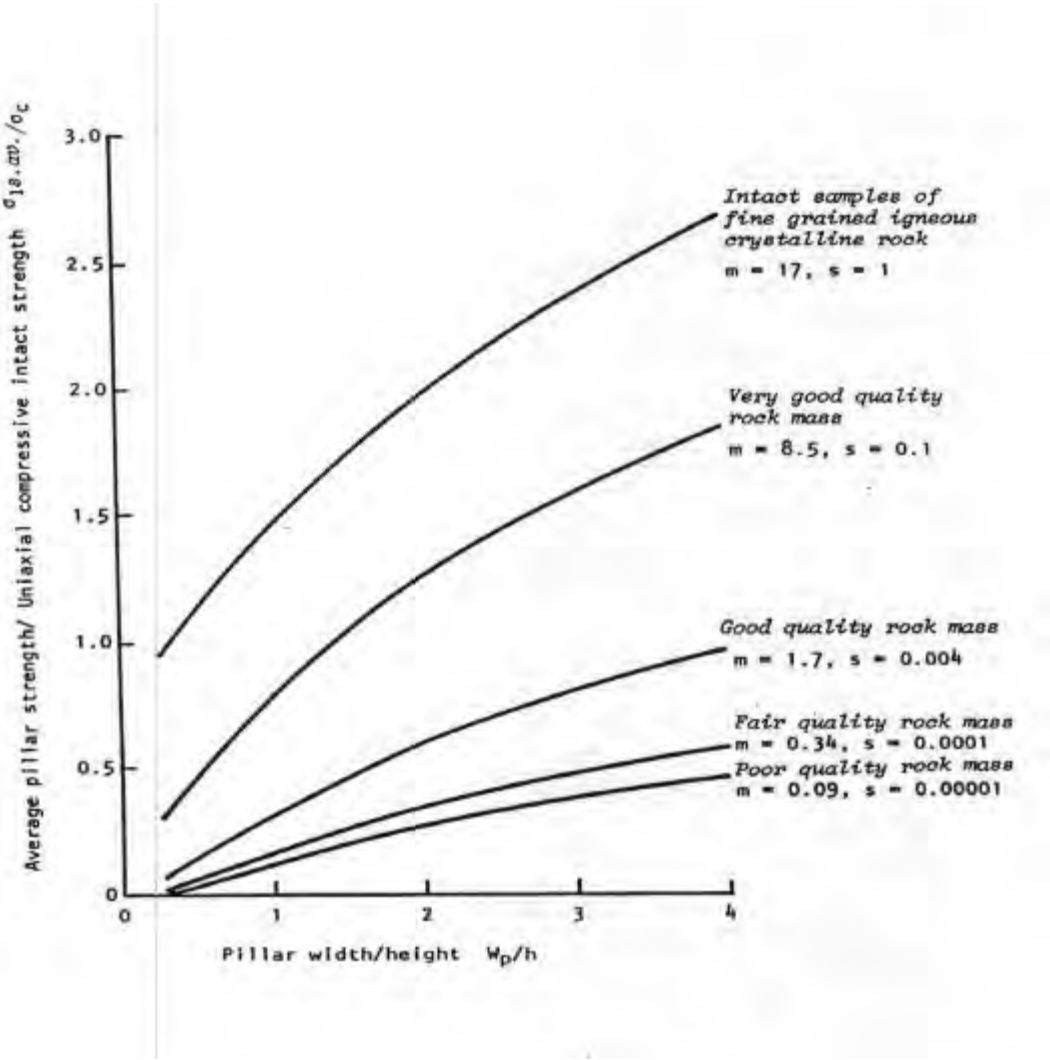

Figure 8-6. Influence of Pillar Width-to-Height Ratio on Average Pillar Strength (After Hoek and Brown

Table 8-5. Stresses Acting Near the Shafts for Proposed Refrigerated Gas Storage Cavern

Property	18-Foot-Diameter Shaft	10-Foot-Diameter Shaft
Radial stress, psi	960	961
Tangential stress, psi	17,220	17,220
Thickness of DRZ, inches	6.2	3.4

To ensure that the estimated strength of the rock mass was not critical to the stability of the shaft, the estimated rock mass strength was reduced to 2,500 psi from 10,000 psi. This resulted in a slight increase in the extent of the DRZ to about 13 inches for the 18-foot-diameter shaft and 7 inches for the 10-foot-diameter shaft.

8.3.5 Shaft Stability — Finite Element Modeling

The thermomechanical finite element program **SPECTROM-32** [Callahan et al., 1989] was used to simulate the elastoplastic response of the granite surrounding the shafts. Unlike the analytical solutions in which an isotropic stress field is assumed, the effect of the anisotropic in situ stress state in the granite could be explicitly simulated using **SPECTROM-32**. Taking advantage of the symmetry about the horizontal principal stress directions, only a quarter of a horizontal section through each shaft was represented in the finite element model. The far-field boundary of each finite element model was set at a radius equal to 20 the radius of the shaft.

An in situ stress state with maximum and minimum horizontal principal stresses of 6,060 and 3,030 psi and a vertical (out-of-plane) stress of 3,030 psi was specified to represent the assumed conditions at a depth of 3,000 feet in granite. Plane-strain conditions were assumed. Failure of the granite was represented using the Mohr-Coulomb criterion with an unconfined compressive strength of 10,000 psi and an internal friction angle of 50^{o}. The residual (postfailure) strength of the granite was represented using the same criterion. The postfailure, plastic strains in the granite were based on the associative flow rule. Consequently, the rock dilated after failure, thereby representing the creation of porosity that is associated with fracturing.

The zones of failure predicted by **SPECTROM-32** are shown in Figures 8-9 and 8-10 for the 10-foot-diameter and 18-foot-diameter shafts, respectively. In these figures, the *x*-direction is parallel to the direction of the maximum horizontal principal stress. Figures 8-9 and 8-10 show that no failure is predicted on the wall of the shaft that is perpendicular to this direction. The depth of the failure zones increase as the angle from the *x*-direction increases until the failure zones are deepest on the wall that is perpendicular to the direction of the minimum horizontal principal stress (the *y*-direction). Even at their deepest, the failure zones predicted for the 10-foot-diameter and 18-foot-diameter shafts are only 4.8 and 9.4 inches deep, respectively. These values are about 50 percent greater than the DRZ predicted by the analytical method discussed above. Consequently, any spalling from the shafts is expected to require minimal support, such as rock bolting and meshing, and a concrete liner is not required to support the walls of the shafts under the assumed conditions.

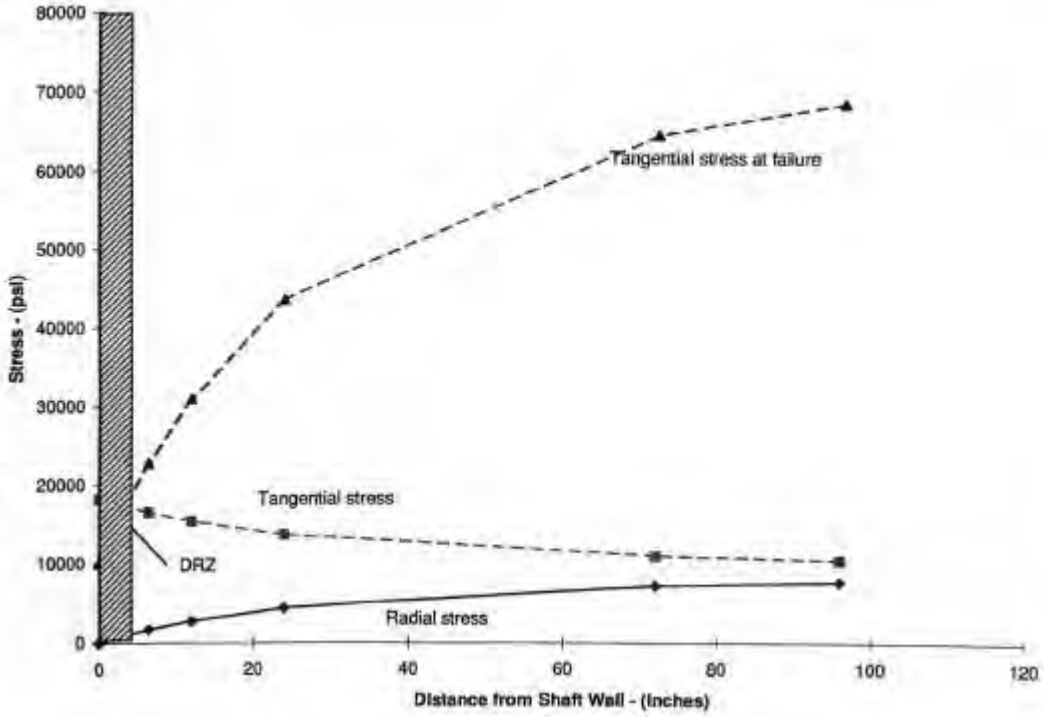
80000
70000
60000
50000
40000
30000
20000
10000
0
Stress - (psi)
Tangential stress at failure
Tangential stress
DRZ
Radial stress
0
20
40
60
80
100
120
Distance from Shaft Wall - (Inches)

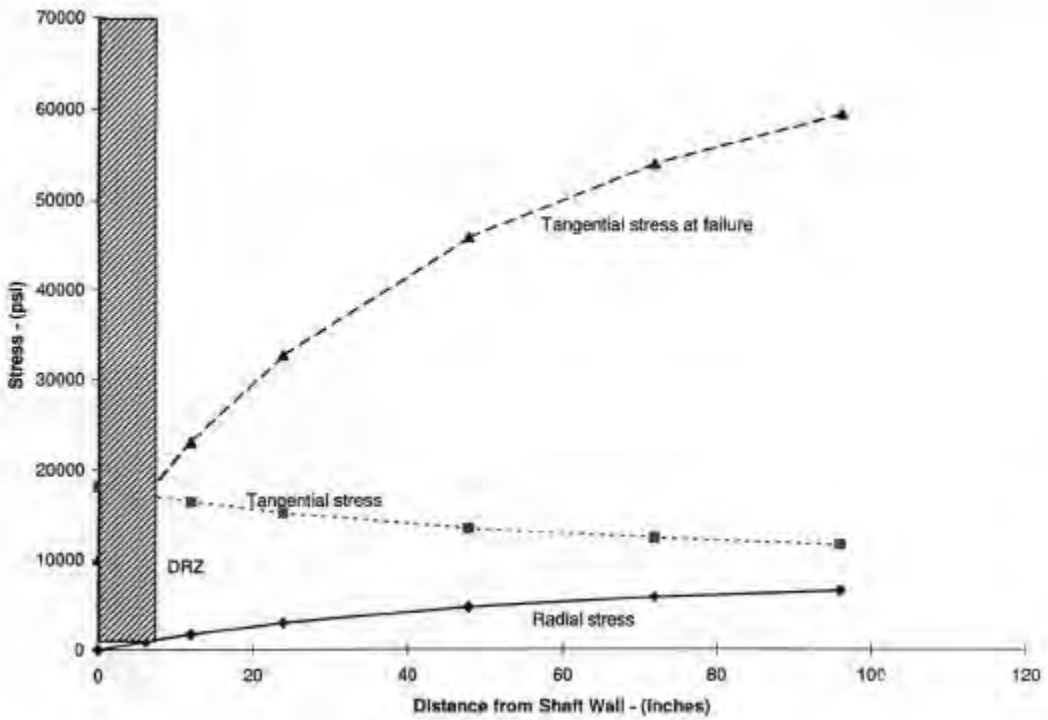
70000
60000
50000
40000
30000
20000
10000
0
Stress - (psi)
Tangential stress at failure
Tangential stress
DRZ
Radial stress
0
20
40
60
80
100
120
Distance from Shaft Wall - (inches)

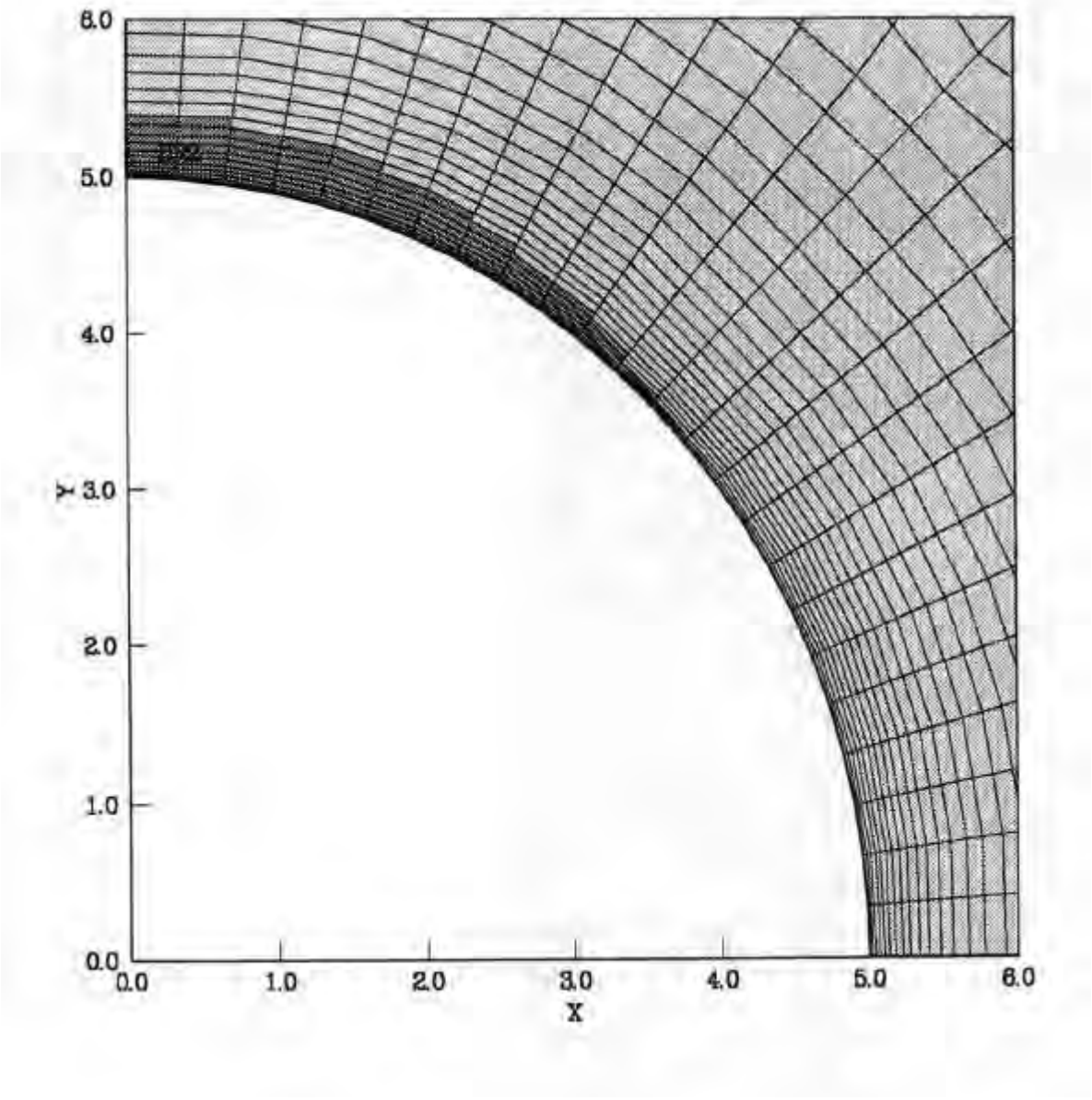

Figure 8-9. Influence of Pillar Width-to-Height Ratio on Average Pillar Strength (After Hoek and Brown) 10,000 psi Granite.

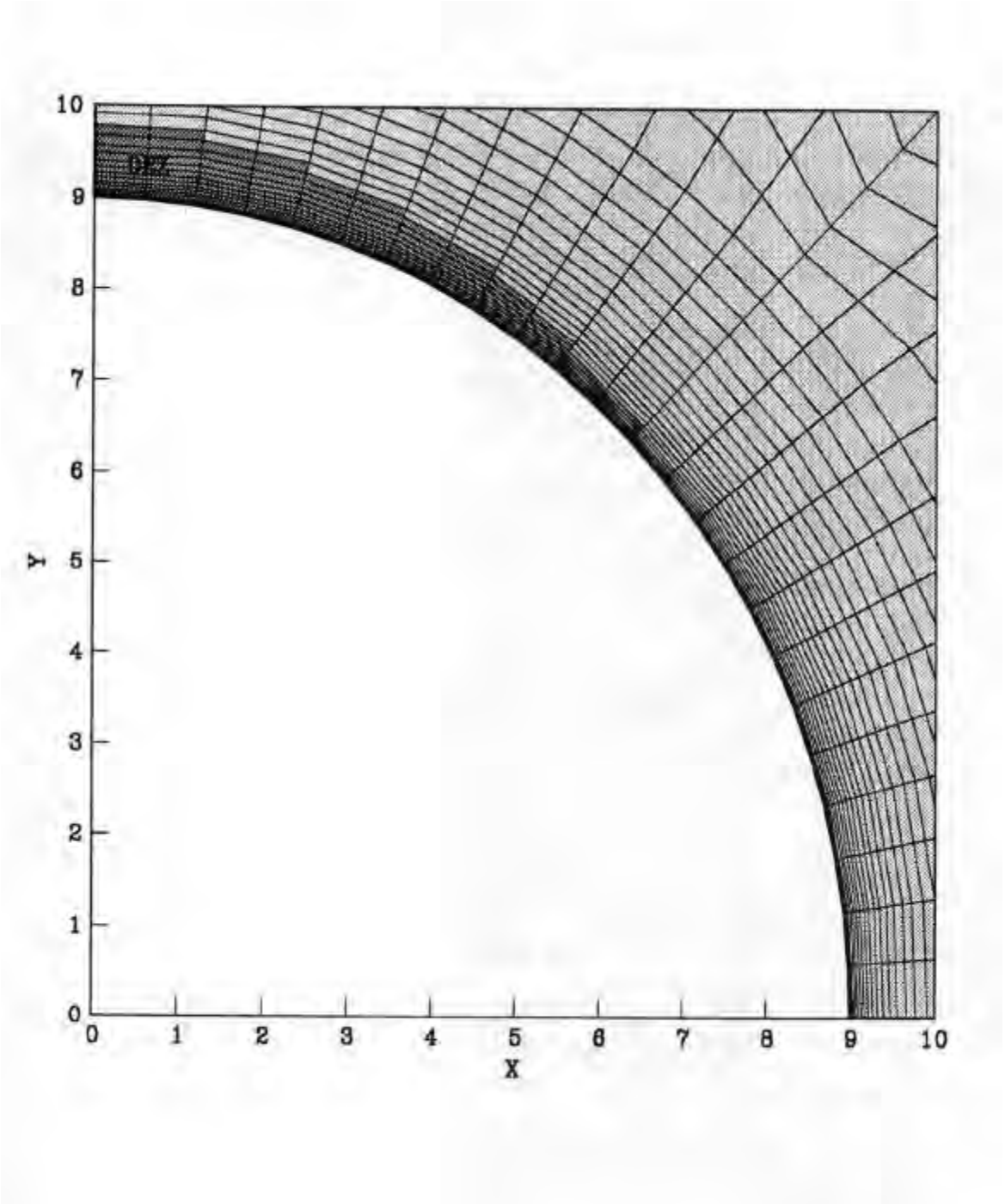

Figure 8-10. DRZ Predicted by SPECTROM-32 Around an 18-Foot-Diameter Shaft at 3,000-Foot Depth in 10,000 psi Granite.

8.3.6 Long-Term Thermal Effects at Minimum Gas Pressure

In this simulation, the mine is modeled at the minimum gas pressure for a period of 5 years. The granite surrounding the gas storage mine is initially at the original in situ temperature. The mine is instantaneously excavated and filled with natural gas at a temperature of –28.9°C (–20°F) at the minimum storage pressure of 2.1 MPa (300 psi). The gas pressure and temperature are held constant. The stresses in the pillars are monitored as the host rock is cooled over a 5-year period. The mine will probably encounter the largest thermal gradients during this initial storage period when most of the surrounding granite is still at the original in situ temperature.

Figures 8-11 and 8-12 show temperature contours predicted by **SPECTROM-41** in the granite surrounding the mine at several times during the 5-year simulation. The temperature gradients are initially very high near the room surfaces and decrease with time as the host rock is cooled. Cooling is a fairly slow process. As shown in Figure 8-12, the temperatures of the center of the pillars are nearly unchanged after 1 year. However, within 5 years, the pillars have cooled significantly and the temperature gradients at the room surfaces are somewhat lower.

Figures 8-13 and 8-14 show contours of the predicted Mohr-Coulomb factors of safety in the pillars at several times during the 5-year simulation. The Mohr-Coulomb factors of safety are based on an unconfined compressive strength of 69 MPa (10,000 psi) and an internal friction angle of 50°. Because the simulations assume no thermal strains at time zero, the factors of safety shown at time zero do not reflect any thermal effects. All of the factors of safety are greater than two. As shown in the figures, the factors of safety near the room surfaces actually increase as the rock is cooled. Factors of safety in the center of the pillar decrease slightly with time.

Figures 8-15 and 8-16 show contours of the predicted maximum principal stress in the granite. A tensile stress is represented by a positive value with the sign convention used. Again, contours shown at time zero do not reflect any thermal effects. The maximum principal stresses are initially all compressive with a least compressive value about equal in magnitude to the gas pressure. However, contraction of the granite surrounding the mine as it cools results in the stresses becoming less compressive. After 1 year, the center of the roof of the centermost room is predicted to have a tensile stress of about 1 MPa. The maximum principal stresses change very little between 1 year and 5 years.

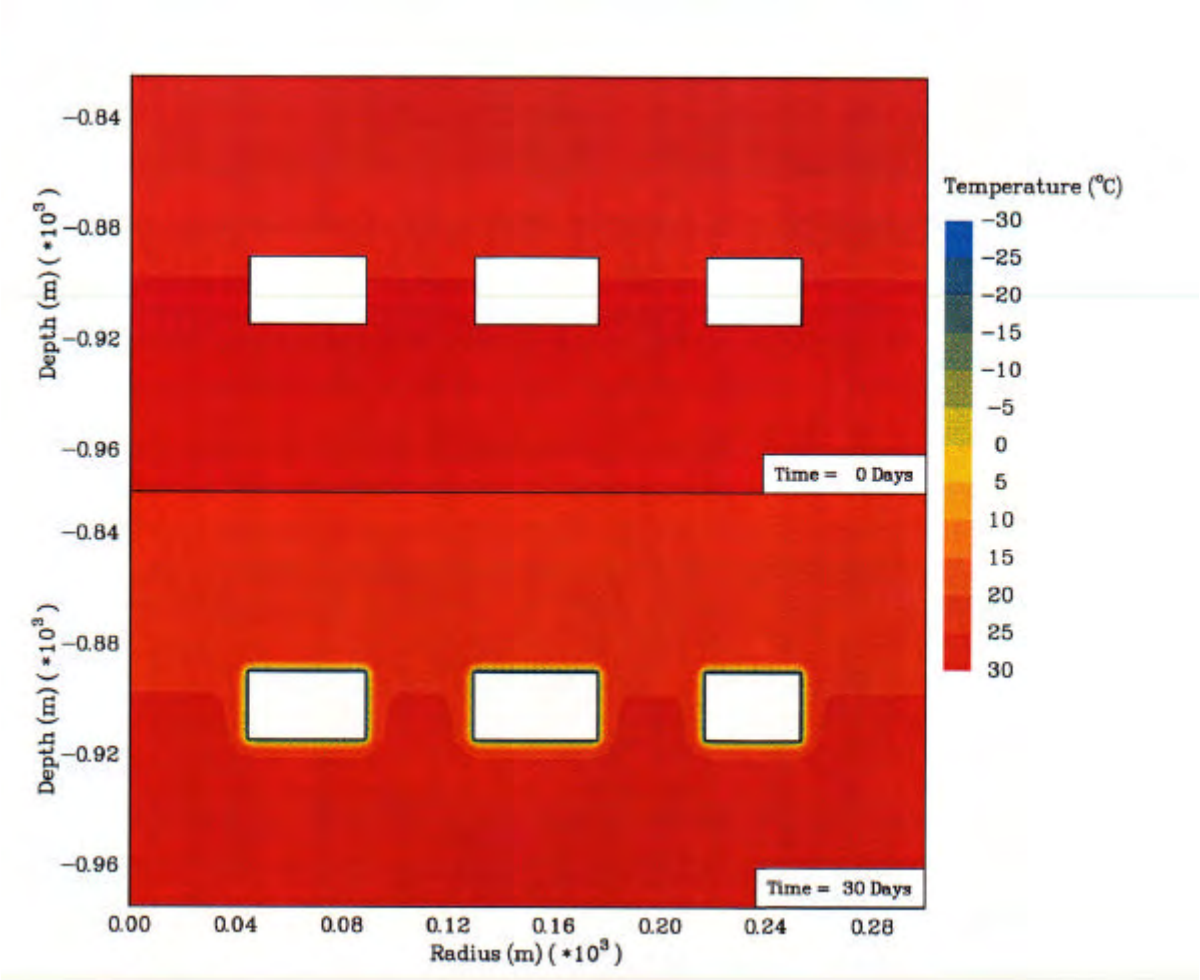

Figure 8-11. Temperature Contours at Time 0 and 30 Days After Filling With Gas at –28.9°C.

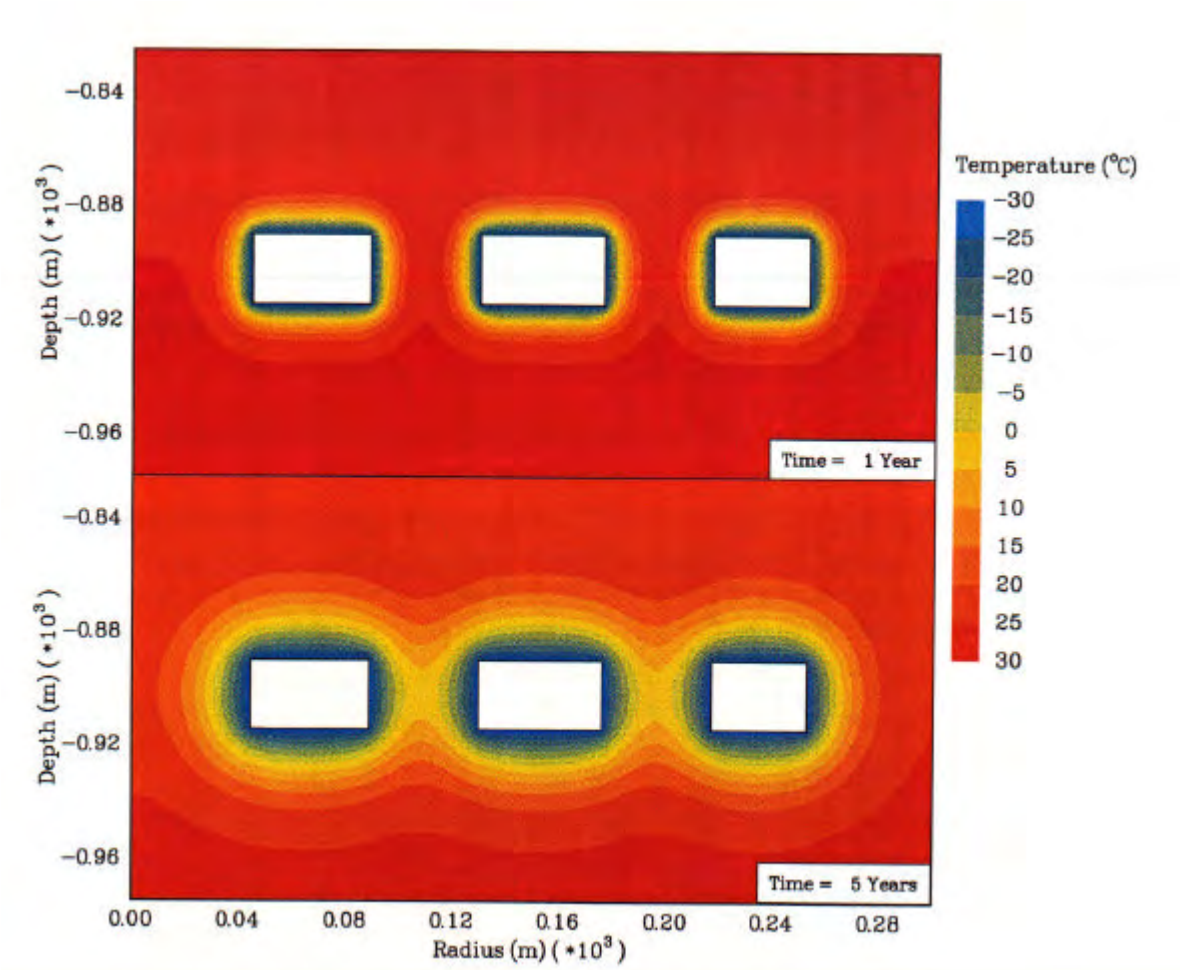

Figure 8-12. Temperature Contours at One and 5 Years After Filling With Gas at –28.9°C.

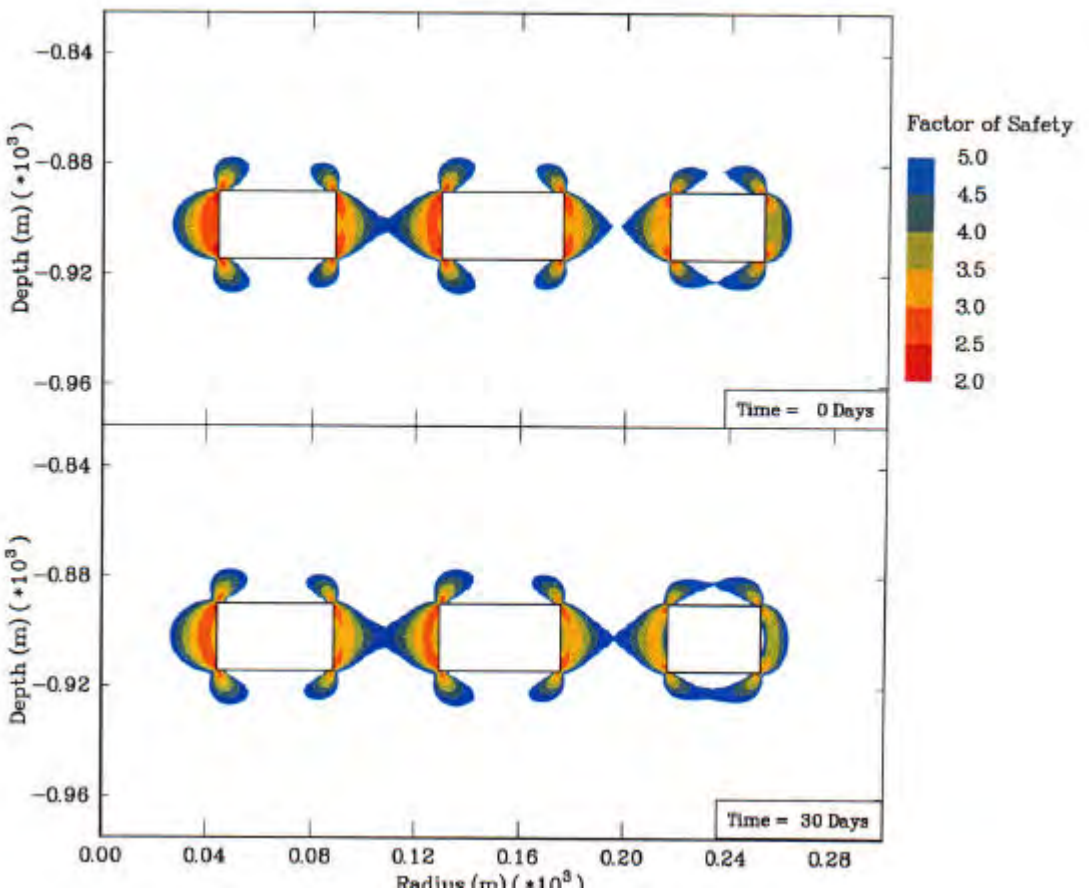

Figure 8-13. Mohr-Coulomb Factor-of-Safety Contours at 0 and 30 Days After Filling With Gas at -28.9°C.

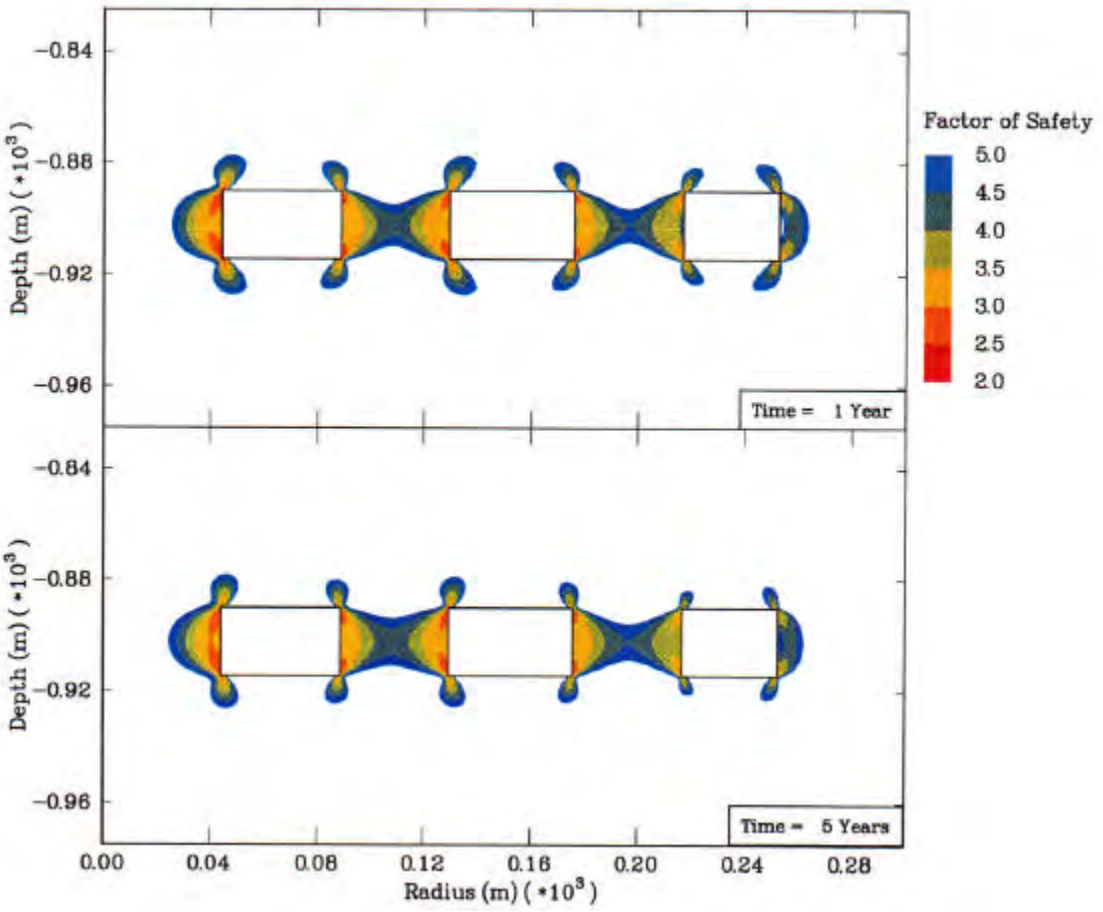

Figure 8-14. Mohr-Coulomb Factor-of-Safety Contours at 1 and 5 Years After Filling With Gas at -28.9°C.

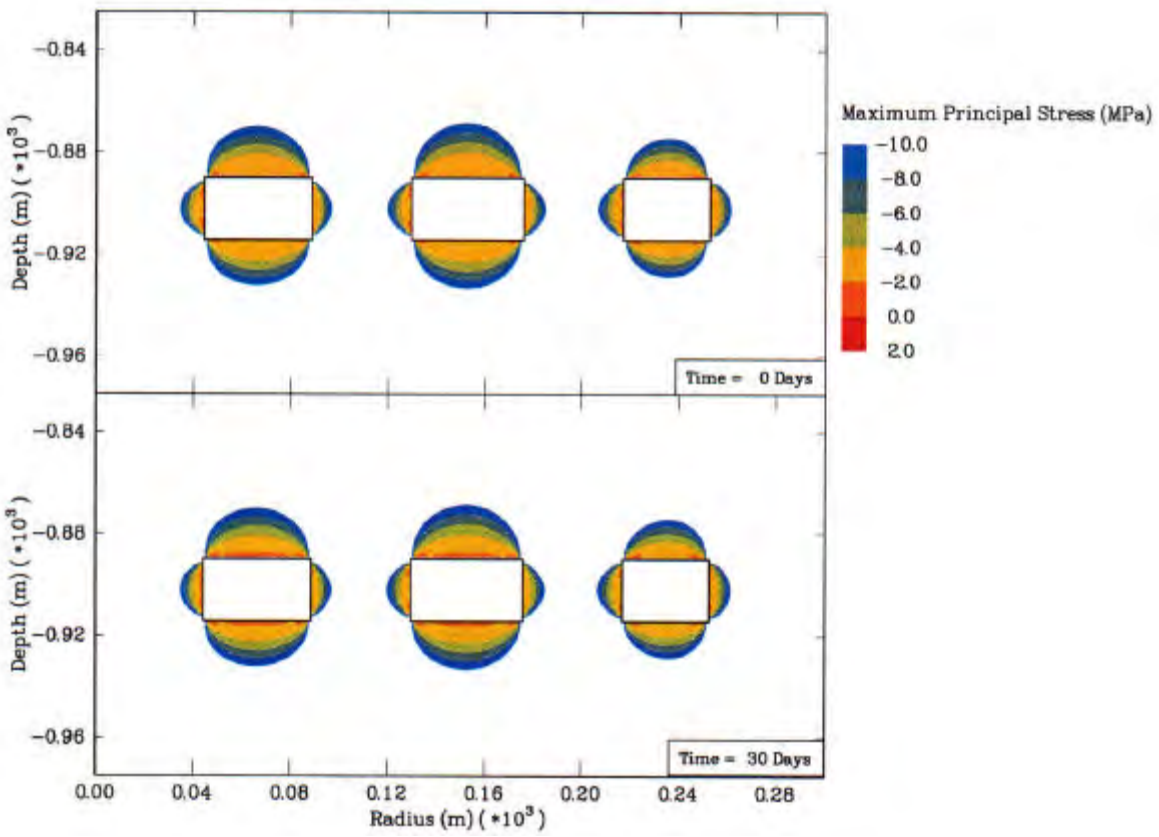

Figure 8-15. Maximum Principal Stress Contours at 0 and 30 Days After Filling With Gas at –28.9°C Compressive Stresses are Negative).

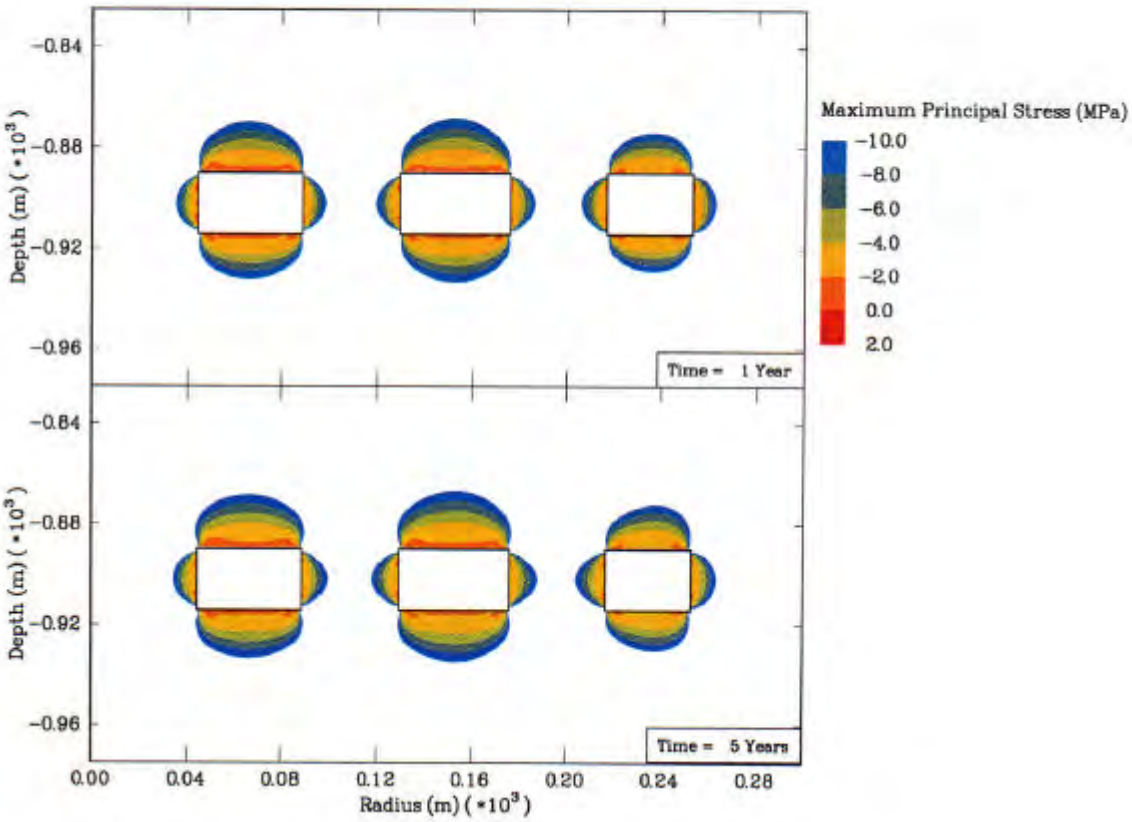

Figure 8-16. Maximum Principal Stress Contours at 1 and 5 Years After Filling With Gas at –28.9°C Compressive Stresses are Negative).

8.3.7 Effect of Gas Withdrawal

The second simulation was used to examine the thermal effects during gas withdrawal. During gas withdrawal, the expansion of the gas in the mine will result in lowering the temperature of the gas. In this simulation, the granite surrounding the gas storage mine is initially at the original in situ temperature. The mine is instantaneously excavated and filled with natural gas at a temperature of –28.9°C (–20°F) at the maximum storage pressure of 7.1 MPa (1,320 psi). The gas pressure and temperature are held constant for 180 days. At 180 days, the pressure is reduced over a 10-day period to the minimum pressure of 2.1 MPa (300 psi). During the withdrawal, the gas temperature is assumed to drop linearly with time to –43.9°C (–47°F). The stability of the mine was monitored during the depressurization.

Figure 8-17 shows contours of the predicted Mohr-Coulomb factors of safety in the pillars just before and at the end of the gas withdrawal. Because the mine is at maximum gas pressure, the factors of safety are all very high at 180 days. The factors of safety are lower after the drawdown but are still greater than 2.5.

Figures 8-18 shows contours of the predicted maximum principal stresses in the granite before and after gas withdrawal. Before the withdrawal, at maximum gas pressure, all of the stresses are highly compressive. However, after the withdrawal, gas pressure is at the minimum value and the temperature in the mine has dropped 15°C. This results in a large portion of the floor and roof of the two centermost rooms having tensile stresses. The maximum tensile stress has a value of about 3.5 MPa, which is lower than the tensile strength of the granite.

8.4 GEOMECHANICAL SUMMARY AND RECOMMENDATIONS

The mine design consists of a room-and-pillar layout with rooms 80 feet wide and 80 feet tall and with 150-foot by 200-foot pillars with a central shaft pillar for the storage of refrigerated natural gas. This design is adequate to develop a long-lasting facility in a granodiorite with the given rock properties.

Before construction is started or the design is finalized, additional geological exploration and geomechanical testing should be conducted. The design then should be refined with more definitive rock properties, including compressive strength, tensile strength, thermal properties, in situ stress state, joint set definition, and hydrologic measurements. The mine pillars, as designed, have a factor of safety in excess of 1.8. The roof span should be reinforced with systematic bolting and shotcrete. Support of the walls should, at a minimum, include bolting of potential loose blocks that result from jointing.

The mine pillars, given the factor of safety, cannot be reduced in width. The room spans can potentially be increased to 130 feet. However, if the room span is increased, the pillar size must also be increased proportionately. The room height could be increased to 100 feet and still maintain the factor of safety in the pillars at 1.75.

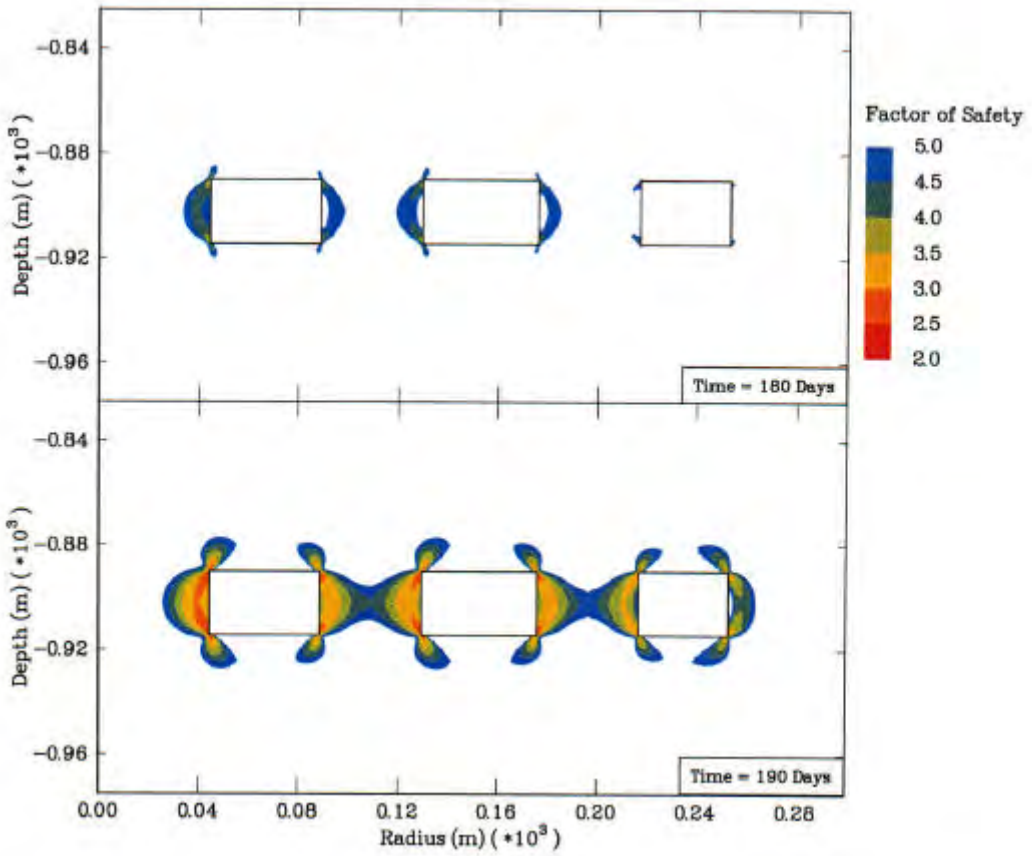

Figure 8-17. Mohr-Coulomb Factor-of-Safety Contours Before and After Drawdown From Maximum to Minimum Gas Pressure.

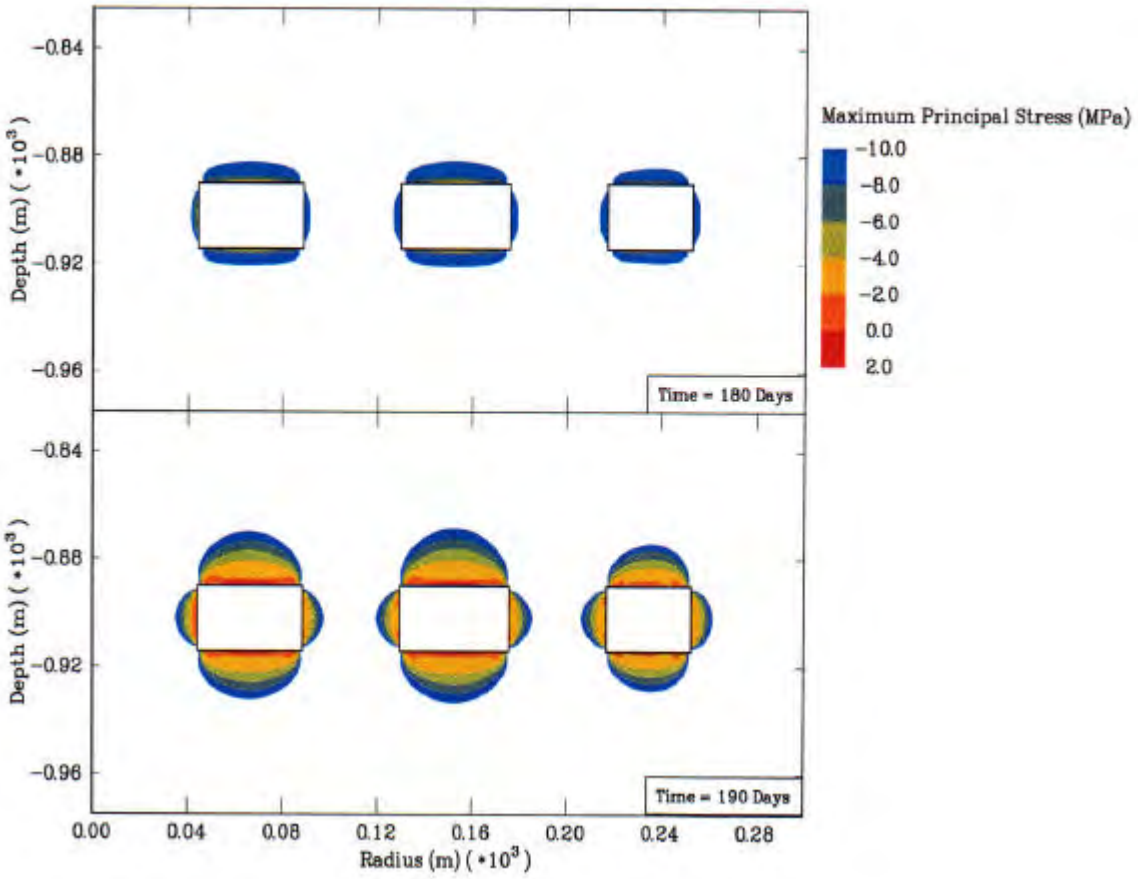

Figure 8-18. Maximum Principal Stress Contours Before and After Drawdown From Maximum to Minimum Gas Pressure.

Based on the assumed rock properties for the site, there is no need to install a lining in the shafts for the refrigerated gas storage cavern. A narrow zone of damaged rock will develop around the shaft walls. This DRZ may require localized minor reinforcement or meshing to prevent spalling rock from injuring miners or damaging hoisting equipment while the storage cavern is being developed.

The results of the two simulations of the thermal effects on the rock strength suggest that the thermal effects do not have a large impact on the mine stability. The Mohr-Coulomb factors of safety were actually improved with time as the granite surrounding the mine cooled from the original in situ temperature. The cooling of the granite did result in some tensile stresses in the roof and floor of the mine. The largest tensile stresses predicted were about 3.5 MPa at the end of the gas withdrawal simulation, which is somewhat less than the 4.8 MPa tensile strength assumed of intact granite.

The actual in situ stress state, which is known to be anisotropic, cannot be represented with axisymmetric models, and was therefore, modeled as being isotropic. Although this assumption may affect the nonthermal results of these simulations, the thermal effects are not believed to be significantly impacted.

This modeling only considers thermal effects due to the expansion (or contraction) of the granite due to temperature changes. It does not consider the effects of freezing groundwater in the pore space of the granite which may have a significant impact on the results.

8.5 CALCULATION OF COOLING LOAD FOR REFRIGERATED NATURAL GAS STORAGE

The following section presents the results of analyses performed to estimate the cooling load required for a refrigerated natural gas storage cavern. The cooling requirements were estimated using finite element simulations of the mine with the heat transfer analysis program **SPECTROM-41** [Svalstad, 1989]. Two sets of calculations were made. The first estimates the overall cooling load required to maintain a gas temperature of –20 ^{o}F. The second estimates the potential beneficial cooling resulting from gas expansion during gas withdrawal.

8.5.1 FINITE ELEMENT MODEL

The geometry of the mined natural gas storage cavern was approximated with an axisymmetric model. The axisymmetric model conserved the actual volume of the mine (37.4 million ft^3) which is represented as three concentric rings at a depth of 3,000 ft, as shown in Figure 8-19. The room width and wall surface area of the mine model are also representative of those in the mine plan. The finite element model of the mine is shown in Fig. 8-20. It contains 6,343 nodes and 2,052 eight-noded elements. The model extends from the ground surface to a depth of 6,000 feet and has an outside radius of 7,500 feet. These extensive boundaries were chosen so that the modeled mine would not be influenced by the boundaries.

The host stratigraphy was assumed to be entirely granite. The thermal material properties used to model the granite are shown in Table 8-6. The assumed initial in situ temperature of the granite as a function of depth is described by the following equation:

$$T = 50.5 + 0.009\,x\,\mathrm{D} \qquad (1)$$

where the temperature is in degrees Fahrenheit and D is the depth in feet. The initial temperature of the granite at the mine level is about 77 ^{o}F.

Table 8-6. Material Properties for Granite

Property	Value	Source
Thermal Conductivity	1.45 Btu/ft-R	Carslaw and Jaeger [1959]
Specific Heat	0.21 Btu/lbm-R	Carslaw and Jaeger [1959]
Density	175 lbm/ft^3	PB-KBB Inc. [1998]

8.5.2 OVERALL COOLING LOAD

The plan for the refrigerated storage cavern is to store natural gas at a temperature of –20 ^{o}F. Because of the large difference between the temperature of the stored natural gas and that of the surrounding granite, a large amount of heat will be transferred from the granite to the stored gas. Through time, the granite surrounding the mine will cool and less heat will be transferred to the gas. External cooling will have to be provided to counteract the heat transferred from the surrounding granite or the temperature of the stored gas will increase.

To estimate the cooling load required to maintain the gas temperature at –20 ^{o}F, a finite element simulation was performed in which the nodes at the mine surface were fixed at –20 ^{o}F and the heat required to maintain this fixed temperature boundary condition was tracked. The cooling load was tracked over a total simulation time of 10 years. Fig. 8-21 shows the cooling load as function of time. The cooling load versus time is nearly linear on the log-log plot, indicating that the cooling load initially drops very quickly when the temperature gradients in the granite are large, but drops much slower as these temperature gradients decrease. Fig. 8-22 shows the temperature gradients surrounding the mine at 1 and 10 years. At the end of the first year, the cooling load is about 10 million Btu/hr, and after 10 years, the cooling load reduced to about 3.7 million Btu/hr.

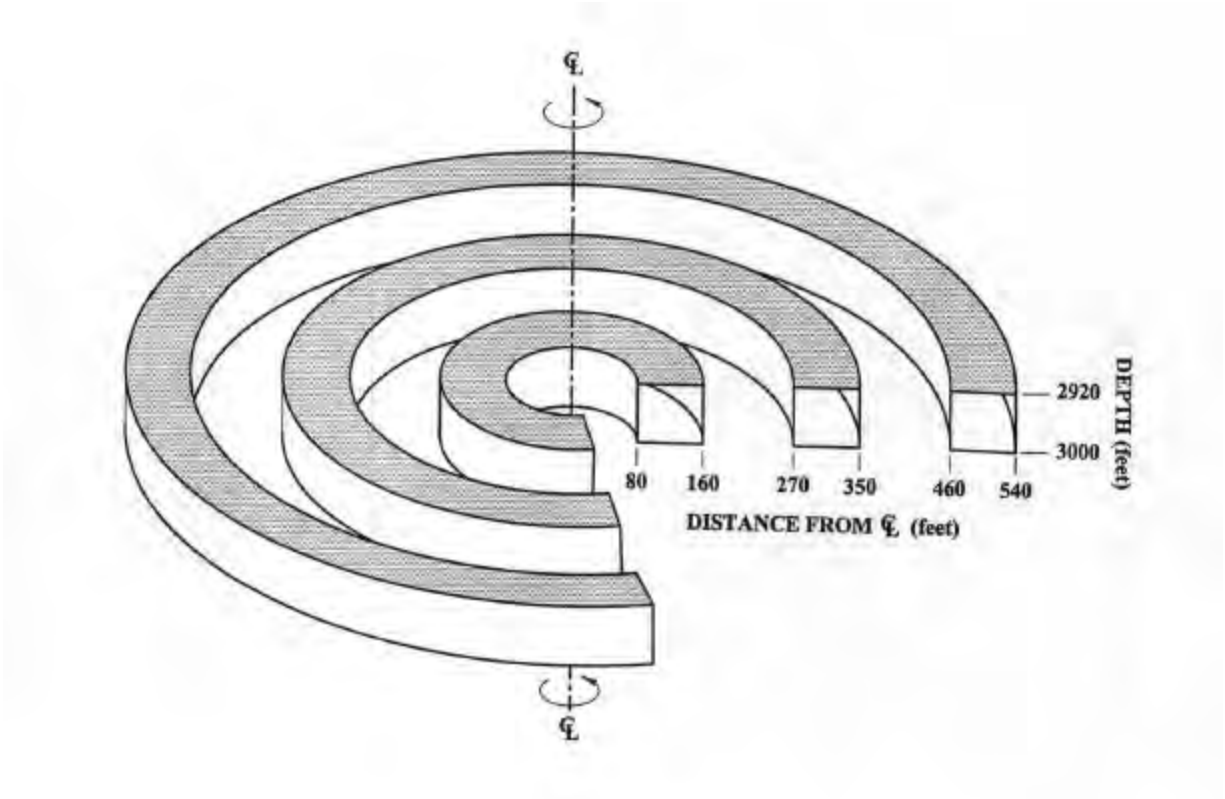

Figure 8-19. Schematic of Axisymmetric Model of Storage Caverns

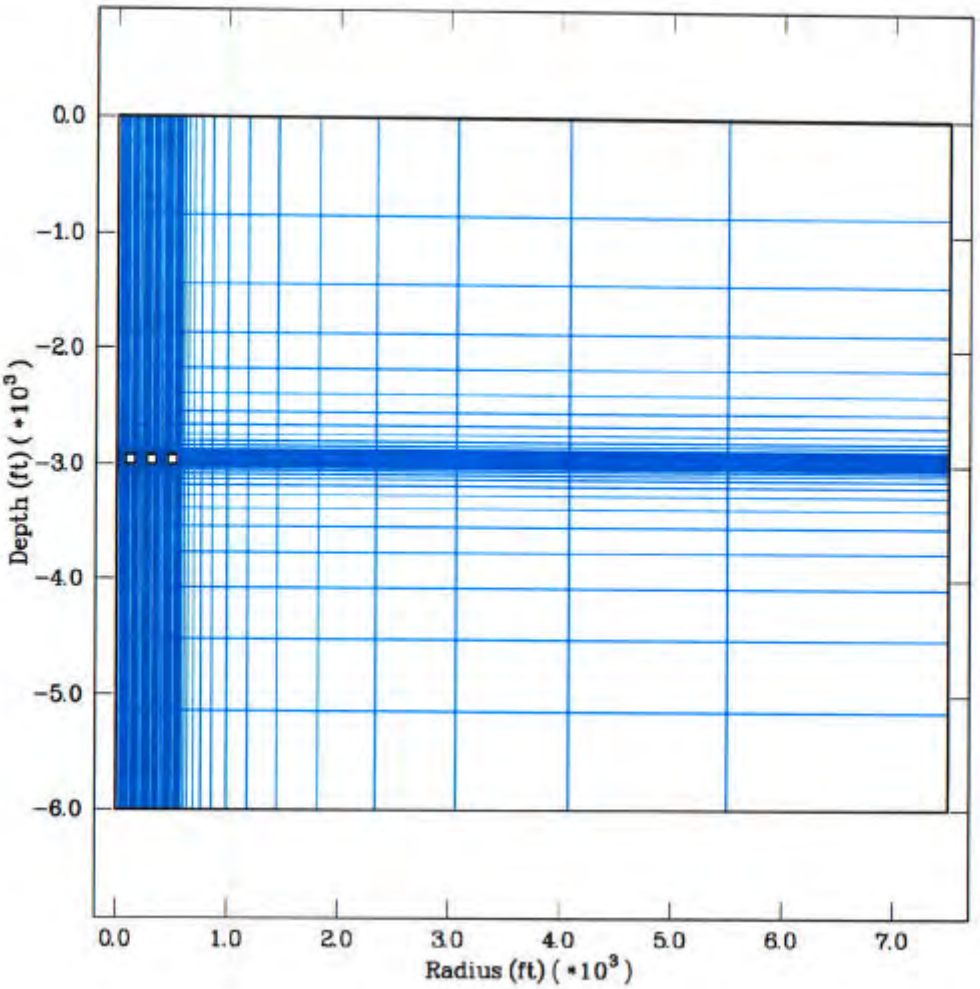

Figure 8-20 Finite Element Model of Storage Cavern

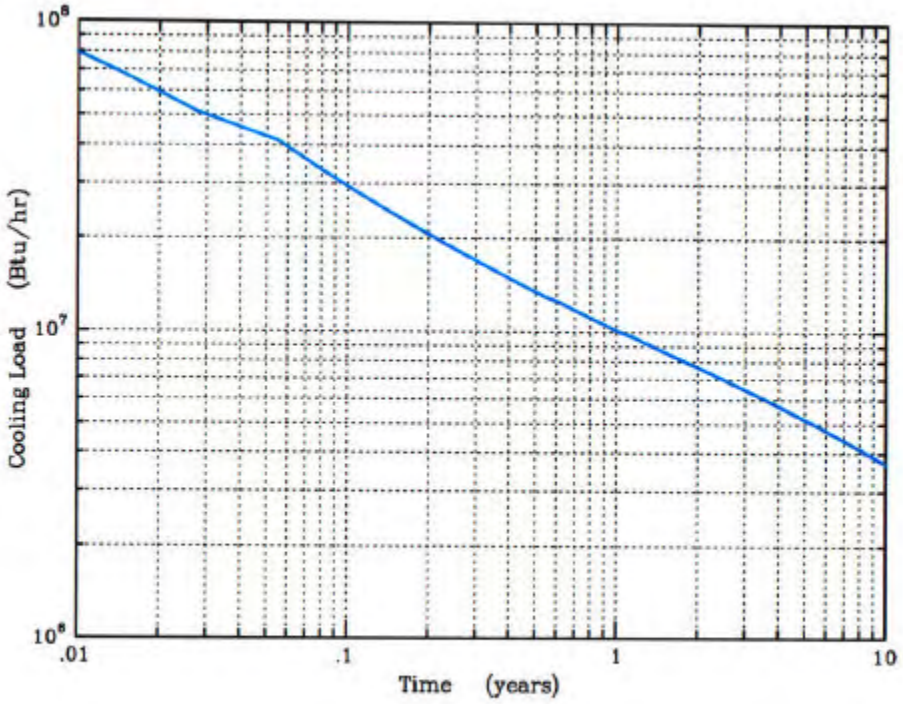

Figure 8-21. Cooling Load Required to Maintain Storage Cavern at –20 F

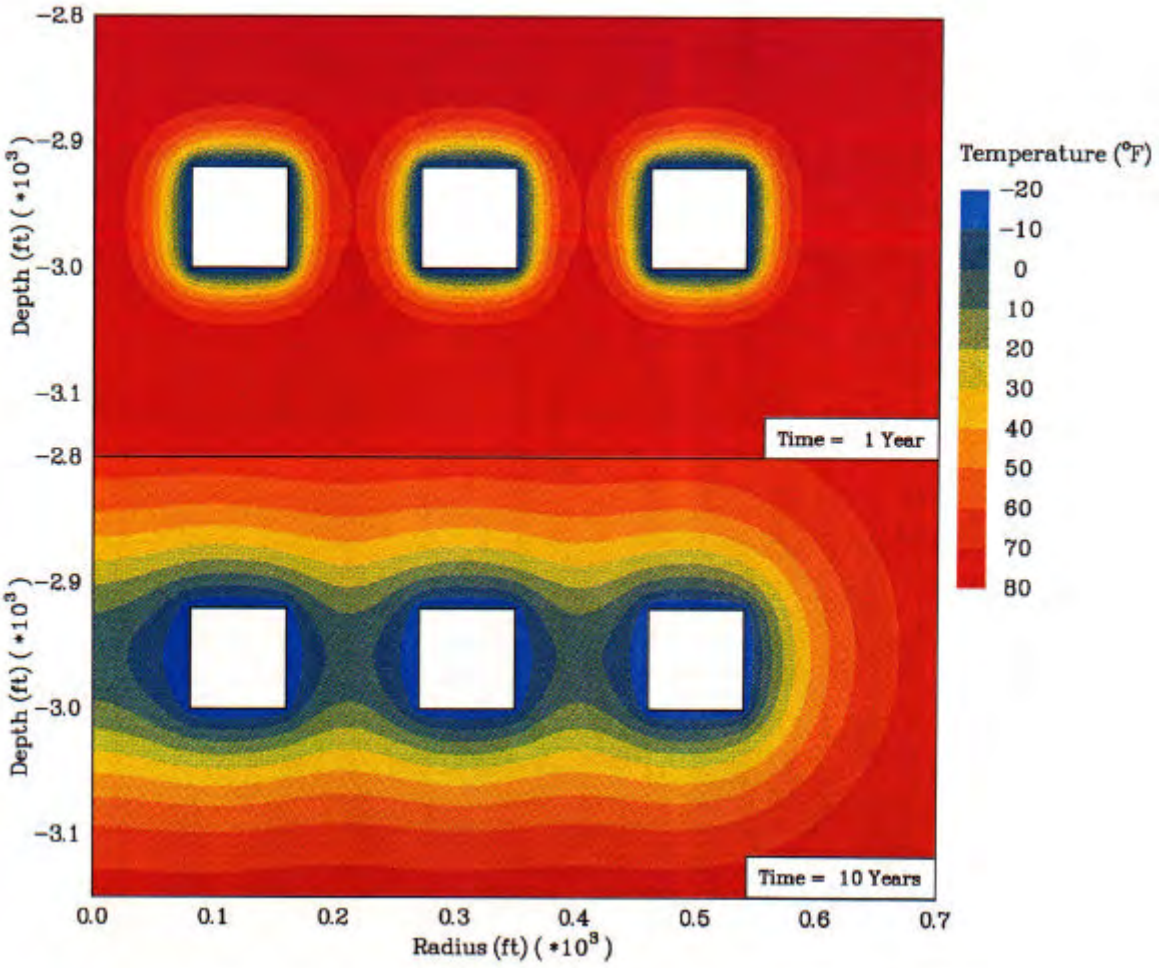

Figure 8-22. Temperature Contours Around Mine at 1 and 10 Years.

8.5.3 EFFECT OF GAS WITHDRAWAL

During gas withdrawal, thermal energy stored in the gas is converted to mechanical energy by depressurization and the associated decrease in density of the gas. The heat that is consumed during withdrawal results in cooling the gas and surrounding granite. The total thermal energy consumed during gas withdrawal based on ideal gas behavior is described by:

$$\bullet q_{ex} = R\,T\,V_c\left(\frac{\partial\, r}{\partial\, t} + \vec{v} \bullet \Delta r\right) \qquad (2)$$

where:

R = gas constant (Btu/lbm- R)

T = temperature (R)

V_c = cavern volume (ft^3)

r = gas density (lbm/ ft^3)

$\vec{v}$ = gas velocity vector.

In this analyses, the gas velocities and the gas density gradients within the cavern are assumed to be small, and thus, the second term of Equation 1 is ignored. To account for the nonideal behavior of the gas, the gas constant was calculated as:

$$R = \frac{Z\ \overline{R}}{M_w} \qquad (3)$$

where:

Z = compressibility factor of the gas

$\overline{R}$ = universal gas constant (1.987 Btu/lb- mole- R) [1]

M_w = molecular weight of the gas.

The compressibility factor, Z, was calculated using an empirical relationship developed by Coker [1993]. The gas was assumed to be pure methane (M_w = 16.04). The resulting equation used to estimate the heat consumed during expansion is given by:

$$\dot{q}_{ex} = \frac{Z\,\bar{R}\,T\,\dot{m}}{M_w} \qquad (4)$$

The gas was initially assumed to be at a pressure of 1,250 psia and a temperature of –20 ^{o}F. The withdrawal rate of 250 million scf/day results in a mass flow rate of about 450,000 lbm/hr. Although the temperature drops during withdrawal using Equation 3, the compressibility factor increases (from about 0.72 to about 0.86), resulting in a nearly constant rate of heat consumed (16.7 million Btu/hr) by gas expansion during the 20-day withdrawal period.

Of the total heat consumed, a portion will be taken from the granite and a portion will be taken from the gas. This heat balance is described by:

$$\dot{q}_{ex} = \dot{q}_{gr} + r\,V_c\,C_p\frac{\Delta T}{\Delta t} \qquad (5)$$

where $\dot{q}_{gr}$ is the heat flow from granite and the second term is the heat flow from the gas. Finite element simulations were made to estimate $\dot{q}_{gr}$, which will reduce the overall cooling load. In the finite element simulations, the total heat consumption rate ($\dot{q}_{ex}$) was represented as a negative heat generation rate in cavern. The heat flow rate from the granite ($\dot{q}_{gr}$) was solved using Equation 5 above. The following assumptions were made in modeling the gas in **SPECTROM-41**:

- Convection in the gas, which could not be simulated, will result in very low thermal gradients within the gas. To account for this, an arbitrarily high value was used for the thermal conductivity of the gas.
- Although the density of the gas decreases during withdrawal, this could not be simulated, and an average density of 3.58 lbm/ft3 was used in the simulations.
- The specific heat (C_p) was assumed to be 0.538 Btu/lbm-R [Van Wylen and Sonntag, 1978].

Finite element simulations of gas withdrawal were performed at various times. In each simulation, the gas temperature was maintained at –20 ^{o}F until the start of the withdrawal period. At the start of the withdrawal period, a negative heat generation rate of 16.7 million Btu/hr was applied in the cavern for the 20-day withdrawal period. The beneficial heat loss from the granite ($\dot{q}_{gr}$) was calculated using Eq. 5 and the predicted temperature change in the gas from the finite element simulation. Table 8-7 shows the estimated cooling benefit from a 20-day gas withdrawal period at various withdrawal initiation times. At times less than 90 days, the heat consumed during withdrawal is not large enough to maintain the gas temperature at –20 ^{o}F. After 90 days, the heat consumed during gas withdrawal is more than enough to maintain the gas temperature, and in fact, lowers the temperature of the gas to below –20 ^{o}F.

Examination of the cooling load plot in Fig. 8-21 and the values from the Table 8-7 suggests that after about 3 years, the cooling provided by gas withdrawal (roughly 14.5 million Btu/hr) is about double the cooling load (about 6.5 million Btu/hr). Thus, if gas were continuously cycled (i.e. continuous 20-day withdrawal, 20-day injection cycles), the gas temperature could be maintained entirely with the cooling provided during the withdrawal periods.

Table 8-7. Cooling Provided During Gas Withdrawal

Time at Initiation of Withdrawal	Cooling Rate (Btu/hr x 10^6) During Withdrawal
30 Days	18.6
90 Days	16.7
180 Days	15.8
1 Year	15.2
5 Years	14.1
10 Years	13.8

8.5.4 SUMMARY

Because of the large difference between the temperature of the stored natural gas and that of the surrounding granite, a large amount of heat will be transferred from the granite to the stored gas. The cooling load after 1 year of storage operations is estimated to be about 10 million Btu/hr. After 10 years of storage operations, the estimated cooling load is reduced to about 3.7 million Btu/hr. The estimated cooling provided during gas withdrawal periods is estimated to be about 15.2 million Btu/hr after 1 year of storage operations and decreases to about 13.8 after 10 years of storage operations. Based on these estimates, and assuming the cavern is active, much of the cooling load will be provided by gas expansion during the withdrawal periods.

Section 9

HEALTH AND SAFETY

The design of the cavern and surface process equipment must reasonably allow for safety during construction and after the facility is commissioned. Of particular concern is underground construction due to an element of unpredictability with respect to geology. Since cavern construction takes place hundreds of feet below ground in confined areas, any mishaps, such as a collapse, can have grave consequences. Many procedures have been developed for minimizing the risks associated with underground construction.

Underground construction standards have been developed over many years, and if followed, allow for safe cavern construction as well as safe operations, once the cavern is constructed. There are construction and operating standards which have been adopted industry-wide and are required by government agencies such as OSHA and MSHA.

The design of the surface process equipment meets or exceeds standards developed by various industry groups. Of these industry groups, the American National Standards Institute (ANSI) and the American Society of Mechanical Engineers (ASME) dominate with respect to setting integrity standards for piping components, pressure vessels, heaters, pumps, compressors, and various types of materials and hardware. Reputable equipment manufacturers follow these and other applicable standards and their equipment is usually inspected and certified by third-party inspectors.

Although process equipment is designed, tested and certified, there is a possibility the equipment may be improperly installed and operated. Proper engineering and a systematic safety analysis (process hazard analysis, known as “PHA” or “HAZOP” will reduce safety risks to acceptable levels. A HAZOP is conducted once a process and instrumentation diagram (“P&ID”) is developed.

During the HAZOP, the P&ID is completely reviewed by engineers and plant operations personnel. What-if scenarios during facility operation are discussed and potential hazards are identified. The process may then be reconfigured to eliminate or reduce the chance of the hazard occurring.

In the case of constructing the surface facilities for a natural gas storage facility, the health and safety risks to construction workers are burns, falls, overexertion, heat exhaustion, radiation exposure, exposure to solvents, electrocution, falling debris and other hazards. Steel erection involves the use of welding machines and cutting torches. Improper or worn out tools and equipment can result in burns to the skin and eyes.

The improper use of or not using respirators when priming and painting steel surfaces can result in overexposure to poisonous solvents. Also, the erection of steel structures with cranes, in the presence of power lines, may pose an electrocution risk.

The erection of process piping also requires welding and torch cutting as does structural steel but also requires the use of x-ray equipment for certifying welding integrity. The x-ray equipment contains a

radioactive (gamma ray) source, which can result in serious injury to construction workers if the material is improperly handled. The exposure to radiation may also have a long-term effect on anyone who is exposed, especially construction workers.

Risks relating to operating the facility may impact operations personnel as well as the general public. Construction personnel may only be exposed to operations-related risks during facility testing and commissioning. The risks, although low, include gas leaks due to ruptured piping, well leaks, equipment malfunction, operator error and other external factors. The gas leaks may result in fires, which may damage adjoining property and subjecting emergency workers to health and safety risks.

Other risks include spills of hazardous chemicals such as used lubricating oil and the glycol used for removing water from the gas. These spills can pollute the ground water with toxic chemicals and potentially carcinogens. However, the inventory of glycol and lubricants is small when compared to a chemical processing plant or petroleum refinery; therefore, any spill would likely be classified as minor.

In summary, an underground natural gas storage facility is relatively safe when compared to other types of hydrocarbon processing facilities. Natural gas contains little, if any, hydrocarbons which are considered poisonous or carcinogenic. Since natural gas is less dense than air at atmospheric conditions, it will rise and disperse if it leaks from the cavern or surface piping/equipment. Industry experience with underground natural gas storage facilities has been quite favorable with respect to immediate and long term safety and health to both facility operators and the general public.

The following cavern safety systems/features are recommended during operations:

1. EMERGENCY SHUTDOWN (ESD) VALVES

   ESD valves must be installed in the piping, either at the top of the cavern wellheads or in the piping within approximately 50 feet of it. ESD valves must be Fail Safe Closed, e.g., valve equipped with air open/spring close pneumatic actuators. Valves should be equipped with valve position indicators to indicate and confirm valve position both locally and in the control room. If actuators are equipped with manual overrides, lock-outs must be provided or handwheels or closing mechanisms removed.

2. ESD VALVE OPERATION

   Product and brine ESD valves can be manually opened and closed independently, as required. However, any ESD condition closes both valves. Valves should remain closed until the system is checked and reset.

3. ESD CONDITIONS

   A. Loss of electrical signal to ESD valves and instrumentation.

B. Loss of ESD valve actuator supply pressure, e.g., pneumatic or hydraulic pressure.

C. Fire in the vicinity of the wells.

D. Manual emergency close from Facility ESD Stations or Control Room.

E. Signal from any one of ESD instruments.

4. ESD INSTRUMENTATION

A. Production System Instrumentation

1. Instrumentation to protect against overpressuring the cavern, e.g., high pressure switch on product line or product injection pump discharge.

2. Instrumentation to detect uncontrolled release of product from the cavern through product system. Minimum of two instruments are recommended to provide redundancy, preferably measuring different parameters. Examples of product system ESD instrumentation are:

- Low pressure
- Excess flow
- Differential pressure, e.g., wellhead vs. meter station pressure

3. Fire detection. Examples of fire detection instrumentation and methods are:

- Fusible fittings in ESD actuator supply tubing. Fire causes fittings to melt, releasing pressure from actuator and closing ESD valve.
- Infrared detectors
- Video surveillance by operator

4. ESD instrument set points should be established a safe margin above or below the maximum or minimum operating levels, respectively.

5. ESD instruments may require field adjustable time delays to prevent nuisance closures.

5. LEAK DETECTORS

Leak detectors, or gas detectors, designed to detect the presence of hydrocarbon vapor in the atmosphere should be located at all transfer areas, e.g., main transmission line to the storage piping, pumps. In general, it is recommended that a low level set point, % Lower Explosive Limit (LEL), initiate an alarm and a high level set point initiate an ESD.

6. MANUAL ESD

Manual ESD stations should be located in the control room, at strategic locations around the facility, and at each storage well. These ESD stations allow the operator to initiate an ESD, in the event of an emergency, either station-wide or at a particular storage well.

7. ESD MANUAL RESET

ESD stations at the storage wells should be equipped with a manual reset, which compels the operator to inspect the well before resetting the system to resume normal operations.

8. ALARMS

Visual alarms and audible alarms for ESD should be provided at the control room and at the storage well areas.

9. WELLHEAD PROTECTION

Barriers or other systems should be installed around wellheads to protect against mechanical damage.

10. MONITORING STORAGE OPERATIONS

All gas injection and withdrawal operations should be continuously monitored by a qualified operator.

11. EMERGENCY RESPONSE PLAN

The facility should have a current emergency response plan in place to give operators the proper direction to follow in the event of an emergency at the facility and to provide important information for emergency response personnel.

12. EMPLOYEE SAFETY TRAINING PLAN

The facility should have a current employee safety training plan to provide training for operators and other site personnel regarding safety designs and procedures.

13. TESTING AND MAINTENANCE PROGRAM

A testing and maintenance program should be established to insure all safety systems are tested regularly and maintained properly.

All pertinent safety standards promulgated by OSHA and MSHA (30 CFR 57) for shaft sinking and development of underground caverns must be followed during the construction of the facility. These standards apply to ground control; fire prevention and control; ventilation and control measures; welding/cutting/and compressed air; explosives; conveying as other transportation systems; drilling; loading,

hauling, and dumping; electricity; machinery and equipment; personal protection; materials storage and handling; lighting; personnel hoisting; and safety programs. Shaft sinking is a specialized work and only well-experienced underground construction companies should be allowed to bid on the cavern construction job. Every person working underground must be well trained in the underground operations. He/she must wear articles of personal protection at all times while underground. This should include hard-toe shoes, safety belt, self-rescuer, safety glasses, hard hat and lighting. Before entering any working place, it must be thoroughly inspected by a responsible person for ventilation, presence of any noxious or flammable gases, any loose rock or other hazardous conditions. Loose rock must be brought down by a scaling bar or a scaling machine.

Section 10

CONSTRUCTION COST ESTIMATES AND SCHEDULE

Cost estimates were prepared for mine shafts to four different depths: 1,500', 2,000', 2,500' and 3,000'. The depths determine the pressure to which the gas can be compressed under the hydraulic seal; greater the depth, greater the confining pressure. The following assumptions were made in preparing these estimates.

1) The shaft collars would extend 150 feet through overburden and weathered rock.

2) All excavations are assumed to be dry and only minor amounts of drill water will be pumped.

3) Each shaft will be lined with 12-inches of plain (non-reinforced) concrete.

4) Domestic and process water will be furnished by others. Sewer service is available for domestic waste water.

5) No allowance has been included for handling or controlling ground water or waste process water.

6) Electricity will be furnished by others.

7) Construction activities will be under the jurisdiction of MSHA rather than OSHA.

8) Waste rock will be hauled to an approved disposal site by a subcontractor. An allowance for haulage is included.

9) All cavern and miscellaneous excavations are supported with 8-foot rock bolts.

10) Performance and payment bonds premiums are not included.

11) On-site explosives storage is permitted.

12) Pollution insurance premiums above our standard $5 million are not included.

13) The direct, fully-burdened labor rate is $35.00 per hour.

14) Transit-mix concrete is available for the delivered-price of $100.00 per yard.

15) Hoisting equipment and head frames will be left in place to install mechanical equipment. The crushing and skip loading equipment will be abandoned in place at the cavern level.

16) There is no salvage value allowed for any equipment acquired for the project.

17) The project will be exempt from sales and use taxes.

18) All permits will have been obtained by others, prior to the start of construction. The contractor will be responsible for his licenses, and explosives used and storage permits.

19) Site preparation, grading and access roads will have been completed prior to contractor mobilization.

20) Design costs for excavations, shaft furnishings, foundations, head frames and the like are not included. No allowance for appropriately-sized hoisting and crushing equipment and head frames is included.

21) There are no costs included for operation of the facility after construction.

22) A mutually-acceptable construction contract will be negotiated.

Table 10-1, Table 10-2, and Table 10-3 provide cost estimates for storage caverns at 1,500, 2,000, and 2,500 ft depth. Table 10-4 provides additional information on man-hours, labor and material cost, EOE and indirect costs, and the assumptions made in arriving at these costs. Table 10-5 provides the cost estimate for a 3,000 ft deep facility.

Schedule

Project duration is driven by the ability to hoist waste rock. It has been assumed that the contractor could hoist at an average rate of 400 tons per hour, 16 hours per day. This rate is conservative, but takes into account that the material handling system requires regular maintenance. The rate also assumes that there will be unscheduled maintenance due to mechanical failure plus the fact there will be times when the material handling system is available, but there is no muck to hoist because of the problems elsewhere in the project.

Table 10-6 provides a schedule for a 2,500 ft deep facility, whereas Table 10-7 provides the schedule for 3,000 ft deep facility. Increasing the depth of the cavern makes it necessary to construct the raisebore in two 1,500 foot lifts. The shaft will be sunk to 1,500 feet, a drift driven to the Service Shaft location and the raise pulled to surface, then lined to the 1,500 ft level. When the Production Shaft has been completed to the 3,000 ft level, the raise will be completed from the 3,000 ft level to the station at 1,500 ft. Table 10-7 reflects this activity.

Table 10-1

Estimated Cost of a Storage Cavern - 1,500-Foot Depth

115.7 Million Cubic Feet Storage

1500 Foot Depth

One 8-20-Ft-Diameter Conventional Shaft

One Ten-Ft-Diameter Raise Bored Shaft

4 Million Cubic Feet Miscellaneous Excavation

Project Duration 80 Months

COST ITEM	QUANTITY	UNITS		UNIT COST	TOTAL
Mobilization	1	LS		7,215,000	7,215,000
Sink & Line Shaft	1,500	LF		6,713	10,069,500
Raise Bore & Line Shaft	1,500	LF		2,613	3,919,500
Material Handling Equipment	1	LS		4,123,000	4,123,000
Assemble Mining Equipment	1	LS		2,695,000	2,695,000
Excavate Top Heading	1,851,300	BCY		46.12	85,381,956
Excavate Bench	2,581,900	BCY		40.21	103,818,199
TOTAL					208,222,155
Contingency					29,101,800
TOTAL PROJECT COST					237,324,000

Table 10-2

Estimated Cost of a Storage Cavern - 2,000-Foot Depth

68.7 Million Cubic Feet Storage

2,000 Foot Depth

One 18-20-Ft-Diameter Conventional Shaft

One Ten-Ft-Diameter Raise Bored Shaft

4 Million Cubic Feet Miscellaneous Excavation

Project Duration 59 Months

COST ITEM	QUANTITY	UNITS		UNIT COST	TOTAL
Mobilization	1	LS		7,215,000	7,215,000
Sink & Line Shaft	2,000	LF		6,713	13,426,000
Raise Bore & Line Shaft	2,000	LF		2,613	5,226,000
Material Handling Equipment	1	LS		4,123,000	4,123,000
Assemble Mining Equipment	1	LS		2,695,000	2,695,000
Excavate Top Heading	1,159,500	BCY		46.12	53,476,140
Excavate Bench	1,385,000	BCY		40.21	55,690,850
TOTAL					141,851,990
Contingency					19,577,100
TOTAL PROJECT COST					161,429,100

Table 10-3

Estimated Cost of a Storage Cavern - 2,500-Foot Depth

47 Million Cubic Feet Storage

2500 Foot Depth

One 18-20-Ft-Diameter Conventional Shaft

One Ten-Ft-Diameter Raise Bored Shaft

4 Million Cubic Feet Miscellaneous Excavation

Project Duration 48 Months

COST ITEM	QUANTITY	UNITS		UNIT COST	TOTAL
Mobilization	1	LS		7,215,000	7,215,000
Sink & Line Shaft	2,500	LF		6,713	16,782,500
Raise Bore & Line Shaft	2,500	LF		2,613	6,532,500
Material Handling Equipment	1	LS		4,123,000	4,123,000
Assemble Mining Equipment	1	LS		2,695,000	2,695,000
Excavate Top Heading	791,400	BCY		46.12	36,502
Excavate Bench	1,137,185	BCY		40.21	45,725,000
TOTAL					119,419
Contingency					15,994,000
TOTAL PROJECT COST					135,413,000

Table 10-4

Cost Estimate Detail for 2,500-Foot Deep Cavern

Bid Item	Qty.	Unit	Mnhrs.	Labor	Materials	EOE	Total	Ind. Cost	Total	Unit Cost
Mobilization	1	LS	22,000	770,000	3,500,000	52,000	4,322,000	2,996,000	7,212,000	7,212,000
Sink & Line Shaft	2,500	LF	70,000	2,450,000	3,385,000	215,000	6,050,000	11,027,000	16,672,000	6,669
Raisebore Shaft	2,500	LF	25,000	875,000	1,804,000	24,000	2,703,000	3,937,000	6,495,000	2,598
Material Handling Eqpt.	1	LS	22,600	791,000	234,000	127,000	1,152,000	3,079,000	4,120,000	4,120,000
Assemble Mining Eqpt.	1	LS	16,000	560,000	32,000		592,000	2,179,000	2,693,000	2,693,000
Exc. Top Heading	791,400	BCY	151,600	5,306,000	4,462,000	3,728,000	13,496,000	23,884,000	36,502,000	46.12
Exc. Bench	1,137,185	BCY	201,600	7,056,000	3,052,000	2,133,000	12,241,000	31,761,000	45,725,000	40.21
Total Field Cost			938,496	38,172,000	28,925,000	8,784000	106,636,000		119,419,000	
Contingency = 15% of the total field cost									15,994,000	
TOTAL PROJECT COST									135,413,000	

NOTES:

1) Direct burdened labor rate is $35.00 per hour.
2) Salaried labor at rates used in ARSCo Bid.
3) Drill steel & bits @ 0.85 per DLF.
4) Loader and truck EOE @ $40.00 per hour.
5) Dynamite @ $1.50 per pound.
6) ANFO @ $1.00 per pound.
7) Drill EOE @ 0.35 per DLF.
8) Raise bore cutters @ $50.00 per LF.
9) Transit-mix concrete @ $100.00 per yard.
10) Electrical service not included.
11) Work scheduled on seven days per week.
12) No bond premium included.
13) Indirect cost include plant & equip., G&A costs, muck haul and margin.
14) Cavern excavation rate based upon hoisting 400 tons per hour.

Table 10-5

Cost Estimate Detail for 3,000-Foot Deep Cavern

Bid Item	Qty.	Unit	Mnhrs.	Labor	Materials	EOE	Total	Ind. Cost	Total	Unit Cost
Mobilization	1	LS	22,000	770,000	3,500,000	52,000	4,322,000	3,498,000	7,212,000	7,212,000
Sink & Line Shaft	3,000	LF	81,000	2,835,000	3,906,000	258,000	6,999,000	14,439,000	21,813,000	7,271
Raisebore Shaft	3,000	LF	28,200	987,000	2,186,000	64,000	3,237,000	5,026,000	8,393,000	2,798
Material Handling Eqpt.	1	LS	22,600	791,000	234,000	127,000	1,152,000	3,594,000	4,120,000	4,120,000
Assemble Mining Eqpt.	1	LS	16,000	560,000	32,000		592,000	2,544,000	2,693,000	2,693,000
Exc. Top Heading	584,765	BCY	105,300	3,685,500	3,298,000	2,754,000	9,737,500	18,772,000	28,996,500	49.59
Exc. Bench	822,642	BCY	148,000	5,180,000	2,205,000	1,547,000	8,932,000	26,385,000	36,002,000	43.76
Total Field Cost (include P&E and G&A costs)			832,000	34,341,500	25,237,000	7,205,000	97,538,500		109,229,500	
Contingency = 15% of the total field cost									14,629,000	
TOTAL PROJECT COST									123,858,500	

NOTES:

1) Direct burdened labor rate is $35.00 per hour.
2) Salaried labor at rates used in ARSCo Bid.
3) Drill steel & bits @ 0.85 per DLF.
4) Loader and truck EOE @ $40.00 per hour.
5) Dynamite @ $1.50 per pound.
6) ANFO @ $1.00 per pound.
7) Drill EOE @ 0.35 per DLF.
8) Raise bore cutters @ $50.00 per LF.
9) Transit-mix concrete @ $100.00 per yard.
10) Electrical service not included.
11) Work scheduled on seven days per week.
12) No bond premium included.
13) Indirect cost include plant & equip., G&A costs, muck haul & margin.
14) Cavern excavation rate based upon hoisting 400 tons per hour.

Activity ID	Activity Description	Orig Dur
100	Mobilize Mine Equipment	120
110	Construct Shaft To Cavern Level	217
120	Construct Access Tunnels To Raise Bore Shaft	22
130	Level and Assemble Mining Equipment	22
140	Mine Service and Access Gallery	43
150	Raise Bore and Finish Service Shaft	120
160	Sink and Line To Bottom	22
170	Install Crusher and Skips	65
180	Excavate Cavern Drifts	476
210	Design Surface Equipment	100
220	Construct Compressor Station and Refrigeration	120
190	Demobilize Excavation Equipment	22
200	PROJECT COMPLETION	0*

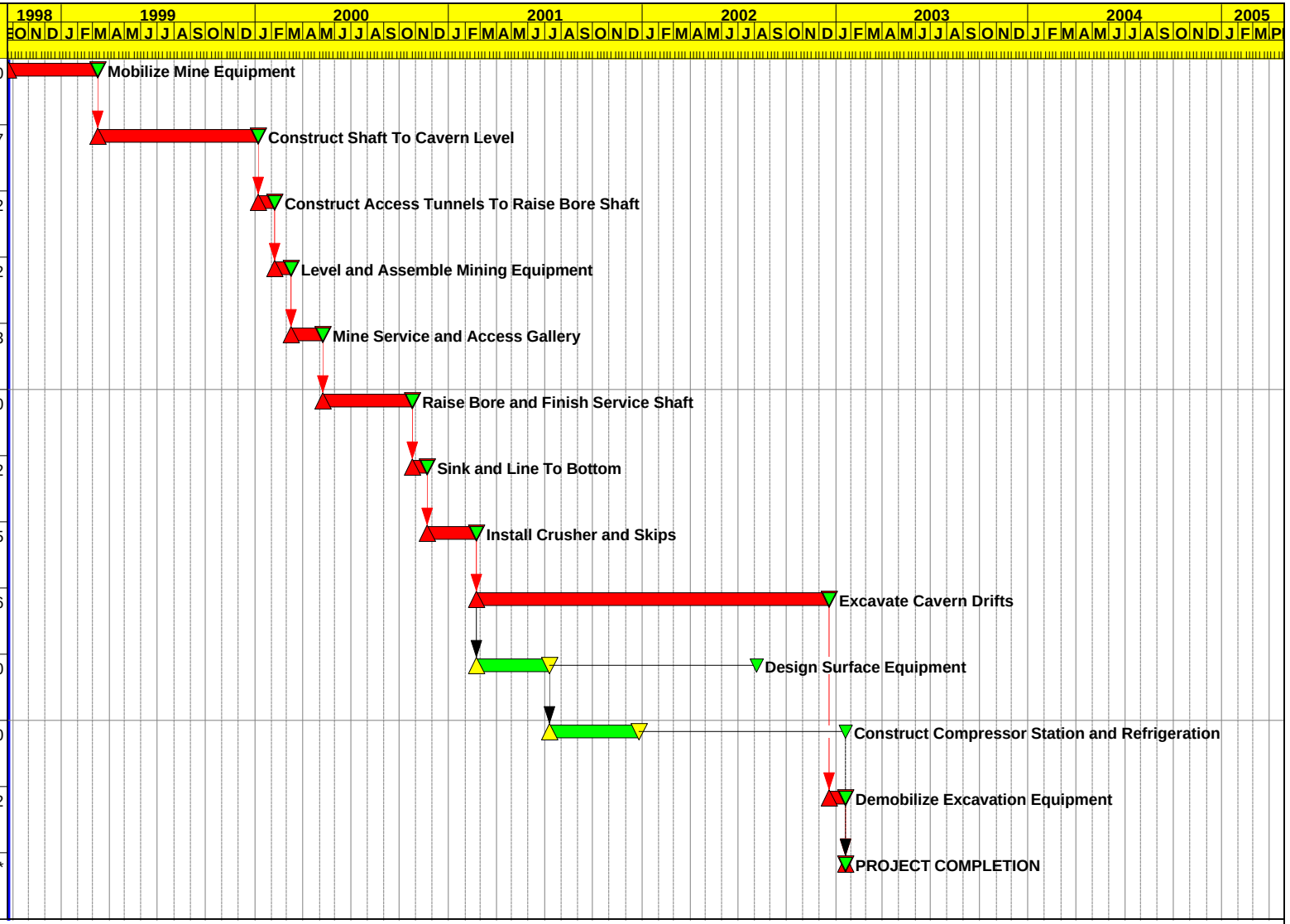

Project Start	23SEP98
Project Finish	20JAN03
Data Date	23SEP98
Run Date	30SEP98

Early Bar
Float Bar
Progress Bar
Critical Activity

MIN2

Sheet 1A of 1B

Department of Energy

ADVANCED UNDERGROUND GAS STORAGE

2,500-ft Cavern Level

Date	Revision	Checked	Approved

Activity ID	Activity Description	Orig Dur	Rem Dur
100	Mobilize Mine Equipment	130	130
110	Construct Shaft To 1500-ft Level	153	153
120	Construct Access Tunnels To Raise Bore Shaft	22	22
130	Lower and Assemble Mining Equipment	22	22
230	Construct Access To Raise Bore Shaft	22	22
140	Mine Service and Access Gallery	108	108
240	Raise and Line to 1,500-ft Level	65	65
150	Raise Bore and Finish Service Shaft	93	93
160	Sink and Line To 3,000-ft	152	152
170	Install Crusher and Skips	65	65
180	Excavate Cavern Driftes	260	260
210	Design Surface Equipment	100	100
220	Construct Compressor Station and Refrigeration	120	120
190	Demobilize Excavation Equipment	22	22
200	PROJECT COMPLETION	0*	0*

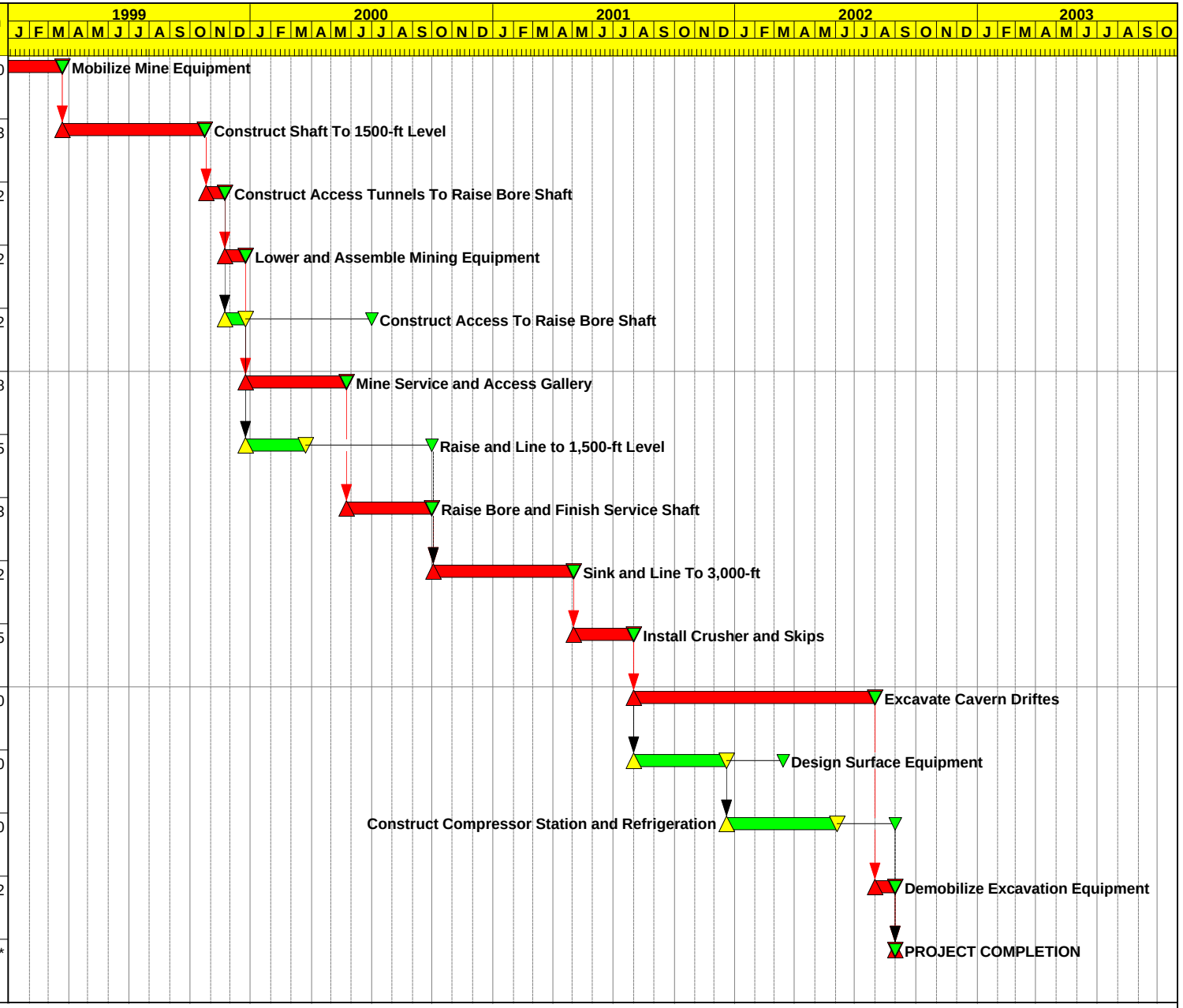

Project Start	23SEP98
Project Finish	29AUG02
Data Date	23SEP98
Run Date	30SEP98

Early Bar
Float Bar
Progress Bar
Critical Activity

MINE

Department of Energy

ADVANCED UNDERGROUND GAS STORAGE

3,000-ft Deep Cavern

Date	Revision	Checked	Approved

Process Equipment Cost

The refrigeration, compressor and process equipment would consist of two 13,000 HP centrifugal gas compressors, three 1300 ton gas turbine refrigeration systems, one 200 HP recirculation gas compressor, one skid-mounted 250 MMSCFD molecular sieve dehydration system, one 66.2 MMBtu/hr line heater, one 1300 psig 250 MMscfd motor skid, four vertical scrubbers (1440 psig MAWP), and miscellaneous gate valves, check valves, pipes, etc. The cost of this equipment is estimated to be $31,971,400.

Table 10-8 provides a complete cost summary of the refrigerated-mined cavern project at the 3,000-foot depth. The costs include the mining costs, process equipment, structures and foundations, and the infrastructure needed at the site.

More details on the costs are presented in the Appendix of this report regarding how the total costs were arrived at.

OPERATING COSTS OF REFRIGERATED MINED CAVERN

The cost of operating the refrigerated cavern storage system is based upon the assumptions listed in the design parameters shownin Section 3. It is further assumed that the maximum number of injection and withdrawal cycles will be completed. With 5 billion standard cubic feet of working gas storage, a maximum flow rate of 250 MMscfd, 9 fill/empty cycles can be completed annually. The costs are based on the cavern being fully injected to 1250 psig, and then emptied to the minimum pressure of 250 psig, at the maximum fill and withdrawal rate of 250 MMscfd.

During injection, the delivery pressure from the transmission lines, is assumed to be 350 psig. Therefore, the injection compressors are utilized for 19 of the 20 days for injection. Deliveries to the transmission lines form the storage cavern are assumed to be at 650 psig. This will require the compressors to be used during the 20 day withdrawal cycles for about 6 days. The refrigeration system will be used during injection to chill the gas to storage temperatures, and will operate continuously at a maintenance level to keep the cavern at -20°F. During the withdrawal cycle, the product gas will be heated to 60°F by the forced draft heater. Additional fuel gas will be required by the dehydration system for regeneration of the molecular sieve beds. There will also be “base load” energy requirements for the facility to operate compressor lubrication systems, air coolers, instrumentation, plant lighting, space heating and cooling, and other miscellaneous plant utilities.

Table 10-8

Cost Summary of Refrigerated Mined Cavern Project

(3,000-Foot Deep Mine)

Working Gas Storage of 5.0 Billion Standard Cubic Feet

Maximum Injection Rate of 250 MMSCFD

Maximum Withdrawal Rate of 250 MMSCFD

Injection Cycle - 20 Days

Withdrawal Cycle - 20 days

Conventional Mining and Shaft Sinking (6,292,335 barrels of space)			112,346,209
Refrigeration System, Compressors, and Process			31,971,424
Electrical and Instrumentation Equipment			2,243,333
Compressor Building (210-feet X 50-feet) and Control			903,540
Compressor Building Foundation and Slab			68,064
Concrete Supports for Compressor Station Piping			19,698
Control Building Foundation			153,256
Mechanical Separators Foundations			5,570
Mole Seives Foundations			4,999
Pressure Reducing Station Foundations			4,999
Gas Storage Facility Final Design (Eight Months)			1,078,342
Gas Storage Facility Construction & Commissioning			4,815,600
SUBTOTAL			**153,615,034**
Contingency on All Costs @ 10%			15,361,503
SUBTOTAL			**168,976,538**
Contractors' Profit at 10% on Surface Facilities			3,537,488
TOTAL PROJECT COST			**172,514,026**
COST OF FACILITY PER MSCF OF BASE GAS STORAGE			**$34.50**
MINING COST PER BARREL OF MINED SPACE			**$20.00**

The following table (Table 10-9) shows the energy costs for the operation of the facility after the startup phase is completed. The table covers a range of gas prices for fuel since the price will vary subject to market conditions and the terms of the supply contract.

Table 10-9

Energy Costs

	Gas Cost - $/MMBtu:	$ 2.00	$ 2.25	$ 2.50	$ 2.75	$ 3.00
20 Day Injection Period	Fuel Required MMBtu's	Energy Cost	Energy Cost	Energy Cost	Energy Cost	Energy Cost
Compression	$9,864.4	$19,729	$22,195	$24,661	$27,127	$29,593
Refrigeration	$16,491.6	$32,983	$37,106	$41,229	$45,352	$49,475
Dehydration	$1,920.0	$3,840	$4,320	$4,800	$5,280	$5,760
Plant Baseline	$1,221.6	$2,443	$2,749	$3,054	$3,359	$3,665
Total Injection	$29,497.6	$58,995	$66,370	$73,774	$81,118	$88,493
20 Day Withdrawal Period						
Compression	$2,748.6	$5,497	$6,184	$6,872	$7,559	$8,246
Refrigeration	$245.0	$490	$551	$613	$674	$735
Gas Heating	$14,928.0	$29,856	$33,588	$37,320	$41,052	$44,784
Plant Baseline	$1,221.6	$2,443	$2,749	$3,054	$3,359	$3,665
Total Withdrawal	$19,143.2	$38,286	$43,072	$47,858	$52,644	$57,430
Total Cost per In/Out Cycle		$97,282	$109,442	$121,602	$133,762	$145,922
Total Energy Cost per Year		$875,534	$984,976	$1,094,418	$1,203,860	$1,313,302

Labor Costs

The labor costs are shown in Table 10-10. These costs are based on the plant being manned 24 hours per day by two operators included is a salaried supervisor and one “day” clerical position. The labor rates and hours assumed are shown in the table. Two relief operators are included for filling operator positions during absenteeism for vacations, sicknesses and other reasons. An overtime rate was assumed for 3% of the work year for the hourly personnel.

Table 10-10

Labor Costs

Position	No.	Hrs/Day	Days/Wk	$/Hr	OH @ 35%	Cost/Yr
Supervisor	1	8	5	35.00	47.25	98,280
Shift Operators	8	12	4	20.00	27.00	488,808
Relief Operators	2	12	4	18.00	24.30	109,982
Clerical	1	8	5	13.00	17.55	37,315
TOTAL						734,385

- 2190 hrs per year on 12 hr shift schedule
- Overtime figured at 3% of annual schedule at base rate.

Maintenance and Operating Supplies

Maintenance and operating supplies for the facility are assumed to be provided on an as-needed basis with maintenance provided by independent contractors. Some routine maintenance items will be performed by the operators and relief operators. The maintenance cost provided is a rough estimate. Experienced operators can provide a more detailed analysis.

Cost Summary

Table 10-11 is a summary of some of the major annual operating costs for the Refrigerated Mined Cavern Gas Storage Facility. Other costs associated with running a facility were not included in the scope of this estimate. Other costs that should be considered include taxes, insurance, depreciation, working capital, management and other overhead charges.

Table 10-11

Annual Operating Costs

Cost Parameter	Monthly Cost	Annual Cost
Labor		
1 Supervisor	$8,190	$98,280
8 Shift Operators	$40,734	$488,808
2 Relief Operators	$9,165	$109,982
1 Clerical	$3,110	$37,315
Labor Subtotal	$61,199	$734,385
Maintenance Mat'l & Labor	$10,000	$120,000
Operating Supplies	$3,000	$36,000
Energy (as fuel gas)*	$91,202	$1,094,418
TOTAL	$165,400	$1,984,803

* Assumes $2.50 per MMBtu.

Section 11
OPTIMIZATION

The conceptual mine design was reviewed in relation to its components, such as drift and pillar size and shaft diameter. Potential savings in the construction cost were considered by modifying dimensions of these variable components.

As far as the underground cavern design is concerned, the two variables that can be changed to affect the cost of the facility are the shafts and underground excavation. Consideration was given to varying the sizes of these components to determine their impact on the total facility cost. Other cost factors, such as "mobilization," "material-handling equipment," and "assembling equipment" are essentially constant, although minor variations could occur. The method of shaft construction also influences the cost. However, as explained in tasks 4 and 6, "constructibility," drilling an 18-ft main shaft for the type of rock in the region under consideration, and at the required depth (in excess of 2,500 ft) was ruled out.

The shaft construction cost can be reduced either by having smaller diameter shafts, or by reducing the depth of the shafts. The size of the shaft is dictated by the amount of rock that has to be excavated for the designed storage capacity. The storage of 5 billion cubic feet of working gas at -20°F at a depth of 2,500 ft, for instance, requires excavation in excess of 50 million cubic feet, or 1.9 million cubic yards of rock. To excavate this large volume underground requires the use of multi-boom jumbo drills, a number of 40-50 ton trucks, front-end loaders with 5-7 yard buckets, jaw crushers, scalers, etc. The shaft size must be at least 18-ft diameter to lower this equipment into the mine. Even with this size shaft, some of the equipment must be cut into smaller pieces, lowered into the cavern, and reassembled by welding, etc., at the shaft bottom. The hoisting rate must be at least 400 tons per hour to remove the excavated material from the cavern to the surface in a reasonable time. The skips for this duty, once again, require an 18-ft shaft. At the rate of 400 tons per hour hoisting for 16 hours per day, cavern construction alone will take about 22 months, with a total construction time of approximately four years. During all this time capital investment will be tied up with no return. If the shaft size were to be made smaller, say 14 ft, the shaft construction cost may be 10% less, but the facility construction time will exceed 5 years, resulting in a corresponding increase in the facility construction cost. Thus, for a reasonable schedule and for economic reasons, the optimum size of one of the shafts should be at least 18 ft. Since the second shaft is needed for ventilation purposes and for providing a second means of ingress/egress to and from the cavern, its size can be reduced for economy. The optimum size of this shaft is approximately 10 ft to fit a mancage within. The most economic method of construction of this size shaft is raise boring. Raise boring cost is about 40% of the conventionally sunk shaft.

Shaft construction cost is approximately 15% of the total cavern development cost. In normal mining operations in massive deposits, shaft depth can be varied to realize economic benefits. However, in this gas storage project, shaft depth is intimately linked to the size of the cavern. The size of the cavern depends

on the compressed volume of the gas to be stored (gas storage pressure). The gas is stored at about 95% of the hydrostatic head (0.433 psi/ft) in order to maintain the hydraulic seal. Hydraulic head is related to the depth of the cavern. Thus, at shallow depths, larger excavated cavern volume is needed than storage at greater depth for the same volume of gas due to lower compression possible.

Previously design relative to 2,500 ft deep shafts and caverns, their constructibility, and costs were described in Section 10. For this optimization study, shaft depths of 1,500 ft, 2,000 ft, and 3,000 ft were also considered and compared to the base case of 2,500 ft.

1,500 ft deep shafts (one 18 ft conventionally sunk shaft and the other 10 ft raise-bored) cost about $9.0 million less than the 2,500 ft deep shafts. Hoisting distance is reduced and as such, hoisting cost per ton is reduced. However, at this depth the gas can be compressed only to less than 645 psi and the storage volume for 5 billion standard cubic feet of working gas, at -20°F increases to 4.4 million cubic yards compared to 1.9 million cubic yards needed at 2,500 ft depth. The cost of cavern excavation increases to $177.2 million. The total cavern development cost at 1,500 ft depth will be approximately $23 million compared to the cavern development cost of $135.4 million at 2,500 ft base case. Additionally, gas taken out of the reservoir will probably need additional compression before delivery to the commercial gas pipelines. The construction schedule would be stretched out to 80 months compared to the base case of 48 months.

The 2,000 ft deep storage cavern will require a storage volume of 2.5 million cubic yards to store 5 billion cft of working gas at approximately 850 psi at a temperature of -20°F. The shaft sinking cost will be reduced by $5 million, but the total cavern development cost will be $157.3 million, about $22 million more than the base case. The construction schedule will be 59 months, or 11 months longer than the base case. The conclusion from the discussion of these two cases is that cavern construction at depths less than 2,500 ft will be more expensive.

A cavern depth of 3,000 ft was then considered. Although it is not a common practice to routinely sink shafts to this depth, some shafts in excess of 3,000 ft depth have been constructed in the U.S. for metal mining. Thus, it will not be beyond the state of the art to sink shafts to this depth for gas storage with a conventional drill and blast method. For raise boring, however, it is the general consensus that 2,500 ft is the limit for a single lift raisebore. However, raise boring can be constructed in multi-lifts for deeper shafts. Thus, a 3,000 ft raisebore can be constructed in two 1,500 ft lifts. For this purpose the main production shaft (18-ft diameter shaft) will initially be sunk to 1,500 ft level. A drift will then be driven to the Service shaft (10 ft diameter shaft) location. The raise will be pulled to the surface, then lined to the 1,500 ft level. When the Production shaft has been completed to the 3000 ft level, the raise will be completed from the 3,000 ft level to the station in the Service shaft at 1,500 ft. Hoisting from 3,000 ft level will take longer. The increased hoisting distance and the weight of the hoisting rope will require greater horsepower hoists, which are available in the market. The dimensions of the rooms and pillars underground will remain the same. The pillar safety factor will be reduced to about 1.9, which is more than adequate. The required storage cavern

volume will be 36 million cft or 1.34 million cyd. Storage cavern at 3,000 ft depth will cost about $124 million, a saving of $11 million over the 2,500 ft deep facility. Cost includes plant and equipment, G&A, removal of excavated material offsite, and margin. The construction schedule will be 47 months, essentially the same as for the 2,500 ft. Further details of the cost and schedule are provided in Table 11-1.

The results of the above discussion for the storage of 5 billion SCF of gas at -20°F are summarized in the following table.

Table 11-1

Comparative Cost and Schedule of Cavern Location

	Shaft Depth 1500 ft	**Shaft Depth 2000 ft**	**Shaft Depth 2500 ft**	**Shaft Depth 3000 ft**
Mobilization	7,215,000	7,215,000	7,212,000	7,212,000
Sink & line 18 ft shaft	10,003,500	13,330,000	16,672,000	21,813,000
Rise-bore shaft	3,897,000	5,196,000	6,495,000	8,393,000
Material handling eqpt.	4,123,000	4,123,000	4,120,000	4,120,000
Assembling mining eqpt.	2,695,000	2,695,000	2,693,000	2,693,000
Cavern Exc.	181,714,000	104,197,640	82,227,000	64,998,500
Total mining cost	209,647,500	136,764,640	119,419,000	109,229,500
Contingency	31,447,125	20,514,696	15,994,000	14,629,000
Total cavern development cost	241,094,625	157,279,336	135,413,000	123,858,500
SCHEDULE	80 months	59 months	48 months	47 months

In addition to compression, the underground cavern volume also depends on the chilled temperature that the gas is subjected to. The cavern volumes and the costs given above are for the storage of gas chilled to a temperature of -20°F. These volumes will be further reduced if the temperatures are reduced.

Calculations were made to determine the required cavern volume if the same quantity of gas could be chilled to -30°F and -40°F and stored at 2500 and 3000 ft depths. (Description: How to accomplish it, its impacts, required changes to the process equipment, etc.). The cavern volumes required for the storage of 5 billion cubic feet of working gas at various depths and temperatures are provided in the following table.

Table 11-2

Required Cavern Volumes at Various Depths and Temperatures

Depth	Cavern Volume at -20°F, million cubic yards	Cavern Volume at-30°F, million cubic yards	Cavern Volume at -40°F, million cubic yards
2500	1.87	1.75	1.56
3000	1.34	1.21	1.08

The process equipment cost was estimated only for chilling the gas to a temperature of -20 ^{o}F for the following reasons.

1. A colder temperature would require possible process design changes regarding refrigerant type and equipment design.
2. The metallurgy for the piping and equipment throughout the chilled system would have to be re-evaluated for service below -20 ^{o}F, including piping in the mined cavern.

Section 12

EVALUATION OF SUCCESS CRITERIA

In preparing an evaluation of the commercial feasibility of any gas storage project, one must evaluate how the project compares with the alternatives available to the market place, both physically, in terms of operational capability, and economically with regard to the relative costs of other services. In order to accomplish this, one must first become familiar with the types of storage available, and the services (and their related costs) that are provided in the market today.

Types of Storage

Natural gas storage has been in widespread use across North America for the better pat of this century, with the development of the Zoar project near Buffalo, New York in 1916 representing the first commercial gas storage development in the United States. At present there are more than 400 operating gas storage projects in the United States.

In general there are three major categories of gas storage projects, each of which tends to lend itself to specific service applications:

- Underground Reservoir Storage
- Underground Storage in Salt Deposits
- Liquefied Natural Gas (LNG) Storage

Underground reservoir storage is by far the most common type of gas storage in the U.S., representing over 98% of installed capacity. The majority of the reservoir storage fields in operation are depleted gas and/or oil fields that have rock properties suitable for the safe containment and redelivery of injected gas volumes. Examples of important rock properties for gas storage development would include a finite containment structure or trap, an impermeable cap rock above the storage zone(s), and a reasonably permeable and porous zone in which the gas will be stored. These fields also tend to make attractive candidates due to the existence in most cases of reservoir data acquired during the production life of the field. The analysis of production and well data from depleted fields is one of the key steps in evaluating the suitability of a candidate field, and in ultimately designing the gas storage facility.

A second type of reservoir storage is in underground aquifers. These tend to be fairly deep (greater than 2,000 ft), salt water aquifers that have little commercial value, but which have rock properties suitable for gas storage. Aquifer storage projects are much less common than depleted gas and/or oil field projects, representing approximately 12% of the total installed capacity in the U.S.[1]

---

[1] Id., p. 46.

Reservoir storage sites tend to provide seasonal gas storage services characterized by fairly long injection and withdrawal cycles and relatively large total stored volumes of gas. Typically, a reservoir storage facility would hold from several to tens of billion cubic feet (BCF) of working or customer gas that would be cycled into and out of the reservoir once annually. The typical operating pattern for these facilities is a 150 to 200 day injection cycle, during the spring and summer months, followed by a winter withdrawal cycle of 120 to 150 days. There are, however, examples of reservoir storage facilities with shorter cycle times (e.g., 30 to 90-day withdrawal cycles) and these generally offer customers more flexibility in terms of daily injection and withdrawal rates.

Natural gas is also commonly stored in underground salt deposits, either in large caverns leached into a salt dome or in bedded salt formations. These facilities tend to be much smaller than reservoir storage sites in terms of overall volume but almost universally provide a higher rate of re-delivery and re-injection per unit volume. The injection and withdrawal characteristics of salt storage are precisely what make this type of storage valuable in the marketplace.

For instance, a typical salt cavern development might have on the order of 3.0 BCF of working gas capacity, with the ability to withdraw the entire volume in 10 days with replacement in 20 days, allowing the customer to cycle the space or inventory approximately once a month on average. This type of operating profile makes salt storage valuable for curing imbalances on the pipeline system and for handling commodity prices in the daily and monthly spot market. Depending on the location of the facility, the storage might also have peaking service benefits (if in the market area) or reliability service benefits (if in either the market area or the production area). In general, a 10-day firm withdrawal service seems to fit the needs of the high deliverability market fairly well -- i.e., for gas balancing, short term price optimization and reliability. In fact, most supply interruption and/or needle peaking events in the gas industry tend to last form a few to several days at most. Our experience has been that salt service customers tend to require a withdrawal to injection ratio of about 1:2 or 1:3.[2]

Imagine, for instance, an electric generation facility in the market area with a variable day-to-day output profile characterized by a high degree of swing in daily gas load. A properly designed salt storage service would enable the generation facility to purchase steady base load gas supplies and swing the imbalance volumes into and out of storage. Moreover, a properly structured storage contract might enable the same customer to purchase interruptible or recall-able supplies and/or transportation, utilizing the storage as a backstopping mechanism to hedge against periods of short-term price increase or interruptions. Overall, the use of salt storage as a supply management tool in this manner can result in the customer achieving

[2]The Hattiesburg Gas Storage project located in Mississippi and developed and operated by the current principals of Brant Energy L.L.C. ("Brant"), provided in its initial phases a 10 day withdrawal and 20 day re-injection service. In marketing a subsequent expansion of that facility we learned that customers believed a 30 day re-injection cycles would be preferable.

significant savings and improvements in supply reliability.[3]

Liquefied natural gas, or LNG, is an expensive form of natural gas storage that is used to meet two market requirements -- needle peaking and/or supply reliability (backstopping). Typical LNG projects are designed to provide between 3 and 10 days of supply per year which is called upon the coldest days of the year and/or when other system supplies are curtailed unexpectedly. Due to the high cost associated with liquefaction, these projects are expensive when compared to other types of storage, but service a niche that often cannot be met with other forms of storage due to location and/or geologic factors. Overall, LNG represents a very minor share of the U.S. market, equating to less than 1 percent of U.S. consumption and 9 percent of underground storage withdrawals in 1993.[4]

On a volume basis, most of the LNG consumed in the U.S. is imported from Algeria into Eastern U.S. markets. The LNG is brought in large shiploads and stored in cryogenic tanks at very low temperatures. The product is then distributed to local satellite storage (tank) systems by truck and vaporized into the pipeline system as it is demanded. However, most U.S. LNG projects, particularly those operating in the Midwest and west involve liquefying and storing relatively small amounts of pipeline supplies during a long, 200+ day liquefaction season that normally occurs during the summer. These projects typically store from about one to five BCF of LNG and offer around 10 days of vaporization service per year.

Comparison to Alternatives

The operating parameters, along with the capital and operating costs, were reviewed for the Refrigerated Mined Cavern (RMC) natural gas storage facility proposed for the Ellicott City area of Maryland. Capital cost numbers were modified to include the following:

Land and storage rights	$0.500 million
Mineral rights	0.500
Permitting and regulatory	0.750
Marketing	0.200
Legal	0.200
Overhead and project management	0.750
Total capital cost additions	**$2.900 million**

[3]A major Hattiesburg combination gas/electric utility would cycle its capacity in precisely this way. Typically, the customer would buy base loaded gas for the month and inject into storage on weekends when the electric plant was off-line, Withdrawals would commence on Monday morning and the ensuing weekday activity would closely track the operating profile of the electric plants served.

[4]EIA, March 1995, p.52.

Including contingencies, this raised the total capital investment to approximately $178 million.

Table 12-1 compares the unit capital costs for several depleted field, aquifer, salt cavern, and LNG projects with the proposed RMC project.

Table 12-1

Representative Unit Capital Costs for New Gas

Storage and LNG Projects

Type of Project	Location	Project Name	Working Gas Capacity (BCF)	Total Cost ($MM)	Unit Cost ($/MCF)	Notes
Depleted Field	California	Putah Sink	15.000	40.000	2.67	(1)
Depleted Field	Colorado	Douglas Creek	10.000	30.000	3.00	(1)
Depleted Field	Utah	Clay Basin Expansion	15.200	49.600	3.26	(1)
Depleted Field	Oklahoma	Manchester	15.000	30.000	2.00	(1)
				Average>>	2.73	
Aquifer	Indiana	Carbon-Calcutta	3.900	12.275	3.15	(1)
Aquifer	Illinois	Hillsborough Expansion	4.500	36.600	8.13	(1)
				Average>>	5.64	
Salt Cavern	Alabama	S. Alabama-McIntosh	2.700	30.000	11.11	(1)
Salt Cavern	Mississippi	Hattiesburg phase 1 & 1A	3.500	47.000	13.43	(2)
Salt Cavern	Louisiana	Napoleonville Phase 1	4.600	45.000	9.78	(1)
				Average>>	11.44	
LNG	North Carolina	Pine Needle	4.000	107.000	26.75	(2)
LNG	Maine	Granite Slate	2.000	44.222	22.11	(2)
				Average>>	24.43	
Refrigerated mined Cavern		Mid-Atlantic	5.000	178.000	35.60	

Notes: (1) EIA/The Value of Underground Storage in Today's Natural Gas Industry.

(2) Brant Energy Data.

Although the capital costs of the RMC project are substantially higher than the others shown, it should be noted that, while LNG peaking service and depleted reservoir storage, which are both typically one-cycle per year, are available to the market area to be served by the RMC project, the multi-cycle service afforded by aquifer and salt cavern storage are not. Operationally, the RMC facility is similar to salt cavern storage - characterized by high deliverability with multiple cycles possible within a given year. Specifically, the RMC facility proposed by PB-KBB has 5.0 BCF of working gas capacity with firm withdrawal capacity of 250 MMCFD and firm injection capacity of 250 MMCFD. This configuration permits the entire facility to be drawn down over a 20 day period and similarly refilled over a 20 day period. The maximum number of physical cycles that can be achieved annually is 9.1.

While the facility physically most resembles salt cavern storage, its proposed location within a "market area" means that it should also be compared to other peaking sources when analyzing the RMC from a service feasibility perspective. The most common market area natural gas peaking service along the Eastern Seaboard is LNG. However, LNG facilities tend to differ from salt caverns and the proposed RMC facility in that they tend to be designed with a single cycle capability, i.e., a very long liquefaction cycle (on the order of 200 days) with a single vaporization cycle (analogous to withdrawal) of approximately 10 days.

In general, the flexibility afforded by market area, multi-cycle, high deliverability gas storage is preferable to the single cycle of an LNG service for several reasons:

Multiple demand peaks can be met within a given year.

While typically the true "peaks" are observed during winter heating season, the increased use of gas fired generation can also create short-term summer demand (air conditioning load) situations where withdrawals form a high deliverability storage facility become economic.

Baseload gas supply planning can be better optimized.

A multi-cycle, high deliverability service means better and more frequent "backstopping" or insurance capability for interruptible supply contracts.

Daily and monthly balancing.

Multi-cycle, high deliverability storage is commonly used for daily and monthly balancing (matching nominations and receipts to deliveries on the pipeline or distribution system), thereby avoiding costly imbalance penalties.

Gas supply cost management

Besides merely allowing for greater interruptibility in flowing supplies, a multi-cycle high deliverability storage service does afford short-term opportunities to capture value associated with gas price volatility that may

be observed within the daily market.

On a unit cost basis, the RMC project is considerably higher than salt cavern storage and somewhat higher than LNG. However, it is Brant's understanding that within the market area of study, there is not adequate salt for the development of an underground natural gas storage project. Hence the higher costs of the RMC project may be justified if multi-cycle, high deliverability services are demanded.

Cost of Service Rate Development

A simplified cost-of-service model was used to take basic capital and operating cost data for the RMC project to develop monthly demand charges and per cycle costs. A fifteen year planning horizon was used to develop annual and levelized rates. Major assumptions include:

- A typical utility or regulated capital structure of 50% debt and 50% equity
- 30 year book depreciation period for the purposes of calculating rates
- Completed capital cost of $178 million
- Income tax rate of 38.25%
- Storage capacity of 5.0 BCF, with injection and withdrawal capacity of 250 MMCF/day

Using these assumptions, preliminary rates have been calculated as follows:

- 15 Year Levelized Demand Charge $9.919 /Mcfd/Mo
- Single Cycle Unit Cost $5.980 /Mcf
- Unit Cost at Maximum Cycles (9.1) $0.681 /Mcf

An advantage that the RMC project has over the most likely competitive service, LNG, is its ability to cycle many times throughout the year. The high capital costs of both services result in fixed demand charges which are substantially higher than reservoir, aquifer or even salt cavern services. Because of the RMC project's ability to cycle gas through the facility several times a year, versus once for LNG service, it is possible to spread these costs over a much larger volume of gas thereby reducing the unit cost of service substantially.

Comparison to Alternatives

Table 12-2 summarizes rates for a series of selected older and newer (proposed) LNG and salt storage projects. The 15-year levelized rate for the RMC project is depicted for comparative purposes.

It would appear that the proposed RMC project falls within the range of rates for projects delivering similar high deliverability services. The 15 year levelized rate developed appears to fall somewhat above market area salt storage and well within the range of existing and proposed LNG facilities. LNG, due to its proximity

to the marketplace, as well as its high deliverability capability, would most likely be the primary competitor for the RMC project. The preliminary RMC rates, which are in the range of LNG service, would appear to enable the project to be competitive in the market.

As stated above, the RMC project, with a 20-day injection an 20-day withdrawal period, tends to resemble high deliverability salt cavern storage service more than LNG service. However, given the possible location of the project within a market area, the project may be able to capture a market value that would represent a hybrid between LNG and salt cavern storage. This would need to be market tested in some detail before drawing definitive conclusions.

Table 12-2

Comparison of Rates for Refrigerated Mined Cavern

Natural Gas Storage vs. Selected LNG and

Underground Salt Cavern Storage Facilities

Existing LNG Facilities	Days of Withdrawal/ Vaporization	Monthly Demand $/dth/day	Monthly Volume Charge $/dth	Variable Withdrawal Charge $/dth	Variable Injection Charge $/dth	Fuel %	Fuel @ $2.50 $/dth	Single Cycle Unit Cost $/dth	Cost/Cycle @ Max. # of Cycles $/dth
Transco LNG @ Carlstadt, NJ	10	0.9058	0.1745	0.2025	0.2025	7.44%	0.186	3.772	n/a
East Tennessee Natural Gas	10	7.1856	0.0000	0.0000	0.0000	15.69%	0.392	9.015	n/a
Eastern Shore Natural Gas	10	8.6701	0.1745	0.2025	0.2025	7.44%	0.186	13.089	n/a
South Caroline Pipeline Co.	10	5.620	0.0000	0.2500	0.0500	0.00%	0.000	7.044	n/a
Proposed LNG Facilities									
Cove Point LNG (MD)	10	4.940	0.0000	0.0005	0.0005	20.50%	0.513	6.442	n/a
Granite State LNG (ME)	10	6.0600	0.0260	0.0000	0.0546	2.20%	0.055	7.682	n/a
Pine Needle LNG (NC)	10	4.850	0.0000	0.0000	0.0000	0.00%	0.000	5.820	n/a
Existing Salt Cavern Storage									
Hattiesburg Gas Storage (MS)	10	2.6300	0.0000	0.0100	0.0100	1.50%	0.038	3.214	0.321
Proposed Salt Cavern Storage									
Avoca Gas Storage (NY)	10	3.7500	0.0000	0.0100	0.0100	2.00%	0.050	4.570	0.563
Tioga Gas Storage (PA)	10	4.200	0.0000	0.0100	0.0100	1.20%	0.030	5.090	0.602
Refrigerated Mined Cavern	**20**	**9.9190**	**0.0000**	**0.0000**	**0.0000**	**1.16%**	**0.029**	**5.980**	**0.681**

APPENDICES

CONCEPTUAL DRAWINGS

DEPARTMENT OF ENERGY

REFRIGERATED MINED CAVERN STORAGE

GENERAL

861-GG-003	LIST OF DRAWINGS
861-GG-001	ELECTRICAL SYMBOL DIAGRAM
861-GG-002	PIPING & INSTRUMENT SYMBOL DIAGRAM
861-GP-001	GENERAL FACILITY LAYOUT
861-GP-002	GENERAL EQUIPMENT LAYOUT

ARCHITECTURAL

861-AC-001	OFFICE/CONTROL BUILDING ELEVATION
861-AC-002	OFFICE/CONTROL BUILDING PLAN

ELECTRICAL

861-ED-001	ONE LINE DIAGRAM - CONCEPTUAL DESIGN (1 OF 3)
861-ED-002	ONE LINE DIAGRAM - CONCEPTUAL DESIGN (2 OF 3)
861-ED-003	ONE LINE DIAGRAM - CONCEPTUAL DESIGN (3 OF 3)

GEOLOGICAL

861-LB-004	TWO SHAFT MINE SHOWING DEVELOPMENT AND BENCHING HEADINGS
861-LB-005	SHAFT OUTFITTING DURING CONSTRUCTION
861-LB-006	MINE GENERAL ARRANGEMENT
861-LB-007	GENERAL CAVERN LAYOUT-2500' DEPTH
861-LB-008	GENERAL CAVERN LAYOUT-3000' DEPTH
861-LB-009	GAS DISTRIBUTION SYSTEM IN MINE-3000' DEPTH
861-LB-010	SECTION 'A-A' 3000' DEPTH

MECHANICAL

861-MD-001	PROCESS FLOW DIAGRAM
861-MD-002	METER SKID
861-MD-003	GAS COMPRESSION SYSTEM
861-MD-004	MOLECULAR SIEVE DEHYDRATOR
861-MD-005	REGENERATION GAS SYSTEM
861-MD-006	REFRIGERATION SYSTEM
861-MD-007	STORAGE CAVERN AND HEATER
861-MP-001	COMPRESSOR BUILDING PLAN & ELEVATION

GENERAL NOTES

REFERENCE DRAWINGS

PROJ. No.	REV. No.	LOC.	REVISIONS	REVISED BY DATE	CHECKED BY DATE	APPROVED BY DATE

THIS DRAWING PREPARED FOR:

DEPARTMENT OF ENERGY

PB-KBB Inc.
Engineering Construction Operations
11757 KATY FREEWAY #600
HOUSTON, TEXAS 77079

TITLE:
REFRIGERATED MINED CAVERN STORAGE
LIST OF DRAWINGS

DESIGN BY: RCR	DATE: 06/98	DRAWN BY: TST	DATE: 06/98	SCALE: NONE	
CHECKED BY: RS	DATE: 06/98	APPROVED BY:	DATE:	PROJECT No.: 861	
FILE NAME: 861GG003.DGN		DRAWING No.: 861-GG-003		REVISION: 0	

H:/PROJECTS/861/DGN/861GG003.DGN

ELECTRICAL SYMBOLS

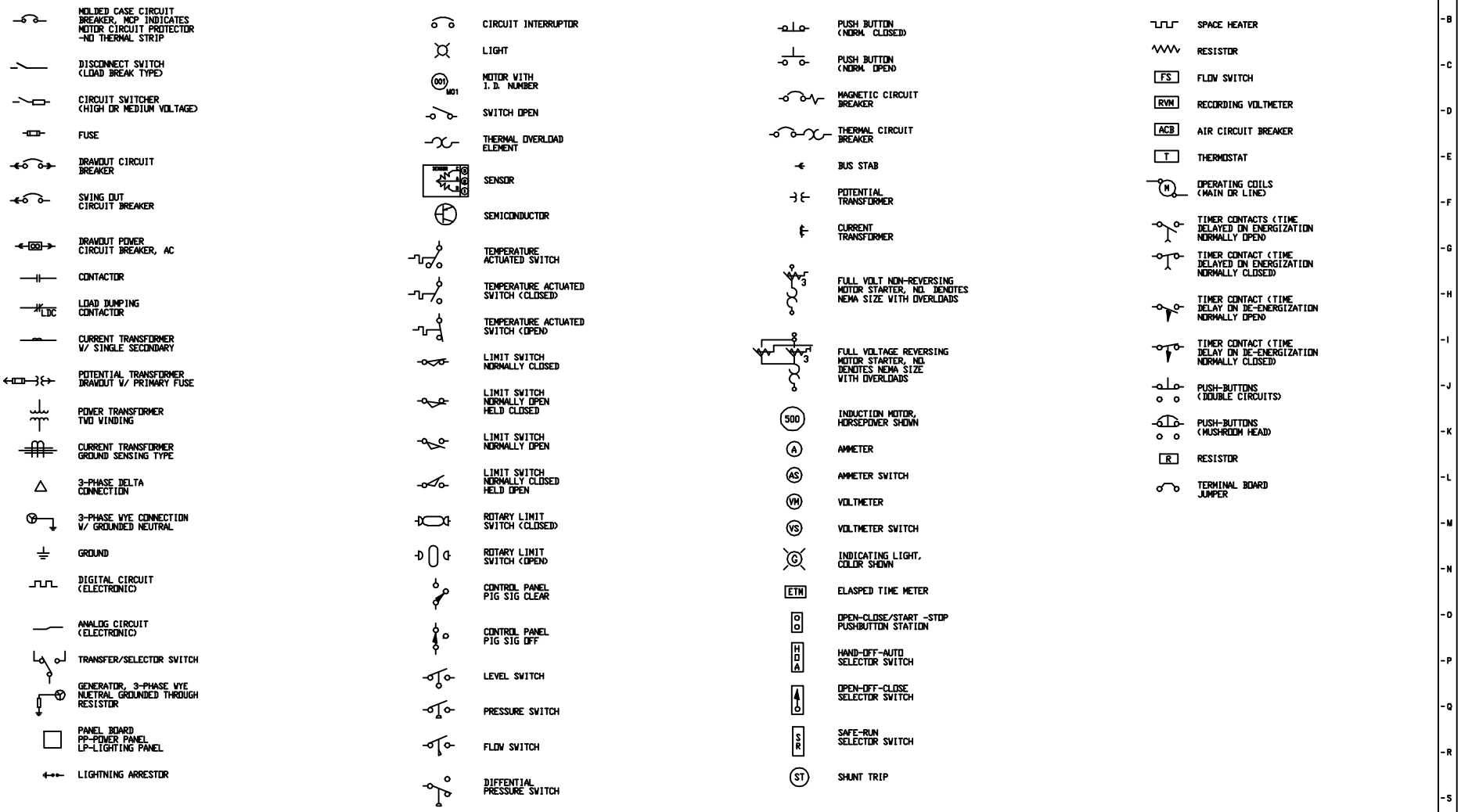

GENERAL NOTES	REFERENCE DRAWINGS

PROJ. No.	REV. No.	LOC.	REVISIONS	REVISED BY DATE	CHECKED BY DATE	APPROVED BY DATE

THIS DRAWING PREPARED FOR

DEPARTMENT OF ENERGY

PB-KBB Inc.
Engineering Construction Operations
11757 KATY FREEWAY #600
HOUSTON, TEXAS 77079

TITLE:

REFRIGERATED MINED CAVERN STORAGE
ELECTRICAL SYMBOL DIAGRAM

DESIGNED BY	DATE	DRAWN BY	DATE	SCALE
RCR	06/98	TST	06/98	NONE
CHECKED BY	DATE	APPROVED BY	DATE	PROJECT NO.
RS	06/98			861
FILE NAME		DRAWING No.		REVISION
861GG001.DGN		861-GG-001		A

H:/PROJECTS/861/DGN/861GG001.DGN

PIPING & INSTRUMENTATION SYMBOLS

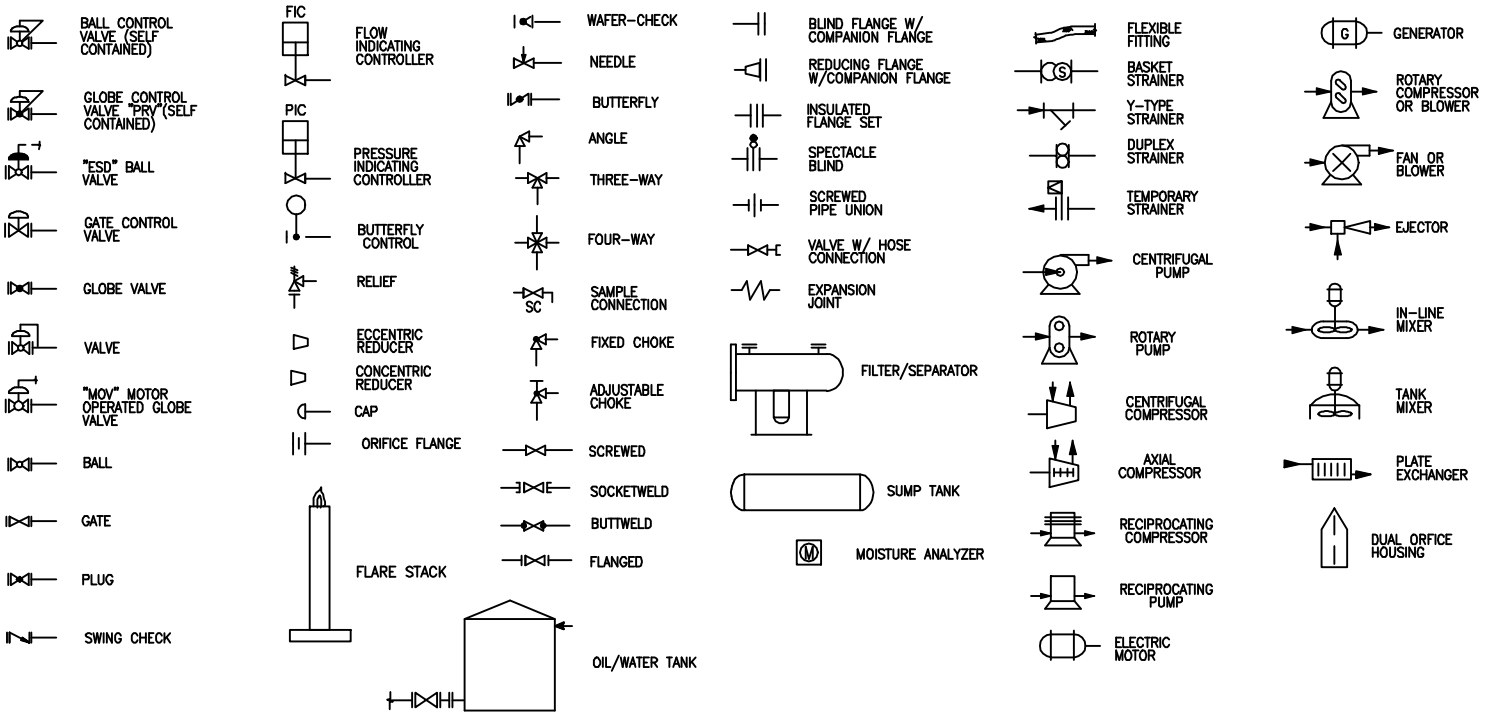

GENERAL NOTES	REFERENCE DRAWINGS

PROJ. No	REV. No.	LOC.	REVISIONS	REVISED BY DATE	CHECKED BY DATE	APPROVED BY DATE

THIS DRAWING PREPARED FOR:

DEPARTMENT OF ENERGY

PB-KBB Inc.
Engineering Construction Operations
11757 KATY FREEWAY #600
HOUSTON, TEXAS 77079

TITLE:
REFRIGERATED MINED CAVERN STORAGE
PIPING & INSTRUMENTATION
SYMBOL DIAGRAM

DRAWN BY RCR	DATE 06/98	DESIGNED BY TST	DATE 06/98	SCALE NONE	
CHECKED BY RS	DATE 06/98	APPROVED BY	DATE	PROJECT No 861	
FILE NAME 861GG002.DGN		DRAWING No 861-GG-002		REVISION 0	

H:/PROJECTS/861/DGN/861GG002.DGN

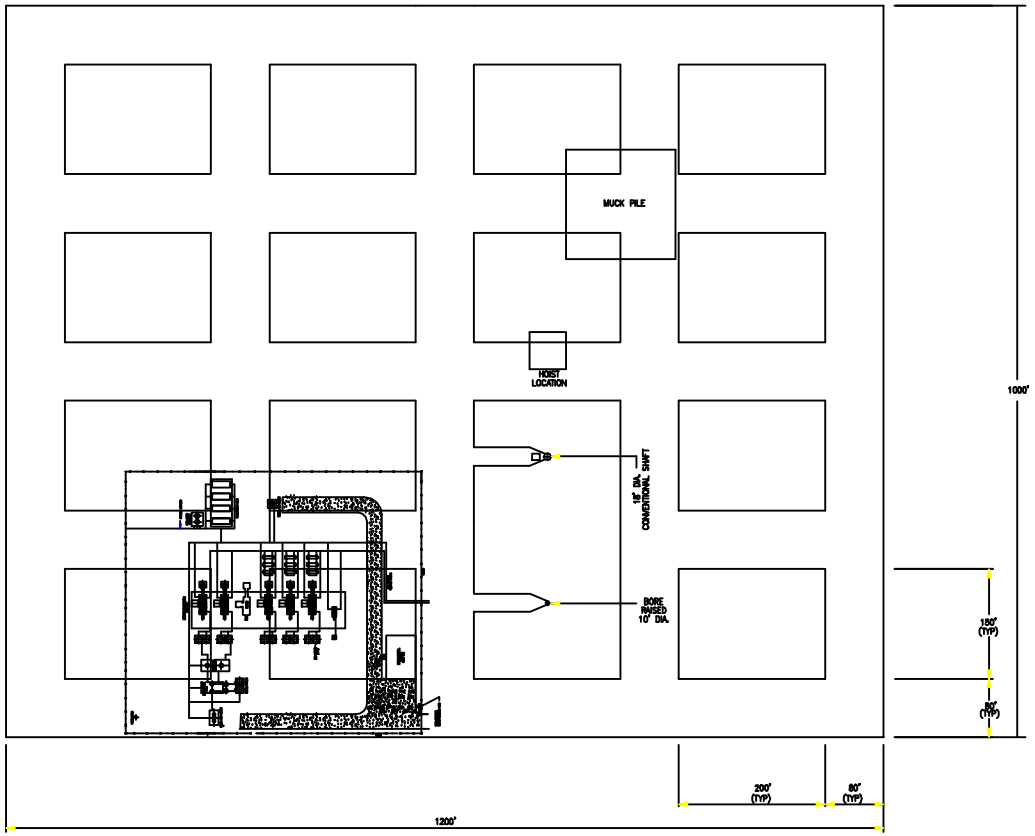

GENERAL NOTES	REFERENCE DRAWINGS

PROJ. No.	REV. No.	LOC.	REVISIONS	REVISED BY DATE	CHECKED BY DATE	APPROVED BY DATE
No.						

THIS DRAWING PREPARED FOR:

DEPARTMENT OF ENERGY

PB-KBB Inc.
Engineering Construction Operations
11757 KATY FREEWAY #600
HOUSTON, TEXAS 77079

TITLE:

REFRIGERATED MINED CAVERN STORAGE GENERAL FACILITY LAYOUT

DRAWN BY	MM	DATE	05/98	SCALE	1"=80'
CHECKED BY	MM	DATE	05/98	PROJECT NO.	861
FILE NAME	861GP001.DGN	DRAWING No.	861-GP-001	REVISION	0

H:/PROJECTS/861/DGN/861GP001.DGN

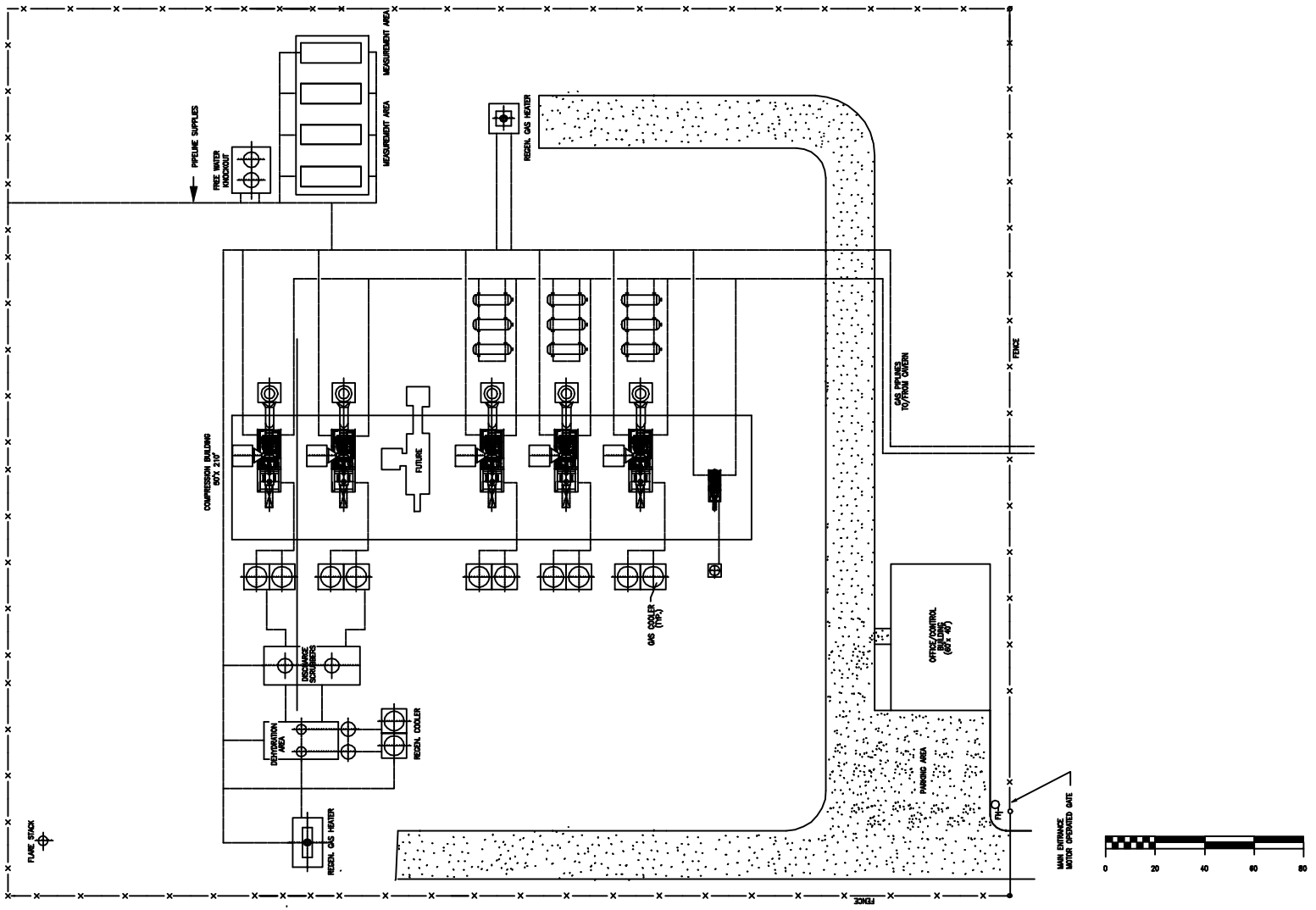

GENERAL NOTES	REFERENCE DRAWINGS

PROJ. No.	REV. No.	LOC.	REVISIONS	REVISED BY DATE	CHECKED BY DATE	APPROVED BY DATE

This Drawing Prepared For:

DEPARTMENT OF ENERGY

PB-KBB Inc.
Engineering Construction Operations
11757 KATY FREEWAY #600
HOUSTON, TEXAS 77079

TITLE:

REFRIGERATED MINED CAVERN STORAGE GENERAL EQUIPMENT LAYOUT

DESIGN BY	DATE	DRAWN BY	DATE	SCALE
MM	05/98	TST	05/98	1"=20'
CHECKED BY	DATE	APPROVED BY	DATE	PROJECT No.
MM	05/98			861
FILE NAME		DRAWING No.		REVISION
861GP002.DGN		861-GP-002		0

H:/PROJECTS/861/DGN/861GP002.DGN

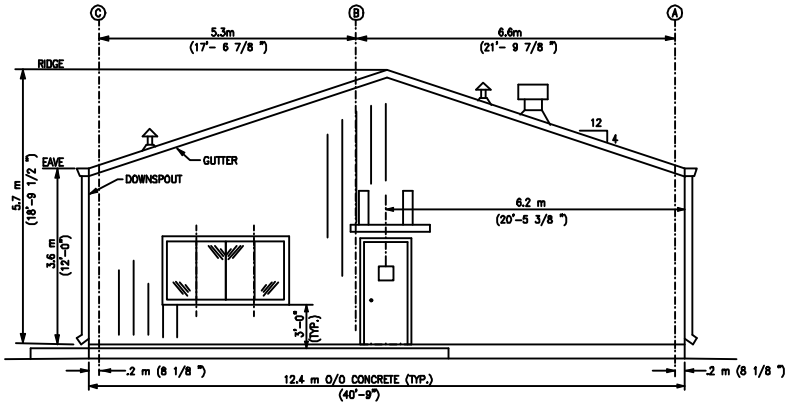

EAST ELEVATION
SCALE: 1/4 "= 1'-0"

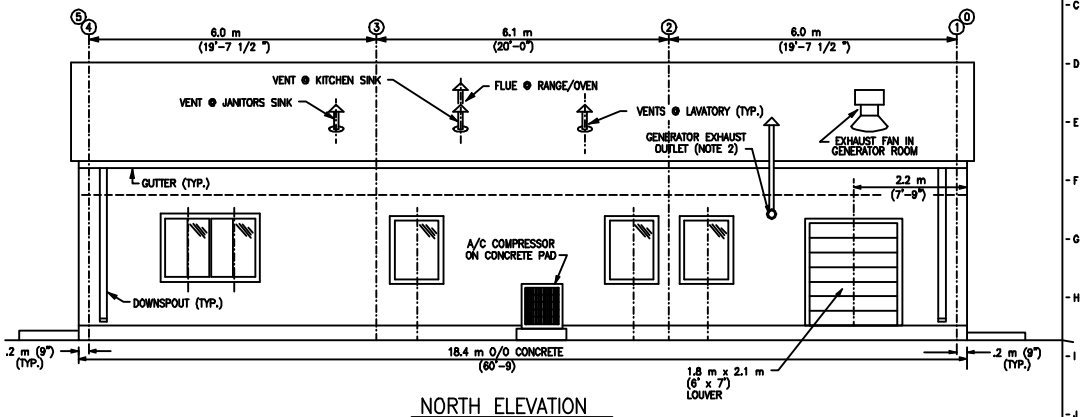

NORTH ELEVATION
SCALE: 1/4 "= 1'-0"

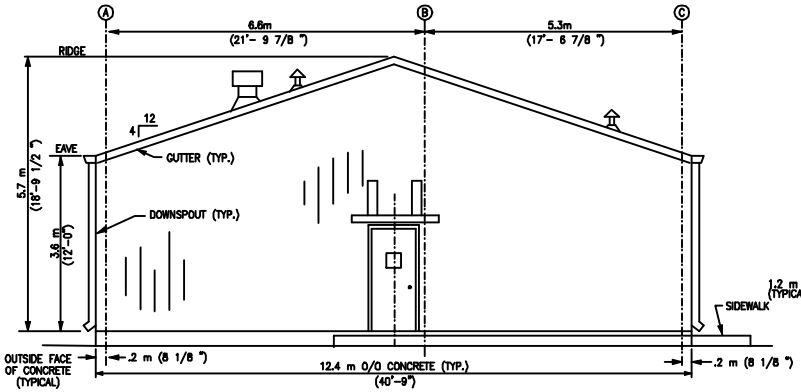

WEST ELEVATION
SCALE: 1/4 "= 1'-0"

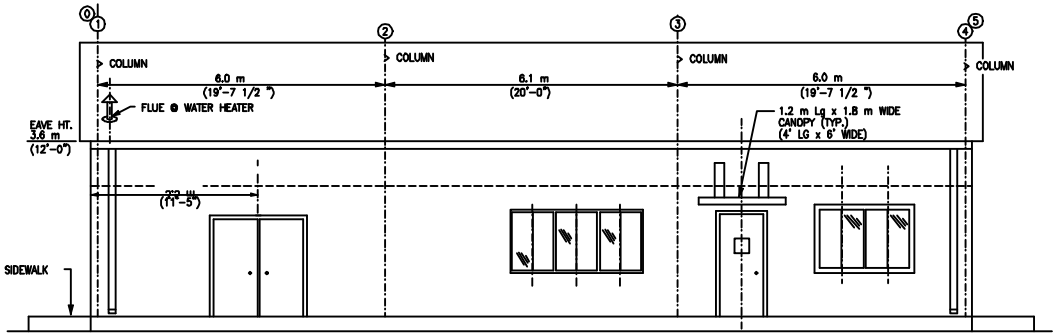

SOUTH ELEVATION
SCALE: 1/4 "= 1'-0"

GENERAL NOTES

1. GENERATOR EXHAUST SIZE, ROUTING, SUPPORT SYSTEM AND BUILDING PENETRATION ARE TO BE DETERMINED BASED UPON SELECTED GENERATOR SUPPLIER SHOP DRAWINGS OF ENGINE EXHAUST SYSTEM.

REFERENCE DRAWINGS

PROJ. No.	REV. No.	LOC.	REVISIONS	REVISED BY DATE	CHECKED BY DATE	APPROVED BY DATE
	1	–	CHANGED DWG TITLE	RCE-11/17/97	LS-11/17/97	RS-11/17/97

THIS DRAWING PREPARED FOR:
DEPARTMENT OF ENERGY

PB-KBB Inc.
Engineering Construction Operations
11757 KATY FREEWAY #600
HOUSTON, TEXAS 77079

TITLE:
REFRIGERATED MINED CAVERN STORAGE
OFFICE/CONTROL BLDG. ELEVATIONS

DESIGN BY	DATE	DRAWN BY	DATE	SCALE
RS	9/98	RCR	04/98	1/4 "=1'-0"
CHECKED BY	DATE	APPROVED BY	DATE	PROJECT No.
NH	04/98			861
FILE NAME		DRAWING No.		CONTRACT NUMBER
861AC001.DGN		861-AC-001		

H:/PROJECTS/861/DGN/861AC001.DGN

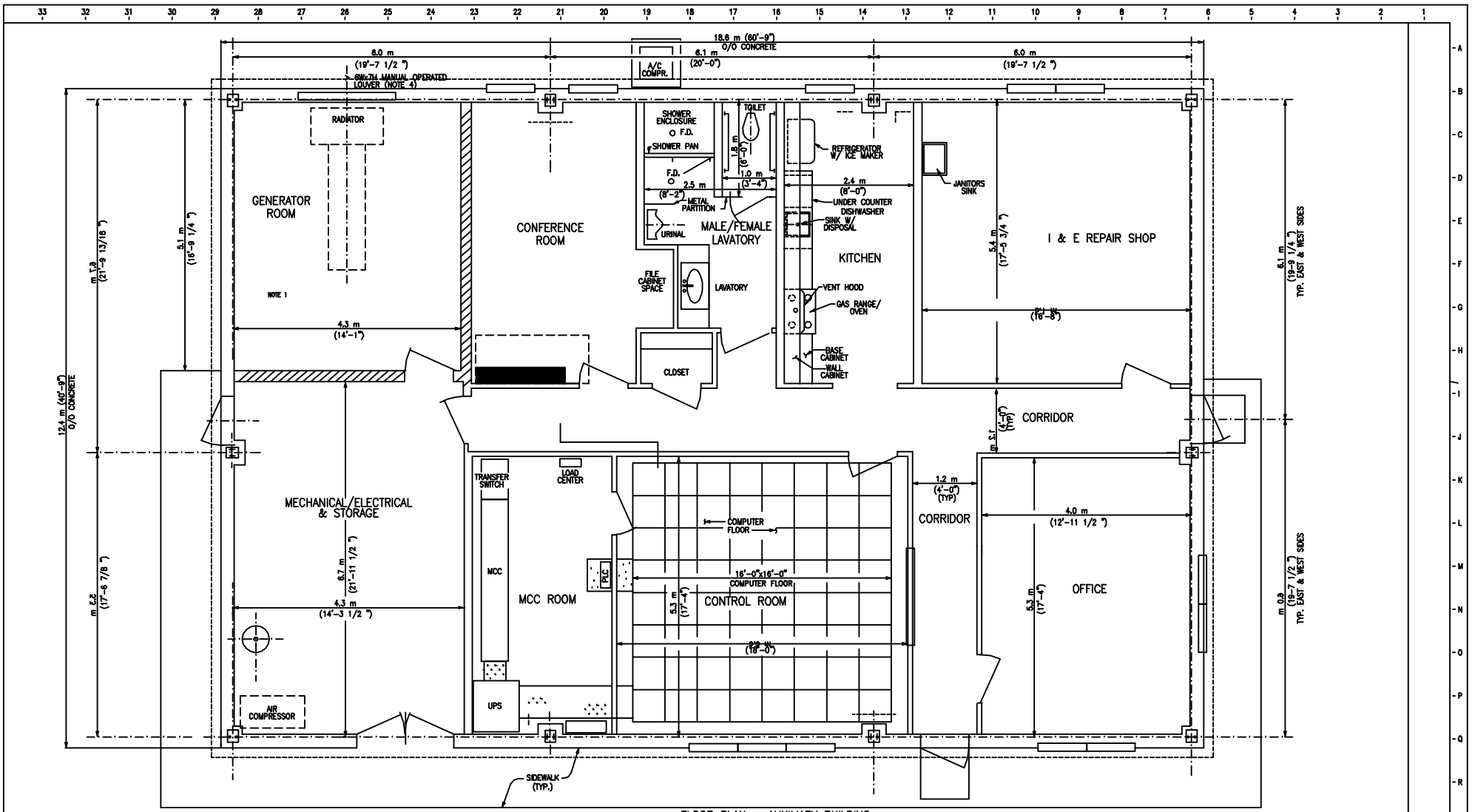

FLOOR PLAN – AUXILIARY BUILDING

SCALE: 3/8 " = 1'-0"

GENERAL NOTES

1. STANDBY GENERATOR IS LOCATED INSIDE THE BUILDING TENTATIVELY. EXACT LOCATION WILL BE DETERMINED DURING DETAILED DESIGN.

PROJ NO.	REV. NO.	LOC.	REVISION	REVISED BY DATE	CHECKED BY DATE	APPROVED BY DATE
	1	-	ADD NOTE 1	WCE-7/97	LS-7-97	RS-7/97
	2	-	CHANGED TITLE	WCE-11/97	LS-11/97	RS-11/97

THIS DRAWING PREPARED FOR

DEPARTMENT OF ENERGY

PB-KBB Inc.
Engineering Construction Operations
11757 KATY FREEWAY 8TH FLOOR
HOUSTON, TEXAS 77079

TITLE:

REFRIGERATED MINED CAVERN STORAGE
OFFICE/CONTROL BUILDING PLAN

DRAWN BY	RS	DATE	11/97	SCALE	3/8 "=1'-0"
DESIGNED BY	NH	DATE	11/97	PROJECT NO.	861
FILE NAME	861AC002.DGN			DRAWING NO.	861-AC-002

H:/PROJECTS/861/DGN/861AC002.DGN

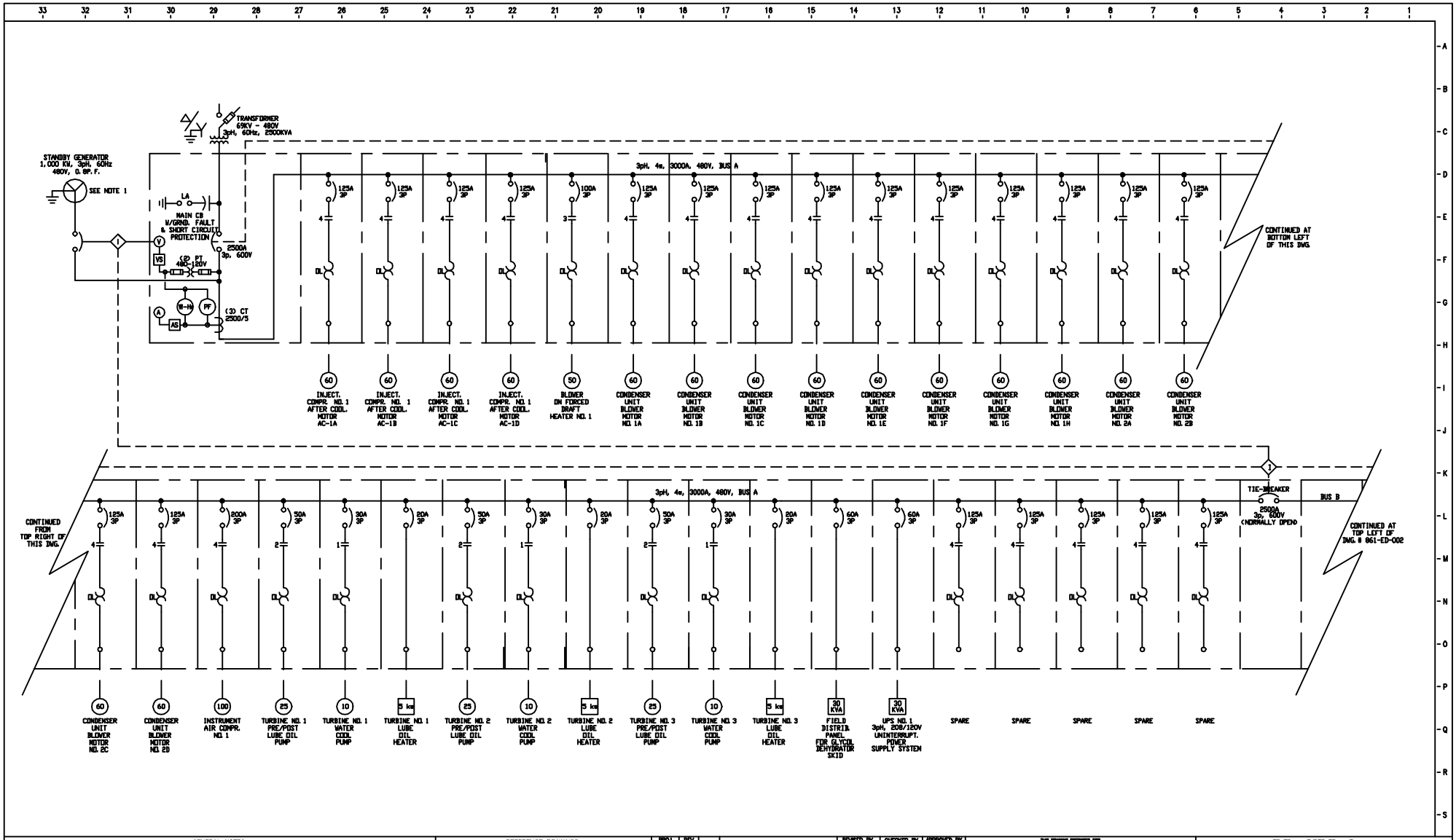

GENERAL NOTES

1. STANDBY GENERATOR IS ELECTRICALLY INTERLOCKED WITH BOTH MAIN CIRCUIT BREAKERS & TIE BREAKERS. IT WILL START ONLY ON LOSS OF UTILITY POWER IN BOTH TRANSFORMERS. TIE BREAKERS SHALL BE OPEN WHEN STANDBY GENERATOR IS RUNNING. MANUAL LOAD SHEDDING IS REQUIRED.

REFERENCE DRAWINGS

PROJ. No.	REV. No.	LOC.	REVISIONS	REVISED BY DATE	CHECKED BY DATE	APPROVED BY DATE

THIS DRAWING PREPARED FOR

DEPARTMENT OF ENERGY

PB-KBB Inc.
Engineering Construction Operations
11757 KATY FREEWAY #400
HOUSTON, TEXAS 77079

TITLE:

REFRIGERATED MINED CAVERN STORAGE
ONE-LINE DIAGRAM
CONCEPTUAL DESIGN(1 OF 3)

DESIGN BY	LS	DATE	05/98	DRAWN BY	TST	DATE	05/98	SCALE	NONE
CHECKED BY	RS	DATE	05/98	APPROVED BY		DATE		PROJECT NO.	861
FILE NAME	861ED001.DGN			DRAWING NO.	861-ED-001			REVISION	0

H:/PROJECTS/861/DGN/861ED001.DGN

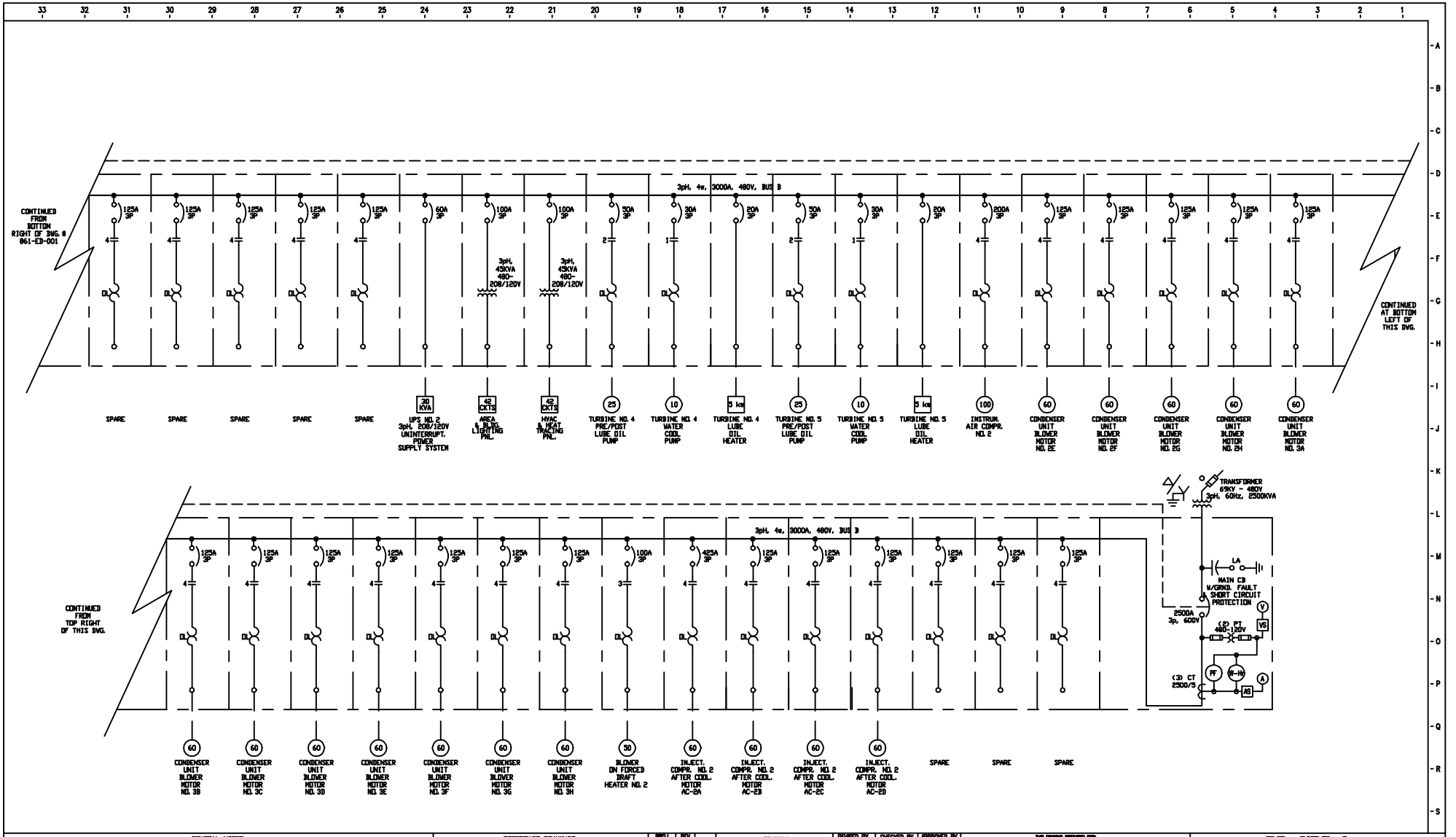

GENERAL NOTES	REFERENCE DRAWINGS

PROJ. No.	REV. No.	LOC.	REVISIONS	REVISED BY DATE	CHECKED BY DATE	APPROVED BY DATE

THIS DRAWING PREPARED FOR:

DEPARTMENT OF ENERGY

PB-KBB Inc.
Engineering Construction Operations
11757 KATY FREEWAY #400
HOUSTON, TEXAS 77079

TITLE:

REFRIGERATED MINED CAVERN STORAGE ONE-LINE DIAGRAM CONCEPTUAL DESIGN(2 OF 3)

DESIGNED BY LS	DATE 05/98	DRAWN BY TST	DATE 05/98	SCALE NONE	
CHECKED BY RS	DATE 05/98	APPROVED BY	DATE	DRAWING No. 861	
FILE NAME 861ED002.DGN		DRAWING No. 861-ED-002		REVISION No. 0	

H:/PROJECTS/861/DGN/861ED002.DGN

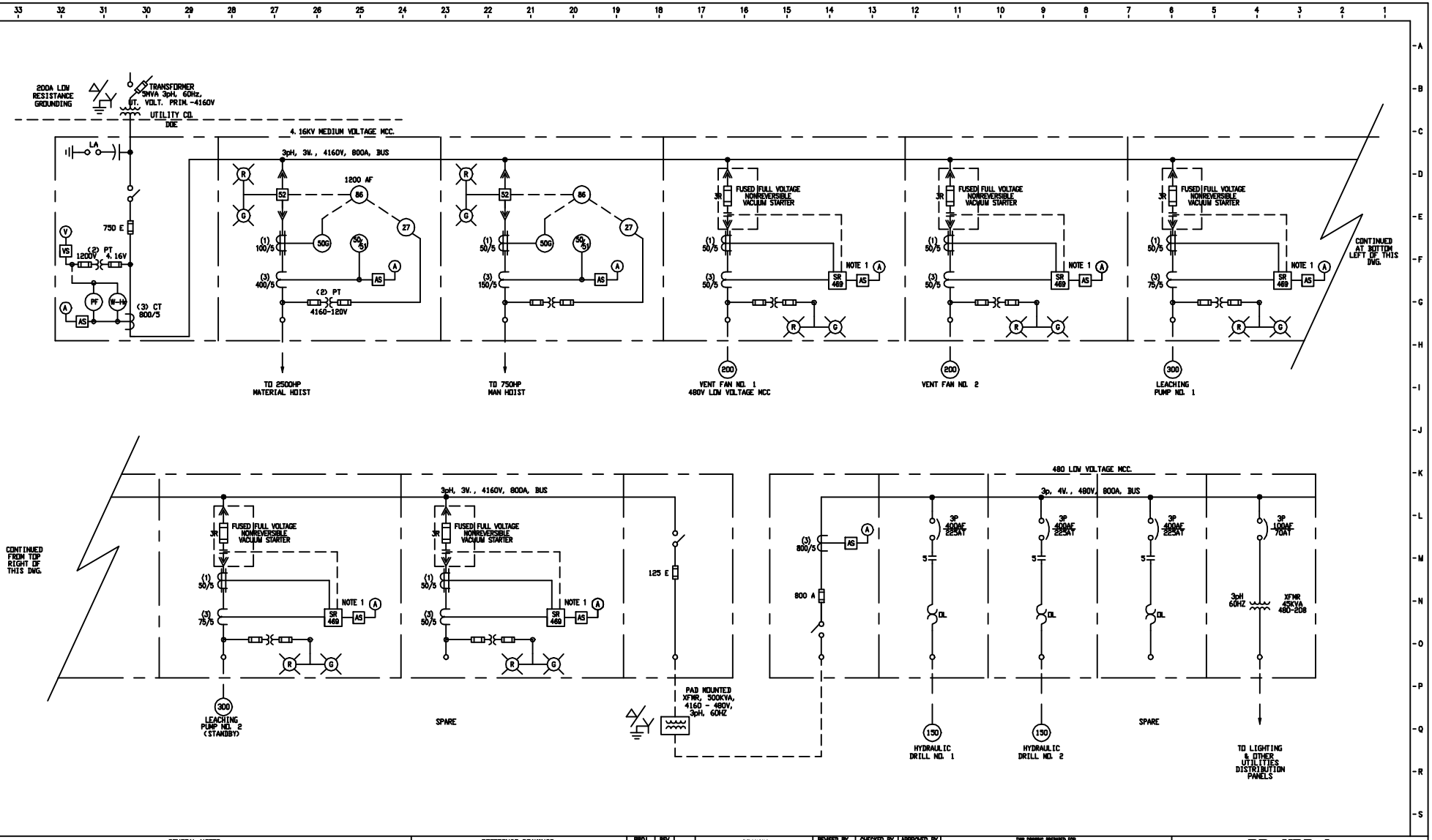

GENERAL NOTES

1. ELECTRONIC MOTOR PROTECTION RELAY SR-K69 (MULTILINE) OR SIMILAR W/FOLLOWING PROTECTION FUNCTIONS: OVERLOAD, GROUND FAULT, SHORT CIRCUIT, SINGLE PHASE, UNDERVOLTAGE.
2. BOTH MEDIUM & LOW VOLTAGE MCC ARE CONSTRUCTED IN NEMA3R ENCLOSURES GOOD FOR OUTDOOR INSTALLATION.
3. POWER SUPPLY ARRANGEMENTS SHOULD BE MADE WITH UTILITY COMPANY SUPPLYING & INSTALLING 5MVA DISTRIBUTION TRANSFORMER FOR CONSTRUCTION POWER.

REFERENCE DRAWINGS

PROJ. No.	REV. No.	LOC.	REVISIONS	REVISED BY DATE	CHECKED BY DATE	APPROVED BY DATE

THIS DRAWING PREPARED FOR
DEPARTMENT OF ENERGY

PB-KBB Inc.
Engineering Construction Operations
11757 KATY FREEWAY #600
HOUSTON, TEXAS 77079

TITLE:
REFRIGERATED MINED CAVERN STORAGE
ELECTRICAL ONE-LINE DIAGRAM
CONCEPTUAL DESIGN(3 OF 3)

DESIGNED BY	DATE	DRAWN BY	DATE	SCALE
LS	0598	TST	06/98	NONE
CHECKED BY	DATE	APPROVED BY	DATE	PROJECT NO.
RS	0598			861
FILE NAME		DRAWING No.		REVISION
861ED003.DGN		861-ED-003		0

H:/PROJECTS/861/DGN/861ED003.DGN

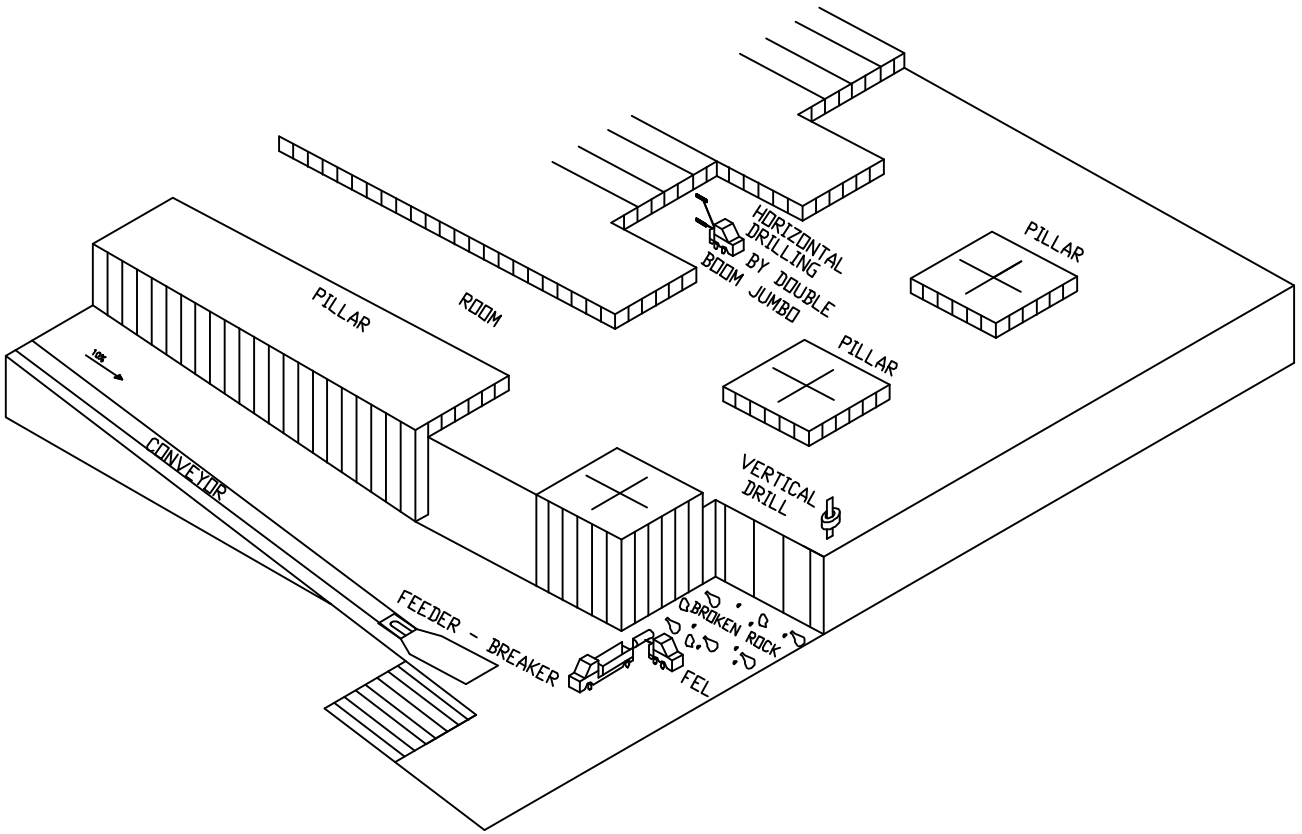

GENERAL NOTES	REFERENCE DRAWINGS

PROJ. No.	REV. No.	LOC.	REVISIONS	REVISED BY DATE	CHECKED BY DATE	APPROVED BY DATE

THIS DRAWING PREPARED FOR:

DEPARTMENT OF ENERGY

PB-KBB Inc.
Engineering Construction Operations
11757 KATY FREEWAY #600
HOUSTON, TEXAS 77079

TITLE:

REFRIGERATED MINED CAVERN STORAGE
TWO SHAFT MINE SHOWING DEVELOPMENT
AND BENCHING HEADINGS

DESIGNED BY	MM	DATE	05/98	DRAWN BY	TST	DATE	05/98	ISSUED	NONE
CHECKED BY	MM	DATE	05/98	APPROVED BY		DATE		PROJECT NO.	861
FILE NAME	861LB004.DGN			DRAWING No.	861-LB-004			REVISION	0

H:/PROJECTS/861/DGN/861LB004.DGN

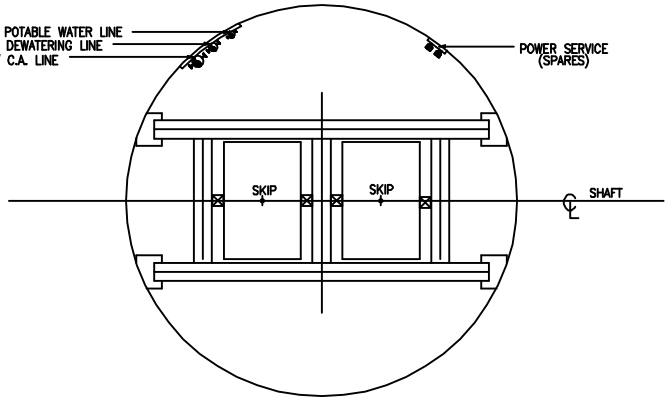

18' DIA. PRODUCTION SHAFT

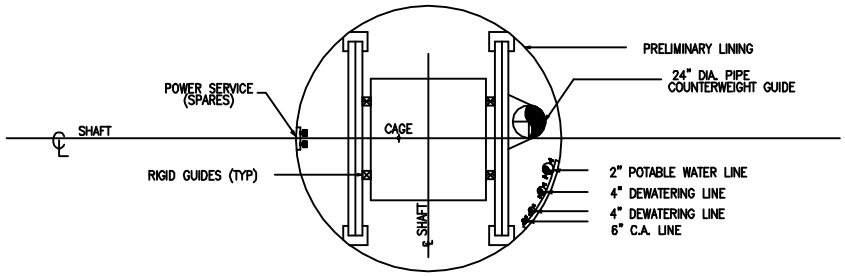

10' DIA. SERVICE SHAFT

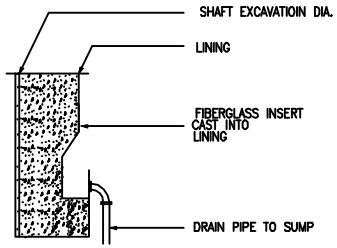

TYPICAL WATER RING DETAIL

(ELEVATION IN SHAFT AS REQUIRED)

GENERAL NOTES	REFERENCE DRAWINGS

PROJ. No.	REV. No.	LOC.	REVISIONS	REVISED BY DATE	CHECKED BY DATE	APPROVED BY DATE

THIS DRAWING PREPARED FOR

DEPARTMENT OF ENERGY

PB-KBB Inc.
Engineering Construction Operations
11757 KATY FREEWAY #600
HOUSTON, TEXAS 77079

TITLE

REFRIGERATED MINED CAVERN STORAGE
SHAFT OUTFITTING DURING CONSTRUCTION

DESIGNED BY	DATE	DRAWN BY	DATE	GROUP
MM	05/98	TST	05/98	NONE
CHECKED BY	DATE	APPROVED BY	DATE	PROJECT NO.
MM	05/98			861

FILE NAME	DRAWING No.	REVISION
861LB005.DGN	861-LB-005	0

H:\PROJECTS\861\DGN\861LB005.DGN

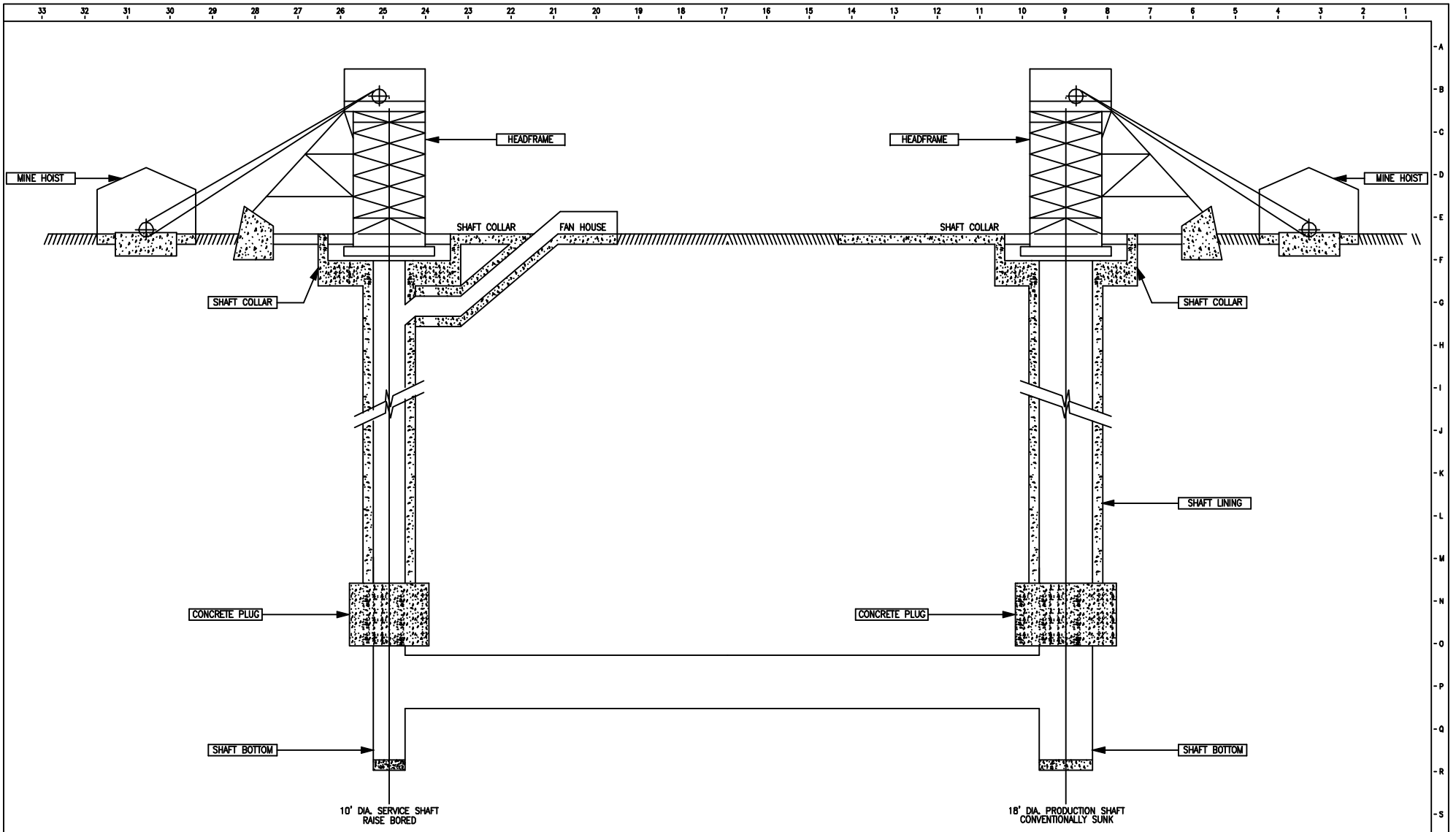

GENERAL NOTES	REFERENCE DRAWINGS

PROJ. NO.	REV. NO.	LOC.	REVISIONS	REVISED BY DATE	CHECKED BY DATE	APPROVED BY DATE

THIS DRAWING PREPARED FOR:

DEPARTMENT OF ENERGY

PB-KBB Inc.
Engineering Construction Operations
11757 KATY FREEWAY #600
HOUSTON, TEXAS 77079

TITLE:

REFRIGERATED MINED CAVERN STORAGE
MINE GENERAL ARRANGEMENT

DESIGN BY	DATE	DRAWN BY	DATE	SCALE
MM	05/98	TST	05/98	NONE
CHECKED BY	DATE	APPROVED BY	DATE	PROJECT NO.
MM	05/98			861
FILE NAME		DRAWING NO.		REVISION
861LB006.DGN		861-LB-006		0

H:/PROJECTS/861/DGN/861LB006.DGN

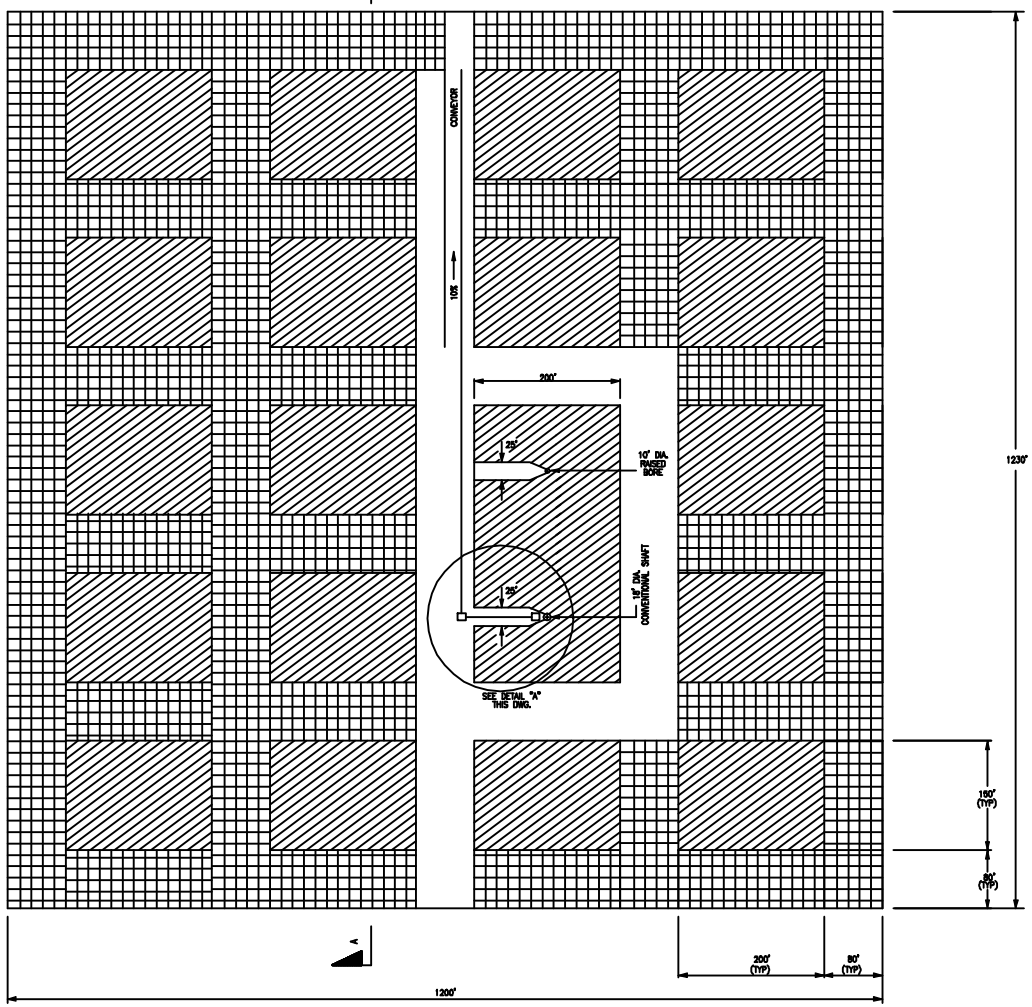

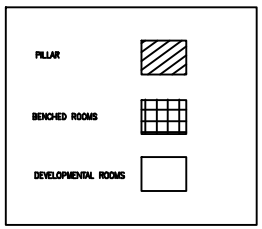

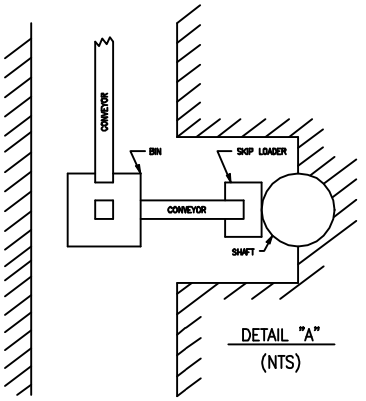

DETAIL "A"
(NTS)

0 80 160 240 320

GENERAL NOTES	REFERENCE DRAWINGS

PROJ. No.	REV. No.	LOC.	REVISIONS	REVISED BY DATE	CHECKED BY DATE	APPROVED BY DATE

THIS DRAWING PREPARED FOR:
DEPARTMENT OF ENERGY

PB-KBB Inc.
Engineering Construction Operations
11757 KATY FREEWAY #600
HOUSTON, TEXAS 77079

TITLE:
REFRIGERATED MINED CAVERN STORAGE
GENERAL CAVERN LAYOUT-2500' DEPTH

DESIGNED BY	DATE	DRAWN BY	DATE	SCALE
MM	05/98	TST	05/98	1"=80'
CHECKED BY	DATE	APPROVED BY	DATE	PROJECT NO.
MM	05/98			861
FILE NAME		DRAWING No.		REVISION
861LB007.DGN		861-LB-007		0

H:/PROJECTS/861/DGN/861LB007.DGN

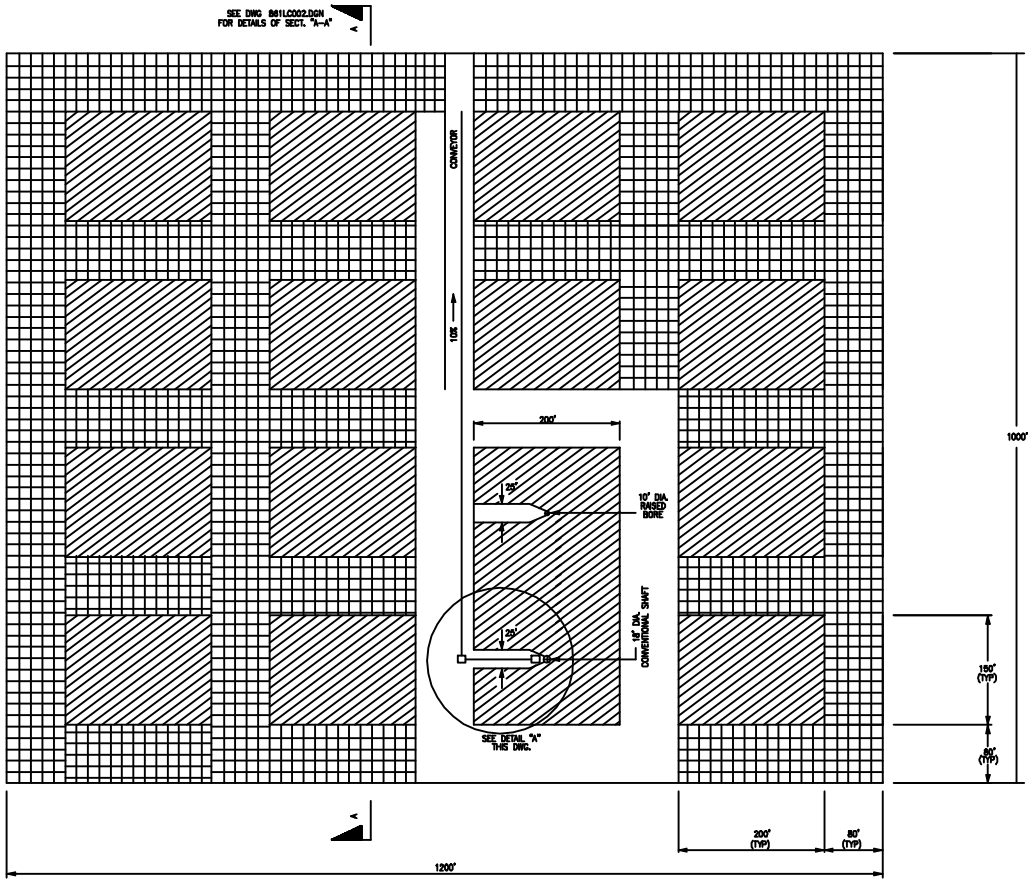

LEGEND

PILLAR

BENCHED ROOMS

DEVELOPMENTAL ROOMS

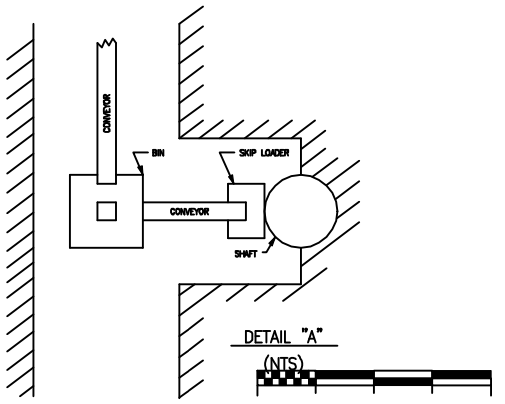

DETAIL "A"
(NTS)

0 80 160 240 360

GENERAL NOTES	REFERENCE DRAWINGS

PROJ. No.	REV. No.	LOC.	REVISIONS	REVISED BY DATE	CHECKED BY DATE	APPROVED BY DATE

THIS DRAWING PREPARED FOR:

DEPARTMENT OF ENERGY

PB-KBB Inc.
Engineering Construction Operations
11757 KATY FREEWAY #600
HOUSTON, TEXAS 77079

TITLE:

REFRIGERATED MINED CAVERN STORAGE
GENERAL CAVERN LAYOUT-3000' DEPTH

DRAWN BY	DATE	DESIGN BY	DATE	SCALE
MM	05/98	TST	05/98	1"=80'
DESIGNED BY	DATE	APPROVED BY	DATE	PROJECT No.
MM	05/98			861
FILE NAME		DRAWING No.		REVISION
861LB008.DGN		861-LB-008		0

H:/PROJECTS/861/DGN/861LB008.DGN

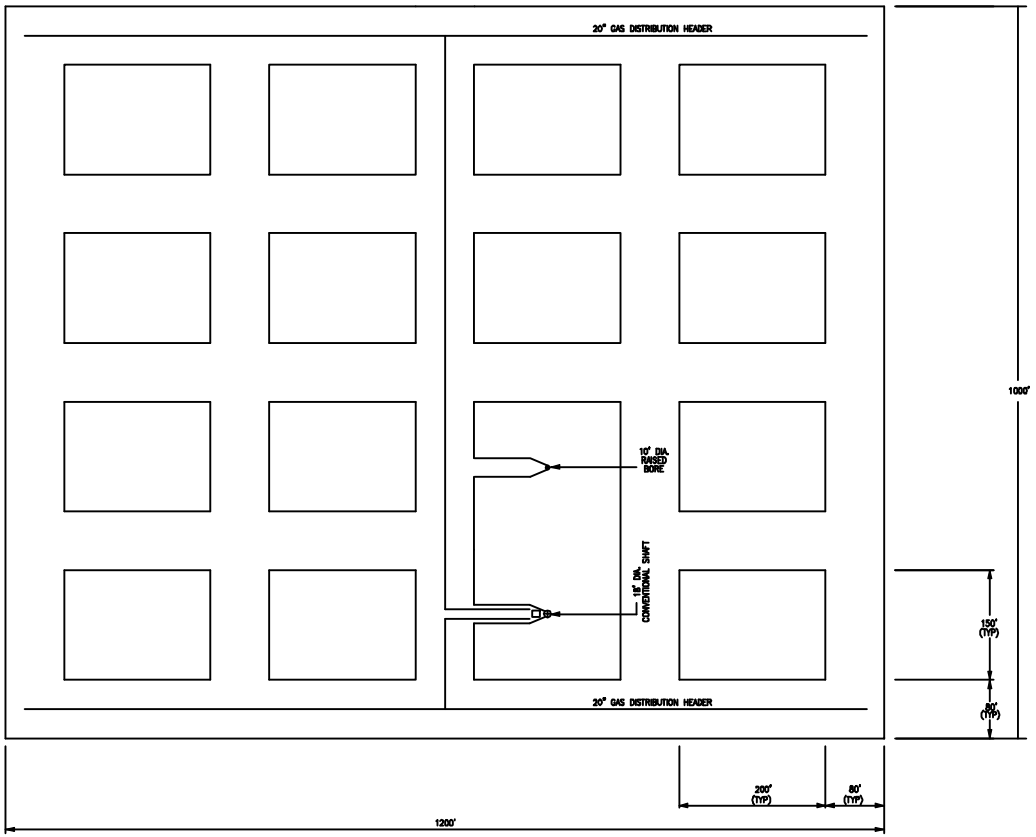

0 80 160 240 360

GENERAL NOTES	REFERENCE DRAWINGS

PROJ. No.	REV. No.	LOC.	REVISIONS	REVISED BY DATE	CHECKED BY DATE	APPROVED BY DATE

THIS DRAWING PREPARED FOR:

DEPARTMENT OF ENERGY

PB-KBB Inc.
Engineering Construction Operations
11757 KATY FREEWAY #600
HOUSTON, TEXAS 77079

TITLE:
REFRIGERATED MINED CAVERN STORAGE
GAS DISTRIBUTION SYSTEM IN MINE
3,000 FT DEPTH

DESIGN BY MM DATE 05/98	DRAWN BY TST DATE 05/98	SCALE 1"=80'	
CHECKED BY MM DATE 05/98	APPROVED BY DATE	PROJECT NO. 861	
FILE NAME 861LB009.DGN	DRAWING NO. 861-LB-009	REVISION NO. 0	

H:/PROJECTS/861/DGN/861LB009.DGN

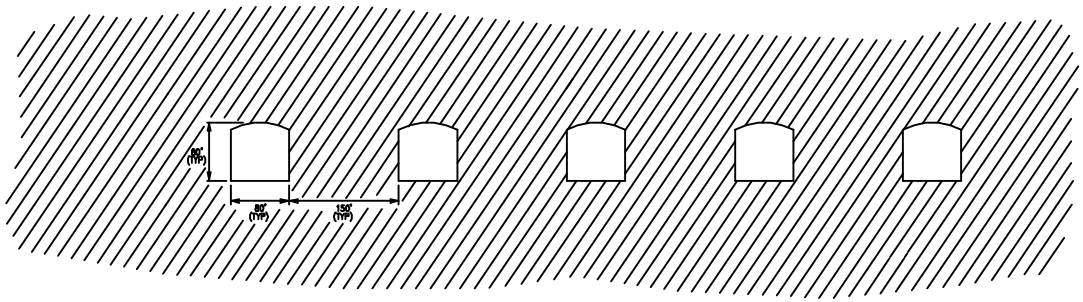

SECTION "A–A" AT 3000' DEPTH

0 80 160 240 360

GENERAL NOTES	REFERENCE DRAWINGS

PROJ. No.	REV. No.	LOC.	REVISIONS	REVISED BY DATE	CHECKED BY DATE	APPROVED BY DATE

THIS DRAWING PREPARED FOR:

DEPARTMENT OF ENERGY

PB–KBB Inc.
Engineering Construction Operations
11757 KATY FREEWAY #600
HOUSTON, TEXAS 77079

TITLE:

REFRIGERATED MINED CAVERN STORAGE
SECTION 'A–A' 3000' DEPTH

DESIGNED BY	DATE	DRAWN BY	DATE	SCALE
MM	05/98	TST	05/98	1"=80'
CHECKED BY	DATE	APPROVED BY	DATE	PROJECT NO.
MM	05/98			861
FILE NAME: 861LB010.DGN		DRAWING No. 861–LB–010		REVISION 0

H:/PROJECTS/861/DGN/861LB010.DGN

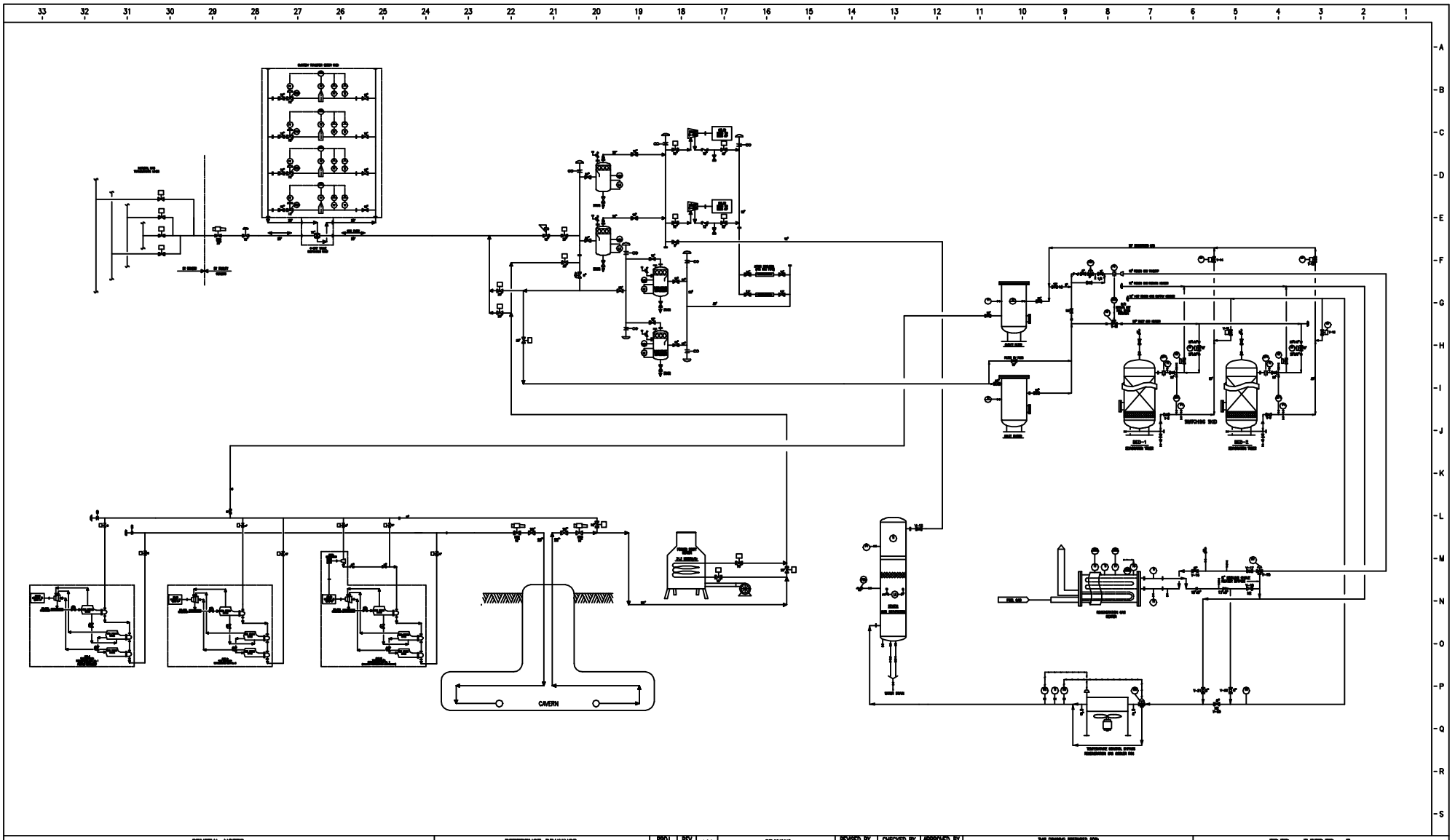

GENERAL NOTES	REFERENCE DRAWINGS

PROJ. No.	REV. No.	LOC.	REVISIONS	REVISED BY DATE	CHECKED BY DATE	APPROVED BY DATE

THIS DRAWING PREPARED FOR:

DEPARTMENT OF ENERGY

PB-KBB Inc.
Engineering Construction Operations
11757 KATY FREEWAY #600
HOUSTON, TEXAS 77079

TITLE:

REFRIGERATED MINED CAVERN STORAGE PROCESS FLOW DIAGRAM

DRAWN BY	DATE	CHECKED BY	DATE	APPROVED BY	DATE	SCALE	PROJECT NO.
WS	06/96	TST	06/96			NONE	861
WS	06/96						

FILE NAME	DRAWING No.	REVISION
861MD001.DGN	861-MD-001	0

H:/PROJECTS/861/DGN/861MD001.DGN

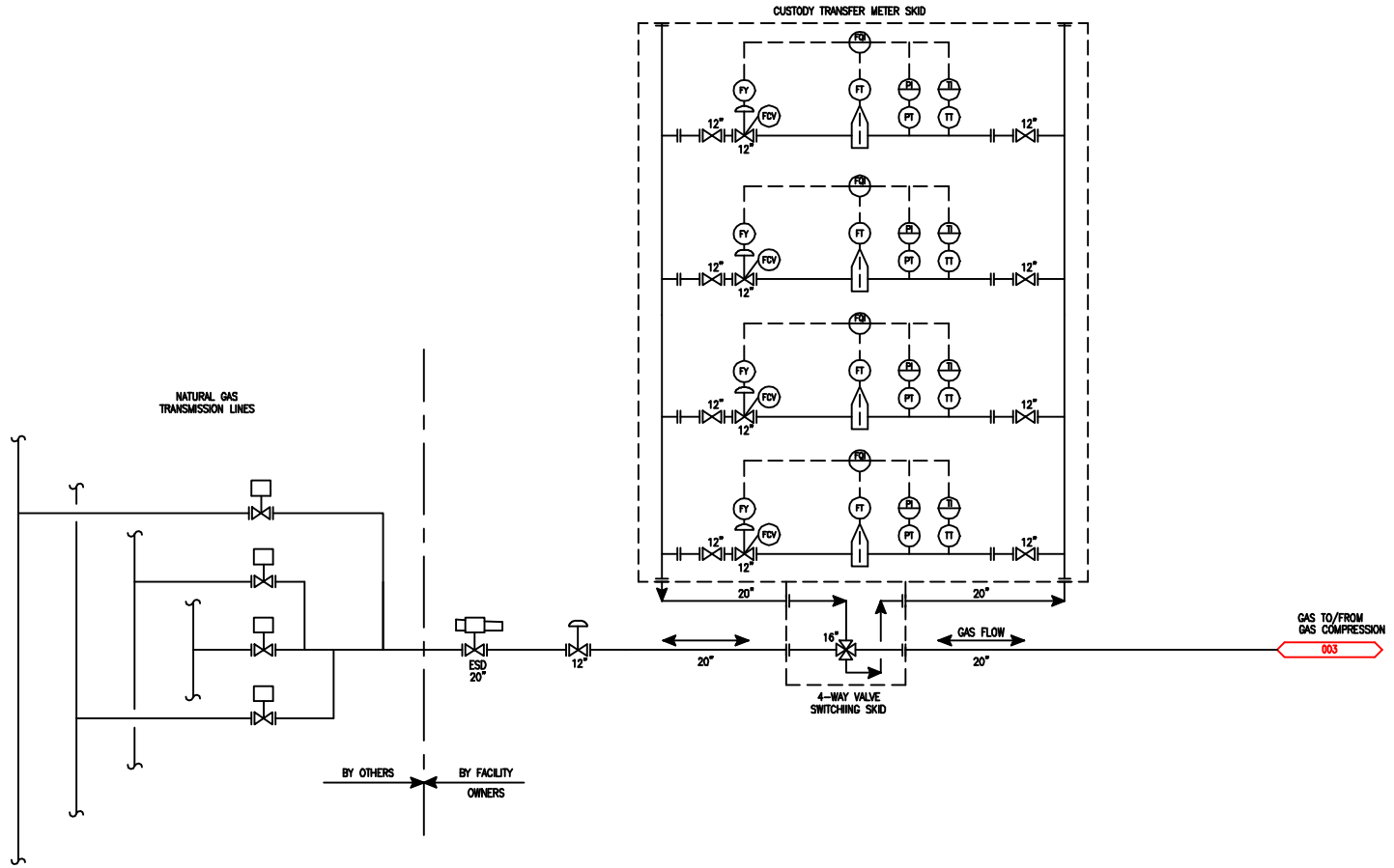

GENERAL NOTES	REFERENCE DRAWINGS

PROJ. No.	REV. No.	LOC.	REVISIONS	REVISED BY DATE	CHECKED BY DATE	APPROVED BY DATE

THIS DRAWING PREPARED FOR:

DEPARTMENT OF ENERGY

PB-KBB Inc.
Engineering Construction Operations
11757 KATY FREEWAY #600
HOUSTON, TEXAS 77079

TITLE:

REFRIGERATED MINED CAVERN STORAGE METER SKID

DRAWN BY	DATE	DRAWN BY	DATE	SCALE
WS	06/98	TST	03/98	NONE
CHECKED BY	DATE	APPROVED BY	DATE	PROJECT NO.
WS	06/98			861
FILE NAME: 861MD002.DGN		DRAWING No. 861-MD-002		REVISION 0

H:/PROJECTS/861/DGN/861MD002.DGN

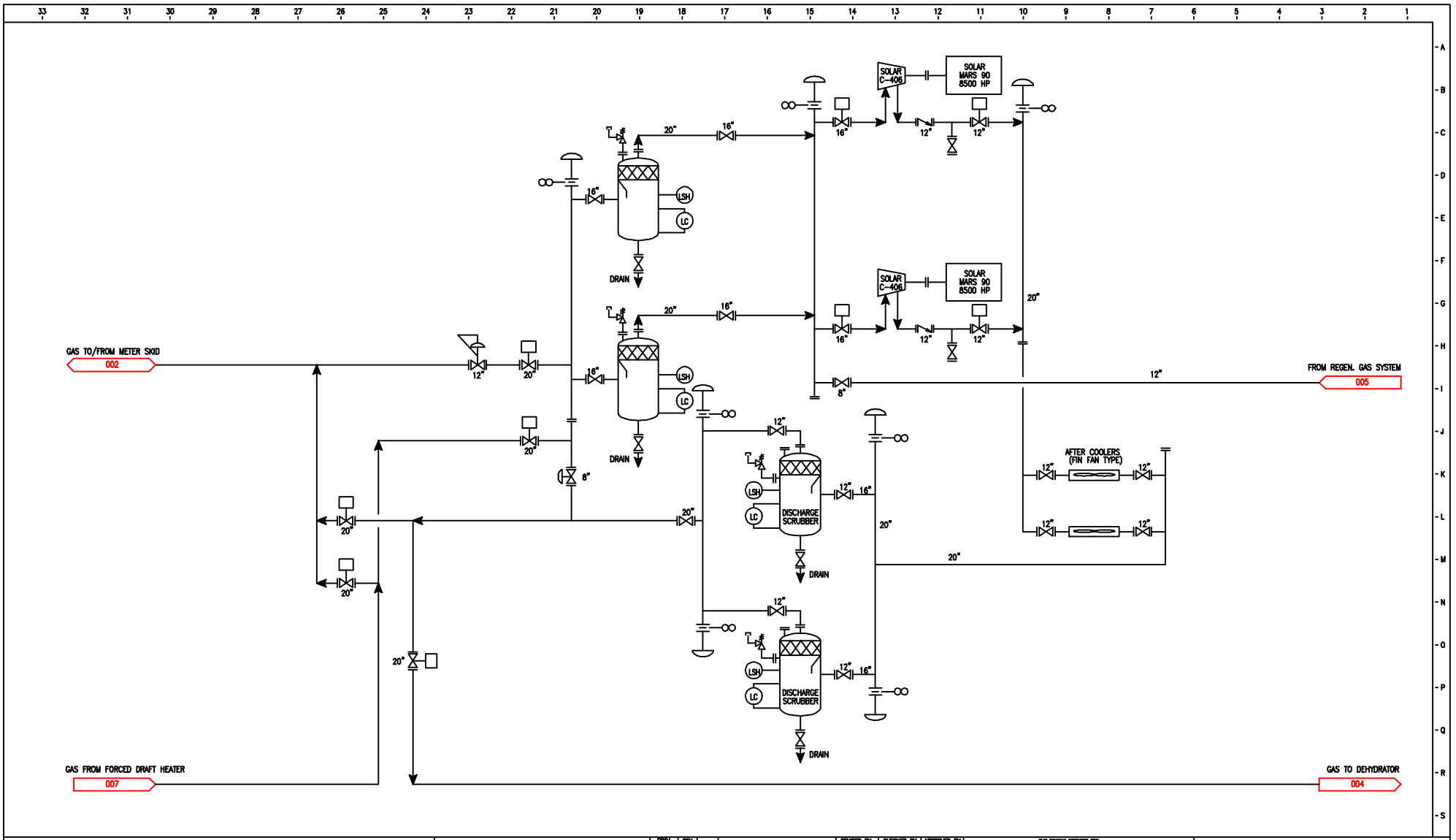

GENERAL NOTES

REFERENCE DRAWINGS

PROJ. No.	REV. No.	LOC.	REVISIONS	REVISED BY DATE	CHECKED BY DATE	APPROVED BY DATE

THIS DRAWING PREPARED FOR

DEPARTMENT OF ENERGY

PB-KBB Inc.
Engineering Construction Operations
11757 KATY FREEWAY #600
HOUSTON, TEXAS 77079

TITLE:

REFRIGERATED MINED CAVERN STORAGE
GAS COMPRESSION SYSTEM

DESIGN BY	WS	DATE	06/98	DRAWN BY	TST
CHECKED BY	WS	DATE	06/98	APPROVED BY	
FILE NAME	861MD003.DGN			DRAWING NO.	861-MD-003
DATE	06/98			PROJECT NO.	861
SCALE	NONE			REVISION	0

H:/PROJECTS/861/DGN/861MD003.DGN

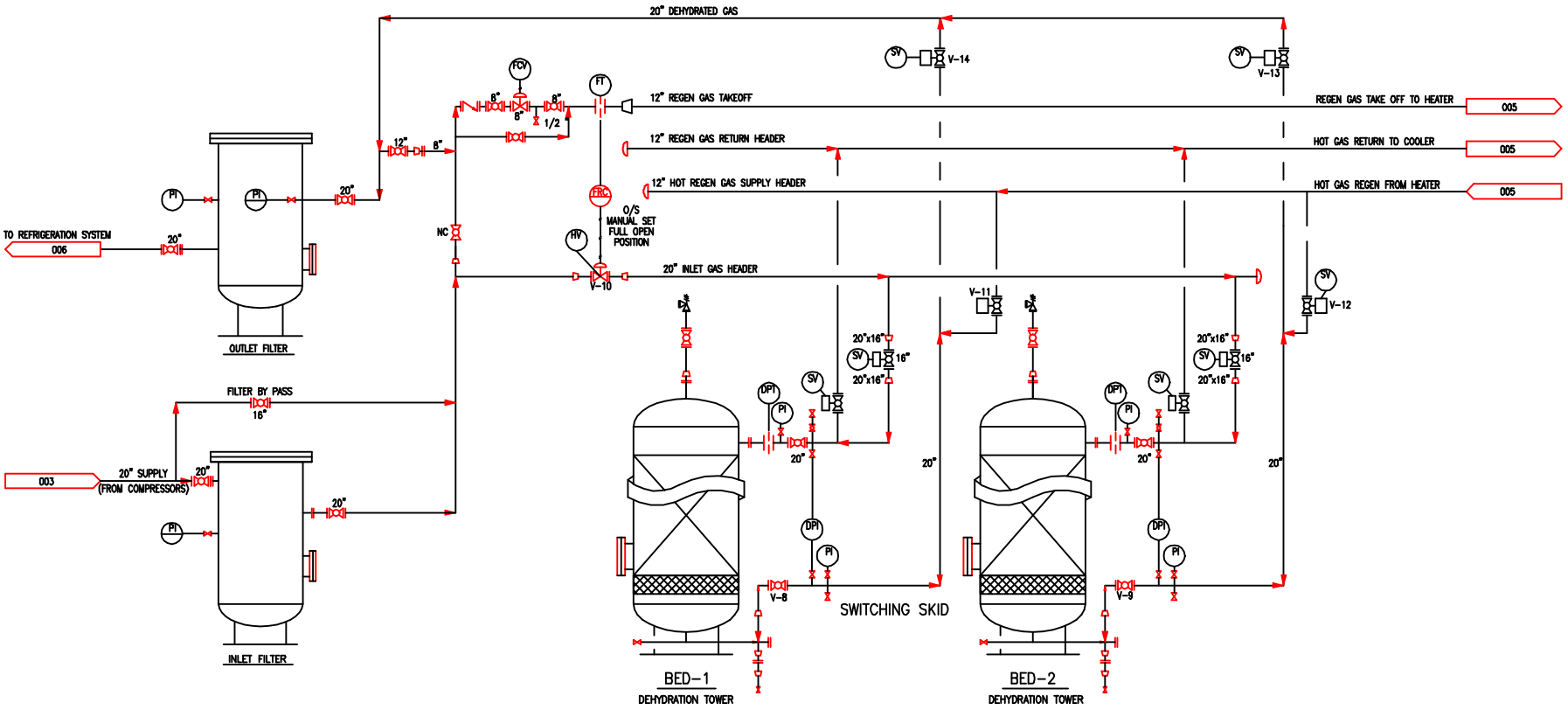

GENERAL NOTES	REFERENCE DRAWINGS

PROJ. No.	REV. No.	LOC.	REVISIONS	REVISED BY DATE	CHECKED BY DATE	APPROVED BY DATE

This drawing prepared for:

DEPARTMENT OF ENERGY

PB-KBB Inc.
Engineering Construction Operations
11757 KATY FREEWAY #600
HOUSTON, TEXAS 77079

TITLE:

REFRIGERATED MINED CAVERN STORAGE
MOLECULAR SIEVE DEHYDRATOR

DRAWN BY	DATE	CHECKED BY	DATE	SCALE
WS	06/98	TST	06/98	NONE
CHECKED BY	DATE	APPROVED BY	DATE	PROJECT NO.
WS	06/98			861
FILE NAME		DRAWING No.		REVISION
861MD004.DGN		861-MD-004		0

H:/PROJECTS/861/DGN/861MD004.DGN

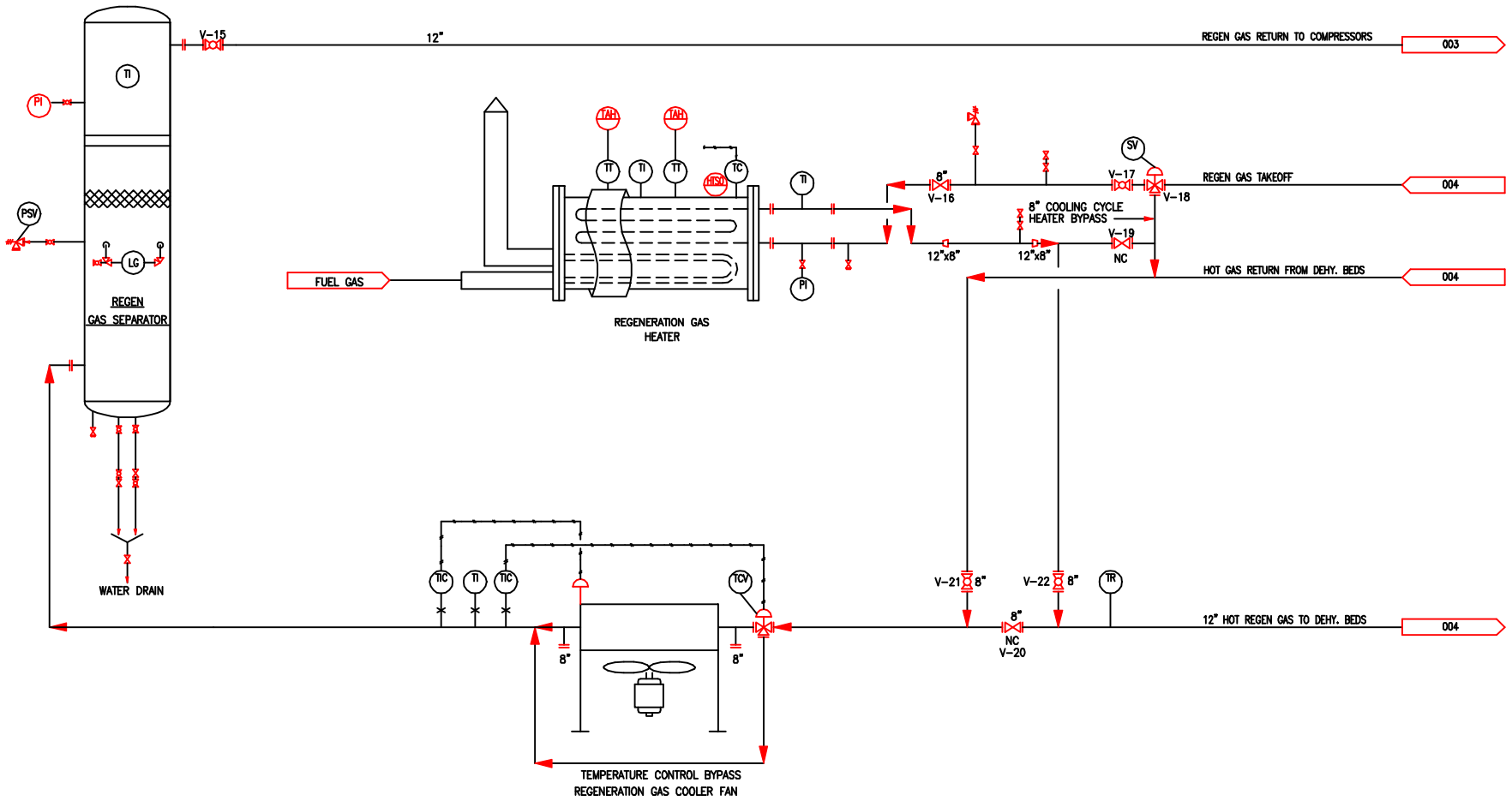

GENERAL NOTES	REFERENCE DRAWINGS

PROJ No.	REV. No.	LOC.	REVISIONS	REVISED BY DATE	CHECKED BY DATE	APPROVED BY DATE

THIS DRAWING PREPARED FOR:

DEPARTMENT OF ENERGY

PB-KBB Inc.
Engineering Construction Operations
11757 KATY FREEWAY 8800
HOUSTON, TEXAS 77079

TITLE:

REFRIGERATED MINED CAVERN STORAGE
REGENERATION GAS SYSTEM

DRAWN BY	DATE	CHKD BY	DATE	SCALE
WS	06/98	TST	06/98	NONE
DESIGNED BY	DATE	APPROVED BY	DATE	PROJECT NO.
WS	06/98			861
FILE NAME		DRAWING NO.		REVISION
861MD005.DGN		861-MD-005		0

H:/PROJECTS/861/DGN/861MD005.DGN

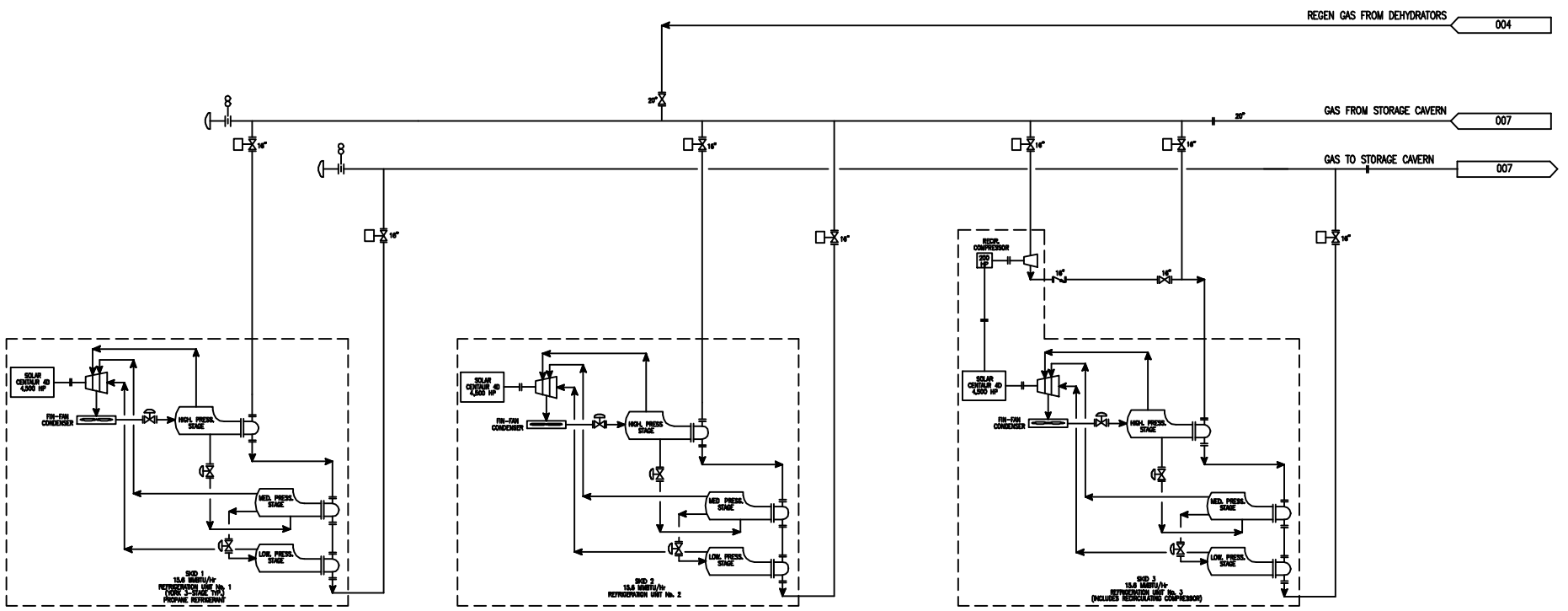

GENERAL NOTES

1. DASHED LINE, (- - - - - - -), REPRESENTS SKID OUTLINE.

REFERENCE DRAWINGS

PROJ. No.	REV. No.	LOC.	REVISIONS	REVISED BY DATE	CHECKED BY DATE	APPROVED BY DATE

THIS DRAWING PREPARED FOR:

DEPARTMENT OF ENERGY

PB-KBB Inc.
Engineering Construction Operations
11757 KATY FREEWAY #600
HOUSTON, TEXAS 77079

TITLE:

REFRIGERATED MINED CAVERN STORAGE
REFRIGERATION SYSTEM

DESIGN BY: WS	DATE: 06/98	DRAWN BY: TST	DATE: 06/98	SCALE: NONE	
CHECKED BY: WS	DATE: 06/98	APPROVED BY:	DATE:	PROJECT NO: 861	
FILE NAME: 861MD006.DGN		DRAWING NO.: 861-MD-006		REVISION: 0	

H:/PROJECTS/861/DGN/861MD006.DGN

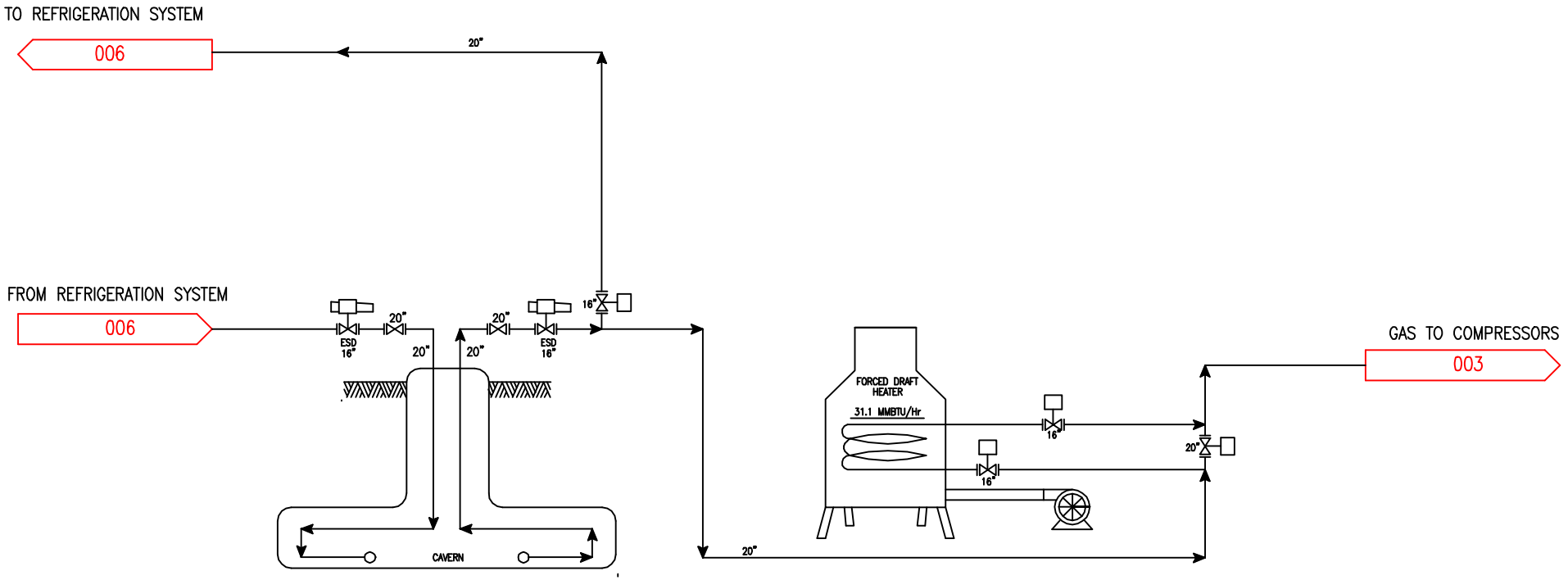

GENERAL NOTES	REFERENCE DRAWINGS
1. DASHED LINE, (- - - - - - -), REPRESENTS SKID OUTLINE.	

PROJ. No.	REV. No.	LOC.	REVISIONS	REVISED BY DATE	CHECKED BY DATE	APPROVED BY DATE

THIS DRAWING PREPARED FOR:

DEPARTMENT OF ENERGY

PB-KBB Inc.
Engineering Construction Operations
11757 KATY FREEWAY #600
HOUSTON, TEXAS 77079

TITLE:

REFRIGERATED MINED CAVERN STORAGE
STORAGE CAVERN AND HEATER

DESIGN BY	DRAWN BY	SCALE
WS 06/98	TST 06/98	NONE
CHECKED BY	APPROVED BY	PROJECT NO.
WS 06/98	DATE	861
FILE NAME	DRAWING No.	REVISION
861MD007.DGN	861-MD-007	0

H:/PROJECTS/861/DGN/861MD007.DGN

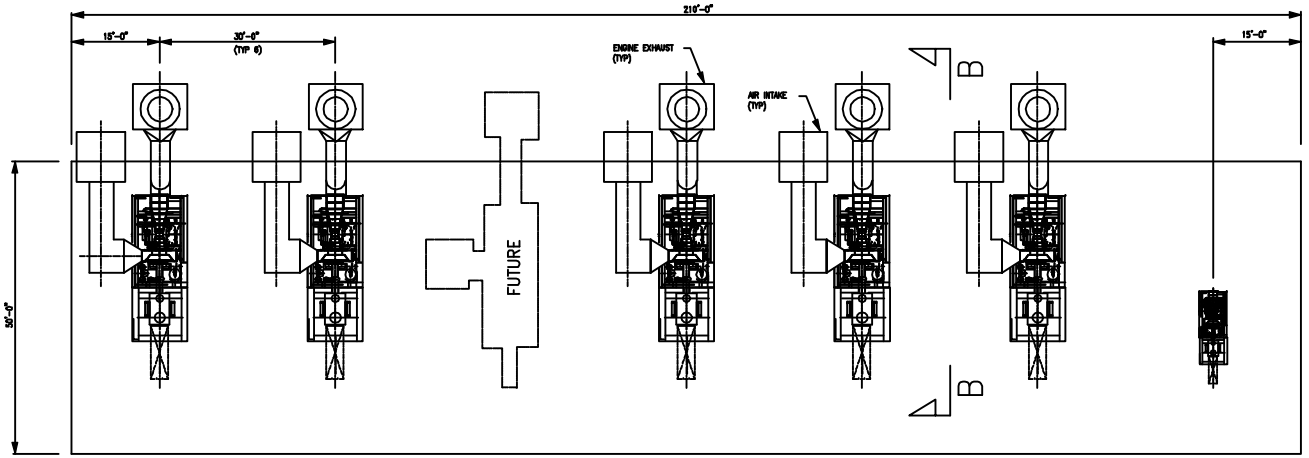

PLAN VIEW

COMPRESSION BUILDING
50'X 210'

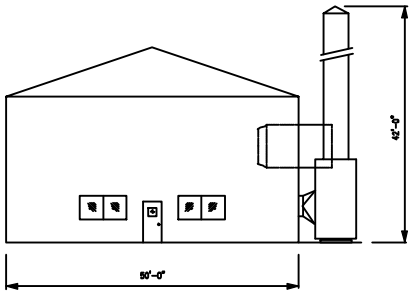

SECTION "A-A"
THIS DWG.

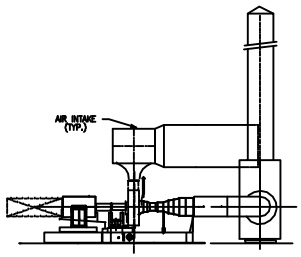

SECTION "B-B"
THIS DWG.

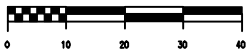

GENERAL NOTES

1. COMPRESSOR-TURBINE UNITS ORIENTATION AND COMPRESSOR BUILDING DIMENSIONS ARE INDICATED TENTATIVELY. THE EXACT ORIENTATION AND DIMENSIONS WILL BE REVISED DURING DETAILED DESIGN IN ACCORDANCE TO THE SELECTED MANUFACTURERS DRAWINGS.

REFERENCE DRAWINGS

PROJ. No.	REV. No.	LOC.	REVISIONS	REVISED BY DATE	CHECKED BY DATE	APPROVED BY DATE
	1	-	REMOVED MCC	WCE-05/97	LS-05/97	RS-05/97
	2	-	MODIFIED COMPRESSOR	WCE-10/97	LS-10/97	RS-10/97

THIS DRAWING PREPARED FOR:

DEPARTMENT OF ENERGY

PB-KBB Inc.
Engineering Construction Operations
11757 KATY FREEWAY #600
HOUSTON, TEXAS 77079

TITLE:

REFRIGERATED MINED CAVERN STORAGE
COMPRESSOR BUILDING
PLAN & ELEVATIONS

DESIGN BY	RS	DATE 3/96	DRAWN BY	RCR	DATE 3/96	SCALE 1"=10'
DESIGNED BY	NH	DATE 3/96	APPROVED BY		DATE	PROJECT NO. 861
FILE NAME	861MP001.DGN		DRAWING NO.	861-MP-001		REVISION NO. 2

H:/PROJECTS/861/DGN/861MP001.DGN

COST ESTIMATE DETAIL

	BASE QUANITY	METRIC/ IMPERIAL	QUANITY	UNIT	UNIT WEIGH	M/I WEIGHT	WEIGHT ADJUS	TOTAL WEIGHT	UNIT MATL	CURRENCY MATERIAL	MATL ADJUST.	TOTAL MATL	UNIT HOURS	HOURS ADJUST	TOTAL HOURS	CREW	LABOR RATE	TOTAL LABOR	UNIT SUBCON	SUBCON ADJUST	TOTAL SUBCON	UNIT EQUIP	CURRENCY EQUIP	TOTAL EQUIP	UNIT OTHER	OTHER ADJUST	TOTAL OTHER	TOTAL	SUBTOTALS
CONVENTIONAL MINING AND SHAFT SINKING (6,292,335 BBLS OF																													
MINING MOBILIZATION	1.00	1.00	1	EA	0.00	1.00	1.00	0	3,500,000	3,500,000	1.00	3,500,000	22,000	1.00	22,000.00	LABOR	35.00	770,000	0.00	1.00	0.00	52,000	52,000	52,000	3,498,000	1.00	3,498,000	7,820,000	
SINK AND LINE MAIN SHAFT; 18-FOOT I.D. CONCRETE LINED; 3,000-FEET	1.00	1.00	1	EA	0.00	1.00	1.00	0	3,906,000	3,906,000	1.00	3,906,000	81,000	1.00	81,000.00	LABOR	35.00	2,835,000	0.00	1.00	0.00	258,000	258,000	258,000	14,439,000	1.00	14,439,000	21,438,000	
RAISEBORE SHAFT; 3,000-FEET, 10-FOOT I.D. CONCRETE LINED	1.00	1.00	1	EA	0.00	1.00	1.00	0	2,186,000	2,186,000	1.00	2,186,000	28,200	1.00	28,200.00	LABOR	35.00	987,000	0.00	1.00	0.00	64,000	64,000	64,000	5,026,000	1.00	5,026,000	8,263,000	
MATERIAL HANDLING EQUIPMENT, MINE HOIST, CRUSHER, HAUL TRUCKS, ECT.	1.00	1.00	1	EA	0.00	1.00	1.00	0	234,000	234,000	1.00	234,000	22,600	1.00	22,600.00	LABOR	35.00	791,000	0.00	1.00	0.00	127,000	127,000	127,000	3,594,000	1.00	3,594,000	4,746,000	
ASSEMBLE MINING EQUIPMENT	1.00	1.00	1	EA	0.00	1.00	1.00	0	32,000	32,000	1.00	32,000	16,000	1.00	16,000.00	LABOR	35.00	560,000	0.00	1.00	0.00	0	0	0	2,544,000	1.00	2,544,000	3,136,000	
EXCAVTE TOP HEADING OF MINE DRIFTS	1.00	1.00	1	EA	0.00	1.00	1.00	0	3,298,000	3,298,000	1.00	3,298,000	105,300	1.00	105,300.00	LABOR	35.00	3,685,500	0.00	1.00	0.00	2,754,000	2,754,000	2,754,000	18,772,000	1.00	18,772,000	28,509,500	
EXCAVATE BENCH OF MINE DRIFTS	1.00	1.00	1	EA	0.00	1.00	1.00	0	2,205,000	2,205,000	1.00	2,205,000	148,000	1.00	148,000.00	LABOR	35.00	5,180,000	0.00	1.00	0.00	1,547,000	1,547,000	1,547,000	26,385,000	1.00	26,385,000	35,317,000	
CONSTRUCTION ELECTRICAL POWER FOR MINE HOIST (50% USAGE FACTOR)	1.00	1.00	34,630,105	KWH	0.00	1.00	1.00	0	0.050	0	1.00	1,731,505	0	1.00	0.00			0	0.00	1.00	0.00	0	0	0	0	1.00	0	1,731,505	
CONSTRUCTION ELECTRICAL POWER FOR VENTILATION AND MINING EQUIPMENT	1.00	1.00	27,704,084	KWH	0.00	1.00	1.00	0	0.050	0	1.00	1,385,204	0	1.00	0.00			0	0.00	1.00	0.00	0	0	0	0	1.00	0	1,385,204	
SUBTOTAL MINING AND SHAFT SINKING																													**112,346,209**
REFRIDGERATION SYSTEM , COMPRSSORS, AND PROCESS																													
GAS COMPRESSORS, CENTRIFUGAL C406 MARS 90 13,000 H.P.	2.00	1.00	2	EA	0.00	1.00	1.00	0	5,400,000	5,400,000	1.00	10,800,000		1.00	0.00	LABOR	35.00	0	0.00	1.00	0.00	0	0	0	0	1.00	0	10,800,000	
REFRIDGERATION SYSTEM, 1300 TON PROPANE REFRIGERANT, GAS TURBINE	3.00	1.00	3	EA	0.00	1.00	1.00	0	3,000,000	3,000,000	1.00	9,000,000		1.00	0.00	LABOR	35.00	0	0.00	1.00	0.00	0	0	0	0	1.00	0	9,000,000	
RECIRCULATION GAS COMPRESSOR, CENTRIFUGAL, 200 H.P. ELECTRIC DRIVE	1.00	1.00	1	EA	0.00	1.00	1.00	0	600,000	600,000	1.00	600,000		1.00	0.00			0		1.00	0.00		0	0		1.00	0	600,000	
MOLECULAR SIEVE DEHYDARATION UNIT, SKID MOUNTED, 250 MMSCFD	1.00	1.00	1	EA	0.00	1.00	1.00	0	1,585,000	1,585,000	1.00	1,585,000		1.00	0.00			0		1.00	0.00		0	0		1.00	0	1,585,000	
LINE HEATER, 66.2 MM BTU/HR, DIRECT FIRED	1.00	1.00	1	EA	0.00	1.00	1.00	0	450,000	450,000	1.00	450,000		1.00	0.00			0		1.00	0.00		0	0		1.00	0	450,000	
METER SKID, 250 MMSCFD, 1300 PSIG	1.00	1.00	1	EA	0.00	1.00	1.00	0	3,630,000	3,630,000	1.00	3,630,000		1.00	0.00			0		1.00	0.00		0	0		1.00	0	3,630,000	
VERTICAL SCRUBBERS, PROCESS VESSELS, 1440 PSIG MAWP	4.00	1.00	4	EA	0.00	1.00	1.00	0	120,000	120,000	1.00	480,000		1.00	0.00			0		1.00	0.00		0	0		1.00	0	480,000	
GATE VALVE, 20-INCH ANSI 600 W/BETTIS OPERATOR	2.00	1.00	2	EA	0.00	1.00	1.00	0	36,000	36,000	1.00	72,000	9	1.00	18.00	MECH1		0		1.00	0.00		0	0		1.00	0	72,000	
GATE VALVE, 20-INCH ANSI 600 W/MOV OPERATOR	5.00	1.00	5	EA	0.00	1.00	1.00	0	29,300	29,300	1.00	146,500	9	1.00	45.00	MECH1		0		1.00	0.00		0	0		1.00	0	146,500	
GATE VALVE, 20-INCH ANSI 600 W/BEVEL GEAR OPERATOR	4.00	1.00	4	EA	0.00	1.00	1.00	0	24,200	24,200	1.00	96,800	9	1.00	36.00	MECH1		0		1.00	0.00		0	0		1.00	0	96,800	
GATE VALVE, 16-INCH ANSI 600 W/BETTIS OPERATOR	3.00	1.00	3	EA	0.00	1.00	1.00	0	36,000	36,000	1.00	108,000	7	1.00	19.80	MECH1		0		1.00	0.00		0	0		1.00	0	108,000	
GATE VALVE, 16-INCH ANSI 600 W/MOV OPERATOR	13.00	1.00	13	EA	0.00	1.00	1.00	0	19,400	19,400	1.00	252,200	7	1.00	85.80	MECH1		0		1.00	0.00		0	0		1.00	0	252,200	
GATE VALVE, 16-INCH ANSI 600 W/BEVEL GEAR OPERATOR	5.00	1.00	5	EA	0.00	1.00	1.00	0	14,600	14,600	1.00	73,000	7	1.00	33.00	MECH1		0		1.00	0.00		0	0		1.00	0	73,000	
CHECK VALVE, 16-INCH ANSI 600 SWING TYPE	1.00	1.00	1	EA	0.00	1.00	1.00	0	17,000	17,000	1.00	17,000	7	1.00	6.60	MECH1	29.11	192		1.00	0.00		0	0		1.00	0	17,192	
GATE VALVE, 12-INCH ANSI 600 W/MOV OPERATOR	2.00	1.00	2	EA	0.00	1.00	1.00	0	14,700	14,700	1.00	29,400	5	1.00	10.40	MECH1		0		1.00	0.00		0	0		1.00	0	29,400	
GATE VALVE, 12-INCH ANSI 600 W/BEVEL GEAR OPERATOR	8.00	1.00	8	EA	0.00	1.00	1.00	0	11,100	11,100	1.00	88,800	5	1.00	41.60	MECH1		0		1.00	0.00		0	0		1.00	0	88,800	
CHECK VALVE, 12-INCH ANSI 600 SWING TYPE	2.00	1.00	2	EA	0.00	1.00	1.00	0	13,000	13,000	1.00	26,000	5	1.00	10.40	MECH1		0		1.00	0.00		0	0		1.00	0	26,000	
GATE VALVE, 8-INCH ANSI 600 W/BEVEL GEAR OPERATOR	1.00	1.00	1	EA	0.00	1.00	1.00	0	4,800	4,800	1.00	4,800	4	1.00	3.80	MECH1		0		1.00	0.00		0	0		1.00	0	4,800	
GATE VALVE, 12-INCH ANSI 600 FINAL CONTROL ELEMENT	2.00	1.00	2	EA	0.00	1.00	1.00	0	43,800	43,800	1.00	87,600	5	1.00	10.40	MECH1	29.11	303		1.00	0.00		0	0		1.00	0	87,903	
PIPE, 20-INCH DIAM., 0.375 WALL, X-60 (PLANT SLEEPERS)	1.00	1.00	300	LF	0.00	1.00	1.00	0	18	18	1.00	5,310	5	1.00	1,560.00	MECH1	29.11	45,412		1.00	0.00		0	0		1.00	0	50,722	
PIPE, 20-INCH DIAM., 0.375 WALL, X-60 (PLANT SLEEPERS INSULATED)	1.00	1.00	3,240	LF	0.00	1.00	1.00	0	18	18	1.00	57,348	5	1.00	16,848.00	MECH1	29.11	490,445		1.00	0.00		0	0		1.00	0	547,793	
PIPE, 20-INCH DIAM., 0.375 WALL, X-60 (MINE SHAFT INSULATED)	1.00	1.00	6,000	LF	0.00	1.00	1.00	0	18	18	1.00	106,200	5	1.00	31,200.00	MECH1	29.11	908,232		1.00	0.00		0	0		1.00	0	1,014,432	
PIPE, 20-INCH DIAM., 0.375 WALL, X-60 (MINE DISTRUBUTION BARE)	1.00	1.00	3,400	LF	0.00	1.00	1.00	0	18	18	1.00	60,180	5	1.00	17,680.00	MECH1	29.11	514,665		1.00	0.00		0	0		1.00	0	574,845	
PIPE, 12-INCH DIAM., 0.375 WALL, GRADE B (PLANT SLEEPERS BARE)	1.00	1.00	820	LF	0.00	1.00	1.00	0	11	11	1.00	9,184	5	1.00	4,264.00	MECH1	29.11	124,125		1.00	0.00		0	0		1.00	0	133,309	
20" SCH .375 FIELD SHOP BUTTWELD A-53/A-106 CARBON STEEL	1.00	1.00	15	EA	0.00	1.00	1.00	0	0	0	1.00	0	8	1.00	123.00	MECH1	29.11	3,581	0.00	1.00	0.00	0	0	0	0	1.00	0	3,581	
20" SCH .375 FIELD SHOP BUTTWELD A-53/A-106 CARBON STEEL	1.00	1.00	162	EA	0.00	1.00	1.00	0	0	0	1.00	0	8	1.00	1,328.40	MECH1	29.11	38,670	0.00	1.00	0.00	0	0	0	0	1.00	0	38,670	
20" SCH .375 FIELD SHOP BUTTWELD A-53/A-106 CARBON STEEL	1.00	1.00	300	EA	0.00	1.00	1.00	0	0	0	1.00	0	8	1.00	2,460.00	MECH1	29.11	71,611	0.00	1.00	0.00	0	0	0	0	1.00	0	71,611	
20" SCH .375 FIELD SHOP BUTTWELD A-53/A-106 CARBON STEEL	1.00	1.00	170	EA	0.00	1.00	1.00	0	0	0	1.00	0	8	1.00	1,394.00	MECH1	29.11	40,579	0.00	1.00	0.00	0	0	0	0	1.00	0	40,579	
12" SCH .375 FIELD SHOP BUTTWELD A-53/A-106 CARBON STEEL	1.00	1.00	41	EA	0.00	1.00	1.00	0	0	0	1.00	0	5	1.00	217.30	MECH1	29.11	6,326	0.00	1.00	0.00	0	0	0	0	1.00	0	6,326	
12" SCH .375 A-53 CS PIPE RUN, OUTSIDE ON SLEEPERS	1.00	1.00	820	LF	49.56	1.00	1.00	40,639	26	26	1.00	21,074	0	1.00	114.31	MECH1	29.11	3,328	0.00	1.00	0.00	0	0	0	0	1.00	0	24,402	
20" SCH .375 A-53 CS PIPE RUN, OUTSIDE ON SLEEPERS	1.00	1.00	3,240	LF	78.60	1.00	1.00	254,664	59	59	1.00	191,160	0	1.00	608.80	MECH1	29.11	17,722	0.00	1.00	0.00	0	0	0	0	1.00	0	208,882	
20" SCH .375 A-53 CS PIPE RUN, MINE SHAFT	1.00	1.00	6,000	LF	78.60	1.00	1.00	471,600	59	59	1.00	354,000	0	1.00	1,127.40	MECH1	29.11	32,819	0.00	1.00	0.00	0	0	0	0	1.00	0	386,819	
20" SCH .375 A-53 CS PIPE RUN, MINE DISTRIBUTION BARE)	1.00	1.00	3,400	LF	78.60	1.00	1.00	267,240	59	59	1.00	200,600	0	1.00	638.86	MECH1	29.11	18,597	0.00	1.00	0.00	0	0	0	0	1.00	0	219,197	
4" THICK URETHANE INSULATION ON 20" COLD PROCESS PIPE	1.00	1.00	9,240	LF	0.00	1.00	1.00	0	43	43	1.00	395,842	2	1.00	16,632.00	INSU1	23.47	390,353	0.00	1.00	0.00	0	0	0	0	1.00	0	786,195	
MISC. PIPE FITTINGS, AND SPECIAL TOOLS @ 1% OF COMPRESSOR AND PIPING	1.00	1.00	1	LUMP	0.00	1.00	1.00	0	316,459	316,469	1.00	316,469	0	1.00	0.00		0.00	0	0.00	1.00	0.00	0	0	0	0	1.00	0	316,469	
SUBTOTAL REFRIDGEATION SYSTEM																													**31,971,424**
ELECTRICAL AND INSTRUMENTATION EQUIPMENT																													
POWER TRANSFORMER, 3 PH, UTILITY VOLT-480V OIL FILLED 2500 KVA	2.00	1.00	2	EA	0.00	1.00	1.00	0	41,000	41,000	1.00	82,000	105	1.00	210.00	ELEC1	50.88	10,685		1.00	0.00		0	0		1.00	0	92,685	
STANDY GERNERATOR, NATURAL GAS FUELED, 3 PHJ, 60 HZ, 1000 KW, 480V	1.00	1.00	1	EA	0.00	1.00	1.00	0	138,000	138,000	1.00	138,000	220	1.00	220.00	ELEC1	50.88	11,194		1.00	0.00		0	0		1.00	0	149,194	
LOW VOLTAGE MCC, 3PH, 4W, 480V, 3000A	1.00	1.00	1	EA	0.00	1.00	1.00	0	94,700	94,700	1.00	94,700	135	1.00	135.00	ELEC1	32.75	4,421		1.00	0.00		0	0		1.00	0	99,121	
UPS SYSTEM 30 KVA, 3PH, 208/120V	1.00	1.00	1	EA	0.00	1.00	1.00	0	27,300	27,300	1.00	27,300	116	1.00	116.00	ELEC1	50.88	5,902		1.00	0.00		0	0		1.00	0	33,202	
UPS DISTRIBUTION PANEL, SPH, 208V, 225 AMP, 42CKTS	1.00	1.00	1	EA	0.00	1.00	1.00	0	2,470	2,470	1.00	2,470	24	1.00	24.00	ELEC1	32.75	786		1.00	0.00		0	0		1.00	0	3,256	
COMPRESSOR BUILDING LIGHTING 120V, 1PH, 250W, SH, EX	5.00	1.00	5	EA	0.00	1.00	1.00	0	1,930	1,930	1.00	9,650	24	1.00	120.00	ELEC1	32.75	3,930		1.00	0.00		0	0		1.00	0	13,580	
EXTERIOR AND AREA LIGHTING, 30 FT TAPPERED STEEL POLESS W/2 AM BRACKETS	14.00	1.00	14	EA	0.00	1.00	1.00	0	825	825	1.00	11,550	3	1.00	42.00	ELEC1	32.75	1,376		1.00	0.00		0	0		1.00	0	12,926	
EXTERIOR FLOOD LIGHT FIXTURE 120V, 400W. 1PH, MH	10.00	1.00	10	EA	0.00	1.00	1.00	0	1,135	1,135	1.00	11,350	10	1.00	100.00	ELEC1	50.88	5,088		1.00	0.00		0	0		1.00	0	16,438	
COMPRESSOR BUILDING LIGHTINGING PROTECTION	20.00	1.00	20	EA	0.00	1.00	1.00	0	335	335	1.00	6,700	4	1.00	80.00	ELEC1	0.00	0	10,820.00	1.00	216,400.00		0	0		1.00	0	223,100	
ELECTRIC/DIESEL FIRE PORTECTION PUMPS	1.00	1.00	1	LUMP	0.00	1.00	1.00	0		0	1.00	0		1.00	0.00	ELEC1	32.75	0	137,650.00	1.00	137,650.00		0	0		1.00	0	137,650	
SITE AND HOISTS GROUNDING PROTECTIONS SYSTEMS	1.00	1.00	1	LUMP	0.00	1.00	1.00	0		0	1.00	0		1.00	0.00	ELEC1	0.00	0	26,642.00	1.00	26,642.00		0	0		1.00	0	26,642	
COMPRESSOR BUILDING LIGHTING AND HVAC	1.00	1.00	1	LUMP	0.00	1.00	1.00	0		0	1.00	0		1.00	0.00	ELEC1	0.00	0	26,642.00	1.00	26,642.00		0	0		1.00	0	26,642	
ELECTRICAL GATE SYSTEM (PERSONNEL AND VEHICLE)	1.00	1.00	1	LUMP	0.00	1.00	1.00	0		0	1.00	0		1.00	0.00	ELEC1	0.00	0	30,860.00	1.00	30,860.00		0	0		1.00	0	30,860	
POWER DISTRIBUTION CONDUIT SYSTEM (OUTDOOR)	1.00	1.00	1	LUMP	0.00	1.00	1.00	0		0	1.00	0		1.00	0.00	ELEC1	0.00	0	37,968.00	1.00	37,968.00		0	0		1.00	0	37,968	
POWER DISTRIBUTION CONDUIT (INDOOR)	1.00	1.00	1	LUMP	0.00	1.00	1.00	0		0	1.00	0		1.00	0.00	ELEC1	0.00	0	16,000.00	1.00	16,000.00		0	0		1.00	0	16,000	
ELECTRICAL OWER AND INSTRUMENTATION CABLE AND WIRING	1.00	1.00	1	LUMP	0.00	1.00	1.00	0		0	1.00	0		1.00	0.00	ELEC1	0.00	0	46,900.00	1.00	46,900.00		0	0		1.00	0	46,900	
EXPOSED PIPES ELECTRICAL HEAT TRACING SYSTEM	1.00	1.00	1	LUMP	0.00	1.00	1.00	0		0	1.00	0		1.00	0.00	ELEC1	0.00	0	28,340.00	1.00	28,340.00		0	0		1.00	0	28,340	
INSTRUMENT DATA SYSTEM (DSC OR PC-PLC BASED)	1.00	1.00	1	LUMP	0.00	1.00	1.00	0		0	1.00	0		1.00	0.00	ELEC1	0.00	0	42,670.00	1.00	42,670.00		0	0		1.00	0	42,670	
INTRUMENTATION DATA SYSTEM SFOTWARE PROGRAMMING AND SYSTEM	1.00	1.00	1	LUMP	0.00	1.00	1.00	0		0	1.00	0		1.00	0.00	ELEC1	0.00	0	22,300.00	1.00	22,300.00		0	0		1.00	0	22,300	
TRUBINE FLOWMETERS- METER STATION	6.00	1.00	6	EA	0.00	1.00	1.00	0	10,200	10,200	1.00	61,200	36	1.00	216.00	ELEC1	38.70	8,359	76,000.00	1.00	456,000.00		0	0		1.00	0	525,559	
PIPELINE FLOWMETERS-INSERTION ULTRASONIC	3.00	1.00	3	EA	0.00	1.00	1.00	0	14,300	14,300	1.00	42,900	28	1.00	84.00	ELEC1	38.70	3,251	126,000.00	1.00	378,000.00		0	0		1.00	0	424,151	
WHELLHEAD INSTRUMENTATION AND FLOWMETERS	1.00	1.00	1	LUMP	0.00	1.00	1.00	0		0	1.00	0		1.00	0.00	ELEC1	0.00	0	56,400.00	1.00	56,400.00		0	0		1.00	0	56,400	
GAS ANALYZER-CHOMATOGRAPH	1.00	1.00	1	EA	0.00	1.00	1.00	0	47,500	47,500	1.00	47,500	48	1.00	48.00	ELEC1	85.00	4,080		1.00	0.00		0	0		1.00	0	51,580	
MOISTURE IN GAS ANALYZER	1.00	1.00	1	EA	0.00	1.00	1.00	0	12,150	12,150	1.00	12,150	40	1.00	40.00	ELEC1	55.00	2,200		1.00	0.00		0	0		1.00	0	14,350	
SITE AND HOISTS COMMUNICATION SYSTEMS	1.00	1.00	1	LUMP	0.00	1.00	1.00	0		0	1.00	0		1.00	0.00	ELEC1	0.00	0	38,500.00	1.00	38,500.00		0	0		1.00	0	38,500	
CLOSED CIRCUIT TV SECURITY SYSTEM	1.00	1.00	1	LUMP	0.00	1.00	1.00	0		0	1.00	0		1.00	0.00	ELEC1	0.00	0	42,500.00	1.00	42,500.00		0	0		1.00	0	42,500	
PRESSURE AND DIFFENTIAL PRESSURE TANSMITTERS	23.00	1.00	23	EA	0.00	1.00	1.00	0	1,120	1,120	1.00	25,760	4	1.00	92.00	ELEC1	55.00	5,060		1.00	0.00		0	0		1.00	0	30,820	
SUBTOTAL ELECTRICAL AND INSTRUMENTATION EQUIPMENT																													**2,243,333**
COMPRESSOR BUILDING (210-FEET X 50-FEET) AND CONTROL																													
TYPE 3 WAREHOUSE SQUARE FOOT BUILDING COST (COMPRESSOR BUILDING)	1.00	1.00	10,500	SF	0.00	1.00	1.00	0	0	0	1.00	0	0	1.00	0.00	NONE		0	50.00	1.00	525,000.00	0	0	0	0	1.00	0	525,000	
TYPE 3 OFFICE BUILDING SQUARE FOOT BUILDING COST (CONTROL BUILDING)	1.00	1.00	4,000	SF	0.00	1.00	1.00	0	0	0	1.00	0	0	1.00	0.00	NONE		0	82.00	1.00	328,000.00	0	0	0	0	1.00	0	328,000	
REM. GRASS 2" DPT. & SHRUBS AT 10' CTRS, 37,000 SF EST. HR. PROD., GR. 3	1.00	1.00	144,990	SF	0.00	1.00	1.00	0	0	0	1.00	0	0	1.00	0.00	NONE		0	0.01	1.00	1,565.89	0	0	0	0	1.00	0	1,566	
1500 CY, GROUP 3, TOPSOIL STRIPPING AND STOCKPILING	1.00	1.00	8,055	CY	0.00	1.00	1.00	0	0	0	1.00	0	0	1.00	0.00	NONE		0	2.95	1.00	23,762.25	0	0	0	0	1.00	0	23,762	
1500 CY, GROUP 6, REPLACING TOPSOIL	1.00	1.00	8,055	CY	0.00	1.00	1.00	0	0	0	1.00	0	0	1.00	0.00	NONE		0	3.13	1.00	25,212.15	0	0	0	0	1.00	0	25,212	
SUBTOTAL COMPRESSOR BUILDING AND CONTROL BUILDING																													**903,540**
COMPRESSOR BUILDING FOUNDATION AND SLAB																													
6" THICK SAND FILL UNDER SLABS ON GRADE .01852 CY/SF	1.00	1.00	10,500	SF	0.00	1.00	1.00	0	0	0	1.00	0	0	1.00	0.00	NONE		0	0.82	1.00	8,568.00	0	0	0	0	1.00	0	8,568	
12" THICK CONCRETE FOR NON-FORMED SLABS ON GRADE .0371 CY/SF	1.00	1.00	389	CY	0.00	1.00	1.00	0	55	55	1.00	21,389	0	1.00	167.61	PLUNC	21.16	3,547	0.00	1.00	0.00	0	0	0	0	1.00	0	24,936	
MECH PLACING OF 15000 CYS OR MORE OF CONC FOR SLABS ON GRADE	1.00	1.00	389	CY	0.00	1.00	1.00	0	0	0	1.00	0	0	1.00	0.00	NONE		0	2.90	1.00	1,128.10	0	0	0	0	1.00	0	1,128	
#3 .375" STR BAR BTM LAYER A615 GR 60 REINF STL FOR SMOG, 0.376#/LF	1.00	1.00	16,582	LB	0.00	1.00	1.00	0	0	0	1.00	4,560	0	1.00	116.07	IRON1	27.23	3,161	0.00	1.00	0.00	0	0	0	0	1.00	0	7,721	
#3 .375" STR BAR TOP LAYER A615 GR 60 REINF STL FOR SMOG, 0.376#/LF	1.00	1.00	16,581	LB	0.00	1.00	1.00	0	0	0	1.00	4,560	0	1.00	140.94	IRON1	27.23	3,838	0.00	1.00	0.00	0	0	0	0	1.00	0	8,398	
8'H x 20' CLEAR OPENING GALVANIZED CHAIN LINK DOUBLE DRIVE GATE	1.00	1.00	1	EA	0.00	1.00	1.00	0	0	0	1.00	0	0	1.00	0.00	NONE		0	650.00	1.00	650.00	0	0	0	0	1.00	0	650	
8' #2 MESH, #9 WIRE VINYL COATED CHAIN LINK FENCE, NO GATES	1.00	1.00	1,526	LF	0.00	1.00	1.00	0	0	0	1.00	0	0	1.00	0.00	NONE		0	10.92	1.00	16,663.92	0	0	0	0	1.00	0	16,664	

	BASE	METRIC/	QUANITY	UNIT	UNIT	M/I	WEIGHT	TOTAL	UNIT	CURRENCY	MATL	TOTAL	UNIT	HOURS	TOTAL	CREW	LABOR	TOTAL	UNIT	SUBCON	TOTAL	UNIT	CURRENCY	TOTAL	UNIT	OTHER	TOTAL	TOTAL	SUBTOTALS
	QUANITY	IMPERIAL			WEIGH	WEIGHT	ADJUS	WEIGHT	MATL	MATERIAL	ADJUST.	MATL	HOURS	ADJUST	HOURS		RATE	LABOR	SUBCON	ADJUST	SUBCON	EQUIP	EQUIP	EQUIP	OTHER	ADJUST	OTHER		
SUBTOTAL COMPRESSOR BUILDING FOUNDATION AND SLAB																													**68,064**
CONCRETE SUPPORTS FOR COMPRESSOR STATION PIPING																													
24" DIA.x .375" A-COATED SONOTUBE FORM FOR RD COLUMN/PIER	600.00	1.00	600	LF	0.00	1.00	1.00	0	8	8	1.00	4,794	0	1.00	139.20	CARP1	41.65	5,797	0.00	1.68	0.00	0	0	0	0	1.00	0	10,591	
#3 .375" SPRRAL FOR RD COL & PIER USING SONOTUBE, 0.376#/LF	225.00	1.00	225	LB	0.00	1.00	1.00	0	0	0	1.00	59	0	1.00	2.03	IRON1	42.98	87	0.00	1.68	0.00	0	0	0	0	1.00	0	146	
24" DIA.x .375" CONCRETE FOR RD COLUMN/PIER .1164 CY/LF	69.84	1.00	70	CY	0.00	1.00	1.00	0	59	59	1.00	4,086	2	1.00	116.49	PLSUC	41.85	4,875	0.00	1.68	0.00	0	0	0	0	1.00	0	8,961	
SUBTOTAL CONCRETE SUPPORTS FOR COMPRESSOR STATION																													**19,698**
CONTROL BUILDING FOUNDATION																													
4" THICK SAND FILL UNDER SLABS ON GRADE .01235 CY/SF	2,400.00	1.00	2,400	SF	0.00	1.00	1.00	0	0	0	1.00	0	0	1.00	0.00	NONE		0	0.59	1.68	2,381.24	0	0	0	0	1.00	0	2,381	
#3 .375" DOWELS A615 GR 60 REINFORCING STEEL FOR SOG, 0.376#/LF	2,400.00	1.00	2,400	LB	0.00	1.00	1.00	0	0	0	1.00	720	0	1.00	18.00	IRON1	42.98	774	0.00	1.68	0.00	0	0	0	0	1.00	0	1,494	
12" EDGE FORMS FOR SLABS ON GRADE	200.00	1.00	200	LF	0.00	1.00	1.00	0	0	0	1.00	60	0	1.00	24.00	CARP1	41.65	1,000	0.00	1.68	0.00	0	0	0	0	1.00	0	1,060	
MECH PLACING OF UNDER 500 CYS OF CONC FOR SLABS ON GRADE	88.89	1.00	89	CY	0.00	1.00	1.00	0	0	0	1.00	0	0	1.00	0.00	NONE		0	10.40	1.68	1,557.25	0	0	0	0	1.00	0	1,557	
20' x 18" SIDE FORM,1 STY BLD CONT INTEGAL FT TW/ 6" TW SLABS ON GR 2 BF/LF	180.00	1.00	180	LF	0.00	1.00	1.00	0	1	1	1.00	95	0	1.00	21.60	CARP1	41.65	900	0.00	1.68	0.00	0	0	0	0	1.00	0	995	
12" THICK CONCRETE FOR NON-FORMED SLABS ON GRADE .0371 CY/SF	192.22	1.00	192	CY	0.00	1.00	1.00	0	55	55	1.00	10,572	0	1.00	82.85	PLUNC	41.85	3,467	0.00	1.68	0.00	0	0	0	0	1.00	0	14,039	
2" x 5,000 - 9,999 SF ASPHALT CONCRETE ON 4" AGGREGATE BASE (ROADS)	1.00	1.00	40,000	SF	0.00	1.00	1.00	0	0	0	1.00	0	0	1.00	0.00	NONE		0	1.96	1.68	131,729.62	0	0	0	0	1.00	0	131,730	
SUBTOTAL CONTROL BUILDING FOUNDATION																													**153,256**
MECNANICAL SEPERATORS FOUNDATION																													
4" THICK SAND FILL UNDER SLABS ON GRADE .01235 CY/SF	864.00	1.00	864	SF	0.00	1.00	1.00	0	0	0	1.00	0	0	1.00	0.00	NONE		0	0.59	1.68	857.25	0	0	0	0	1.00	0	857	
#3 .375" DOWELS A615 GR 60 REINFORCING STEEL FOR SOG, 0.376#/LF	864.00	1.00	864	LB	0.00	1.00	1.00	0	0	0	1.00	259	0	1.00	6.48	IRON1	42.98	279	0.00	1.68	0.00	0	0	0	0	1.00	0	538	
12" EDGE FORMS FOR SLABS ON GRADE	118.00	1.00	118	LF	0.00	1.00	1.00	0	0	0	1.00	35	0	1.00	14.16	CARP1	41.65	590	0.00	1.68	0.00	0	0	0	0	1.00	0	625	
MECH PLACING OF UNDER 500 CYS OF CONC FOR SLABS ON GRADE	32.00	1.00	32	CY	0.00	1.00	1.00	0	0	0	1.00	0	0	1.00	0.00	NONE		0	10.40	1.68	560.61	0	0	0	0	1.00	0	561	
20' x 18" SIDE FORM,1 STY BLD CONT INTEGAL FT TW/ 6" TW SLABS ON GR 2 BF/LF	118.00	1.00	118	LF	0.00	1.00	1.00	0	1	1	1.00	63	0	1.00	14.16	CARP1	41.65	590	0.00	1.68	0.00	0	0	0	0	1.00	0	652	
12" THICK CONCRETE FOR NON-FORMED SLABS ON GRADE .0371 CY/SF	32.00	1.00	32	CY	0.00	1.00	1.00	0	55	55	1.00	1,760	0	1.00	13.79	PLUNC	41.85	577	0.00	1.68	0.00	0	0	0	0	1.00	0	2,337	
SUBTOTAL MECNANICAL SEPERATORS FOUNDATION																													**5,570**
MOLE SEIVES FOUNDATIONS																													
4" THICK SAND FILL UNDER SLABS ON GRADE .01235 CY/SF	640.00	1.00	640	SF	0.00	1.00	1.00	0	0	0	1.00	0	0	1.00	0.00	NONE		0	0.59	1.68	635.00	0	0	0	0	1.00	0	635	
#3 .375" DOWELS A615 GR 60 REINFORCING STEEL FOR SOG, 0.376#/LF	640.00	1.00	640	LB	0.00	1.00	1.00	0	0	0	1.00	192	0	1.00	4.80	IRON1	42.98	206	0.00	1.68	0.00	0	0	0	0	1.00	0	398	
12" EDGE FORMS FOR SLABS ON GRADE	168.00	1.00	168	LF	0.00	1.00	1.00	0	0	0	1.00	50	0	1.00	20.16	CARP1	41.65	840	0.00	1.68	0.00	0	0	0	0	1.00	0	890	
MECH PLACING OF UNDER 500 CYS OF CONC FOR SLABS ON GRADE	23.70	1.00	24	CY	0.00	1.00	1.00	0	0	0	1.00	0	0	1.00	0.00	NONE		0	10.40	1.68	415.27	0	0	0	0	1.00	0	415	
20' x 18" SIDE FORM,1 STY BLD CONT INTEGAL FT TW/ 6" TW SLABS ON GR 2 BF/LF	168.00	1.00	168	LF	0.00	1.00	1.00	0	1	1	1.00	89	0	1.00	20.16	CARP1	41.65	840	0.00	1.68	0.00	0	0	0	0	1.00	0	929	
12" THICK CONCRETE FOR NON-FORMED SLABS ON GRADE .0371 CY/SF	23.70	1.00	24	CY	0.00	1.00	1.00	0	55	55	1.00	1,304	0	1.00	10.22	PLUNC	41.85	428	0.00	1.68	0.00	0	0	0	0	1.00	0	1,731	
SUBTOTAL MOLE SEIVES FOUNDATIONS																													**4,999**
PRESSURE REDUCING STATION FOUNDATIONS																													
4" THICK SAND FILL UNDER SLABS ON GRADE .01235 CY/SF	600.00	1.00	600	SF	0.00	1.00	1.00	0	0	0	1.00	0	0	1.00	0.00	NONE		0	0.59	1.68	595.31	0	0	0	0	1.00	0	595	
#3 .375" DOWELS A615 GR 60 REINFORCING STEEL FOR SOG, 0.376#/LF	600.00	1.00	600	LB	0.00	1.00	1.00	0	0	0	1.00	180	0	1.00	4.50	IRON1	42.98	193	0.00	1.68	0.00	0	0	0	0	1.00	0	373	
12" EDGE FORMS FOR SLABS ON GRADE	110.00	1.00	110	LF	0.00	1.00	1.00	0	0	0	1.00	33	0	1.00	13.20	CARP1	41.65	550	0.00	1.68	0.00	0	0	0	0	1.00	0	583	
MECH PLACING OF UNDER 500 CYS OF CONC FOR SLABS ON GRADE	22.22	1.00	22	CY	0.00	1.00	1.00	0	0	0	1.00	0	0	1.00	0.00	NONE		0	10.40	1.68	389.31	0	0	0	0	1.00	0	389	
20' x 18" SIDE FORM,1 STY BLD CONT INTEGAL FT TW/ 6" TW SLABS ON GR 2 BF/LF	110.00	1.00	110	LF	0.00	1.00	1.00	0	1	1	1.00	58	0	1.00	13.20	CARP1	41.65	550	0.00	1.68	0.00	0	0	0	0	1.00	0	608	
12" THICK CONCRETE FOR NON-FORMED SLABS ON GRADE .0371 CY/SF	22.22	1.00	22	CY	0.00	1.00	1.00	0	55	55	1.00	1,222	0	1.00	9.58	PLUNC	41.85	401	0.00	1.68	0.00	0	0	0	0	1.00	0	1,623	
SUBTOTAL PRESSURE REDUCING STATION FOUNDATIONS																													**4,172**
GAS STORAGE FACILITY FINAL DESIGN (EIGHT MONTHS DURATION)																													
MECHANICAL ENGINEER	2.00	1.00	2	MANHOUR		1.00	1.00	0	0	0	1.00	0	1,280	1.00	2,560.00		82.60	211,456		1.00	0.00		0	0	0	1.00	0	211,456	
CIVIL ENGINEER	1.00	1.00	1	MANHOUR		1.00	1.00	0	0	0	1.00	0	1,280	1.00	1,280.00		82.60	105,728		1.00	0.00		0	0	0	1.00	0	105,728	
ELECTRICAL ENGINEER	2.00	1.00	2	MANHOUR		1.00	1.00	0	0	0	1.00	0	1,280	1.00	2,560.00		82.60	211,456		1.00	0.00		0	0	0	1.00	0	211,456	
MINING ENGINEER	1.00	1.00	1	MANHOUR		1.00	1.00	0	0	0	1.00	0	1,280	1.00	1,280.00		82.60	105,728		1.00	0.00		0	0	0	1.00	0	105,728	
CHEMICAL ENGINEER	1.00	1.00	1	MANHOUR		1.00	1.00	0	0	0	1.00	0	1,280	1.00	1,280.00		82.60	105,728		1.00	0.00		0	0	0	1.00	0	105,728	
CAD OPERATOR	1.00	1.00	1	MANHOUR		1.00	1.00	0		0	1.00	0	1,280	1.00	1,280.00		51.92	66,458		1.00	0.00		0	0		1.00	0	66,458	
PROCUREMENT MANAGER	1.00	1.00	1	MANHOUR		1.00	1.00	0	0	0	1.00	0	1,280	1.00	1,280.00		82.60	105,728		1.00	0.00		0	0		1.00	0	105,728	
PROJECT COST AND SCHEDULING	1.00	1.00	1	MANHOUR		1.00	1.00	0	0	0	1.00	0	1,280	1.00	1,280.00		63.72	81,562		1.00	0.00		0	0		1.00	0	81,562	
PROJECT SECRETARY	1.00	1.00	1	MANHOUR		1.00	1.00	0	0	0	1.00	0	1,280	1.00	1,280.00		28.32	36,250		1.00	0.00		0	0		1.00	0	36,250	
PRCUREMENT CLERK	1.00	1.00	1	MANHOUR		1.00	1.00	0	0	0	1.00	0	1,280	1.00	1,280.00		28.32	36,250		1.00	0.00		0	0		1.00	0	36,250	
OFFICE PHONE	6.00	1.00	6	PER MONTH		1.00	1.00	0	0	0	1.00	0	500	1.00	3,000.00		0.00	0	500.00	1.00	3,000.00		0	0		1.00	0	3,000	
TRAVEL AND OVERNIGHT	5.00	1.00	5	EACH		1.00	1.00	0	0	0	1.00	0	1,500	1.00	7,500.00		0.00	0	1,500.00	1.00	7,500.00		0	0		1.00	0	7,500	
OFFICE SUPPLIES	5.00	1.00	5	PER MONTH		1.00	1.00	0		0	1.00	0	300	1.00	1,500.00		0.00	0	300.00	1.00	1,500.00		0	0		1.00	0	1,500	
SUBTOTAL FINAL DESIGN																													**1,078,342**
GAS STORAGE FACILITY CONSTRUCTION AND COMMISIONING (50	1.00	1.00	1	MANHOUR		1.00	1.00	0	0	0	1.00	0	8,000	1.00	8,000.00		82.60	660,800		1.00	0.00		0	0		1.00	0	660,800	
FIELD SUPERINTENDENT	1.00	1.00	1	MANHOUR		1.00	1.00	0	0	0	1.00	0	8,000	1.00	8,000.00		82.60	660,800		1.00	0.00		0	0		1.00	0	660,800	
FIELD SUPERINTENDENT ASSISTANT	1.00	1.00	1	MANHOUR		1.00	1.00	0	0	0	1.00	0	8,000	1.00	8,000.00		82.60	660,800		1.00	0.00		0	0		1.00	0	660,800	
FIELD MINING ENGINEER	1.00	1.00	1	MANHOUR		1.00	1.00	0	0	0	1.00	0	8,000	1.00	8,000.00		82.60	660,800		1.00	0.00		0	0		1.00	0	660,800	
FIELD OFFICE CLERK	1.00	1.00	1	MANHOUR		1.00	1.00	0	0	0	1.00	0	8,000	1.00	8,000.00		82.60	660,800		1.00	0.00		0	0		1.00	0	660,800	
FIELD INVENTORY CLERK	1.00	1.00	1	MANHOUR		1.00	1.00	0	0	0	1.00	0	8,000	1.00	8,000.00		82.60	660,800		1.00	0.00		0	0		1.00	0	660,800	
CONSTRUCTION INSPECTOR	1.00	1.00	1	MANHOUR		1.00	1.00	0	0	0	1.00	0	8,000	1.00	8,000.00		82.60	660,800		1.00	0.00		0	0		1.00	0	660,800	
FIELD OFFICE PHONE	50.00	1.00	50	PER MONTH		1.00	1.00	0	0	0	1.00	0	0	1.00	0.00		0.00	0	500.00	1.00	25,000.00		0	0		1.00	0	25,000	
TRAVEL AND OVERNIGHT	1,500.00	1.00	1,500	PER DAY		1.00	1.00	0	0	0	1.00	0	0	1.00	0.00		0.00	0	100.00	1.00	150,000.00		0	0		1.00	0	150,000	
FIELD OFFICE SUPPLIES	50.00	1.00	50	PER MONTH		1.00	1.00	0	0	0	1.00	0	0	1.00	0.00		0.00	0	300.00	1.00	15,000.00		0	0		1.00	0	15,000	
SUBTOTAL CONSTRUCTION SUPERVISION																													**4,815,600**
																													153,614,207

REFERENCES

REFERENCES FOR SECTION 8 GEOMECHANICAL

Abel, J. F., J. E. Dowis, and D. P. Richards, 1979. "Concrete Shaft Lining Design," *Proceedings, 20th U.S. Symposium on Rock Mechanics*, University of Texas-Austin, Austin, TX, June 4-6, Center for Earth Sciences and Engineering, University of Texas-Austin, Austin, TX, pp. 627–633.

Barton, N., 1976. "Recent Experiences With the Q-System of Tunnel Support Design," *Proceedings, Symposium on Exploration for Rock Engineering*, Johannesburg, Vol. 1, pp. 107-117.

Barton, N., R. Lien, and J. Lunde, 1974. "Engineering Classification of Rock Masses for the Design of Tunnel Support," *Rock Mechanics*, Vol. 6, pp. 189–236.

Barton, N., T. L. By, P. Chryssanthakis, L. Tunbridge, J. Kristiansen, F. Løset, R. K. Bhasin, H. Westerdahl, and G. Vik, 1994. "Predicted and Measured Performance of the 62 m Span Norwegian Olympic Ice Hockey Cavern at Gjøvik,"*International Journal of Rock Mechanics and Mining Science and Geomechanics Abstracts*, Vol. 31, No. 6, pp. 617–641.

Bieniawski, Z. T., 1976. "Rock Mass Classification in Rock Engineering," *Proceedings, Symposium on Exploration for Rock Engineering*, Johannesburg, Vol. 1, pp. 97–106.

Callahan, G. D., A. F. Fossum, and D. K. Svalstad, 1989. *Documentation of **SPECTROM-32**: A Finite Element Thermomechanical Stress Analysis Program*, DOE/CH/10378-2, prepared by RE/SPEC Inc., Rapid City, SD, for the U. S. Department of Energy, Chicago Operations Office, Argonne, IL, Vol. I and II.

Carslaw, H. S. and J.C. Jaeger, 1959. *Conduction of Heat in Solids*, 2nd Edition, Oxford University Press, Walton Street, Oxford, United Kingdom.

Hoek, E., 1979. "The Role of Modeling in the Design of Nuclear Waste Repositories – The Design Engineer's Viewpoint," *Proceedings, Workshop on Thermomechanical Modeling for a Hardrock Waste Facility*, UCAR 10043, Lawrence Livermore Laboratories, Lawrence, CA, pp. 33–43.

Hoek, E. and E. T. Brown, 1980. "Underground Excavations in Rock," *The Institution of Mining and Metallurgy*, London.

Kuriyagawa, M., I. Matsunaga, N. Kinoshita, and K. Hibi, 1977. "Rock Behavior of Underground Cavern With the Storage of Cryogenic Liquified Gas," *Subsurface Space (Rockstore 80)*, S. Magnus Bergman (ed.), Pergamon Press, New York, NY, pp. 665–672.

Lama, R. D. and V. S. Vutukuri, 1978. *Handbook on Mechanical Properties of Rocks*, Vol. IV., Trans Tech Publications, Clausthal, Germany.

Lindner, E. N. and J. A. Halpern, 1978. "In Situ Stress in North America: A Compilation," *International Journal of Rock Mechanics and Geomechanical Abstracts*, Vol. 15, pp. 183–203.

Mirza, M., 1998. *Rock Mechanics*, letter to J. L. Ratigan, RE/SPEC Inc., Rapid City, SD, from PB-KBB Inc., Houston, TX, February 13.

Ostrowski, W. J. S., 1972. "Design Considerations for Modern Shaft Lining," *Transactions of the Canadian Institute of Mining and Metallurgy*, Vol. LXXV, pp. 184–198.

PB-KBB Inc., 1997. *Literature Search for Selecting Target Areas — Task 1*, report to Federal Energy Technology Center, Houston, TX, December 24.

Richards, D. P. and J. F. Abel, 1981. "Shaft Lining Design in Rock," *Transactions of AIME,* Vol. 270, pp. 1801–1805.

Selmer-Olsen, R. and E. Broch, 1977. "General Design Procedure for Underground Openings in Norway," *Storage in Excavated Caverns (Rockstore 77)*, S. Bergman (ed.), Vol. 2, Pergamon Press, Elmsford, NY, pp. 219–226.

Svalstad, D. K., 1989. *Documentation of **SPECTROM-41**: A Finite Element Heat Transfer Analysis Program*, DOE/CH/10378-1, prepared by RE/SPEC Inc., Rapid City, SD, for the U.S. Department of Energy, Chicago Operations Office, Argonne, IL.

University of Karlsruhe, 1998. *World Stress Map*, on the Internet at http://www-gpi.physik.uni-lar;srije.de/wsm/.

Zoback, M. L. and M. Zoback, 1980. "State of Stress in the Conterminous United States," *Journal of Geophysical Research*, Vol. 85, pp. 6113–6156.

REFERENCES FOR COOLING LOAD CALCULATIONS (SECTION 8)

Carslaw, H. W. and J. C. Jaeger, 1959. *Conduction of Heat in Solids*, 2nd Edition, Oxford University Press, Walton Street, Oxford, United Kingdom.

Coker, A. K., 1993. ``Program Calculates Z-Factor for Natural Gas," *Oil & Gas Journal*, pp. 74 75.

PB-KBB Inc., 1998. Personal communication with PB-KBB Inc., Houston, TX.

Svalstad, D. K., 1989. *Documentation of SPECTROM-41: A Finite Element Heat Transfer Analysis Program*, DOE/CH/10378-1, prepared by RE/SPEC Inc., Rapid City, SD, for the U.S. Department of Energy, Chicago Operations Office, Argonne, IL.

Van Wylen, G. J. and R. E. Sonntag, 1978. *Fundamentals of Classical Thermodynamics*, 2nd Edition, John Wiley & Sons, New York, NY.

Chilled Gas Storage in Mined Caverns Workshops

November 3, 1998 — Houston, Texas
November 5, 1998 — Pittsburgh, Pennsylvania

As part of the Department of Energy's Federal Energy Technology Center (FETC) Advanced Natural Gas Storage Concepts program, PB-KBB Inc. of Houston, Texas, completed an engineering and economic evaluation of storing chilled natural gas in a conventionally mined hard rock cavern.

FETC sponsored two technology transfer workshops to present the design, construction, projected operating costs, and other technical aspects of storing chilled natural gas in a 5 billion cubic foot (Bcf), mined, rock cavern facility. Four presentations from the workshops are available in Adobe Acrobat portable document format (PDF) below. To view the presentations, click on the titles.

Welcome, Project Background, and Economic Analysis — Roger Schalge, PB-KBB Inc.

DOE's Advanced Natural Gas Storage Concepts Program Description — Gary Sames, Federal Energy Technology Center

Mined Gas Storage Concepts and Site Selection — Bruce Russell, PB-KBB Inc.

Surface Facilities Design — Walter J. Swartz, PB-KBB Inc.

Chilled Gas Storage In Mined Caverns Work Shop

THE DEPARTMENT OF ENERGY AND PB-KBB INC.

WELCOMES AND THANKS YOU FOR COMING

PRESENTATION OF PROJECT BACKGOUND, OUTLINE, RESULTS

- Roger Schalge
- Bachelor of Science Degree in Mechanical Engineering
- Polytechnic Institute of Brooklyn
- Graduated 1965
- Employed by PB-KBB inc. Since 1978 (20 years)
- Manager of Projects
- Member of SPE and ASME
- Member of Mechanical Engineers National Honor Society

Doe Advanced Natural Gas Storage Concepts Program

CHILLED GAS STORAGE IN MINED ROCK CAVERNS

Technology Transfer

PB-KBB INC.
11757 KATY FREEWAY
HOUSTON, TEXAS
281 589-5833

DEPARTMENT OF ENERGY
FEDERAL ENERGY
TECHNOLOGY CENTER
MORGANTOWN, WV

Department Of Energy Representative

- Mr. Gary Sames
- Project Manager
- Chilled gas storage in mined caverns
- Geologist
- DOE’s Advanced Natural Gas Storage Concepts program description

PB-KBB Representative And Speaker

- Mr. Bruce Russell
- Chief Geologist
- Professional degree in Geological Engineering
- Colorado School of Mines, 1958
- Society of Mining Engineers of AIME
- Employed by PB-KBB since 1972 (26 years)
- Responsible for geological investigation of underground storage caverns
- Has selected sites for many mined storage caverns
- Bruce will present mined gas storage concepts and site selection

PB-KBB Representative And Speaker

- Mr. Walter (Wally) J. Swartz
- Manager of Storage Operations
- B.S. In Chemical Engineering
- University of Detroit, 1973
- Master of Engineering
- University of Detroit, 1974
- Employed by PB-KBB since 1997
- Previously Assistant Facilities Manager - Diamond Shamrock Mount Belvieu Storage Facility
  - 30 salt dome storage caverns and surface facilities
- Wally will present surface facilities design

PB-KBB FACILITATOR

- Mr. Dan Tolleson
- Business Development Manager
- Employed by PB-KBB since 1989
- Dan will direct discussion groups at the completion of the presentation

WORK SHOP ORGANIZATION

- Miss Ginny Wetzel
- Ginny was the publisher for the brochure, prepared the Work Shop programs, arranged the accommodation, meals, travel, and everything else that matters.
- Ginny will be available the rest of the day to assist

PARTICIPATING SUBCONTRACTORS

- Merimack Energy -- Market Analysis
- Frontier-Kemper -- Mining Contractor, Construct-Ability and Cost Estimating
- RE/Spec -- Rock Mechanics and Mine Thermodynamics
- Department of Energy -- Program Management

Doe Advanced Natural Gas Storage Concepts Program
Next Speaker - Gary Sames

CHILLED GAS STORAGE IN MINED ROCK CAVERNS

Technology Transfer

PB-KBB INC.
11757 KATY FREEWAY
HOUSTON, TEXAS
281 589-5833

DEPARTMENT OF ENERGY
FEDERAL ENERGY
TECHNOLOGY CENTER
MORGANTOWN, WV

PROJECT OBJECTIVES AND OVERVIEW

- Provide storage that is competitive with alternative available high deliverable storage methods
- Available alternatives are salt cavern storage and LNG
- Provide natural gas storage with multiple cycles per year
- Provide high deliverability
- DOE identified five areas that do not have favorable geological conditions of storage such as salt, depleted gas fields, and aquifers
- The areas were New England, Mid-Atlantic (NY/NJ), South Atlantic (DL/MD/VA) South East Atlantic (NC/SC/GA), and the Pacific Northwest (WA/OR)
- Of the five, one was selected for the conceptual design based on pipelines interconnects and future market growth
- The area selected was Howard and Montgomery Counties, Maryland
- The area is near Baltimore and Washington, D.C.

PROJECT SCOPE OF WORK - MINING

- Select area for mined storage cavern
- Conceptual design of cavern and access shafts
- Rock Mechanics evaluation of mine openings and shaft
- Thermodynamics evaluation of stored gas
- Effect of temperature on mined cavern stability
- Conceptual design of surface facilities such as refrigeration equipment, compressor station, and ancillary equipment
- Prepare conceptual design drawings
- Prepare cost and schedule for complete facility
- Complete a final report on all activities
- Conduct Technology Transfer to industry via Work Shops
- The scope did not include a financial model, return on investment

PROJECT CONCEPT

- Chilling natural gas increase it's density
- The increased density decrease the spatial volume required to storage a cubic foot gas
- Natural gas compressibility decrease to a minimum at temperatures of about -40 ^{o} F and 1,800 psia.
- The Z factor, gas compressibility, at the above conditions is equal to about , Z = 0.5053
- This factor in combination with the reduced temperature can reduce the mined cavern spatial volume by up to 50 %
- Gas has already stored in mined cavern
- PB-KBB has constructed about 80 mined caverns for the storage of LPG which is a combination of vapor and liquid

PROJECTED MARKET AREA STORAGE REQUIREMENTS

Table 2-2
1994 Edition of the Baseline Projection

	New Peaking/Market Area Storage Needs, 2010 (1) (MMCFD)	New Annual Delivery Capacity Needs, 2010 (MMCFD)	Planned or Completed Pipeline & Expansion Projects, 1994-1997 (2) (MMCFD)	Net Requirement (MMCFD)
New England (ME/VT/NH/MA/CT/RI)	269	1,130	978	421
Mid Atlantic (NY/NJ)	1,412	1,158	2,650	(80)
South Atlantic (DL/MD/VA)	450	803	272	981
South Atlantic (NC/SC/GA)	1,190	688	11,197	681
Pacific Northwest (WA/OR/ID)	401	366	695	73

Note: (1) Assumed “high bound” on peak shaving
(2) DOE/EIA Natural Gas 1996 Issues and Trends (December, 1995) and in-house data.

PROJECTED MARKET AREA STORAGE REQUIREMENTS

Table 2-1
Summary of 2010 Peaking and Market Area Gas Storage Requirements of Selected Regions of the US (1994)

Region	Peaking/Market Area Storage Needs (MMCF/day)
New England	269
Mid Atlantic (NY/NJ)	1,352
South Atlantic (DL/MD/VA)	450
South Atlantic (NC/SC/GA)	1,190
Pacific Northwest (WA/OR)	401

Source: GRI Topical Report – Future Seasonal Natural Gas Loads and Gas Delivery Capacity Requirements in the Lower 48 United States (1/94)

A TYPICAL MINE DRIFT

TYPICAL MINED CAVERN DRIFT OR TUNNEL

A TYPICAL MINED CAVERN DRIFT OF TUNNEL

A TYPICAL MINED CAVERN DRIFT OR TUNNEL

ADVANTAGES OF Z FACTOR AND TEMPERATURE

- Using the equation of state (Perfect Gas Law):
- **$pV = n*Z*R*T$**
  - Where:
  - p = pressure in psia
  - V = Volume in cubic feet
  - n = moles of gas
  - Z = gas compressibility
  - R = Universal gas constant (10.73)
  - T = Temperature in degrees Rankine
- Substitution using Charles and Boyles Law results in:
- **$V_{std} = V_c * [P_c / (T_c * Z_c)] * (T_{std} * Z_{std}) / p_{std}$**
  - Where:
  - V_{std} = Standard cubic feet of gas in storage
  - V_c = Cavern volume in cubic feet
  - P_c = Cavern gas pressure in pisa
  - T_c = Cavern temperature in degrees Rankine
  - Z_c = Cavern gas compressibility at cavern temperature and
  - T_{std} , Z_{std}, and p_{std} are condition a atmospheric conditions; constants

ADVANTAGE OF Z FACTOR AND TEMPERATURE

- The term (T_{std} * Z_{std}) / p_{std} is a constant; C_{std} = 35.3
- Therefore, to simplify :
- **$V_{std} = V_c * [p_c / (T_c * Z_c)] * C_{std}$**
- The variables that can be manipulated to increase V_{std} are:
- V_c ,cavern volume, p_c ,cavern pressure, and T_c ,cavern gas temperature
- Any increase in the cavern pressure p_c is limited by geology for a mined cavern to the hydrostatic head or possible advantages of chilling the gas to be discussed later
- Increasing V_c is related to economic of construction and also depth; the deeper the cavern the higher the cost
- Since Z_c and T_c are in the denominator of the equation any decrease in these values increase V_{std}
- As an example, if T_c for a normal mined storage cavern is
  - 150º F (610 º R) then **Z_c = 0.9046**,
  - giving **$p_c / (T_c * Z_c) = p_c * 0.0018$**
- Reducing T_c to
  - -20 º F (440 º R) makes **Z_c = 0.6151,**
  - giving; **$p_c / (T_c * Z_c) = p_c * 0.0037$**
- **0.0037 / .0018 = 2.0556, increases V_{std} by a factor of 2.0556**

PROJECT CONCEPT BASED ON TEMPERATURE AND COMPRESSIBILITY

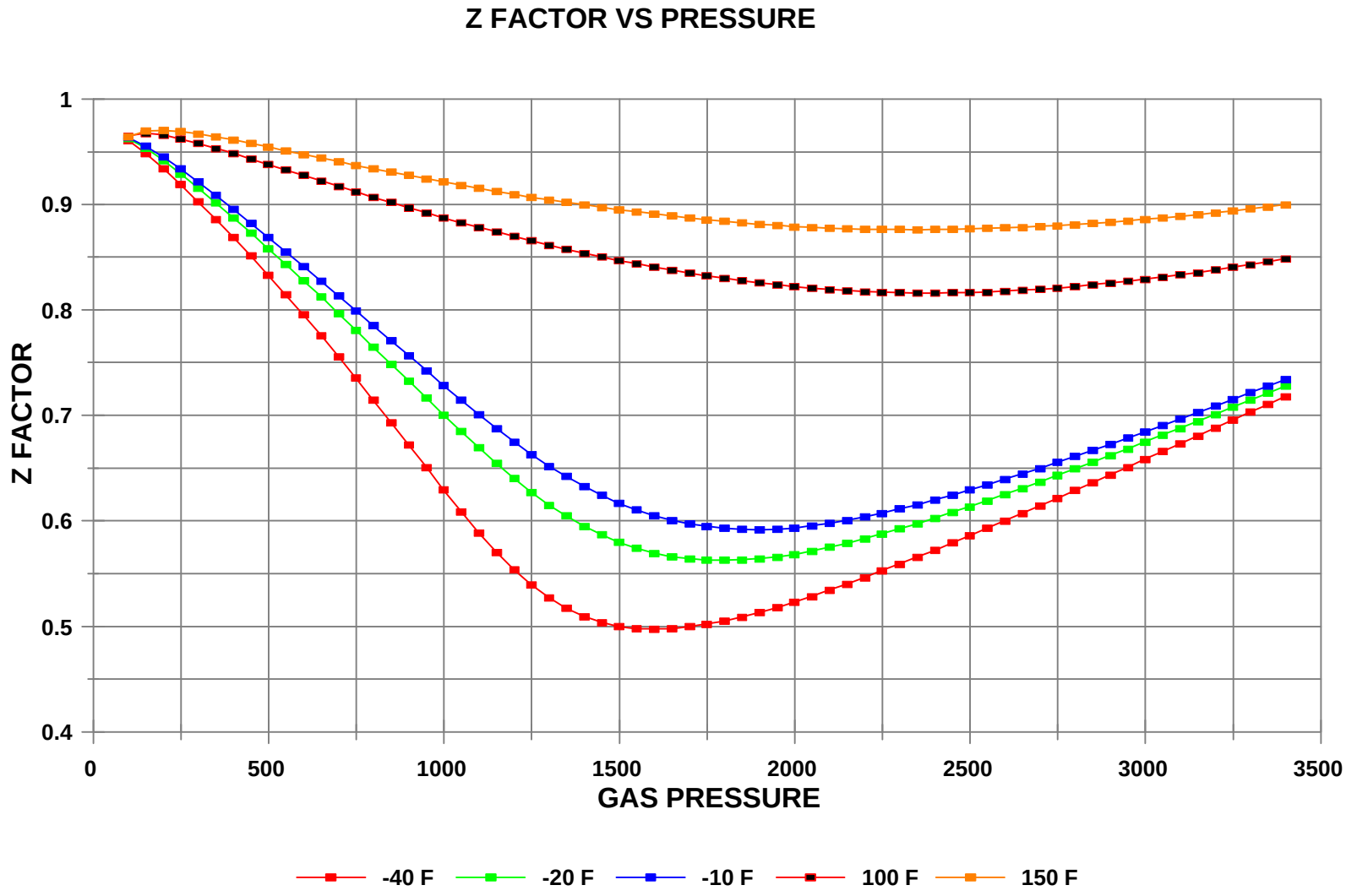

FIGURE 2.0

GRAPH OF GAS VOLUME VS PRESSURE

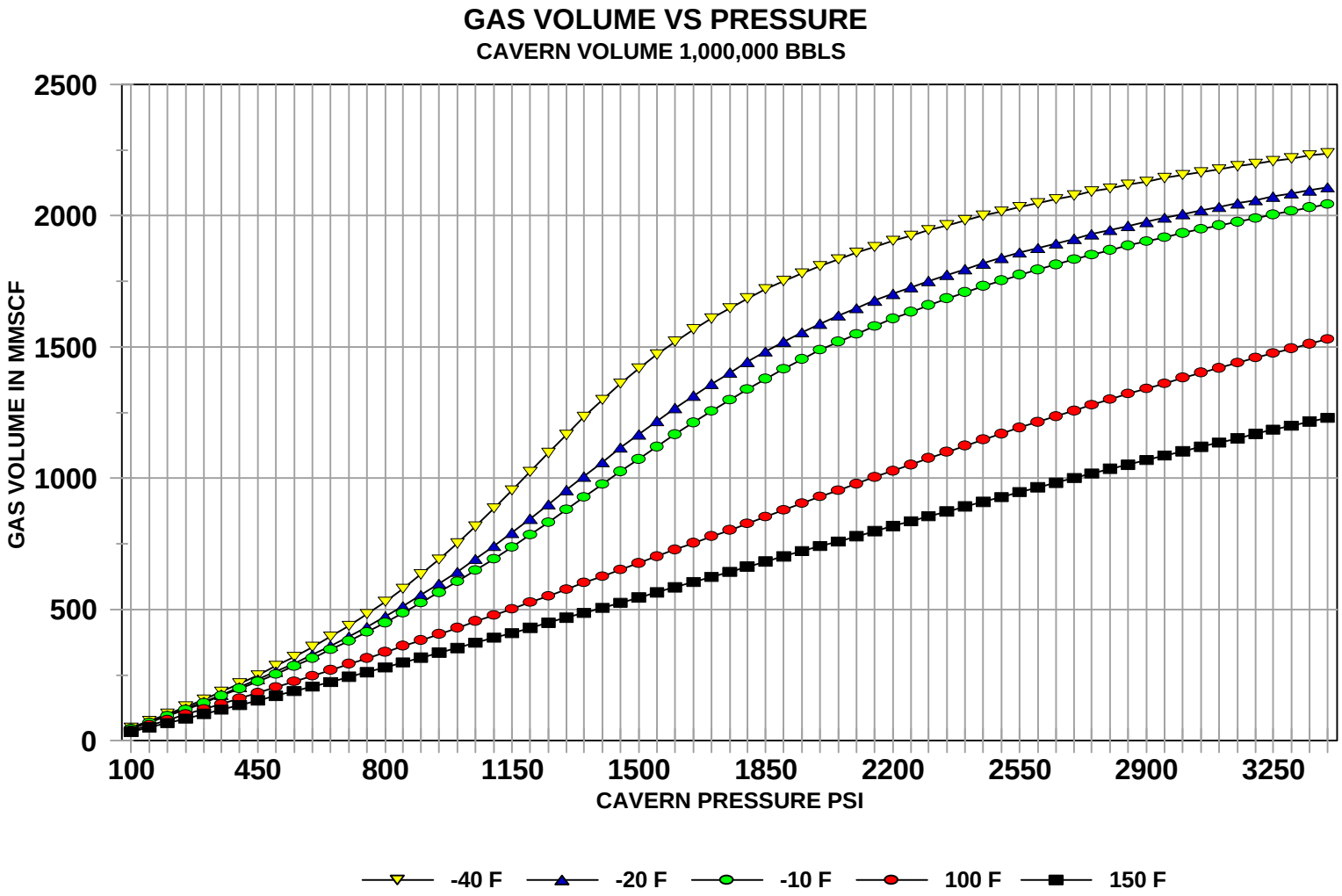

FIGURE 1.0

SELECTED PROCESS AND CAVERN DESIGN PARAMETERS

The process design parameters selected for this study are as follows:

Maximum gas pressures:	1,080 - 1,250 psi
Minimum gas pressures:	250 psig and 100 psig
Operating temperatures:	-20°F, 0°F and +20°F
Cavern depth:	2,500 - 3,000 feet
Operating pressure gradient:	0.433 psi/ft
Working gas volume:	5 Billion Standard Cubic Feet (BSCF)
Gas withdrawal rate:	250 Million Standard Cubic Feet per Day (MMSCFD)
Gas injection rate:	250 MMscfd
Incoming gas temperature:	50°F to 80°F
Dehydration:	Water content reduction from 7 lbm/MMscf to < 1 lbm/MMscf prior to chilling (TEG or Mole Sieve-type)
Production casing diameter:	20 inch OD (0.500" wall)

COMPLETION OF PROJECT OVERVIEW

- It is now time for the Mid-Morning break
- The next speaker will be Mr. Bruce Russell
- Mr. Russell will present site selection, site geology, and some principles on gas storage in mined caverns

Doe Advanced Natural Gas Storage Concepts Program
Next Speaker - Roger Schalge

CHILLED GAS STORAGE IN MINED ROCK CAVERNS

Technology Transfer

PB-KBB INC.
11757 KATY FREEWAY
HOUSTON, TEXAS
281 589-5833

DEPARTMENT OF ENERGY
FEDERAL ENERGY
TECHNOLOGY CENTER
MORGANTOWN, WV

PRESENTATION ON MINING

- Roger Schalge

GOETECHNICAL ASSUMPTION FOR CONCEPTUAL DESIGN OF CAVERN

Geotechnical Assumptions for Conceptual Design of Refrigerated Natural Gas Storage Cavern

1. Geological Column

0 - 50'	Overburden
50 - 150'	Weathered crystalline rock (igneous or metamorphic)
150 - 3000'	Unweathered crystalline rock (igneous or metamorphic)

2. Rock Properties and Hydrologic Conditions

Unconfined Compressive Strength: . . 2,000 - 20,000 psi (average 10,000 psi)
Tensile Strength: . . . . . 700 psi
Young's Modulus . . . . . .7,500,000 psi
Poisson's Ratio: 0.27
Bulk Density: . . . . . .2.80 g/cc
Porosity: 1%
Hydraulic Conductivity (K): . . . . . 10^{-7} cm/sec at 2500-ft. depth
Temperature at 2500' Depth: . . . . . 73°F
Temperature Gradient: . . . . . .0.64°F/100 feet
Water Table: . . . . . ± 30 feet below surface (in gentle hilly terrain); Near surface (in valley bottoms)

Average RQD index value: . . . . . 85 at 2500-ft. depth

GEOLOGICAL COLUMN MATERIAL PROPERTIES AND ASSUMPTIONS

Depth	Material
0-50 feet	Overburden
50-150 feet	Weathered crystalline rock
150-3,000 feet	Unweathered crystalline rock

Table 8-2. Properties of Unweathered Crystalline Rock

Property	Value
Unconfined compressive strength	2,000-20,000 psi; Average = 10,000 psi
Tensile strength	700 psi
Young? s modulus	7,500,000 psi
Poisson? s ratio	0.27
Bulk density	2.80 g/cc
Porosity	1%
Temperature at 3,000-foot depth	73 ^{o}F
Average RQD index value	85 at 3,000-foot depth
Water table	Within 30 feet of surface
Hydraulic conductivity	10^{-7} cm/sec at 3,000-foot depth

GAS OPERATING CONDITIONS

Table 8-3. Gas Operating Conditions

Property	Value
Gas storage pressure, maximum	1,370 psi
Gas storage pressure, minimum	250 psi
Refrigerated gas temperature	-20 ^{o}F

THERMAL PROPERTIES OF GRANITE

Table 8-4. Thermal Properties of Granite

Property	Value
Coefficient of thermal expansion	3.75×10^{-6}
Specific heat	880 J/kg-K
Thermal conductivity	2.51 W/m-K

REQUIRED CAVERN VOLUMES AT VARIOUS DEPTH AND TEMPERATURES

Table 11-2
Required Cavern Volumes at Various Depths and Temperatures

Depth	Cavern Volume at -20°F, million cubic yards	Cavern Volume at-30°F, million cubic yards	Cavern Volume at -40°F, million cubic yards
2500	1.87	1.75	1.56
3000	1.34	1.21	1.08

The process equipment cost was estimated only for chilling the gas to a temperature of -20 ^{o}F for the following reasons.

1. A colder temperature would require possible process design changes regarding refrigerant type and equipment design.
2. The metallurgy for the piping and equipment throughout the chilled system would have to be re-evaluated for service below -20 ^{o}F, including piping in the mined cavern.

TEMPERATURE DISTRIBUTION IN MINE

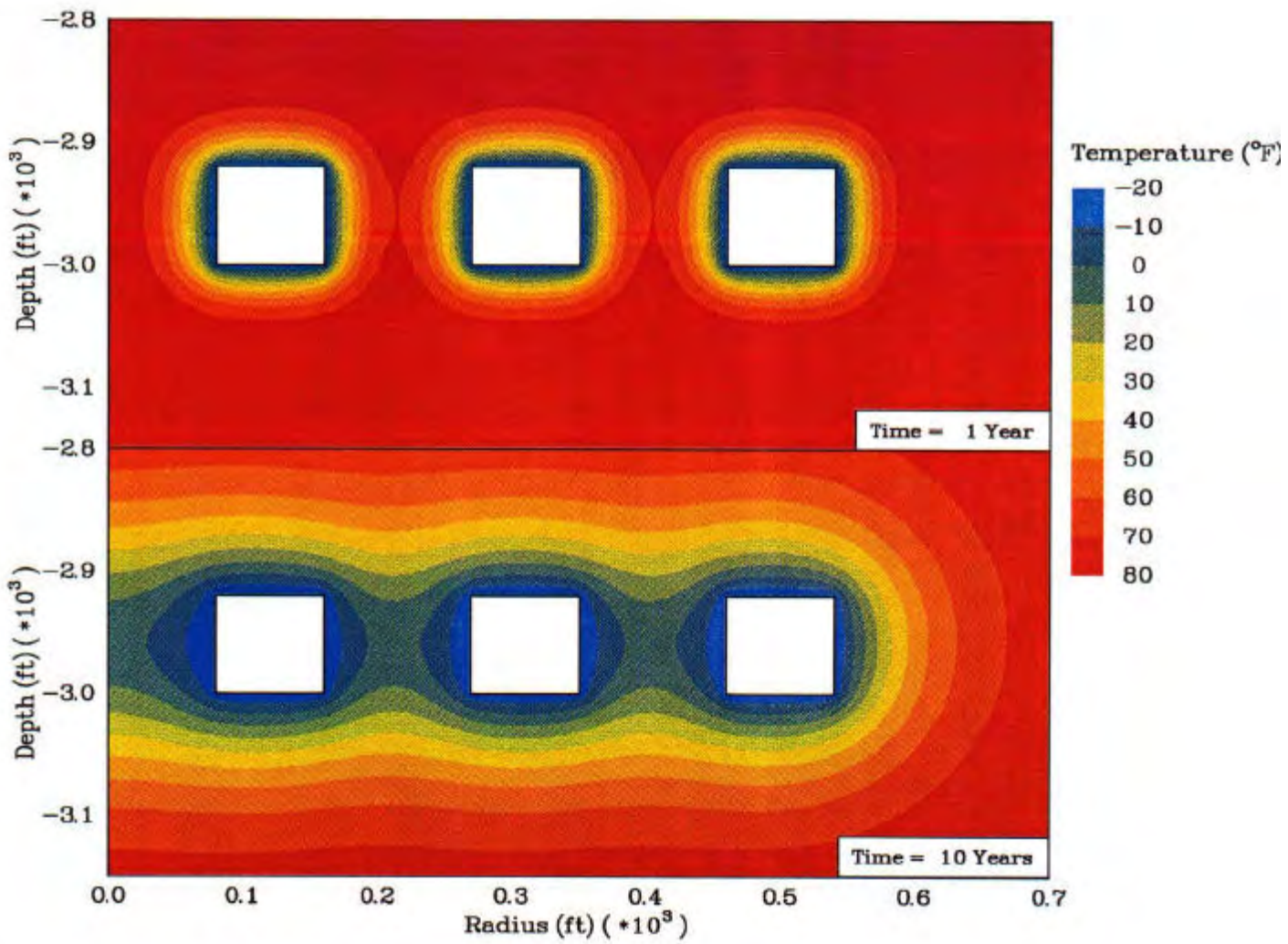

COOLING LOAD IN MINE TO MAINTAIN TEMPERATURE

- COOLING LOAD IN BTU's per hour VS TIME IN YEARS

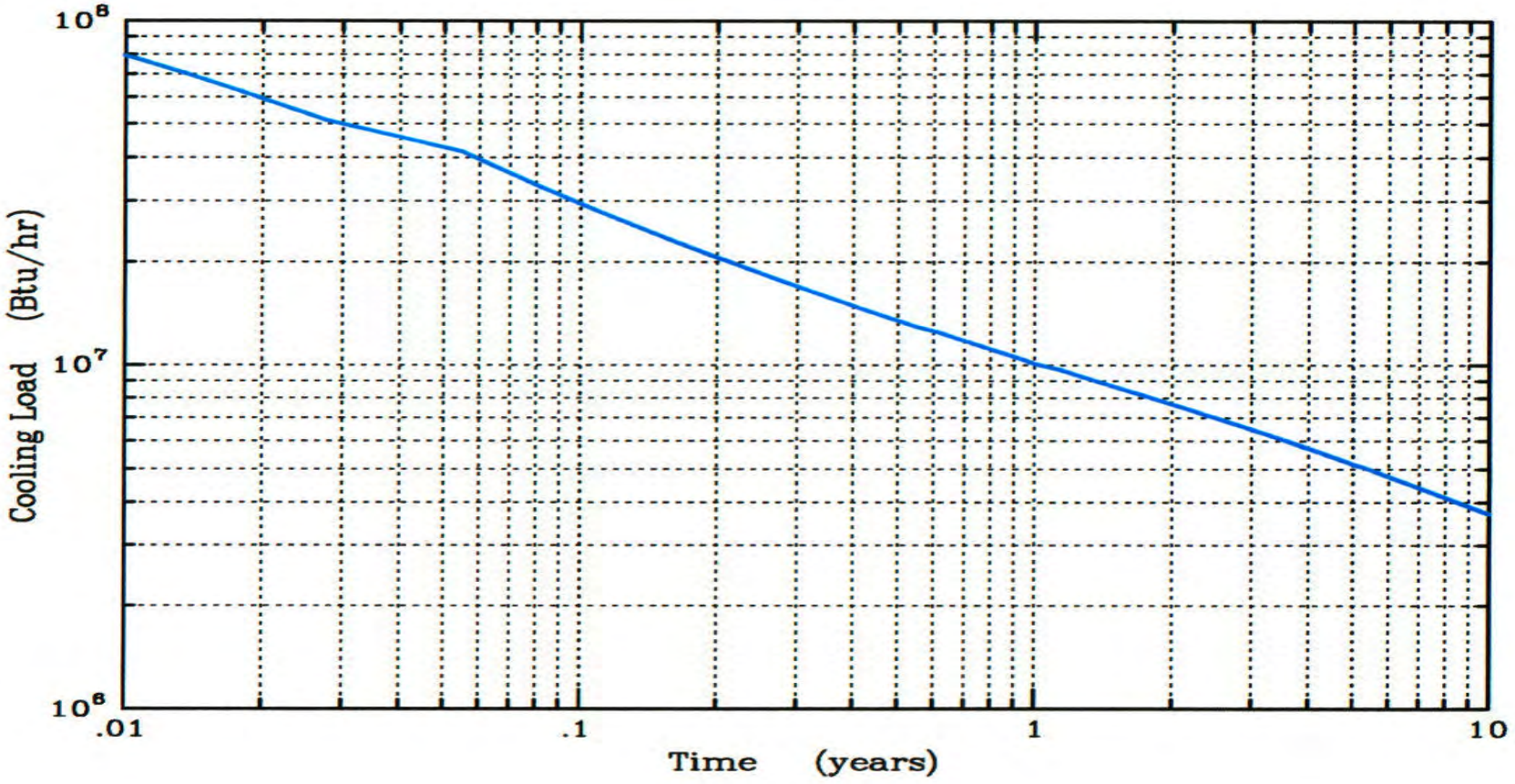

RECIRCULATION COOLING LOAD TO MAINTAIN GAS IN MINE @ - 20 ^{0} F

- ONE MONTH — 30 MM BTU / HR
- ONE YEAR — 10 MM BTU / HR
- TEN YEARS — 3.7 MM BTU / HR

MOHR-COULOMB FACTOR-OF-SAFETY CONTOURS BEFORE AND AFTER DRAWDOWN FROM MAXIMUM TO MINIMUM GAS PRESSURE

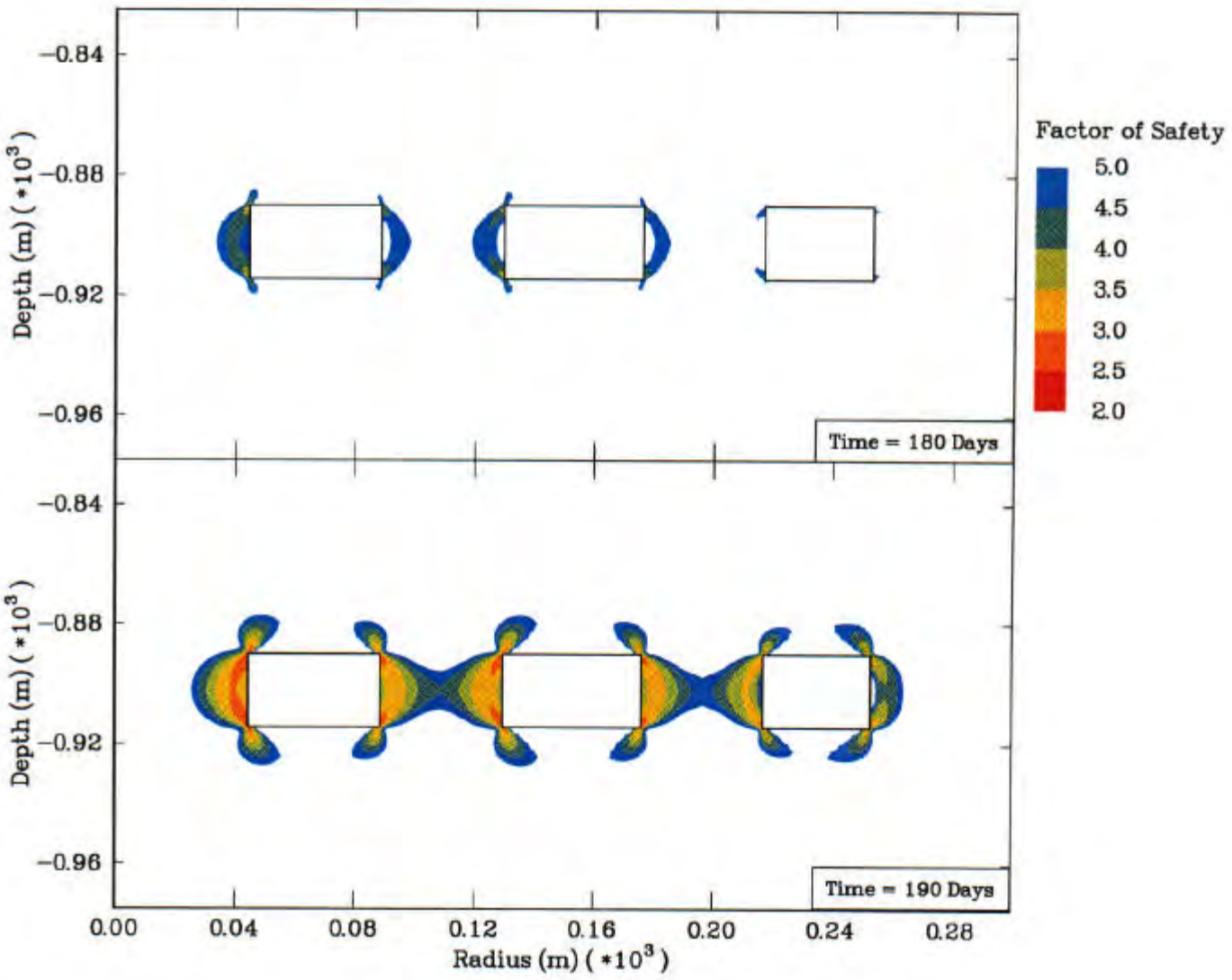

MOHR-COULOMB FACTOR-OF-SAFTEY CONTOURS AT 1 AND 5 YEARS AFTER FILLING WITH GAS AT 29 ^{O} C

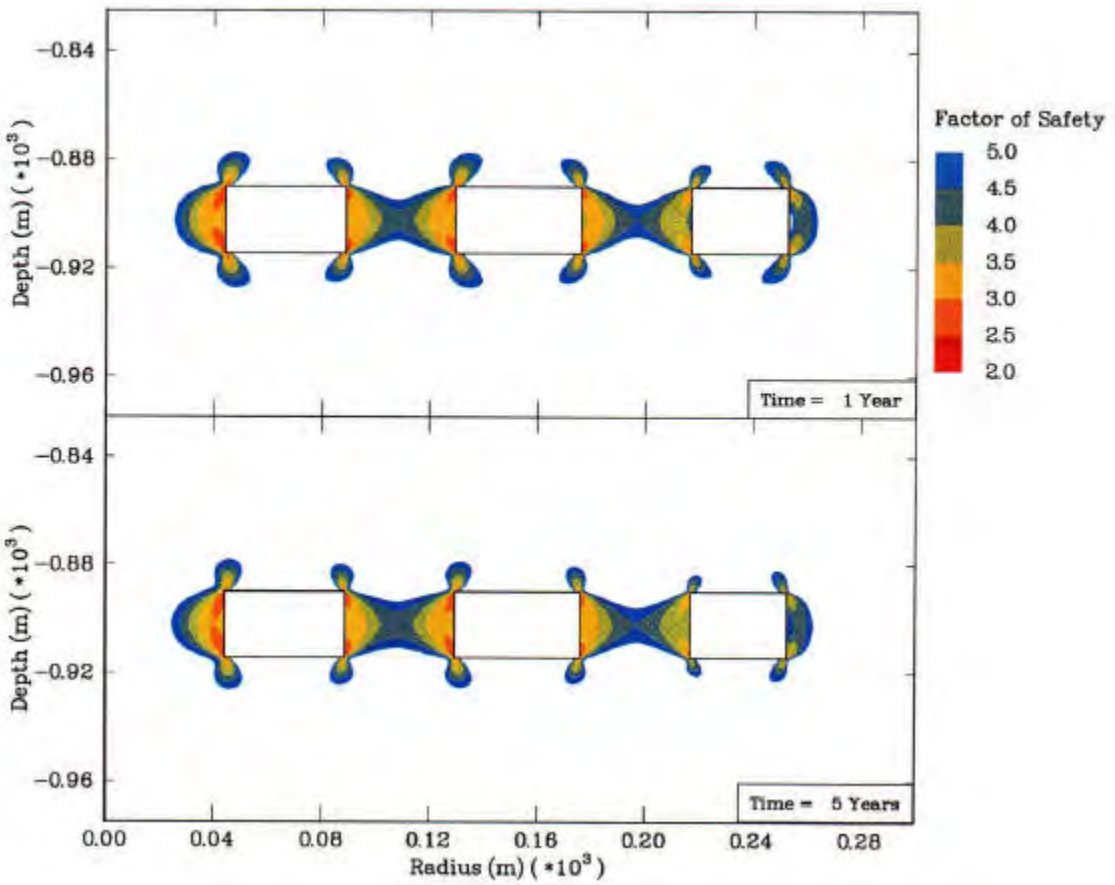

MINE GENERAL LAYOUT

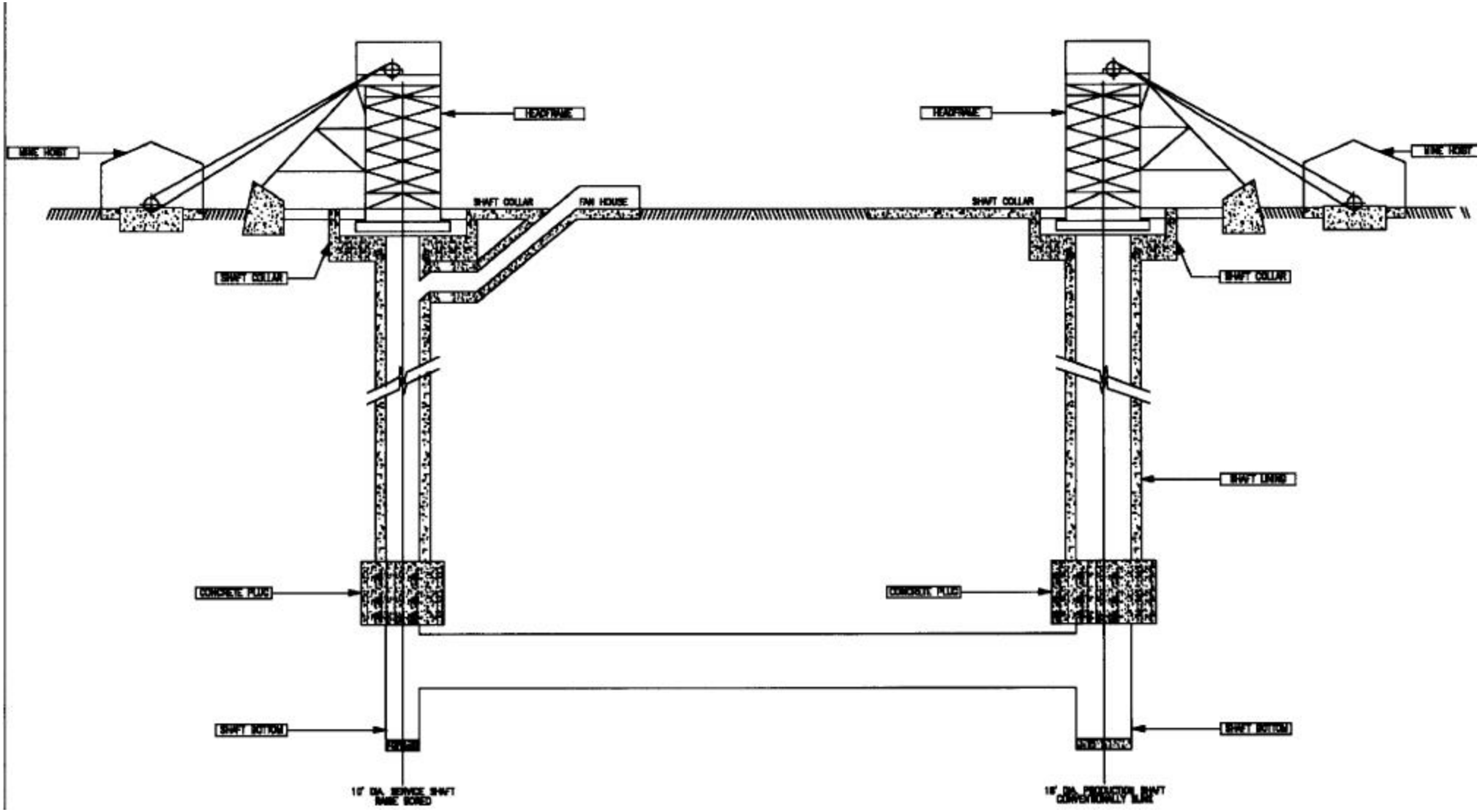

MINING EQUIPMENT REQUIRED FOR CAVERN CONSTRUCTION

Construction Equipment

The following construction equipment will be required for the gas storage cavern:

- Double-Drum with Clutch Hoist for Production Shaft
- Single Divided Drum Hoist for Men and Material Shaft
- One Work Stage
- Two 20-ton Skips
- Mancage
- Two Double (or Triple) Boom Electrohydraulic Jumbo Drills
- One Vertical Drill
- ANFO Loading and Blasting Rig
- Two Front-End Loaders (Cat 990 or equivalent)
- Two 40-ton Trucks
- One Roof Bolter
- One Rigid Boom Scaler (Gradall)
- One 80' high Cherry Picker for Handscaling
- Jaw Crusher
- Conveyors and Hoppers
- Power Distribution System
- Compressor and Compressed Air Distribution System
- Dewatering Pump
- Construction Fan with Tubing for Shaft Sinking
- Lubrication Truck
- 300,000 cfm Fan for Cavern Ventilation
- One 5-Stage Centrifugal Compressor (900 HP) for Evacuating Air
- Five Inert Gas Generators (120,000 scfh/unit) with Cooling Towers

MINED CAVERN AT 3,000 - FOOT LEVEL (ROOM AND PILLAR)

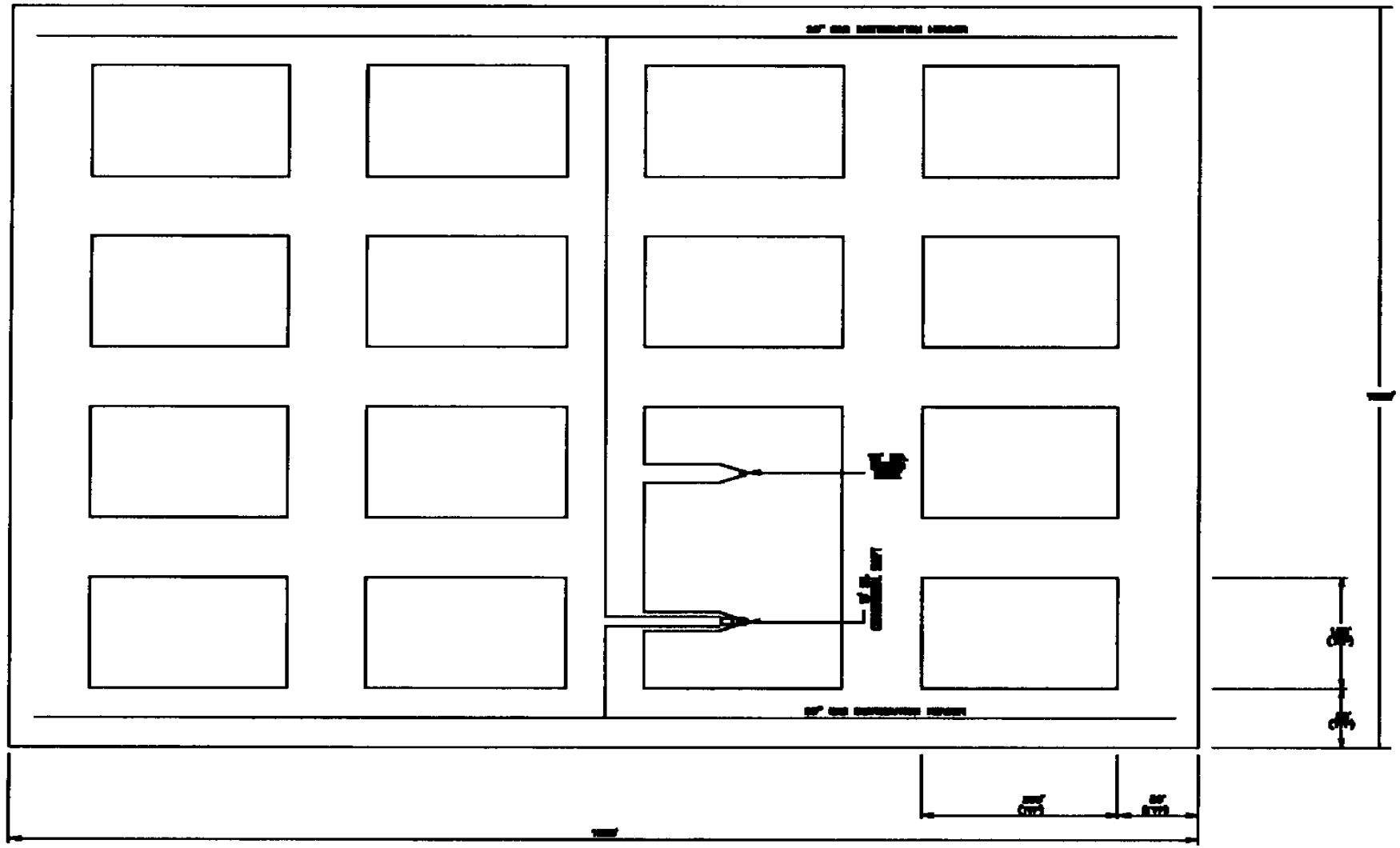

MINE DEVELOPMENT SHOWING BENCHING AND HEADINGS

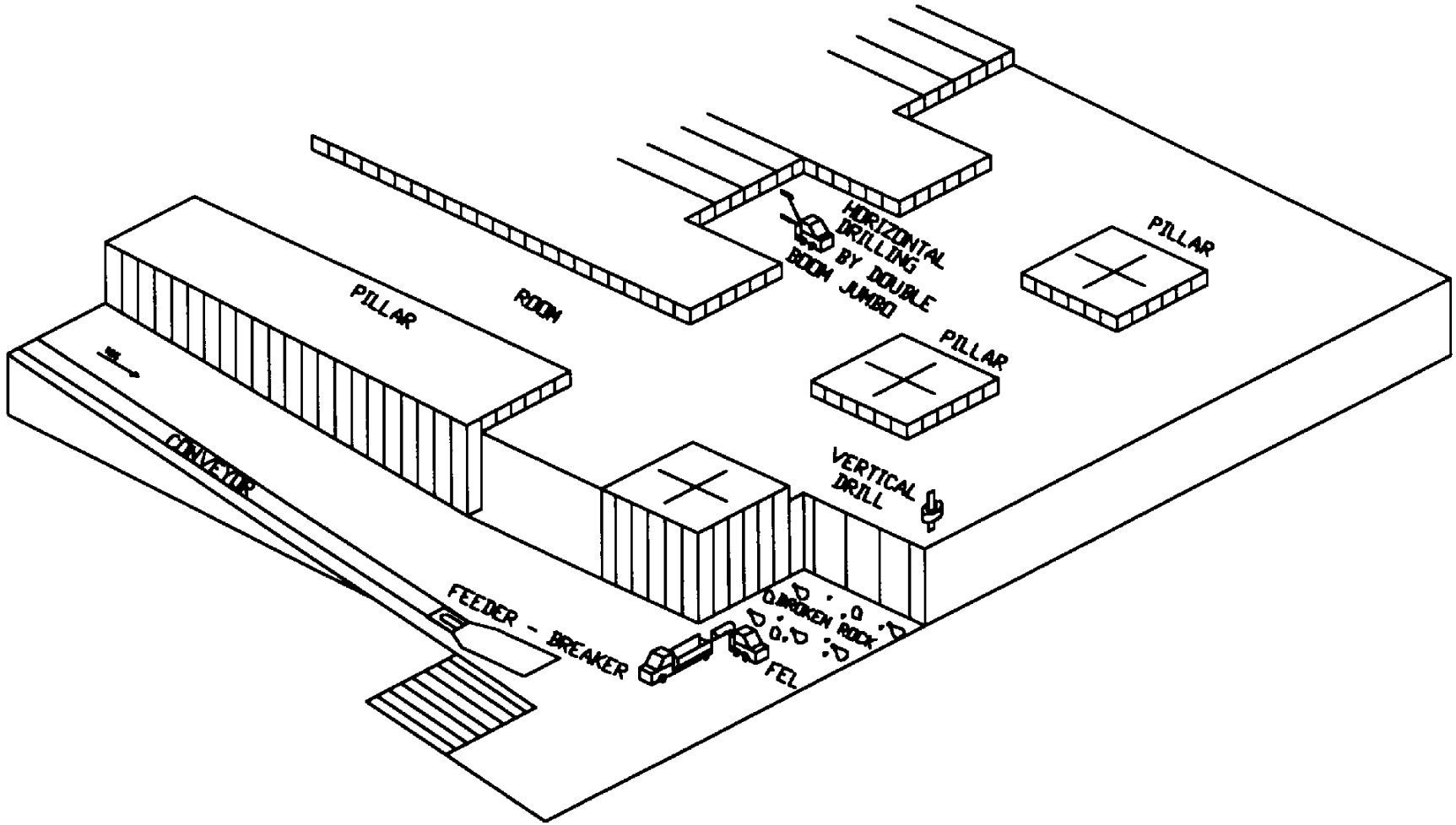

HEADING AND BENCHING MINING METHOD

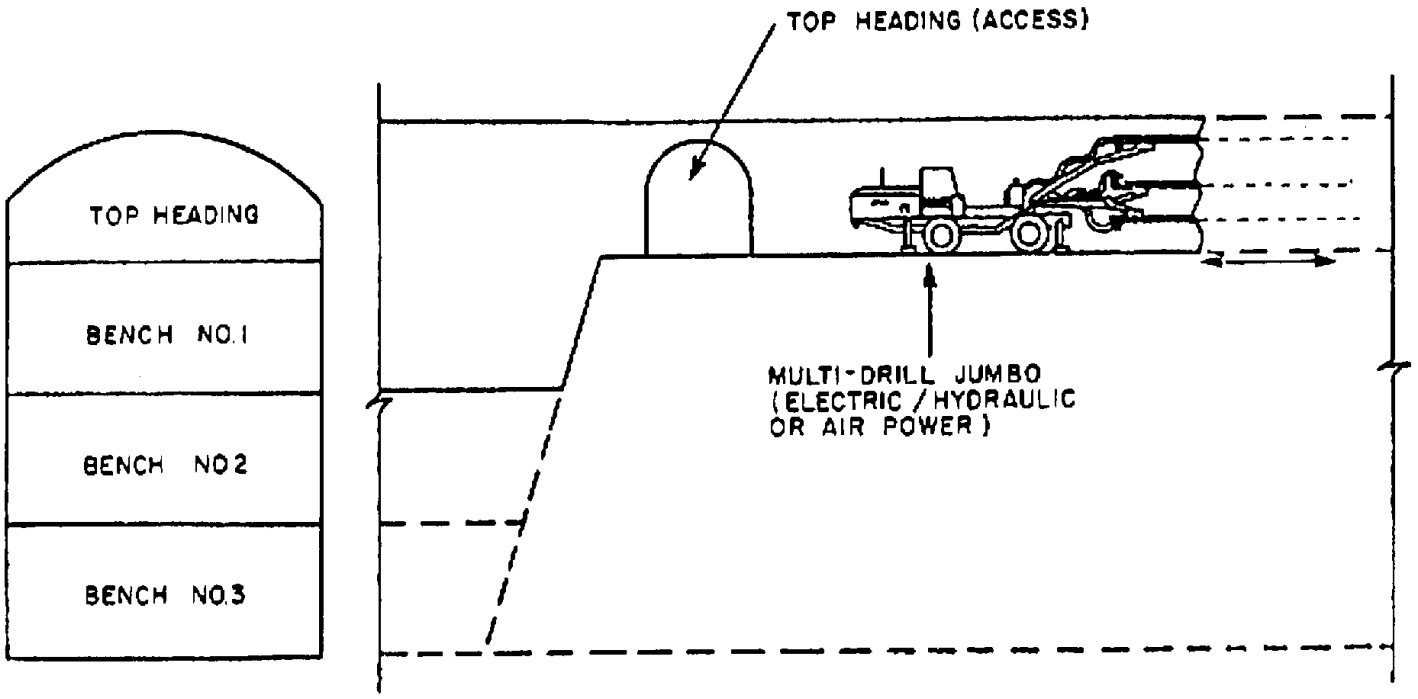

VIEW OF UNDERGROUND MINING

RAISE BORING METHOD

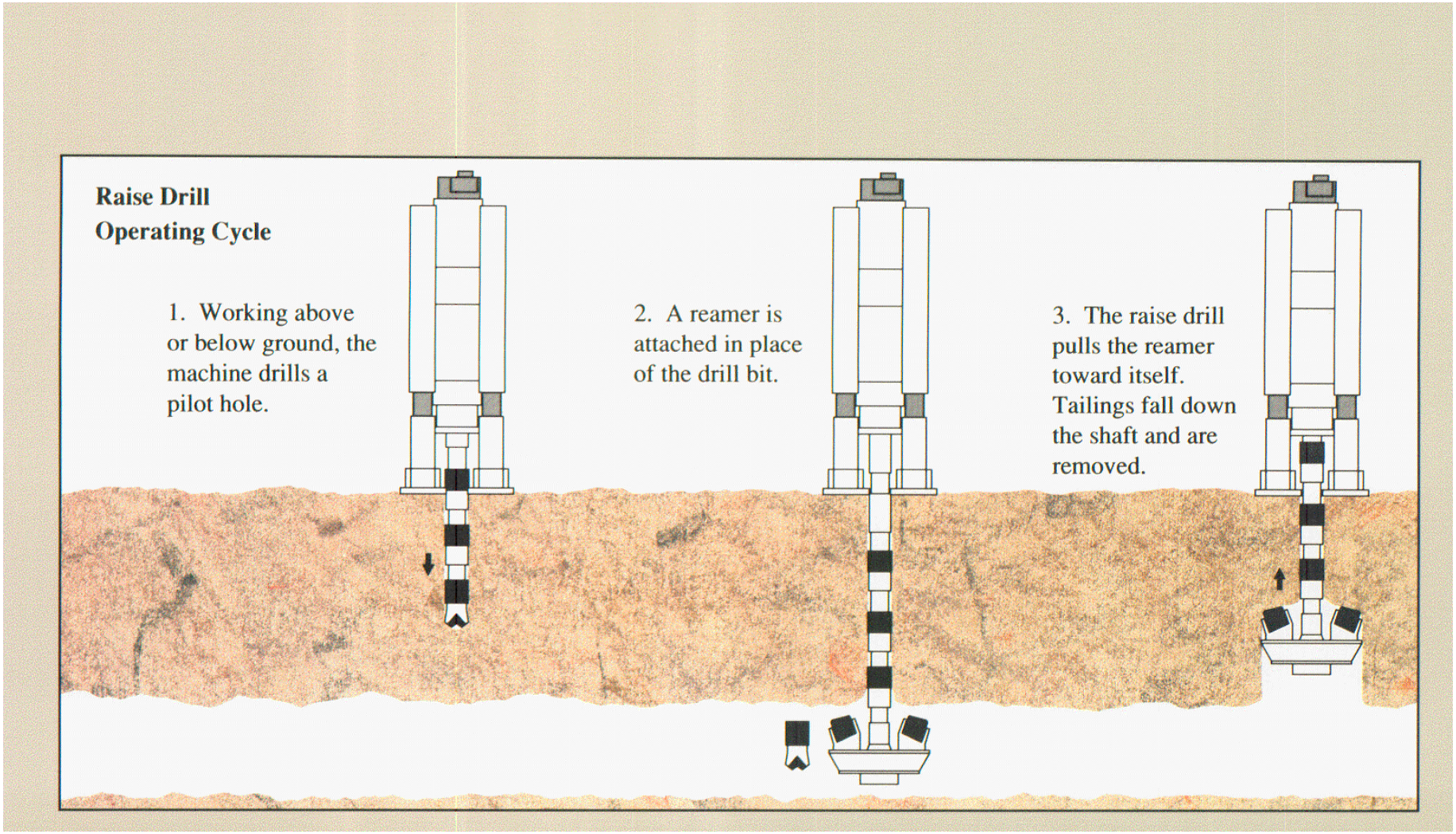

RAISE BORING AT SURFACE AND UNDERGROUND

VIEW UP A LINED SHAFT AND DOWN

MINING HEAD FRAME AND FRONT END LOADER


35

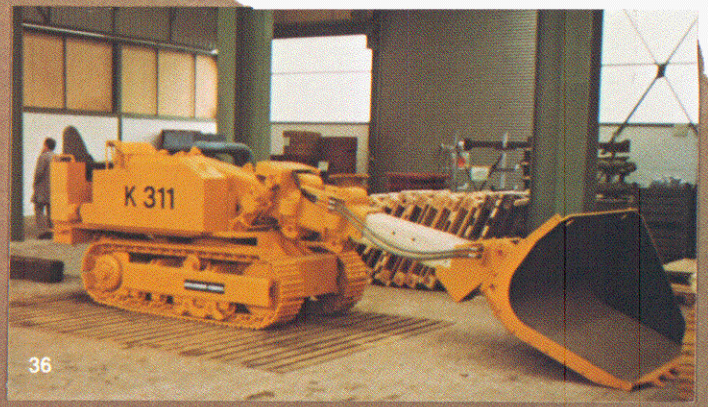

36

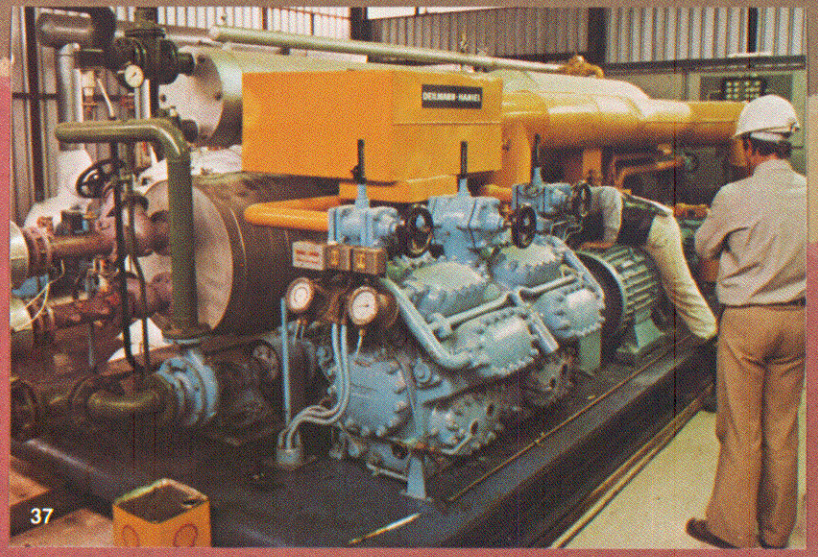
37

ELEVATION VIEW OF MINED CAVERN AT 3,000 - FOOT LEVEL

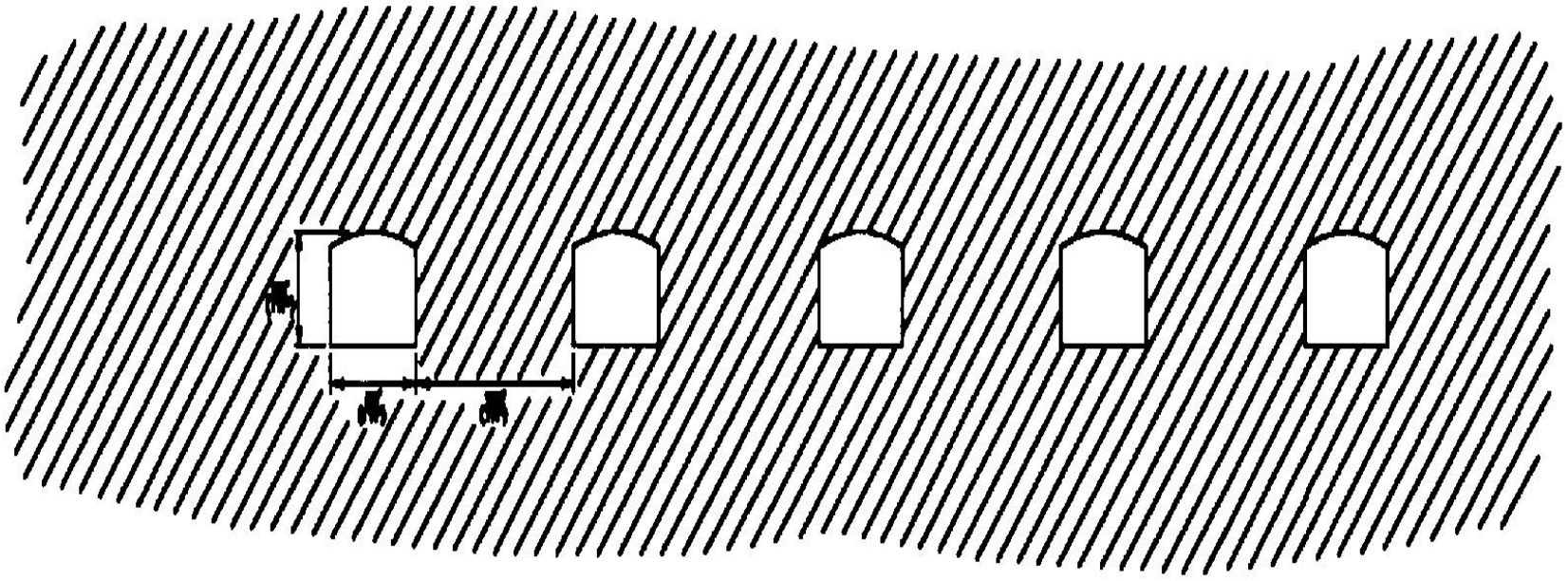

SECTION "A-A" AT 3000' DEPTH

MINED CAVERN CONCEPT PRESENTATION COMPETION

- The next presentation will be on the conceptual design of the surface facilities
- The speaker is Mr. Wally Swartz

Doe Advanced Natural Gas Storage Concepts Program

CHILLED GAS STORAGE IN MINED ROCK CAVERNS

Technology Transfer

PB-KBB INC.
11757 KATY FREEWAY
HOUSTON, TEXAS
281 589-5833

DEPARTMENT OF ENERGY
FEDERAL ENERGY
TECHNOLOGY CENTER
MORGANTOWN, WV

CONCLUSIONS (COST AND SCHEDULE)

- Mining and surface facilities cost and schedule

MINING LABOR COSTS

Table 10-10
Labor Costs

Position	No.	Hrs/Day	Days/Wk	$/Hr	OH @ 35%	Cost/Yr
Supervisor	1	8	5	35.00	47.25	98,280
Shift Operators	8	12	`4	20.00	27.00	488,808
Relief Operators	2	12	4	18.00	24.30	109,982
Clerical	1	8	5	13.00	17.55	37,315
TOTAL						734,385

- 2190 hrs per year on 12 hr shift schedule
- Overtime figured at 3% of annual schedule at base rate.

ESTIMATED COST OF CAVERN - 1,500 FOOT DEPTH

Table 10-1
Estimated Cost of a Storage Cavern - 1,500-Foot Depth

115.7 Million Cubic Feet Storage
1500 Foot Depth
One 8-20-Ft-Diameter Conventional Shaft
One Ten-Ft-Diameter Raise Bored Shaft
4 Million Cubic Feet Miscellaneous Excavation
Project Duration 80 Months

COST ITEM	QUANTITY	UNITS		UNIT COST	TOTAL
Mobilization	1	LS		7,215,000	7,215,000
Sink & Line Shaft	1500	LF		6,713	10,069,500
Raise Bore & Line Shaft	1500	LF		2,613	3,919,500
Material Handling Equipment	1	LS		4,123,000	4,123,000
Assemble Mining Equipment	1	LS		2,695,000	2,695,000
Excavate Top Heading	1851300	BCY		46.12	85,381,956
Excavate Bench	2581900	BCY		40.21	103,818,199
TOTAL					208,222,155
Contingency					29,101,800
TOTAL PROJECT COST					237,324,000

SUMMARY ESTIMATED COST OF CAVERN - 1,500 FT

Bid Item	Total	Unit Cost
Mobilization	7,212,000	7,212,000
Sink & Line Shaft (per ft)	10,069,500	6,713
Raise Bore Shaft (per ft)	3,919,500	2,613
Material Handling Equipment	4,120,000	4,120,000
Assemble Mining Equipment	2,693,000	2,693,000
Excavate Top Heading(CY)	85,381,956	46.12
Excavate Bench (CY)	103,818,199	40.21
Total Field Cost	208,222,155	
Contingency = 15% of the total field cost	29,101,800	

TOTAL PROJECT COST $237,324,000

ESTIMATED COST OF STORAGE CAVERN - 2,000 - FOOT DEPTH

Estimated Cost of a Storage Cavern - 2,000-Foot Depth

68.7 Million Cubic Feet Storage
2,000 Foot Depth
One 18-20-Ft-Diameter Conventional Shaft
One Ten-Ft-Diameter Raise Bored Shaft
4 Million Cubic Feet Miscellaneous Excavation
Project Duration 59 Months

COST ITEM	QUANTITY	UNITS		UNIT COST	TOTAL
Mobilization	1	LS		7,215,000	7,215,000
Sink & Line Shaft	2000	LF		6,713	13,426,000
Raise Bore & Line Shaft	2000	LF		2,613	5,226,000
Material Handling Equipment	1	LS		4,123,000	4,123,000
Assemble Mining Equipment	1	LS		2,695,000	2,695,000
Excavate Top Heading	1159500	BCY		46.12	53,476,140
Excavate Bench	1385000	BCY		40.21	55,690,850
TOTAL					141,851,990
Contingency					19,577,100
TOTAL PROJECT COST					161,429,100

SUMMARY ESTIMATED COST OF STORAGE CAVERN - 2,000 - FOOT DEPTH

Bid Item	Total	Unit Cost
Mobilization	7,212,000	7,212,000
Sink & Line Shaft (per ft)	13,426,000	6,713
Raise Bore Shaft (per ft)	5,226,000	2,613
Material Handling Equipment	4,123,000	4,123,000
Assemble Mining Equipment	2,693,000	2,693,000
Excavate Top Heading(CY)	53,476,140	46.12
Excavate Bench (CY)	55,690,850	40.21
Total Field Cost	141,851,990	
Contingency = 15% of the total field cost	19,577,100	
TOTAL PROJECT COST	$161,429,100	

ESTMATED COST OF STORAGE CAVERN - 2,500-FOOT DEPTH

Table 10-3
Estimated Cost of a Storage Cavern - 2,500-Foot Depth

47 Million Cubic Feet Storage
2500 Foot Depth
One 18-20-Ft-Diameter Conventional Shaft
One Ten-Ft-Diameter Raise Bored Shaft
4 Million Cubic Feet Miscellaneous Excavation
Project Duration 48 Months

COST ITEM	QUANTITY	UNITS		UNIT COST	TOTAL
Mobilization	1	LS		7,215,000	7,215,000
Sink & Line Shaft	2500	LF		6,713	16,782,500
Raise Bore & Line Shaft	2500	LF		2,613	6,532,500
Material Handling Equipment	1	LS		4,123,000	4,123,000
Assemble Mining Equipment	1	LS		2,695,000	2,695,000
Excavate Top Heading	791,400	BCY		46.12	36,502
Excavate Bench	1137185	BCY		40.21	45,725,000
TOTAL					119,419
Contingency					15,994,000
TOTAL PROJECT COST					135,413,000

COST ESTIMATE DETAIL FOR 2,500 - FOOT DEEP CAVERN

Table 10-4

Cost Estimate Detail for 2,500-Foot Deep Cavern

Bid Item	Qty.	Unit	Mnhrs.	Labor	Materials	EOE	Total	Ind. Cost	Total	Unit Cost
Mobilization	1	LS	22,000	770,000	3,500,000	52,000	4,322,000	2,996,000	7,212,000	7,212,000
Sink & Line Shaft	2,500	LF	70,000	2,450,000	3,385,000	215,000	6,050,000	11,027,000	16,672,000	6,669
Raisebore Shaft	2,500	LF	25,000	875,000	1,804,000	24,000	2,703,000	3,937,000	6,495,000	2,598
Material Handling Eqpt.	1	LS	22,600	791,000	234,000	127,000	1,152,000	3,079,000	4,120,000	4,120,000
Assemble Mining Eqpt.	1	LS	16,000	560,000	32,000		592,000	2,179,000	2,693,000	2,693,000
Exc. Top Heading	791,400	BCY	151,600	5,306,000	4,462,000	3,728,000	13,496,000	23,884,000	36,502,000	46.12
Exc. Bench	1,137,185	BCY	201,600	7,056,000	3,052,000	2,133,000	12,241,000	31,761,000	45,725,000	40.21
Total Field Cost			938,496	38,172,000	28,925,000	8,784000	106,636,000		119,419,000	
Contingency = 15% of the total field cost									15,994,000	
TOTAL PROJECT COST									135,413,000	

NOTES:

1) Direct burdened labor rate is $35.00 per hour.
2) Salaried labor at rates used in ARSCo Bid.
3) Drill steel & bits @ 0.85 per DLF.
4) Loader and truck EOE @ $40.00 per hour.
5) Dynamite @ $1.50 per pound.
6) ANFO @ $1.00 per pound.
7) Drill EOE @ 0.35 per DLF.
8) Raise bore cutters @ $50.00 per LF.
9) Transit-mix concrete @ $100.00 per yard.
10) Electrical service not included.
11) Work scheduled on seven days per week.
12) No bond premium included.
13) Indirect cost include plant & equip., G&A costs, muck haul and margin.
14) Cavern excavation rate based upon hoisting 400 tons per hour.

SUMMARY COST ESTIMATE FOR 2,500 FOOT DEEP CAVERN

Bid Item	Total	Unit Cost
Mobilization	7,212,000	7,212,000
Sink & Line Shaft (LF)	16,672,000	6,669
Raise Bore Shaft (LF)	6,495,000	2,598
Material Handling Equipment	4,120,000	4,120,000
Assemble Mining Equipment	2,693,000	2,693,000
Excavate Top Heading (CY)	36,502,000	46.12
Excavate Bench (CY)	45,725,000	40.21
Total Field Cost	$119,419,000	
Contingency = 15% of the total field cost	15,994,000	
TOTAL PROJECT COST	135,413,000	

PROJECT SCHEDULE FOR 2,500 - FOOT DEEP CAVERN

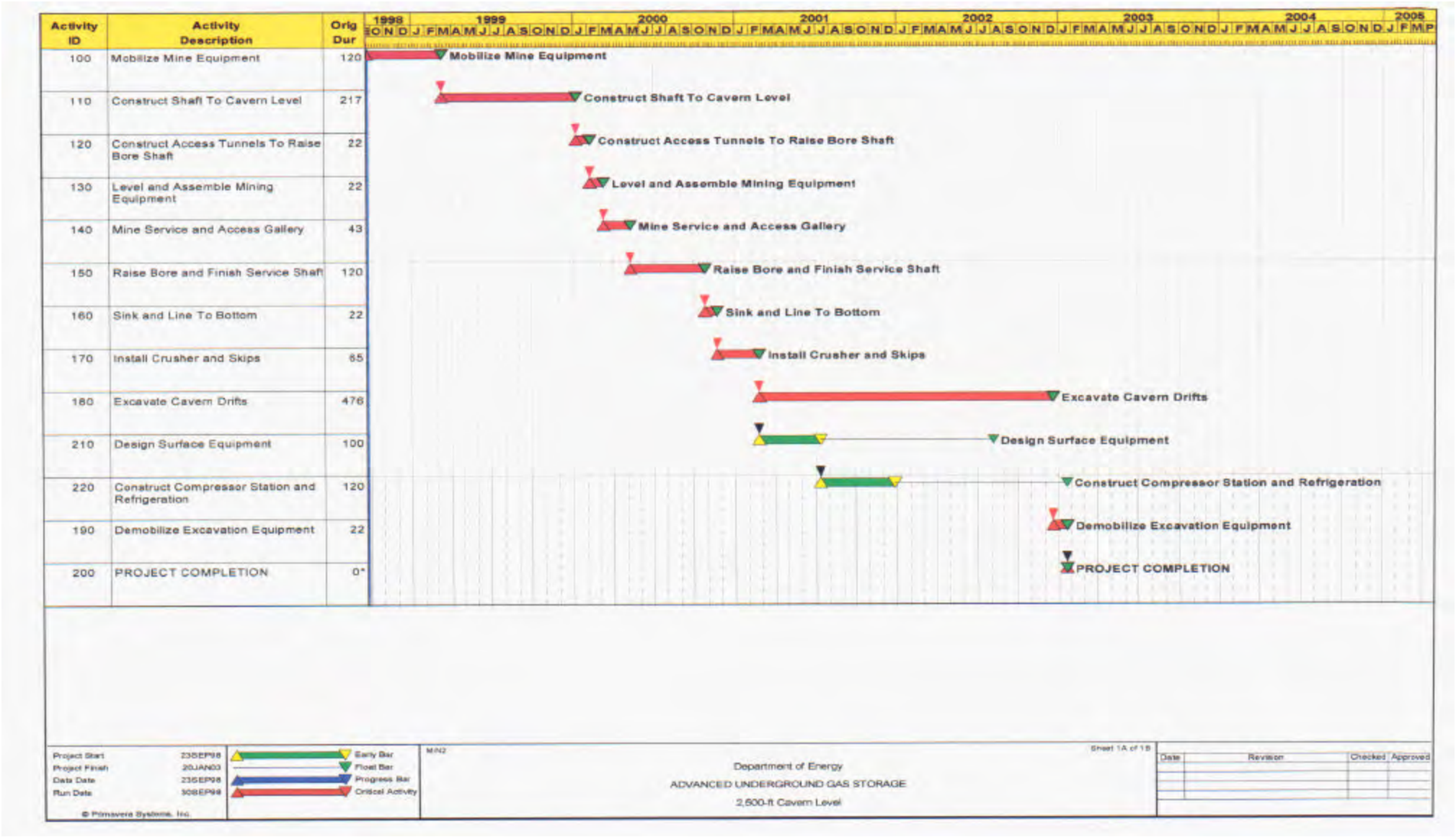

REPRESENTATIVE UNIT COSTS FOR NEW GAS STORAGE AND LNG PROJECTS

Table 12-1
Representative Unit Capital Costs for New Gas Storage and LNG Projects

Type of Project	Location	Project Name	Working Gas Capacity (BCF)	Total Cost ($MM)	Unit Cost ($/MCF)	Notes
Depleted Field	California	Putah Sink	15.000	40.000	2.67	(1)
Depleted Field	Colorado	Douglas Creek	10.000	30.000	3.00	(1)
Depleted Field	Utah	Clay Basin Expansion	15.200	49.600	3.26	(1)
Depleted Field	Oklahoma	Manchester	15.000	30.000	2.00	(1)
				Average>>	2.73	
Aquifer	Indiana	Carbon-Calcutta	3.900	12.275	3.15	(1)
Aquifer	Illinois	Hillsborough Expansion	4.500	36.600	8.13	(1)
				Average>>	5.64	
Salt Cavern	Alabama	S. Alabama-McIntosh	2.700	30.000	11.11	(1)
Salt Cavern	Mississippi	Hattiesburg phase 1 & 1A	3.500	47.000	13.43	(2)
Salt Cavern	Louisiana	Napoleonville Phase 1	4.600	45.000	9.78	(1)
				Average>>	11.44	
LNG	North Carolina	Pine Needle	4.000	107.000	26.75	(2)
LNG	Maine	Granite Slate	2.000	44.222	22.11	(2)
				Average>>	24.43	
Refrigerated mined Cavern		Mid-Atlantic	5.000	178.000	35.60	

Notes: (1) EIA/The Value of Underground Storage in Today's Natural Gas Industry.
(2) Brant Energy Data.

SUMMARY OF UNIT COST FOR VARIOUS STORAGE METHODS

TYPE STORAGE	LOCATION	$/MSCF
Depleted Field	California	$2.67
Depleted Field	California	3.00
Depleted Field	Utah	3.26
Depleted Field	Oklahoma	2.00
Aquifer	Indiana	3.15
Aquifer	Illinois	8.13
Salt Cavern	Alabama	11.11
Salt Cavern	Miss.	13.43
Salt Cavern	Napoleonville, La	9.78
LNG	North Carolina	22.11
LNG	Maine	24.43
Chilled Gas	Many Places	35.90

REPRESENTATIVE UNIT CAPITAL COSTS FOR STORAGE

TYPE OF STORAGE		AVG. UNIT COST $ / MCF
DEPLETED GAS FIELD		2.73
AQUIFER		5.64
SALT CAVERNS		11.44
LNG		24.43
CHILLED GAS		35.6
AVOCA & TIOGA		32.00 to 34.00

COST ESTIMATE DETAIL FOR 3,000 - FOOT DEEP CAVERN

Table 10-5

Cost Estimate Detail for 3,000-Foot Deep Cavern

Bid Item	Qty.	Unit	Mnhrs.	Labor	Materials	EOE	Total	Ind. Cost	Total	Unit Cost
Mobilization	1	LS	22,000	770,000	3,500,000	52,000	4,322,000	3,498,000	7,212,000	7,212,000
Sink & Line Shaft	3,000	LF	81,000	2,835,000	3,906,000	258,000	6,999,000	14,439,000	21,813,000	7,271
Raisebore Shaft	3,000	LF	28,200	987,000	2,186,000	64,000	3,237,000	5,026,000	8,393,000	2,798
Material Handling Eqpt.	1	LS	22,600	791,000	234,000	127,000	1,152,000	3,594,000	4,120,000	4,120,000
Assemble Mining Eqpt.	1	LS	16,000	560,000	32,000		592,000	2,544,000	2,693,000	2,693,000
Exc. Top Heading	584,765	BCY	105,300	3,685,500	3,298,000	2,754,000	9,737,500	18,772,000	28,996,500	49.59
Exc. Bench	822,642	BCY	148,000	5,180,000	2,205,000	1,547,000	8,932,000	26,385,000	36,002,000	43.76
Total Field Cost (include P&E and G&A costs)			832,000	34,341,500	25,237,000	7,205,000	97,538,500		109,229,500	
Contingency = 15% of the total field cost									14,629,000	
TOTAL PROJECT COST									123,858,500	

NOTES:

1) Direct burdened labor rate is $35.00 per hour.
2) Salaried labor at rates used in ARSCo Bid.
3) Drill steel & bits @ 0.85 per DLF.
4) Loader and truck EOE @ $40.00 per hour.
5) Dynamite @ $1.50 per pound.
6) ANFO @ $1.00 per pound.
7) Drill EOE @ 0.35 per DLF.
8) Raise bore cutters @ $50.00 per LF.
9) Transit-mix concrete @ $100.00 per yard.
10) Electrical service not included.
11) Work scheduled on seven days per week.
12) No bond premium included.
13) Indirect cost include plant & equip., G&A costs, muck haul & margin.
14) Cavern excavation rate based upon hoisting 400 tons per hour.

SUMMARY COST ESTIMATE DETAIL FOR 3,000 - FOOT DEEP CAVERN

Bid Item	Total	Unit Cost
Mobilization	7,212,000	7,212,000
Sink & Line Shaft (per ft)	21,813,000	7,271
Raise Bore Shaft (per ft)	8,393,000	2,798
Material Handling Equipment	4,120,000	4,120,000
Assemble Mining Equipment	2,693,000	2,693,000
Excavate Top Heading(CY)	28,996,500	49.59
Excavate Bench (CY)	36,002,000	43.76
Total Field Cost	109,229,500	
Contingency = 15% of the total field cost	14,629,000	

TOTAL PROJECT COST $123,858,500

COST SUMMARY OF REFIRGERATED MINED CAVERN AT 3,000-FOOT DEPTH

Working Gas Storage of 5.0 Billion Standard Cubic Feet

Maximum Injection Rate of 250 MMSCFD

Maximum Withdrawal Rate of 250 MMSCFD

Injection Cycle - 20 Days

Withdrawal Cycle - 20 days

Conventional Mining and Shaft Sinking (6,292,335 barrels of space)			112,346,209
Refrigeration System, Compressors, and Process			31,971,424
Electrical and Instrumentation Equipment			2,243,333
Compressor Building (210-feet X 50-feet) and Control			903,540
Compressor Building Foundation and Slab			68,064
Concrete Supports for Compressor Station Piping			19,698
Control Building Foundation			153,256
Mechanical Separators Foundations			5,570
Mole Seives Foundations			4,999
Pressure Reducing Station Foundations			4,999
Gas Storage Facility Final Design (Eight Months)			1,078,342
Gas Storage Facility Construction & Commissioning			4,815,600
SUBTOTAL			**153,615,034**
Contingency on All Costs @ 10%			15,361,503
SUBTOTAL			**168,976,538**
Contractors' Profit at 10% on Surface Facilities			3,537,488
TOTAL PROJECT COST			**172,514,026**
COST OF FACILITY PER MMSCF OF BASE GAS STORAGE			**$34.50**
MINING COST PER BARREL OF MINED SPACE			**$20.00**

COST SUMMARY OF REFIRGERATED MINED CAVERN AT 3,000 - FEET

Conventional Mining and Shaft Sinking (6,300,000 BBLS)		112,346,209
Surface Compressor and Refrigeration Equipment		41,268,825
SUBTOTAL		153,615,034
Contingency on All Costs @ 10%		15,361,503
SUBTOTAL		168,976,538
Contractors Profit @ 10%	on Surface Facility	3,537,488
TOTAL PROJECT COST		$172,514,026
COST OF FACILITY PER MSCF STORED		34.50
MINING COST PER BARREL OF MINED SPACE		20.00

Required Cavern Volume (BBLS)

Depth	Cavern Volume @ -20 ^{0} F	Cavern Volume @ - 40 ^{0} F
1500’	21,200,000	Not calculated
2000’	12,000,000	Not calculated
2500’	9,000,000	7,510,000
3000’	6,500,000	5,200,000

PROJECT SCHEDULE FOR 3,000 - FOOT DEEP CAVERN

Activity ID	Activity Description	Orig Dur	Rem Dur
100	Mobilize Mine Equipment	130	130
110	Construct Shaft To 1500-ft Level	153	153
120	Construct Access Tunnels To Raise Bore Shaft	22	22
130	Lower and Assemble Mining Equipment	22	22
230	Construct Access To Raise Bore Shaft	22	22
140	Mine Service and Access Gallery	108	108
240	Raise and Line to 1,500-ft Level	65	65
150	Raise Bore and Finish Service Shaft	93	93
160	Sink and Line To 3,000-ft	152	152
170	Install Crusher and Skips	65	65
180	Excavate Cavern Drifts	260	260
210	Design Surface Equipment	100	100
220	Construct Compressor Station and Refrigeration	120	120
190	Demobilize Excavation Equipment	22	22
200	PROJECT COMPLETION	0*	0*

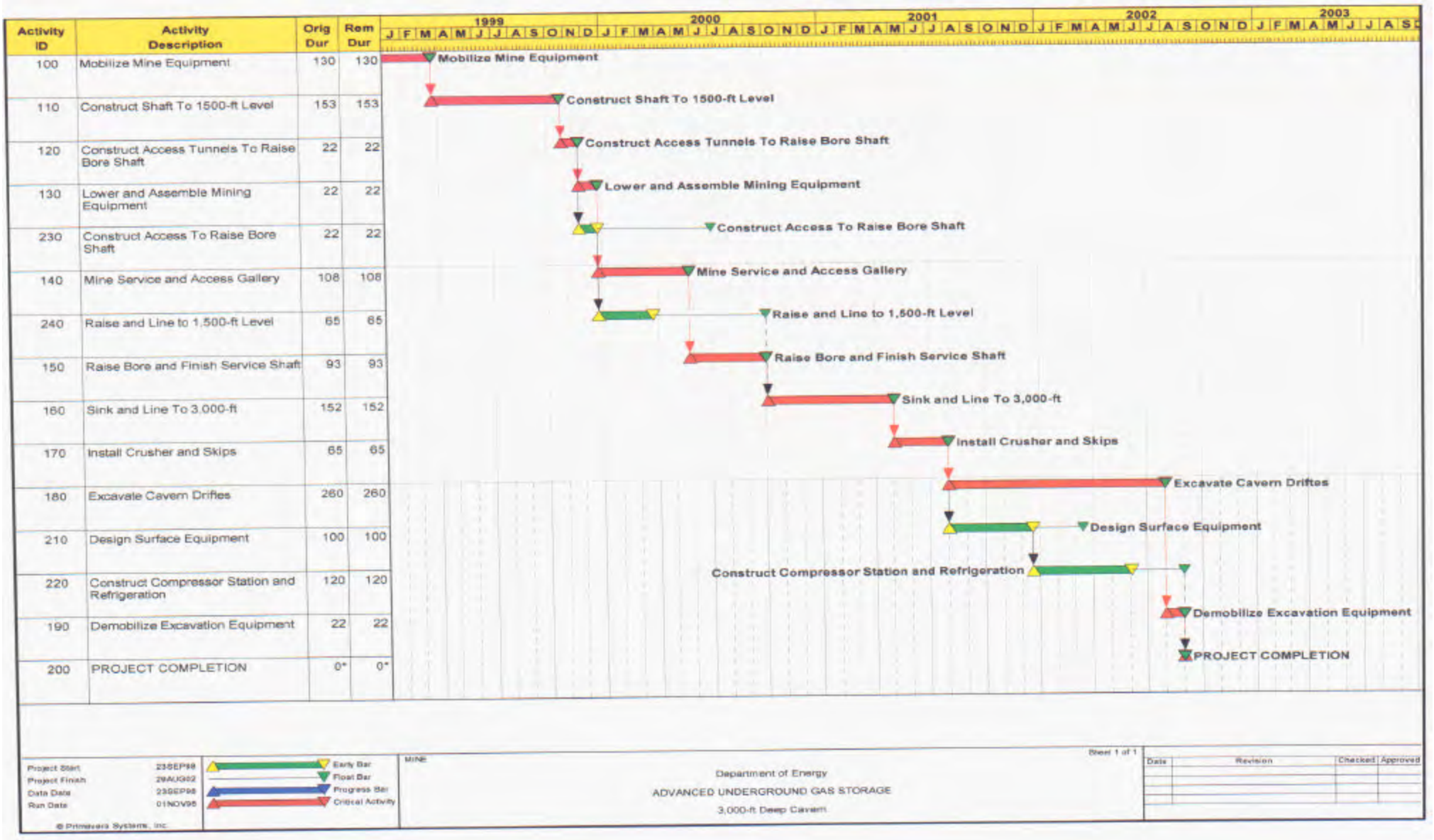

COMPARATIVE COST AND SCHEDULE OF CAVERN DEPTHS

Table 11-1
Comparative Cost and Schedule of Cavern Location

	Shaft Depth 1500 ft	Shaft Depth 2000 ft	Shaft Depth 2500 ft	Shaft Depth 3000 ft
Mobilization	7,215,000	7,215,000	7,212,000	7,212,000
Sink & line 18 ft shaft	10,003,500	13,330,000	16,672,000	21,813,000
Rise-bore shaft	3,897,000	5,196,000	6,495,000	8,393,000
Material handling eqpt.	4,123,000	4,123,000	4,120,000	4,120,000
Assembling mining eqpt.	2,695,000	2,695,000	2,693,000	2,693,000
Cavern Exc.	181,714,000	104,197,640	82,227,000	64,998,500
Total mining cost	209,647,500	136,764,640	119,419,000	109,229,500
Contingency	31,447,125	20,514,696	15,994,000	14,629,000
Total cavern development cost	241,094,625	157,279,336	135,413,000	123,858,500
SCHEDULE	80 months	59 months	48 months	47 months

ANNUAL OPERATING COSTS

Table 10-11
Annual Operating Costs

Cost Parameter	Monthly Cost	Annual Cost
Labor		
1 Supervisor	$8,190	$98,280
8 Shift Operators	$40,734	$488,808
2 Relief Operators	$9,165	$109,982
1 Clerical	$3,110	$37,315
Labor Subtotal	$61,199	$734,385
Maintenance Mat'l & Labor	$10,000	$120,000
Operating Supplies	$3,000	$36,000
Energy (as fuel gas)*	$91,202	$1,094,418
TOTAL	$165,400	$1,984,803

* Assumes $2.50 per MMBtu.

ENERGY COST FOR FACILITY

Table 10-9
Energy Costs

	Gas Cost - $/MMBtu:	$ 2.00	$ 2.25	$ 2.50	$ 2.75	$ 3.00
20 Day Injection Period	Fuel Required MMBtu's	Energy Cost	Energy Cost	Energy Cost	Energy Cost	Energy Cost
Compression	$9,864.4	$19,729	$22,195	$24,661	$27,127	$29,593
Refrigeration	$16,491.6	$32,983	$37,106	$41,229	$45,352	$49,475
Dehydration	$1,920.0	$3,840	$4,320	$4,800	$5,280	$5,760
Plant Baseline	$1,221.6	$2,443	$2,749	$3,054	$3,359	$3,665
Total Injection	$29,497.6	$58,995	$66,370	$73,774	$81,118	$88,493
20 Day Withdrawal Period						
Compression	$2,748.6	$5,497	$6,184	$6,872	$7,559	$8,246
Refrigeration	$245.0	$490	$551	$613	$674	$735
Gas Heating	$14,928.0	$29,856	$33,588	$37,320	$41,052	$44,784
Plant Baseline	$1,221.6	$2,443	$2,749	$3,054	$3,359	$3,665
Total Withdrawal	$19,143.2	$38,286	$43,072	$47,858	$52,644	$57,430
Total Cost per In/Out Cycle		$97,282	$109,442	$121,602	$133,762	$145,922
Total Energy Cost per Year		$875,534	$984,976	$1,094,418	$1,203,860	$1,313,302

COMPARISON OF STORAGE RATES FOR REFRIGERATED MINED CAVERN VS SELECTED LNG AND OTHER UNDERGROUND STORAGE FACILITIES

Existing LNG Facilities	Days of Withdrawal/ Vaporization	Monthly Demand $/dth/day	Monthly Volume Charge $/dth	Variable Withdrawal Charge $/dth	Variable Injection Charge $/dth	Fuel %	Fuel @ $2.50 $/dth	Single Cycle Unit Cost $/dth	Cost/Cycle @ Max. # of Cycles $/dth
Transco LNG @ Carlstadt, NJ	10	0.9058	0.1745	0.2025	0.2025	7.44%	0.186	3.772	n/a
East Tennessee Natural Gas	10	7.1856	0.0000	0.0000	0.0000	15.69%	0.392	9.015	n/a
Eastern Shore Natural Gas	10	8.6701	0.1745	0.2025	0.2025	7.44%	0.186	13.089	n/a
South Caroline Pipeline Co.	10	5.620	0.0000	0.2500	0.0500	0.00%	0.000	7.044	n/a
Proposed LNG Facilities									
Cove Point LNG (MD)	10	4.940	0.0000	0.0005	0.0005	20.50%	0.513	6.442	n/a
Granite State LNG (ME)	10	6.0600	0.0260	0.0000	0.0546	2.20%	0.055	7.682	n/a
Pine Needle LNG (NC)	10	4.850	0.0000	0.0000	0.0000	0.00%	0.000	5.820	n/a
Existing Salt Cavern Storage									
Hattiesburg Gas Storage (MS)	10	2.6300	0.0000	0.0100	0.0100	1.50%	0.038	3.214	0.321
Proposed Salt Cavern Storage									
Avoca Gas Storage (NY)	10	3.7500	0.0000	0.0100	0.0100	2.00%	0.050	4.570	0.563
Tioga Gas Storage (PA)	10	4.200	0.0000	0.0100	0.0100	1.20%	0.030	5.090	0.602
Refrigerated Mined Cavern	**20**	**9.9190**	**0.0000**	**0.0000**	**0.0000**	**1.16%**	**0.029**	**5.980**	**0.681**

SUMMARY OF COMARATIVE UNIT COST

Existing LNG Facilities	Single Cycle U.C. $/dth
Transco LNG @ Carlstadt, NJ	3.772
East Tennessee Natural Gas	9.015
Eastern Shore Natural Gas	13.089
South Caroline Pipeline Co.	7.044
Proposed LNG Facilities	
Cove Point LNG (NC)	6.442
Granite State LNG (ME)	7.682
Pine Needle LNG NC)	5.820
Existing Salt Cavern Storage	
Hattiesburg Gas Storage (MS)	3.214
Proposed Salt Cavern Storage	
Avoca Gas Storage (NY)	4.570
Tioga Gas Storage (PA)	5.090
Refrigerated Mined Cavern	5.980

CONCLUSIONS

- Store 5.0 BSCF of natural gas
- Multiple cycles per year, 20 days injection and 20 days withdrawal
- Storage is comparable to costs of LNG
- Storage cost is slightly more than two proposed salt cavern projects in the North East (NY/PA)
- The two salt cavern storage facilities were fully subscribed
- Can construct facility for about $172,000,000
- Unit cost is about 34.50 per thousand cubic feet of gas stored
- Can be located in many areas of the United States
- It may be possible to increase the storage pressure after the water around the cavern freezes
- Innovative use of existing technology
- Technically feasible

NEXT SPEAKER

NATURAL GAS STORAGE

Presented by:

Christopher J. Freitas

Office of Natural Gas & Petroleum Technology

Doe Advanced Natural Gas Storage Concepts Program
Next Speaker - Dan Tolleson

CHILLED GAS STORAGE IN MINED ROCK CAVERNS

Technology Transfer

PB-KBB INC.
11757 KATY FREEWAY
HOUSTON, TEXAS
281 589-5833

DEPARTMENT OF ENERGY
FEDERAL ENERGY
TECHNOLOGY CENTER
MORGANTOWN, WV

BREAK INTO TEAMS FOR DISCUSSION

- Mr. Dan Tolleson

  - Technical Questions
  - Positive / Negative Comments
  - Future Possibilities
    - Economics
    - Market
    - Technology

Questions from Houston

- What is the next step? Is there a follow up study?
- Could this technology be used in depleted mines?
- At a lower temperature (less than -20 F) what would the problems be?
- Applicable in CAES?
- Did the schedule include Geotechnical and Environmental schedule or just a construction schedule?
- In determining the depth relative to the safety factor - What are the environmental issues?
- Could you go through the refrigeration process starting from cavern completion?
- How does this compare to traditional LPG costs?
- Is this economically feasible?

Questions from Houston (continued)

- What is the DOE web site address and when will the CD's be available? www.fetc.doe.gov
- Are 9 cycles a year feasible?
- Can you make water tight seals around the shaft?
- With a total project of 6 to 8 years, who would invest?
- How do you get rid of the rock?
- How do you prove mechanical integrity?
- How can you accurately predict the cost estimate?
- Can this work in salt?
- Does the natural gas market support this?
- What is the pay out? How many years?
- How do you get the equipment in the mine?

Questions from Houston (continued)

- What are the effects of freezing on cavern / internal pressure?
- What are the future expansion possibilities?
- How do you purge the cavern?
- Monitor wells?

Department of Energy
Fossil Energy Natural Gas Program
Natural Gas Storage Research

Federal Energy Technology Center
Gas Storage and Deliverability Team

- DOE has supported a $1 million per year program in Gas Storage since 1993
- FETC an Implementing Organization for the Department's Energy Policy

Why a Federal Gas Storage Program? Federal Policy

- **Congress and Administration Agree:**
  - Gas storage is an important piece of nation's critical infrastructure, and as such important to the health and safety of the American people
  - Gas storage plays a critical role in the ability of the U.S. to increase use of natural gas as both an environmentally friendly fuel and as a key to greater energy independence

Gas Storage Program Goals

- Promote the development of advanced natural gas storage technologies necessary to improve storage and delivery of natural gas
- Increase confidence in the long term availability, reliability and safety of the natural gas system

4 Focus Areas in Gas Storage and Deliverability

- Deliverability Enhancement
- Reservoir Management
- Gas Measurement
- Advanced Storage Concepts

Deliverability Enhancement Core Area

- **RD&D efforts in the deliverability enhancement project area are focused to provide cost-effective means to increase the deliverability of the natural gas storage system**
- **Specific projects include:**
  - advanced fracture stimulation technology
  - improved remedial treatment technologies

Reservoir Management
Core Area

- **RD&D efforts are focused to increase the efficiency of storage operations through industry and FETC partnerships (CRADAs)**
- **Specific projects include:**
  - reservoir characterization and engineering assessment studies to optimize field performance
  - demonstrate the ability of horizontal wells to increase deliverability

Gas Measurement

- **RD&D efforts will provide improved accuracy and real-time measurement of both gas volume and energy content at gas storage facilities**
- **Specific projects include:**
  - an assessment of the state-of-technology for energy flow meters
  - testing and evaluation of correlating sound speed measurements to heating value
  - testing and evaluation of the application of a thermal micro-sensor to measure thermodynamic properties that may be correlated to heating value

Advanced Storage Concepts Program
National Storage Needs:

- With gas use predicted to increase by 5 Tcf by 2010, more peaking and base load balancing capacity is necessary to build confidence in the ability of natural gas to provide reliable service
- Many important regions of the U.S. where natural gas has the greatest growth potential lack conventional storage geology

FETC

Advanced Storage Concepts Program

DOE's first attempt to address factors that currently limit future growth of natural gas use in residential service, as an industrial fuel, and in electric power generation in many areas of the U.S.

Procurement of Research and Development Announcemnt (PRDA)

- A PRDA calling for unique or innovative gas storage technologies to meet the future growth potential of natural gas in "geologically challenged" areas of the country was issued
- Economic and engineering feasibility studies required for proposed technologies

4 Respondents Selected for Funding

- PB-KBB's "Refrigerated-Mined Cavern Storage"
- Sofregaz, U.S.'s "Gas Storage in Lined Rock Caverns"
- RE/SPEC's "Improved Modeling of Salt Cavern Storage"
- Mississippi State University's "Natural Gas Storage as Hydrates"

Lined Rock Caverns

- **Steel Lining**
  - serves as gas-tight seal and pressure containment
- **Concrete Layer**
  - transfers stress from lining to rock
- **Rock**
  - absorbs the stress
- **Drainage System**
  - handle ground water influx
- **Interconnected pipeline to caverns**

Lined Rock Caverns

- Diameter: 100 - 120 ft
- Height: 120 - 240 ft
- Pressure: 2,200 - 3,600 psi
- Working Gas: 300 - 500 MMcf per cavern
- Depth: 300 - 500 ft

Lined Rock Caverns

- **Grangesberg, Sweden test plant**
- **3 caverns at 1/8 scale**
  - 16 ft diameter
  - 33 ft height
  - 160 ft below surface
- **Tested different lining materials**
- **Maximum pressure reached was 7,500 psi**
- **Planning 1/4 scale demonstration plant**

Lined Rock Caverns

- **LRC Topical Report completed**
- **Geological cases selected**
  - Boston (4-cavern plant / 2 Bcf working gas)
  - Atlanta (8-cavern plant / 4 Bcf working gas)
- **Anticipated completion: April 1999**

Advanced Design Criteria for Salt Caverns

- Study to evaluate the feasibility of using an advanced constitutive geomechanical model for rock salt in gas storage cavern design
- Goal: reduction of minimum allowable gas pressure would increase working gas volume
- Modeling effort seeks to assess damages to cavern under cycling and lower pressures

Advanced Design Criteria for Salt Caverns

- **Method: Modeling existing caverns**
- **Damage Potential Method**
  - Based on stress states
- **Multimechanism Deformation Coupled Fracture Method**
  - Based on stress states and stress history
  - Quantifies the degree of dilation
- **In situ stress >> cavern pressure**
  - Dilation (microfracturing)
  - Macrofracturing can lead to spalling of roof or walls

Cavern Characteristics

Cavern A

- Depth (top): 2,009 ft
- Total Depth: 3,438 ft
- Max. Diameter: 350 ft
- Min. Pressure: 603 psi
- Max. Press: 1,707 psi
- Working Gas: 7.3 Bcf
- Cushion Gas: 3.3 Bcf

Cavern B

- Depth (top): 4,088 ft
- Total Depth: 5,080 ft
- Max. Diameter: 200 ft
- Min. Press: 1,200 psi
- Max. Press: 3,475 psi
- Working Gas: 3.2 Bcf
- Cushion Gas: 1.8 Bcf

Phase I Results

- Predicted dilatancy boundaries can differ significantly for the two methods
- The MDCF model shows that healing will occur at maximum pressure
- Less damage was predicted for the shallower cavern in this study
- Lower minimum gas pressure can be used without jeopardizing cavern stability

Advanced Design for Salt Caverns
Phase 2

- **Determination of an efficient test matrix**
  - constitutive model parameter vs. test type
  - design of test matrix
  - acquisition of data
  - fitting of model to data
- **Temperature effects/healing characteristics**
- **Pore pressure effects**
- **Cost analysis**
- **Anticipated completion: April 1999**

Gas Storage as Hydrates

- **Determine the technical and economical feasibilty of storing natural gas as hydrates**
- **Rate of formation**
  - atomizing water into a chilled gas
  - use of surfactant
- **Rate of decomposition**
  - irradiation with microwaves
  - heating coils
- **Storage stability**

Gas Storage as Hydrates

- **Hydrate formation**
  - Order of magnitude increase with surfactant (sodium lauryl sulfate)
  - Form quickly in a stagnant system as a concentric cylinder of solids
  - Storage may not require moving mechanical parts
  - General rate of formation equation being developed
  - www.che.msstate.edu/doe_msu1.html

Gas Storage as Hydrates

- **Recent work**
  - Runs with natural gas (90% C1, 6% C2, 4% C3)
  - Induction time longer for natural gas than ethane
  - Withdrawal composition beome leaner in methane upon decomposition
  - Current experiments show storage capacity of 165 scf/ ft^3; theoretical maximum of 181 scf/ft^3

Gas Storage as Hydrates
What's next?

- Phase II - Engineering feasibility and economic analysis
- Expected completion in May 1999

FETC

BRUCE RUSSELL

CHIEF GEOLOGIST

PB-KBB Inc.

TOPICS OF DISCUSSION

I. BACKGROUND OF GAS STORAGE IN MINED CAVERNS

II. SITE SELECTION AND VERIFICATION PROCESS (Geotechnical Feasibility Study)

III. MARYLAND STUDY AREA GEOLOGY AND SELECTION OF PROSPECTIVE CAVERN AREA

I. BACKGROUND OF GAS STORAGE IN MINED CAVERNS

- NATURAL GAS SUPPLY/DEMAND
- SURFACE VS. UNDERGROUND STORAGE
- TYPES OF UNDERGROUND STORAGE
  - POROUS MEDIA
  - SALT CAVERNS (Solution Mined)
  - ROCK CAVERNS (Conventionally Mined)
    - Igneous Rock - Dolomite
    - Metamorphic Rock - Anhydrite
    - Limestone - Shale
- BASIC GEOLOGICAL AND HYDROLOGICAL REQUIREMENTS FOR ROCK CAVERNS
- EXAMPLES OF GAS STORAGE IN MINED CAVERNS

BASIC GEOLOGICAL AND HYDROLOGICAL REQUIREMENTS

- ADEQUATE ROCK STRUCTURAL STRENGTH
- LOW ROCK PERMEABILITY
- ADEQUATE GROUND WATER PRESSURE OVER CAVERN (See Figures)
- CAVERN ROCK NONREACTIVE WITH STORED PRODUCT
- CAVERN ROCK NOT WATER SENSITIVE

BASIC HYDROLOGIC GAS CONTAINMENT PRINCIPLE

(Natural Gas Illustration)

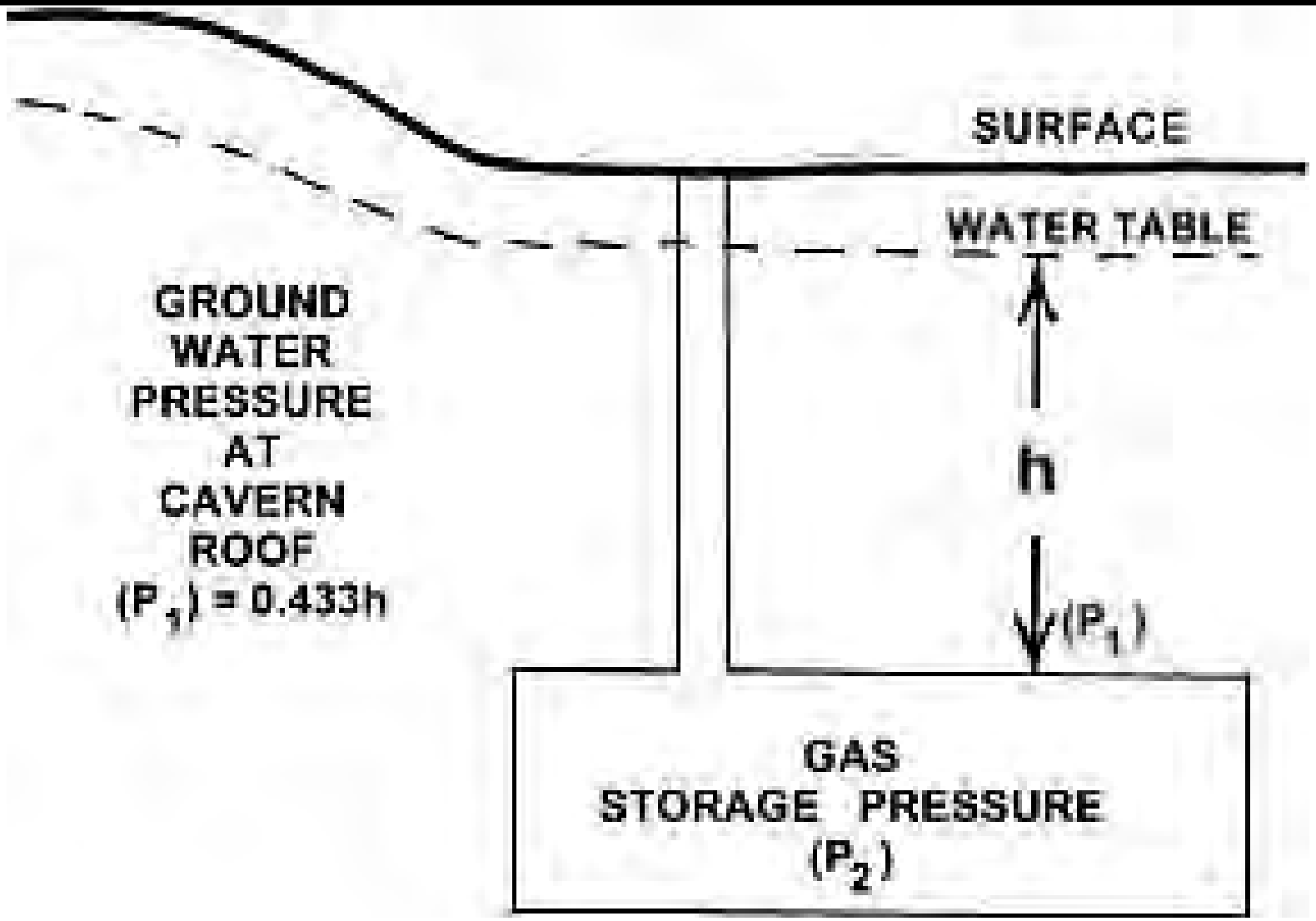

HYDROLOGIC CONTAINMENT REQUIREMENT: $P_1 > P_2$

BASIC HYDROLOGIC GAS CONTAINMENT PRINCIPLE

(LP - Gas Illustration)

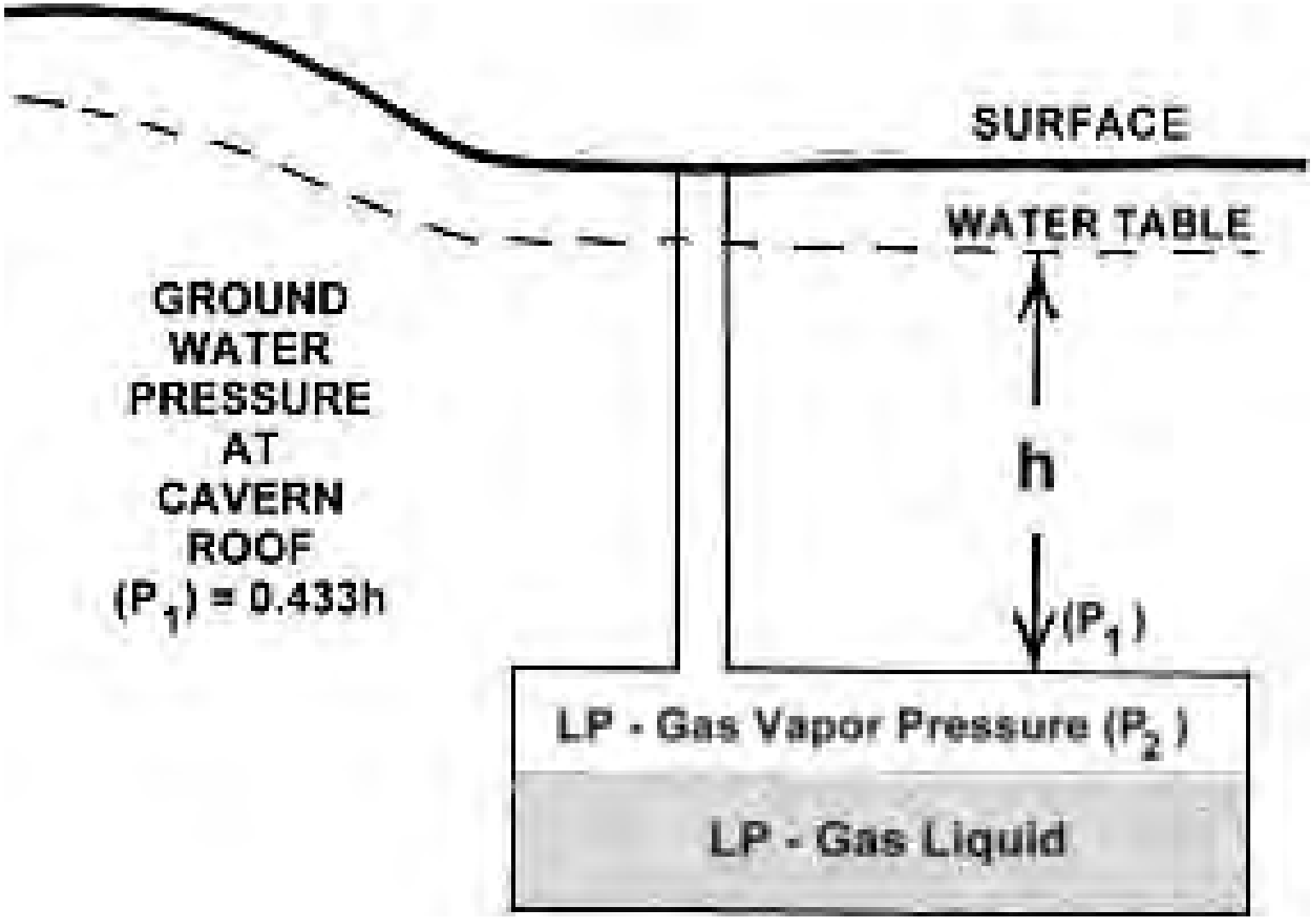

HYDROLOGIC CONTAINMENT REQUIREMENT: $P_1 > P_2$

EXAMPLES OF GAS STORAGE IN MINED CAVERNS

- COMPRESSED AIR STORAGE IN MINES
- LIGHT HYDROCARBON LIQUID STORAGE IN CAVERNS
  - LP-GAS
  - OLEFINS
  - ANHYDROUS AMMONIA
- NATURAL GAS STORAGE IN COAL MINES
- COMPRESSED AIR CUSHION CHAMBERS FOR UNDERGROUND HYDROPOWER PLANTS

BASIC HYDROLOGIC GAS CONTAINMENT PRINCIPLE

(LP - Gas Illustration)

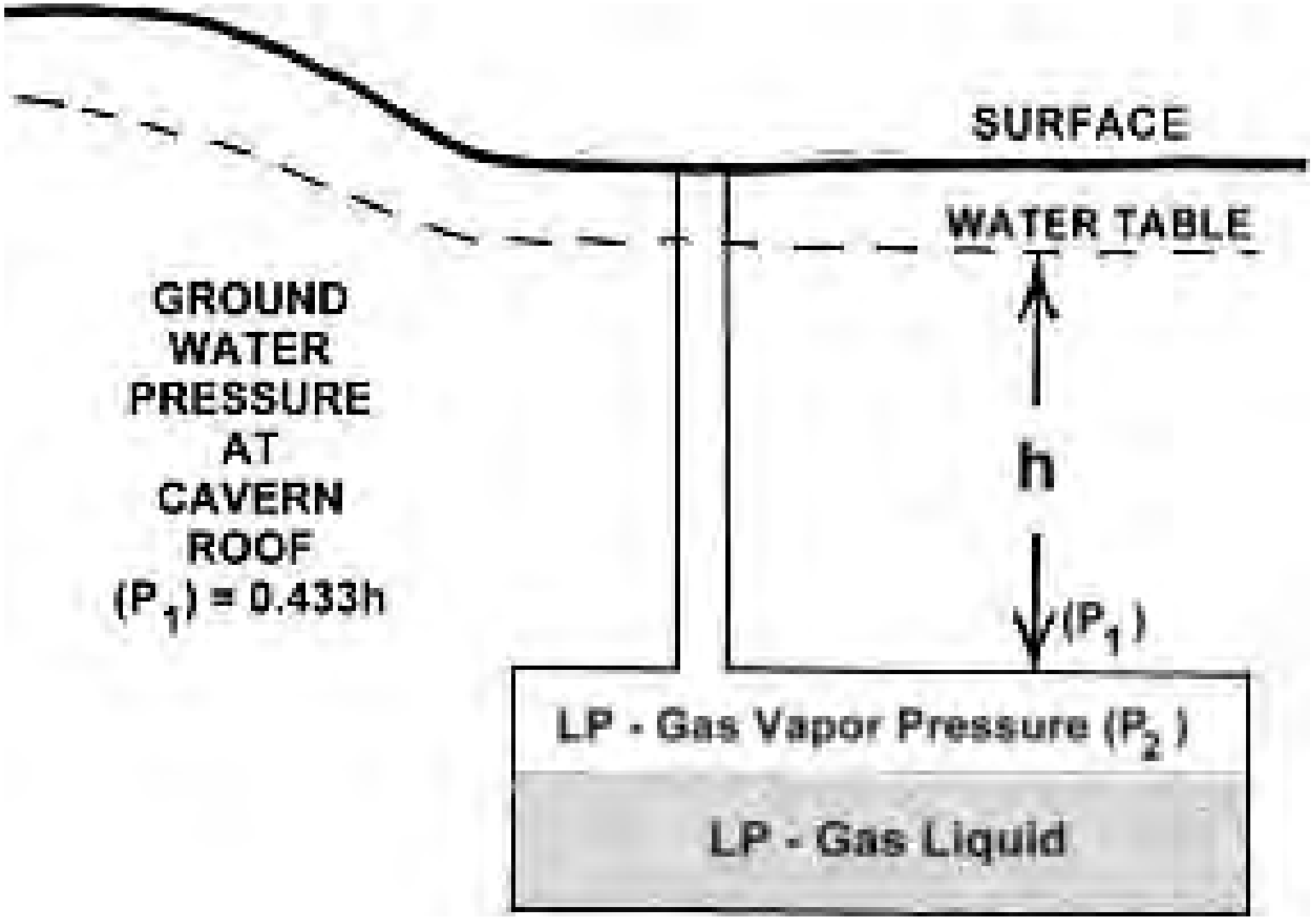

HYDROLOGIC CONTAINMENT REQUIREMENT: $P_1 > P_2$

II. SITE SELECTION AND VERIFICATION PROCESS

(Geotechnical Feasibility Study)

- PRELIMINARY GEOTECHNICAL INVESTIGATIONS
- INTERMEDIATE GEOTECHNICAL INVESTIGATIONS
- DETAILED GEOTECHNICAL INVESTIGATIONS

PRELIMINARY GEOTECHNICAL INVESTIGATIONS

- SCOPE OF PROJECT DETERMINATION
- STUDY AREA SELECTION
- GEOLOGICAL/GEOPHYSICAL/HYDROLOGICAL INFORMATION SEARCH
- PRELIMINARY SEISMIC RISK EVALUATION
- PRELIMINARY STUDY AREA INSPECTION AND SITE SELECTION
- PRELIMINARY BUDGET CONSTRUCTION COST ESTIMATE

INTERMEDIATE GEOTECHNICAL INVESTIGATIONS

- PHOTOGEOLOGIC INSPECTION
- GEOLOGIC MAPPING
- SURFACE GEOPHYSICAL SURVEYING
- FINAL SELECTION OF PREFERRED SITE
- PLANNING OF CORE DRILLING AND TESTING PROGRAM
- SELECTION OF CORE DRILLING AND LABORATORY CONTRACTORS

DETAILED GEOTECHNICAL INVESTIGATIONS

- CORE DRILLING
- CORE LOGGING
- CORE HOLE HYDROLOGIC TESTING
- CORE HOLE GEOPHYSICAL LOGGING
- IN SITU STRESS DETERMINATION
- LABORATORY TESTING OF REPRESENTATIVE CORE SAMPLES
- PREPARATION OF GEOTECHNICAL FEASIBILITY REPORT
- CONCEPTUAL STORAGE FACILITY DESIGN AND COST ESTIMATE

III. MARYLAND STUDY AREA GEOLOGY AND SELECTION OF PROSPECTIVE CAVERN AREA

- SUMMARY OF PRELIMINARY GEOTECHNICAL INVESTIGATION
- MARYLAND PHYSIOGRAPHIC PROVINCES (See Figure)
- GEOLOGY AND PROSPECTIVE CAVERN AREA - Howard and Montgomery Counties (See Figure)
- GEOTECHNICAL ASSUMPTIONS FOR CONCEPTUAL CAVERN DESIGN

MARYLAND PHYSIOGRAPHIC PROVINCES

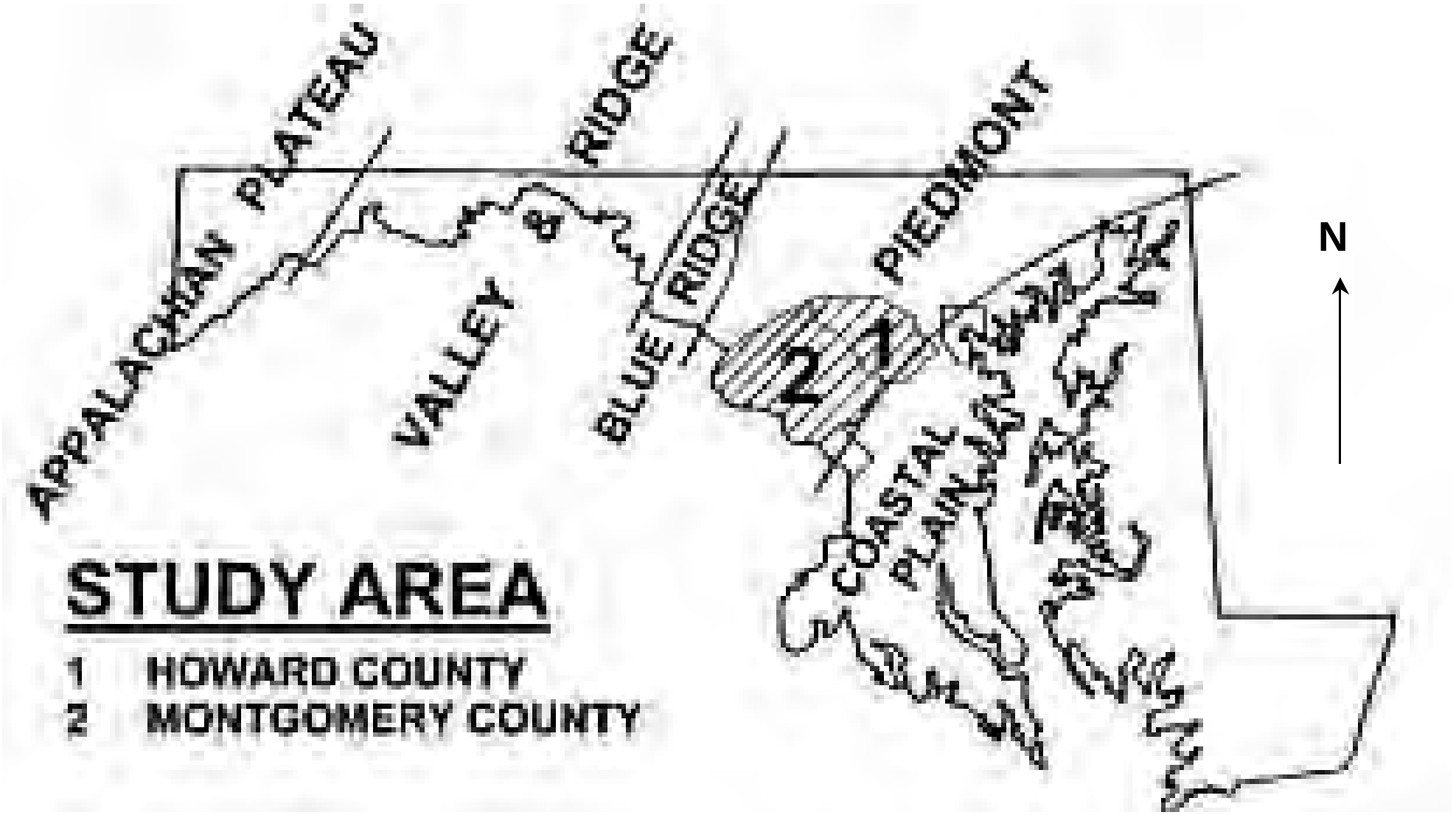

GEOLOGY AND PROSPECTIVE CAVERN AREA

Howard and Montgomery Counties

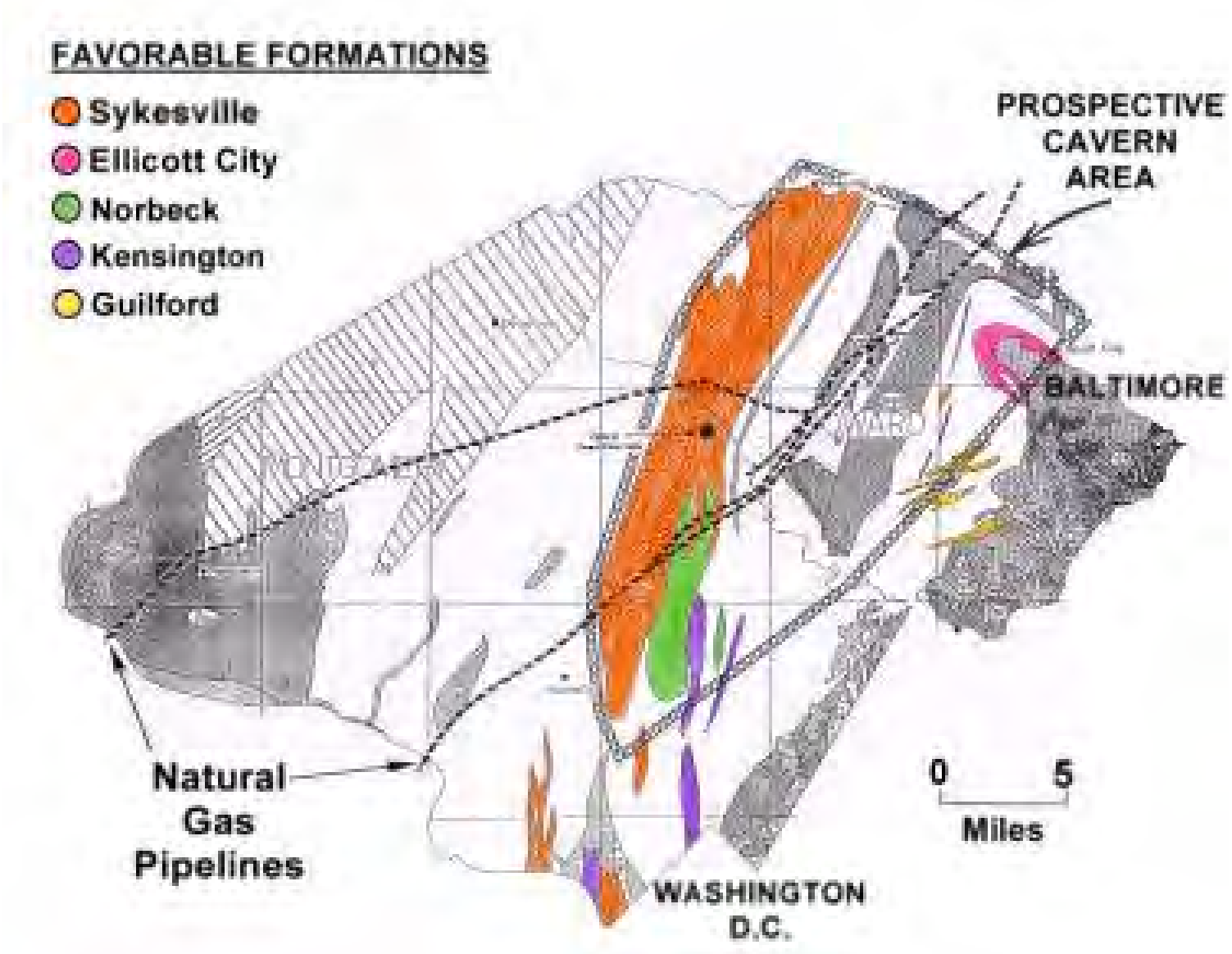

GEOLOGICAL CONCLUSION

- GOOD QUALITY ROCK SUITABLE FOR DEEP REFRIGERATED CAVERN CONSTRUCTION APPEARS TO EXIST IN STUDY AREA

SURFACE FACILITIES

Wally Swartz
Manager of Storage Operations

Surface Facilities

- Purpose of the Surface Facilities Analysis
- Design Basis of the Process
- Process Conceptual Design
- Plant Site
- Operating Costs

Purpose of the Surface Facilities Analysis

- Develop a plant and process conceptual design
- Estimate the cost of construction
- Estimate the cost of operation
- Compare the costs to alternative methods of gas storage

Design Basis

- The following conditions were selected from the range of parameters for the plant design:
  - Working gas storage of 5 BCF
    - 37 million cubic feet of spatial volume
    - Maximum cavern pressure of 1250 psig
    - Minimum cavern pressure of 250 psig
  - 250 MMSCFD maximum injection and withdrawal rates (20 day fill or empty cycle)

Design Basis (Cont.)

- Natural Gas storage at -20 ^{o}F
  - Refrigeration considerations
  - Metallurgy
- Incoming gas temperature of 50 to 80 ^{o}F
- Water content of incoming gas
  - 7lbm/MMSCF
- Water content of gas to the cavern
  - less than 1 lbm/MMSCF

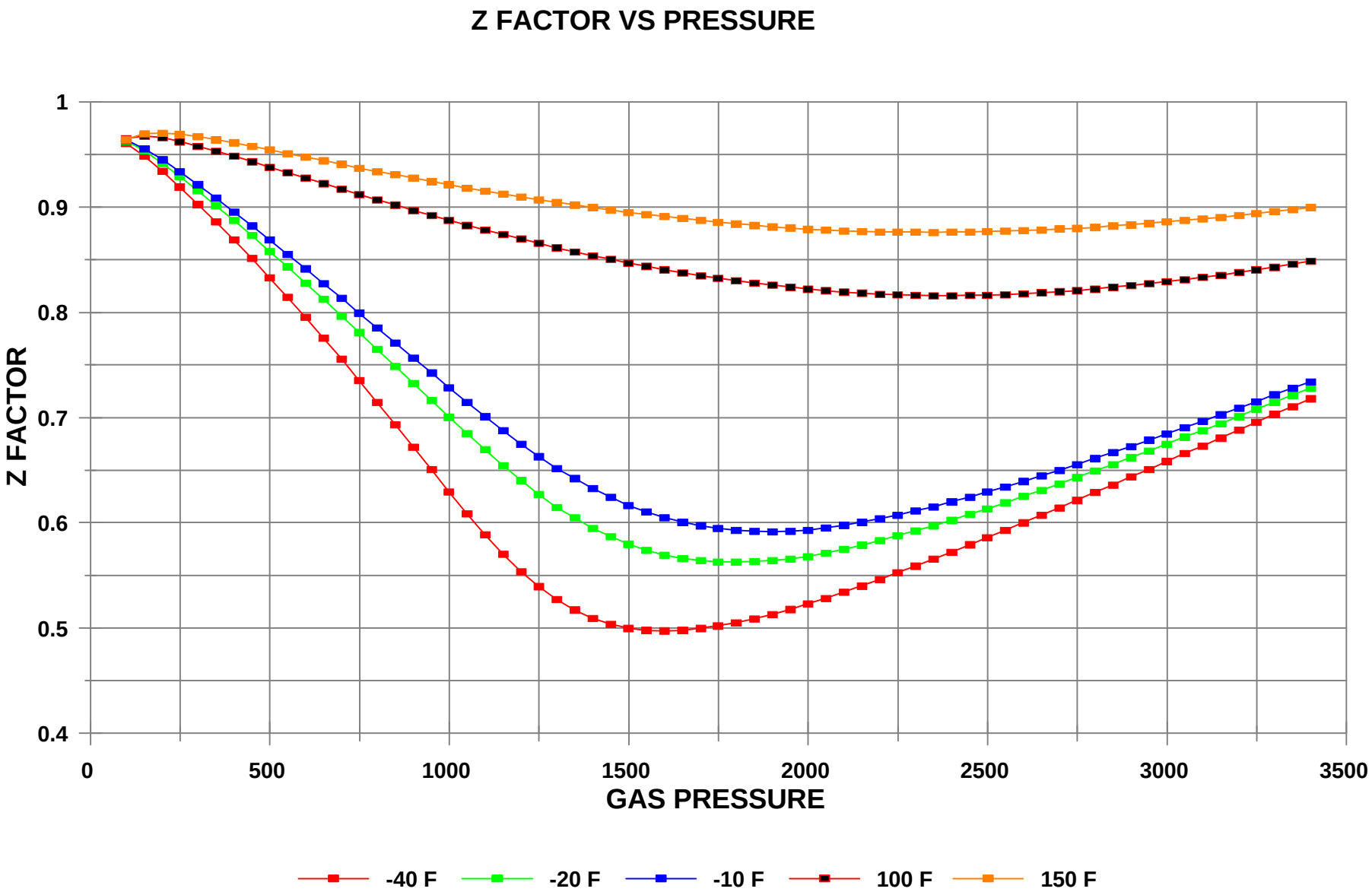
Z FACTOR VS PRESSURE
Z FACTOR
1
0.9
0.8
0.7
0.6
0.5
0.4
0
500
1000
1500
2000
2500
3000
3500
GAS PRESSURE
-40 F
-20 F
-10 F
100 F
150 F

FIGURE 2.0

Process Conceptual Design

Six Major Process Steps

- Gas Measurement for Receipt and Delivery
- Compression
- Dehydration
- Refrigeration
- Storage Cavern
- Gas Heater

Gas Measurement

- Pipeline quality gas at 400 to 600 psig
- Cavern pressure 250 to 1250 psig
- Multiple pipeline connections
- Automated Parallel Orifice Meters
- Instrument Building with data system

Gas Measurement

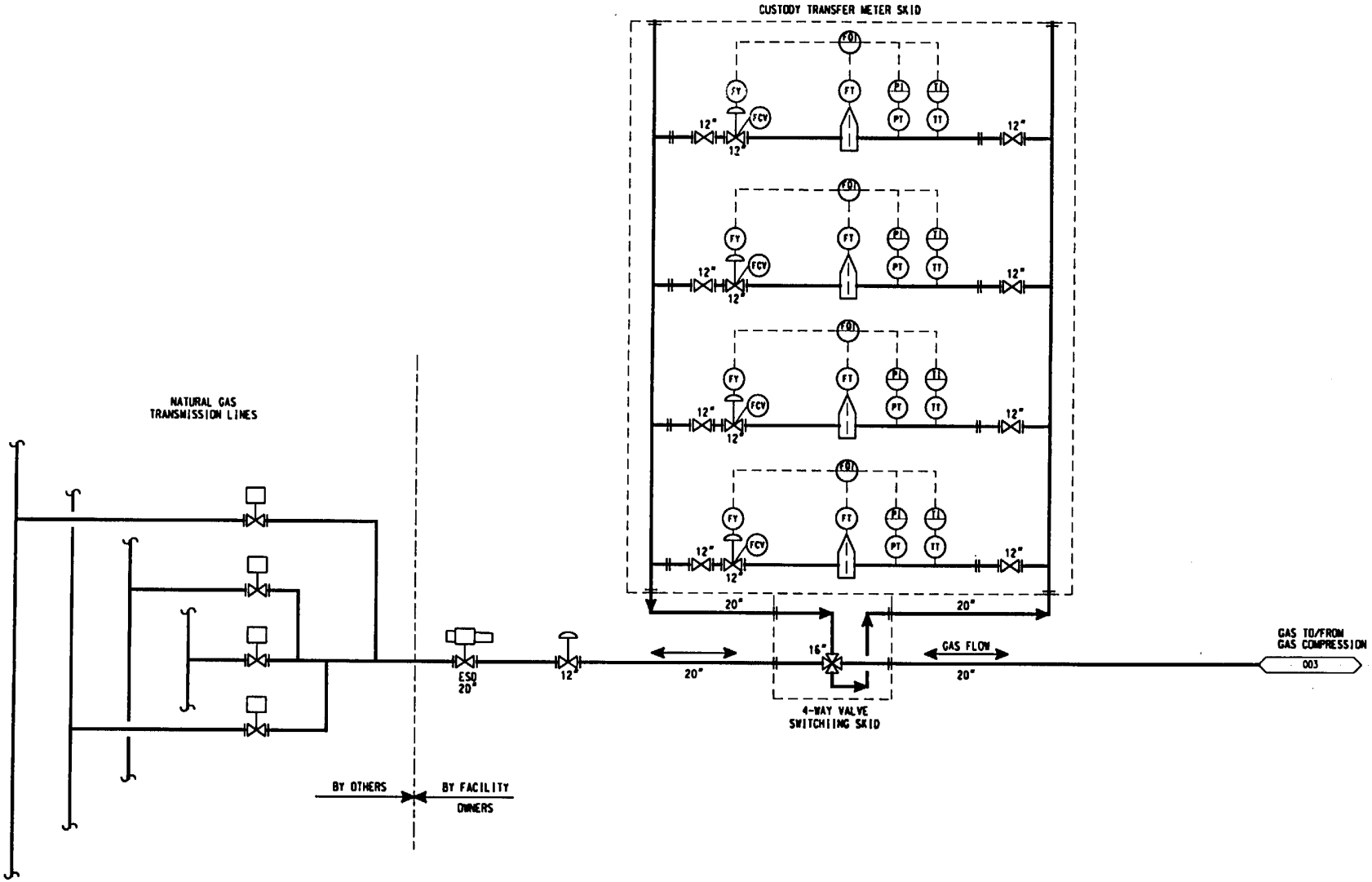

Compression

- Pipeline gas at 400 to 600 psig
- Cavern pressure from 250 to 1250 psig
- Maximum flow rate of 250 MMSCFD
- Two Solar C406 Compressors
- Mars 90 Gas Turbines - 20,000 HP
- Maximum injection conditions require 17,000 HP
- Maximum withdrawal conditions require 15,000 HP
- 200 HP recycle compressor

Gas Compression

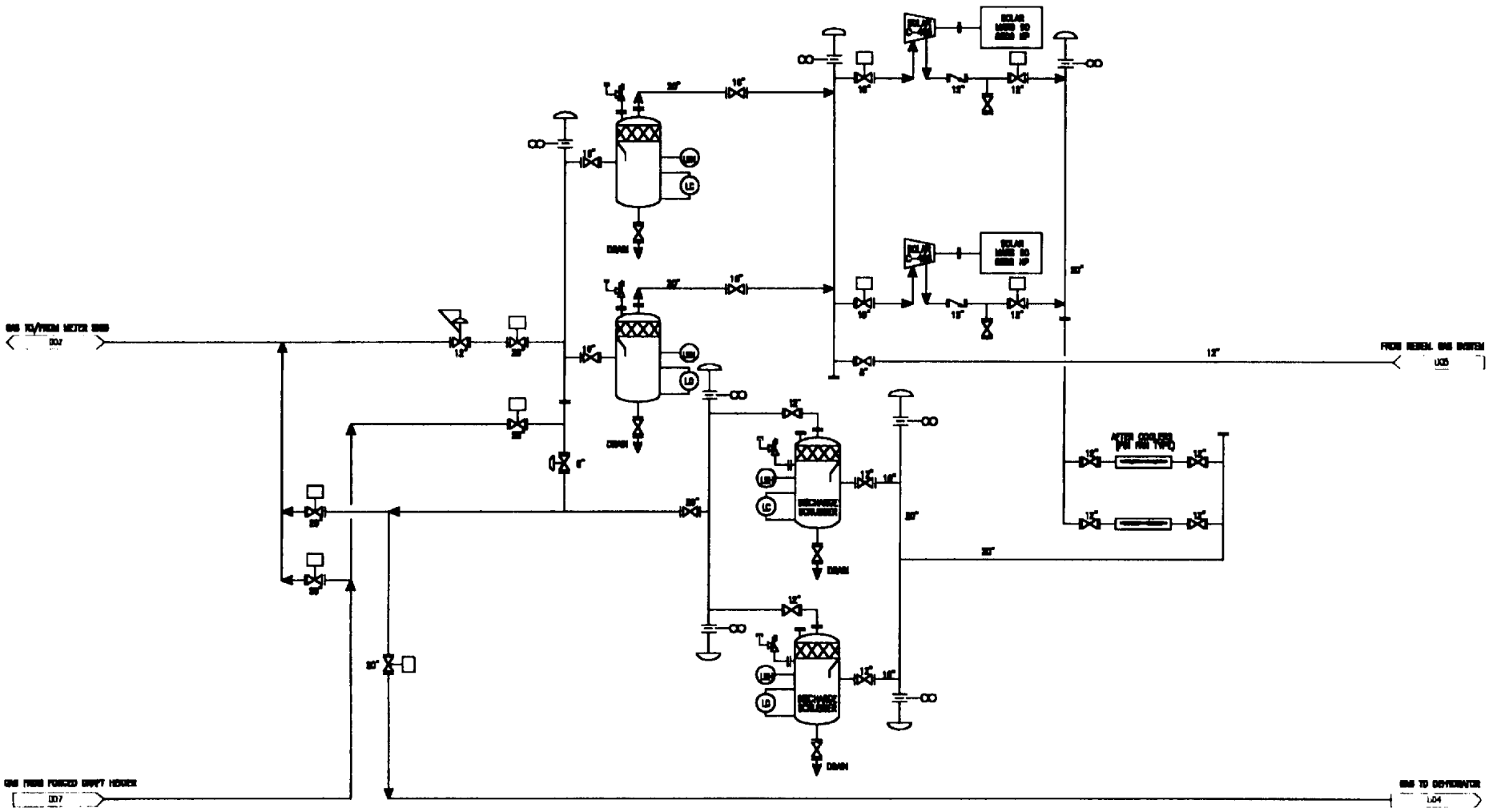

Dehydration

- Minimize hydrate formation after chilling to -20 ^{o}F
- Vendor’s sizing and budgetary estimate of automated molecular sieve dehydration skid
- Regeneration system and PLC controller
- < 1 lbm/MMSCF gas
- Skid mounted, PLC automated

Dehydration - Mole Sieve

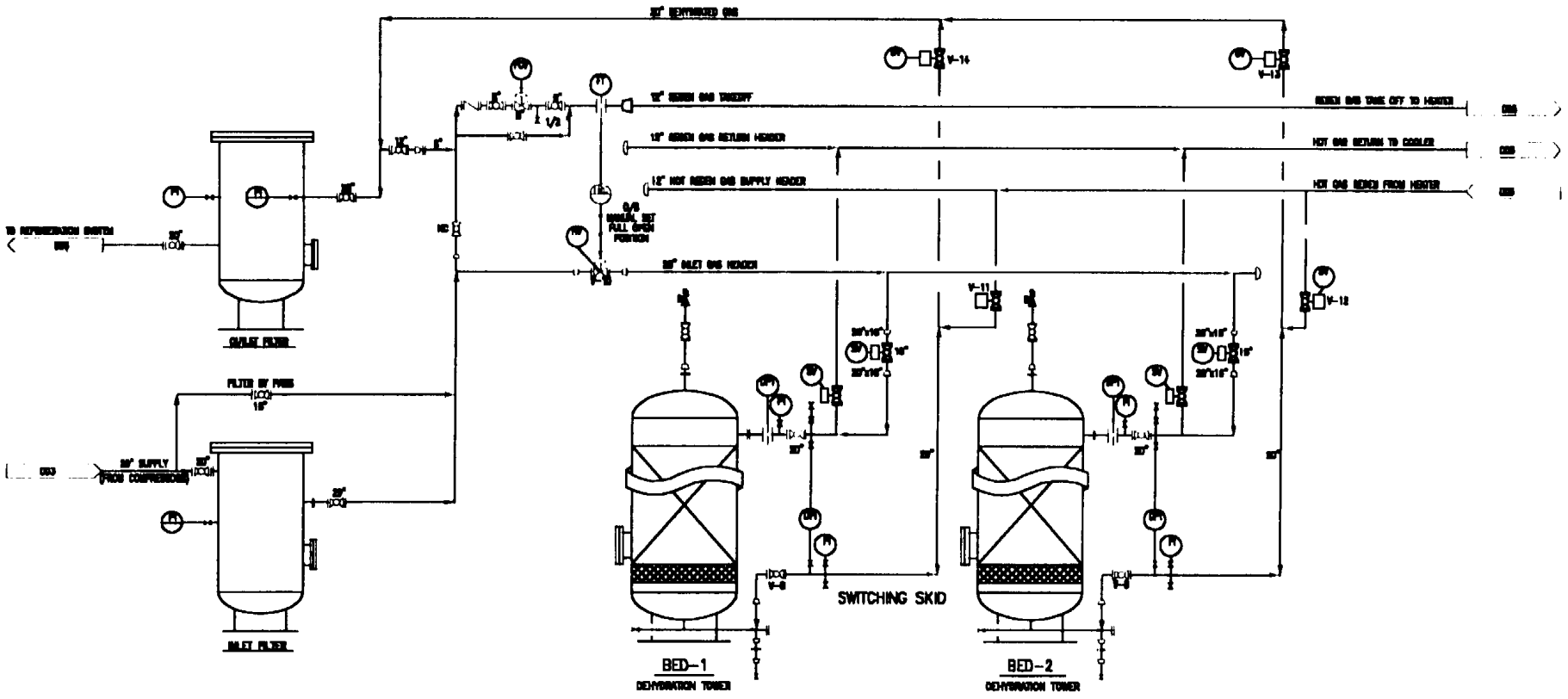

Mole Sieve - Regeneration

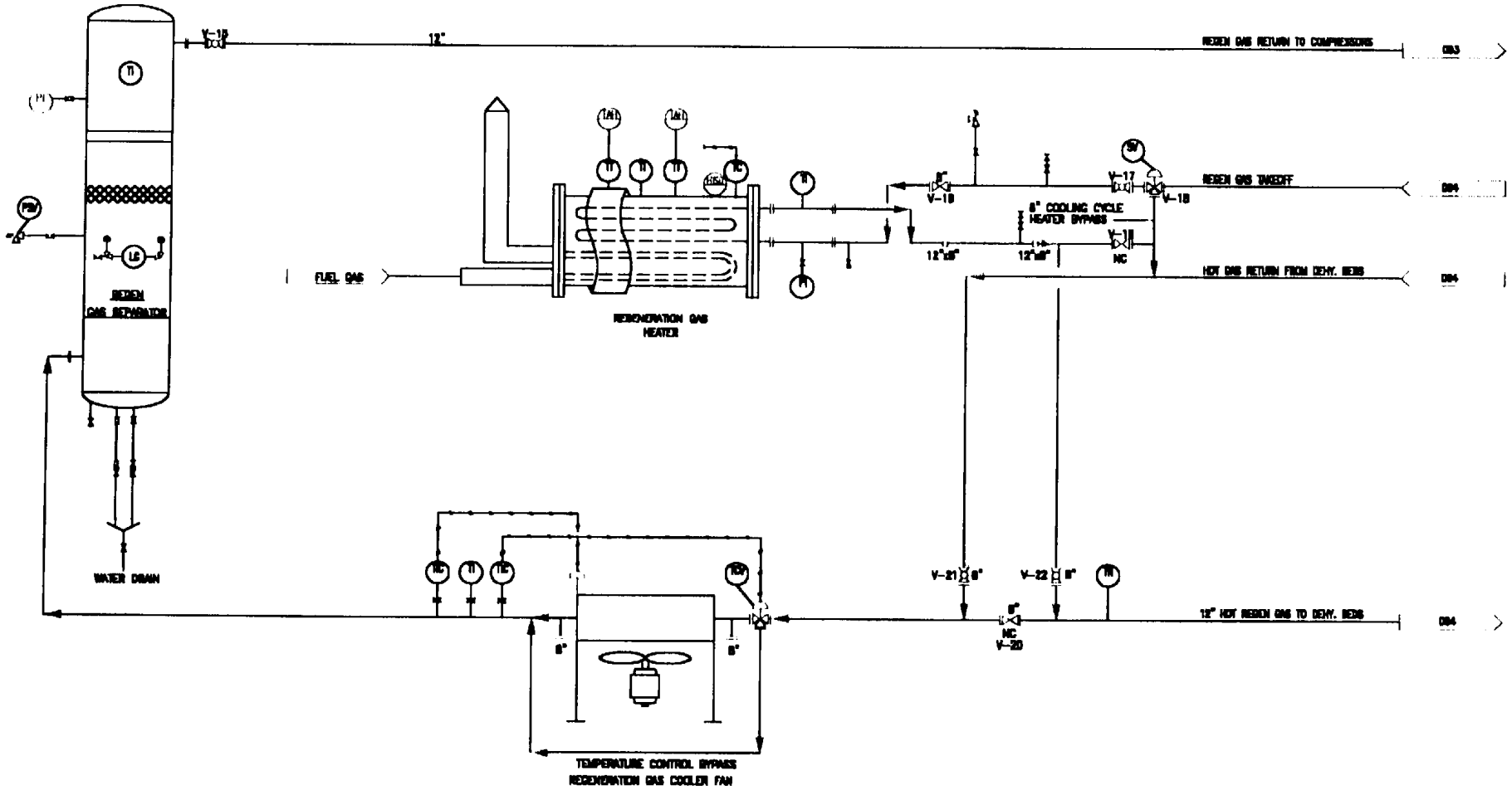

Refrigeration

- Three stage cycle
- Propane refrigerant
- Pipeline temperature to -20 ^{o}F
- Three Compressors with Gas turbine drivers - 4500 HP each
- Kettle type shell and tube heat exchangers
- 3900 Tons Refrigeration

Refrigeration

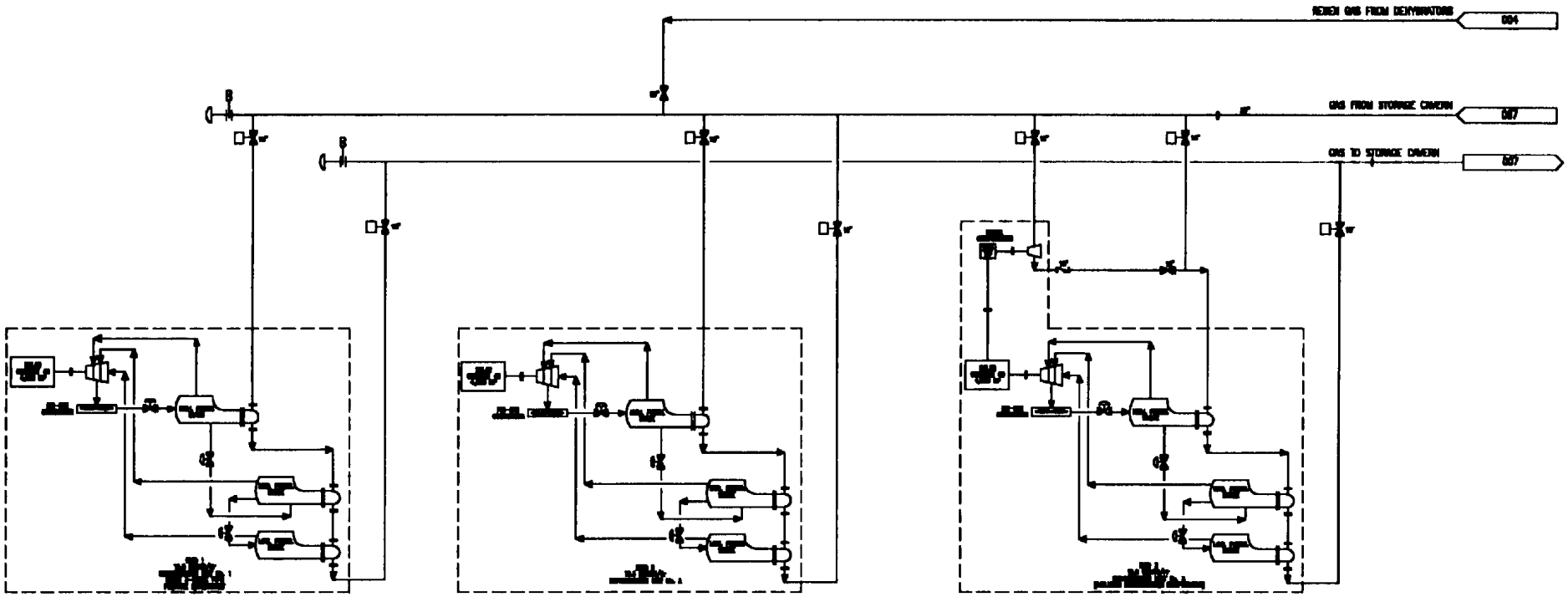

Cavern and Gas Heating

- 20 inch insulated line to cavern
- Cavern distribution system for refrigeration
- Gas fired convection heater for warming the withdrawal stream to the pipeline
- Maintenance cooling and dehydration may be required due to rock temperatures
- Heat balance will be affected by the injection withdrawal cycle
- Estimated cooling required after 1 year is 10 million BTU per hour
- The beneficial cooling of the withdrawal cycle is estimated to be 15 million BTU per hour

COOLING LOAD VS. TIME

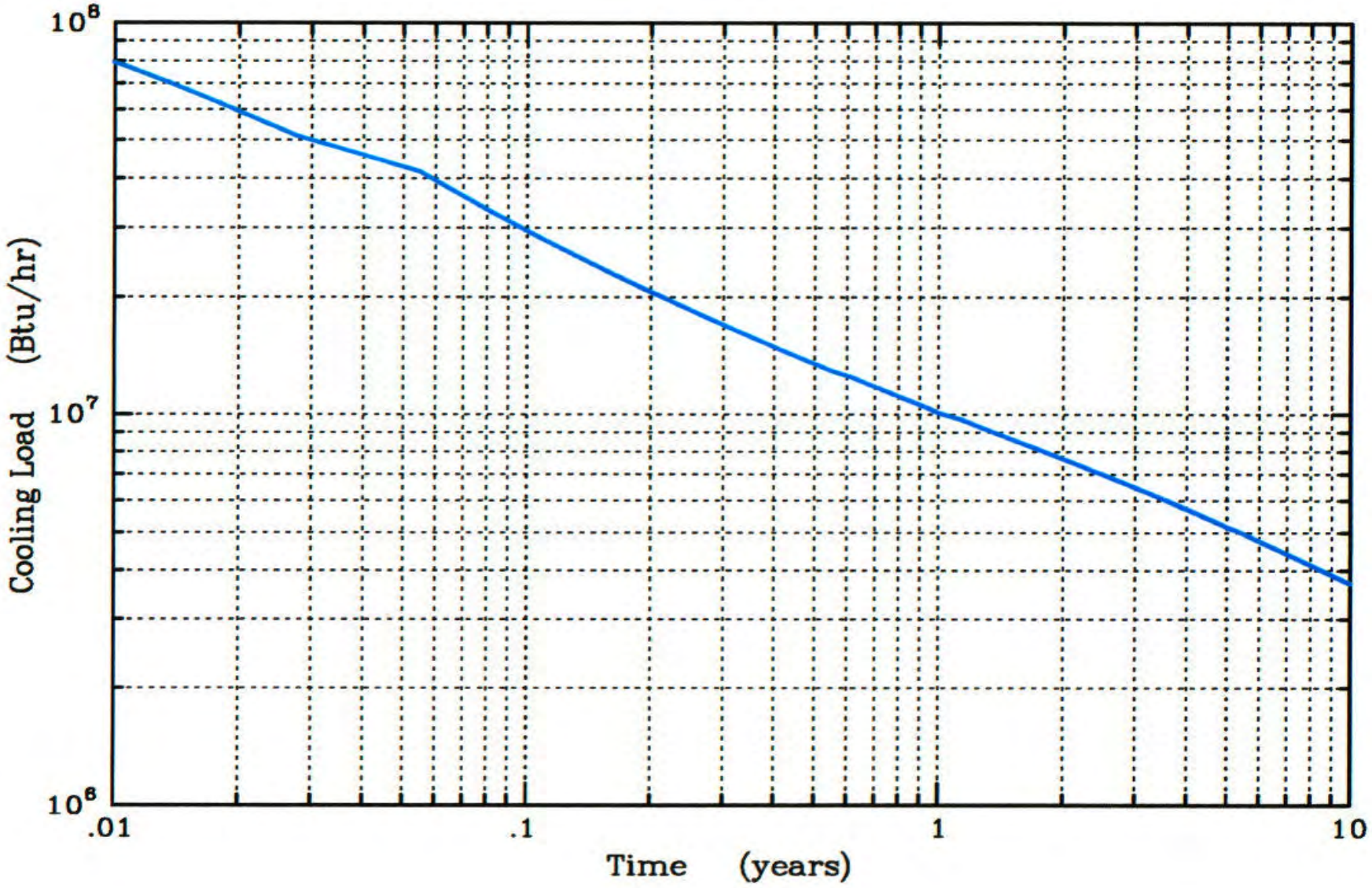

Cavern and Gas Heating

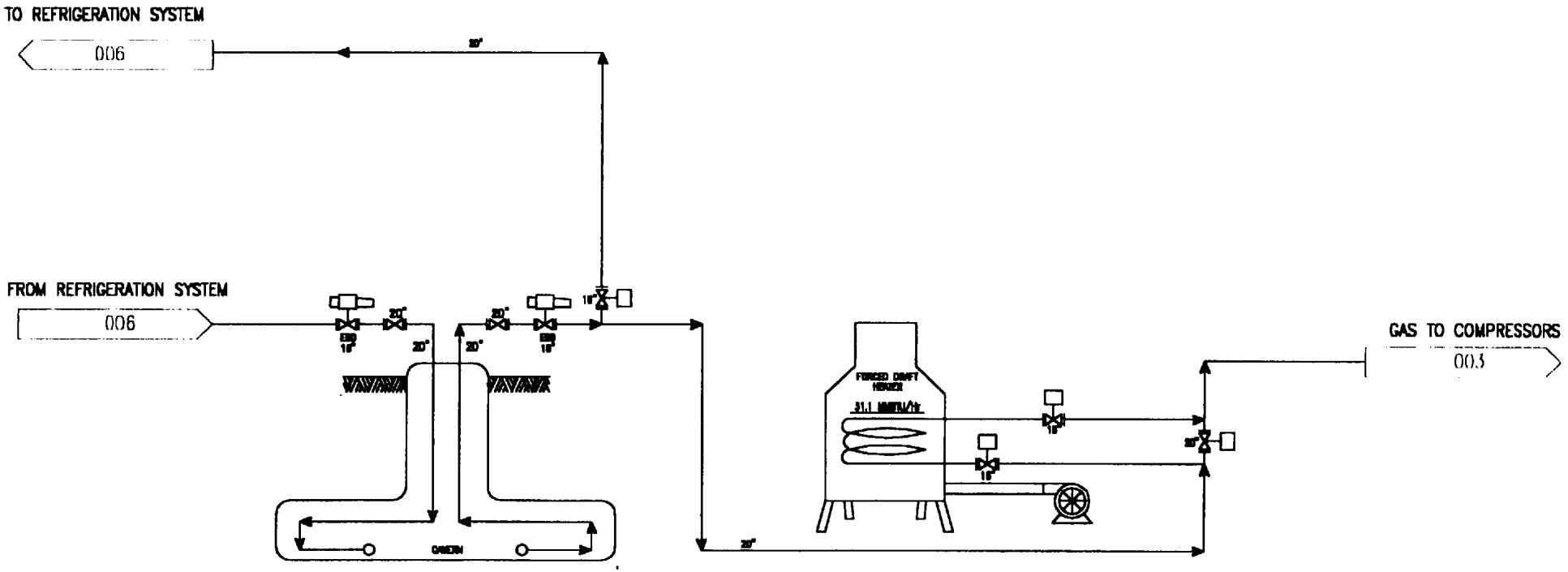

Plant Site

- Cavern occupies approximately 27 acres
- The process plant covers 4 acres
- Mining operation requires an additional 3 to 4 acres

Plant Site

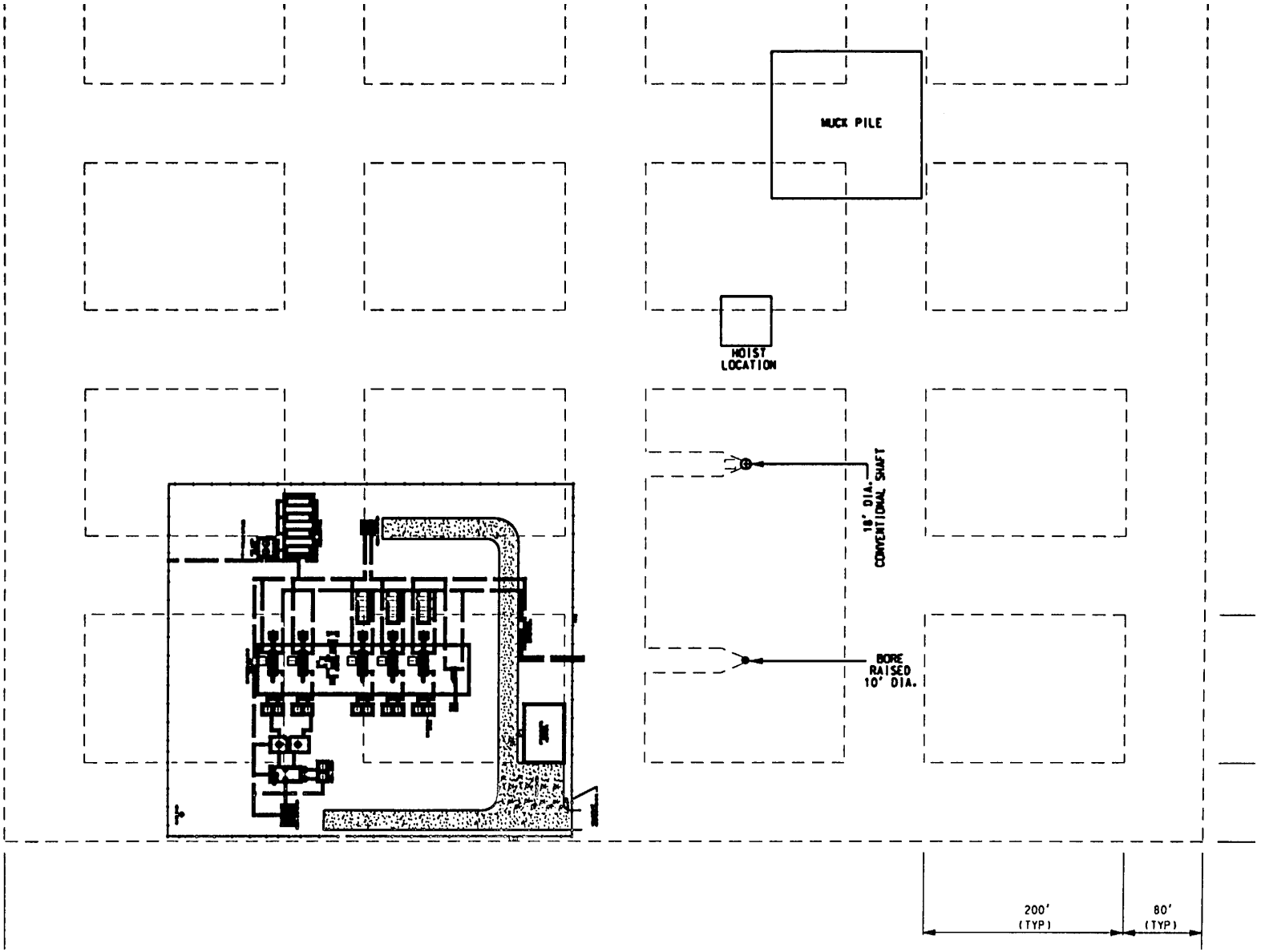
MUCK PILE
HOIST LOCATION
18' DIA. CONVENTIONAL SHAFT
BORE RAISED 10' DIA.
200' (TYP)
80' (TYP)

Plant Layout

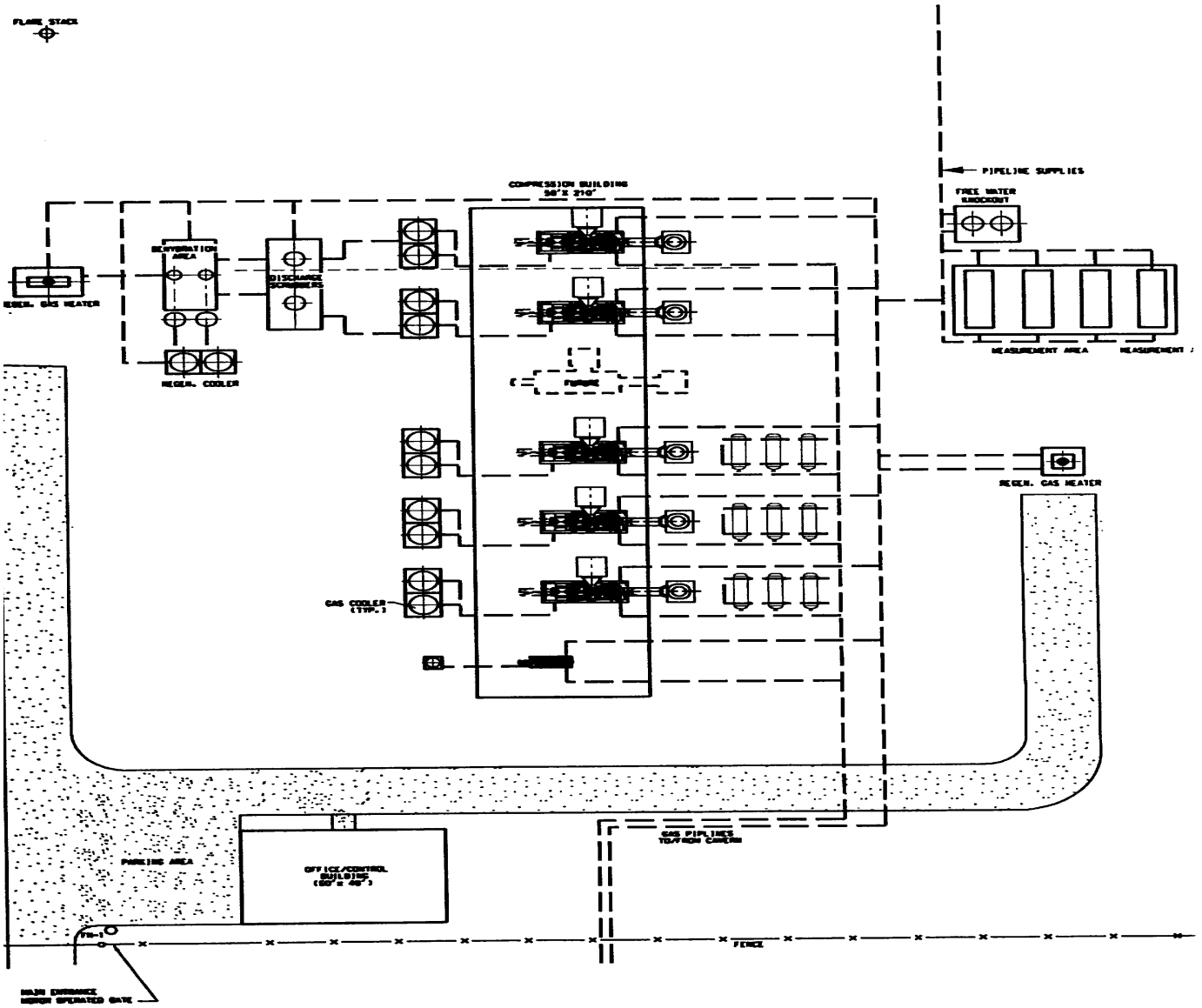

Plant Energy Costs

Energy Costs

Gas Cost - $/MMBTU:		$ 2.00	$ 2.25	$ 2.50	$ 2.75	$ 3.00
20 Day Injection Period	Fuel Required MMBTUs	Energy Cost	Energy Cost	Energy Cost	Energy Cost	Energy Cost
Compression	9,864.4	$ 19,729	$ 22,195	$ 24,661	$ 27,127	$ 29,593
Refrigeration	16,491.6	$ 32,983	$ 37,106	$ 41,229	$ 45,352	$ 49,475
Dehydration	1,920.0	$ 3,840	$ 4,320	$ 4,800	$ 5,280	$ 5,760
Plant Baseline	1,221.6	$ 2,443	$ 2,749	$ 3,054	$ 3,359	$ 3,665
Total Injection	29,497.6	$ 58,995	$ 66,370	$ 73,744	$ 81,118	$ 88,493
20 Day Withdrawal Period						
Compression	2,748.6	$ 5,497	$ 6,184	$ 6,872	$ 7,559	$ 8,246
Refrigeration	245.0	$ 490	$ 551	$ 613	$ 674	$ 735
Gas Heating	14,928.0	$ 29,856	$ 33,588	$ 37,320	$ 41,052	$ 44,784
Plant Baseline	1,221.6	$ 2,443	$ 2,749	$ 3,054	$ 3,359	$ 3,665
Total Withdrawal	19,143.2	$ 38,286	$ 43,072	$ 47,858	$ 52,644	$ 57,430
Total Cost Per In/Out Cycle		$ 97,282	$ 109,442	$ 121,602	$ 133,762	$ 145,922
Total Energy Cost Per Year		$ 875,534	$ 984,976	$ 1,094,418	$ 1,203,860	$ 1,313,302

Operating Costs

Cost Summary			
Cost Parameter	Monthly Cost	Annual Cost
Labor		
1 Supervisor	$ 8,190	$ 98,280
8 Shift Operators	$ 40,734	$ 488,808
2 Relief Operators	$ 9,165	$ 109,982
1 Clerical	$ 3,110	$ 37,315
Labor Subtotal	$ 61,199	$ 734,385
Maintenance Mat'l & Labor	$ 10,000	$ 120,000
Operating Supplies	$ 3,000	$ 36,000
Energy (as fuel gas)*	$ 91,202	$ 1,094,418
Total	$ 165,400	$ 1,984,803
* Assumes $ 2.50 per MMBTU		

Summary

- Conceptual design based upon cavern conditions
- Conventional processing equipment
- Surface site requirements
- Construction and operating costs

Doe Advanced Natural Gas Storage Concepts Program
Lunch Break

CHILLED GAS STORAGE IN MINED ROCK CAVERNS

Technology Transfer

PB-KBB INC.
11757 KATY FREEWAY
HOUSTON, TEXAS
281 589-5833

DEPARTMENT OF ENERGY
FEDERAL ENERGY
TECHNOLOGY CENTER
MORGANTOWN, WV

Natural Gas Hydrates Storage Project

Final Report
1 October 1997 - 31 May 1999

Principal Investigator
R. E. Rogers
March 26, 1999

Contract DE-AC26-97FT33203

Mississippi State University
P.O. Box 9595
129 Etheredge-Hardy Road
Mississippi State, MS 39762

Natural Gas Hydrates Storage Project
PHASE II.
Conceptual Design
and
Economic Study

Final Report
9 June - 10 October 1999

Principal Investigator
R.E. Rogers
Graduate Research Assistant
Yu Zhong
September 27, 1999

Contract DE-AC26-97FT33203

Mississippi State University
P.O. Box 9595
129 Etheredge-Hardy Road
Mississippi State, MS 39762

NATURAL GAS HYDRATES STORAGE PROJECT

FINAL REPORT
1 October 1997 - 31 May 1999

Principal Investigator

R. E. Rogers

March 26, 1999

Contract DE-AC26-97FT33203

Mississippi State University
P.O. Box 9595
129 Etheredge-Hardy Road
Mississippi State, MS 39762

ABSTRACT

Since economical and environmental conditions could be positively affected by greater use of natural gas, especially for peak-loading events of power plants, the feasibility of overcoming a major impediment of safe, aboveground storage in heavily populated areas was sought in the work funded by DE-AC26-97FT33203. Principal deterrent to utilizing natural gas to its fullest is the difficulty of on-site storage; principal incentive to utilizing natural gas to its fullest is its clean-burning quality and its relatively low cost.

Storage of natural gas in gas hydrates would have distinct inherent advantages of safety (stored gas would be essentially encased in ice), slow dissipation of gas in case of tank failure, and low operating pressures.

Greatly improved formation rates, packing density and process simplification were achieved in the subject study by incorporating sodium dodecyl sulfate in water at concentrations above the critical micellar concentration. Natural gas storage capacities of 155 vol-gas/vol-hydrate were demonstrated at 3.89 MPa (565 psia) and 275.4 K (36°F) in a quiescent system in less than 3 hours after hydrate initiation. The surfactant also causes hydrate adsorption and packing on the test-cell walls as the hydrates form. The process was shown to be technically feasible in the laboratory work.

To be feasible economically, a hydrate-storage process must be simple to minimize labor, maintenance, and equipment costs. The process envisioned from the laboratory work appears attractive in its simplicity. Development of design concepts and economic analysis are recommended as the next step.

TABLE OF CONTENTS

LIST OF FIGURES

LIST OF TABLES

EXECUTIVE SUMMARY

Although the unique gas-storage property of hydrates has long been known, their use industrially to store gas has never been utilized. The subject study was made to determine industrial potential of hydrates for gas storage; specifically, the study was to determine the feasibility of gas-hydrate storage for electric power plants to help meet peak-load fuel needs.

A breakthrough was achieved early in the study when the extraordinary effects of surfactant on the process were discovered. Thereafter, efforts centered on developing a surfactant-water based system to form the hydrates.

The surfactant sodium dodecyl sulfate (biodegradable, nontoxic, cheap) in hydrate-forming water concentrations as low as 286 ppm was found to resolve three major processing problems: (1) Hydrate formation rates were increased by a factor of about 700. (2) Hydrate particles formed, adsorbed, and packed on the tank walls--avoiding a technically difficult and economically forbidding mechanical separation and packaging step of removing hydrate particles from a water slurry. (3) Free water trapped between hydrate particles adsorbed on the vessel walls continued to occlude gas to full utilization of free water to provide a maximum packing density. (4) Processing was simplified: forming and storing hydrates in the same tank, reusing water in the storage tank without removing from that vessel, injecting gas and forming hydrates in a quiescent state, separating and packing of storage particles without mechanical assistance.

The presence of propane is necessary for lower-pressure Type II hydrates; both propane and ethane facilitate low-pressure processing. A gas mixture of 90% methane, 6% ethane and 4% propane was used in the experiments as a typical feed-gas composition representing relative amounts of the three hydrocarbons in natural gas. It was determined that 155 vol/vol of natural gas of this composition could be stored in hydrates at 3.89 MPa (550 psig) and 564.9 K (36°F). Or at a lower processing pressure of 3.57 MPa (518.3 psia), 148 vol-gas/vol-hydrate could be stored. Moreover, formation rates are such that 86% of the theoretical maximum storage capacity could be achieved within 2 ½ hours, thus allowing a complete cycle of gas-hydrate formation, decomposition, and turn-around-time within a 24-hour period.

With surfactant, a hydrate storage process becomes technically feasible. The simplicity of the process with surfactant improves the probability of an economically-viable process. Based on the laboratory data, a design concept of a formation/storage tank is presented. It is recommended to develop a final process design and economic study in a follow-on, option phase of this study.

INTRODUCTION

A. Historical, State-of-the Art

Gas hydrates were discovered in 1810 by Davy, chlorine gas being occluded in those first hydrates. Although their unique storage capabilities were recognized, they remained a laboratory curiosity. Expanded interest and research developed in about 1940 prompted mainly by hydrates' nuisance in the oil field. Consequently, the thrust of research became to develop means to prevent hydrate occurrence in hydrocarbon transmission lines through arctic regions and subsea. In the 1980s and 1990s discoveries of large quantities of gas stored in naturally-occurring hydrates on the sea floor, perhaps as much as 1116 trillion cubic meters (tcm) of hydrocarbon gases, was a major impetus in the current acceleration of hydrate research. The subject DOE grant is the first serious attempt to utilize the unique properties of hydrates to store natural gas for applications such as peak loads of electric power plants. The objective of this contract DE-AC26-97FT33202 was to determine the technical feasibility of using gas hydrates to store natural gas aboveground for peak loading of electric power plants; if found feasible, a follow-on phase would develop a conceptual design of a large-scale process and would determine the economic viability of such a process.

At the beginning of the current work, November 1997, hydrate state-of-the-art recognized positive and negative factors regarding feasibility of gas storage in hydrates.

The positive factors known at project initiation were the following: (1) 180+ vol-gas/vol-hydrate could be stored. (2) Safety of storing natural gas in hydrates was unmatched, for gas would be essentially encased in ice. (3) Gas could be stored in the hydrates at relatively low pressures. (4) The slow release of gas from hydrates in the event of storage-tank rupture enhances safety. (5) Vast quantities of gas stored in naturally-occurring hydrates were known.

Also, at the beginning of the project, the following negative factors diminished feasibility prospects: (1) The formation of hydrates in a quiescent pure water-hydrocarbon gas was extremely slow at hydrate-forming temperatures and pressures. Historically, hydrate formation in the laboratory with a rocking cell apparatus had been cumbersome and slow. (The rocking motion establishes enough turbulence to periodically sweep away the hydrate film that forms on the water surface preventing contact with the gas.) (2) The state-of-the-art process was complex for scaleup, especially if a mechanically stirred reactor became necessary to achieve acceptable formation rates. (3) The slurry separation and packing of hydrate particles formed in a mechanically-stirred reactor seemed prohibiting. (4) When hydrate particles form, much free water is trapped in the interstices of particles. Therefore, free water between particles would occupy much of the expensive storage tank. (5) A storage process for hydrates had never been demonstrated.

These negative factors had to be overcome to develop a feasible process.

B. Structure, Properties of Hydrates

Natural gas hydrates are crystalline inclusion compounds formed when natural gas under pressure comes into contact with water at low temperatures. Through hydrogen bonding, the host water molecules form a lattice structure resembling a cage. The hydrate lattices contain large vacancies or cavities. These cavities are at least partially occupied by small gas molecules such as CH_4, C_2H_6, C_3H_8, I-C_4H_{10}, n-C_4H_{10}, N_2, and CO_2 to stabilize the lattice structure. (Sloan, 1991; Tse et al., 1983; Wilcox et al., 1941) Normally, hydrates are formed in one of two types of repeating crystal structures. The basic water configuration from which the two hydrate structures are formed has 12 faces with 5 sides per face. Links between the vertices of this basic configuration result in type I hydrate structure, while structure II is produced by the coupling of the faces (Sloan, 1990). Each unit cell of a hydrate of structure I consists of 46 water molecules which form two small and six large cavities. The unit cell of a hydrate of structure II consists of 16 small and eight large cavities formed by 136 water molecules.

Each of the two hydrate structures, I and II, accommodates two sizes of molecules. In structure I, gases with molecular diameters up to 5.8 Angstroms can fit in the large cavities, while only molecules of diameter less than 5.2 Angstroms can fit in the small cavities or have the option of filling both cavity sizes. A similar arrangement occurs with the structure II hydrate that has cavities of 4.8 Angstroms and 6.9 Angstroms. If gases such as propane are present with 5.8>diameter#6.9 Angstroms, then structure II must form to accommodate the larger molecules (Makogon, 1981; Sloan, 1991). Pentane (C_5H_{12}) and heavier hydrocarbons do not form hydrate because of their size (Carson and Katz, 1941).

Generally, the hydrate number n (ratio of water to gas molecules in the hydrates) is used to express the composition of gas hydrates. The higher the hydrocarbon concentration, the lower the hydrate number n. For structure I, the lowest hydrate number is 5.75 (7.67 if only the large cavities are filled). For structure II, the minimum hydrate numbers are 5.67 if all cavities are filled or 17.0 if only the large ones are occupied. The packing of gas molecules in a hydrate structure approaches that of liquid form (Makogon, 1981).

The volume of gas stored in a given volume of hydrates under hydrate formation conditions of pressure and temperature is calculated using Eq. (1) (Makogon, 1981).

$$V_{GH} = (V \tilde{n} V_G 10^3)/M_h \qquad (1)$$

The equation for the molecular weight M_h of the hydrates reads

$$M_h = M + 18.02\ n \qquad (2)$$

The hydrate number n is given by Eqs. (3) and (4) for structures I and II, respectively. (Spontak, 1986; Sloan, 1990)

$$n = 46/(2\grave{e}_{sm} + 6\grave{e}_{bg}) \quad (3)$$

or

$$n = 136/(16\grave{e}_{sm} + 8\grave{e}_{bg}) \quad (4)$$

A detailed discussion on the determination of the fractional fillings $\grave{e}_{sm}$ and $\grave{e}_{bg}$ of the small and large cavities is given by Makogon (1981) and Sloan (1990).

The density of hydrates formed by gas mixtures is given by Eq. (5) (Makogon, 1981)

$$\tilde{n} = [\sum N_i (M_i + 18.02 n_i)] / \sum 18.02 N_i V_i n_i \quad (5)$$

Where

M = molecular weight of gas mixture
M_h = molecular weight of hydrate
M_i = molecular weight of hydrate forming gas I
V = volume of hydrate (m^3)
V_{GH} = volume of gas stored in hydrate (m^3)
V_i = specific volume of water in hydrate formed by component I (m^3/kg)
V_g = percentage of volume of gas stored in hydrates, nondimensional
n = hydrate number, nondimensional
$\tilde{n}$ = density (kg/m^3)
$\grave{e}_{bg}$, $\grave{e}_{sm}$ = fractional filling of large and small cavities, nondimensional

C. Rate of Hydrate Formation

The basic rate equation for hydrate formation relates pressure, temperature, degree of supercooling, and water-gas interface area (Vysniauskas and Bishnoi, 1983). In eq. (6) A represents a lumped pre-exponential constant, a_s is the water-gas interfacial area, ΔE_a is the activation energy for hydrate formation, R is the universal gas constant, T represents absolute temperature, P represents system pressure, a and b are arbitrary constants and $\tilde{a}$ is the overall order of reaction with respect to pressure.

$$r ' A a_s \exp(-\frac{\Delta E_a}{RT}) \exp(-\frac{a}{\Delta T^b}) P^{\tilde{a}} \qquad (6)$$

The parameters in the equation have been established for a methane-pure water system (Vysniauskas and Bishnoi, 1983) and ethane-pure water system (Vysniauskas and Bishnoi, 1985) in which the water was mechanically stirred. It is useful to keep in mind eq. (6) as the effects of surfactants on the rate of formation are discussed.

The interfacial area between the liquid water and gas is generally established in laboratory experimentation by vigorously agitating the test cell contents as hydrates form, continually regenerating the contact surface of gas and water. For example, in the experimental apparatus of Narita (1996) an impeller speed of 500 rpm gave a maximum hydrate reaction rate. At 500 rpm, Vysniauskas and Bishnoi (1983) estimated a surface area of the gas/water interface as 106 cm^2 for their system. For rapid hydrate formation, a renewable surface is necessary because a thin film of hydrates which forms on the water surface isolates the gas from the water to decrease gas absorption rate into the free water (Herri *et al*., 1996). Therefore, hydrate formation rate in a quiescent system is extremely slow and controlled by the diffusion rate of the gas as well as the water through the thin hydrate film (Mori and Mochizuk, 1996).

A latent heat of formation of about 65.4 kJ/mol (Sloan, 1990) is released at the water-gas interface when hydrates form, introducing heat transfer rate as a factor in hydrate formation rate as it affects the temperature terms in eq. (6). The relatively large release of heat creates an experimental problem of determining a true interfacial temperature. Stainless steel surfaces increase formation rates by their conductive removal of heat from the interface and facilitate hydrate formation by being a promoter of nucleation.

D. Formation Mechanism, Quiescent State

The mechanism of hydrate formation in a quiescent pure water-gas system is that water molecules first form clusters by hydrogen bonding in the liquid phase, proceeding to cluster and occlude gas until a critical concentration and size of the clusters is reached which is the critical nuclei for hydrate formation (Vysniauskas and Bishnoi, 1983). After an induction time of 20 minutes or less, depending on system conditions, particle agglomeration of these nuclei proceeds at the water-gas interface, resulting in a thin film of hydrates on the surface that isolates the liquid from the gas, drastically slowing the rate of formation. Gas and water then must diffuse through the thin film to perpetuate crystal growth.

In the mechanism of hydrate formation in a quiescent system, free water is trapped between solid hydrate particles. This water may represent a large percentage of the hydrate volume. Englezos (1996) found only 1.4% to 14% of the water in an experimental cell (based on maximum amount that could form hydrates and dependent on the guest molecular identity) was bound in the hydrate structure while

most of the water was trapped between solid particles. The entrapment has been a deterrent to practical use of the hydrates. For example, if gas storage in hydrates for industrial use were the goal, appreciable volumes of the storage tank would be occupied by the trapped water, decreasing storage capacity and rendering hydrates as a gas storage means impractical.

E. Test Apparatus

The experimental apparatus used in the subject grant is sketched in Fig. 1.

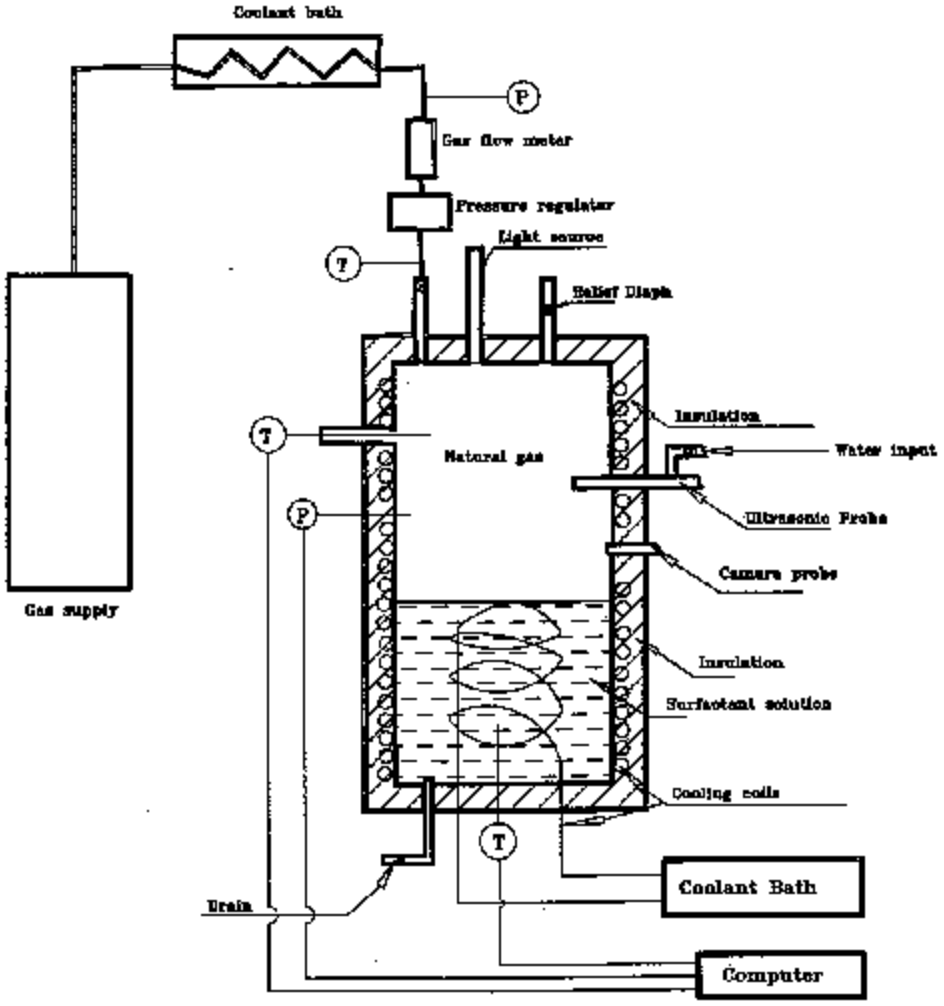

Fig. 1. Sketch of test apparatus.

The 304 stainless steel test cell has a capacity of 3800 cm^3. Both ends are sealed with blank flanges bolted to the cell; the flanges have phonographic serrated raised faces with 0.79 mm concentric grooves to accommodate sealing with 2.4 mm thick Teflon gaskets. Each blank flange has appropriate ports for access to the interior; additional ports exist along the sides of the cell. Inside the lower half of the cell is a coil of 9.5 mm diameter 316 ss tubing through which is circulated cooling water with enough ethylene glycol to depress the water's freezing point to 253 K. The coolant is circulated from a refrigerated bath capable of maintaining bath temperature within ±0.01 K of the set point to a low temperature capability of 253 K. Around the exterior of the cell is also coiled 9.5 mm diameter stainless steel tubing through which the coolant is circulated. The cell and cooling coils are enclosed with insulation. An ultrasonic probe and atomizer extend into the cell from a side port. One RTD probe extends into the bottom of the cell; a second RTD probe extends into the gas phase at the top. One pressure transducer extends into the cell from a side port, and a second transducer monitors pressure in the feed reservoir vessel. A piston metering pump with a maximum pressure capability of 5.52 MPa and a flow rate of 31 ml/min allows metering water solutions into the cell under pressure.

The cell interior is viewed during operation in one of two ways. One choice is to view the interior or take still camera photographs through a 101.6 mm diameter x 50.8 mm thick quartz window secured in a blind flange bolted onto the top of the cell. A second choice is that depicted in Fig. 1. Two 9.5 mm i.d. viewing wells extend into the cell from the top and side of the cell. One well allows light input from a 150 watt halogen light source transmitted by fiber optics light guide. The wells are sealed with transparent sapphire windows pressure checked to 16 MPa. The second well accommodates a Model 702-023K black and white video camera with the image transmitted to either a video cassette recorder for taping and a television monitor for viewing while running or directly to the computer for digital processing. The viewing system was supplied by Instrument Technology, Inc.

A Model FMA-8508 mass gas flowmeter from Omega Engineering, Inc. was used to measure gas added to the cell during hydrate formation. The flowmeter has a capability of 0-5000 sccm, at an accuracy within 1% of full scale and a repeatability of within 0.25% of flow rate. A Tescom Corporation model 26-1026 constant pressure regulator can maintain constant pressure in the cell within ±6.9 kPa.

Outputs from the mass flowmeter, RTDs and pressure transducers are recorded and displayed on computer by Omega software and an Omega data acquisition system.

Double-distilled water was used in all experiments. Sodium dodecyl sulfate (SDS), molecular weight of 288.4 g/mole, was purchased from Strem Chemicals, Inc. SDS in powder form was 98%+ pure with no alcohols in the residuals. Surfactant was weighed by means of a Model AG 204 Mettler analytical balance and added to the desired volume of water.

Ethane gas was purchased from Matheson Gas Products. Analysis with the gas chromatograph established an ethane purity of 99.6%. A primary gas mixture of methane, ethane and propane was

purchased from Matheson to give representative and relative quantities of these three major hydrate formers of natural gas. The gas mixture contained 90.01% methane, 5.99% ethane and 4.00% propane. Gases were analyzed by means of a Model 6890 Hewlett-Packard gas chromatograph, using a HPPLOT-Q column and a flame ionization detector. Ethane was used at the lower pressures in the experiments to establish a procedure, and then the natural gas mixture was used in verification and expansion of the data.

F. Test Procedure

A typical procedure was as follows. Initially, surfactant-water solution was pumped into the empty cell to displace all gases. The hydrocarbon gas was then injected to displace water to a predetermined water level. For example, the level could be selected to be along the line of sight of the camera probe in which case liquid completely covered the internal cooling coils. With a pressure below where hydrates could form, the system was cooled to 275 K- 278 K. Pressure was then raised to the operating pressure over a 2-3 minute span by flowing precooled gas into the cell; measurement of gas mass admitted was made with the flowmeter. After reaching desired pressures, constant pressure was maintained as hydrates formed. Hydrate formation was followed by the temperatures, pressures, and mass flows continuously displayed and recorded on the computer. During each experimental run, the inside of the cell was observed on a tv monitor and the video recorded with commentary on video tape.

A second procedure was similar except hydrates formed under a decreasing pressure because occluded gas was not being replenished during the process. In this procedure, the constant-pressure regulator and mass flowmeter were not used; gas contents were followed with gas-law calculations.

In comparing the two foregoing procedures, a faster hydrate formation rate and a larger fraction of the crystal cavities filled when the initial high pressure was kept constant throughout the process.

Two procedures were also used in obtaining photographs for the subject report. In one procedure, camera shots were made through the 101.6 mm (4 in.) diameter quartz window on top of the cell. These give excellent views of hydrate crystal development with and without surfactant. Later in the work, the transparent top was replaced with a fiber-optics/camera system that allowed video tape recording of the action inside the cell. Excellent film was obtained on VHS tape. However, transferring part of the film to still photographs for this report proved difficult in maintaining clarity. The best procedure turned out to be photographing the images on the monitor while playing the film; three photographs in the report were thus taken and presented with the reminder that the video tape is clearer. Excellent footage was recorded on tape.

RESULTS AND DISCUSSION

It is the objective of the study to determine the feasibility of utilizing gas hydrates to store natural gas for industrial use.

I. Surfactant Effects

At the beginning of the study it was apparent that technical breakthroughs would be necessary in several areas before hydrates could be successfully used to store natural gas in a large-scale process. Those breakthroughs needed were the following: improved packing fraction of gas in the hydrate mass, faster formation rate of the hydrates, means to collect hydrate particles from water slurry, and process simplification.

A breakthrough came with the introduction of small quantities of an anionic surfactant sodium dodecyl sulfate into the water from which hydrates were to be formed. A dramatic improvement was realized in gas packing fraction, formation rate, collection of particles and process simplification.

A. Storage Capacity with Surfactant

There are two separate problems in realizing the highest possible storage capacity of gas in hydrates. The first problem is to fill the cavities of the crystal with gas. The second problem is to increase the packing fraction of hydrate particles.

The first problem may be succinctly stated as follows. Ultimate storage capacity of gas in the hydrates is limited by thermodynamics to about 181 vol-gas/vol-hydrate. That is, all cavities in the hydrate are then filled with natural gas components. As pressure of the system increases, the fraction of filled cavities increases. To establish a practical, cost-effective process for hydrate storage of gas, therefore, one must optimize the pressure, since costs of processing and storage increase with pressure. There must be a tradeoff between added costs of higher pressures and the cost benefits of a larger fraction of cavities filled.

The second problem in establishing practical storage capacity results from the entrapment of free water between hydrate particles. The solid mass of frozen hydrates entrap a large amount of water between particles so that the bulk of hydrate mass formed in a vessel, for example, would contain a large volume of water trapped and isolated from contact with gas. In other words, much of the storage space in the tank would be occupied by water not containing gas. The packing fraction of gas in the frozen mass of hydrates could be low even though the cavities in the hydrate crystals of that mass were mostly filled with occluded gas.

The first problem mentioned above will be discussed in another section; it is thermodynamically limited and not affected by surfactant. The second problem will be addressed at this point because the use of surfactant in the water solves that problem.

(1) Conversion of Interstitial Water in Batch Process

The entrapped water problem was addressed in a series of experimental runs with natural gas (90.01% methane, 5.99% ethane, 4.00% propane) in which pressure was allowed to decline in the test cell as hydrates formed in a batch-type process. The system conditions were a quiescent state, pressure initially at 3.57 Mpa (518.3 psia), temperature at 274.8- 277.6 K (35-40°F), and 286 ppm SDS in double-distilled water. As pressure approached equilibrium from the first batch of gas, free water was drained from the bottom of the cell. Another batch of gas was added to bring the pressure back to 3.57 MPa. Five such additional batch loadings of gas were made, and each loading was returned to 3.57 MPa at its beginning. With this scenario, hydrate particles formed on the first loading with attendant free water trapped between particles. Since the free water in the bottom of the cell had been drained, any hydrates formed in subsequent loadings necessarily originated from water trapped between hydrate particles. A mass balance using the gas laws revealed how much gas went into hydrates for each loading; along with the time measurement during each loading, the rate of formation was also calculated for each loading.

In Fig. 2 is presented data for natural gas that shows the packing fraction of each loading. Note that the last four loadings represented by the lightly-shaded areas were obtained by extrapolating the data, since the experiments were stopped after six loadings. (The moles of gas found to be in the frozen mass divided by the theoretical moles of gas in the frozen mass if all water was converted to hydrates and all cavities filled with gas is referred to as the packing fraction.)

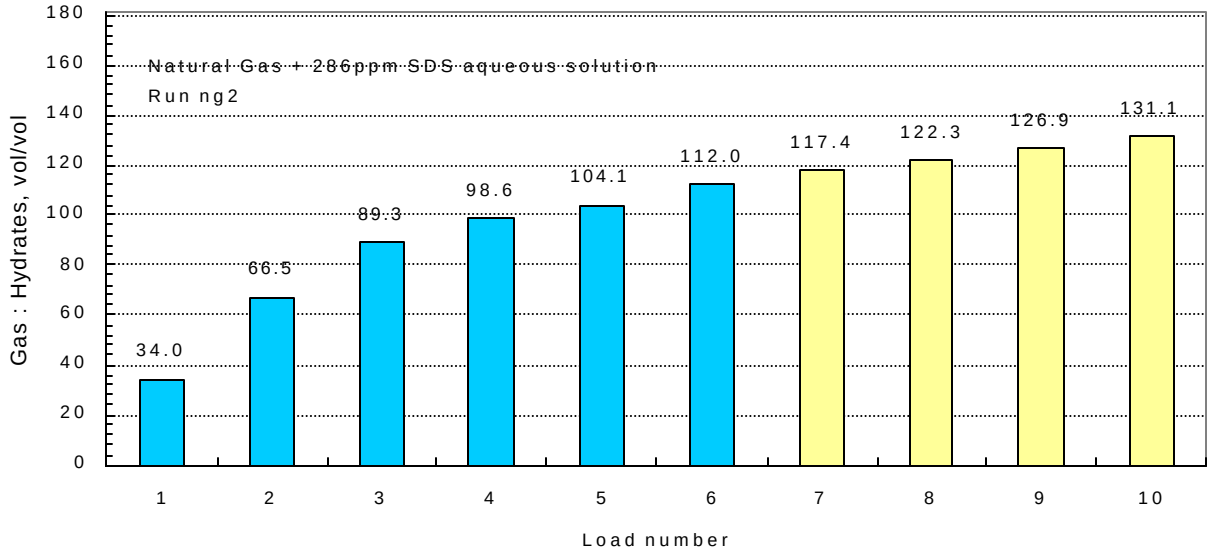

Fig. 2. Natural gas storage capacity, batch process.

To reiterate, the water trapped between particles was converted to hydrates in successive loadings after the free water had been drained from the cell. Our data showed about 62% of maximum packing after the six loadings and about 72% extrapolated to ten loadings for a batch-type process. To achieve a higher packing fraction, therefore, it is advisable to go from a batch process to a semi-continuous process where the maximum gas pressure would be maintained during hydrate formation.

(2) Conversion of Interstitial Water in Semi-continuous Process

The conversion of interstitial water to hydrates was further demonstrated in another experimental run representing a semi-continuous process containing natural gas, water, and 286 ppm SDS. Gas was continuously added to the cell, as needed, to maintain a constant pressure as gas was being occluded during hydrate formation. At the higher constant pressure of a semi-continuous process, a greater fraction of the cavities fill. Natural gas in our test cell was maintained at 3.57 MPa (518.3 psia) with assistance of a constant- pressure regulator; gas added to the cell was measured with a mass flowmeter. All of the free water initially in the bottom of the cell was first converted to hydrates, and then the interstitial water was converted to hydrates. Results showed a 82% achievement of theoretical capacity when processing pressure was maintained at 3.57 MPa. See Fig. 3. At a pressure of 3.89 MPa, 86% of theoretical capacity was achieved. A semi-continuous process would offer a better hope for an economically-viable industrial application.

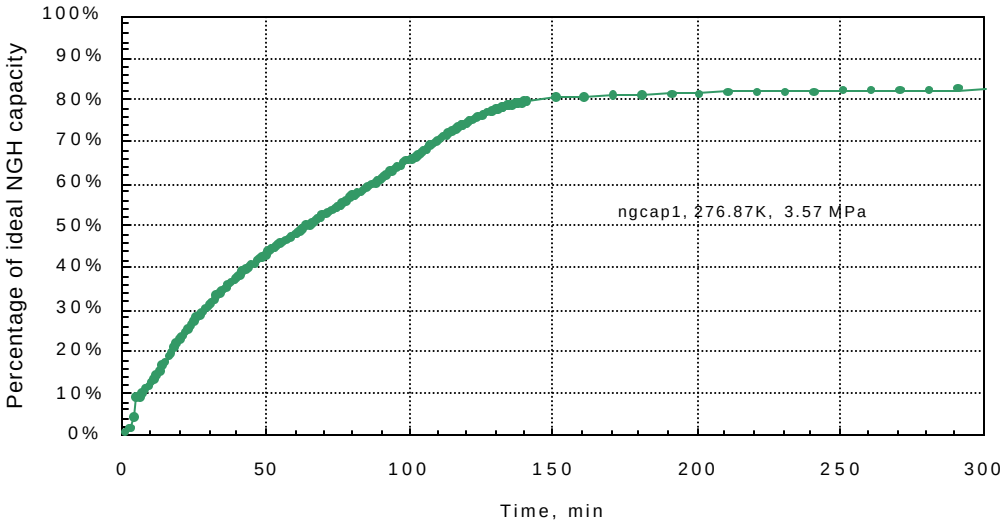

Fig. 3. Interstitial water conversion at constant high pressure.

(3) Surfactant Improvement of Attainable Storage Capacity

Surfactant facilitates the packing of the hydrate particles as they form. The hydrate particles move from the water slurry to the surface of the water because of their buoyancy (specific gravity is less than 1).

Near the water surface, the particles move to the stainless steel walls and are adsorbed on the walls of the container, building inwardly from the walls in a concentric cylinder. Practically, this means that an expensive processing step is avoided of separating particles from a water slurry and packing them in a storage container. Furthermore, space is maximized when the surfactant-laden particles build inwardly from the container walls. Note in the photograph of Fig. 4 taken from the test cell how the hydrates have packed all available space in the cell, leaving a small borehole down the center. In Fig. 4, ethane gas had kept being added to achieve a maximum packing; hydrates filled the cell at the conclusion.

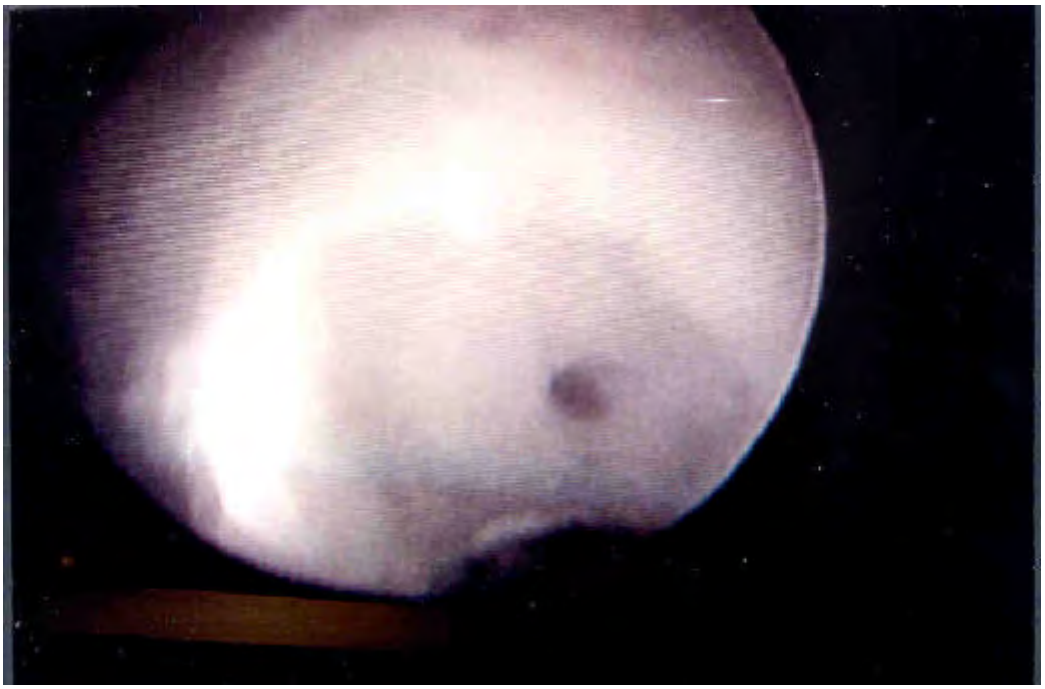

Fig. 4. Photograph of ethane packing test cell to maximum loading.
(Photographed from VHS film.)

B. Formation Rate with Surfactant

(1) Formation Rates in Batch System

Hydrates form very slowly in a quiescent system of pure water- hydrocarbon gas. However, the addition of 286 ppm of sodium dodecyl sulfate to the water increases the formation rate in a quiescent system by a factor of about 700. This is evident in Fig. 5 where rate, as represented by the moles of ethane gas occluded per mole of water in our system, is plotted versus time after pressure and temperature had been brought to the hydrate formation conditions.

After about 10 days, the system without surfactant was far from the hydrate capacity reached in less than 3 hours in a 286 ppm SDS surfactant-water system. (Note that the data was taken in a batch system, i.e., gas was not replenished in the cell as pressure declined.) The results are especially striking when the rapidity of hydrate formation in a surfactant system is viewed on the video film which was taken during some experimental runs.

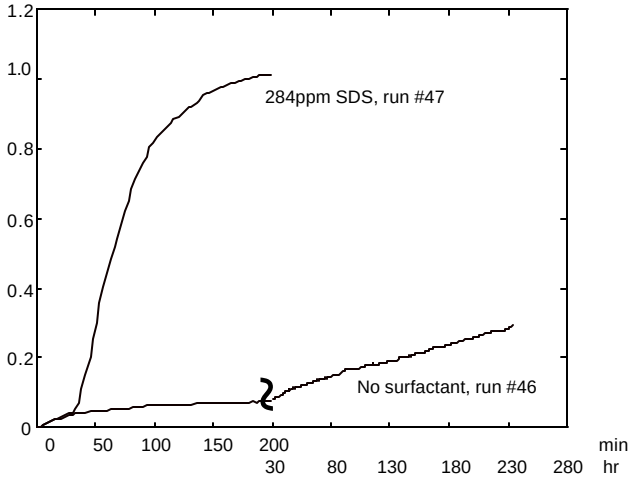

Fig. 5. SDS surfactant increases hydrate formation rate.

As mentioned before and as other researchers have mentioned, free water becomes trapped between hydrate particles upon formation. What is the rate of hydrate formation from the trapped water during each loading and what is the mechanism? The effect of the renewed interfacial surface area between water and gas may be anticipated from Equation 6, which is the rate expression for hydrates forming for a single species of gas or for a gas mixture with a constant composition (Vysniauskas and Bishnoi, 1983).

$$r = A a_s \exp\left(-\frac{\Delta E_a}{RT}\right) \exp\left(-\frac{a}{\Delta T^b}\right) P^{\tilde{a}} \qquad (6)$$

Where

A = lumped pre-exponential constant
a_s = water- gas interfacial area
a,b = arbitrary constants
ΔE_a = activation energy for hydrate formation
P = system pressure

R = universal gas constant
r = rate of hydrocarbon gas consumption during hydrate formation
T = absolute temperature
ã = overall order of reaction with respect to pressure

From Equation 6, one expects that increasing the water-gas interfacial area increases the rate of hydrate formation linearly. (Keep in mind that this interfacial area must continually be renewed so that a film of hydrates does not isolate fresh water surface from free gas contact.) With surfactant present, the mechanism is altered, for then discrete particles of hydrates form and surrounding surfactant moves with the particle to adsorb on the vessel walls; water and surfactant are attached to the particle's outer surface. Gas can diffuse through this porous network on the cell walls and thus contact a large surface area of fresh water-surfactant. In summary, surfactant excluded from the hydrate structure concentrates in the trapped water to promote continued hydrate formation as the interstitial water forms hydrates.

Surface tension effects on the formation rate are embodied in the *A* term of the equation. The pressure and temperature effects on the formation rate as predicted by eq (6) remain unaltered by surfactants.

A series of experiments was run with natural gas that gives insight into the rate of hydrate formation from the interstitial water. The series involved a batch process, i.e., gas was not continuously replenished to the cell but each gas loading was allowed to approach equilibrium before the next was added. Free water was drained from the bottom of the cell after the first loading of gas so that subsequent hydrate formation occurred from the interstitial water. Temperature was kept constant. With these considerations, view Fig. 6 where rate of formation of natural gas hydrates from interstitial water is superposed on the gas-capacity data of Fig. 2 over the six discrete gas loadings.

Note that the rate of formation of natural gas hydrates increases in going from the first to the second loading but decreases as the interstitial water reacts further even though the interfacial area could be expected to increase. Why?

The following figure illustrates the effect of interstitial water on the formation rate.

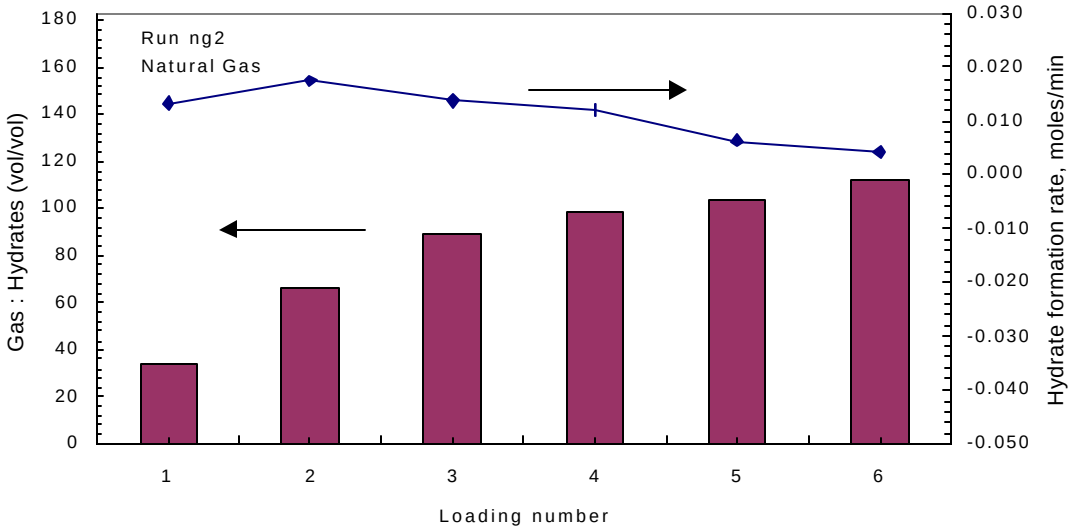

Fig. 6. Storage capacity and rate of natural gas hydrates

To delve into the reason further, consider Fig. 7 in which successive loadings of ethane gas were made rather than successive loadings of a mixture of natural gas.

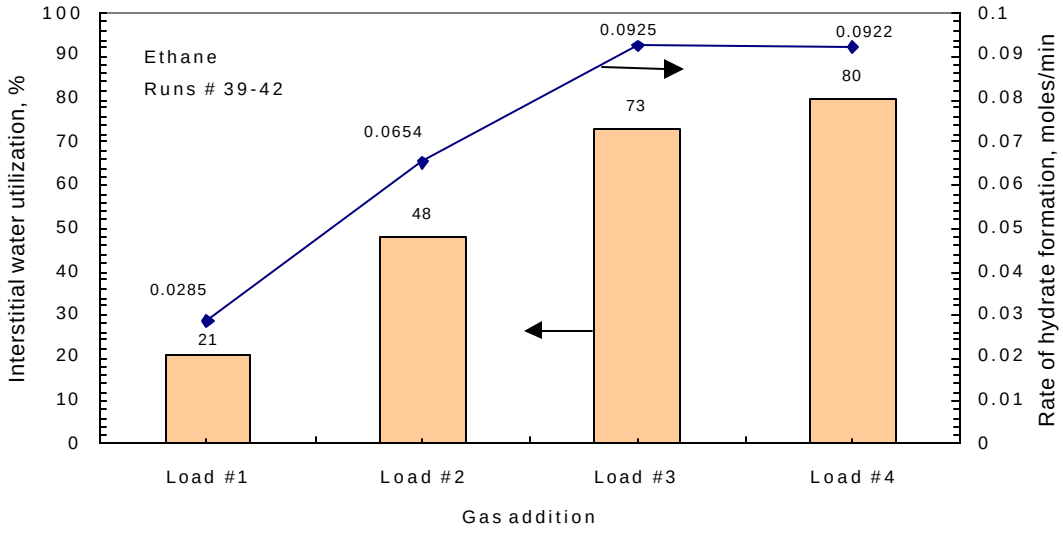

Fig. 7. Interstitial water converted at high rate.

It is seen from Fig. 7 that the rate of formation increases as the interstitial water reacts to form ethane hydrates. When most of the trapped water has reacted (approximately 73%), the formation rate remains constant thereafter. This indicates a lower permeability as interstices become filled with hydrates; mass transfer limits the rate even though interfacial area may be increasing.

It is concluded that three opposing steps determine the rate of hydrate formation from the interstitial water: (1) As more interstitial water is converted, the interfacial area increases between water on the hydrate-particle surfaces and gas, tending to increase the rate.
(2) As more interstitial water is converted, the propane and ethane concentration of the free natural gas decreases, tending to decrease the rate of formation under the falling pressures of this batch process.
(3) As more interstitial water is converted, permeability of the mass of hydrate particles eventually decreases, tending to decrease formation rate.

Therefore, semi-continuous process is suggested by the data for further improvement.

(2) Formation Rates in Semi-Continuous System

The procedure of adding gas to the cell batchwise and then allowing pressure to decline to equilibrium, as presented in Fig. 6 and Fig. 7, results in a lower formation rate and a lower storage capacity than if gas could be continually replenished as hydrates formed to maintain an initial high pressure. In order to verify this, a constant pressure regulator and mass flow meter were installed in the laboratory apparatus. Results from the semi-continuous process were positive and are given later in the report. Such a semi-continuous process is also highly desirable for scale-up of the process.

C. Process Simplification and Economy with Surfactant

The feasibility of a practical, economical hydrate storage process depends on simplicity. For the sake of simplicity, it would be preferable to have no moving parts in the hydrate formation-storage tank in order to reduce maintenance, labor, operating difficulties, and capital investment. For example, it has been our experience in the laboratory that flow problems abound with hydrates blocking flow lines; this was the case in the beginning of the work upon attempting to spray the water into the gas-pressurized formation tank to create with droplets a large, renewable interface area for faster hydrate formation. Also, serious maintenance and operating problems would arise in a large-scale operation by vigorously stirring the water as hydrates form: How could one provide proper and lasting sealing of the agitator to prevent gas leaks from the pressurized tank? How would one stir the progressively increasing viscosity of the water-hydrate slurry as the solid content increased? How would one pack the hydrate particles formed in an agitated system?

Surfactant in the water solution simplifies the process in three main ways. First, the surfactant causes rapid and complete hydrate formation. Second, the surfactant causes hydrates to form in a

stagnant system. Third, the surfactant attached to hydrates migrate to the cell walls where they are adsorbed and packed.

(1) Simplification from High Formation Rate

In the first simplification, hydrates form rapidly and completely. About 86% of the theoretical limit of gas storage was reached in our test cell within 3 hours of hydrate initiation at 3.89 MPa (564.9 psia) and 275.4 K (36° F). See Fig. 17. This means that with proper design of the formation-storage vessel, a formation-decomposition cycle including turnaround time should be achieved within a 24-hour period. A design concept will be proposed for a process with short turnaround times in the contract option phase.

(2) Simplification from Quiescent System

In the second simplification, surfactant allows the hydrates to be formed in a quiescent system. The alternatives would impose more complex processing steps. One alternative would be to increase water-gas interfacial area by atomizing the water into a pressurized chilled gas to achieve sufficient rate of formation. Another alternative would be to mechanically stir the water-hydrate slurry as hydrates form. Surfactant eliminates the need to impose water flow or moving parts during formation. As a consequence, complexity of the formation/storage tanks would be reduced; in fact, hydrate formation-storage-decomposition would be accomplished in the same vessel. Surfactant would allow reuse of the process water: after decomposition the water and surfactant would remain in the storage tank, and the next formation cycle would proceed by repressurizing with gas. The simplified process greatly enhances the prospects for an economical large-scale process.

(3) Simplification--Cell Wall Buildup

An important simplification from the use of surfactant is that small amounts of SDS in the water cause the hydrate mass to collect on the stainless-steel test cell walls as the hydrate forms. The mechanism will be explained in Section D of *Results and Discussion*. The following photographs emphasize the effect.

The stark difference between a quiescent pure water-gas system and a quiescent water-surfactant-gas system can be seen from photographs taken of the inside of the test cell. First consider hydrates formed in a quiescent system without surfactant in Fig. 8 where the photograph was taken through the transparent quartz top of the pressurized cell. The hydrate crystal growth developed with ethane at 2.41 MPa (350 psi) and 277.6 K (40°F). Note the random growth of the crystals generally extend from one cold metal surface to another, not necessarily associated with the wall surface. The darker mass in the bottom of the cell is free water covered by a sheet of hydrates.

Figure 8 follows.

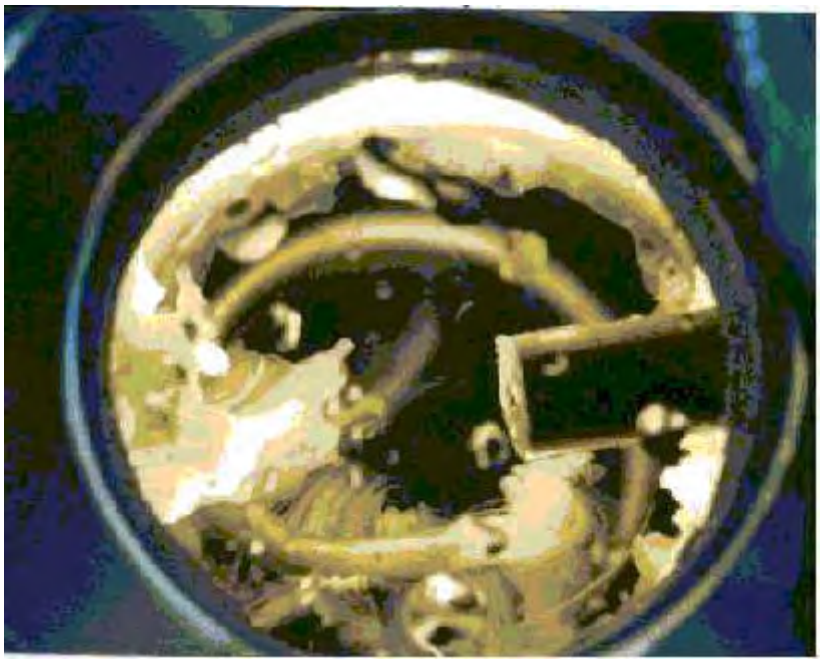

Fig. 8. Beginning growth of hydrate crystals-pure water/ethane.

In Fig. 9 is the same set of ethane-pure-water crystals 5 days after initiation, still slowly extending their random growth. As the crystals grow, they are trapping free water between particles. Also, as they grow their packing is not such that the space in a storage vessel could be efficiently used. If hydrates were to be utilized in this form to store gas, several processing steps would be necessary to crush and repack the solid-solution mass while maintaining adequate pressure and temperature.

Figure 9 illustrates the slow and random growth of hydrate crystals in a pure water system.

Fig. 9. Developed growth of hydrate crystals--pure water/ethane
(5 days after hydrate initiation)

However, when sodium dodecyl sulfate is used in water concentrations as low as 286 ppm under similar conditions of pressure and temperature, a different packing occurs in the test cell. Hydrates rapidly grow inwardly from the stainless steel walls of the cell in a concentric cylinder.

As the water level in the cell drops during hydrate formation, the cooling coils become exposed in the bottom of the cell and hydrates then collect around that stainless steel tubing. A photograph taken at the beginning of hydrate formation from a surfactant solution is given in Fig. 10. The photograph was taken only 6.5 minutes after hydrates began to form at a pressure of 2.31 MPa and a temperature near 282 K.

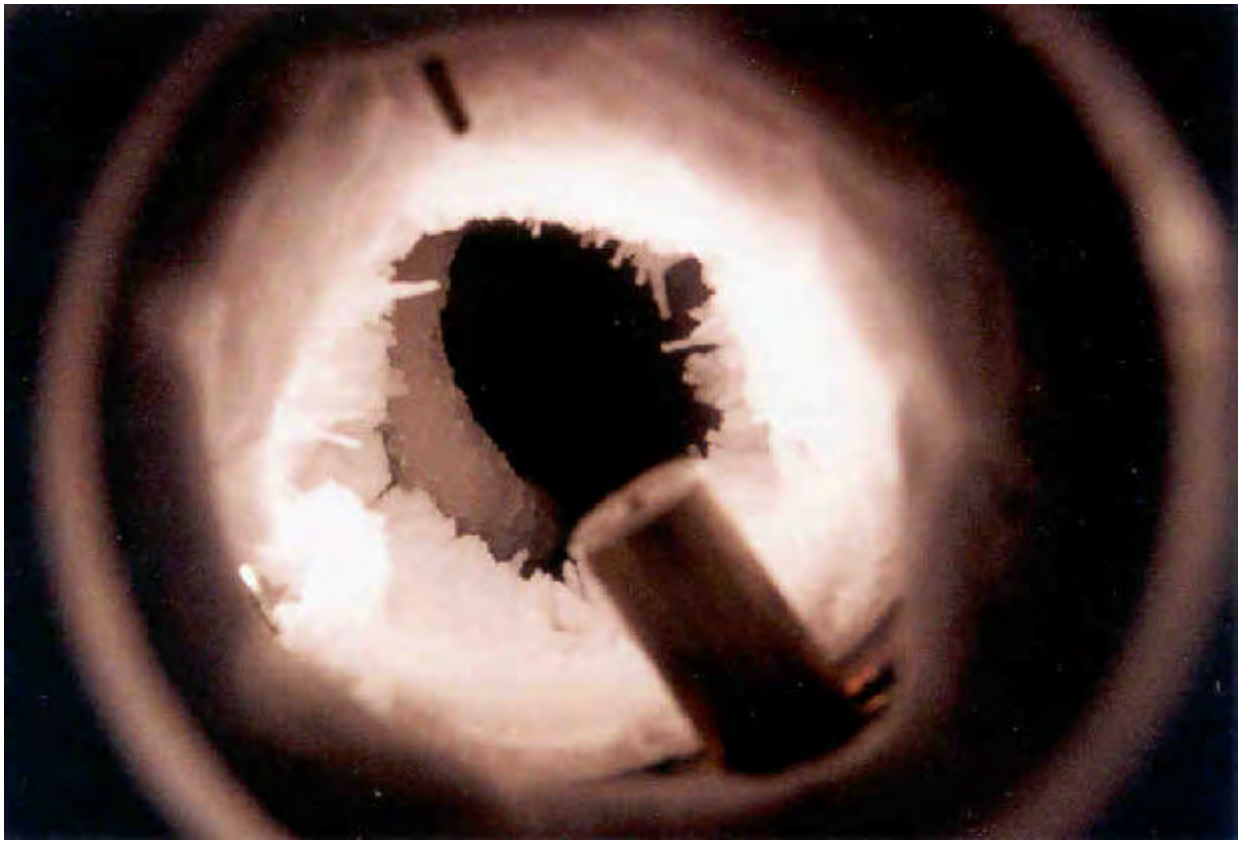

Fig. 10. Beginning growth of hydrate crystals--surfactant/water/ethane.
(Run #DOE 44)

In Fig. 11 is a photograph of the hydrates formed from a surfactant-water system after much more gas has been occluded. When the free water is depleted in the bottom of the cell, water-surfactant

trapped between hydrate particles on the walls continue forming hydrates.

This hydrate formation from interstitial water increases the bulk density of the hydrate packing, which results in a very efficient packing for storage as can be seen in Fig. 11. The packing appears denser and whiter when compared to Fig. 10, indicating more of the interstitial water has been converted to hydrates. Also, note the stalactite-type protrusions of forming hydrates on the inner surface.

Fig. 11. Developed growth of hydrate crystals--surfactant/water/ethane, Run #34.
(Some water drops on quartz window are also visible. Taken 3 ½ hours after hydrate initiation.)

The packing arrangement and appearance near ultimate capacity of natural gas in hydrates in our test cell may be viewed in Fig. 12. The photograph was taken after the maximum capacity of natural gas had been loaded into the test cell and occluded in the water-SDS solution. Note that this photograph of near-theoretical-capacity was taken only 3 hours, 57 minutes after hydrate initiation. Also, the solid mass filled the entire cell by growing inwardly from the walls until the cylindrical void in the mass remained slightly off-center; the bottom of the test cell can be seen through the void visible in Fig. 12.

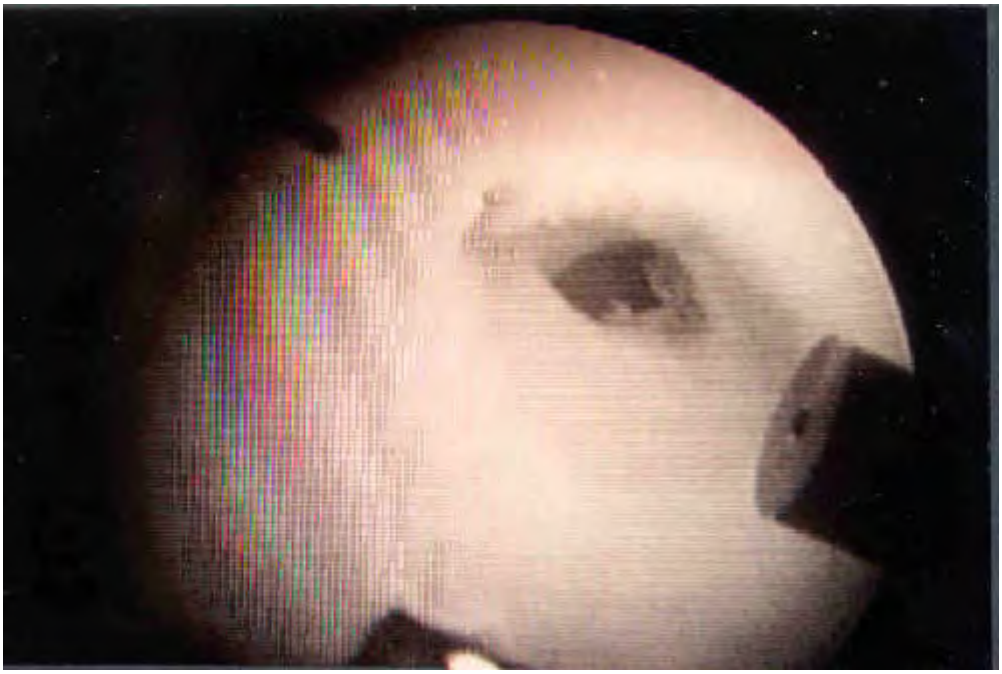

Fig. 12. Growth of hydrate crystals--surfactant/water/natural gas.
(Photo taken from VHS tape)

The packing arrangement of the hydrate particles formed from the surfactant-water system suggests some cost-effective ways to design a formation-storage tank for natural gas storage in hydrates.

D. Hydrate Formation Mechanism

(1) *Surfactant Alteration of Hydrate Formation Mechanism*

Based on MacKerell's simulation of the SDS micelle configuration (MacKerell, 1995) and our observation of hydrate formation in a water-SDS-ethane system, the micelle model of Fig. 13 for occurrence in a hydrate-forming system is concluded.

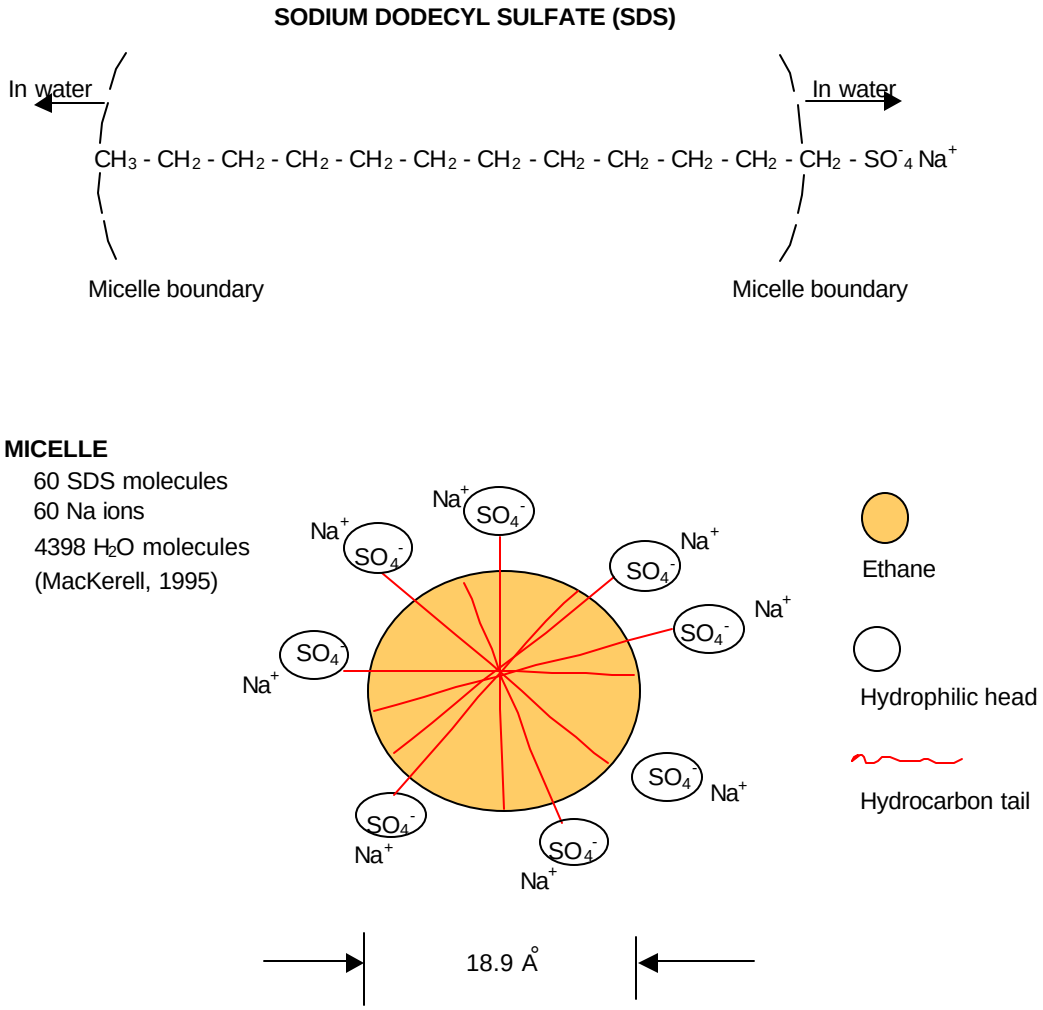

Fig. 13. Model of micelle in hydrate-forming system

Our observations indicate that surfactant micelles facilitate hydrate formation from natural gas

components by concentrating methane, ethane, and propane in the micelle, effectively increasing hydrocarbon solubility in the water; the twelve-carbon tail of the surfactant would solubilize the hydrocarbon gases into the micelle sphere; the proximity to the micelle-water boundary of the terminal methyl groups of SDS helps scavenge the methane, ethane, and propane molecules from the water. Water is excluded from the interior of the micelle sphere where the hydrocarbon gases are concentrated by the saturated hydrocarbon components of SDS. Thus, the gas is brought into intimate contact with the surrounding water, and the micelles act as nucleation sites congregating the water-cluster precursors of hydrates at the surface of the micelle sphere. These sites are located subsurface of the bulk water in the cell as well as on the surface of the bulk water.

In our test cell, hydrate particles were viewed by the fiber optics-camera arrangement and filmed on VHS tape forming below the water surface as depicted in Fig. 14. The camera probe was inserted into the well on the side of the test cell so that the initial water level split the viewing port; one-half of the probe was above water, the other one-half below water. Upon forming subsurface, the particles moved rapidly upward to the water surface and then to the test cell walls. This was a rapid movement of large particle agglomerates.

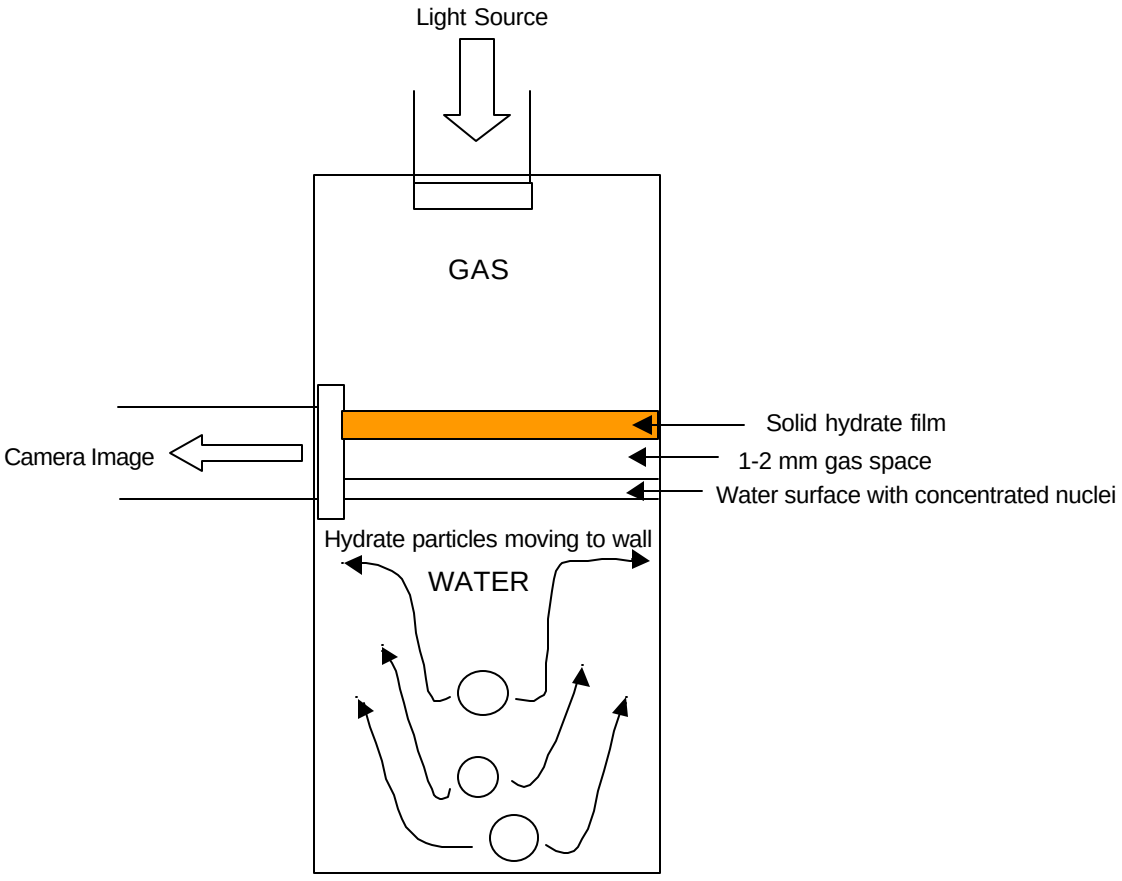

Fig. 14. Observed hydrate formation subsurface with surfactant.

The subsurface hydrate-formation phenomenon in the presence of surfactant is explained by the model of the micelles. The driving force for upward movement of hydrate particles would be buoyancy because hydrate particles are less dense than the water; driving force for their movement to the walls would be their adsorption on that solid surface. Surfactant adsorption at solid-liquid-gas interfaces is common with the micelle structure intact (Wanless and Ducker, 1996). Note that surfactant molecules would be excluded from the hydrate structure, but probably remain oriented at the particle surface and the attraction of surfactant molecules to the stainless-steel surfaces would provide the driving force to move the particles to the walls.

The cylindrical mass buildup of hydrates on the surfactant-wetted, stainless-steel walls continued as water level dropped in the cell.

The boost to gas solubility by micelles and the subsurface migration of the hydrate particles, thereby not creating an obstruction to further hydrate formation, partly account for the 700-fold increase of hydrate formation rate when surfactant is present.

(2) CMC At Hydrate-Forming Conditions

Critical micellar concentration (CMC) refers to a threshold level of surfactant concentration necessary for micelles to form. Above CMC some physical properties of a solution abruptly change. The sodium dodecyl sulfate (SDS) used in the experimentation was checked for the critical micellar concentration in water. The determination was first made by preparing multiple concentrations of SDS/water solutions and then determining the surface tension at each concentration with a capillary-rise apparatus at ambient temperature and atmospheric pressure. Surface tension is one of the physical properties that sharply changes at the CMC. The results are presented in Fig. 15.

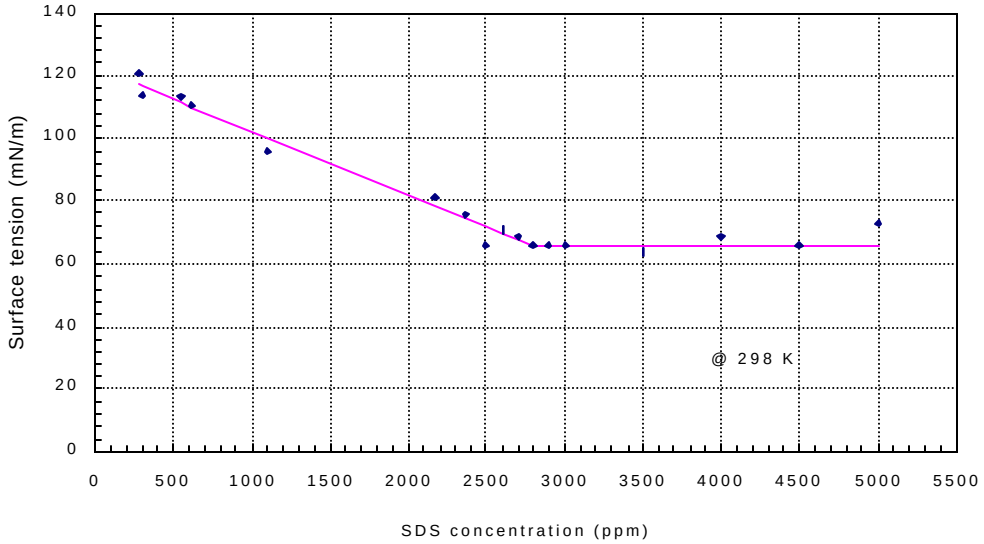

Fig. 15. Critical micellar concentration of sodium dodecyl sulfate, 1 atm.

It is apparent that the CMC at 298 K (77°F) and 1 atm for our solution occurred at 2700 ppm of SDS. However, when using the same surfactant in the chilled and pressurized test cell, hydrates rapidly form at 286 ppm instead of the 2700 ppm. In explanation, CMC is a function of temperature and the amount of gas dissolved in the water (Rosen, 1978). At hydrate-forming conditions the temperature is about 275.4 K (36°F). Gas solubility would be greater at the lower temperature, but hydrocarbon gas solubility increases more rapidly just prior to hydrate formation. Therefore, in order to get a better estimate of CMC at our test conditions, we made multiple runs with ethane in the test cell, varying SDS concentration, attempting to determine the true CMC of the system. The results are given in Fig. 16.

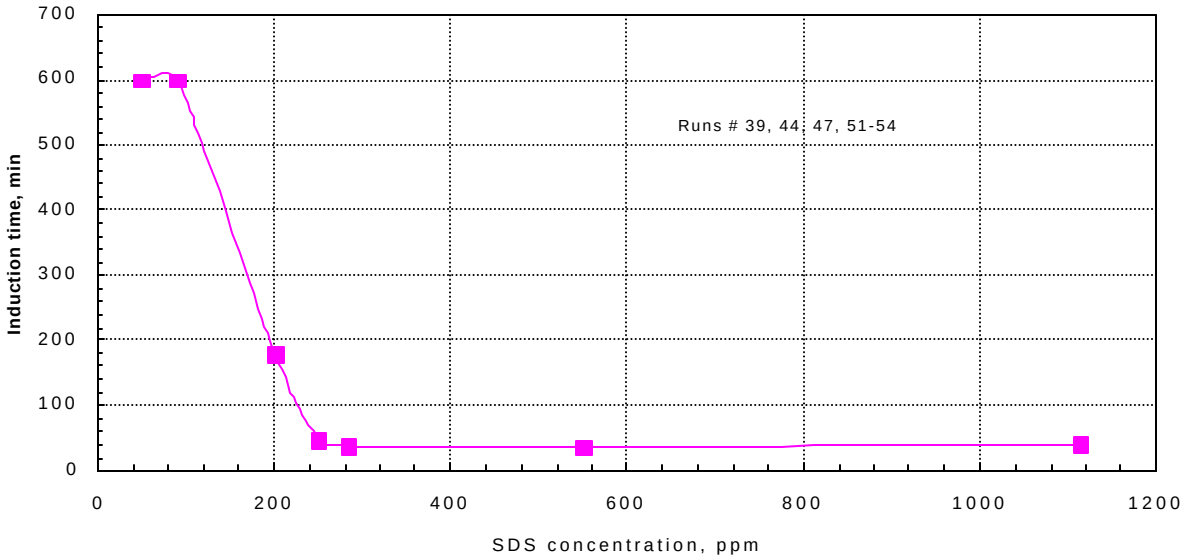

Fig. 16. Hydrate induction time defines CMC.

Note the very sharp break in the curve at 242 ppm, representing the CMC at hydrate-forming conditions for ethane. Induction time gave the most sensitive indication of the breakpoint, although amount of gas occluded at a specific time would also have worked.

The conclusion from Fig. 16 is that a SDS surfactant solution concentration at the CMC of 242 ppm or greater will provide the desired benefits to the hydrate gas-storage process.

II. Pressure Effects

The storage capacity of natural gas in gas hydrates for large-scale use depends on obtaining a high bulk-density of hydrate particles in the storage vessel and on filling a high fraction of cavities in each individual hydrate crystal. The maximum bulk density can be accomplished with

the addition of surfactant to the water solution, but filling the crystal cavities depends on system pressure.

With our test-gas composition of 90.01% methane, 5.99% ethane and 4.00% propane, the fraction of cavities estimated to be filled as a function of pressure is calculated by the statistical thermodynamics program of Sloan (Sloan, 1992). The results are given in Table I and Table II.

TABLE I. Fraction of small and large cavities filled
(free gas composition 90.01% CH_4)

		Percent of small cavity filled			Percent of large cavity filled		
P, MPa	T, K	Methane	Ethane	Propane	Methane	Ethane	Propane
2.86	11.5	0.766027	0	0	0.062497	0.074237	0.858711
3.21	12.4	0.779095	0	0	0.065831	0.075830	0.853912
3.57	13.3	0.790729	0	0	0.069241	0.077395	0.849043

Note: For equilibrium vapor composition: 90.01%, 5.99%, 4%

TABLE II. Fraction of small and large cavities filled
(free gas composition 99.1% CH_4)

		Percent of small cavity filled			Percent of large cavity filled		
P, MPa	T, F	Methane	Ethane	Propane	Methane	Ethane	Propane
2.86	2.4	0.834662	0	0	0.617589	0.101905	0.249471
3.21	3.6	0.843456	0	0	0.630381	0.100669	0.239494
3.57	4.5	0.85131	0	0	0.642563	0.099396	0.229982

Note: For equilibrium vapor composition: 99.1%, 0.8%, 0.1%

At a free-gas composition of 90.01% methane, for example, the fraction of small voids filled with methane increases from 76.6% to 79.1% in going from 2.86 MPa (415 psia) to 3.57 MPa (518 psia), while over the same range the large voids remain filled to capacity (99.5%). Therefore, the effect of going to higher pressures is to improve the fractional filling of small cavities with methane.

The amount of natural gas that could be stored in hydrates at practical processing pressures and times was determined. Three experimental runs were made in which temperature was held constant at 275.4 K (36°F), and the surfactant concentration was maintained at 286 ppm; procedure and other conditions except pressure were repeated. Hydrates were formed in the cell until all of the water became tied up in the hydrate structure, i.e., interstitial water also formed hydrates. Individual runs were made at pressures of 3.89, 3.47, 3.11, 2.76 MPa (550.2, 503.6, 451.2, and 400.5 psig). The chosen pressure

was kept constant throughout the run with the constant pressure regulator, and the rate of gas occluded was measured with the gas mass-flow meter. Such a procedure gives a greater storage capacity than when pressure is allowed to drop and would be a preferred procedure in a large-scale process.

The storage capacity of the gas hydrates as a function of time after hydrate initiation is given in Fig. 17.

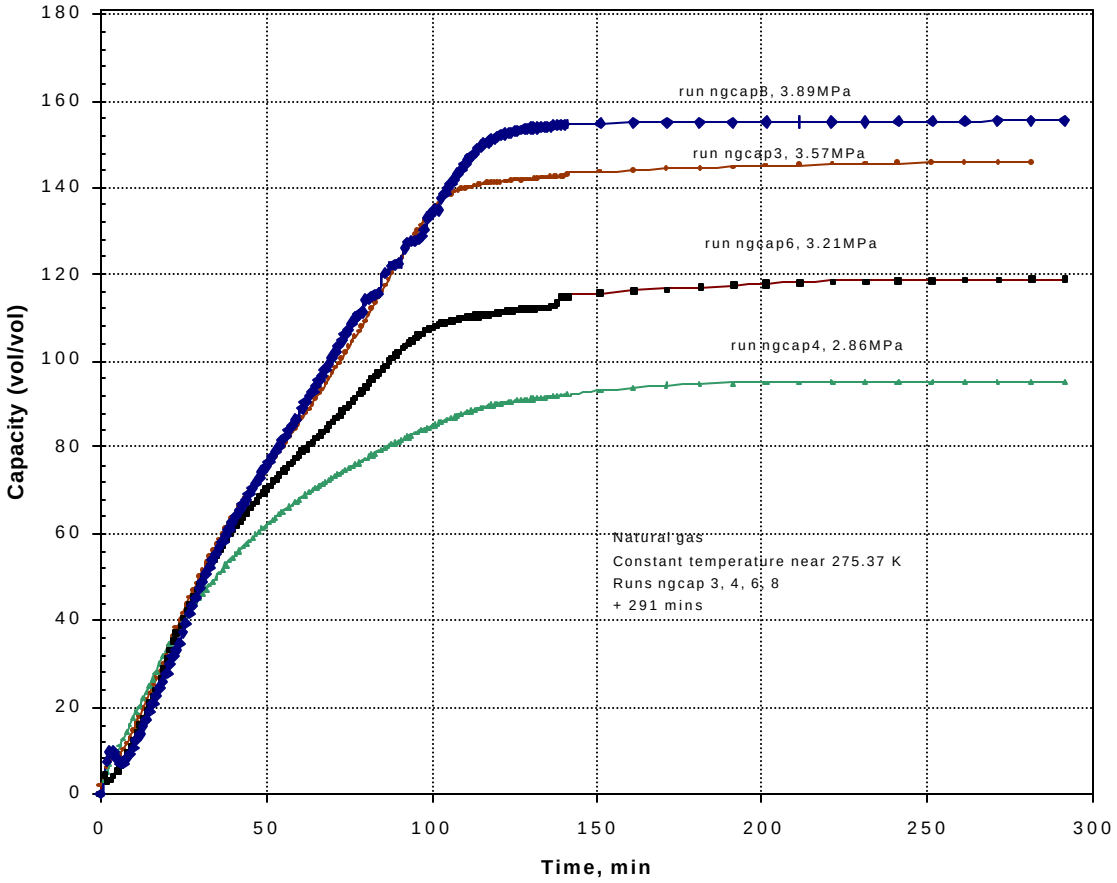

Fig. 17. Pressure increases natural gas storage capacity.

The results reflect an increase of storage capacity as pressure increases, since higher pressures cause more cavities in each crystal to be filled with gas and the interstitial water to be fully reacted.

These results show that 155 (vol gas)/(vol hydrate) storage capacity is achieved at a processing pressure of 3.89 MPa (564.9 psia). Furthermore, this much gas is incorporated into the hydrates in less than 3 hours of processing time. The 155 vol/vol represents 86% of the theoretical storage capacity if all cavities were filled. The results emphasize the technical feasibility of the process.

If a common time during formation is taken in Fig. 17, 291 minutes for example, the storage capacity is seen to increase with pressure as given in Fig. 18. At the 3.57 MPa (518 psia), a storage of 148.4

vol/vol is achieved; at 3.89 MPa (564.9 psia), a storage capacity of 155 vol/vol is achieved. One can anticipate that even higher pressures would improve capacity further, but the higher pressures would necessarily increase storage tank costs.

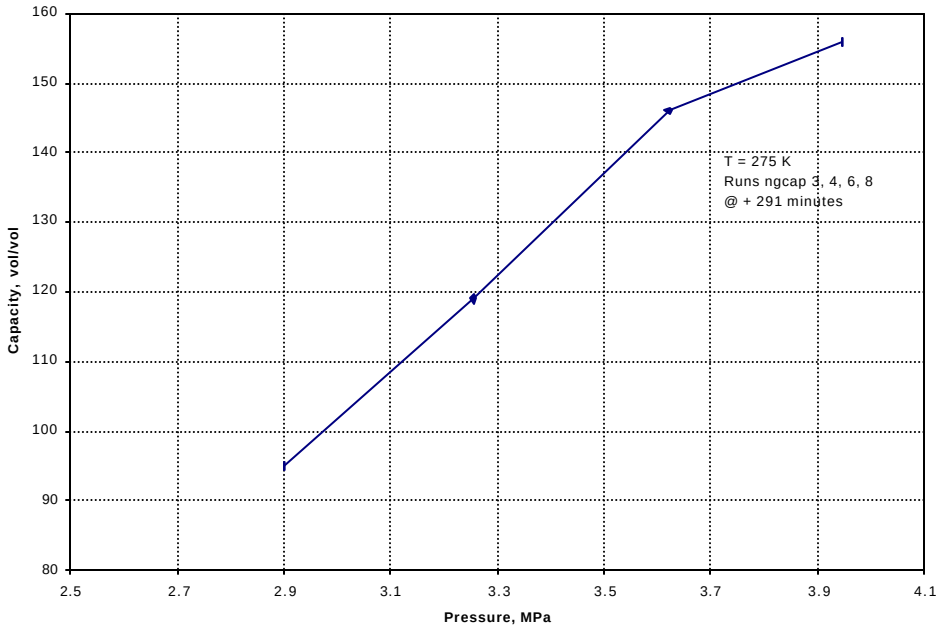

Fig. 18. Pressure trends of natural gas storage capacity.

From Equation (6) if surface tension, gas-water interfacial area, temperature, and degree of supercooling are kept constant, as in the runs of Fig. 18, then the equation reduces to

$$r \propto C P^{\tilde{a}} \qquad (7)$$

where

r = rate of hydrate formation
C = a constant
P = pressure
ã = overall order of reaction with respect to pressure

Therefore, as our data supports, the rate of hydrate formation is a function of pressure with the surfactant-water-natural gas system.

III. Temperature Effects

A latent heat of formation of about 65.4 kJ/mol (Sloan, 1990) is released at the water-gas interface when hydrates form, introducing heat transfer rate as a factor in the formation rate as it affects the temperature terms in eq. (6). The relatively large release of heat creates an experimental problem of determining a true interfacial temperature. Stainless steel surfaces increase formation rates by their conductive removal of heat from the interface and facilitate formation by being a promoter of nucleation.

The release of latent heat during hydrate formation is illustrated in Fig. 19 as a comparison of liquid-phase and gas-phase temperatures in the laboratory test cell. In this run, cell and water contents at ambient temperature were pressurized with natural gas initially and then cooled to 277.1 K (39°F); pressure decreased according to the gas law until hydrates began forming whereupon pressure dropped precipitously. Note that the RTD probe in the gas phase is much more sensitive to the release of the latent heat in our laboratory test cell. It illustrates the difficulty of measuring a true interfacial temperature which would have a value somewhere between the two traces in the figure below.

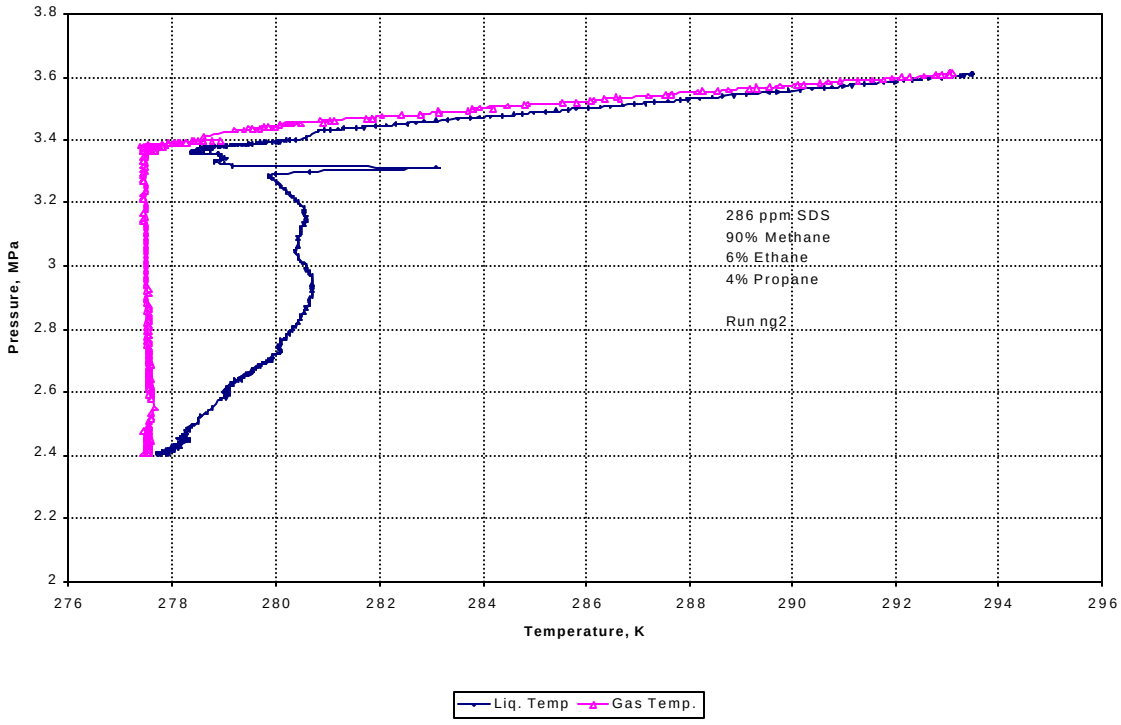

Fig. 19. Gas-phase temperature more sensitive to natural gas hydrate formation.

IV. Natural Gas Composition Effects

A. Formation Compositions

Of the hydrocarbon gases present in natural gases, only methane will fit into the smallest cavities of Type I and help stabilize the crystal. Propane is necessary to stabilize the Type II hydrate crystal, although methane will fit into all three sizes of cavities in Type I and Type II hydrates. Therefore, storage of natural gas must involve forming Type II hydrate crystals, which means having propane present, in order to perform the process at practical pressures.

For a given temperature, hydrates are formed at lowest pressures from propane and the pressure gets progressively higher in the order propane-ethane-methane. Then, it is to be expected that for a mixture of the three gases, occlusion would be preferentially in the order propane-ethane-methane. Table III illustrates this.

TABLE III. Summary of occluded and free gas compositions.

Load #	P (MPa)	T (^oK)	Calculated Occluded Gas Composition %			GC Free Gas Measured %		
			CH_4	C_2H_6	C_3H_8	CH_4	C_2H_6	C_3H_8
1. Begin	3.51	293.1	68.3	3.5	28.2	90.01	5.99	4.00
1. End	2.30	277.6	80.7	5.6	13.3	98.1	1.7	0.2
2. Begin	3.37	282.1	65.5	3.4	31.1	94.0	4.0	2.0
2. End	2.67	276.8	81.2	4.5	14/3	98.6	1.2	0.2
3. Begin	3.34	278.8	66.5	3.7	29.8	95.6	3.1	1.3
3. End	2.88	276.9	87.3	3.8	9.0	99.1	0.8	0.1
4. Begin	3.34	279.6	76.9	3.7	19.3	98.2	1.4	0.4
4. End	3.14	277.5	86.6	5.0	8.4	98.8	1.1	0.1
5. Begin	3.34	278.7	79.1	3.7	17.2	98.5	1.2	0.3
5. End	3.22	277.7	86.7	5.0	8.3	98.8	1.1	0.1
6. Begin	3.34	278.4	82.2	4.4	13.4	98.6	1.2	0.2
6. End	3.16	277.4	87.4	3.76	8.86	99.1	0.8	0.1

The data in Table III was taken in six successive batch loadings of the gas mixture of 90.01% methane, 5.99% ethane, and 4.00% propane. As hydrates formed from an initial pressure of

about 3.34 MPa (485 psia), pressure in the test cell declined to near equilibrium, whereupon more gas of the original composition was added to bring the pressure back up to about 3.34 MPa. This was repeated five times. Free-gas compositions in the test cell were determined at the beginning and ending of each loading by gas chromatography; occluded-gas composition at equilibrium in the hydrates of the test cell were calculated by statistical thermodynamics (Sloan, 1992).

Note that the free gas in the test cell becomes progressively richer in methane; the free gas concentration of methane increases from 90.01% initially to 99.1% at the end of the sixth loading, whereas propane concentration in the free gas decreases from 4.00% to 0.10%. The first gas occluded in the hydrates contains 68.3% methane and the last hydrates formed have 87.4% methane. If withdrawal of gas with changing composition creates any difficulty in end-use, a surge-mixing tank could be installed on the outlet gas stream.

Some important applications to large-scale storage of natural gas in hydrates are derived from the data of Table III: (1) Lower storage/formation pressures of the natural gas will be realized with increasing propane and ethane concentrations in the natural gas. (2) If the free gas rich in methane were to be withdrawn from the formation vessel for some auxiliary use, substantially lower storage pressures would be realized. (3) Higher formation rates and greater storage capacity would be realized if feed gas were to be admitted to the hydrate tank at an initial pressure that remained constant in a semi-continuous process.

B. Withdrawal Compositions

The withdrawal gas composition will result from combining occluded gas released from hydrates and free gas above the hydrates. The occluded gas becomes leaner in methane as decomposition of the hydrates proceeds. In Table IV is summarized the composition as analyzed with the gas chromatograph of the withdrawn gas from the test cell at three stages of decomposition: start, midway, end. The changing composition reflects the scavenging effect of the hydrates for propane and ethane.

Again, if withdrawal of gas with changing composition creates a difficulty in end-use, a surge-mixing tank could be installed on the outlet gas stream.

TABLE IV. Natural gas withdrawal compositions.

Component	Begin	Midway	End No Hydrates Remain
Methane	99.1	94.1	76.5
Ethane	0.8	5.2	12.4
Propane	0.1	0.7	11.1
	458 psia 39.5 F	227.7 psia 38.6 F	207.1 psia 76.1 F

V. Decomposition

A. Hysteresis of Formation/Decomposition

Decomposition of the hydrates proceeds as rapidly as heat can be transferred to the solid mass for the latent heat of the phase change. In our test cell with the cooling/heating coils inside the cell in direct contact with the water and solids, decomposition rate was limited only by the capability to dispose of the liberated gases. Since the hydrocarbon gases removed from the cell in the laboratory were always mixed with nitrogen to a composition beyond the flammability limit, the hydrate decomposition rate was necessarily limited by our disposal rate. Therefore, the decomposition rate was studied by retaining liberated gases in the test cell and allowing cell pressure to rise. The decomposition rate is sufficient to meet process requirements under these conditions, although higher rates could be achieved if pressure was decreased and gases removed as would occur in a large-scale process. Also, the decomposition rate proved sufficient with a moderate temperature of 294.3 K (70^{o}F) in the circulating water; therefore, in a large scale process a low-quality heat source could serve to decompose the 274.8-277.6 K (35-40^{o}F) hydrate particles. For example, water from a power plant at 311 K (100^{o}F) normally sent to a cooling tower to lower temperature for reuse would suffice.

In Fig. 20 is the formation and decomposition curves for ethane hydrates in a quiescent system of pure water-ethane. (No surfactant was present.) The pressurized system was cooled to form the hydrates and then allowed to decompose as pressures and temperatures were monitored.

Note that the equilibrium curve is superposed as the dotted line in Fig. 20.

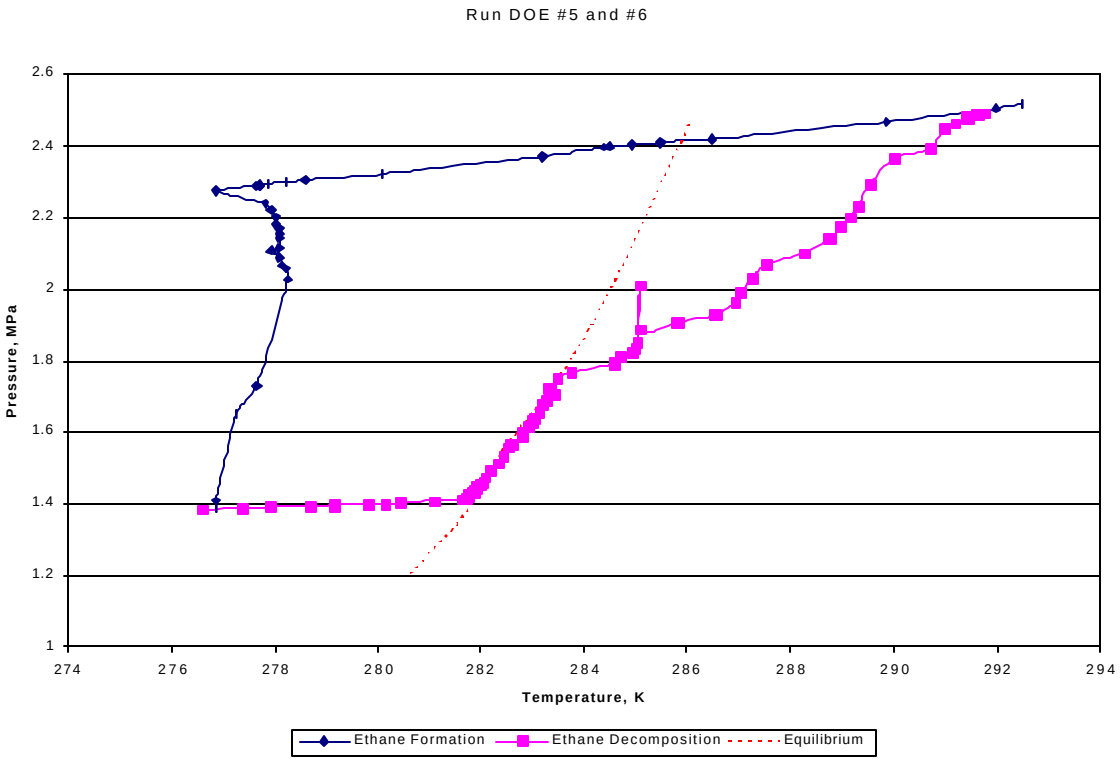

Fig. 20. Hysteresis of formation/decomposition cycle.

Note that as the temperature decreases below the equilibrium curve at about 285.4 K (54°F), a faster drop in pressure occurs as hydrate nuclei begin to form in the cell. The net effect as the nuclei form is an apparent increase in the solubility of ethane in water. After supercooling, hydrates particles formed and pressure dropped steeply. If formation had been allowed to continue past 1.38 Mpa (200 psia), the equilibrium curve eventually would have been approached. On adding heat to the system, the solid particles first warmed to near the equilibrium temperature without decomposition, decomposition followed the equilibrium curve, and then the system returned to the original temperature and pressure when all of the hydrates had been decomposed. The hysteresis observed in Fig. 20 is typical.

Afterwards, in another experimental run with SDS surfactant in the water, the cell was packed to near capacity with hydrates. Then, the hydrate decomposition inside the pressurized cell was captured on VHS video film. It is interesting that the gas evolved from the hydrates remained intact as bubbles as it moved through the gas above the hydrates. The movement of the bubbles appeared similar to gas bubbling through liquid water, although there was no free water present in the cell. An explanation is offered that the occluded gas is surrounded by the hydrogen-bonded-water-cage which has on its outer surface the surfactant excluded from the hydrate structure; possibly, upon decomposition the released gas expands to form a bubble with the released water-surfactant forming the boundary. The movement

of the bubbles is vividly seen on the video tape, although capturing a still photograph from the film for this report was only partially successful. Figure 21 is a camera photograph from the monitor while playing the film from a VCR.

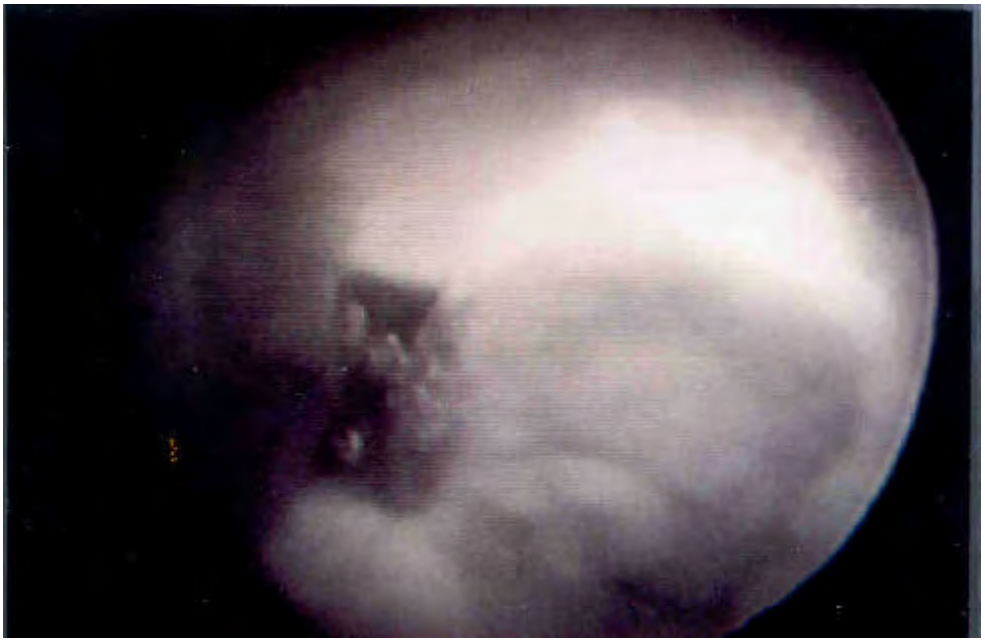

Fig. 21. Photograph of gas bubbles during decomposition.
(Photo from VHS film)

Installing a demister on the exit line of any storage tank during decomposition should be a simple solution to an implied problem of entrained water.

B. Effect of Total Pressure on Decomposition

After the hydrocarbon gases are occluded in the solid matrix of the hydrate, the stability can be maintained at that temperature as long as the total pressure is maintained at the equilibrium point, or higher. That is, an inert gas could be used to displace the free hydrocarbon gas and maintain the total pressure above the natural gas hydrate during storage, for example, in cases of long-term storage or when extreme precautions against tank leakage were desired during the storage period.

C. Decomposition with Microwaves

Microwaves were investigated for decomposing hydrates. Pressure transducer and RTD probes were positioned in the test cell as in other tests of this report. It was necessary to have at least a 7.62 cm (3 in) diameter quartz transparent window through which to inject the microwaves. A 5.08 cm (2 in) thick quartz was necessary to contain up to 6.89 Mpa (1000 psi) gases in the test cell. An adapter was designed and fabricated to attach the quartz window on the top of the cell and seal it to prevent gas leakage at the high pressure. A 10.2 cm (4 in) i.d. aluminum elbow connected the cell to the microwave generator. The microwave generator was a Gerling Laboratories, Model GL 114 at an operating frequency of 2450 MHz. Microwave power can be adjusted up to 1500 watts; amount of energy reflected in the delivery train is monitored and the difference between generated and reflected power is that injected into the cell. A 1.83 m (6-ft) wire screen around the apparatus was used as added protection of personnel.

The tests were run before the discovery of the beneficial effects of surfactant upon hydrate formation rate, so that the hydrates prepared for the microwave tests had been slowly grown over a period of about 4 days and were present in a random mass of solid crystals above the water in the bottom of the cell as seen in Fig. 9. No free water was visibly exposed to microwaves; the hydrates gave a solid covering of the free water in the bottom of the cell.

In Fig. 22 is a sketch of the experimental setup.

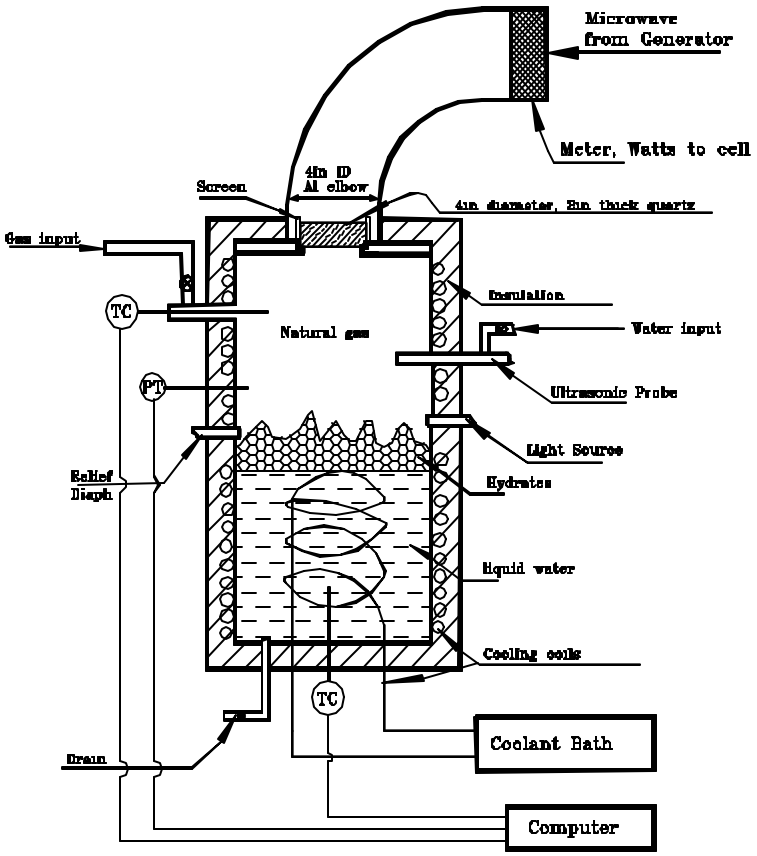

Fig. 22. Apparatus for microwave injection.

As indicated on the sketch of the apparatus, pressures and temperatures in the test cell were continuously recorded on the computer as the microwave tests were run.

A standard effect was established of microwaves on pure water in the cell pressurized to about 1.99 MPa (289 psi) with nitrogen chilled to 286.5 K (56° F). Microwaves were injected in 30-second pulses with 2 minutes between pulses. The schedule of microwave pulses was 100 watt increments from 60 to 860 watts. Pressure showed stepwise increases as microwave pulses vaporized some of the liquid.

Figure 23 shows the standard effect of microwaves.

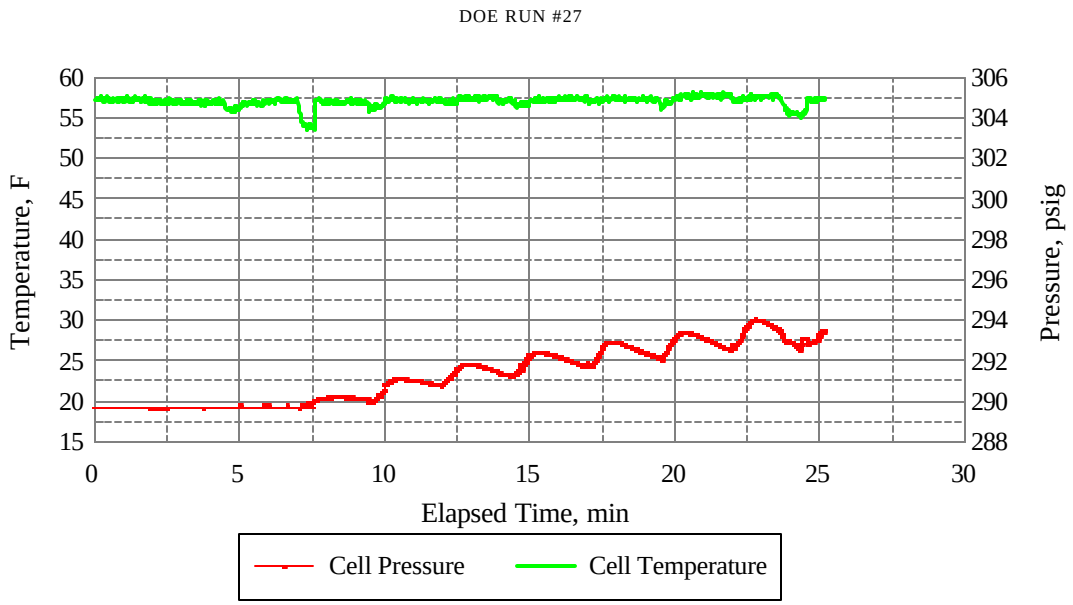

Fig. 23. Microwave response with water in system.

From a similar schedule of microwave pulses into the cell containing hydrates at 1.99 MPa (289 psi) and 285.4 K (54° F), resulting temperatures and pressures are presented in Fig. 24. Note that steeper pressure steps resulted and pressure spikes formed on each microwave input. One surmises that additional gases were evolved as well as hydrate-structure-water being vaporized, i.e., hydrates were dissociated. Water associated with the hydrate matrix would have also vaporized to give similar peaks to the liquid water standard. Again, the liquid water in the bottom of the cell was covered by the mass of hydrates and not irradiated.

Also note in Fig. 24 some difference in the gas temperature behavior. At about 190 watts of microwave input, positive temperature spikes occurred upon injection, whereas at lower wattage negative spikes resulted. It is speculated that excessive energy entered the cell above 190 watts to be dissipated in the gas phase.

Note that the peaks in Fig. 24 include water from the hydrate structure and gas released from the hydrate structure.

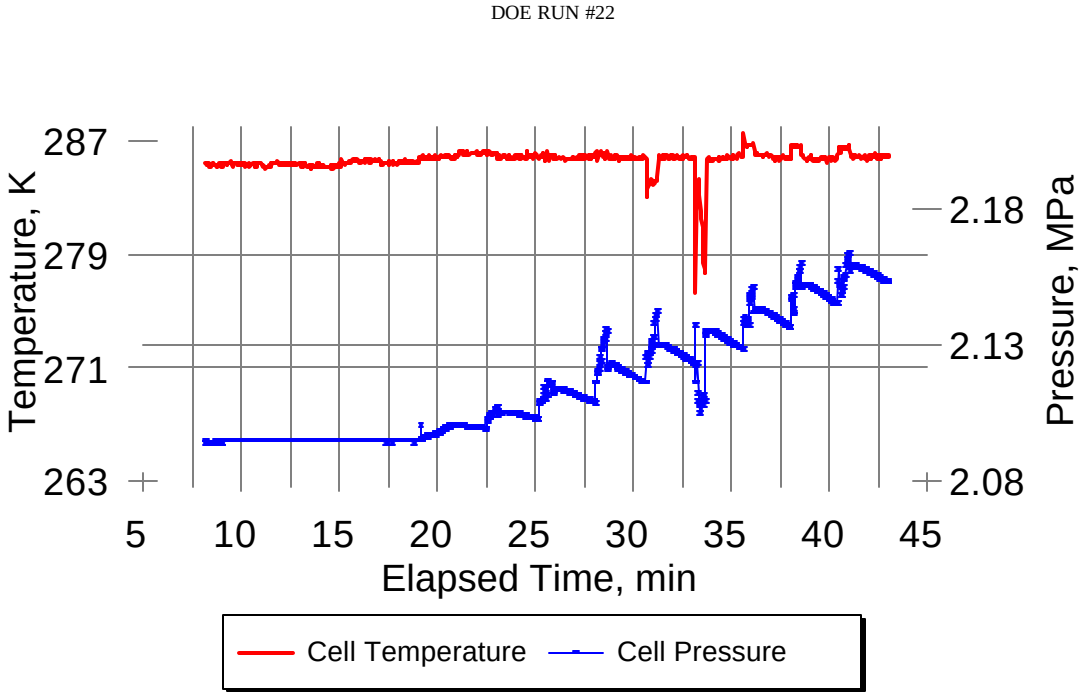

Fig. 24. Hydrate decomposition with cascading microwave pulses.

Input wattage of the microwaves was increased stepwise. Results are given in Fig. 25.

The gas released from hydrates as a function of power input was than calculated.

An optimum wattage seemed to exist as given in Fig. 25. Above the 190 watts, gas liberated per watt decreased.

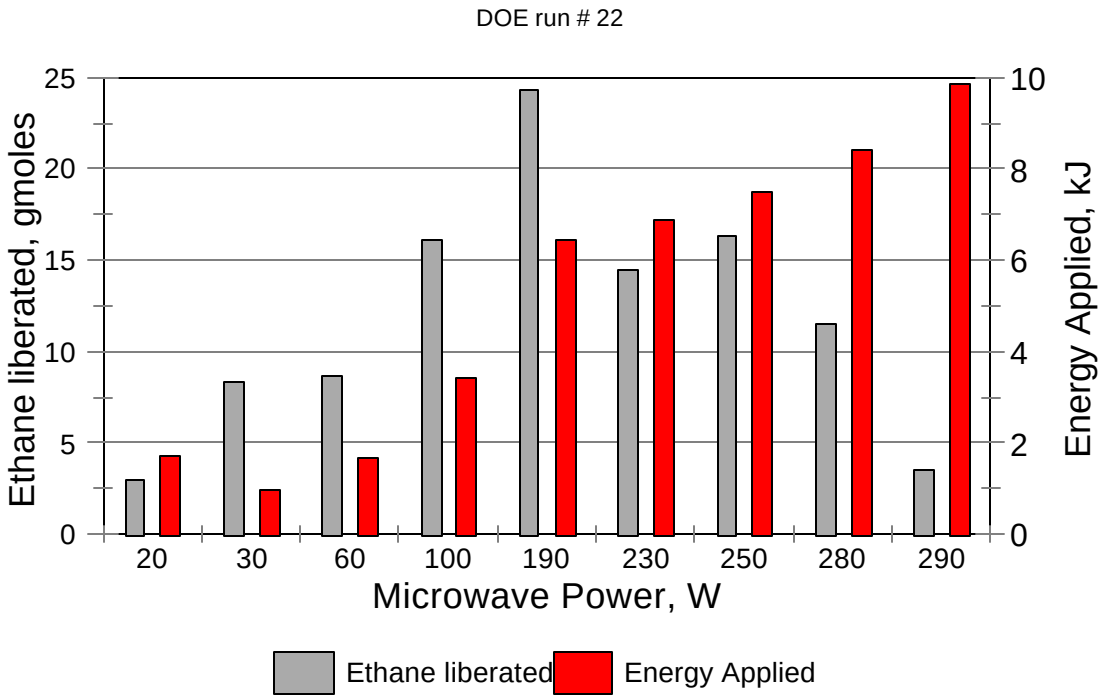

Fig. 25. Optimum microwave wattage for hydrate decomposition

The microwave experiments were not continued because decomposition of hydrates in a large scale process could be achieved very cheaply, especially near a power plant, with low-grade water of 376.5 K (110 F) or cooler that would ordinarily be sent to a cooling tower, anyhow. However, the results are kept in mind for possible specialty applications in this process.

VI. Impact of Study on Hydrate Storage Feasibility

A. Statement of Process Technical Need and Capability

The feasibility of gas hydrates for storing natural gas was studied because of their potential storage capacity of 180+ vol/vol and their inherent safety of essentially gas encased in ice at relatively low pressures. Furthermore, large quantities of natural gas are known to be stored this way naturally in ocean sediments and arctic regions.

Since hydrates have never been used for the industrial storage of gas, the feasibility study began with some major questions about such a process involving gas hydrates. Could the hydrates be formed rapidly enough? Prior to this study, formation of hydrates was a slow process in the laboratory, especially if using the simplest of systems--quiescent water and gas. Although hydrate formation had been shown by numerous people before the study to be rapid if mechanical stirring was used in the laboratory, a mechanically-stirred system under pressure at low temperatures on a large scale would not be practical from the standpoint of maintenance, initial equipment costs, labor, and leakage. Another question was whether a high bulk density of the hydrates could be realized? Or could a process step to collect the hydrate crystals from the water and pack them be practical? These were imposing questions, for water was known to be trapped inefficiently between solid hydrate particles and made inaccessible to further hydrate formation in previous laboratory work. In a scale-up, because of tank size and cost, one could not tolerate approximately 80% of the storage space to be occupied by unreacted water, as had been reported. Finally, could the process be made simple enough to be practical and economical?

A breakthrough occurred early in the work that provided answers to the preceding questions. By using the surfactant sodium dodecyl sulfate in concentrations as low as 286 ppm in water, the desired properties are achieved: (1) Hydrates form rapidly--about 700 times faster than without surfactant. (2) Free water trapped between particles is fully utilized to give a high bulk density. (3) Particles move from the water solution as they form and deposit (pack) on the chamber walls. (4) Hydrates form in a simple quiescent system. (5) 86% of the theoretical storage capacity can be achieved within 3 hours of hydrate initiation. (6) 155 vol-gas/vol-hydrate can be stored at 3.89 Mpa (564.9 psia) and 275.4 K (36^{o}F).

These experimental observations suggest ideas for a practical design for large-scale natural gas storage in hydrates.

B. Hydrate Formation/Storage Tank

(1) Characteristics to incorporate.

The interpretation of the laboratory observations relate to a design concept for a hydrate formation/storage/ decomposition tank as follows.

1. A single tank would serve for forming the hydrates as well as storing and decomposing them. This would negate the need for a tricky process step of pumping a cold liquid slurry of water-hydrate particles under pressure.
2. The hydrate particles form subsurface in water when it contains surfactant. This allows the formation process to proceed with a stagnant, unstirred water-surfactant solution. The many attendant problems of mechanical agitation of a thickening slurry under pressure are avoided. One would only admit more gas to the tank as it is occluded into the hydrates.
3. The hydrate particles move from the surfactant solution as they form and pack on the tank walls because of the adsorption of surfactant on the walls. This means no separation steps to remove hydrate particles from the water and pack them for storage is necessary. The particles pack into a desired arrangement as they form.
4. The free water trapped between hydrate particles on the tank walls continues to form hydrates because surfactant is excluded from the hydrate structure and transferred to the surrounding water. In fact, the rate of formation increases because of the greater surface area as more hydrates form--up to the point where a decreasing permeability slows the rate. Therefore, a high bulk density is achieved in the packing.
5. The rate of formation is high with surfactant present in the water. Our laboratory data indicate 86% of theoretical storage capacity is achieved within 3 hours after hydrate initiation. Moreover, this rate occurs in a quiescent system. The high rate indicates that a complete formation-decomposition cycle with adequate turnaround time could be achieved well within a 24- hour period at a very low labor requirement.
6. Water-surfactant solution wets the walls of the storage vessel. As particles collect on the walls, the water level drops, so that at the end when the last free water is in the cell, the hydrate mass is above the free water in the cell bottom.
7. Decomposition could be realized with heat transfer from a relatively low-temperature medium.
8. A substantial latent heat must be accommodated in the phase change.

(1) Sketch of tank concept.

The following Fig. 26 of a concept of a hydrate formation/storage/decomposition tank is suggested. (Zhong, et al., 1998)

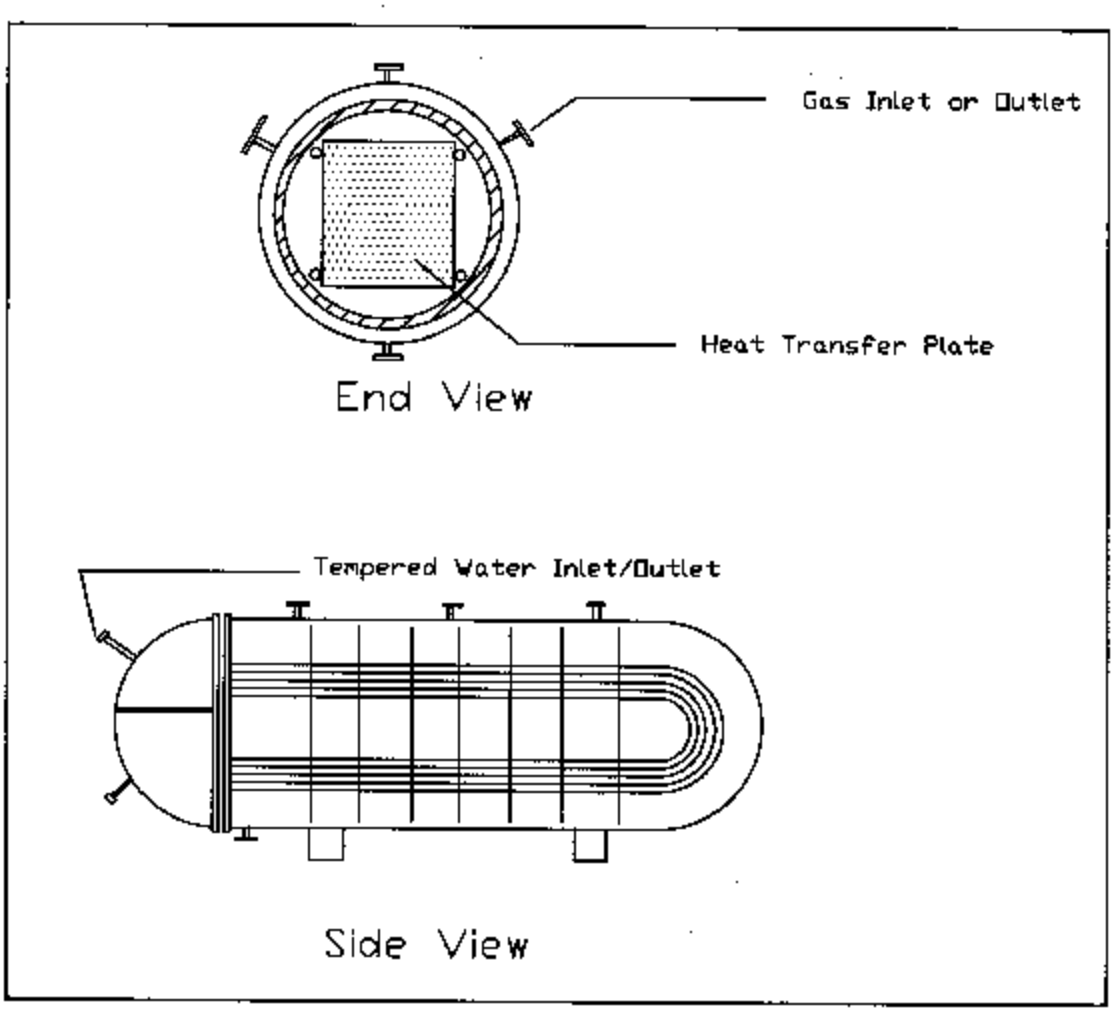

Fig. 26. Hydrate formation/storage/decomposition tank (Zhong, Montgomery, Pitman, Bounds).

To incorporate the findings of the laboratory test cell, the storage tank for an industrial-size facility features 9 thin stainless-steel plates 0.813 mm (0.032" thick) attached as a unit to tubing for a closed-loop flow of cooling or heating fluid, depending upon whether a formation or decomposition step is in progress. The plates and tubing are suspended on a rack that can be pulled as a unit from the horizontal tank for maintenance.

During hydrate formation, cooling fluid would circulate through the tubing to remove latent heat of hydrate formation. Heat transfer would be by conduction from direct contact of tubing with

plate and by conduction-convection to the water surrounding the tubing and plates. Gas would be admitted or withdrawn through the top ports. Gas hydrates would form on both sides of all plates and on the inside walls of the tank. The nine plates and inside surface area of the tank give an equivalent volume-surface ratio as was present in the laboratory test cell.

A time sequence depicting hydrate formation on the heat-transfer plates of the tank is given in Fig. 27.

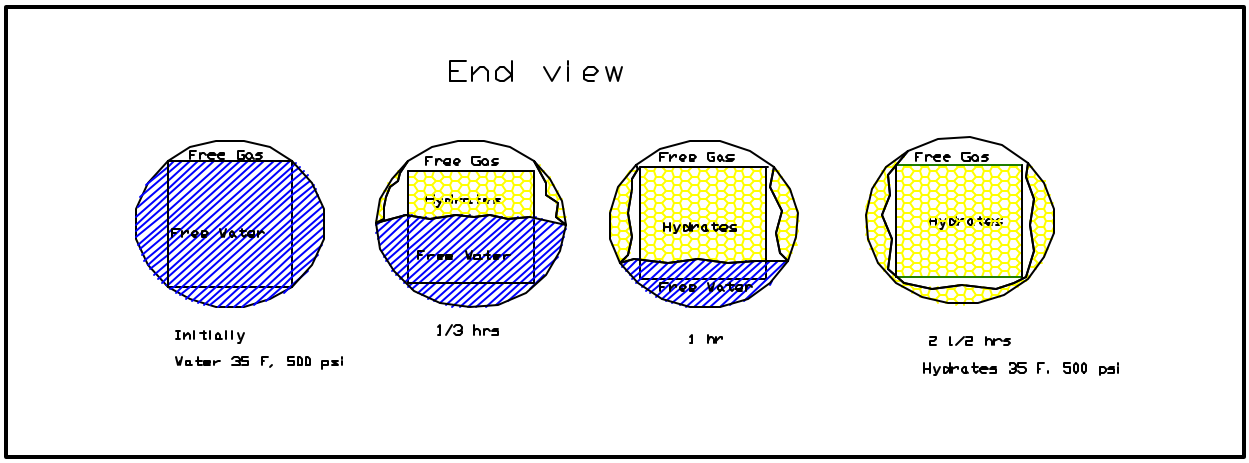

Fig. 27. Time sequence of hydrate formation in storage tank.

Water-surfactant are envisioned as initially submerging the plates. Free gas at 3.89 Mpa (564.9 psia) is admitted continuously. Hydrate forms on all the metal surfaces and the water level drops. Gas is replenished to maintain initial pressure. All of the free water is tied up by the fourth frame. Gas continues to form hydrates from trapped interstitial water until 86% of the theoretical gas capacity of hydrate storage is reached in about 2 ½ - 3 hours.

Decomposition is a reversal of these steps as warm water is passed through the heat-transfer coils.

In Fig. 28 is a side-view depiction of how hydrate particles would build on the inside surfaces of the formation tank and plates.

The sketch is based on observations of the particle build up in the laboratory test cell.

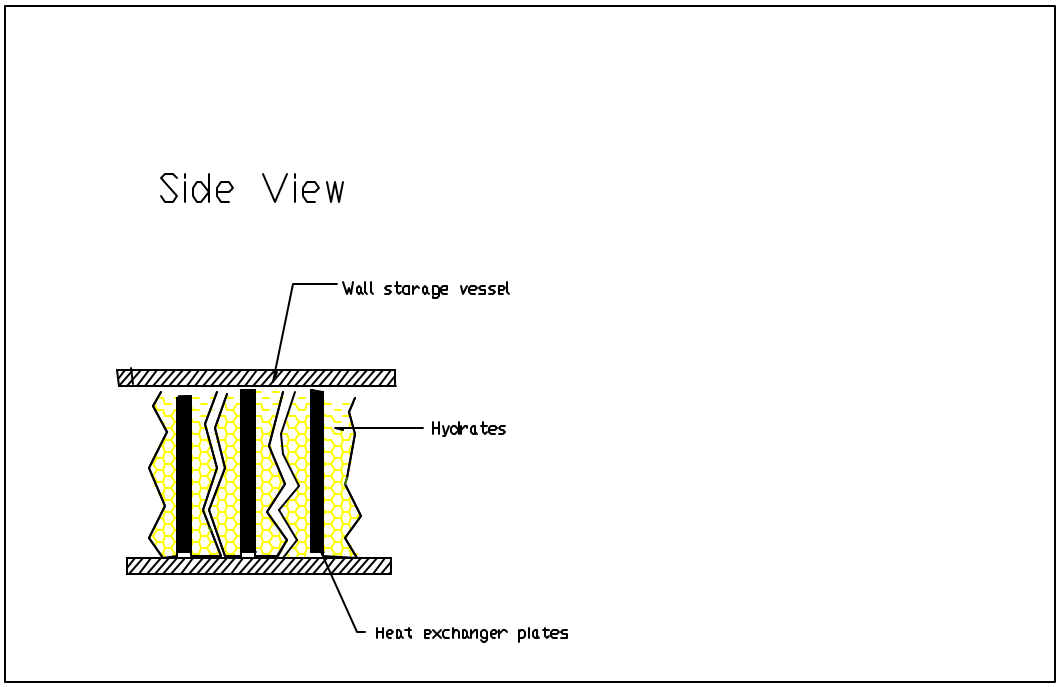

Fig. 28. Concept of hydrate accumulation in storage tank.

These ideas for a storage tank design would be pursued in the follow-on study to establish a final design and determine the economics of a large-scale hydrate storage process.

VII. CONCLUSIONS

The following major conclusions pertaining to the feasibility of storing natural gas in gas hydrates are made as a result of studies under the contract DE-AC26-97FT33203.

1. It is technically feasible to store natural gas in hydrates on a scale for industrial applications.

2. At a pressure of 3.89 Mpa (550 psig) and a temperature of 276.0 K (37°F), 155 (volume gas at standard temperature and pressure)/(volume hydrate) can be stored from a feed gas typified by 90% methane, 6% ethane, and 4% propane.

3. Concentrations of surfactant in the water above the critical micellar concentration (242 ppm) enhances process feasibility greatly:

   A. Increases formation rate of the hydrates by a factor of about 700.
   B. Causes the hydrate particles to adsorb on the tank walls as the hydrate forms, thus eliminating the need for separation of particles from the cold water-hydrate slurry.
   C. Maximizes gas content of the packed hydrate particles, as trapped free water between packed particles continues to form hydrates after adsorption on the vessel wall until complete utilization of trapped water is approached.
   D. Simplifies process. Allows a quiescent system to form hydrates.
   E. The surfactant is cheap; small amounts are required; it is nontoxic, biodegradable.

4. The rate of hydrate decomposition can be controlled by the heat transfer rate to the hydrate particles. An ambient temperature heating medium can be used to give an adequate decomposition rate.

5. Propane concentrations of at least 1- 4% must exist in the feed gas along with the methane in order to adequately store gas below 3.89 Mpa (550 psig) as Type II hydrates. As ethane and propane concentrations in the feed gas are increased, required formation and storage pressures decrease.

6. Occluded gas composition depends on feed gas composition.

7. A storage tank design can be devised from knowledge of the experimental results.

VIII. RECOMMENDATIONS

The use of surfactants makes a process for storing natural gas in hydrates technically feasible. The next step should be to develop a design for a large-scale process based on the laboratory results. In conjunction with the design, an economic study should be made estimating total capital investment, production costs, and storage costs per volume of gas per cycle over the life of the facility.

BIBLIOGRAPHY

Carson, B.D., and Katz, L.D., "Natural Gas Hydrates," *AIMME Tech. Pub*. No. 1371 (1941).

Englezos, P., "Nucleation and Growth of Gas Hydrate Crystals in Relation to 'Kinetic Inhibition'", *2nd International Symposium on Gas Hydrates*, Toulouse (1996) 147-153.

Herri, J., Gruy, F., and Cournil, M., "Kinetics of Methane Hydrate Formation," *2nd International Symposium on Gas Hydrates*, Toulouse (1966) 243-250.

MacKerrell, A.D., Jr., "Molecular Dynamics Simulation Analysis of a Sodium Dodecyl Sulfate Micelle in Aqueous Solution: Decreased Fluidity of the Micelle Hydrocarbon Interior," *J. of Phys. Chem.*, **99** (1995) 1846-1855.

Makogon, Y.F., *Hydrates of Natural Gas*, PennWell Books (1981).

Marita, H., and Uchida, T., "Studies on Formation/Dissociation Rates of Methane Hydrates," *2nd International Symposium on Gas Hydrates*, Toulouse (1996) 191-197.

Mori, Y., and Mochizuki, T., "Modeling of Mass Transport across a Hydrate Layer Intervening between Liquid Water and 'Guest' Fluid Phases," *2nd International Symposium on Gas Hydrates*, Toulouse (1996) 267-274.

Sloan, D.E., Jr., *Clathrate Hydrates of Natural Gases*, Marcel Dekker Inc., New York, NY, (1990).

Sloan, D.E., Jr., "Natural Gas Hydrates," *J. Petroleum Technology*, **43**, No. 12 (1991) 1414-1417.

Spontak, R.J., "Determination of Volumetric Properties for Systems Containing Structure I Gas Hydrates," *Industrial Engineering and Chemistry Process Design Development*, **25**, No. 4 (1986) 1030-33.

Tse, J.S., et al., "Molecular Dynamics Studies of Ice and Structure I Clathrate Hydrate of Methane," *J. of Physics and Chem*, **87** (1983) 4198-4203.

Vysniauskas, A., and Bishnoi, P.R., "Kinetics of Ethane Hydrate Formation," *Chemical Engineering Science*, **40** (1985) 299-303.

Vysniauskas, A., and Bishnoi, P.R., "A Kinetic Study of Methane Hydrate Formation," *Chemical Engineering Science*, **38** (1983) 1061-1072.

Wilcox, W.I., Carson, D.B., and Katz, D.L., "Natural Gas Hydrates," *Industrial and Engineering Chem*, **33**, No. 5 (1941) 662-65.

Zhong, Y., Montgomery, R., Pitman, R. And Bounds, M., *Plant Design*, Senior chemical engineering project assignment, Mississippi State U., Dept. of Ch.E., Nov. 1998.

LIST OF ACRONYMS AND ABBREVIATIONS

SDS	The anionic surfactant sodium dodecyl sulfate.
CMC	The critical micellar concentration. A threshold of surfactant concentration in water solution, at which point many physical properties abruptly change.
RTD	Resistance temperature detector.

NATURAL GAS HYDRATES STORAGE PROJECT
PHASE II. CONCEPTUAL DESIGN AND ECONOMIC STUDY

FINAL REPORT
9 June - 10 October 1999

Principal Investigator
R.E. Rogers

Graduate Research Assistant
Yu Zhong

September 27, 1999

Contract DE-AC26-97FT33203

Mississippi State University
P.O. Box 9595
129 Etheredge-Hardy Road
Mississippi State, MS 39762

ABSTRACT

DOE Contract DE-AC26-97FT33203 studied feasibility of utilizing the natural-gas storage property of gas hydrates, so abundantly demonstrated in nature, as an economical industrial process to allow expanded use of the clean-burning fuel in power plants. The laboratory work achieved breakthroughs: (1) Gas hydrates were found to form orders of magnitude faster in an unstirred system with surfactant-water micellar solutions. (2) Hydrate particles were found to self-pack by adsorption on cold metal surfaces from the micellar solutions. (3) Interstitial micellar-water of the packed particles were found to continue forming hydrates. (4) Aluminum surfaces were found to most actively collect the hydrate particles.

These laboratory developments were the bases of a conceptual design for a large-scale process where simplification enhances economy. In the design, hydrates form, store, and decompose in the same tank in which gas is pressurized to 550 psi above unstirred micellar solution, chilled by a brine circulating through a bank of aluminum tubing in the tank employing gas-fired refrigeration. Hydrates form on aluminum plates suspended in the chilled micellar solution. A low-grade heat source, such as 110^{o}F water of a power plant, circulates through the tubing bank to release stored gas. The design allows a formation/storage/decomposition cycle in a 24-hour period of 2,254,000 scf of natural gas; the capability of multiple cycles is an advantage of the process.

The development costs and the user costs of storing natural gas in a scaled hydrate process were estimated to be competitive with conventional storage means if multiple cycles of hydrate storage were used. If more than 54 cycles/year were used, hydrate development costs per Mscf would be better than development costs of depleted reservoir storage; above 125 cycles/year, hydrate user costs would be lower than user costs of depleted reservoir storage.

TABLE OF CONTENTS

LIST OF FIGURES

LIST OF TABLES

Page

EXECUTIVE SUMMARY

The feasibility of storing natural gas in gas hydrates was demonstrated in the laboratory during Phase I of this contract. Although 180+ (vol gas @ STP in hydrates)/(vol hydrates) at equilibrium was known to be possible prior to the study, serious problems had to be overcome to realize the potential in a practical process: (1) Free water when trapped between forming hydrate particles become isolated from gas and unreactive. (2) Mechanical stirring required for rapid formation created scaleup problems. (3) Hydrate formation was too slow in an unstirred system to be practical. (4) Filtering and packing hydrate particles from a cold, pressurized slurry is difficult, requiring excessive labor for an economical process.

In Phase I of the study, these problems were resolved in the laboratory by using a 242+ ppm of a surfactant sodium dodecyl sulfate that formed micelles to solubilize the hydrocarbon gas: (1) Rates were increased by a factor of greater than 700. (2) Hydrates formed subsurface and the surfactant moved the particles to the stainless steel walls to be adsorbed. (3) Entrained water in the interstices of adsorbed hydrate particles rapidly converted to hydrates. Consequently, hydrates were formed to 86% of theoretical gas capacity in a quiescent system which self-collected and self-packed in the test cell within 3-hours of hydrate initiation.

Based on the laboratory findings, Phase II prepared a conceptual design and an economic analysis of a large-scale process, which are contained in the subject report. To process 2,254,000 scf-natural-gas/cycle, 3 carbon-steel tanks are proposed of 10 ft diameter by 60 ft length designed for a 550 psig operating pressure with retrievable aluminum adsorption plates supported in the tank. A refrigerated brine heat-transfer medium for hydrate formation flows through 500 aluminum tubes, 3/4" diameter, 14 Birmingham Wire Gauge (BWG). The tubing extends parallel through the length of the tank. Water from the power plant at 110^{o} F would flow through the tubing to decompose the hydrates. A vacuum-enclosed fiber-glass insulation on the tank exterior cuts heat gain costs to a minimum during storage. A natural-gas-fired refrigeration system is integral to the design to reduce costs and to utilize methane-rich gas above the hydrates.

A single formation/decomposition cycle can be achieved within 24 hours: 7 2/3 hours for the formation in each of 3 storage tanks filled in series and 1 hour for the decomposition. The limiting factor in filling each tank with hydrates is the heat-transfer rate to remove the latent heat of hydrate formation, not the formation rate or mass transfer rate of the hydrates. The aluminum plates and aluminum tubing arrangement allows relatively rapid hydrate-filling of the tanks even though it is the pacing step in the process. Consequently, a daily cycle of formation/storage/decomposition would be possible.

An economic analysis of a large-scale process concluded that the development costs per 1000 scf for gas hydrate storage can be competitive with liquefied natural gas (LNG), salt caverns and depleted reservoirs by using at least 4, 14 and 54 cycles/year, respectively. The user costs can be competitive with conventional storage above 13 cycles/year; above 125 cycles/year hydrate costs are superior to all.

I. INTRODUCTION

A. Needs for Gas Storage

Natural gas offers clean-burning fuels, abundant domestic supply, existing distribution infrastructure, and a low-price energy source. For some applications, however, use is limited by current storage choices of mainly salt caverns and depleted gas reservoirs, choices that geologically exclude some major markets. Compressing and liquefying natural gas encounter safety and economy problems. Therefore, the subject work was undertaken to study the feasibility of a novel way to store natural gas, namely, occluded in gas hydrates.

Natural gas storage in gas hydrates is novel in the sense that industry has never made use of the potentially high gas storage capacity of hydrates. However, it is not novel considering that some 100,000- 300,000 trillion cubic feet (tcf) of natural gas (Collett, 1996; Kvenvolden, K.A., 1993), multiple times the entire conventional supply of hydrocarbons, are estimated to be naturally stored in gas hydrates onshore and offshore in the United States. Historically, hydrate research has dwelt on preventing hydrate occurrence in the oilfield, while research on utilizing hydrate storage properties for industry has been negligible. It was therefore appropriate to engage in this feasibility study.

As the first serious attempt to utilize the unique properties of hydrates to store natural gas, the objective was to determine the technical feasibility of commercial storage and, if found feasible, develop a conceptual design and determine an economic viability of a large-scale process.

B. Advantages of Gas Hydrate Storage

Prior to the subject study, the known advantages of gas hydrates for storing natural gas were the following: 1. Gas in excess of 180 (vol gas @ standard conditions)/(vol of hydrates) could be packed into the gas hydrate crystals. (2) Natural gas stored in hydrates would be inherently safer because gas is essentially encased in ice. (3) Natural gas stored in hydrates would be released slowly, in case of storage tank rupture. (4) Gas could be stored in hydrates at relatively low pressures. (5) Vast quantities of gas are stored in naturally-occurring hydrates. These properties suggested a possibility of safe storage of natural gas aboveground at sites whose geology limits conventional underground storage.

Also, prior to the subject study, the following known negative factors diminished feasibility prospects: (1) The formation of hydrates in a quiescent pure water-hydrocarbon gas system was extremely slow at hydrate-forming temperatures and pressures in laboratories. (2) A dynamic process was complex for scale-up, especially if a mechanically-stirred reactor became necessary to achieve acceptable formation rates. (3) The slurry separation and packing of hydrate particles formed in a stirred reactor seemed economically prohibitive. (4) Excessive free water typically trapped between hydrate particles would diminish gas-packing density, thus increasing storage tank size and cost. (5) A storage process for hydrates had never been demonstrated.

C. Results of Feasibility Study

Phase I of the contract demonstrated in the laboratory the feasibility of a hydrate storage process. A review of those results follows.

(1) Experimental

A stainless steel cell of 3900 cm^3 was constructed and equipped with two RTD probes, pressure transducer, and relief valve. Cooling coils were placed inside the cell and around the exterior walls; a gas mass flowmeter, a constant pressure regulator, and a computerized Omega data-collection system were installed. Video capture of hydrate formation was made with still photographs taken through a 2" thick, 3" diameter pure quartz disk sealing the top of the cell and with an invasive fiber optics/camera system viewed through sapphire-windowed ports in the side of cell; activities inside the cell could be viewed on a monitor screen and/or filmed with VHF video cassette recording.

(2) Hydrate Storage Capacity and Formation Rate

A breakthrough occurred early in the laboratory work that provided answers to multiple problems regarding commercial storage of gas hydrates. A surface active agent was found to solve the problems of achieving high storage capacities in a short period of time while facilitating packing the hydrate particles from an unstirred system. Consider the results presented in Fig. I.C.1 of three experimental runs made to determine attainable capacity; temperature was held constant at 275.4 K (36°F), and a sodium dodecyl sulfate (SDS) surfactant concentration was maintained at 286 ppm; procedure and other conditions except pressure were repeated. Hydrates were formed in the cell until all of the water became tied up in the hydrate structure, i.e., interstitial water also formed hydrates. Individual runs were made at pressures of 3.89, 3.47, 3.11, 2.76 MPa (550.2, 503.6, 451.2, and 400.5 psig), where the chosen pressure was kept constant throughout each run with a constant pressure regulator, and the rate of gas occluded was measured with a gas mass-flowmeter. Such a constant-pressure procedure in a semi-continuous process would be preferred in an industrial operation.

The results presented in Fig. I.C.1 show that 155 (vol gas)/(vol bulk hydrate) storage capacity is achieved at a processing pressure of 3.89 MPa (550 psig). Furthermore, as a result of surfactant in the water, this much gas is incorporated into the hydrates in less than 3 hours of processing time, a rate of hydrate formation about 700 times faster than in a pure water system. The 155 vol/vol represents 86% of the theoretical storage capacity if all cavities were filled, including hydrates formed from interstitial water.

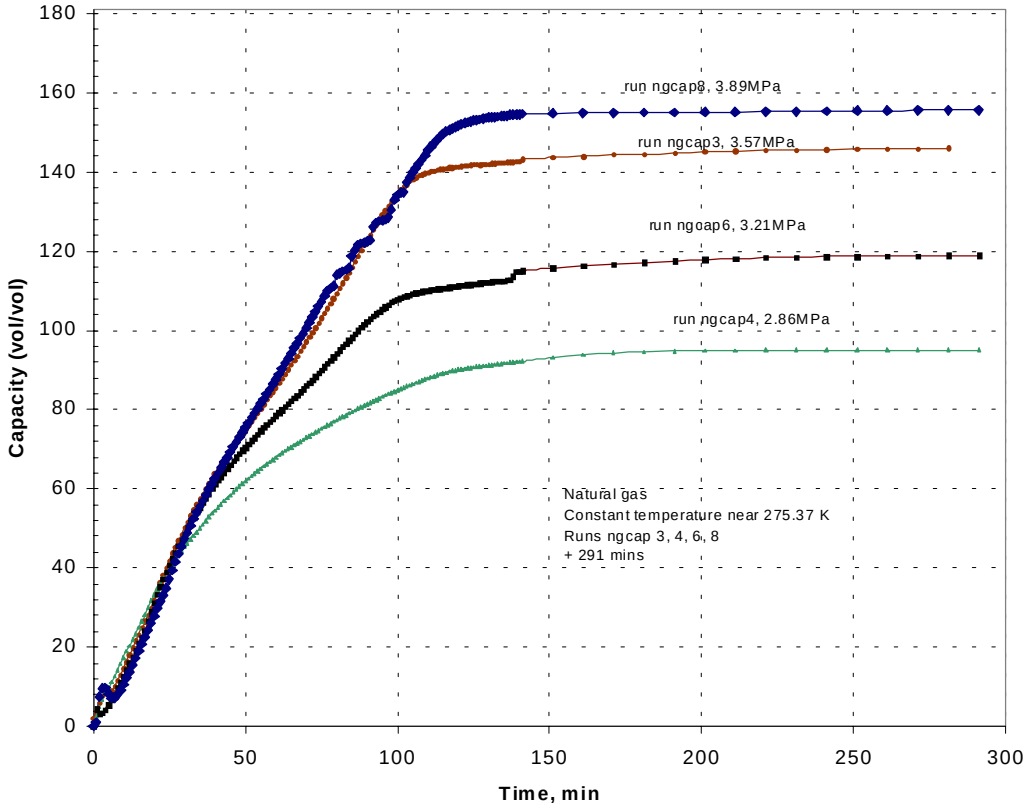

Fig. I.C.1. High storage capacity in less than 3 hours

At a common time after hydrate initiation is taken, 291 minutes for example, the storage capacity is seen to increase with pressure as given in Fig. I.C.2. Therefore, a processing pressure of 3.89 MPa (550 psig) is suggested for a large-scale process.

It was found in later experiments that aluminum was better than stainless steel or copper as a surface to adsorb and retain hydrate particles as they form from micellar solution. Fortunately, aluminum also would have a lighter weight, better heat conduction, and more favorable economy as adsorption plates in a large-scale process.

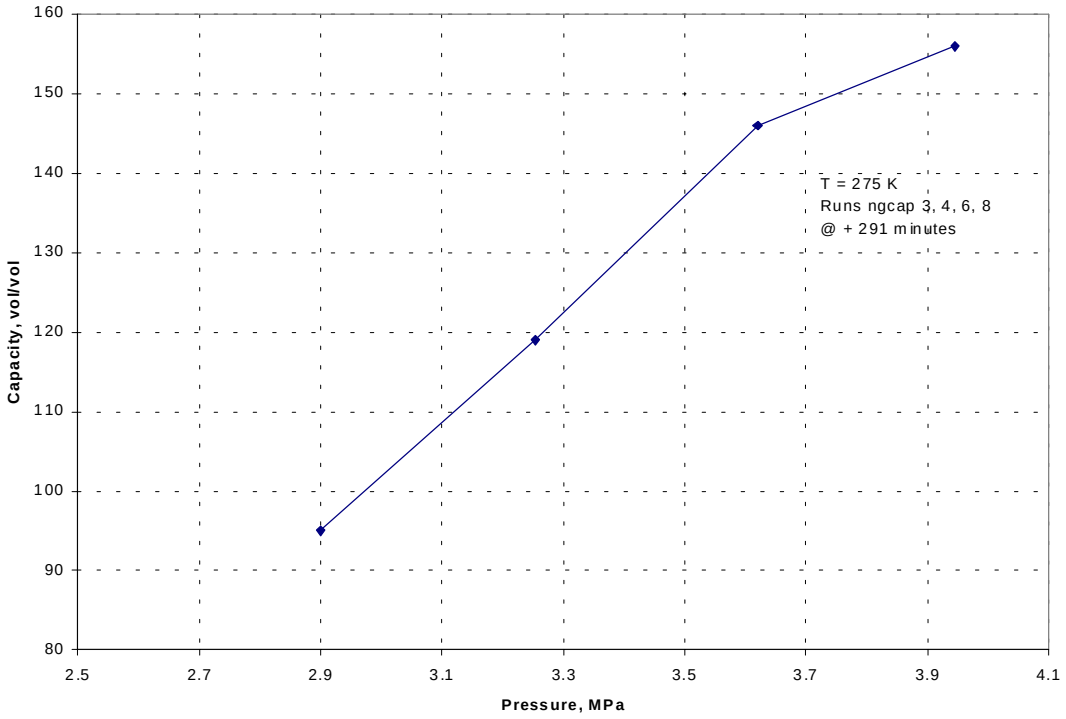

Fig. I.C.2. Processing pressure of 550 psi chosen

The rate of hydrate formation was increased by adding surfactant to achieve the critical micellar concentration (CMC). The formation rate became elevated to the extent that the reaction rate would no longer be controlling. Instead, the heat-transfer rate of removing latent heat of formation would limit rate of filling a storage tank in a large-scale process.

(*3) Packing of Hydrate Particles*

The inherent problem of packing hydrate particles in an industrial size process was addressed. It was found that SDS surfactant facilitates the packing of hydrate particles as formed. By situating a camera at the water-gas interface, VHS film captured the formation of the hydrate particles subsurface and their movement (specific gravity is less than 1) from the water slurry to the surface of the water. Near the water surface, the particles moved to the stainless steel walls to be adsorbed, building inwardly from the walls in a concentric cylinder. The natural gas hydrates symmetrically pack in the cell, leaving open only a small cylindrical void slightly off-center through which the bottom of the cell is visible. Practically, this means that an expensive processing step of separating particles from a water slurry and packing them in a storage container is preempted. Furthermore, storage space is maximized when the surfactant-laden particles build inwardly from the container walls.

(4) Conversion of Interstitial Water

The conversion to hydrates of interstitial water was achieved in a semi-continuous process with a system containing natural gas, water, and 286 ppm of SDS. Gas was continuously added to the cell to replenish gas being occluded and to maintain a constant pressure during hydrate formation; gas flow was controlled by a constant-pressure regulator and flow measured by a gas mass flowmeter. At the higher constant pressure, a greater fraction of the cavities fill than if gases were added batchwise. Natural gas in our test cell was maintained at 3.89 MPa (550 psig). Hydrates were allowed to form until all of the free water initially in the bottom of the cell was dissipated into the hydrate structure or as free water in the interstices; then the free water remaining in the interstices was converted to hydrates. Results showed that within 3 hours, 86% of theoretical capacity was achieved. Hydrate formation rates remained high as interstitial water was converted.

(5) Process Simplification

For a hydrate storage process to be economical, it must be simple. Labor must be minimal. Preferably, there would be no moving parts in the hydrate formation-storage tank, and maintenance, labor, operating difficulties, and capital investment would be reduced.

Surfactant in the water solution simplifies the process four ways: (1) Hydrates form rapidly. (2) Hydrates form in a quiescent system. (3) Hydrate particles migrate to the cell walls where they self-adsorb and self-pack. (4) Interstitial water forms hydrates. In the first simplification, hydrates form in the presence of surfactant greater than 700 times faster than in a quiescent, pure-water/gas system. Therefore, with proper design of the formation-storage vessel, a formation-decomposition cycle including turnaround time could be achieved within a 24-hour period. In the second simplification, surfactant causes hydrates to be formed in a quiescent system, eliminating the need to impose water flow, movement, or mechanical stirring. Consequently, complexity of the formation/storage tanks would be reduced; in fact, hydrate formation-storage-decomposition could be accomplished in the same vessel. Surfactant allows reuse of the process water: after hydrate decomposition, the water and surfactant would remain in the storage tank, and the next formation cycle would proceed by repressurizing with gas. In the third and fourth simplifications, difficult intermediate process steps of collecting and packing hydrate particles in a storage vessel are eliminated, because the particles form in the cell in an ordered and packed manner. After packing, the interstitial water is converted to hydrates at a high rate.

The simplifications greatly enhance the prospects for an economical large-scale process.

(6) Critical Micellar Concentration for Hydrate Formation

Critical micellar concentration (CMC) refers to a threshold level of surfactant concentration in water necessary for micelles to form, and above which some physical properties of a solution abruptly change. To determine concentration levels needed to influence hydrate formation and to give insight into the mechanism of hydrate formation, surface tension was measured for

numerous concentrations of SDS/water solutions; the CMC at 298 K (77°F) and 1 atm for our solution occurred near 2700 ppm of SDS.

However, when using the same surfactant in the chilled and pressurized test cell, hydrates rapidly formed at lower SDS concentrations than 2700 ppm, indicating a lower CMC. In explanation, CMC is a function of temperature and the amount of gas dissolved in the water. In order to get a better estimate of CMC at test conditions, multiple runs were made with a pressurized and chilled water/ethane system in the test cell while varying SDS concentration. The results are given in Fig. I.C.3.

In Fig. I.C.3 the very sharp break in the curve at 242 ppm represents the CMC at ethane hydrate-forming conditions for SDS. Hydrate induction time gave the most sensitive indication of the breakpoint, although amount of gas occluded at a specific time would also have sufficed.

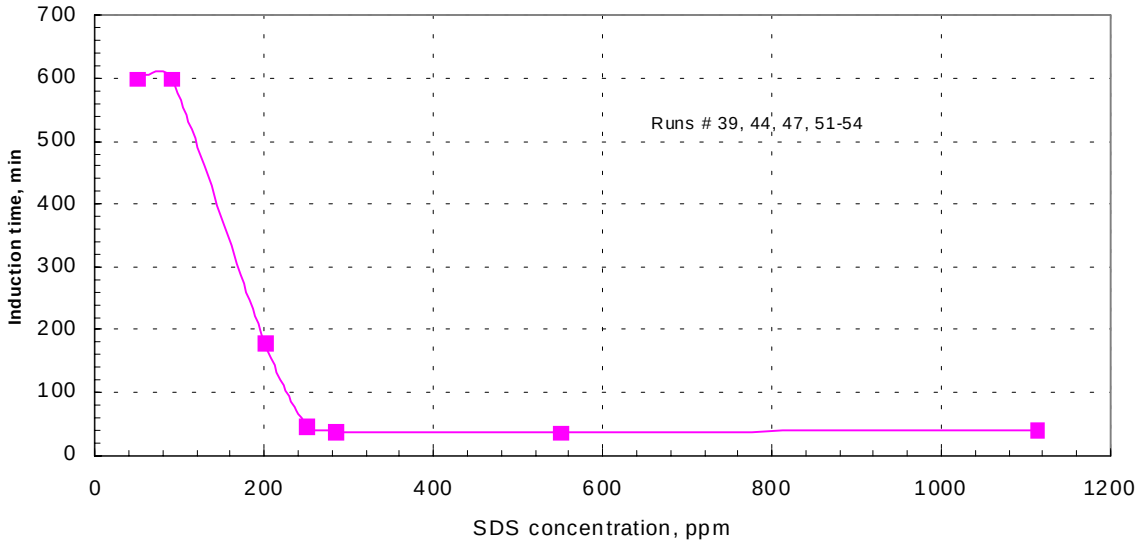

Fig. I.C.3. Critical micellar concentration threshold for hydrate formation

The conclusion from Fig. I.C.3 is that a SDS surfactant solution concentration above the CMC greatly enhances the hydrate gas-storage process. The micellar configuration is sketched in Fig. I.C. 4.

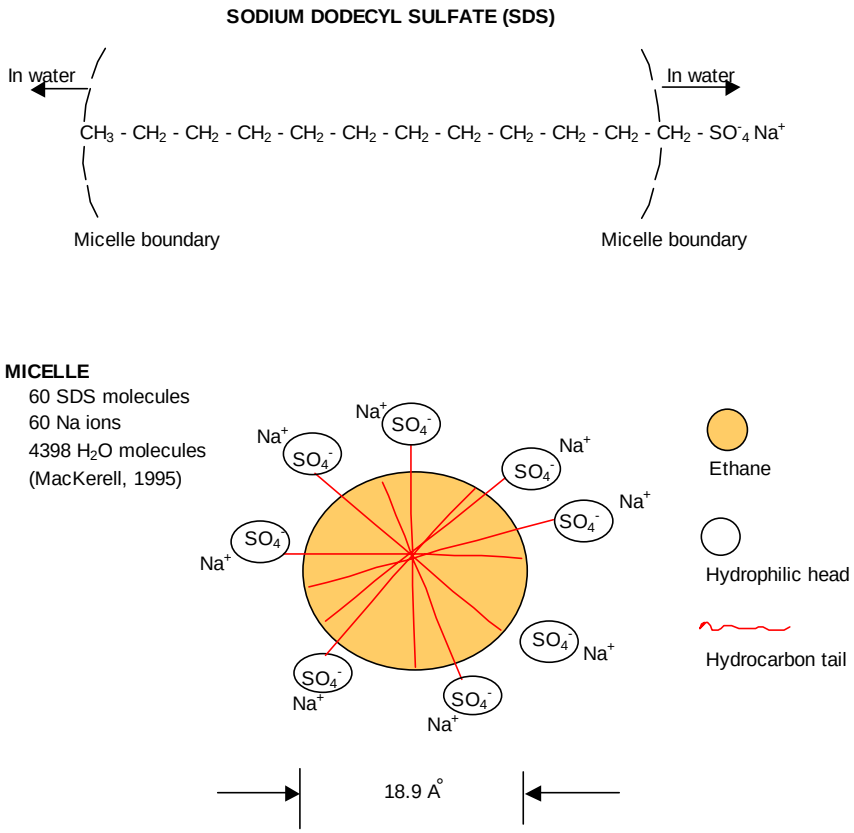

Fig. I.C.4. Micelles solubilize natural gas, forming hydrates subsurface

These experimental observations make possible a practical design for large-scale natural gas storage in hydrates in which natural gas is solubilized in the micelles and facilitates hydrate formation subsurface.

II. CONCEPTUAL DESIGN HYDRATE STORAGE PROCESS

The following is the concept of a large-scale process based on the data obtained in the feasibility phase.

A. Process Flow Diagram

A block diagram of the envisioned scaled up process for gas hydrate storage of natural gas is given in Fig. II.A.1.

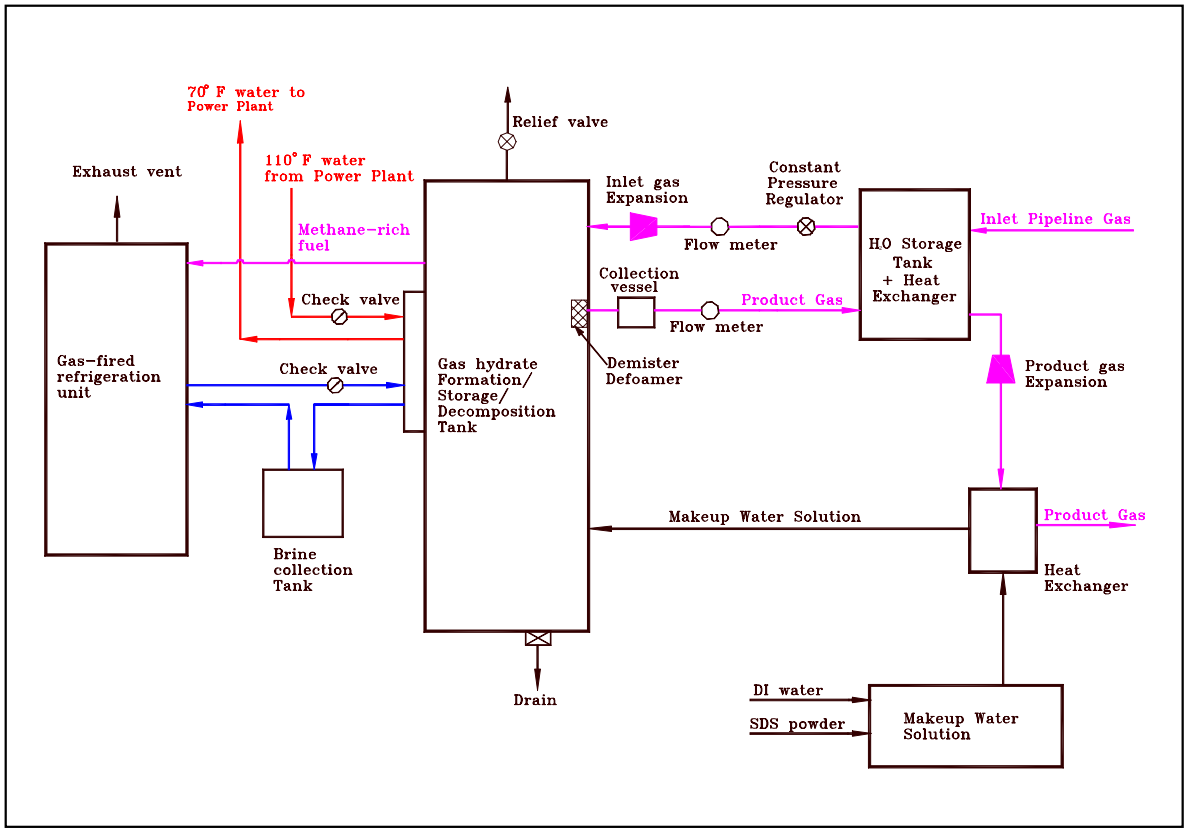

Fig. II.A.1. Block diagram hydrate storage process

The process was designed to fill 3 tanks in series with hydrates in a 23-hour period and then decompose all 3 tanks in parallel within a 1-hour period. The formation tanks also serve for storage and decomposition. Heat transfer fluid flowing through tubing in the tank would alternately come from a refrigeration unit for formation or from the adjacent power plant for decomposition. Feed gas flows into the formation tank from a pipeline at pressures ranging from 600 to 700 psig; feed gas in the formation tank is controlled to a constant 550 psig. Makeup water to replace moisture entrained with the outlet gas is cooled by the exiting cold gas; a demister-defoamer and collection vessel remove entrained water in the exiting gas stream. A gas-fired refrigeration unit cools a circulating brine that removes latent heat of formation; the refrigeration unit uses methane-rich gases from the storage tank as fuel.

B. Formation/Storage/Decomposition Tank

(1) Storage Tank Design

Hydrate formation, storage and decomposition is performed in the same tank; it has an operating pressure of 550 psig. Laboratory studies demonstrated that hydrates form rapidly from the micelles of sodium dodecyl sulfate and, just as importantly to the success of the process, the surfactant adsorbs on a metal surface and there packs the hydrates. The laboratory work showed aluminum to be the best surface for adsorption and retention of the hydrates. This is fortunate because of aluminum's higher thermal conductivity, lighter weight, and lower cost. Therefore,

aluminum adsorption plates rest on supports and traverse the length of the tank; they can be individually removed. Eighteen total vertical and horizontal aluminum supports accommodate the weight of the hydrate mass.

Aluminum heat exchange tubing extends the length of the tank and heating/cooling mediums make one-pass through each tube. Heat transfer results from conduction and convection from the tubes immersed in water and contacting the plates and supports.
The tank's drain and gas ports are Teflon coated to prevent buildup of hydrates.

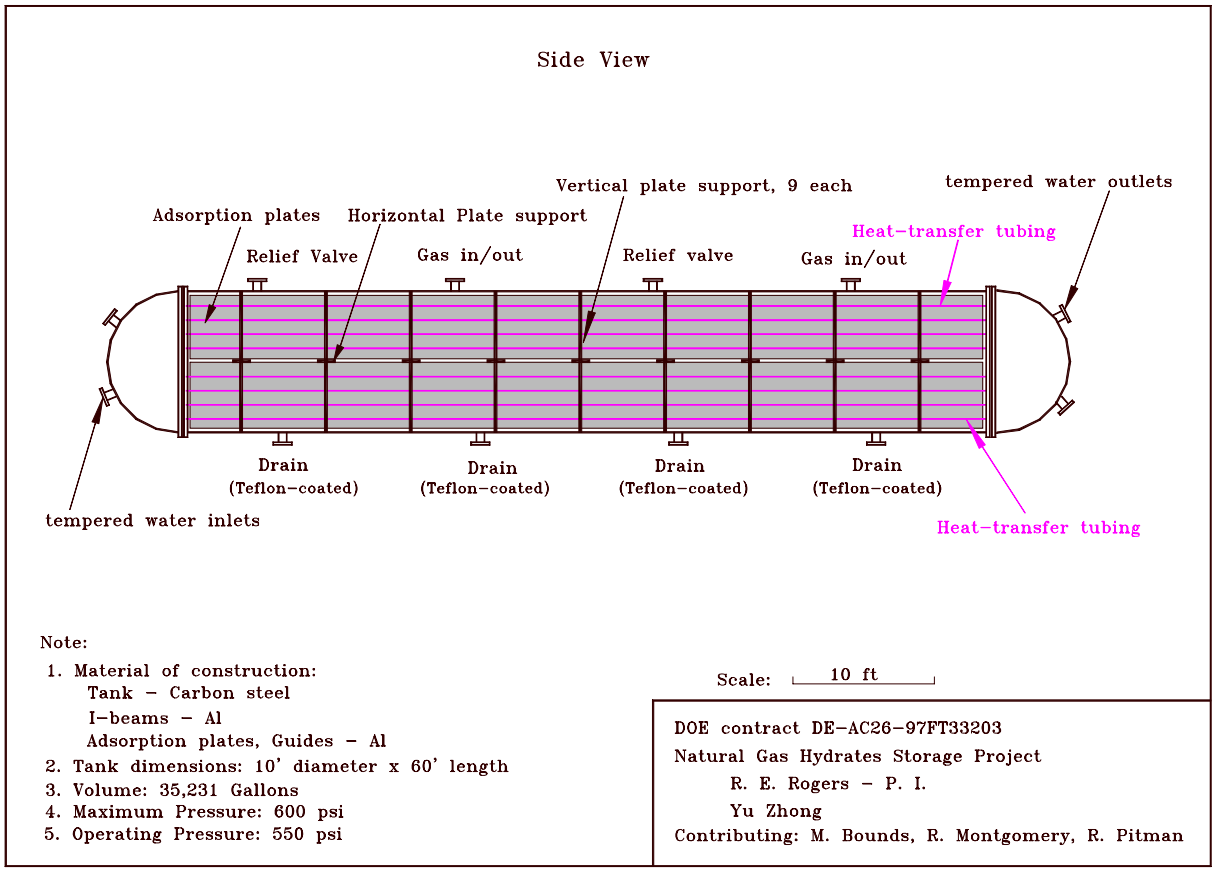

Fig. II.B.1. Hydrate formation/storage/decomposition tank

(2) Hydrate Adsorption Plates

The rate of hydrate formation with SDS micellar solution depends upon the surface area of the adsorption plates (DOE Monthly Status Report, Aug. 1999). Therefore, for the scaled formation tank to exhibit at least a hydrate formation rate as rapid as achieved in the laboratory unit, equivalence of volume/surface area would be required. By using this scale factor, the 10-ft diameter tank would require an adsorption plate surface area at least 1879 ft^2. The proposed design, however, establishes a plate surface area of 7,995 ft^2. Although this is an over design on

surface area, the additional plates are needed to support the weight of the hydrates. A sketch of the plates is presented in Fig. II.B.2.

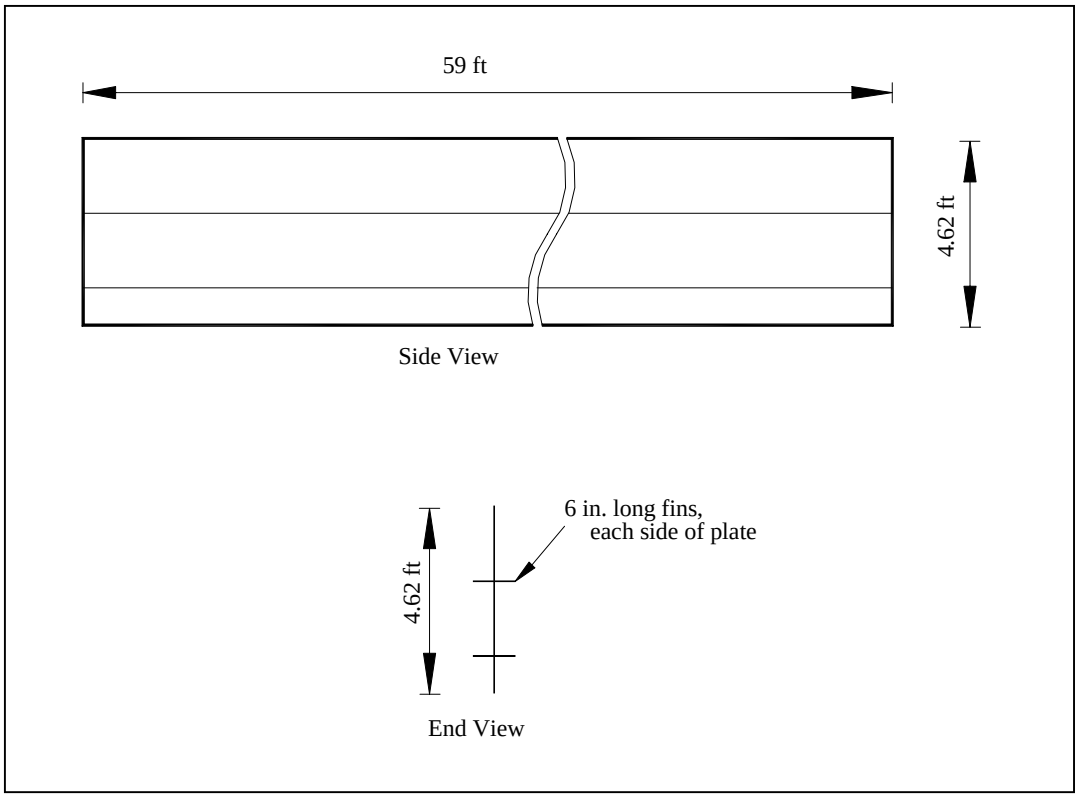

Fig. II.B.2. Sketch of largest adsorption plate.

Fins are added to support the weight of the hydrates that build outwardly from the plates, but they also provide additional surface area for adsorption. Twenty plates run the length of the tank. Each plate may be pulled separately from the tank. The heat transfer tubes run parallel to the plates and rest on the aluminum cross-supports.

In Fig. II.B.3. is sketched the pattern of plates for a quadrant of the formation tank; the sizes and numbers of plates would be repeated in each quadrant.

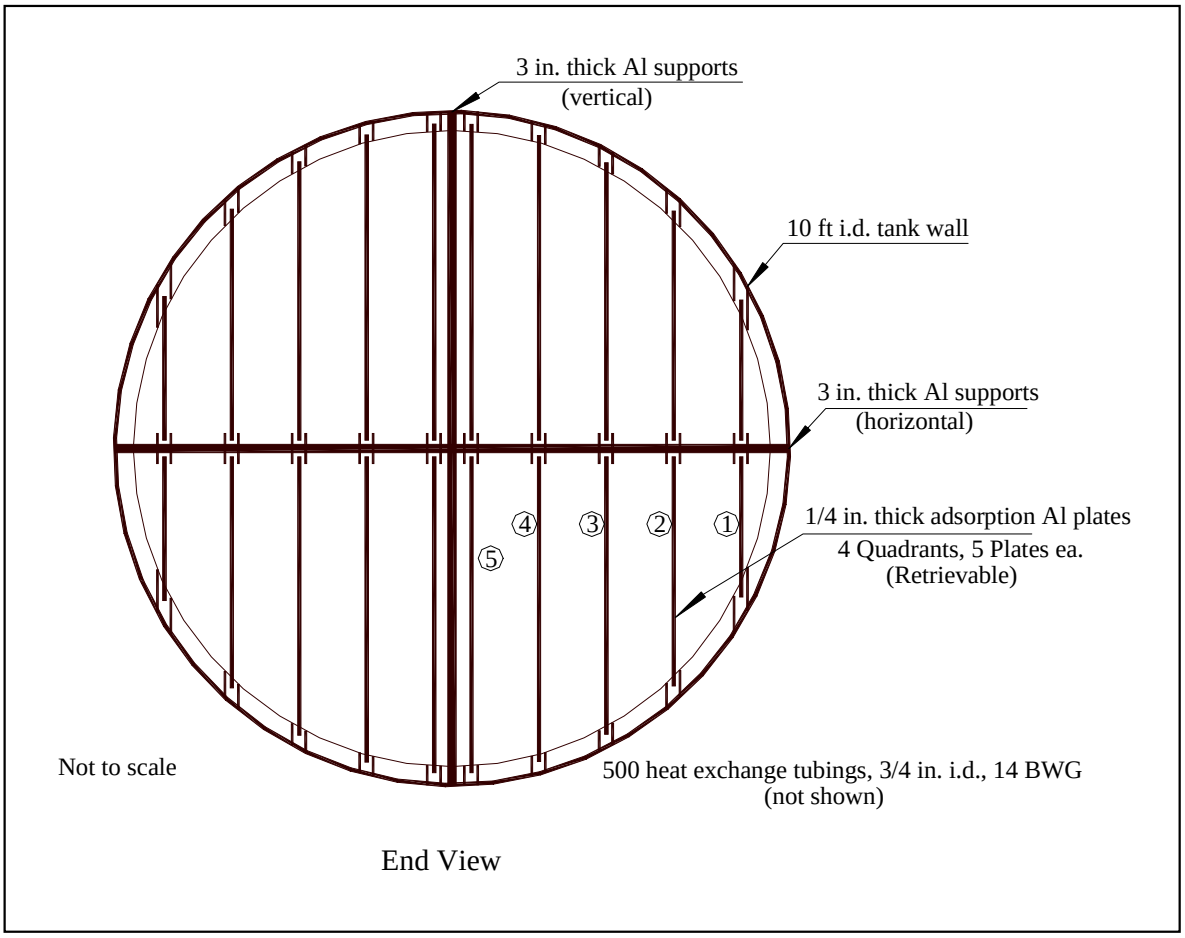

Fig. II.B.3. Plate pattern in storage tank (tubing not shown)

Note that plate guides keep the plates in place and allow each to be removed from the tank. Again, the simplicity of the design promotes economy and easy maintenance.

Each of the twenty plates would be 59 ft long and 1/4" thick aluminum. In Table II.B.1. is summarized plate dimensions.

TABLE II.B.1. Summary of adsorption plate description

Plate No.	L (ft)	W (ft)	Thick (in)	No. of Plates	Surf. Area, ft^2	Vol, ft^3/plate
1	59	2.45	1/4	4	289.2	3.01
2	59	3.53	1/4	4	416.3	4.34
3	59	4.15	1/4	4	489.8	5.10
4	59	4.50	1/4	4	530.6	5.53
5	59	4.62	1/4	4	545.5	5.68

(3) Plate Supports.

Hydrates adsorb on the plates and build outwardly, their mass kept in place by the overlapping fins. According to the laboratory runs, hydrates will fill the space between plates as the water level lowers. In Fig. II.B.4 is sketched a representation of the nine horizontal supports for the plates, each 3 in. thick aluminum alloy; nine vertical supports and the horizontal supports are paired at equal distances along the longitudinal axis. The supports are designed to withstand the hydrate load with a maximum deflection of only 0.5 in. over their entire length. Note that the aluminum heat-transfer tubing is in direct contact with the supports.

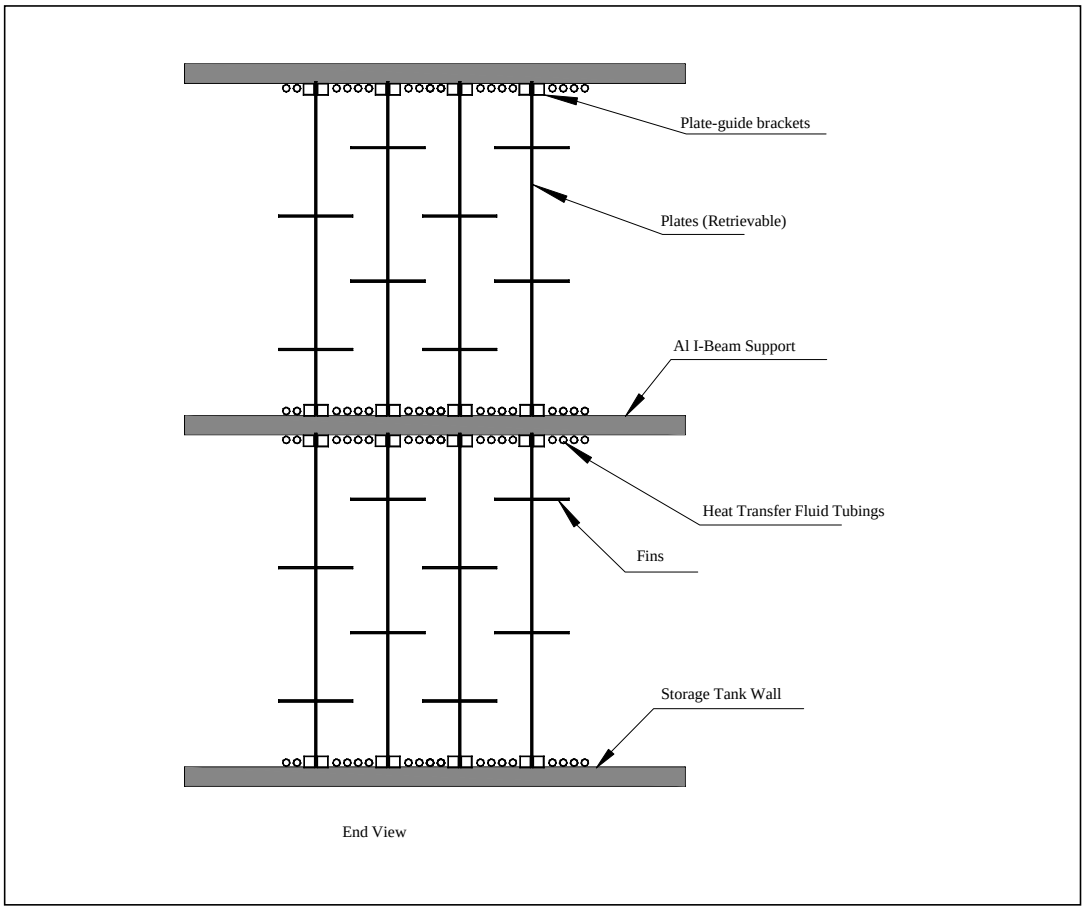

Fig. II.B.4. Plate and holder system

(4) Insulation

The hydrates would be formed and stored at a temperature between 35°F and 40°F. Heat gains would be prohibitive without exceptional insulation. It is proposed to use a super insulation employed in the insulation of liquefied gases: oxygen, nitrogen, argon, helium. The insulation has exceptionally low thermal conductivity. Small-diameter fibers of about 1 micron are bonded with melamine resin to form a fiber glass blanket that exhibits minimal out gassing under vacuum at low temperatures. (Johns Manville, Lydall Inc., 1998)

The insulation is available in 1" thick sheets and has a nominal density of l lb_m/ft^3. At a tank temperature of -153°F, the material has a rated thermal conductivity of only 0.0023 Btu/hr-ft-°F under 0.1 mm Hg of pressure.

Three layers of the insulation to give a 3" thickness would be installed around the circumference of the approximately 60 ft cylindrical tank length and then sealed to hold vacuum.

(5) Heat Transfer Tubing

A means of forming hydrates rapidly with micellar solutions was developed in the laboratory, making a bulk storage process feasible. It was demonstrated that the rate of hydrate formation can be further increased with larger surface areas available for adsorption/packing of the hydrate crystals. Further, aluminum was found to facilitate the formation and collection the best. By inserting aluminum plates into the laboratory test cell, the hydrate formation became exceptionally fast. After making heat-transfer calculations, it became apparent that the large-scale formation rate would be limited by the heat transfer rate that dispels the latent heat of hydrate formation. Consequently, the problem of removing the heat of formation in a large scale process becomes paramount. A full tank of hydrates will require almost 50 million Btu to be removed during the formation cycle.

The large unit as designed provides aluminum plates for formation and collection of hydrates with surface area/tank-volume ratio 5 ½ times greater than the laboratory test cell. The large surface area is provided primarily to collect and support the hydrate crystals, but in so doing, it elevates the formation rate. Moreso, then, will the hydrate formation rate be limited by the heat transfer rate from these plates. Therefore, the design establishes banks of heat transfer tubes traversing the length of the 60 ft long tank. Heat transfer by convection will result from those tubes submerged in the formation waters. Conduction will also result from direct contact with the plate supports.

Heat transfer calculations were made to configure the tube bank. (See Appendix.) The following design parameters resulted from the calculations:

1. Aluminum tubing; 500 tubes; 3/4" o.d., 59 ft length; 14 BWG.
2. Diameter and wall thickness of tubing provides adequate stress against collapse for a maximum pressure difference of 550 psi in the tank and an extreme occurrence of 1 atm inside the tubing. A stress safety factor of 3 resulted.
3. Maximum fluid velocity of 7 ft/sec in the tubing.
4. Maximum pressure drop of 12 psi in the tubing.
5. Overall heat transfer coefficient of 479 Btu/ft^2-^oF.
6. Chilled brine flow rate of 2,960 gal/min.

With these parameters, the approximately 50 million Btu could be removed from the tank in 7 hours--establishing the formation segment of the hydrate-storage cycle-time. This time compares with a formation time in the laboratory test cell of about 3 hours, even though the laboratory cell has a 5.5 times lower surface/volume ratio. It should be noted that there is space to add more than the designed 500 tubes to the large-scale tank design.

A sketch of the plates, heat-transfer tubes, supports, and tank are given in Fig. II.B.5.

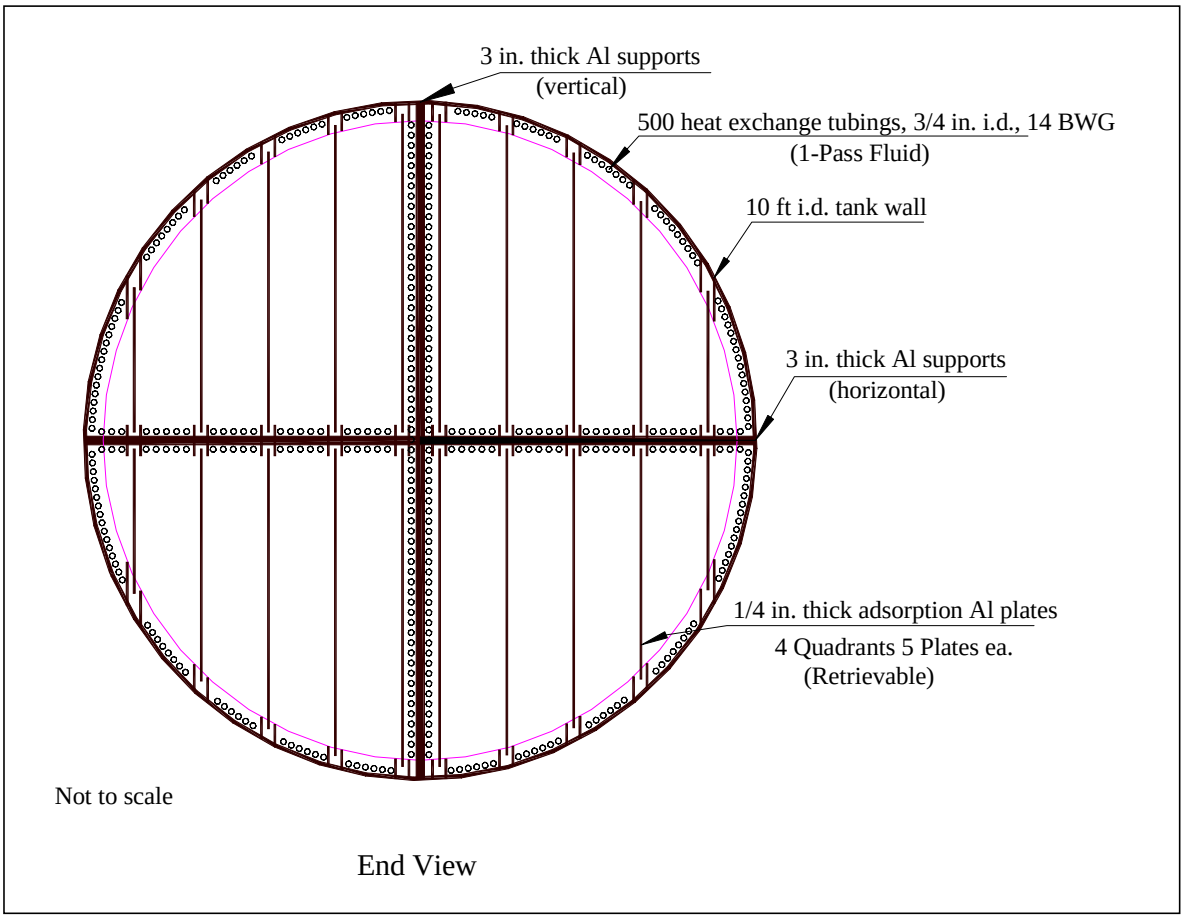

Fig. II.B.5. Heat-transfer tubing arrangement

III. MASS AND ENERGY REQUIREMENTS

The major energy and mass flowrates for a single hydrate storage tank is shown in Fig. III.1. The sketch applies to one tank out of the three tanks that are involved in a cycle of formation/storage/decomposition.

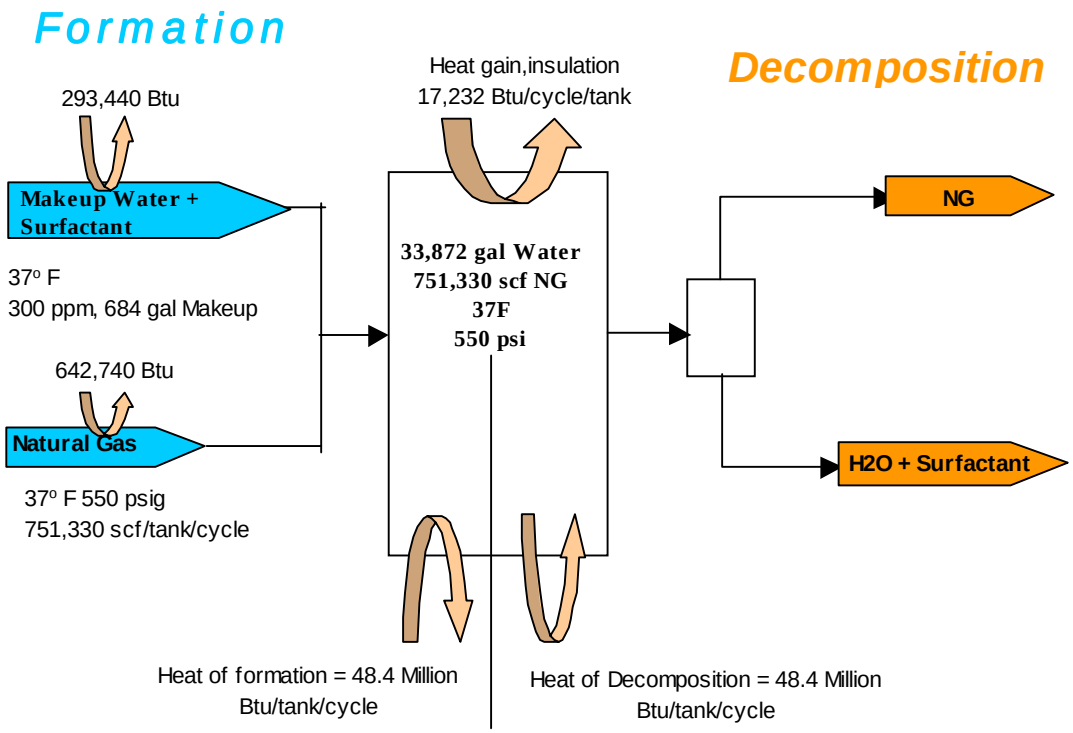

Fig. III.1. Mass and energy requirements, 1 storage tank
(Bounds, Montgomery, Pitman, Zhong, 1998)

Enough sensible heat of the entering makeup water and gas charge must be removed to bring them to 37°F. To assist in the sensible heat removal of these two streams, heat exchange with the cold exiting gas is made to lower the temperature of both entering streams to 53°F, the temperature at which hydrate nuclei began to form in the laboratory test cell, which prevents hydrates forming in any flow lines before the fluid reaches the formation tank. The major energy concern of the process is the latent heat of 49.3 million Btu that must be removed to form each tank of hydrates. The like amount of energy added to decompose is less demanding because the decomposition can be affected with a low-grade energy source at a reduced system pressure. The heat gain by the hydrates during storage can be kept to relatively low values with the super insulation commercially available for cryogenic storage. For one tank of a single cycle 738,700 scf of gas would be stored in the hydrates with an additional 12,600 scf compressed in free space of the tank; thus, for one cycle of 3 tanks 2,254,000 scf of gas would be stored.

The calculations to determine hydrate formation energy requirements are given in the Appendix. A basis was used of one formation/storage/decomposition tank of 10 ft diameter by 60 ft length. Any larger-scale process can be found then as an integer multiple of the base unit requirements. The following heat removal from one hydrate tank during formation and storage would be necessary: a. Latent heat of water, b. Gas sensible heat, c. Makeup water sensible heat, d. Initial water charge sensible heat, and e. Insulation losses. The initial water charge sensible heat would only be removed upon startup of the plant. These refrigeration needs could be partly offset by heat exchange with the exiting product gas and the Joules-Thomson effect of expanding feed gases.

TABLE III.B.1. Energy requirements to form hydrates, 1 tank.

Process Step	**Cooling, Btu/cycle/tank**
Latent Heat of Formation Water	48,372,800
Feed Gas Sensible Heat	642,700
Makeup Water Sensible Heat	39,502
Initial Water Charge Sensible Heat	253,900
Insulation Loss	17,237
Total	49,326,200

As expected, the latent heat extracted to form the hydrates is the overriding energy requirement. See Fig. III.B.1

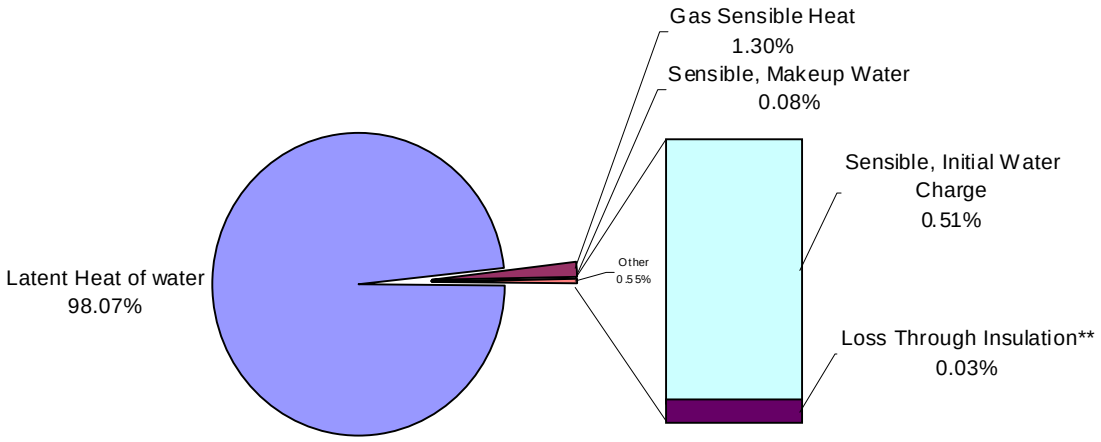

Fig. III.B.1. Cooling requirements for a cycle.

Some of the items in Table III.B.1 depend upon the number of cycles per year. The effect becomes less significant after about 10 cycles.

IV. ECONOMIC ANALYSIS

A. Equipment Costs

A tabulation is made for all equipment needed to conduct the process where 3 storage tanks operated in series comprise 1 cycle. That is, 3 storage tanks and the attendant processing equipment form a unit, and the entire unit would be involved in a single cycle of hydrate formation/storage/decomposition. Therefore, if a larger-scale process is desired, the costs and equipment listed in this report may be approximated from multiplication by an appropriate integer.

The listing and estimated pricing of equipment for the gas hydrate storage process is given in Table IV.A.1.

Table IV.A.1. Equipment list. (Bounds, Montgomery, Pitman, and Zhong)

Equipment Description	Quantity (1)	Size	Matl Construction	Unit Cost $	Cost 1 Tank, $	Total Cost 3 Tanks, $
Hydrate Formation, Storage, Decomposition Tank	1	10' D x 60' L	Carbon Steel, Lined	$300,000	$300,000	$900,000
Natural Gas Fired Refrig System	1	596 tons (2)	N/A	$682,744	$682,744	$682,744
Adsorption Plates	20	9,086 ft^2	Aluminum (4)	$1,357	$27,146	$81,439
Heat-Transfer Tubing	500	59' L x 3/4" o.d., 14 gauge	Aluminum (3)	$127	$63,720	$191,160
Surfactant Soln Storage Tank With Agitator	1	2734 gal Serves 3 Hyd Tanks	Carbon steel (6)	$9,702	$9,702	$9,702
Water Deionization Unit (7)	3	2,734 gal/60 min	n/a	$62	$62	$187
Insulation for Tank	3""	72"x50'x1" rolls	Cryogenic fiberglass	$4,970	$4,970	$14,910
Support System, Hydrate Tank	1	Aluminum	Construction of Support	$25,000	$25,000	$75,000
Feed Soln (makeup) Pump	1 (10)	205 gpm, P=50	Cast-Steel, Centrifugal	$7,546	$7,546	$7,546
Tempered Water Circulation Pump	1 (11)	2920 gpm, P=12	316 ss, Centrifugal	$12,600	$12,600	$37,800
Surfactant Soln Transfer Pump	1	273 gpm, P=20	Ductile Iron Casing, Cent.	$2,156	$2,156	$2,156
Insulation Vacuum Pump	3	0.75 hp	Cast Steel	$2,500	$2,500	$7,500
Brine Collection Tank (8)	1	1,014	Gallons, 304 ss	$8,948	$8,948	$8,948
Constant Pressure Regulator	1/tank	5"D	SS Flow Control	$8,624	$8,624	$25,872
Check Valves	2/tank (13)	8" D	Carbon Steel , Flanged	$485	$970	$2,910
Relief Valves	2/tank	5"D	SS Relief	$8,624	$17,248	$51,744
Heat Exchanger, Makeup H20	1/3 tanks	1000 ft^2	Carbon Steel	$30,000	$30,000	$30,000
Heat Exchanger, Feed Gas	1/three tanks	1000 ft^2	Carbon Steel	$30,000	$30,000	$30,000
Demister, Defoamer	1/tank	Vane-type (12)	6" Thick, Coalescing Type	$500	$500	$1,500
Foam, Mist Collection Vessel	1/three tanks (9)	8,117	Gallons, Carbon Steel	$19,404	$19,404	$19,404
Electrical-driven Refrigeration	1			$1,000	$1,000	$3,000
Hydrate Tank Supports	1	3"x3"x10'	Aluminum (5)	$3,222	$3,222	$9,667
Tank, to cool entering gas	1	2000 gal	carbon steel (14)	$9,000	$9,000	$9,000
			TOTAL =	$1,168,573	$1,267,063	$2,202,189

Notes:

1. Process is designed around equipment for a 24-hour cycle, with three tanks, 1 refrigeration unit, etc.
2. See Refrig section of calculations in Appendix.
3. Aluminum tubing cost = $2.16/linear ft.
4. Total wt of plates (Plates:h35 =n33) + fins * $1.70/lb alum.
5. Support cost = total no. supports of 18(Supports:b43)*Wt/bm*$1.70/lb alum
6. From Timmerhaus, 4th ed., See Tank, Appendix.
7. Water deionization for makeup water. Per personal conversation w/Hoppenjans, Ecolochem, Inc., $8,000/350,000 gals at 1000 gpm general surface supply water.
8. Brine collection tank used to collect brine used in hydrate formation phase. Tank holds brine during decomposition phase when cooling tower water flows thru tubing. 25% free space, for tubing in all 3 hydrate tanks; Timmerhaus, p.539.
9. 2% of hydrate tank water and surfactant removed from exiting gas. Size carbon steel vessel to collect 3 cycles of the solution from all 3 hydrate tanks.
10. Size for makeup water volumetric flow rate, p.527 Timmerhaus, all 3 tanks, to be filled in 10 minutes with a 50 psig pressure drop in lines, once per cycle.
11. Brine flow rate limiting. Tubing:d193 gives gpm/tube * Tubing:e197 no. tubes. Timmerhaus, p. 527, 1.8 factor for 316 ss, 12 psi drop through tubing.
12. Petroleum Engineer's Handbook; similar to gas-liquid separators. Use coalescing type, 6" thick vane-type. Effective for entrained liquid as well as foam removal. Centrifugal device on gas inlet.
13. Timmerhaus, p511. Flanged valves.
14. Carbon steel tank to store water for heat exchange, exiting gas and entering gas.

Therefore, $2,202,000 would be the purchased equipment cost for a gas hydrate storage facility that would form/store/decompose 2,254,000 scf of gas per cycle; the equipment would be amortized over a 20-year life. One cycle could be performed in a time as short as 24 hours; otherwise, the cycle duration would be determined by the time desired for storage.

The effect of equipment on gas-storage costs is given in Fig. IV.A.1.

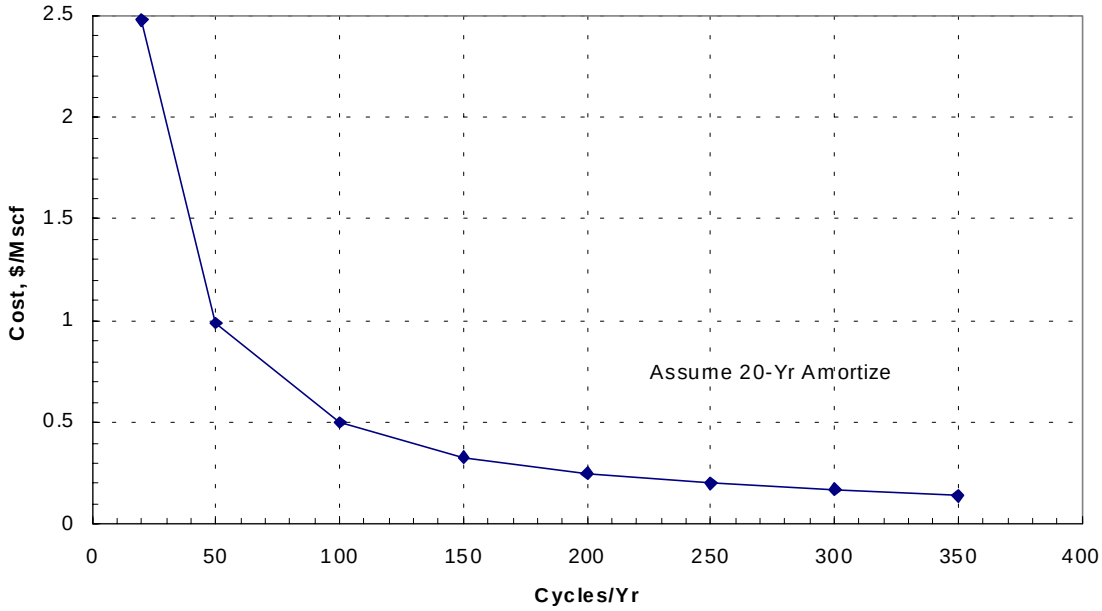

Fig. IV.A.1. Equipment impact on gas storage cost

B. Fixed Capital Investment

The fixed capital investment to install a gas hydrate storage process that could store 2,254,000 scf per cycle is presented in Table IV.B.1. The fixed capital investment is determined by the method of percentage of purchased equipment cost where factors found to be applicable in the chemical process industries for a solid/fluid plant cost are multiplied times the purchased equipment cost to give the other costs of the capital investment. That is, the equipment cost is first estimated, and then the factor in the second column of Table IV.B.1 is multiplied times that equipment cost to determine the capital cost item of the first column.

With a calculated equipment cost of $2,202,000 the fixed capital investment would be $6,893,000 to process the gas of three storage tanks over a 20-year life of the equipment.

TABLE IV.B.1. Fixed capital investment

Item	Factor	Cost
Direct Costs		
Purchased equipment, delivered	1	$2,202,189
Equipment installed	0.39	$858,854
Instrument., controls installed	0.13	$286,285
Piping installed	0.31	$682,679
Electrical installed	0.1	$220,219
Buildings	0.29	$638,635
Yard Improvements	0.1	$220,219
Total Direct Plant Cost		**$5,109,079**
Indirect Costs		
Engineering and supervision	0.1	$220,219
Construction expenses	0.17	$374,372
Total Direct and Indirect Costs		**$5,703,670**
Contractor's fee	0.18	$396,394
Contingency	0.36	$792,788
Fixed Capital Investments		$6,892,852

C. Labor Costs

The three largest costs of the hydrate storage process are refrigeration, equipment, and labor. One of the most important developments of the feasibility study was a simple, rapid formation process that could be performed in a quiescent system by just pressurizing the tank containing formation waters without mechanical stirring or circulating of processing fluids, and the hydrates would self-collect and self-pack in the container. As a consequence, labor requirements are reduced to a low value. The semi-continuous process operates with controls that admit feed gas to maintain a constant pressure in the forming stage. In a process where labor costs can make it economically unacceptable, the laboratory findings are pivotal in developing a practical process.

An estimate of labor requirement to operate the hydrate plant for a year was made by the method of Turton (Turton, 1998). It was assumed that the plant would be similar to a typical chemical plant and operate 24 hours per day with 3 shifts/day. The number of operators per shift was estimated on the basis of each major item of equipment. (See Appendix.) For this continuous operation, 5 operators would be necessary with an annual labor cost of $257,400.

D. Energy Costs

A fiber glass blanket insulation where the glass fibers are bonded with melamine resin is taken as representative of a super insulation that would be used on hydrate storage tanks. Such an insulation is used on cryogenic tanks. (John Manville, distributed by Lydall, Inc.)

As insulation thickness increases, its capital cost increases, but the heat gain of the cold hydrate tank decreases. These calculations are summarized in Table IV.D.1. Note the large decrease in heat gain to the tank from no insulation to 3 in. of insulation.

TABLE IV.D.1. Determining insulation thickness.

Ins. Thickness, in.	Heat Loss Btu/hr/tank	Heat Loss Btu/year/tank	20-Yr Loss, $ per tank	Insulation Cost, $ per tank	ROI, %
0	18,254,348	159,908,085,491	$74,986,207	0	11,303,600
0.2	10,550	92,419,318	$43,338	663	3,267
0.4	5,284	46,291,434	$21,708	1325	1,088
0.6	3,528	30,909,505	$14,494	1988	545
0.8	2,650	23,217,392	$10,887	2650	326
1	2,123	18,601,740	$8,723	3313	218
1.2	1,772	15,524,465	$7,280	3976	156
1.4	1,521	13,326,318	$6,249	4638	117
1.6	1,333	11,677,650	$5,476	5301	91
1.8	1,187	10,395,313	$4,875	5963	73
2	1,070	9,369,413	$4,394	6626	59
2.2	974	8,530,018	$4,000	7289	50
2.4	894	7,830,504	$3,672	7951	42
2.6	826	7,238,591	$3,394	8614	36
2.8	768	6,731,223	$3,156	9276	31
3	718	6,291,493	$2,950	9939	

ROI = Incremental Return on Investment
Assume a return on investment of 25% is required.

ROI = Incremental increase in energy savings/incremental cost of insulation * 100

By taking an incremental Return on Investment (ROI) as the incremental energy savings divided by the incremental cost of insulation as insulation thickness is increased, it is determined that an insulation thickness of 3 in. would be desirable. See Fig. IV.D.1.

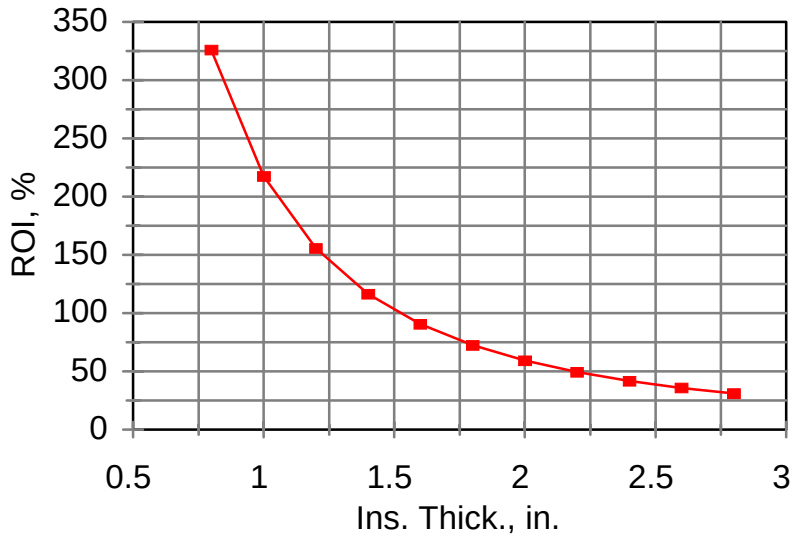

Fig. IV.D.1. Choosing insulation based on Return on Investment.

Because of the low heat gains through the insulation, storage temperatures of the gas hydrates can be maintained with a household-size electrical refrigeration unit on each storage tank. Overwhelmingly, the primary refrigeration demand comes from removing the latent heat of hydrate formation. A large gas-fired refrigeration unit would add the costs per 1000 scf of natural gas stored as given in Fig. IV.D.2.

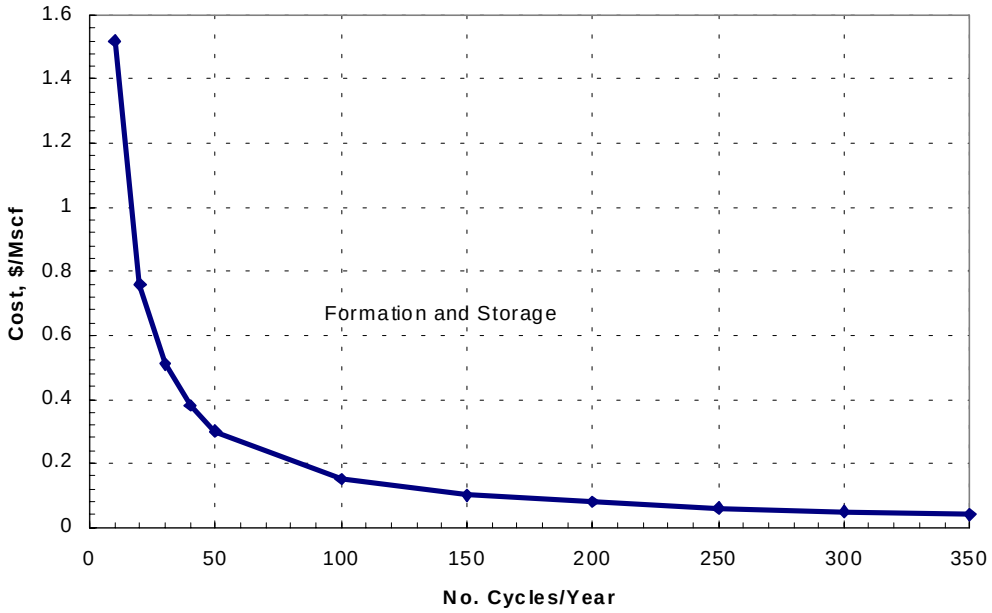

Fig. IV.D.2. Refrigeration costs

E. Cycling Effects

The fixed capital investment to process 2,254,000 scf of natural gas in one cycle was estimated to be $6,893,000. One cycle covering formation to decomposition can be achieved in 24 hours. A larger-scale operation would involve integer multiples of these costs and storage capacities. In other words, the equipment and facilities would be repeated with this unit cost if larger operations were wanted.

(1) Development costs

The fixed capital investment, which includes direct and indirect costs, represents the development costs for a gas hydrate storage facility. Based on a 20-year life of the facility and the fixed capital investment being amortized over the 20-year life, the development cost per 1000 scf of gas was determined. See Fig. IV.E.1

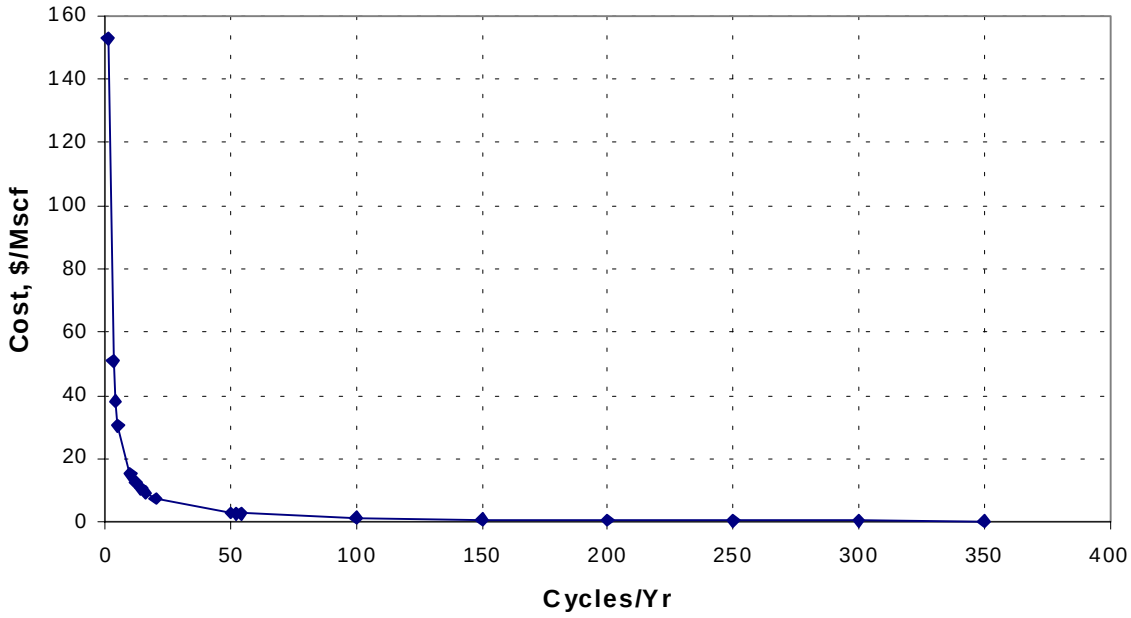

Fig. IV.E.1. Development costs of gas-hydrate storage facility

It is evident that the development cost is prohibitive for one cycle per year. However, the cost drops precipitously as the number of cycles increases. Since the shortest achievable cycle time in the design is 24 hours, it is possible to have 300 cycle per year, if an 18% downtime is assumed.

Therefore, the process becomes attractive for meeting frequent demands for stored gas but it is economically not attractive for bulk storage in 1 or 2 cycles per year.

(2) User Costs

The operating costs to store natural gas in hydrates are summarized in Table IV.E.1. See the Appendix for the calculations.

TABLE IV.E.1. Product or user costs (Timmerhaus, 1990)

ITEM	DETERMINED BY	COST	BASIS
Raw Matls	Calculate	$181	per cycle
Operating Labor	Calculate	$257,400	per year
Utilities	Calculate	$1,888	per cycle
Supervisory Labor	15% Operating Labor	$38,610	per year
Maintenance and Repair	6% Fixed Capital Investment	$20,679	per year
Operating Supplies	15% Maintenance and Repairs	$3,102	per year
Laboratory Charges	15% Operating Labor	$38,610	per year
Depreciation	Calculate	$110,109	per year
Property Taxes	4% Fixed Capital Investment	$27,571	per year
Insurance	1% Fixed Capital Investment	$3,446	per year
Plant Overhead	70% Operating Labor+Supervision+ Maintenance	$221,682	per year
Administrative	25% Operating Labor	$64,350	per year
Contingency	1% Total Product Cost	$7,876	per year

Labor is minimized in the process because of forming the hydrates from a quiescent system. That is, no mechanical stirring and no processing steps to collect/pack the hydrate particles; the action of the surfactant accomplishes these functions. Nevertheless, labor is still the largest user cost. In one regard, the results in the table emphasize that the process could not be competitive if labor costs were not kept low by use of surfactant and adsorption plates.

If one takes the approach that the storage facility is operated as a chemical plant in which 24-hour shifts operate 300 days per year (65 days downtime), then operating costs per 1000 scf of gas

decline precipitously with the number of cycles per year. Then, the operating costs decrease as given in Fig. IV.E.2.

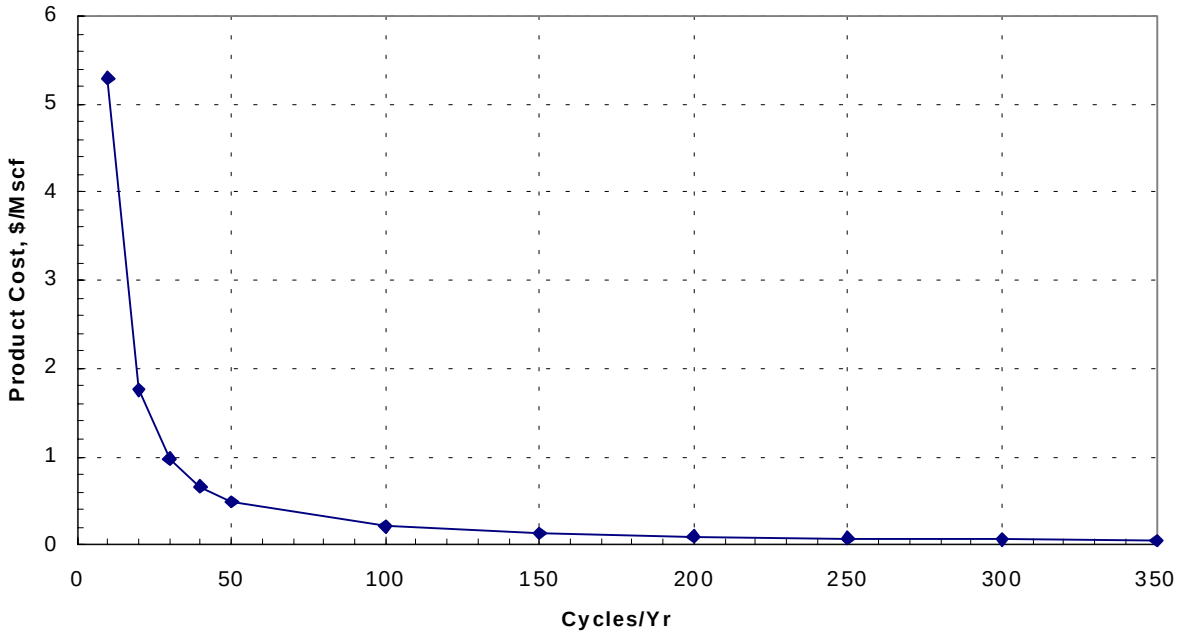

Fig. IV.E.2. Product (user) costs of stored hydrate gas

F. Economic Comparison Hydrate Storage with Conventional Storage Means

Estimates of development and user costs are reported for conventional methods of storing natural gas. Here, these two costs are calculated for hydrate storage and compared to conventional methods.

(1) Development Costs

The development costs per 1000 scf of gas were compared to conventional storage development costs. Conventional storage costs are given in Table IV.F.1.

TABLE IV.F.1. Approximate costs of natural gas storage by conventional means. (Beckman, 1997)

Type Storage	Development Cost, $/Mcf	User Cost, Single-cycle, $/Mcf
Depleted Reservoir	2- 3.50	0.20- 1.50
Salt Cavern	7- 14.00	0.80- 4.50
Aquifer	2- 4	0.60- 1.75
LNG	25- 40	10+

The comparison is best made by viewing Fig. IV.G.1.

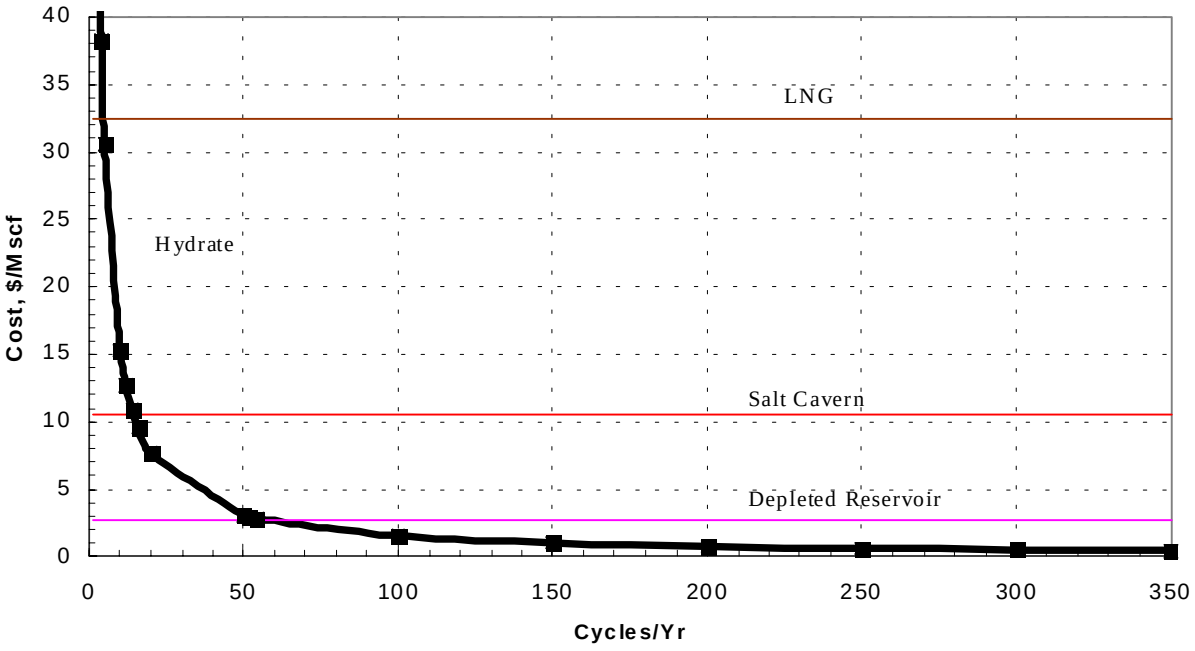

Fig. IV.G.1. Comparison of development costs

Note that the gas-hydrate process becomes competitive with LNG when 4 cycles or more per year are made. From the standpoint of development costs, the hydrate process becomes competitive with salt cavern and depleted reservoir storage for cycling above 14 and 54 cycles/year, respectively.

(2) User costs

The cost of storing the natural gas in hydrates, i.e., the user cost that must be charged the customer, was determined, and the calculations are included in the Appendix. Also, see Table IV.E.1. How these user costs compare to conventional storage user costs is shown in Fig. IV.G.2.

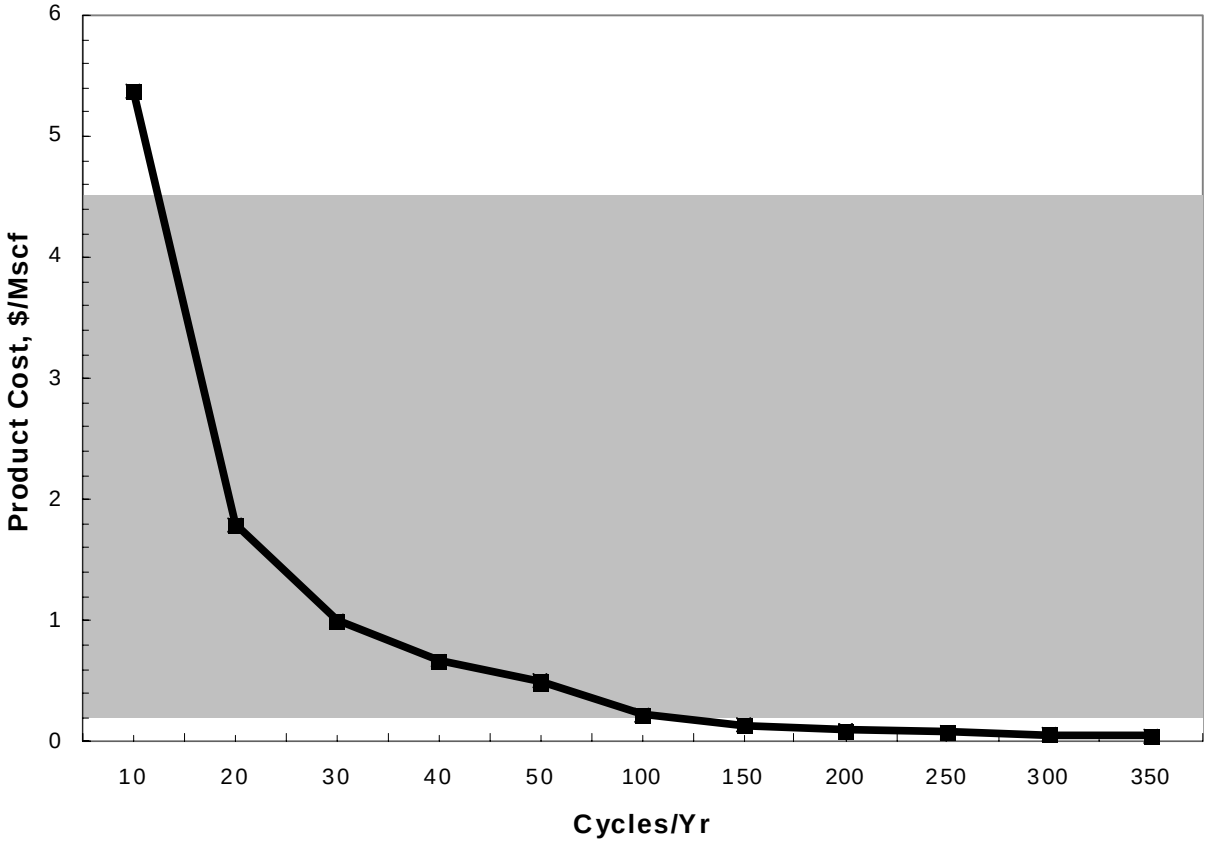

Fig. IV.G.2. Comparison of hydrate user costs with conventional storage

It is observed in Fig. IV.G.2 that less than 13 cycles of hydrate storage per year would not be economically competitive with conventional storage from the standpoint of user costs. In the range of 13 to 125 cycles per year, the hydrate storage is competitive. Above 125 cycles per year, the hydrate storage user costs become less than conventional storage.

V. Extensions and Limitations of Proposed Design

Gas-Fired Refrigeration-- The design includes gas-fired refrigeration to remove the latent heat of hydrate formation. The natural gas refrigeration unit is important for two reasons: economy of

fuel usage and utilization of methane-rich gas that accumulates in the process. The two reasons are very much related because the hydrates as they form occlude gas leaner in methane than the free gas from which they form; the free gas in the formation tank above the forming hydrates, therefore, becomes richer in methane as the process develops. While gas-fired refrigeration would use this accumulating methane-richer gas to supply cheaper cooling to the process, reducing methane-rich gas above the hydrates would also result in lower operating and storage pressures for the process. (The benefits of lower pressures from rich methane use were not included in the design.)

Some background information on the refrigeration unit may be obtained in the final report entitled "Development of a Gas Fired Absorption Chiller for the United States Market" by Carrier Corporation for the Gas Research Institute (Decker, 1992).

Larger or Smaller Scales-- The concept submitted in this report is for a design that is modular in the sense that a scale larger than the 2,254,000 scf of gas stored per cycle could be approximated by integer multiples of the given equipment and cost. Of course, a larger-size operation would be somewhat cheaper per unit of gas stored because of the "0.6 rule-of-thumb" in scaleup of some equipment without purchasing duplicate equipment and because labor costs per Mscf would be lower.

Also, the conceptual process would be versatile enough to serve on a smaller scale or in remote areas for other applications. For example, cost savings could result from its location near a gas source of higher pressure where the gas expansion would reduce refrigeration costs.

Basic design of the process would remain the same for larger- or smaller- scale versions in applications other than a power plant.

Rate of Hydrate Decomposition-- Any low-grade heat source at ambient or higher temperatures could be used to decompose the hydrates. In the proposed process 110^{o} F water from the power plant, ordinarily going to a cooling tower, would be used to decompose hydrates. (The minor cost savings to the hydrate process by circumventing the cooling tower was not included in the economic calculations.) In another setting the process could use surface water, or even ambient air, to circulate through the heat transfer tubing and decompose the hydrates. With reduced pressures and a relatively low equilibrium temperature, the hydrate decomposition rate is high.

The proposed process involves decomposing the hydrate contents of the three parallel storage tanks, and calculations show that the decomposition could be done in one hour. However, removing the gas in that time frame could cause excessive foaming problems and excessive gas velocities. In such case the cycle time could be extended above 24 hours, an arbitrary choice, or the formation time could be lowered by several means to allow more time for decomposition while maintaining a 24-hour cycle.

A pilot-plant scale would be particularly useful in verifying the practical decomposition time.

Hydrate Formation Time-- In a micellar solution, hydrate formation rate in the large-scale process is not limited by reaction rate. Heat transfer to remove the latent formation heat limits. In the calculations, enough tubes were inserted (500) to give the necessary heat transfer in 7 2/3 hours to fill each tank with hydrates, there being three tanks to fill in series per cycle. Since there is sufficient tank space for more heat-transfer tubes, the cycle time could be shortened by adding more tubes at the expense of more tons of refrigeration.

Gas Purity-- No methyl alcohol must be in the entering gas stream because of its retardation of hydrate formation.

V. CONCLUSIONS

The project established the feasibility of a new natural gas storage method for either large-scale commercial applications or smaller applications in remote areas. This is significant because of the limited number of methods that are available. A breakthrough occurred in Phase I that overcame some seemingly insurmountable technical and economic problems involving hydrate storage of natural gas. Namely, surfactant micellar solution was found to form hydrates rapidly in a quiescent system, self-pack crystals by adsorption as the hydrates form, and convert interstitial water of packed particles to hydrates. By this simplification, manual labor is minimized and equipment maintenance is minimized in a hydrate-storage process. For example, the lack of mechanically moving parts (quiescent system, no mechanical stirring) and the lack of a hydrate-particle separation step from the slurry (particles adsorb and build on metal surfaces) reduce maintenance and labor.

A conceptual design and an economic analysis were made. The economic analysis showed the major contributor to user cost to be refrigeration to remove latent heat of hydrate formation. High gas-supply pressure, gas-fired refrigeration unit, super insulation, and energy exchange of process streams in a large-scale facility would reduce refrigeration costs. The major contributor to development cost is the equipment capital investment, namely, the formation/storage/decomposition tank. When all of the costs are considered, hydrate storage becomes competitive for multiple cycles.

Therein is a distinct advantage of the hydrate storage process as designed: a formation/decomposition cycle can be accomplished within a 24-hour period and numerous storage cycles can be performed in a year. Advantages of the proposed hydrate storage process are the following:

1. Safety of storage. Gas is essentially encased in ice with a slow release if the tank ruptures. (Conceivably, the hydrates could be stabilized indefinitely by pressurizing with an inert gas or water to enhance safety. Crystal stability depends upon the total pressure and not partial pressure of the occluded gas. This step was not proposed in the conceptual design.)
2. Low-pressure storage. A pressure of 550 psig was used as the basis of the design to optimize gas capacity with costs. (Conceivably, the hydrates could be formed at 550 psig but stored near atmospheric pressure if a storage temperature of -20°C to 0°C were maintained. But the conceptual design is based on a 550 psig formation/storage pressure and a storage temperature of 37°F.)
3. Aboveground storage.
4. Attractiveness of economy increases as the number of storage cycles is increased.
5. Size of storage facility can be any multiple or fraction of the size of the conceptual unit presented in this report.
6. Application versatility. Size, location, safety, simplicity make possible a wide variety of applications ranging from large power plants to remote units of a small-scale application.

VI. RECOMMENDATIONS

Demonstrate a small pilot plant of the process. For the process to be available for industrial use, a demonstration of the conceptual design beyond the laboratory would be needed. The pilot would necessarily be an outside unit, possibly on the grounds of a power plant.

Secondarily, concurrent with the pilot plant, further laboratory evaluations could assist in evaluation of data for the pilot plant, as needed.

BIBLIOGRAPHY

Beckman, K.L. and Determeyer, P.L., "Natural Gas Storage: Historical Development and Expected Evolution", *Gas Tips- Gas Research Institute,* **3**, 2, (1997) 13-22.

Bradley, H.B., ed., Petroleum Engineering Handbook, Society of Petroleum Engineers, Richardson, TX, 1989.

Cengel, Y.A., and Boles, M.A., Thermodynamics: An Engineering Approach, 2nd ed., McGraw-Hill, Inc., New York, NY, 1994.

Collett, T."Geologic assessment of the natural gas hydrate resources in the onshore and offshore regions of the United States," *2nd International Symposium on Gas Hydrates*, Toulouse, France, (1966) 499-506.

Decker, M., "Development of a Gas-Fired Absorption Chiller for the United States Market," Carrier Corporation, New York, Report No. GRI-92/0334 (1992).

Ecolochem, Inc., Hoppenjans personal communication.

Flinn, R.A., and Trojan, P.K., Engineering Materials and Their Applications, 3rd ed., Houghton Mifflin Co., Boston, MA, 1986.

Handa, Y.P., "Compositions, enthalpies of dissociation, and heat capacities in the range 85 to 270 K for clathrate hydrates of methane, ethane, and propane, and enthalpy of dissociation of isobutane hydrate, as determined by a heat-flow calorimeter", *J. Chem. Thermo*., **18** (1986) 915-921.

Himmelblau, D.M., Basic Principles and Calculations in Chemical Engineering, 3rd ed., Prentice-Hall, Upper Saddle River, NJ, 1974.

Johns Manville, Lydall Inc., Corporate brochure and personal communication, 1998.

Kvenvolden, K.A., "A Primer on Gas Hydrates," The Future of Energy Gases, ed., D.G. Howell, U.S. Geological Survey Professional Paper 1570.

Lide, D.R., ed., Handbook of Chemistry and Physics, 74th ed., CRC Press, Boca Raton, Fla., 1993.

Perry, J.H., Green, D.W., and Maloney, J.O., eds., Chemical Engineers' Handbook, McGraw-Hill Book Co., Inc., New York, NY, 1984, 23-58.

Peters, M.S., and Timmerhaus, K.D., Plant Design and Economics for Chemical Engineers, 4th ed., McGraw-Hill, Inc., New York, NY, 1991.

Rogers, R.E., “Natural Gas Hydrates Storage Project,” *DOE Monthly Status Reports*, Contract DE-AC26-97FT33203, October 1997- May 1999.

Turton, et al., Analysis, Synthesis, and Design of Chemical Processes, Prentice-Hall, Inc., Upper Saddle River, NJ, 1998.

Zhong, Y., Montgomery, R., Pitman, R. and Bounds, M., *Plant Design*, Senior chemical engineering project assignment, Mississippi State U., Dept. of Ch.E., Nov. 1998.

APPENDIX

(Calculations)

III.Economic Analysis of an Industrial-Size Gas Hydrate Storage Process

F. Insulation

Calculations:

TABLE III.F.1. Determining insulation thickness

Ins. Thickness, in.	Heat Loss Btu/hr/tank	Heat Loss Btu/year/tank	20-Yr Loss, $ per tank	Insulation Cost, $ per tank	ROI, %
0	18,254,348	159,908,085,491	$74,986,207	0	11,303,600
0.2	10,550	92,419,318	$43,338	663	3,267
0.4	5,284	46,291,434	$21,708	1325	1,088
0.6	3,528	30,909,505	$14,494	1988	545
0.8	2,650	23,217,392	$10,887	2650	326
1	2,123	18,601,740	$8,723	3313	218
1.2	1,772	15,524,465	$7,280	3976	156
1.4	1,521	13,326,318	$6,249	4638	117
1.6	1,333	11,677,650	$5,476	5301	91
1.8	1,187	10,395,313	$4,875	5963	73
2	1,070	9,369,413	$4,394	6626	59
2.2	974	8,530,018	$4,000	7289	50
2.4	894	7,830,504	$3,672	7951	42
2.6	826	7,238,591	$3,394	8614	36
2.8	768	6,731,223	$3,156	9276	31
3	718	6,291,493	$2,950	9939	

ROI = Incremental Return on Investment

Assume a return on investment of 25% is required.

ROI = Incremental increase in energy savings/incremental cost of insulation * 100

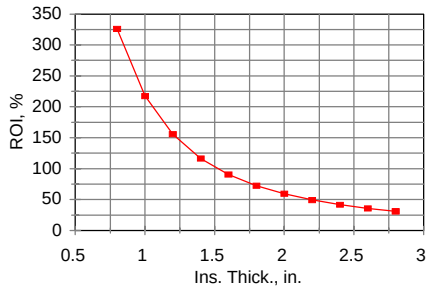

Cryo-Lite cryogenic insulation fibler glass blanket marketed by Lydall, Inc.

Reference: Personal conversation D.A. Armstrong of Lydall, Inc. It has

low thermal conductivity (0.0192 Btu/hr-ft-R) at 1 atm and 80F. Under

vacuum (p<0.001 mm Hg) its thermal conductivity can go as low as 0.0021 Btu/hr-ft-R.

It is made of high quality fine fibers bonded with a melamine resin.

Properties:

Light weight (1 lb/ft^3)
Flexibility (easy to cut and fit)
Fast pumpdown times
Flame resistant
Stable
Oxygen compatibility

If 3 inches (3 layers) of insulation is wrapped around the storage tank (total surface area is 1991 ft^2/tank)

Price = $249.60 per roll of 72" x 50' x 1" = $0.83 per ft^2 per inch thickness

Total price for insulating 1 tank = $4,970 per tank

Total price for insulating 3 tanks = $14,909 per 3 tanks

Plate Design

II.B.2. Plate Volumes and Weights

Plate Vol = L*W*T/12

where
L= length, ft.
W = Width, ft
T = Thickness, in.

Wt. Plate = W = Plate Vol*(specific gravity)*(density water)
W = V*SG*D

Adsorp Surface = L*W*2
Specific Grav, Al = 2.7

Note: Fins add to weight, area, volume of plates.

Table II.B.1. Plate and fins sizes, weights, volumes

Plates								Fins					
Thick, in.	No.	Length, ft.	Width, ft.	No. of Plates	Adsorp Surf ft**2/plate	Volume, cu ft/plate	Weight, lb/plate	No./plate	Length, ft.	Width, in.	Volume, cu ft	Weight, lb/plate	Adsorp Surface, ft**2/fin
0.25	1	59	2.451	4	289.22	3.01	507.58	1	59	6.25	0.32	4	61.46
0.25	2	59	3.528	4	416.30	4.34	730.61	1	59	6.25	0.32	4	61.46
0.25	3	59	4.151	4	489.82	5.10	859.63	1	59	6.25	0.32	4	61.46
0.25	4	59	4.497	4	530.65	5.53	931.28	1	59	6.25	0.32	4	61.46
0.25	5	59	4.623	4	545.51	5.68	957.38	1	59	6.25	0.32	4	61.46
			Total =	20	9,086	94.65	15,946	20			1.60	22	1,229

Vol, Plates + Fins = 96 cu ft

Wt, Plates + Fins = 15,968 lbs

Adsorp Surf, Plates + Fins = 10,315 ft**2

Note: The thickness of the support beams is 3 in.
The distance between the edge of the adsorption plate and the tank wall is 3 in. all the way around.

Scale Factors for Test Cell to Plant Scale

Surf area lab cell/Volume lab cell = 4/D Note: No plates present.

To achieve at least the rate of hydrate formation in the large-scale tank as in the lab test cell, one must have at least a surface area/volume ratio equal to the test cell.

Diameter of large-scale tank= 10 ft
To make the large-scale equivalent to the laboratory cell:
Surf area large tank = 4*vol large tank/dia large tank
Surf area large scale tank = 1,884 ft^2 Note: If equivalent to test cell.

Calculated Surface Area of plates of large tank = 10,315 ft^2 Note: Not counting inside surface of tank or supports.

Therefore, Large tank surface area is over-designed by a factor = 5.48

II.B.1. Tank Design

Hydrate Tank Volume & Weight

Vol tank = 3.14*D**2*L/4

D = 10 ft

L = 60 ft

Vol tank = 4710 cu ft

Vol tank = 35,231 gal

Water in Hydrate Tank, Volume & Weight

Vol Water = Vol Tank - Vol Tubing - Vol Plates - Vol Fins - Vol supports

Vol Tank =	c8	ft^3
Vol Tubing =	Tubing:C18	ft^3
Vol Plates =	Plates:H34	ft^3
Vol Fins =	Plates:m33	ft^3
Vol supports =		ft^3

Vwater = 4,522 ft^3 = 33,822 gals

Weight water = Ww = Volume water*62.4 lbf

Wwater = 282,154 lbf

Makeup Water Soln Storage Tank

Estimate the required volume of water and surfactant to store enough makeup water for 3 tanks of 1 cycle.

Assume: 2% of water in tanks entrained with gas when hydrates are decomposed.

Volume of Water in 1 tank = 33,822 gals Hydrate tank

Vol Makeup Water, 1 tank = 676 gals

Assume 300 ppm SDS surfactant , 0.3 g/l

Wt surfactant per makeup vol, 1 tank = 1.69 lbs

Wt surfactant makeup, 3 tanks = 5.08 lbs

Vol makeup H20, 1 tank = 902 gals (with 25% free space)

Vol makeup H20, 3 tanks = 2,706 gals (with 25% free space)

$9,702 Cost of carbon steel tank corrected to 1998 prices. Tank agitated. From Timmerhaus, 4th ed. p. 539.

II.B. Tubing for Heat Transfer

Calculate Volumes and Weights

Assume: Tubing would be placed side by side on supports and inside surface of tank.
Tubing would enter one end of tank and exit at the head of the other end.
Each tube would extend the length of the tank. Tubing made of aluminum.

	No. tubes= n	500		
	o.d, in.	0.75		
	Length, ft.	59		
	i.d., in.	0.459		
	Thick, in.	0.083		
	Sp. Gv.	2.7		
outside	Vol 1 Tubing =	0.18	ft^3	Vol = Pi/4*o.d.^2*L/144
outside	Vol all tubing =	90.46	ft^3	Vtot = vol*n
	Wt 1 Tubing =	63.08	lbf	Wt(tub) = Length*Pi*(o.d.-i.d.)*thickness*sp.gv.*62.4/144 lbf
	Wt all tubing =	31,538	lbf	

Calculate Velocities in Cylindrical Aluminum Tubing --1st approximation.

Aluminum alloys have unusual ability to maintain strength and shock resistance at temperatures as low as -250C (-425F). Good corrosion resistance and relatively low cost make these alloys very popular for low-temperature equipment. For most welded construction the 5000-series aluminum alloys are widely used.

Perry's ChE Handbook, 1984, p. 23-58.

Modulus of Elalsticity of Aluminum Alloys 5052 and 5454 = 10,500,000 psi at about 32F

Specification Minimum Tensile Strength, 5052 Al plate = 25,000 psi
Specification Minimum Yield Strength, 5052 alloy plates = 9,500 psi

Reference: ASME Boiler and Pressure Vessel Code, an American National Standard,
Section VIII, Rules for Construction of Pressure Vessels, 1986 ed., p. 128.

Specification Minimum Tensile Strength, 5454 alloy, seamless extruded tube = 31,000
Specification Minimum Yield Strength, 5454 alloy, seamless extruded tube = 12,000

Aluminum heat exchanger tube dimensions given in Perry's.

o.d., in.	i.d., in.	Wall, in.	BWG	Velocity @ 1 ft/s, Capacity, gal/min
0.125	0.084	0.083	14	0.0175
0.125	0.206	0.022	24	0.1037
0.375	0.209	0.083	14	0.1068
0.375	0.331	0.022	24	0.2679
0.5	0.334	0.083	14	0.273
0.5	0.43	0.035	20	0.4528
0.625	0.459	0.083	14	0.5161
0.75	0.584	0.083	14	0.8348

Rule of Thumb: Limit velocity of liquids (water) in metal pipes to less than 5 ft/sec

to prevent erosion and water hammer.

Acceptable range of pressure drops in a heat exchanger: for a

system pressure >10 psig, pressure drop range can be 5 psi up

to 50% of system gauge pressure.

A tube-side velocity of 1-10 ft/s is selected, with a typical value of 4 ft/s for heat exchangers>'

Process Design Principles, Seider, 1999, p307

Practical Process Engineering, Sandler, Luckiewicz, 1987.

tube o.d., in.	tube i.d., in.	Velocity, ft/sec	No. Tubes	Vol Flow, gal/min	Inlet Press, psia	Reynolds No.,	f	Press drop, psia	Stress, psi	Safety Factor
0.125	0.084	2	20	8.22	50	761	0.01	10	2,006	5
0.375	0.209	3	20	30.68	50	2,840	0.007	6	1,596	6
0.5	0.334	5	20	81.72	50	7,563	0.0062	9	1,986	5
0.625	0.459	6	20	134.76	50	12,473	0.0059	9	2,388	4
0.75	0.584	7	20	200.03	50	18,514	0.0055	9	2,794	3

Vol flow, gpm = No. tubes*pi/4*(id)^2/144*velocity*60*7.48

Press Drop = [2*2fLV^2/Dgc] per tube

where f = Fanning friction factor

L = 2*length of the tank

Reynolds No. = DV*density/viscosity

Note: Velocities in table above kept below 10 ft/s and pressure drop below 10 psi.

Stress = P*2b^2/(b^2-a^2)

This stress is that from a pressure external to the tubing.

P= 550 psi which is max pressure when inside p=1 atm.

b = in. which is od of tubing

a = in. which is i.d. of tubing

Note the safety factors in the above table are conservative since only atmospheric

pressure was assumed to exist on the inside of the tubing.

Calculate No. Tubes Needed for Heat Transfer, Hydrate Formation --1st Approximation

q = U*A*(Change in temp of cooling water)

where,

U = 200 Btu/(h*ft^2*F) An approximation. See Sandler, p. 508.

A = ft^2 inside area of tubing.

A = (no. tubes)*2*L*Pi*id/12

T2 = temp brine in tubes = 28F (corresponds to lab test cell)

T1 = temp of water in tank forming hydrates = 37F

T2-T1 = 9 F degree temp between hydrate tank and brine

tube i.d., in.	Vol Flow, gal/min	U, Btu/ft^2hrF	A, ft^2	Q Btu/hr	Req. Time, hrs
0.084	8.22	200	51.87	93,371	526
0.209	30.68	200	129.06	232,316	211
0.334	81.72	200	206.26	371,261	132
0.459	134.76	200	283.45	510,206	96
0.584	200.03	200	360.64	649,151	76

Heat to Remove from Tank During Hydrate Formation = (Latent heat of water forming hydrates)
and + (sensible heat of makeup water) + (heat gained from outside during form)
and + (sensible heat of gas)

Latent Heat =	48,372,778	Btu/cycle
Sens. Makeup=	39,502	Btu/cycle
Sens. Gas =	642,740	Btu/cycle
Insulation =	17,237	Btu/cycle
Total =	**49,072,256**	**Btu/cycle**

To meet this requirement, a cycle must be the time given in the above table.
As seen in the table the cycle time is not practical, so more tubes needed.

What flow rate of water necessary to absorb the the heat of c136?
Q = mCp(T2 brine - T1 brine)
m = Q/(Cp*deltaT*8.33)

m =	841,575	gal/cycle

Assume the formation part of the cycle is 4 hours.
From the above table, it is evident that the flow rate must be much larger than supplied by 20 tubes.
The flow rate must be about 47 times greater than supplied by 20 of the 1/2" tubing.
i.e., about 1000 of the 1/2" tubes would be needed.

Assuming a 4 hour cycle time, the following number of tubes are approximated:

o.d., in.	with 20 tubes Vol flow, gal/min	Vol flow, gal/hr	4-hr cycle Vol Flow, gal	No. tubes needed
0.125	8.22	493	1,973	8,532
0.375	30.68	1,841	7,363	2,286
0.5	81.72	4,903	19,613	858
0.625	134.76	8,086	32,342	520
0.75	200.03	12,002	48,007	351

Therefore, the 3/4" o.d. tubes are needed to supply the needed flow rate, pressure drop,
velocity, and stress safety factor with enought room to place them in the tank.

Finally, is the assumed value of 200 Btu/ft^2-hr-F valid?

hi = 0.023*k/D*(DG/viscosity)^.8 *(Cp*viscosity/k)^.333
hi = 0.023 *k/D*(Re)^.8 * (Pr)^.333
Where,

G = mass velocity lb/ft^2-sec			
Cp =	1	Btu/lb-F	
k =	0.32	Btu/ft/hr/F	at 32F
Viscosity =	0.001205568	lb/ft-sec	at 32F
Re =	18,514	from i84	
Pr =	13.56		
hi =	934.82	Btu/ft^2-hr-F	

Ui = overall coefficient = 1 / [(1/hi) + (xw/km * id/avg d)]

xw =	0.01383333333	ft.	from d84 and c84
km =	12.46	Btu/ft-hr-F	for Aluminum 5052 alloy
ln mean d =	0.66		
Ui =	488.55	Btu/ft^2-hr-F	

Final Interation -- Calculation of Cycle Time, Hydrate Formation

Given:
1. 3/4" o.d. tubing, Aluminum 14 BWG
2. Velocity cooling brine = 7 ft/sec
3. Pressure drop in tubing = 12 psi
4. Reynolds No. in tubing = 17,633
5. Maximum stress on tubing = 2,794 psi a safety factor of 3.
6. Volumetric flow rate/tube= 5.84 gpm/tube
7. Heat to remove in hydrate formation = 53,719,256 Btu/cycle

Find:
1. Maximum # tubes from tank geometry.
   Max Allowable 3/4" o.d. tubing = 500
2. Find gpm flow rate satisfying tubing size and velocity.
   GPM = No. tubes*pi/4*(i.d.)^2/144*velocity*60*7.48 = 2,920 gal/min
3. hi = 899.03 Btu/ft^2-hr-F
4. Ui = 478.60 Btu/ft^2-hr-F
5. Pressure Drop in Tubing = 12 psi 2fLV^2/(D/12*gc)*density

Time/Cycle, hrs	Total gals all tubes	Hydrate Energy Req	Cum Heat Transfer	H20 temp rise, F
1	175,229	49,072,256	1.94e+07	33.62
2	350,457	49,072,256	3.88e+07	16.81
3	525,686	49,072,256	5.82e+07	11.21
4	700,914	49,072,256	7.76e+07	8.40
5	876,143	49,072,256	9.70e+07	6.72
6	1,051,372	49,072,256	1.16e+08	5.60
7	1,226,600	49,072,256	1.36e+08	4.80
8	1,401,829	49,072,256	1.55e+08	4.20

Therefore, from the table above, 7 hours would be the needed cycle time
in order to raise the temperature of the cooling brine from only 28-33 F.
Note that the mass flow rate of cooling brine is set by tube size and no.
The amount of heat transferred is set by the hydrate formation demand.
The rate of heat transferred is set by the heat transfer coefficient , surf area,
and temperature difference driving force. The pressure drop inside the
tubing would be 12 psi.

Calculation of Heat Transfer for Hydrate Decomposition

Assume use water from turbine of power plant at 110 F to decompose hydrates.

Avg Hot Water Temp = 80 F Using a conservative avg temp in line.
Hydrate Temperature = 37 F
Velocity water = 7 ft/sec
Pressure Drop of Water = 10 psi
Density heating water = 62.3 lbm/ft^3
Viscosity heating water = 0.982 cp
Btu/(ft-hr-F)
k m = 12.46

Reynolds No. = DV*Dens/Visc = 32,162
Prandtl No. = 7.30

hi = 0.023*k/D*(Re)^0.8*(Pr)^0.333 = 1,183 Btu/ft^2-hr-F

Ui = 549 Btu/ft^2-hr-F

Q = Ui*A*(t2-t1)*time

Flow Time	Btu Q required	Btu Q transferred
1	48,372,778	136,601,420

Therefore, heat can be transferred to decompose the hydrates in less than 1 hour.

Hydrates: volumes, weights, gas content

Sp Gv Hydrates =	0.92	
Thick, hyd on plates =	0.5	ft
Adsorp surf, plates =	Plates:g33	
Vol fins	Plates:m33	ft^3
Gas content, hydrates =	155	vol/vol

Total vol hyd on plates = Vhp = [Total adsorp surf area of plates*thick hydrates on plates - vol fins]/sp.gv.*0.95 (95% coverage)

Vhp	=	4,689	ft^3
Vhp	=	33,324	gal

Note: This gives a 95% coverage of the plates.

Hydrates on Each Plate, Summary

Plates					Adsorp	4-Plate	4_plate	Hydrate	Hydrate	Gas	Gas
Thick, in.	No.	Length, ft.	Width, ft.	No. of Plates	Surf ft**2/plate	Vol Hyd ft^3	Wt Hyd lbf	Vol/plate ft^3/plate	Wt/plate lbf/plate	content/ plate, scf	Content/ 4 plates, scf
0.125	1	59	2.451	4	289.22	590.69	33,173	147.67	8,293	22,889	91,557
0.125	2	59	3.528	4	416.30	859.76	48,284	214.94	12,071	33,316	133,263
0.125	3	59	4.151	4	489.82	1011.58	56,810	252.90	14,203	39,199	156,795
0.125	4	59	4.497	4	530.65	1095.90	61,546	273.97	15,386	42,466	169,864
0.125	5	59	4.623	4	545.51	1126.60	63,270	281.65	15,818	43,656	174,624
			Total =	**20**	**9,086**	4684.53	263,083	1171.13	65,771	181,526	**738,716**

Calculate Free Gas Compressed in Void Space of Tank

Given:

1. Plates 95% covered to leave 5% void space.
2. Plates 59 ft length, leaving 1 ft free space on ends
3. Pressure in tank = 550 psig.

Volume of tank =	4710	ft^3 from C8 of tank section.
Free Vol of tank =	235.5	ft^3 which is 5% of tank volume uncovered plates
Free Vol, end tank =	78.5	ft^ 3 which is the 1 ft of length of tank free.
Total Free Vol, tank=	**314**	ft^3 tank vol occupied by compressed gas.

scf compress gas = 12,614 scf to be added to that stored in hydrates

Calculations for Plate Support Network

Reference:
Flinn, Trojan, Engineering Materials and Their Applications, 3rd ed.
p.433

Deflection of a Beam = WL^3/(4Ebh^3)

where,

W= concentrated load at center
L = lenght of span
E = molulus of elasticity
I = moment of inertia, bh^3/12

W =			weight of hydrates on 10 ft of 10 plates + wt plates + wt tubing, all for 1 quadrant
b =	3	in.	(width of the support beam.)
E =	10500000	psi	(for aluminum alloy, page 71 Flinn)
L =	10	ft.	(Length of beam = diameter of the tank)
h =	3	in.	(thickness of 3"x3" Al support beam.)

Table I. Vary beam width and thickness for imposed weight.

Deflection in.	Weight, lbf	Length, L, ft.	Width, b, in.	Thick,h, in.
0.492999011683	7,765	5	3	3
2.49580749664	7,765	5	2	2
39.9329199463	7,765	5	1	1

Note: The cross beam supports are located every 6 ft down the length of the tank.
The vertical supports anchor the cross beam supports every 6 ft in the center of tank.
The sides of the tank anchor the cross beam supports on each end.
Therefore, 5 ft of beam supported on both ends supports the plate weight and hydrate weight of 6 ft of each quadrant.

No. Beams	Beam Volume ft^3		Beam Wt lb/beam	Total Beam Weight, lb
18	0.625		105.3	1,895

Note: Beams are each 3" x 3" x 10' and a total of 9 horiz + 9 vertical
Specific gravity aluminum = 2.7

Wt Beam = 2.7*62.4* beam volume

IV.D.2. Latent heat

Note: Heats of hydrate formation is taken from Handa for individual gases.
Heat of formation of the typical gaseous mixture is calculated with mole fraction as weighting factor.
9.486E-4 Btu = 1 J
Handa, Y.P., "Compositions, enthalpies of dissociation, and heat capacities in the range 85 to 270 K for clathrate hydrates of methane, ethane, and propane, and enthalpy of dissociation of isobutane hydrate, as determined by a heat-flow calorimeter",
J. Chemical Thermodynamics, 1986, vol 18, 915-921.

TABLE EN#1. Calculate latent heat hydrate formation

Gas Component	mole fraction	Heat of Formation, kJ/mol gas	Gas mix, kJ/mol gas	Gas mix, Btu/mol gas	Gas mix, Btu/lb-mol gas	Gas mix, Btu/scf gas	Gas mix, Btu/lb-mol H20	Gas mix, Btu/lb H20
methane	0.894	54.2	48.45	45.96	20,868	55.06	3,478	193.22
ethane	0.063	71.8	4.52	4.29	1,948	5.14	325	18.04
propane	0.035	129.2	4.52	4.29	1,947	5.14	325	18.03
isobutane	0.008	133.2	1.07	1.01	459	1.21	76	4.25
	1		58.57	55.56	25,222	66.55	4,204	233.54

Example calc of table:
48.7 kJ/mol gas * (0.9486 Btu/1 KJ) = 46.20 Btu/mol-gas
46.2 Btu/moles-gas * (454 g-mol gas/lb-mol gas) = Btu/lb-mol gas=
20,975 Btu/lb-mol gas
Putting on a basis of Btu/scf gas
20,975 Btu/lb-mol gas / 379 scf/lbmol = 55.3 Btu/scf
Putting on a basis of Btu/lb-mol H20,
20,975 Btu/lb-mol gas/(5.7 l-mol H20/lb-mol gas)= 3680 Btu/lb-mol H20
Putting on a basis of Btu/lb-H20,
3680 Btu/lb-mol H20/18 lb H20/lb-mol H20 = 143 Btu/lb H20
As a comparison from Chem & Physics Handbook, Heat fusion ice = 6.01 kJ/mol water = 143 btu/lb-H20
On a hydrate basis: 6.01kJ/mol water *6 mol water/mol gas = 34.7 kJ/mol gas

Iculation of Latent Energy to Form 1 Tank of Hydrates Ca

Assume volume of gas occluded in hydrates is 155 scf gas/ft^3 hydrates

Vol hydrates on plates = [Total adsorpt surf area of plates* thick hydrates on plate - vol fins]/sp. gv.
See Hydrates, D13
Latent Heat To Fill 1 Tank= (Btu/scf gas)*(ft^3 hydrates on plates)*155 scf/cuft

Latent Heat to Fill 1 Tank = **48,372,778** Btu
Gas Occluded in 1 Tank = **738,716** scf (includes compressed gas in tank)

Calculation of Sensible Heat to Cool Gas from Ambient to 37F.

Assume: Gas enters at 60F.
Assume: Cool gas to 37F.

Energy to cool= (cp of gas)*(60-37 F)*(Gas occluded in 1 tank + compressed gas)
Note: Heat capacities from Himmelblau, D.M., Basic Principles and Calculations in Chemical Engineering, 3rd ed., 1974, Prentice-Hall.
cp = a+bt+ct^2+dt^3 J/mol-C
Note: Calculate the mean heat capacity at the mean temperature and use mole fraction as weighting factor.

Gas mol fract.		a	b	c	d	Cp @ 45F J/mol-C	Cp@ 45F Btu/lb-F	Cp mix @ 45F Btu/lb-F	Avg Mol Wt., lb/lbmol
0.894	methane	34.31	0.05469	0.000003661	-0.000000011	34.71	0.52	0.46	30.67
0.063	ethane	49.37	0.1392	-0.00005816	0.0000000073	50.37	0.75	0.05	3.11
0.035	propane	68.032	0.2259	-0.0001311	0.0000000317	69.66	1.04	0.04	2.38
0.008	i-butane	89.46	0.3013	-0.0001891	0.0000000499	91.63	1.37	0.01	0.72
1								**0.56**	**36.88**

Enthalpy of cooling by removal of sensible heat of occluded gas =
Cp*(53-37F)*(Molec Wt)*scf/379 Note: leaving decomposed gas cools entering gas to 53F, just above hydrate condition.)

Enthalpy = **642,740** Btu (to fill 1 tank with the gas to be occluded.
Also includes sensible heat for
compressed gas in tank not occluded.)

Calculation of Sensible Heat to Remove in Cooling Water Charge Initially

Water Charged to Tank = 282,154 lbf (See Tank page, c25)

Cp = 1 Btu/lb/F (Water)

Q = mCp(60F-37F)

Sensible Heat to Cool Initial Water Charge = 6,489,536 Btu

Calculation of Sensible Heat to Remove in Makeup Water

Assume: 2 mass% of initial water is entrained with the gas upon withdrawal.

Makeup Water = 5,643 lbm

Heat exchange between produced cold gas and entering warm water cools H20 to 53F
Just above hydrate forming temperature.

Sensible Heat to Cool Makeup Water = 39,502 Btu

Summary of Energy Requirements

Item	Refrig. Require., Btu/cycle/ 1 tank	
Latent Heat of Water	48,372,778	
Gas Sensible Heat	642,740	
Sensible, Makeup Water	39,502	
Sensible, Initial Water Charge	253,938	90% of initial charge water cooled down from 38 to 37F
Loss Through Insulation**	17,237	
Total Energy =	**49,326,195**	**Btu/cycle/tank**

Assume** : The heat gain through the insulation must be removed by refrigeration.
Each cycle will be 24 hours of formation/decomposition. Therefore,
this heat gain applied to a 24 hour span of
1 cycle/tank.

Cooling Requirements
(Hydrate Formation)

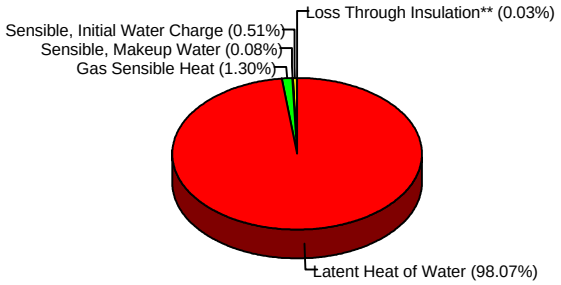

Item	Refrig. Require., Btu/cycle				
No. of Cycles ---------->	1	10	50	100	365
Latent Heat of Water	48,372,778				
Gas Sensible Heat	738,716				
Sensible, Makeup Water	39,502				
Sensible, Initial Water Charge*	253,938	253,938	253,938	253,938	253,938
Loss Through Insulation**	314,575	31,457	6,291	3,146	862
Total =	49,719,509	49,436,391	49,411,225	49,408,080	49,405,796
Total MM =	49.72	49.44	49.41	49.41	49.41

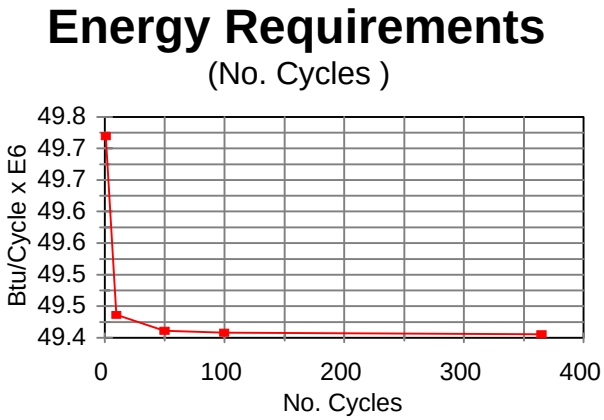

Refrigeration Costs

A. Formation of Hydrates

TABLE I. Costs based on 1 cycle of stated duration and 1 tank.

Item		Time Duration of one cycle, hours 1	2	3	4	5	6	7	8	9	10	24
		BTU/min for the given cycle										
Latent Heat, Water	48,372,778	806,213	403,106	268,738	201,553	161,243	134,369	115,173	100,777	89,579	80,621	33,592
Sensible Heat, Gas	738,716	12,312	6,156	4,104	3,078	2,462	2,052	1,759	1,539	1,368	1,231	513
Sensible Makeup Water	39,502	658	329	219	165	132	110	94	82	73	66	27
Sensible, Initial H20 Charge	253,938	4,232	2,116	1,411	1,058	846	705	605	529	470	423	176
Insulation Loss	314,575	5,243	2,621	1,748	1,311	1,049	874	749	655	583	524	218
Total =	49,719,509	828,658	414,329	276,219	207,165	165,732	138,110	118,380	103,582	92,073	82,866	34,527

Cengel and Boles, Thermodynamics, An Engineering Approach, 2nd ed., p. 585:
Cooling capacity of a refrigeration system is often expressed as tons of refrigeration.
It is the capacity that can freeze 2000 lbs of water at 32F in 24 hours.
1 ton refrigeration = 200 Btu/min.
The cooling load of a typical 200-m^2 residence is in the 3-ton (10-kW) range.

Item		Time Duration of one cycle, hours 1	2	3	4	5	6	7	8	9	10	24
		Tons of Refrigeration										
Latent Heat, Water	48,372,778	4031.06	2015.53	1343.69	1007.77	806.21	671.84	575.87	503.88	447.90	403.11	167.96
Sensible Heat, Gas	738,716	61.56	30.78	20.52	15.39	12.31	10.26	8.79	7.70	6.84	6.16	2.57
Sensible Makeup Water	39,502	3.29	1.65	1.10	0.82	0.66	0.55	0.47	0.41	0.37	0.33	0.14
Sensible, Initial H20 Charge	253,938	21.16	10.58	7.05	5.29	4.23	3.53	3.02	2.65	2.35	2.12	0.88
Insulation Loss	314,575	26.21	13.11	8.74	6.55	5.24	4.37	3.74	3.28	2.91	2.62	1.09
Total ----->	49,719,509	4,143	2,072	1,381	1,036	829	691	592	518	460	414	173

Note: 1. Assume each cycle is 24 hours.
2. Assume that 3 tanks could be filled (7 hrs set by heat transfer rate) and 7 2/3/hrs tank on refrigeration.
3. Assume 1 hour for decomposition of all 3 tanks.
4. Therefore, filling/decomposition of 3 tanks could be done in a 24-hour period.
5. Refrigeration would be selected to fill 1 tank in 7 2/3 hours.

To refrigerate 3 tanks in a cycle would require = 543 tons

B. Refrigeration to replace heat gain through insulation.

Heat gain, 3" insulation = 718 Btu/hr/tank
Btu/min/tan
Heat gain, 3" insulation = 12 k
Heat gain, 3" insulation = 35.9 Btu/min/3 tanks
Tons Refrig for ins. loss = 0.18 tons refrig.

Note this would need to be a separate small unit that would run during storage only.

C. Capital Cost of Refrigeration Equip. for Formation
Gas Powered

50-ton unit cost = $149,000 (1989 pric)
Reference: Decker, GRI-92/0334
Assuming six-tenths rule for cost of other sizes,

Cost larger unit = (596/50)^.6 * $149,000
Cost larger unit = $622,971
Using the Ch.E. Plant Cost Index to correct for inflation of CPI equipment:
1989 Index = 355.4
1998 Index = 389.5

Current Cap. Cost Refrig = $682,744 for refrig of 543 tons of refrig for formation.
which will service 3 tanks in one 24-hr cycle

D. Capital Cost for Refrigeration Unit for Insulation Gains
Electrical Power-Driven
Refrig for unit for ins gains
of 0.18 tons refrig/24 hours storage period in 3 tanks for 1 cycle .

Cost Refrig for Ins Gain = **$1,000** Cap Cost for refrig equip.

E. Fuel Costs for Refrigeration
1. Refrig Unit for Hydrate Formation

Full-load demand for 50-ton gas-fired refrig unit =1.35 MM Btu/hr (GRI report).
Required for size calcd for storage (See Refrig Costs:d44)
Example: (596 tons/50 tons)*1.35 MM Btu/hr = 16.1 MM Btu/hr
Btu content of natural gas = 1,000 Btu/scf = 1 MM Btu/Mscf
16.1 MM Btu/hr * scf/1000 Btu = 16.1 Mscf/hr
Assume 44% efficiency of the conversion; 16.1/.44= 36.6 Mscf/hr
Use gas price of $2.70/Mscf,
NG cost = $2.70*36.6= $98.82 /hr

ng cost for refrig = $90 per hr for ng to drive refrig.

Plots of Costs of Hydrate Storage Process

$682,744 is the cost of a gas-powered refrig unit that will remove the heat to fill 3 tanks with hydrates in a 24-hr cycle.

Assume the life of the refrigeration unit is 20 years.

$1,000 is the cost of a small refrig unit to replace heat gain through the insulation during the storage phase of each cycle.
Assume life of the small unit is 5 years.

is the cost of the natural gas to drive the refrigeration unit each cycle.
Assumes an efficiency of 44% of the conversion.

738,716 is the scf of gas to be stored in each tank in hydrates.
2,216,148 is the scf of gas to be stored per cycle (i.e. 3 tanks)
12,614 is the scf of gas stored in each tank, compressed in void space.
37,841 is the scf of gas stored in each tank, compressed in 3 tanks
2,253,990 is the total scf of gas stored per cycle in the 3 tanks

Table I. Refrig equp cost per cycle to form 3 tanks of hydrates

No. cycles per year	Cost/cycle Refrig Equip	Cost/cycle Small unit	scf/cycle	Refrig. Cost/ Mscf
1	$34,137	$200	2,253,990	15.23
2	$17,069	$100	2,253,990	7.62
3	$11,379	$67	2,253,990	5.08
4	$8,534	$50	2,253,990	3.81
5	$6,827	$40	2,253,990	3.05
10	$3,414	$20	2,253,990	1.52
20	$1,707	$10	2,253,990	0.76
30	$1,138	$7	2,253,990	0.51
40	$853	$5	2,253,990	0.38
50	$683	$4	2,253,990	0.30
100	$341	$2	2,253,990	0.15
150	$228	$1	2,253,990	0.10
200	$171	$1	2,253,990	0.08
250	$137	$1	2,253,990	0.06
300	$114	$1	2,253,990	0.05
350	$98	$1	2,253,990	0.04

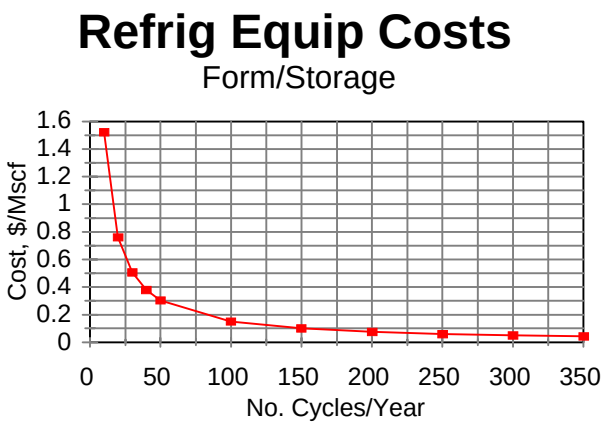

Fuel Costs for Refrigeration Units

Gas-Powered Unit

Full-load gas demand for a 50-ton gas-powered refrigeration unit would be about
1.35 MM Btu/hr = 22,500 Btu/min. Ref.: Report on gas-powered refrig units.

The above statement would indicate a 44% efficiency of energy conversion.

Assume: 7 2/3 hrs/tank each cycle. Refrigeration required = 596 tons to process
3 tanks in series for a 24-hour cycle.

Refrig. Required = 596 tons * 200 Btu/min = 108,510 Btu/min

Assume: Btu value of methane = 1000 Btu/scf
Then, Btu value of 1000 scf = 1,000,000 Btu/Mscf where the natural gas used
would be the methane-rich portion that grows as hydrates form.

scf natural gas required = 0.108509868009 Mscf/min
scf natural gas required = 6.51059208055 Mscf/hr

Assume: cost of natural gas = $2.75 per Mscf

Natural Gas Fuel Cost= $17.90 per hr

Length of one cycle = 24 hours (3 tanks in series, each filled in 7 2/3 hours)
Fuel Costs per tank = $137.32
Fuel Cost/Mscf stored = $0.19

Electrical-Powered Small Units

Note: One small refrigeration unit would be needed for each tank to remove
heat gained through the insulation.

718 Btu/hr/tank heat gained thru ins. (see Costs:c48)
16,521 Btu/tank/cycle = B103*7.67 hr/tank *3

scf stored/tank/cycle = 738,716 scf per Hydrates:o31

22.36 Btu/Mscf the energy loss by each tank per gas stored in it over a 24-hr cycle.

Assume: Cost of electricity = $0.08/ kW-hr
9.486 Btu = 2.778 E-3 kW-hr

Assume: 40% efficiency.
0.0013099 dollars/Mscf of gas stored in a single tank over a 24 hr cycle
$0.97 per tank per 24 hour cycle to remove heat gained thru insulation

Equipment Costs as a Function of Life and Cycles/Yr

Gas Stored/Cycle = 2,216,148 scf for 3 tanks

Equipment Cost = $2,202,189 for 3 tanks and supporting equipment

Assume either a 10-year life of the equipment or a 20-year life.

No. Cycles Per Year	Equip Cost, 10-Yr Life	Equip Cost, 20-Yr Life	Cost, $/MSCF 10-Yr Life	Cost, $/MSCF 20-Yr Life
1	$220,219	$110,109	99.37	49.69
5	$44,044	$22,022	19.87	9.94
10	$22,022	$11,011	9.94	4.97
20	$11,011	$5,505	4.97	2.48
50	$4,404	$2,202	1.99	0.99
100	$2,202	$1,101	0.99	0.50
150	$1,468	$734	0.66	0.33
200	$1,101	$551	0.50	0.25
250	$881	$440	0.40	0.20
300	$734	$367	0.33	0.17
350	$629	$315	0.28	0.14

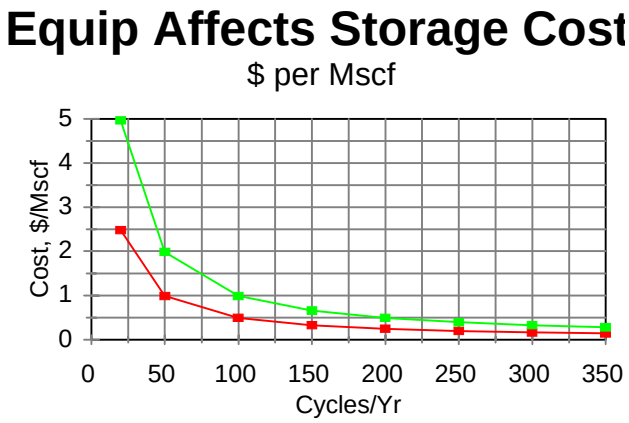

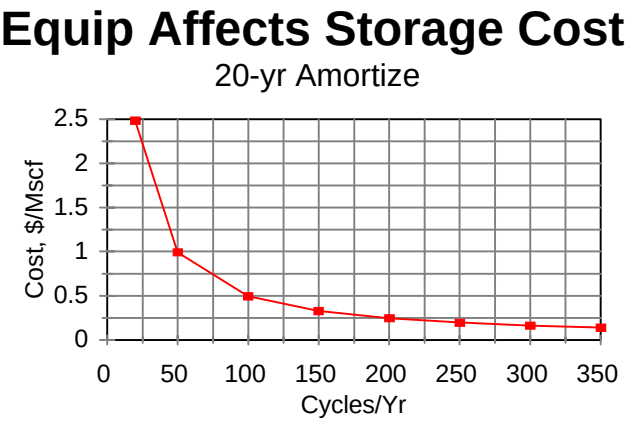

Development Costs as a Function of Cycles

Assume: Development costs is the fixed capital investment.

Life of plant would be 20 years and FCI amortized over 20 years.

No. Cycles per Year	FCI Amortiz 20 Years	Cost, $/Mscf 20-Yr Life	Development $ Depleted Res.	Development $ Salt Cavern	Development $ LNG
1	$344,643	$152.90	2.72	10.5	32.5
3	$114,881	$50.97	2.72	10.5	32.5
4	$86,161	$38.23	2.72	10.5	32.5
5	$68,929	$30.58	2.72	10.5	32.5
10	$34,464	$15.29	2.72	10.5	32.5
12	$28,720	$12.74			32.5
14	$24,617	$10.92			32.5
16	$21,540	$9.56			32.5
20	$17,232	$7.65	2.72	10.5	32.5
50	$6,893	$3.06	2.72	10.5	32.5
52	$6,628	$2.94			
54	$6,382	$2.83			
100	$3,446	$1.53	2.72	10.5	32.5
150	$2,298	$1.02	2.72	10.5	32.5
200	$1,723	$0.76	2.72	10.5	32.5
250	$1,379	$0.61	2.72	10.5	
300	$1,149	$0.51	2.72	10.5	
350	$985	$0.44	2.72	10.5	

Development Costs

Fixed Capital Investment

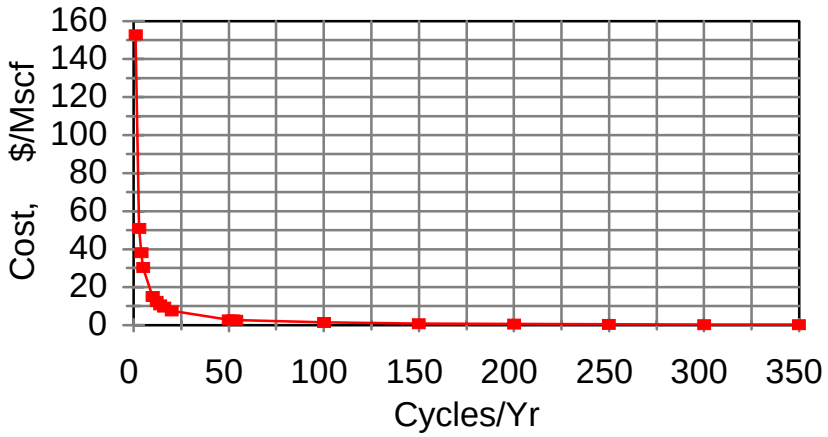

Development Costs

Hydrate Storage Process

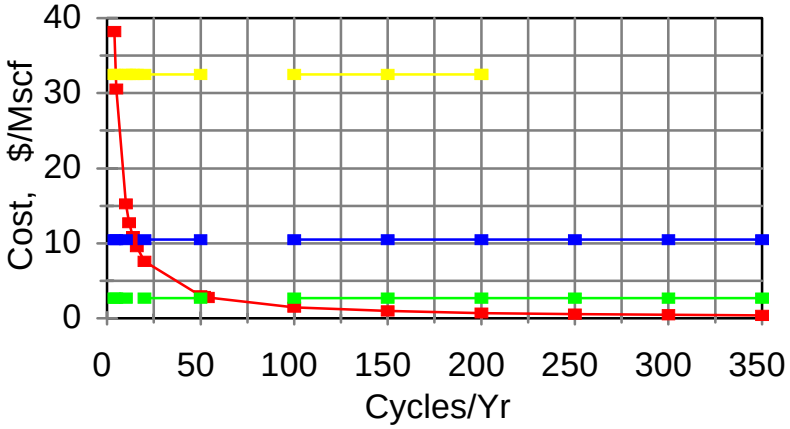

Product Costs

What would be the user cost for storing the natural gas in hydrates?

The product cost (user cost) will be comprised of the following:

TABLE I. Product Costs

		Cost/Cycle		
Raw Matls	Calculate	$181	per cycle	
Operating Labor	Calculate	$257,400	per year	
Utilities	Calculate	$1,888	cycle	
Supervisory Labor	15% Operating Labor	$38,610	per year	
Maintenance and Repair	6% Fixed Capital Investment	$20,679	per year	
Operating Supplies	15% Maintenance and Repairs	$3,102	per year	
Laboratory Charges	15% Operating Labor	$38,610	per year	
Depreciation	Calculate	$110,109	per year	
Property Taxes	4% Fixed Capital Investment	$27,571	per year	
Insurance	1% Fixed Capital Investment	$3,446	per year	
Plant Overhead	70% Operating Labor+Supervision+Maintenance	$221,682	per year	
Administrative	25% Operating Labor	$64,350	per year	
Contingency	1% Total Product Cost	$7,876	per year	
	Total =	$793,436	per yr	(Divide by no. cycles and add+Raw matls +Utili*21 hrs*no. cycles

Notes for calculation of Table I:

Raw Matls: Makeup water + initial water/20 yrs + surfactant

			Cost
Initial water =	33,822	gals/1 tank	$778
Initial water =	101,467	gals/3 tank	$2,334
Makeup W=	676	gals/1 tank	$16
Makeup W =	2,029	gals/3 tank	$47
Initial surf =	85	lbs/1 tank @300 ppm	$85
Initial surf =	254	lbs/3 tank @300 ppm	$254
Makeup Surf=	1.69	lb/1 tank @ 300 ppm	$2
Makeup Surf=	5.08	lb/3 tank @ 300 ppm	$5

Total Raw Matl Cost per Cycle (3 tanks) = $181 Assumes initial spread over 20 year life of plant

Unit Cost H20, deionized =	$0.02	per gal deionize
Unit Cost SDS Surfactant =	$1.00	per lb
Unit Cost H20, not deionized =	$0.10	per 1000 gal (Timmerhaus, p. 200)

Operating Labor:

Reference: Turton, et al., Analysis, Synthesis, and Design of Chemical Processes, Printice-Hall, 1998, p. 84.
Labor requirements broken down into how many operators typically needed to run specific items of equipment.

Item	Operators/ shift/ equip	No. Equip Items, Hydrate Process/cycle	Operators/ shift
Refrig Unit	0.5	1	0.5
Reactors	0.5	1	0.5
Ht Exchangers	0.1	2	0.2
		Total =	1.2

Note: A single operator works 49 wks/yr; 5 8-hr shifts/wk = 245 shifts/op/yr
Plant operates 24-hrs/day = 365 days/yr * 3 shifts/day = 1095 operator shifts/yr
4.5 operators are hired for each operator needed in plant at any time (1095/245)
Typical chem. plant operator makes $21/hr = 46,800/yr in 1996 = $51,480 currently.

Operating Labor =	5.4	That is, 4.5*no. operators
	5	Operators
Labor Costs, current =	**$257,400**	for entire year

Table II. Product costs per Mscf as a function of no. cycles/yr

No. cycles	Prod Costs/ Year	Gas stored Mscf/yr	Prod cost/Mscf
1	$833,261	2,254	$369.68
2	$436,543	4,508	$96.84
3	$304,304	6,762	$45.00
4	$238,184	9,016	$26.42
5	$198,513	11,270	$17.61
10	$119,169	22,540	$5.29
20	$79,497	45,080	$1.76
30	$66,273	67,620	$0.98
40	$59,661	90,160	$0.66
50	$55,694	112,699	$0.49
100	$47,760	225,399	$0.21
150	$45,115	338,098	$0.13
200	$43,793	450,798	$0.10
250	$42,999	563,497	$0.08
300	$42,470	676,197	$0.06
350	$42,092	788,896	$0.05

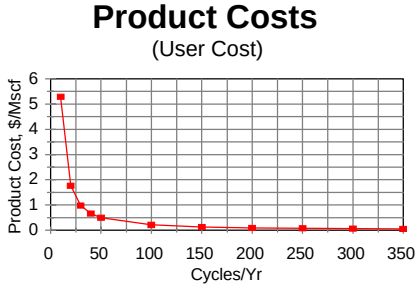

Purchased Equipment Cost

Table III. Equipment list. (Bounds, Montgomery, Pitman, and Zhong)

Equipment Description	Quantity (1)	Size	Matl Construction	Unit Cost $	Cost 1 Tank, $	Total Cost 3 Tanks, $
Hydrate Formation, Storage, Decomposition Tank	1	10' D x 60' L	Carbon Steel, Lined	$300,000	$300,000	$900,000
Natural Gas Fired Refrig System	1	596 tons (2)	N/A	$682,744	$682,744	$682,744
Adsorption Plates	20	9,086 ft^2	Aluminum (4)	$1,357	$27,146	$81,439
Heat-Transfer Tubing	500	59' L x 3/4" o.d., 14 gauge	Aluminum (3)	$127	$63,720	$191,160
Surfactant Soln Storage Tank With Agitator	1	2734 gal Serves 3 Hyd Tanks	Carbon steel (6)	$9,702	$9,702	$9,702
Water Deionization Unit (7)	1	2,734 gal/60 min	n/a	$62	$62	$187
Insulation for Tank	3"	72"x50'x1" rolls	Cryogenic fiberglass	$4,970	$4,970	$14,910
Support System, Hydrate Tank	1	Aluminum	Construction of Support	$25,000	$25,000	$75,000
Feed Soln (makeup) Pump	1 (10)	205 gpm, P=50	Cast-Steel, Centrifugal	$7,546	$7,546	$7,546
Tempered Water Circulation Pump	1 (11)	2920 gpm, P=12	316 ss, Centrifugal	$12,600	$12,600	$37,800
Surfactant Soln Transfer Pump	1	273 gpm, P=20	Ductile Iron Casing, Cent.	$2,156	$2,156	$2,156
Insulation Vacuum Pump	3	0.75 hp	Cast Steel	$2,500	$2,500	$7,500
Brine Collection Tank (8)	1	1,014	Gallons, 304 ss	$8,948	$8,948	$8,948
Constant Pressure Regulator	1/tank	5"D	SS Flow Control	$8,624	$8,624	$25,872
Check Valves	2/tank (13)	8" D	Carbon Steel , Flanged	$485	$970	$2,910
Relief Valves	2/tank	5"D	SS Relief	$8,624	$17,248	$51,744
Heat Exchanger, Makeup H20	1/3 tanks	1000 ft^2	Carbon Steel	$30,000	$30,000	$30,000
Heat Exchanger, Feed Gas	1/three tanks	1000 ft^2	Carbon Steel	$30,000	$30,000	$30,000
Demister, Defoamer	1/tank	Vane-type (12)	6" Thick, Coalescing Type	$500	$500	$1,500
Foam, Mist Collection Vessel	1/three tanks (9)	8,117	Gallons, Carbon Steel	$19,404	$19,404	$19,404
Electrical-driven Refrigeration	1			$1,000	$1,000	$3,000
Hydrate Tank Supports	1	3"x3"x10'	Aluminum (5)	$3,222	$3,222	$9,667
Tank, to cool entering gas	1	2000 gal	carbon steel (14)	$9,000	$9,000	$9,000
			TOTAL =	$1,168,573	$1,267,063	$2,202,189

Notes:

1. Process is designed around equipment for a 24-hour cycle, with three tanks, 1 refrigeration unit, etc.
2. See Refrig section of calculations in Appendix.
3. Aluminum tubing cost = $2.16/linear ft.
4. Total wt of plates (Plates:h35 =n33) + fins * $1.70/lb alum.
5. Support cost = total no. supports of 18(Supports:b43)*Wt/bm*$1.70/lb alum
6. From Timmerhaus, 4th ed., See Tank, Appendix.
7. Water deionization for makeup water. Per personal conversation w/Hoppenjans, Ecolochem, Inc., $8,000/350,000 gals at 1000 gpm general surface supply water.
8. Brine collection tank used to collect brine used in hydrate formation phase. Tank holds brine during decomposition phase when cooling tower water flows thru tubing. 25% free space, for tubing in all 3 hydrate tanks; Timmerhaus, p.539.
9. 2% of hydrate tank water and surfactant removed from exiting gas. Size carbon steel vessel to collect 3 cycles of the solution from all 3 hydrate tanks.
10. Size for makeup water volumetric flow rate, p.527 Timmerhaus, all 3 tanks, to be filled in 10 minutes with a 50 psig pressure drop in lines, once per cycle.
11. Brine flow rate limiting. Tubing:d193 gives gpm/tube * Tubing:e197 no. tubes. Timmerhaus, p. 527, 1.8 factor for 316 ss, 12 psi drop through tubing.
12. Petroleum Engineer's Handbook; similar to gas-liquid separators. Use coalescing type, 6" thick vane-type. Effective for entrained liquid as well as foam removal. Centrifugal device on gas inlet.
13. Timmerhaus, p511. Flanged valves.
14. Carbon steel tank to store water for heat exchange, exiting gas and entering gas.

Fixed Capital Investment

Use typical ratios found to be applicable for estimating capital investment items based on delivered-equipment cost for a solid-fluid processing plant. Ref: Timmerhaus, p. 183.

Table 2. Fixed capital investment

Item	Factor	Cost
Direct Costs		
Purchased equipment, delivered	1	$2,202,189
Equipment installed	0.39	$858,854
Instrument., controls installed	0.13	$286,285
Piping installed	0.31	$682,679
Electrical installed	0.1	$220,219
Buildings	0.29	$638,635
Yard Improvements	0.1	$220,219
Total Direct Plant Cost		**$5,109,079**
Indirect Costs		
Engineering and supervision	0.1	$220,219
Construction expenses	0.17	$374,372
Total Direct and Indirect Costs		**$5,703,670**
Contractor's fee	0.18	$396,394
Contingency	0.36	$792,788
Fixed Capital Investments		$6,892,852

COMMERCIAL POTENTIAL OF NATURAL GAS STORAGE IN LINED ROCK CAVERNS (LRC)

Final Report SZUS-0005

by

Sofregaz US Inc.
200 WestLake Park Boulevard
Suite 1100
Houston, Texas 77079
UNITED STATES
and
LRC
S-205 09 Malmö, Sweden
Carl Gustafsväg 4
SWEDEN

prepared for

U.S. Department of Energy
Federal Technology Center
P.O. Box 880
Morgantown, West Virginia 26507-0880

November 1999

DOE-SPONSORED WORKSHOP ON ALTERNATIVE GAS STORAGE TECHNOLOGIES

February 17, 2000

Greentree Holiday Inn – Pittsburgh, PA

Introduction to the Lined Rock Cavern (LRC) Gas Storage Concept
JoeRatigan
(Sofregaz)

Concept Development, Design Principles and Below Ground Design
PerTenborg
(SYCON)

Storage Use and Alternatives, Above Ground, Cost, and Comparisons to Other Technologies
Ola Hale
(SYCON)

U.S. Department of Energy/National Energy Technology Laboratory
Gas Storage Program Overview

SZUS-0005

COMMERCIAL POTENTIAL OF NATURAL GAS STORAGE IN LINED ROCK CAVERNS (LRC)

COMMERCIAL POTENTIAL OF NATURAL GAS STORAGE IN LINED ROCK CAVERNS (LRC)

Final Report SZUS-0005

prepared for

U.S. Department of Energy
Federal Energy Technology Center
P.O. Box 880
Morgantown, West Virginia 26507
UNITED STATES

November 1999

SOFREGAZ US Inc.

COMMERCIAL POTENTIAL OF NATURAL GAS STORAGE IN LINED ROCK CAVERNS (LRC)

Final Report SZUS-0005

by

Sofregaz US Inc.
200 WestLake Park Boulevard
Suite 1100
Houston, Texas 77079
UNITED STATES

and

LRC
S-205 09 Malmö, Sweden
Carl Gustafsväg 4
SWEDEN

prepared for

U.S. Department of Energy
Federal Energy Technology Center
P.O. Box 880
Morgantown, West Virginia 26507
UNITED STATES

November 1999

FOREWORD

This report presents the results of a study performed by Sofregaz US, Houston, Texas, and LRC, a consortium composed of Gaz de France International S.A., Paris, France, and Sydkraft AB, Malmo, Sweden. In cooperation with LRC, NYSEG, Binghamton, New York, and ANR Storage Company of Detroit, Michigan, have reviewed the report. In addition to LRC, Acres American Inc., Buffalo, New York, and SPS Inc., Houston, Texas, contributed to the study effort in assessing state and federal permitting requirements and mapping pipelines, respectively. Dr. Joe L. Ratigan was Project Manager for Sofregaz US and Mr. Ola Hall was Project Manager for LRC.

EXECUTIVE SUMMARY

The geologic conditions in many regions of the United States will not permit the development of economical high-deliverability gas storage in salt caverns. These regions include the entire Eastern Seaboard; several northern states, notably Minnesota and Wisconsin; many of the Rocky Mountain States; and most of the Pacific Northwest. In late 1997, the United States Department of Energy (USDOE) Federal Energy Technology Center engaged Sofregaz US to investigate the commercialization potential of natural gas storage in Lined Rock Caverns (LRC). Sofregaz US teamed with Gaz de France and Sydkraft, who had formed a consortium, called LRC, to perform the study for the USDOE.

Underground storage of natural gas is generally achieved in depleted oil and gas fields, aquifers, and solution-mined salt caverns. These storage technologies require specific geologic conditions. Unlined rock caverns have been used for decades to store hydrocarbons - mostly liquids such as crude oil, butane, and propane. The maximum operating pressure in unlined rock caverns is limited, since the host rock is never entirely impervious. The LRC technology allows a significant increase in the maximum operating pressure over the unlined storage cavern concept, since the gas in storage is completely contained with an impervious liner.

The LRC technology has been under development in Sweden by Sydkraft since 1987. The development process has included extensive technical studies, laboratory testing, field tests, and most recently includes a storage facility being constructed in southern Sweden (Skallen). The LRC development effort has shown that the concept is technically and economically viable. The Skallen storage facility will have a rock cover of 115 meters (375 feet), a storage volume of 40,000 cubic meters (250,000 petroleum barrels), and a maximum operating pressure of 20 MPa (2,900 psi).

There is a potential for commercialization of the LRC technology in the United States. Two regions were studied in some detail - the Northeast and the Southeast. The investment cost for an LRC facility in the Northeast is approximately $182 million and $343 million for a 2.6-billion cubic foot (bcf) working gas facility and a 5.2-bcf working gas storage facility, respectively. The relatively high investment cost is a strong function of the cost of labor in the Northeast. The labor union-related rules and requirements in the Northeast result in much higher underground construction costs than might result in Sweden, for example.

The LRC technology gas storage service is compared to other alternative technologies. The LRC technology gas storage service was found to be competitive with other alternative technologies for a variety of market scenarios.

TABLE OF CONTENTS

TABLE OF CONTENTS
(Continued)

TABLE OF CONTENTS
(Continued)

TABLE OF CONTENTS
(Continued)

LIST OF TABLES

LIST OF FIGURES

LIST OF FIGURES
(Continued)

LIST OF FIGURES
(Continued)

FIGURE **PAGE**

1.0 INTRODUCTION AND SCOPE

In late 1997, Sofregaz US was engaged by the Federal Energy Technology Center (FETC) to investigate the commercialization potential of natural gas storage in Lined Rock Caverns (LRC). Sofregaz US teamed with Gaz de France and Sydkraft to perform the study for the Department of Energy.

The geologic conditions in many regions of the United States will not permit the development of economical high-deliverability gas storage in salt caverns. These regions include the entire Eastern Seaboard; several northern states, notably Minnesota and Wisconsin; many of the Rocky Mountain states; and most of the Pacific Northwest. This study addresses the development of a design and associated cost estimate for lined rock caverns for these regions of the United States. The study addresses the development of LRC at two locations: one along the Southeastern Coast and the other in the Northeast.

In Chapter 2.0, the state-of-the-art in LRC technology is described. Chapter 3.0 provides a summary of the market data for conventional storage alternatives in the area in which the LRC technology is being proposed. The two geologic sites are described in Chapter 4.0, and the conceptual LRC design is presented in Chapter 5.0. Chapters 6.0 and 7.0 present the cost estimate and a comparison to conventional alternatives for storage. Chapter 8.0 provides a very brief review of the environmental issues associated with the LRC and the permitting issues that need to be addressed with such a development. The report concludes with cited references and several appendices with detailed information.

2.0 DESCRIPTION OF THE LINED ROCK CAVERN TECHNOLOGY

2.1 BACKGROUND

Underground storage of natural gas is conventionally achieved in depleted oil and gas fields, aquifers, and solution-mined salt caverns. It requires specific geological conditions not available everywhere. Alternatives to conventional underground storage are LNG and propane-air peak-shaving facilities. However, these alternatives are costly. The LRC technology is a new alternative to conventional underground storage of natural gas.

Unlined rock caverns have been used for decades to store a wide range of low vapor pressure products, mostly liquids such as crude oil, butane, and propane. Since the host rock is never completely impervious, product confinement within the cavern is sometimes achieved through the water curtain technique. The idea is to have water continuously flowing toward the cavern from outside so that the stored product can never escape and migrate out of the cavern. The cavern must be sited deep enough to make sure that the water hydraulic pressure in the fractures of the rock around the cavern is always higher than the vapor pressure of the product stored in the cavern. The water pressure is maintained by injecting water into the rock through horizontal water holes above the cavern ("the water curtain") in order to maintain a stable groundwater table level. Figure 2-1 illustrates the storage concept of an unlined rock cavern with a water curtain. The same concept of unlined rock with a water curtain has been envisaged for air and even natural gas, but it becomes uneconomical as soon as large storage capacity is required. Indeed, unlined rock caverns must be sited very deep to enable a sufficiently high storage pressure. With the new LRC concept, this constraint can be alleviated since gas containment within the cavern is ensured by the lining.

The LRC technology has been under development by Sydkraft in Sweden since 1987. There are no suitable geological conditions for conventional underground gas storage in Scandinavia. The geology of those countries (Finland, Sweden, and Norway), with the exception of Denmark, is largely dominated by crystalline bedrock. Since the penetration of natural gas into the energy market is growing, it has become critical for Scandinavian gas companies to find a way to store natural gas underground. Sydkraft, the largest private energy group in Sweden in the field of electricity, natural gas, LPG and heating systems, has taken the lead for development of the new technology adapted to the Scandinavian geology; the LRC technology. The LRC development program began in 1987 with Sydkraft in a leading role and with the participation of several Scandinavian entities; among them: Neste, Skanska, Statoil, Swedgas, and Vattenfall. Sydkraft entered into a partnership agreement with Gaz de France in 1995 to jointly evaluate the feasibility for an LRC demonstration plant in Sweden. The feasibility study involving the construction of an LRC demonstration plant is now complete and construction has started.

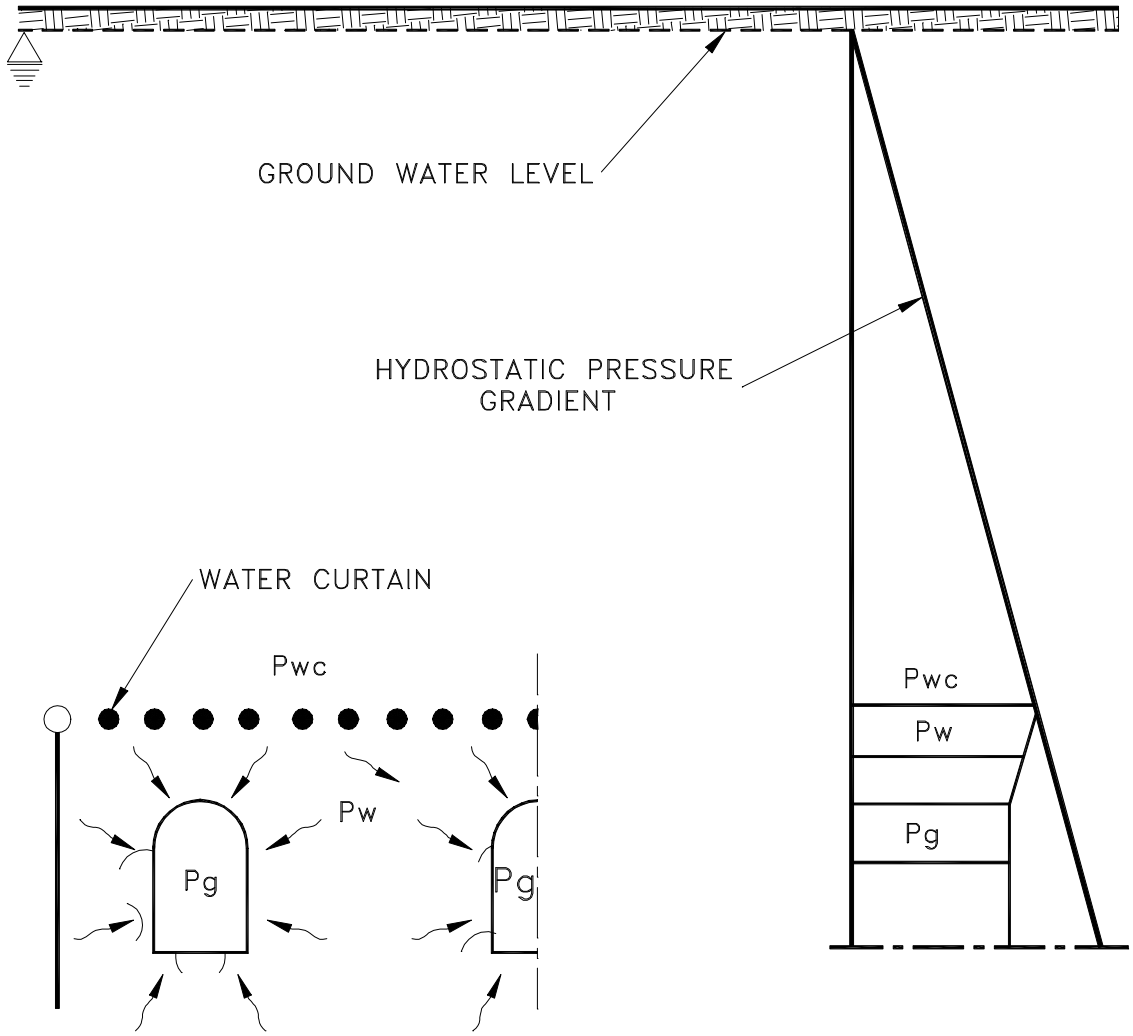

Figure 2-1. Concept of Unlined Rock Cavern With a Water Curtain.

2.2 THE LRC STORAGE CONCEPT

2.2.1 Overall Description

Figure 2-2 illustrates the LRC storage concept. The underground facility consists of one or more storage caverns, a vertical shaft, and a system of tunnels connecting the caverns with the ground surface. The storage caverns are excavated in rock as vertical cylinders.

Caverns are planned to be located at a depth of about 100-200 meters below ground (300-600 feet). The maximum storage pressure will be in the range of 15-30 MPa (2,200-4,350 psi), with typical cavern dimensions of 35-40 meters (100-120 feet) in diameter, 60-100 meters (200-340 feet) in height, and 12-30 million Nm^3 (400-1,100 million cubic feet (MMcf)) of natural gas storage (working volume) capacity.

The aboveground facility includes a compressor station, heating equipment, piping, valves, metering, and control system. A dehydration unit will only be needed on a temporary basis upon initiating gas storage service. Injection into the cavern is done directly from the pipeline by flow control when the storage pressure is lower than the pipeline pressure. When the cavern pressure is higher than the pipeline pressure, compression is used to boost gas pressure. Before being injected into the cavern, the gas is cooled (after compression) by an air or water cooler. During gas injection, when the pressure is higher in the cavern than in the pipeline, some gas will be withdrawn from the cavern by a separate compressor, circulated through a cooler, and injected back into the cavern. This will increase the working gas volume in the cavern. In order to further enhance the working gas capacity, the recirculated gas can be cooled to a lower temperature by means of a refrigeration unit.

Withdrawal is normally done by free flow from the cavern to the transmission line. Compression is used when the storage pressure falls below the pipeline pressure. To avoid too low of a gas temperature in the cavern at the end of withdrawal, gas can be heated in a heat exchanger and recirculated into the cavern. The gas also needs to be heated before pressure reduction in the withdrawal mode when the difference in pressure between the cavern and the pipeline is high.

The LRC design is based on the combination of a few key components:

- The surrounding rock mass to absorb the forces
- A concrete layer serving as a base for the lining and as a load transfer media between the gas pressure forces and the rock
- A thin lining enclosing the gas in the cavern.

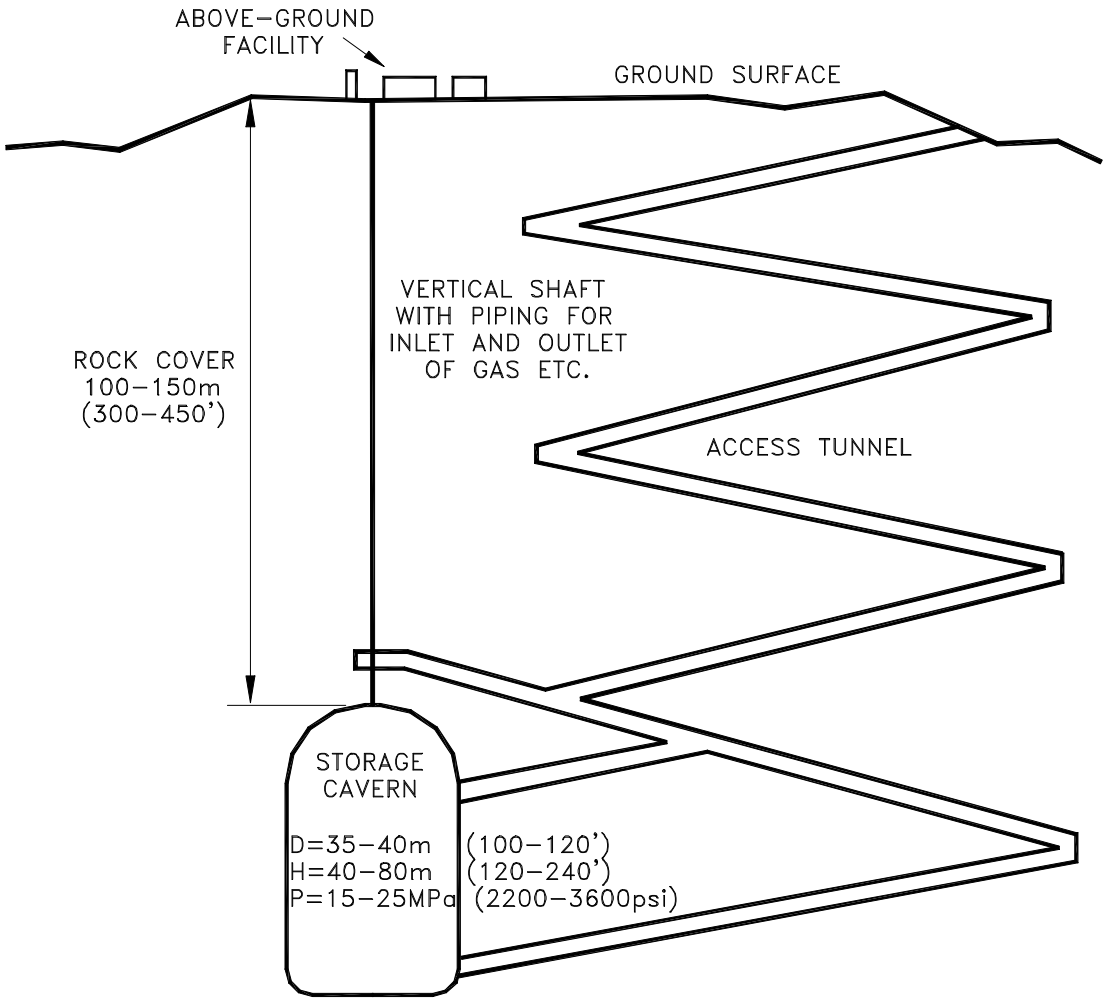

Figure 2-2. Schematic Illustration of the Lined Rock Cavern Concept.

A fourth component, the drainage system between the cavern wall and liner, has been added to handle groundwater influx. Figure 2-3 illustrates the design of the cavern wall, liner, and drainage system.

2.2.2 Pressure-Absorbing Rock Mass

The rock mass surrounding the cavern is the pressure-absorbing medium, and thus, the pressure vessel. Typically, for most common rocks contemplated so far for LRC, the surrounding rock mass starts to deform both elastically and plastically at pressures over about 4 MPa (600 psi). The magnitude of these early deformations is critical since it contributes to the ultimate strain of the lining.

A certain thickness of rock coverage is required to prevent the rock mass from uplifting when gas is pressurized in the cavern. Figure 2-4 illustrates a simple model for calculating the uplift effect and implies how much rock coverage must be taken for a given cavern diameter and maximum operating pressure. This model includes rock characteristics (α), in situ depth conditions (σ_η), cavern depth (z) and geometry (D), and operating parameters (p).

2.2.3 Pressure-Transferring Concrete Layer

A concrete layer is cast between the lining and the rock. The purpose of this concrete layer is twofold:

1. Transfer the load generated by the gas pressure in the cavern to the surrounding rock mass.
2. Provide a smooth base for the lining.

The concrete layer also has a role to minimize the strain in the lining. The large cracks that can be generated by the lining deformation result in a number of smaller cracks in the concrete; thus, producing a strain in the lining.

Concrete reinforcement may vary, depending on the geological conditions and the type of lining. The need for concrete reinforcement will decrease with a higher rock mass strength. However, if the frequency of fractures is too low (e.g., only of few larger fractures), increased reinforcement has to be incorporated. The amount of reinforcement is also related to the liner. With a thin liner, the allowance for the maximum width of cracks is lower than for a thick liner. The crack width is controlled by the amount of the reinforcement.

2.2.4 Gas-Tight Lining

The lining material must be gas-tight and chemically resistant to gas and to the possible condensates and impurities that it may contain, as well as to the outside environment. From a structural standpoint, the lining is not supposed to carry primary loads as it is supported by the

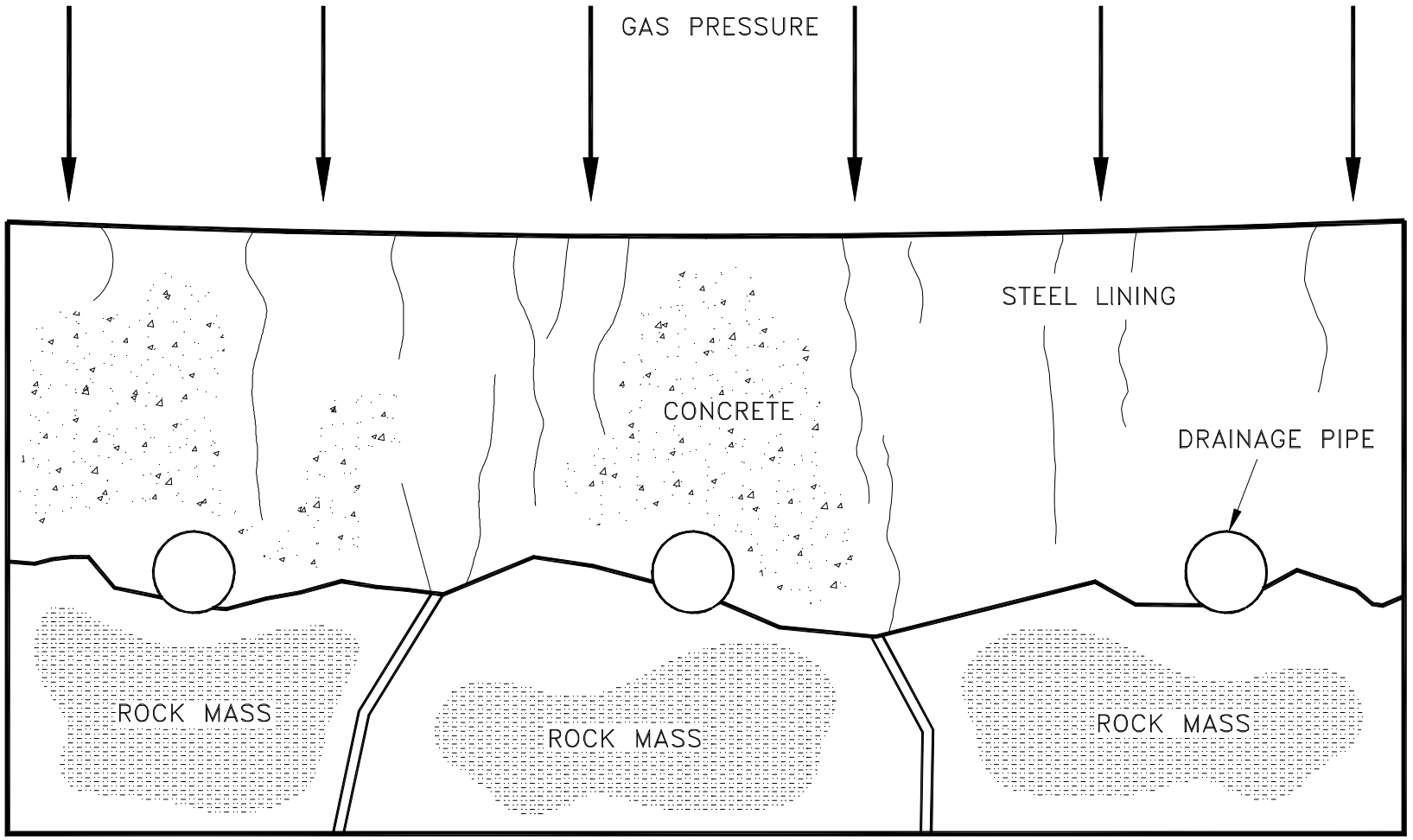

Figure 2-3. Cavern Wall Design in the LRC.

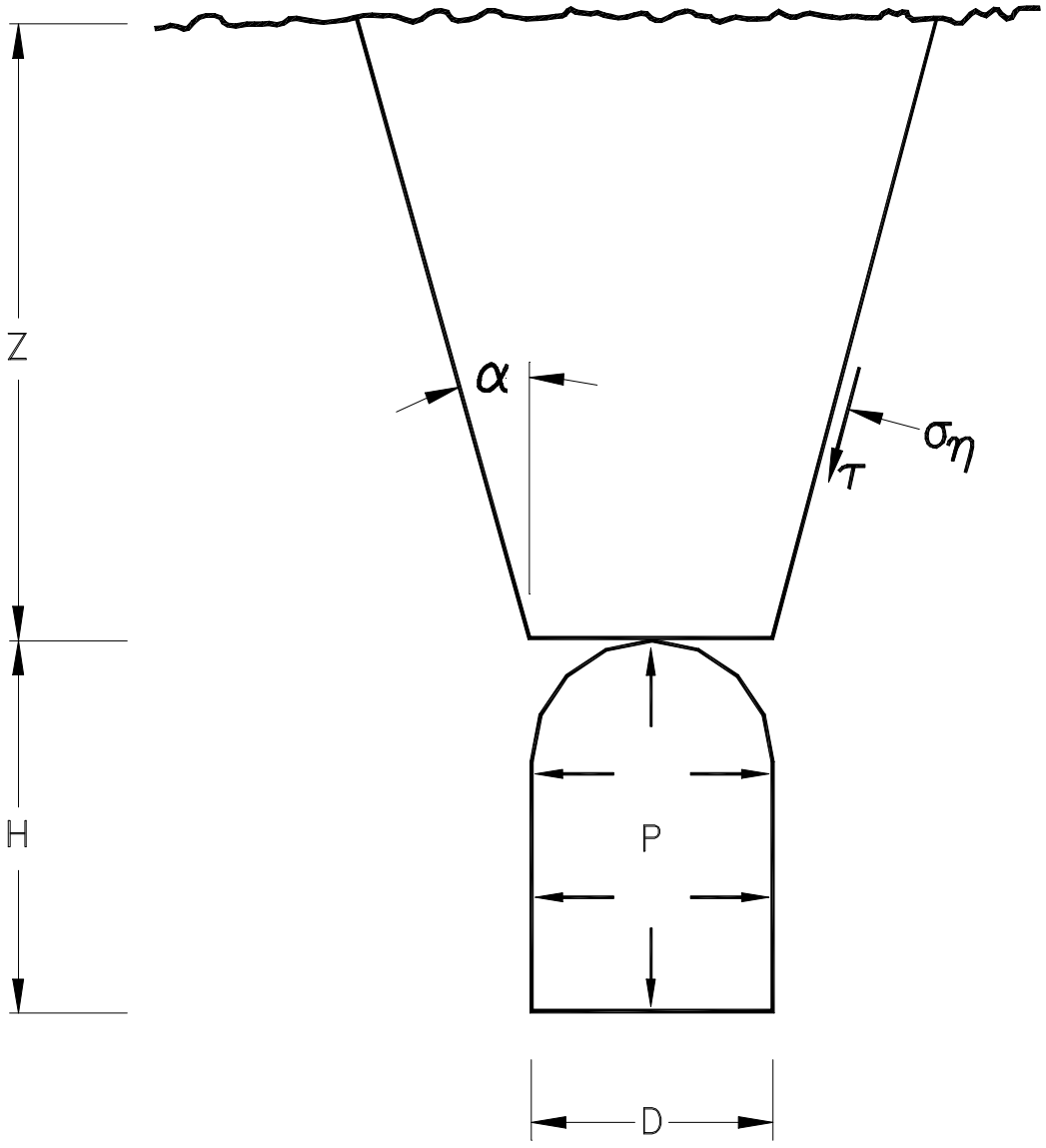

Figure 2-4. Simple Model for Calculating the Uplift Effect.

concrete layer, which in turn, is supported by the surrounding rock mass. The lining shall, however, be able to resist the stress and strain caused by the general elastic and plastic deformation of the cavern wall. In addition, with increasing gas pressure, fractures and cracks will open up in the rock mass. These will initiate smaller cracks in the concrete layer. The liner must then have the capacity to withstand the strain resulting from the spanning of the largest of those cracks. Experiments have shown that many lining materials can support crack spans of up to 2 millimeters in the concrete layer without any problem.

The maximum operating pressure permissible for the storage depends on the lining characteristics and the geological conditions. It must be set at a value such that the induced deformation in the rock mass and the concrete layer does not result in a strain in the lining in excess of its capacity for deformation.

Another issue to consider when designing the lining of the cavern wall is its durability in terms of resistance to repeated mechanical deformation and to chemical aggressiveness. Numerous materials have been tested by the Geotechnical Engineering Department of the Chalmers Technological University of Gothenburg, Sweden. Two categories of material were tested:

- Plastic materials
- Steel.

A number of plastic lining materials have been tested in the laboratory, including polyethylene (PE), poly-vinyl chloride (PVC), and butyl. Low-density polyethylene (LDPE) and PVC show better deformation capabilities than high-density polyethylene (HDPE). Those materials are flexible enough to be used on irregular surfaces. However, it is known that some of the condensates contained in natural gas may soften plastic materials, and long-term imperviousness cannot be guaranteed. Of the common plastic materials, only certain polypropylenes have been classified to be chemically stable and impervious in the long term.

In addition to plastic materials, both carbon steel and thin stainless steel linings have been studied. The carbon steel concept can be described as a conventional storage tank placed in a rock cavern with the space between the tank and the rock filled in with concrete. Stainless steel is more resistant to corrosion than carbon steel. The stainless steel selected for the tests and for further consideration is an austenitic steel, which is ductile and has the ability to bridge over cracks.

2.2.5 Drainage System

Since the lined rock caverns are planned to be placed at 100-200 meters (300-600 feet) in depth, the hydrostatic pressure outside of the cavern due to the column of groundwater can be 1-2 MPa (150-300 psi). If the operating gas pressure within the cavern is expected to be lower

than the hydrostatic pressure outside the cavern, or if the cavern is depressurized to the atmospheric pressure for inspection and/or maintenance, the lining could be exposed to a load from the outside. A drainage system installed outside the cavern, within its wall, could have the function of reducing that hydrostatic pressure by draining the flowing groundwater.

2.3 THE LRC TECHNOLOGY EIGHT-STEP DEVELOPMENT

The LRC technology has been developed step-by-step over a period of more than 10 years, since the initial step in 1987. Seven steps have already been completed, and the eighth and final step, the construction of the demonstration plant, was started in 1998 by the partners in the project: Sydkraft and Gaz de France.

- **Step 1 - Conceptual Studies [Sydgas et al., 1987a, 1987b, 1989; Sydgas, 1990a, 1990b, 1992; Sydkraft and Vattenfall, 1992]**

The first step consisted of basic conceptual studies and was conducted from 1987 through 1992 by a combination of Scandinavian companies, including Sydkraft, Sydgas, Swedgas, and Vattenfall. These studies principally addressed the issue of the cavern lining and its tightness to gas.

- **Step 2 - Experimental Tests [Stille et al., 1994]**

During the second step, from 1990 to 1994, the two concepts of gas storage in rock caverns with a water seal and storage at low temperature (chilled storage) were studied through a series of tests performed in the Röda Sten experimental rock cavern.

- **Step 3 - Grängesberg Pilot Plant [Stille et al., 1994]**

A pilot plant was constructed in 1988-1989 at Grängesberg and was used for testing from 1989 through 1993. The purpose was to experiment with different linings, to test the cavern under pressure and evaluate the effect of increasing pressure, to test the benefit of reduced storage temperature, to further investigate the feasibility of stainless steel lining, to better understand the fracture mechanism in the surrounding rock, and to test the consequence of leakage in the liner at high pressure. The results of this pilot plant at Grängesberg are presented in Section 2.4.

- **Step 4 - Test Plant Results Interpretation**

The fourth step consisted of compiling and analyzing the test plant results and was completed in 1995.

- **Step 5 - Technical Studies [Sydkraft and Skanska, 1995a; 1995b; 1995c; 1995d; 1995e; 1995f; 1995g; 1995h; 1995i; 1995j]**

The fifth step, implemented in 1994-1995, included various technical studies, such as definition of operating conditions, siting criteria, risk analysis, modeling of sandwich wall

construction and drainage system, rock mechanics studies, quality assurance, creation of the circulation system, and development of an aboveground plant simplified design.

- **Step 6 - Engineering Studies**

During the sixth step, from 1994-1996, engineering work was accomplished, including optimization of costs, design of sandwich wall and drainage system, gas leakage detection, study of high withdrawal and injection rates, quality control, and market analysis.

- **Step 7 - Risk Assessment and Preliminary Design [Sydkraft and Gaz de France, 1996a; 1996b; 1997]**

The seventh step, started in 1996, was completed in 1997. It addressed mostly the risk assessment and the preliminary design of the demonstration plant.

- **Step 8 - Demonstration Project**

Implementation of the eighth step was approved by the partners in October 1997. This step consists of building and testing a demonstration plant of industrial scale. The construction work started in the fall of 1998, and commissioning is scheduled for the beginning of 2001. The storage will be located at Skallen near Halmstad in southern Sweden. The geometric volume will be 40,000 m^3 (1.4 MMcf or 250,000 barrels (bbls)), which is about one-half the size of a commercial cavern.

2.4 SUMMARY OF THE GRÄNGESBERG PILOT PLANT RESULTS

2.4.1 Test Plan General Description

The LRC concept was successfully tested in the pilot plant of Grängesberg between 1988 - 1992 (e.g., Stille et al. [1994]). This was a critical step before deciding on building a full-scale demonstration plant. Grängesberg is situated in central Sweden, 250 kilometers west of Stockholm. The predominant type of rock in the area is medium-grained granite. The plant construction was started in 1988 and was completed in 1989. Three test rooms were excavated as vertical cylinders. The schematic of a typical test room is shown in Figure 2-5. Each test room is 4.4 meters in diameter (14 feet) and 9 meters high (28 feet). The rock overburden above the test rooms is 50 meters (179 feet) thick. The rooms are lined on the inside with concrete and steel.

2.4.2 Test Plan Objectives

The main objectives of the test plan were as follows:

- Test the entire system under realistic load conditions.
- Test and evaluate different lining materials.

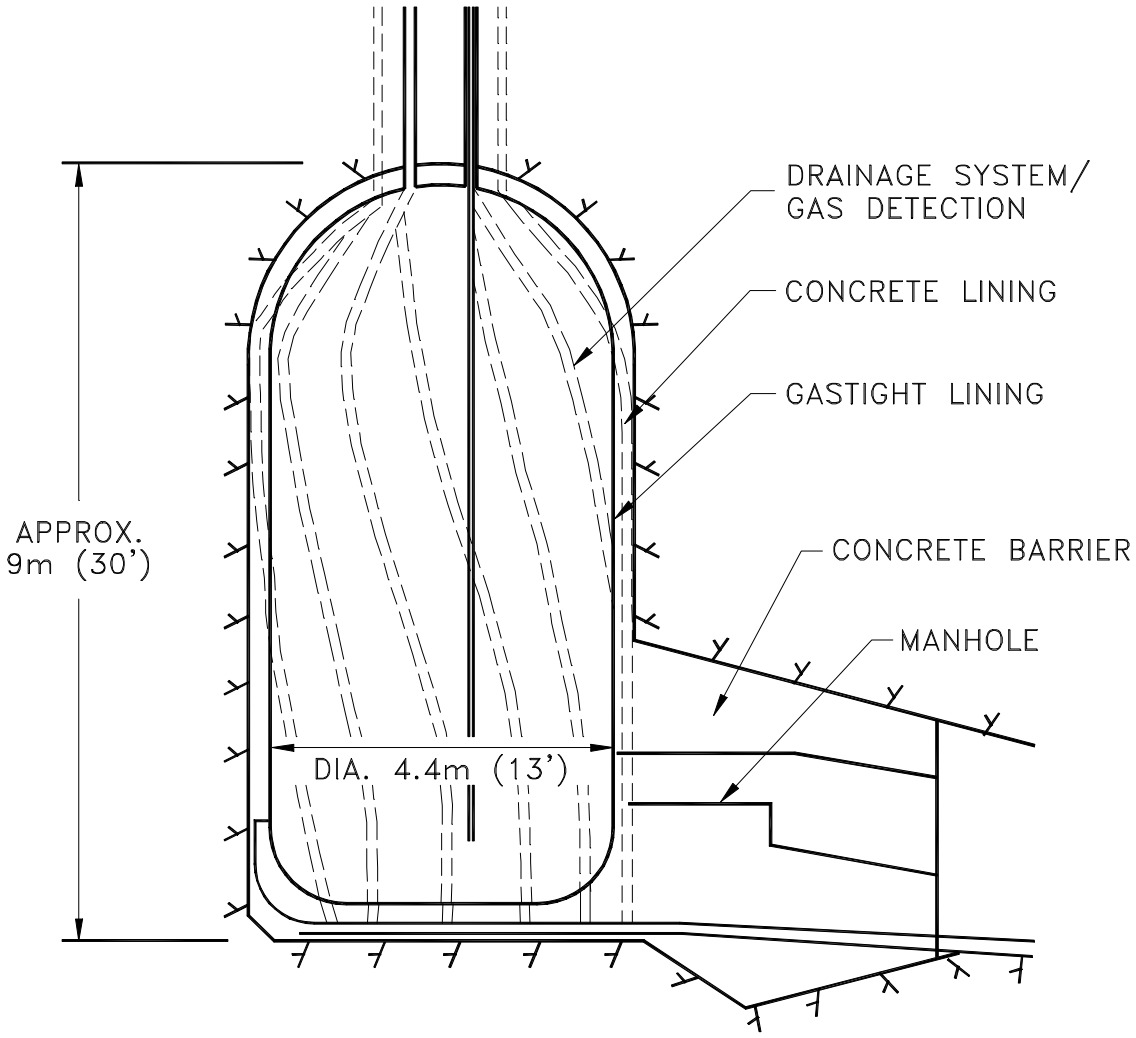

Figure 2-5. Schematic Illustration of a Typical Test Room at Grängesberg, Sweden.

- Analyze bedrock behavior under different pressure and temperature conditions.
- Test the drainage system.
- Demonstrate the viability of the LRC concept on a small scale.

In order to achieve those objectives, each of the test rooms was heavily equipped with instrumentation for several different independent measurement systems, including:

- Extensometers measuring movements in the rock radially and vertically
- Mini-extensometers measuring movement at the interface between rock and concrete
- Convergence meters measuring the remaining deformation after each test
- Measurement to determine the remaining deformation in the lining
- Convergence measurement to determine deformation in the concrete barriers and in the adjacent tunnels
- Continuous monitoring of pressure and temperature in the test rooms and continuous temperature monitoring in the concrete layer and the rock.

2.4.3 Test Program

Tests were carried out in four phases during 1989-1993. Room #1 was lined with thin stainless steel. Room #2 was lined with carbon steel. Room #3 was initially lined with polypropylene which ruptured in an early stage of the test, and the room was later relined with thin stainless steel.

Limited pressure tests have been carried out in Room #1 with a maximum pressure of 14 MPa (2,000 psi). In Room #2, comprehensive pressure tests have been carried out, including more than 200 load cycles up to a maximum pressure of 52 MPa (7,500 psi). Room #3 has been subjected to a great number of load cycles up to a maximum pressure of 26 MPa (3,800 psi).

2.4.4 Test Results

The deformations measured in the surrounding rock, the concrete layer, and the lining were relatively small considering the high-pressure levels experienced. The rock mass accounted for 50 percent of the total radial deformation in the lining. The remaining 50 percent was absorbed by the concrete layer and the transition zone between the concrete and the rock. The concrete layer, when inspected after dismantling the steel liner, was relatively intact. Cracks and crack zones were formed, but no large pieces of loose concrete nor crushed zones were found. Strains in the steel higher than the yield point were observed. However, the metallurgic analysis performed on samples showed that the structure and properties of the steel had not been modified by the high-pressure loading.

The most important result from the Grängesberg tests was that the rock mass proved its function as a pressure vessel at pressure levels comparable to those intended for a commercial storage plant. The maximum operating pressure of the commercial plant has to be selected according to the surrounding rock mass mechanical properties so that the capacity of deformation of the liner is not exceeded.

2.5 SUMMARY

The LRC technology has been developed step-by-step over a period of 10 years and has been proven technically feasible through the various tests performed at the Grängesberg Pilot Plant. The LRC storage concept has the following advantages compared to the conventional underground storage of natural gas:

- The size of the LRC storage can be customized to specific needs and can be then expanded by phases, if needed.
- Provided that adequate geology is present, LRC storage can be located at gas consumption centers.
- Gas is never in contact with groundwater, and dehydration during the withdrawal mode is unnecessary.
- LRC storage is structurally stable and the base gas requirement is minimal.
- LRC storage possesses the same ability as a salt cavern to deliver high withdrawal rates and to be cycled several times in a year.

3.0 MARKET DATA COLLECTION FOR CONVENTIONAL ALTERNATIVES

3.1 STORAGE DEMANDS

The storage alternatives that LRC has to compete with are depleted fields, aquifers, salt caverns, and LNG. When comparing different alternatives, several aspects have to be considered, depending on the end customers' need. The customer profile and transportation profile will create the type of service needed from the storage; thus, determining which cost aspect is the most important for the storage to possess: low cost per working gas, low cost per deliverability, or low cost for swing service and multiple cycles.

The customer profile is determined by the type of customer and the type of service needed from storage. The main customers for an underground storage service are:

- Local Distribution Companies (LDC)
- Power generation companies
- Transportation companies
- Marketers.

The LDCs supply residential and commercial customers in their territory. They have a monopoly for that service, but there is an ongoing process of dissolving this monopoly. The LDCs mainly have two types of variations in demand to consider:

1. Seasonal variations between winter and summer
2. Peak variations due to extreme weather conditions.

The power generation companies are anticipated to cause the major growth in gas consumption along the Atlantic coast. If a power plant is not a base-load plant, the plant will need to face several variations in their load:

- Seasonal variation with winter and summer peaks (air conditioning)
- Weekly, daily, and hourly variations due to lower power demand during weekends and peak demands during mornings and evenings.

The short-term variations require close proximity between the power plant and the storage to be able to deliver the high amounts at a very short notice. If the distance between the storage and the power plant is too long, a short-term peak demand can cause a pressure drop in the supplying pipeline; thus, reducing the transportation capacity in the pipeline that supplies the power plant as well as other customers with natural gas.

The transportation companies need to balance swing in pipeline demand in order to maximize annual transmission capacity. They also provide "no-notice" and other swing services, creating variations that can be balanced with storage.

Marketers are used more and more by LDCs and power generation companies to coordinate the supply and transportation arrangements from the gas supply areas to the market. In that role, they have the same basic needs for storage as the LDC or power generation company. Often, a marketer tries to optimize the supply portfolio by utilizing short-term contracts and futures; thus, taking opportunities from the prevailing market. These activities also result in a demand for short-term storage (i.e., parking and loaning).

Based on the background given above, storage cost is interesting to study from different perspectives, depending on the customer demand. The different types of storage have different profiles, which makes them more or less attractive, depending on the anticipated service. Cost parameters of interest to study when comparing different types of storage are:

- Investment cost/cost of service
  - per working gas
  - per deliverability
  - per swing
  - for multiple cycles
- Operational cost.

Figure 3-1 shows typical performance for different types of storage. This figure illustrates the base for the storage cost profile for the different types of storage user. From the matrix, one can see that salt cavern and LRC are interesting for relatively small volumes and have good injection and withdrawal performance, which means they are suitable for peak service, swing service, parking and loaning, and balancing in pipelines and power generation.

3.2 GENERAL INVESTMENT COST PROFILE FOR UNITED STATES UNDER-GROUND NATURAL GAS STORAGE

In order to provide a picture of average levels of United States' storage investment costs, the capital investment cost data for projects available from the Energy and Environmental Inc. [1994] and Thompson [1997] are presented in Figures 3-2 through 3-7. The different storage types have been divided into three major groups based on their working gas capacity. In order to reflect the full range of the costs, all projects are represented by the light-colored bar.

RSI-835-99-084

Characteristics						Depleted Reservoir	Aquifer	Salt Cavern	LNG	LRC
Working gas (WG) (Bcf)	<2	2–10	>10							
Injection rate % of WG/day	<1	1–5	>5							
Possible annual cycles	<=1	Some	Several							
Possible location in market (New storage)	Rare	Some	Good							
Swing possibilities	None	Some	High							
Expansion possibilities	None	Some	Good							

Figure 3-1. Matrix Showing Characteristics for Different Types of Storage.

RSI-835-99-085

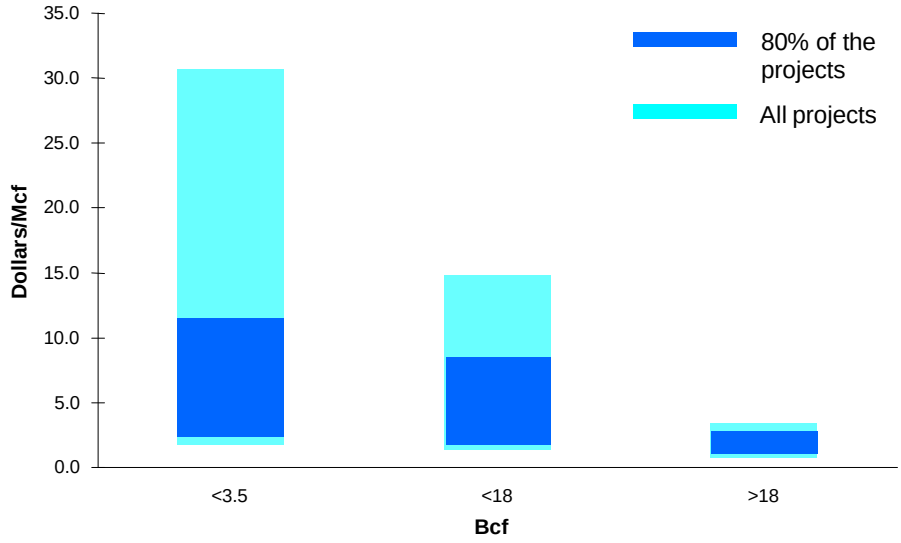

No. of projects = 41
Median costs for capacity for sizes:
<3.5 Bcf = $5/Mcf
<18 Bcf = $3/Mcf
>18 Bcf = $2/Mcf

Figure 3-2. Depleted Field Investment Cost per Unit Working Gas Volume.

RSI-835-99-086

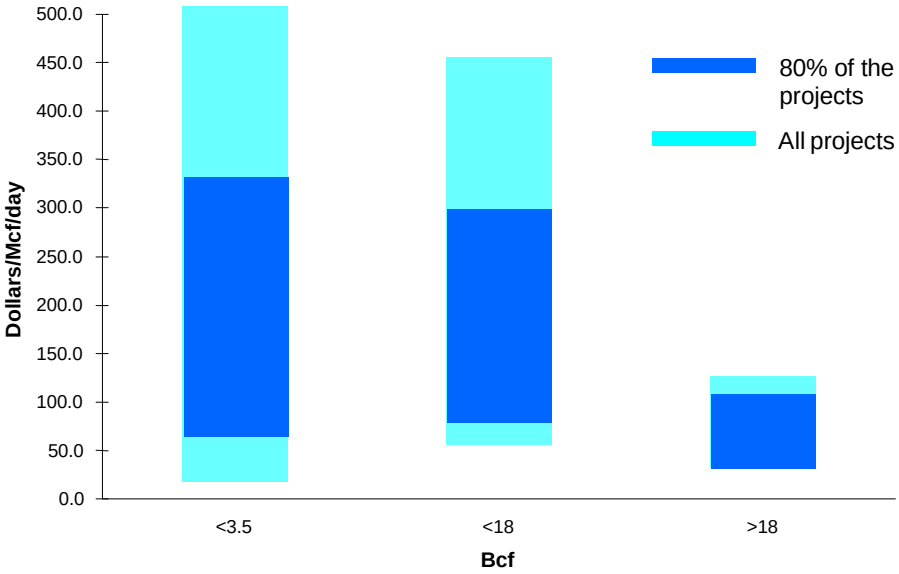

No. of projects = 41
Median costs for withdrawal rates for capacity sizes:
<3.5 Bcf = $150/Mcf/day
<18 Bcf = $140/Mcf/day
>18 Bcf = $100/Mcf/day

Figure 3-3. Depleted Field Investment Cost per Unit Withdrawal Rate.

RSI-835-99-087

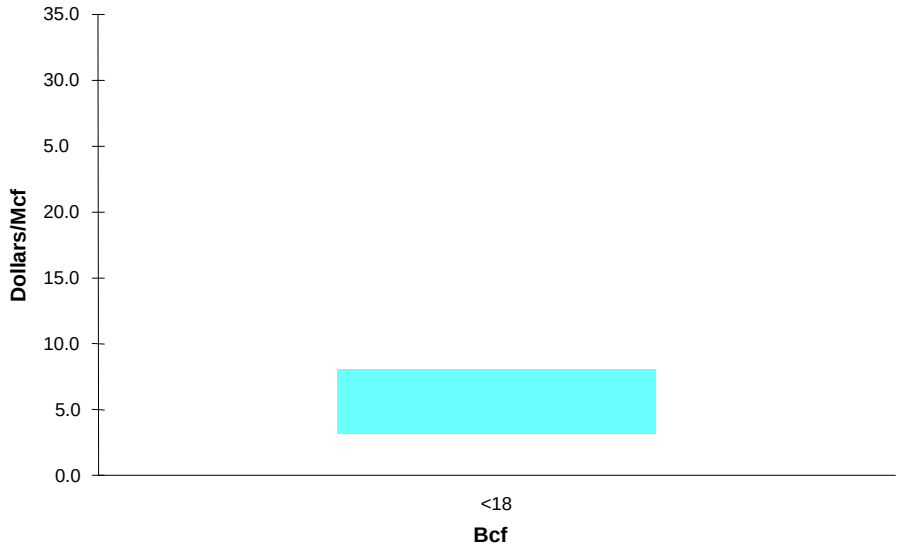

No. of projects = 3
Median costs per capacity size:
<18 Bcf = $4/Mcf

Figure 3-4. Aquifer Storage Investment Cost per Unit Working Gas Volume.

RSI-835-99-088

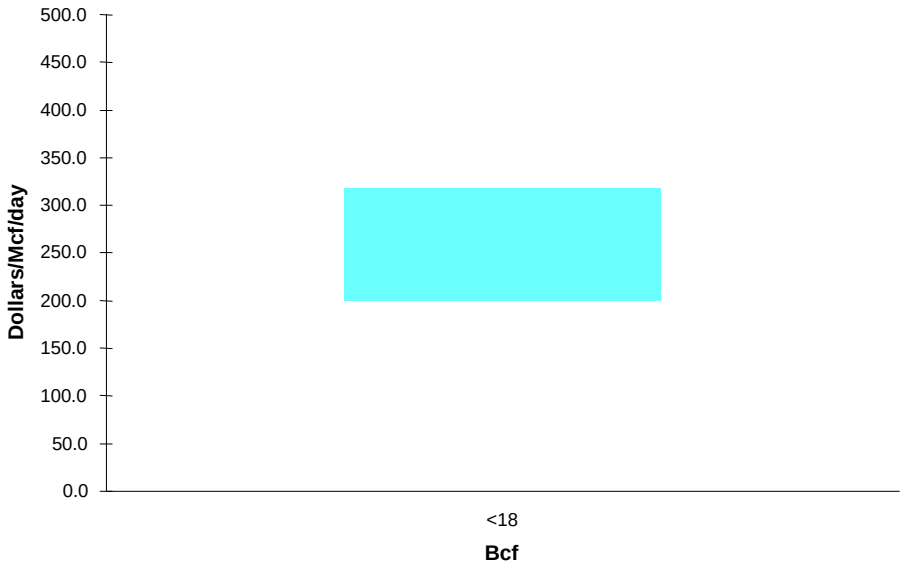

No. of projects = 3
Median costs per withdrawal rate for capacity size:
<18 Bcf = $290/Mcf/day

Figure 3-5. Aquifer Storage Investment Cost per Unit Withdrawal Rate.

RSI-835-99-089

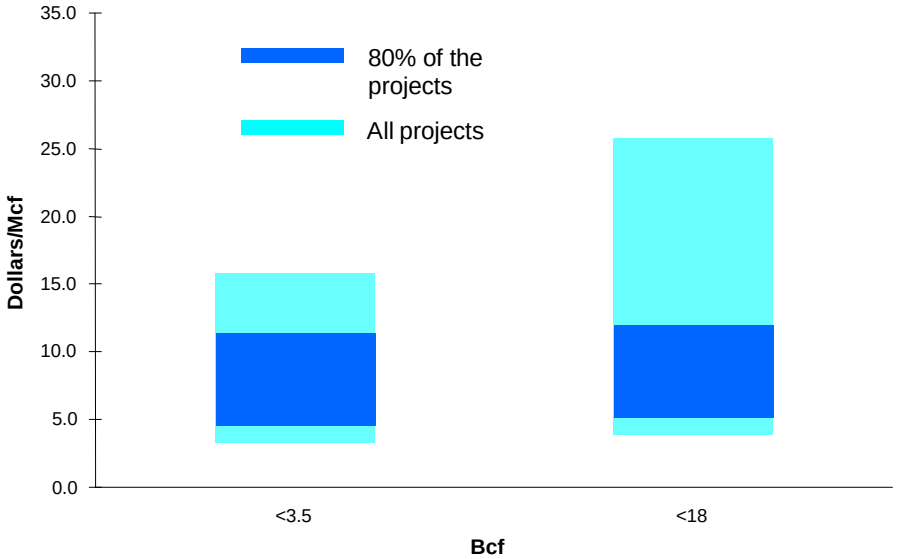

No. of projects = 24
Median costs for capacity sizes:
<3.5 Bcf = $8.6/Mcf
<18 Bcf = $8.2/Mcf

Figure 3-6. Salt Cavern Investment Cost per Unit Working Gas Volume.

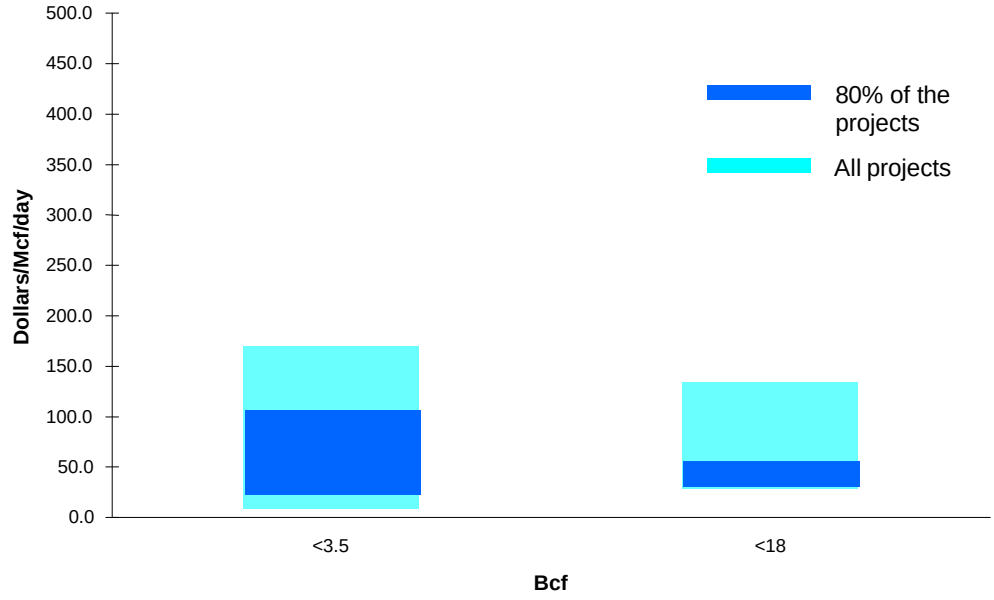

No. of projects = 24
Median costs per withdrawal rates for capacity sizes:
<3.5 Bcf = $52/Mcf/day
<18 Bcf = $57/Mcf/day

Figure 3-7. Salt Cavern Investment Cost per Unit Withdrawal Rate.

To get a better feeling for the most likely cost, a second grouping of projects, including 80 percent of the total number of projects, are represented by the dark bar. The dark bar shows the cost range if 10 percent of the storage projects with the highest and lowest cost are excluded.

The investment cost data are summarized in Tables 3-1 and 3-2. The main conclusion that can be drawn from this information is that the cost of storage depends to a large extent on the utilization of the storage. If the need is a seasonal storage with a large working gas capacity, then depleted fields and aquifers offer the lowest cost. On the other hand, if high withdrawal rates are needed for peaking services, then salt caverns offer the lowest cost.

Table 3-1. Summary of Median Size and Investment Cost per Unit Working Gas Volume

Type	No. of Projects	Median Size (Bcf)	Median Cost ($/Mcf)
Aquifer	3	9	4.0
Depleted Field	41	6	3.3
Salt Cavern	24	5	8.3

Table 3-2. Summary of Median Size and Cost per Unit Withdrawal Rate

Type	No. of Projects	Median Size (Mcf/Day)	Median Cost ($/Mcf/Day)
Aquifer	3	81	292
Depleted Field	41	61	137
Salt Cavern	24	506	55

For salt caverns, there is a link between the high cost for working gas and the high cost for deliverability. For depleted fields, it is often the demand for high deliverability that causes an increased cost for working gas due to more wells and more compressor power.

It also has to be kept in mind that cavern storage can be cycled several times per year, which essentially increases the available working gas capacity. If the storage is located where this multiple-cycling capability can be utilized, it will decrease the unit cost for the available working gas volume considerably. There is a clear trend in the United States for an increasing demand for cavern storage because of the high flexibility and lower cost for deliverability.

4.0 IDENTIFICATION AND SELECTION OF TWO GEOLOGIC CASES

4.1 OVERVIEW

Figure 4-1 illustrates the major pipelines and salt basins in the United States, as well as the outcrops of Precambrian and Premesozoic rocks. The latter are candidate formations for LRC. Clearly, sites for LRC are principally in the East.

Two areas in the eastern United States were selected for LRC assessment: New England and the Southeast area. These two areas do not have the potential for conventional storage within or reasonably close to their market areas and are in primarily igneous and metamorphic geologic terrain. In addition, they are both at the eastern end of the national gas transmission system. Both of these areas depend upon LNG for a portion of their supply to meet peak-day (needle peaking) needs. Both areas would benefit greatly from market area, multicycle cavern storage.

Geological data were collected from published sources and summarized to portray the geology in and around each of the two selected areas. The locations of pipelines supplying each area were plotted on the geological maps.

The geology of the United States East Coast is almost entirely igneous and metamorphic terrain except for coastal plain sedimentary cover in the Southeast and portions of the Upper East Coast. None of the coastal plain sediments have been found to be useful for gas storage. There is only one reservoir storage facility on the East Coast located in the western part of the state of Maryland - the Accident Field with 15.3 billion cubic feet (bcf) of working gas, 62 bcf total capacity. The two regional areas studied are in crystalline igneous or metamorphic rocks adjacent to major supply pipelines and in close proximity to city gates. Both sites are described in more detail below.

4.2 BEDROCK GEOLOGY OF NEW ENGLAND

The geology of New England is both complex and diverse. Major geologic features of the area are summarized below and are illustrated in Figure 4-2.

4.2.1 Regional Geology

Eastern Massachusetts is composed of two terrains which differ in stratigraphy, metamorphism, and plutonism. These are the Nashoba zone and the Milford-Dedham zone. The Nashoba zone, which is bounded on the northwest by the Clinton-Newbury fault and on the

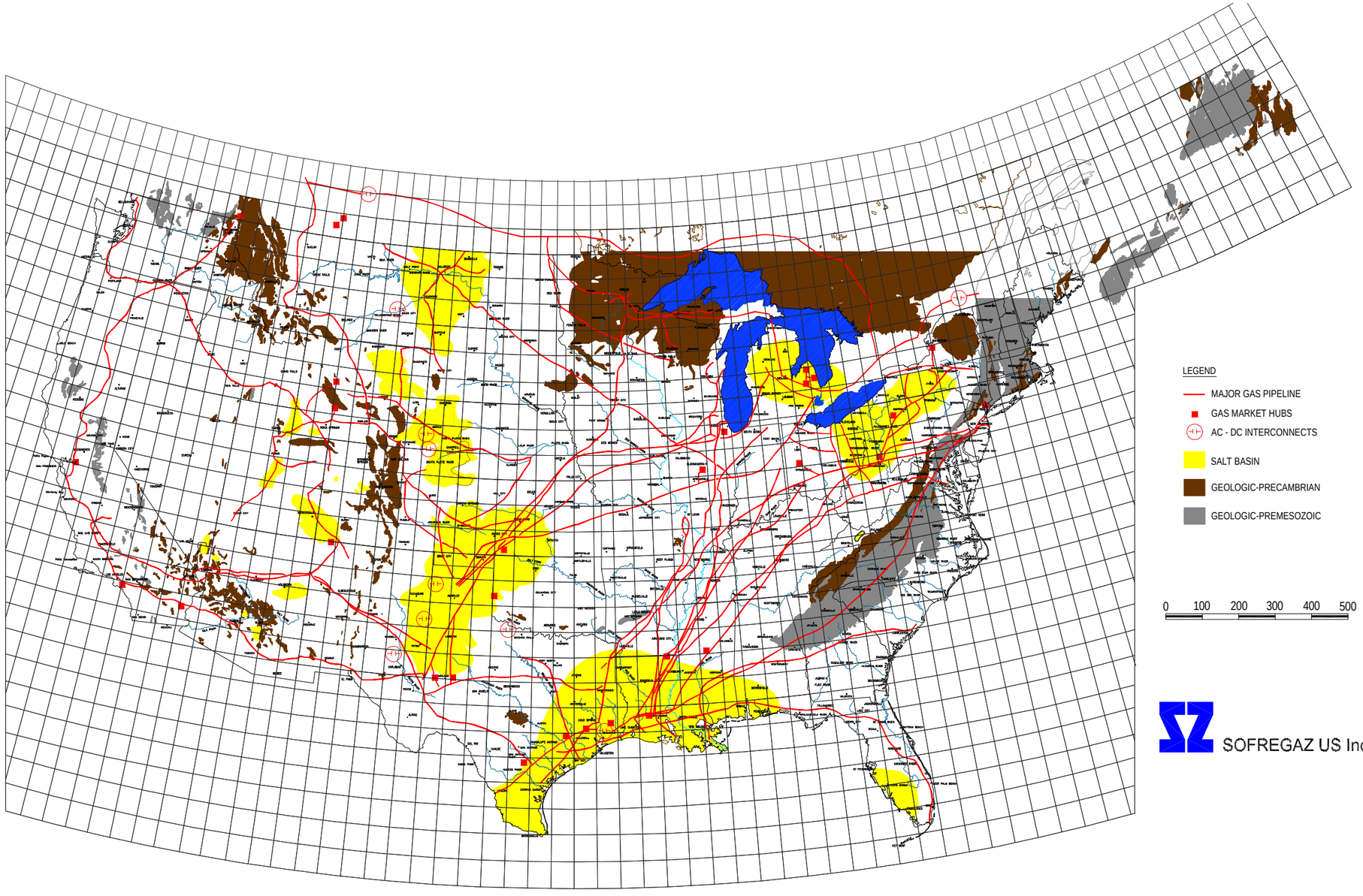

Figure 4-1. Major Pipelines, Salt Basins, and Precambrian and Premesozoic Outcrops in the United States.

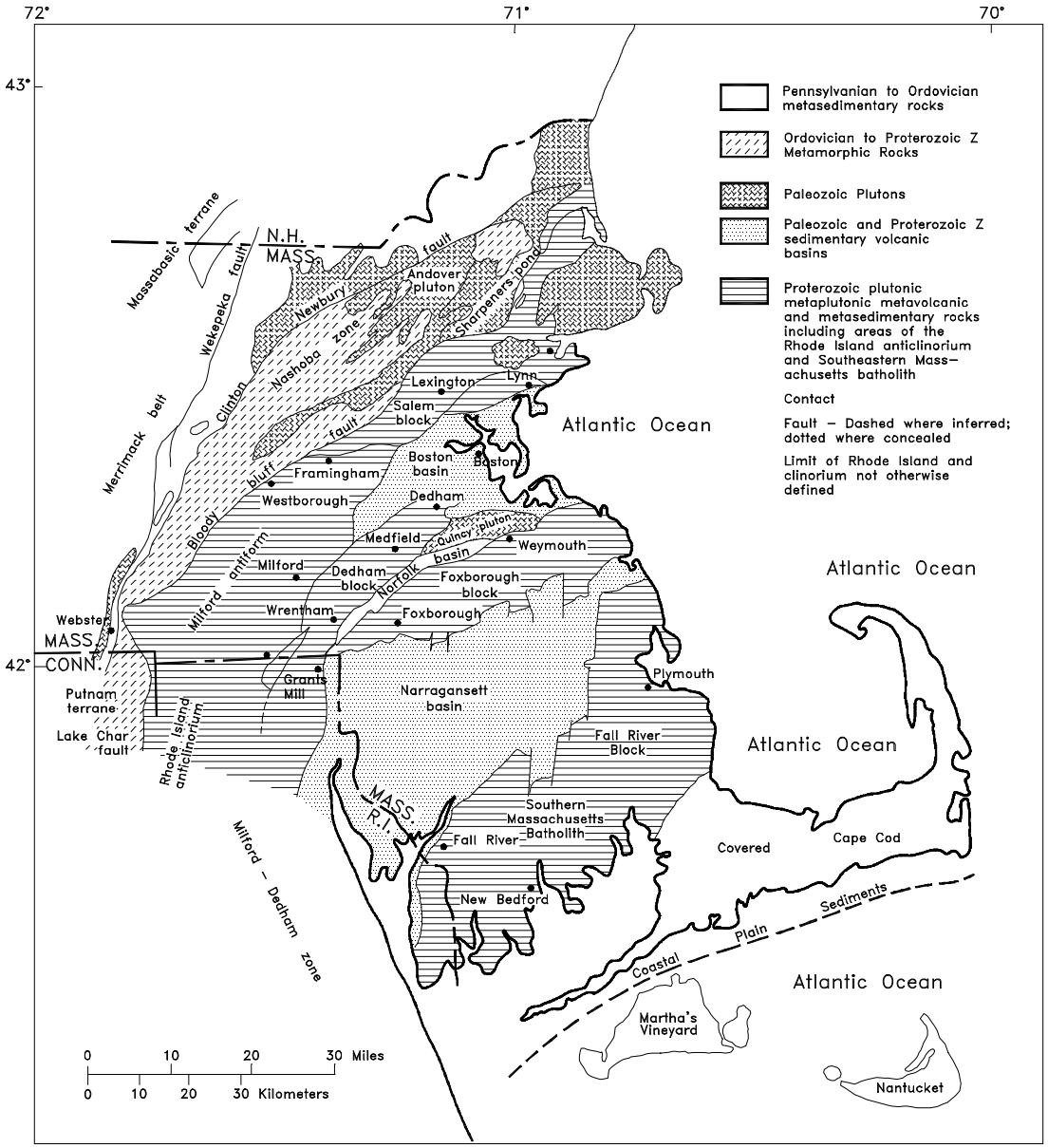

Figure 4-2. Index Map and Major Structural Features of Eastern Massachusetts (After Goldsmith [1987]).

southeast by the Bloody Bluff fault, is a high-grade metamorphic belt composed of steeply dipping Proterozoic Z age schist, paragneiss, and rocks intruded by Ordovician, Silurian, and Devonian age plutons. The Milford-Dedham zone, which is bounded on the west and northwest by the Bloody Bluff fault and on the east by an offshore extension of the Meguma terrain of Nova Scotia, consists of mostly crystalline Proterozoic Z age plutonic and metamorphic basement rock which have been intruded by younger Proterozoic Z granite and granodiorite batholiths.

Nashoba Zone

The Nashoba zone is a northeast trending belt approximately 25 kilometers wide and 100 kilometers long. The Clinton-Newbury fault, which defines the northwestern boundary of the zone, extends from the Massachusetts-Connecticut border to the Gulf of Maine. The southeastern boundary of the Nashoba zone, which is defined by the Bloody Bluff fault, approximately parallels the Clinton-Newbury fault and is located 20 kilometers northwest of the center of the city of Boston. The Nashoba zone appears to be synformal with only a few large-scale folds identified; however, the zone contains many small-scale easterly trending folds. The zone is cut by many northeast-trending longitudinal faults which are post-Silurian, possibly Mesozoic in age. Older faulting within the zone and in the Clinton-Newbury fault system are west-dipping, low-angle thrust and reverse faults which are possibly of Acadian age. The younger faulting tends to be steeply dipping and is characterized by brecciation and gouge along the fault trace, while the older faults are characterized by mylonite or microbrecciation.

The Nashoba zone lies in a narrow belt of high-grade metamorphism, which consists of pelitic rocks of the Nashoba Formation, Fish Brook Gneiss, Shawsheen Gneiss, Tadmuck Brook Schist, and the Marlboro Formation. These rocks are of Proterozoic Z age (580-730 million years) and represent sedimentation and volcanism within a basin forming adjacent to a volcanic arc. The pelitic rocks of the Nashoba, Shawsheen, and the eastern part of the Tadmuck Brook contain sillimanite-muscovite and sillimanite-orthoclase mineral assemblages, while the pelitic rocks of the Marlboro and western part of the Tadmuck Brook contain mineral assemblages of staurolite and andalucite. The rocks assemblage described have been placed in the sillimanite-almadine-orthoclase subfacies of the highly metamorphosed almadine-amphibolite facies. The mineral associations of the Nashoba belt suggest that these rocks recrystalized at a temperature of 625-650°C and a pressure of 6 kilobars, indicating a burial depth of approximately 23 kilometers. In the northern portion of the Nashoba zone, evidence suggests that additional thermal metamorphism occurred contemporaneous with the emplacement of the Ordovician age Andover Granite. The later emplacement of the Sharpners Pond Diorite during the Silurian and a Devonian age Andover Granite appears to have little additional metamorphic effect.

The intrusive rocks of the Nashoba zone range in age from Ordovician to Devonian and are largely massed in the northern portion of the zone. The Andover Granite intruded in two phases: the Ordovician age Andover Granite (450 million years) covers an area of

approximately 200 square kilometers and is a light-colored, muscovite-garnet-bearing gneissic granite which intruded the formations of the Nashoba zone at all scales. The Sharpners Pond Diorite (430 million years) covers an area of approximately 150 square kilometers and is an hornblende diorite to granodiorite. The Straw Hollow Diorite and Assabet Quartz Diorite, which appear to be slightly older than the Sharpners Pond Diorite, cover an area of approximately 26 square kilometers and are gray to green colored, weakly foliated hornblende diorite to granodiorite. The Devonian age Andover Granite (410 million years) is a light-colored nongneissic binary granite, and in addition, a nongneissic pegmatitic granite which intrudes both the gneissic Andover Granite and the Sharpners Pond Diorite.

Milford-Dedham Zone

The Milford-Dedham zone has been broken by normal and reverse faults into upthrown blocks of Proterozoic age plutonic and metamorphic basement rock and downthrown blocks containing sedimentary and volcanic cover rocks of Proterozoic Z, Cambrian, Silurian-Devonian, Pennsylvanian, Triassic, and Jurassic age. The major upthrown blocks are the Milford antiform, the Salem block, and the southeastern Massachusetts batholith, which is subdivided into the Dedham, Foxborough, and Fall River blocks. The downthrown blocks are the Newbury, Middleton, Boston, Norfolk, Bellingham, and Narragansett basins.

The Milford antiform consists of gneissic plutonic rocks of the Proterozoic Z Sterling Plutonic Suite, Milford Granite, metasedimentary and metavolcanic rocks of the Plainfield and Westboro Formations and the Blackstone Group. The metasedimentary and metavolcanic formations are largely in the amphibole facies of metamorphism and are thought to have undergone metamorphism prior to the intrusion of the plutonic rocks. In general, the Milford antiform is divided into two areas of varying deformation. An extension of the Northern Border fault, which is the boundary between the Milford antiform and the Boston basin, separate the variably deformed amphibole facies plutonic, quartzitic, and paragneissic rocks of the west from the fractured, brittlely deformed greenschist facies plutonic, metasedimentary, and meta-volcanic rocks.

The Milford Granite is located near the town of Milford and occupies an area of approximately 100 square kilometers. The Milford is divided into two phases: a light-colored pink granite and a darker-colored granodiorite. The Milford Granite, along with the Esmond Granite, form the core of the Milford antiform and are relatively undeformed.

The Salem block, which is located north of the Milford antiform, consists primarily of Proterozoic Z age mafic plutonic rocks, mafic to felsic metavolcanic rocks, and minor metasedimentary rocks. These rocks have been intruded by the younger Proterozoic Z age Dedham Granite and Topsfield Granodiorite and by early and middle Paleozoic alkalic granite and gabbro. The metavolcanic and metasedimentary rocks contain assemblages typical of the amphibole facies metamorphism, while the Dedham Granite and Topsfield Granodiorite exhibit metamorphism no higher than the greenschist facies. The Paleozoic age Peabody Granite forms

the core of the Peabody pluton, which has an area of approximately 50 square kilometers. The Peabody Granite is a light-gray to green-colored, weathered granite consisting of alkali feldspar, quartz, and ferrohornblende. The Cape Ann pluton consists of the Ordovician-Silurian age Cape Ann Granite, the Beverly Syenite, and the Squam Granite. Together, these members occupy an area of approximately 385 square kilometers. The Cape Ann Granite is a grayish-green, medium- to coarse-grained granite to quartz syenite. The term Beverly Syenite refers to rocks similar to the Cape Ann but completely absent of quartz. The Squam Granite is a gray to brown, fine- to medium-grained, porphyritic alkalic granite and occupies only an area of 5 square kilometers within the overall Cape Ann Complex.

The Dedham, Foxborough, and Fall River blocks are located southeast of the Milford antiform and Salem block and form the Proterozoic Z age southeastern Massachusetts batholith. The Dedham and Foxborough blocks consist almost entirely of plutonic basement rock; metasedimentary and metavolcanic rocks are rare and are only found as inclusions within the plutonic rock. The plutonic rocks of the Dedham and Foxborough blocks are similar in composition and texture as the Proterozoic Z plutonic rocks of the Salem block, except as a whole, they are significantly less deformed, fractured, or altered. The Fall River block is separated from the Foxborough block by the Narragansett basin. The plutonic rocks are similar in composition and texture to that of the Foxborough block. The Fall River block contains significantly more metasedimentary and metavolcanic basement rock, which grade from the low-grade greenschist facies of metamorphism in the northern part of the block to a high-grade amphibole facies in the south.

The Newbury basin is a small wedge-shaped lenticular basin located between the Nashoba zone and the northern part of the Salem block. The basin is believed to have formed as a graben within the Bloody Bluff fault complex during Paleozoic time. The strata is unmetamorphosed Silurian-Devonian marine sediments and volcanic rocks, which have subsequently been overturned. The Middleton basin lies in the same structural zone as the Newbury basin and includes an area no greater than 6 kilometers long and 0.5 kilometer wide. This basin is filled with Triassic-Jurassic redbed deposits.

The Boston basin, which is separated from the Milford antiform and Salem blocks on the north and west by the Northern Border fault and the Dedham and Foxborough blocks on the south by the Mount Hope and Blue Hills faults, contains unmetamorphosed Proterozoic Z sedimentary and volcanic rocks of the Boston Bay Group overlying basement rocks of the Milford antiform, Salem, and Dedham blocks. The Northern Border fault is a reverse fault approximately 38 kilometers long that has thrust the Salem block and Melrose subblock southeastward over the Boston Bay Group. The throw on this fault is estimated to be 1,300 meters. The Mount Hope fault, which is the northeastern border of the Dedham block, is believed to be a northward-directed thrust fault which has subsequently been rotated to near vertical. The maximum throw on the fault is estimated at 350 meters. The Blue Hill fault, which forms the boundary between the Boston Basin and the Foxborough block, is thought to be

a northward-directed thrust fault which has been subsequently rotated and tilted. The throw on this fault is estimated at 5,000 meters. The Quincy pluton is located on the southern border of the Boston basin and is composed of the Silurian-Ordovician age Quincy Granite and Blue Hills Granite. The pluton occupies an area of approximately 55 square kilometers and is described as a light brown to pink, fine- to coarse-grained hornblende granite.

The Norfolk basin is located between the Dedham and Foxborough blocks and is similar to the Narragansett basin in that it is composed largely of unmetamorphosed Pennsylvanian age marine and nonmarine sediments overlying Proterozoic Z basement rocks. The basin is fault bounded with throws estimated at 400 meters.

The Bellingham basin, which is located on the Massachusetts-Rhode Island border, is a fault-bounded graben composed primarily of slightly metamorphosed (greenschist facies) Pennsylvanian age nonmarine pebbles to conglomeratees clastic deposits.

The Narragansett basin is located between the Foxborough and Fall River blocks and is composed largely of the unmetamorphosed fine- to medium-grained Pennsylvanian age marine and nonmarine sedimentary rocks. The Pennsylvanian rests nonconformably on the Proterozoic basement rocks. The basin is estimated to be 2,000 meters thick with the maximum subsidence occurring at the northern and southern borders.

4.2.2 Potential Storage Sites

Numerous potential storage sites for LRC exist in the Northeast. From a geomechanics standpoint, evaluation of the Rock Mass Rating (RMR) is perhaps the most expedient method for determining site suitability. Other important site selection factors include pipeline access, ease of permitting, groundwater conditions, local faulting, and access.

4.3 BEDROCK GEOLOGY OF THE SOUTHEAST AREA

The geology of the Southeast United States is nearly as diverse as the Northeast. The major geologic features of the area are summarized below and illustrated in Figure 4-3.

4.3.1 Regional Geology

Northern Georgia encompasses four geographical regions: Cumberland Plateau, Valley and Ridge, Blue Ridge Mountains, and Piedmont Plateau. These geographical regions, except the Piedmont Plateau, are included as part of the Appalachian Mountains. The Cumberland Plateau, which is located in the extreme northwestern corner of the state, is characterized by narrow infertile valleys bordered by high, steep ridges. The Valley and Ridge region lies to the east of the Cumberland Plateau and is characterized by wide, flat fertile valleys separated by

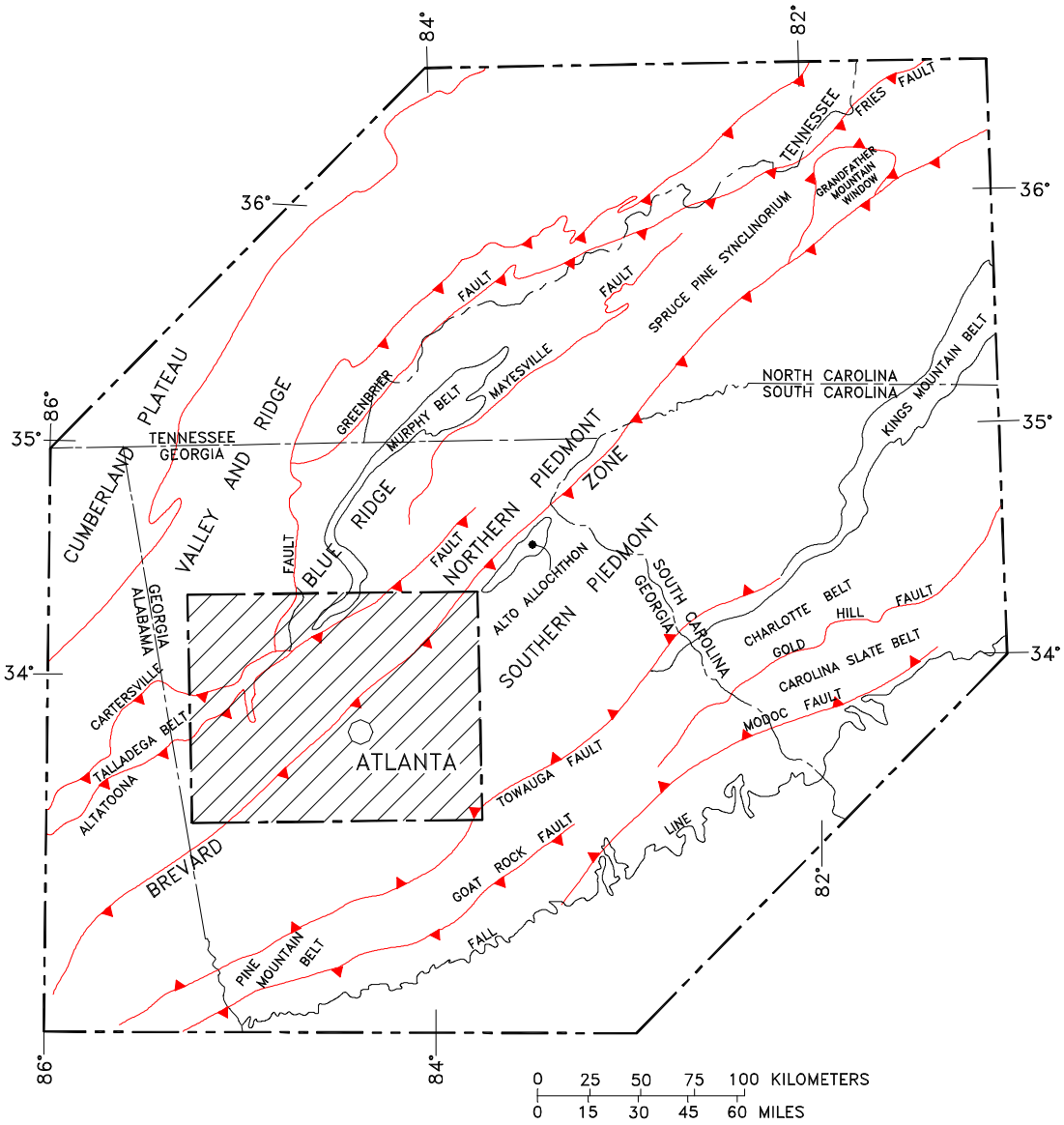

Figure 4-3. Regional Location Map Showing Boundaries of the Greater Atlanta Regional Map and Regional Setting of Map Area (After McConnell and Costello [1982]).

narrow, steep-sided ridges. The Blue Ridge Mountains region is characterized by rounded forested mountains separated by narrow valleys underlain by crystalline bedrock. The Piedmont Plateau makes up most of the northern one-half of the state and is characterized by rolling hills also underlain by crystalline bedrock.

Rocks of the Atlanta region area are divided into three major geologic provinces: Valley and Ridge, Blue Ridge, and Piedmont. The Valley and Ridge Geologic Province is composed of unmetamorphosed to weakly metamorphosed (greenschist facies) Paleozoic age rocks of the foreland thrust and fold belt. The Blue Ridge Geologic Province is composed of metamorphosed Proterozoic Y basement rocks and Proterozoic Z age to early Paleozoic age metasedimentary rocks. The Piedmont Geologic Province is composed of Proterozoic Z age to early Paleozoic age metasedimentary and plutonic rocks. The Piedmont Geologic Province is subdivided into the Northern and Southern Piedmont Provinces and is composed of Proterozoic Z to early Paleozoic metasedimentary, metavolcanic, and plutonic rocks.

Valley and Ridge Province

The Valley and Ridge Province is defined as that region located between the Cumberland Plateau and the Blue Ridge Mountains. The boundary between the Valley and Ridge Province and the Blue Ridge Province corresponds with the trace of the Cartersville fault. Rocks ranging in age from Lower Cambrian to Pennsylvanian are present in this region, but only rocks of Lower Cambrian age are present in the immediate Atlanta area. The oldest rocks in the province are represented by the Chilhowee Group, Cochran Formation, Nichols Formation, Wilson Ridge Formation, and Weisner Formation.

The Wilson Ridge and Weisner Formations are the only members of the Chilhowee Group present in the Atlanta area. Rocks of the Wilson Ridge Formation are described as fine- to coarse-grained, moderately well-sorted orthoquartzite. Overlying the Wilson Ridge is the Weisner Formation, which is composed of rocks described as very fine- to fine-grained orthoquartzite, cross-bedded fine- to coarse-grained orthoquartzite, conglomerate and grayish-green mudstone.

Overlying the Weisner is the Shady Dolomite, which is described as a thin, dark gray to black, fine-grained dolomite having paper-thin shale lamellae. The Rome Formation overlies the Shady Dolomite and is described as a red- to green-colored, fine-grained, slight calcareous sandstone with some thin layers of limestone present.

Blue Ridge Province

The Blue Ridge Province is defined as those rocks present between the Cartersville fault on the north and the Allatoona fault on the south. The Blue Ridge portion of the Atlanta region area is dominated by two structural features: the Salem Church anticlinorium and the Murphy synclinorium.

The Salem Church anticlinorium is composed of the Proterozoic Y (1,000 million years) age Corbin Gneiss Complex and the Proterozoic Z age Ocoee SuperGroup: Snowbird Group, Walden Creek Group, and Great Smoky Group. Rocks comprising the Corbin Gneiss Complex form the core of the Salem Church anticlinorium and consists of a paragneiss described as a coarse-grained, quartz-monzonitic orthogeneiss- medium- to coarse-grained, orthoclase-mica gneiss and metaigneous granite and granodiorite. The Snowbird Group consists of the Pinelog Formation, which unconformably overlies the Corbin Gneiss. The Pinelog Formation is described as poorly sorted quartz-pebble metaconglomerate, metasandstone, metasiltstone, and metashale. Rocks of the Pinelog Formation are erosional in origin and are derived from the granitic Corbin Gneiss facies. Overlying the Pinelog is the Wilhite Formation of the Walden Creek Group, which consists of a think sequence of metasandstone, sandy marble, and calcareous metasiltstone. The Great Smoky Group is the uppermost member of the Ocoee SuperGroup and consists of the Etowah Formation, Sweetwater Creek Formation, and the Dean Formation. The Etowah Formation lies conformably on the Wilhite Formation and consists of a monotonous sequence of interlayered metasandstones and meta-argillite with small lenses of calc-silicate granofels. Overlying the Etowah is the Sweetwater Creek Formation which consists of poorly sorted coarse-grained conglomeritic metasandstone with thin interbeds of graphitic phyllite. The Dean Formation is the uppermost member of the Great Smoky Group and consists of a moderately well sorted quartz-pebble metaconglomerate.

Within the Murphy synclinorium, the Dean Formation is overlain by Lower Paleozoic age rocks of the Murphy Belt Group: Nantahala Formation, Brasstown Formation, Murphy Marble, Marble Hills Hornblende Schist, and the Mineral Bluff Formation. The Nantahala Formation is predominantly a carbonaceous phyllite to laminated argillite with interbeds of fine- to medium-grained metasandstone. Overlying the Nantahala is the Brasstown Formation which consists of interlayered gray schists and micaceous quartzites. The Murphy Marble, which is a fine- to medium-grained calcitic to dolomitic marble, overlies the Brasstown and is a high-quality commercial quarried commodity. The Murphy Marble grades upward culminating in the Marble Hills Hornblende Schist. A relatively thin transition zone is considered the formation boundary. The Mineral Bluff Formation is the uppermost member of the Murphy Belt Group and is described as a thick sequence of pelitic rocks with included garnet-quartz-sericite schist and pure-sericite schist.

Northern Piedmont Province

The Northern Piedmont Province includes all rocks lying between the Allatoona fault and the Brevard fault and includes the late Precambrian age New Georgia and Sandy Creek Groups. In the Atlanta region area, the New Georgia Group is characterized by the dominance of metavolcanic rocks over metasedimentary rocks. The Sandy Creek Group is the opposite and is characterized by the dominance of metasedimentary rocks over metavolcanic rocks.

The New Georgia Group is exposed in outcrop along a belt 22 kilometers wide and 210 kilometers long and contains most of the base and precious metal deposits in the region. The New

Georgia Group is composed of intermingled beds of metamorphosed felsic and mafic volcanic rocks, plutonic rocks, and a small amount of sedimentary rocks. Metamorphism and intense deformation have obliterated the original sedimentary and volcanic textures, making the internal stratigraphy of the New Georgia Group very difficult. However, portions of the New Georgia Group in the Atlanta region area are well known and have been extensively studied. These stratigraphic units and areas include the Mud Creek Formation in the Villa Rica area, the Pumpkinvine Creek Formation to the northeast of the Villa Rica area, and the Univeter Formation near the town of Univeter.

The Mud Creek Formation is composed of garnetiferous, hornblende-plagioclase amphibolite gneiss interlayered with garnet-biotite schist and gneiss and banded-magnetite quartzite. The Pumpkinvine Formation is composed of hornblende-quartz-plagioclase gneiss interlayered with biotite-muscovite-plagioclase gneiss and amphibolite. The Univeter Formation is composed of a sequence of amphibolite, hornblende gneiss, garnet-biotite-muscovite schist, garnet-chlorite schist, and banded-magnetite quartzite.

The Sandy Springs Group overlies the New Georgia Group and represents the most areally extensive rock group in the Northern Piedmont Province. The Sandy Springs Group is divided into rocks of the eastern belt and the western belt. The Sandy Springs (eastern belt) consists of three formations: Powers Ferry Formation, Chattahoochee Palisades Quartzite, and Factory Shoals Formation. The Powers Ferry Formation is the oldest unit in the Sandy Springs Group and is composed of interlayered gneiss, schist, and amphibolite. Overlying the Powers Ferry is the Chattahoochee Palisades Quartzite, which is described as a massive white to yellowish, sugary to vitreous quartzite containing mica and garnet. Overlying the Chattahoochee Palisades is the Factory Shoals Formation, which is composed of garnet-biotite-oligoclase, which varies from a kyanite-quartz schist to a staurolite-muscovite-quartz schist.

The Sandy Springs (western belt) consists of three formations: Dog River Formation, Andy Mountain Formation, and Bill Arp Formation. The Dog River Formation is composed of interbedded muscovite-biotite-quartz-feldspar gneiss, garnet-muscovite schist, amphibolite, and thin beds of magnatite quartzite. Overlying the Dog River is the Andy Mountain Formation, which is composed of garnet-muscovite-quartz schist and sugary quartzite. The Bill Arp Formation is the uppermost member of the Sandy Springs (western belt) Group and consists of interlayered garnet-biotite-muscovite-plagioclase-quartz schist and metagraywacke.

Southern Piedmont Province

The city of Atlanta is located within the Southern Piedmont Province. The Southern Piedmont Province is defined as those rocks lying between the Brevard fault and the Atlantic Coastal Plain and includes late Proterozoic Z to early Paleozoic rocks of the Atlanta Group. The similarity of the rock units and stratigraphic sequence indicates the rocks of the Atlanta Group are equivalent to those of the New Georgia and Sandy Springs Group. The Southern Piedmont Province has been complicated by intrusion of late Paleozoic plutons but is currently accepted

that the rocks south of the Brevard fault were deposited in similar environments as the rocks north of the Brevard fault. In general, the Camp Creek and Big Cotton Indian Formations of the Southern Piedmont are equivalent to the New Georgia Group. The Clarkston, Stonewall, Wahoo Creek, Clairmont, Norcross Gneiss, and Promise Land Formations of the Southern Piedmont are equivalent to the Powers Ferry Formation of the Sandy Springs Group. The Lanier Mountain Quartzite of the Southern Piedmont is equivalent to Chattahoochee Palisades Quartzite, and the Norris Lake Schist is equivalent to the Factory Shoals Formation.

Plutonic Rocks

Post Grenville (Proterozoic Y) age-intrusive rocks are generally limited to the Piedmont Provinces, although numerous pegmatites occur in the Blue Ridge Province. Plutons of Grenville age or older are limited to the Corbin Gneiss Complex in the Blue Ridge Province. Paleozoic-intrusive rocks in the Piedmont Provinces are divided into three categories: premetamorphic, presynmetamorphic, and postmetamorphic. Paleozoic metamorphism is not exactly known or defined but has been interpreted to have occurred at approximately 265 million years.

Intrusive rocks in the Piedmont Provinces that were emplaced prior to metamorphism and subsequent deformation have lost most of their original fabric and texture; however, several premetamorphic plutons are recognized in the Atlanta region area. The Villa Rica Gneiss, Laura Lake Mafic Complex, Acworth Gneiss, Kellogg Creek Mafic Complex, and Galts Ferry Gneiss are members of the premetamorphic category north of the Brevard fault. Biotitic-plagioclase gneisses of the Big Cotton Indian, Camp Creek, possibly Promise Land and Norcross Gneiss formations are premetamorphic intrusives found south of the Brevard fault.

Presynmetamorphic intrusive, like those intrusives in the premetamorphic category, retain deformational fabrics associated with Paleozoic metamorphism. However, unlike those premetamorphic plutons, presynmetamorphic intrusives, they show no direct relationship to surrounding extrusive rocks. In general, presynmetamorphic intrusives contain far more potassium and are considered as peraluminous to meta-aluminous. The Austell, Sand Hill, and Mulberry Rock Gneiss are intrusives found north of the Brevard fault while the Union City Complex is the only intrusive in this category found south of the Brevard fault.

Postmetamorphic-intrusive rocks in the Atlanta region area can be divided into two subdivisions: those emplaced 300-325 million years and those emplaced 180-230 million years. The older of the two subdivisions is represented by large felsic plutons, such as the Stone Mountain, Ben Hill, Panola, and Palmetto Granites, and are limited to the Southern Piedmont Province. These large plutons are similar in texture and composition and are characteristically medium- to coarse-grained porphyritic granites composed of biotite-muscovite-quartz-plagioclase-microcline. These plutonic rocks show no metamorphic overprint or fabric deformation. Intrusives of the younger subdivision are Jurassic-Triassic age diabase dikes and

are also limited to the Southern Piedmont Province except one small diabase dike located in the Blue Ridge Province.

4.3.2 Potential Storage Sites

As with the Northeast, many potential LRC sites exist in the Southeast. Again, evaluating the RMR is perhaps the most expedient method for accessing site suitability from a geomechanics perspective. The groundwater, pipeline access, ease of permitting, and access will also play important roles in siting an LRC in the Southeast.

5.0 CONCEPTUAL DESIGN FOR LRC

5.1 DESIGN PRINCIPLES

Certain aspects of the LRC technology or technology development that were discussed in Chapter 2.0 are discussed again below in more detail to more fully explain the LRC design principles.

5.1.1 Historical Background

More than 10 years of research and development have been invested in the LRC concept. The development work can briefly be described by looking at the eight major steps taken during this period to advance the development of the LRC concept. A brief description of the eight major steps discussed previously in Chapter 2.0 is summarized below.

- **Step 1 - Conceptual Studies**

The first step consisted of basic conceptual studies and was conducted from 1987 through 1992 by a combination of Scandinavian companies, including Sydkraft, Sydgas, Swedgas, and Vattenfall. These studies principally addressed the issue of the cavern lining and its tightness to gas.

- **Step 2 - Experimental Tests**

During the second step, from 1990 to 1994, two concepts of gas storage in rock cavern using a water seal and storage at low temperature (chilled storage) were studied through a series of tests performed in the Röda Sten experimental rock cavern.

- **Step 3 - Grängesberg Pilot Plant**

A pilot plant was constructed in 1988-1989 at Grängesberg in Sweden and used for testing from 1989 through 1993. The purpose was to experiment with different linings and evaluate the effect of increasing pressure, to test the benefit of reduced storage temperature, to further investigate the feasibility of stainless steel lining, to better understand the fracture mechanism in the surrounding rock, and to test the consequence of leakage in the liner at high pressure.

- **Step 4 - Test Plant Result Interpretation**

The fourth step consisted of compiling and analyzing the test plant results and was completed in 1995.

- **Step 5 - Technical Studies**

Technical studies, such as operational conditions, siting criteria, risk analysis, modeling of sandwich wall construction, drainage system, rock mechanics studies, quality assurance,

creation of the circulation system, and aboveground plant simplified design were implemented 1994-1995.

- **Step 6 - Engineering Studies**

During the sixth step, from 1994-1996, engineering work had been accomplished, including design of sandwich wall and drainage system, gas leakage detection, study of high withdrawal and injection rates, quality control, and market analysis.

- **Step 7 - Risk Assessment and Preliminary Design**

The seventh step, started in 1996, was completed in 1997. It addressed mostly the risk assessment and the preliminary design of the demonstration plant. These studies were carried out jointly by the present LRC partners: Gaz de France and Sydkraft.

- **Step 8 - Demonstration Project**

The eighth step, whose implementation was approved by the partners in October 1997, consists of building and testing a demonstration plant of industrial scale. The construction work started in the fall of 1998, and commissioning is scheduled for the beginning of 2001. The storage will be located at Skallen near Halmstad in southern Sweden. The geometric volume will be 40,000 m^3 (1.4 MMcf or 250,000 bbls), which is one-half the size of a commercial cavern.

Besides development of the concept, the efforts made in cooperation with the Royal Institute of Technology in Stockholm, Sweden, and the Chalmers Institute of Technology, Gothenburg, Sweden, have contributed to the knowledge of strength and general behavior of the rock mass that is subjected to the high gas storage pressures.

5.1.2 General Rock Mechanics Aspects

This section will describe general rock mechanical aspects which constitute the basis for the behavior of the rock mass, and thus, the design. The presentation is related to the test plant in Grängesberg which was used for verification and development of the theories behind the LRC concept.

The general approach for the Grängesberg pilot tests was to use established and well-known methods to classify the rock mass in order to establish the rock mass parameters. The parameters were used together with rock mechanics principals for prediction of deformations. The logic chain of the approach is shown in Figure 5-1.

5.1.2.1 Expected General Behavior of the Rock Mass

The expected deformation of the rock mass in the Grängesberg Pilot Plant (see Figure 5-2) was based on the rock mechanics principles (e.g., Brown et al. [1983]; Stille [1984]). The rock mechanics approach, termed here as the "elasto-plastic" approach, is the normal approach for

rock mechanic applications commonly used in Sweden. At low pressures, an elastic behavior is expected. At higher pressures, tensile stresses will occur, starting in the rock surface. When the strength of the rock mass is exceeded, shearing and compression takes place in the joints leading to plastic or irreversible deformations.

RSI-835-99-091

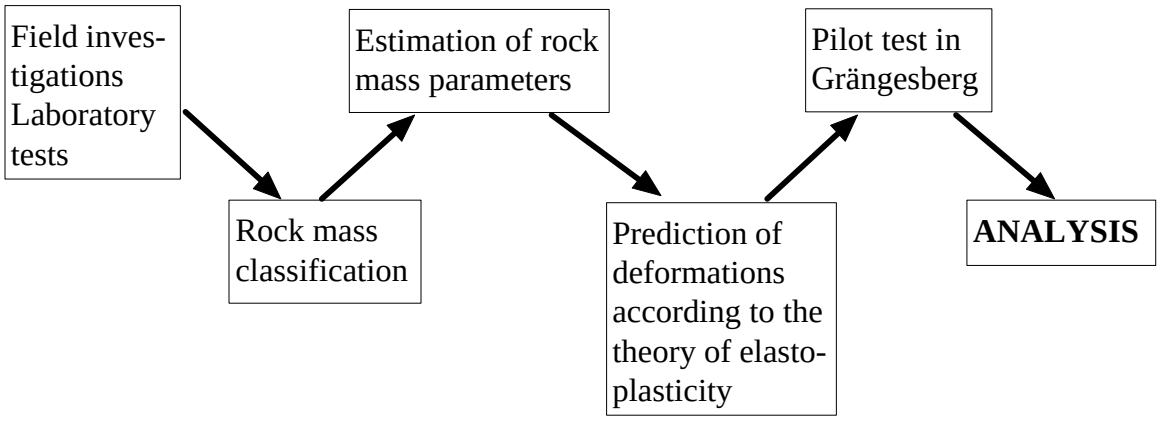

Figure 5-1. The Logic Chain of the Approach Adopted for the Grängesberg Pilot Plant Tests.

RSI-835-99-092

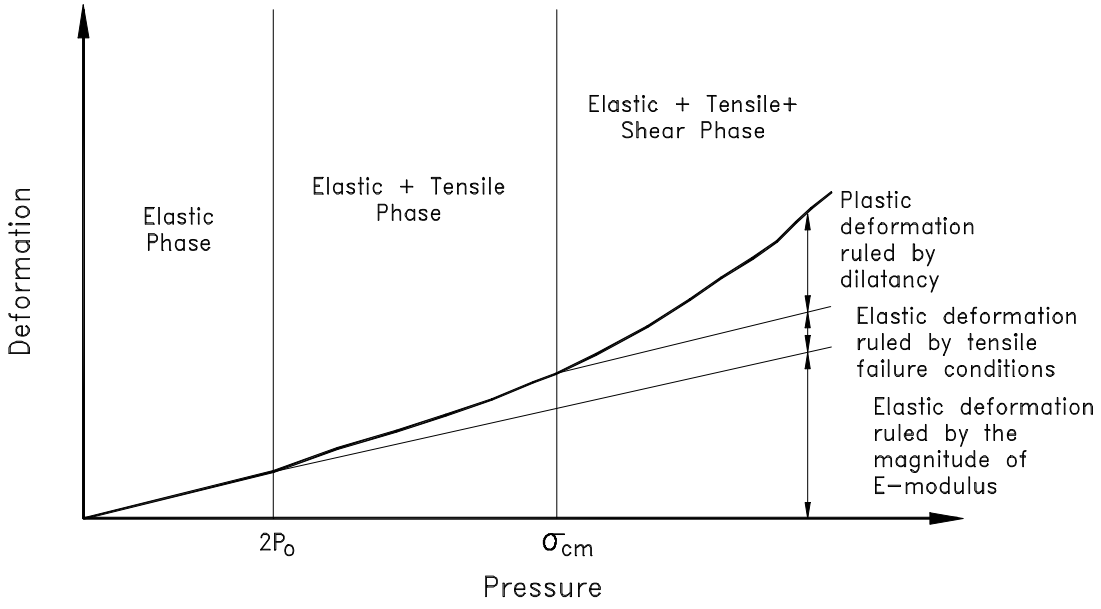

Figure 5-2. Expected Principal Elasto-Plastic Behavior of the Rock Mass. Tensile Stresses in the Rock Surface Occur at Twice the Initial In Situ Stress, $2P_0$ (for an Isotropic Stress Field). Plastic Deformations Occur When the Compressive Strength of the Rock Mass, $\sigma_{c,m}$, Is Exceeded.

At high pressures, three deformation zones will develop around the cavern, as illustrated in Figure 5-3. The radius and the thickness of each zone depends on the strength of the rock mass and the initial in situ stress field. A weaker rock will result in a larger plastic zone.

RSI-835-99-093

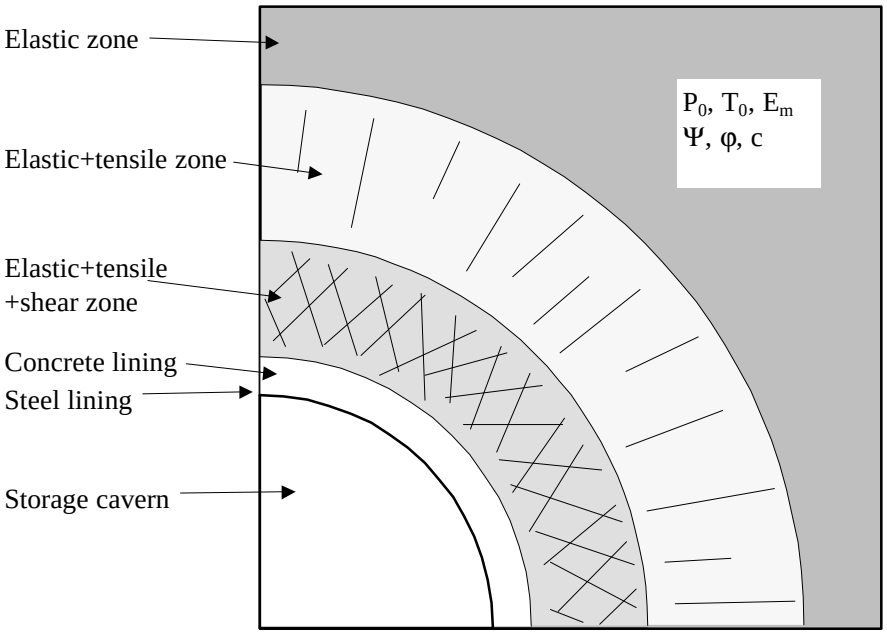

Figure 5-3. Illustration of the Different Deformation Zones Around a Pressurized LRC.

An isotropic elasto-plastic behavior is relevant when studying large volumes of a rock mass with several joint sets. This is, for example, the case for the Grängesberg Pilot Plant. If a rock mass contains only a few sets of discontinuities, then when looking at the detailed behavior of single rock blocks and joints, a more anisotropic behavior must be considered, as the mechanical properties will vary in different directions.

5.1.2.2 Rock Mass Classification and Properties

The Grängesberg Pilot Plant is located in an area dominated by a medium-grained granitic rock (for intact rock: σ_c = 340 MPa, E = 56 GPa). Steep joints are found in mainly three directions in the area. Horizontal joints occur only sparsely. The initial horizontal stresses are low (1-4 MPa). During the investigation phase, geological information was gathered from the following activities:

- **Field observations** relating to joint spacing and orientation, joint roughness, joint filling materials, and groundwater flow.
- **In situ stress measurements** to determine the principal stresses of the rock mass.

- **Core drilling** to determine the Rock Quality Designation (RQD).
- **Laboratory tests** on core samples for determining uniaxial compressive strength, elastic modulus, density, and Poisson's ratio of the intact rock.

The geological information gathered above was used to classify the rock mass according to two different methods: the geomechanics Rock Mass Rating (RMR) system and the Q (Tunneling Quality Index) method. Both of these methods are standard methods in Sweden, are internationally recognized, and have been used for the design of underground excavations all over the world.

The RMR system [Bieniawski, 1973] uses six parameters to classify a rock mass:

1. Uniaxial compressive strength of the intact rock
2. RQD
3. Spacing of discontinuities
4. Condition of discontinuities
5. Groundwater conditions
6. Orientation of discontinuities.

The Q method [Barton et al., 1974] is based on a large number of case histories. The rating is based on the following six parameters:

- RQD
- Joint set number, J_n
- Joint roughness number, J_r
- Joint alteration number, J_a
- Joint water reduction factor, J_w
- Stress reduction factor, SRF.

In order to estimate the mechanical properties; i.e., the compressive strength (characterized with cohesion, c, and the angle of internal friction, ϕ) and the E modulus of the rock mass in Grängesberg, several empirical methods were used. The methods are based on or related to the rock mass classification. Methods used in Grängesberg are listed in Table 5-1.

As a result of the site investigation, the rock mass classification and the estimation of the mechanical properties, the values for the important parameters shown in Table 5-2 were obtained.

Table 5-1. Methods Used in Grängesberg Pilot Plant to Estimate the Mechanical Properties of the Rock Mass

Parameter	Methods	Methods Based on
Compressive strength of rock mass (c, ϕ)	Hoek and Brown [1980] Bieniawski [1978] Stille et al. [1982]	RMR value RMR value RMS value (modified RMR)
E modulus of rock mass	Bieniawski [1978] Stille et al. [1982] Serafim and Pereira [1983] Grimstad and Barton [1993]	RMR value RMR value RMR value Q value

Table 5-2. Parameters Used to Describe the Grängesberg Pilot Plant Site

Parameter	Estimation Based on	Estimated Value
E modulus (rock mass)	Methods indicated in Table 5-1	30 GPa
Uniaxial compressive strength (rock mass), $\sigma_{c,m}$	Methods indicated in Table 5-1	9 MPa
Dilatancy, ψ	Conservative assumption	10°
Angle of internal friction, ϕ	Methods indicated in Table 5-1	35°
Cohesion, c	Methods indicated in Table 5-1	2.3 MPa
Tensile strength (rock mass), $\sigma_{t,m}$	Conservative assumption	0 MPa
Poisson's ratio, ν	Reasonable assumption	0.1
Density, δ	Lab test on core samples	2700 kg/m^3
Largest horizontal stress, σ_H	In situ stress measurements	2.5 MPa
Smallest horizontal stress, σ_h	In situ stress measurements	1.3 MPa
Vertical stress, σ_v	$\rho \times g \times h$	1.3 MPa

5.1.2.3 Predicting the Deformation for the Grängesberg Pilot Plant

The parameter values from Table 5-2 were used for calculating the deformations with a finite element code known as **JOBFEM** (see Appendix A). With this code, the rock mass is modeled as an axially symmetric continuum. Calculations were made for the two different horizontal (radial) stress conditions: 1.3 and 2.5 MPa. The modeling included the excavation phase.

The predicted total radial deformation at the cavern boundary (for either of the two horizontal in situ stress conditions) in Test Room 2 (Grängesberg Pilot Plant) due to pressurization is shown in Figure 5-4. Also shown is the expected spread in deformation of ±1 millimeter due to local behavior of single rock blocks and joints.

RSI-835-99-094

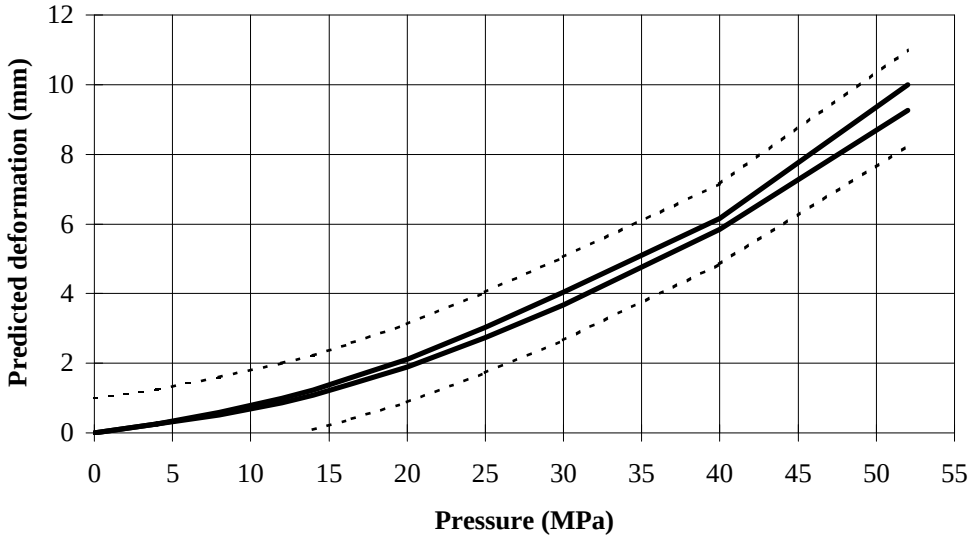

Figure 5-4. Predicted Radial Deformations in Test Room 2 (for Horizontal Stress Conditions of 1.3 and 2.5 MPa), Grängesberg Pilot Plant. Expected Spread in Deformation Is Set at ±1 Millimeter.

The **JOBFEM** calculations were also used for predicting how far out from the cavern the rock mass will be affected by the cavern pressure. The deformations were expected to be exponentially decreasing with the distance from the cavern. Figure 5-5 shows the predicted distribution of radial deformation along a 11.5-meter-long extensometer for different pressures. The length of the extensometer is measured from the rock surface outward.

5.1.2.4 Measured Deformations in Grängesberg Pilot Plant

The total radial deformations measured in all three test rooms in Grängesberg Pilot Plant for different cavern pressures are shown in Figure 5-6. Figure 5-7 shows the measured distribution of radial deformation along a 11.5-meter-long extensometer. The length of the extensometer is measured from the rock surface outward.

RSI-835-99-095

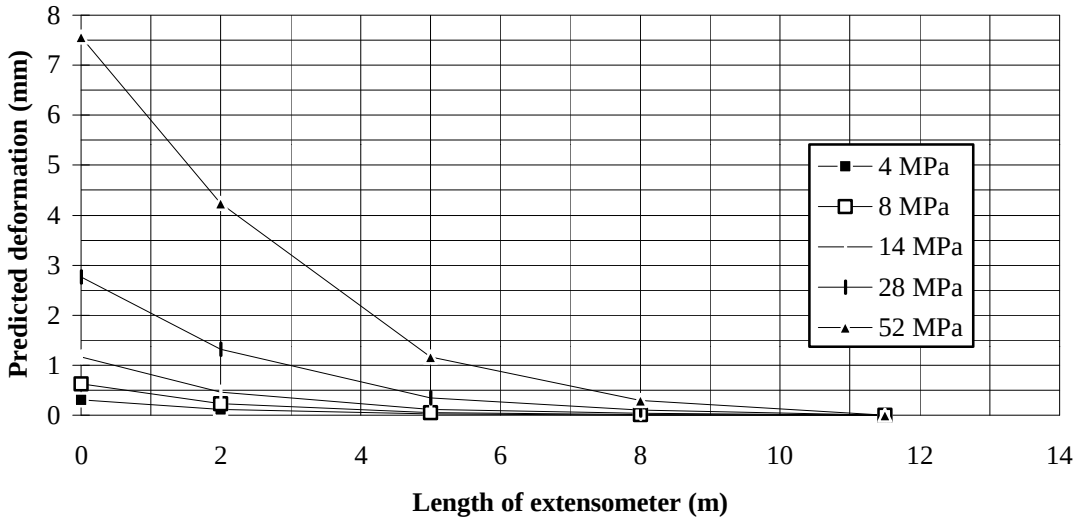

Figure 5-5. Predicted Distribution of Radial Deformation Along an 11.5-Meter-Long Extensometer.

RSI-835-99-096

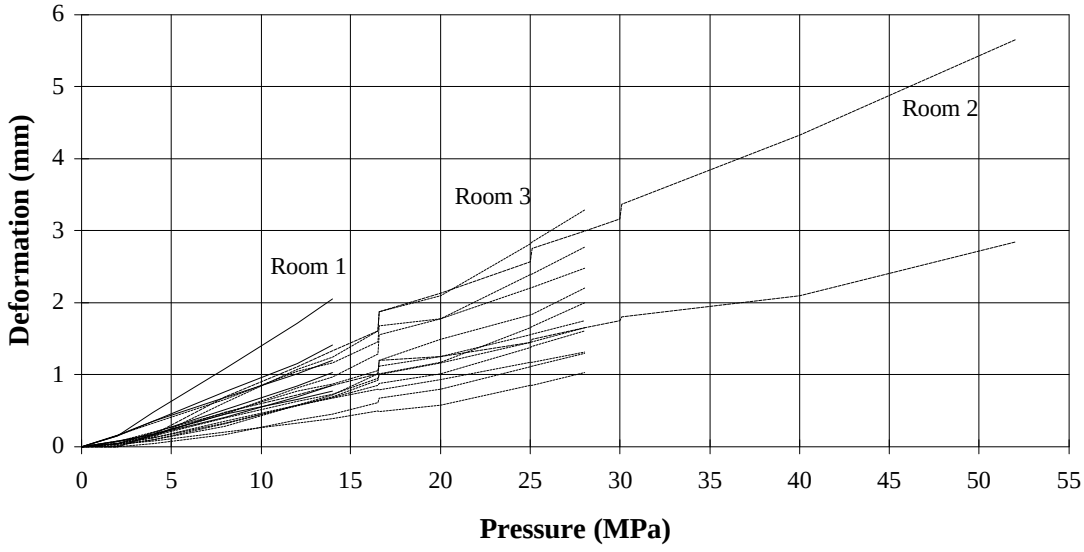

Figure 5-6. Total Radial Deformations Measured in all Three Test Rooms (Grängesberg Pilot Plant).

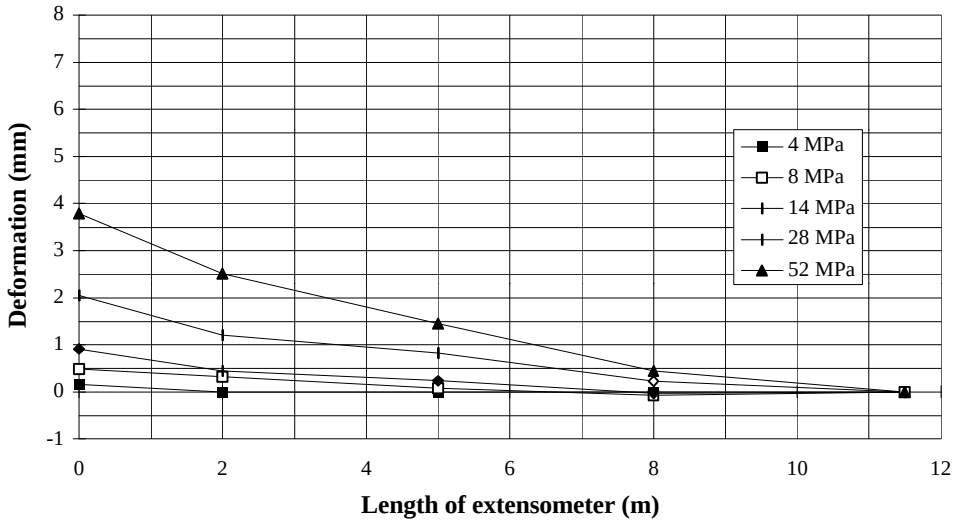

Figure 5-7. Measured Distribution of Radial Deformation Along an 11.5-Meter-Long Extensometer.

5.1.2.5 Comparison Between Predicted and Measured Behavior

Figure 5-8 shows the predicted radial deformations (for either of the two horizontal stress conditions) along with the measured deformations in all installed horizontal extensometers (a combination of Figures 5-4 and 5-6). The predicted deformation span and the measured deformations show good agreement for the intended maximum storage pressure range; i.e., 20-25 MPa. No measured deformation has exceeded the upper limit of the predicted span.

At high-pressure levels, the measured deformations are considerably smaller than the predicted deformations. The explanation to this is to be found both in a built-in conservatism in the methods used for estimating the mechanical properties and in the conservative approach adopted by design engineers with little previous experience in the field of high-pressure storage in an LRC.

The evaluation of the distribution of deformation along the length of all the installed extensometers shows that approximately 90 percent of the radial deformation at 28 MPa takes place within a distance of two diameters from the cavern wall (see the example in Figure 5-7).

The analysis of the results has shown that the *E* modulus generally was underestimated at the initial prediction. The results at 52 MPa also indicate that the *E* modulus is different in different directions (the deformations were measured in two perpendicular directions). The main reason for the large discrepancy at high pressures, however, has to do with the underestimation of the rock mass strength in the finite element model.

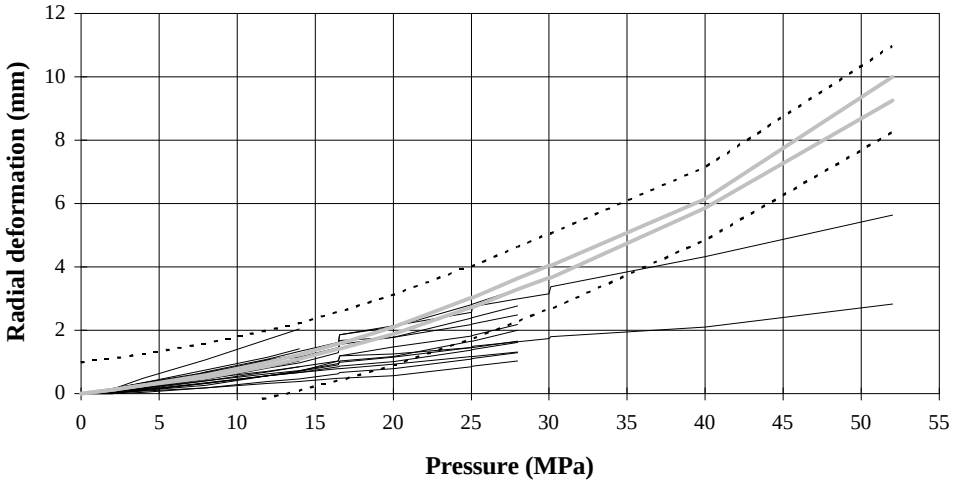

Figure 5-8. Deformations in all Horizontal Extensometers in the Three Test Caverns Along With the Predicted Deformations According to **JOBFEM** (Two Thick Lines for Two Different Horizontal Stress Conditions). The Expected Spread Was Set at ±1 Millimeter.

5.1.2.6 Behavior During Multiple Cycles

Knowledge about the long-term behavior is essential when designing peak-shaving facilities; i.e., storage caverns subjected to a very large number of cyclic loads. Several hundreds of cyclic loads to high-pressure levels have been performed in the Grängesberg Pilot Plant test rooms to evaluate the impact of the long-term deformations. Figure 5-9 shows the measured change in height (K7) and diameter (K8, K9) in Test Room 2 during 50 pressure cycles between 15 and 30 MPa. The duration of each cycle was 1 to 1.5 hours.

The general conclusion from the cyclical tests is that no significantly escalating deformations have occurred. On the contrary, a hardening behavior has been recorded; see Figure 5-10 showing the additional rock deformation in Test Room 2 during 100 pressure cycles between 1 and 16.5 MPa. This is explained by the fact that the rock mass closest to the cavern is probably compacted as rock joints are closed and sheared.

The main part of the additional deformation arises during the first 50 cycles. The total increase in the radial deformation from the 100 cycles is only about 17 percent. Pressure cycle tests performed in Test Room 3 show the same behavior. The increase in deformation due to pressure cycles is thus very limited and diminishing with the number of cycles for this case. This conclusion is assumed to be valid also for a peak-shaving facility subjected to ten complete pressure cycles a year (500 cycles over a lifetime of 50 years).

RSI-835-99-099

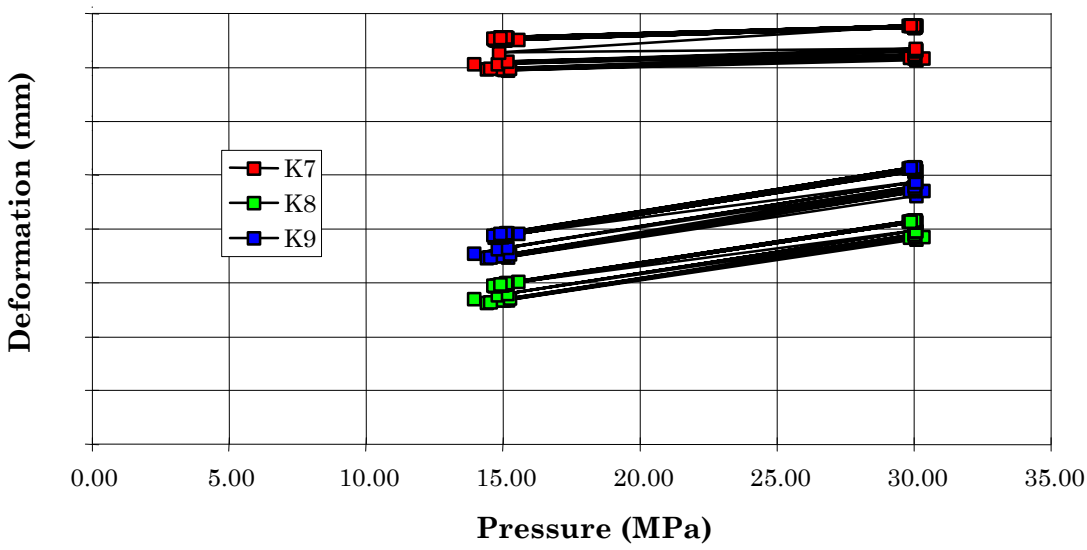

Figure 5-9. Measured Change in Diameter (K7, K8) and Height (K9) of Test Room 2 During 50 Cyclic Pressure Loads Between 15 and 30 MPa.

RSI-835-99-100

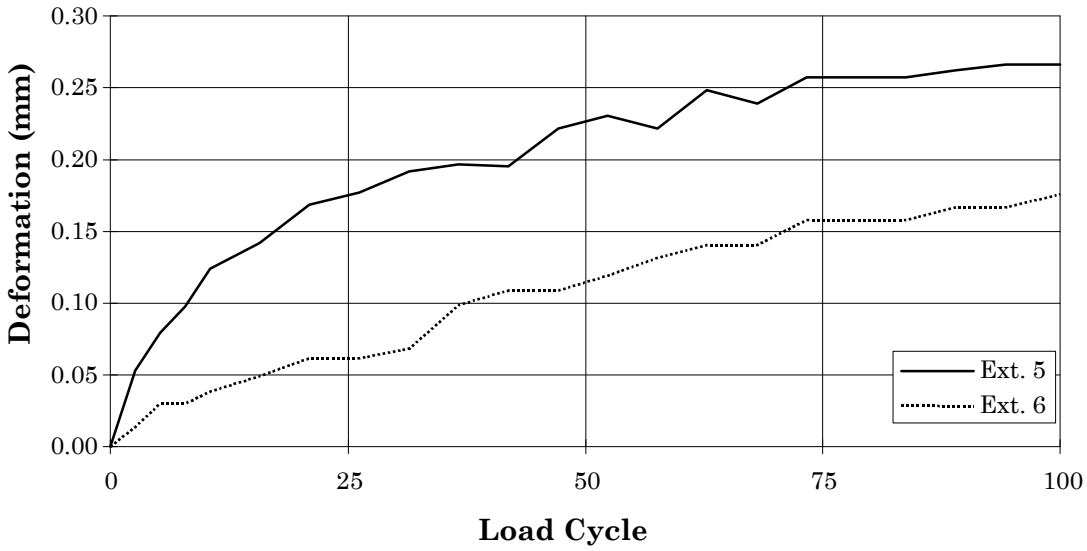

Figure 5-10. Additional Rock Deformation Registered in Test Room 2 During 100 Pressure Cycles Between 1 and 16.5 MPa.

5.1.2.7 Summary

The general behavior of the rock mass in the Grängesberg Pilot Plant follows the expected rock mechanics behavior. The predictions made for the Grängesberg Pilot Plant regarding deformations (made with the best knowledge available at that time) have proven to be very conservative. Evaluation of the Grängesberg test results have helped to improve the empirical relationship used to estimate the mechanical properties of the rock mass and will enable design engineers to obtain better estimates; thus, optimizing the storage design. The tests in the Grängesberg Pilot Plant are probably the largest in situ tests of this type in the world for hard rock caverns and will contribute to the improvement of the methods used for estimating rock mass strength.

5.1.3 Safety Against Uplift

5.1.3.1 Theoretical Background

As there is limited experience regarding the safety against uplift for shallow, high-pressure rock caverns, the problem has to be approached with numerical models in combination with mechanical analogies. The prediction for the Grängesberg Pilot Plant was established with the aid of both analytical and numerical calculations combined with assumptions based on experiences from other analog applications.

The first approach uses the analogy of the resistance against uplift for flat, cylindrical anchor-plates placed in a material characterized with a cohesion of c and an angle of internal friction of ϕ (see Figure 5-11). This has been studied both theoretically [Vesic, 1971] and experimentally [Harvey and Burley, 1973]. To calculate the resistance against uplift (P_u), the following parameters were used:

- cohesion (c)
- angle of internal friction (ϕ)
- density of material (γ)
- depth beneath the surface (H) (corresponds to rock cover for LRC)
- diameter of the anchor plate (D) (corresponds to cavern diameter for LRC).

The second approach uses the method of calculating the weight of a rock overburden shaped like a cone (see Figure 5-12). The weight of the cone, and thereby also the resistance, depends on the angle α. The shear strength of the rock mass is ignored. In rock mechanical applications (e.g., bolts anchored in rock), an angle of 30-45° is generally used to describe the failure [Littlejohn and Bruce, 1975]. It is reasonable to assume that the angle should be in the same range for this case. Uplift failure will occur if the storage pressure exceeds the weight of the rock mass cone. The result of the calculations made with the anchor plate method and the cone

method for the Grängesberg Pilot Plant, using angles in the range of 30-45°, are shown in Figure 5-13.

RSI-835-99-101

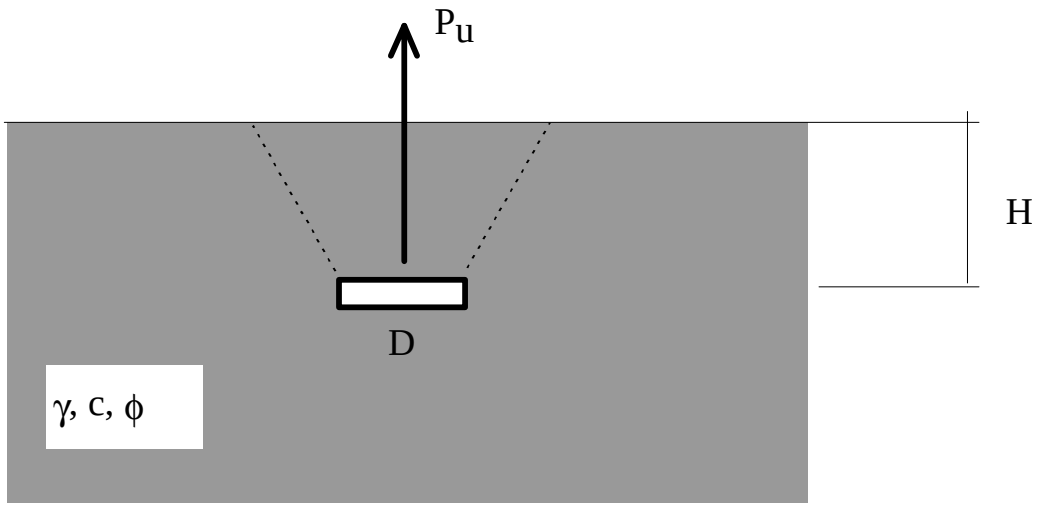

Figure 5-11. Uplift of Cylindrical Anchor Plates.

RSI-835-99-102

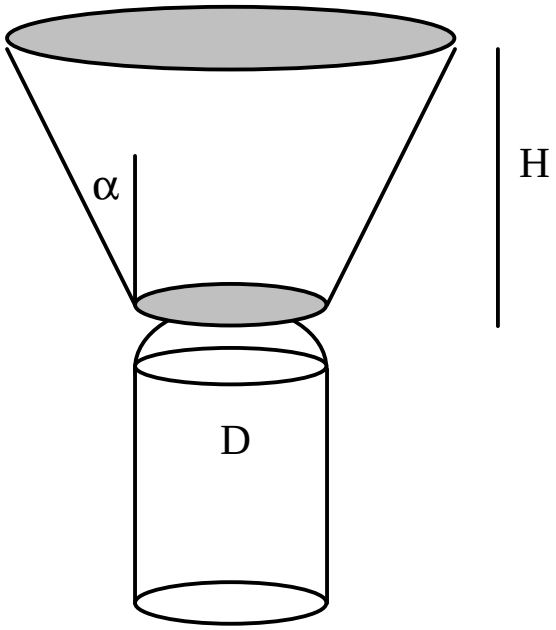

Figure 5-12. Resistance Against Uplift With a Cone-Shaped Rock Overburden.

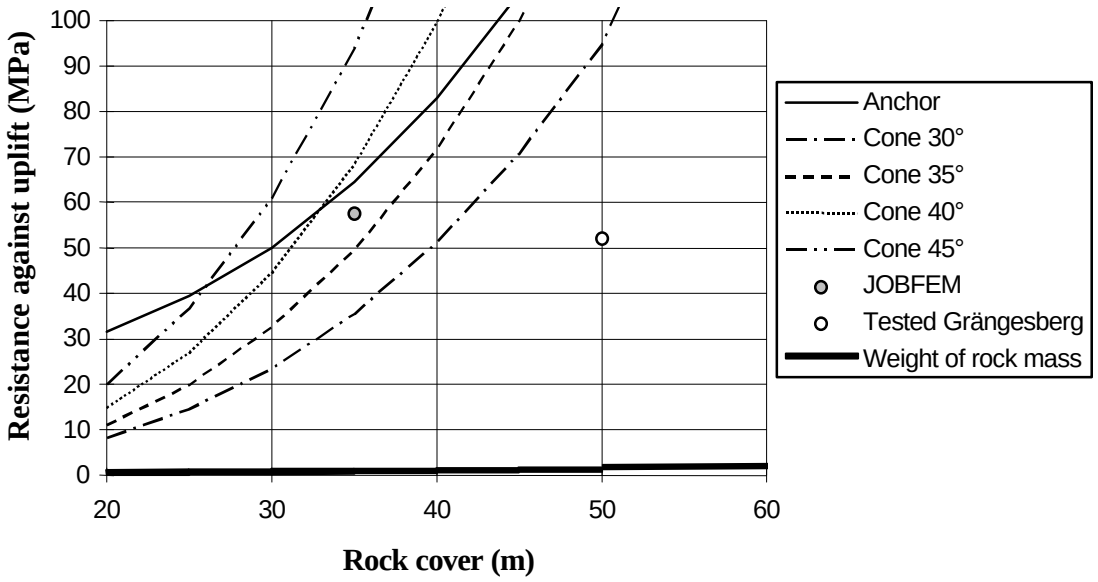

Figure 5-13. The Resistance of the Rock Mass Against Uplift Calculated With Three Different Methods for the Grängesberg Pilot Plant (Cavern Diameter 4.4 Meters and Actual Rock Cover 50 Meters).

The third method involved is a finite element modeling using the **JOBFEM** code. The principal input parameters for Grängesberg are those previously presented in Table 5-2. The results of the **JOBFEM** calculation are also shown in Figure 5-13.

5.1.3.2 Study of Uplift in the Grängesberg Pilot Plant

Figure 5-13 summarizes the calculations of safety against uplift made for the Grängesberg Pilot Plant as well as the weight of the vertical rock mass directly above the cavern.

The vertical weight of the rock mass directly above the cavern corresponds only to a pressure of 1.3 MPa. The **JOBFEM** calculation was made for a rock cover of 35 meters[1], indicating an uplift failure at 57.5 MPa. As shown in Figure 5-13, the uplift resistance calculated with the anchor analogy, the cone theory (with α = 35-40°), and the **JOBFEM** code are approximately equal at a rock cover of 35 meters. This indicates a resistance against uplift in the range of 50-70 MPa.

Test Room 2, located with a rock cover of 50 meters, was successfully pressurized to 52 MPa without any observed tendency for uplift. As indicated in Figure 5-13, this point is far below

[1] The **JOBFEM** calculations were carried out before the final location of the storage rooms was finalized. Due to local geologic reasons, the final location selected has a rock cover of 50 meters.

the estimated resistance against uplift. Extrapolating along the calculated results in Figure 5-13 to the actual rock cover of 50 meters, the resistance against uplift for the Grängesberg case would be expected to be approximately 135 MPa.

5.1.4 Design Loop

The LRC concept is characterized by a high degree of flexibility with respect to siting. The concept has been primarily developed and demonstrated to function well in Swedish bedrock of normal quality (Grängesberg). However, locations within geological formations of considerably lower quality are possible. The minimum requirements on rock mass quality are connected with the requirement to excavate and to maintain a large-scale rock cavern (diameter of 20-40 meters). If this basic requirement is fulfilled, an LRC storage may be constructed. However, to make the storage economically feasible, the storage pressure must, of course, be relatively high. The maximum storage pressure is dictated by the chosen lining material and the actual geological conditions. The deformations must not exceed the maximum strain capacity of the lining material. This leads to a design loop where the design parameters are optimized in relation to each other within the frame of the geological conditions (see Figure 5-14).

RSI-835-99-104

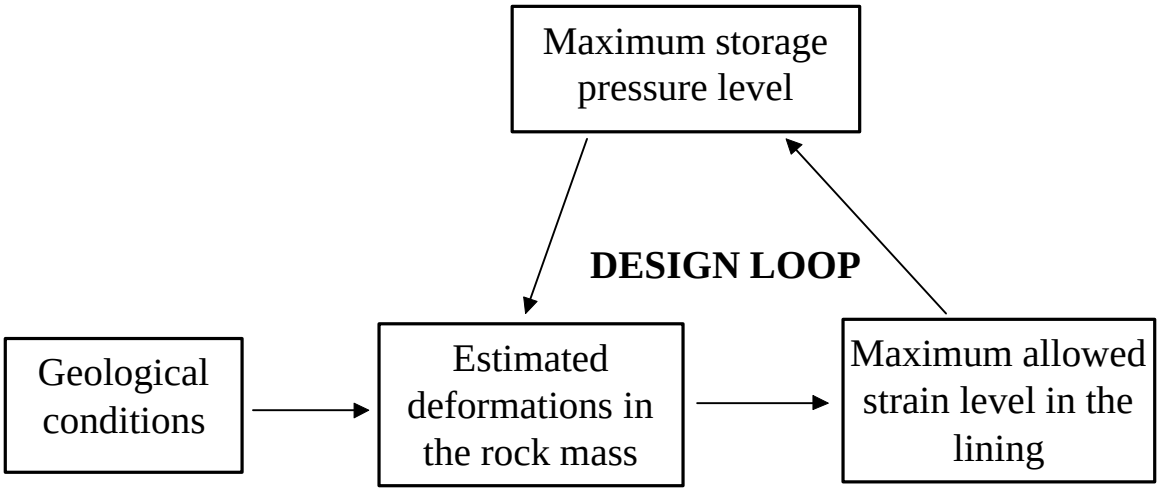

Figure 5-14. Design Loop for Technical and Economical Optimization of a Lined Rock Cavern for Storage of Gas.

With the knowledge of rock quality, the degree of homogeneity, and the initial state of stress, the same rock mechanical approach used for the Grängesberg Pilot Plant can be used for any other location to estimate the deformation caused by high gas storage pressures. A maximum allowable cavern pressure can then be determined, depending on the cavern size and the lining material according to the previously described design loop. When the maximum cavern pressure has been determined, the minimum required rock cover can also be determined.

Screening criteria for siting LRC storage have been developed as a result of the evaluation of the Grängesberg Pilot Plant. The only geological input-data needed are the rock mass rating according to the RMR or the Q methods. As the rock mass rating often is well known from other underground excavations in many candidate areas, a first estimate of the suitability of the intended location may normally be possible without any significant site investigations.

Application of the RMR method for establishing cavern storage pressures is illustrated in Figure 5-15. With a knowledge of the RMR value, the storage pressure can be determined from the graph in Figure 5-15. For example, with an RMR value of 70, a storage pressure in the range up to 34 MPa can be expected to be acceptable.

RSI-835-99-105

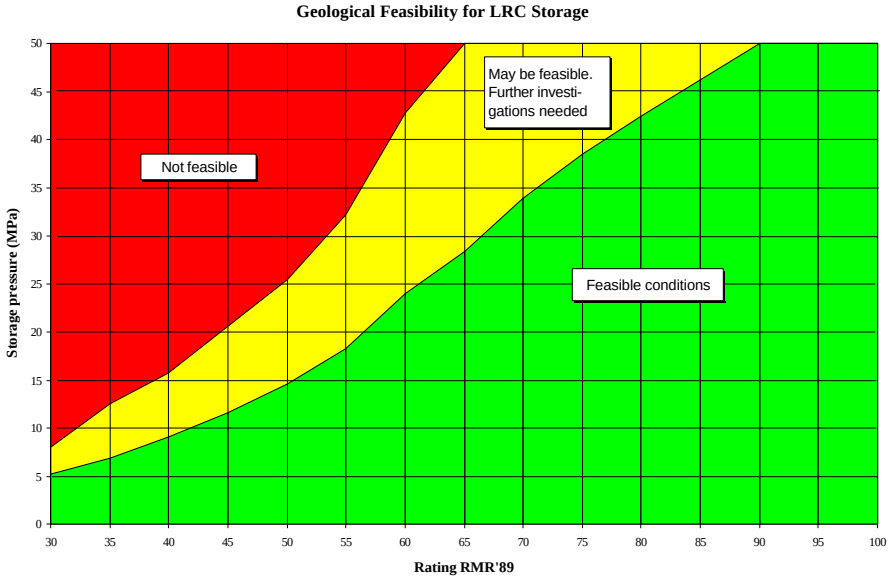

Figure 5-15. Method for Judging the Potential of a Site for LRC Storage.

If a site is judged to have potential for LRC storage, the suitability has, of course, to be further analyzed in order to make a final decision. The key to an accurate evaluation of rock mass behavior and LRC suitability is the mechanical properties estimation. This is done by using the empirical relations described in Section 5.1.2.2.

To determine the values of the relevant parameters needed for establishing a suitable predictive model, a range of field test methods and laboratory tests must be executed.

5.1.5 Cavern Wall Principles

The LRC concept is based on the interaction of four elements, as shown in Figure 5-16:

1. steel liner
2. concrete layer
3. surrounding rock
4. drainage system.

RSI-835-99-106

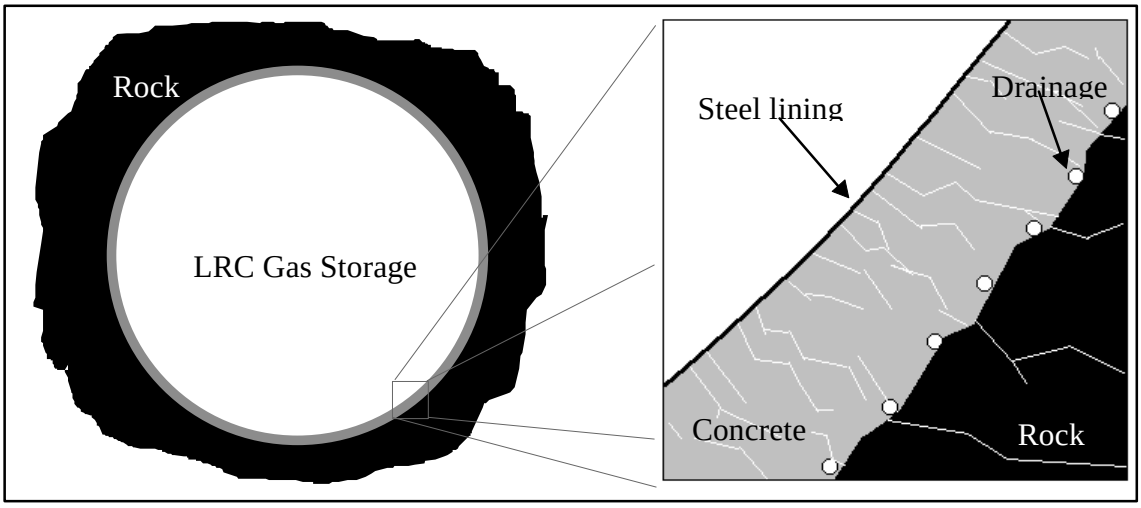

Figure 5-16. Horizontal Projection of Storage Showing the Sandwich Wall.

The **steel liner** will be made of carbon steel. The test in the Grängesberg Pilot Plant has shown that this is the most successful of the materials tested. The role of the steel liner is to achieve gas tightness. It is able to bridge minor cracks in the concrete.

The **concrete layer** is an intermediate layer and is located between the steel liner and the rock. Its main purpose is to transmit the gas pressure in the cavern to the rock and to distribute it uniformly across cracks. At the same time, it will serve as a smooth base for the steel liner.

The **surrounding rock mass** will support the gas pressure load on the wall, thus acting as a pressure absorber.

The **drainage system** consists of perforated drainpipes fixed at an oblique angle to cross horizontal and vertical cracks in the concrete and the rock. The drainage system allows the water pressure against the steel liner to be lowered when the gas pressure in the cavern is low, thus avoiding the risk of liner buckling.

5.1.6 Thermodynamic Behavior

The temperature response of gas in LRC storage is a bit different than for other storage concepts. The main reason is the depth, and thus, the surrounding rock temperature. An LRC cavern will be located at approximately 150 meters (500 feet) below ground. At this depth, the temperature of the rock will be about 17°C (62°F). This is a great difference compared to domal salt caverns that are located at a depth of 1,000-1,500 meters (3,300-4,900 feet) where the temperature of the surrounding rock may be 50-60°C (120-140°F).

A sample calculation of the temperature of gas in storage is shown in Appendix B. During the rapid withdrawals (anticipated for LRC to be 10 days or less), the gas temperature will go below 0°C (32°F). The worst case is a withdrawal after a quiescent period in the storage in which the temperature will have gone down by cooling from the ambient rock temperature. After a 3-month quiescent period, the temperature after withdrawal will go down to -18°C (0°F).

The transient temperature distribution can have a negative impact on the steel liner and the concrete. A low temperature at the end of the withdrawal results in an increase in the residual gas volume in the cavern, thus increasing the base gas requirement and can also cause gas hydrate formation to occur. If repeated freezing and thawing occurs, it could have a negative impact on the concrete outside the steel liner. After many years of operation, the concrete might degrade.

Depending on the water content of the gas, hydrates may form toward the end of the gas withdrawal cycle. During gas injection, the reaction is, of course, the opposite. Gas will be cooled after the compressor, but the compression inside the cavern will develop heat that will increase the temperature inside the cavern, and thus, limit the working gas volume in the cavern. At the end of a 20-day injection, the cavern temperature is approximately 43°C (108°F) (see Appendix B).

In order to increase the working gas volume and avoid the risks associated with low temperature described above, a circulation system was created. With the circulation system, gas inside the cavern will be cooled during injection and heated during withdrawal. The temperature after injection will be equal to the ambient rock temperature, 17°C (62°F), and the temperature after withdrawal will be a minimum of 0°C (32°F). The working gas will increase approximately 30 percent with the circulation system compared to an unheated/uncooled LRC storage system. The circulation system is further described in Section 5.2.6.

5.2 CONCEPTUAL DESIGN

The storage consists of four rock caverns located at a depth of approximately 150 meters (500 feet). Caverns are excavated through an access tunnel. Each cavern will have a separate

shaft for connection to the aboveground facilities. Drawing No. EXGAZ-16 (see Appendix C) shows the cavern and access tunnel configuration.

5.2.1 Storage Performance

The storage will have the following characteristics:

Number of caverns	4	
Geometric volume	320,000 (11.3 MMcf)	m^3
Working gas	74×10^6 (2.6 Bscf)	m^3
Gas withdrawal, maximum	7.4×10^6 (260 MMscf/d)	m^3/d
Gas injection	3.7×10^6 (130 MMscf/d)	m^3/d
Gas circulation, maximum	7.4×10^6 (260 MMscf/d)	m^3/d
Cycles	Several	
Duration of withdrawal	10	day
Duration of injection	20	day
Pipeline pressure	84 (1,220 psi)	bar
Maximum storage pressure	230 (3,330 psi)	bar
Minimum storage pressure	38 (550 psi)	bar
Storage temperature after injection	20 (68°F)	°C
Inlet gas temperature	10 (50°F)	°C
Minimum storage temperature	0 (32°F)	°C
Compressibility (@ p = 230 bar, T = 20°C)	0.82	
Compressibility (@ p = 38 bar, T = 0°C)	0.90	
Compressor injection power	8.8 (12,000 hp)	MW
Compressor circulation power	0.625 (850 hp)	MW
Refrigeration compressor power	1.9 (2,600 hp)	MW
Connection pipe diameter	DN 400 (16")	
Shaft pipes, inlet	DN 250 (10")	
outlet	DN 300 (12")	

The performance corresponds to a cavern storage design with 10-day withdrawal and 20-day injection.

5.2.2 Site Description

The LRC is a challenge from both a design and construction perspective due to the scale of the rock caverns. A cavern is a 95-meter-high (312-foot-high) standing cylinder with a diameter of approximately 37 meters (121 feet).

The minimum depth of the caverns is estimated as approximately 150 meters (500 feet). The final decision will be made based on:

1. The local geology, which means that the vertical placement of the caverns will be made to avoid geological weak zones in the roof section of the caverns.
2. Rock mechanical properties. Minor geological weakness zones might be present in the wall sections, but larger weakness zones should be avoided.

The local topography will be used in such a way that the access tunnel length will be minimized. It is not unrealistic to assume that a difference in height of about 50-70 meters (160-230 feet) or more will be present at any site chosen. This will shorten the access tunnel and/or minimize the declination of the tunnel.

The aboveground facilities need to be considered when planning the needed space in the site selection process. This includes space not only for the machinery and pipe installations, but also the space needed for excavated rock and waste water treatment.

The geological environment that will be sought during the site selection process will consist of primarily crystalline rock; e.g., granite and granodiorite. The rock mechanical properties of this rock will be classified according to the RMR system [Hoek et al., 1997]. The major part of the rock mass investigated should have an RMR value of 60 and above. Most likely, the average RMR value will be around 80.

5.2.3 General Layout

The general layout of the facility shows a system of four caverns, shaped as standing cylinders (see Drawing No. EXGAZ-15 and EXGAZ-16, Appendix C). Each cylinder has a diameter of approximately 37 meters (121 feet) and a height of approximately 95 meters (312 feet). Each cavern should be placed with a distance of at least 100 meters between the cavern walls to avoid interaction effects in the rock mass when pressurizing the caverns. This approach has been verified in a test facility in Sweden [Isander, 1994]. The roofs of the caverns are to be shaped as semispherical domes in order to be stable during rock excavation and steel liner construction while the bottom portions of the caverns will be more flattened but still with a somewhat rounded shape. An access tunnel from the surface will spiral down to the levels where the caverns are entered. The connection between the caverns and the surface, as far as gas transportation is concerned, will consist of separate shafts for each cavern.

5.2.4 Rock Excavation

The main rock engineering components of the LRC concept are the excavation of the access tunnels, the storage cavern, the shaft for the gas pipes, and the grouting and rock supporting operations.

5.2.4.1 Excavation of the Tunnel Entrance

The tunnel entrance will be excavated using conventional drill-and-blast methods. This means that the work needs to be planned carefully to avoid inconveniences regarding vibrations, noise, dust, and air pressure waves to people, the surrounding structures, and other concerns that might be sensitive. The entrance will be planned in such a way that the amount of excavated rock will be minimized, although this is dependent on the local geology and rock mechanical features.

5.2.4.2 Excavation of the Tunnels

The excavation will be performed as conventional drill-and-blast operations, and the tunnels will be made in a horseshoe shape, although the shape might vary slightly due to local geological and rock mechanical conditions. The final shape of the tunnels should not be less than the theoretical section and the excess excavation should be limited. Controlled blasting techniques will be utilized throughout construction to minimize overbreak damage to the remaining rock mass. The drilling pattern and the charge plan will be adapted to suit the local geology and to meet the demands set out regarding the damaged zone around the tunnel as well as to minimize the overbreak of rock.

The tunnels will be excavated with a minimum of excess rock. The cross section of the tunnels at straight stretches should be around 25 square meters (270 square feet) and in curves around 43 square meters (463 square meters). The tunneling operations will need niches along the tunnel to allow for vehicles turning. Temporary pump pits will also be made, as well as meeting places for vehicles.

Rock support will be used when needed; i.e., spot bolting. The bolting will be performed with grouted rebar. Use of temporary support might be needed; e.g., friction bolts or anchored bolts, but will not be included in the final support. Systematic bolting can occur as well as shotcrete with or without steel fibers, depending on the local geological and rock mechanical conditions.

In certain portions of the facility, systematic bolting and shotcrete can be used, such as where the tunnel splits in two or at the position of pump pits. Systematic bolting may also be needed at sections with poor Rock Mass Quality.

Grouting will be needed to minimize the amount of groundwater leaking into the tunnel, in order to optimize the pumping equipment as well as to reduce the influence on the groundwater level. Grouting operations will primarily use cement-based grout. The grout curtain will be designed to suit the local geology and might vary during the excavation of the tunneling works. The design of the grouting will include specification of the number of holes, lengths, and directions. The grouting operations will need careful monitoring as the tunneling proceeds. Change of the drilling pattern might also be necessary.

5.2.4.3 Excavation of the Shafts

Two types of shafts will be excavated in the LRC facility. The locations and functions of the various shafts are described below. One shaft type is the shorter shaft, 15-20 meters (49-66 feet) in length, which will be excavated by the drill-and-blast method. Drilling can be performed as long-hole drilling, after which blasting can be performed either as retreat blasting or in one single blast. The choice is dictated by the quality demands that are made and on the local geological and rock mechanical conditions.

Longer shafts can be made by using raise-boring techniques. Shafts with a length of more than 40 meters (131 feet) and with a diameter of less than 5 meters (16 feet) can easily be made by raise boring at competitive costs. Rock support costs will be lower using the raise-boring method, compared to conventional drill-and-blast methods. When raise boring a shaft, it is important to be able to control ingress of groundwater into the shaft. Therefore, it is advised to drill long holes at the position of the shaft where grouting can be performed.

Support might be needed in the shafts, even if raise boring is used. These supports will most likely be limited to shorter rock bolts and shotcrete, possibly fiber reinforced.

5.2.4.4 Installation Chambers Above the Caverns

Above each cavern, a small chamber will be made. It will be used for pregrouting above the cavern and pouring concrete. The chamber will be approximately 7 × 7 meters (23 × 23 feet) and some 6-7 meters (20-23 feet) high. The shaft down to the cavern has to be adapted to the concrete plug needed to seal the cavern. The distance between the cavern and the tunnel above is around 15-20 meters (49-66 feet). This dimension might change, however, due to local geological conditions. The shaft can be made by raise boring or by using the drill-and-blast method, the latter being the most efficient.

5.2.4.5 Excavation of the Rock Caverns

The excavation of the caverns can be made in different ways and the decision on what method to use will be based on the experience and capability of the different contractors (e.g., Sturk and Stille [1995]; Sagefors and Daerga [1996]).

Before the excavation work starts inside the caverns, grouting operations will take place from the small chambers above the caverns. Long drillholes will be made in a fan shape into the rock mass above the caverns. These drillholes will be grouted, using cement, to ensure that the groundwater movements in the rock mass around the caverns will be kept as small as possible during excavation.

The access tunnels will enter the planned cavern at two or more points. From these entrance points, the excavation will proceed in a manner that will be both safe and economical. The height of the caverns makes it necessary to have the highest level of safety during the operations, and the excavation sequence will be planned in such a way that exposure to hazardous situations is minimized.

The more traditional way of excavating the caverns would be to enter the cavern at the top and to excavate the cupola. This operation puts very high demands on accuracy when drilling and blasting, as the roof is a sensitive part of the construction. From the entrance level, a spiralling ramp is made upward as the roof section is excavated. As the cupola is half-spherical, it puts special demands on the excavation technique used. Once the roof is excavated and secured with systematic bolting and shotcrete, the ramp is removed and the wall reinforced accordingly. The barrier position at the top of the cavern will be finally shaped from inside the cavern as the excavation work is being done in the cavern cupola.

The cavern would also be entered at the bottom where a level for mucking out the waste rock would be established. The shape of this level might vary, depending on what excavation sequence is chosen. One possible scenario is to excavate a small chamber at the center of the cavern at the lower entrance level. A raise-bored shaft could then be made from the upper access level. This shaft might be enlarged to a suitable diameter as it would be used as a rock pass into which the waste rock will be dumped. The rock would be loaded and hauled to surface.

The remaining rock in the cylindrical part of the cavern will be slashed into the shaft as the excavation operation proceeds downward in a spiral. The size of the blasts will depend on local geological factors, as well as on the methods used by the contractor. Reinforcement of the cavern walls will be carried out, using rockbolts and shotcrete, as the excavation proceeds. Additional grouting of the walls might be necessary to avoid wet working conditions inside the cavern and to facilitate later casting of concrete against the walls.

The last part of the rock cavern to be excavated is the bottom. The most optimal shape would be to make the same shape as the roof, which is half-spherical. The problems encountered doing that in the bottom of the cavern are so significant that a compromise has to be made, allowing the bottom to be rounded but not in a perfect half-sphere. The excavation proceeds in the same way as earlier; i.e., a spiralling ramp is used to reach the correct level.

5.2.4.6 Excavation of the Barrier Positions

The barrier or seal positions are to be blasted with extra care to create a smooth surface with as few fractures as possible. The barriers will be placed at the tunnel entrances in connection with the concrete wall inside the caverns. The barriers will be approximately 4-6 meters (13-20 feet) long. The blasting procedure will include making a pilot tunnel along the length of the

barrier, after which slashing of the walls will be made in shorter sections. At the position of the barrier, the tunnel will be made wedge shaped to increase the pressure-absorbing capability of the barrier.

The same technique will be used at the top of the cavern where the shaft will enter the cavern. The smooth blasting of the barrier position will be made from inside the cavern. This section of the shaft will also be made wedge shaped.

5.2.4.7 Excavation of the Pump Pits

Pump pits of a conventional type will be needed at one or more positions within the facility. The excavation of these pits will be made using the conventional drill-and-blast method, after which concrete casting works will take place.

At the bottom of the access tunnels at the lower parts of the caverns, a pump pit will be made. It will be made to a depth lower than the bottom of the cavern to ensure that the drainage water from the cavern will be transported to the pump pit. The connection between the pump pit and the cavern will be through one or more drillholes from the bottom of the caverns to the bottom of the pump pit.

5.2.4.8 Excavated Rock Treatment

The calculated amount of excavated rock for a four-cavern facility is approximately 400,000 m^3 (14 million cubic feet). Assuming a swelling factor of 1.6 results in a total volume of 640,000 m^3 (22.6 million cubic feet) of excavated rock to be deposited, sold, or used in the construction works.

The rock produced at the construction site will be of good quality and there should be several ways of using it in the construction work at the site. The rock can be used for aggregates in the concrete production and for the foundation of the surface structures. If not used on site, the produced aggregates should hold a commercial value in a favorable market, provided other construction projects are occurring in the same area. The value of the aggregates decreases very quickly with required haulage distance.

If the excavated rock is not being used for construction work, it has to be deposited on site. Even if the excavated rock is being used, a temporary deposit area needs to be established, although not of the same size as if all rock has to be deposited.

A permanent deposit area needs to be designed to accommodate the local demands. Consideration has to be taken of the surrounding landscape and vegetation as far as the visual perception of the deposit is concerned. The effects on vegetation and groundwater must also be taken into consideration as far as water treatment is concerned. Other factors, such as dust,

noise, and visual impact on the site, must be considered. If the deposit is placed in remote areas with little or no population, the environmental effects should be limited.

5.2.4.9 Treatment of Leakage Water

A certain amount of groundwater will leak into the tunnel system of the facility. This water has to be pumped to the surface and processed before passing it on to any natural recipient. This treatment will most likely consist of sedimentation dams to allow any rock particles present in the water to settle. These sediments are being produced mainly in the drilling operations of the rock excavation. Other materials can be present in the leakage water, such as cement from the grouting and casting operations. This will be treated in the same way as described above. If any oil is present in the leakage water, an oil separator must be installed.

5.2.5 Cavern Wall

5.2.5.1 Concrete Wall

A concrete layer will be cast between the lining and the rock. The purpose of this concrete layer is twofold:

1. Transfer the load generated by the gas pressure in the cavern to the surrounding rock mass.
2. Provide a smooth base for the steel lining.

The concrete layer also has a role to minimize the strain in the lining. The large cracks that can be generated by the deformation result in a number of smaller cracks in the concrete, thus, limiting the local strain in the lining.

The selection of concrete quality should be made carefully. The concrete lining must be of sufficient strength to facilitate the distribution of cavern pressure to the rock walls. The proposed procedure to construct the wall after excavation is to start with the steel lining followed by the concrete wall.

The primary concerns related to the construction of the concrete casting are:

- Support for the form pressure
- Transportation and distribution of concrete
- Need for working space inside the formwork
- Coordination with the steel lining construction.

Support for the form pressure

There will be a considerable height to the wall being casted. The pressure of the concrete needs to be balanced by some kind of support from inside the liner.

A special concern has to do with the support needed when pouring concrete under the bottom part of the steel lining. The upward lift of the concrete will be very large, and the only method for having a counterforce is to use dead weight in the form of water filling of the lining.

Transportation and distribution of concrete

The total concrete volume needed for one cavern wall is of the order of 7,000 m^3 (245,000 cubic yards), which results in a total of 28,000 m^3 (980,000 cubic yards) for a four-cavern facility. To ensure a steady supply, a concrete mixing plant is needed on site (or in the near vicinity). The concrete will be transported by truck into the tunnels and might be pumped the last part of the way.

Other concrete works in the facility include the casting of pump pits and the barriers to the caverns. The amount of concrete for these works is small in comparison with the needs for the cavern wall lining, but are estimated at approximately 3,500 m^3 (120,000 cubic yards) for a four-cavern facility.

5.2.5.2 Steel Lining

The steel lining will provide the primary guarantee of gas tightness in the cavern. The lining material must be resistant to gas and the possible condensates and impurities that it may contain, as well as to the environment to which the outer surface is exposed.

From the structural standpoint, the lining is not intended nor designed to carry primary loads, as the concrete layer supports the lining, which in turn, is supported by the surrounding rock mass. The lining should, however, be able to withstand the stress and strain caused by the general elastic and plastic deformation of the cavern wall. In addition, with increasing gas pressure, fractures and cracks will open up in the rock mass. These will initiate smaller cracks in the concrete layer. The liner must then have the capacity to withstand the strain resulting from the spanning of the largest of those cracks.

The maximum operating pressure allowed for the storage depends on the lining characteristics and the geological conditions. It must be set at a value such that the induced deformation in the rock mass and the concrete layer does not result in the strain of the lining in excess of its capacity for deformation.

The quality of the steel lining is of primary importance for a successful LRC. It must, therefore, have the highest priority, and every effort must be put into creating the best possible

conditions for the emplacement of the lining. The different steps in the steel lining construction work are:

- Transportation and placing of the steel plates
- Welding, including pretreatment of joint surfaces and posttreatment of weld surfaces
- Quality control regarding strength
- Quality control regarding gas tightness.

Each one of these work steps will constitute a separate workstation with specialized personnel and equipment. The main question for the choice of construction method is where to put these workstations and how the work should be carried out at these workstations.

Another important choice is the decision as to whether the welds are to be made with automatic or manual welding. Automatic welding (e.g., Submerged Arc Welding (SAW)) is expected to give a higher production rate and a uniform and high weld quality, and is, therefore, preferred. There will probably, however, always remain some welds that are not suitable to automate.

5.2.5.3 Drainage System

The hydrostatic pressure outside of the cavern due to the column of groundwater can be 1.5-2.5 MPa (220-360 psi). The drainage system is a part of the general groundwater management plan. This plan consists of three major parts:

1. During construction of the cavern, the rock mass is grouted in the cavern roof and wall in order to minimize groundwater inflow to the cavern. This is needed both for construction and operation purposes.
2. During concrete placement for the cavern wall, water influx is prevented by the drainage system.
3. During operation, when gas pressure within the cavern is lower than the hydrostatic pressure outside the cavern, or when the cavern is depressurized to atmospheric pressure for inspection and/or maintenance, the lining can then be exposed to a load from the outside. This is prevented by lowering the pressure through the drainage system.

During construction, the drainage system is in operation, draining all groundwater so as to not damage the steel lining. When the construction is completed, the drainage system is closed, and full groundwater pressure is allowed (1.5-2.5 MPa). The groundwater pressure must never be allowed to be higher than the storage pressure inside the cavern.

The movements of the groundwater are to be minimized during operation of the LRC. This restriction is intended to reduce the risk for chemical and bacterial obstruction in the system, as well as to avoid lowering of the groundwater table.

5.2.6 Storage Operation

A flow diagram for the aboveground facilities is shown in Drawing No. EXGAZ-01 (see Appendix C). The operating principles for the aboveground facilities are described below. The different operational cases for the aboveground facilities are shown in Drawing No. EXGAZ-02 to 06 (see Appendix C).

5.2.6.1 Injection With Flow Control

Drawing No. EXGAZ-02 (see Appendix C) illustrates injection with flow control. When the pipeline pressure is above the cavern pressure, gas will be injected with flow control. The gas flow is measured during injection in an ultrasonic flow meter before the flow control valve. The inlet gas is analyzed in a gas chromatograph and a dew point meter. The gas will pass through a filter to capture rust and other particles coming from the pipeline.

5.2.6.2 Injection With Compression

Drawing No. EXGAZ-03 (see Appendix C) illustrates injection with compression. When the pressures in the pipeline and the cavern are equalized, injection continues by means of the injection compressors. The injection rate is 3.7×10^6 m^3/day (130 MMcf/day) at an inlet pressure of 700 psi and an outlet pressure of 3,330 psi. Gas is cooled in an air cooler down to the ambient temperature of about +38°C (100°F). The cooling will continue by means of a refrigeration unit down to a temperature of 10°C (50°F). At the same time, gas is circulated from the caverns by means of the circulation compressor through an air cooler and a refrigeration unit, in order to cool the storage gas; thus, increasing the working gas volume. The circulation flow rate is maximum at 260 MMcf/day, and the temperature of the gas going back to the storage is 10°C (50°F). The goal is to have a final gas temperature close to the ambient rock temperature (see Section 5.1.6). In order to achieve maximum efficiency, the cool gas is injected at the bottom of the cavern and warmer gas is taken out at the top (see Figure 5-17).

5.2.6.3 Withdrawal With Reduction

Drawing No. EXGAZ-04 (see Appendix C) illustrates withdrawal with pressure reduction. During withdrawal, gas is removed from the cavern by free flow down to the pipeline pressure. The withdrawal capacity is 7.4×10^6 m^3/day (260 MMscf/day). At the same time, the same amount of gas is circulated and heated in order to maintain a temperature above 0°C inside the

cavern. During the circulation, warm gas is injected at the bottom of the cavern in order to avoid any cold areas (see Figure 5-18).

RSI-835-99-107

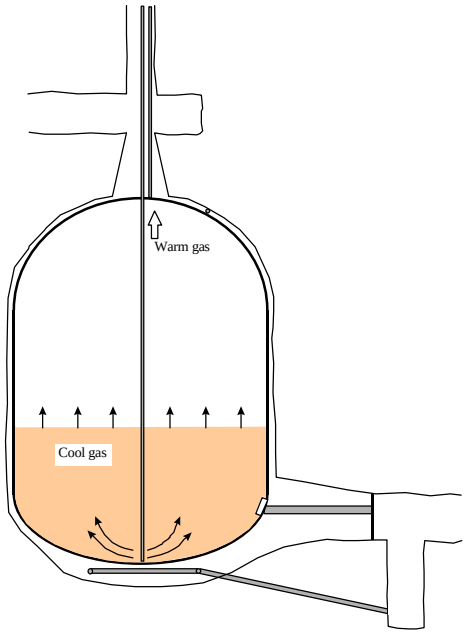

Figure 5-17. Circulation Cooling During Injection.

RSI-835-99-108

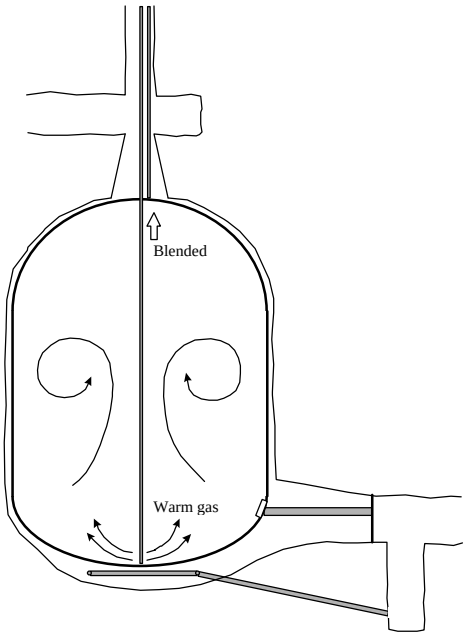

Figure 5-18. Circulation Heating During Withdrawal.

Before pressure reduction, the gas flows through a filter, protecting the pressure reduction valves from water or rust particles. The gas is heated before the pressure reduction to avoid low temperatures in the pipeline.

5.2.6.4 Withdrawal With Compression

Drawing No. EXGAZ-05 (see Appendix C) illustrates withdrawal with compression. When the cavern pressure level reaches the pipeline pressure, gas will continue to be withdrawn by means of the main compressors. In this case, the installed compressor power is utilized to reduce the base gas requirement by going below the pipeline pressure in the cavern. The compressors can be utilized to withdraw gas down to a pressure of 38 bar (555 psi) and inject it into the pipeline at a maximum pressure of 84 bar (1,215 psi).

5.2.6.5 Circulation Cooling/Heating

Drawing No. EXGAZ-06 (see Appendix C) illustrates circulation cooling and heating. This case is used if the temperature for some reason should need to be adjusted. This can be used for optimization of the storage operation.

5.2.7 Aboveground Facilities Layout and Main Equipment

The layout for the aboveground facilities is shown in Drawing No. EXGAZ-07 (see Appendix C). The facility consists of four headshafts - one for each cavern. The shafts contain two gas pipes: one for injection and one for withdrawal. Each cavern can be operated separately.

The compressor station consists of two electric motor-driven, two-stage reciprocating compressors for injection and one circulation compressor. Adjacent to the compressors, air coolers for cooling by ambient air are installed. In line with the air cooler, the refrigeration unit, which is cooling the gas to 10°C, is installed.

The metering and pressure reduction consists of two outlet trains with filters, heaters, and pressure reduction valves. "Slam-shuts" will ensure that the storage pressure does not overpressure the pipeline. Heat for warming the gas is provided from a boiler central with a water/glycol system. Gas analysis instruments are installed to measure the gas composition and the dew point.

The facility is controlled from a control room which also includes staff facilities. The operation is controlled by a PLC system. Electricity is supplied through a high-voltage transformer and switch gear. The aboveground facilities will include the support systems listed below:

- Air compressors for instrument air
- ESD system, including venting of the compressor system
- Gas detectors
- Fire detectors
- Lubrication oil storage tank
- Glycol system
- Waste oil tank
- UPS system.

6.0 COST ESTIMATE

6.1 INTRODUCTION

This chapter gives the investment and operational cost for a four- and an eight-cavern LRC storage facility. A time schedule for the project is also presented. The costs are believed to be accurate for December 1998 for a location in New England. The New England area is selected for the cost estimate as it is the most promising area from a market point of view (see Chapter 7.0). The primary difference between the cost of an LRC in New England and the Southeast would relate to differences in labor rates.

To be able to handle all uncertainties linked to the cost, a probabilistic approach has been chosen for presenting the cost. The result is a cost-versus-probability curve that is believed to give a truer cost picture than just one single value.

The cost achieved in the United States for the rock excavation has been compared with the Scandinavian cost for similar excavation. This comparison is presented in Section 6.2.6.

A cost estimate that is 100 percent accurate is impossible to develop for any major project. The cost level will depend on design parameters but also local geological conditions as well as the competition and the general situation in the construction market. A probabilistic model called Multirisk is used to handle the uncertainties. Multirisk has been used by Sycon in many projects in the past.

The general factors that will impact the cost level of an LRC storage include:

1. Design
2. Geology
3. Production methods
4. Permitting
5. Competition
6. Location.

The anticipated **design** of a four-cavern storage for the cost estimate is presented in Chapter 5.0.

The anticipated **geology** is described in Chapters 4.0 and 5.0. An RMR value of at least 70 is anticipated. This represents competent rock with a low requirement for rock support. The water influx is anticipated to be low.

The **production methods** used are well recognized by United States rock excavation contractors. Improvements can be made using, for example, Scandinavian methods.

The cost for **permitting** is based on "normal" requirements for underground storage.

The cost estimate is made without consideration of **competition**. It is, therefore, likely that the cost can be lowered when the project is ready to be bid.

An LRC project is a very labor-intensive construction project. The **location** where the LRC is being constructed will, therefore, have a significant impact on construction costs because of variations in labor union issues. This uncertainty is handled in the probabilistic model at a general influence level.

The costs for the LRC facility are divided into three groups: preconstruction cost, below ground cost, and aboveground cost. For the calculation of these costs, each item in each group has been assigned a low, likely, and high value. The items are regarded as independent of each other. To combine the items for a total project cost, Multirisk has been used. For the below ground group, general conditions are also applied for competition and location impact.

6.2 INVESTMENT COST FOR A FOUR-CAVERN FACILITY

The four-cavern storage facility will have the characteristics below:

Number of caverns	4	
Geometrical volume	320,000 (11.3 MMcf)	m^3
Working gas	74×10^6 (2.6 Bscf)	m^3
Gas withdrawal, maximum	7.4×10^6 (260 MMscf/d)	m^3/d
Gas injection	3.7×10^6 (130 MMscf/d)	m^3/d
Gas circulation, maximum	7.4×10^6 (2.60 MMscf/d)	m^3/d

The calculated investment cost for the three groups: preconstruction, below ground, and aboveground, is presented below. The cost is presented as a probabilistic S-curve. In the curve, the cost will depend on the confidence level that is chosen for the project. An 80 percent probability is what is normally chosen for investment decisions. This means that the probability that the cost is lower than this value is 80 percent. The graphs below show the S-curves for the three groups of costs. Also, the top ten uncertainties are indicated. These are the items in the cost calculation in which the cost portion combined with the uncertainty create the greatest impact on the total cost.

6.2.1 Preconstruction Cost

The preconstruction cost consists of:

- Permits
- Design and tender documents
- Site selection and geologic evaluation.

The S-curve for the preconstruction cost is presented in Figure 6-1, and the top ten risks are presented in rank-order in Figure 6-2. The cost with 80 percent probability for preconstruction is $5,800,000. The most uncertain item is the cost for permitting.

RSI-835-99-109

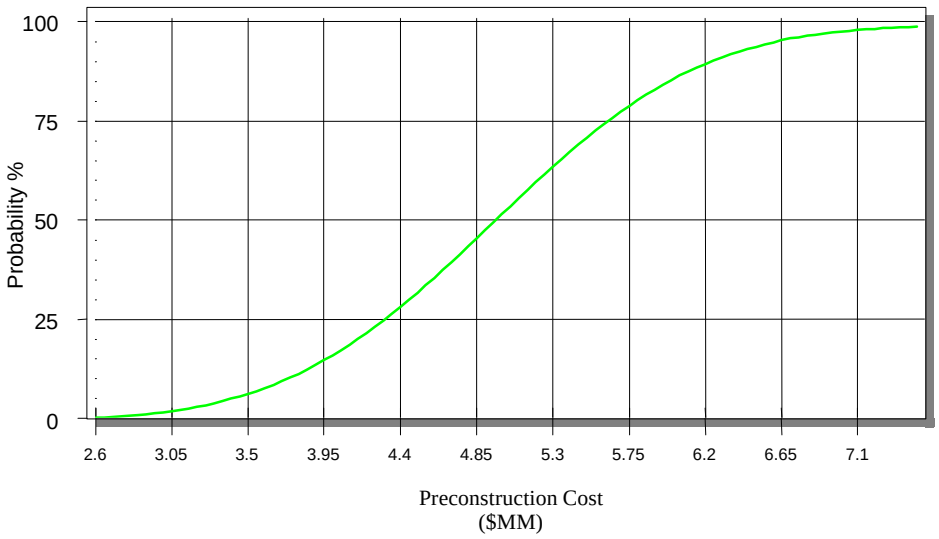

Figure 6-1. Preconstruction Investment Cost.

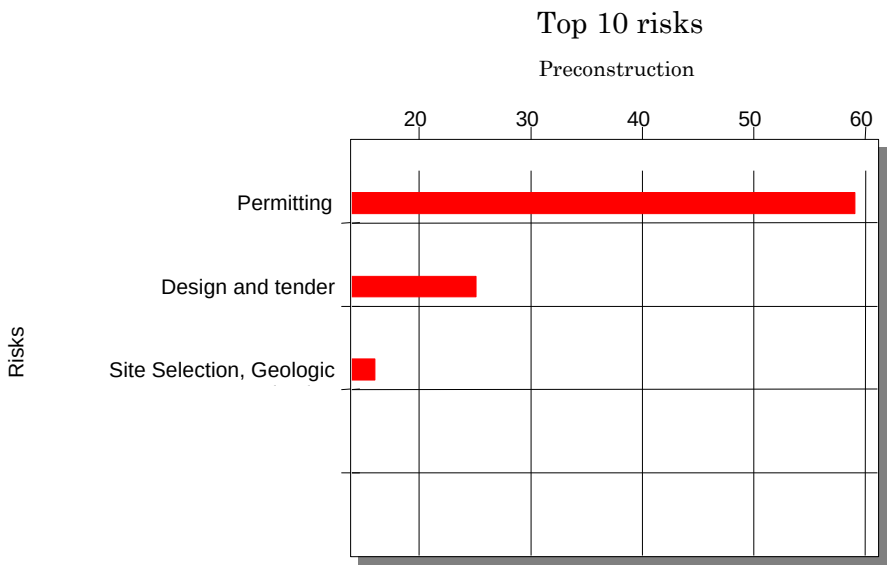

Figure 6-2. Uncertainties for Preconstruction Cost.

6.2.2 Below Ground Cost

The below ground cost includes:

- Site preparation
- Spiral access tunnels
- Cavern access tunnels
- Above cavern tunnels
- Caverns
- Cavern shafts
- Concrete barriers
- Water drainage pipes
- Rock support
- Shotcrete
- Grouting

- General service
- General and administrative labor
- General and administrative expenses
- Insurance and bonding
- Equipment purchase and rent
- Electrical consumption
- Water treatment plant.

The S-curve for the below ground portion of the LRC project is illustrated in Figure 6-3 and shows that the cost with 80 percent probability for below ground construction is $125,500,000.

RSI-835-99-111

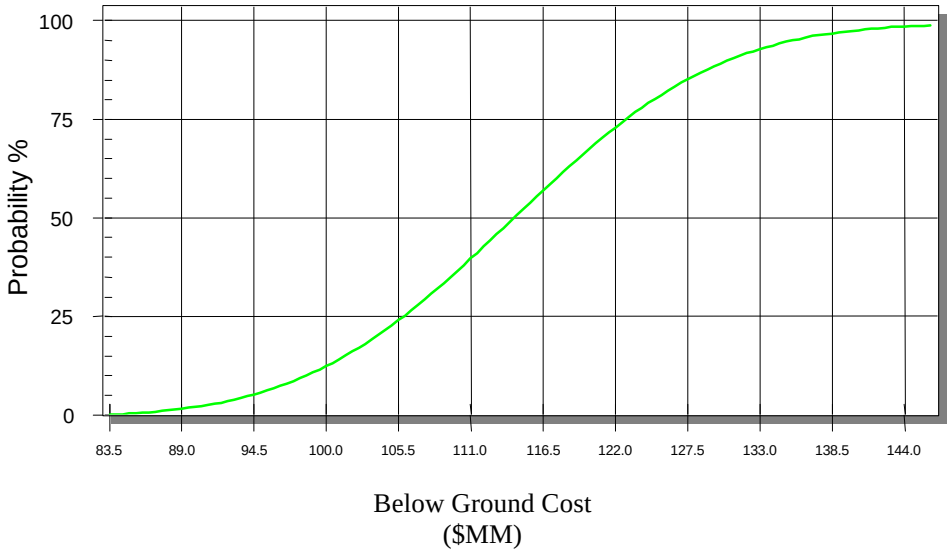

Figure 6-3. Below Ground Investment Cost.

The three dominating uncertainties shown in Figure 6-4 are competition, location, and the steel lining. In a tender procedure, there is always a span between the highest and lowest bid. A 30 percent span between the highest and the lowest is not unusual. Since the cost estimation is done without any competition, it is reasonable to believe that the cost will go down during bidding. In the model, a likely reduction has been set to 5 percent with a span from -15 percent to +10 percent.

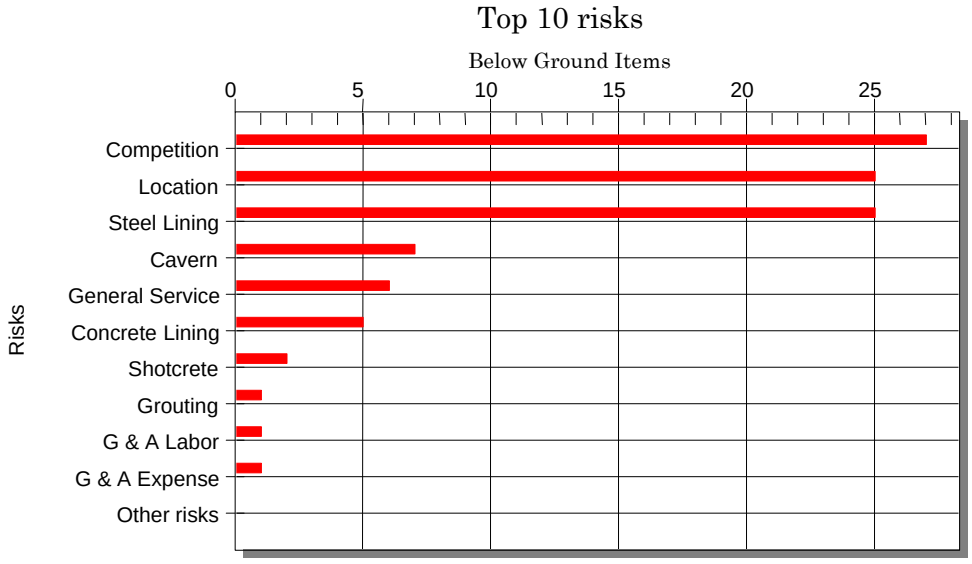

Figure 6-4. Largest Uncertainties for Below Ground Cost.

The second major uncertainty factor has to do with the project location. This parameter is related to the labor union situation and the wages at the location where the project might be built. It is anticipated that there will be a difference between the individual states in New England. In the model, a likely reduction has been set to 0 percent with a span from -15 percent to +10 percent.

The third major uncertainty concerns the steel liner. This uncertainty is related to the production cost of the liner. This type of liner has never been developed before; thus, there is no experience base. The first steel liner will be built in the demonstration plant in Sweden.

The analysis is based on the assumption that the site has been selected and the geologic investigations are made in the preconstruction phase. The uncertainties associated with rock excavation are higher prior to the geological investigation.

6.2.3 Aboveground Cost

The aboveground facilities cost includes:

- Pipeline connection of one-half mile
- Power supply

- Compressor station
- Station piping
- Workshops and warehouses
- Permits, legal fees, insurance.

The cost with 80 percent probability for aboveground construction is $31,000,000 (see Figure 6-5). The largest uncertainty, as shown in Figure 6-6, is related to the compressor equipment and installation of equipment and piping in the compressor station as these are the dominating costs.

RSI-835-99-113

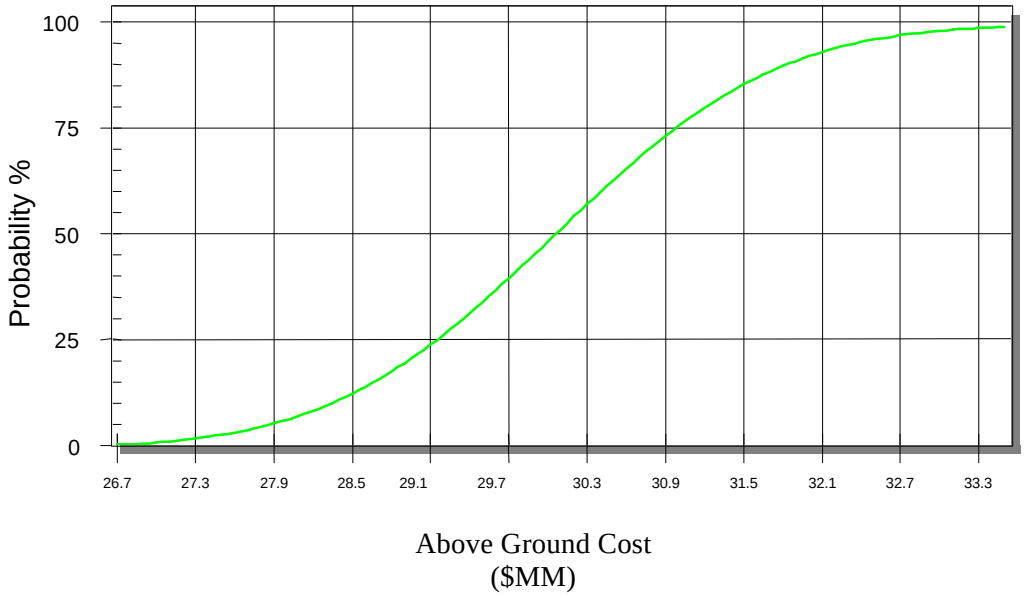

Figure 6-5. Aboveground Investment Cost.

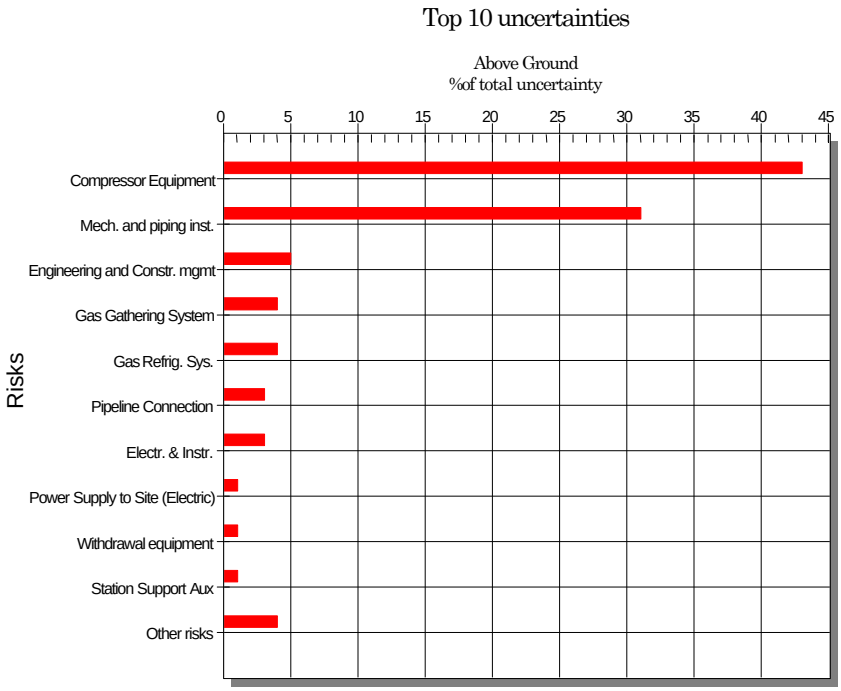

Figure 6-6. Largest Uncertainties for Aboveground Cost.

6.2.4 Total Investment Cost for a Four-Cavern Storage Facility

The total investment cost includes the cost from each of the three main cost groupings: preconstruction, below ground, and aboveground, together with base gas cost and Allowance for Funds During Construction (AFDC). The base gas cost of $1,250,000 is calculated assuming a gas volume of 0.5 bcf and a gas price of $2.5. The AFDC is calculated assuming an interest rate 7.5 percent and the project time schedule in Section 6.2.1. The total investment cost for a four-cavern storage facility (with an 80 percent probability) is shown in Table 6-1.

Table 6-1. Investment Cost for a Four-Cavern LRC Facility

Cost Component	Investment Cost ($1,000)
Preconstruction	5,800
Below ground	125,550
Aboveground	31,000
Base gas	1,250
AFDC	18,700
Total	**182,300**

6.2.5 Operating Cost for a Four-Cavern Storage Facility

The operating cost for a four-cavern storage facility with one cycle is presented in Table 6-2. With several cycles, the fixed operational cost will be constant except for compressor maintenance, which will increase with the run time. The variable cost is proportional to the number of cycles.

Table 6-2. Annual Operating Cost for a Four-Cavern LRC Facility

Cost Component	Annual Operating Cost ($1,000)
Fixed cost:	
Personnel (7)	600
Maintenance compressors	200
Insurance	100
Fixed maintenance	100
Variable cost for one cycle:	
Electricity for injection and cooling plus fuel gas	500
Total cost for one cycle	**1,500**

The Skallen demonstration plant in Sweden will be built with a remote-control capability. Personnel operating the main pipeline will also operate the storage. This manpower approach is also possible with a four-cavern facility, which would cut the cost for personnel shown.

6.2.6 Total Investment Cost for an Eight-Cavern Storage Facility

The eight-cavern storage facility will have the characteristics below:

Number of caverns	8	
Geometrical volume	640 000 (22.6 MMcf)	m^3
Working gas	148×10^6 (5.2 Bscf)	m^3
Gas withdrawal, maximum	14.8×10^6 (560 MMscf/d)	m^3/d
Gas injection	7.4×10^6 (260 MMscf/d)	m^3/d
Gas circulation, maximum	14.8×10^6 (560 MMscf/d)	m^3/d

The design will basically include two modules of four caverns each with a separate access tunnel. The two four-cavern modules can be built simultaneously or sequentially. The cost estimate has been revised for an eight-cavern based on the two four-cavern modules being built at the same time. This will create some synergies regarding indirect construction cost that are more related to the construction time than to the size; e.g., supervision, general service, water treatment, and operation. The cost increase for preconstruction of an eight-cavern facility instead of a four-cavern facility is small. The cost estimate for an eight-cavern facility, with an 80 percent probability, is presented in Table 6-3, together with the four-cavern facility cost multipliers.

Table 6-3. Investment Cost for an Eight-Cavern LRC Facility

Cost Component	Investment Cost ($1,000)	Four-Cavern Facility Multiplier
Preconstruction	7,000	1.21
Below ground	239,000	1.90
Aboveground	60,000	1.94
Base gas	2,500	2.00
AFDC	35,200	1.88
Total	**343,700**	**1.89**

6.2.7 Operating Cost for an Eight-Cavern Storage Facility

The operating cost for an eight-cavern storage facility is presented in Table 6-4. The operating cost is 1.87 times the four-cavern facility cost.

Table 6-4. Annual Operating Cost for an Eight-Cavern LRC Facility

Cost Component	Annual Operating Cost ($1,000)
Fixed cost:	
Personnel (11)	1,700
Maintenance compressors	400
Insurance	150
Fixed maintenance	150
Variable cost for one cycle:	
Electricity for injection and cooling plus fuel gas	1,100
Total cost for one cycle	**2,800**

6.2.8 Comparison of Investment Cost in the United States to Investment Cost in Scandinavia

The investment cost for a four-cavern facility in the United States has been compared to the cost for a similar facility in Scandinavia. The Scandinavian cost was calculated with the SECON-model (see Chapter 7.0 and Appendix D). The cost comparison is presented in Table 6-5.

Table 6-5. Investment Cost Comparison for LRC Storage Between the United States and Scandinavia

Cost Component	U.S. Cost	Scandinavian Cost	Ratio of U.S. Cost to Scandinavian Cost
	$1,000		
Preconstruction Cost	5,800	5,800	1.00
Below Ground Cost	125,550	54,600	2.33
Aboveground Cost	31,000	34,000	0.91
Total	**162,350**	**94,400**	**1.72**

As shown in Table 6-5, there is a great difference in the below ground cost between the United States and Scandinavia. The cost differences for some of the more significant cost items are illustrated in Table 6-6.

Table 6-6. Cost Comparison for LRC Storage Between the United States and Scandinavia for Certain Below Ground Components

Facility Component	United States/ Scandinavia Cost
Tunnels	3.21
Caverns	3.39
Shafts	1.66

The cost differences are caused mainly by different union rules in the United States compared to Scandinavia. These rules significantly impact a labor-intensive project such as excavation of a rock cavern. The tables above indicated that there is a great potential for reducing the project cost. There should be some room for negotiating labor union contracts.

6.2.9 Cost of Service

The cost of service is calculated using the model presented in Chapter 7.0 and Appendix D. The cost of service calculation shown in Table 6-7 is based on the following conditions:

Interest rate	8.4%
Return on equity	14.0%
Equity debt ratio	25/75
Federal tax	36.0%
State tax	8.25%
Property tax	1.0% (Calculated on the entire investment, including that below ground)

Cost of electricity and fuel are included in the cost of service shown in Table 6-7.

Table 6-7. Cost of Service per Deliverability for LRC Storage

Facility	Deliverability MMcf/d	$/Mcf/d/Month	Annual Cost for Capacity at 1 Cycle ($/Mcf)	Annual Cost for Capacity at 12 Cycles ($/Mcf)
Four-cavern facility	260	$9.79	11.75	1.28
Eight-cavern facility	520	$9.23	11.07	1.21

6.2.10 Cost Reduction Potential

Sycon and Gaz de France are presently working with cost reductions for the LRC concept. The evaluations include changes in design, such as increased height and width of the caverns, as well as more economical production methods for mining of the caverns. Options with gas cooling and higher gas pressure are also being evaluated.

The design changes are evaluated technically and economically in an ongoing process with a feasibility target price of $8/Dth/d/month.

6.2.11 Project Schedule

Figure 6-7 illustrates the project schedule for a four-cavern storage facility. The schedule is based on a project construction start in January 1999. The project schedule for the LRC demonstration plant in Sweden is also shown for information.

The total project time is about 6 years. However, two caverns can be commissioned approximately 1 year before total project completion.

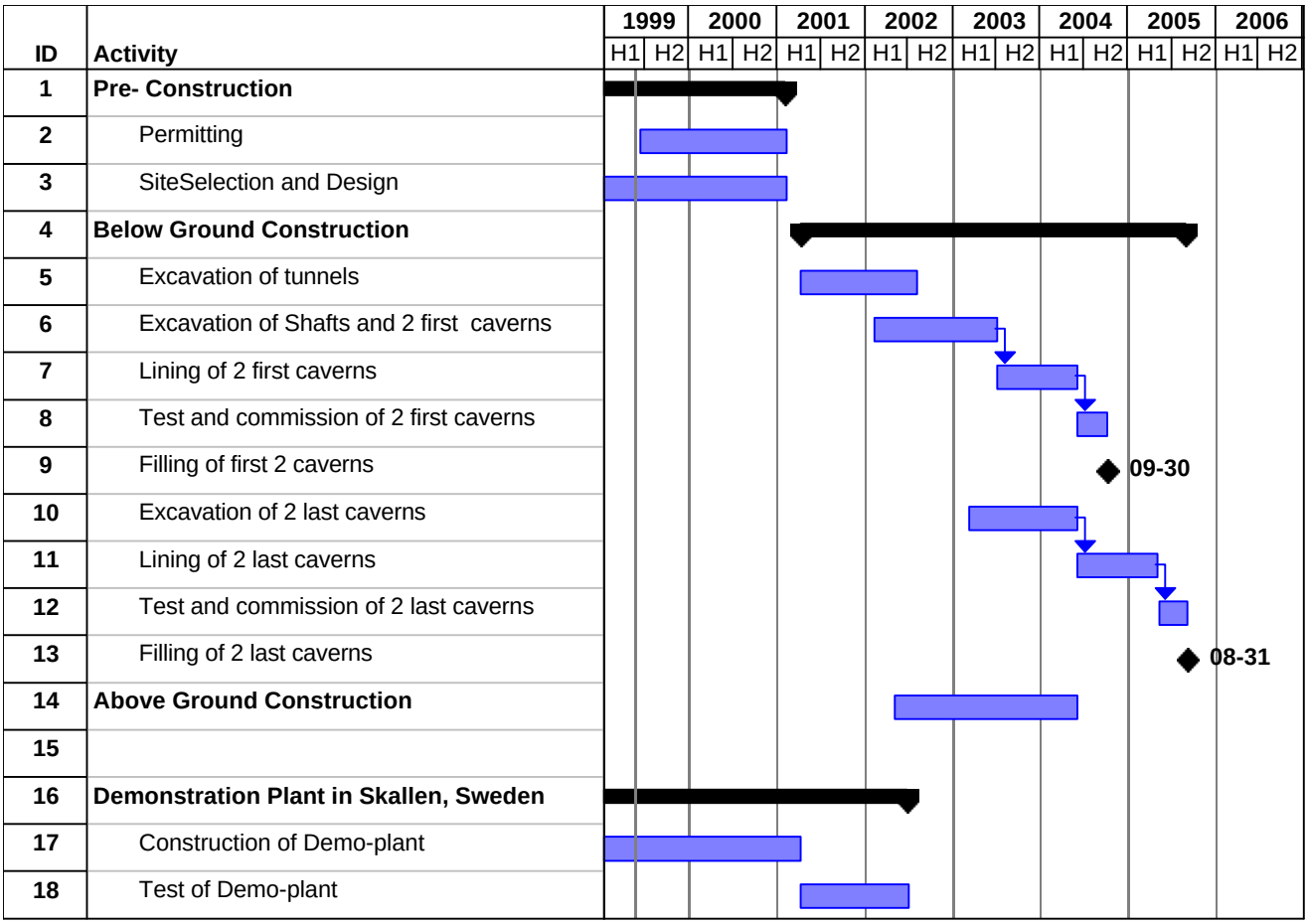

Figure 6-7. Time Schedule for a Four-Cavern LRC Storage.

7.0 ECONOMIC COMPARISON OF LRC TO ALTERNATIVES

7.1 INTRODUCTION

In this chapter, the LRC is compared to other storage alternatives and pipeline transportation. The comparison is made for two regions: the Northeast, covering New England, and the Southeast, covering Georgia, North Carolina, and South Carolina. Both of these areas have geology suitable for LRC and both are facing the highest gas consumption rates in the country, leading to a tremendous increase in the need for flexibility and modulation. The growth is mainly driven by power generation and climate conditions that generate strong peak demands either in winter (Northeast and Southeast) or both in winter and in summer (Southeast).

The Northeast area is located at the far end of the transmission pipeline systems that originate in the gas production regions of the Gulf of Mexico. The gas has to be transported over long distances to reach the East Coast market. Thus, it is expensive to transport the gas with a low load factor; i.e., it is uneconomical to cover the consumption variation with the pipeline. The distance to the Southeast area is shorter, but the pipeline transportation capacity is limited.

There is no salt cavern storage in the two subject areas. The closest salt storage is located in the middle Atlantic for the Northeast and in Louisiana, Mississippi, and Alabama for the Southeast. Furthermore, storage for modulation of a power plant has to be located very close to the facility to be able to function properly. Long transmission distances will create problems in the gas supply due to pressure drop in the system.

LNG peak-shaving facilities, which have been the only storage means in the two areas for a long time, have three major drawbacks:

1. The cost is high.
2. They are not very well perceived by the population, making approval for new projects difficult.
3. An LNG liquefaction plant can generally only provide one cycle per year, depending on the investment for liquefaction equipment. Vaporization plants, which are recharged by truck delivery, can be cycled. However, they then have to rely on a larger liquefaction unit or an import terminal located within a reasonable distance.

7.2 THE NEW ENGLAND AREA

Four pipelines run from the Gulf of Mexico to supply the area: The Tennessee pipeline, the Transcontinental/Algonquin pipeline, the Texas Eastern/Algonquin pipeline, and the Colombia Gulf/Colombia Gas/Algonquin pipeline. Another line, the Iroquois pipeline, supplies New England through the Canadian border from the TransCanada pipeline. The PNGTS receives gas from the TransCanada pipeline via the Montreal pipeline. One more line from Canada is projected: the M&E pipeline. The M&E pipeline will transmit gas from the Sable Island Project.

The storage option available today for the Northeast consumers (besides the option of buying peak gas from LNG) is to utilize storage located in the Middle Atlantic.

7.3 THE SOUTHEAST AREA

The Transcontinental pipeline supplies this area with gas from the Gulf of Mexico. The SONAT pipeline also provides the states of Georgia and South Carolina with gas. The lack of storage facilities in the Southeast is even more evident than in the Northeast. The storage that can be utilized is located in northern West Virginia or in Louisiana, Mississippi, or Alabama. This situation has favored the construction of the Pine Needle LNG plant.

7.4 CASE STUDIES

The economics of LRC will depend on the customers' load profile. To illustrate LRC use with different customer requirements, two cases have been evaluated. The cases are:

Case 1: Peak storage for one cycle each year. The most likely customers are marketers or LDCs that want to cover the risk associated with severe weather conditions.

Case 2: Multiple cycle storage that could be utilized by all types of customers: LDCs, transmission companies, power plants, or marketers. The average number of cycles for the five highest cycling facilities in the United States was between 3 and 3.5 cycles, for the heating season 97-98 [Energy Information Administration, 1998]. The number of cycles for the most active facilities has increased sharply during the 90s. During the heating season of 90-91, the average number of cycles for the five highest cycling facilities was 0.3 cycle. For this case, a three-cycle scenario is chosen.

The cases have been evaluated for the two areas encompassing New England and the Southeast. The economic model presented in Appendix D was utilized for the evaluation.

The cost utilized in this comparison for LRC is the forecasted cost of $8/Dth/d/month. This is a targeted cost for LRC, as discussed in Chapter 6.0.

7.4.1 New England Area

For this area, the possible pipeline transportation alternatives have been listed in Table 7-1.

Table 7-1. Cost Comparison for Various Storage Technologies

In State	Cost Basis	Cost ($/Dth/d/Month)
Maine	Tennessee+Granite	19.82
New Hampshire	Tennessee	17.15
	Col.Gulf/Col.Gas/Tennessee	14.96
Massachusetts	Tennessee	17.15
	Col.Gulf/Col.Gas/Tennessee	16.02
	Texas Eastern/Algonquin	27.53
	TransCanada/Iroquois/Tennessee	33.18
	TransCanada/Iroquois/ Algonquin	39.86
Connecticut	Tennessee	17.15
	TransCanada/Iroquois	33.61
	Col.Gulf/Col.Gas/Tennessee	16.02
	Texas Eastern/Algonquin	27.53

A comparison has been made for a typical customer needing a deliverability of 30 MDth/d. When comparing pipeline transportation and storage utilization, the Tennessee pipeline transportation rate has been utilized. The proposed storage in salt caverns at Tioga and the proposed LNG storage in Wells, Maine, have been used for the storage alternatives. It should be noted that the proposed LNG facility in Wells has been canceled. However, it should nonetheless serve as a reasonable comparison for possible alternatives. A small local LNG satellite tank has also been included for comparison. The satellite can only supply 6 MDth/d with refilling every day. The assumptions made for the evaluation of Cases 1 and 2 are given in Tables 7-2 and 7-3, respectively. The results of the evaluations are shown in Tables 7-4 and 7-5 for Cases 1 and 2, respectively.

Table 7-2. Assumptions for Case 1

Quantity	Value	Units
Needed deliverability	30	MDth/d
Yearly gas volume	300	MDth
Storage withdrawal time	10	d
Storage injection time	200	d
Storage rates:		
LRC	8.0	$/Dth/d/month
Salt storage:		
Tioga (Zone 4)	4.2	$/Dth/d
LNG:		
Wells, Maine (Zone 6)	6.4	$/Dth/d/month
LNG Satellite	9.7	$/Dth/d/month
Transportation of LNG (Truck @ $2.00/Dth)	1.7	$/Dth/d/month
Long haul firm transportation rate on Tennessee (Zone 0-6)	17.15	$/Dth/d/month

Table 7-3. Assumptions for Case 2

Quantity	Value	Units
Needed deliverability	30	MDth/d
Yearly gas volume	900	MDth
Storage withdrawal time	10	d
Storage injection time	200	d
Storage rates:		
LRC	8.0	$/Dth/d/month
Salt storage:		
Tioga (Zone 4)	4.2	$/Dth/d/month
LNG:		
Wells, Maine (Zone 6)	6.4	$/Dth/d/month
Transportation of LNG (Truck @ $2.00/Dth)	1.7	$/Dth/d/month
Long haul firm transportation rate on Tennessee (Zone 0-6)	17.15	$/Dth/d/month

Table 7-4. Comparison of Transportation Cost of 300 MDth Yearly at a Deliverability of 30 MDth/d - Case 1

	Long-Haul Firm Transportation	Tioga Storage	Wells LNG	LNG Satellite[(a)]	LRC
Transportation to storage	-	233,000	600,000	600,000	308,000
Storage Cost	-	1,512,000	2,304,000	3,500,000	2,880,000
Transportation to end customer	6,174,000	2,225,000	1,217,000	-[(a)]	1,217,000
Total annual cost	**6,174,000**	**3,970,000**	**4,121,000**	-[(a)]	**4,405,000**
Total cost (per yearly gas volume)	**20.6**	**13.2**	**13.7**	-[(a)]	**14.7**
Cost compared to long-haul firm transportation		**-2,204,000**	**-2,053,000**	-[(a)]	**-1,767,000**
Total annual cost, Direct connection				**4,100,000**	**3,188,000**
Cost compared to long haul firm transportation with direct connection				**-2,074,000**	**-2,986,000**
Total cost (per yearly gas volume)				**13.7**	**10.63**

(a) Max 6 MDth/d.

The cost for injection and withdrawal are comparably small for all alternatives, and are thus, neglected in this comparison.

The conclusions that can be drawn from these tables are:

- LRC has possibilities to lower the cost for transportation of gas from the Gulf of Mexico to the New England area.
- The cost for LRC is a bit higher than the proposed alternatives for a one-cycle operation. However, for some operations, such as power plant hourly peaks, salt caverns located in Tioga may cause problems for the transmission company due to pressure drop in the transmission line. LRC could then be used for pipeline pressure balancing.
- For the three-cycle case, LRC competes with firm transportation and LNG.
- If the LRC storage can be located so that a direct connection with the end customer, or if back haul delivery can be utilized, the LRC storage competes with all of the alternatives.

Table 7-5. Comparison of Transportation Cost of 900 MDth Yearly at a Deliverability of 30 MDth/d - Case 2

	Long-Haul Firm Transportation	Tioga Storage	Wells LNG	LNG Satellite[(a)]	LRC
Transportation to storage	-	233,000	1,800,000	1,800,000	308,000
Storage Cost	-	1,512,000	2,304,000	3,500,000	2,880,000
Transportation to end customer	6,174,000	2,225,000	1,217,000	-[(a)]	1,217,000
Total annual cost	**6,174,000**	**3,970,000**	**5,321,000**	-[(a)]	**4,405,000**
Total cost (per yearly gas volume)	**6.9**	**4.4**	**5.9**	-[(a)]	**4.9**
Cost compared to long-haul firm transportation		**-2,204,000**	**-853,000**	-[(a)]	**-1,767,000**
Total annual cost, Direct connection				**5,300,000**	**3,188,000**
Cost compared to long haul firm transportation with direct connection				**-874,000**	**-2,986,000**
Total cost (per yearly gas volume)				**5.9**	**3.5**

(a) Max 6 MDth/d.

7.4.2 Southeast Area

Fewer specific alternatives exist in the Southeast for cost comparison. However, it is clear that the Southeast area is closer to the Gulf of Mexico; thus, the transportation cost for gas from the production area to the southern market is lower than transportation to the New England market.

The TRANSCO rates for firm transportation from production areas (Zone 1-3) are $6-7 Dth/d/month for transportation into Alabama and Georgia (Zone 4). Transportation costs into South Carolina and North Carolina (Zone 5) are $9-10 Dth/d/month. Transportation cost inside Zone 4 is $5 Dth/d/month, and the cost inside Zone 5 is $4 Dth/d/month.

The available storage alternative in the southern market area is the Pine Needle LNG storage. The demand charge for this storage is $4.85 Dth/d/month.

The conclusions for the Southeast area are:

- LRC will not compete with firm transportation in Georgia but will in South Carolina and North Carolina. However, connection directly to an end customer or back haul delivery is needed to compete.
- LRC will not compete with LNG for the single cycle of Case 1. However, LRC will compete in Case 2, with a three-cycle operation. This could be of interest for pipeline balancing and power generation.

8.0 ENVIRONMENTAL IMPACT AND PERMITTING ISSUES

8.1 SUMMARY OF ENVIRONMENTAL IMPACT

Construction of the LRC facility will last approximately 4-5 years. Conventional techniques will be used to construct tunnels and rooms in the rock; i.e., drill-and-blast. Electrical drilling machines will be used, which implies that new electric cables must be supplied to the working area. There will be minor ground vibrations from the construction. However, the vibration will be very small and contained within approximately 200 meters (650 feet) from the construction area.

Some of the rock mass can be used for site preparation in connection with the facility and in production of concrete for the storage. Remaining rock aggregate will be piled or sold on the market. Traffic will mainly occur in connection with disposal of crusher material. The rock aggregate used for construction purposes may be crushed in a mobile crusher near the pile. The total amount of rock aggregate from the excavation will be approximately 600,000 m^2 (21 million cubic feet) for a four-cavern facility.

In this chapter of the report, a very brief summary of the potential environmental impacts (both during and after construction) is provided.

8.1.1 Environmental Effects During the Construction Period

Effects on the environment during the construction of the plant can be divided into two main categories: (1) influence from rock excavation work and (2) influence from construction of the connecting pipeline. Pipeline connection is a well-known technology, and is, therefore, not discussed here.

Landscape

The landscape will be influenced from establishing the working site and construction of the plant. Trailers for workers, warehouse, and workshop will be placed at the tunnel entrance. Areas for parking and arrangements for trailers will be made adjacent to the entrance.

Rock aggregate that is placed permanently or temporarily can affect the landscape. Vegetation in the rock aggregate area has to be cut. Access roads will also be developed.

Ground

Within the working area for the storage, there will be an impact on soil because of the traffic. There will be effects on the forestry in the area that is affected by the workings.

Certain work near the working site will be limited. The damage incurred is estimated to be moderate and restoration will be done after the construction is finished.

Vegetation

No affect is assumed on the vegetation due to eventual lowering of the water table in the area. Other damages to the vegetation are estimated only to be in the areas of the buildings and the tunnel entrance.

Animals

The animals in the area may be disturbed by the construction. After some work progress, the rock excavating will be done at greater depths and the disturbance on the ground will be minimized. Other work on the ground may also disturb the animal life, but this disturbance is expected to be very low.

Groundwater

An eventually lower water table will be very local and presumably will only exist for a very short time. Eventually, a well very near the working site could be influenced by a lower water table. However, this is estimated only to occur for short periods of time.

The technique of constructing the storage cavern is based on limiting the inflowing water in the tunnel system. This will be done by grouting; i.e., injection of a cement slurry in the rock cracks.

The water that is still leaking into the tunnel system and cavern room will be pumped up to the ground and be cleaned. Some water will be reused in the building process and some will be disposed. As an alternative, the water can be injected back into the ground.

Watercourses and wetlands

A very small influence is expected on watercourses and wetlands in the area.

Recreation

Recreation in the area around the working site may be disturbed because of the noise from work at the plant and from the traffic. This is expected to be contained within 200-500 meters (650-1,640 feet), depending on the site topography. At large distances, the influence will be small. Certain restrictions can be put in place concerning trespass on ground areas near the working site.

Noise and vibration on the ground

It is a matter of course that a construction site of this size will generate noise. This noise is caused by excavation, transportation, and the ventilation plant for the tunnel. Disturbing noise

levels from the excavation will only be present during the first 3-4 weeks. After this, the excavation will have gone so far into the rock that almost no noise can be heard on the ground.

Dust

Dust arises in connection with vehicular travel. The amount of dust from vehicles should be very small, depending on the condition of the roads. Dust from excavation near the ground is limited in both time and space.

Discharge

The risk of discharge in the surroundings is regarded as small. A source of discharge that can be identified is from the vehicles that are used at the site. Exhaust from these vehicles can, however, be cleaned effectively. Eventual discharge of oil will be limited by demands on the contractor.

8.1.2 Environmental Effects After the Construction Period

Landscape

The plant will have three to four smaller buildings that will be built within an area that will be fenced. A small parking space will be built in connection with the aboveground plant. Existing vegetation and trees shall, as far as possible, be left to minimize the impact on the landscape.

Ground

The use of ground for forestry and farming will be influenced in the area where the aboveground plant is situated. The aboveground plant will be fenced.

Animals

Noise from compressors may disturb sensitive animal life. However, this is not different from existing storage alternatives.

Groundwater

An eventually lower level of groundwater around the storage will be very local and limited during a very short time.

The technique of constructing the storage is based on limiting the inflowing water in the tunnel system. This will be done by grouting; i.e., injection of cement slurry in the rock cracks. The rock mass can be expected to be very dense and no large problems with groundwater loss is expected.

Watercourses and wetlands

A very small influence is expected on watercourses and wetlands.

Recreation

There will be local noise from compressors. Area for the aboveground plant will be fenced. However, this is no different from existing storage alternatives.

Cultural environment

No influence is expected.

Noise

There will be noise from the compressor station. The compressors will be isolated to minimize the noise.

Dust

Dust will practically not exist.

Emission

Emission of natural gas will only occur during maintenance of the aboveground facilities or in an emergency situation.

8.2 PERMIT SUMMARY

Tables 8-1 and 8-2 identify the federal and state regulations (Massachusetts and Georgia) that are or may be applicable to the LRC technology. Regulations and permits required in each state are principally driven by federal legislation, and are, therefore, generally similar.

A column is included in both tables that is entitled "Relevance to LRC Technology." This column indicates whether a specific permit is required, likely to be required, or unlikely to be required. Many of the permit requirements are site specific. It is, therefore, important to consider all potential permit requirements in the site selection and design phases of the work.

Factors which will affect the permitting schedule and cost for an LRC storage facility in each state are highly site specific and should be an important consideration during the site selection process. For example, locating an LRC facility near a valuable and protected resource, such as a wild and scenic river, will result in an increase in the time required and cost for permitting. In addition, a river basin commission authorization may also be required based on the proposed location of the LRC facility and the potential impacts of dewatering operations on area groundwater.

Table 8-1. Federal and State Regulations That are or may be Applicable to the LRC Technology in Massachusetts (Page 1 of 5)

Type	Citation	Agency	Description and Requirements	Relevance to LRC Tech.
	18 CFR Part 157 & 284[a]	FERC	**7(C) Certificates of the Natural Gas Act** Certificates are required to demonstrate or receive: • public convenience and necessity • provision of storage and transportation services • approval of market-based rates • confidential treatment Typical permit application requirements include the following descriptions or evaluations: • project • water use & quality • vegetation & wildlife • cultural resources • socioeconomics • geology • soils • land use, recreation, and aesthetics • air & noise quality • alternatives • reliability & safety • engineering design.	Yes
Regulatory Affairs	301 CMR 11.00[b]	MEPA (State)	**Massachusetts Environmental Policy Act** Environmental Notification Form (ENF) to be filed with the Massachusetts Environmental Policy Act (MEPA) Office. Agency and public comment period follow. Environmental Impact Report (EIR) may be required. Agency and public comment periods follow with a statement issued at the end of the process.	Likely Unlikely
Air Quality Control	310 CMR 6.00, 7.00, & 8.00	MADEP (State)	**Air Permits** Air Plan approval required for construction of certain projects: • fuel utilization facility with energy input above certain threshold limits • construction in nonattainment areas • certain boilers, stationary engines, & emergency generators. Relevant Permits: BWP AQ 02 (Nonmajor comprehensive approval) BWP AQ 03 (Major comprehensive approval)	Likely Unlikely

Table 8-1. Federal and State Regulations That are or may be Applicable to the LRC Technology in Massachusetts (Page 2 of 5)

Type	Citation	Agency	Description and Requirements	Relevance to LRC Tech.
Industrial Wastewater Management	314 CMR	MADEP (State)	**NPDES Permits - Industrial Wastewater**	
	314 CMR 3,00, 4.00 & 12.00		BWP IW 18 Permit required for industrial wastewater discharge to surface waters (no threshold limits based on discharge volume or rate).	Possible
	314 CMR 7.00 & 12.00		BWP IW 12 (Type I Facility) Permit and Plan approval required for industrial wastewater discharge to MA sewer system.	Possible
	314 CMR 5.00 & 6.00		BWP IW 24 (Type I Facility) - plan approval only.	Possible
	314 CMR 12.00		BWP IW 05 (Type I Facility) Permit to discharge industrial wastewater to groundwater.	Unlikely
			Permits required to store industrial wastewater on site in a holding tank with disposal via POTW. No thresholds based on amount of discharge.	
			BWP IW 01 (Permit to construct & install a non-hazardous holding tank).	Unlikely
			BWP IW 28 (Permit to convert an existing tank to a nonhazardous holding tank).	Unlikely
Water Pollution Control	310 CMR 15.00 (Title 5 Regulations)	Municipal Board of Health	**Sanitary Sewage Systems** Disposal Works Construction Permit is required from the local municipal Board of Health for septic systems <10,000 gpd.	Possible
	314 CMR 7.00 & 12.00	MADEP (State	State permits are required for sanitary sewage disposal systems >10,000 gpd. BWP WP 01 Title 5 Plan Approval BWP WP 02 Title 5 Variance BWP WP 03 Approval of miscellaneous sewage treatment systems BWP WP 04 Permit to pump sewage prior to entrance to septic tank BWP WP 10 Permit for discharge to groundwater (includes noncontact cooling water >2,000 gpd, - stormwater, construction dewatering, & other discharges with certain limited treatment	Unlikely

Table 8-1. Federal and State Regulations That are or may be Applicable to the LRC Technology in Massachusetts (Page 3 of 5)

Type	Citation	Agency	Description and Requirements	Relevance to LRC Tech.
Water Pollution Control	314 CMR 7.00 & 12.00	MADEP (State)	**Sewer Connection to Public System** Permits are required for the following public sewer connections. BRP WP 14 Sewer extension ≤2,500 feet & with flows <50,000 gpd or connected to a pump station.	Possible
	314 CMR 7.00 & 12.00	MADEP (State)	BRP WP 55 Permit for sewer extension or industrial wastewater connection (not covered under Industrial Wastewater Management Program) for flows ≥15,000 gpd.	Unlikely
			Industrial Wastewater Holding Tank BRP WP 56 Permit for industrial wastewater holding tank for a facility without a safer alternative.	Unlikely
Watershed Management	40 CFR 122-125 31 CMR 3.00 & 4.00	USEPA & MADEP (State)	**NPDES Permits - Surface Water Discharge** NOTE: Massachusetts is not a delegated state under the Clean Water Act; therefore, a USEPA General Permit is required for Stormwater (Notice of Intent), construction site dewatering, noncontact cooling water, & minor nonprocess wastewater. An approved storm water management plan is required. MADEP review will not being until after a draft permit has been received from USEPA. The permit program is administered jointly with the USEPA.	
			BWP WM 06 (Type I Surface Water Discharge). BWP WM 08 (EPA General Permit (NOI), Stormwater). BWP WM 09 (Approval of Stormwater Management Plan). BWP WM 10 (EPA General Permit, Construction Site Dewatering). BWP WM 11 (EPA General Permit, Noncontact Cooling Water). BWP WM 13 (EPA General Permit, Minor Nonprocess Wastewater).	Unlikely Yes Yes Yes Unlikely Possible
Watershed Management	310 CMR 4.00 & 36.00	MADEP (State	**Surface Water & Groundwater Withdrawal** BRP WM 03 Permit required for surface water or groundwater withdrawal from river basins at a rate >100,000 gpd or >9 million gal/3 mos.	Unlikely

Table 8-1. Federal and State Regulations That are or may be Applicable to the LRC Technology in Massachusetts (Page 4 of 5)

Type	Citation	Agency	Description and Requirements	Relevance to LRC Tech.
Water Supply	310 CMR 27.00	MADEP (State)	**Underground Injection Control**	
			BRP WS 06 Permit required for Class V well (underground injection).	Possible
			NOTE: A recharge well(s) used to replenish water in an aquifer is classified as Class V.	
Wetlands & Waterways	310 CMR 9.00 & 10.00	MADEP (State)	**401 Water Quality Certification**	Possible
			Required under the Federal Clean Water Act for certain activities in wetlands and waters. Massachusetts has the authority to review projects that must obtain federal licenses or permits that result in discharges to state waters. This applies to dredging, disposal of dredged material, & placement of fill in vegetated wetlands or waters subject to federal jurisdiction.	
			An optional Determination of Applicability (BRP WW 04) for projects can be made by the Waterways Regulations Program.	
			Relevant license, permit, or certificate of compliance required for wetlands or waterways work include:	
			BRP WW 01 Waterways license - required for projects involving the placement of structures & fill in nontidal rivers & streams and other categories.	Unlikely
			Waterways permit - required for projects not involving fill or placement of structures in waterways (such as dredging).	Possible
			BRP WW 11 Project certification required for minor fill or excavation (loss up to 5,000 ft^2 of bordering & isolated wetland).	Unlikely
			BRP WW 08 Project certification required for minor dredging (between 100 yd^3 and 5,000 yd^3).	Unlikely
			BRP WW 05 Certificate of Compliance required within 60 days of completion of the project.	Possible
		USACOE	**Section 404 Permit (Federal)**	
			Needed for a proposed activity that involves filling and construction in any waterway or wetland.	Likely
		USACOE	**Section 10 Permit (Federal)**	
			Needed for dredging, filling, or construction & repair of structures in navigable waters.	Unlikely

Table 8-1. Federal and State Regulations That are or may be Applicable to the LRC Technology in Massachusetts (Page 5 of 5)

Type	Citation	Agency	Description and Requirements	Relevance to LRC Tech.
Wetlands & Waterways	310 CMR 10.00	Local Conservation Commission	**Wetlands Protection** Wetlands protection is administered by local conservation commissions. A Notice of Intent (NOI) and permit (Order of Conditions) is required from the local conservation commission for removing, dredging, filling, or other altering of a wetland.	Possible
Hazardous Materials	40 CFR 262 310 CMR 30.00	USEPA MADEP (State)	**Hazardous Waste Generators** Registration required for hazardous waste generators (LQG, SQG, & VSQG). • EPA ID Number required for LQG & SQG (except waste oil) • MADEP registration required for VSQG & waste oil SQG. NOTE: Waste oil is classified as hazardous in MA. Hazardous materials recycling permit required for >27 gal. hazardous waste per month.	Possible Unlikely
Toxics Use Reporting	310 CMR 40.00, 41.00, & 50.00	MADEP (State)	Regulations which apply to facilities that use at least 10,000 lbs. of any chemical listed on EPA's Toxic Release Inventory (Section 313 - Emergency Planning and Right-to-Know and CERCLA).	Unlikely
Solid Waste Management	310 CMR 16.00 & 19.00	MADEP (State)	**Solid Waste Management Facilities** NOTE: A comprehensive site assessment is required for a solid waste management facility permit. Permits (or other) are required for the following categories: BWP SW 17 Determination of Need, Small Operation Site Assignment. BWP SW 27 Permit for new landfill between 25 & 250 acre feet (volume). BWP SW 28 Permit for new landfill <25 acre feet (volume) BWP SW 10 Permit to receive authorization to operate a new landfill. BWP SW 01 Permit to establish a new solid waste facility.	Unlikely

(a) Code of Federal Regulations.

(b) Code of Massachusetts Regulations.

Table 8-2. Federal and State Regulations That are or may be Applicable to the LRC Technology in Georgia (Page 1 of 4)

Type	Citation	Agency	Description and Requirements	Relevance to LRC Tech.
	18 CFR Part 157 & 284[a]	FERC	**7(C) Certificates of the Natural Gas Act** Certificates are required to demonstrate or receive: • public convenience and necessity • provision of storage and transportation services • approval of market-based rates • confidential treatment Typical permit application requirements include the following descriptions or evaluations: • project • water use & quality • vegetation & wildlife • cultural resources • socioeconomics • geology • soils • land use, recreation, and aesthetics • air & noise quality • alternatives • reliability & safety • engineering design.	Yes
Underground Storage	OCGA Section 46-4-50 to 46-4-62	GA Public Service Comm. (State)	**Underground Gas Storage** Requirements & regulations which apply to utilities desiring to use or operate an underground reservoir. An order approving the project is required from the Public Service Commission. • The application shall include a legal description of all proposed improvements, maps showing the proposed facilities and underground reservoir, and other information to provide a clear and concise presentation.	Yes
Surface Mining	Chapter 390-3-3[b], Surface Mining	GDNR (EPD) (State)	**Surface Mining** Permit and Mine Land Use Plan required for surface mining. The Mine Land Use Plan shall include: • Engineering drawings, plans, specifications, maps, or other attachments • A specific plan of action • Description of the company • Mining methods & lands to be affected • Reclamation objective & schedule • Affected acreage • Protection of contiguous natural resources & property on the National Register of Historic Places • Erosion & siltation control.	Likely

Table 8-2. Federal and State Regulations That are or may be Applicable to the LRC Technology in Georgia (Page 2 of 4)

Type	Citation	Agency	Description and Requirements	Relevance to LRC Tech.
Eminent Domain	Chapter 391-3-23, Petroleum Pipeline Eminent Domain Procedures	GDNR (EPD) (State)	**Petroleum Pipeline Eminent Domain** A Certificate of Public Convenience and Necessity is needed from the Commissioner followed by a permit. Permit application requirements include: • Certificate of Public Convenience • Property information (inc. consultations with owners) • Environmental effects report • Background engineering reports.	Possible
Air	Chapter 391-3-1, Air Quality Control	GDNR (EPD) (State)	**Air Permits** Title V Program Permit, application requirements include: • Facility-wide information • Emission unit information • Emissions data • Monitoring program • Compliance program (for existing facilities not in compliance) • Accidental release prevention program. NOTE: Applicant may be able to combine groups of emissions units.	Likely
Water	Chapter 391-3-16.03 Federal Water Pollution Control Act, Sections 301-303, 306 & 307	GDNR (EPD) (State) USACOE (Federal) USACOE (Federal)	**Joint Application** 401 Certification of Water Quality State program is coordinated with USACOE (Savanna Dist.) via a Memorandum of Understanding. Federal Water Pollution Control permits through USACOE are typically included. **Section 404 Permit (Federal)** Needed for a proposed activity that involves filling and construction in any waterway or wetland. **Section 10 Permit (Federal)** Needed for dredging, filling, or construction of structures in navigable waters.	Likely Likely Unlikely

Table 8-2. Federal and State Regulations That are or may be Applicable to the LRC Technology in Georgia (Page 3 of 4)

Type	Citation	Agency	Description and Requirements	Relevance to LRC Tech.
Water	Chapter 391-3-6, Water Quality Control	GDNR (EPD) (State)	**NPDES Permitting** Authority delegated to state by USEPA. State regulations pursuant to the GA Water Quality Control Act. NPDES permits are required for the following categories: • Storm water associated with industrial activity • Nonstorm water (general or individual) • Storm water associated with construction • Underground Injection Control • Land disposal & treatment systems • Land application facilities. Permit application requirements include: Storm Water (industrial activity) Notice of Intent, pollution prevention plant, engineering report(s), plans & specifications, monitoring program, notice & public participation. Storm Water (construction) Nonstorm Water Notice of Intent, engineering report(s), plans, specifications & related materials, notice & public participation.	Likely Yes Possible
Groundwater	Chapter 391-3-2, Groundwater Use	GDNR (EPD) (State)	**Groundwater Withdrawal** The state regulates groundwater withdrawal and/or use at rate of >100,000 gpd. A permit is required for consumptive or nonconsumptive use. Permit requirements include: • State concurrent on well construction • Documentation • Proposed groundwater injection well information • Aquifer characteristics • Drilling & well construction information.	Unlikely
Hazardous Waste	Chapter 391-3-11, Solid Waste Management 40 CFR 262	GDNR (EPD) (State) USEPA	**Hazardous Waste Generators** Registration, storage, handling, shipping, and treatment/disposal requirements for hazardous waste generators (LQG & SQG). • EPA ID Number required for LQG & SQG generators.	Possible

Table 8-2. Federal and State Regulations That are or may be Applicable to the LRC Technology in Georgia (Page 4 of 4)

Type	Citation	Agency	Description and Requirements	Relevance to LRC Tech.
Solid Waste Management	Chapter 391-3-4, Solid Waste Management	GDNR (EPD) (State)	**Solid Waste Management Landfills** Permit required for construction & operation of a solid waste landfill. Landfill siting requirements include: • Site assessment report geologic, hydrologic, & env. resources) • Application of specific design criteria • Approved monitoring program • Closure requirements.	Unlikely
Underground Storage Tank Management	Chapter 391-3-15, Underground Storage Tank Management	GDNR (EPD) (State)	**Underground Storage Tank Registration** Annual registration required for underground storage tanks.	Possible

(a) Code of Federal Regulations.

(b) Rules of the Georgia Department of Natural Resources, Environmental Protection Division.

Overall, a rough estimate of the time required to obtain necessary permits in these states will generally range between 18 and 24 months, based on the following assumptions:

- An Environmental Impact Statement (EIS) is not required (site location is critical for this issue).
- Site selection, property acquisition (excluding pipeline right-of-ways, if required), and preliminary design are substantially complete at the onset of permit studies and applications.

It should be further noted that the following issues may increase the permitting schedule:

- If the project is opposed by the agencies, special interest groups, or intervenors.
- Construction and/or project health and safety reviews, as may be required by the Occupational Safety and Health Administration (OSHA) or Mine Safety and Health Administration (MSHA) may be required.
- Local municipal reviews and approvals will be required.

As far as costs for licensing and permitting, project specifics, such as length of pipeline tie-ins, proximity to environmentally sensitive areas, and level of opposition to the project, greatly impact the costs of permitting and licensing. Therefore, a range of $2-10 million for permitting activities would not be unreasonable.

9.0 REFERENCES

Barton, N., R. Lien, and J. Lunde, 1974. "Engineering Classification of Rock Masses for the Design of Tunnel Support," *Rock Mechanics*, Springer Verlag, Vol. 6, pp. 189-236.

Bieniawski, Z. T., 1973. "Engineering Classification of Jointed Rock Masses," *Trans. South African Inst. Civ. Eng.*, Vol. 15, No. 12, pp. 335-344.

Bieniawski, Z. T., 1978. "Determining Rock Mass Deformability - Experiences From Case Histories," *International Journal of Rock Mechanics and Mining Science & Geomechanics Abstracts*, Vol. 15, pp. 237-247.

Brown, E. T., J. W. Bray, B. Ladanyi, and E. Hoek, 1983. "Ground Response Curves for Rock Tunnels," *Journal of Geotechnical Engineering,* ASCE 109, pp. 15-39.

Energy and Environmental Inc., 1994. *Cost of New Underground Natural Gas Storage Facilities in the Lower 48 States,* final report submitted to United States Department of Energy and the Energy Information Administration.

Energy Information Administration, 1998. *Natural Gas 1998: Issues and Trends.*

Goldsmith, R., 1987. *The Bedrock Geology of Massachusetts*, U.S. Geologic Survey Professional Paper 1366-E-J.

Grimstad, E. and E. Barton, 1993. "Updating of the Q-System for NMT," *Proceedings, International Symposium on Sprayed Concrete - Modern Use of Wet Mixed Sprayed Concrete for Underground Support, Fagernes*, Eds. Kompen Opsahl och Berg. Norwegian Concrete Association, Oslo, Norway.

Harvey, R. C. and E. Burley, 1973. "Behaviour of Shallow Inclined Anchorages in Cohesionless Sand," *Ground Engineering*, Vol. 6, pp. 48-55.

Hoek, E., and E. T. Brown, 1980. "Underground Excavations in Rock," *Institute of Mining and Metallurgy*, London.

Hoek, E., P. K. Kaiser, and W. F. Bawden, 1997. *Support of Underground Excavations in Hard Rock,* A. A. Balkema.

Isander, A., 1994. "Rock Mechanical Results From a Research Facility for Storage of Natural Gas in Lined Rock Caverns," *ISRM International Symposium*, Santiago, Chile.

Littlejohn, G. S. and D. A. Bruce, 1975. "Rock Anchors - State of the Art," *Ground Engineering*, May.

McConnell, K. I. and J. O. Costello, 1982. "Guide to Geology Along a Traverse Through the Blue Ridge and Piedmont Provinces of North Georgia," *Excursions in Southeastern Geology,* R. W. Frey (ed.), American Geological Institute, Vol. 1, pp. 241-258.

Sagefors, I. and P-A. Daerga, 1996. "An Excavation Method for Large Vertical Cylindrical Caverns," *Tunnelling and Underground Space Technology*, Vol. 11, No. 3, pp. 279-285.

Serafim, J. L. and J. P. Pereira, J. P., 1983. "Consideration of the Geomechanical Classification of Bieniawski," *Proceedings, International Symposium on Engineering Geology and Underground Construction*, Lisbon 1(II), pp. 33-44.

Stille, H., 1984. *Rock Bolting - Analysis Based on the Theory of Ground Reaction Curve*, Report 151:1/84, Swedish Rock Engineering Research, SveBeFo, Stockholm, Sweden.

Stille, H., A. Fredriksson, and T. Groth, 1982. *FEM-Analys Av Bergmekaniska Problem Med JOBFEM*, BeFo Nr. 307:1/82.

Stille, H., J. Johansson, and R. Sturk, 1994. "High Pressure Storage of Gas in Lined Rock Caverns - Results From Field Tests," *Proceedings, EUROCK'94 International Conference*, Delft, Balkema, Rotterdam.

Sturk, R. and H. Stille, 1995. "Design and Excavation of Rock Caverns for Fuel Storage - A Case Study From Zimbabwe," *Tunneling and Underground Space Technology*, Vol. 10, No. 2, pp. 193-201.

Sydgas, 1990a. *Catastrophic Case for Lined Rock Caverns,* Internal report.

Sydgas, 1990b. *Simulation of Natural Gas Dispersion at Leakage From a Rock Storage,* Internal report.

Sydgas, 1992. *Initial Risk Analysis for Lined Rock Caverns Storage for Natural Gas,* Internal report.

Sydgas and Vattenfall, 1992. *Swedgas' Storage Project, Technology and Costs, Summary,* Internal report.

Sydgas, Sydkraft, Vattenfall, and Swedgas, 1987a. *Lined Rock Caverns: Project Carbon Steel Lining,* Internal report.

Sydgas, Avesta Lining, and Swedgas, 1987b. *Stainless Steel for Lining of Rock Cavern for Storing of Pressurized Natural Gas*, Internal report.

Sydgas, Sydkraft, Avesta Lining, and Vattenfall, 1989. *Sydgas Natural Gas Storage - Phase 1*, Internal report.

Sydkraft and Gas de France, 1996a. *Basic Design Report,* Internal report.

Sydkraft and Gas de France, 1996b. *Final Risk Asssessment,* Internal report.

Sydkraft and Gas de France, 1997. *Elaboration of Detailed Demonstration Program,* Internal report.

Sydkraft and Skanska, 1995a. *Authority Standards,* Internal report.

Sydkraft and Skanska, 1995b. *Operational Conditions,* Internal report.

Sydkraft and Skanska, 1995c. *Site Specific Conditions,* Internal report.

Sydkraft and Skanska, 1995d. *Technical Criteria for Localization,* Internal report.

Sydkraft and Skanska, 1995e. *Risk Analysis,* Internal report.

Sydkraft and Skanska, 1995f. *Modelling of Sandwich Wall Construction,* Internal report.

Sydkraft and Skanska, 1995g. *System for Water and Gas Drainage for Lined Gas Storage,* Internal report.

Sydkraft and Skanska, 1995h. *Supplementary Rock Mechanical Studies,* Internal report.

Sydkraft and Skanska, 1995i. *Strategy and Program for Quality Assurance,* Internal report.

Sydkraft and Skanska, 1995j. *Simplified Above Ground Plant,* Internal report.

Thompson, J. M., 1997. "U.S. Underground Storage of Natural Gas in 1997: Existing and Proposed," *Natural Gas Monthly*, September.

Vesic, A. S., 1971. "Breakout Resistance of Objects Embedded in Ocean Bottom," *Journal of Soil Mechanics and Foundation Division*, ASCE, Vol. 97, No. SM9, pp. 1183-1205.

APPENDIX A

DESCRIPTION OF JOBFEM FINITE ELEMENT SOFTWARE

APPENDIX A
DESCRIPTION OF JOBFEM FINITE ELEMENT SOFTWARE

A FINITE ELEMENT COMPUTER PROGRAM FOR ANALYSIS OF SOIL AND ROCK STRUCTURES

JOBFEM is a finite element program specially designed to simulate soil and rock structures and offers the following features:

- Material behaviors, such as elasto-plasticity with Mohr-Coulomb failure criteria, multi-laminate materials, hyperbolic stress-strain relationship, and a joint model.
- Excavation, filling, variable pore pressure, and temperature loads.
- Calculation of transient and steady state groundwater head or temperature flow.
- Three- and four-node area elements and a four-node joint element.
- The application of support elements such as tensioned and untensioned rock bolts, linings, beams, and shells.
- Analysis of either two-dimensional (plane strain, plane stress) or axisymmetrical problems.

The program system **JOBFEM** includes a preprocessor for mesh generation and mesh plotting and postprocessors for plotting the results of the analysis in different forms.

JOBFEM was developed at the Department of Soil and Rock Mechanics at the Royal Institute of Technology in Stockholm. The program has been used in Sweden for several years in practical design. A manual in English is available.

APPENDIX B

LRC GAS TEMPERATURE CALCULATIONS

APPENDIX B
LRC GAS TEMPERATURE CALCULATIONS

1. Temperature and pressure initialization

During the commissioning procedure, it is planned to pressurize the cavern with water. Therefore, temperature simulations can be initiated with a water-filled cavern. The cavern is assumed to be filled with water for 60 days for the tests. The dewatering phase will last approximately 1 month. The initial conditions are as follows:

Water temperature	11°C (51°F)
Rock temperature	17°C (62°F)

2. Cavern Characteristics

The cavern geometric characteristics are as follows:

Midcavern depth	200 m
Volume	80 000 m^3
Diameter	35 m
Height	83 m

3. Thermal characteristics for the surrounding rock mass

The rock thermal properties are as follows:

Conductivity	3.5 W/m/K
Spec. weight	2,700 kg/m^3
Spec. heat	800 J/kg/K
Geothermal Gradient	0.03 K/m

4. Gas Characteristics

The thermodynamic functions of the gas are calculated by using norm AGA8.

5. Cavern performance

The cavern performance characteristics are as follows:

Working gas	$14.3 \times 10^6 m^3$ (0.50 Bscf)
Gas withdrawal, maximum	$1.4 \times 10^6 m^3$/day (50 MMscf/day)
Gas injection	$0.7 \times 10^6 m^3$/day (25 MMscf/day)
Time of withdrawal	10d

Time of injection	20d
Pressure after injection	230 bar (3,330 psi)
Pressure after withdrawal	38 bar (550 psi)
Gas injection temperature is equal to	10°C (50°F).

RESULTS

The results of the thermal simulation are shown in Figure B-1. The first injection starts at Day 11 and lasts for 20 days. After that, there is a quiescence period of 20 days before the 10-day withdrawal starts. The temperature for this cycle varies from a maximum of +43°C (108°F) after injection to -18°C (0°F).

The second injection cycle starts directly after the withdrawal. At the end of the 20-day injection, the cavern temperature is 37°C (99°F). The preceding 10-day withdrawal starts immediately after the injection. The temperature after withdrawal is -18°C (0°F). The cycle is repeated again with the same results.

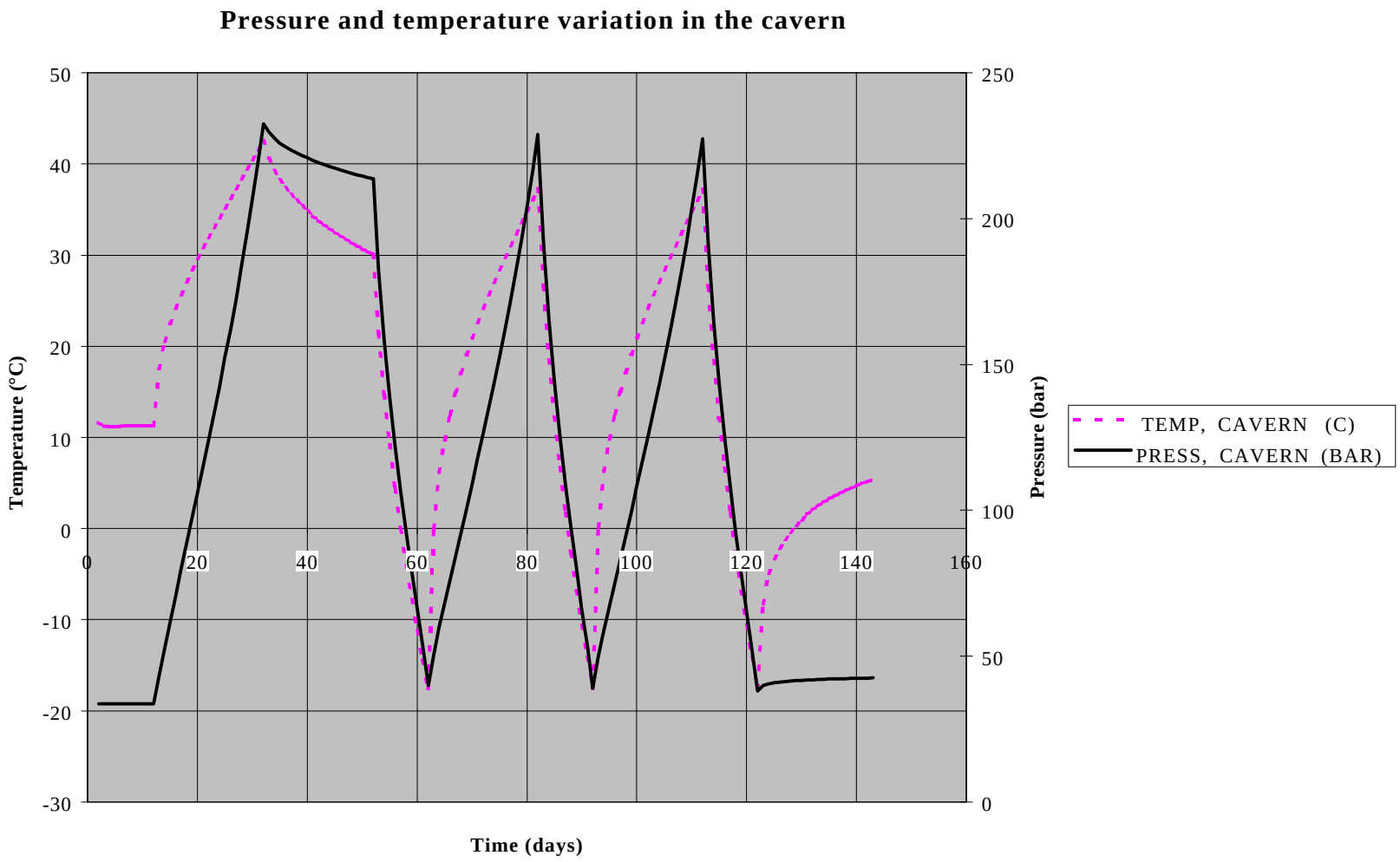

Figure B-1. Pressure and Temperature Variation in the Cavern.

APPENDIX C

DESIGN DRAWINGS

APPENDIX C
DESIGN DRAWINGS

DRAWING LIST
DEPARTEMENT OF ENERGY
LRC NATURAL GAS STORAGE Date 1999-01-31

Drawing No.		Date	Name	Rev	Date	Remark
EXGAZ	-01	980831	PROCESS DIAGRAM	A	990121	
EXGAZ	-02	980831	PROCESS DIAGRAM LOADING WITH REDUCTION	A	990121	
EXGAZ	-03	980831	PROCESS DIAGRAM LOADING WITH COMPRESSION	A	990121	
EXGAZ	-04	980831	PROCESS DIAGRAM WITHDRAWAL WITH REDUCTION	A	990121	
EXGAZ	-05	980831	PROCESS DIAGRAM WITHDRAWAL WITH COMPRESSION	A	990121	
EXGAZ	-06	980831	PROCESS DIAGRAM CIRCULATION COOLING/HEATING	A	990121	
EXGAZ	-07	980902	NEW ENGLAND LAY-OUT	-		
EXGAZ	-08	980902	PIPING IN STORAGE ROOM	-		
EXGAZ	-12	990128	STORAGE ROOM, SECTION SITE 2	-		
EXGAZ	-13	990128	ROCK REINFORCEMENT	-		
EXGAZ	-14	990128	ACESS TUNNEL, SECTION STRAIGHT, CURVE	-		
EXGAZ	-15		GENERAL LAYOUT	-		
EXGAZ	-16		CAVERN AND TUNNELLING CONFIGURATION	-		

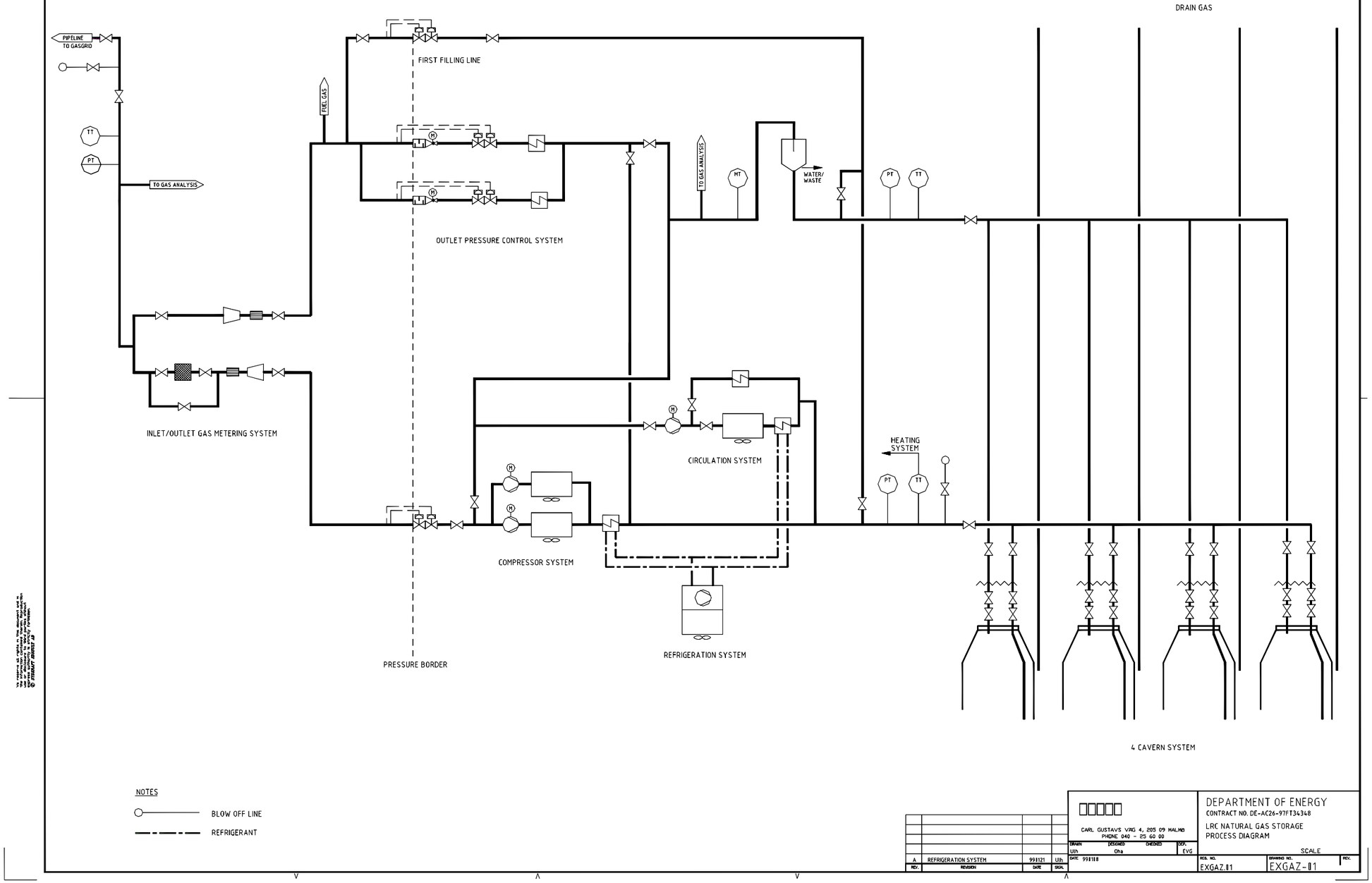
PIPELINE
TO GASGRID
TT
PT
TO GAS ANALYSIS
INLET/OUTLET GAS METERING SYSTEM
FUEL GAS
FIRST FILLING LINE
OUTLET PRESSURE CONTROL SYSTEM
COMPRESSOR SYSTEM
PRESSURE BORDER
CIRCULATION SYSTEM
REFRIGERATION SYSTEM
TO GAS ANALYSIS
MT
WATER/
WASTE
PT
TT
HEATING
SYSTEM
PT
TT
DRAIN GAS
4 CAVERN SYSTEM
NOTES
BLOW OFF LINE
REFRIGERANT
CARL GUSTAVS VÄG 4, 205 09 MALMÖ
PHONE 040 - 25 60 00
DRAWN
DESIGNED
CHECKED
DEPT.
Ulh
Ohs
EVG
DATE 991118
DEPARTMENT OF ENERGY
CONTRACT NO. DE-AC26-97FT34348
LRC NATURAL GAS STORAGE
PROCESS DIAGRAM
SCALE
REG. NO.
EXGAZ.11
DRAWING NO.
EXGAZ-11
REV.
A
REFRIGERATION SYSTEM
991121
Ulh
REV.
REVISION
DATE
SIGN.

1. LOADING WITH REDUCTION

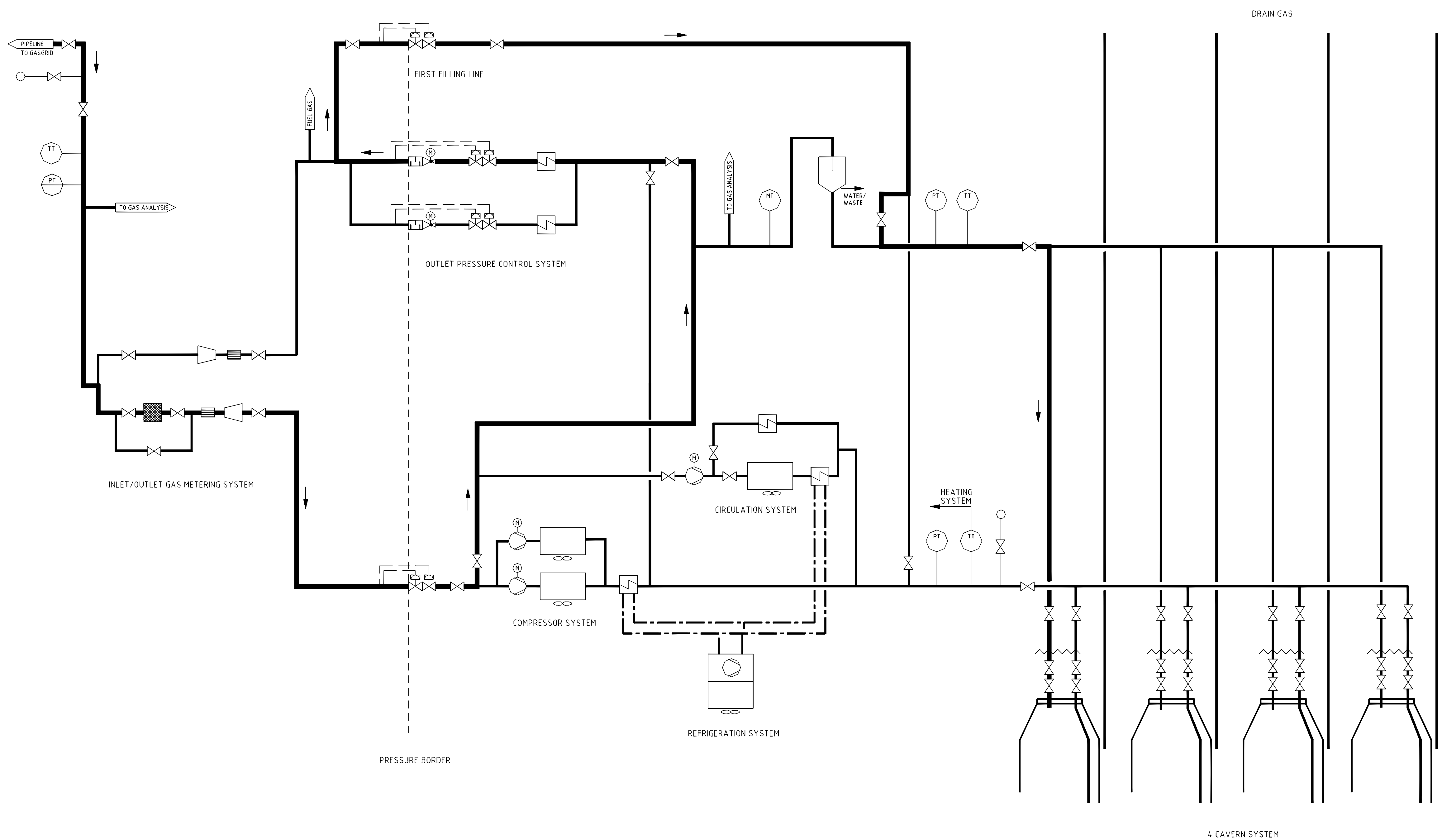

NOTES

BLOW OFF LINE

REFRIGERANT

REV.	REVISION	DATE	SIGN.
A	REFRIGERATION SYSTEM	990121	Ulh

CARL GUSTAVS VÄG 4, 205 09 MALMÖ
PHONE 040 - 25 60 00

DRAWN	DESIGNED	CHECKED	DEP.
Ulh	Oha		EVG

DATE 990108

DEPARTMENT OF ENERGY
CONTRACT NO. DE-AC26-97FT34348
LRC NATURAL GAS STORAGE
PROCESS DIAGRAM
LOADING WITH REDUCTION
SCALE

REG. NO.	DRAWING NO.	REV.
EXGAZ.01	EXGAZ-02	

2. LOADING WITH COMPRESSION

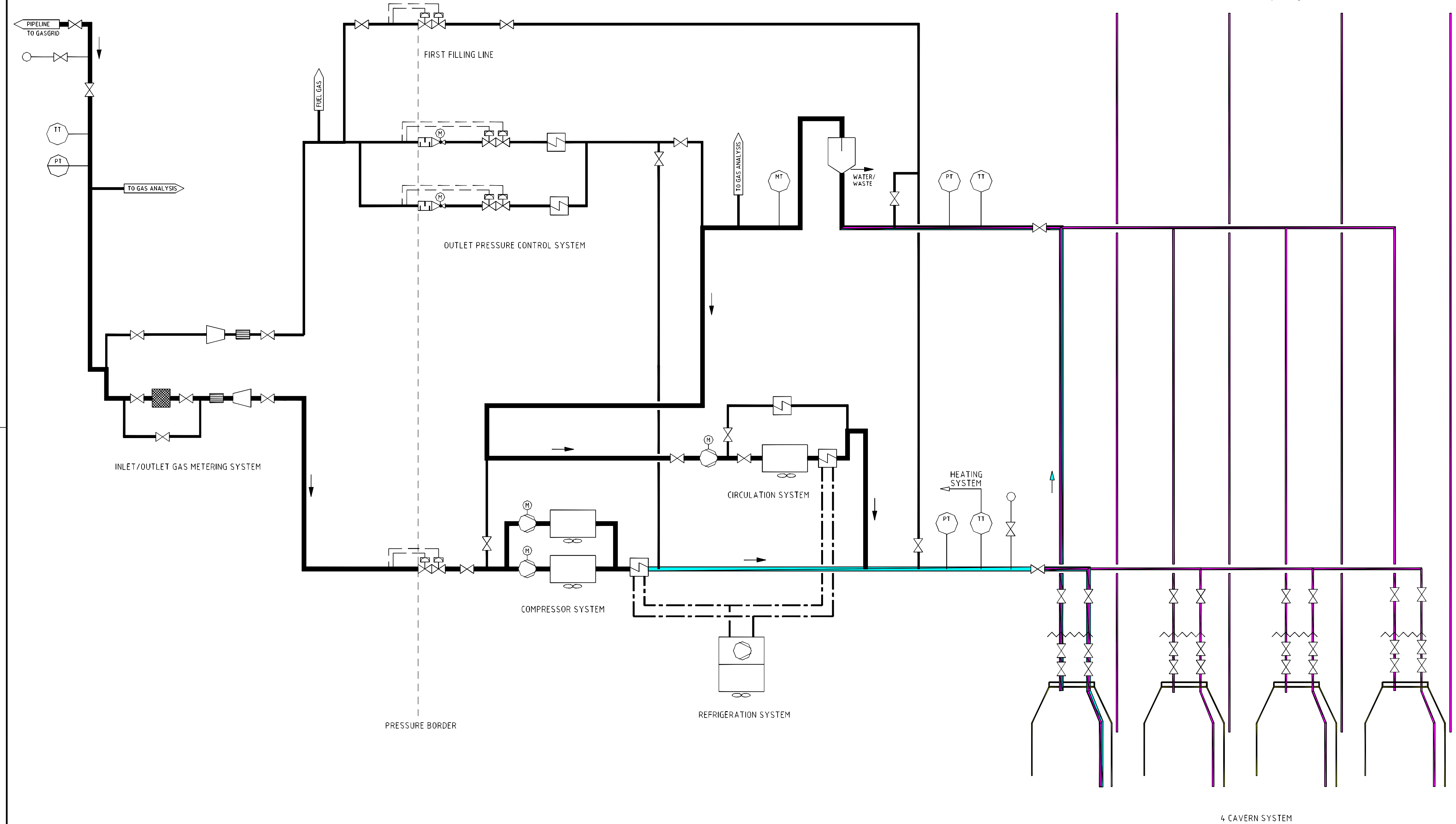

NOTES

- BLOW OFF LINE
- REFRIGERANT

REV.	REVISION	DATE	SIGN.
A	REFRIGERATION SYSTEM	990121	Ulh

CARL GUSTAVS VÄG 4, 205 09 MALMÖ
PHONE 040 - 25 60 00

DRAWN: Ulh DESIGNED: Oha CHECKED: DEP.: EVG
DATE: 990108

DEPARTMENT OF ENERGY
CONTRACT NO. DE-AC26-97FT34348
LRC NATURAL GAS STORAGE
PROCESS DIAGRAM
LOADING WITH COMPRESSION
SCALE

REG. NO. EXGAZ.01
DRAWING NO. EXGAZ-03
REV.

3. WITHDRAWAL WITH REDUCTION

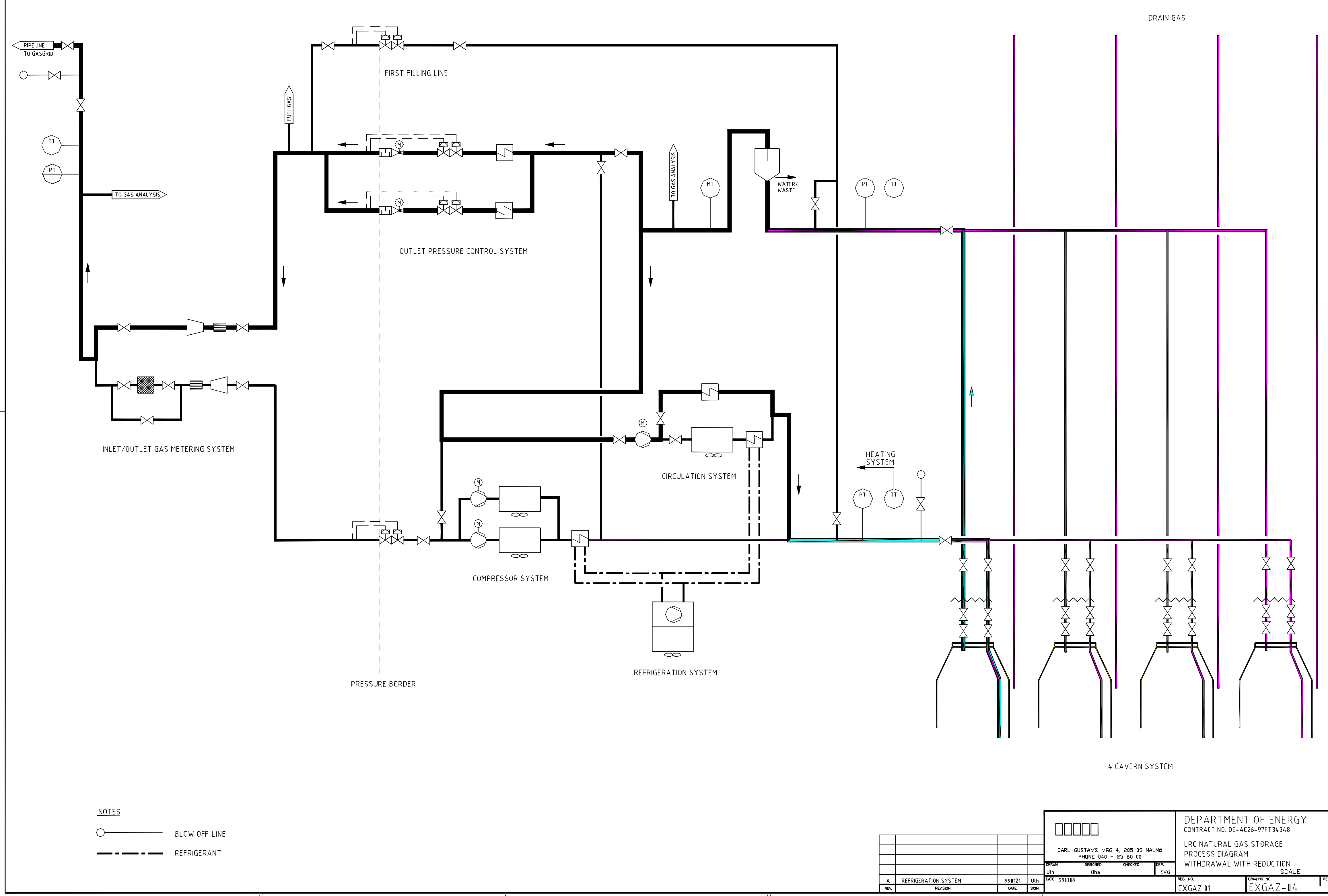

4. WITHDRAWAL WITH COMPRESSION

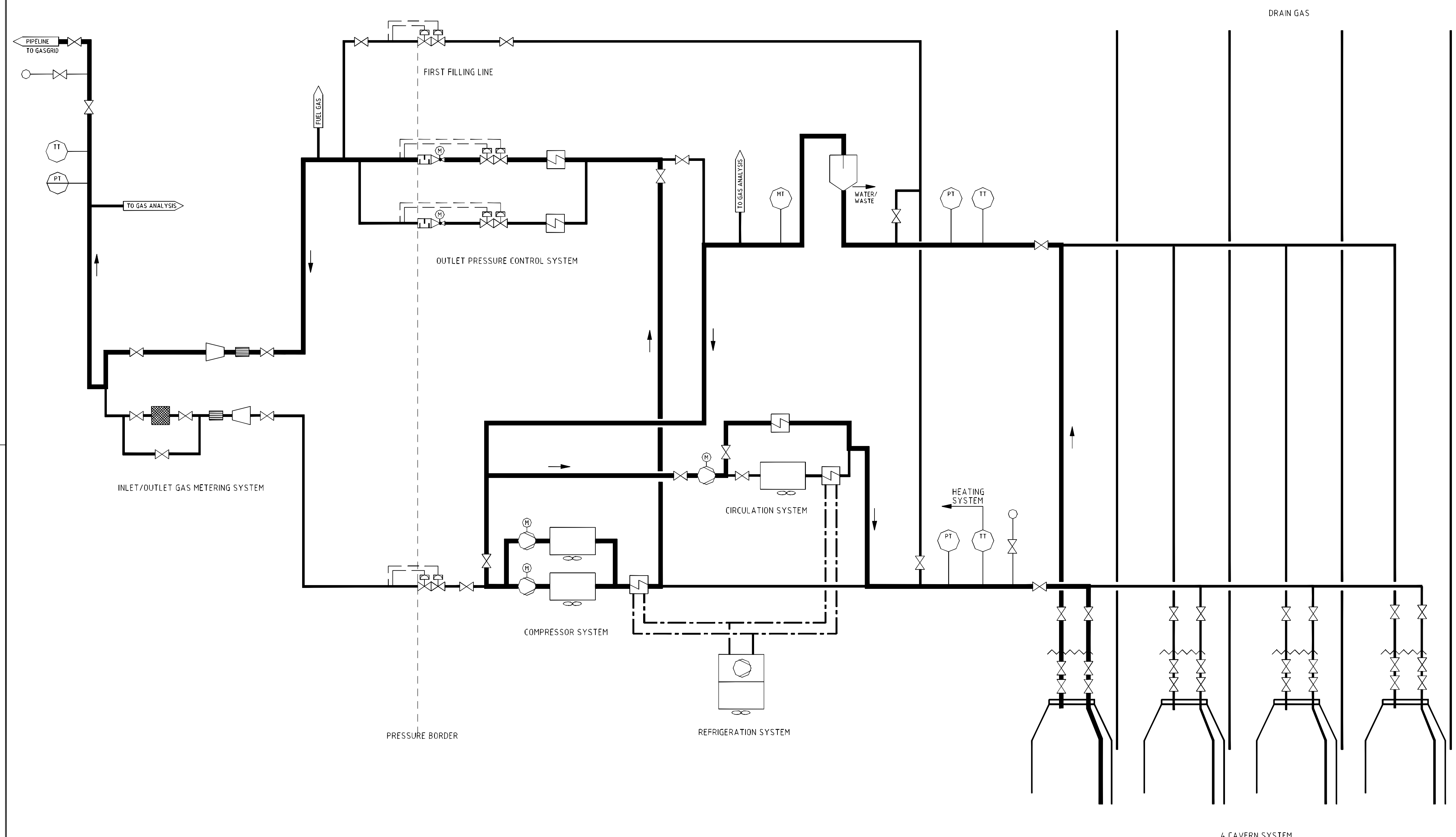

NOTES

- BLOW OFF LINE
- REFRIGERANT

REV.	REVISION	DATE	SIGN.
A	REFRIGERATION SYSTEM	990121	Ulh

CARL GUSTAVS VÄG 4, 205 09 MALMÖ
PHONE 040 - 25 60 00

DRAWN	DESIGNED	CHECKED	DEP.
Ulh	Oha		EVG

DATE 990108

DEPARTMENT OF ENERGY
CONTRACT NO. DE-AC26-97FT34348

LRC NATURAL GAS STORAGE
PROCESS DIAGRAM
WITHDRAWAL WITH COMPRESSION
SCALE

REG. NO.	DRAWING NO.	REV.
EXGAZ.01	EXGAZ-05	

5. CIRCULATION COOLING/HEATING

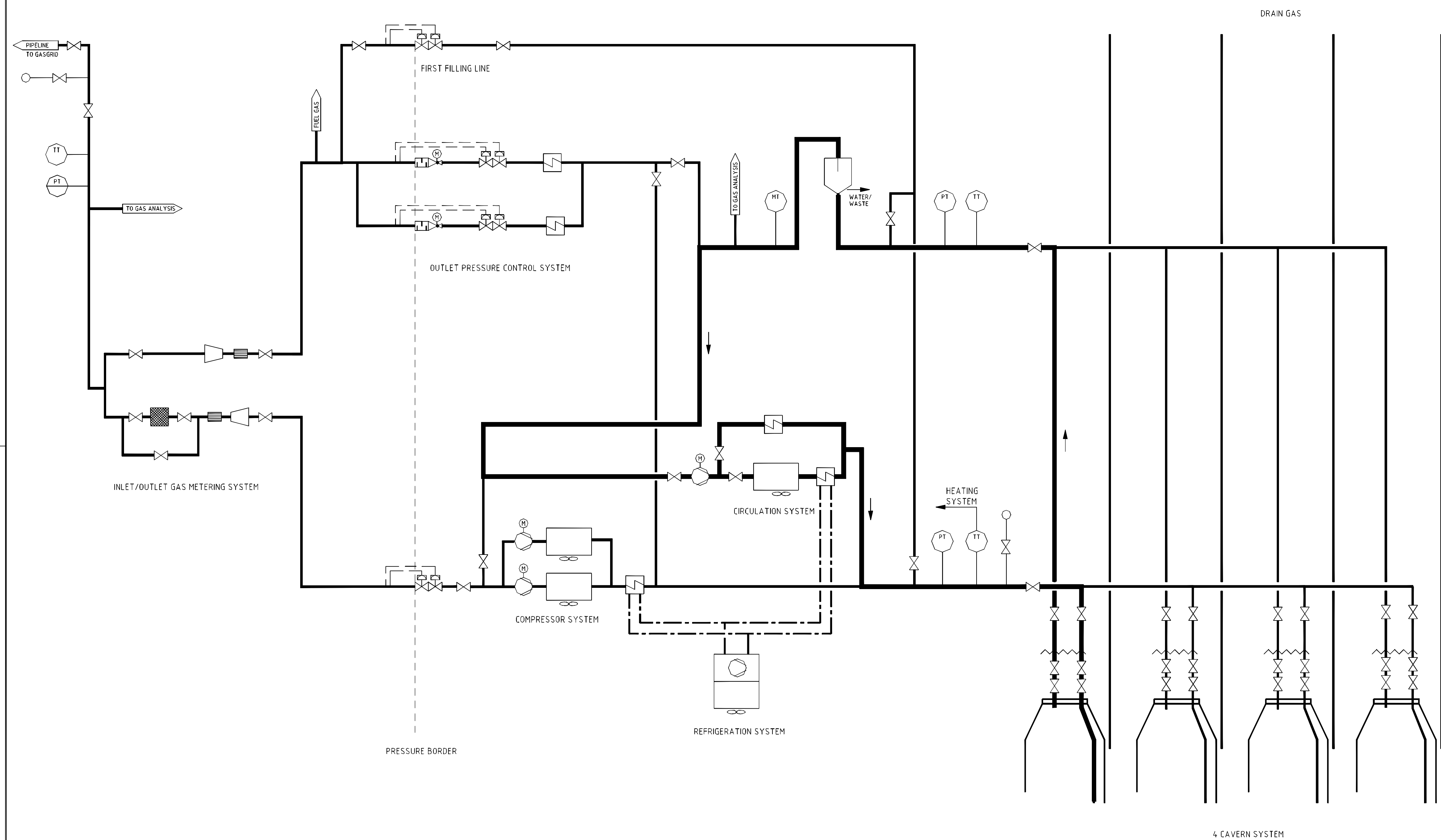

NOTES

BLOW OFF LINE

REFRIGERANT

REV.	REVISION	DATE	SIGN.
A	REFRIGERATION SYSTEM	991121	Ulh

CARL GUSTAVS VÄG 4, 205 09 MALMÖ
PHONE 040 - 25 60 00

DRAWN	DESIGNED	CHECKED	DEP.
Ulh	Oha		EVG

DATE 991118

DEPARTMENT OF ENERGY
CONTRACT NO. DE-AC26-97FT34348
LRC NATURAL GAS STORAGE
PROCESS DIAGRAM
CIRCULATION COOLING/HEATING
SCALE

REG. NO.	DRAWING NO.	REV.
EXGAZ.01	EXGAZ-06	

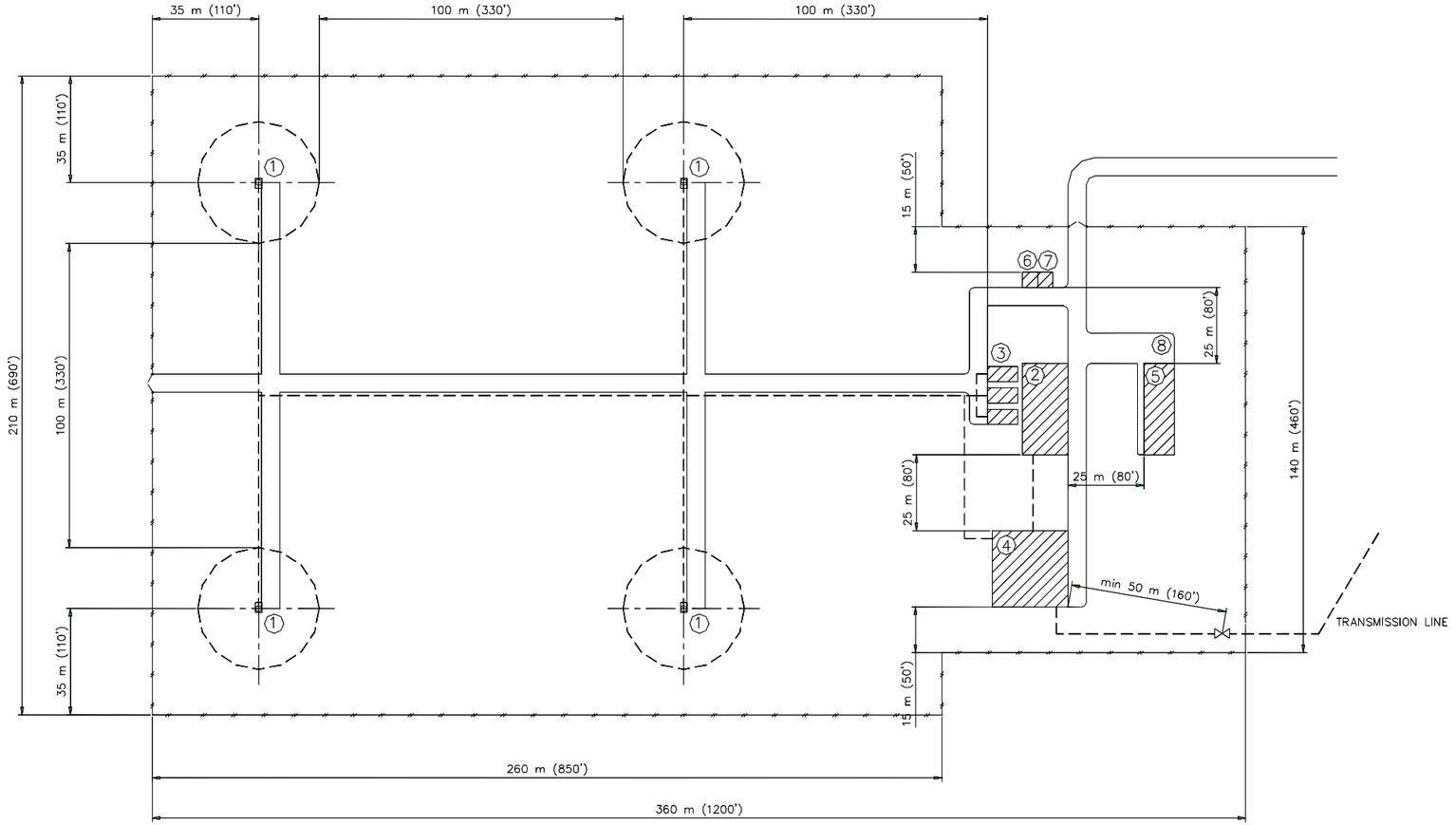

1. SHAFT HEAD
2. COMPRESSORS 15 x 30 m (50'W x 100'L)
3. AIR COOLERS 20 x 10 m (70'W x 30'L)
4. METERING, PRESSURE REDUCTION AND HETING 25 x 25 m (80'W x 80'L)
5. CONTROL AND FACILITIES FOR STAFF 10 x 30 m (30'W x 100'L)
6. ELECTRIC SWITCH GEAR
7. ELECTRIC TRANSFORMER
8. PARKING

LAND REQUIREMENT 68600 m2 (17 acres)

SYCON
CARL GUSTAVS VÄG 4, 205 09 MALMÖ
PHONE 040 - 25 60 00

DRAWN	DESIGNED	CHECKED	DEP.
Ulh	Oha		EVG

DATE 990108

DEPARTMENT OF ENERGY
CONTRACT NO. DE-AC26-97FT34348
NEW ENGLAND
LRC NATURAL GAS STORAGE
LAY-OUT
SCALE

REG. NO.	DRAWING NO.	REV.
EXGAZ.01	EXGAZ-07	

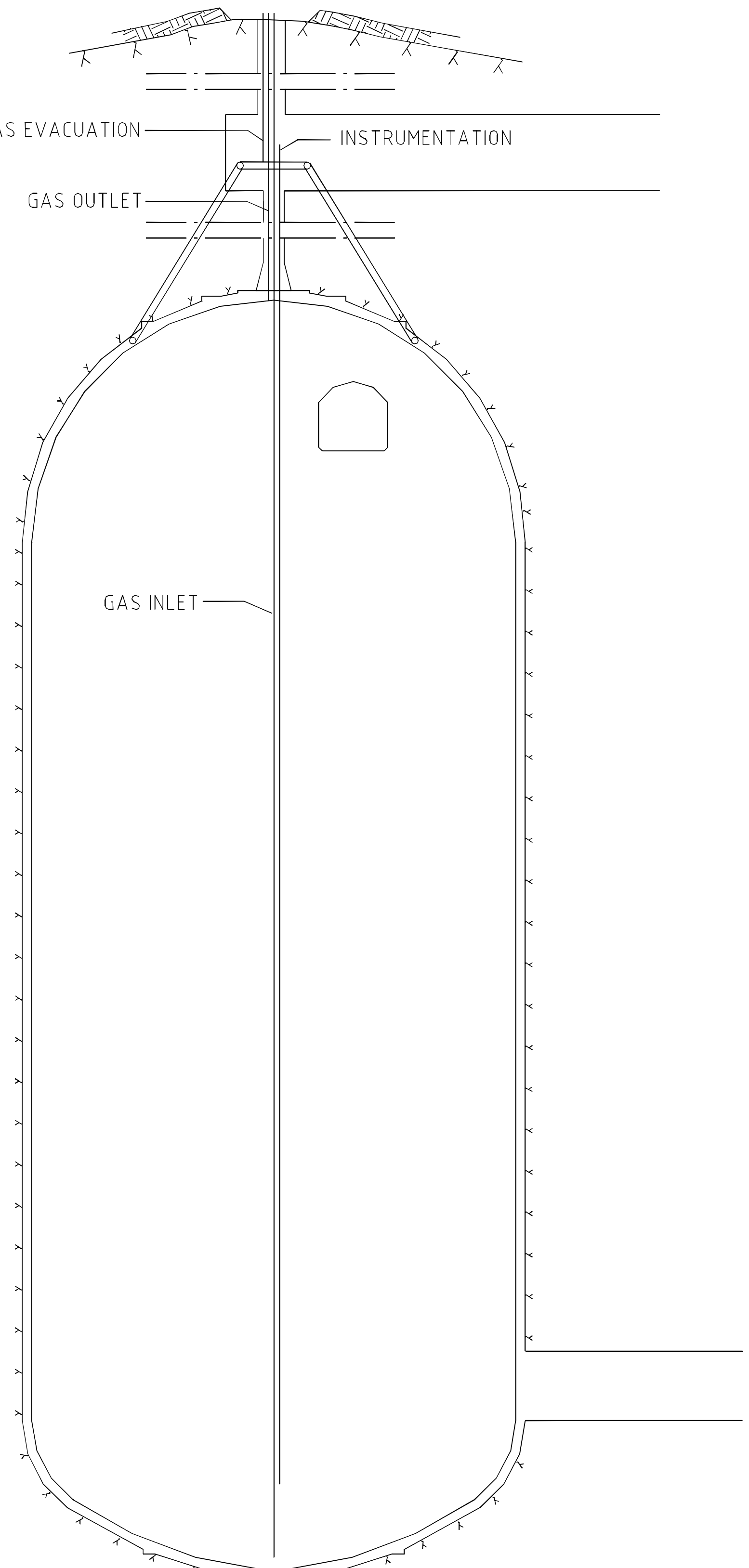

SYCON
CARL GUSTAVS VÄG 4, 215 09 MALMÖ
PHONE 040 - 25 61 00

DRAWN	DESIGNED	CHECKED	DEP.
Ulh	Oha		EVG

DATE 990108

DEPARTMENT OF ENERGY
CONTRACT NO. DE-AC26-97FT34348

LRC NATURAL GAS STORAGE
PIPING IN STORAGE ROOM

SCALE

REG. NO.	DRAWING NO.	REV.
EXGAZ.01	EXGAZ-08	

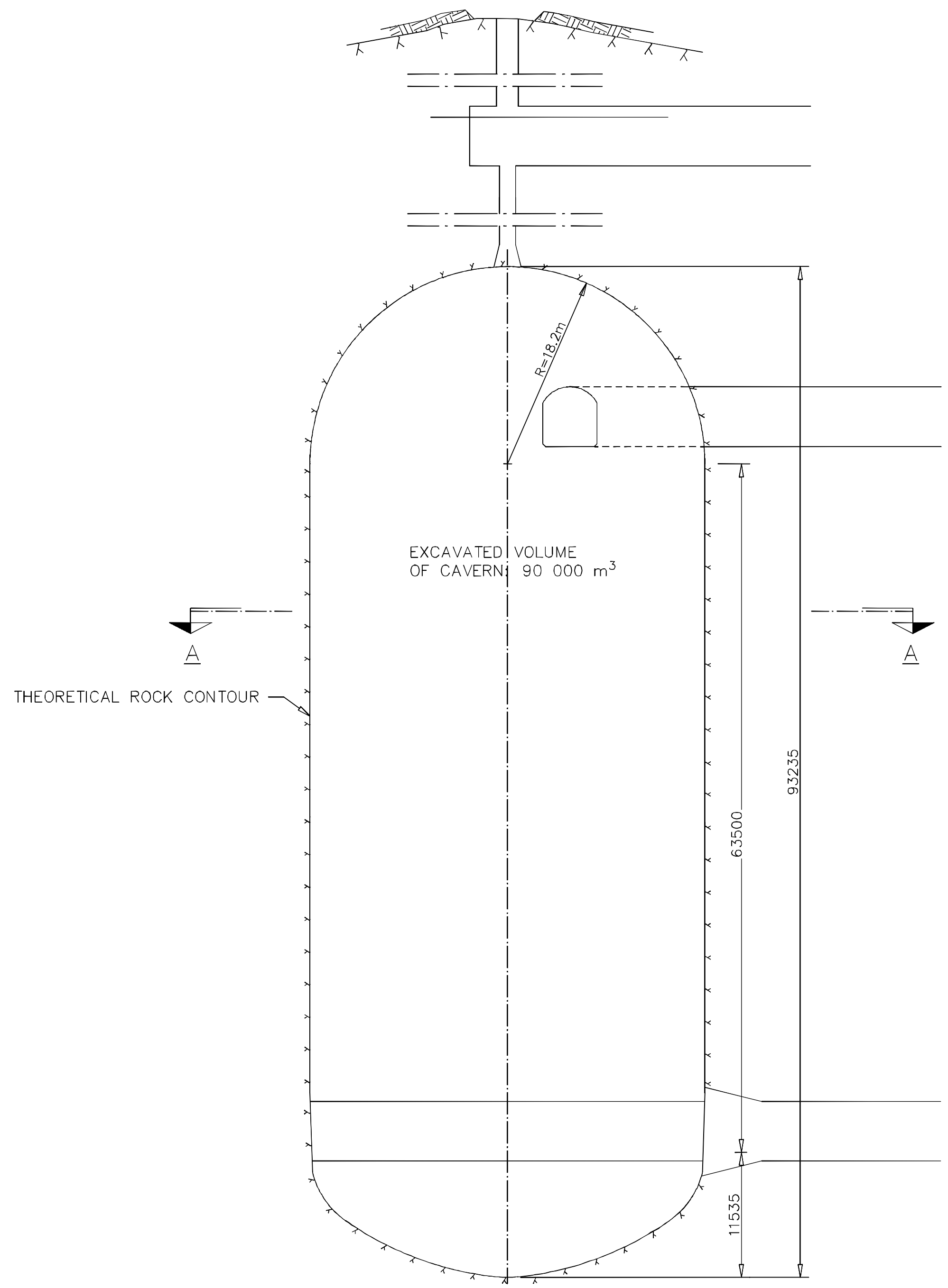

STORAGE ROOM, VERTICAL SECTION

1:250

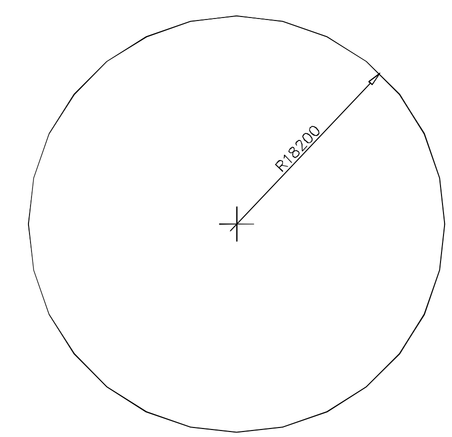

A–A STORAGE ROOM, HORIZONTAL SECTION

1:250

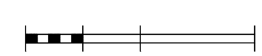

SYCON CARL GUSTAVS VÄG 4, 205 09 MALMÖ PHONE 040 – 25 60 00	DEPARTMENT OF ENERGY CONTRACT NO. DE-AC26-97FT34348 LRC NATURAL GAS STORAGE STORAGE ROOM, SECTION SITE 02 SCALE 1:250
DRAWN Ulh · DESIGNED Ais · CHECKED · DEP. EVG	
DATE 990128	REG. NO. EXGAZ.01 · DRAWING NO. EXGAZ–12 · REV.

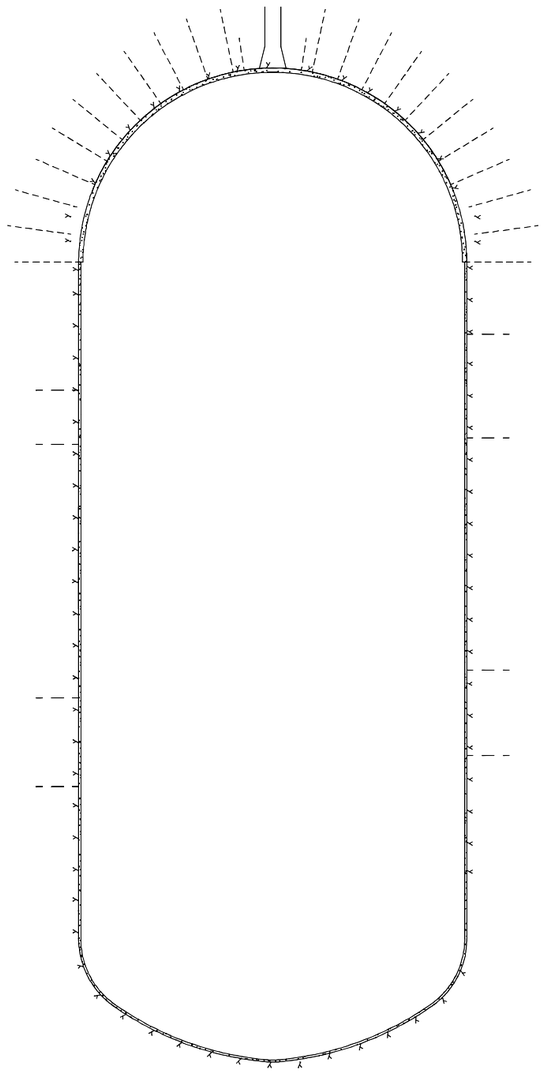

DIRECTIONS

EXPLANATIONS

SHOTCRETE

BOLT

REINFORCEMENT OF ROCK CAVERN

1: 200

0 10 20m

SYCON
CARL GUSTAVS VÄG 4, 205 09 MALMÖ
PHONE 040 - 25 80 00

Drawn	DESIGNED	CHECKED	DEP.
Ulh	Als		EVG

DATE 990128

DEPARTMENT OF ENERGY
CONTRACT NO. DE-AC26-97FT34348

LRC NATURAL GAS STORAGE
ROCK REINFORCEMENT
ROCK CAVERN

SCALE 1: 200

REL. NO. EXGAZ.01

DRAWING NO. EXGAZ-13 REV.

DIRECTIONS

INSTRUCTIONS

TUNNEL DIMENSIONS CORRESPONDS TO THEORETICAL ROCK CONTOUR

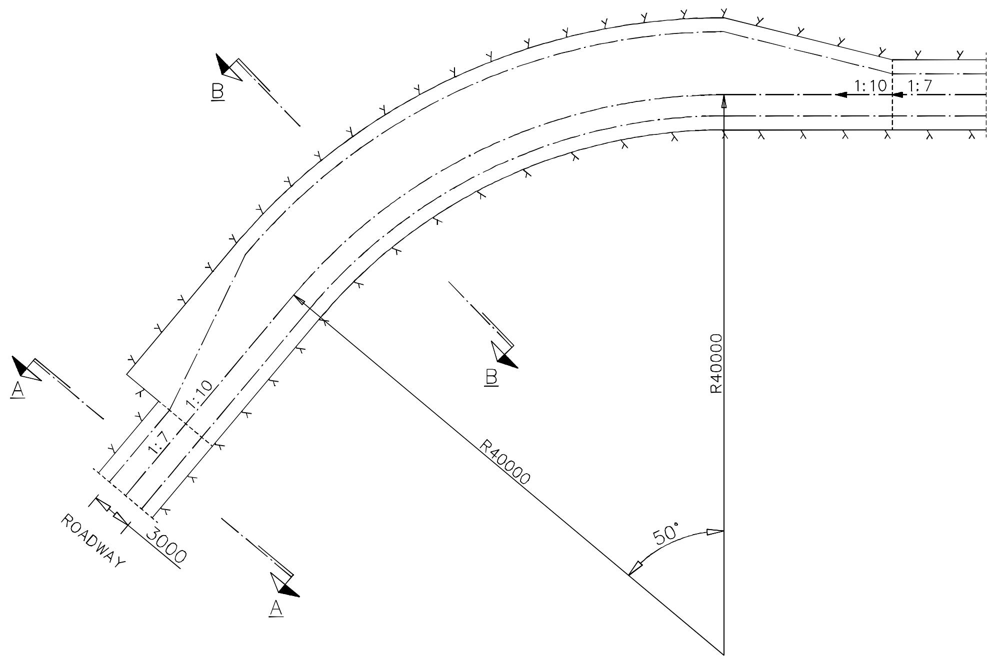

PASSING POINT CURVE

1: 200

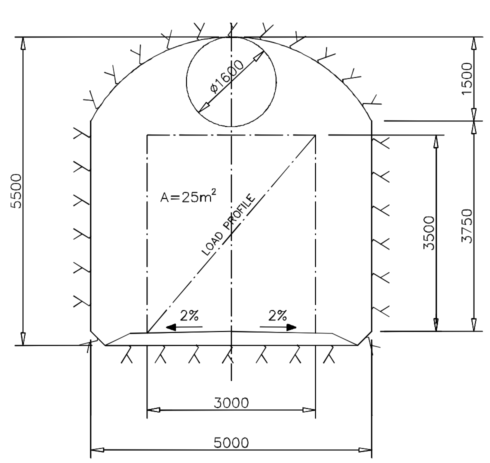

A–A – TYPE SECTION OF SUPERSTRUCTURE ACCESS TUNNEL STRAIGHT (CAMBER 2%)

1: 50

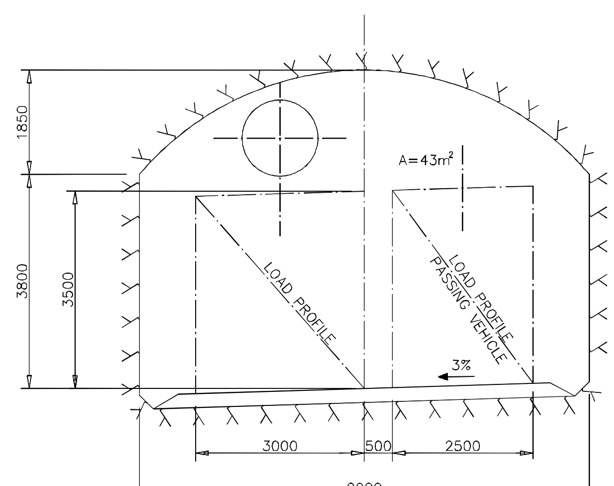

B–B – TYPE SECTION OF SUPERSTRUCTURE, CROSSING POINT CURVE (WARPING 3%)

1: 50

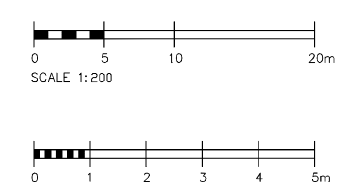

SYCON CARL GUSTAVS VÄG 4, 205 09 MALMÖ PHONE 040 – 25 60 00	DEPARTMENT OF ENERGY CONTRACT NO. DE–AC26–97FT34348
DRAWN Ulh / DESIGNED Ais / CHECKED / DEP. EVG	LRC NATURAL GAS STORAGE ACESS TUNNEL, SECTION STRAIGHT, CURVE SCALE 1: 50 / 1: 200
DATE 990128	REG. NO. EXGAZ.01 / DRAWING NO. EXGAZ–14 / REV.

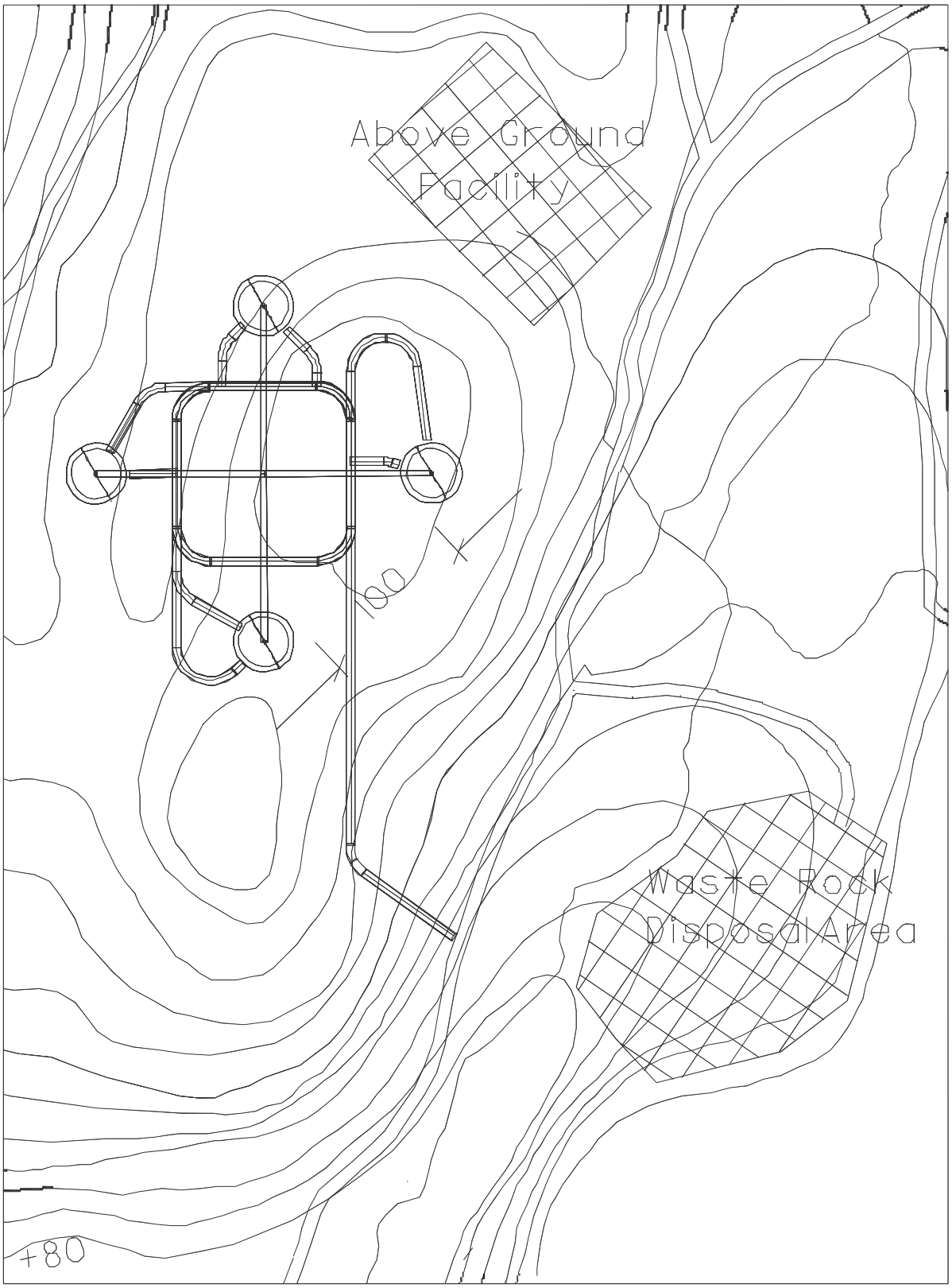

Drawing No. EXGAZ-15. General Layout.

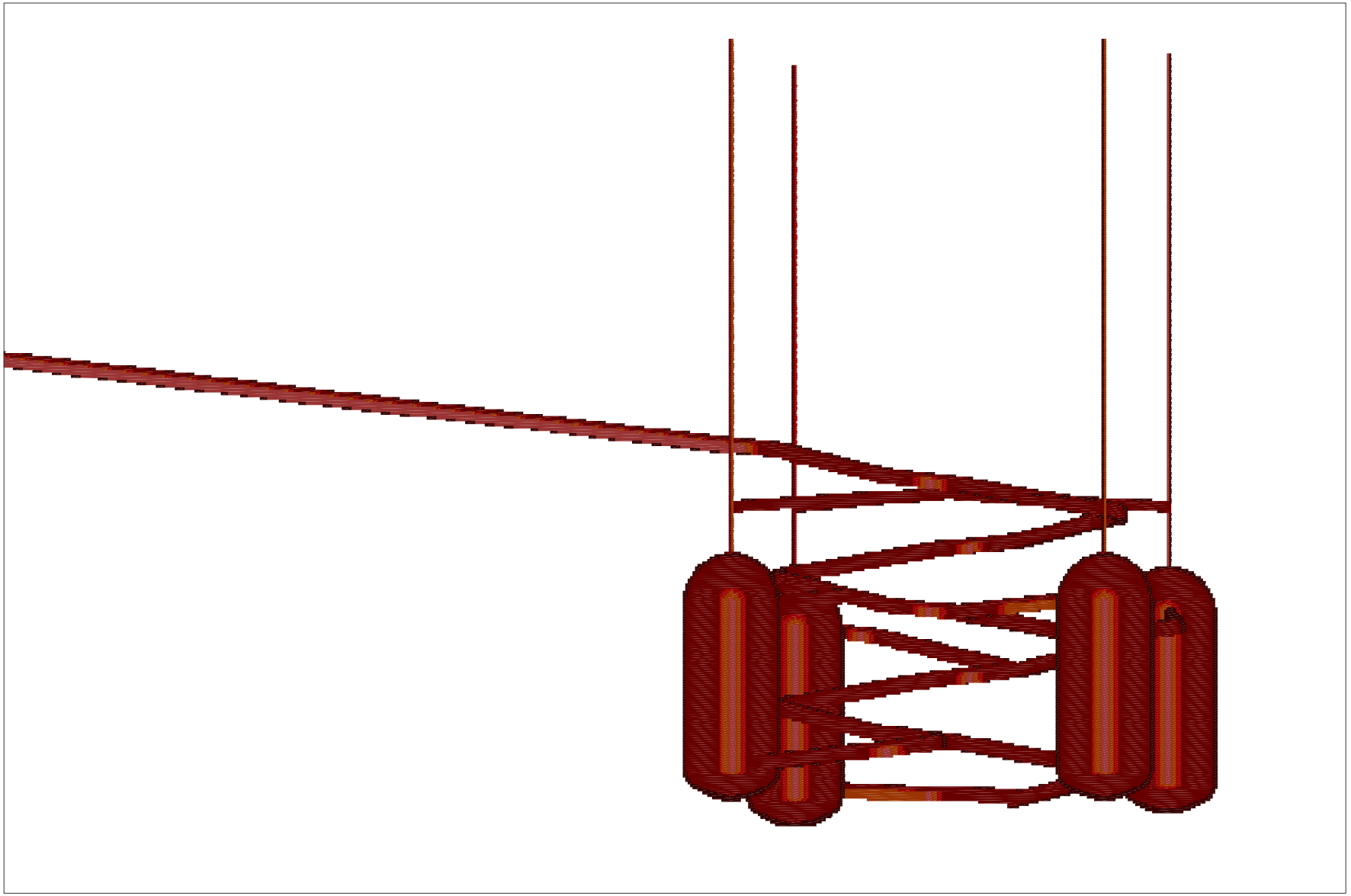

Drawing No. EXGAZ-16. Cavern and Tunneling Configuration.

APPENDIX D

MANUAL FOR ECONOMIC MODEL

Natural Gas Transportation & Storage Model

DRAFT VERSION 1.0

END USER INPUT DATA		
Delivery zone	0	
Receipt zone	6	
Deliverability	260	MDTH/d
Yearly volume	5200	MDTH

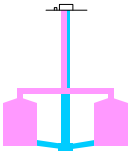

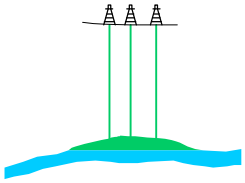

APPENDIX D
MANUAL FOR ECONOMIC MODEL

D.1 INTRODUCTION

This economic model was developed by Sycon Energikonsult©, Sweden. It is developed in Microsoft Excel 97, SR-2.

The economic model can be used for two types of investigations:

1. Evaluation of investment and operating cost for an LRC storage facility.
2. Evaluation of a cost estimate for transportation of natural gas between different parts of the eastern United States gas grid.

A natural gas customer may wish to buy a certain yearly volume of gas and may have a certain need for deliverability. The gas is consumed in one zone and supplied in another. The gas has to be transported from the delivery zone to the receipt zone. As shown in Figure D-1, this can be done in two ways; either directly by pipeline or via storage. You can choose different storage types and they can be placed in different zones. With the model, alternatives can be compared and the most favorable alternative can be chosen.

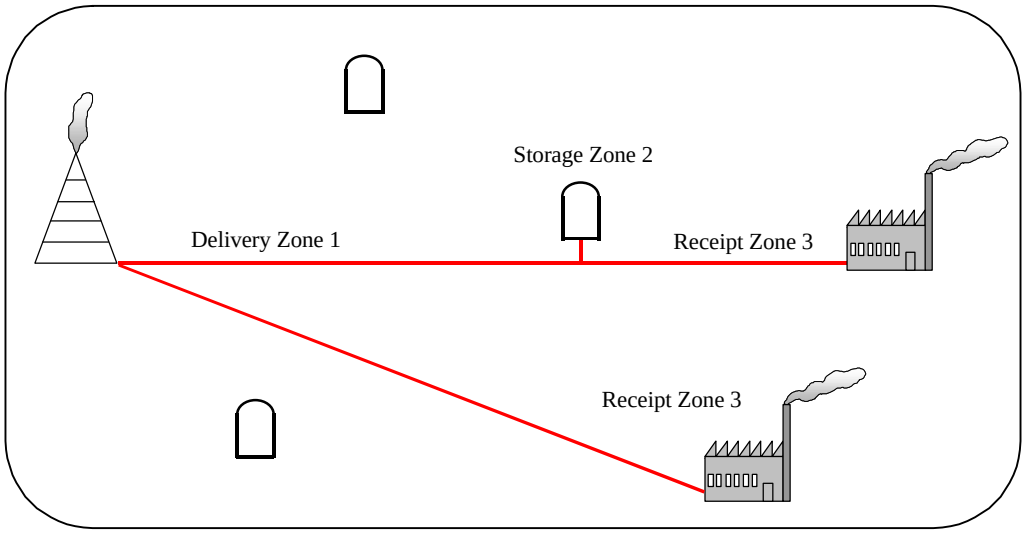

Figure D-1. Alternatives for Gas Transportation.

The different types of storage that are handled by the model are:

- Salt cavern
- Depleted fields
- LRC
- LNG.

D.2 BACKGROUND

Storage costs for salt caverns and depleted fields are based on the study *U.S. Underground Storage of Natural Gas in 1997: Existing and Proposed*. The proposed storage projects in the study reflect the costs for building new storage projects.

Storage costs for LRC are based on the SECON model. The SECON model was developed by Sycon Energikonsult AB and was originally designed to calculate the costs for building LRC storage in Sweden. The costs in the model have been revised to match the United States' conditions.

LNG storage costs are based on the study titled *Advanced Underground Gas Storage Concepts Refrigerated-Mined Cavern Storage, DOE Contract Number DE-AC26-97FT34349.*

Transportation rates are those of the Tennessee Gas Pipeline Company.

D.3 INSTRUCTIONS

Cells used for input data in the spreadsheet model are yellow. In the model, the user can select the eight sheets noted below:

1. End User Input Data
2. Transportation Cost
3. Cost Comparison Graph
4. LRC Investment Cost
5. Storage Rate
6. i-Data
7. i-Model Transportation Rate
8. i-COS LRC.

Some sheets in the model have a name that begins with "i;" for example, i-Data. These sheets give background information only.

D.3.1 End User Input Data (Sheet 1)

In this sheet, the user must insert the delivery zone and the receipt zone. The user will also have to insert the deliverability volume and the yearly volume to be transported, as illustrated in Figure D-2. As mentioned above, the cells with yellow cover are for inserting data.

END USER INPUT DATA		
Delivery zone	0	
Receipt zone	6	
Deliverability	520	MDTH/d
Yearly volume	62400	MDTH

Figure D- 2. End User Input Data.

D.3.2 Transportation Cost (Sheet 2)

In this sheet, the model calculates (1) the transportation cost directly by pipeline to the end user and (2) in the other alternative, via storage. The user must also give the size and performance for the LRC investment cost calculation on this sheet.

D.3.2.1 Transportation Cost to End User (1.)

The model calculates the cost for transportation of gas directly to the end user by pipeline. The model uses a firm transportation rate based on the chosen delivery and receipt zone. If the user wishes to use the calculated value from the model, the calculated value must be inserted in the cell for "Actual Transportation Rate." If another transportation rate is to be used, that value needs to be input in the cell for "Actual Transportation Rate" and the model will use that value instead. The user must always insert a value in the cell for "Actual Transportation Rate."

The model shows the yearly transportation cost. It also shows transportation cost per yearly gas volume and yearly transportation cost per deliverability, as shown in Figure D-3.

D.3.2.2 Pipeline + Storage (2.)

The next step in the modeled process is to calculate the cost for transportation of gas, including storage.

1. PIPELINE TRANSPORTATION TO END USER		
TRANSPORTATION COST TO END USER		
Model transportation rate	18,81	USD/DTH/d/month
Actual transportation rate	18,81	USD/DTH/d/month
Yearly transportation cost	**117 374 400**	**USD**
Transportation cost per yearly gas volume	**2**	**USD/DTH**
Yearly transportation cost per deliverability	**19**	**USD/DTH/d/month**

Figure D-3. Transportation Cost to End User.

Transportation Cost to Storage

The model calculates the yearly transportation cost to the storage facility. The model uses a firm transportation rate based on the chosen delivery and storage zone. If the calculated value from the model is to be used, it should be input in the cell for "Actual Transportation Rate." If another transportation rate is to be used, it should be input in the cell for "Actual Transportation Rate" and the model will use that value instead. The user must always insert a value in the square for "Actual Transportation Rate" as shown in Figure D-4.

TRANSPORTATION COST TO STORAGE					
Storage injection rate	50	50	50	13	MDTH/d
Storage feeding time	1248	1248	1248	4800	d
Model transportation rate	14,61	16,23	18,81	18,81	USD/DTH/d/month
Actual transportation rate	14,61	16,23	18,81	14,61	USD/DTH/d/month
Yearly transportation cost	8 766 000	9 738 000	11 286 000	2 279 160	USD

Figure D-4. Transportation Cost to Storage.

Storage Cost

The model calculates the yearly storage cost for the different types of storage based on calculated or inserted storage rates. The user must insert the storage zone for the different types of storage.

The model calculates the storage rates based on the investment and operating cost for salt caverns, depleted fields, and LRC. The investment cost for salt caverns is based on projects listed in the i-Data sheet. For LRC, the model calculates the investment cost. The storage rates are calculated based on the development cost in sheet i-Data (salt and depleted fields) or calculated (LRC) with the cost of service model. For LNG, a number of storage rates are included in the model. The model will pick the relevant rate, depending on the given storage zone.

If the user wishes to use the calculated value from the model, this rate should be input in the cell for "Actual Storage Rate." A numerical value must always be input for "Actual Storage

Rate" except for LRC. For LRC, there is no actual storage rate, so the model will always use the calculated storage rate.

If the user wishes to use an actual storage rate, that rate must be input in the cell for "Actual Storage Rate" and the model will calculate with that value instead.

For LRC, various working gas volumes, deliverability, injection rate, and number of cycles can be input to obtain the best option for minimizing the transportation cost. The calculated storage rate is presented in the "Transportation Cost" sheet (see Figure D-5). The investment cost is detailed in the "LRC-Investment Cost" sheet (described in Section D.3.6).

STORAGE COST					
Type of Storage	**Salt Cavern**	**Depleted Field**	**LRC**	**LNG**	
Storage zone	4	5	6	6	
Deliverability	260	260	260	260	MDTH/d
Injection rate			130		MDTH/d
Withdrawal time			10		d
Working gas			2,6		Bcf
No. of cycles			2		
No of caverns			4		
Calculated storage rate	6,8	19,1	10,1	6,4	USD/DTH/d/month
Actual storage rate	6,4	19,1		6,4	USD/DTH/d/month
Yearly storage cost	19 968 000	59 592 000	31 534 767	39 936 000	USD

Figure D-5. Storage Cost.

Transportation Cost to End User

The model calculates the yearly cost for transportation of gas from the storage facility to the end user. The model uses a transportation rate based on the chosen storage zone and the chosen receipt zone. If the user wishes to use the calculated value from the model, this rate must be input in the cell for "Actual Transportation Rate." If the user wishes to calculate with another transportation rate, that rate must be input in the cell for "Actual Transportation Rate" and then the model will use that value instead.

If the user inputs a "Y" in the cell for "Customer Connected Directly to Storage," then the model will not account for any cost for transportation from storage to the end user.

The model shows the total yearly cost for the different alternatives with storage. It also shows the total cost per yearly gas volume and per deliverability.

Finally, the yearly cost difference between using pipeline transportation plus different storages and alternative pipeline transportation directly to the end user is provided as shown in Figure D-6.

TRANSPORTATION COST TO END USER					
Customer connected directly to storage (Y/N)	N	N	N	N	
Model transportation rate	7,81	6,82	5,01	7,81	USD/DTH/d/month
Actual transportation rate	7,81	6,81	5	7,8	USD/DTH/d/month
Yearly transportation cost	48 734 400	42 494 400	31 200 000	48 672 000	USD
Total yearly cost	**97 436 400**	**171 416 400**	**118 642 987**	**500 231 160**	**USD**
Total cost per yearly gas volume	**1,6**	**2,7**	**1,9**	**8,0**	**USD/DTH**
Total yearly cost per deliverability	**15,6**	**27,5**	**19,0**	**80,2**	**USD/DTH/d/month**
Yearly cost difference 2-1	**-19 938 000**	**54 042 000**	**1 268 587**	**382 856 760**	**USD**

Figure D-6. Transportation Cost to End User.

D.3.3 Cost Comparison Graph

In the cost comparison graph, the transportation cost for the different alternatives and the allocation of transportation costs are illustrated in Figure D-7.

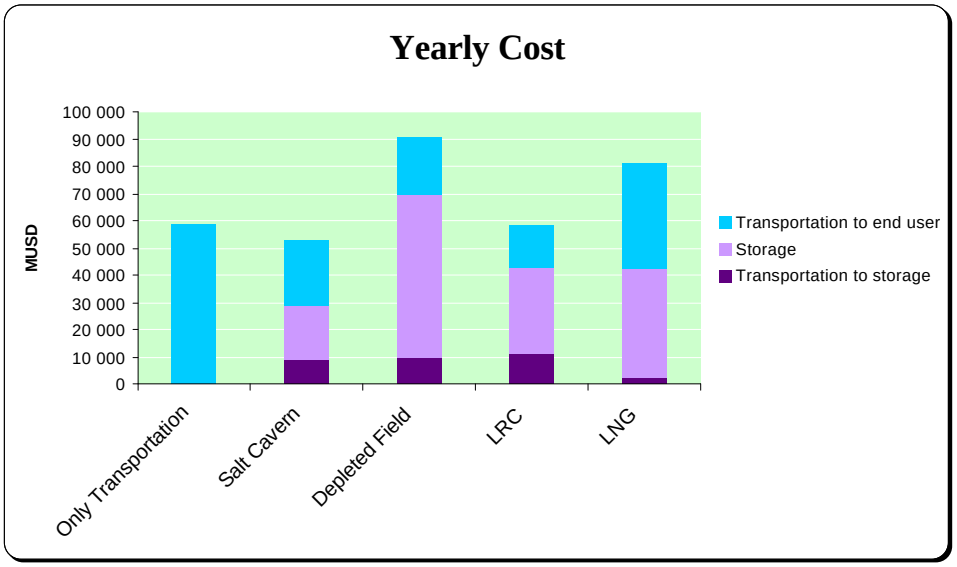

Figure D-7. Cost Comparison Graph.

D.3.4 Storage Rate

As shown in Figure D-8, the actual storage rate and the calculated storage rate for the different storage types in the selected storage zone are illustrated by the model.

D.3.5 LRC Investment Cost

The model shows the investment costs for LRC, based on the working gas volume, deliverability, injection rate, and number of cycles that are input to the model, as shown in Figure D-9.

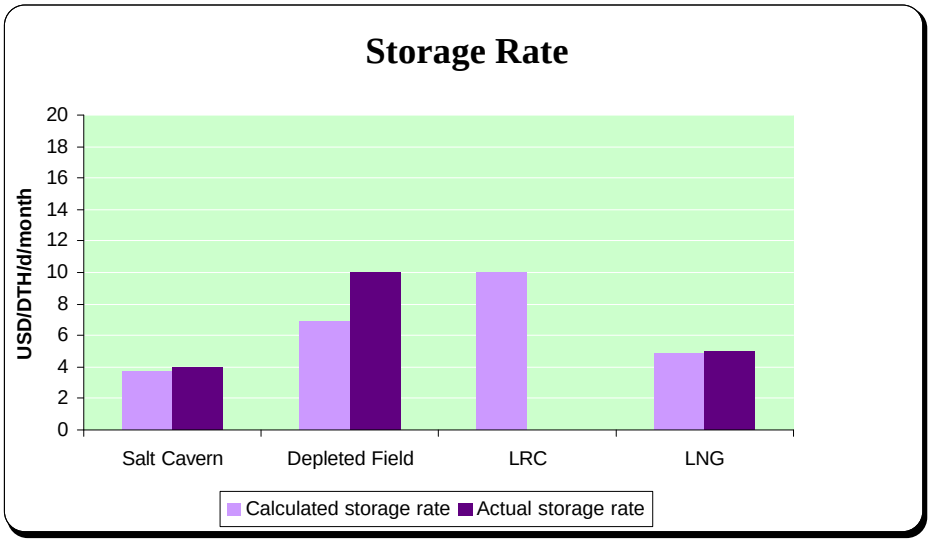

Figure D-8. Storage Rate.

Deliverability	6	MDTH/d
Working gas	5,2	Bcf
Injection rate	260	MDTH/d
No. of cycles	12	
Pre-Construction	**7 000**	MUSD
Below Ground Cost	**239 480**	MUSD
Above Ground	**62 000**	MUSD
Base Gas	**2 500**	MUSD
Subtotal	**310 980**	MUSD
AFUDC	**35 189**	MUSD
Total	**346 169**	MUSD

Figure D-9. LRC Investment Cost.

DOE-SPONSORED WORKSHOP ON ALTERNATIVE GAS STORAGE TECHNOLOGIES

February 17, 2000

Greentree Holiday Inn – Pittsburgh, PA

The United States Department of Energy (DOE), National Energy Technology Laboratory, sponsored four projects relating to Alternative Storage Technologies for Natural Gas Storage. DOE will host a workshop from 8:30 a.m. to 4:30 p.m. on February 17, 2000, in Pittsburgh, Pennsylvania, to present two of the technologies to industry – (1) *Commercial Potential of Natural Gas Storage in Lined Rock Caverns (LRC)* and (2) *Advanced Design Criteria to Improve the Working Gas Capacity of Natural Gas Storage Caverns in Salt Deposits*. Sofregaz US, with SydKraft and Gaz de France as major subcontractors, performed the LRC project, and RESPEC performed the salt cavern project. Both projects are described briefly below.

LRC Project

The LRC technology provides an alternative to salt for many regions in the United States, including the Northeast. The gas storage chamber is constructed by first excavating a vertical cylinder in the relatively shallow subsurface. A steel liner is then placed in the excavated cylinder while a special concrete structure is installed between the liner and the excavated rock surface. The LRC concept has been developed in Scandinavia. A field experimental and demonstration site in Sweden was utilized to help develop the concept. Currently, a demonstration facility is being constructed in southern Sweden. The DOE-sponsored LRC project addressed the current state-of-the-art in the LRC concept, market data for conventional alternative storage in the Northeast, identification and selection of two generic geologic sites, conceptual design for the LRC, cost estimate, economic comparison of LRC to alternatives, and environmental impact and permitting issues.

Introduction to the Lined Rock Cavern (LRC) Gas Storage Concept	*JoeRatigan (Sofregaz)*
Concept Development, Design Principles and Below Ground Design	*PerTenborg (SYCON)*
Storage Use and Alternatives, Above Ground, Cost, and Comparisons to Other Technologies	*Ola Hale (SYCON)*

SOFREGAZ US

Joe L. Ratigan
Sofregaz US

Project Manager

SOFREGAZ US

Project Team

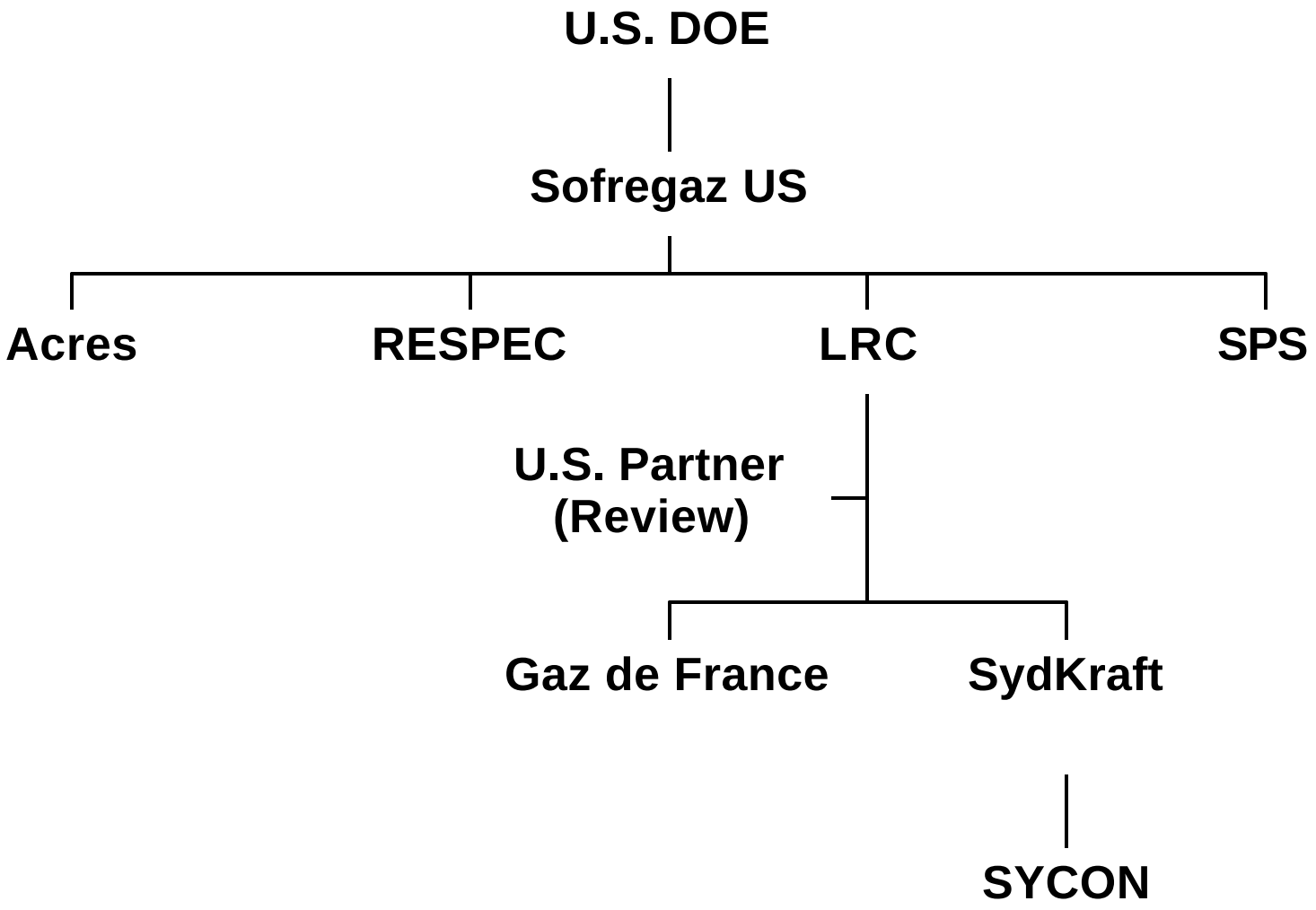

SOFREGAZ US

LRC Rock Formations

SOFREGAZ US

Typical Excavation in Hardrock

SOFREGAZ US

LRC Rock Characterization

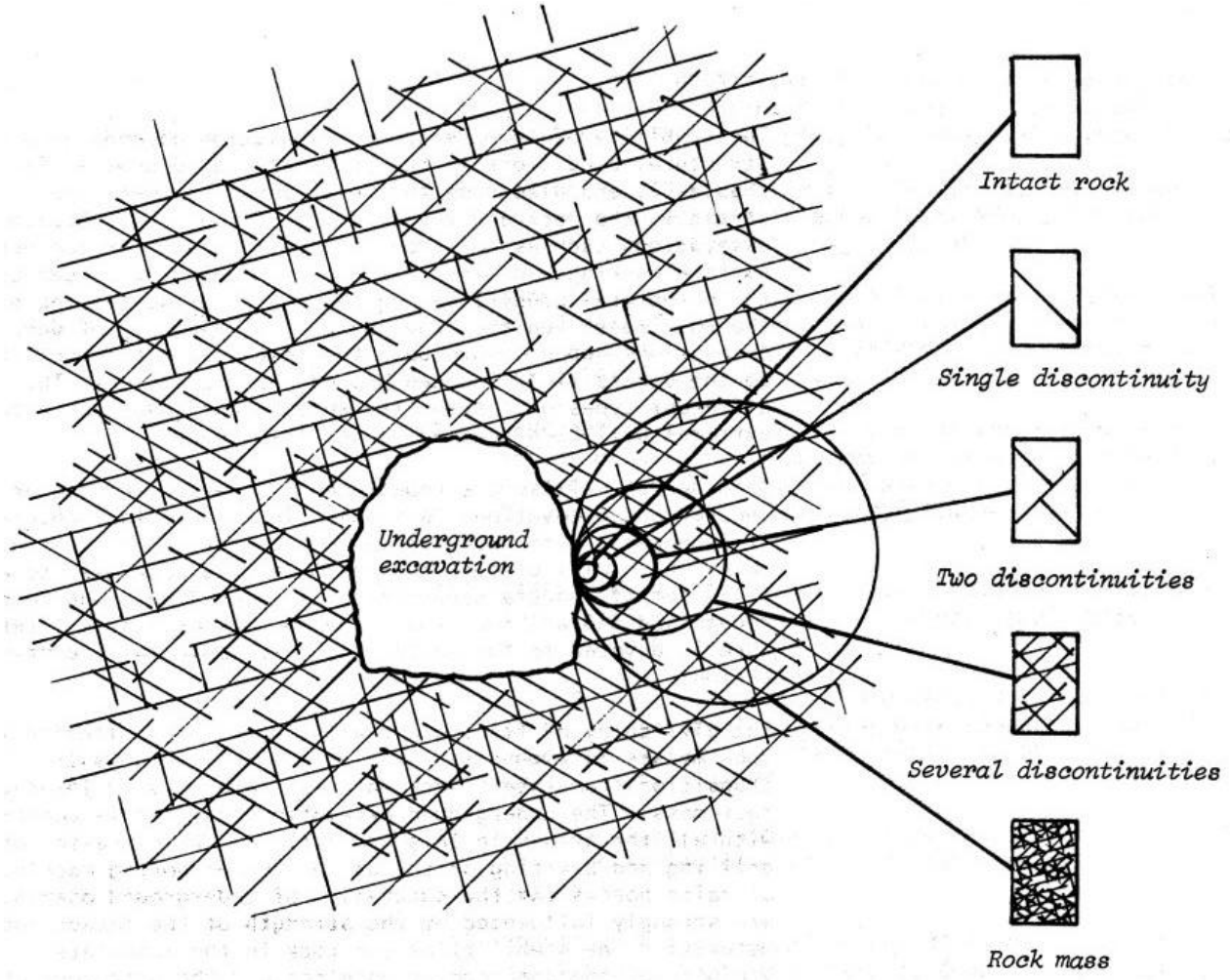

Per Tengborg

PROJECT LEADER

SYCON

SWEDEN

LRC- Concept

The Eight Development Steps

⌘ Conceptual studies	1987-1997
⌘ Experimental Tests	1990-1994
⌘ Grängesberg Pilot Plant	1988-1993
⌘ Test plant result interpretation	1993-1995
⌘ Technical studies	1994-1995
⌘ Engineering studies	1994-1996
⌘ Risk assessment and preliminary design	1997
⌘ Demonstration project	1998-2002

Natural Gas in Sweden

First introduced in 1985

Storage demand has to be met

No geological conditions for:

- aquifers
- salt caverns
- depleted oil- or gasfields

Storage in excavated rock caverns

- lined shallow rock caverns
- unlined rock caverns at great depths
- Low temperature (chilled storage)

The Grängesberg Pilot Plant

- Built in 1988 by a group of Nordic companies
- Situated 250 km W Stockholm
- Tests i four phases 1989-93

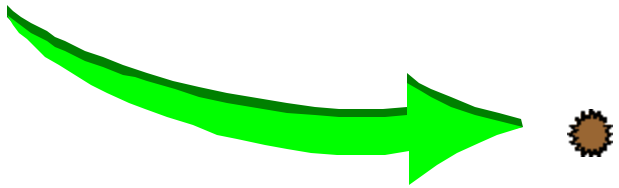

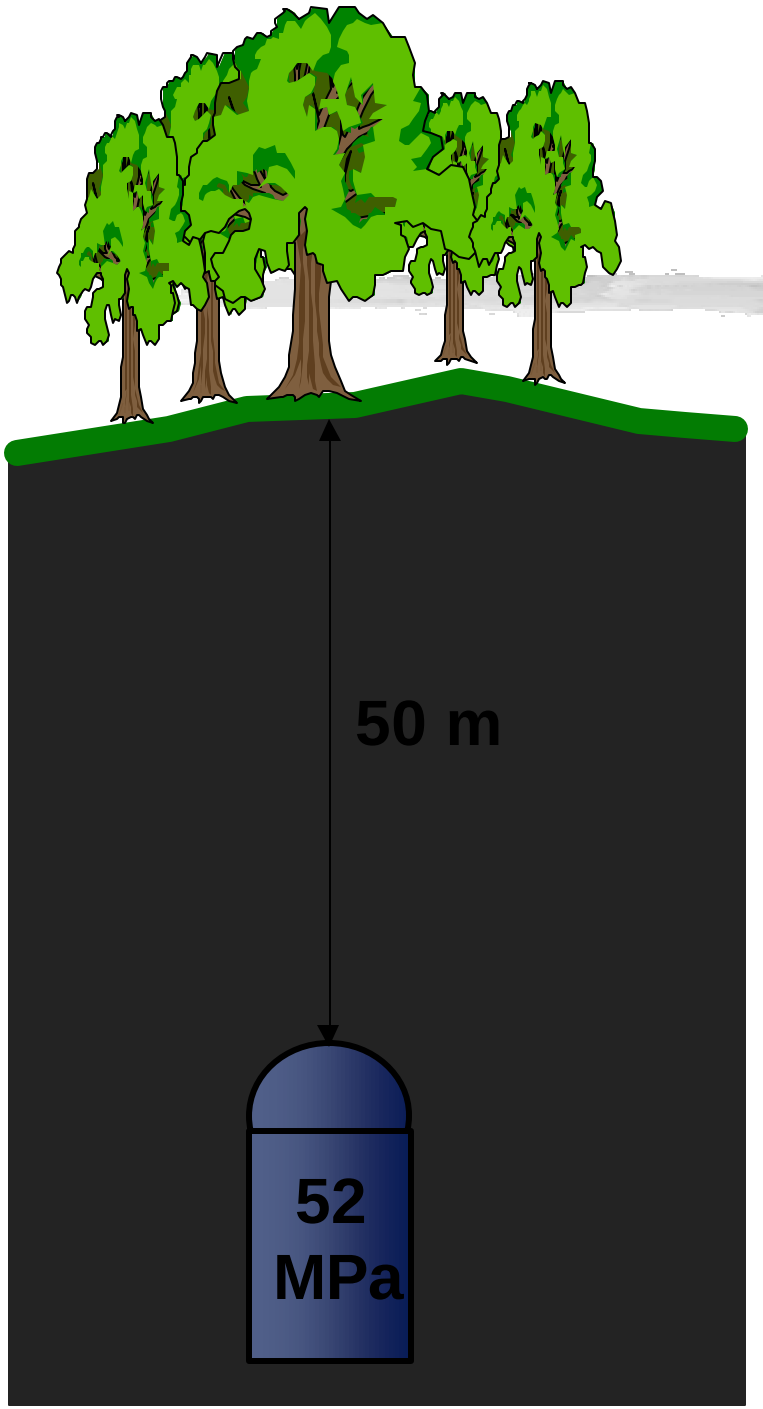

Conclusions

- The rock mass has proven its function as pressure vessel
  - Mostly linear deformations
  - No tendency of up-lift
- The concrete lining has proven its function as pressure distributor
- The steel lining has proven its function as gas container

Approach for Pilot Plant

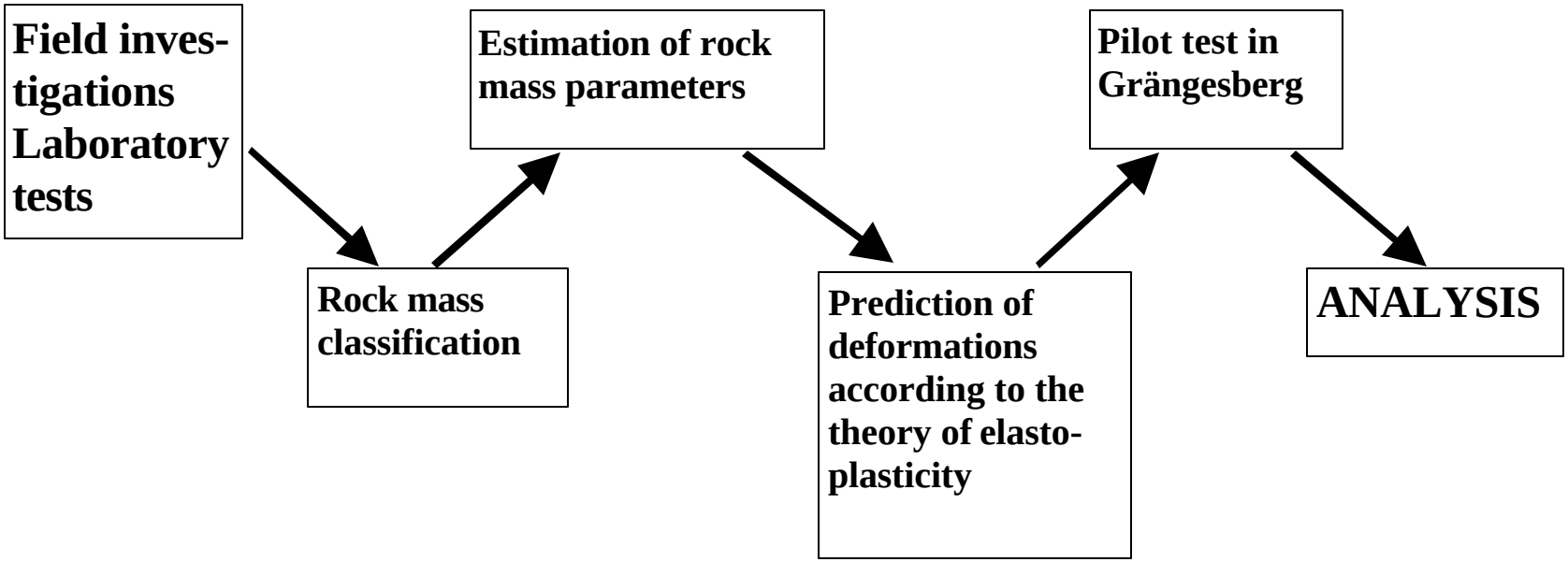

The Grängesberg Pilot Plant - Layout

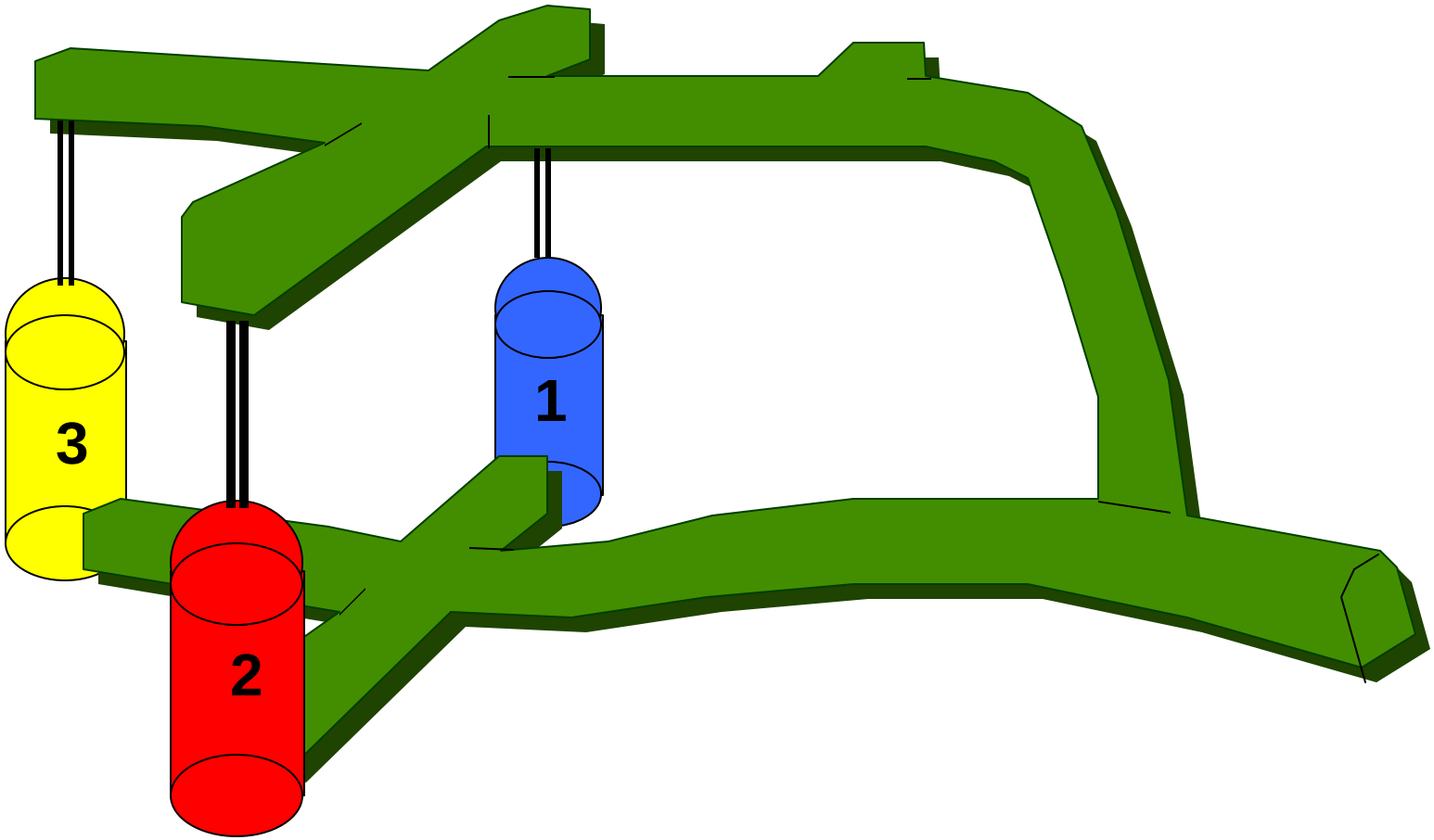

General Layout of Testroom 2

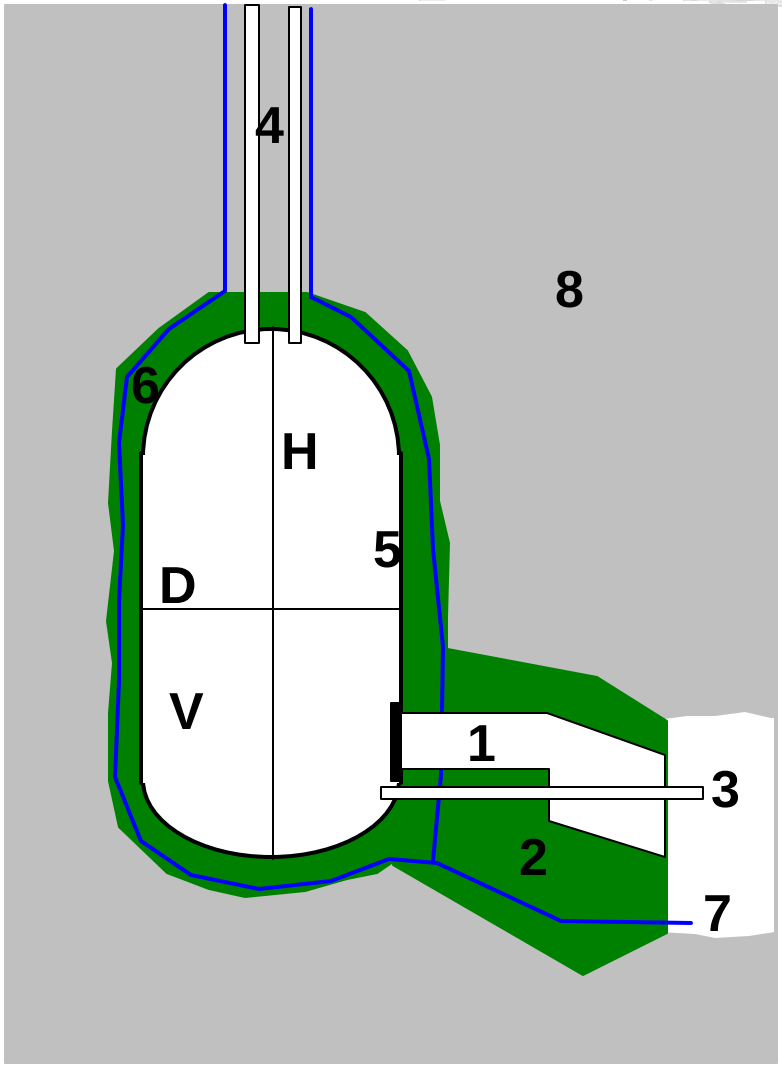

H = 9 m, D = 4.4 m, V = 120 m^3

1. **Access tube**
2. **Concrete plug**
3. **Water fill**
4. **Gas fill**
5. **Steel lining**
6. **Concrete lining**
7. **Drainage system**
8. **Rock mass**

Monitoring System

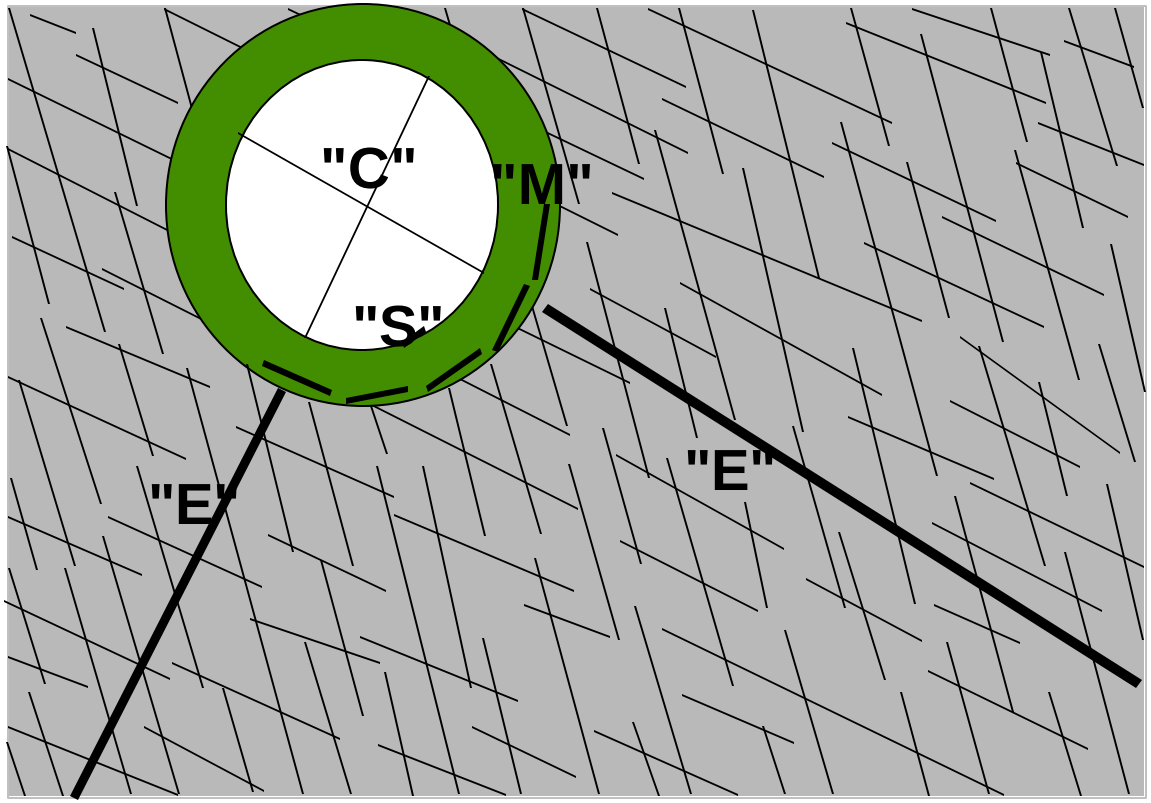

"E" Multiple extensometer

"M" Mini-extensometer

"C" Convergence line

"S" Strain meter

Cavern Wall

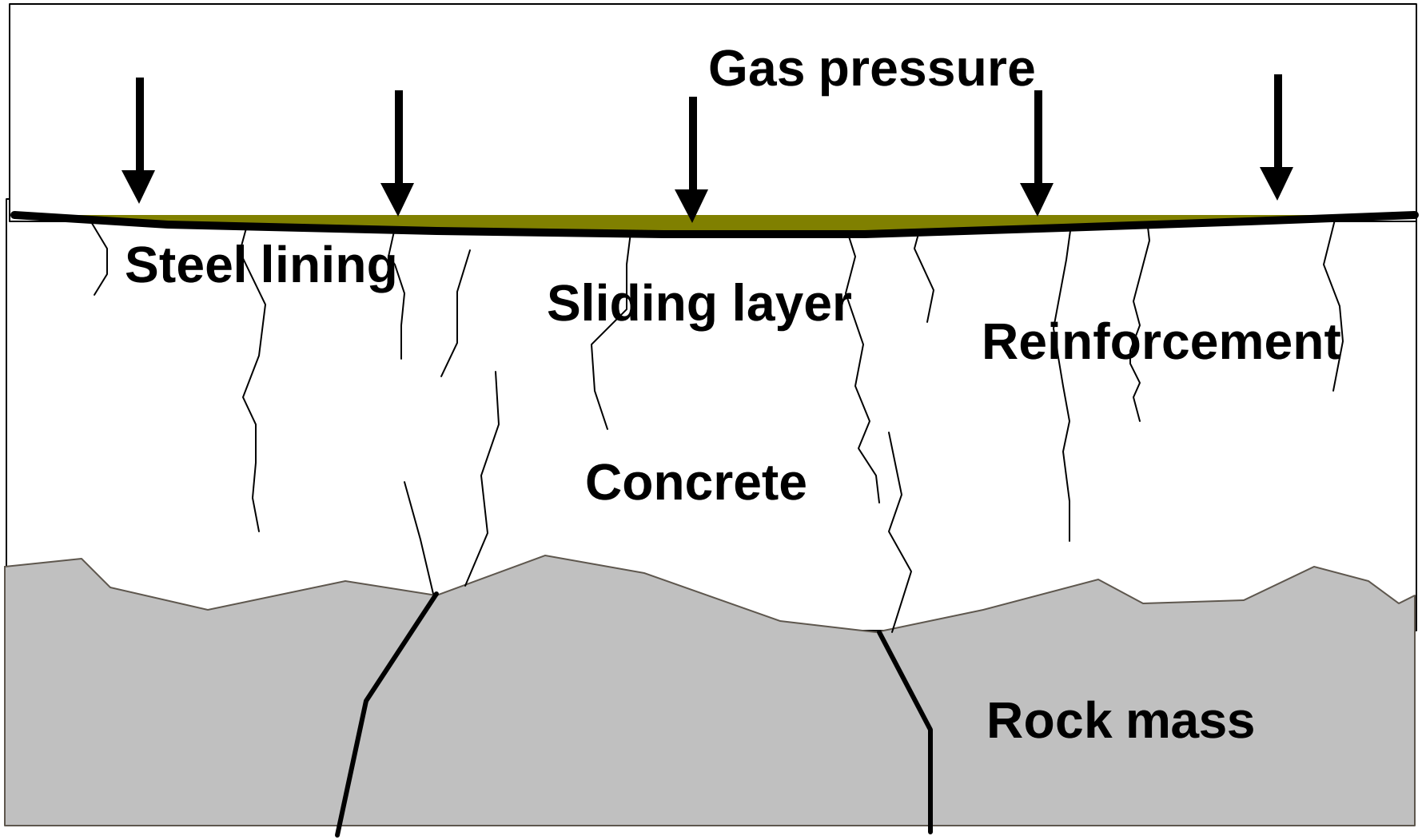
Gas pressure
Steel lining
Sliding layer
Reinforcement
Concrete
Rock mass

Elasto-Plastic Behavoir

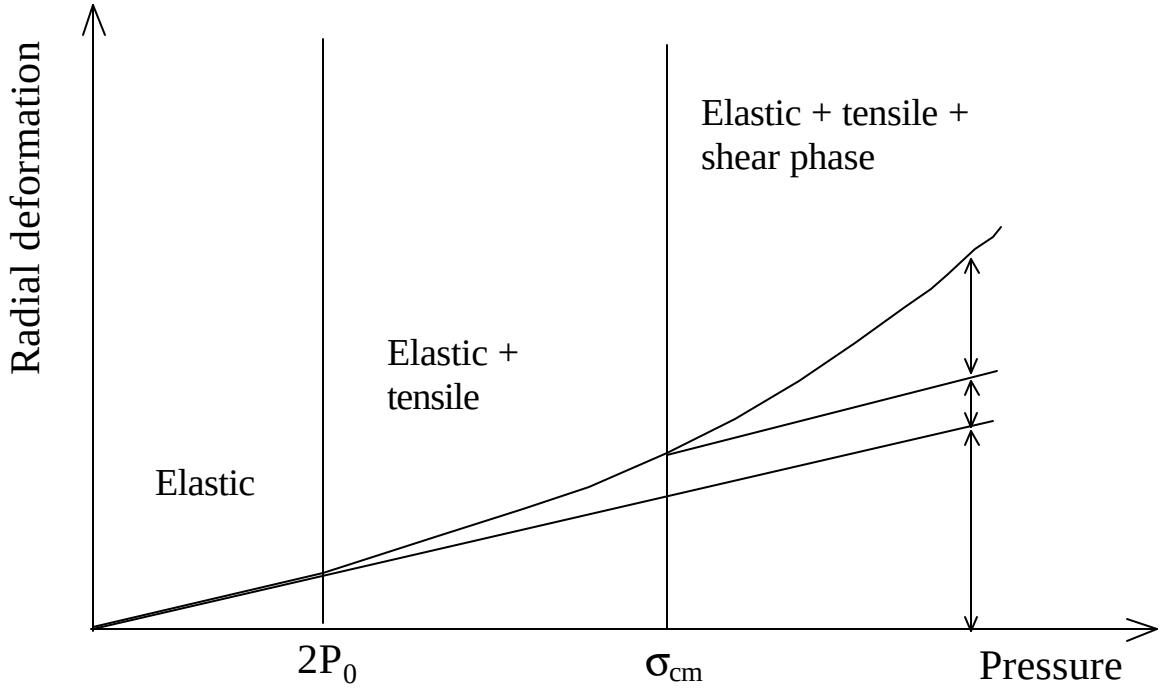

General Deformation

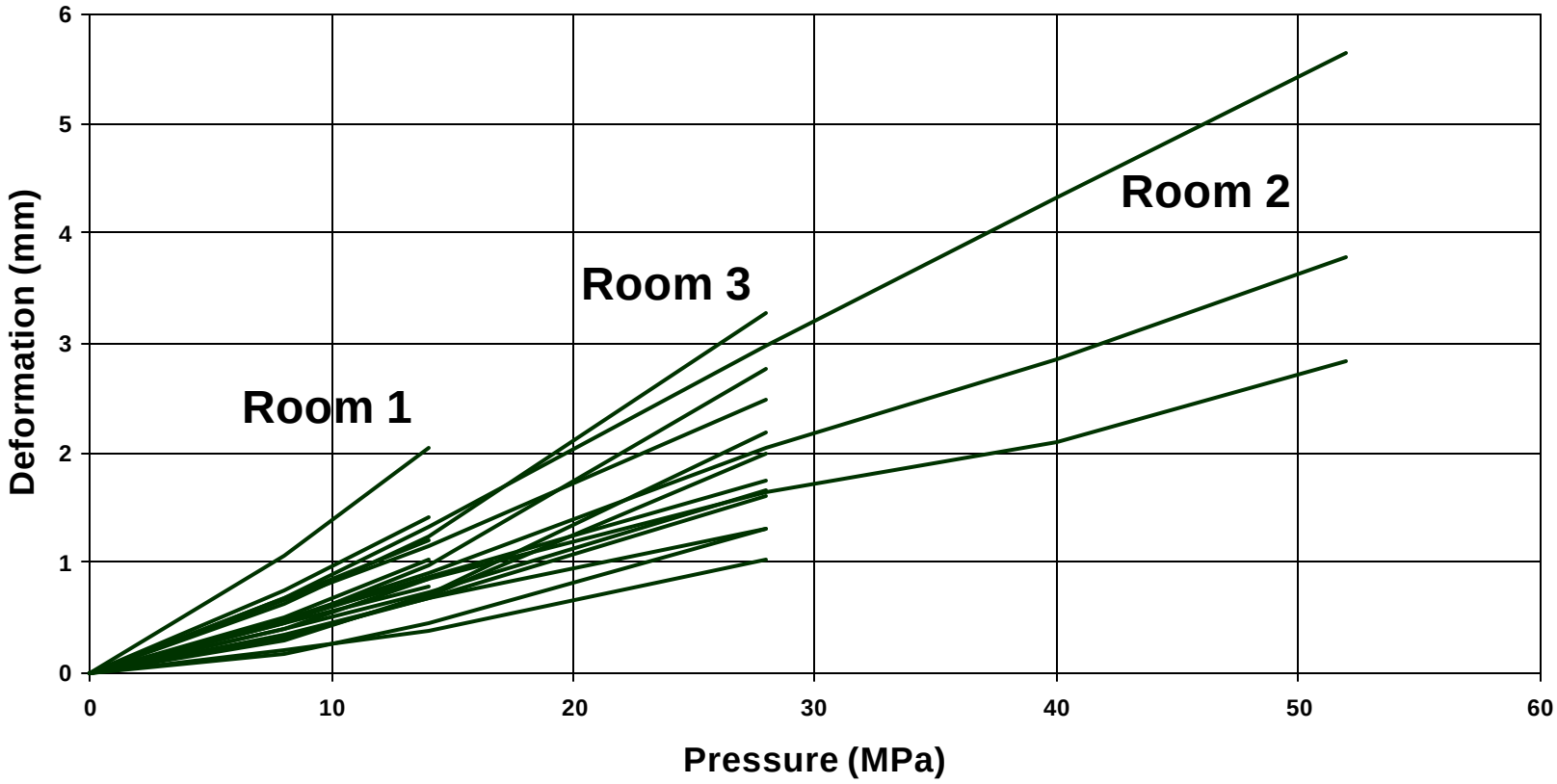

Pressure Tests in Room 2

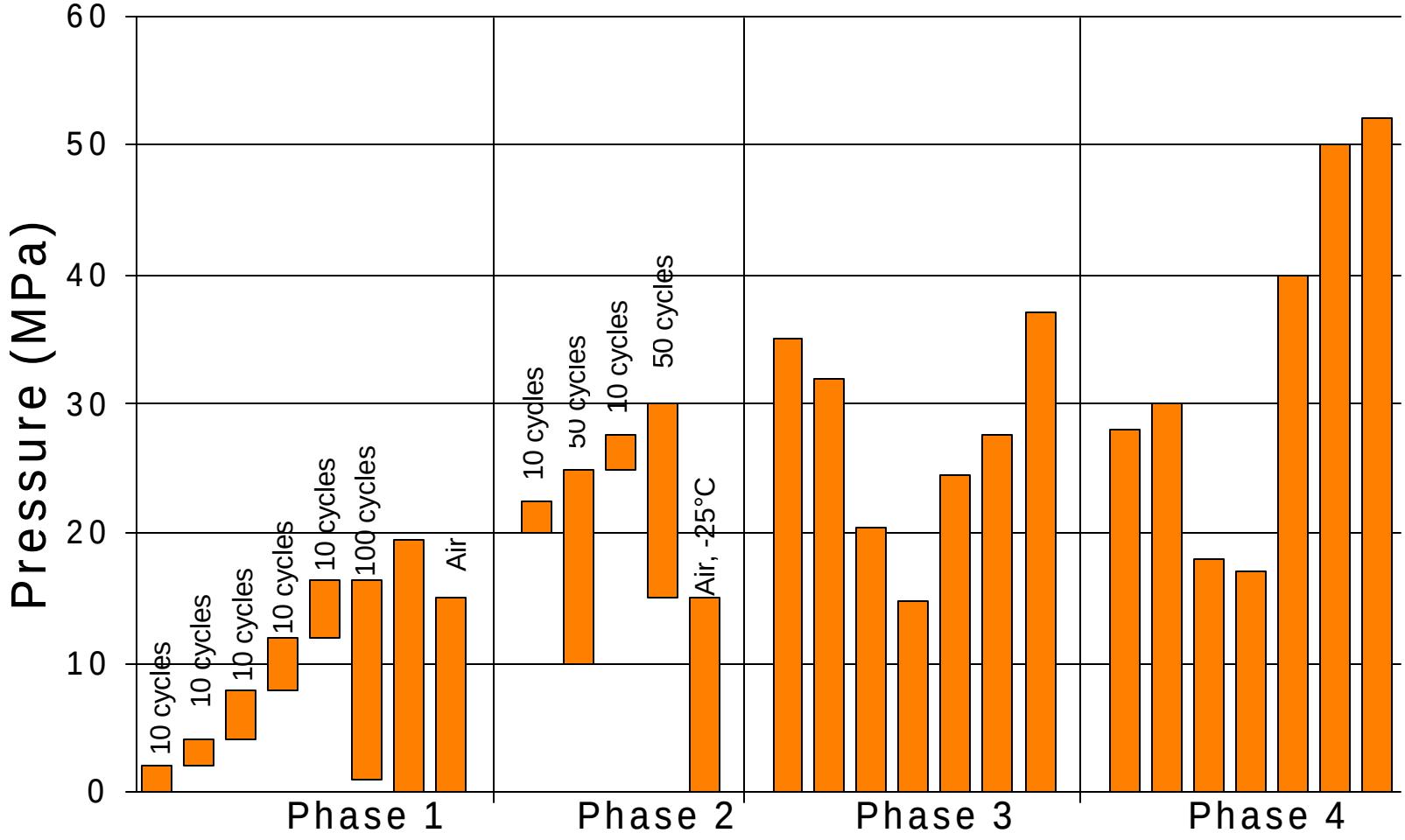

Demonstration Project

- Built and demonstrated by Sydkraft and Gaz de France
- Present activity is the cavern excavation
- Demonstration planned to start in October 2001
- The project i partially financed by the European Union

LRC Demonstration Project Technical Data

- Cavern diameter, D=115 ft
- Height, H=160 ft
- Gas Pressure, p=2900 psi
- Working Gas Volume,WG=300MMcf
- Base Gase Volume, VG_b= 60MMcf (20MMcf)
- Deliverability Working Gas, qw_w= 30MMcf/d
- Injection Rate, qi=15MMcf/d

LRC Demo in Sweden

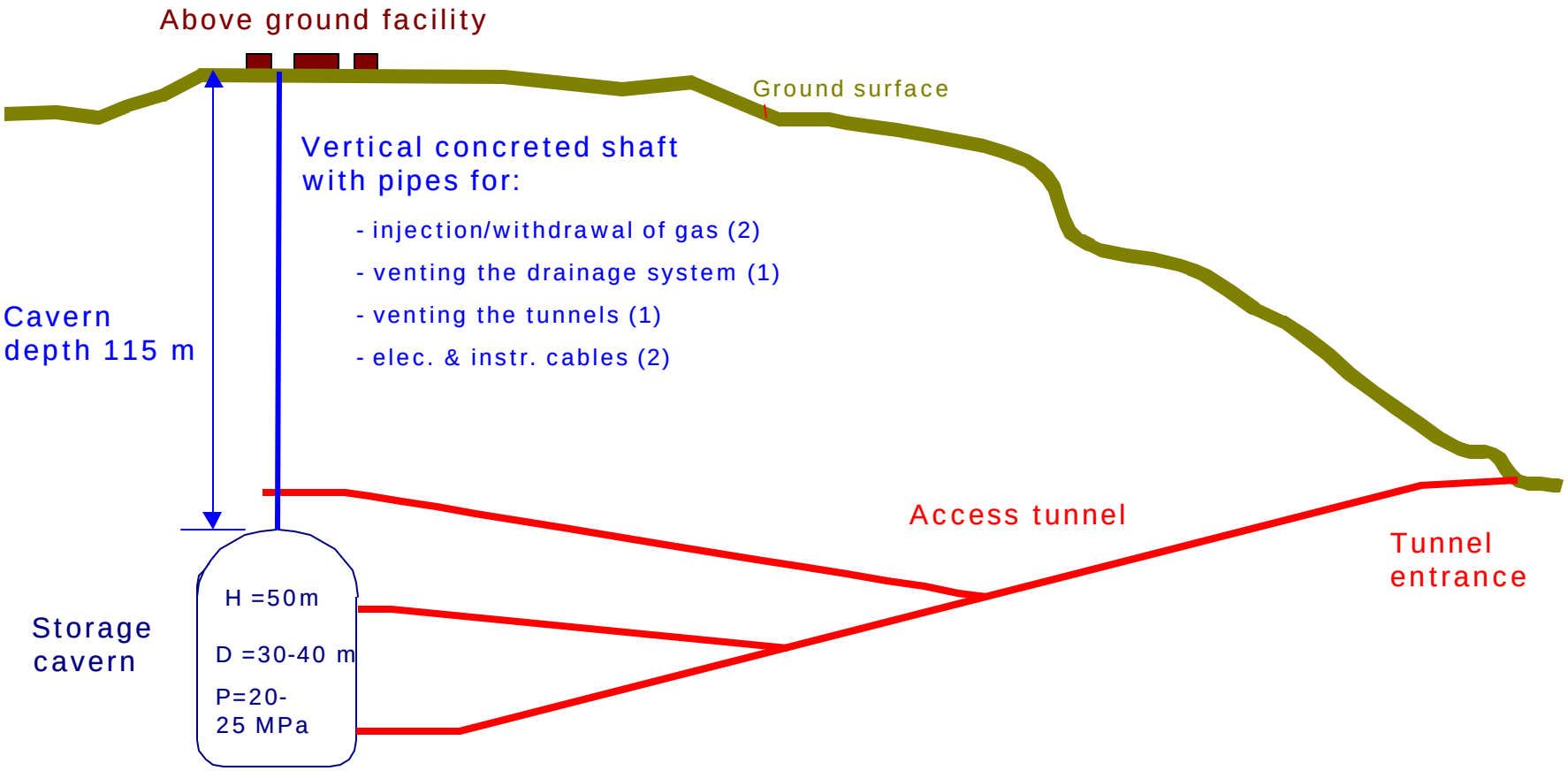

Siting Methodology Step

- Customers, pipelines, general geology
- Feasibility for LRC and max pressure based on FLRC1 and economic evaluation
- Desk-top studies geology
- Field investigation 3-5 sites
- Site selection
- Geologic investigation: rock mass parameter variation

Siting Methodology Step

- Technical potential based on FLRC2 and determination of depth
- Decision to build
- Detail design
- Start of construction
- Updating of prognosis by FLRC2
- Acceptance test for specified pressure and commissioning

Geological Feasibili

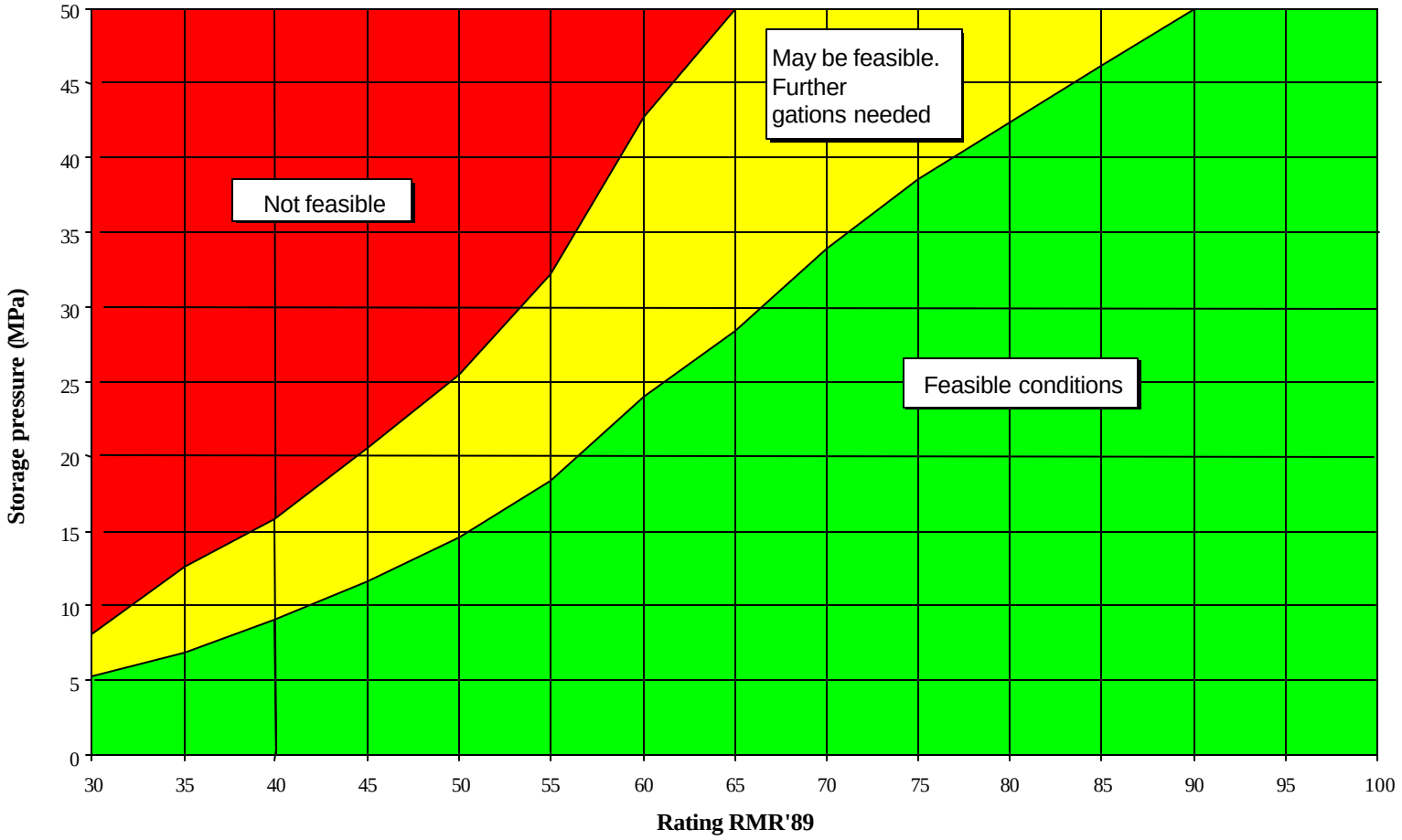

determination of depth

MAIN RULES

- The storage shall be placed below the non robust zone
- Probabilistic design

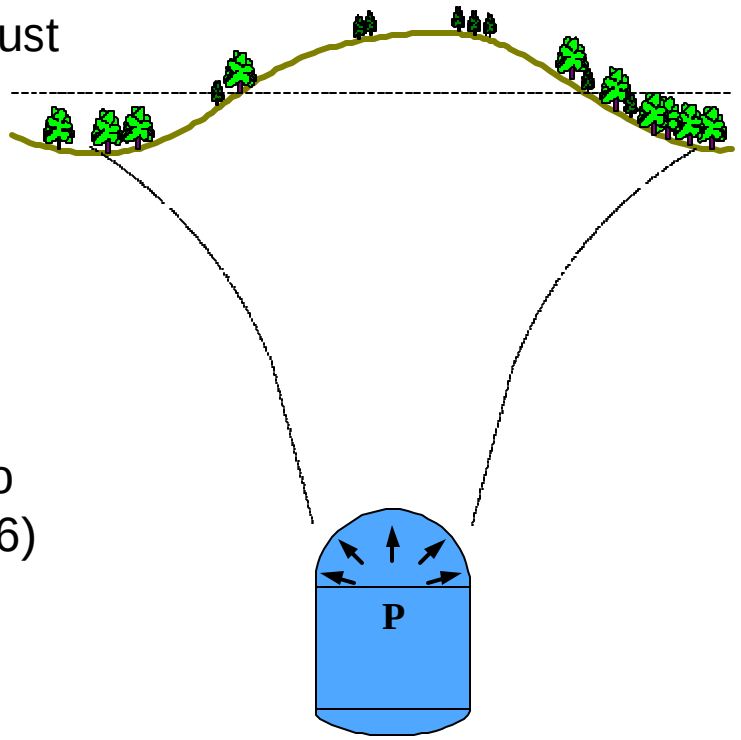

FOUR DESIGN STEPS

- Determine the necessary depth with regards to rock mass failure (probability of failure < 10E-6)
- Determine the extent of the non robust zone
- Evaluate the geology with regards to the existence of larger weakness zone
- Chose the design depth to be at least as low as the lowest of the above

Cone Theory

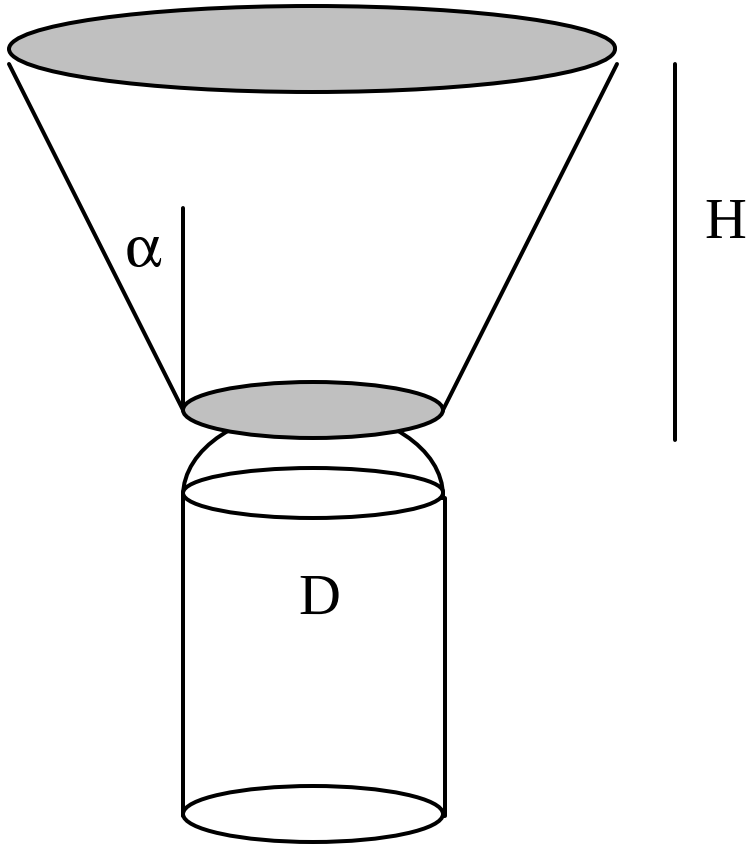

Safety against uplift

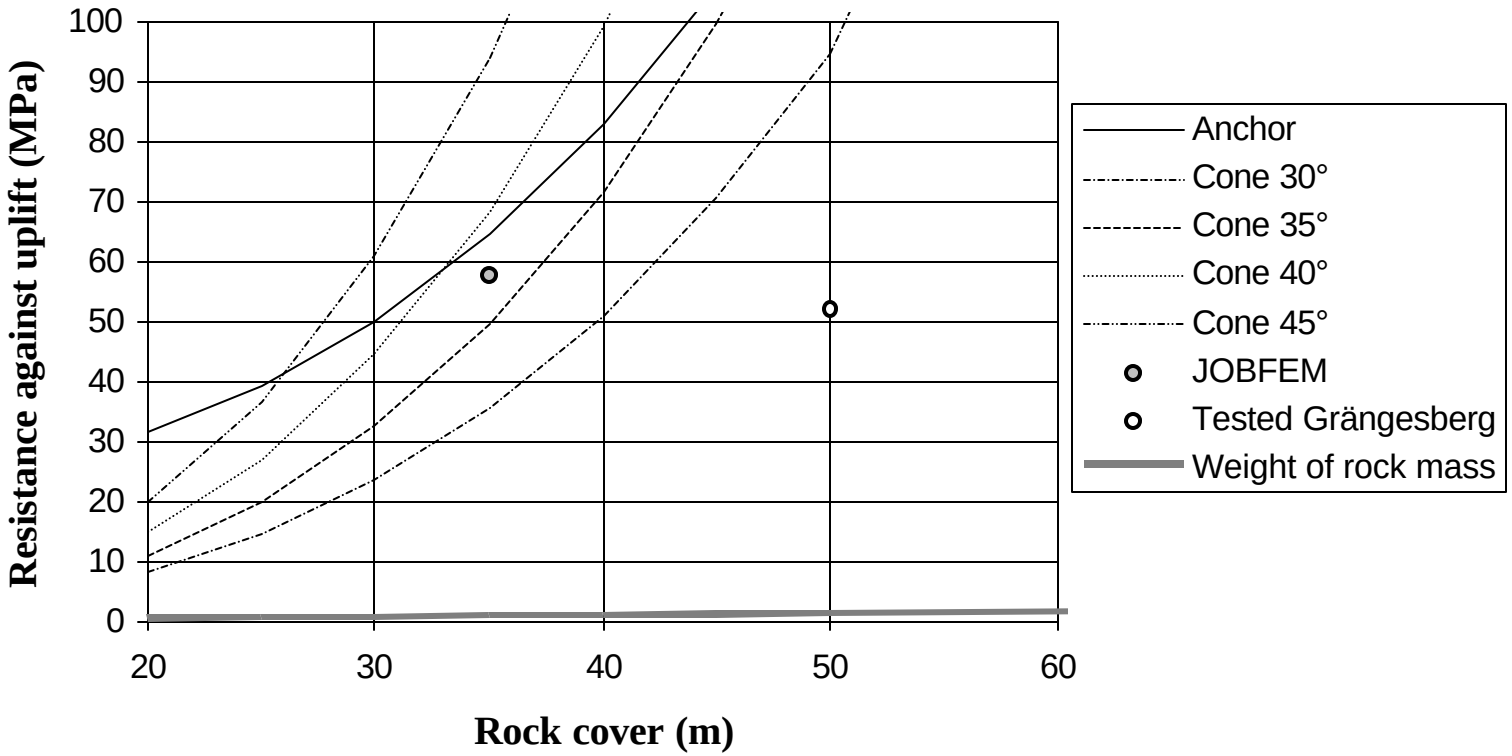

Rock Mass Parameters

Parameter	Methods	Methods based on
Compressive strength of rock mass (c, ϕ)	Hoek & Brown, 1980 Bieniawski, 1978 Stille et al., 1982	RMR-value RMR-value RMS-value (modified RMR)
E-modulus of rock mass	Bieniawski, 1978 Stille et al., 1982 Serafim & Pereira, 1983 Grimstad & Barton, 1993	RMR-value RMR-value RMR-value Q-value

Probabilistic Design

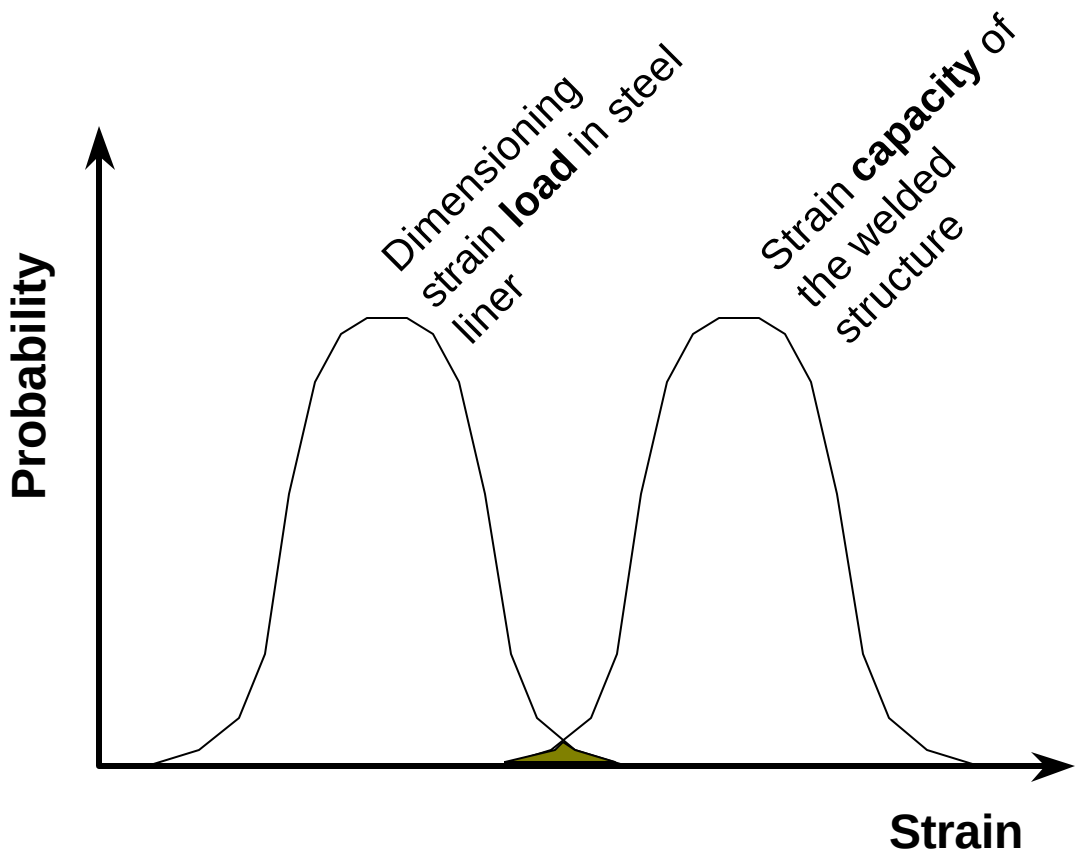

General Layout

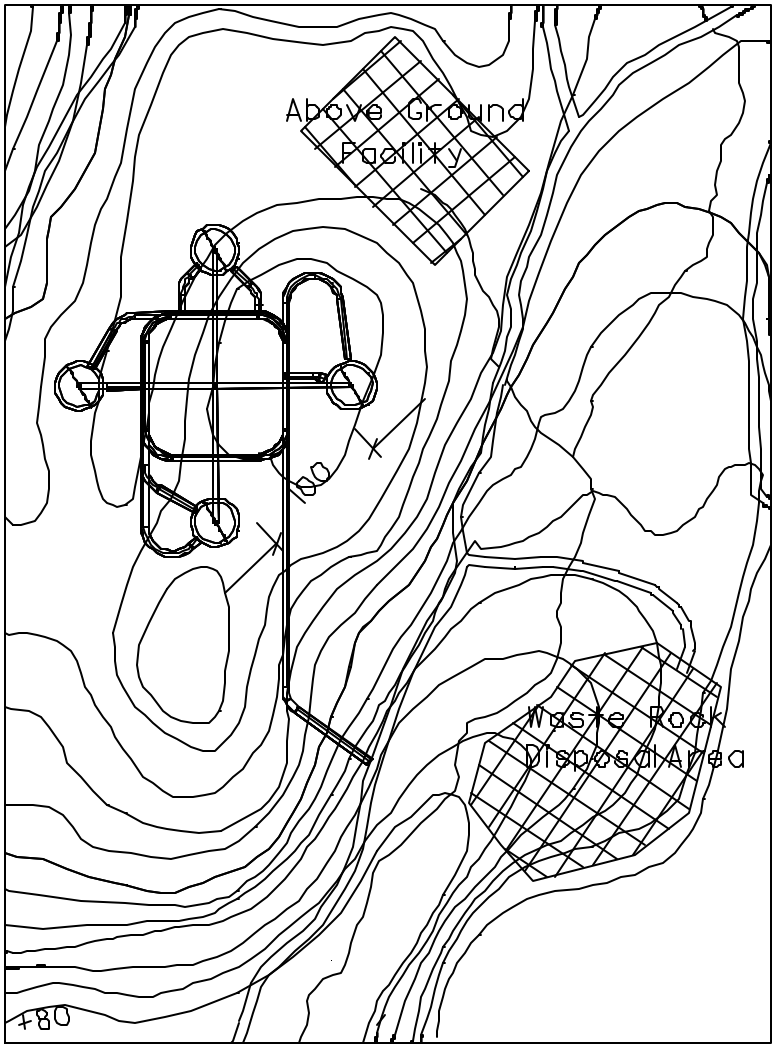

Tunnels

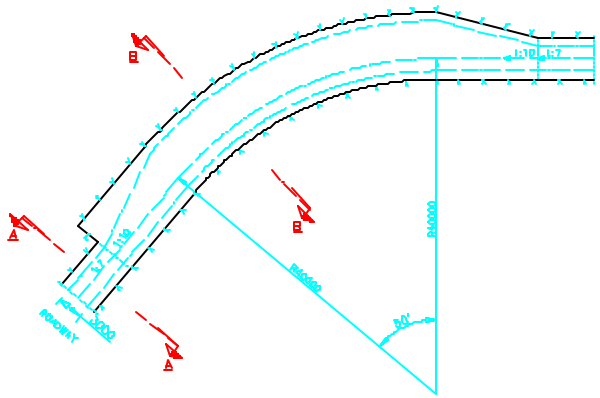

DIRECTIONS

INSTRUCTIONS

TUNNEL DIMENSIONS CORRESPONDS TO THEORETICAL ROCK CONTOUR

PASSING POINT CURVE
1:200

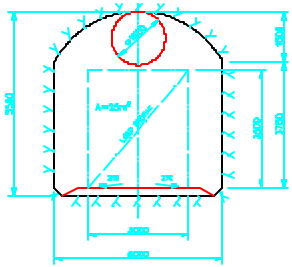

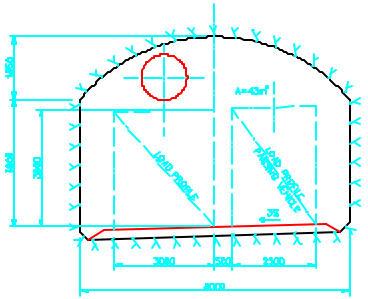

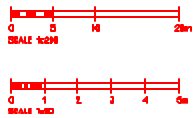

Rock Cavern

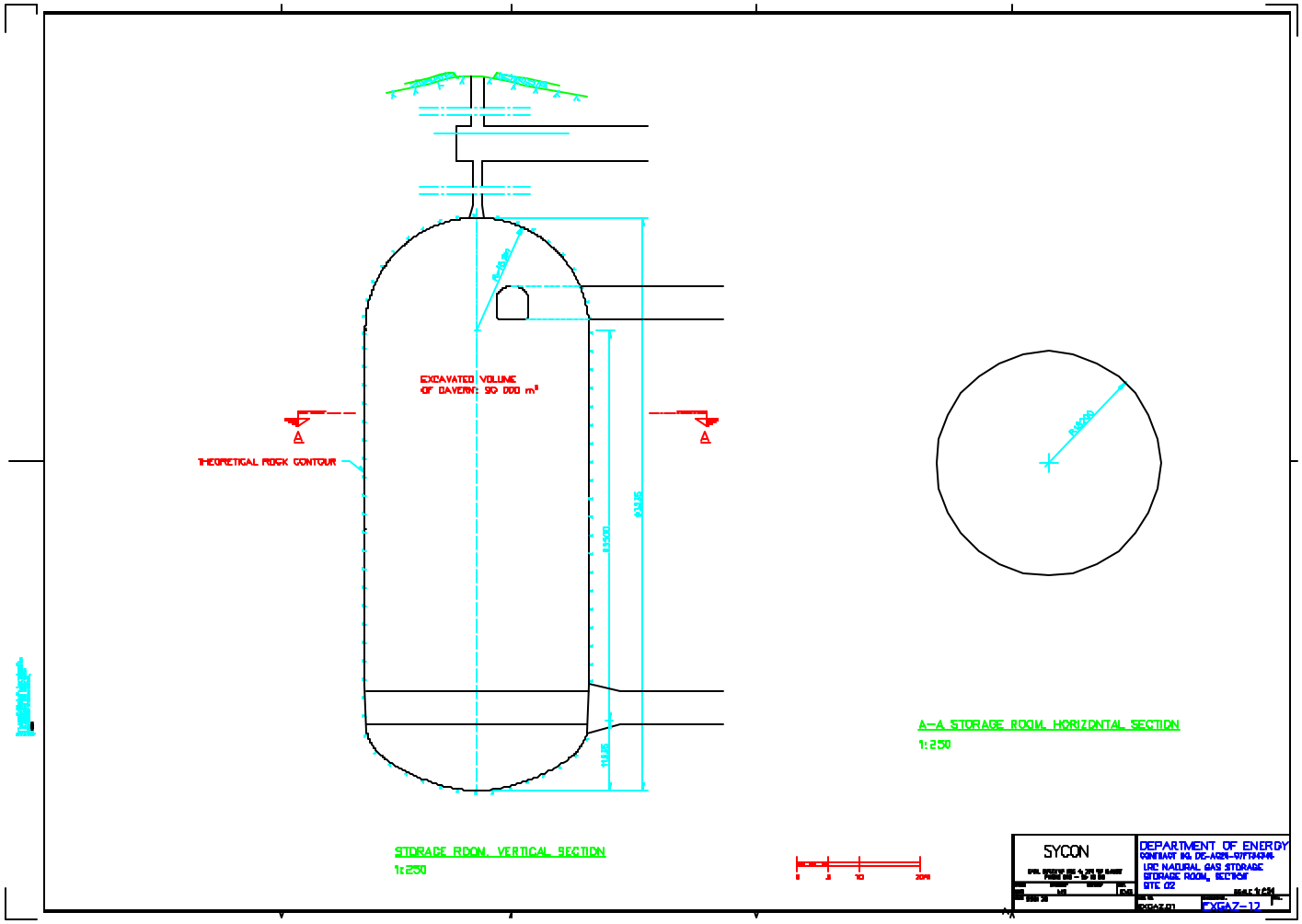
EXCAVATED VOLUME
OF CAVERN: 90 000 m³
THEORETICAL ROCK CONTOUR
A
A
STORAGE ROOM, VERTICAL SECTION
1:250
A–A STORAGE ROOM, HORIZONTAL SECTION
1:250
SYCON
DEPARTMENT OF ENERGY
LRC NATURAL GAS STORAGE
STORAGE ROOM, SECTION
SITE 02
EXGAZ-12

Rock Cavern Excavation

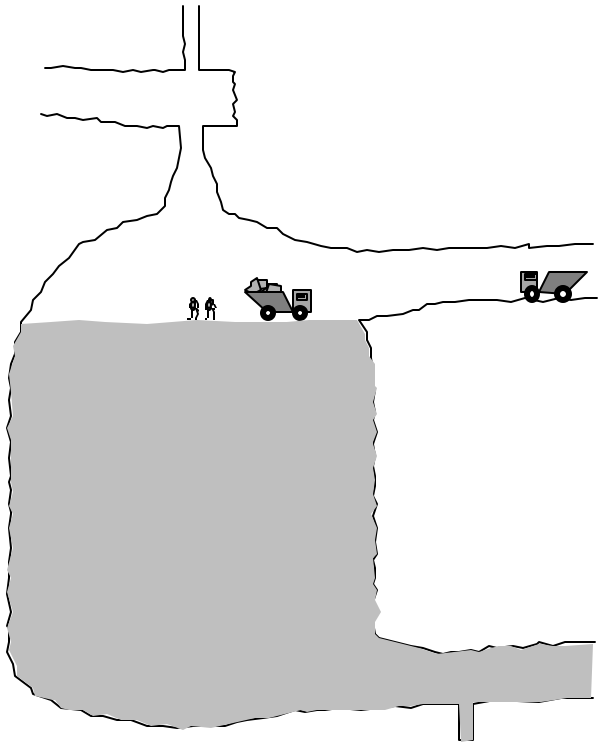

Excavation of top tunnel, cavern dome and shaft

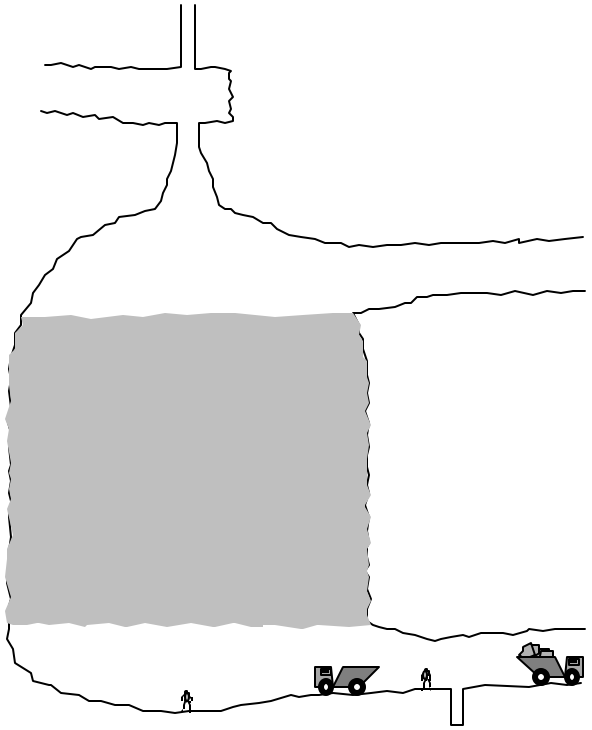

Excavation of bottom tunnel and cavern bottom

Rock Cavern Excavation

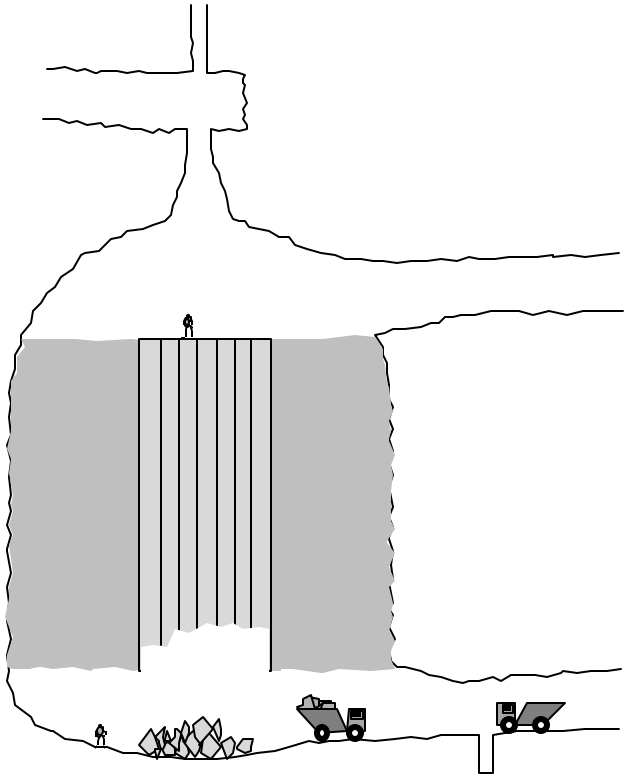

Excavation of central shaft in caven centre w long hole drilling/blasting

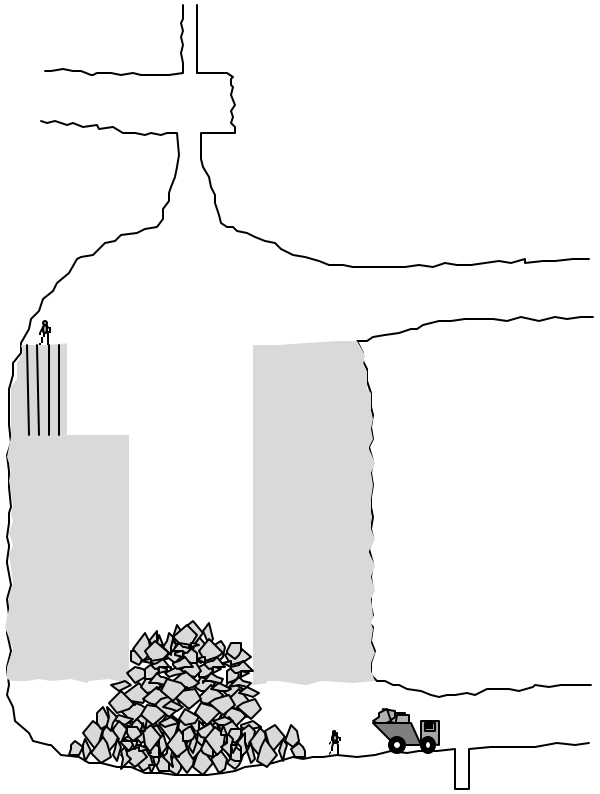

Bench blasting blasting of remaining part

Wall Structure

- Rock mass : pressure absorption
- Concrete layer :
  - Pressure transfer
  - Deformation distribution
  - Smooth basis for the liner
- Steel liner : gas tightness

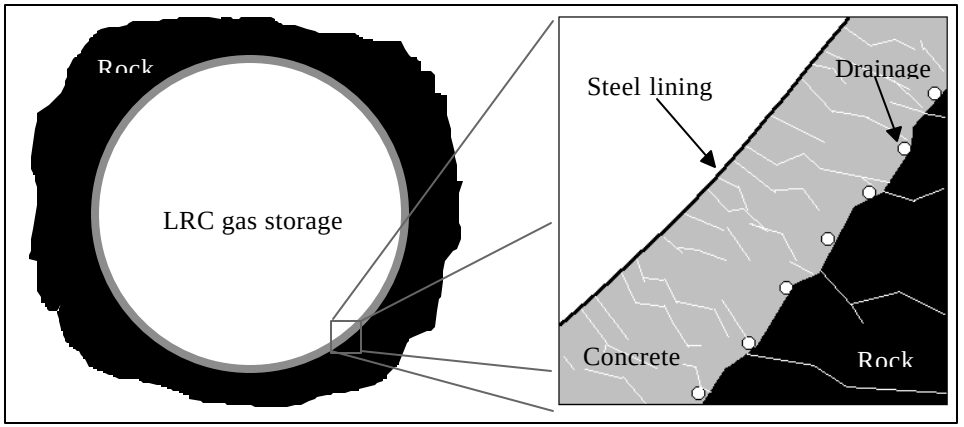

OLA HALL

SENIOR ADVISOR
&
PROJECT MANAGER

SYCON

SWEDEN

Why Storage?

* Reliability 

* Minimization of transportation cost 

* Price Arbitrage 

Storage Customers

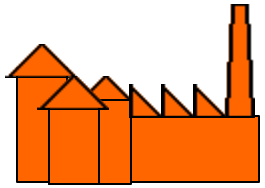

Local Distribution Companies

-Seasonal variations between winter and summer
-Peak variations due to extreme weather conditions

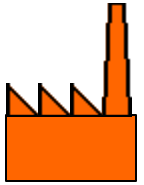

Power Generation Companies

-Seasonal variations with winter and summer
-Weekly- daily- and hourly variations

Transmission Companies

-Net balancing service

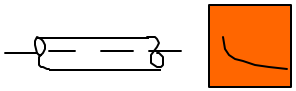

Marketers

-Short term contracts
-Parking
-Loaning

Storage Characteristics

Characteristics	Low	Medium	High	**Reservoir**	**Salt cavern**	**LRC**
Typical working gas size (WG) (Bcf)						
Injection rate % of WG/day						
Deliverability % of WG/day						
Possible annual cycles						
Possible location in market (New storage)						
Swing possibilities						
Expansion possibilities						

Reservoir, Investment Cost per Working Gas Unit

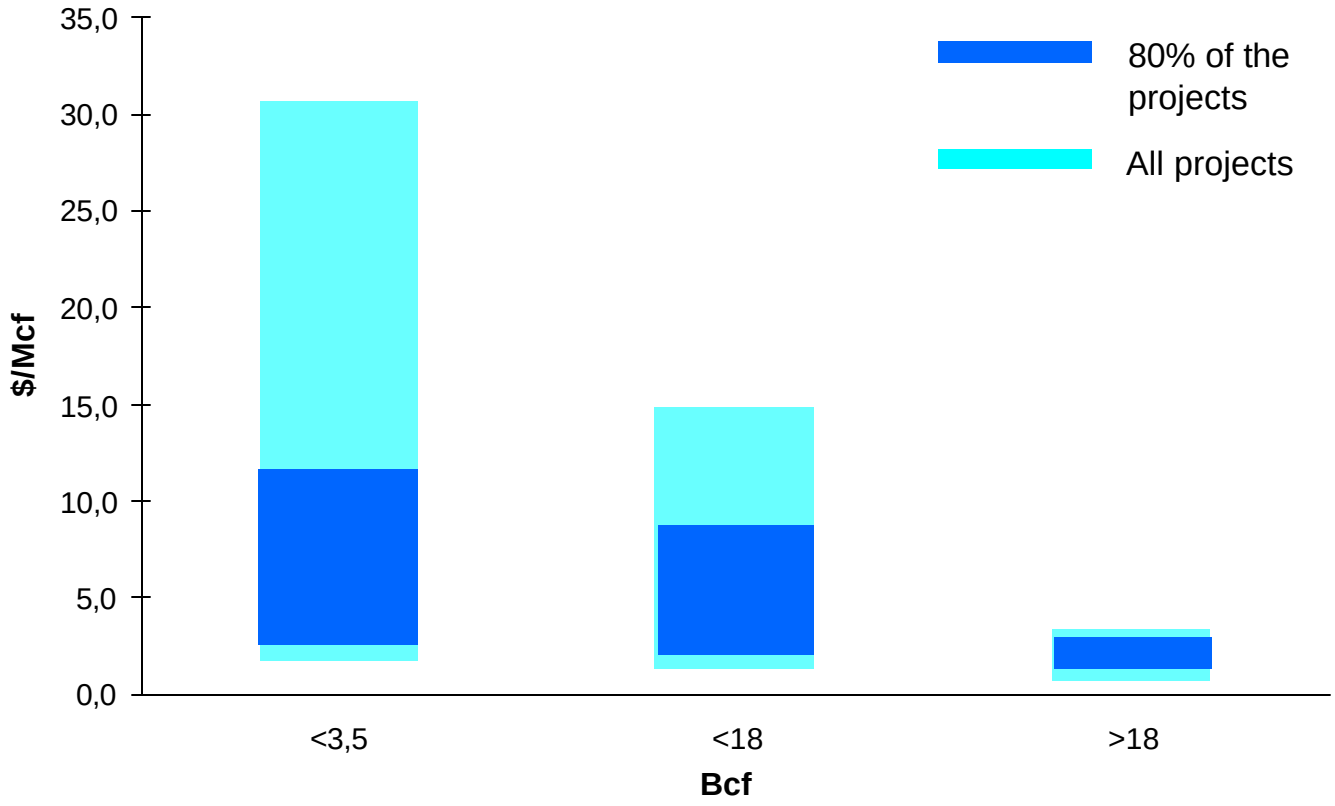

Salt Cavern, Inv. Cost per Working Gas Unit

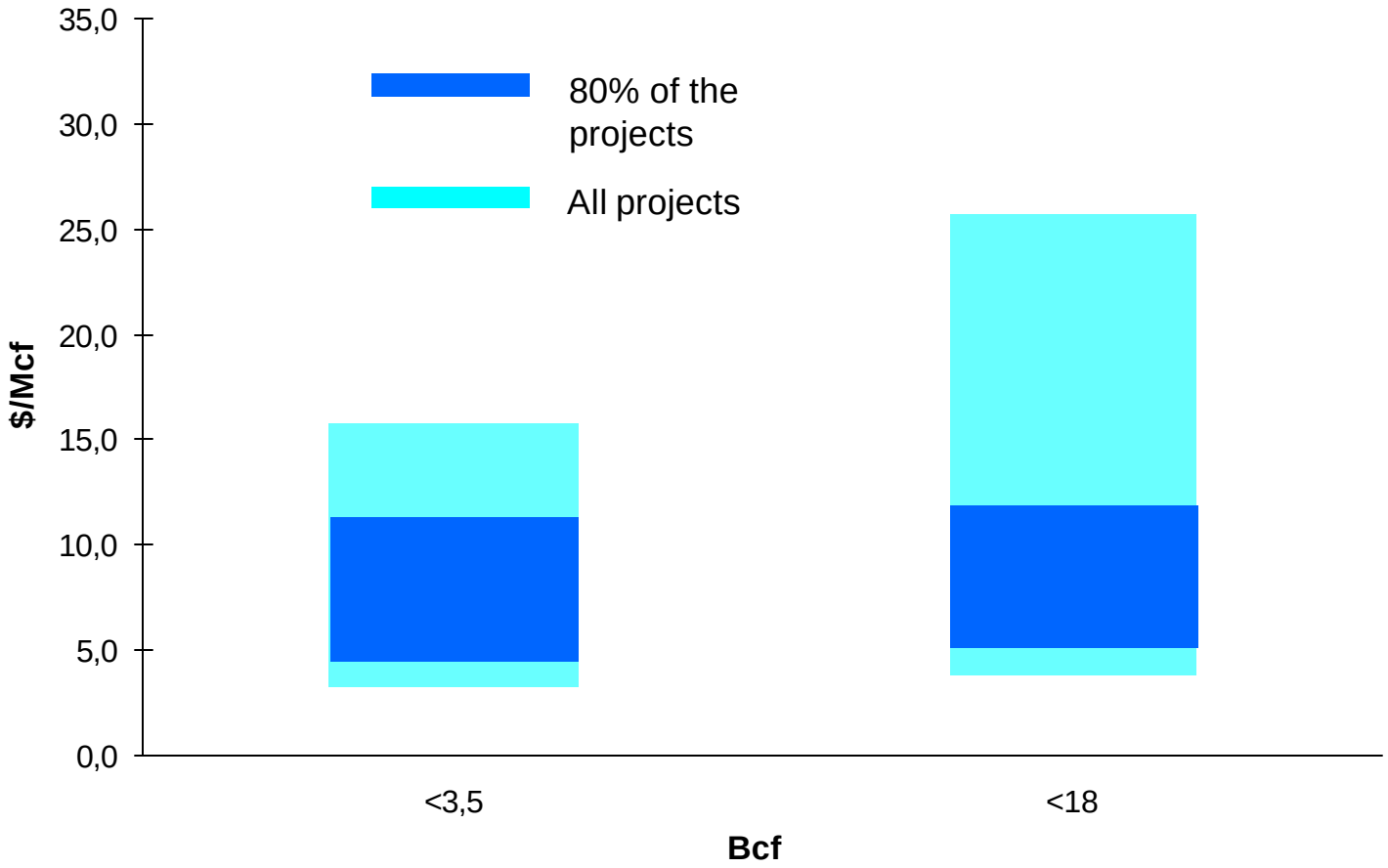

Reservoir, Investment Cost per Deliverability

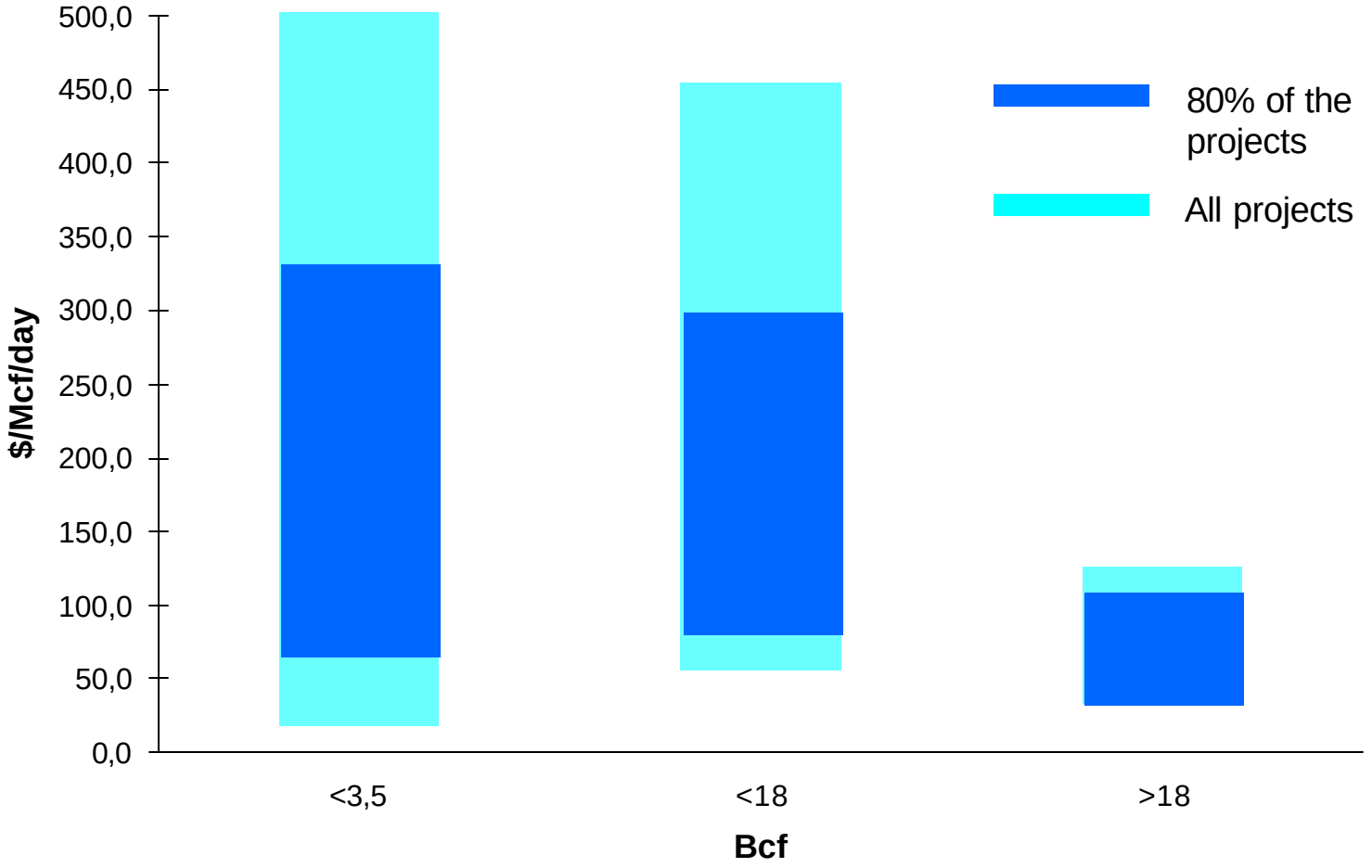

Salt Cavern, Inv. Cost per Deliverability

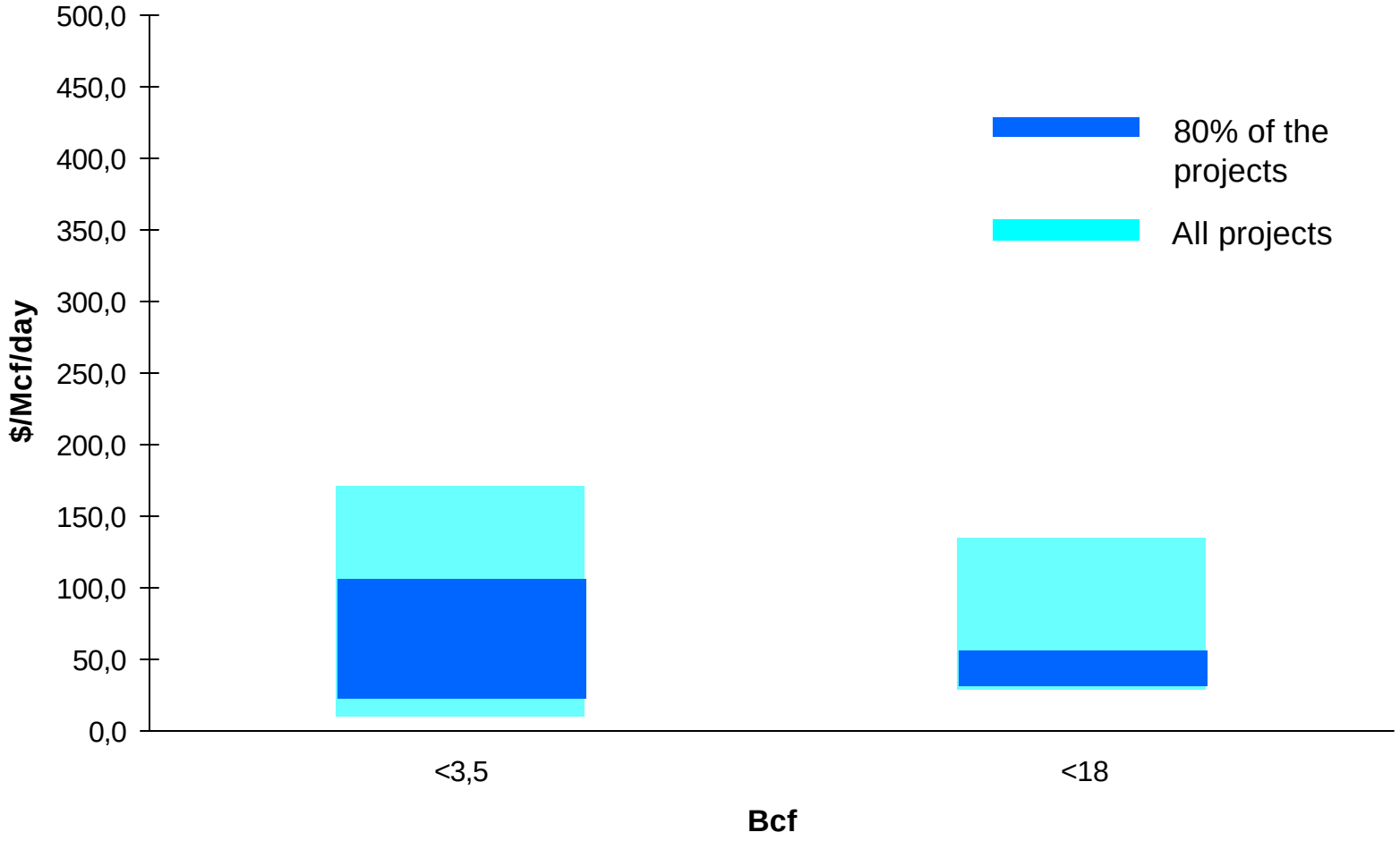

Unit Cost per Working Gas Volume

Type	No. of Projects	Median Size (Bcf)	Median Cost ($/Mcf)
Aquifer	3	9	4.0
Depleted Field	41	6	3.3
Salt Cavern	24	5	8.3

Unit Cost per Deliverability

Type	No. of Projects	Median Size (Mcf/Day)	Median Cost ($/Mcf/Day)
Aquifer	3	81	292
Depleted Field	41	61	137
Salt Cavern	24	506	55

Storage Cost & Customer Puzzle

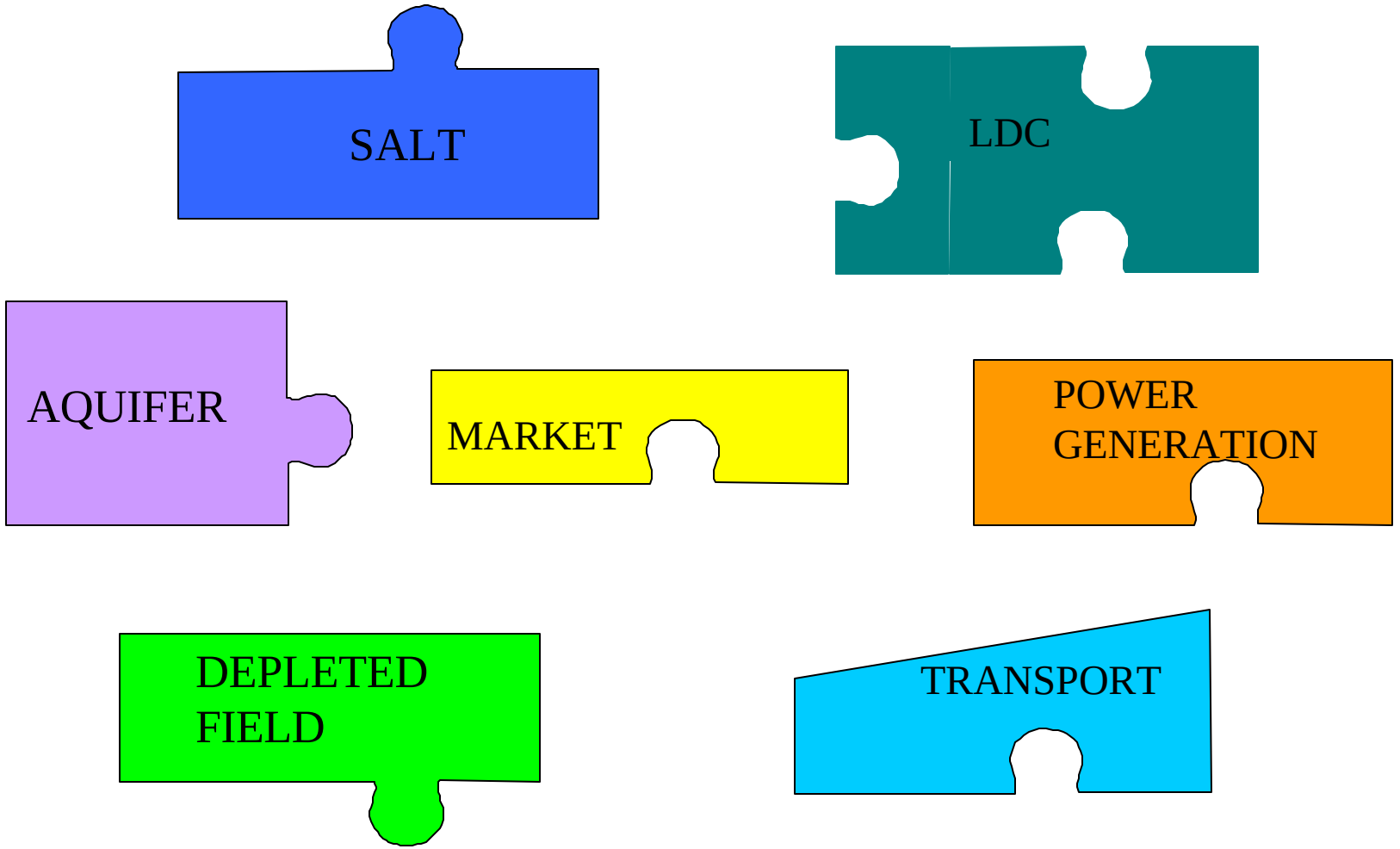

Storage Performance

- Working Gas Capacity 2.6Bscf
- Deliverability 260MMscf/d
- Gas Injection 130MMsc/d
- Max. Pressure 3,330 psi
- Min. Pressure 555 psi
- No. of Possible Cycles 12

Cavern Temperature Calculation

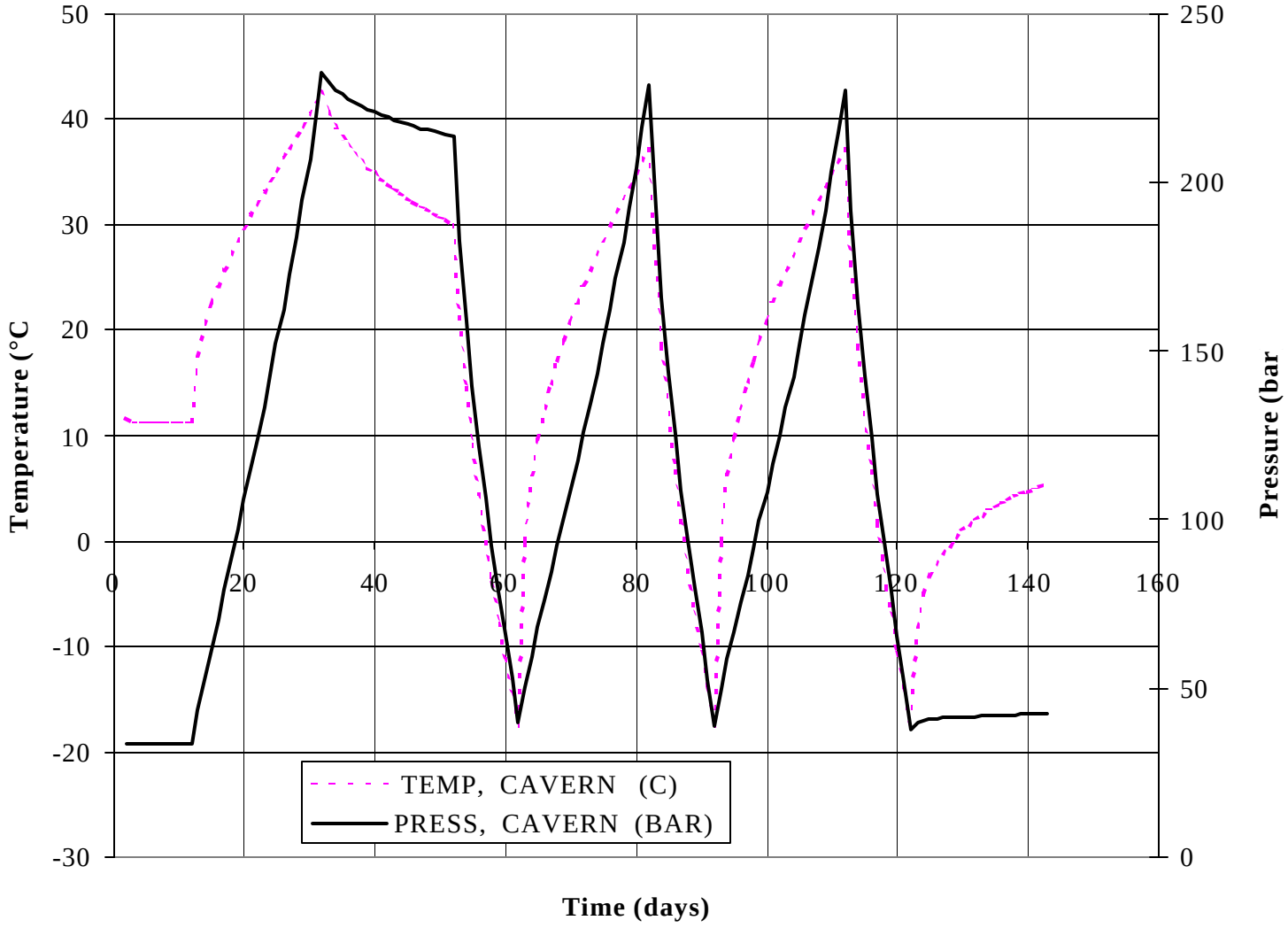

Circulation System

Injection

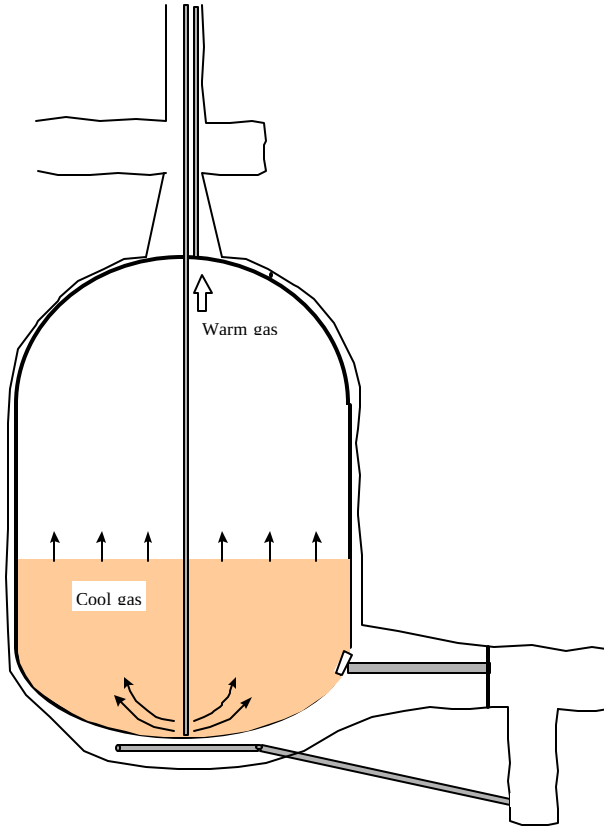

Withdrawal

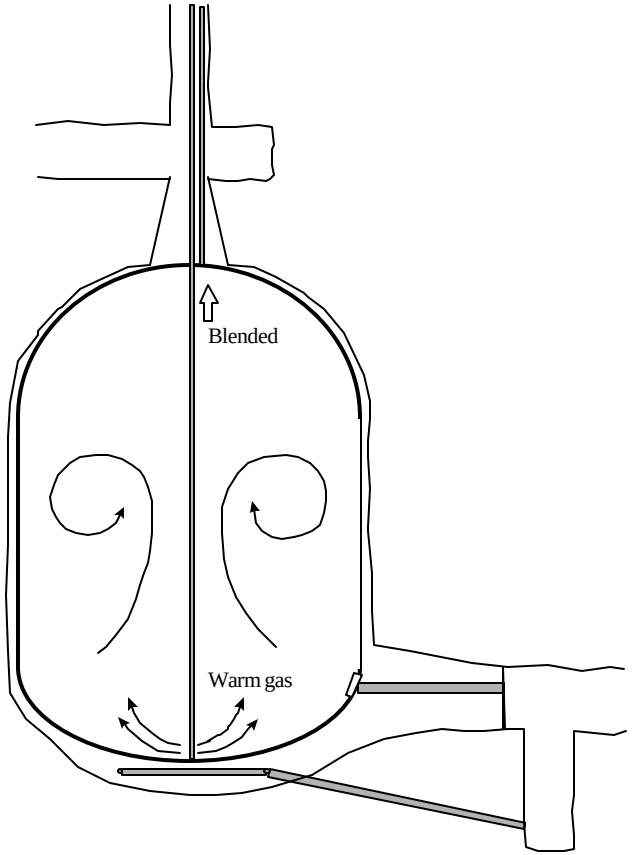

Operational cases

- Injection With Flow Control
- Injection With Compression
- Withdrawal With Reduction
- Withdrawal With Compression
- Circulation Cooling/Heating

PFD-Diagram

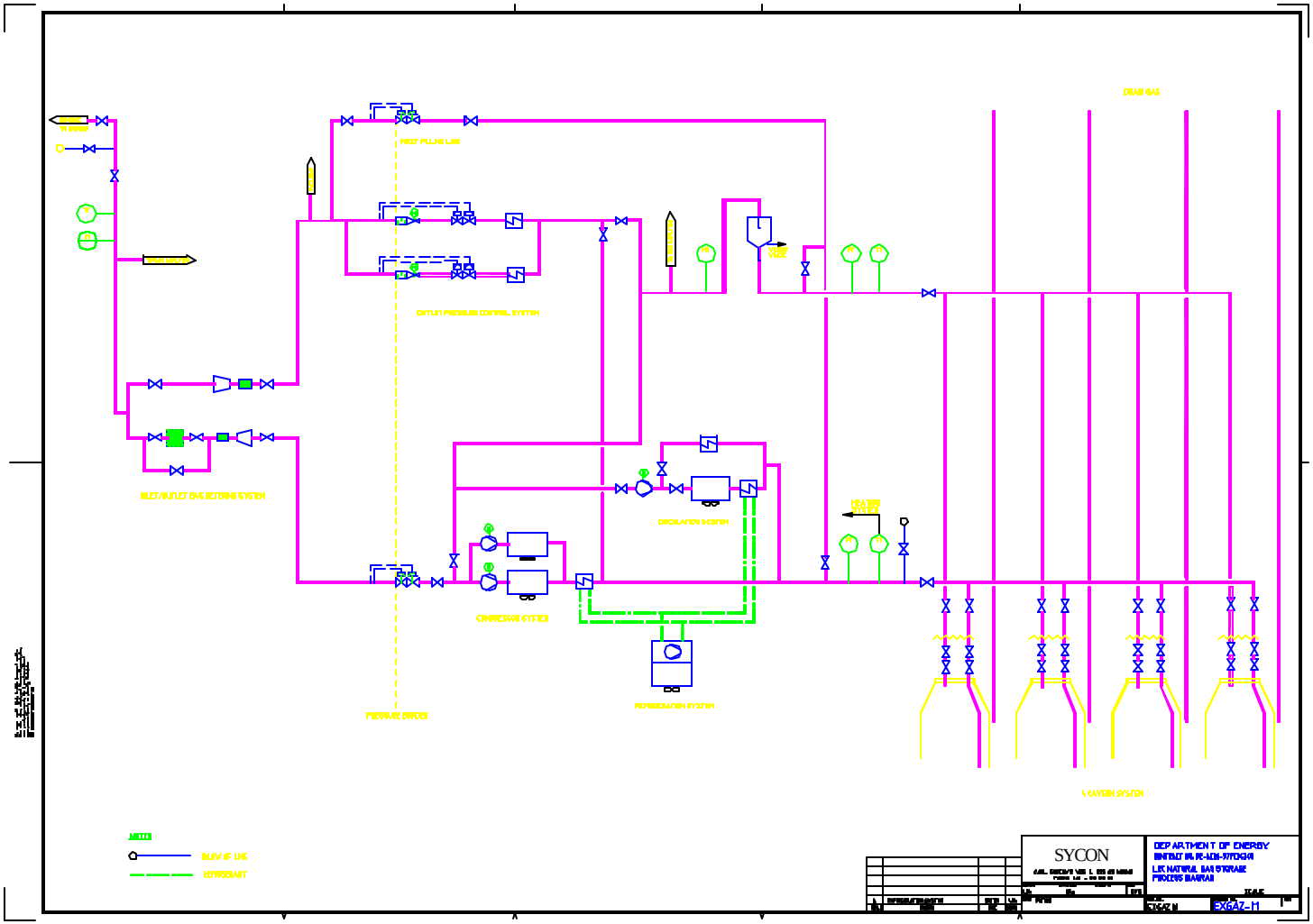
SYCON
DEPARTMENT OF ENERGY
LRC NATURAL GAS STORAGE
PROCESS DIAGRAM
EXAMPLE-1

Lay-Out

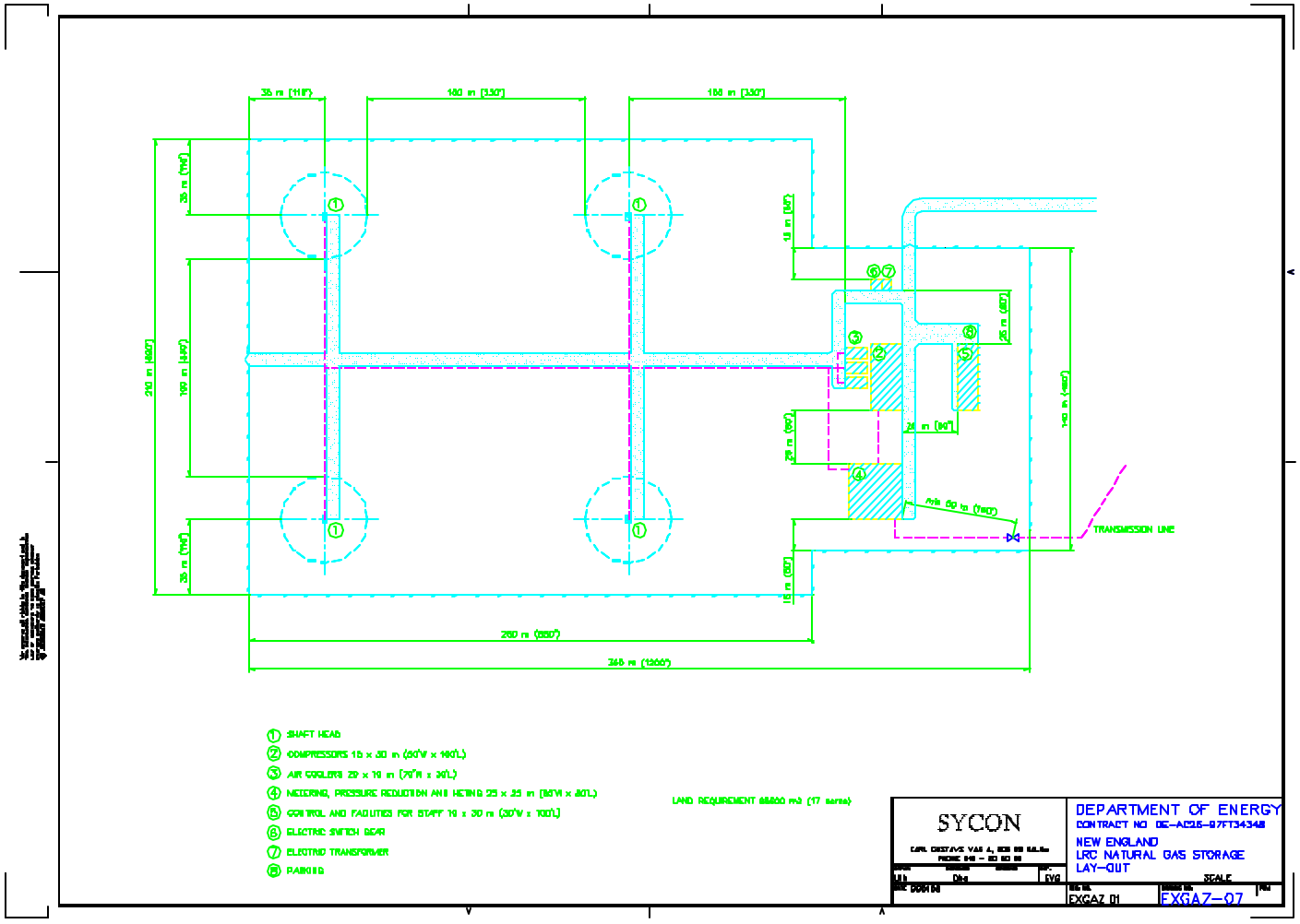
TRANSMISSION LINE
① SHAFT HEAD
② COMPRESSORS 15 x 30 m (50'W x 100'L)
③ AIR COOLERS 20 x 70 m (70'W x 30'L)
④ METERING, PRESSURE REDUCTION AND HEATING 25 x 35 m (80'W x 80'L)
⑤ CONTROL AND FACILITIES FOR STAFF 70 x 30 m (30'W x 100'L)
⑥ ELECTRIC SWITCH GEAR
⑦ ELECTRIC TRANSFORMER
⑧ PARKING
LAND REQUIREMENT 68800 m2 (17 acres)
SYCON
DEPARTMENT OF ENERGY
NEW ENGLAND
LRC NATURAL GAS STORAGE
LAY-OUT
EXGAZ 01
EXGAZ-07

Environmental Impact During Construction

- Conventional Excavation Technique is Used
- Excavated Rock Will be Piled or Sold
- Water Table Level Will be Controlled
- Drain Water Will be Purified

Environmental Impact During Operation

- No Contact Between Gas and Ground Water
- Same Impact as From a Compressor Station

Investment Cost Parts

- Pre-Construction Cost
- Below Ground Cost
- Above Ground cost

Probabilistic Approach

- Multi Risk Model
- High,Low and Likely Value
- General Conditions
  - Competition
  - Localisation

Pre-Construction Cost

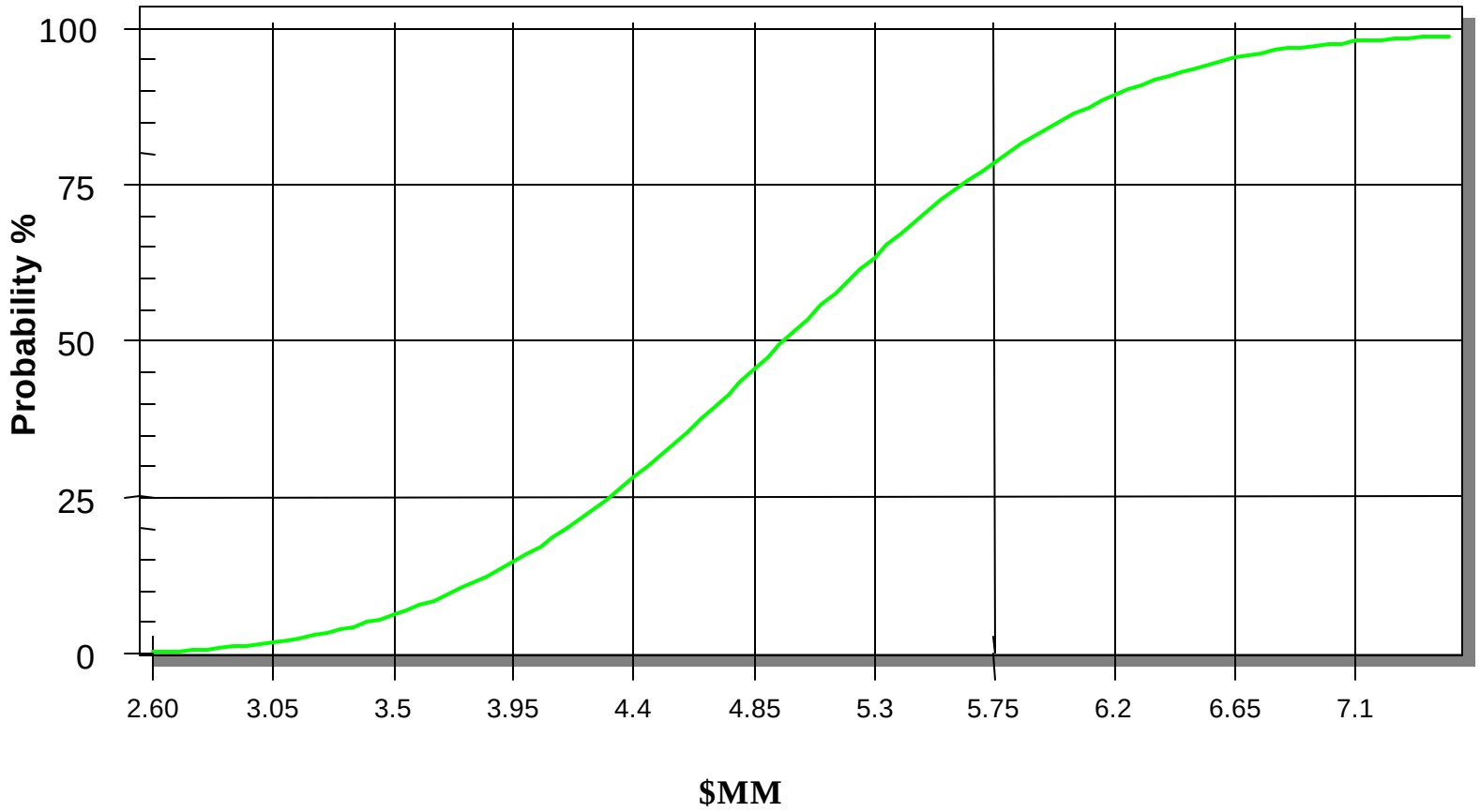

Main Uncertainties in Pre-Construction Cost

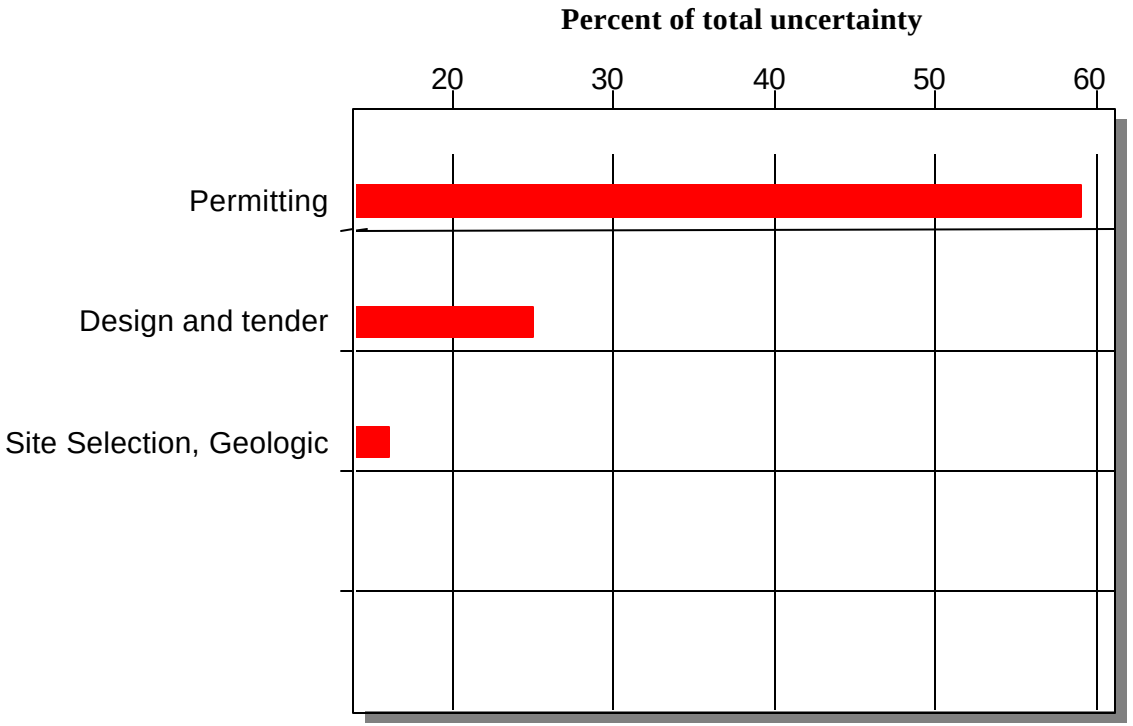

Below Ground Cost

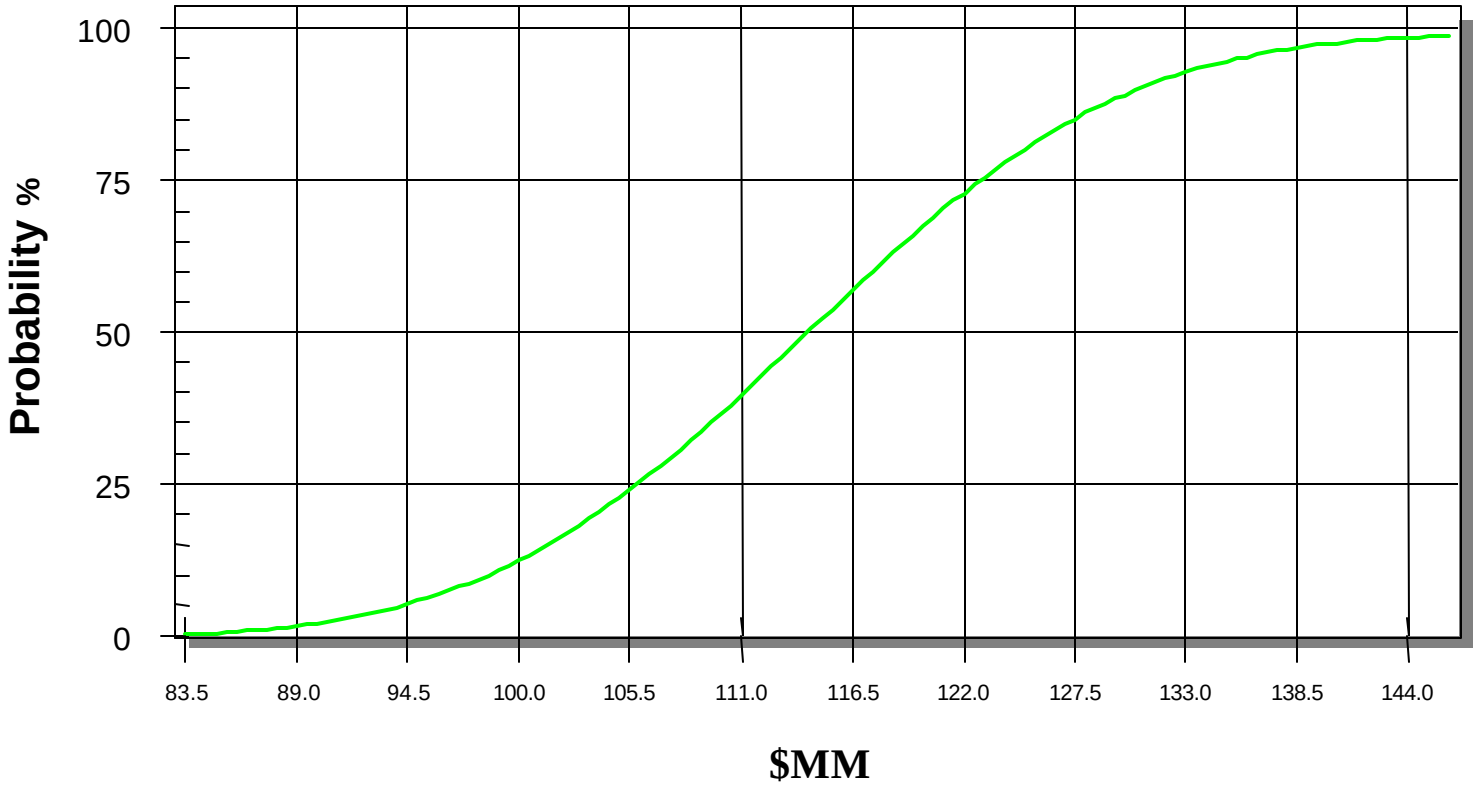

Main Uncertainties in Below Ground Cost

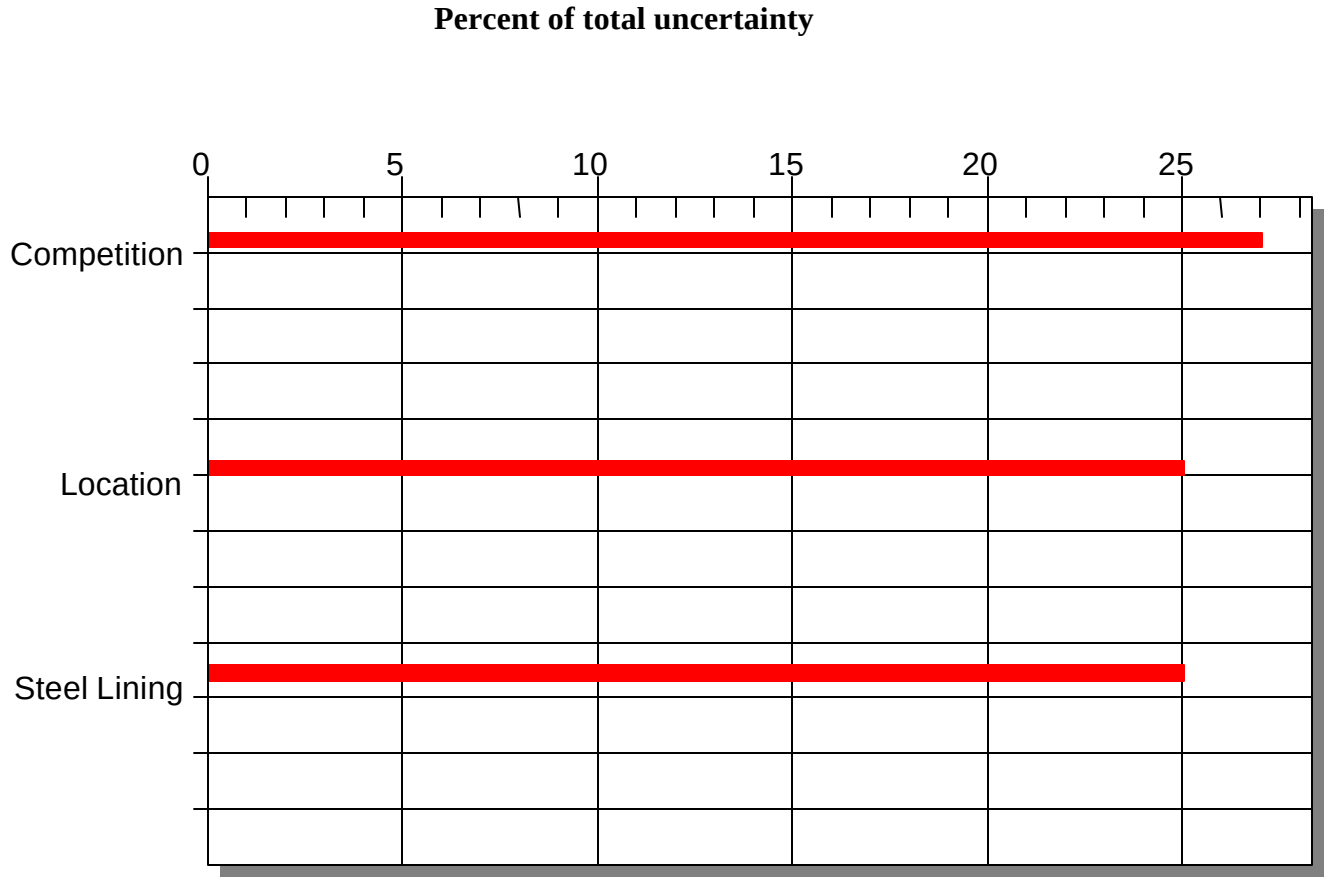

Above Ground Cost

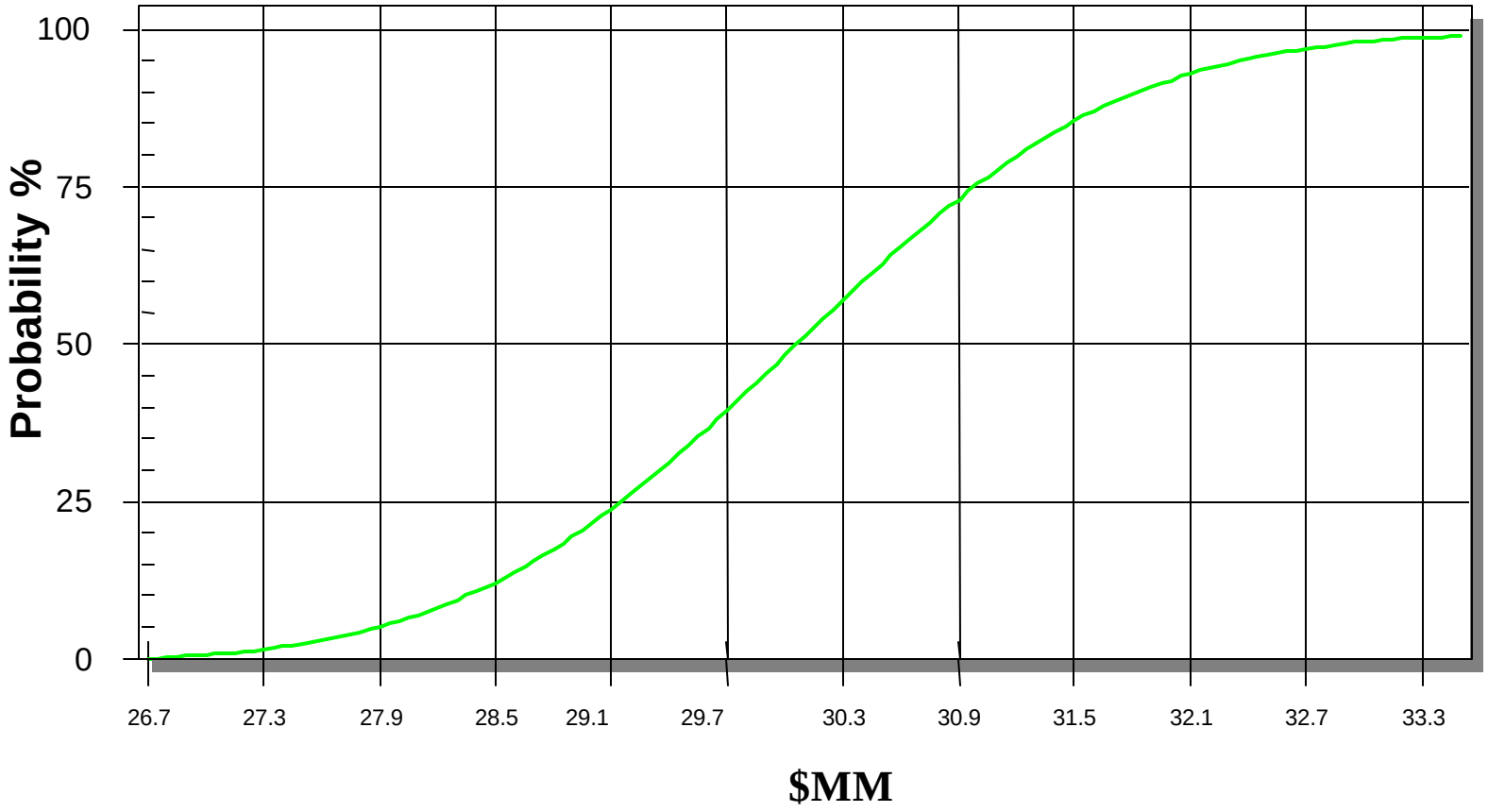

Total Investment Cost

	$1,000
Pre-construction	5,800
Below ground	125,550
Above ground	31,000
Base gas	1,250
AFDC	18,700
Total	**182,300**

Yearly Operating Cost

	Yearly Operating Cost $1,000
Fixed cost:	
Personnel (7)	600
Maintenance compressors	200
Insurance	100
Fixed maintenance	100
Variable cost for one cycle:	
Electricity for injection and cooling plus fuel gas	500
Total cost one cycle	**1,500**

US v.s. Scandinavian Cost

	U.S. Cost	Scandinavian Cost	Factor
	$1,000		
Pre-Construction Cost	5,800	5,800	1.00
Below Ground Cost	125,550	54,600	2.33
Above Ground Cost	31,000	34,000	0.91
Total	**162,350**	**94,400**	**1.72**

Cost of Service

	Deliverability MMcf/d	**$/Mcf/d /month**	**Yearly cost for capacity, 1 cycle, ($/Mcf)**	**Yearly cost for capacity, 12 cycles, ($/Mcf)**
Four-cavern facility	260	$9.79	11.75	1.28
Eight-cavern facility	520	$9.23	11.07	1.21

Time Schedule

ID	Activity
1	**Pre- Construction**
2	Permitting
3	SiteSelection and Design
4	**Below Ground Construction**
5	Excavation of tunnels
6	Excavation of Shafts and 2 first caverns
7	Lining of 2 first caverns
8	Test and commission of 2 first caverns
9	Filling of first 2 caverns
10	Excavation of 2 last caverns
11	Lining of 2 last caverns
12	Test and commission of 2 last caverns
13	Filling of 2 last caverns
14	**Above ground**
15	
16	**Demonstration Plant in Skallen, Sweden**
17	Construction of Demo-plant
18	Test of Demo-plant

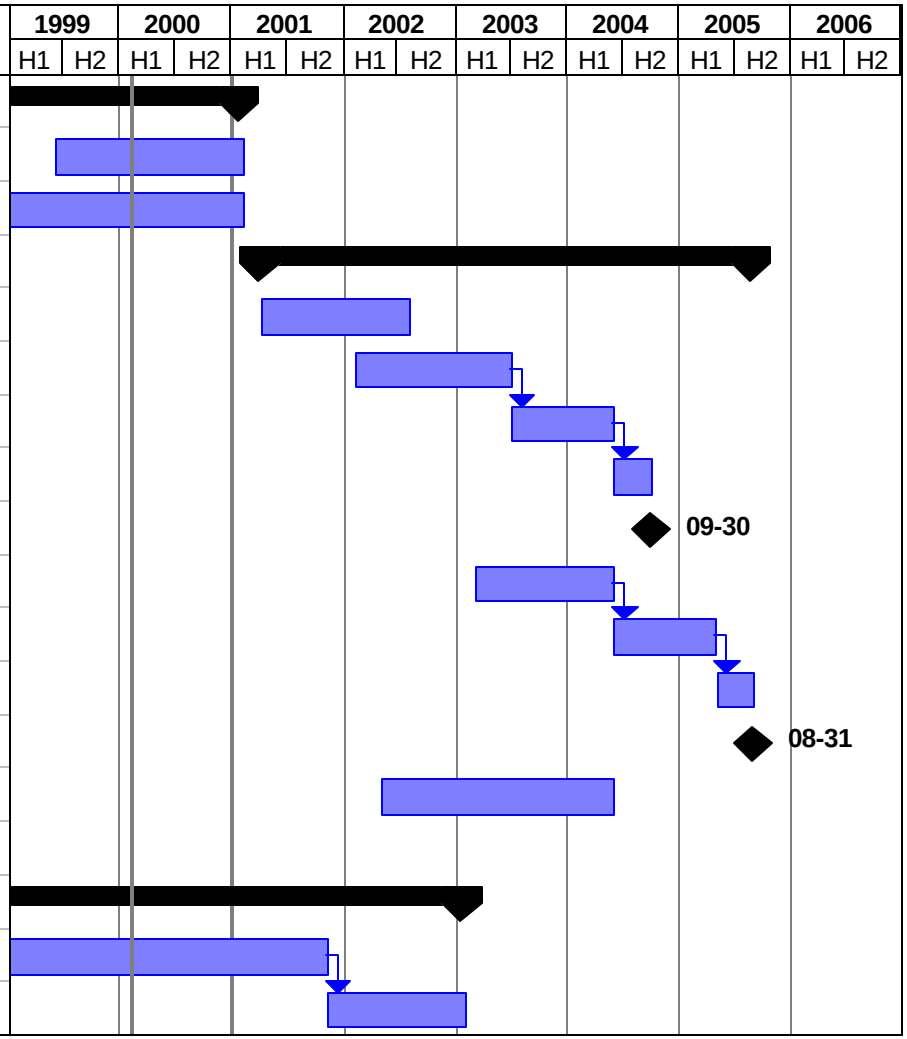

LRC US Group

Cost Reduction Work

- Increased Cavern Diameter and Height
- Two Caverns Instead of Four
- Shorter Access Tunnels
- Implementing More Efficient Production Methods

Performance and Cost of Revised Concept

⌘ Working Gas Volume	3Bscf
⌘ Deliverability	300MMscf/d
⌘ Injection Rate	150MMscf/d
⌘ Cost of Service	$8/dth/d/month
⌘ In Service	December 2005

LRC Market Target

Geologic flexibility

High deliverability

Multiple cycles

LRC Working Gas Cost

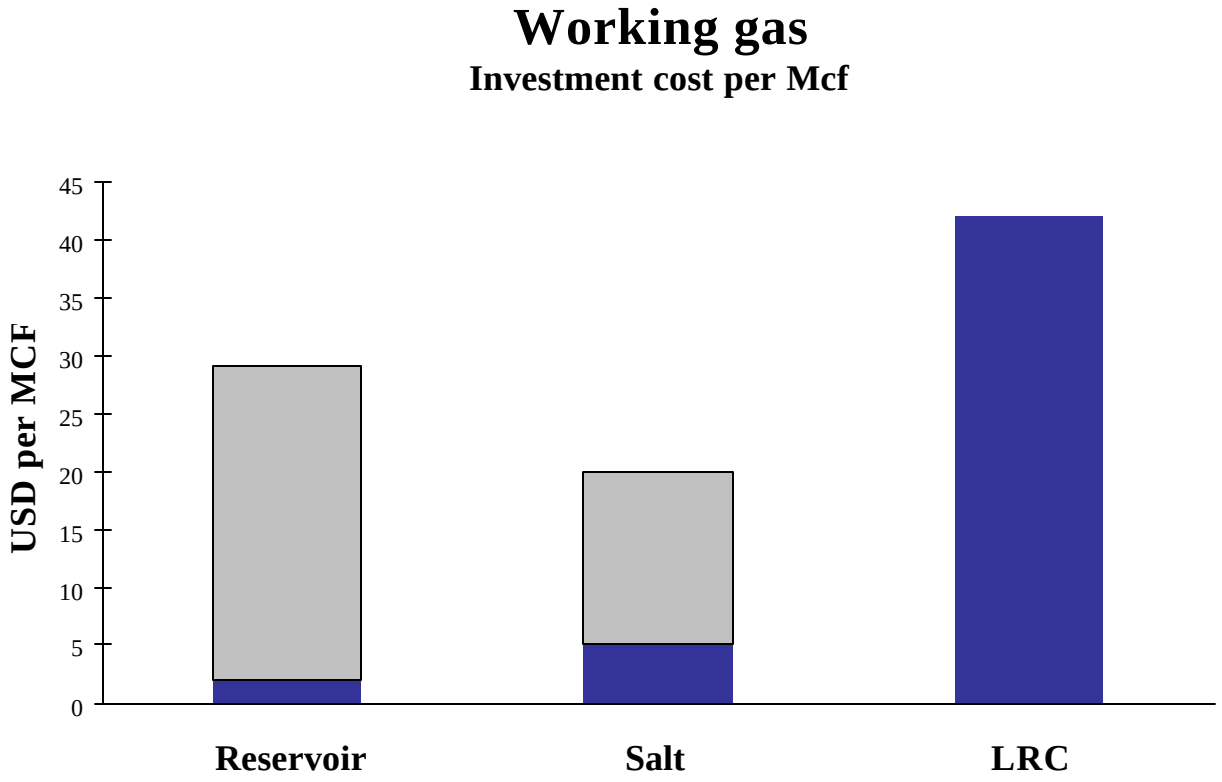

LRC Deliverability Cost

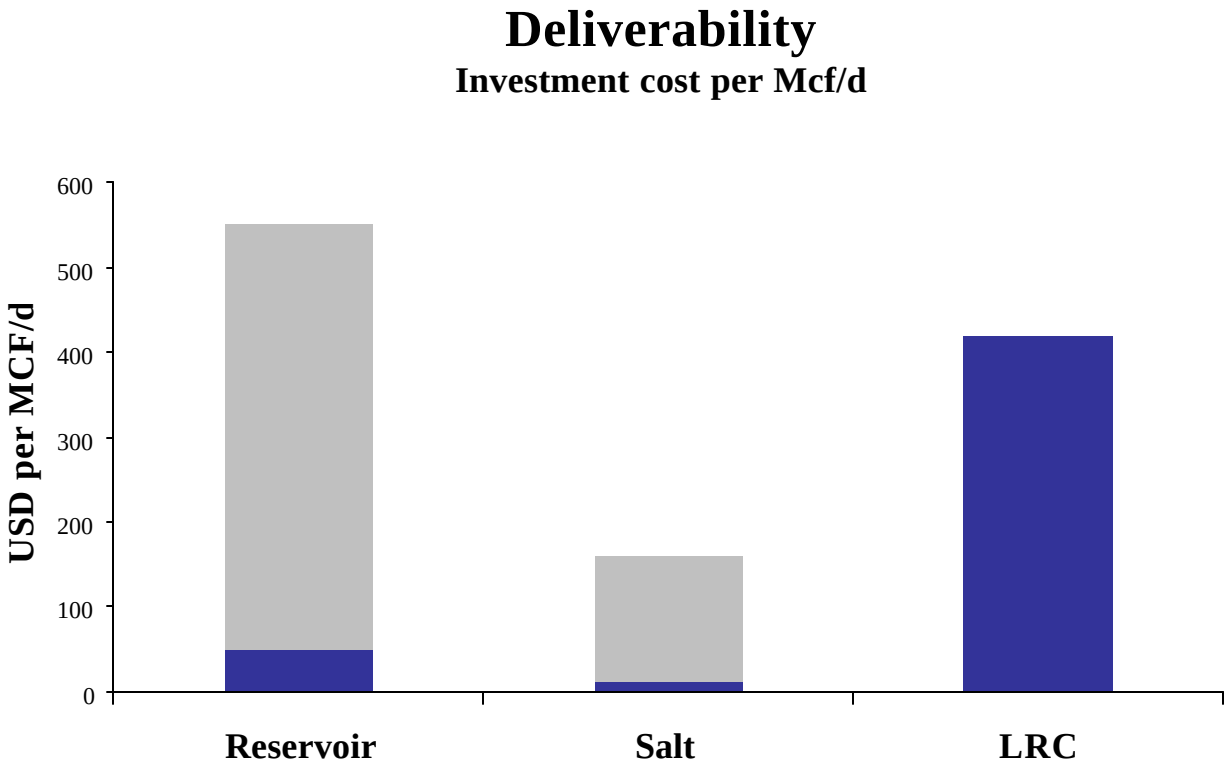

LRC Multiple Cycles Cost

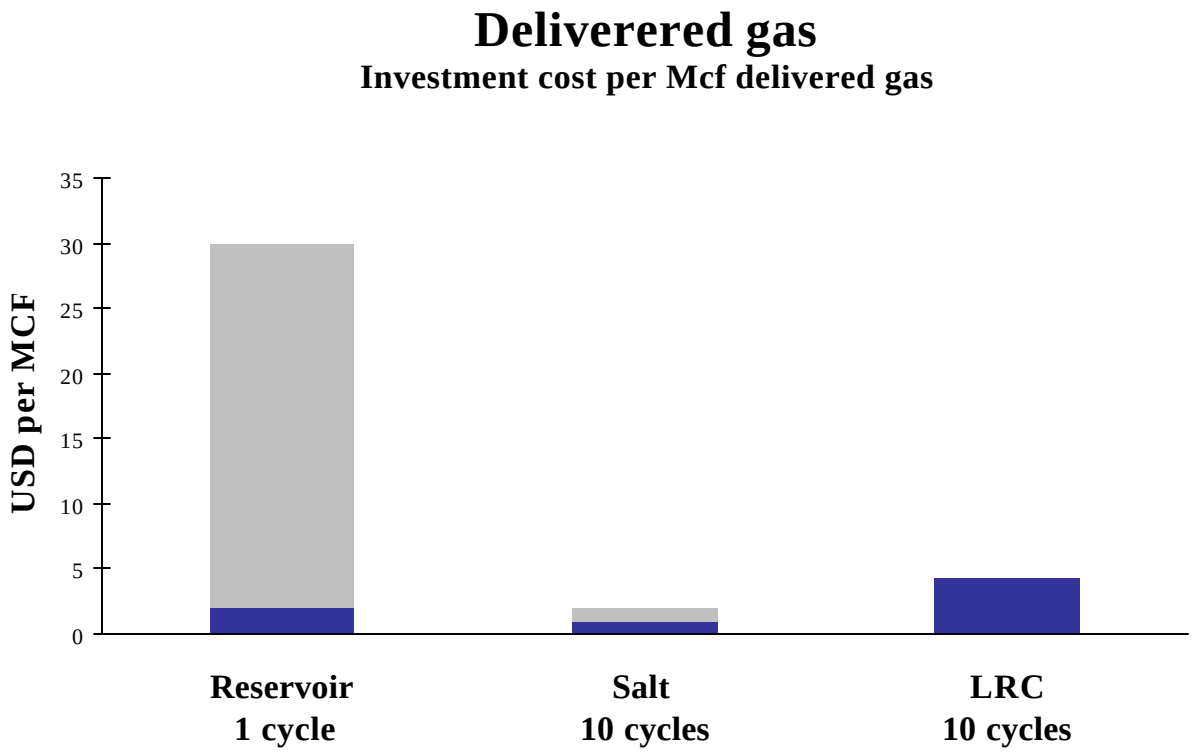

Cost of 300Mdth Yearly 30Mdth/d in 1 Cycle

	Long haul firm transportation	Tioga Storage	Wells LNG	LNG Satellite [(a)]	LRC
Transportation to storage	-	233 000	600 000	600 000	308 000
Storage Cost	-	1 512 000	2 304 000	3 500 000	2 880 000
Transportation to end customer	6 174 000	2 225 000	1 217 000	0	1 217 000
Total annual cost	**6 174 000**	**3 970 000**	**4 121 000**		**4 405 000**
Yearly Unit Cost	***20.6***	***13.2***	***13.7***		***14.7***
Cost Difference		**-2 204 000**	**-2 053 000**		**-1 767 000**
Direct Connection					
Total annual cost				**4 1000 000**	**3 188 000**
Cost Difference				**-2 074 000**	**-2 986 000**
Yearly Unit Cost				***13.7***	***10.63***

(a) Max 30Mdt/d

Cost of 900Mdth Yearly 30Mdth/d in 3 Cycles

	Long haul firm transportation	Tioga Storage	Wells LNG	LNG Satellite [(a)]	LRC
Transportation to storage	-	233 000	1 800 000	1 800 000	308 000
Storage Cost	-	1 512 000	2 304 000	3 500 000	2 880 000
Transportation to end customer	6 174 000	2 225 000	1 217 000	0	1 217 000
Total annual cost	**6 174 000**	**3 970 000**	**5 321 000**		**4 405 000**
Yearly Unit Cost	***6.9***	***4.4***	***5.9***		***4.9***
Cost Difference		**-2 204 000**	**-853 000**		**-1 767 000**
Direct Connection					
Total annual cost				**5 3000 000**	**3 188 000**
Cost Difference				**-874 000**	**-2 986 000**
Yearly Unit Cost				***5.9***	***3.5***

(a) Max 30Mdt/d

New England Market Possibilities

- Lower Cost for Long Haul Transportation by De-contracting
- Possible to Cycle Thus Competing with LNG
- Can be Used for Pipeline Pressure Balancing

South East Market Possibilities

- Difficult to Compete With Long Haul Transportation by De-contracting
- Possible to Cycle Thus Competing with LNG
- Can be Used for Pipeline Pressure Balancing

Economic Model

Natural Gas
Transportation & Storage
Model

VERSION 1.1

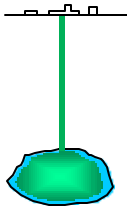

END USER INPUT DATA		
Delivery zone	0	
Receipt zone	6	
Deliverability	260	MDTH/d
Yearly volume	2600	MDTH

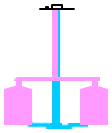

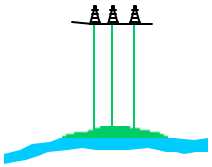

Model Principles

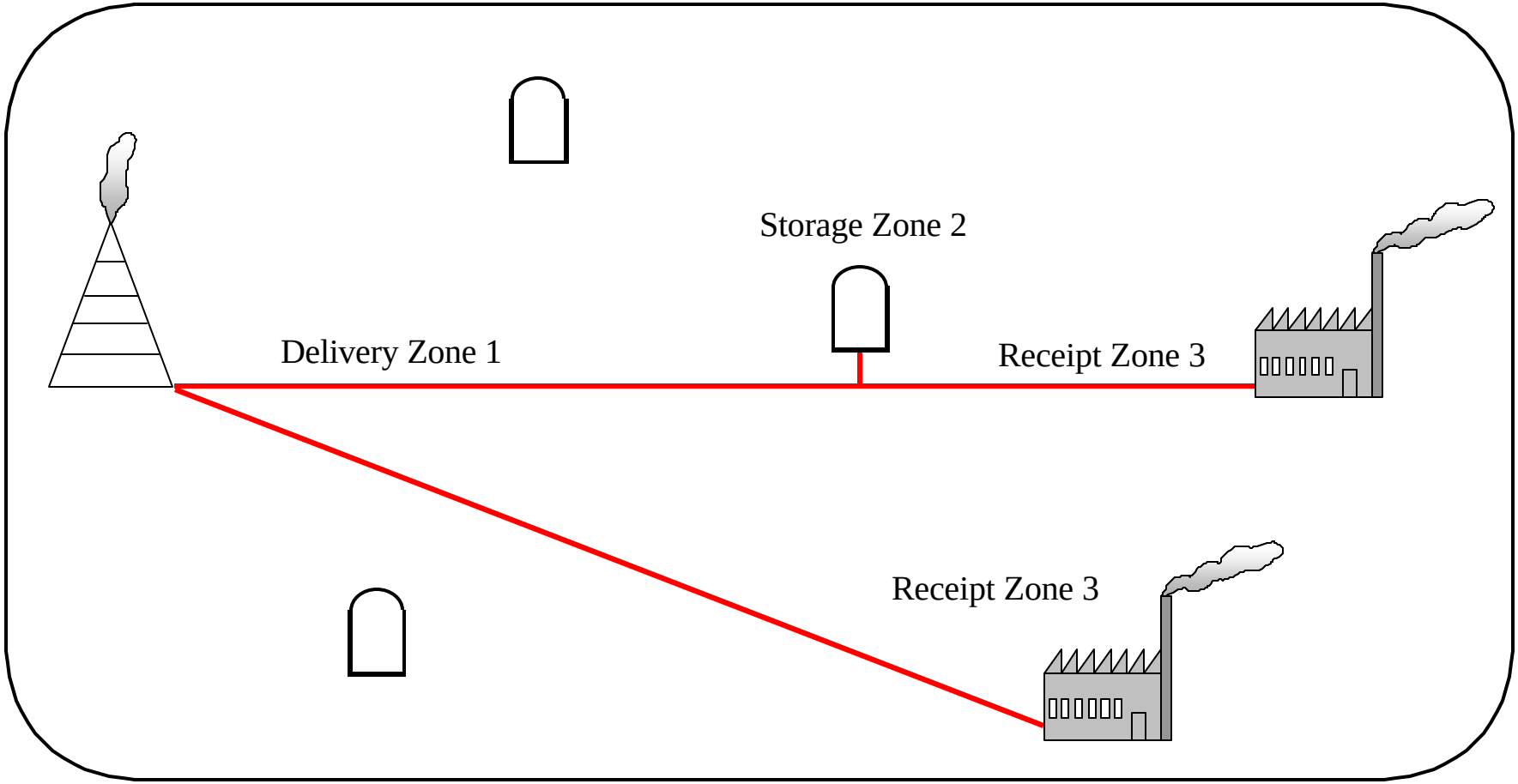

Model Outcome

- Indication of LRC Cost
- Comparison With Other Alternatives
- Given Location, Deliverability and Annual Gas Consumption

Cost Comparison Example

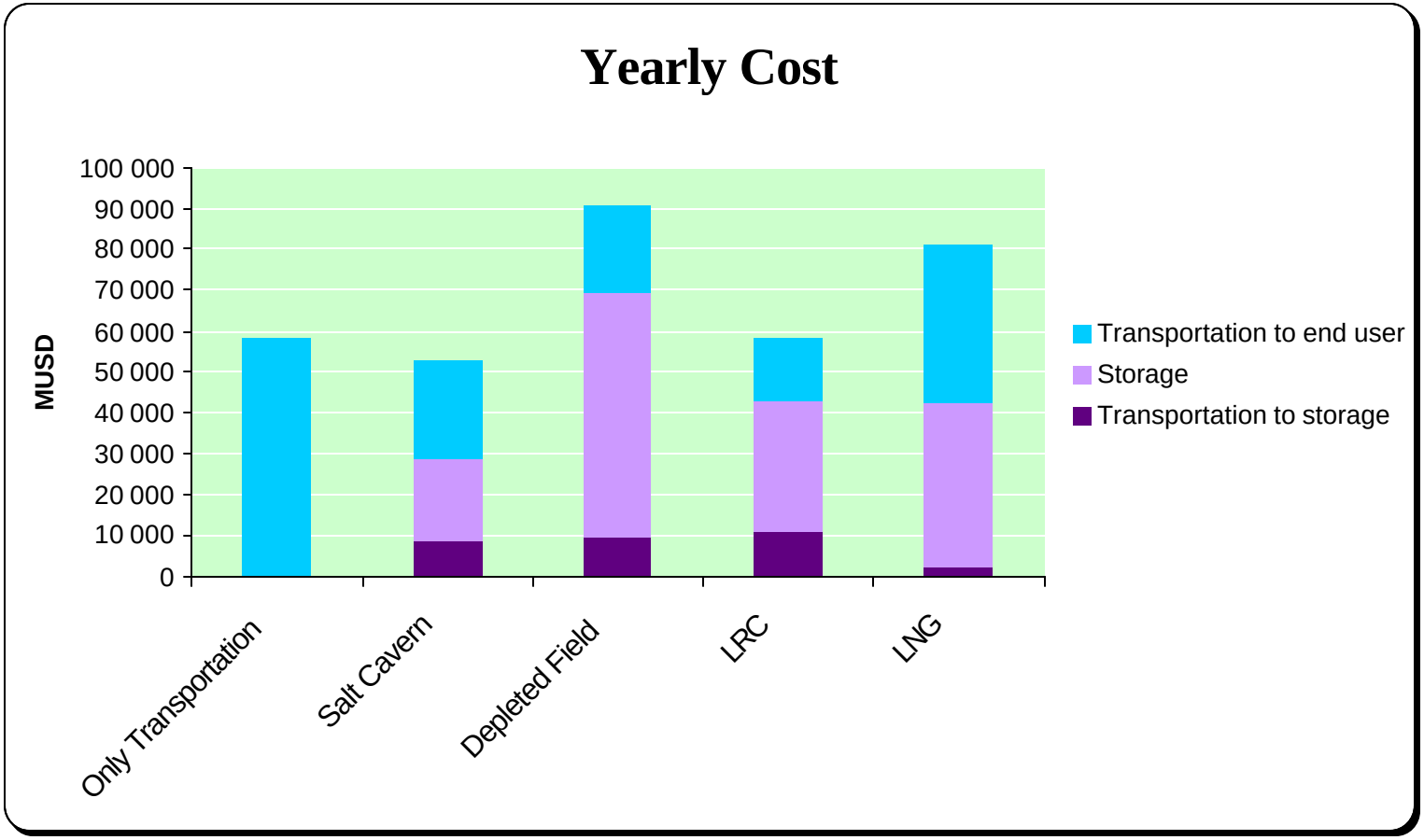

Advanced Storage Concepts Workshop:

Advanced Design Criteria for Salt Caverns

RESPEC

Lined Rock Cavern Storage

Sofregaz U.S., Inc.

February 17, 2000

Sponsored by:

National Energy Technology Laboratory

U.S. Department of Energy
Office of Fossil Energy

Overview of Department of Energy's Gas Storage Program

National Energy Technology Laboratory Gas Storage and Deliverability Team

- **Fossil Energy has supported a modest $1 million per year program in Gas Storage since 1993.**
  - HQ Program Manager - Christopher Freitas
  - NETL Product Manager - Brad Tomer
  - Implementing Team Members
    - Gary Sames
    - James Ammer
    - Thomas Mroz

Gas Storage

The Federal Role:

- Gas storage is a vital component of the nation's critical infrastructure, and as such reliability and system performance is important to the health and safety of the American people.
- Gas storage plays a critical role in the ability of the U.S. to increase use of natural gas as both an environmentally friendly fuel and as a key to greater energy independence.
- Improved gas storage technologies are necessary to enable the advanced and distributed power systems of the future envisioned in other program areas.

Gas Storage Program Purpose

- Promote the development of the advanced natural gas storage technologies necessary to improve storage and delivery of natural gas.
- Increase confidence in the long term availability, reliability, and safety of the natural gas system.

4 Focus Areas in Gas Storage and Deliverability

- Deliverability Enhancement
- Gas Measurement
- Reservoir Management
- Advanced Storage Concepts

Natural Gas Storage Schedule and Milestones

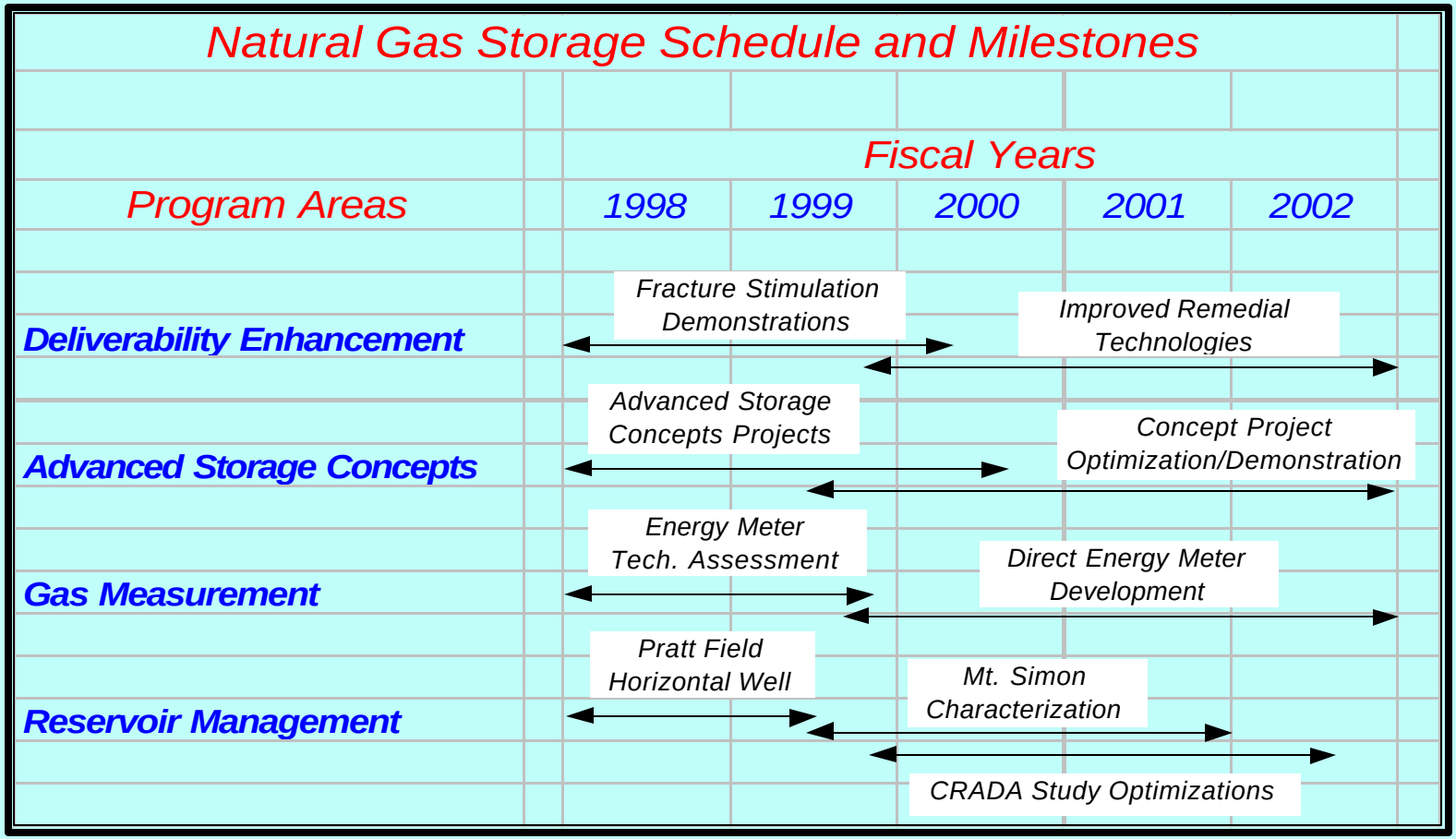

Deliverability Enhancement

- **Conduct RD&D efforts to provide cost-effective means to both maintain and increase the deliverability of the natural gas storage system.**

Deliverability Enhancement Timeline

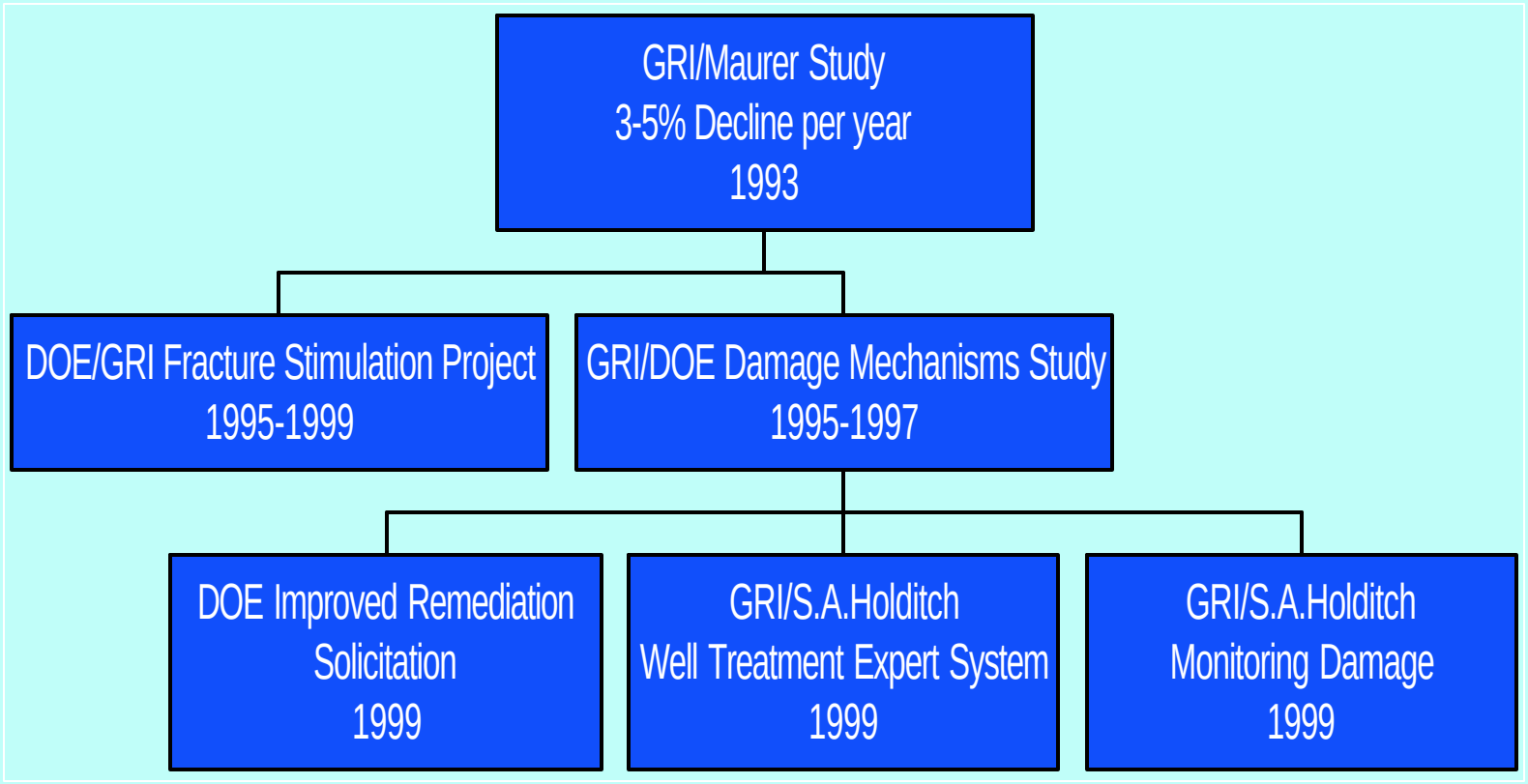

New and Novel Fracture Stimulation Project

Advanced Resources International

- **GOAL: Demonstrate New and Novel Fracture Stimulation Technologies for Restoring Lost Deliverability in Gas Storage Wells**

Accomplishments

- **31 Fracture Stimulation Treatments**
- **4 Stimulation Types**
  - Liquid CO2 Sand
  - Tip-Screenout
  - Extreme Overbalanced (EOB)
  - Propellant
- **8 Storage Fields**
- **5 States**

LOCATION OF TEST SITES

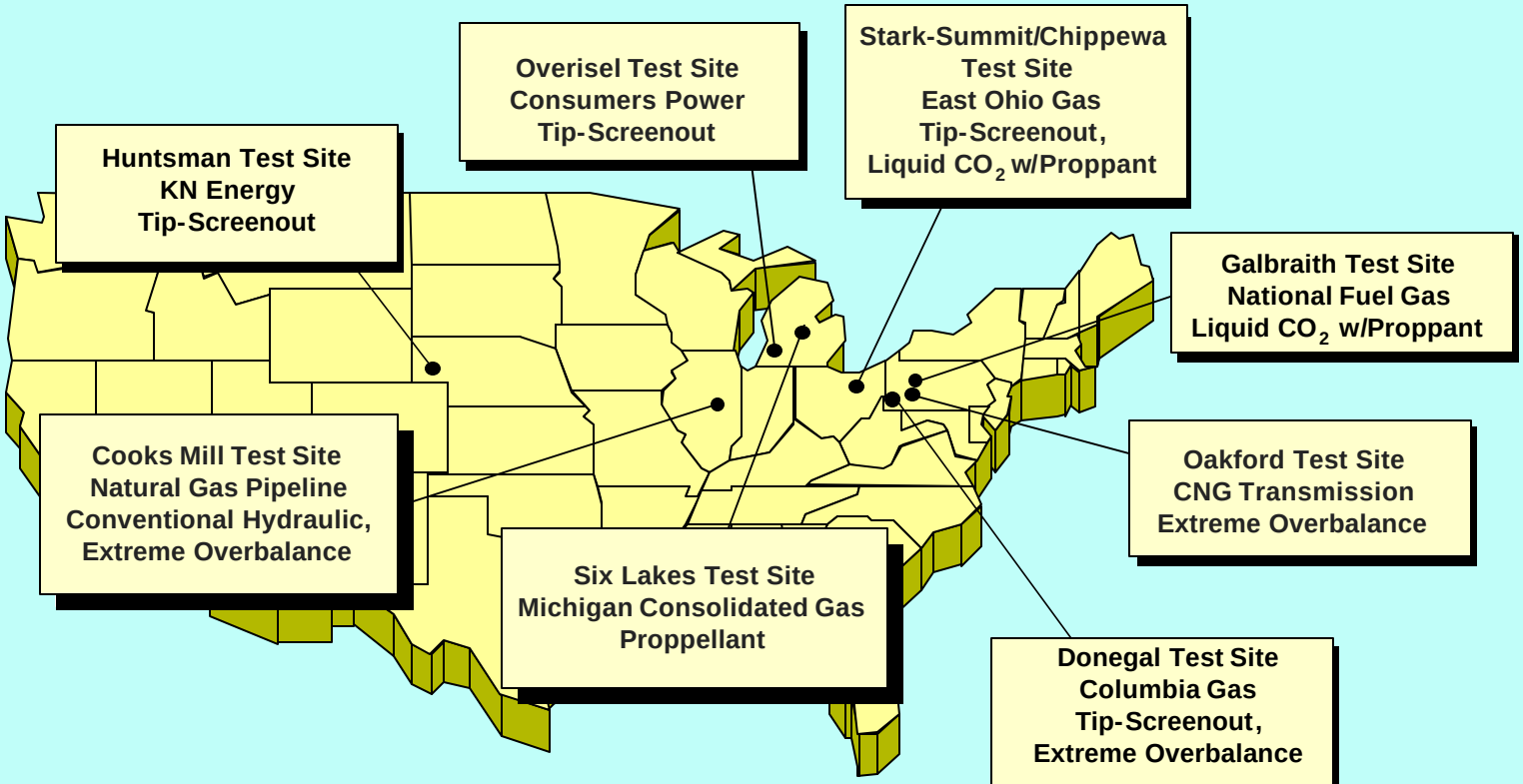

Accomplishments

- **First Liquid CO2 Sand Fracs in Storage Wells**
- **First Downhole Treatment Records in Storage**
  - Liquid CO2 Sand
  - EOB
  - Propellant
- **Side-by-Side Comparison of Aqueous and Non-Aqueous Fracturing Fluids**
- **Enhancements to Simulator for Design and Execution of EOB Fracturing**

Accomplishments

- **Major Diagnositics Collected**
  - Over 110 Modified Isochronal Multi-Point Pressure Transient Tests (Pre, Post, and 1-year Anniversary)
  - Over 50 Other Diagnostics
    - Downhole Camera
    - Tracer Surveys
    - Mini-fracs
    - Bottomhole Treating Records
    - Temperature and Acoustic Logs
    - Step Rate Tests

Major Findings

- **Fracturing Technologies can Provide Attractive Deliverability Enhancement but are not a Cure-All**

- **Gas Storage Formations are Highly Sensitive to Any Amount of Aqueous Liquids**
  - Results of Liquid CO2 Sand Fracs indicate that this technology provides immediate benefits

Major Findings

- **Several Technology/Methodology Advances are Needed:**
  - Additional downhole data, modeling improvements for design and analysis, and overall understanding of:
    - Liquid CO2 Sand
    - EOB
    - Propellant
  - Candidate selection
  - Economic evaluation of treatment success vs. other alternatives, especially long term

Improved Natural Gas Storage Well Remediation

- **Support research to develop effective, economic remediation technologies for damage mechanisms identified in previous DOE/GRI study as prevalent causes of shallow wellbore damage:**
  - 1) Inorganic precipitates (gypsum, carbonates, etc)
  - 2) Hydrocarbons, organic residues, production chemicals
  - 3) Bacterial fouling and plugging
  - 4) Particulate fouling and plugging
- **Demonstrate the improved remedial technologies tailored for these specific damage mechanisms in the field**

Improved Remedial Design Projects

- **Objective:** Demonstrate improved remedial technologies tailored for specific damage mechanisms
- **Key Features:**
  - Phase 1: Characterization of geochemical environment(s) and damage mechanism(s); laboratory validation of mitigation strategies
  - Phase 2: Field verification of proposed techniques

Treatment of Storage Well HOPS Damage through Application of CO_2

Advanced Resources International

- **Summary:**
  - Addresses damage caused by Hydrocarbons, Organic Residues, and Production Chemicals (HOPs)
  - Will treat HOPs using CO_2 as the primary treatment fluid
- **Key Technical Partners:**
  - Stim-Lab

Damage Characterization and Removal in Gas Storage Reservoirs

Holditch-Reservoir Technologies

- **Summary:**
  - Addresses damage caused by Hydrocarbons, Organic Residues, and Inorganic Precipitates
  - Innovative laboratory characterization effort and strong field testing plan
  - Presents synergy opportunity with GRI work
- **Key Technical Partner:**
  - Penn State

Sonication Tool Development for Treating Storage Well Damage

Furness-Newburge, Inc

Summary:

- Develop integrated sonication remediation tool to both identify and treat storage well damage (including inorganic precipitates, particulate fouling, organic residues)

Key Technical Partners:

- Argonne National Lab, Nicor Technologies, Inc.

Gas Measurement

Goals:

- Conduct RD&D efforts to provide improved accuracy and real-time measurement of both gas volume and energy content at gas storage facilities.

Ultrasonic Meter Testing and Evaluation for Gas Storage Application

Southwest Research Institute - Phase I

- **Ultrasonic Meters Can Provide the Required Accuracy for Gas Storage Facilities**
  - Extremely accurate at high flow rates
  - Accurate in both flow directions
    - Effect of thermowell upstream is very small
  - Basically insensitive to changes in temperatures
  - Higher measurement error at low flow rate is offset by the small overall volume at these rates

Ultrasonic Meter Testing and Evaluation for Improved Accuracy

M98001157C

A Technology Assessment and Feasibility Evaluation of Natural Gas Energy Flow Measurement Alternatives

Southwest Research Institute - Phase II

Phase II Results

- **A Gross Inferential Approach to Energy Measurement was Identified**
- **Feasibility was Demonstrated**
- **Potential to Upgrade Any Flow Meter to Energy Measurement**
  - Order-of-magnitude lower cost than traditional composition assay

Development of a Low Cost Inferential Natural Gas Energy Flow Rate Prototype Retrofit Module

Phase III - Initiated June 1999

Southwest Research Institute

Co-funded by Gas Research Institute

Reservoir Management

Goals:

- Conduct RD&D efforts to increase the efficiency of storage operations through industry and FETC partnerships (CRADAs).

Modeling Studies

- **Objective: Demonstrate the importance of geologic modeling and reservoir simulation for optimizing the development and operation of gas storage fields**
- **Main Focus: Horizontal Wells**
- **Cooperative Research and Development Agreements (CRADAs) Have Been the Mechanism**
  - National Fuel Gas Supply Corporation
  - Equitrans, Inc.
  - Northern Indiana Public Service Company

Results

- **National Fuel**
  - Horizontal wells would provide better efficiency and cost savings (SPE 31002)
- **Equitrans**
  - Remediation of well damage and horizontal wells would help provide a 10-day or 30-day peaking service (DOE Natural Gas Conference Proceedings)
  - Horizontal well drilled July 1999
- **NIPSCO**
  - Still under investigation

Advanced Storage Concepts

- **The Advanced Storage Concepts Program is DOE's first attempt to address storage issues that can limit the future growth of natural gas use in residential service, as an industrial fuel, and in electric power generation in many important regions of the U.S.**

Advanced Storage Concepts

Goals:

- **Build the peaking and base load balancing capacity that is necessary to enable natural gas to provide reliable service in a future where gas use is predicted to increase by 5 Tcf by 2010.**
- **Provide storage alternatives for the many important regions of the U.S. where natural gas has the greatest growth potential, but that lack conventional storage geology.**

Summary of 2010 Peaking and Market Area Gas Storage Requirements of Selected Regions of the US (1994)

Region	Peaking/Market Area Storage Needs (MMCF/day)
New England	269
Mid Atlantic (NY/NJ)	1,352
South Atlantic (DL/MD/VA)	450
South Atlantic (NC/SC/GA)	1,190
Pacific Northwest (WA/OR)	401

Source: GRI Topical Report ♦Future Seasonal Natural Gas Loads and Gas Delivery Capacity Requirements in the Lower 48 United States (1/94)

Advanced Storage Concepts

Projects:

Refrigerated-Mined Cavern Storage

Lined Rock Cavern Storage

Gas Storage as Hydrates

Advanced Design Criteria for Salt

Chilled Gas Storage in Bedded Salt Caverns

Gas Storage in Basalt

Refrigerated-Mined Cavern Storage

Project Partners

- PB-KBB -- Prime Contractor, Facility Design
- Merimack Energy -- Market Analysis
- Frontier-Kemper -- Mining Contractor, Construct-Ability and Cost Estimating
- RESPEC -- Rock Mechanics and Mine Thermodynamics
- Department of Energy -- Program Management

Project Overview

- DOE solicitation identified five areas that do not have favorable geological conditions of storage such as salt, depleted gas fields, and aquifers
- The areas were New England, Mid-Atlantic (NY/NJ), South Atlantic (DL/MD/VA) South East Atlantic (NC/SC/GA), and the Pacific Northwest (WA/OR)
- Of the five, one was selected for the conceptual design based on pipelines interconnects and future market growth
- The area selected was Howard and Montgomery Counties, Maryland, near both Baltimore and Washington, D.C.

Project Overview - cont.

- Provide storage that is competitive with alternative available high deliverable storage methods
- Available alternatives considered are salt cavern storage and LNG
- Provide natural gas storage with multiple cycles per year
- Provide high deliverability

1994 EIA Baseline Projection

	New Peaking/Market Area Storage Needs, 2010 (1) (MMCFD)	New Annual Delivery Capacity Needs, 2010 (MMCFD)	Planned or Completed Pipeline & Expansion Projects, 1994-1997 (2) (MMCFD)	Net Requirement (MMCFD)
New England (ME/VT/NH/MA/CT/RI)	269	1,130	978	421
Mid Atlantic (NY/NJ)	1,412	1,158	2,650	(80)
South Atlantic (DL/MD/VA)	450	803	272	981
South Atlantic (NC/SC/GA)	1,190	688	11,197	681
Pacific Northwest (WA/OR/ID)	401	366	695	73

Note: (1) Assumed "high bound" on peak shaving
(2) DOE/EIA Natural Gas 1996 Issues and Trends (December, 1995) and in-house data.

Refrigerated-Mined Cavern Storage

- **Hard Rock**
- **Cavern Volume: 50 Million Cu Ft**
  - 80 ft by 80 ft rooms
  - 7 tunnels of 1,000 ft length
- **Pressure: 1,250 psi**
- **Temperature: -20 ºF**
- **Depth: 3,000 ft**
- **Working Gas: 5 Bcf**
- **20 Day Injection, 20 Day Withdrawal**

Representative Unit Capital Costs for New Gas Storage and LNG Projects

Type of Project	Location	Project Name	Working Gas Capacity (BCF)	Total Cost ($MM)	Unit Cost ($/MCF)	Notes
Depleted Field	California	Putah Sink	15.000	40.000	2.67	(1)
Depleted Field	Colorado	Douglas Creek	10.000	30.000	3.00	(1)
Depleted Field	Utah	Clay Basin Expansion	15.200	49.600	3.26	(1)
Depleted Field	Oklahoma	Manchester	15.000	30.000	2.00	(1)
				Average>>	2.73	
Aquifer	Indiana	Carbon-Calcutta	3.900	12.275	3.15	(1)
Aquifer	Illinois	Hillsborough Expansion	4.500	36.600	8.13	(1)
				Average>>	5.64	
Salt Cavern	Alabama	S. Alabama-McIntosh	2.700	30.000	11.11	(1)
Salt Cavern	Mississippi	Hattiesburg phase 1 & 1A	3.500	47.000	13.43	(2)
Salt Cavern	Louisiana	Napoleonville Phase 1	4.600	45.000	9.78	(1)
				Average>>	11.44	
LNG	North Carolina	Pine Needle	4.000	107.000	26.75	(2)
LNG	Maine	Granite Slate	2.000	44.222	22.11	(2)
				Average>>	24.43	
Refrigerated mined Cavern		Mid-Atlantic	5.000	178.000	35.60	

Notes: (1) EIA/The Value of Underground Storage in Today's Natural Gas Industry.
(2) Brant Energy Data.

SUMMARY OF UNIT COST FOR VARIOUS STORAGE METHODS

Depleted Field	California	$2.67/mcf
Depleted Field	California	3.00
Depleted Field	Utah	3.26
Depleted Field	Oklahoma	2.00
Aquifer	Indiana	3.15
Aquifer	Illinois	8.13
Salt Cavern	Alabama	11.11
Salt Cavern	Miss.	13.43
Salt Cavern	Napoleonville, La	9.78
LNG	North Carolina	22.11
LNG	Maine	24.43
Chilled Gas	Many Places	35.90

Refrigerated-Mined Cavern Storage Status

- **Workshops**
  - November 3, 1998: Houston
  - November 5, 1998: Pittsburgh
- **Final Report Available on CD-ROM**
- **Cost Comparison Showed that RMC can Provide Similar Cost of Service to LNG for Single Cycle and Better Cost of Service for Multiple Cycles**

Gas Storage as Hydrates

Mississippi State University

- **Determine the Technical and Economical Feasibility of Storing Natural Gas as Hydrates**
- **Improve Rate of Formation**
- **Improve Rate of Decomposition**
- **Investigate Storage stability**
- **Conceptual Design and Costs**

Gas Storage as Hydrates Status

- Phase I Feasibility Completed May 1999
- Phase II Conceptual Design Completed December 1999

Hydrate Storage Process

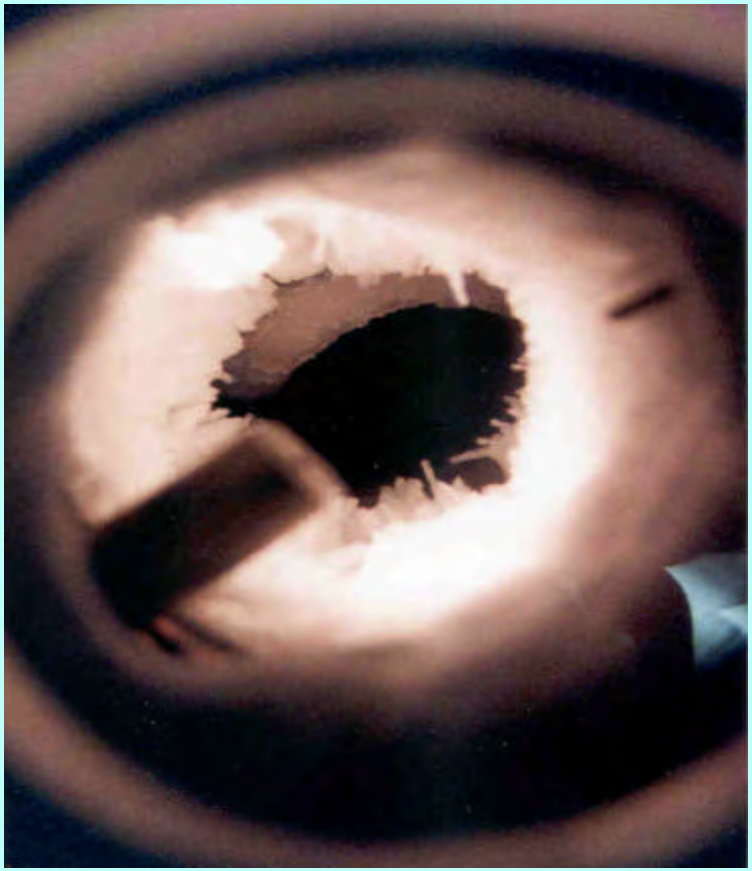

Hydrates adsorb on walls of test cell:

- Quiescent water and natural gas system
- 286 ppm surfactant increases hydrate formation rate 700x

550 psi, 37°F

Hydrate Storage Process

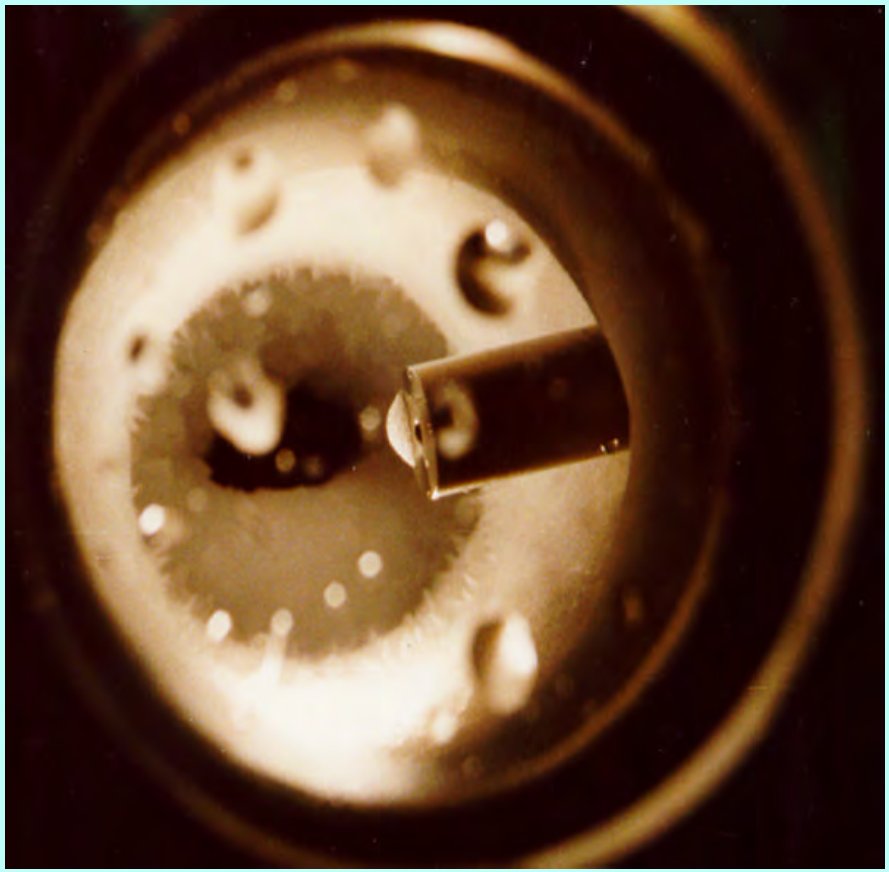

High rate of hydrate formation continues as interstitial water converts to hydrates.

Hydrate particles pack symmetrically on walls with high gas density.

Hydrate Storage Process

Hydrates continue to build concentrically on test cell wall as water level drops and gas is added to solid structure of hydrates.

(Black area of center = bottom of test cell.)

Hydrate Storage Process

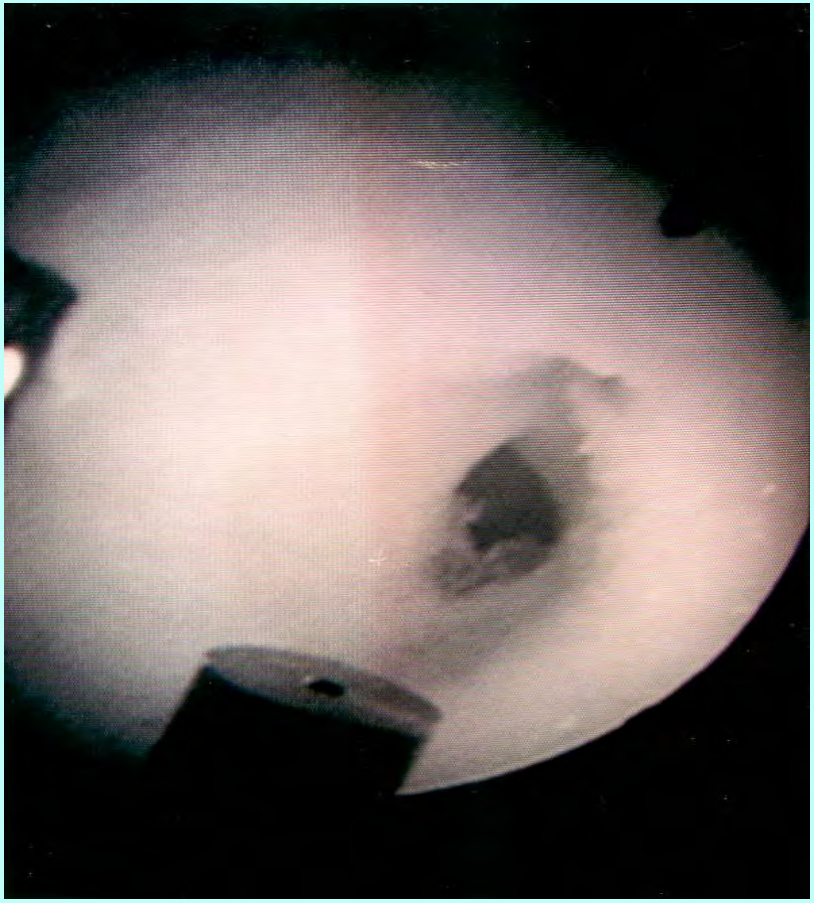

Test cell nears capacity.

Note: Symmetry maintained such that cell bottom still visible.

156 vol gas (STP)/vol hydrate stored and packed at 550 psig and 37°F in <3 hours, no mechanical stirring; 86% of theoretical capacity.

System Design

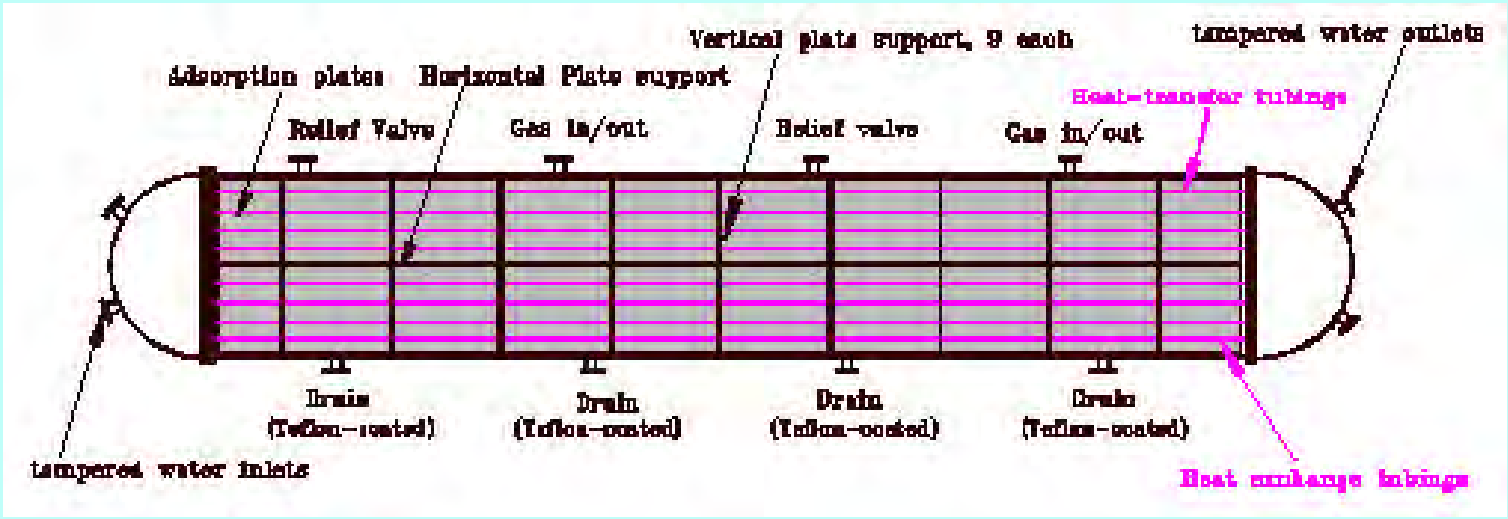

System Design - cont.

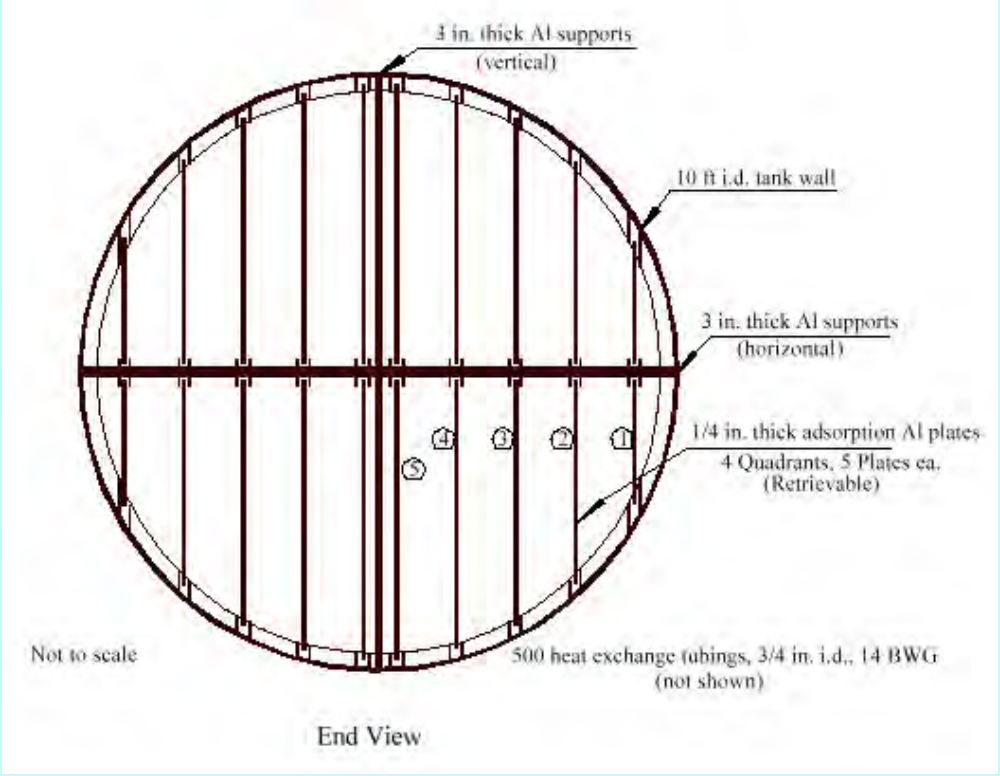

Capital Investment for 2.25 Mmcf Storage Facility

Item	Factor	Cost
Direct Costs		
Purchased equipment, delivered	1	$2,202,189
Equipment installed	0.39	$858,854
Instrument., controls installed	0.13	$286,285
Piping installed	0.31	$682,679
Electrical installed	0.1	$220,219
Buildings	0.29	$638,635
Yard Improvements	0.1	$220,219
Total Direct Plant Cost		**$5,109,079**
Indirect Costs		
Engineering and supervision	0.1	$220,219
Construction expenses	0.17	$374,372
Total Direct and Indirect Costs		**$5,703,670**
Contractor's fee	0.18	$396,394
Contingency	0.36	$792,788
Fixed Capital Investments		$6,892,852

Operating Costs for Hydrate Storage

ITEM	DETERMINED BY	COST	BASIS
Raw Matls	Calculate	$181	per cycle
Operating Labor	Calculate	$257,400	per year
Utilities	Calculate	$1,888	per cycle
Supervisory Labor	15% Operating Labor	$38,610	per year
Maintenance and Repair	6% Fixed Capital Investment	$20,679	per year
Operating Supplies	15% Maintenance and Repairs	$3,102	per year
Laboratory Charges	15% Operating Labor	$38,610	per year
Depreciation	Calculate	$110,109	per year
Property Taxes	4% Fixed Capital Investment	$27,571	per year
Insurance	1% Fixed Capital Investment	$3,446	per year
Plant Overhead	70% Operating Labor+Supervision+Maintenance	$221,682	per year
Administrative	25% Operating Labor	$64,350	per year
Contingency	1% Total Product Cost	$7,876	per year

Operating Costs per Mcf per Number of Cycles

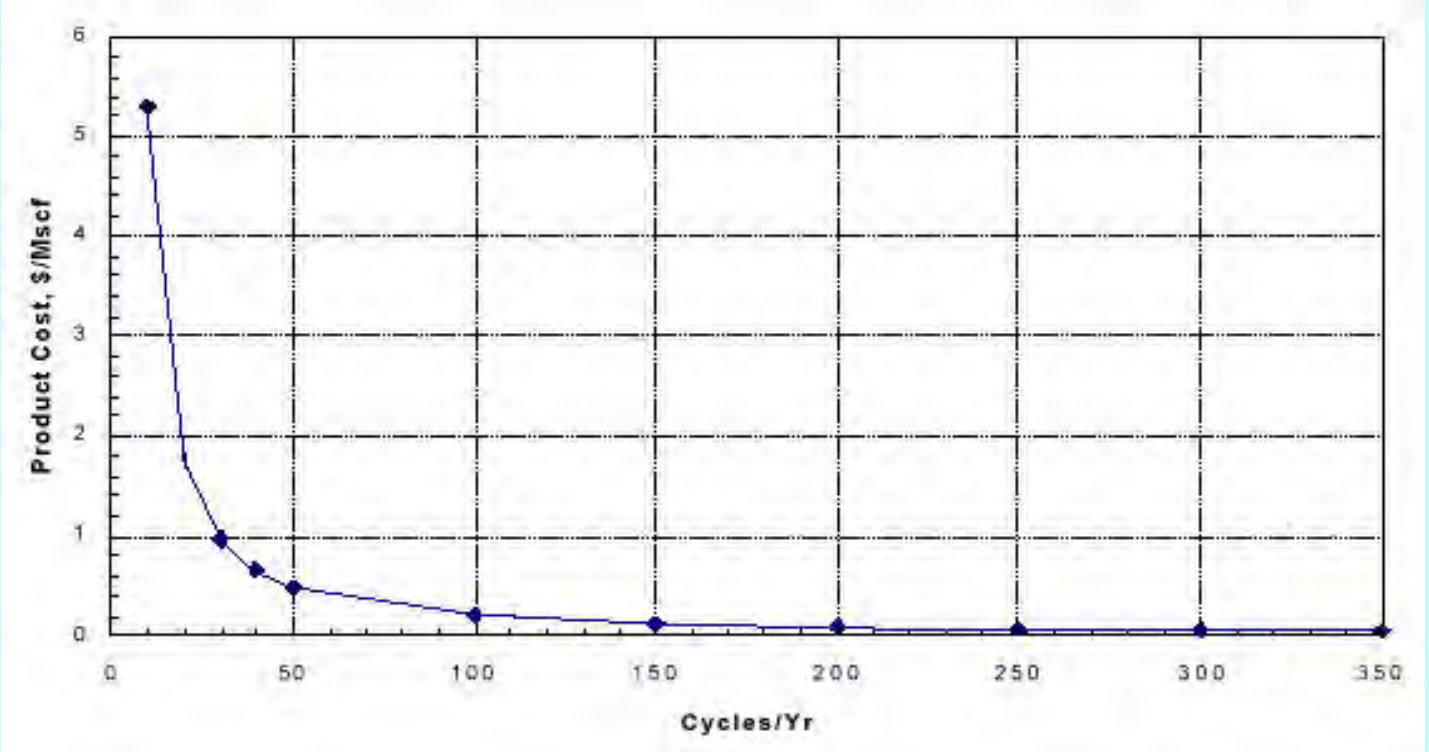

Gas Storage in Basalt

- Industry Partner - Pacific Gas Transmission
- Performing Partner - Pacific Northwest National Laboratory
- Hydrogeologic characterization of Columbia River Basalt aquifers for natural gas storage

Basalt Plans

- Hydrogeologic characterization through cross hole pump tests
- “How To” report for evaluating the feasibility of storing natural gas in Columbia River basalts.
- Report will have universal application in other basaltic volcanic enviromnments

Basalt Study

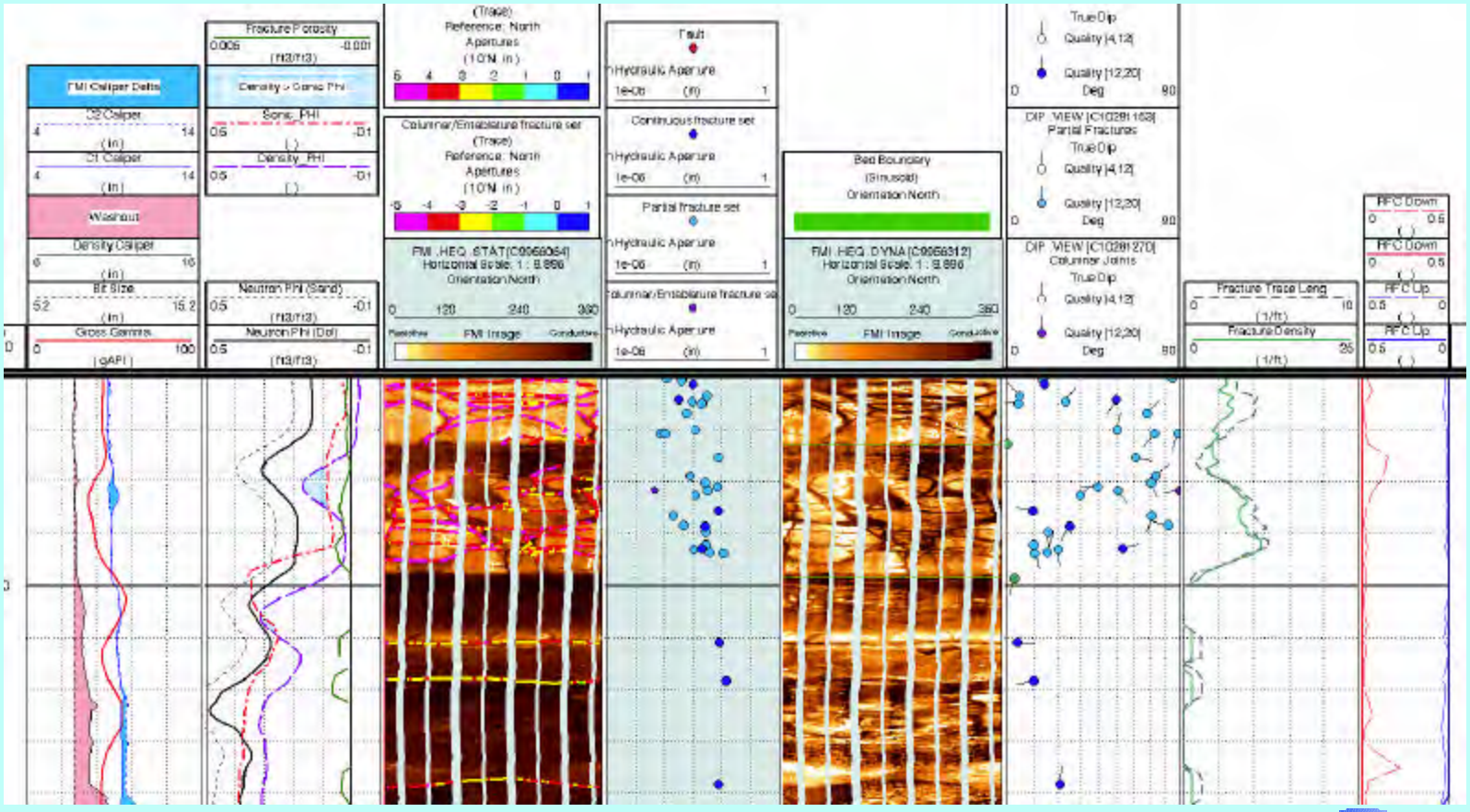

Chilled Gas Storage in Bedded Salt Caverns

RESPEC

- **Objective: Evaluate the feasibility of storing chilled gas in bedded salt deposits**
  - Bedded salt is of interest because of brine disposal limitations
  - It may be possible to dramatically increase working gas capacity of a given storage volume in planned or existing bedded salt caverns

Project Work Plan - Phase I

- **Laboratory evaluation of low-temperature thermal properties of salt**
  - Thermal conductivity to predict temperature distribution, thermally induced stress, and cooling load requirements in salt caverns.
- **Evaluate cooling load requirements to maintain a design temperature**
  - Finite element modeling of injection-withdrawal scenarios for cooling equipment requirements
- **Preliminary Design and Cost Analysis**
  - Capital and Operating costs in dollars per unit increase in working gas capacity

Project Work Plan - Phase II

- **Laboratory determination of low-temperature mechanical properties of salt**
  - Effects of reducing ambient conditions on strength and creep properties
- **Thermomechanical analysis of salt stability in chilled bedded salt caverns**
  - Finite element simulations of temperature and stress distributions at -20^{o}F design temperature
  - Assess potential for tensile fracturing and strength reduction through intergranular microfracturing

Questions?

FEASIBILITY STUDY FOR LOWERING THE MINIMUM GAS PRESSURE IN SOLUTION-MINED CAVERNS BASED ON GEOMECHANICAL ANALYSES OF CREEP-INDUCED DAMAGE AND HEALING Topical Report RSI-0969 DE-AC26-97FT34350 *by* Kerry L. DeVries Joel D. Nieland Joe L. Ratigan RESPEC P.O. Box 725 Rapid City, South Dakota 57709-0725 *prepared for* U.S. Department of Energy Federal Technology Center P.O. Box 880 Morgantown, West Virginia 26507-0880 December 1998	**PHASE II FEASIBILITY STUDY FOR LOWERING THE MINIMUM GAS PRESSURE IN SOLUTION-MINED CAVERNS BASED ON GEOMECHANICAL ANALYSES OF CREEP-INDUCED DAMAGE AND HEALING** Topical Report RSI-1165 DE-AC26-97FT34350 *by* Joel D. Nieland Kerry L. DeVries Kirby D. Mellegard RESPEC P.O. Box 725 Rapid City, South Dakota 57709-0725 *prepared for* U.S. Department of Energy Federal Energy Technology Center P.O. Box 880 Morgantown, West Virginia 26507-0880 July 1999

DOE-SPONSORED WORKSHOP ON ALTERNATIVE GAS STORAGE TECHNOLOGIES
February 17, 2000
Greentree Holiday Inn – Pittsburgh, PA

U.S. Department of Energy/National Energy Technology Laboratory
Gas Storage Program Overview

FEASIBILITY STUDY FOR LOWERING THE MINIMUM GAS PRESSURE IN SOLUTION-MINED CAVERNS BASED ON GEOMECHANICAL ANALYSES OF CREEP-INDUCED DAMAGE AND HEALING

Topical Report RSI-0969
DE-AC26-97FT34350

by

Kerry L. DeVries
Joel D. Nieland
Joe L. Ratigan

RESPEC
P.O. Box 725
Rapid City, South Dakota 57709-0725

prepared for

U.S. Department of Energy
Federal Technology Center
P.O. Box 880
Morgantown, West Virginia 26507-0880

December 1998

EXECUTIVE SUMMARY

This report presents the results of a study to evaluate the potential of increasing the working gas volume of new and existing compressed natural gas (CNG) storage caverns by using an advanced constitutive model for rock salt in the cavern design procedure. Geomechanical finite element analyses were made to determine the minimum gas pressure allowable based on an existing stress-based criterion (the Damage Potential method) and an advanced constitutive model (the Multimechanism Deformation Coupled Fracture (MDCF) model) capable of modeling damage and healing in rock salt. The MDCF model is a constitutive model developed by Sandia National Laboratories and their subcontractors to provide a description of damage, healing, and deformation of salt for safe disposal of radioactive waste at the Waste Isolation Pilot Plant. The MDCF model has the capability to track damage development and healing and to provide a quantitative measure for the damage. Additionally, the healing behavior of the salt (included with the MDCF model) was to be analyzed to determine if complete healing of the damaged rock zone would occur during the time period when the cavern was at maximum gas pressure.

In order to demonstrate the capability of the MDCF model to predict the evolution of damage and healing around CNG storage caverns, geomechanical analyses were performed of two actual CNG storage caverns. The two caverns, referred to as Cavern A and Cavern B, have different depth, volume, geometry, temperature, and proximity to other caverns. Cavern depth is nominally 2,000 and 4,000 feet to the casing shoe for Cavern A and Cavern B, respectively. Two natural gas service cycles were used in the simulations and are referred to as Case 1 and Case 2. Both cycles are initiated at maximum gas pressure and are drawn down to minimum gas pressure over a 10-day period. The Case 1 gas pressure cycle is held at minimum gas pressure for a period of 10 days, and the Case 2 gas pressure cycle is held at minimum gas pressure for 100 days. After the minimum pressure service, both cycles repressurize to maximum gas pressure over a 10-day period. Both cycles are then held at maximum gas pressure for 100 days. The scenarios simulated for each of the caverns include:

- A 10-day gas withdrawal from maximum gas pressure to atmospheric pressure to determine the minimum gas pressures that ensure no salt dilation based on the Damage Potential method and the MDCF model with various salt impurity levels.[1] The pressures determined with the Damage Potential method were designated the *baseline* minimum gas pressures.
- Simulations with 5-day and 20-day gas withdrawal periods to evaluate the impact of the gas withdrawal rate.

[1] The salt "impurity level" is an input quantity in the MDCF model. Throughout this study, the "impurity level" should actually be thought of as a porosity level.

- A single Case 1 gas cycle was simulated at minimum gas pressures equal to 50 and 90 percent of the baseline minimum gas pressure to examine the sensitivity to the minimum gas pressure.
- A long-term simulation at minimum gas pressure to determine the maximum allowable time at minimum gas pressure. Minimum gas pressures of both 50 and 90 percent of the baseline minimum gas pressure were evaluated.
- Simulations of five consecutive gas pressure cycles were made to evaluate long-term damage accumulation and healing. The simulations were made with both Case 1 and Case 2 gas pressure cycles. The simulations were made with a minimum gas pressure equal to 50 percent of the baseline minimum gas pressure.

During the first part of this study, the minimum gas pressure that would completely suppress dilation of the salt was determined using the Damage Potential method and the MDCF model with impurity levels of 0, 1, 2, and 3 percent. The minimum gas pressures to completely suppress dilation predicted using the Damage Potential method were 0.14 and 0.22 psi/foot of depth at the casing shoe for Cavern A and Cavern B, respectively. The minimum gas pressure predicted by the MDCF model that completely suppresses dilation of the salt for Cavern A ranged from 0.0 to 0.73 psi/foot of depth at the casing shoe. Similarly, the minimum gas pressure predicted by the MDCF model ranged between 0.12 and 0.63 psi/foot of depth at the Cavern B casing shoe. Impurity levels of 0, 1, and 2 percent resulted in minimum gas pressures lower than that predicted using the Damage Potential method for Cavern A. However, for Cavern B, only impurity levels of 0 and 1 percent resulted in minimum gas pressures less than that predicted using the Damage Potential method.

The minimum gas pressure necessary to suppress salt dilation predicted by the MDCF model is greater than that predicted by the Damage Potential method for salt containing high levels of impurities (typically greater than 2 percent). This does not imply that the MDCF model predicts the cavern will become unstable if the gas pressure is dropped below the pressure that is needed to completely suppress dilation. It simply means that microcracking and dilation of the salt can be expected and that the size and severity of the damaged zone will depend on the stress conditions, temperature, and length of time the salt is subjected to a condition that is conducive to damage development.

In order to assess the stability of the salt on the periphery of the storage caverns using the MDCF model, a criterion was established as the limiting value that should not be exceeded. It was assumed here that the salt surrounding the caverns will remain stable if it does not reach the tertiary creep stage. Geomechanical analyses of the two CNG storage caverns were performed to determine the stability of the caverns based on the aforementioned design criterion using the MDCF model. Results of these analyses showed that if the caverns are operated and held at a minimum gas pressure of 50 percent of the minimum pressure determined using the Damage Potential method, the salt surrounding Cavern A will not reach the design limit until about 7 years at the minimum pressure. However, only 12 days were required for a volume of

salt in Cavern B to exceed the design limit at a minimum gas pressure of 50 percent of the baseline minimum pressure. If a minimum gas pressure of 90 percent of the baseline pressure is specified, the salt around Cavern B will not exceed the design limit until approximately 65 days at minimum gas pressure. *Thus, a gas pressure lower than that determined by the existing Damage Potential method can be allowed for a short period of time while maintaining cavern stability.* The maximum time that the cavern can be held at minimum pressure will vary, depending on the damage characteristics of the salt and operating conditions of the cavern.

Gas storage caverns are not typically held at minimum pressure for extended periods of time. It was shown in this study that damaged salt (salt that has experienced dilation) could be healed when the cavern is held at maximum gas pressure. The time required to heal the salt (reduce the porosity to its initial level) increases for increasingly lower minimum gas pressures and longer periods of operation at minimum gas pressure. Complete healing of the salt was predicted within the 100-day period at maximum gas pressure for both Cavern A and Cavern B after the caverns had experienced a 10-day period at minimum gas pressure. Complete healing of the salt was also predicted within 100 days for Cavern A following a 100-day period at minimum pressure, but not for Cavern B. This is because higher levels of damage were predicted in the salt surrounding Cavern B during the period the cavern was held at minimum pressure.

It was demonstrated in this study that if a conservative dilation boundary and damage criterion are specified for the MDCF model, it is still possible to use a lower minimum gas pressure than that predicted by the Damage Potential method without jeopardizing cavern stability. However, site-specific evaluation of the damage and healing characteristics of salt core should be undertaken and further refinements in the MDCF model are recommended.

TABLE OF CONTENTS

TABLE OF CONTENTS
(Continued)

LIST OF TABLES

LIST OF FIGURES

LIST OF FIGURES
(Continued)

FIGURE **PAGE**

LIST OF FIGURES
(Continued)

FIGURE **PAGE**

1.0 INTRODUCTION

1.1 BACKGROUND

With the projected growth in natural gas demand exceeding the current pipeline and underground storage capacities, innovative concepts are being sought to meet the needs of the natural gas industry and end-use markets. Much of the growth will be met through increased pipeline capacity and conventional storage. Typically, natural gas is stored underground in depleted oil and gas fields, aquifers, and salt caverns. The purpose of this report is to investigate advanced design techniques for salt caverns which could potentially increase the working gas capacity of new and existing natural gas storage caverns in salt formations.

The storage of compressed natural gas (CNG) in salt caverns is a growing industry. According to statistics provided by the Gas Research Institute (GRI), there are 25 salt cavern CNG facilities, consisting of 127 individual caverns, in the United States and Canada as of April 1995 [Harrison and Ellis, 1995]. Product movement to and from CNG storage caverns is accomplished simply by compression and expansion of the stored gas. Consequently, the internal pressure on the walls of a CNG storage cavern can vary considerably. Since a minimum level of internal pressure is necessary to ensure cavern stability, a certain quantity of gas must always remain in a cavern. This gas is referred to as the base or cushion gas. The quantity of gas that can be withdrawn from a cavern is referred to as the working gas volume.

The economics of CNG storage in salt caverns are largely dependent on maximizing the ratio between the working gas and the cushion gas volumes. This ratio depends directly on the relative values of the maximum and minimum gas pressures permitted in the storage cavern. The maximum storage pressure is limited to a fraction of the weight of the overburden (typically 0.75–0.85 of the vertical stress) in order to prevent fracturing and loss of containment. The minimum pressure required to ensure the structural stability of the cavern is much more difficult to determine, and numerical simulations of cavern response during typical gas service cycles and conservative design criteria are used to evaluate the cavern stability at the minimum gas pressure (e.g., Ratigan et al. [1993]). Advanced constitutive models for salt that incorporate damage accumulation and healing have not been used in these simulations. Application of these advanced constitutive models may indicate that the minimum gas pressure can be decreased in many CNG storage caverns without compromising the stability of the surrounding salt. If this proves to be the case, the working gas capacity and the economics of CNG storage in salt caverns can be improved.

1.2 SCOPE

Over the last few years, research has been performed to develop a theoretical model based on experimental data of damage accumulation and healing for disposal of radioactive waste at the Waste Isolation Pilot Plant (WIPP) near Carlsbad, New Mexico. This research has led to the development of an advanced constitutive model that provides a more accurate description of the behavior of rock salt. The objective of this report is to determine if this advanced technology can be transferred to the natural gas storage industry. Before this technology can be transferred to the CNG industry, both technical and economical issues must be answered to determine the feasibility of using the advanced constitutive model. This study provides a preliminary assessment for use of the model by the CNG industry.

Geomechanical analyses of two typical natural gas storage caverns were performed to determine if the constitutive model developed for the WIPP is potentially feasible for use in the CNG industry. The analyses were performed using both the advanced constitutive model developed for the WIPP and the current approach used to evaluate cavern stability (e.g., Ratigan et al. [1993]). The purpose of these analyses is to determine if the working gas volume of the caverns can be increased by reducing the minimum storage pressures, without jeopardizing cavern stability, based on a more accurate prediction of the salt.

1.3 REPORT ORGANIZATION

This report contains nine chapters and three appendices. Chapter 2.0 discusses cavern stability requirements. The technical approach used to predict cavern stability is presented in Chapter 3.0. Chapter 4.0 describes the finite element computer program and the geomechanical models used in the analysis. Chapter 5.0 presents the cavern stability results based only on dilatancy boundaries. The cavern stability results based on damage accumulation and healing are presented in Chapter 6.0. Chapter 7.0 provides a summary of the study and the conclusions drawn from it. Chapter 8.0 describes future work required to make the use of the Multimechanism Deformation Coupled Fracture (MDCF) model viable and is followed by a list of references (Chapter 9.0). Appendix A gives a full description of the MDCF model. The MDCF model parameters used for the two cavern sites are given in Appendix B. Appendix C describes how natural gas and brine were modeled in the simulations.

2.0 ROCK MECHANICS ISSUES AND CAVERN STABILITY

2.1 BACKGROUND

The development of storage caverns in salt for the containment of liquids (e.g., brine, oil, etc.) has been a popular alternative to surface storage since the early 1950s and is also becoming common practice for the containment of gaseous fluids such as natural gas, compressed air, etc. Natural rock salt is an excellent containment medium because of the extremely low permeability ($<1 \times 10^{-21}$ m^2) that results from the low porosity and tightly bonded grain boundaries of the salt and the lack of large fluid-conducting fractures within the formation comprising the salt.

The development of caverns disturbs the natural stress state that exists in the salt before cavern development and induces deviatoric (or shear) stresses in the salt near the cavern, as shown in Figure 2-1, where J_2 is the second invariant of the deviatoric stress tensor.[2] The deviatoric stresses are highest near the cavern walls, especially at abrupt changes in geometry, but decrease with distance away from the cavern. Furthermore, the magnitude of the deviatoric stresses is proportional to the cavern depth and inversely proportional to the cavern pressure.

Deviatoric stress states activate three general deformation mechanisms in salt: (1) instantaneous elastic deformation, (2) inelastic viscoelastic deformation, and (3) inelastic brittle deformation. Both inelastic deformation mechanisms are time-dependent which gives salt its well known creep characteristics; however, the mechanisms differ in two important aspects. First, the inelastic brittle deformation mechanism induces microcracks in the salt which produce a volume increase or *dilation*. In contrast, the viscoelastic deformation mechanism occurs without changes in salt volume. Second, the brittle mechanism is activated only when the magnitude of the deviatoric stress is high relative to the mean stress (average of the three principal stresses). In contrast, viscoplastic deformation occurs virtually whenever a deviatoric stress is induced, regardless of the magnitude of the mean stress.

Even though salt has low porosity and provides good containment of fluids in most applications, there are conditions that produce damage in salt which, in turn, lead to an increase in salt porosity, an enhancement in salt permeability, and a degradation in strength. Under these conditions, stability of the cavern and/or the ability of the salt to contain liquid or gaseous fluids within a storage cavern may be compromised, and as such, must be considered in the cavern design process.

[2] Before a cavern is created, the deviatoric or shear stress is assumed to be zero.

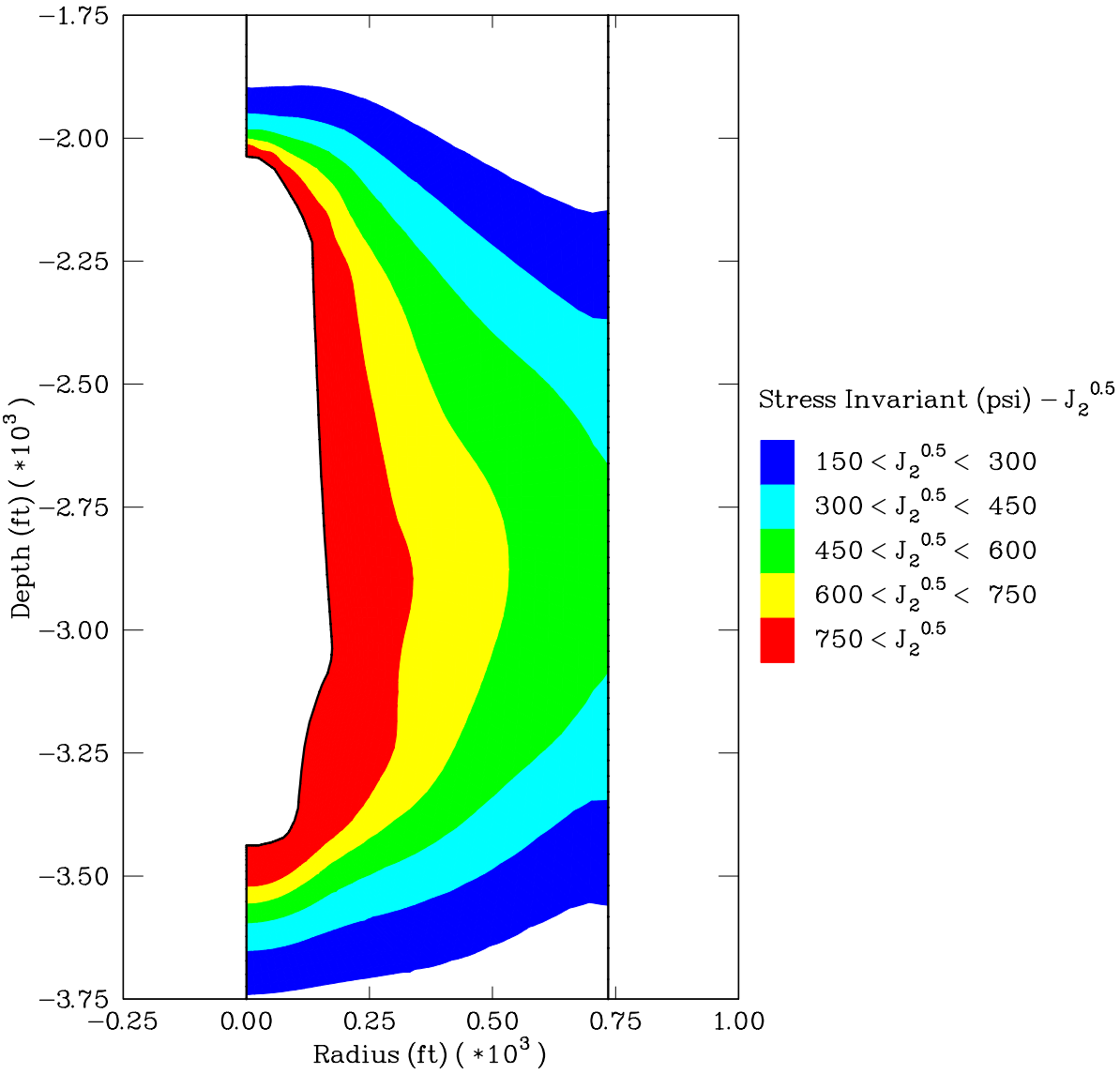

Figure 2-1. Shear Stress Regions Around a Typical Cavern in Salt Expressed in Terms of the Second Invariant of the Deviator Stress Tensor.

2.2 DESIGN CONSTRAINTS

The approach generally used in the geomechanics evaluation of a salt cavern to be used for CNG storage is to determine an acceptable operating pressure range while meeting various design constraints [Ratigan et al., 1993]. These constraints typically include the following:

- Negligible potential for salt dilation that can lead to spalling in the cavern roof and/or walls and subsequent damage to the cavern or hanging string(s).
- Acceptable closure rates which will not result in excessive subsidence and/or damage to adjacent caverns and well casings.
- For bedded salts, an acceptable factor of safety in the overlying nonsalt layers to prevent roof collapse.
- Sufficient cavern spacing to negate cavern connectivity during (1) normal operations and (2) Mechanical Integrity Testing of the subject well or adjacent wells.

Of these constraints, the first is often the one that limits the minimum gas pressure in a natural gas storage cavern. When the deviatoric stress state (caused by the difference between the gas pressure inside a cavern and the in situ stress of the surrounding salt) becomes too large, dilation (microfracturing resulting in increased porosity) occurs in the salt. Spalling of the salt along the roof or wall of a cavern can occur when the dilation in the salt becomes severe enough to initiate macrofracturing.

2.3 DAMAGE VARIABLES

The onset of damage (or dilatant volumetric strain) in salt, as well as damage accumulation, is affected by a number of variables, including the following:

- Mean stress
- Time
- Porosity
- Temperature
- Pore pressure.

The effect that each of these variables has on damage is described below.

2.3.1 Mean Stress

High mean stress is known to suppress brittle deformations in most rocks, including salt. Examples of the effect of mean stress on dilatant volumetric strain are shown in Figure 2-2. This figure shows axial and volumetric strain as a function of time for four creep tests conducted

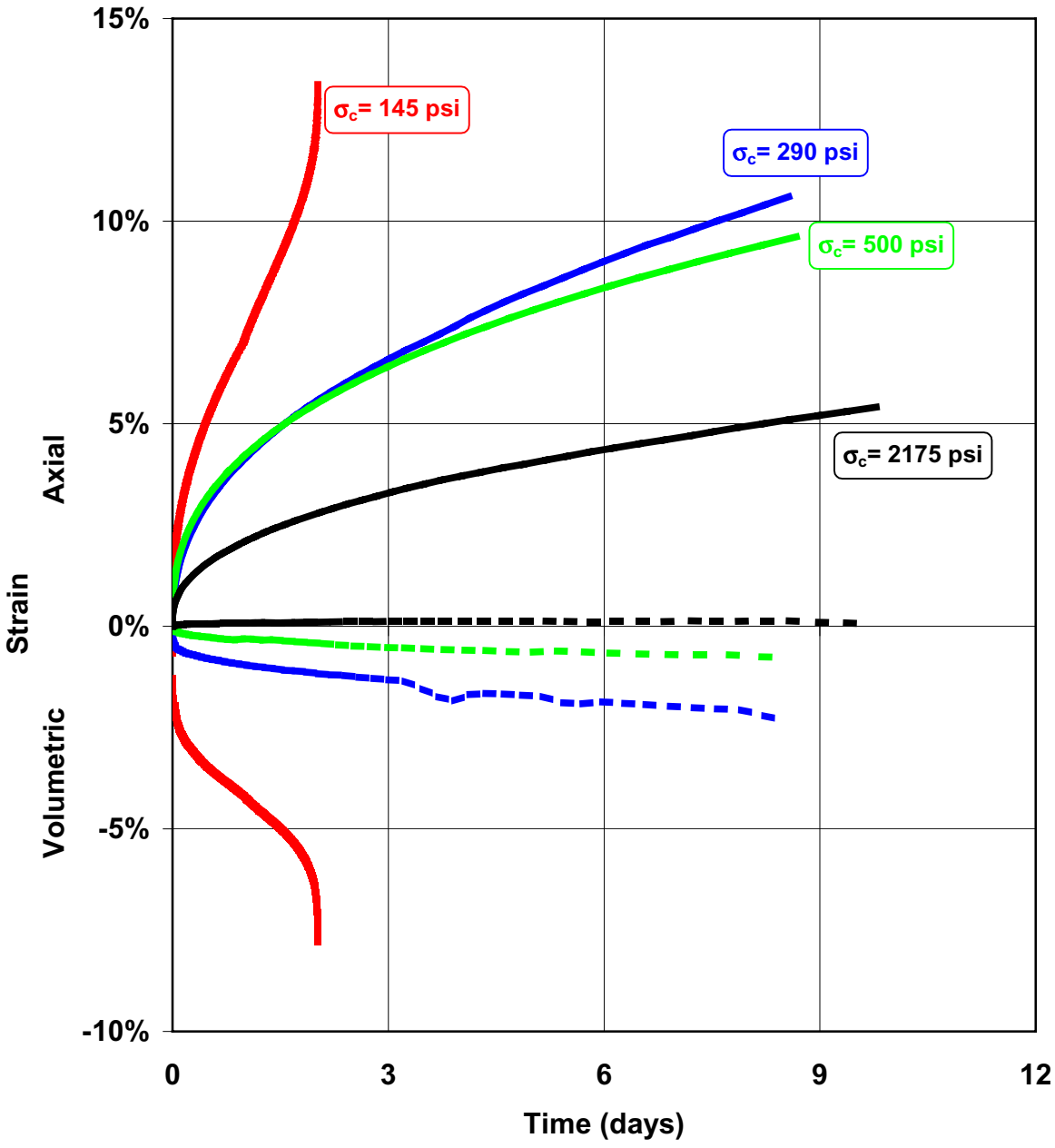

Figure 2-2. Effect of Mean Stress on Salt Dilation During Creep.

at identical stress differences (3,625 psi) and temperatures (77°F), but at different confining pressures; i.e., 145, 290, 500, and 2,175 psi. At the highest confining pressure (i.e., 2,175 psi), the dilatant volumetric strain is completely suppressed so only constant-volume deformation occurs. In subsequent tests at lower confining pressures (or mean stresses), dilatant volumetric strain accumulates at increasingly higher rates, and in some cases, actually leads to rupture at the lowest confining pressures.

2.3.2 Time

Assuming the dilation stress has been exceeded in a creep test, the dilatant volumetric strain accumulates with time, as shown in the creep curves provided in Figure 2-2. The dilatant volumetric strain continues to accumulate until one of the following occurs: (1) the salt ruptures/fails or (2) the stress state is changed so that the dilation stress is no longer exceeded. In the latter case, evidence exists that damage can actually heal under conditions approaching hydrostatic compression [Costin and Wawersik, 1980; Brodsky, 1990; Pfeifle and Hurtado, 1998].

2.3.3 Porosity

Pfeifle and Hurtado [1998] have recently presented evidence from creep tests that suggests that salt damage (in terms of dilatant volumetric strain) increases with the initial porosity of the salt. These data are reproduced in Figure 2-3 which shows results for initial porosity levels of 0.62 percent to 3.22 percent. These results are consistent with Chan et al. [1996a] who have suggested that dilatant volumetric strain increases as a function of soft impurity content (e.g., clay minerals). The explanation for this relationship is that the interface between the salt and clay particles is weak such that all particles debond from the salt matrix, resulting in a distribution of pores containing detached clay particles.

2.3.4 Temperature

Although no direct evidence was found in the literature to assess the effect of temperature on damage in salt, it is well known that salt becomes much more ductile at elevated temperature. Based on this observation, it is assumed that the damage in salt will be suppressed under conditions of elevated temperature.

2.3.5 Pore Pressure

Fokker [1995] has shown that salt dilates in laboratory fracture tests at pore pressures that approach and/or exceed the confining pressure level used during the tests. If the Terzaghi effective stress concept (effective stress is equal to the difference between the total applied stress and the pore pressure) is invoked, then the effect of pore pressure on damage may be incorporated with the mean stress variable described above. That is to say, the effective mean stress could be substituted for the mean stress because pore pressure does not affect the manner in which stress difference is defined.

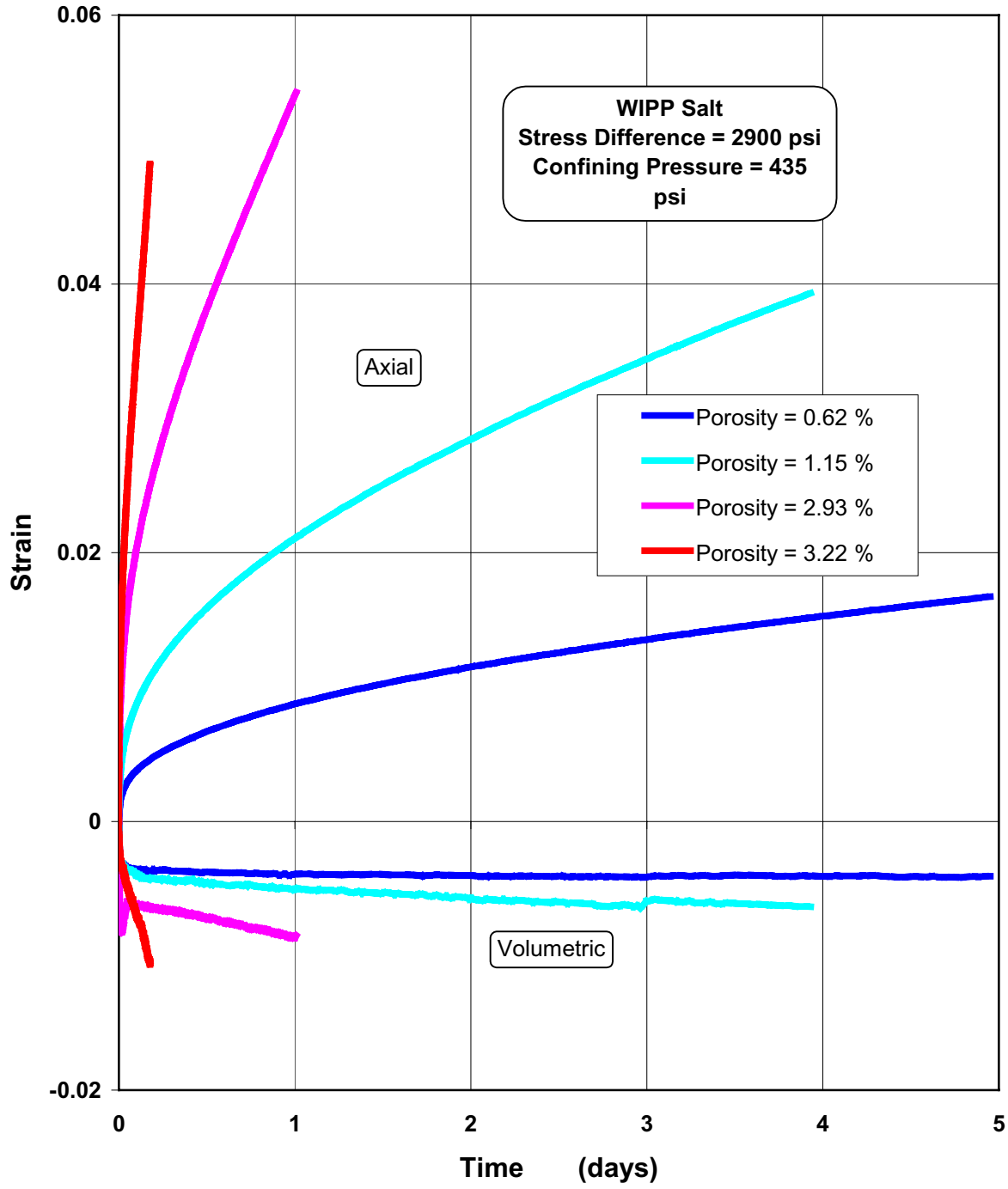

Figure 2-3. Axial and Volumetric Strain Versus Time for Salt Depicting Effect of Initial Porosity on Dilation.

3.0 TECHNICAL APPROACH FOR PREDICTING CAVERN STABILITY

Currently, two methods are available to estimate the potential for salt dilation. The Damage Potential method indicates whether or not salt could dilate based only on the stress states in the salt [Ratigan et al., 1991]. This method has been used extensively in the last several years for estimating the potential for salt dilation around salt storage caverns (e.g., Ratigan et al. [1993]) and dry-mined excavations in salt at the WIPP in New Mexico (e.g., Hansen et al. [1993]; Lin and Van Sambeek [1992]; Van Sambeek et al. [1993]). The Multimechanism Deformation Coupled Fracture (MDCF) method [Chan et al., 1992] is based not only on the stress state, but also the stress history. This model not only gives an indication of whether or not the salt may dilate (or heal), but also quantifies the degree of dilation.

The idea that the minimum gas pressure in CNG salt caverns may be reduced with a different design analysis method is based on the concept that a more accurate prediction of the behavior of salt can be obtained by an advanced model that tracks the history of damage and healing within the salt. This is in contrast to the Damage Potential method approach which simply indicates whether or not the salt has experienced a stress state that could cause dilation. By incorporating damage accumulation and healing in the dilation model, some of the uncertainty can be reduced, and a more accurate dilation criterion may be established. If a more precise design criterion could be established for cavern analysis, the uncertainty in the minimum gas pressure requirement would also be reduced. This reduction of uncertainty may allow less conservative estimates of minimum gas pressure to be made, which could result in increased economic benefits for the CNG storage industry.

The key to demonstrating that the MDCF model is technically and economically feasible for use in the CNG industry requires that the new approach be compared to the current approach. This comparison is an analytical exercise that requires a geomechanics evaluation of typical CNG storage caverns using the Damage Potential method and the MDCF model to evaluate the cavern stability. The following two sections describe these two methods in more detail.

3.1 DAMAGE POTENTIAL METHOD

The Damage Potential method is based on the stress states that result in the dilation of rock salt in laboratory experiments. Ratigan et al. [1991] show that potential for dilation in the salt surrounding an underground opening in salt can be described as:

$$\text{damage potential} = \frac{\sqrt{J_2}}{I_1} \qquad (3\text{-}1)$$

where I_1 is the first invariant of the stress tensor and J_2 is the second invariant of the deviatoric stress tensor. These stress measures are defined as follows:

$$I_1 = \sigma_1 + \sigma_2 + \sigma_3 \tag{3-2}$$

$$\sqrt{J_2} = \left(\frac{1}{6} \left[(\sigma_1 - \sigma_2)^2 + (\sigma_1 - \sigma_3)^2 + (\sigma_2 - \sigma_3)^2 \right] \right)^{1/2} \tag{3-3}$$

where:

σ_1, σ_2, σ_3 = principal stresses.

Based on creep tests on salt from the WIPP site and the Avery Island salt mine, dilation is expected when the damage potential is greater than about 0.27. This value of the damage potential defines the dilation boundary and differentiates between dilating and nondilating stress states. This boundary is shown by the straight line in Figure 3-1. Salt with stress states in the region above this boundary are expected to dilate; those that are below the boundary are not expected to dilate. The Damage Potential method does not quantify the degree of dilation or microfracturing. Although this criterion is based on only WIPP and Avery Island salt, it has been found to characterize many Gulf Coast domal salts reasonably well [Ratigan et al., 1993].

3.2 MDCF CONSTITUTIVE MODEL FOR ROCK SALT

Considerable improvements in the ability to predict the deformation and deformation rate around underground openings in salt deposits have been obtained as a result of research efforts in various countries related to the permanent disposal of radioactive waste. Most of the constitutive models formulated have assumed that during creep deformation, the volume of the rock salt is constant and driven by deviatoric stresses induced by the excavation, independent of mean stress. The coupling of creep deformation and damage on the creep response of rock salt is treated by only a few constitutive models (e.g., Cristescu and Hunsche [1992]; Chan et al. [1996a; 1996b]; Aubertin et al. [1993]). The MDCF constitutive model given by Chan et al. [1996a; 1996b] is used here to describe the time-dependent inelastic deformation of rock salt.

3.2.1 Background

Development of the MDCF model was an evolutionary process. In the first published paper of the MDCF model, Chan et al. [1992] formulated a damage-based kinematic equation which was added to the dislocation-based kinetic equation of the multimechanism deformation (M-D) model given by Munson et al. [1989]. Thus, the MDCF model is an extension of the M-D model, which was developed to provide an accurate constitutive model for the constant-volume creep response of rock salt. Like the MDCF model, development of the M-D model was motivated by the need to develop a predictive technology for the safe disposal of radioactive waste for the

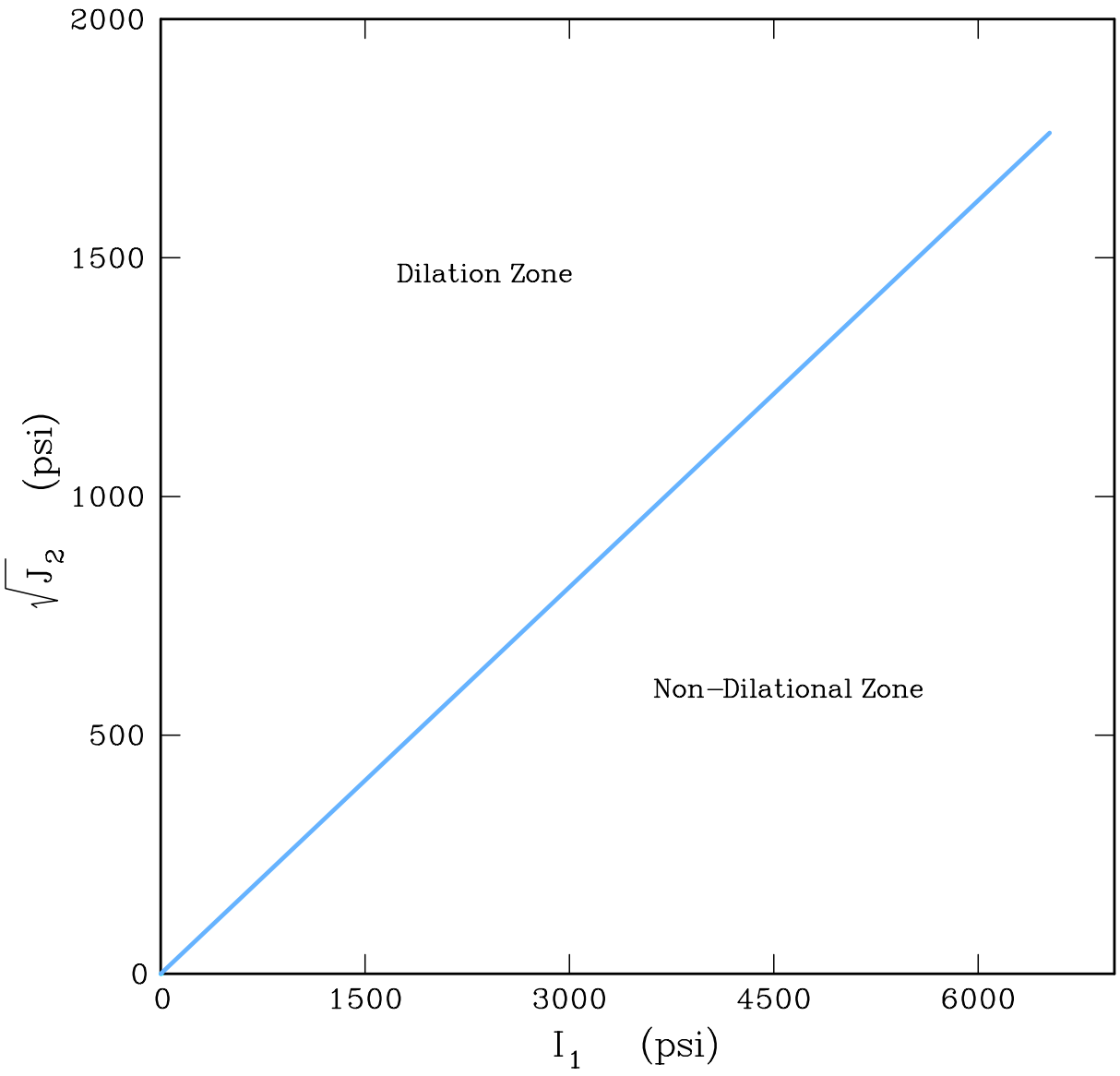

Figure 3-1. Dilation Boundary for Damage Potential Method (Developed by Ratigan et al. [1991]).

WIPP. Therefore, a description of the MDCF model begins with a brief discussion of the M-D model.

3.2.2 M-D Model

The M-D model is based on micromechanistic concepts using the deformation mechanism map constructed by Munson [1979]. A deformation mechanism map is a representation in stress and temperature space of those micromechanical mechanisms controlling the deformation. Each mechanism has a constitutive equation that specifies the deformation or strain rate as a function of the imposed conditions of stress and temperature and the material properties. The deformation mechanism map constructed by Munson [1979] from available theoretical and experimental information on steady-sate creep of salt is shown in Figure 3-2. The map plots the dimensionless quantities of normalized stress (shear stress/shear modulus) against the homologous temperature (temperature/melting temperature). Five regimes are identified in this figure where separate mechanism dominate the deformation of salt: (1) defectless flow, (2) dislocation glide, (3) dislocation climb creep with two subregimes denoted by volume and pipe self diffusion, (4) diffusional creep with two subregimes denoted by volume and grain boundary self diffusion, and (5) a regime whose creep mechanism is undefined. The undefined mechanism has no micromechanical model, but is empirically well defined on the basis of laboratory testing.

In Figure 3-2, boundaries or portions of boundaries whose locations are confirmed by experimental evidence are shown as solid lines, boundaries whose locations are the result of calculations based on constitutive equations are shown as dashed lines, and boundaries whose locations are based on interpolation or extrapolation are shown as dotted lines. Inclusion of a question mark means the boundary is based on conjecture only. Constant strain-rate trajectories are shown on the map for strain rates of 10^{-12}, 10^{-10}, and 10^{-8}/s as determined by the micromechanistic models using site-specific parameter estimates established for rock salt. The constant strain-rate trajectories were placed on the deformation map by Munson [1979] for illustrative purposes since strain rate is specified for many laboratory applications.

Munson [1979] identified the probable WIPP repository stress and temperature conditions on the deformation mechanism map. As shown in Figure 3-2, only three mechanisms need to be incorporated into the constitutive model for the expected repository conditions. These three mechanisms are also applicable for the conditions expected for most, if not all, CNG storage caverns. Based on the deformation mechanism map and the three rate-controlling mechanisms, a constitutive model was proposed by Munson and Dawson [1979] which was later called the M-D model. The model assumes that each of the three mechanism act in parallel; thus, the total steady-state creep rate is just the sum of the creep rates of the individual mechanism. Primary (transient) creep was incorporated into the model by multiplying the steady-state creep rate by a transient function which was later modified as described by Munson et al. [1989]. The transient function is composed of a work-hardening branch, equilibrium branch, and a recovery branch for an internal variable whose development is governed by a separate evolution equation. This model provides the framework for the development of the MDCF model which extends the

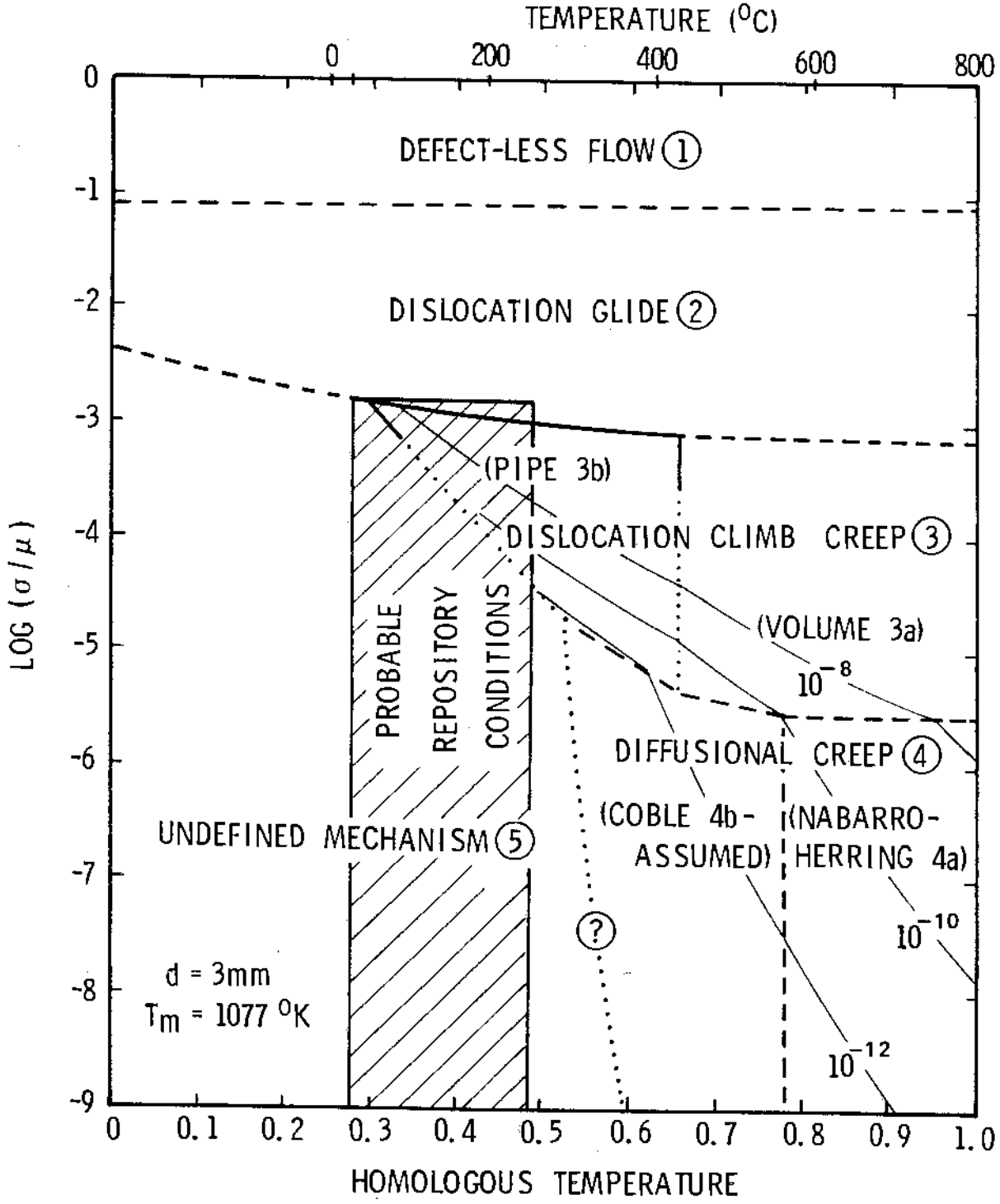

Figure 3-2. Deformation Mechanism Map for Salt (After Munson [1979]).

M-D model by incorporating an expression for describing the contribution of cavities or microcracks to the macroscopic inelastic strain rate.

3.2.3 Extension of the M-D Model

Several papers have been published since the initial paper by Chan et al. [1992] documenting enhancements and revisions of the MDCF model (e.g., Chan et al. [1994; 1995a; 1995b; 1996a; 1996b; 1996c; 1997]). Modifications and enhancements include, among others, development of a nonassociated damage-induced flow law, clay particle function, cleavage fracture mechanism, and healing mechanism. The latest known version of the model was used in this study with minor exceptions as described below.

The total inelastic strain rate in the MDCF model is represented by two components, dislocation creep and creep-induced damage, that contribute to the macroscopic strain rate. Two kinetic equations describe the damage component of the model, one for shear-induced damage and one for cleavage fracture. These kinetic equations account for creep-induced damage during the transient, steady-state, and tertiary creep stages, with the damage that accumulates in the transient creep region not leading to tertiary creep immediately. Important characteristics of the model include the ability to predict pressure-dependent flow and plastic dilatancy.

3.2.4 Dilatancy Boundary

Based on laboratory experiments, damage-induced inelastic flow in rock salt is nonassociated, dilational, and contributes significantly to the macroscopic strain rate at low confining pressures. The inelastic strain rate and volumetric strain due to damage decreases with increasing confining pressures and is suppressed at sufficiently high confining pressures. Unlike the Damage Potential method, a dilatancy boundary is not given in terms of the second invariant of the deviatoric stress tensor and the first invariant of the Cauchy stress tensor. Instead, the MDCF model was formulated using a work-conjugate stress measure (damage stress) to determine dilational stress states in terms of principal stresses. Dilation is expected when the damage stress measure is greater than zero. The damage stress is given by:

$$\sigma_{eq}^{\omega} = \left|\sigma_1 - \sigma_3\right| + \left(1 - p_1\rho\right) x_2 x_7 sgn\left(I_1 - \sigma_3\right) \left[\frac{I_1 - \sigma_3}{3\, x_7 sgn\left(I_1 - \sigma_3\right)}\right]^{x_6} + x_1 \sigma_1 H\left(\sigma_1\right) \quad (3\text{-}4)$$

where I_1 is the first invariant of the Cauchy stress tensor; the x's and p_1 are material constants; ρ is the impurity (clay) content; and σ_1 and σ_3 are the maximum and minimum principal stress; respectively, with compression assumed to be negative. The first term represents the driving force for shear-induced damage, which leads to the opening of "wing-tip" microcracks or grain boundary cracks. The second term in Equation 3-4 represents the suppression of microcrack growth by a confining pressure. This term was recently extended to account for the increase in damage accumulation associated with increasing impurity of clay content [Chan et al., 1996a]. The third term represents the opening of microcracks by the maximum tensile

stress, σ_1. Given the parameter x_1 is positive and the Heaviside step function $\langle H(\sigma_1) \rangle$, the damage stress measure is positive whenever the maximum principal stress is tensile.

A dilatancy boundary for the MDCF model can be presented in terms of J_2 and I_1 if the intermediate principal stress is expressed in terms of the minimum or maximum principal stress. In Figure 3-3, dilation boundaries are presented for salt at the WIPP site that have been categorized as clean and argillaceous. The boundaries were calculated using Equation 3-4, assuming values for ρ of 0.0 percent for clean salt and 2.9 percent for argillaceous salt. The dilation boundaries presented in this figure assume stress states where the two maximum principal stresses are equal (i.e., triaxial test condition). However, the dilation boundaries do not differ significantly when three-dimensional stress states or varying load paths are considered. Again, salt is expected to dilate when the stress state is above the dilation boundary. Likewise, no dilation is expected for stress states below the dilation boundary corresponding to a stress measure given by Equation 3-4 that is equal or less than zero. The dilation boundary determined using the Damage Potential method is included in Figure 3-3 for comparative purposes. As shown in Figure 3-3, the dilatancy boundary is very sensitive to the value specified for the clay content parameter ρ. The clay particle function is discussed in more detail in the following section.

3.2.5 Clay Particle Function

The MDCF model contains a clay particle function to account for the possible effects of soft impurity content on the creep and damage responses in argillaceous salt. The clay particle function was developed, in part, based on the results reported by Nemat-Nasser [1983] of brittle materials with embedded inclusions. The experimental evidence indicated that the weak damage process associated with pores, holes, and inclusions was the nucleation of microcracks by tensile stresses induced at the poles. Chan et al. [1996a] assumed that the interface between the clay particles and salt is weak such that all particles are debonded from the salt matrix, resulting in a distribution of pores containing detached clay particles.

As mentioned in Chapter 2.0, Pfeifle and Hurtado [1998] have recently presented evidence from creep tests that suggests that salt damage (in terms of dilatant volumetric strain) increases with the initial porosity of the salt. This data was shown in Figure 2-3 for porosity levels up to 3.22 percent. These results are consistent with Chan et al. [1996a] for similar values of percent clay content. Conversely, Pfeifle and Hurtado [1998] did not observe a strong correlation between clay content and salt damage. However, limited data are available to characterize the damage response of impure salt and is the subject of future research. Therefore, it is postulated here that the increase in the inelastic strain rate and dilatant volumetric strain observed for impure salt results from pores or inclusion, either brine filled, gas filled, or soft impurity content, that is weakly bonded to the salt matrix. For this reason, the term *impurity content* is used in this report instead of *volume fraction of clay* to describe the behavior of salt with pores, holes, and/or inclusions.

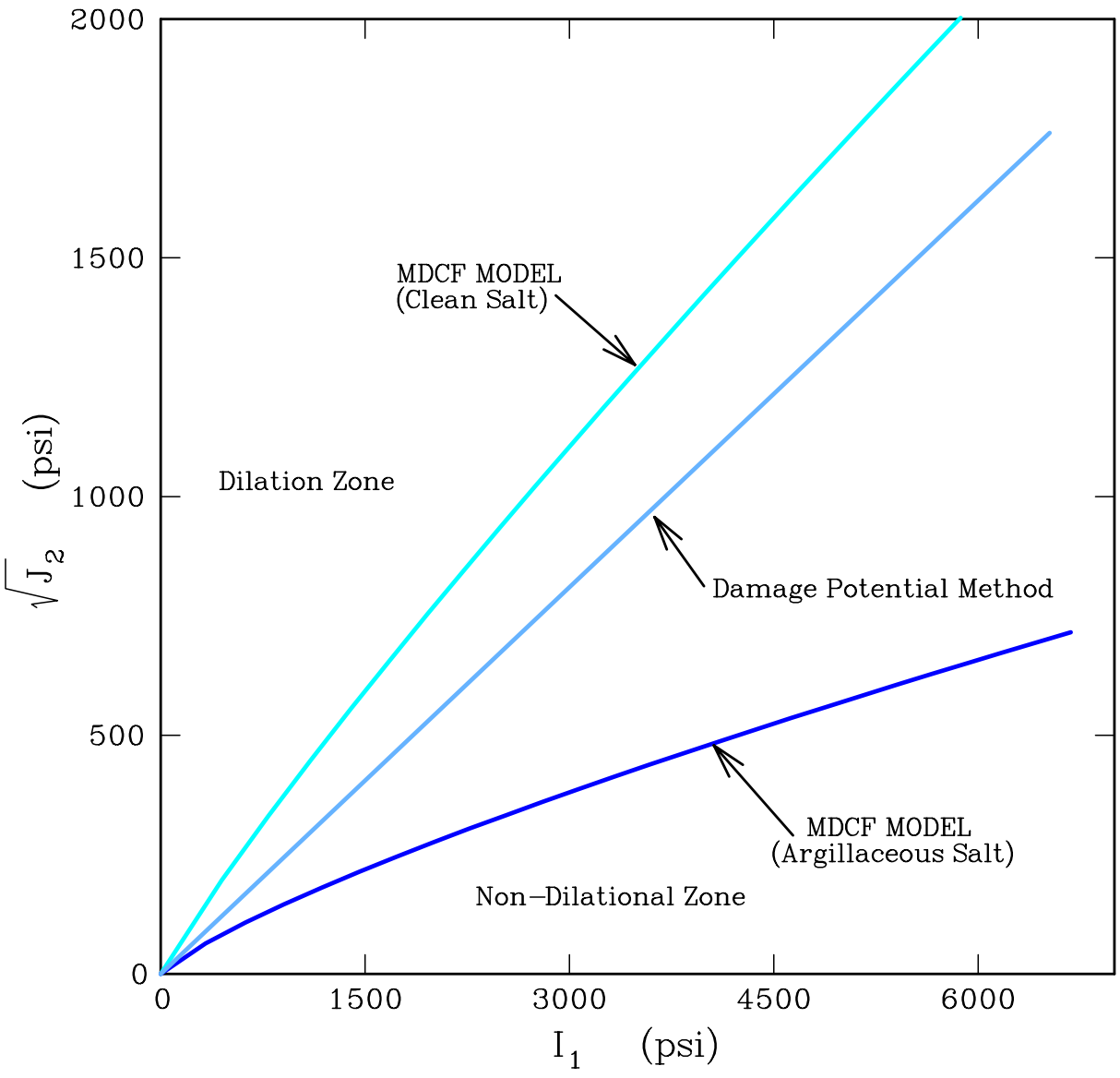

Figure 3-3. Comparison of Dilation Boundaries Predicted Using the MDCF Model for WIPP Salt.

3.2.6 Damage Variable

In addition to a direct contribution to the inelastic strain rate, the MDCF model was formulated such that damage also produces a softening effect as proposed by Kachanov [1958]. The Kachanov damage variable reduces the load-bearing capacity through a reduction in the effective area using a continuum damage mechanics approach. For the MDCF model, the Kachanov damage variable (ω) is determined from an evolutionary equation and provides a scalar measure for the level of damage. In addition to the damage state variable, damage is quantified through model prediction of dilatant volumetric strain.

3.2.7 Cavern Stability Design Criterion

Coupling of creep and damage in the MDCF model allows calculation of the entire creep curve, including tertiary creep. The onset of tertiary creep is traditionally defined as the time the minimum strain rate is observed in a creep test. Experimental evidence shows that the time to the onset of tertiary creep and the strain to creep rupture increases with confining pressure at a constant stress difference. The mechanical strength of salt decreases rapidly during the tertiary creep stage; consequently, the stability of a storage cavern in salt could be jeopardized if the salt undergoes tertiary creep. Chan et al. [1996c; 1997] have proposed using critical values of the damage variable, ω, as indicators of the onset of tertiary creep and creep rupture. Chan et al. [1996c; 1997] estimate critical damage values of 0.015 and 0.15 to represent the onset of tertiary creep and creep rupture in WIPP salt, respectively.

A comparison of the measured and calculated time-to-rupture responses of WIPP salt in triaxial compression is shown in Figure 3-4. The experimental results shown in this figure were obtained from triaxial compression creep tests conducted on cylindrical specimens at 77°F and a stress difference of 3,625 psi under various confining pressures. Test points indicated by closed circles indicate rupture, while those with an arrow did not fail at the time the test was terminated. Based on this figure, a critical damage value of 0.015 may not be a conservative estimate for the onset of tertiary creep because two of the eight experimental tests ruptured before the model predicted the onset of tertiary creep. A more conservative estimate for the time-to-creep rupture is obtained with a critical damage value of 0.0025. Comparison of calculated and experimental creep rupture times using a critical damage values of 0.0025 is shown in Figure 3-4. As shown in this figure, the time predicted by the MDCF model to obtain a damage level of 0.0025 is less than the measured time-to-rupture for all of the experiments. Therefore, a critical damage value of 0.0025 is proposed as the design criterion to be used here for evaluating the stability of CNG storage caverns.

The rate of evolution of the damage variable depends on a number of variables, including stress, impurity content, and material parameters. Because of the variability of salt and limited availability of data, additional research is warranted to increase confidence in the limiting value of the damage variable for evaluating cavern stability. However, the proposed critical damage value of 0.0025 should provide a conservative estimate for material damage that does not

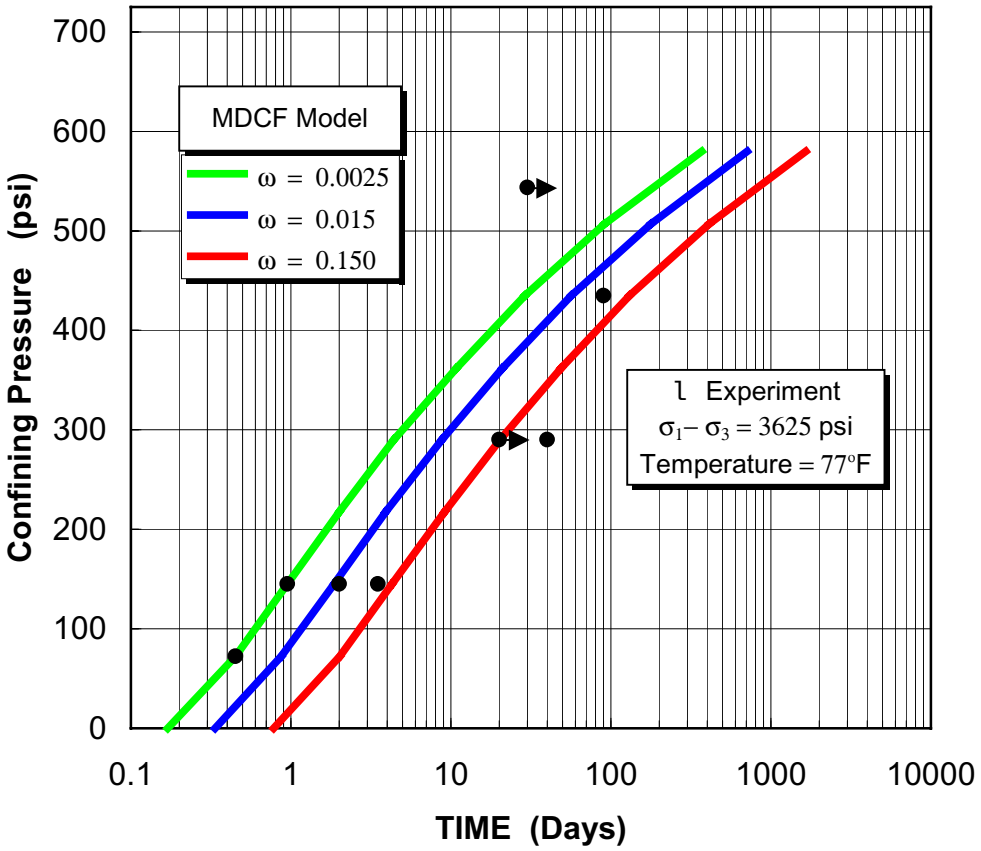

Figure 3-4. Comparison of Calculated and Measured Time-to-Rupture Results of WIPP Salt as a Function of Confining Pressure.

greatly influence the structural integrity of salt using parameter estimates established for the WIPP.

3.2.8 Damage Healing

The work of Chan et al. [1995b] represents one of the first steps in simulating the healing of salt. Development of the healing term was based largely on the results of a series of hydrostatic compression tests performed by RESPEC on WIPP salt at 68, 115, and 158°F and reported by Brodsky and Munson [1994]. In these experiments, damage was introduced by straining cylindrical specimens with a constant axial strain rate to 1.5 percent axial strain at low confining pressure (72.5 psi). The predamaged specimens were then compressed under a hydrostatic pressure of 2,175 psi to isolate the damage healing processes from dislocation creep. The amount of volumetric strain recovered by damage healing was quite rapid during the early stages of these tests and nearly the same magnitude for all the tests regardless of the temperature. The rapid healing behavior is thought to arise from the closure of open microcracks. During the later stages of the healing tests, the rate of healing was much slower; the amount of volumetric strain recovered increased with temperature and with the time of healing, consistent with sintering of microcracks by a diffusion controlled process.

Figure 3-5 shows a plot of the normalized volumetric strain measurements versus time for one of the hydrostatic compression tests reported by Brodsky and Munson [1994]. In this figure, normalized volumetric strain is presented in terms of the volumetric strain due to healing $\left(\varepsilon_v^h\right)$ and the initial volumetric strain at the beginning of the healing process $\left(\varepsilon_{vo}\right)$. Two healing mechanisms are indicated in this figure by the bilinear plots of two different slopes. It has been suggested that Mechanisms 1 and 2 correspond to closing and healing of microcracks, respectively [Chan et al., 1995b] and can be represented by identical kinetic equations with different time constants.

Instead of having separate terms for individual healing mechanisms, the current form of the MDCF model [Chan et al., 1996b] uses a single healing term. To account for the experimental observation of two characteristic times (two healing mechanism rates), a variable time constant is used that is a function of the volumetric strain. When the volumetric strain is relatively large, the value of the time constant represents the characteristic time constant for damage healing by crack closure. As the volumetric strain becomes small, the value of the time constant is increased to correspond to the characteristic time constant for Mechanism 2.

Both isotropic and anisotropic healing behavior can be described by the MDCF model. The healing inelastic damage flow is anisotropic in nature because damage will typically accumulate normal to the major principal stress (compression negative). To implement the anisotropic nature of the healing, Chan et al. [1996b] have developed the flow potential based on stress-induced anisotropy. However, the state of stress does not provide information regarding the direction of damage. For this reason, isotropic flow based only on mean stress was adopted for this study.

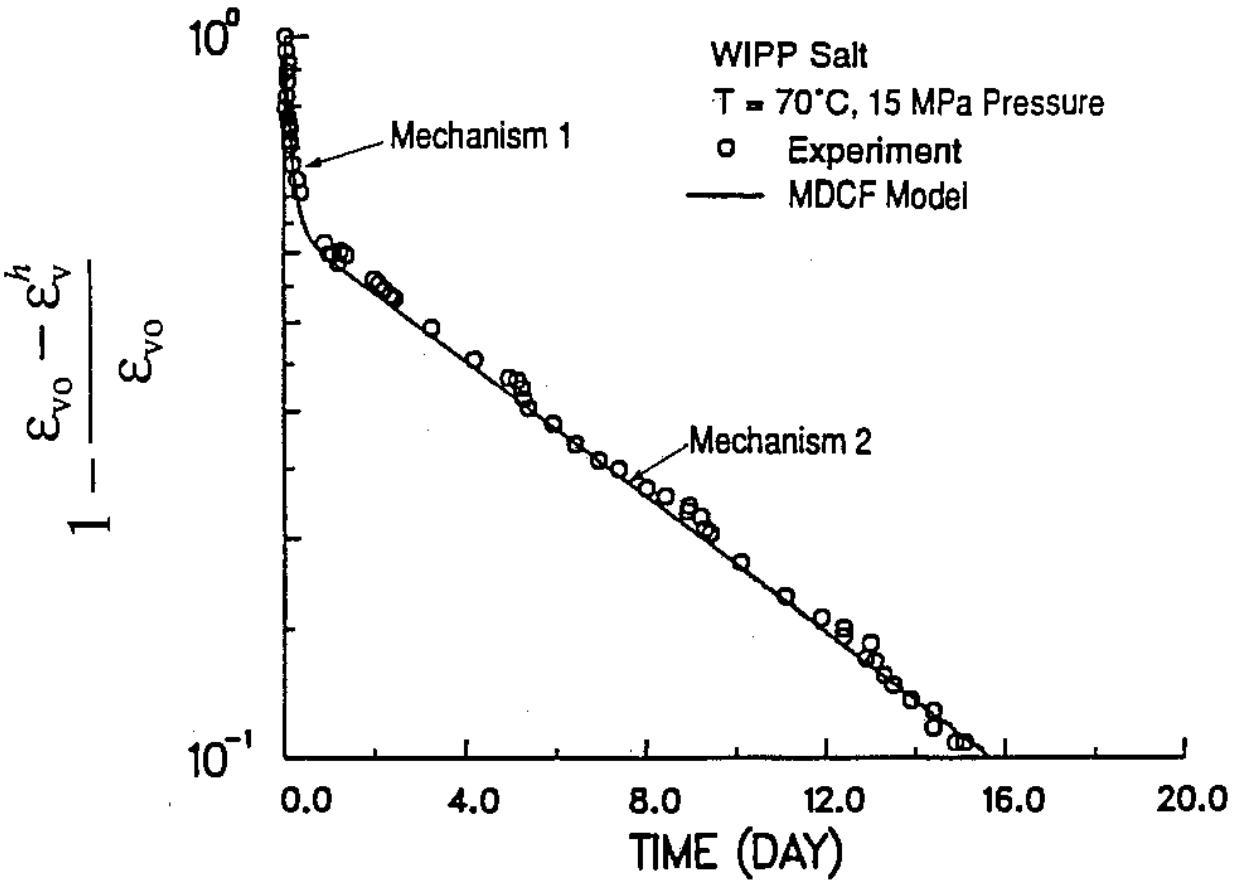

Figure 3-5. A Semilog Plot of Normalized Volumetric Strain Versus Time for Damage Healing of WIPP Salt at 70°C (158°F) Under a Hydrostatic Pressure of 15 MPa (2,175 psi) (After Chan et al. [1996b]).

3.2.9 Constitutive Model Equations

The MDCF model incorporated into the finite element code **SPECTROM-32** [Callahan et al., 1989] follows the work of Chan et al. [1996a] and includes an extension of the model to represent damage healing given by Chan et al. [1996b] with minor exceptions. A detailed description of the model used in this study is provided in Appendix A.

4.0 FINITE ELEMENT PROGRAM AND GEOMECHANICAL MODELS

The finite element method was used to predict the minimum gas pressure and continuum damage around two natural gas storage caverns at different depths. Axisymmetric models were developed for both of the caverns used in this study to demonstrate the applicability of the MDCF model to predict the minimum gas pressure of CNG storage caverns. A description of the finite element program, the modeled geometry, in situ conditions, and fluid properties of the two natural gas storage caverns used for demonstrative purposes is described below.

4.1 FINITE ELEMENT PROGRAM

The finite element program **SPECTROM-32** [Callahan et al., 1989] was used to model the mechanical behavior of the two CNG storage caverns. **SPECTROM-32** is a thermomechanical, finite element program that has been developed by RESPEC for the solution of rock mechanics problems. It was designed specifically for the simulation of underground openings and structures. **SPECTROM-32** not only has the capability to model the elastic-plastic response that is commonly associated with brittle rock types, but it also has the capability to simulate the viscoplastic behavior that is observed in salt. The features and capabilities of **SPECTROM-32** that were required specifically for the simulation of the storage caverns include:

- Options for two-dimensional and axisymmetric geometries.
- Kinematic and traction boundary conditions.
- MDCF constitutive model for viscoplastic behavior of salt, including damage.
- Capability to represent arbitrary in situ stress and temperature fields.
- Capability to simulate excavation or solution-mining operations.

4.2 GEOMECHANICAL MODELS OF STORAGE CAVERNS

A geomechanics evaluation of a storage well field is usually a three-dimensional problem. However, it is not usually practical to solve three-dimensional rock mechanics problems using the finite element method when the material displays time-dependent deformation (creep). Practical solutions can be realized if the problem can be reduced to one or more two-dimensional problems. For the caverns used in this study, axisymmetric models are a very good representation of the in situ geometry. The geometry and depth of the models used in this study represent existing storage caverns in domal salt. Site-specific material properties were used where possible to provide a realistic example of the expected results for these caverns. The geometry and in situ conditions for the two caverns are discussed separately below.

4.2.1 Cavern A

Cavern A is a natural gas storage cavern located in a salt dome that includes a number of other caverns used for storage or brine production. A few of these caverns are in close proximity to Cavern A such that their presence will have an impact on the stress state of the salt near Cavern A. The finite element mesh for Cavern A is shown in Figure 4-1, and specific characteristics are listed in Table 4-1. The cavern is modeled between the depth interval 2,009 and 3,438 feet below ground surface. The geometry (radius as a function of depth) for this cavern was determined based on a design solution-mining simulation. The model extends vertically from the top of the salt dome at a depth of 669 feet to a depth of 7,000 feet. Because the cavern is located in a salt dome, no stratigraphic members are included in the model and each element represents a volume of salt. An outer radius of 735 feet was specified for this model to approximate the effects of other storage caverns that are in near proximity to Cavern A. The mesh contains 4,639 nodes and 1,480 eight-noded elements. Elements near the cavern walls are very finely subdivided with the first layer of elements having a thickness of only about 3 feet. This extremely fine subdivision was used to accurately represent the large stress gradients anticipated near the cavern.

4.2.1.1 In Situ Temperature Profile

Although the circulation of brine during leaching of the well and the compression and decompression of gas during natural gas storage would perturb the ambient temperature distribution in the immediate vicinity of the well, these perturbations were assumed to have negligible effects on the mechanical behavior of the well and were not modeled. A temperature gradient that is constant with depth was assumed for analyses of Cavern A. The temperature as a function of depth is given by:

$$T = 79.3 + 0.0106z \tag{4-1}$$

where T is the temperature in degrees Fahrenheit and z is the depth in feet. This temperature profile results in a temperature of approximately 100°F and 115°F at the top and bottom of Cavern A, respectively.

4.2.1.2 In Situ Stress Distribution

The in situ stress distribution was assumed to be isotropic and equal to the weight of the overburden. The top of the salt above Cavern A is at a depth of approximately 669 feet below ground surface. The caprock and sediment overlying the salt were modeled as a pressure traction boundary and were estimated based on an average density of 161.6 pcf. The resulting overburden pressure at the top of the salt dome is 749 psi. The density of the salt was assumed to be 135 pcf, which results in a vertical gradient in stress of 0.94 psi/foot below the top of the salt dome. Consequently, the in situ stress distribution prior to solutioning of the well was assumed to be:

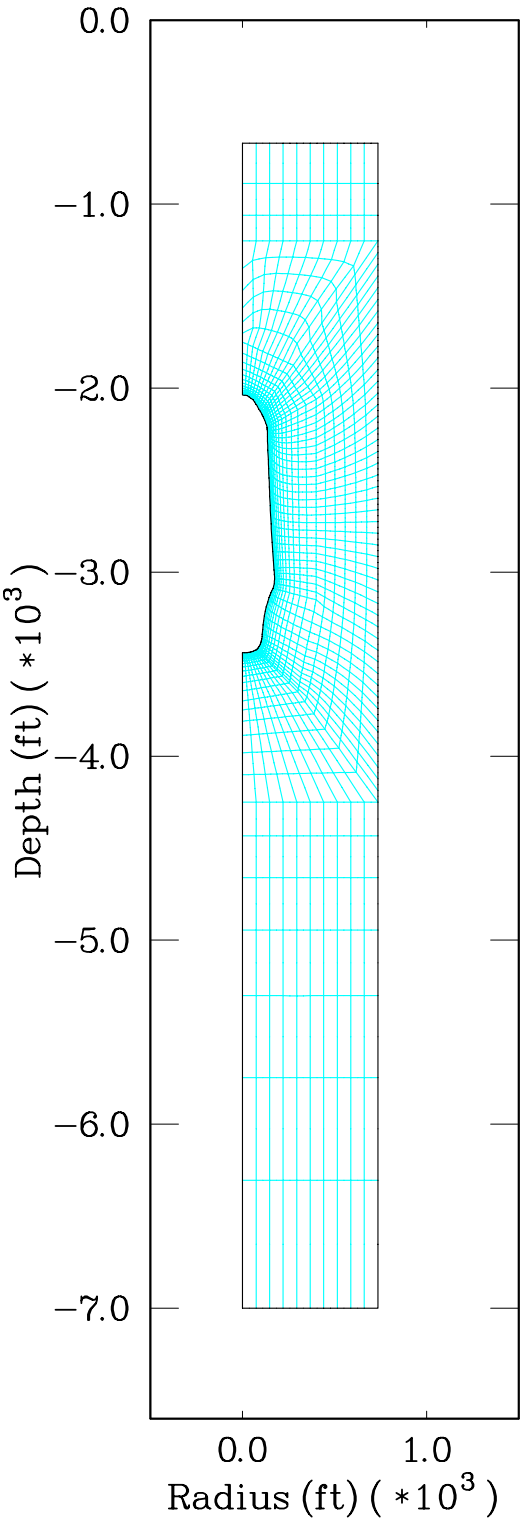

Figure 4-1. Cavern A Finite Element Mesh.

$$\sigma_r = \sigma_\theta = \sigma_z = 0.94(z - 669) + 749 \quad (4\text{-}2)$$

where σ_r, σ_θ,and σ_z are the radial, tangential, and vertical stress components in psi, and z is the depth in feet. At the casing shoe depth (2,009 feet), the vertical stress is estimated to be about 2,009 psi based on Equation 4-2.

Table 4-1. Characteristics of Gas Storage Caverns

Cavern Characteristic	Cavern	
	A	B[(a)]
Casing Shoe Depth (ft)	2,009	4,088
Approximate Cavern Total Depth (ft)	3,438	5,080
Approximate Cavern Maximum Diameter (ft)	350	200
Approximate Cavern Volume (MMbbls)[(b)]	15.2	3.7
Approximate Design Minimum Cavern Pressure at the Casing Shoe (psig)	603	1,200
Approximate Design Maximum Cavern Pressure at the Casing Shoe (psig)	1,707	3,475
Approximate Maximum Working Gas Volume (Bcf)[(c)]	7.3	3.2
Approximate Minimum Cushion Gas Volume (Bcf)	3.3	1.8
Approximate Total Gas Volume (Bcf)	10.6	5.0

(a) The minimum cavern pressure, working gas volume, and cushion gas volume for this well were incorrectly listed in Ratigan [1997].

(b) Millions of petroleum barrels.

(c) Billion standard cubic feet.

4.2.2 Cavern B

The finite element mesh for Cavern B is shown in Figure 4-2. The cavern is modeled between the depth interval of 4,088 and 5,080 feet. This mesh contains 7,247 nodes and 2,340 eight-noded elements. The model extends vertically from the top of the salt at a depth of 1,680 feet to a depth of 7,100 feet. Because Cavern B is essentially isolated from other caverns, an outer radius of 1,500 feet was used to approximate an infinite boundary. Again, elements near the cavern walls are very finely subdivided to accurately represent the large stress gradients anticipated near the caverns. Specific characteristics for this cavern are listed in Table 4-1.

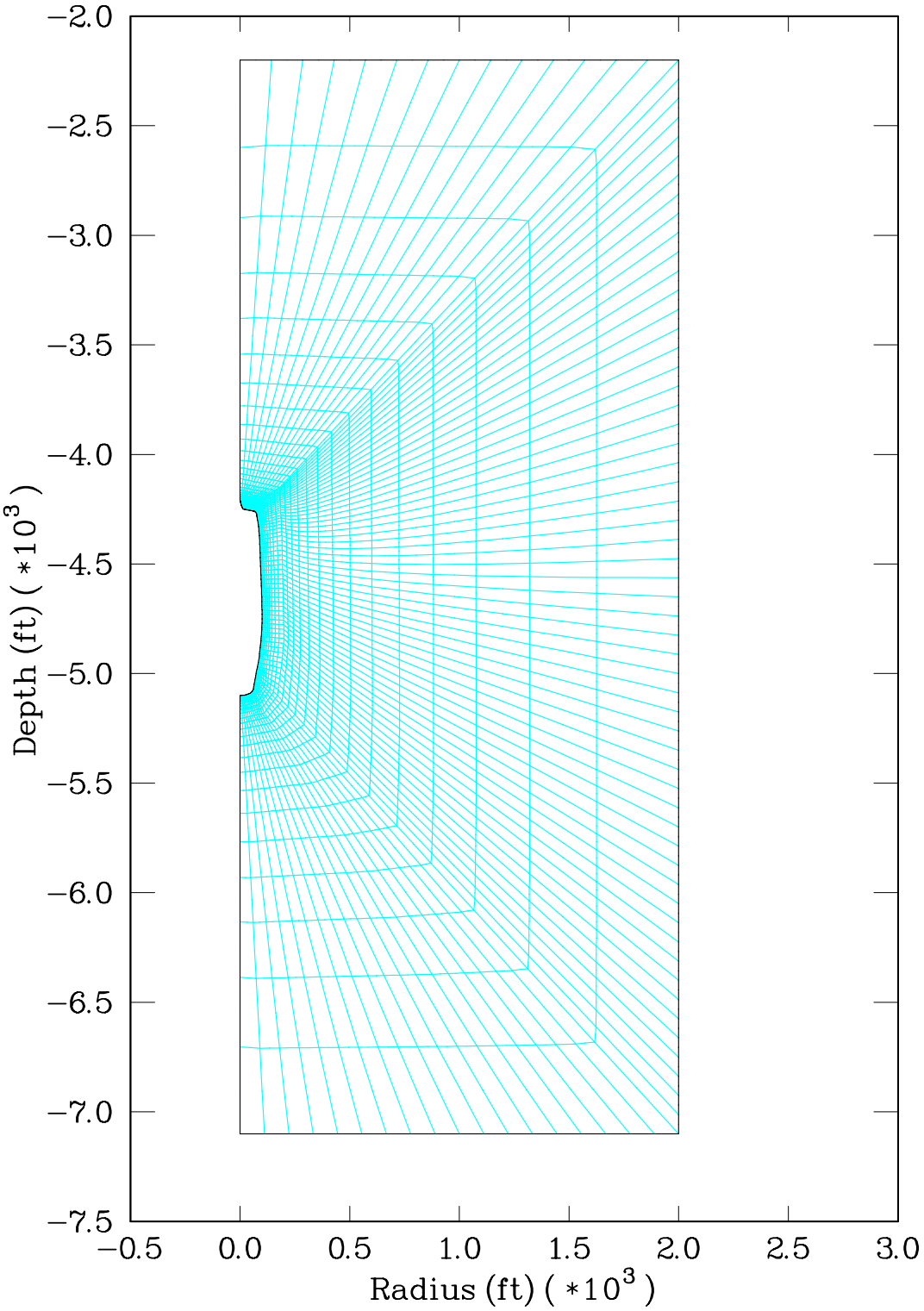

Figure 4-2. Cavern B Finite Element Mesh.

4.2.2.1 In Situ Temperature Profile

Although leaching of the well and normal movement of product would perturb the ambient temperature distribution in the immediate vicinity of the well, these perturbations were assumed to have negligible effects on the mechanical behavior of the well and were not modeled. A temperature gradient that is constant with depth was assumed for analyses of Cavern B. The temperature as a function of depth is given by:

$$T = 102.9 + 0.005662z \tag{4-3}$$

where T is the temperature in degrees Fahrenheit and z is the depth in feet. This temperature profile results in a temperature of approximately 126°F and 132°F at the top and bottom of Cavern B, respectively.

4.2.2.2 In Situ Stress Distribution

The in situ stress distribution was assumed to be isotropic and equal to the weight of the overburden. The density of the salt was assumed to be 135 pcf, which results in a vertical gradient in stress of 0.94 psi/foot below the top of the salt above Cavern B. The caprock and sediment overlying the salt were modeled as a pressure traction boundary and were assumed to have an average density of 144 pcf, which results in an overburden stress of 1,680 psi at the top of the salt. Consequently, the in situ stress distribution prior to leaching of the well was assumed to be:

$$\sigma_r = \sigma_\theta = \sigma_z = 0.94(z - 1{,}680) + 1{,}680 \tag{4-4}$$

where σ_r, σ_θ,and σ_z are the radial, tangential, and vertical stress components in psi and z is the depth in feet.

4.2.3 Cavern A and Cavern B Model Boundary Conditions

The kinematic boundary conditions specified along the sides of the axisymmetric models for Cavern A and Cavern B were:

- No radial displacement along the centerline.
- No radial displacement along the outer radius.
- No vertical displacement along the bottom surface.

The upper surfaces of the models are free to move in both the radial and vertical directions. After the excavation of the salt was simulated, normal tractions were specified along the surface of the cavern to simulate the fluid pressure inside the cavern. The magnitudes of these tractions are equal to the hydrostatic pressure based on the densities of the fluids in the cavern plus the pressure specified at the wellhead.

4.3 PROPERTIES OF WELL FLUIDS

The mechanical response of the storage caverns not only depends on the material properties of the salt surrounding the well but also on the material properties of the fluids inside the well. The wells were assumed to be filled with saturated brine before being dewatered. The wells are subsequently filled with compressed natural gas. In the simulations, these fluids are represented by their pressures applied as normal tractions to the surfaces of the well. An equation of state relating the fluid's pressure to its density and temperature was assumed for each fluid. The assumed equations of state used to predict the resultant vertical pressure gradients for brine and natural gas used in this study are provided in Appendix C.

5.0 NUMERICAL RESULTS OF CAVERN STABILITY BASED ON DILATANCY BOUNDARIES

5.1 PROBLEM DESCRIPTION

In this chapter, the dilatancy boundary predicted with the Damage Potential method is compared to that of the MDCF model. Finite element models were used to make the comparison of the boundaries of the two methods during simulated gas withdrawal from the two subject caverns.

In Figure 5-1, the dilation boundaries based on the MDCF model and the Damage Potential method are shown in I_1-$\sqrt{J_2}$ stress space. The Damage Potential method dilation boundary is represented by a straight line, as described in Section 3.1. The four MDCF dilation boundaries shown are based on Equation 3-4 with impurity or porosity levels between 0 and 3 percent. Also shown in Figure 5-1 are test data on salt samples from each of the cavern sites. Tests on salt from the Cavern A site include both Standard Triaxial Compression (STC) tests in which the confining pressure is held constant as the axial load is increased and Constant Mean Stress (CMS) tests where the confining pressure is decreased as the axial load is increased. Creep tests were used to determine the dilation boundary for salt from the Cavern B site. Because the stress state is held constant in creep tests, these test data only determine whether or not dilation is occurring at a given stress state; a single test cannot be used to determine the dilation boundary.

Finite element simulations were used to demonstrate the use of dilation boundaries in developing minimum gas pressure design constraints for natural gas storage caverns. Typically, using the Damage Potential method, the design minimum gas pressure for a cavern is determined by simulating gas withdrawal from the cavern while monitoring the magnitude and location of the damage potential values. As gas is withdrawn from the cavern, the difference between the cavern pressure and the in situ stress state in the salt surrounding the cavern increases, resulting in higher damage potential values. The design minimum gas pressure is determined when the damage potential values in the salt surrounding the cavern reach the value determined through laboratory testing which results in dilation of the salt or a value which represents the desired factor of safety with respect to this value. Typically, only the salt surrounding the upper portion of the cavern is evaluated since dilation in the lower portion of a cavern generally does not have an adverse impact on cavern stability.

In the finite element simulations used to compare the salt dilation boundaries, cavern development was simulated by instantaneously excavating the cavern with a brine pressure head and allowing the surrounding salt to creep for a time equal to the actual solutioning period. After the solutioning period, dewatering of the caverns was simulated. Cavern A was dewatered at maximum gas pressure. Cavern B was dewatered at a pressure less than the

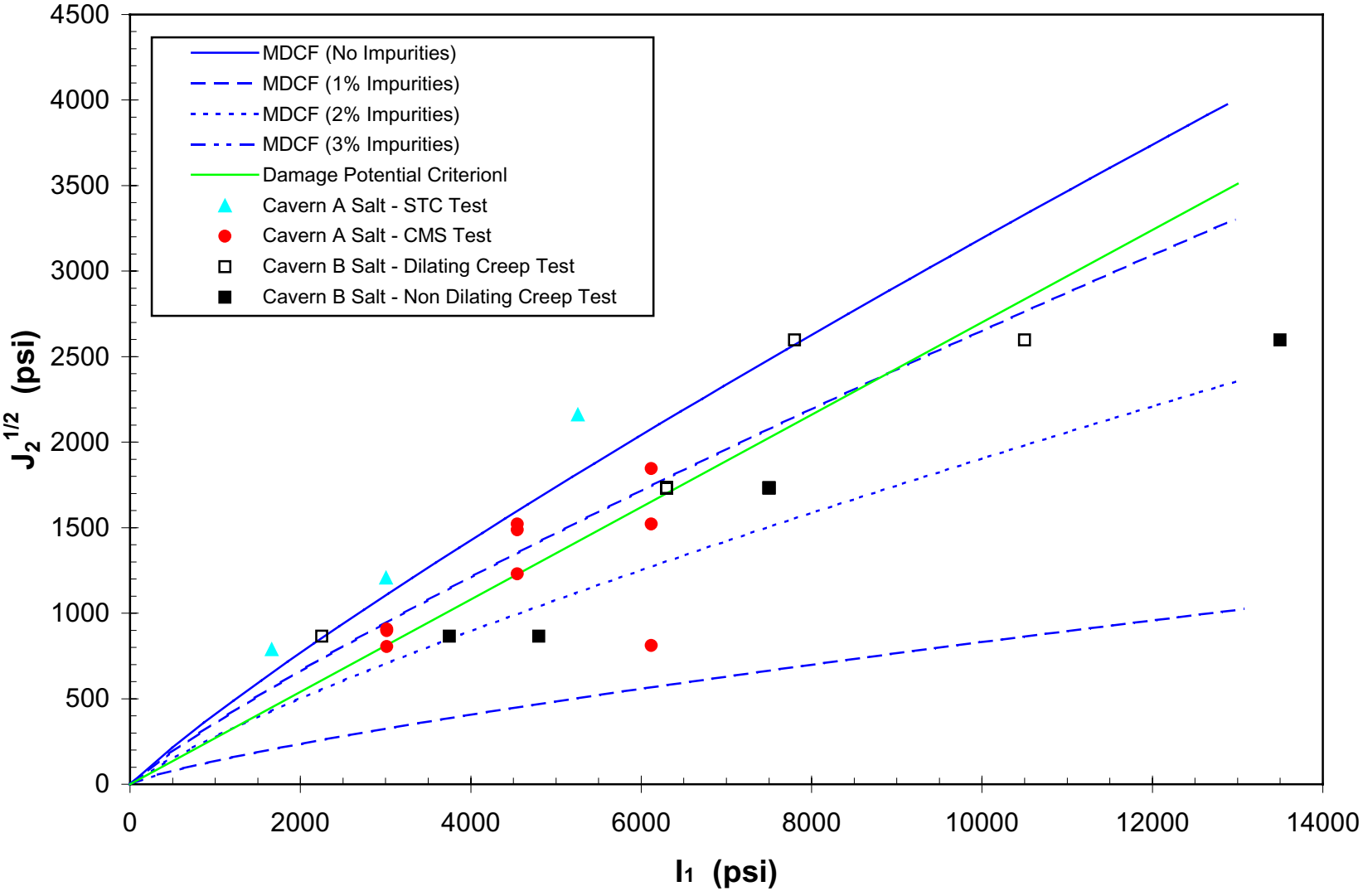

RSI-621-98-011

Figure 5-1. Dilation Boundaries Based on the MDCF and the Damage Potential Methods.

maximum, then pressurized to the maximum gas pressure immediately after dewatering. The maximum gas pressure for both caverns is 0.85 psi/foot of depth at the casing shoe.

The simulations for both caverns were then initiated with the caverns at maximum gas pressure. The gas in the caverns was completely withdrawn over a period of 10 days. For each cavern, the volume of dilating salt above the cavern midheight was calculated based on both the Damage Potential method and on the MDCF model with impurity levels of 0, 1, 2, and 3 percent. Also, because of the significant difference in volume between the two caverns, the volume of dilating salt was normalized by dividing by the cavern volume.

5.2 MODELING RESULTS

Figures 5-2 and 5-3 show the predicted normalized dilational salt volume above the cavern midheight versus gas pressure at the casing shoe for Cavern A and Cavern B, respectively. The predicted dilation volumes are significantly higher for Cavern A which is not as deep, but several times as large as Cavern B. For the MDCF model, there is a large difference between the 2 and 3 percent impurity levels in the predicted volumes of dilation for both caverns. The difference in predicted dilation volumes for impurity levels between 0 and 2 percent is much smaller. For both caverns, the dilation volume predicted with the Damage Potential method is between the dilation volumes predicted with the MDCF model with 1 and 2 percent impurities levels. Table 5-1 summarizes the casing shoe pressures at which salt dilation begins based on both dilation criteria (the Damage Potential method and the MDCF model method).

Figures 5-4 through 5-8 show the regions of predicted salt dilation based on the Damage Potential method and the MDCF model for the four impurity levels evaluated for Cavern A at a gas pressure of 0.07 psi/foot of depth at the casing shoe. This pressure represents 50 percent of the pressure required to initiate salt dilation in Cavern A with the Damage Potential method and is used as the minimum gas pressure for most of the simulations presented in Chapter 6.0. As shown in the figures, the volumes of salt predicted to dilate at this pressure are quite small for the Damage Potential method and also the MDCF model with impurity levels of 0 and 1 percent. In fact, as shown in Figure 5-2, none of the salt above the cavern midheight is predicted to dilate by the MDCF model with impurity levels of 0 and 1 percent. For the MDCF model with an impurity of 2 percent, a small volume of salt above the midheight is expected to dilate. At an impurity level of 3 percent, the volume of salt expected to dilate is substantially larger and surrounds the entire cavern.

Figures 5-9 through 5-13 show the regions of predicted salt dilation for Cavern B at a gas pressure of 0.11 psi/foot of depth at the casing shoe. This pressure represents 50 percent of the pressure required to initiate salt dilation in Cavern B with the Damage Potential method and is used as the minimum gas pressure for most of the simulations presented in Chapter 6.0. Again, the volumes of salt predicted to dilate at this pressure are quite small for the Damage Potential method and also the MDCF model with impurity levels of 0 and 1 percent. Only very

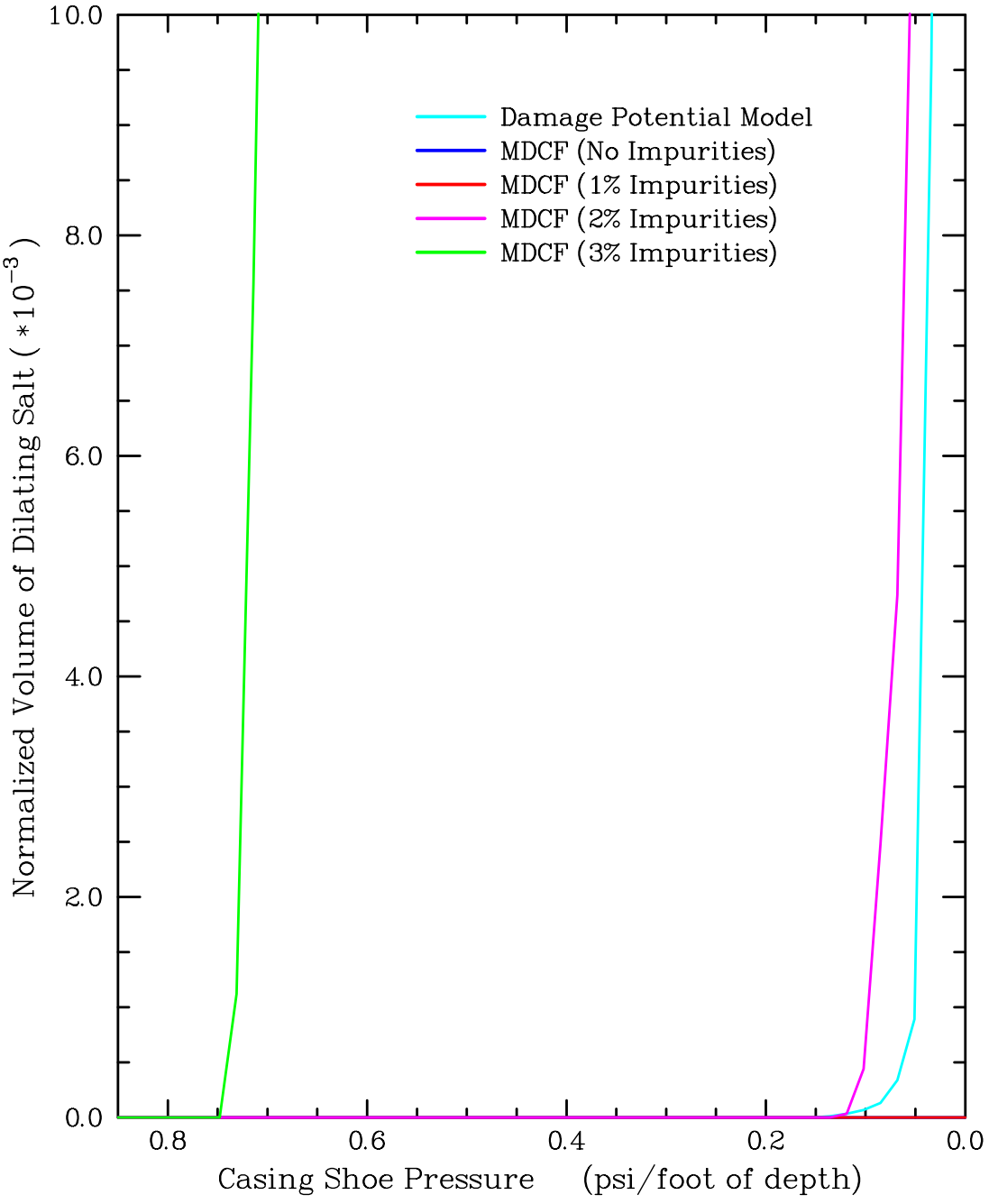

Figure 5-2. Predicted Normalized Volume of Dilating Salt Above Cavern A Midheight Versus Gas Pressure at the Casing Shoe.

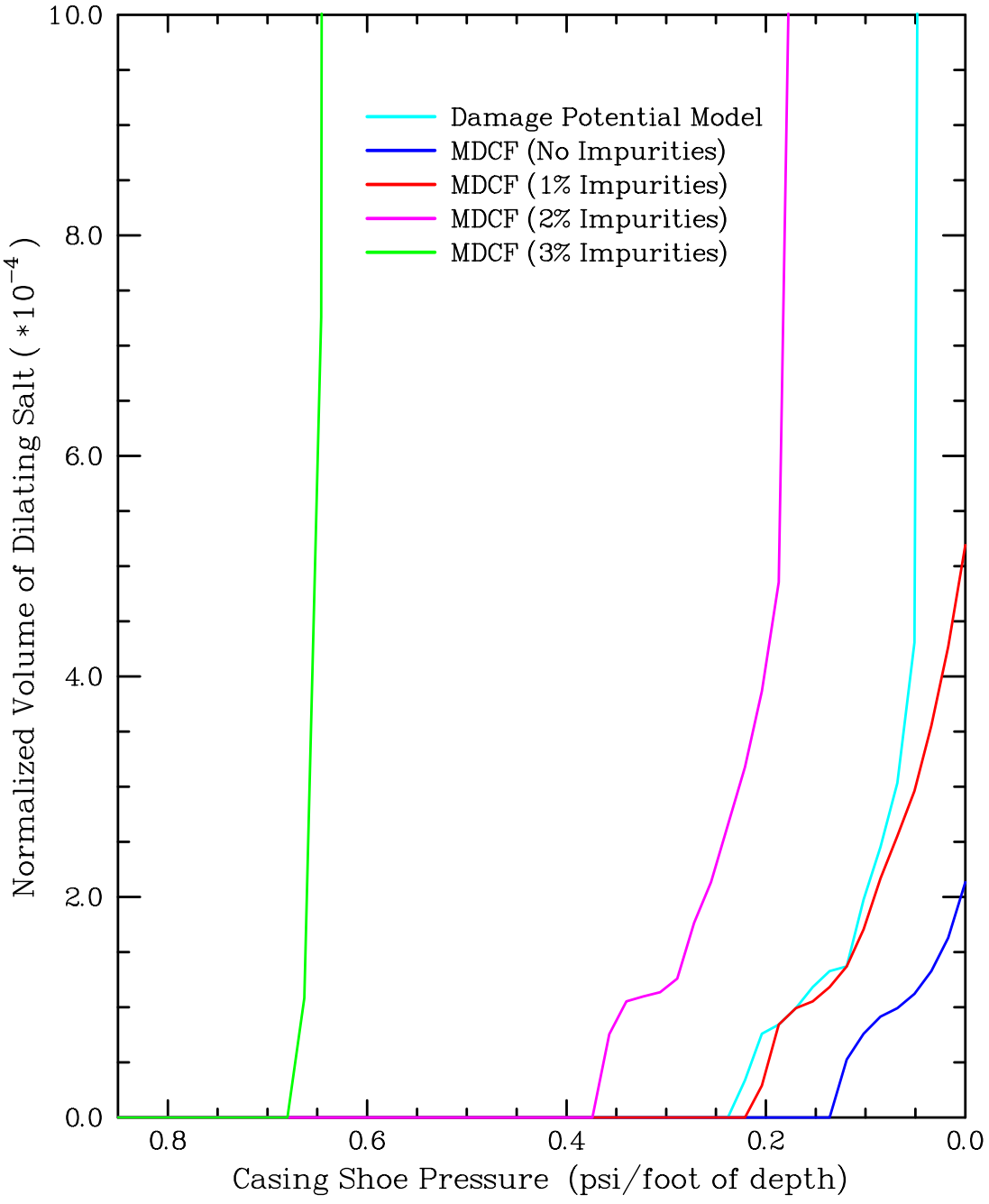

Figure 5-3. Predicted Normalized Volume of Dilating Salt Above Cavern B Midheight Versus Gas Pressure at the Casing Shoe.

small volumes of salt near the top of the cavern are predicted to dilate under these model assumptions. For the MDCF model with an impurity of 2 percent, a thin skin of salt around most of the cavern is predicted to dilate. As with Cavern A, at an impurity level of 3 percent, the volume of salt expected to dilate is very large and surrounds the entire cavern.

Table 5-1. Casing Shoe Pressures (psi/Foot of Depth) at Which Dilation Begins

Dilation Boundary Criterion		Cavern A	Cavern B
Damage Potential Method		0.14	0.22
MDCF Model	No Impurities	(a)	0.12
	1% Impurities	(a)	0.20
	2% Impurities	0.12	0.36
	3% Impurities	0.73	0.63

(a) No elements exceeded the dilation boundary criterion.

To ensure that the dilatancy boundary results presented here are not significantly impacted by the gas withdrawal rate used in the simulations, similar analyses were made with withdrawal periods of 5 days and 20 days. The predicted normalized volume of dilating salt above the cavern midheight versus gas pressure for Cavern A using the Damage Potential method dilatancy boundary is shown in Figure 5-14 for each of the three withdrawal periods evaluated. Figure 5-15 shows similar graphs for Cavern B. As shown in the figures, the results are nearly the same for all three withdrawal rates. Although not shown in the figures, results for the MDCF dilatancy boundaries also show very little dependence on the gas withdrawal rate.[3]

[3] The thermodynamics of the gas withdrawal are not included in these simulations. The change in gas temperature associated with rapid withdrawals could have an impact on the cavern periphery and well casings.

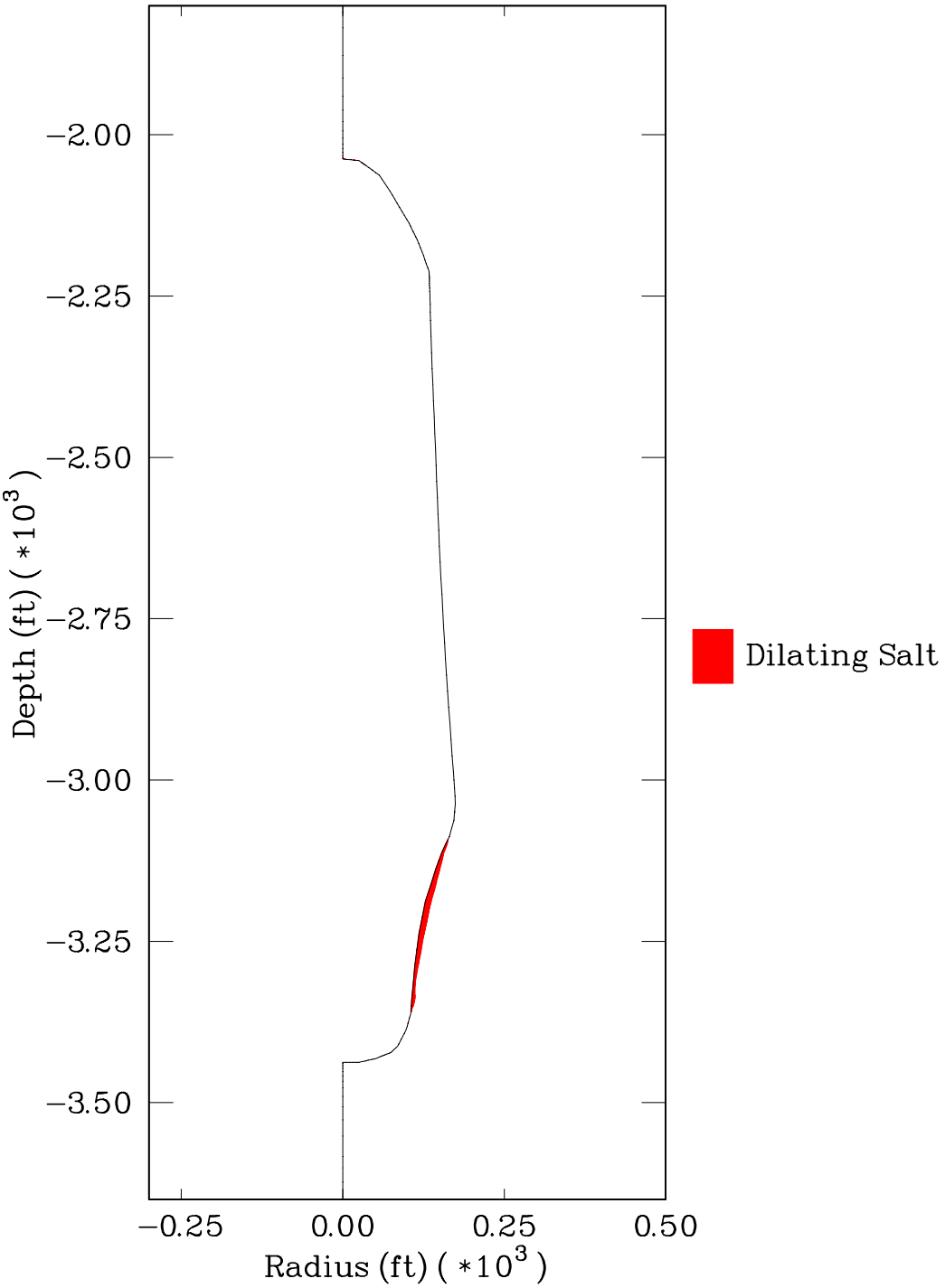

Figure 5-4. Regions of Predicted Salt Dilation Based on the Damage Potential Method for Cavern A at a Gas Pressure of 0.07 psi/Foot of Depth at the Casing Shoe.

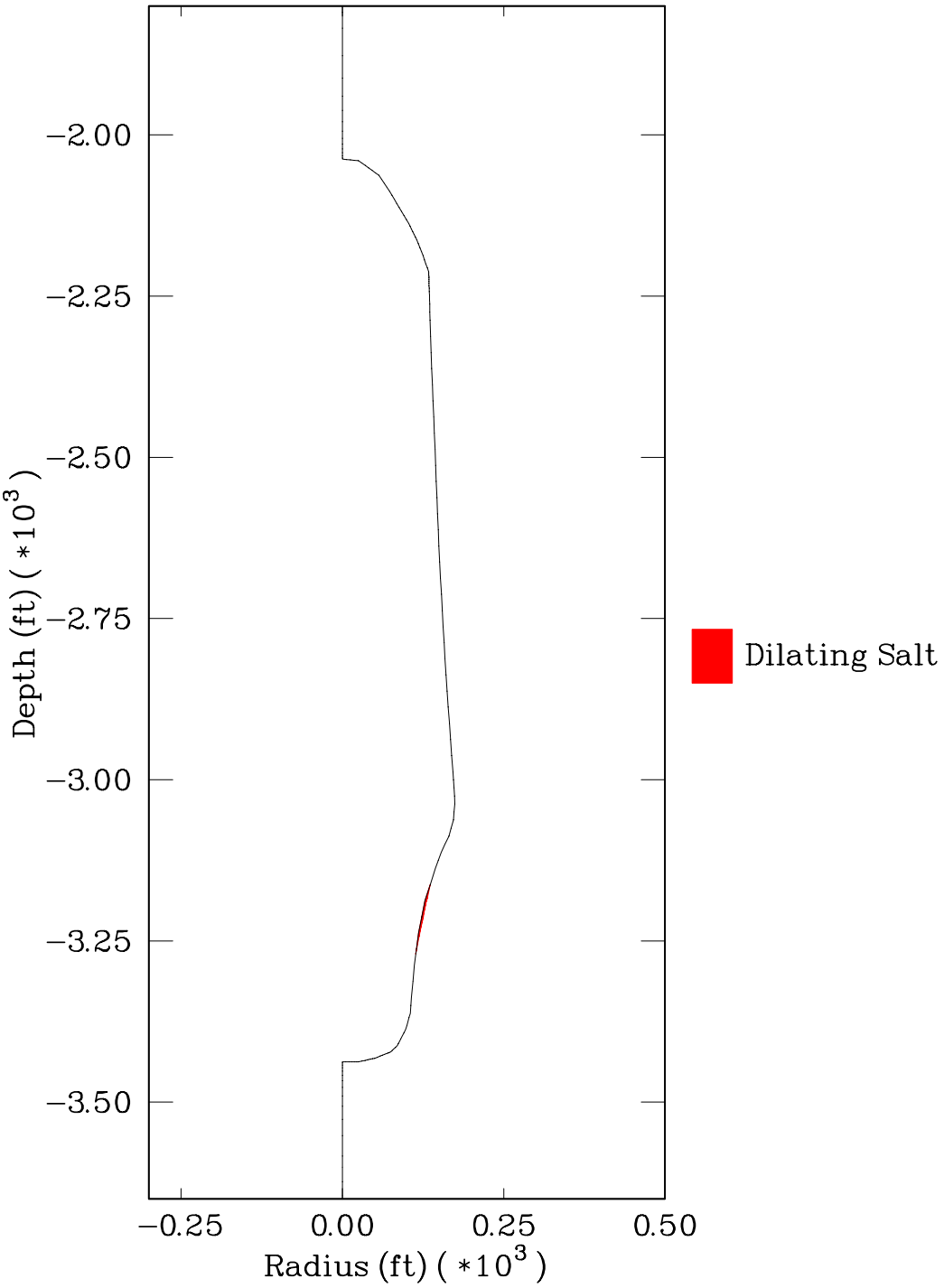

Figure 5-5. Regions of Predicted Salt Dilation Based on the MDCF Model With no Salt Impurity for Cavern A at a Gas Pressure of 0.07 psi/Foot of Depth at the Casing Shoe.

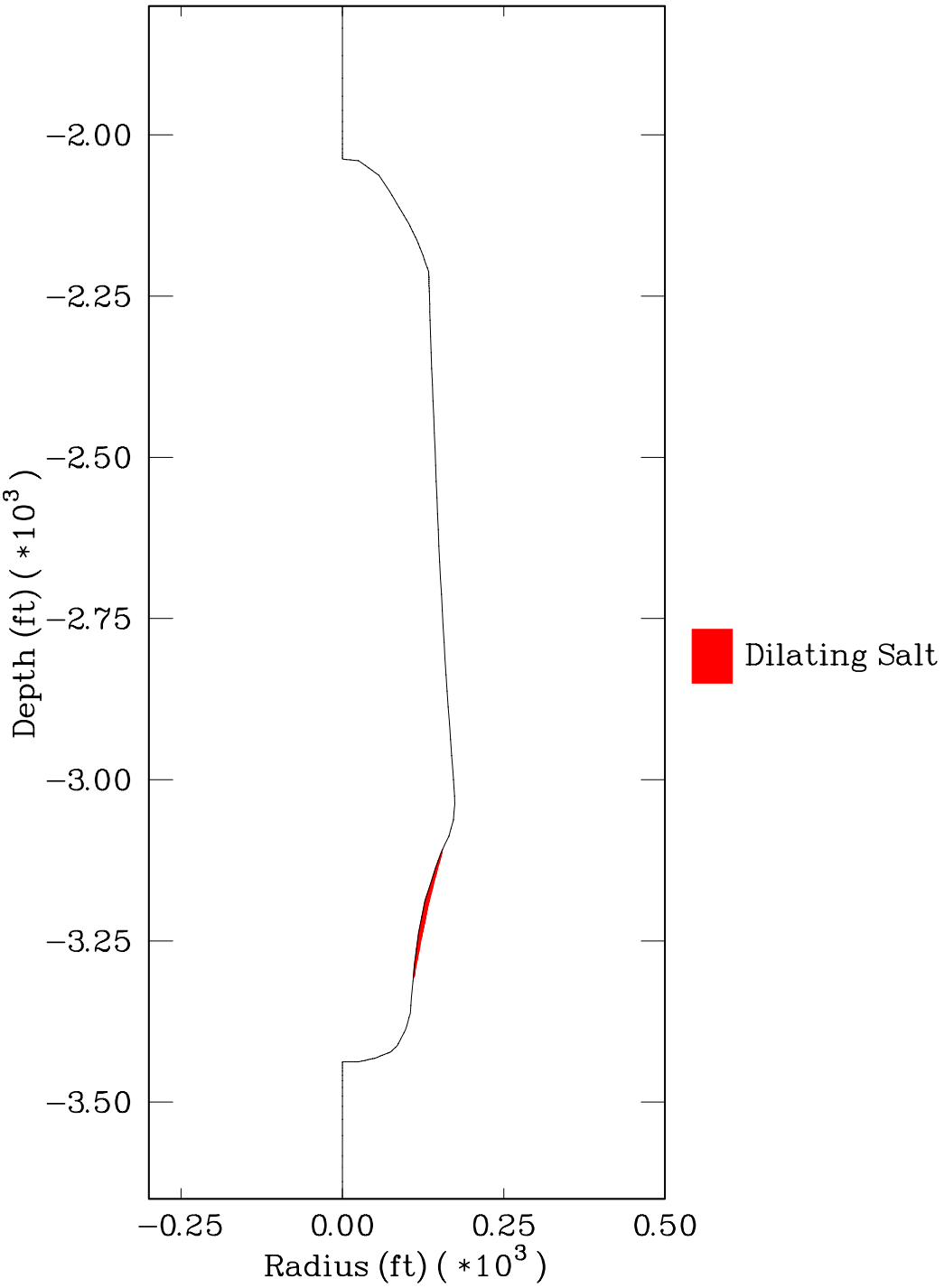

Figure 5-6. Regions of Predicted Salt Dilation Based on the MDCF Model With a Salt Impurity of 1 Percent for Cavern A at a Gas Pressure of 0.07 psi/Foot of Depth at the Casing Shoe.

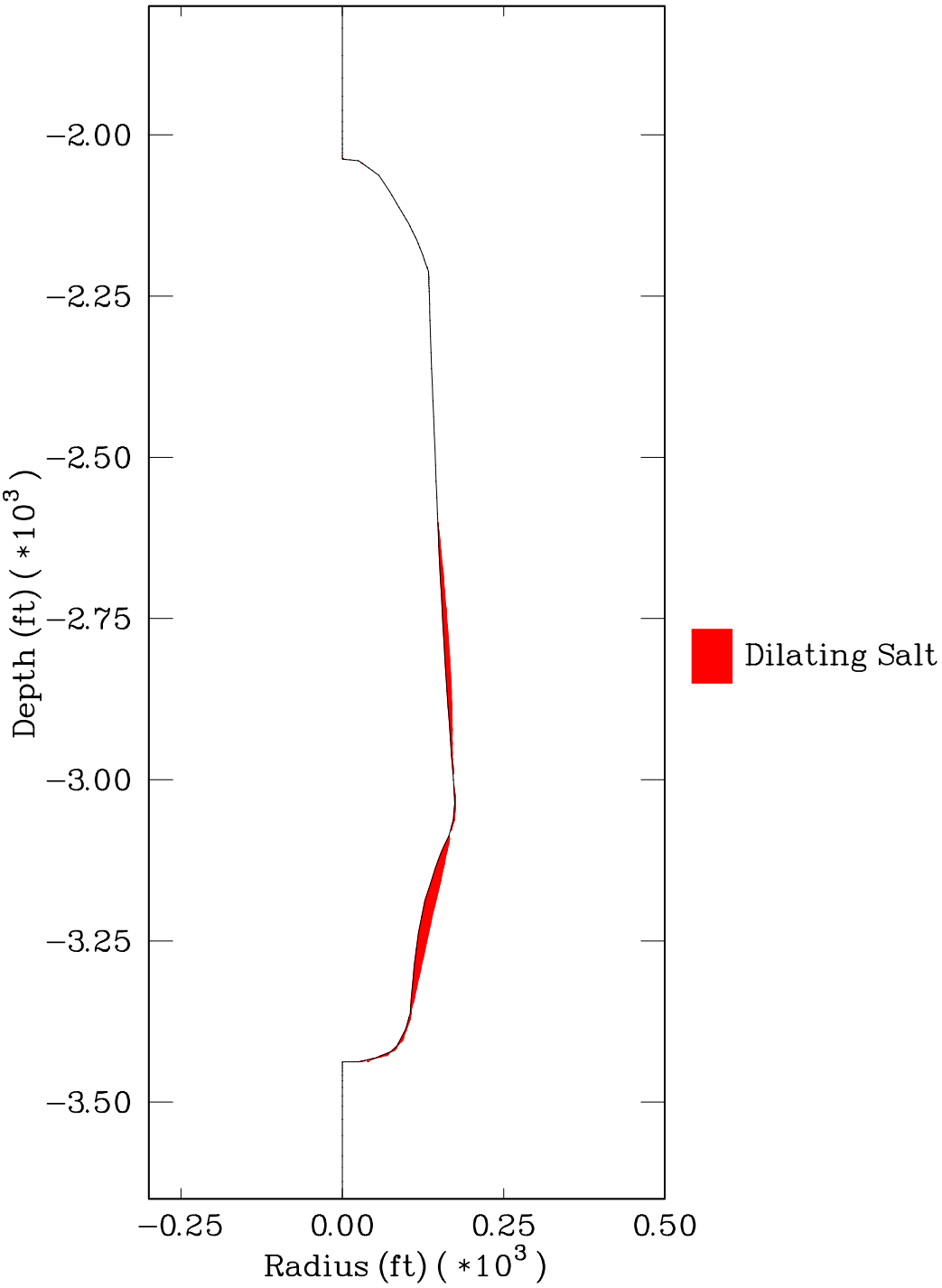

Figure 5-7. Regions of Predicted Salt Dilation Based on the MDCF Model With a Salt Impurity of 2 Percent for Cavern A at a Gas Pressure of 0.07 psi/Foot of Depth at the Casing Shoe.

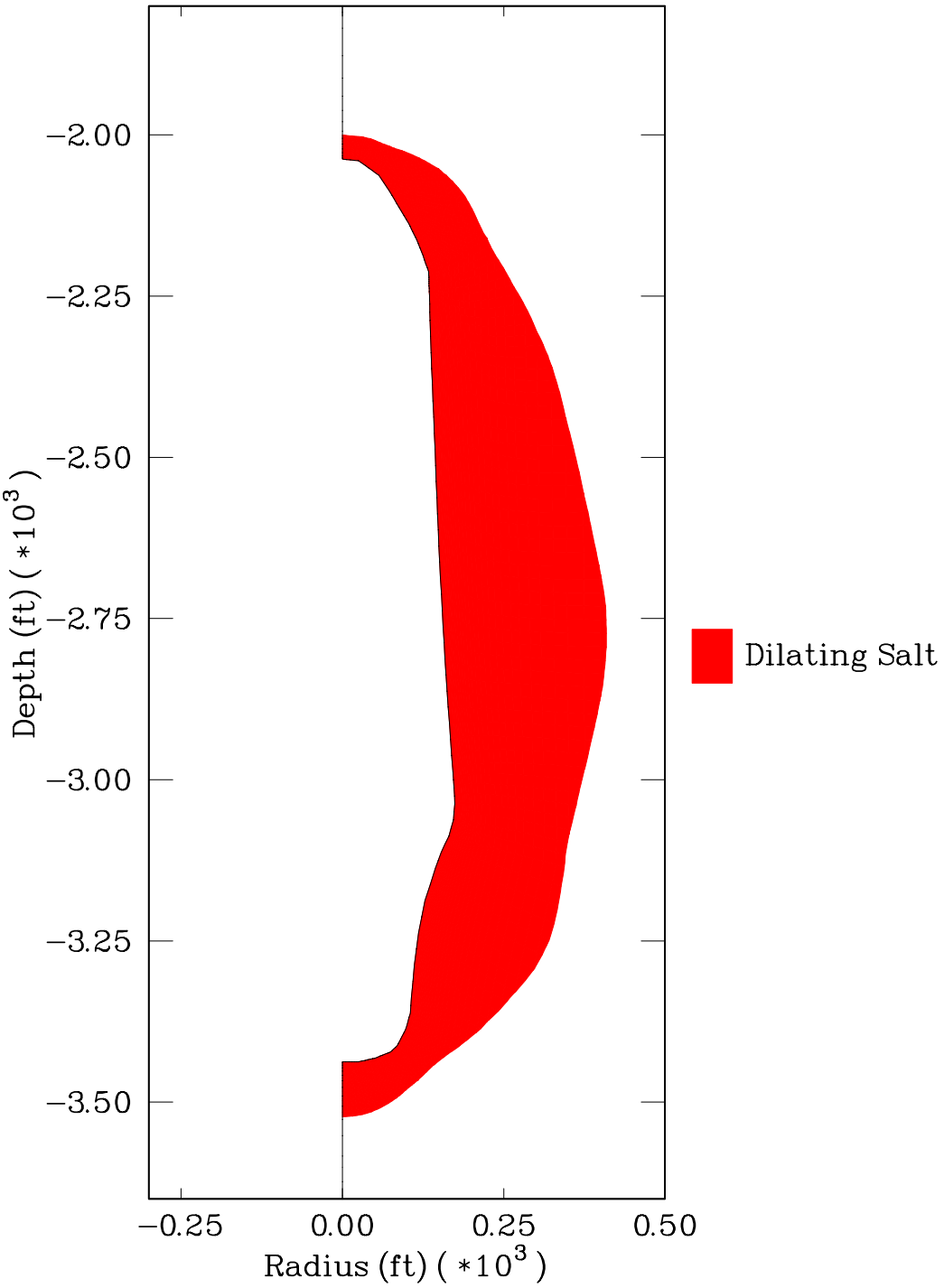

Figure 5-8. Regions of Predicted Salt Dilation Based on the MDCF Model With a Salt Impurity of 3 Percent for Cavern A at a Gas Pressure of 0.07 psi/Foot of Depth at the Casing Shoe.

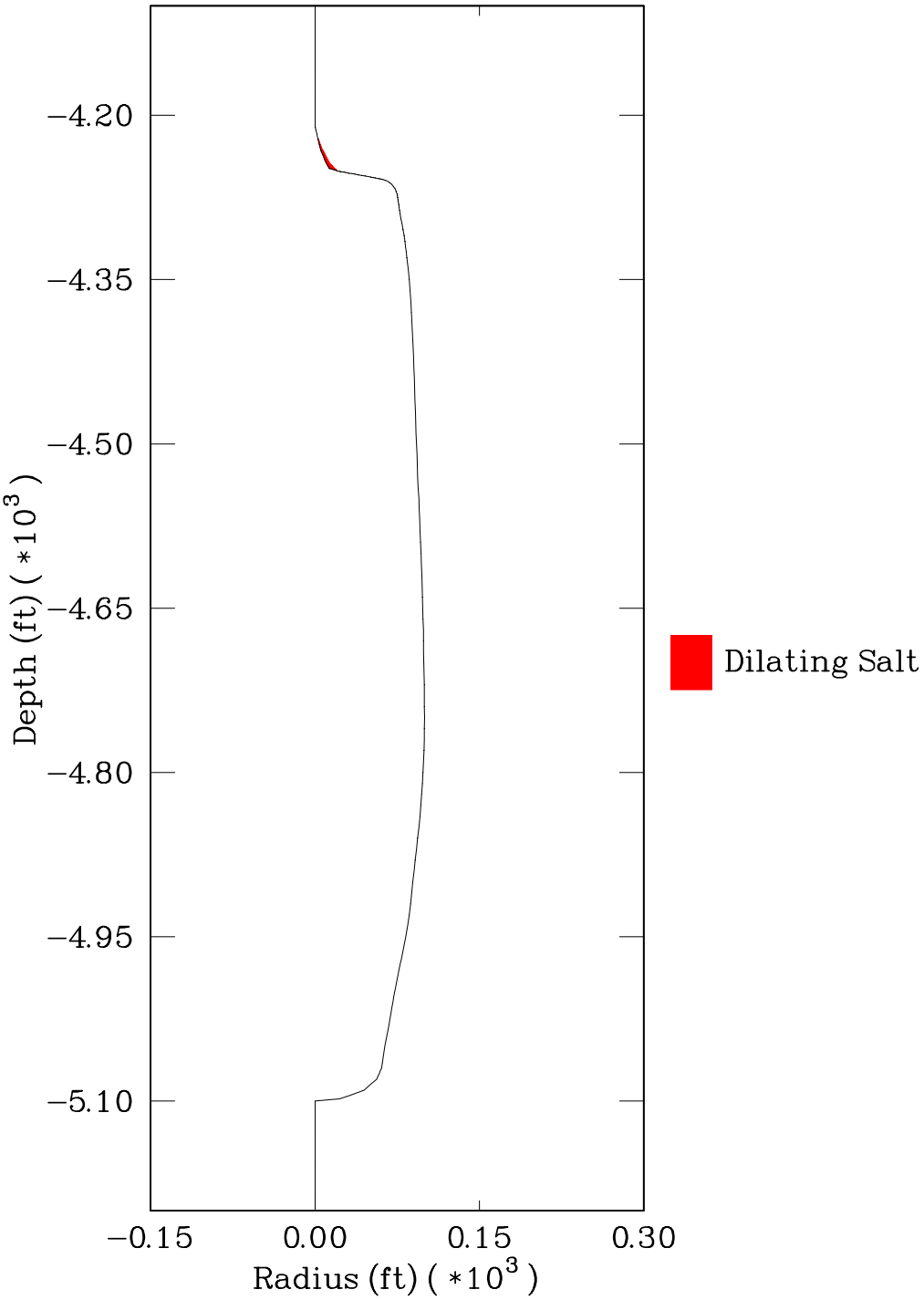

Figure 5-9. Regions of Predicted Salt Dilation Based on the Damage Potential Method for Cavern B at a Gas Pressure of 0.11 psi/Foot of Depth at the Casing Shoe.

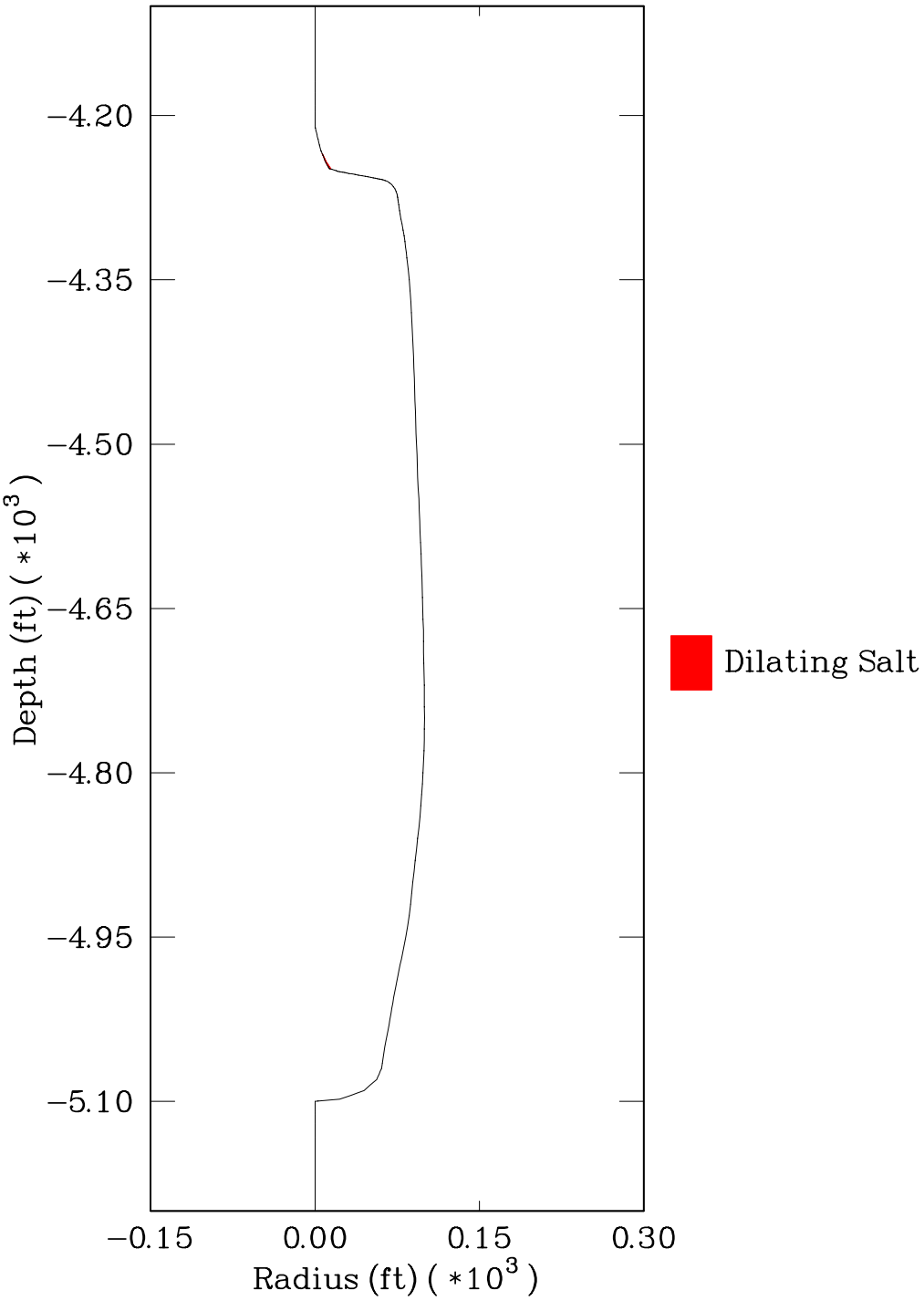

Figure 5-10. Regions of Predicted Salt Dilation Based on the MDCF Model With no Salt Impurity for Cavern B at a Gas Pressure of 0.11 psi/Foot of Depth at the Casing Shoe.

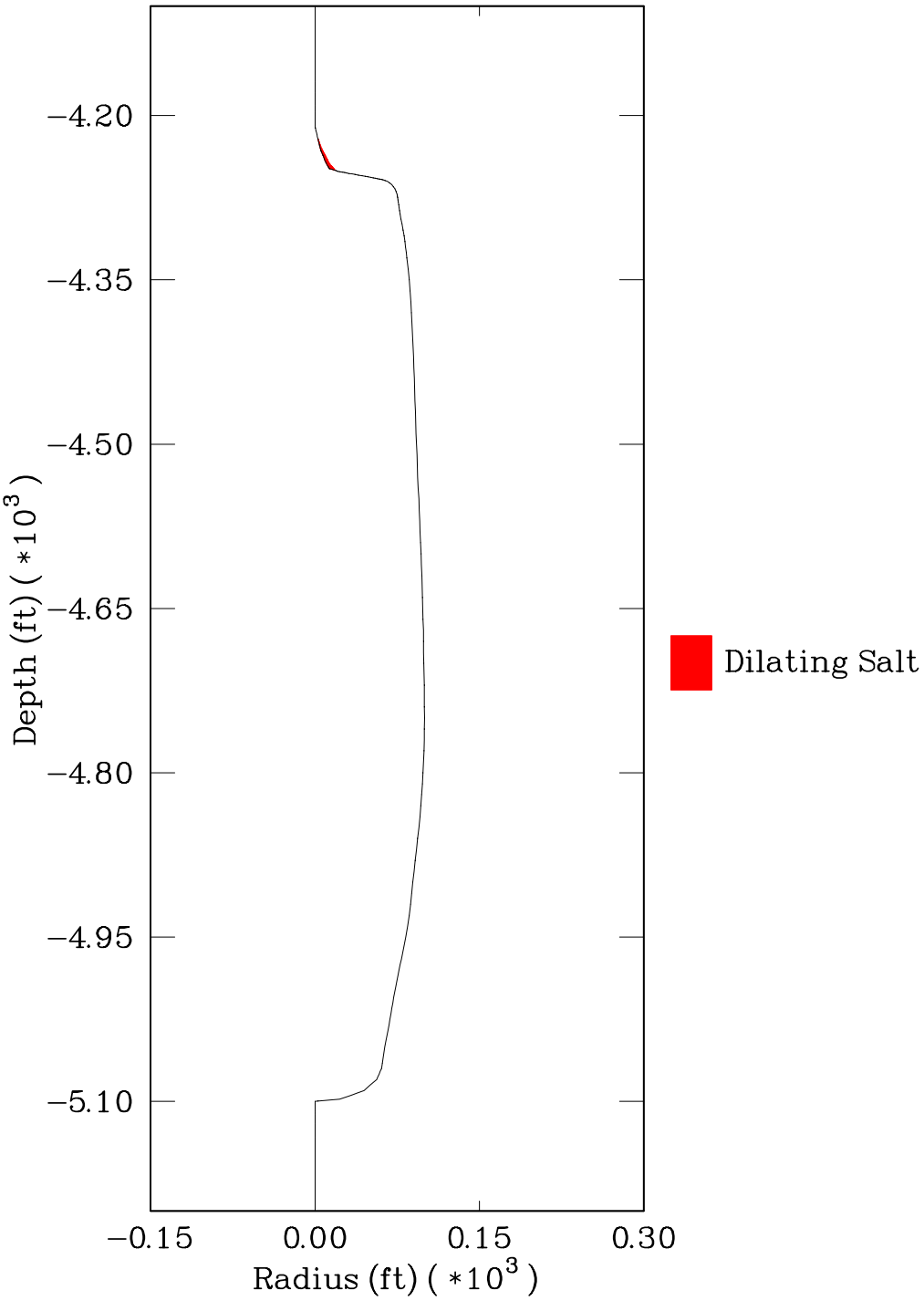

Figure 5-11. Regions of Predicted Salt Dilation Based on the MDCF Model With a Salt Impurity of 1 Percent for Cavern B at a Gas Pressure of 0.11 psi/Foot of Depth at the Casing Shoe.

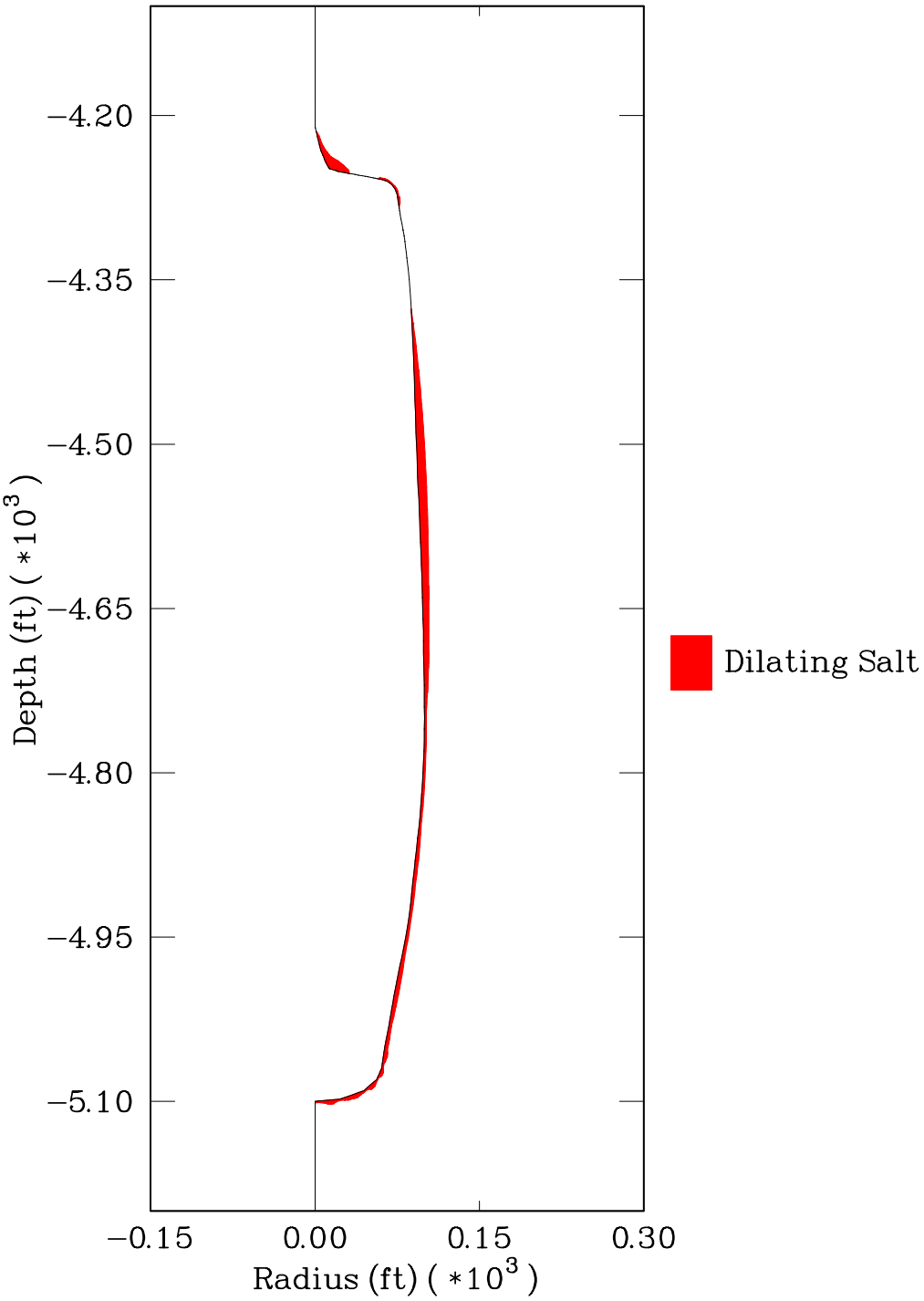

Figure 5-12. Regions of Predicted Salt Dilation Based on the MDCF Model With a Salt Impurity of 2 Percent for Cavern B at a Gas Pressure of 0.11 psi/Foot of Depth at the Casing Shoe.

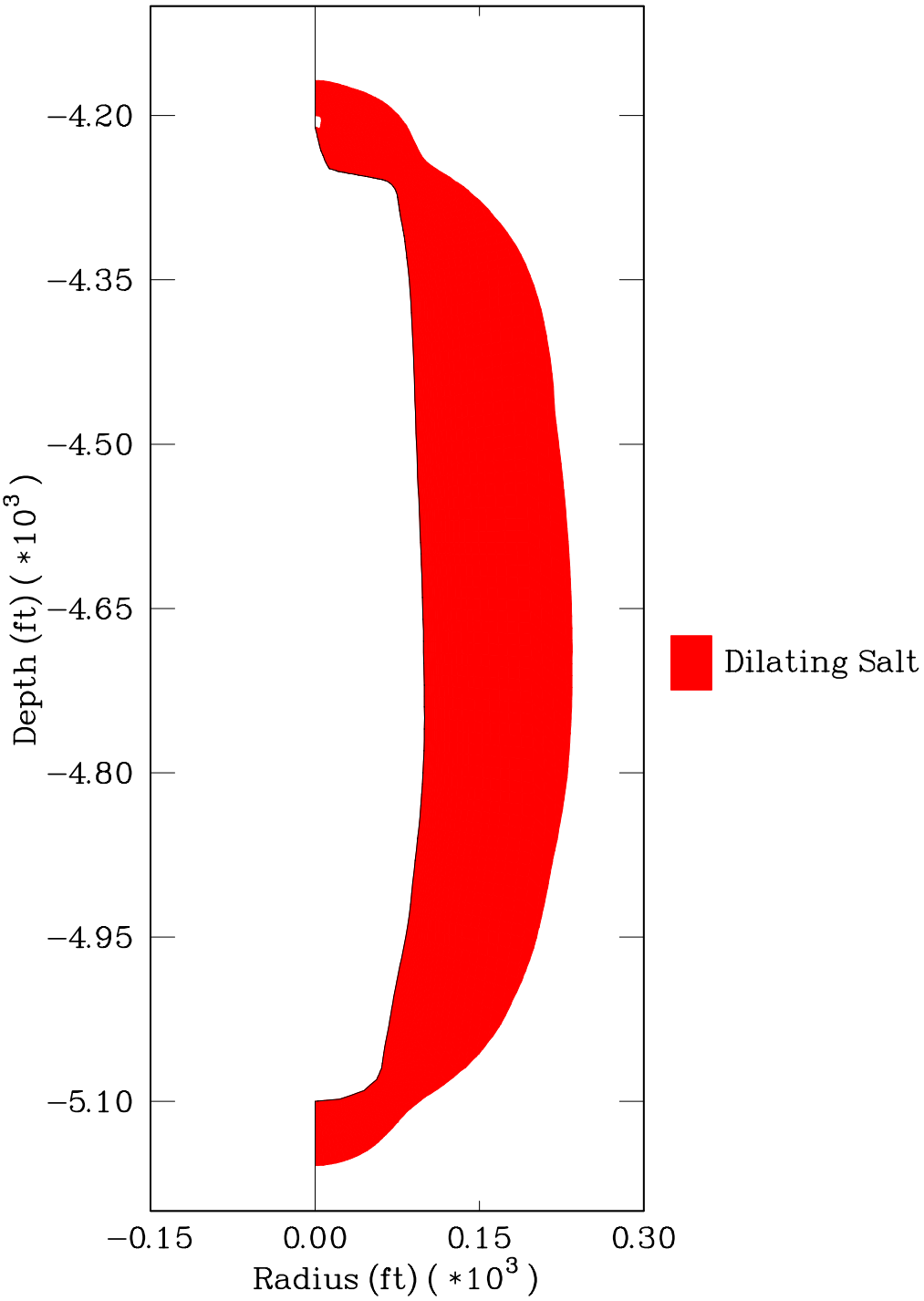

Figure 5-13. Regions of Predicted Salt Dilation Based on the MDCF Model With a Salt Impurity of 3 Percent for Cavern B at a Gas Pressure of 0.11 psi/Foot of Depth at the Casing Shoe.

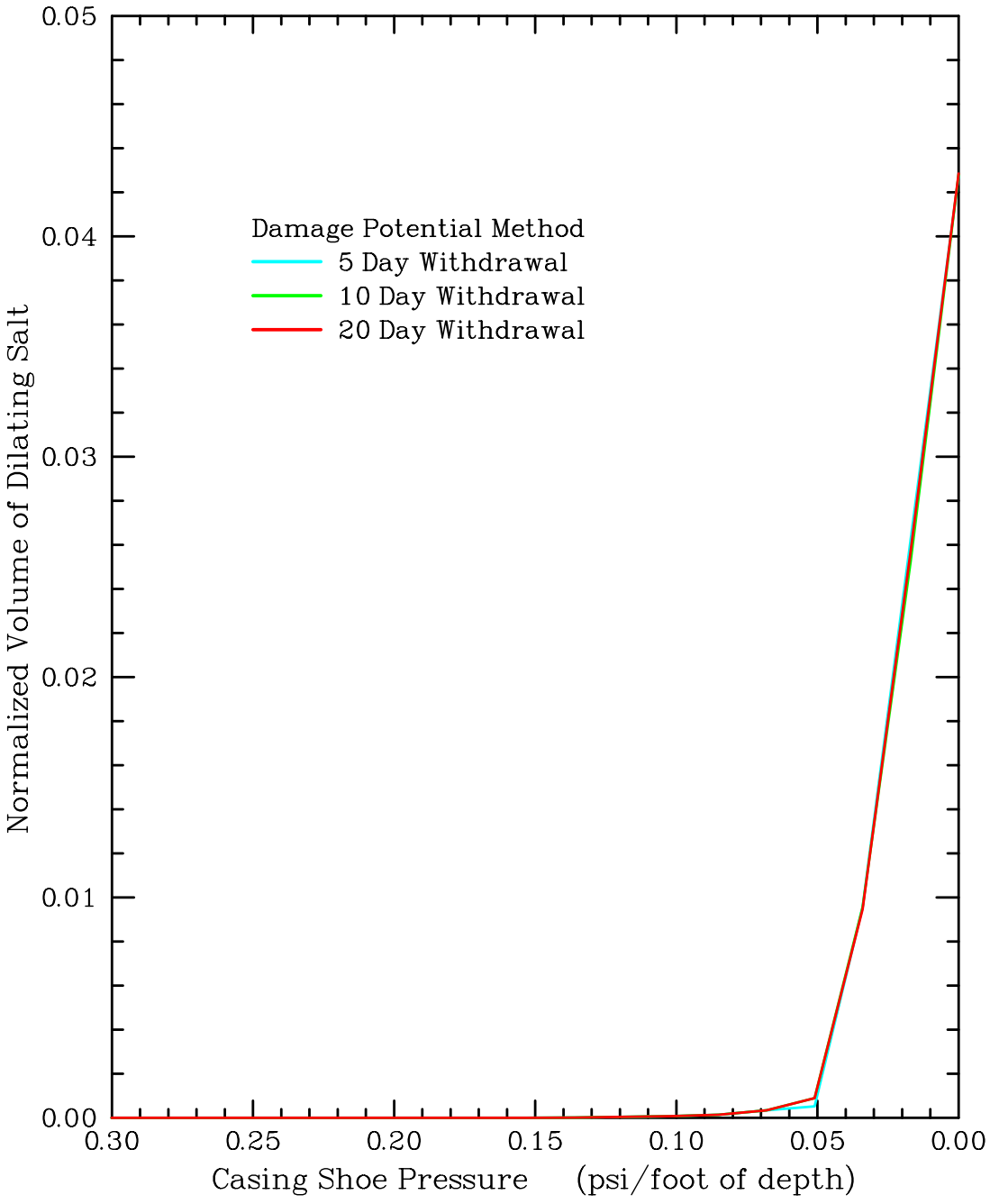

Figure 5-14. The Predicted Normalized Volume of Dilating Salt Above the Cavern Midheight Versus Gas Pressure for Cavern A Using the Damage Potential Method Dilatancy Boundary for Three Different Withdrawal Rates.

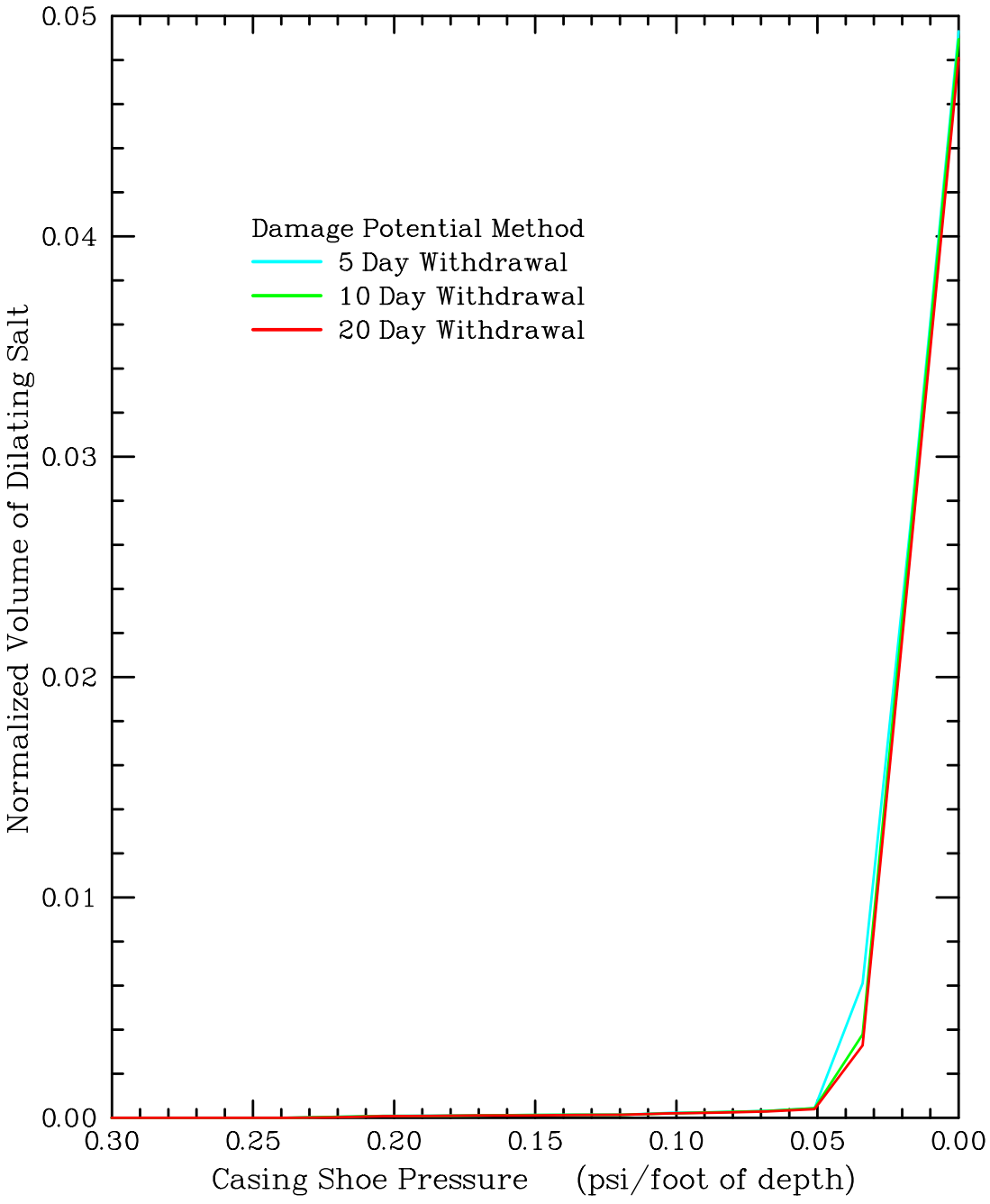

Figure 5-15. The Predicted Normalized Volume of Dilating Salt Above the Cavern Midheight Versus Gas Pressure for Cavern B Using the Damage Potential Method Dilatancy Boundary for Three Different Withdrawal Rates.

6.0 NUMERICAL RESULTS OF CAVERN STABILITY BASED ON DAMAGE QUANTIFICATION

6.1 PROBLEM DESCRIPTION

Cavern simulations were made in which both of the caverns are drawn down to pressures below that required to initiate dilation in the salt surrounding the caverns. As a conservative measure, the MDCF model was used with an impurity of 3 percent. As shown in the previous chapter, significant volumes of salt in both caverns are predicted to dilate at this impurity level. The dilatant volumetric strain was used to track accumulated dilation or damage and also healing in the salt surrounding the caverns during simulated natural gas storage cycles. The following were evaluated:

- Sensitivity to the minimum gas pressure.
- Time required to heal damaged salt.
- Maximum allowable time at minimum pressure.
- Long-term accumulation of salt damage.

Two natural gas service cycles were used in this study to evaluate the use of the MDCF constitutive model (see Figure 6-1). These cycles are referred to as Case 1 and Case 2 throughout this report. Both cycles start at the maximum gas pressure of 0.85 psi/foot of depth at the casing shoe and are drawn down to the minimum gas pressure over a period of 10 days. The Case 1 gas pressure cycle is held at minimum pressure for 10 days, and the Case 2 gas pressure cycle is held at minimum gas pressure for 100 days. After storage service at minimum gas pressure, both cycles repressurize the caverns back to maximum gas pressure over a 10-day period. Both cycles then hold maximum gas pressure for 100 days.

6.2 MODELING RESULTS

6.2.1 Evaluation of Minimum Gas Pressure

In the previous chapter, it was shown that using the Damage Potential dilation boundary, that salt dilation is expected when the minimum gas pressure at the casing shoe is 0.14 psi/foot of depth and 0.22 psi/foot of depth for Cavern A and Cavern B, respectively. These pressures were used as the baseline minimum gas pressures for use with the MDCF model simulations. To evaluate the effect of minimum pressure on damage and healing, simulations with the MDCF model were made at minimum gas pressures that are 50 and 90 percent of these baseline values.

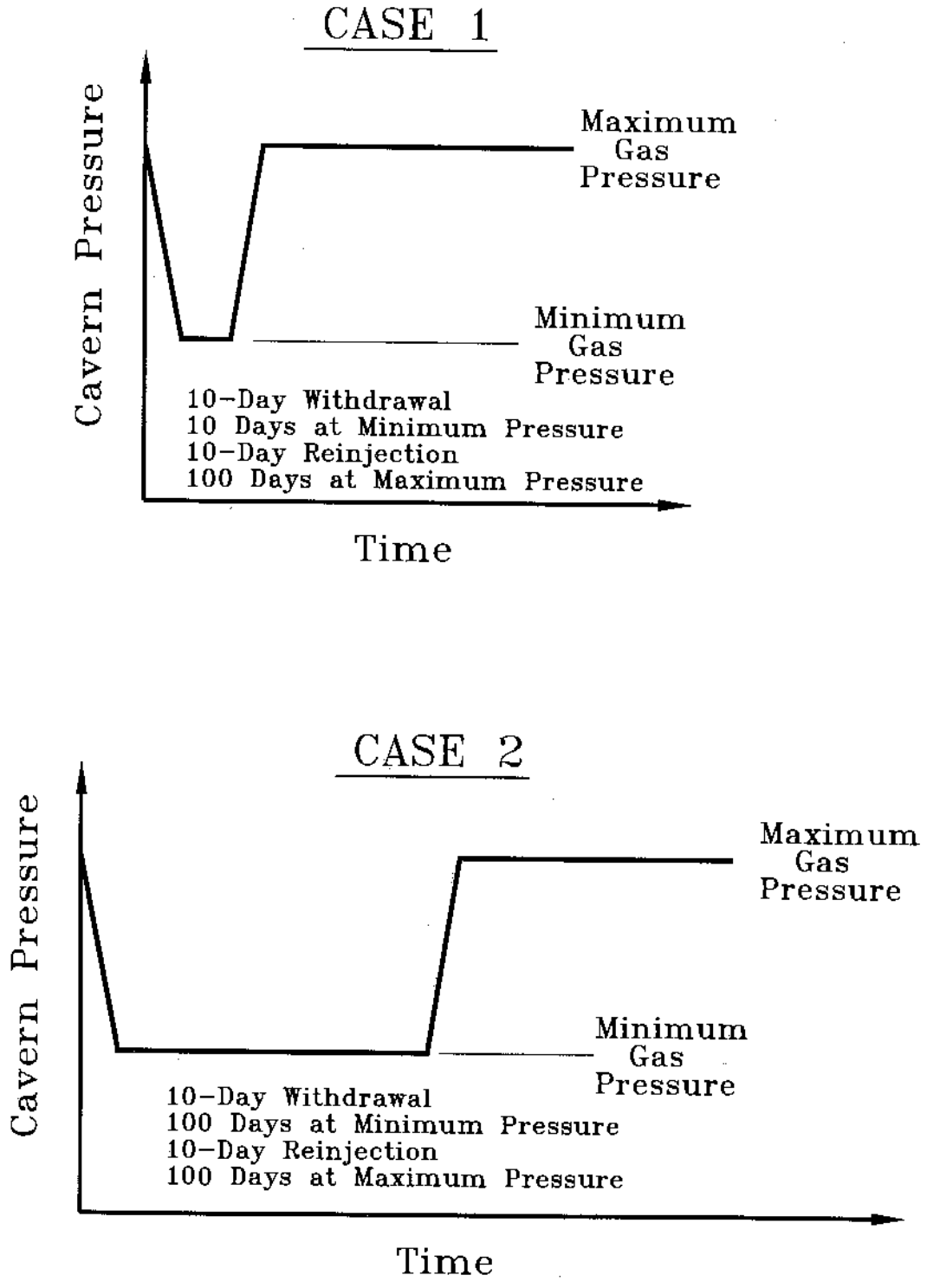

Figure 6-1. Natural Gas Service Cycles Analyzed.

Figure 6-2 shows the normalized volume of salt above the cavern midheight which exceeds 0.1 με (microstrains) throughout a single Case 1 gas pressure cycle for Cavern A. No dilatant volumetric strain occurs until about halfway into the 10-day pressure drawdown. The volume of salt with dilatant volumetric strain greater than 0.1 με then rapidly increases throughout the rest of the withdrawal period. This volume continues to increase at a somewhat slower rate during the 10-day period at minimum pressure. The maximum volume of salt with dilatant volumetric strains occurs at the end of the 10-day period at minimum pressure. This volume then starts to decrease about midway into the 10-day repressurization when the stresses are conducive to healing. At the end of the repressurization, the healing rate decreases considerably. As shown in the figure, the volume of salt which experiences dilatant volumetric strain is strongly dependent on the minimum gas pressure. The maximum volume of salt during the cycle which experiences a dilatant volumetric strain of more than 0.1 με is about 20 percent higher for the simulation with a minimum gas pressure that is 50 percent of the baseline pressure than for that which is at 90 percent of the baseline pressure. Likewise, the time until complete healing of the dilatant volumetric strain is dependent on the minimum gas pressure. The volumetric strain for the simulation with a minimum pressure of 50 percent of the baseline was completely healed about 80 days after repressurization; whereas, the simulation with a minimum gas pressure of 90 percent of the minimum only required about 40 days to completely heal the dilatant strain.

Figure 6-3 shows the normalized volume of salt above the cavern midheight which exceeds 0.1 με throughout a single Case 1 gas pressure cycle for Cavern B for the two minimum pressures evaluated. Although the results are similar, larger differences are seen between the two pressures modeled. For Cavern B, the maximum volume of salt that experiences more than 0.1 με is about 50 percent larger for the simulation with a minimum gas pressure of 50 percent of the baseline pressure than that with a minimum gas pressure of 90 percent of the baseline pressure. The volumetric strain for the simulation with a minimum pressure of 50 percent of the baseline was completely healed about 70 days after repressurization; whereas, the simulation with a minimum gas pressure of 90 percent of the minimum only required about 40 days to completely heal the dilatant strain.

It is interesting to note that after repressurization of Cavern B, there is a period where no healing takes place. This occurs because the MDCF damage stress measure actually increases during the later portion of the repressurization. Recall from Section 3.2.4 that damage occurs when the damage stress measure is greater than zero and that healing occurs when it is less than zero. Figure 6-4 shows the MDCF damage stress measure along with the radial, vertical, and tangential stresses for an element in the cavern wall during the gas cycle. At any given time, the maximum principal stress is essentially equal to the largest of the three stress components, and the minimum principal stress is equal to the smallest of the three stress components. As shown in the figure, the damage stress measure nearly tracks the maximum principal stress. During drawdown and the period at minimum pressure, the maximum principal stress is equal to the radial stress. This is also true at the start of the repressurization period. However, as the gas pressure is increased, the tangential stresses around the

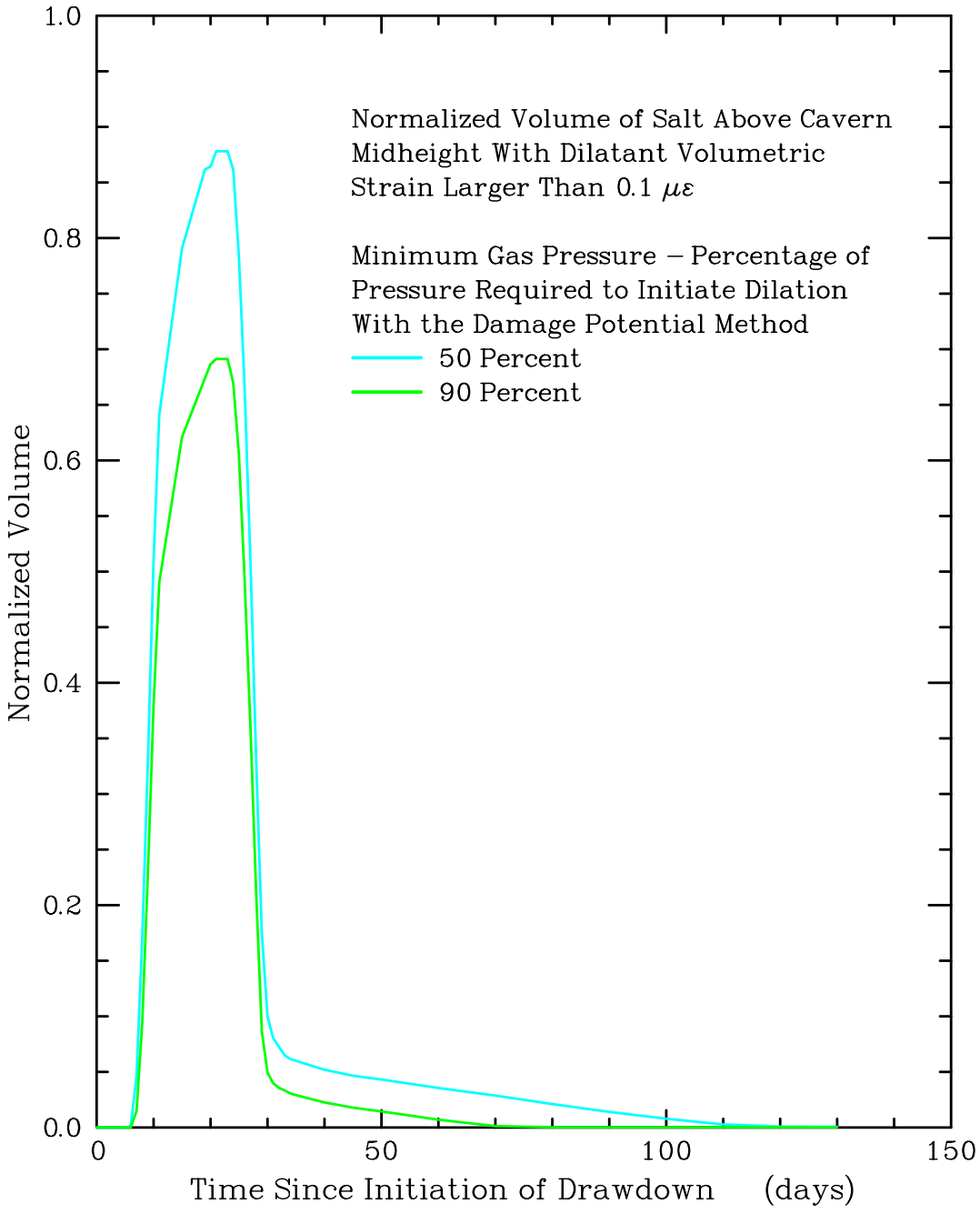

Figure 6-2. Normalized Volume of Salt Above the Cavern Midheight With Dilatant Volumetric Strain Greater Than 0.1 με Throughout a Single Case 1 Gas Pressure Cycle for Cavern A.

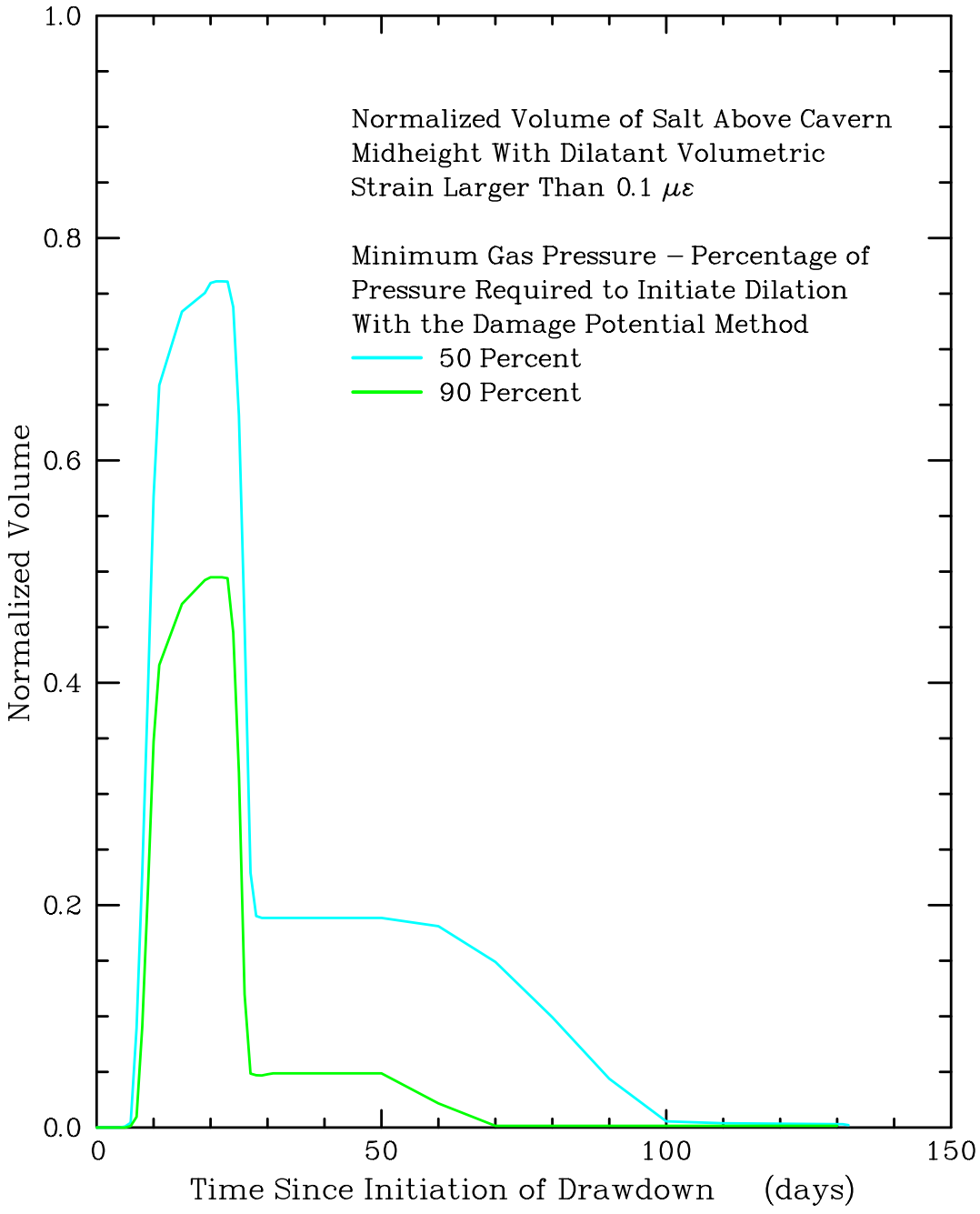

Figure 6-3. Normalized Volume of Salt Above the Cavern Midheight With Dilatant Volumetric Strain Greater Than 0.1 με Throughout a Single Case 1 Gas Pressure Cycle for Cavern B.

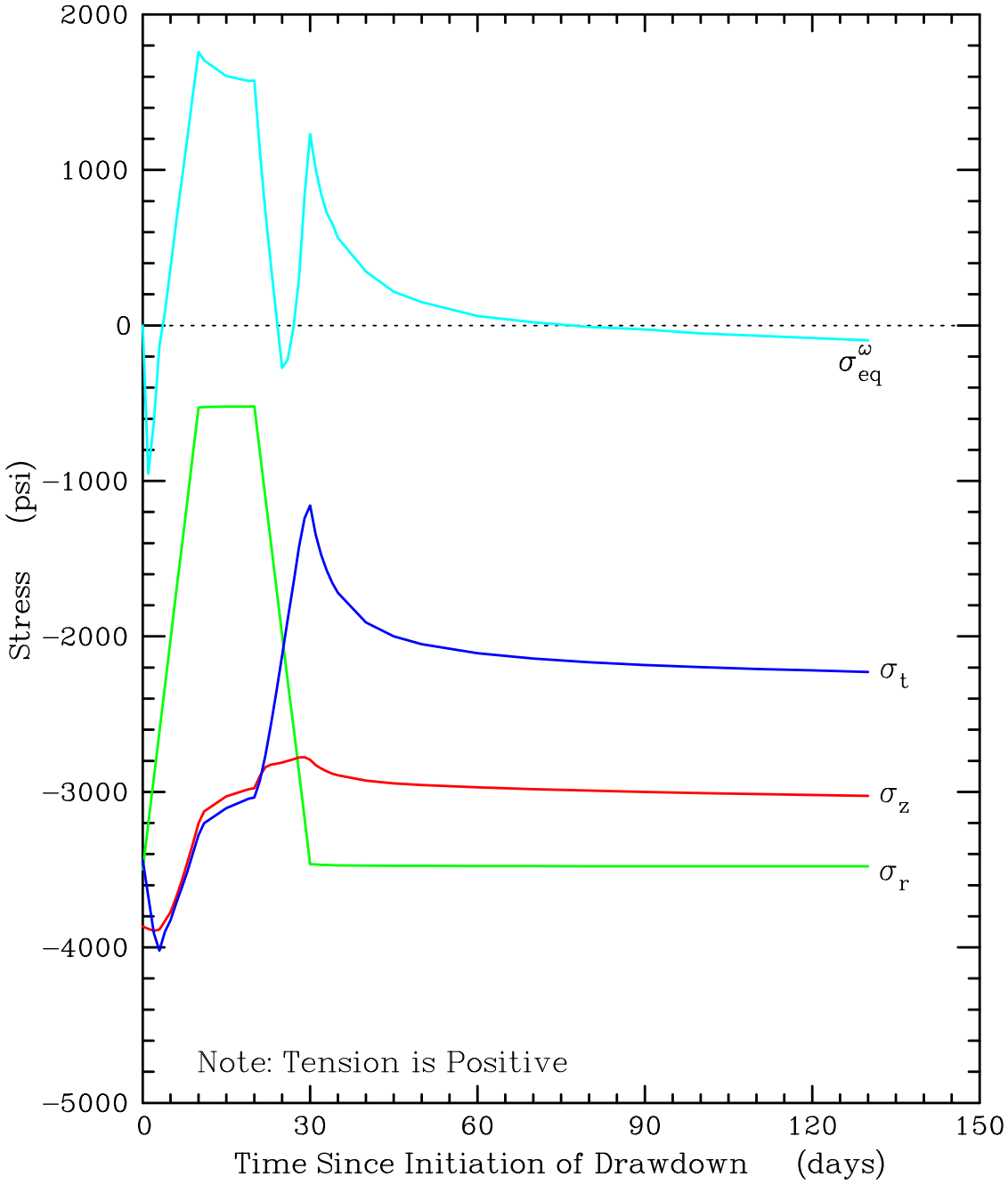

Figure 6-4. MDCF Damage Stress Measure and the Radial, Vertical, and Tangential Stresses for an Element in the Cavern Wall During a Single Case 1 Gas Pressure Cycle.

cavern become less compressive than the radial stress which is becoming more compressive. At the point where these stresses cross, the maximum principal stress begins to increase. The damage stress measure also increases to the point where healing is stalled. After the cavern is fully pressurized, the maximum principal (tangential) stress becomes more compressive as the salt creeps to equalize the stresses. As the maximum principal stress becomes more compressive, the damage stress measure drops below zero and healing commences. This same phenomenon occurs in Cavern A, but not severely enough to stop healing during pressurization. The reverse phenomenon is seen during the drawdown periods of consecutive gas cycles.

6.2.2 Maximum Allowable Time at Minimum Gas Pressure

The maximum allowable time at minimum gas pressure was evaluated by monitoring the value of the MDCF damage state variable, ω, as a function of time with the caverns at minimum gas pressure. As ω increases, the creep rate also increases, and eventually tertiary creep occurs, followed by creep rupture. In Section 3.2.7, it was shown that based on laboratory testing, an ω value of 0.0025 can be used as a conservative measure of the point at which creep rupture occurs. To eliminate the geometrical effects, ω was monitored at a location on the cavern wall in the upper portion of each cavern. For these simulations, the gas pressure was reduced from maximum to minimum over a 10-day period and then held at the minimum value for the remainder of the simulation. Figure 6-5 shows the ω value for this location in Cavern A as a function of time at minimum gas pressure for the two minimum gas pressures evaluated. With a minimum gas pressure of 90 percent of the baseline pressure, damage accumulates very slowly and does not exceed the creep rupture value during the entire 10-year period at minimum pressure. At a minimum gas pressure of 50 percent of the baseline pressure, the salt does not reach the rupture limit until about 2,550 days or about 7 years at minimum pressure. The results are significantly different for Cavern B, as shown in Figure 6-6. In Cavern B, creep rupture occurs after about 12 and 65 days at minimum gas pressure for minimum gas pressures of 50 and 90 percent of the baseline pressure, respectively.

6.2.3 Long-Term Damage Accumulation

Several simulations were made to evaluate the accumulation of damage over several natural gas cycles. For each cavern, five consecutive cycles of both Cycle 1 and Cycle 2 were simulated for each cavern. The minimum gas pressure used in the simulations was 50 percent of the baseline minimum gas pressure.

Figures 6-7 and 6-8 show the normalized volume of salt above the cavern midheight with a dilatant volumetric strain greater than 0.1 $\mu\varepsilon$ for Cavern A for five consecutive Case 1 and Case 2 cycles, respectively. For the Case 1 cycles with a 10-day period at minimum gas pressure, all of the salt has a dilatant volumetric strain of less than 0.1 $\mu\varepsilon$ at the end of the first cycle. However, after subsequent cycles, a small volume of salt still has a dilatant volumetric strain exceeding 0.1 $\mu\varepsilon$. In fact, the volume of dilated salt at the end of each cycle

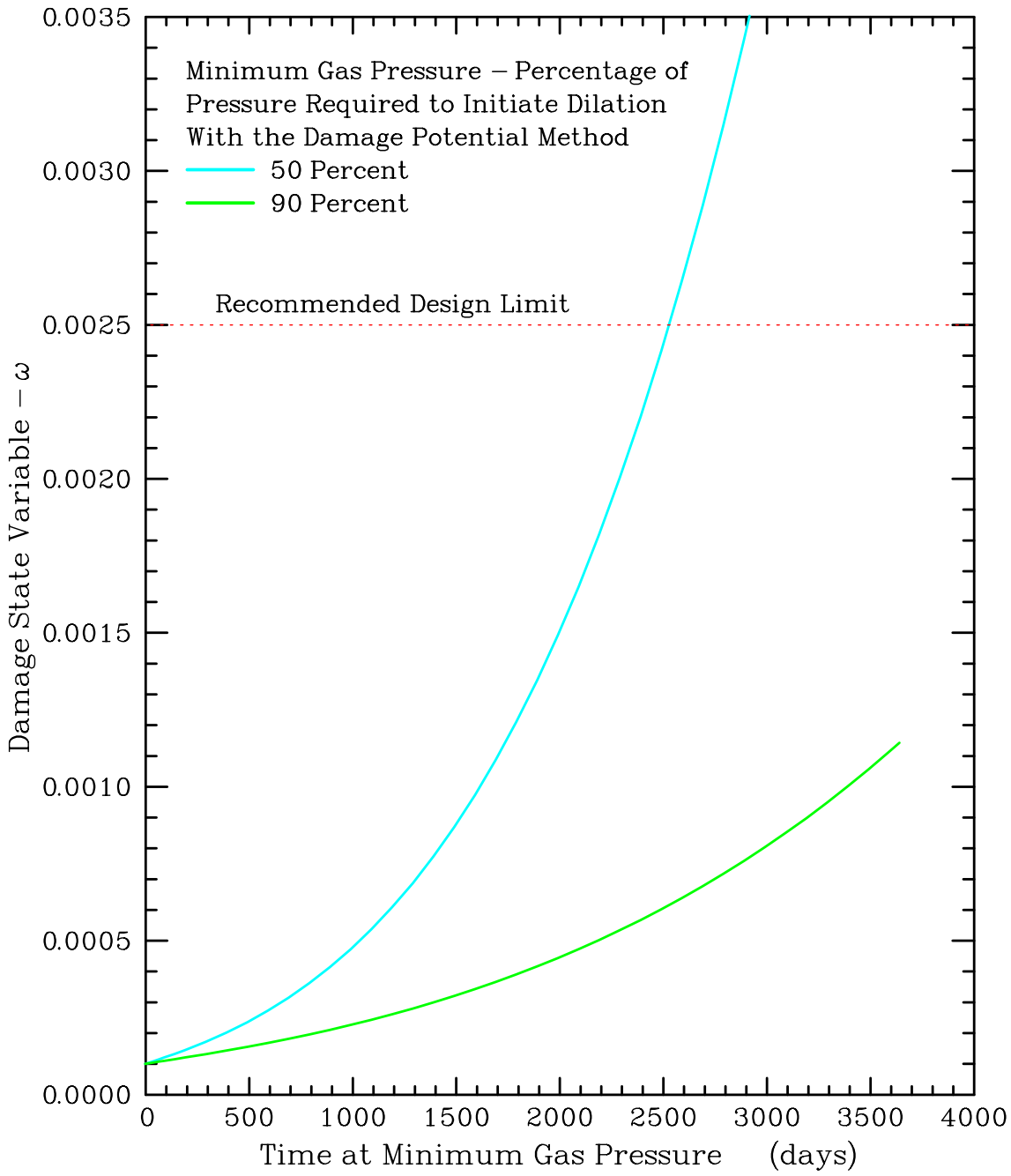

Figure 6-5. MDCF Damage State Variable in the Wall of Cavern A as a Function of Time at Minimum Gas Pressure for the Two Minimum Gas Pressures Evaluated.

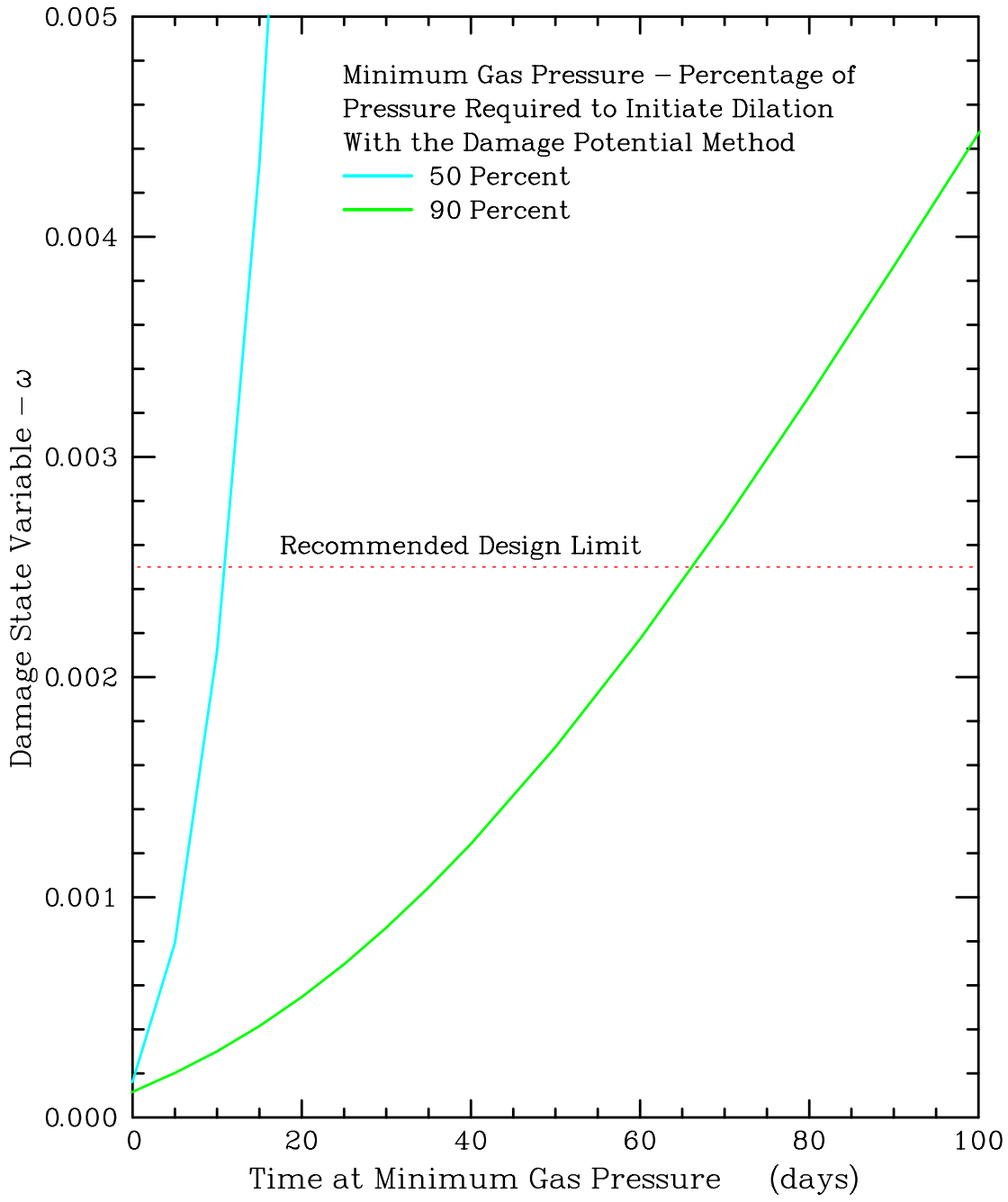

Figure 6-6. MDCF Damage State Variable in the Wall of Cavern B as a Function of Time at Minimum Gas Pressure for the Two Minimum Gas Pressures Evaluated.

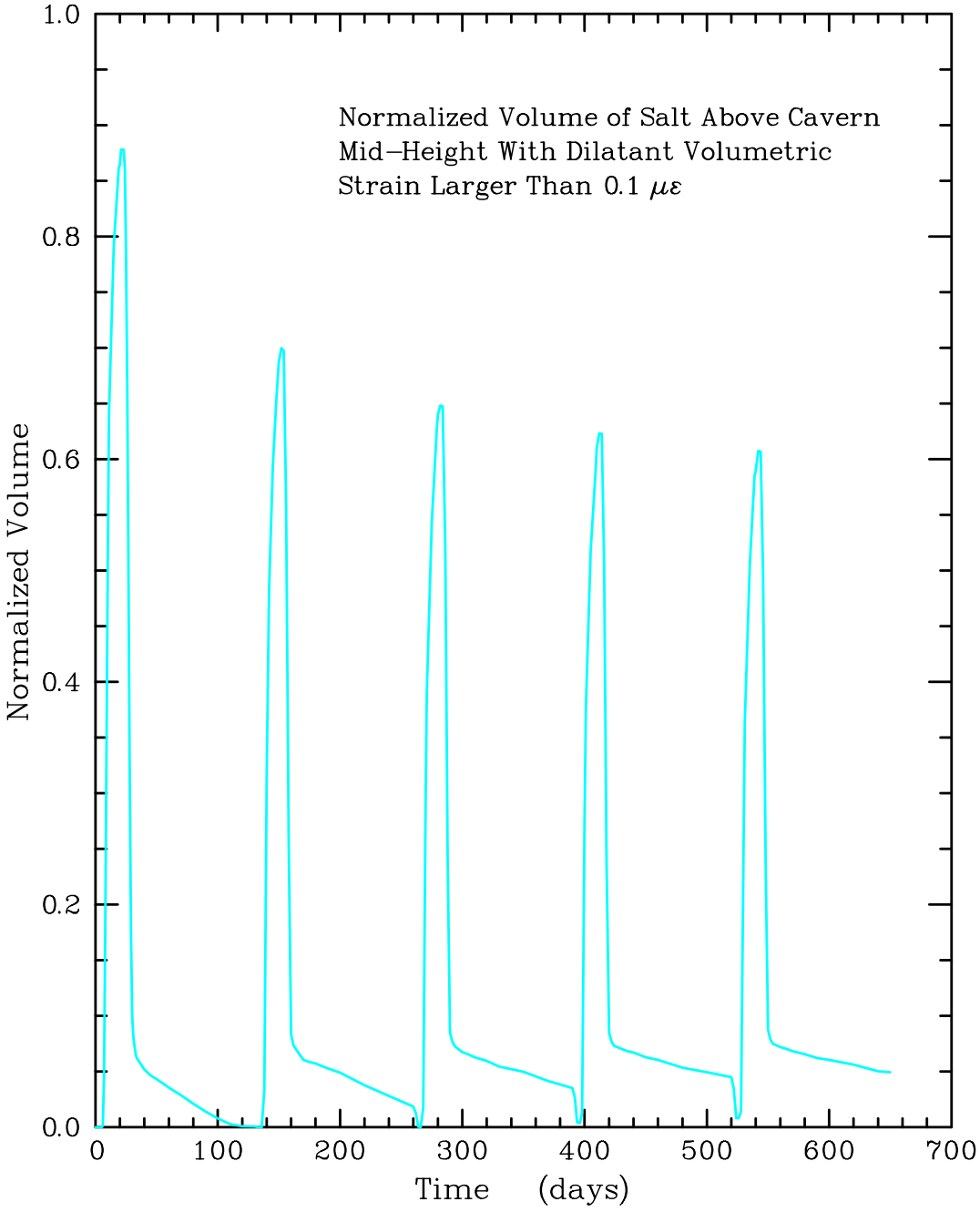

Figure 6-7. Normalized Volume of Salt Above the Cavern Midheight With Dilatant Volumetric Strain Greater Than 0.1 με for Cavern A Throughout Five Consecutive Case 1 Gas Pressure Cycles.

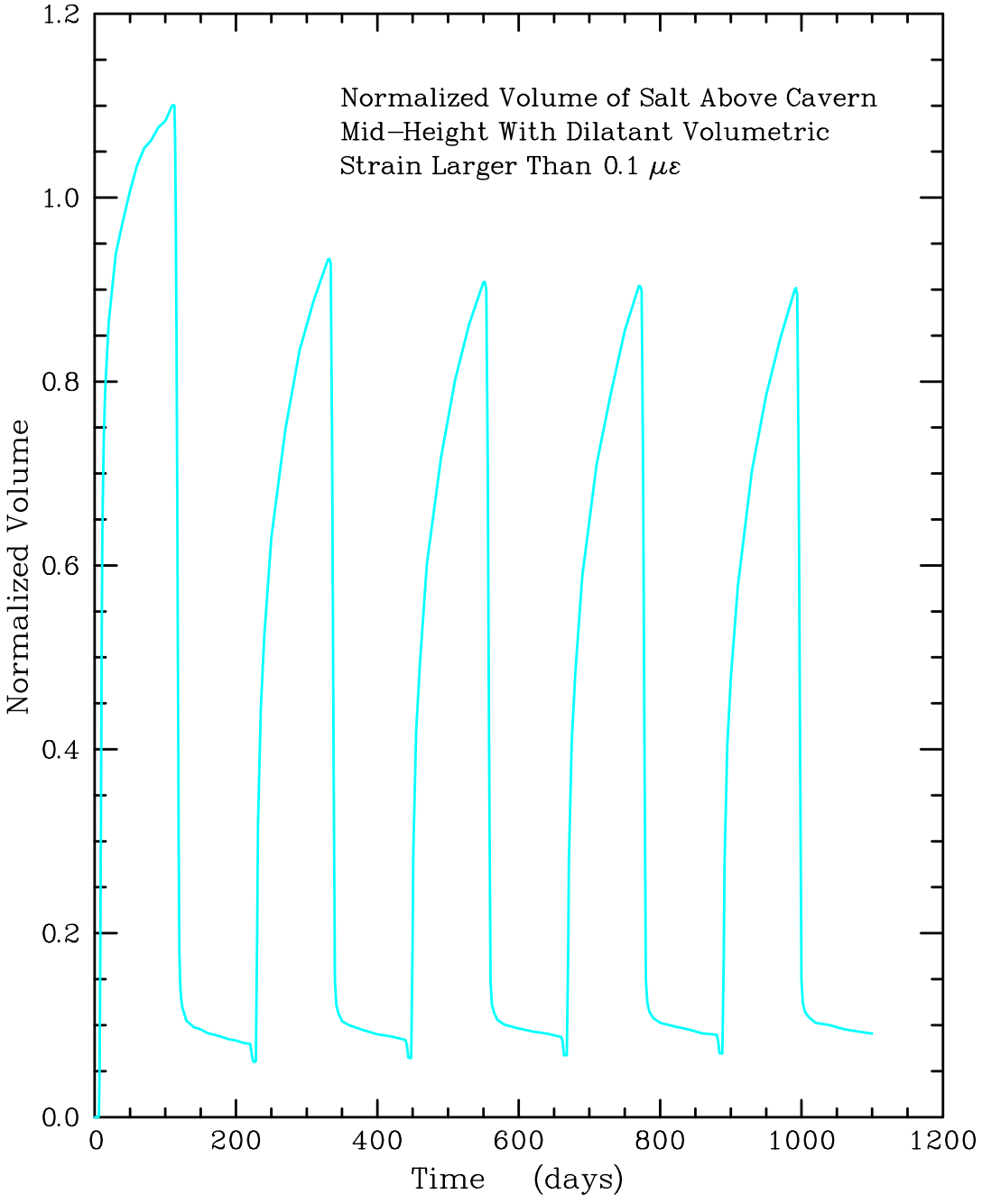

Figure 6-8. Normalized Volume of Salt Above the Cavern Midheight With Dilatant Volumetric Strain Greater Than 0.1 με for Cavern A Throughout Five Consecutive Case 2 Gas Pressure Cycles.

increases slightly with each cycle. This is also evident in Figures 6-9 and 6-10, which show contours of the dilatant volumetric strain in the salt surrounding Cavern A for the Case 1 cycle at the end of the first cycle and at the end of the fifth cycle. For the Case 2 cycles with a 100-day period at minimum gas pressure, the salt is not completely healed by the end of the first cycle, and again, the volume of the salt that is not completely healed increases slightly with each consecutive gas cycle. This is because the Kachanov damage variable and the inelastic volumetric strain are independent of each other during damage healing. As a result, even though the dilatant volumetric strain became vanishingly small, the value of ω, although reduced, did not reach the initial value of undamaged rock salt during the healing stage. Therefore, the predicted results differ during each subsequent cycle due to the softening effect introduced by the damage variable.

For both the Case 1 and Case 2 simulations, the maximum volume of salt with dilatant volumetric strain greater than 0.1 $\mu\varepsilon$ during each cycle decreases with each cycle. This is the result of strain hardening occurring during the periods at low gas pressure. This is also demonstrated in Figures 6-11 and 6-12, which show contours of the dilatant volumetric strain in the salt surrounding Cavern A for the Case 1 cycle at the end of the 10-day period at minimum gas pressure during the first cycle and fifth cycle, respectively. It is also interesting to note that at the beginning of the cycles, during the first part of the gas withdrawal, the volume of salt that exceeds 0.1 $\mu\varepsilon$ actually decreases. This is the result of the same phenomenon seen during the pressurization of Cavern B, except in reverse. As the gas pressure is decreased, the tangential stresses around the cavern become more compressive than the radial stresses, which are becoming less compressive, resulting in a short period of increased healing.

Figures 6-13 and 6-14 show the normalized volume of salt above the cavern midheight with a dilatant volumetric strain greater than 0.1 $\mu\varepsilon$ for Cavern B for five consecutive Case 1 and Case 2 cycles, respectively. Unlike Cavern A, nearly all of the dilatant volumetric strain is healed by the end of the each cycle. Figures 6-15 and 6-16 show contours of the dilatant volumetric strain in the salt surrounding Cavern B for the Case 1 cycle at the end of the first cycle and at the end of the fifth cycle, respectively. As shown in these figures, the only accumulated damage is in small regions around *corners* in the cavern. This is true for both the Case 1 and Case 2 cycles. Like the Cavern A results, strain hardening results in decreasing the maximum volume of salt with dilatant volumetric strain greater than 0.1 $\mu\varepsilon$ with each cycle. This is also revealed in Figures 6-17 and 6-18, which show contours of the dilatant volumetric strain in the salt surrounding Cavern B for the Case 1 cycle at the end of the 10-day period at minimum gas pressure during the first cycle and fifth cycle, respectively.

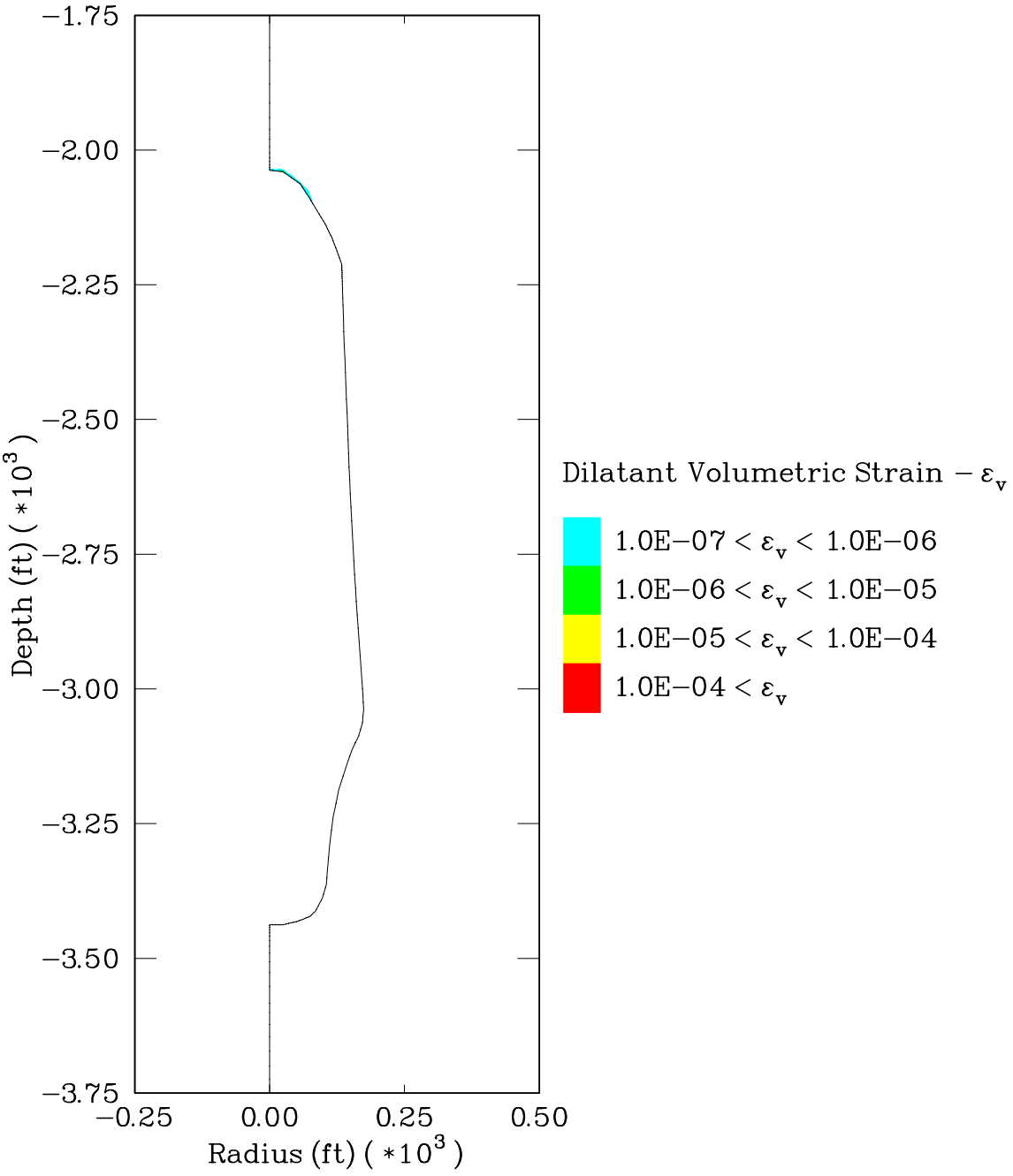

Figure 6-9. Contours of the Dilatant Volumetric Strain in the Salt Surrounding Cavern A at the End of the First Case 1 Gas Cycle.

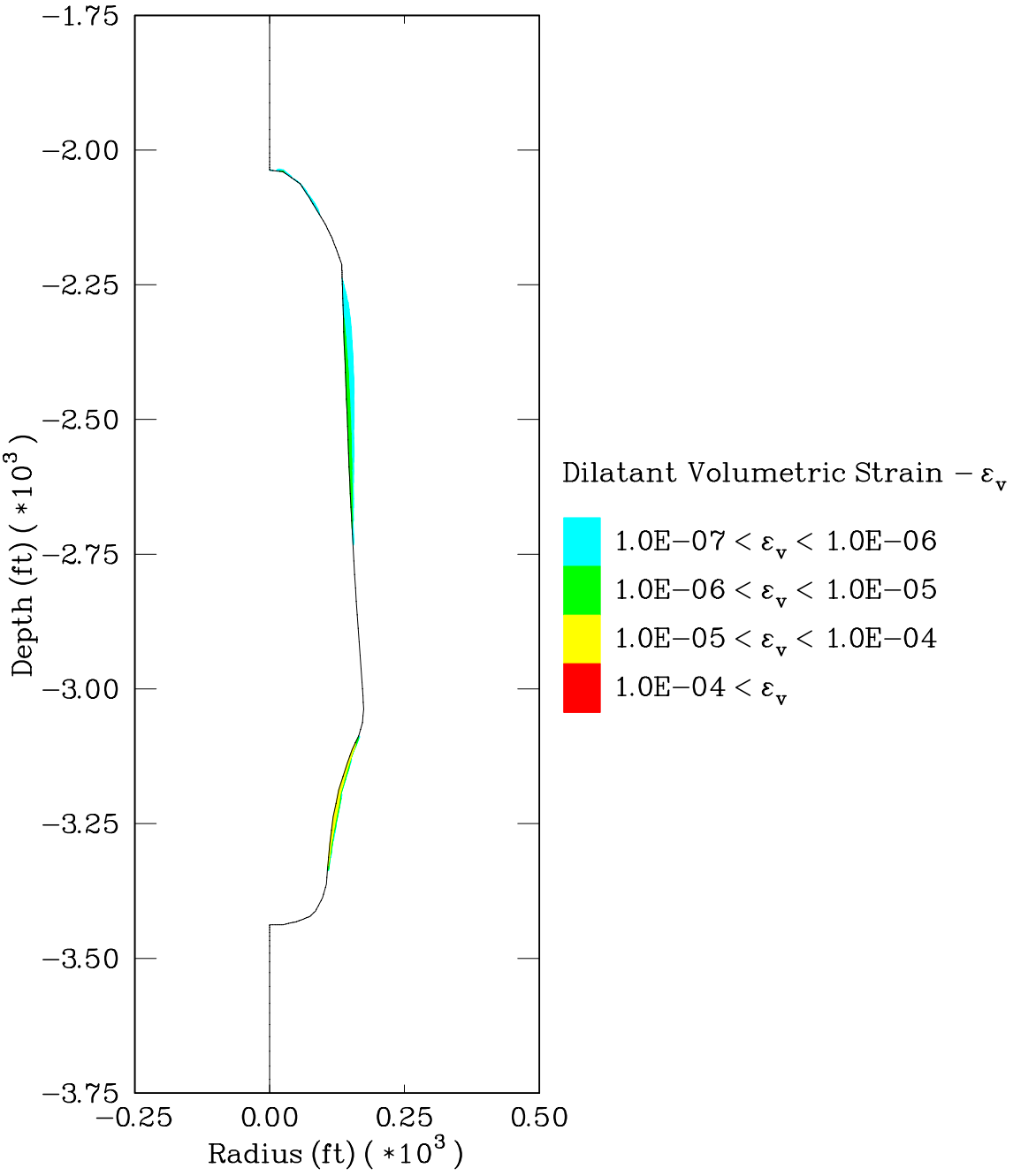

Figure 6-10. Contours of the Dilatant Volumetric Strain in the Salt Surrounding Cavern A at the End of the Fifth Case 1 Gas Cycle.

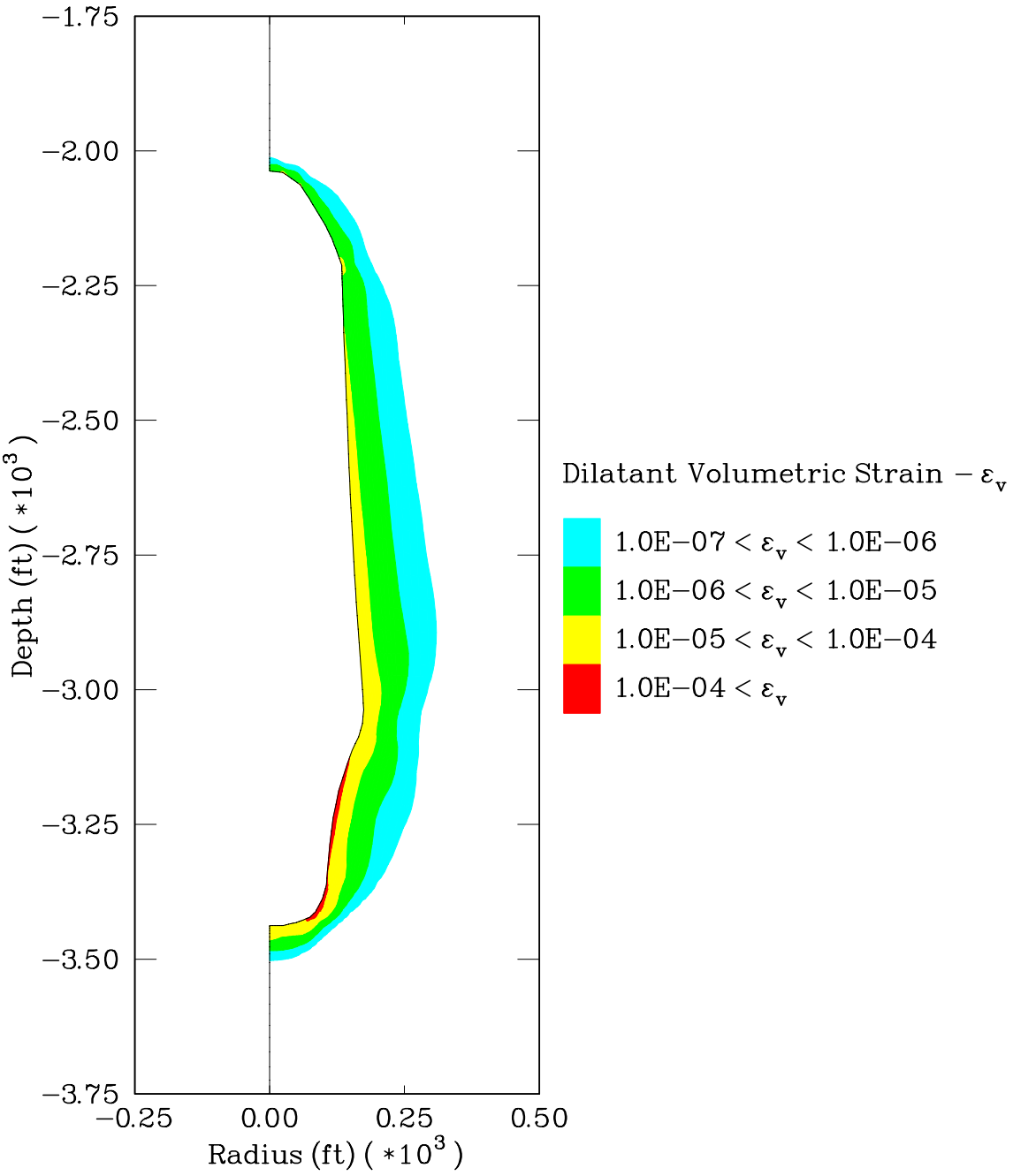

Figure 6-11. Contours of the Dilatant Volumetric Strain in the Salt Surrounding Cavern A at the End of the 10-Day Period at Minimum Gas Pressure During the First Case 1 Gas Cycle.

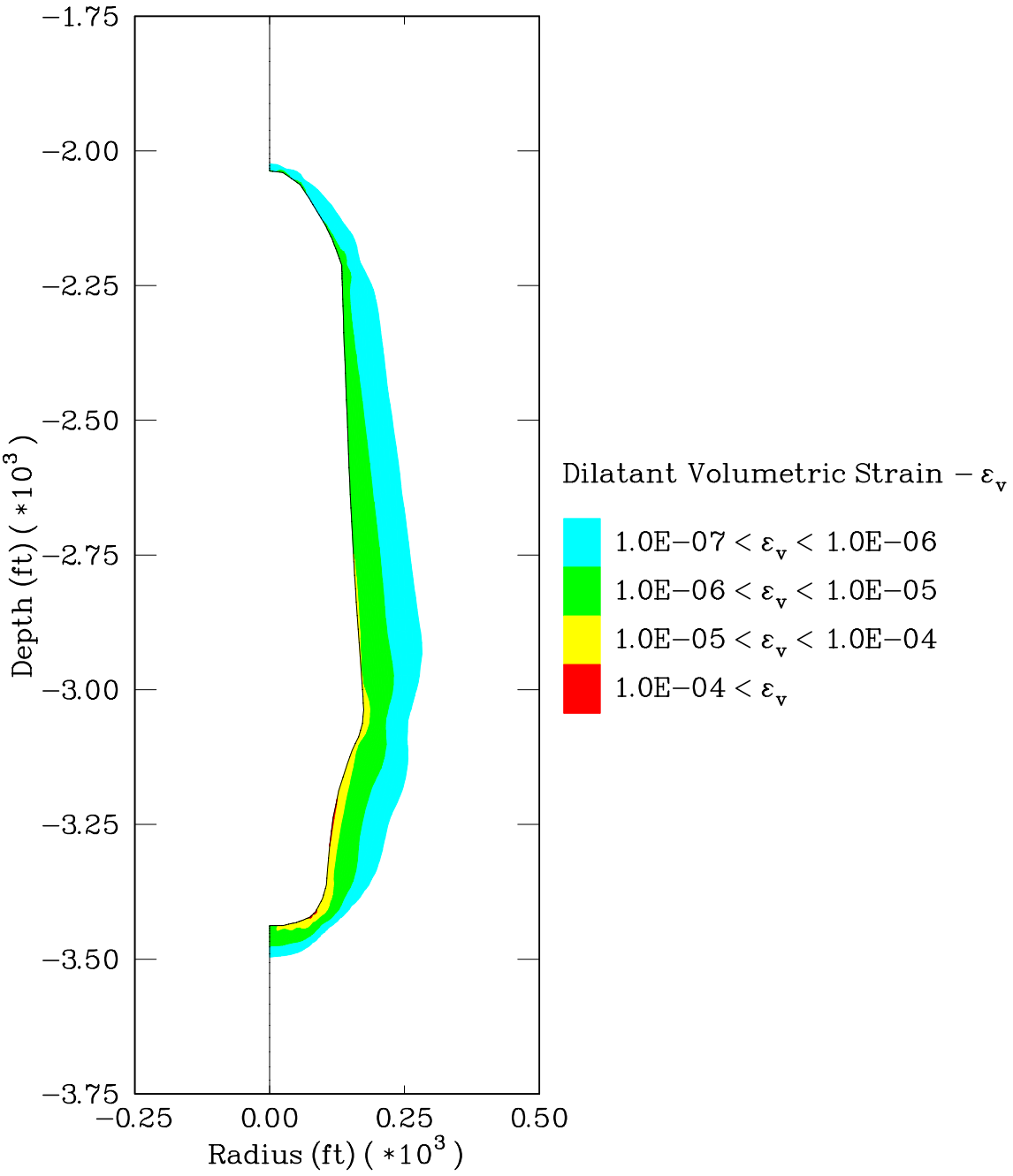

Figure 6-12. Contours of the Dilatant Volumetric Strain in the Salt Surrounding Cavern A at the End of the 10-Day Period at Minimum Gas Pressure During the Fifth Case 1 Gas Cycle.

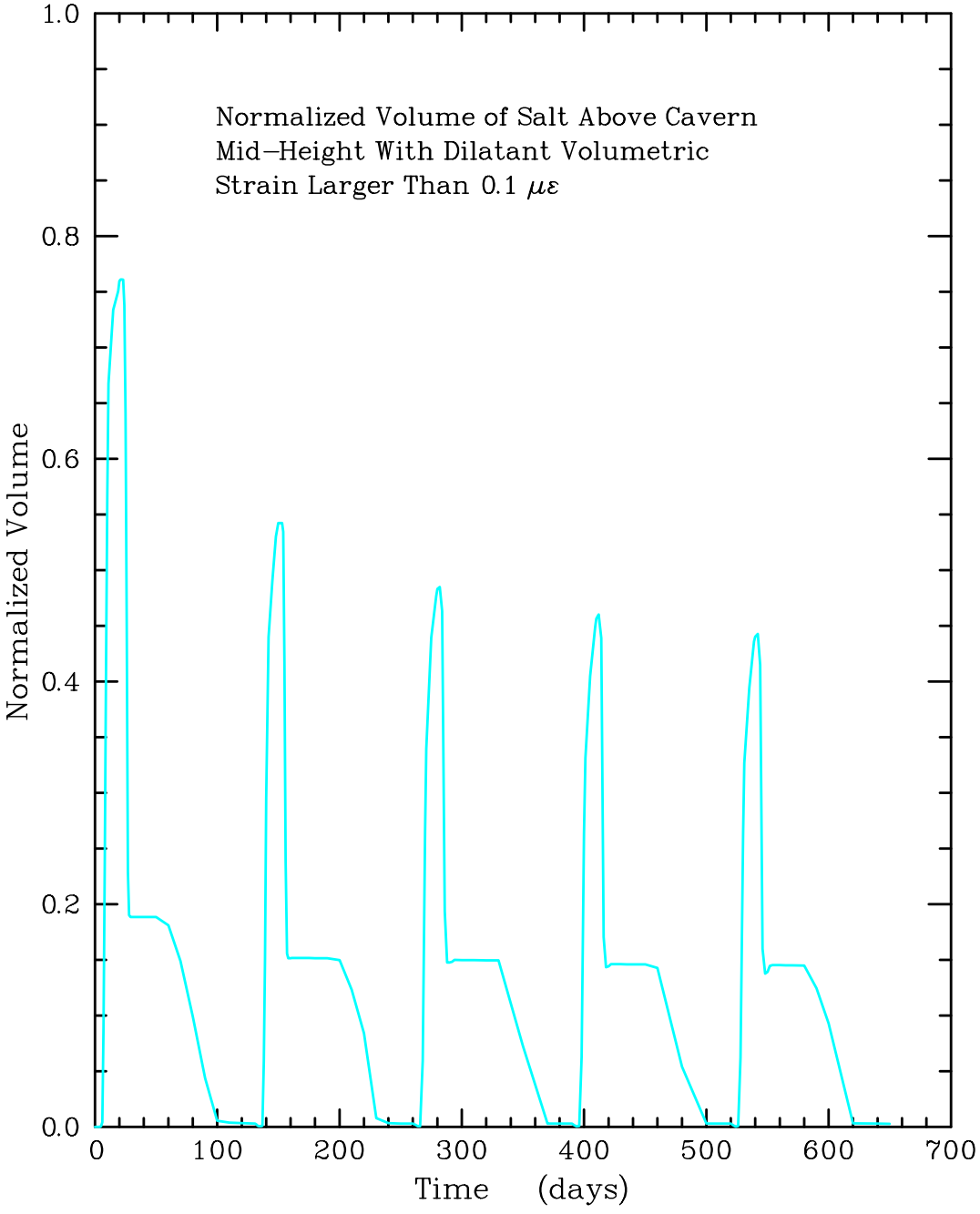

Figure 6-13. Normalized Volume of Salt Above the Cavern Midheight With Dilatant Volumetric Strain Greater Than 0.1 με for Cavern B Throughout Five Consecutive Case 1 Gas Pressure Cycles.

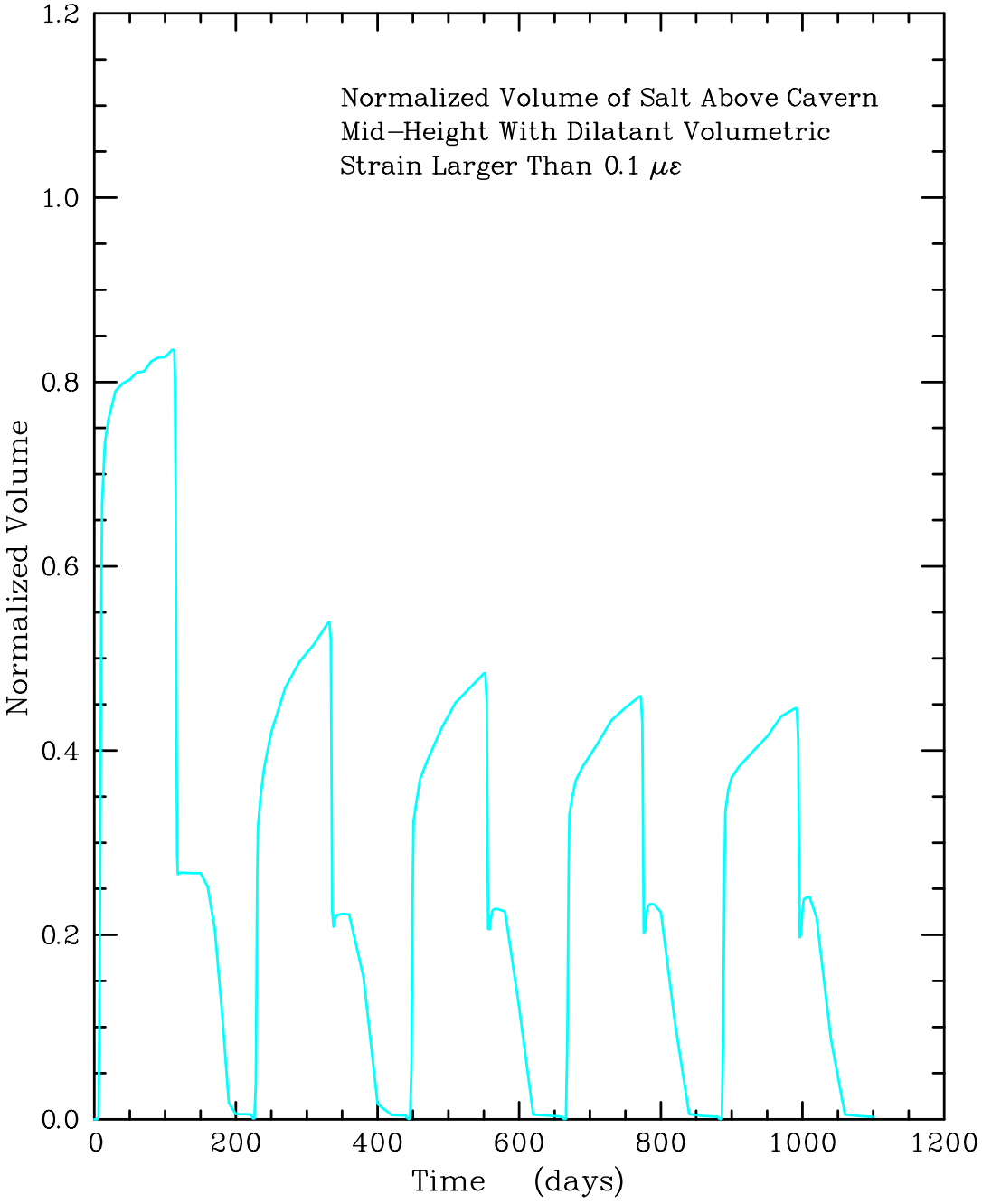

Figure 6-14. Normalized Volume of Salt Above the Cavern Midheight With Dilatant Volumetric Strain Greater Than 0.1 με for Cavern B Throughout Five Consecutive Case 2 Gas Pressure Cycles.

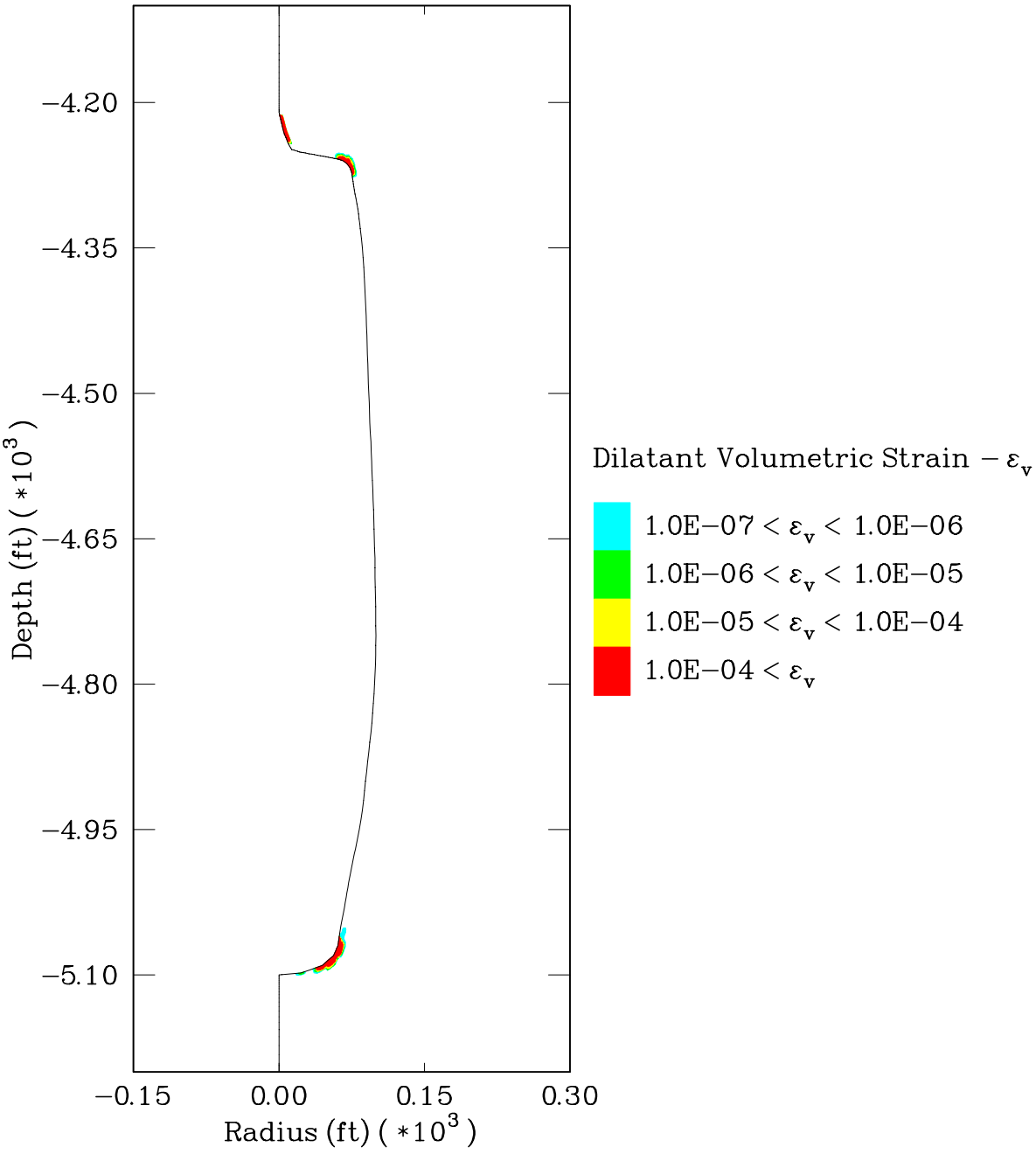

Figure 6-15. Contours of the Dilatant Volumetric Strain in the Salt Surrounding Cavern B at the End of the First Case 1 Gas Cycle.

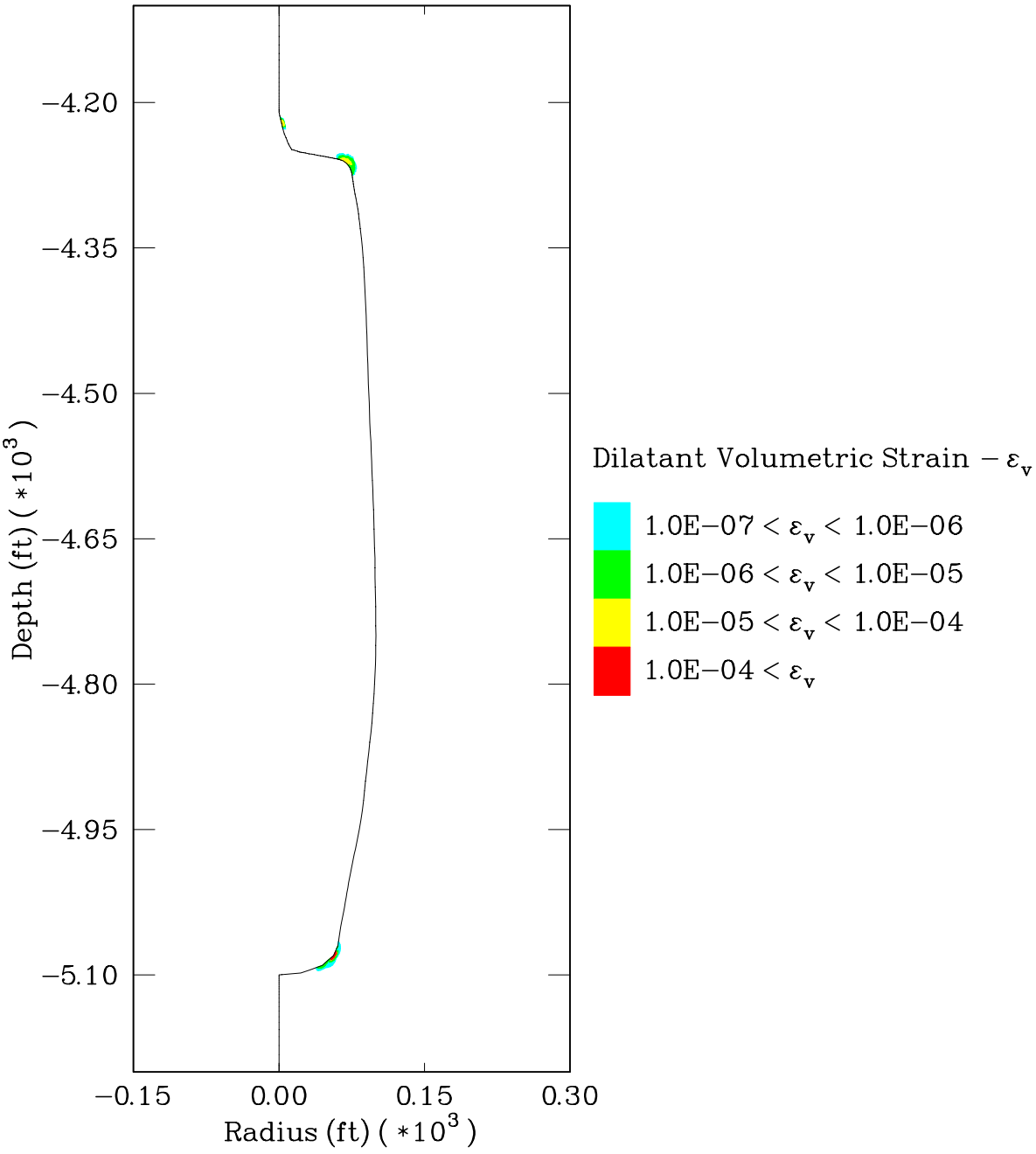

Figure 6-16. Contours of the Dilatant Volumetric Strain in the Salt Surrounding Cavern B at the End of the Fifth Case 1 Gas Cycle.

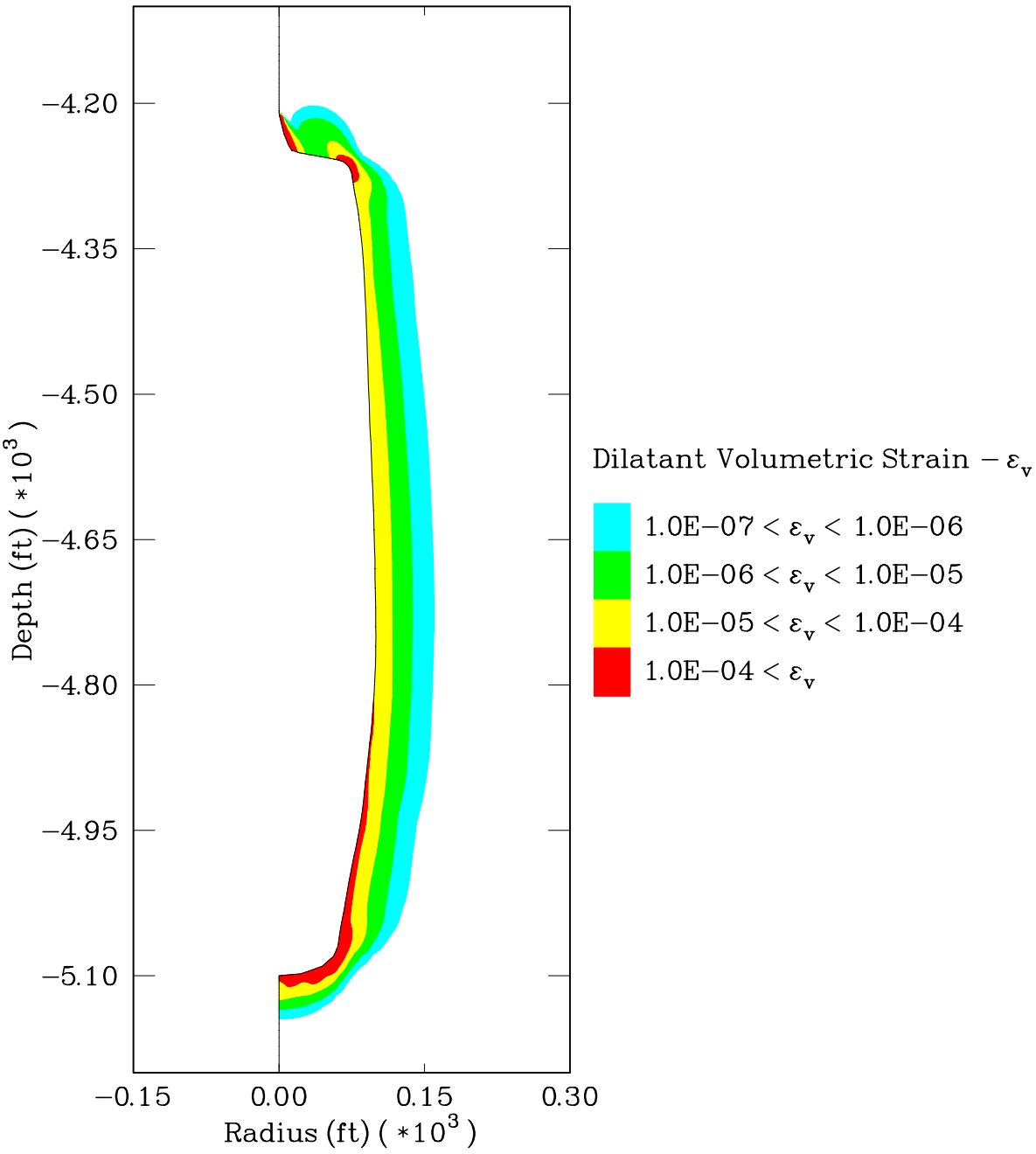

Figure 6-17. Contours of the Dilatant Volumetric Strain in the Salt Surrounding Cavern B at the End of the 10-Day Period at Minimum Gas Pressure During the First Case 1 Gas Cycle.

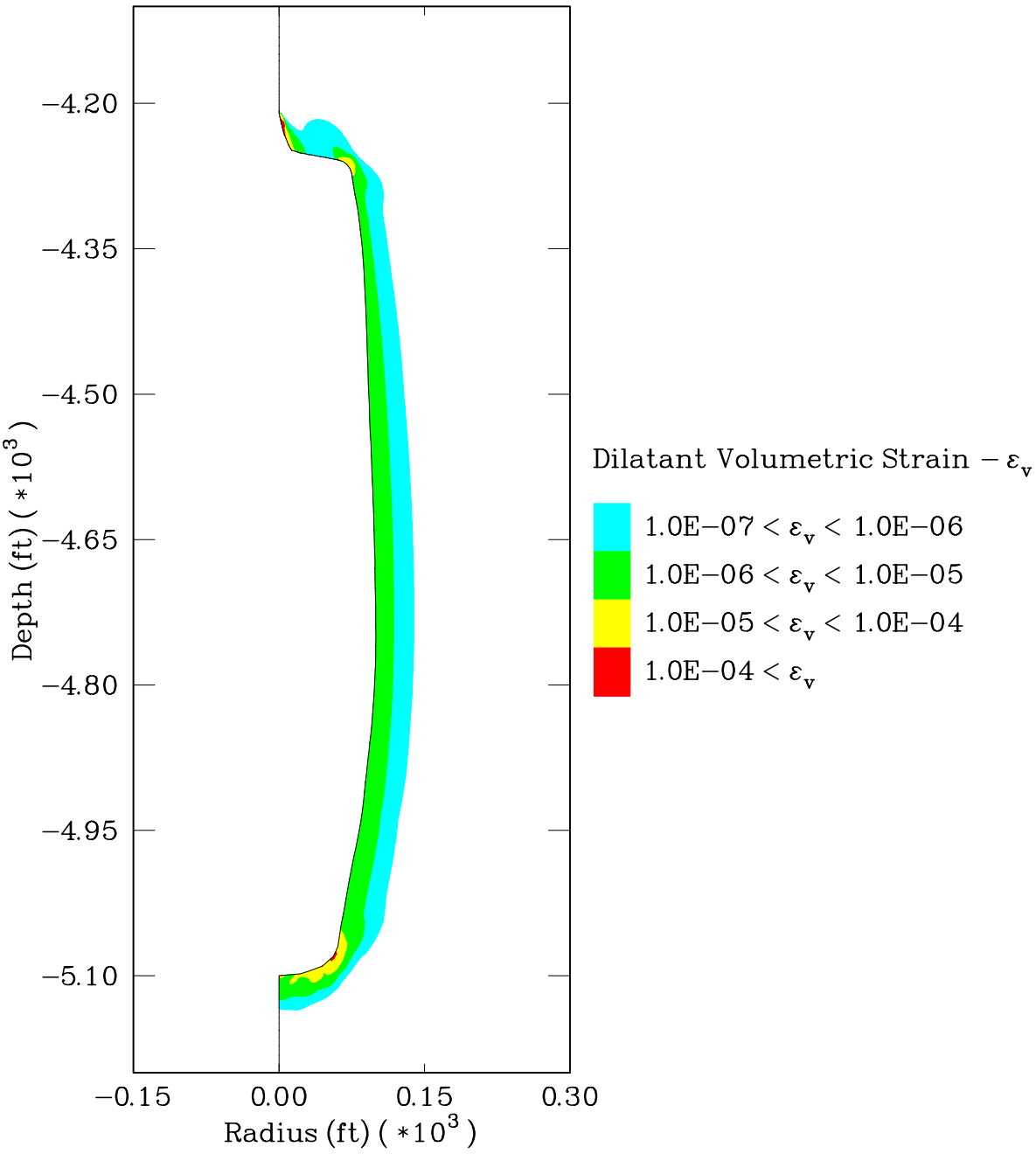

Figure 6-18. Contours of the Dilatant Volumetric Strain in the Salt Surrounding Cavern B at the End of the 10-Day Period at Minimum Gas Pressure During the Fifth Case 1 Gas Cycle.

7.0 SUMMARY AND CONCLUSIONS

Geomechanical analyses were made to determine the minimum gas pressure allowable based on an existing stress-based criterion (Damage Potential) and an advanced constitutive model (MDCF model) capable of quantifying the level of damage and healing in rock salt. The MDCF model is a constitutive model developed for the WIPP to provide a continuum description of the dislocation and damage deformation of salt. The purpose of this study was to determine if the MDCF model is applicable for evaluating the minimum gas pressure of CNG storage caverns. Specifically, it was to be determined if this model would predict that the minimum gas pressure in the caverns could be lowered without compromising the stability of the cavern. Additionally, the healing behavior of the salt was analyzed to determine if complete healing of the damaged rock zone would occur during the period the cavern was at maximum gas pressure. Significant findings of this study include:

1. The predicted dilatancy boundaries for the Damage Potential method and the MDCF model can differ significantly,depending on the stress state and impurity content (porosity) of salt.
2. Based on a conservative design criterion, the MDCF model predicts that a lower minimum gas pressure can be specified without jeopardizing cavern stability than that predicted by the Damage Potential method provided the cavern is not maintained at minimum pressure for an extended period of time.
3. Based on the MDCF model, healing of the dilatant volume of salt will occur at maximum gas pressure.
4. If damage develops during a gas service cycle, sufficient time should be allowed for healing to occur after the cavern is repressurized before the next service cycle to prevent continued damage development during subsequent cycles.
5. Less damage is predicted by the MDCF model around the shallow cavern than in the salt around the deeper cavern for the minimum gas pressures and impurity content specified in this study. Unlike the Damage Potential method, the MDCF dilatancy boundary is not a linear function of the stress invariants; therefore, the potential for damage development is predicted to increase with depth.
6. Further studies are necessary to better characterize the healing response of salt.

8.0 FUTURE WORK

8.1 DETERMINATION OF AN EFFICIENT TEST MATRIX

The mechanical behavior of salt is known to vary from site to site. Therefore, the constitutive model parameter values determined for the WIPP site may not be reliable for evaluating the material behavior of salt at other locations. Thus, the MDCF model should not be used to determine the acceptable operating pressure range for a CNG storage cavern unless site-specific properties or parameters are used. Advanced constitutive models for salt, such as the MDCF model, are highly nonlinear and contain many parameters. As discussed by Senseny and Fossum [1995], evaluation of parameters in such models is not a trivial matter because the parameters often do not have physical meaning (such as yield or failure stress do). In these cases, estimation of the parameters often requires a more rigorous approach which includes three distinct phases: (1) the design of an experimental program or test matrix comprising laboratory tests, (2) the acquisition of data from laboratory tests, and (3) the fitting of the model to the acquired data to determine estimates of the model parameters. The design of the test matrix requires the identification of test types that impose load or strain histories in which the material behavior is dominated by phenomenology that is characterized by the parameters of the model.

A methodology for determining the necessary parameter values of the MDCF model should be developed. The MDCF model parameter values have been determined for the WIPP based on laboratory tests. However, an extensive testing program such as that developed for the WIPP would not be feasible for designing CNG storage caverns because of the excessive duration of the program and the exorbitant cost. However, it may be feasible to determine parameter estimates for the MDCF model if the necessary laboratory tests required to evaluate the MDCF model parameters are minimized. An efficient test matrix can be developed by choosing tests in which the sensitivity coefficient of each parameter of the MDCF model is significantly higher than that of other parameters for a part of the test, or at least is one of the high sensitivity coefficients in some tests so that the parameter's contribution to material behavior can be determined. The estimated cost of determining the parameter estimates of the MDCF model should be evaluated against the added benefit provided by the model and potential savings.

8.2 TEMPERATURE EFFECTS AND HEALING CHARACTERISTICS

The database of laboratory tests used for the development of the MDCF model dislocation creep mechanisms is quite extensive. However, these tests do not provide information suitable for characterizing creep-induced damage because they were specifically performed under conditions that suppress microcracking. Therefore, development of the damage model required that the existing database used to develop the M-D model be supplemented with tests from which damage development and healing can be inferred. This supplemental database is not as

extensive as the database developed to characterize the dislocation creep processes, and in the case of damage healing, is probably not sufficient to validate model. Additionally, very little data were collected at elevated temperatures. The influence of temperature on damage accumulation and healing should be investigated further since CNG storage caverns can operate at temperatures outside the range used to develop the MDCF model.

8.3 PORE PRESSURE EFFECTS

Damage, such as the type that forms in the disturbed rock zone (DRZ) around storage caverns, is known to heal under hydrostatic conditions (e.g., Brodsky [1990]). Stress states near hydrostatic can be obtained in the salt around CNG storage caverns when operated at maximum gas pressure. However, because the salt near the cavern walls could have an enhanced permeability, the gas pressure may actually gain access to the porosity created by the damaging process, and therefore, may not produce the desired effect; i.e., a compressive pressure acting over the full boundary of the cavern. If gas pressure is allowed to access the DRZ, pore pressures will build in the DRZ, and these pore pressures may reduce the potential for healing and/or increase the potential for damage because they will likely lower the overall effective mean stress (i.e., mean stress minus the pore pressure) induced in the DRZ. If the hydrologic characteristics (e.g., permeability, pore pressure, etc.) of the salt influence the mechanical behavior of the salt, the actual behavior of the salt may not be accurately described by the MDCF model. If this is the case, there is a need to understand the coupling between the hydrological and structural characteristics of the DRZ to predict the damage/healing process more accurately.

9.0 REFERENCES

Aubertin, M., J. Sgaoula, and D. E. Gill, 1993. "A Damage Model for Rocksalt: Application to Tertiary Creep," *Proceedings, Seventh Symposium on Salt*, H. Kakihana, H. R. Hardy, Jr., T. Hoshi, and K. Toyokura (eds.), Elsevier, Amsterdam, Vol. 1, pp. 117–125.

Brodsky, N. S., 1990. *Crack Closure and Healing Studies in WIPP Salt Using Compressional Wave Velocity and Attenuation Measurements: Test Methods and Results*, SAND90-7076, prepared by RE/SPEC Inc., Rapid City, SD, for Sandia National Laboratories, Albuquerque, NM.

Brodsky, N. S. and D. E. Munson, 1994. "Thermomechanical Damage Recovery Parameters for Rocksalt From the Waste Isolation Pilot Plant," *Proceedings, 1st North American Rock Mechanics Symposium*, University of Texas–Austin, Austin, TX, June 1–3, P. P. Nelson and S. E. Laubach (eds.), A. A. Balkema, Rotterdam, pp. 731–738.

Callahan, G. D., A. F. Fossum, and D. K. Svalstad, 1989. *Documentation of SPECTROM-32: A Finite Element Thermomechanical Stress Analysis Program*, DOE/CH/10378-2, prepared by RE/SPEC Inc., Rapid City, SD, for the U.S. Department of Energy, Chicago Operations Office, Argonne, IL, Vol. I and II.

Chan, K. S., S. R. Bodner, A. F. Fossum, and D. E. Munson, 1992. "A Constitutive Model for Inelastic Flow and Damage Evolution in Solids Under Triaxial Compression," *Mechanics of Materials*, Vol. 14, pp. 1–14.

Chan, K. S., N. S. Brodsky, S. R. Bodner, A. F. Fossum, and D. E. Munson, 1994. "Damage-Induced Nonassociated Inelastic Flow in Rock Salt," *International Journal of Plasticity*, Vol. 10, pp. 623–642.

Chan, K. S., K. L. DeVries, S. R. Bodner, A. F. Fossum, and D. E. Munson, 1995a. "A Damage Mechanics Approach to Life Prediction for a Salt Structure," *Proceedings of ICES '95, Computational Mechanics*, S. N. Atluri, G. Yagawa, and T. A. Cruse (eds.), Springer, Berlin, pp. 1140–1145.

Chan, K. S., S. R. Bodner, A. F. Fossum, and D. E. Munson, 1995b. "Constitutive Representation of Damage Healing in WIPP Salt," *Proceedings, 35th U.S. Symposium on Rock Mechanics*, University of Nevada, Reno, NV, June 5–7, J. J. K. Daemen and R. A. Schultz (eds.), A. A. Balkema, Rotterdam, pp. 485–490.

Chan, K. S., S. R. Bodner, D. E. Munson, and A. F. Fossum, 1996a. "Inelastic Flow Behavior of Argillaceous Salt," *International Journal of Damage Mechanics*, Vol. 5, No. 3, July, pp. 292–314.

Chan, K. S., D. E. Munson, A. F. Fossum, and S. R. Bodner, 1996b. "A Constitutive Model for Representing Coupled Creep, Fracture, and Healing in Rock Salt," *Proceedings, Fourth Conference of The Mechanical Behavior of Salt*, École Polytechnique de Montréal, Mineral Engineering Department, Québec, Canada, June 17 and 18, M. Aubertin and H. R. Hardy Jr. (eds.), Penn State University, Trans Tech Publications, Clausthal, Germany, 1998, pp. 221–234.

Chan, K. S., D. E. Munson, S. R. Bodner, and A. F. Fossum, 1996c. "Cleavage and Creep Rupture of Rock Salt," *Acta Metallurgica et Materialia*, Vol. 44, No. 9, pp. 3553–3565.

Chan, K. S., S. R. Bodner, A. F. Fossum, and D. E. Munson, 1997. "A Damage Mechanics Treatment of Creep Failure in Rock Salt," *International Journal of Damage Mechanics*, Vol. 6, April, pp. 121–152.

Costin, L. S. and W. R. Wawersik, 1980. *Creep Healing of Fractures in Rock Salt*, SAND80-0392, Sandia National Laboratories, Albuquerque, NM.

Cristescu, N. D. and U. Hunsche, 1992. *Finite Inelastic Deformation-Theory and Application*, D. Desdo and E. Stein (eds.), Springer-Verlag, Berlin, Germany, pp. 511–523.

Fokker, P. A., 1995. *The Behavior of Salt and Salt Caverns*, Ph.D. Dissertation, Technische Universiteit Delft.

Hansen, F. D., M. J. Leroch, L. L. Van Sambeek, and M. S. Lin, 1993. "Gas Barrier Design for the WIPP," *Proceedings, 34th U.S. Symposium on Rock Mechanics*, University of Wisconsin–Madison, Madison, WI, June 27–30, B. C. Haimson (ed.), International Journal of Rock Mechanics and Mining Sciences & Geomechanics Abstracts, Pergamon Press, Vol. 30, No. 7, pp. 1515–1518.

Harrison and Ellis, 1995. *Risk Assessment of Converting Salt Caverns to Natural Gas Storage*, GRI-95/0377, prepared by Radian Corporation, Austin, TX, for the Gas Research Institute, Chicago, IL.

Kachanov, L. M., 1958. "On the Creep Fracture Time," *Izv. Akad. Nauk, USSR, Otdgel. Tekh, Nauk.*, Vol. 8, p. 26.

Lin, M. S. and L. L. Van Sambeek, 1992. *Waste Isolation Pilot Plant Alcove Gas Barrier Final Design Report*, SAND92-7307, prepared by Parsons Brinckerhoff Quade & Douglas, Inc., San Francisco, CA, and RE/SPEC Inc., Rapid City, SD, for Sandia National Laboratories, Albuquerque, NM.

Munson, D. E., 1979. *Preliminary Deformation-Mechanism Map for Salt (With Application to WIPP)*, SAND79-0076, Sandia National Laboratories, Albuquerque, NM.

Munson, D. E. and P. R. Dawson, 1979. *Constitutive Model for the Low Temperature Creep of Salt (With Application to WIPP)*, SAND79-1853, Sandia National Laboratories, Albuquerque, NM.

Munson, D. E., A. F. Fossum, and P. E. Senseny, 1989. *Advances in Resolution of Discrepancies Between Predicted and Measured In Situ WIPP Room Closures*, SAND88-2948, Sandia National Laboratories, Albuquerque, NM.

Nemat-Nasser, S. 1983. *Proceeding, ICF International Symposium on Fracture Mechanics*, Beijing Science Press, Beijing, China, pp. 185–97.

Pfeifle, T. W. and L. D. Hurtado, 1998. "Permeability of Natural Rock Salt From the Waste Isolation Pilot Plant (WIPP) During Damage Evolution and Healing," *Proceedings, 3rd North American Rock Mechanics Symposium*, Cancún, Mexico, June 3–5.

Ratigan, J. L., L. L. Van Sambeek, K. L. DeVries, and J. D. Nieland, 1991. *The Influence of Seal Design on the Development of the Disturbed Rock Zone in the WIPP Alcove Seal Tests*, RSI-0400, prepared by RE/SPEC Inc., Rapid City, SD, for Sandia National Laboratories, Albuquerque, NM.

Ratigan, J. L., J. D. Nieland, and J. D. Osnes, 1993. "Rock Mechanics Aspects of Natural Gas Storage in Domal Salt," presented at the *Solution Mining Research Institute Fall Meeting*, Lafayette, LA, October 25–26.

Senseny, P. E. and A. F. Fossum, 1995. "On Testing Requirements for Viscoplastic Constitutive Parameter Estimation," *Journal of Engineering Materials and Technology*, Vol. 117, April, pp. 151–154.

Van Sambeek, L. L., D. D. Luo, M. S. Lin, W. Ostrowski, and D. Oyenuga, 1993. *Seal Design Alternatives Study*, SAND92-7340, prepared by Parsons Brinckerhoff Quade & Douglas, San Francisco, CA, and RE/SPEC Inc., Rapid City, SD, for Sandia National Laboratories, Albuquerque, NM.

APPENDIX A

SUMMARY OF THE MDCF MODEL

APPENDIX A

SUMMARY OF THE MDCF MODEL

The MDCF model is a constitutive model that provides a continuum description of the creep response and the associated damage evolution and healing of rock salt. Both dislocation motion and creep-induced damage are assumed to contribute directly to the macroscopic inelastic strain rate. In addition to a direct contribution to the inelastic strain rate, the MDCF model was formulated such that damage also produces a softening effect as proposed by Kachanov [1958]. The Kachanov damage variable, ω, reduces the load-bearing capacity through a reduction in the effective area using a continuum damage mechanics approach. The damage variable is determined from an evolutionary equation and provides a measure for the level of damage. For the MDCF model, the contribution of creep-induced damage and healing to the inelastic strain rate is incorporated through additional kinetic equations that are independent of the kinetic equation for dislocation mechanisms. The terms are combined using the approach given by Fossum et al. [1988] to derive a proper three-dimensional generalization using classical thermodynamic principles. The generalized form of the MDCF model is given by:

$$\dot{\varepsilon}^{i}_{ij} = \frac{\partial \sigma^{c}_{eq}}{\partial \sigma_{ij}} \dot{\varepsilon}^{c}_{eq} + \frac{\partial \sigma^{\omega_s^*}_{eq}}{\partial \sigma_{ij}} \dot{\varepsilon}^{\omega_s}_{eq} + \frac{\partial \sigma^{\omega_t}_{eq}}{\partial \sigma_{ij}} \dot{\varepsilon}^{\omega_t}_{eq} + \frac{\partial \sigma^{h}_{eq}}{\partial \sigma_{ij}} \dot{\varepsilon}^{h}_{eq} \qquad \text{(A-1)}$$

where σ^{c}_{eq}, $\sigma^{\omega_s^*}_{eq}$, $\sigma^{\omega_t}_{eq}$, σ^{h}_{eq}, $\dot{\varepsilon}^{c}_{eq}$, $\dot{\varepsilon}^{\omega_s}_{eq}$, $\dot{\varepsilon}^{\omega_t}_{eq}$, and $\dot{\varepsilon}^{h}_{eq}$ are power-conjugate equivalent stress measures and equivalent inelastic strain rates for the dislocation creep (*c*), shear damage (ω_s), tensile damage (ω_t), and damage healing (*h*) mechanisms, respectively. Details of the power-conjugate stress measures, kinetic equations, the flow laws, and the evolution equation for damage in the MDCF model are summarized below. Note that compression is taken to be negative.

Kinetic Equation for Dislocation Flow

The kinetic equation representing the creep rate, $\dot{\varepsilon}^{c}_{eq}$, due to dislocation mechanisms is based on the modified M-D model [Munson et al., 1989]. The formulation remains unchanged with the exception that the six occurrences of the effective stress are divided by the term $(1 - \omega)$, which represents the reduction in the effective load-bearing area caused by the presence of damage. The kinetic equation for the dislocation mechanisms is:

$$\dot{\varepsilon}^{c}_{eq} = F \dot{\varepsilon}_{s} \qquad \text{(A-2)}$$

where *F* is the transient function representing transient creep behavior, and $\dot{\varepsilon}_{s}$ is the steady-state strain rate. The steady-state creep of salt is the sum of three dominant mechanisms: (1) a high temperature, low stress regime controlled by dislocation climb; (2) a low temperature, low stress regime controlled by an undefined mechanism; and (3) a high stress regime controlled by

various possible dislocation slip mechanisms. The steady-state creep rates of the three relevant mechanisms, respectively, are given by:

$$\dot{\varepsilon}_{s_1} = A_1 e^{-Q_1/RT} \left(\frac{\sigma_{eq}^c}{\mu(1-\omega)} \right)^{n_1} \tag{A-3}$$

$$\dot{\varepsilon}_{s_2} = A_2 e^{-Q_2/RT} \left(\frac{\sigma_{eq}^c}{\mu(1-\omega)} \right)^{n_2} \tag{A-4}$$

$$\dot{\varepsilon}_{s_3} = |H| \left(B_1 e^{-Q_1/RT} + B_2 e^{-Q_2/RT} \right) \sinh \left[\frac{q \left(\frac{\sigma_{eq}^c}{(1-\omega)} - \sigma_0 \right)}{\mu} \right] \tag{A-5}$$

where the *A*'s and *B*'s are constants, *Q*'s are activation energies, *T* is the absolute temperature, *R* is the universal gas constant, μ is the shear modulus, *n*'s are the stress exponents, *q* is the stress constant, and σ_0 is the stress limit of the dislocation slip mechanism. $|H|$ is a Heaviside step function with the argument $(\frac{\sigma_{eq}^c}{1-\omega} - \sigma_0)$. The transient creep function *F* is given by:

$$F = \begin{cases} \exp\left[\Delta \left(1 - \frac{\zeta}{\varepsilon_t^*} \right)^2 \right], & \zeta < \varepsilon_t^* \\ 1, & \zeta = \varepsilon_t^* \\ \exp\left[-\delta \left(1 - \frac{\zeta}{\varepsilon_t^*} \right)^2 \right], & \zeta > \varepsilon_t^* \end{cases} \tag{A-6}$$

which is composed of a work-hardening branch, an equilibrium branch, and a recovery branch, respectively. In Equation A-6, Δ and δ represent the work-hardening and recovery parameters, respectively, and ε_t^* is the transient strain limit. The transient strain limit is a function of temperature and stress and is represented by:

$$\varepsilon_t^* = K_0 e^{cT} \left(\frac{\sigma_{eq}^c}{\mu(1-\omega)} \right)^m \tag{A-7}$$

where K_0, *c*, and *m* are constants. The work-hardening and recovery parameters are functions of stress given by:

$$\Delta = \alpha_w + \beta_w \log\left(\frac{\sigma_{eq}^c}{\mu(1-\omega)}\right) \tag{A-8}$$

$$\delta = \alpha_r + \beta_r \log\left(\frac{\sigma_{eq}^c}{\mu(1-\omega)}\right) \tag{A-9}$$

where the α's and β's are constants with the subscripts denoting either work-hardening (w) or recovery (r). δ was taken as a constant in this paper since insufficient experimental data are available to determine the stress dependency of the recovery parameters, and little of the salt surrounding the underground cavern is expected to be in recovery for the service cycle simulated. The evolution rate, $\dot{\zeta}$, of the internal variable ζ is governed by:

$$\dot{\zeta} = (F - 1)\,\dot{\varepsilon}_s \tag{A-10}$$

which diminishes to zero when the steady-state condition is achieved.

The maximum shear stress or Tresca criterion is used here for dislocation-induced flow. The power-conjugate equivalent stress measure, σ_{eq}^c, for the dislocation mechanisms, assuming the Tresca criterion, is given by:

$$\sigma_{eq}^c = 2\cos\psi\sqrt{J_2} = \sigma_1 - \sigma_3 \tag{A-11}$$

where ψ is the Lode angle, J_2 is the second invariant of the deviatoric stress tensor, and σ_1 and σ_3 are the maximum and minimum principal stresses, respectively.

Flow Law for Dislocation Deformation

The shear-induced dislocation flow of rock salt is assumed to be associative. The flow potential is an important factor in extending data obtained from constant stress laboratory creep tests to generalized three-dimensional states of stress. Differentiation of the power-conjugate stress given by Equation A-11 with respect to stress leads to:

$$\frac{\partial \sigma_{eq}^c}{\partial \sigma_{ij}} = \left[\frac{\cos 2\psi}{\cos 3\psi}\right]\frac{s_{ij}}{\sqrt{J_2}} + \left[\frac{\sqrt{3}\sin\psi}{J_2\cos 3\psi}\right] t_{ij} \tag{A-12}$$

where s_{ij} is the deviatoric stress tensor and $t_{ij} = s_{ip}\,s_{pj} - \frac{2}{3}J_2\delta_{ij}$. Equation A-12 is indeterminate when $\psi \rightarrow \pm\pi/6$. To eliminate this problem computationally, the flow potential is taken as the average of the flow potentials on either side of the indeterminacy and evaluated

in the limit as $\psi \rightarrow \pm\pi/6$ whenever the lode angle is within 0.25 degree of the indeterminacy. For both conditions, the result is:

$$\frac{\partial \sigma_{eq}^{c}}{\partial \sigma_{ij}} = \frac{s_{ij}}{2\sqrt{3 J_2}} \tag{A-13}$$

Thus, at the corners of the Tresca potential, the indeterminacies are removed by assuming a von Mises flow which makes the direction of straining unique.

Kinetic Equations for Damage-Induced Flow

The kinetic equations for damage-induced flow are similar in nature to dislocation flow in that damage-induced transient creep is accommodated in the model through a multiplier on the kinetic equations for damage-induced flow during steady-state creep. The model was developed assuming damage can occur in compression as a result of sliding of microcracks by shear and the opening of wing-tip cleavage cracks that develop on some of the shear cracks. Tensile creep damage is also accounted for in the model and is based on the formation of cleavage microcracks aligned normal to the tensile stress. The kinetics of tensile damage in salt are substantially faster than shear damage and is therefore treated as a separate term. The equations describing the shear-induced (*s*) and tension-induced (*t*) damage are similar in form. Thus, the subscript *i* is used to represent *s* and *t* in the equations to follow. The equivalent inelastic strain rate is given by:

$$\dot{\varepsilon}_{eq}^{\omega_i} = F^{\omega_i} \dot{\varepsilon}_{s}^{\omega_i} \tag{A-14}$$

where:

$$F^{\omega_s} = F \exp\left[\frac{c_4\left(\sigma_{eq}^{c} - c_5\right)}{\sigma_0\left(1 - \rho\right)}\right] \tag{A-15}$$

$$F^{\omega_t} = F \exp\left[\frac{c_4\left(\sigma_{eq}^{\omega_t} - c_5\right)}{\sigma_0\left(1 - \rho\right)}\right] \tag{A-16}$$

are the functions that account for the damage-induced inelastic strain rate in the transient region and ρ is the volume fraction of clay particles. The kinetic equation for damage-induced flow during steady-state creep is given by:

$$\dot{\varepsilon}_s^{\omega_i} = c_1 \omega_o \exp(c_3 \omega) \left[\sinh \left(\frac{c_2 \sigma_{eq}^{\omega_i} H\left(\sigma_{eq}^{\omega_i}\right)}{(1 - \omega)(1 - \rho)\mu} \right) \right]^{n_3} \tag{A-17}$$

with:

$$c_1 = c_0 \left(B_1 e^{(-Q_1/RT)} + B_2 e^{(-Q_2/RT)} \right) \tag{A-18}$$

where the c's and n_3 are material constants, ω_0 is the initial value of the damage variable (ω) and the B's and Q's are constants of the dislocation glide mechanisms. As shown in Equation A-16, the Heaviside step function prevents accumulation of damage whenever the power-conjugate equivalent stress measure is negative.

The power-conjugate equivalent stress measures are given by:

$$\sigma_{eq}^{\omega_s} = |\sigma_1 - \sigma_3| + f_p x_2 x_7 \operatorname{sgn}(I_1 - \sigma_3) \left(\frac{I_1 - \sigma_3}{3 x_7 \operatorname{sgn}(I_1 - \sigma_3)} \right)^{x_6} \tag{A-19}$$

$$\sigma_{eq}^{\omega_t} = x_1 \sigma_1 H(\sigma_1) \tag{A-20}$$

where x_1, x_2, x_6, and x_7 are material constants of the damage model; I_1 is the first stress invariant; and σ_1 and σ_3 are the maximum and minimum principal stresses, respectively, with compression assumed to be negative. The first term in Equation A-19 represents the driving force for shear-induced damage, which leads to the opening of "wing-tip" microcracks or grain boundary cracks. The second term in Equation A-19 represents the suppression of microcrack growth by a confining pressure. This term was recently extended to account for the increase in damage accumulation associated with increasing impurity of clay content [Chan et al., 1996a]. The material parameter f_p is related to the impurity content by:

$$f_p = 1 - p_1 \rho \tag{A-21}$$

where ρ is the clay content parameter and p_1 is a material parameter, which is analogous to a local stress intensity factor.

The preceding equations include the damage (ω), which is described in terms of an evolutionary equation. The damage evolution equation is taken as:

$$\dot{\omega} = \dot{\omega}_s + \dot{\omega}_t - \dot{h} \tag{A-22}$$

where the damage rate components for the shear-induced and tension-induced damage are given by:

$$\dot{\omega}_s = \frac{x_4}{t_0}\omega\left[\ln\left(\frac{1}{\omega}\right)\right]^{\frac{x_4+1}{x_4}}\left[\frac{\sigma_{eq}^{\omega_s} H\left(\sigma_{eq}^{\omega_s}\right)}{(1-\rho)\xi_s}\right]^{x_{3s}} \tag{A-23}$$

$$\dot{\omega}_t = \frac{x_4}{t_0}\omega\left[\ln\left(\frac{1}{\omega}\right)\right]^{\frac{x_4+1}{x_4}}\left[\frac{\sigma_{eq}^{\omega_t} H\left(\sigma_{eq}^{\omega_t}\right)}{(1-\rho)\xi_t}\right]^{x_{3t}} \tag{A-24}$$

where x_4, x_{3s}, x_{3t}, ξ_s, ξ_t, and t_0 are material constants. The parameter ξ_s may have different values according to the magnitude of the effective shear-induced damage stress; i.e.,

$$\begin{aligned} \xi_s &= \xi_s^1 \quad \text{for } \sigma_{eq}^c/(1-\omega) > \sigma_0 \\ \xi_s &= \xi_s^2 \quad \text{for } \sigma_{eq}^c/(1-\omega) \le \sigma_0 \end{aligned} \tag{A-25}$$

The healing term or damage recovery rate is discussed later under the discussion of the kinetic equation for healing.

Flow Law for Damage-Induced Inelastic Deformation

The shear-induced inelastic damage flow is assumed to be nonassociative. The flow potential power-conjugate stress measure for shear-induced damage is given by (cf. Equation A-19):

$$\sigma_{eq}^{\omega_s^*} = \left|\sigma_1 - \sigma_3\right| + \frac{x_2 x_8}{3}\left(I_1 - \sigma_3\right) \tag{A-26}$$

where x_8 is a material constant. Differentiation of the power-conjugate stress given by Equation A-26 with respect to stress leads to:

$$\frac{\partial\sigma_{eq}^{\omega_s^*}}{\partial\sigma_{ij}} = b_1\frac{s_{ij}}{\sqrt{3J_2}\cos 3\psi} + b_2\frac{t_{ij}}{J_2\cos 3\psi} + 2b_4\frac{\delta_{ij}}{3} \tag{A-27}$$

where:

$$b_1 = \sqrt{3}\cos 2\psi - b_4\sin\left(2\psi - \frac{\pi}{3}\right) \tag{A-28}$$

$$b_2 = \sqrt{3}\sin\psi - b_4\cos\left(\psi + \frac{\pi}{3}\right) \tag{A-29}$$

$$b_4 = \frac{x_2 x_8}{3} \tag{A-30}$$

The flow potential power-conjugate stress measure for tension-induced damage is given by:

$$\sigma_{eq}^{\omega_t} = x_1 \sigma_1 \; H(\sigma_1) \tag{A-31}$$

where x_1 is a material constant. Differentiation of the work conjugate stress given by Equation A-31 with respect to stress leads to:

$$\frac{\partial \sigma_{eq}^{\omega_t}}{\partial \sigma_{ij}} = x_1 \; H(\sigma_1) \left[\sin\left(2\psi + \frac{\pi}{3}\right) \frac{s_{ij}}{\sqrt{3 J_2}\cos 3\psi} + \cos\left(\psi - \frac{\pi}{3}\right) \frac{t_{ij}}{J_2 \cos 3\psi} + \frac{\delta_{ij}}{3} \right] \tag{A-32}$$

Reviewing the flow laws for the shear-induced and tension-induced damage, one observes an indeterminacy when $\psi = \pm\pi/6$. To eliminate this problem computationally, the flow potential is taken as the average of the flow potentials on either side of the corner and evaluated in the limit as $\psi \rightarrow \pm\pi/6$. Performing this limiting operation as ψ approaches $\pi/6$ (the triaxial compression corner), Equation A-27 for the shear-induced damage term becomes:

$$\frac{\partial \sigma_{eq}^{\omega_s^*}}{\partial \sigma_{ij}} = b_1' \left(\frac{s_{ij}}{\sqrt{3 J_2}} - \frac{t_{ij}}{2 J_2} \right) + 2 b_4 \frac{\delta_{ij}}{3} \tag{A-33}$$

where:

$$b_1' = 1 + \frac{2 b_4}{3} \tag{A-34}$$

and at the triaxial extension corner ($\psi = -\pi/6$):

$$\frac{\partial \sigma_{eq}^{\omega_s^*}}{\partial \sigma_{ij}} = b_1'' \left(\frac{s_{ij}}{\sqrt{3 J_2}} + \frac{t_{ij}}{2 J_2} \right) + 2 b_4 \frac{\delta_{ij}}{3} \tag{A-35}$$

where:

$$b_1'' = 1 + \frac{b_4}{3} \tag{A-36}$$

which are used in **SPECTROM-32** when the Lode angle is within 0.25 degree of ±30 degrees.

Performing this limiting operation as ψ approaches $\pi/6$ (the triaxial compression corner), Equation A-32 for the tension-induced damage term becomes:

$$\frac{\partial \sigma_{eq}^{\omega_t}}{\partial \sigma_{ij}} = \frac{x_1 \; H(\sigma_1)}{3} \left(\frac{s_{ij}}{\sqrt{3 J_2}} - \frac{t_{ij}}{2 J_2} + \delta_{ij} \right) \tag{A-37}$$

and at the triaxial extension corner ($\psi = -\pi/6$):

$$\frac{\partial \sigma_{eq}^{\omega_t}}{\partial \sigma_{ij}} = \frac{2 \, x_1 \; H(\sigma_1)}{3} \left(\frac{s_{ij}}{\sqrt{3 J_2}} + \frac{t_{ij}}{2 J_2} + \frac{\delta_{ij}}{2} \right) \tag{A-38}$$

which are used in **SPECTROM-32** when the Lode angle is within 0.25 degree of ±30 degrees

Kinetic Equation for Damage Recovery Flow (Healing)

Reduction of damage in rock salt can occur by the closure of open microcracks and the sintering of microcracks. The kinetic equation representing the healing or damage recovery gives the total inelastic healing rate as follows:

$$\dot{\varepsilon}_{ij}^{h} = \dot{\varepsilon}_{eq}^{h} \frac{\partial \sigma_{eq}^{h^*}}{\partial \sigma_{ij}} \tag{A-39}$$

where $\sigma_{eq}^{h^*}$ and $\dot{\varepsilon}_{eq}^{h}$ are the power-conjugate equivalent stress measure and the equivalent inelastic strain rate for the healing mechanisms, respectively.

The equivalent inelastic healing strain rate in Equation A-39 is given as [Chan et al., 1996b]:

$$\dot{\varepsilon}_{eq}^{h} = \frac{\varepsilon_{kk}^{i} \left(\sigma_{eq}^{h} - \sigma_b \right) H\left(\sigma_b - \sigma_{eq}^{h} \right)}{\tau \, \mu} \tag{A-40}$$

where ε_{kk}^{i} is the inelastic volumetric strain, τ is a characteristic time constant, and μ is the shear modulus. $H()$ is the Heaviside function; thus, the healing rate is zero if the equivalent stress measure σ_{eq}^{h} is less than σ_b. The equivalent stress measure used to describe the magnitude of the healing strain rate is different than the power-conjugate equivalent stress measure used to describe the flow potential (nonassociative formulation) and is given by:

$$\sigma_{eq}^{h} = \frac{1}{3} \left(I_1 - \sigma_3 \right) \tag{A-41}$$

The value for σ_b is determined from Equation A-19 by solving for the value of σ_{eq}^{h} when $\sigma_{eq}^{\omega_s} = 0$, which is given by:

$$\sigma_b = -x_7 \left[\frac{\sigma_1 - \sigma_3}{f_p x_2 x_7} \right]^{\frac{1}{x_6}} \tag{A-42}$$

Then the quantity $\sigma_{eq}^h - \sigma_b$ overlays the curve that describes the damage so that damage accumulation occurs above the curve and damage recovery (healing) occurs below the curve. The characteristic time constant (τ) is taken to be a function of the inelastic volumetric strain and is written as:

$$\tau = \tau_0 \exp\left(- k_1 \varepsilon_{kk}^i \right) + \tau_1 \tag{A-43}$$

where k_1 is a material constant and τ_0 and τ_1 are characteristic time constants. When the volumetric strain is large, the exponential term becomes insignificant and the limiting value for τ is τ_1. τ_1 is then the characteristic time associated with microcrack closure when the level of damage is high. When the inelastic volumetric strain becomes small, the limiting value of τ is $\tau_0 + \tau_1$, which is the characteristic time constant associated with crack sintering.

The damage variable (ω) is described in terms of the evolutionary equation given in Equation A-22. The healing portion of the equation (modified with the initial damage Heaviside) is taken from [Chan et al., 1996b]:

$$\dot{h} = \frac{\omega \, H(\omega - \omega_0) \left(\sigma_{eq}^h - \sigma_b \right) H\left(\sigma_b - \sigma_{eq}^h \right)}{\tau \, \mu} \tag{A-44}$$

Flow Law for Healing-Induced Inelastic Deformation

The healing (damage recovery) inelastic damage flow is anisotropic in nature because damage will typically accumulate normal to the major principal stress (compression negative). To implement the anisotropic nature of the healing, Chan et al. [1996b] have developed the flow potential based on stress-induced anisotropy. However, the state of stress does not provide information regarding the direction of damage. In addition, Chan's development includes indeterminant conditions under hydrostatic states of stress. Also, under triaxial extension test conditions, Chan's flow potential predicts axial shortening; whereas, under triaxial compression test conditions, axial lengthening is predicted. This condition creates deformation in the opposite direction of loading regardless of the magnitude of the load. For these reasons, a simple isotropic flow based only on mean stress was adopted. Thus, the power-conjugate effective stress measure describing the flow potential is:

$$\sigma_{eq}^{h^*} = \sigma_m \tag{A-45}$$

and flow potential is given by:

$$\frac{\partial \sigma_{eq}^{h^*}}{\partial \sigma_{ij}} = \frac{\delta_{ij}}{3} \tag{A-46}$$

References

Chan, K. S., S. R. Bodner, D. E. Munson, and A. F. Fossum, 1996a. "Inelastic Flow Behavior of Argillaceous Salt," *International Journal of Damage Mechanics*, Vol. 5, No. 3, July, pp. 292–314.

Chan, K. S., D. E. Munson, A. F. Fossum, and S. R. Bodner, 1996b. "A Constitutive Model for Representing Coupled Creep, Fracture, and Healing in Rock Salt," *Proceedings, Fourth Conference of The Mechanical Behavior of Salt*, École Polytechnique de Montréal, Mineral Engineering Department, Québec, Canada, June 17 and 18, M. Aubertin and H. R. Hardy Jr. (eds.), Penn State University, Trans Tech Publications, Clausthal, Germany, 1998, pp. 221–234.

Fossum, A. F., G. D. Callahan, L. L. Van Sambeek, and P. E. Senseny, 1988. "How Should One-Dimensional Laboratory Equations be Cast Into Three-Dimensional Form?," *Proceedings, 29th U.S. Symposium on Rock Mechanics*, University of Minnesota, Minneapolis, MN, June 13–15, P. A. Cundall, R. L. Sterling, and A. M. Starfield (eds.), A. A. Balkema, Rotterdam, pp. 35–41.

Kachanov, L. M., 1958. "On the Creep Fracture Time," *Izv. Akad. Nauk, USSR, Otdgel. Tekh, Nauk.*, Vol. 8, p. 26.

Munson, D. E., A. F. Fossum, and P. E. Senseny, 1989. *Advances in Resolution of Discrepancies Between Predicted and Measured In Situ WIPP Room Closures*, SAND88-2948, Sandia National Laboratories, Albuquerque, NM.

APPENDIX B

MDCF PARAMETER VALUES

APPENDIX B

MDCF PARAMETER VALUES

In order to provide the most accurate description of the mechanical response of the two storage caverns evaluated in this study, site-specific parameter values were used where available. Elastic properties and parameter estimates for the MDCF model dislocation mechanisms have been determined in separate studies for both Cavern A and Cavern B. The elastic properties and parameter values for the dislocation mechanisms of the MDCF model are presented in Table B-1. Parameter values for the damage mechanisms have only been determined for WIPP salt. Without experimental evidence, determination of the parameter values for the damage model is impossible. Therefore, parameter values determined for WIPP salt are used in this study. The parameter values for the damage mechanism for pure halite are presented in Table B-2. All of the parameter values were obtained from laboratory experiments on WIPP salt, independent of field measurements. These tables contain the necessary information to define the inelastic deformation of salt using the MDCF model with one exception. The remaining variable necessary to define the inelastic deformation of salt is the impurity content (ρ). In this study, the impurity content was varied to provide a range for the dilatancy boundary that would encompass expected variances in material properties for domal salt.

Table B-1. MDCF Elastic and Dislocation Creep Model Constants

Parameter	Units	Cavern A	Cavern B
Elastic Parameter Values			
E	psi	3.59×10^{6}	2.63×10^{6}
ν	—	0.30	0.18
Dislocation Creep Parameter Values			
A_1	day^{-1}	5.87×10^{27}	3.82×10^{27}
A_2	day^{-1}	3.19×10^{15}	2.07×10^{15}
Q_1/R	R	2.27×10^{4}	2.27×10^{4}
Q_2/R	R	1.17×10^{4}	1.17×10^{4}
n_1	—	5.5	5.5
n_2	—	3.73	3.68
B_1	day^{-1}	1.67×10^{12}	1.08×10^{12}
B_2	day^{-1}	5.30×10^{4}	3.44×10^{4}
q	—	3,330	2,800
σ_o	psi	1,930	1,280
μ	psi	1.40×10^{6}	1.40×10^{6}
m	—	3	3
K_o	—	3.73×10^{6}	5.27×10^{4}
c	R^{-1}	5.11×10^{-3}	5.11×10^{-3}
α	—	–1.25	–10.39
β	—	–2.07	–6.17
δ	—	0.2417	0.2417

Table B-2. MDCF Damage Model Constants

Parameter	Units	Cavern A	Cavern B
x_1	—	6	6
x_2	—	9	9
x_{3s}	—	5.5	5.5
x_{3t}	—	40	40
x_4	—	3	3
ξ_s^1	psi	3.35×10^4	3.35×10^4
ξ_s^2	psi	5.09×10^4	5.09×10^4
ξ_t	psi	2,197	2,197
x_6	—	0.75	0.75
x_7	psi	145	145
x_8	—	0.1	0.1
x_{10}	—	1	1
t_0	day	1.16×10^{-5}	1.16×10^{-5}
τ_0	day	4.34	4.34
τ_1	day	2.17×10^{-4}	2.17×10^{-4}
c_0	—	50,000	50,000
c_2	—	850	850
c_3	—	10	10
c_4	—	6	6
c_5	psi	3,626	3,626
n_3	—	3	3
k_1	—	5,000	5,000
σ_{th}	psi	–508	–508
p_1	—	28	28
ω_0	—	0.0001	0.0001
ρ	—	0 to 0.03	0 to 0.03

APPENDIX C

PROPERTIES OF WELL FLUIDS

APPENDIX C

PROPERTIES OF WELL FLUIDS

The mechanical response of natural gas storage caverns depends not only on the material properties of the salt surrounding the cavern but also on the material properties of the fluids inside the cavern. It is assumed that the cavern will be filled with saturated brine after solutioning is complete and before the cavern is dewatered. The cavern will subsequently be filled with compressed natural gas. In the simulations of the cavern, these fluids are represented by their pressures applied as normal tractions to the surfaces of the cavern. An equation of state relating the fluid's pressure to its density and temperature was assumed for each fluid. In the following two subsections, the assumed equations of state used to predict the vertical pressure gradients are presented for natural gas and for saturated brine.

Natural Gas Characteristics

The gas pressure, P, in a well can be described as:

$$P = P_0 + \int_0^z \rho g \, dz \qquad \text{(C-1)}$$

where:

P_o = the wellhead pressure

ρ = the density of the gas

g = the gravitational acceleration

z = the depth below wellhead.

The density of natural gas is dependent on pressure and temperature, both of which change with depth. A compressibility equation for natural gas described by Coker [1993] was used to calculate the density as a function of pressure and temperature. Equation C-1 was integrated numerically to determine the pressure versus depth data to determine a linear pressure gradient for the gas at the various pressures simulated.

Brine Characteristics

Because of the very small compressibility of brine, approximately $1.9(10^{-6})$/psi, the increase in brine density associated with the hydrostatic pressure increases over the height of the cavern is negligible (about 0.1 percent change per 1,000 feet). Consequently, the brine density was assumed to remain a constant 75 pcf, resulting in a vertical pressure gradient of 0.52 psi/foot.

References

Coker, A. K., 1993. "Program Calculates Z-Factor for Natural Gas," *Oil & Gas Journal*, February 15, pp. 75–75.

PHASE II FEASIBILITY STUDY FOR LOWERING THE MINIMUM GAS PRESSURE IN SOLUTION-MINED CAVERNS BASED ON GEOMECHANICAL ANALYSES OF CREEP-INDUCED DAMAGE AND HEALING

Topical Report RSI-1165
DE-AC26-97FT34350

by

Joel D. Nieland
Kerry L. DeVries
Kirby D. Mellegard

RESPEC
P.O. Box 725
Rapid City, South Dakota 57709-0725

prepared for

U.S. Department of Energy
Federal Energy Technology Center
P.O. Box 880
Morgantown, West Virginia 26507-0880

July 1999

ABSTRACT

This is the second phase of a two-phase study to evaluate the feasibility of lowering the minimum gas pressure in solution-mined caverns through the use of an advanced constitutive model for salt in cavern design. The purpose of this study is twofold: (1) to develop an efficient laboratory test matrix that can be used to determine the site-specific model parameter values for the Multimechanism Deformation Coupled Fracture (MDCF) constitutive model and (2) to estimate the potential cost benefits gained as a result of using the MDCF model in cavern design. The sensitivity of test specimen response to each of the MDCF model parameters was estimated using numerical simulations of laboratory tests. The results of the sensitivity analysis were used to provide guidance in designing an efficient test matrix comprised of load paths and boundary conditions attainable in most modern laboratory facilities. The resulting test matrix includes 27 tests to determine constitutive parameters, 12 tests to determine strength properties, and ten mineralogic analysis tests to determine salt impurity content. The possible cost benefits of using the MDCF model in cavern design are the result of lowering the minimum gas pressure and thus maximizing the working gas to cushion gas ratio. The cost benefits are analyzed by comparing the reduced storage costs to the additional cost of using the more advanced MDCF constitutive model. It is estimated that even a small decrease in the minimum gas pressure will cover the costs of adopting the MDCF constitutive model within the first year or two of operation.

EXECUTIVE SUMMARY

This report presents the Phase II results of a feasibility study for lowering the minimum gas pressure in solution-mined compressed natural gas (CNG) caverns through the use of an advanced constitutive model for salt. In Phase I of this project, it was demonstrated that the minimum gas pressures in CNG caverns could be reduced (compared to conventional design practices) without compromising the stability of the surrounding salt by using the Multimechanism Deformation Coupled Fracture (MDCF) model for salt. The purpose of this Phase II study is twofold: (1) to develop an efficient laboratory test matrix that can be used to determine the site-specific model parameter values for the MDCF constitutive model and (2) to estimate the potential cost benefits gained as a result of using the MDCF model in cavern design.

BACKGROUND

The storage of CNG in salt caverns is a growing industry. Product movement to and from CNG storage caverns is accomplished simply by compression and expansion of the stored gas. Consequently, the internal pressure on the walls of a CNG storage cavern can vary considerably. Since a minimum level of internal pressure is necessary to ensure cavern stability, a certain quantity of gas must always remain in a cavern. This gas is referred to as the base or cushion gas. The quantity of gas that can be withdrawn from a cavern is referred to as the working gas volume.

The economics of CNG storage in salt caverns are largely dependent on maximizing the ratio between the working gas and the cushion gas volumes. This ratio depends directly on the relative values of the maximum and minimum gas pressures permitted in the storage cavern. The maximum storage pressure is limited by regulation to a fraction of the weight of the overburden (typically 0.75 to 0.85 of the vertical stress) in order to prevent hydraulic fracturing of the salt and/or cemented casing and loss of containment. The minimum pressure required to ensure the structural stability of the cavern is much more difficult to determine. Conventional practice requires the use of both conservative design criteria and numerical simulations of typical gas service cycles comprising different minimum operating gas pressures to predict the states of stress in the salt surrounding the cavern. The predicted states of stress are compared to states of stress known to cause damage (microcracking that produces salt dilation or volume expansion); and then, the minimum gas pressure is established as the lowest pressure that can be achieved without inducing stresses in the salt that cause dilation.

It is well known that some damage or dilation is permissible without compromising the mechanical integrity of the salt. In addition, salt damage is known to be recoverable under

hydrostatic and/or high mean stress conditions. In gas storage caverns, high mean stress conditions are induced in the salt when the gas storage pressures are high, e.g., during maximum storage pressure conditions. Therefore, any damage induced in the salt surrounding the cavern at low storage pressures is likely to be recovered or healed at high storage pressures. The conventional design criteria do not allow for any salt damage nor do they account for salt healing. Advanced constitutive models (e.g., the MDCF model) for salt have been developed which do address the shortcomings of the conventional method, and when used in storage cavern design, may allow lower minimum gas pressures without affecting the structural stability of the cavern. In Phase I of this project, the advanced MDCF model was used to demonstrate that minimum gas pressures in CNG caverns could be reduced (compared to conventional design practices) without compromising the stability of the surrounding salt.

The site-to-site variation in the mechanical behavior of salt requires that laboratory testing be performed to determine site-specific properties for the MDCF model. Because of the complexity of the MDCF model, tests providing load or strain histories that isolate material behavior dominated by one or only a few model parameters must be identified. The design of an efficient test matrix for evaluation of parameters in the MDCF model was guided by a sensitivity analysis which shows the influence of each of the model parameters on specimen response. An efficient test matrix is then developed by choosing tests and test conditions for which the sensitivity coefficient of each parameter that needs to be determined is sufficiently large to confidently determine the parameter value.

The possible cost benefits of using the MDCF model in cavern design are the result of lowering the minimum gas pressure and thus maximizing the working gas to cushion gas ratio. The cost benefits are analyzed by comparing the reduced storage costs to the additional cost of using the more advanced MDCF constitutive model.

RESULTS

Simulations of laboratory tests on salt were made to aid in the design of an efficient test matrix for the purpose of determining site-specific parameter values for the MDCF constitutive model. The MDCF model was first examined to determine which of the parameters can be fixed based on theoretical or other considerations and which parameters must be treated as free parameters. Sensitivity coefficients for each of the free model parameters were calculated for each of the test simulations. Based on the results of the sensitivity analysis and laboratory test constraints, an efficient test matrix was determined. Finally, the potential cost benefits associated with the reduction in required cushion gas were compared to the additional testing and analysis costs required to evaluate the parameters for the MDCF model.

The MDCF model was initially developed to model the extreme conditions expected at the Waste Isolation Pilot Plant (WIPP) nuclear waste repository in salt. The MDCF constitutive model contains 41 parameters. However, because of the limited range of stress and temperature conditions experienced in the salt surrounding CNG storage caverns, it is not necessary to determine all of the parameters in the MDCF model. Also, several parameters have a theoretical basis or are determined by mineralogy. The parameters that do not need to be evaluated on a site-specific basis for CNG storage caverns can be treated deterministically and can be assigned typical values. Based on these considerations, 12 of the 41 model parameters were treated as deterministic parameters, reducing the number of free parameters to 29.

Numerical simulations were made of the available laboratory test types using two different parameter sets. The creep properties used are based on laboratory testing of salt from the Cavern A and Cavern B sites. However, because neither salt was tested to determine damage parameters, the damage parameters for both salts were assumed to be the same as those determined for WIPP salt. The sensitivity of the simulated measured response to each free parameter was calculated for each of the test simulations. The sensitivity results were very similar for both salts. However, it is likely that the sensitivity results for salts with significantly different creep and damage characteristics than those examined here may be different.

Ideally, it should be possible to find load paths in which the material behavior is dominated by one or only a few of the model parameters. However, the sensitivity coefficients determined for some of the parameters are very small for all of the load paths simulated. The parameters with very little or no influence include A_2, B_1, B_2, x_{3s}, ξ_s^1, ξ_s^2, t_0, x_4, t_0, c_0, c_3, and x_7. If the load paths simulated encompass those that will exist around the actual cavern, then determination of these parameters is not necessary because they do not significantly affect the response of the constitutive model. It is also likely that some of the parameters will be difficult to determine from laboratory test data because of correlation with other variables. Correlation between variables is evident when sensitivity coefficients for two or more variables have similar trends during a given load path.

The results of the sensitivity analysis were used to provide guidance on designing an efficient test matrix comprised of load paths and boundary conditions attainable in most modern laboratory facilities. The types of tests being proposed were chosen based on two criteria: (1) they had to be conventional tests that most laboratories could perform and (2) they had to incorporate load paths where at least some of the constitutive model parameters displayed high sensitivity coefficients. A total of 37 tests is proposed. A single testing temperature is proposed because the effects of thermal gradients at most sites are expected to be relatively small. Five types of tests are proposed for estimating the parameters in the MDCF model. The proposed test matrix includes:

- Nine Constant Stress Creep Tests - In a creep test, the axial stress is maintained at a higher level than the radial stresses and the stress state is held constant over a long period of time while the principal strains are monitored. Damage can be either suppressed or enhanced depending on the applied stress difference and mean stress. The tests would be performed at three stress differences and three mean stress levels. Creep tests provide data for estimating creep and damage parameters of the MDCF model.
- Six Constant Mean Stress Tests - In a constant mean stress test, deviatoric stress is increased while maintaining a constant mean stress. This test provides a means for introducing controlled damage in a specimen and is especially good for determining the onset of damage.
- Six Constant Axial Strain Rate Tests - In a constant axial strain rate test, the axial strain is at a specified rate while the confining pressure is held constant. This load path is typically used in strength testing, and can be used to induce controlled levels of damage. If unload/reload cycles are performed, then elastic properties can be determined from the test.
- Six Hydrostatic Compression Tests - In a hydrostatic compression test, the axial stress is maintained at the same level as the radial stresses and the stress state is held constant over a long period of time while the principal strains are monitored. This load path will be performed at lithostatic pressure on specimens predamaged in the other load paths and completely isolates the healing parameters from the creep and damage parameters of the MDCF model.
- Ten Mineralogic Analyses Tests - Mineralogic analysis will be used to determine the impurity content (ρ) of the salt.

In addition, the unconfined compressive strength and the indirect tensile strength can be easily estimated using the relatively inexpensive laboratory tests known as the unconfined compression test and the indirect tension test. Six of each of these tests are recommended to determine these properties.

The total laboratory-related cost estimate is $89,200, which includes $75,000 for the MDCF constitutive parameters testing, $4,200 for material strength properties testing, and $10,000 for data analysis and model fitting. These costs are based on our experience within the RESPEC laboratory and our interactions with other similar laboratory operations and assume that testable specimens are already available to the laboratory. The cost of performing a geomechanical analysis of a storage cavern can range between $25,000 and $75,000, depending on the complexity of the site. Thus, the approximate total cost for adopting the MDCF model to determine the minimum design gas pressure is expected to be between $115,000 and $165,000.

Determining the total potential savings to the CNG industry that could be attributed to adopting the MDCF model depends on future expectations that are unknown, such as the actual cavern service cycles and outcome of the geomechanical analyses using the MDCF model. It is believed that use of the MDCF model will provide a more accurate prediction of salt behavior. As a result, less conservative estimates for the minimum gas pressure can be determined. A reduction in the minimum gas pressure allowable in salt storage caverns can benefit the CNG storage industry in several ways.

- Increase deliverable gas without an increase in storage requirements.
- Increase peaking service.
- Reduce capital expenditure.
- Lower storage costs.
- Reduce storage construction cost.

The cost savings to industry will depend on how much the working gas capacity can be safely increased for each storage cavern and if this increased capacity is utilized. In this study, cost savings were estimated as the reduced capital expense resulting from a reduction in cushion gas volume, the lower storage costs related to the increase in working gas storage space available for lease, and the lower construction costs of a new facility. Examples of the cost savings are given for Cavern A and Cavern B.

If it is possible to lower the minimum gas pressure of a cavern, the operator is able to recoup the capital cost associated with the reduction in volume of the required cushion gas. Based on the analyses of Cavern A and Cavern B, only a small reduction in the design minimum gas pressure (approximately 0.01 psi/ft at the casing shoe) is necessary to offset the price of adopting the new design criterion.

By increasing the working gas volume, storage operators can also benefit through the sale of larger or more contracts and/or reduced penalty risk. Cost savings estimates for Cavern A and Cavern B, assuming a storage lease rate of $0.07 per MMBtu s per month, suggest annual cost savings of $83,500 and $163,000, respectively, for a reduction in the design minimum gas pressure of 0.01 psi/ft at the casing shoe.

In estimating the reduction in construction costs for a new facility, cost savings were based on the reduced cavern size required when the MDCF model is used in cavern design. Based on a conservative construction cost of $3 per thousand cubic feet of working gas, it was estimated that every 1 psi decrease in the design minimum gas wellhead pressure could reduce the construction cost of Cavern A by $15,900 and Cavern B by $3,300. Using these estimates, only a small reduction in the design minimum gas pressure (10 psi for Cavern A and 50 psi for Cavern B) is necessary to offset the $115,000 to $165,000 cost of adopting the new design criterion.

TABLE OF CONTENTS

TABLE OF CONTENTS
(Continued)

LIST OF TABLES

LIST OF FIGURES

LIST OF FIGURES
(Continued)

FIGURE **PAGE**

1.0 INTRODUCTION

1.1 BACKGROUND

With the projected growth in natural gas demand exceeding the current pipeline and underground storage capacities, innovative concepts are being sought to meet the needs of the natural gas industry and end-use markets. Much of the growth will be met through increased pipeline capacity and conventional storage. Conventional storage includes underground storage in depleted oil and gas fields, aquifers, and salt caverns.

The storage of compressed natural gas (CNG) in salt caverns is a growing industry. Product movement to and from CNG storage caverns is accomplished simply by compression and expansion of the stored gas. Consequently, the internal pressure on the walls of a CNG storage cavern can vary considerably. Since a minimum level of internal pressure is necessary to ensure cavern stability, a certain quantity of gas must always remain in a cavern. This gas is referred to as the base or cushion gas. The quantity of gas that can be withdrawn from a cavern is referred to as the working gas volume.

The economics of CNG storage in salt caverns are largely dependent on maximizing the ratio between the working gas and the cushion gas volumes. This ratio depends directly on the relative values of the maximum and minimum gas pressures permitted in the storage cavern. The maximum storage pressure is limited by regulation to a fraction of the weight of the overburden (typically 0.75 to 0.85 of the vertical stress) in order to prevent hydraulic fracturing of the salt and/or cemented casing and loss of containment. The minimum pressure required to ensure the structural stability of the cavern is much more difficult to determine. Conventional practice requires the use of both conservative design criteria (e.g., Ratigan et al., 1991) and numerical simulations of typical gas service cycles comprising different minimum operating gas pressures to predict the states of stress in the salt surrounding the cavern. The predicted states of stress are compared to states of stress known to cause damage (microcracking that produces salt dilation or volume expansion); and then, the minimum gas pressure is established as the lowest pressure that can be achieved without inducing stresses in the salt that cause dilation.

It is well known that some damage or dilation is permissible without compromising the mechanical integrity of the salt. In addition, salt damage is known to be recoverable under hydrostatic and/or high mean stress conditions. In gas storage caverns, high mean stress conditions are induced in the salt when the gas storage pressures are high; e.g., during maximum storage pressure conditions. Therefore, any salt damage induced in the salt surrounding the cavern at low storage pressures is likely to be recovered or healed at high storage pressures. The conventional design criteria do not allow for any salt damage nor do they account for salt healing. Advanced constitutive models (e.g., the Multimechanism

Deformation Coupled Fracture (MDCF) model [Chan et al., 1992]) for salt have been developed which do address the shortcomings of the conventional method, and when used in storage cavern design, may allow lower minimum gas pressures without affecting the structural stability of cavern. In Phase I of this project, DeVries et al. [1998] used the advanced MDCF model to demonstrate that minimum gas pressures in CNG caverns could be reduced (compared to conventional design practices) without compromising the stability of the surrounding salt.

1.2 SCOPE

The purpose of Phase II of this project is twofold: (1) to develop an efficient laboratory test matrix that can be used to determine the site-specific model parameter values for the MDCF constitutive model and (2) to estimate the potential cost benefits gained as a result of using the MDCF model in cavern design.

The site-to-site variation in the mechanical behavior of salt requires that laboratory testing be performed to determine site-specific properties for the MDCF model. Because of the complexity of the MDCF model, tests providing load or strain histories that isolate material behavior dominated by one or only a few model parameters must be identified. The design of an efficient test matrix for evaluation of parameters in the MDCF model will make use of the approach followed by Senseny and Fossum [1995]. In their study, Senseny and Fossum used sensitivity coefficients to show the influence of each parameter in a highly nonlinear material model on the specimen response as a function of load history. An efficient test matrix is then developed by choosing tests and test conditions in which the sensitivity coefficient of each parameter that needs to be determined is sufficiently large to confidently determine the parameter value.

The possible cost benefits of using the MDCF model in cavern design are the result of lowering the minimum gas pressure and thus maximizing the working gas to cushion gas ratio. The cost benefits are analyzed by comparing the reduced storage costs to the additional cost of using the more advanced MDCF constitutive model.

1.3 REPORT ORGANIZATION

This report contains eight chapters. Chapter 2.0 discusses the current and proposed methods of CNG cavern design. The MDCF constitutive model, and how it can be simplified when used for the CNG cavern design, is presented in Chapter 3.0. Chapter 4.0 describes the possible laboratory techniques that can be used in testing salt. The sensitivity analysis and test matrix design is presented in Chapter 5.0. Chapter 6.0 presents the cost analysis. Conclusions are given in Chapter 7.0, and are followed by a list of references in Chapter 8.0.

2.0 COMPRESSED NATURAL GAS CAVERN DESIGN

2.1 TYPICAL CONDITIONS AND DESIGN CONSIDERATIONS

Salt domes and bedded salt deposits are found throughout the world. In the United States, large salt deposits are found in the Gulf Coast, the Great Lakes, and the Midwest regions. The development of storage caverns in salt for the containment of liquids (e.g., brine, oil, etc.) has been a popular alternative to surface storage since the early 1950s and is also becoming common practice for the containment of gaseous fluids such as natural gas, compressed air, etc. Natural rock salt is an excellent containment medium because of its extremely low permeability. Important factors for design consideration include cavern shape, cavern depth, in situ temperatures, and gas pressure cycles.

The development of caverns disturbs the natural stress state that exists in the salt before cavern development and induces deviatoric (or shear) stresses in the salt near the cavern. The deviatoric stresses are highest near the cavern walls, especially at abrupt changes in geometry, but decrease with distance away from the cavern. Furthermore, the magnitude of the deviatoric stresses is proportional to the cavern depth and inversely proportional to the cavern pressure.

Caverns designed for CNG storage are typically cylindrically shaped to maximize site usage. However, many natural gas caverns are converted from brine mining operations or caverns that have been used for other storage operations so their shapes may differ from the typical cylindrical shape. The depth to the top of storage caverns is generally between 1,000 and 7,000 feet. To maximize storage capacity, it is desirable to have the cavern as deep as possible because the maximum allowable gas pressure is generally about 75 to 85 percent of the overburden stress. However, the deviatoric stresses created by the difference in cavern pressure and in situ stresses increase with depth. Cavern heights vary considerably and can range from tens of feet in bedded formations to thousands of feet in salt domes.

Temperature also plays an important role in cavern design because the mechanical properties of salt are strongly temperature dependent. Typical in situ temperature gradients in Gulf Coast salt domes range from about 0.01°F/ft to about 0.015°F/ft [Law Engineering Testing Company, 1983]. Temperature gradients in bedded formations are more variable and range from about 0.005°F/ft to about 0.025°F/ft [Hardy, 1982].

Operating conditions also impact cavern design. Generally, minimum and maximum gas pressures are the products of cavern design. As mentioned above, the maximum gas pressure is generally required by law to be less than some fraction of the overburden stress. This requirement is to prevent the possibility of hydrofracturing the salt and exposing the

environment to product. The design minimum gas pressure is usually dictated by cavern closure rates and cavern stability.

2.2 CAVERN DESIGN AND EVALUATION

The approach generally used in the geomechanics evaluation of a salt cavern to be used for CNG storage is to determine an acceptable operating pressure range while meeting various design constraints [Ratigan et al., 1993]. These constraints typically include the following:

- Negligible potential for salt dilation that can lead to spalling in the cavern roof and/or walls and subsequent damage to the cavern or hanging string(s).
- Acceptable closure rates that will not result in excessive subsidence and/or damage to adjacent caverns and well casings.
- For bedded salts, an acceptable factor of safety in the overlying nonsalt layers to prevent roof collapse.
- Sufficient cavern spacing to negate cavern connectivity during (1) normal operations and (2) Mechanical Integrity Testing of the subject well or adjacent wells.

Of these constraints, the first is often the one that limits the minimum gas pressure in a natural gas storage cavern. When the deviatoric stress (caused by the difference between the gas pressure inside a cavern and the in situ stress of the surrounding salt) becomes too large, dilation (increased porosity) occurs in the salt. Spalling of the salt along the roof or wall of a cavern can occur when the dilation in the salt becomes severe enough to initiate macrofracturing.

The potential for salt dilation is typically evaluated using the Damage Potential method. The Damage Potential method indicates whether or not salt could dilate based only on the stress states in the salt [Ratigan et al., 1991]. However, with the development of advanced constitutive models, it may be possible to predict more accurately the cavern pressures and pressure cycles that will result in dilation and ultimately cavern failure. The following two sections describe the Damage Potential method and advanced design analysis.

2.2.1 Damage Potential Method

The Damage Potential method is based on the stress states that cause dilation of rock salt in laboratory experiments. This method has been used extensively in the last several years for estimating the potential for salt dilation around salt storage caverns (e.g., Ratigan et al. [1993]) and dry-mined excavations in salt at the Waste Isolation Pilot Plant (WIPP) in New Mexico (e.g., Hansen et al. [1993]; Lin and Van Sambeek [1992]; Van Sambeek et al. [1993]). Ratigan et

al. [1991] show that the potential for dilation in the salt surrounding an underground opening in salt can be described as:

$$\text{damage potential} = \frac{\sqrt{J_2}}{I_1} \tag{2-1}$$

where I_1 is the first invariant of the stress tensor and J_2 is the second invariant of the deviatoric stress tensor. These stress measures are defined as follows:

$$I_1 = s_1 + s_2 + s_3 \tag{2-2}$$

$$\sqrt{J_2} = \left(\frac{1}{6}\left[(s_1 - s_2)^2 + (s_1 - s_3)^2 + (s_2 - s_3)^2\right]\right)^{\frac{1}{2}} \tag{2-3}$$

where:

$$s_1, s_2, s_3 = \text{principal stresses.}$$

Based on creep tests on salt from the WIPP site and the Avery Island salt dome, dilation is expected when the damage potential is greater than about 0.27. This value of the damage potential defines the dilation boundary and differentiates between dilating and nondilating stress states. This boundary is shown by the straight line in Figure 2-1. Salt subjected to stress states in the region above this boundary is expected to dilate; those stress states below the boundary are not expected to produce dilation in salt. The Damage Potential method does not quantify the degree of dilation or microfracturing. Although this criterion is based on only WIPP and Avery Island salt, it has been found to characterize many Gulf Coast domal salts reasonably well [Ratigan et al., 1993].

2.2.2 Advanced Design Analysis

The Damage Potential method described above only defines stress states that result in dilation. However, by using an advanced constitutive model such as the MDCF model [Chan et al., 1992], the amount of dilation and also the healing of dilation can be estimated. It is possible that by having a more accurate prediction of the behavior of the salt, the minimum gas pressure in CNG salt caverns may be reduced. By incorporating damage accumulation and healing in the dilation model, some of the uncertainty and conservatism of the Damage Potential method can be reduced, and a more accurate dilation criterion may be established. If a more precise design criterion can be established for cavern analysis, the uncertainty in the minimum gas pressure requirement would also be reduced. This reduction of uncertainty may allow more accurate estimates of minimum gas pressure to be made, which could result in increased economic benefits for the CNG storage industry because of lower cushion gas volume requirements. A full description of the MDCF constitutive model is given in Chapter 3.0.

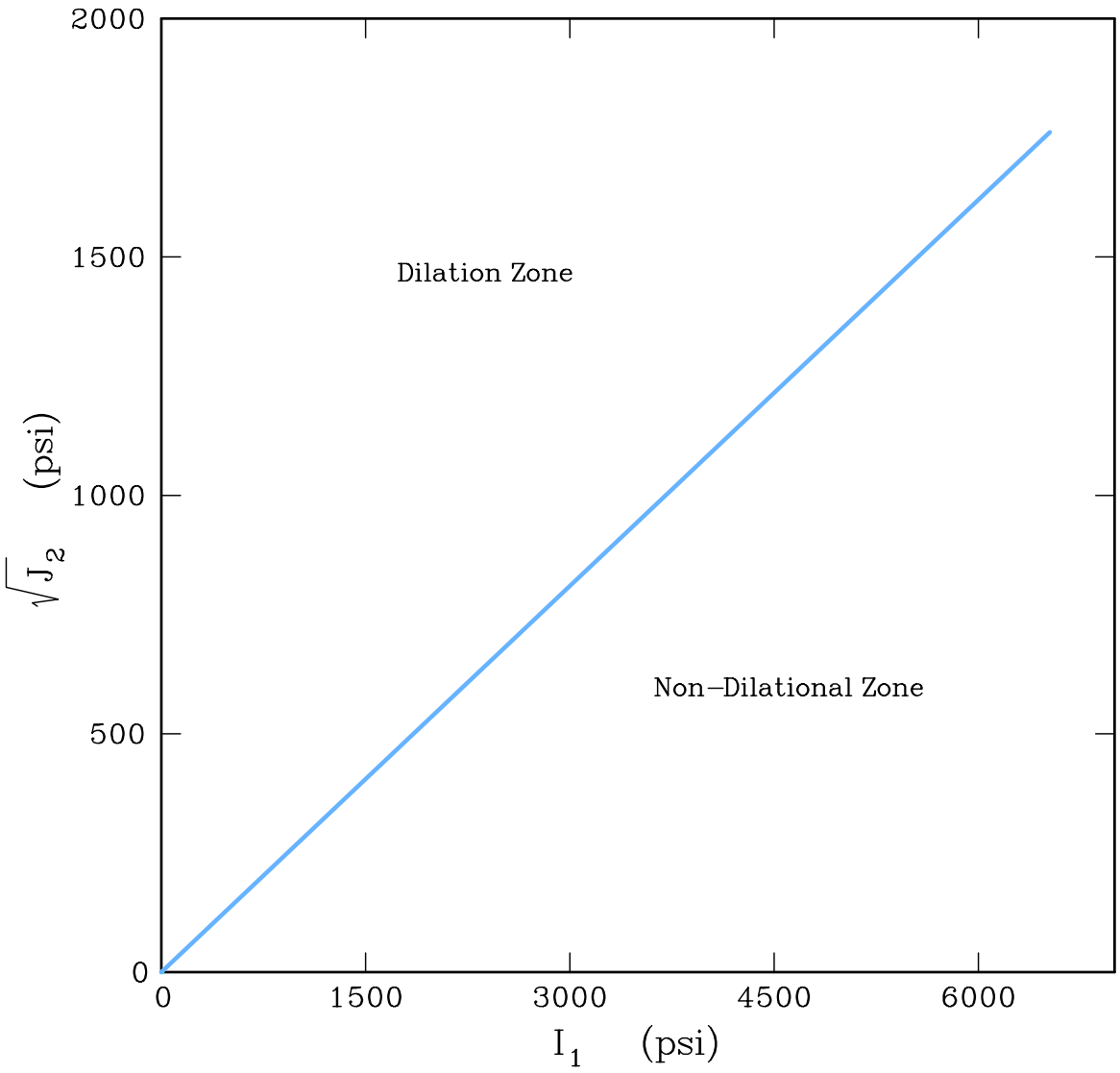

Figure 2-1. Dilation Boundary for Damage Potential Method (Developed by Ratigan et al., [1991]).

3.0 MULTIMECHANISM DEFORMATION COUPLED FRACTURE CONSTITUTIVE MODEL

Development of the MDCF model was an evolutionary process. In the first published paper of the MDCF model, Chan et al. [1992] formulated a damage-based kinetic equation which was added to the dislocation-based kinetic equation of the multimechanism deformation (M-D) model given by Munson et al. [1989]. Thus, the MDCF model is an extension of the M-D model, which was developed to provide an accurate constitutive model for the constant volume creep response of rock salt. Like the M-D model, development of the MDCF model was motivated by the need to develop a predictive technology for the safe disposal of radioactive waste for the WIPP.

3.1 MDCF MODEL DESCRIPTION

The MDCF model is a constitutive model that provides a continuum description of the creep response and the associated damage evolution and healing of rock salt. Both dislocation motion and creep induced damage are assumed to contribute directly to the macroscopic inelastic strain rate. In addition to a direct contribution to the inelastic strain rate, the MDCF model was formulated such that damage also produces a softening effect as proposed by Kachanov [1958]. The Kachanov damage variable reduces the load-bearing capacity through a reduction in the effective area using a continuum damage mechanics approach. The damage variable is determined from an evolutionary equation and provides a measure for the level of damage. For the MDCF model, the contribution of creep-induced damage and healing to the inelastic strain rate is incorporated through additional kinetic equations that are independent of the kinetic equation for dislocation mechanisms. The terms are combined using the approach given by Fossum et al. [1988] to derive a proper three-dimensional generalization using classical thermodynamic principles. The generalized form of the MDCF model is given by:

$$\dot{\varepsilon}_{ij}^{\,i} = \frac{\partial \sigma_{eq}^{c}}{\partial \sigma_{ij}} \dot{\varepsilon}_{eq}^{c} + \frac{\partial \sigma_{eq}^{\omega_s^*}}{\partial \sigma_{ij}} \dot{\varepsilon}_{eq}^{\omega_s} + \frac{\partial \sigma_{eq}^{\omega_t}}{\partial \sigma_{ij}} \dot{\varepsilon}_{eq}^{\omega_t} + \frac{\partial \sigma_{eq}^{h}}{\partial \sigma_{ij}} \dot{\varepsilon}_{eq}^{h} \tag{3-1}$$

where $\dot{\varepsilon}_{ij}^{\,i}$ is the inelastic strain and $\sigma_{eq}^{c}, \sigma_{eq}^{\omega_s^*}, \sigma_{eq}^{\omega_t}, \sigma_{eq}^{h}, \dot{\varepsilon}_{eq}^{c}, \dot{\varepsilon}_{eq}^{\omega_s}, \dot{\varepsilon}_{eq}^{\omega_t}$, and $\dot{\varepsilon}_{eq}^{h}$ are power-conjugate equivalent stress measures and equivalent inelastic strain rates for the dislocation creep (*c*), shear damage (ω_s), tensile damage (ω_t), and damage healing (*h*) mechanisms, respectively. Details of the power-conjugate stress measures, kinetic equations, flow laws, and evolution equation for damage in the MDCF model are summarized below. Note that compression is taken to be negative.

Kinetic Equation for Dislocation Flow

The kinetic equation representing the isochoric creep rate, $\dot{\varepsilon}_{eq}^{c}$, i.e., dislocation flow, is based on the modified M-D model [Munson et al., 1989]. The formulation remains unchanged with the exception that the six occurrences of the effective stress are divided by the term $(1-\omega)$, which represents the reduction in the effective load-bearing area caused by the presence of damage. The kinetic equation for the dislocation mechanisms is:

$$\dot{\varepsilon}_{eq}^{c} = F\dot{\varepsilon}_{s} \tag{3-2}$$

where F is the transient function representing transient creep behavior, and $\dot{\varepsilon}_{s}$ is the steady-state strain rate. The steady-state creep of salt is the sum of three dominant mechanisms: (1) a high temperature, low stress regime controlled by dislocation climb, (2) a low temperature, low stress regime controlled by an undefined mechanism, and (3) a high stress regime controlled by various possible dislocation slip mechanisms. The steady-state creep rates of the three relevant mechanisms, respectively, are given by:

$$\dot{\varepsilon}_{s_1} = A_1 e^{-Q_1/RT}\left(\frac{\sigma_{eq}^{c}}{\mu(1-\omega)}\right)^{n_1} \tag{3-3}$$

$$\dot{\varepsilon}_{s_2} = A_2 e^{-Q_2/RT}\left(\frac{\sigma_{eq}^{c}}{\mu(1-\omega)}\right)^{n_2} \tag{3-4}$$

$$\dot{\varepsilon}_{s_3} = \left|H\left(\frac{\sigma_{eq}^{c}}{1-\omega}-\sigma_0\right)\right|\left(B_1 e^{-Q_1/RT}+B_2 e^{-Q_2/RT}\right)\sinh\left[\frac{q\left(\frac{\sigma_{eq}^{c}}{1-\omega}-\sigma_0\right)}{\mu}\right] \tag{3-5}$$

where the A's and B's are constants, Q's are activation energies, T is the absolute temperature, R is the universal gas constant, μ is the shear modulus, n's are the stress exponents, q is the stress constant, and σ_0 is the stress limit of the dislocation slip mechanism. $|H|$ is a Heaviside step function. The transient creep function F is given by:

$$F = \begin{cases} \exp\left[\Delta\left(1-\frac{\varsigma}{\varepsilon_t^*}\right)^2\right] & \text{for } \varsigma < \varepsilon_t^* \\ 1 & \text{for } \varsigma = \varepsilon_t^* \\ \exp\left[-\delta\left(1-\frac{\varsigma}{\varepsilon_t^*}\right)^2\right] & \text{for } \varsigma > \varepsilon_t^* \end{cases} \tag{3-6}$$

which is composed of a work-hardening branch, an equilibrium branch, and a recovery branch, respectively. In Equation 3-6, Δ and δ represent the work-hardening and recovery parameters, respectively, and ε_t^* is the transient strain limit. The transient strain limit is a function of temperature and stress and is represented by:

$$\varepsilon_t^* = K_0 e^{cT} \left(\frac{\sigma_{eq}^c}{\mu(1-\omega)} \right)^m \tag{3-7}$$

where K_0, c, and m are constants. The work-hardening and recovery parameters are functions of stress given by:

$$\Delta = \alpha_w + \beta_w \log\left(\frac{\sigma_{eq}^c}{\mu(1-\omega)} \right) \tag{3-8}$$

$$\delta = \alpha_r + \beta_r \log\left(\frac{\sigma_{eq}^c}{\mu(1-\omega)} \right) \tag{3-9}$$

where the α's and β's are constants with the subscripts denoting either work-hardening (w) or recovery (r). The evolution rate, $\dot{\varsigma}$, of the internal variable ς, given in Equation 3-6 is governed by:

$$\dot{\varsigma} = (F-1)\,\dot{\varepsilon}_s \tag{3-10}$$

which diminishes to zero when the steady-state condition is achieved.

The maximum shear stress or Tresca criterion is used here for dislocation-induced flow. The power-conjugate equivalent stress measure, σ_{eq}^c, for the dislocation mechanisms, assuming the Tresca criterion, is given by:

$$\sigma_{eq}^c = 2\cos\psi\sqrt{J_2} = \sigma_1 - \sigma_3 \tag{3-11}$$

where ψ is the Lode angle, J_2 is the second invariant of the deviatoric stress tensor, and σ_1 and σ_3 are the maximum and minimum principal stresses, respectively.

Flow Law for Dislocation Deformation

The shear-induced dislocation flow of rock salt is assumed to be associative. The flow potential is an important factor in extending data obtained from constant stress laboratory creep tests to generalized three-dimensional states of stress. Differentiation of the power-conjugate stress given by Equation 3-11 with respect to stress leads to:

$$\frac{\partial \sigma_{eq}^{c}}{\partial \sigma_{ij}} = \left[\frac{\cos 2\psi}{\cos 3\psi}\right]\frac{s_{ij}}{\sqrt{J_2}} + \left[\frac{\sqrt{3}\sin\psi}{J_2 \cos 3\psi}\right] t_{ij} \tag{3-12}$$

where s_{ij} is the deviatoric stress tensor and $t_{ij} = s_{ip}s_{pj} - 2/3 J_2 \delta_{ij}$. Equation 3-12 is indeterminate when $\psi \rightarrow \pm\pi/6$. To eliminate this problem computationally, the flow potential is taken as the average of the flow potentials on either side of the indeterminacy and evaluated in the limit as $\psi \rightarrow \pm\pi/6$ whenever the lode angle is within 0.25 degree of the indeterminacy. For both conditions, the result is:

$$\frac{\partial \sigma_{eq}^{c}}{\partial \sigma_{ij}} = \frac{s_{ij}}{2\sqrt{3J_2}} \tag{3-13}$$

Thus, at the corners of the Tresca potential, the indeterminacies are removed by assuming a von Mises flow which makes the direction of straining unique.

Kinetic Equations for Damage-Induced Flow

The kinetic equations for damage-induced flow are similar in nature to dislocation flow in that damage-induced transient creep is accommodated in the model through a multiplier on the kinetic equations for damage-induced flow during steady-state creep. The model was developed assuming damage can occur in compression as a result of sliding of microcracks by shear and the opening of wing-tip cleavage cracks that develop on some of the shear cracks. Tensile creep damage is also accounted for in the model and is based on the formation of cleavage microcracks aligned normal to the tensile stress. The kinetics of tensile damage in salt are substantially faster than shear damage and is therefore treated as a separate term. The equations describing the shear-induced (*s*) and tension-induced (*t*) damage are similar in form. Thus, the subscript *i* is used to represent *s* and *t* in the equations to follow. The equivalent inelastic strain rate is given by:

$$\dot{\varepsilon}_{eq}^{\omega_i} = F^{\omega_i}\dot{\varepsilon}_{s}^{\omega_i} \tag{3-14}$$

where:

$$F^{\omega_s} = F\ \exp\left[\frac{c_4\left(\sigma_{eq}^{c} - c_5\right)}{\sigma_0\left(1-\rho\right)}\right] \tag{3-15}$$

$$F^{\omega_t} = F\ \exp\left[\frac{c_4\left(\sigma_{eq}^{\omega_t} - c_5\right)}{\sigma_0\left(1-\rho\right)}\right] \tag{3-16}$$

are the functions that account for the damage-induced inelastic strain rate in the transient region and ρ is the volume fraction of clay particles. The kinetic equation for damage-induced flow during steady-state creep is given by:

$$\dot{\varepsilon}_s^{\omega_i} = c_1 \omega_0 \exp(c_3 \omega) \left[\sinh\left(\frac{c_2 \sigma_{eq}^{\omega_i} H\left(\sigma_{eq}^{\omega_i}\right)}{(1-\omega)(1-\rho)\mu} \right) \right]^{n_3} \tag{3-17}$$

with:

$$c_1 = c_0 \left(B_1 e^{(-Q_1/RT)} + B_2 e^{(-Q_2/RT)} \right) \tag{3-18}$$

where the *c*'s and n_3 are material constants, ω_0 is the initial value of the damage variable (ω) and the *B*'s and *Q*'s are constants of the dislocation glide mechanisms. As shown in Equation 3-17, the Heaviside step function prevents accumulation of damage whenever the power-conjugate equivalent stress measure is negative.

The power-conjugate equivalent stress measures are given by:

$$\sigma_{eq}^{\omega_s} = \left|\sigma_1 - \sigma_3\right| + f_p x_2 x_7 \operatorname{sgn}(I_1 - \sigma_3) \left(\frac{I_1 - \sigma_3}{3 x_7 \operatorname{sgn}(I_1 - \sigma_3)} \right)^{x_6} \tag{3-19}$$

$$\sigma_{eq}^{\omega_t} = x_1 \sigma_1 H(\sigma_1) \tag{3-20}$$

where x_1, x_2, x_6, and x_7 are material constants of the damage model; I_1 is the first stress invariant; and σ_1 and σ_3 are the maximum and minimum principal stresses, respectively, with compression assumed to be negative. The first term in Equation 3-19 represents the driving force for shear-induced damage, which leads to the opening of wing-tip microcracks or grain boundary cracks. The second term in Equation 3-19 represents the suppression of microcrack growth by a confining pressure. This term was recently extended to account for the increase in damage accumulation associated with increasing impurity of clay content [Chan et al., 1996a]. The material parameter f_p is related to the impurity content by:

$$f_p = 1 - p_1 \rho \tag{3-21}$$

where ρ is the impurity content parameter and p_1 is a material parameter, which is analogous to a local stress intensity factor.

The preceding equations include the damage variable (ω), which is described in terms of an evolutionary equation. The damage evolution equation is taken as:

$$\dot{\omega} = \dot{\omega}_s + \dot{\omega}_t - \dot{h} \tag{3-22}$$

where the damage rate components for the shear-induced and tension-induced damage are given by:

$$\dot{\omega}_s = \frac{x_4}{t_0}\omega\left[\ln\left(\frac{1}{\omega}\right)\right]^{\frac{x_4+1}{x_4}}\left[\frac{\sigma_{eq}^{\omega_s} H\left(\sigma_{eq}^{\omega_s}\right)}{(1-\rho)\xi_s}\right]^{x_{3s}} \tag{3-23}$$

$$\dot{\omega}_t = \frac{x_4}{t_0}\omega\left[\ln\left(\frac{1}{\omega}\right)\right]^{\frac{x_4+1}{x_4}}\left[\frac{\sigma_{eq}^{\omega_t} H\left(\sigma_{eq}^{\omega_t}\right)}{(1-\rho)\xi_t}\right]^{x_{3t}} \tag{3-24}$$

where x_4, x_{3s}, x_{3t}, ξ_s, ξ_t, and t_0 are material constants. The parameter ξ_s may have different values according to the magnitude of the effective shear-induced damage stress; i.e.,

$$\begin{aligned} \xi_s &= \xi_s^1 \text{ for } \sigma_{eq}^c/(1-\omega) > \sigma_0 \\ \xi_s &= \xi_s^2 \text{ for } \sigma_{eq}^c/(1-\omega) \le \sigma_0 \end{aligned} \tag{3-25}$$

The healing term or damage recovery rate is discussed later under the discussion of the kinetic equation for healing.

Flow Law for Damage-Induced Inelastic Deformation

The shear-induced inelastic damage flow is assumed to be nonassociative. The flow potential power-conjugate stress measure for shear-induced damage is given by (cf. Equation 3-19):

$$\sigma_{eq}^{\omega_s^*} = \left|\sigma_1 - \sigma_3\right| + \frac{x_2 x_8}{3}\left(I_1 - \sigma_3\right) \tag{3-26}$$

where x_8 is a material constant. Differentiation of the power-conjugate stress given by Equation 3-26 with respect to stress leads to:

$$\frac{\partial \sigma_{eq}^{\omega_s^*}}{\partial \sigma_{ij}} = b_1 \frac{s_{ij}}{\sqrt{3J_2}\cos 3\psi} + b_2 \frac{t_{ij}}{J_2 \cos 3\psi} + 2b_4 \frac{\delta_{ij}}{3} \tag{3-27}$$

where:

$$b_1 = \sqrt{3}\cos 2\psi - b_4 \sin\left(2\psi - \frac{\pi}{3}\right) \tag{3-28}$$

$$b_2 = \sqrt{3}\sin\psi - b_4 \cos\left(\psi + \frac{\pi}{3}\right) \tag{3-29}$$

$$b_4 = \frac{x_2 x_8}{3} \tag{3-30}$$

The flow potential power-conjugate stress measure for tension-induced damage is given by:

$$\sigma_{eq}^{\omega_t} = x_1 \sigma_1 H(\sigma_1) \tag{3-31}$$

where x_1 is a material constant. Differentiation of the work conjugate stress given by Equation 3-31 with respect to stress leads to:

$$\frac{\partial \sigma_{eq}^{\omega_t}}{\partial \sigma_{ij}} = x_1 \; H(\sigma_1)\left[\sin\left(2\psi + \frac{\pi}{3}\right)\frac{s_{ij}}{\sqrt{3J_2}\cos 3\psi} + \cos\left(\psi - \frac{\pi}{3}\right)\frac{t_{ij}}{J_2 \cos 3\psi} + \frac{\delta_{ij}}{3}\right] \tag{3-32}$$

Reviewing the flow laws for the shear-induced and tension-induced damage, one observes an indeterminacy when $\psi = \pm \pi/6$. To eliminate this problem computationally, the flow potential is taken as the average of the flow potentials on either side of the corner and evaluated in the limit as $\psi \to \pm \pi/6$. Performing this limiting operation as ψ approaches $\pi/6$ (the triaxial compression corner), Equation 3-27 for the shear-induced damage term becomes:

$$\frac{\partial \sigma_{eq}^{\omega_s^*}}{\partial \sigma_{ij}} = b_1' \left(\frac{s_{ij}}{\sqrt{3J_2}} - \frac{t_{ij}}{2J_2}\right) + 2b_4 \frac{\delta_{ij}}{3} \tag{3-33}$$

where:

$$b_1' = 1 + \frac{2b_4}{3} \tag{3-34}$$

and at the triaxial extension corner ($\psi = -\pi/6$):

$$\frac{\partial \sigma_{eq}^{\omega_s^*}}{\partial \sigma_{ij}} = b_1'' \left(\frac{s_{ij}}{\sqrt{3J_2}} + \frac{t_{ij}}{2J_2}\right) + 2b_4 \frac{\delta_{ij}}{3} \tag{3-35}$$

where:

$$b_1'' = 1 + \frac{b_4}{3} \tag{3-36}$$

which are used when the Lode angle is within 0.25 degree of ±30 degrees.

Performing this limiting operation as ψ approaches $\pi/6$ (the triaxial compression corner), Equation 3-32 for the tension-induced damage term becomes:

$$\frac{\partial \sigma_{eq}^{\omega_t}}{\partial \sigma_{ij}} = \frac{x_1 H(\sigma_1)}{3}\left(\frac{s_{ij}}{\sqrt{3J_2}} - \frac{t_{ij}}{2J_2} + \frac{\delta_{ij}}{2}\right) \tag{3-37}$$

and at the triaxial extension corner $(\psi = -\pi/6)$:

$$\frac{\partial \sigma_{eq}^{\omega_t}}{\partial \sigma_{ij}} = \frac{2x_1 H(\sigma_1)}{3}\left(\frac{s_{ij}}{\sqrt{3J_2}} + \frac{t_{ij}}{2J_2} + \frac{\delta_{ij}}{2}\right) \tag{3-38}$$

which are used when the Lode angle is within 0.25 degree of ±30 degrees.

Kinetic Equation for Damage Recovery Flow (Healing)

Reduction of damage in rock salt can occur by the closure of open microcracks and the sintering of microcracks. The kinetic equation representing the healing or damage recovery process gives the total inelastic healing rate as follows:

$$\dot{\varepsilon}_{ij}^{h} = \dot{\varepsilon}_{eq}^{h} \frac{\partial \sigma_{eq}^{h^*}}{\partial \sigma_{ij}} \tag{3-39}$$

where $\sigma_{eq}^{h^*}$ and $\dot{\varepsilon}_{eq}^{h}$ are the power-conjugate equivalent stress measure and the equivalent inelastic strain rate for the healing mechanisms, respectively.

The equivalent inelastic healing strain rate in Equation 3-39 is given as [Chan et al., 1996b]:

$$\dot{\varepsilon}_{eq}^{h} = \frac{\varepsilon_{kk}^{i}\left(\sigma_{eq}^{h} - \sigma_b\right) H\left(\sigma_b - \sigma_{eq}^{h}\right)}{\tau\mu} \tag{3-40}$$

where $\dot{\varepsilon}_{kk}^{i}$ is the inelastic volumetric strain, τ is a characteristic time constant, and μ is the shear modulus. *H()* is the Heaviside function; thus, the healing rate is zero if the equivalent stress measure σ_{eq}^{h} is less than σ_b. The equivalent stress measure used to describe the magnitude

of the healing strain rate is different than the power-conjugate equivalent stress measure used to describe the flow potential (nonassociative formulation) and is given by:

$$\sigma_{eq}^{h} = \frac{1}{3}\left(I_1 - \sigma_3\right) \tag{3-41}$$

The value for σ_b is determined from Equation 3-19 by solving for the value of σ_{eq}^{h} when $\sigma_{eq}^{\omega} = 0$, which is given by:

$$\sigma_b = -x_7\left[\frac{\sigma_1 - \sigma_3}{f_p x_2 x_7}\right]^{\frac{1}{x_6}} \tag{3-42}$$

Then the quantity $\sigma_{eq}^{h} - \sigma_b$ overlays the curve that describes the damage so that damage accumulation occurs above the curve and damage recovery (healing) occurs below the curve. The characteristic time constant (τ) is taken to be a function of the inelastic volumetric strain and is written as:

$$\tau = \tau_0 \exp\left(-k_1 \varepsilon_{kk}^{i}\right) + \tau_1 \tag{3-43}$$

where k_1 is a material constant and τ_0 and τ_1 are characteristic time constants. When the volumetric strain is large, the exponential term becomes insignificant and the limiting value for τ is τ_1. τ_1 is then the characteristic time associated with microcrack closure when the level of damage is high. When the inelastic volumetric strain becomes small, the limiting value of τ is $\tau_0 + \tau_1$, which is the characteristic time constant associated with crack sintering.

The damage variable (ω) is described in terms of the evolutionary equation given in Equation 3-22. The healing portion of the equation (modified with the initial damage Heaviside) is taken from [Chan et al., 1996b]:

$$\dot{h} = \frac{\omega\, H\left(\omega - \omega_0\right)\left(\sigma_{eq}^{h} - \sigma_b\right) H\left(\sigma_b - \sigma_{eq}^{h}\right)}{\tau\, \mu} \tag{3-44}$$

Flow Law for Healing-Induced Inelastic Deformation

The healing (damage recovery) inelastic damage flow is anisotropic because damage will typically accumulate normal to the major principal stress (compression negative). To implement the anisotropic nature of the healing, Chan et al. [1996b] have developed the flow potential based on stress-induced anisotropy. However, the state of stress does not provide information regarding the direction of damage. In addition, Chan's development includes indeterminant conditions under hydrostatic states of stress. Also, under triaxial extension test

conditions, Chan's flow potential predicts axial shortening; whereas, under triaxial compression test conditions, axial lengthening is predicted. This condition creates deformation in the opposite direction of loading regardless of the magnitude of the load. For these reasons, a simple isotropic flow based only on mean stress was adopted. Thus, the power-conjugate effective stress measure describing the flow potential is:

$$\sigma_{eq}^{h^*} = \sigma_m \tag{3-45}$$

and the flow potential is given by:

$$\frac{\partial \sigma_{eq}^{h^*}}{\partial \sigma_{ij}} = \frac{\delta_{ij}}{3} \tag{3-46}$$

3.2 MDCF MODEL PARAMETERS

The two caverns modeled in Phase I of this project, Cavern A and Cavern B, are located in two different salt domes. The salts from the sites of Cavern A and Cavern B are referred to as A-salt and B-salt, respectively. The MDCF parameters used to model the mechanical response of the salt at these two sites are given in Table 3-1. The dislocation creep properties are based on creep tests on salt from each of the salt domes. No testing was performed to determine the damage and healing parameter values. Therefore, the damage and healing parameter values determined for WIPP salt were used.

3.3 REDUCTION OF MODEL PARAMETERS

As mentioned above, the MDCF model was initially developed to model the extreme conditions expected at the WIPP. The MDCF constitutive model has a total of 41 parameters. However, because of the limited range of stress and temperature conditions experienced in the salt surrounding CNG storage caverns, it is not necessary to determine all of the parameters in the MDCF model. The parameters that do not need to be evaluated on a site specific basis for CNG storage caverns are treated deterministically and can be assigned typical values (such as the values determined for WIPP salt). Table 3-2 lists the parameters according to their role in the MDCF model and whether they are treated as free or deterministic parameters.

The parameter, *m*, which is an exponent in the transient strain limit equation (Equation 3-7), has a theoretical value of 3 and can be treated deterministically. The parameter, ρ, in the damage equations, is the impurity content of the salt. This parameter is determined by the mineralogy of the salt, not by mechanical testing of salt. An impurity content of 0.02 was used as a representative value in this analysis. The parameter μ is a stress-scaling factor and it is typically assigned a value of 1.4×10^6 psi. Since the internal damage variable must be nonzero to grow, the initial damage parameter, ω_0, is assigned a negligible value of 0.0001. Also, β_r was

assumed to be zero, (thus $\delta = \alpha_r$) because insufficient test data were available to determine the stress dependency of the recovery parameter for either of the sites.

The steady-state dislocation creep portion of the MDCF model is comprised of three mechanisms. The first mechanism (Equation 3-3) is only dominant at temperatures and deviatoric stresses much higher than those expected near a CNG storage cavern. For example, using the parameters determined for the sites of Caverns A and B at a temperature of 120°F, the first mechanism only accounts for about 1 to 3 percent of the steady-state strain rate in the range of expected deviatoric stresses. Thus, the parameters A_1, Q_1/R, and n_1 can be treated as deterministic properties.

Table 3-1. MDCF Model Parameter Values (Page 1 of 2)

Parameter	Units	Cavern A	Cavern B
Elastic Parameter Values			
E	psi	3.59×10^6	2.63×10^6
v	-	0.30	0.18
Dislocation Creep Parameter Values			
A_1	day^{-1}	5.87×10^{27}	3.82×10^{27}
A_2	day^{-1}	3.19×10^{15}	2.07×10^{15}
Q_1/R	R	2.27×10^4	2.27×10^4
Q_2/R	R	1.17×10^4	1.17×10^4
n_1	-	5.5	5.5
n_2	-	3.73	3.68
B_1	day^{-1}	1.67×10^{12}	1.08×10^{12}
B_2	day^{-1}	5.30 x 10^4	3.44×10^4
q	-	3,330	2,800
σ_0	psi	1,930	1,280
μ	psi	1.40×10^6	1.40×10^6
m	-	3	3
K_0	-	3.73×10^6	5.27×10^4
c	R^{-1}	5.11×10^{3}	5.11×10^{-3}
α	-	-1.25	-10.39
β	-	-2.07	-6.17
δ	-	0.2417	0.2417

Table 3-1. MDCF Model Parameter Values (Page 2 of 2)

Parameter	Units	Cavern A	Cavern B
Damage and Healing Parameter Values			
x_1	-	6	6
x_2	-	9	9
x_{3s}	-	5.5	5.5
x_{3t}	-	40	40
x_4	-	3	3
ξ_s^1	psi	3.35×10^4	3.35×10^4
ξ_s^2	psi	5.09×10^4	5.09×10^4
ξ_t	psi	2,197	2,197
x_6	-	0.75	0.75
x_7	psi	145	145
x_8	-	0.1	0.1
t_0	day	1.16×10^{-5}	1.16×10^{-5}
τ_0	day	4.34	4.34
τ_1	day	2.17×10^{-4}	2.17×10^{-4}
c_0	-	50,000	50,000
c_2	-	850	850
c_3	-	10	10
c_4	-	6	6
c_5	psi	3,626	3,626
n_3	-	3	3
k_1	-	5,000	5,000
p_1	-	28	28
ω_0	-	0.0001	0.0001
r	-	0 to 0.03	0 to 0.03

In most cases, the test matrix can be reduced significantly without compromising cavern integrity by assuming typical temperature dependencies in the MDCF model. By making this assumption, the parameters Q_1/R, Q_2/R, and c do not need to be determined. Based on the typical in situ temperature gradients in Gulf Coast salt domes, a 1,000-foot-tall cavern has a temperature difference of only about 10°F across the height of the cavern. To minimize the

error in making this temperature-dependence assumption, tests should be conducted at a temperature equal to the in situ temperature at the cavern midheight. However, for very tall caverns or sites with an exceptionally high geothermal gradient, conducting tests at various temperatures may need to be considered.

Table 3-2. Functional Characteristics of MDCF Parameters

Function	Free Parameters	Deterministic Parameters
Transient Creep	a, b, K_0, d	m, c
Steady-State Creep	A_2, B_1, B_2, n_2, σ_0, q	A_1, n_1, Q_1/R, Q_2/R, μ
Shear Damage	x_{3s}, x_8, ξ_s^1, ξ_s^2	
Tension Damage		x_1, x_{3t}, ξ_t
Healing	k_1, τ_0, τ_1	
Shear and Tension Damage	x_4, t_0, c_0, c_2, c_3, c_4, c_5, n_3	
Damage and Healing	x_2, x_6, x_7, p_1	ω_0, ρ

It is a rare occurrence for the stresses in the salt surrounding a CNG storage cavern to become tensile. In fact, because of the low tensile strength of salt (usually less than 300 psi), cavern design constraints require that no tensile stresses exist in the salt surrounding a cavern. Thus, the potential for damage under tensile stress states is eliminated and the tension damage parameters (x_1, x_{3t}, and ξ_t) can be treated as deterministic.

4.0 LABORATORY TECHNIQUES

4.1 LOAD PATH CONSIDERATIONS

This chapter outlines the various constant-temperature load paths that are available in the laboratory. The load paths being considered are those generally available when using computerized test systems equipped with pressure vessels that can accommodate conventional, right-circular, cylindrical, solid specimens. The load paths are presented as simple functions that can be combined in various ways to effect different kinds of laboratory tests. For example, a creep test is generally thought of as a simple constant stress load path, but in fact, a creep test is a combination of at least four unique load paths: (1) initial hydrostatic loading (2) constant hydrostatic stress, (3) axial stress difference, loading, and (4) constant stress creep at the applied stress difference. Additional load paths could be encountered in the creep test during multistage testing, or during unloading, when the test is terminated.

The load path descriptions designate which variables are being controlled. For our purposes, the set of controllable variables will be constrained to total stresses, total stress rates, total strains, and total strain rates. This constraint means that constant temperature is being assumed. If required, temperature effects could be investigated by running the load paths at different levels of constant temperature. The total stress/stress-rate constraint means that pore pressures are presumed to be zero, which eliminates the use of effective stress measures. This constraint is convenient because the force and pressure measurements made during a test represent total stresses. The total strain/strain-rate constraint means that the strain measurements made during a test always contain both elastic and inelastic strain components. The exception is for specific load paths where one of the strain components can safely be assumed as zero; e.g., the elastic strain rate is zero when the stress rate is zero. In addition to the constraints on controllable variables, there are additional conditions that are generally accepted in routine laboratory testing. For example, the instrumentation applied to the specimen is generally oriented along the principal axes of the specimen. Then, the reasonable assumption is that the measured stresses and strains are principal stresses and strains so long as the deformed specimen maintains a right-circular, cylindrical shape.

4.2 SIMPLE LOAD PATHS

When defining a load path, one must identify the variables that are being controlled versus the response variables that are simply being measured. Most common test systems have two axes of control; one axis of control dedicated to the axial principal direction and the second axis of control dedicated to the radial principal direction. Thus, in a typical configuration, the axial force (axial stress) may be controlled on one axis with the confining pressure (radial stress)

being controlled on the other axis, while the axial and radial strains are measured as response variables. In other configurations, the axial strain rate can be controlled on one axis and the confining pressure held constant with the other axis, leaving the axial stress and radial strain as the response variables. The best test systems allow the operator to specify either stress or strain as the feedback signal for controlling the axial force axis, with the capability of switching between the two feedback signals while the test is running. This feature is commonly known as *mode switching* and allows the operator to change from a stress-controlled path to a strain-controlled path (or vice versa) without the necessity of reconfiguring the test system or disassembling the test apparatus.

Assuming two axes of control, one dedicated to the axial principal direction and the other dedicated to the radial principal direction, a matrix of typical test configurations is formed as shown in Table 4-1. The test configurations in Table 4-1 are generally available at any materials testing laboratory using computerized test systems that are equipped for performing triaxial compression tests on cylindrical specimens. The stress and strain symbols used in Table 4-1 are defined as:

σ_a = axial stress
$\dot{\sigma}_a$ = axial stress rate
ε_a = axial strain
$\dot{\varepsilon}_a$ = axial strain rate
σ_r = radial stress
$\dot{\sigma}_r$ = radial stress rate
ε_r = radial strain
$\dot{\varepsilon}_r$ = radial strain rate.

Table 4-1. Matrix of Typical Test Configurations

		Axial Control Axis			
		σ_a	$\dot{\sigma}_a$	ε_a	$\dot{\varepsilon}_a$
Radial Control Axis	σ_r	A	B	C	D
	$\dot{\sigma}_r$	-	E	-	-
	ε_r	-	F	-	G
	$\dot{\varepsilon}_r$	-	-	-	-

The variables being controlled or measured along the axial axis are listed in the top row of the matrix in Table 4-1. The variables being controlled or measured in the radial direction are listed in the column at the left edge of the matrix. The alphabetic symbols located at some of

the row and column intersections indicate typical combinations of axial and radial control modes used in many common laboratory tests. For example, the symbol *B* at the intersection of axial stress rate and radial stress indicates a load path where the axial stress rate is controlled to a constant value and the radial stress is controlled to a constant value. This would be a typical load path used for strength testing; i.e., load-controlled testing at a constant confining pressure. Further details on each of the intersection symbols are given in the following sections. All discussions of load path assume the conventional rock mechanics sign convention; that is, compression is positive. Furthermore, except where noted in discussions, most test systems require that all stresses be compressive (nonnegative) to prevent separation at the interfaces between the specimen and the platens and jackets through which the loads are applied.

4.2.1 Intersection A: Axial Stress and Radial Stress Control

The axial stress level and the radial stress level are held at constant values over some period of time. If the axial stress level equals the radial stress level, then the stress state would represent hydrostatic. If the axial stress is greater (more compressive) than the radial stress, the stress state represents a triaxial compression creep test. The counterpart to the triaxial compression creep test is the triaxial extension creep test wherein the axial stress is less than the radial stress. If noncylindrical specimens are used (commonly known as dog-bone specimens), the axial stresses may actually become tensile in a triaxial extension test.

4.2.2 Intersection B: Axial Stress Rate and Radial Stress Control

The axial stress is applied at a constant rate while the confining pressure is held constant. This is a typical triaxial compression strength test technique. If the confining pressure is at the specific value of zero, then the test is commonly called an unconfined compression test. This particular load path is also commonly encountered during the initiation of a creep test where the axial stress is increased to some prescribed value below the specimen s compressive strength while the confining pressure is held constant.

4.2.3 Intersection C: Axial Strain and Radial Stress Control

The axial strain and the radial stress are both held at constant values. This control state is usually imposed after the specimen has been loaded to some prescribed axial strain value under one of the other load path designations. When this control state is imposed, the axial stress will either remain constant (i.e., material is elastic), begin to decrease (under conditions of triaxial compression), or begin to increase (under conditions of triaxial extension). A change in axial stress and radial strain over time indicates the material is creeping. When the axial stress is decreasing, the test is commonly known as a stress relaxation test and is the counterpart to the conventional constant stress creep test described at intersection *A*.

4.2.4 Intersection D: Axial Strain Rate and Radial Stress Control

This load path is the counterpart to the one described at intersection *B*. Where the former test was performed at a constant axial stress rate, this test is performed at a constant axial strain rate. Both types of tests are commonly used for strength testing.

4.2.5 Intersection E: Axial Stress Rate and Radial Stress Rate Control

This load path is used in proportional loading tests where the axial and radial stress rates may be different, but constant. One common proportional loading test is known as the hydrostatic compression test where the axial and radial stress rates are equal. A less common proportional loading test is known as the constant mean stress test where the axial and radial stress rates are unequal, but controlled at constant rates that result in a constant mean stress. By increasing the axial stress at twice the rate the radial stress is decreased, a deviatoric stress is imposed while maintaining a constant mean stress. This load path is available only after the specimen has been brought to a hydrostatic stress state from which the axial and radial stress rates can be initiated. The constant mean stress test has proven useful for testing of materials that dilate. Dilation is the phenomenon exhibited by many rocks wherein crystalline microcracking induced by deviatoric loading eventually leads to macroscopic cracking as a precursor to material failure. Both the micro- and macrocracking cause the void space to increase, which is reflected in the strain measurements as an increase in specimen volume (dilation). By following a load path wherein the mean stress is held constant while deviatoric stress is increased, the volume of the specimen should remain constant until the onset of dilation.

4.2.6 Intersection F: Axial Stress Rate and Radial Strain Control

This load path is not commonly used, but is available on test systems with computerized control. The axial stress is increased at a constant rate while the radial strain is held at a constant value, usually zero. By holding the radial strain at zero, the load path represents a uniaxial strain test where the axial strain is the only component of the volumetric strain. In order to keep the radial strain at zero during loading, the radial strain transducer is used to provide a feedback signal to the control axis that guides the confining pressure. As axial stress increases, the confining pressure is increased to maintain a zero radial strain. This test could also be performed in triaxial extension by first bringing the specimen to an elevated hydrostatic stress state. The axial stress would be decreased to provide an extensile axial stress condition and the radial strain transducer feedback would cause a corresponding decrease in confining pressure to prevent a change in the radial strain.

4.2.7 Intersection G: Axial Strain Rate and Radial Strain Control

This load path is similar to the one just described for intersection *F*. The only difference is that the axial loading proceeds under a constant axial strain rate instead of a constant axial stress rate.

4.2.8. Other Intersections and Specialty Load Paths

The other intersections in Table 4-1 are not discussed in detail here because the load paths already described are generally sufficient to estimate constitutive parameters. However, the unexplored intersections are still available load paths that can be used if the need should arise. The load paths specifically labeled in Table 4-1 represent the most common uses of traditional test systems, but specialty load paths may also be devised when required. One example of a special load path uses the radial strain axis to control the loading in the axial direction. This path represents a triaxial compression strength test (similar to intersection *D*), but the test is run at a constant radial strain rate instead of a constant axial strain rate. This path is useful for investigating the postpeak behavior of brittle materials, where pronounced dilation is observed. The dilation has a dramatic effect on the radial strain and minimal effect on the axial strain, so use of the radial strain measurement as the controlling feedback signal provides much better system response in the postpeak regime.

4.3 COMPLEX LOAD PATHS

The simple load paths presented in Table 4-1 can be appended to each other for the purpose of applying a series of known, controlled, boundary conditions to a test specimen. In the practical sense, the combining of the simple load paths is required to effect most types of tests. This section will portray some of the typical tests performed in the laboratory and illustrate how those tests are constructed of the simple load paths described in the previous section. The list of test configurations given here is not exhaustive because there are ample resources in most modern laboratories to vary the types and locations of instrumentation and control axes; however, the list does give a good representation of anticipated testing efforts directed at estimating constitutive model parameters. The test types presented here assume the use of instrumentation for measuring axial stress, radial stress, axial strain, radial strain, and time. Temperature could also be measured, but this discussion is limited to isothermal experimentation. Finally, the control axes are as given in Table 4-1; i.e., one axis for the axial principal direction and one axis for the radial principal direction.

4.3.1 Triaxial Compression (Axial Stress or Axial Strain Rate Control)

The triaxial compression test begins with path *E* by applying a hydrostatic stress ramp to the desired confining pressure. Upon reaching the desired pressure, the specimen may then be

subjected to a short application of path *A*, which is a condition of constant hydrostatic compression. The application of path *A* is usually neglected because it typically is of very short duration or the specimen does not exhibit significant deformations. If the test is being performed at a pressure of zero, then paths *E* and *A* are not required. At the conclusion of path *A*, the primary portion of the test begins by following either path *B* or path D. Along path B, the axial stress is increased at a constant rate, while along path D the axial strain is increased at a constant rate. In either case, the confining pressure is held constant. Loading continues until the specimen fails or some other limiting condition is encountered. The loading may continue monotonically until failure, or in a variation of the test, the loading may be reversed and then reapplied periodically to create an unload/reload cycle in the load path. The data from the unload/reload cycle(s) are often used to estimate linear elastic moduli for ductile materials or materials that deform with time. A typical load path for a stress-rate controlled triaxial compression test is shown in Figure 4-1. A typical load path for a strain-rate controlled triaxial compression test is shown in Figure 4-2.

4.3.2 Constant Stress Creep

The triaxial compression creep test begins with path *E* by applying a hydrostatic stress ramp to the desired confining pressure. Upon reaching the desired pressure, the specimen may then be subjected to a short application of path *A*, which is a condition of constant hydrostatic compression. The application of path *A* is usually neglected because it typically is of very short duration or the specimen does not exhibit significant deformations. If the test is being performed at a pressure of zero, then paths *E* and *A* are not required. At the conclusion of path *A*, the primary portion of the test begins by following path *B* (or path D) where the axial stress is increased while the confining pressure is held constant. Loading continues until the prescribed axial stress difference is imposed. This stress state is then held constant (path A) over an extended period of time while the strain response is monitored. A typical load path for a constant stress triaxial compression creep test is shown in Figure 4-3.

4.3.3 Stress Relaxation

The triaxial compression stress relaxation test begins with path *E* by applying a hydrostatic stress ramp to the desired confining pressure. Upon reaching the desired pressure, the specimen may then be subjected to a short application of path *A*, which is a condition of constant hydrostatic compression. The application of path *A* is usually neglected because it typically is of very short duration or the specimen does not exhibit significant deformations. If the test is being performed at a pressure of zero, then paths *E* and *A* are not required. At the conclusion of path *A*, the primary portion of the test begins by following either path *B* or path D. Along path B, the axial stress is increased at a constant rate, while along path D the axial strain is increased at a constant rate. In either case, the confining pressure is held constant. Loading continues until a prescribed axial strain level is imposed. A mode switch is

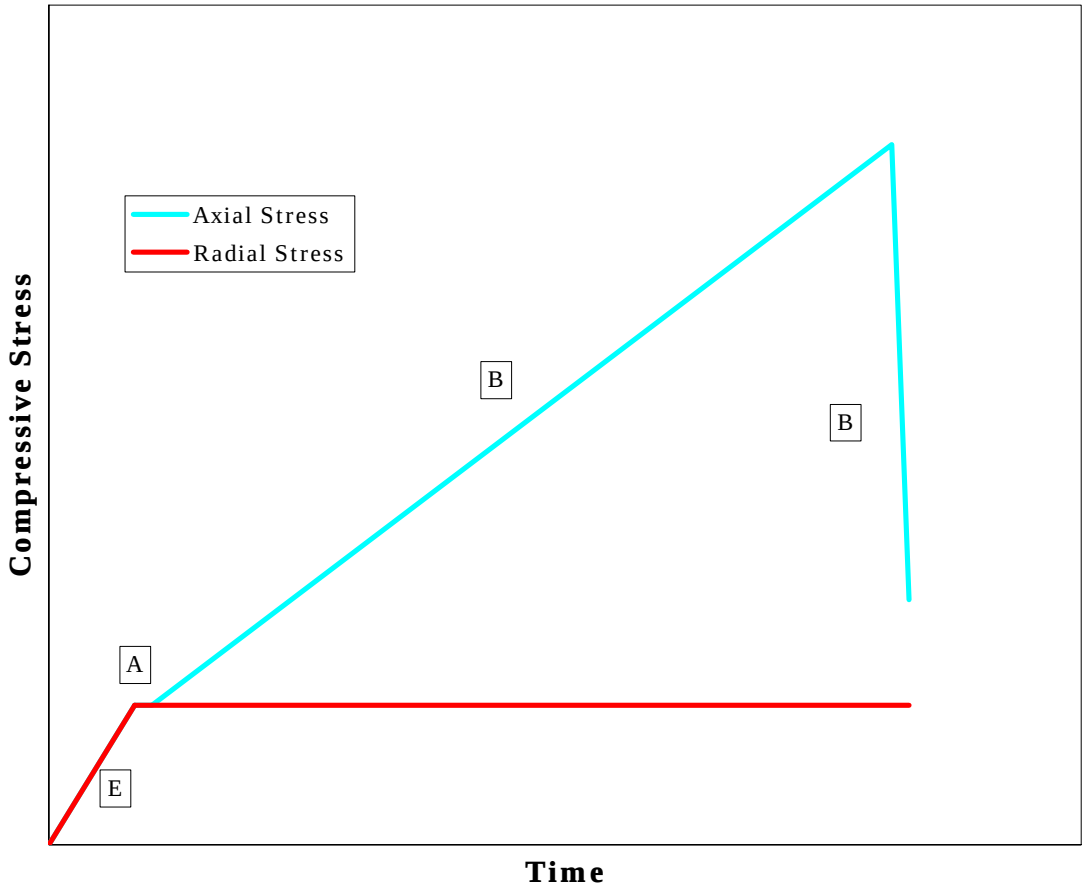

Figure 4-1. Triaxial Compression Under Axial Stress Rate Control.

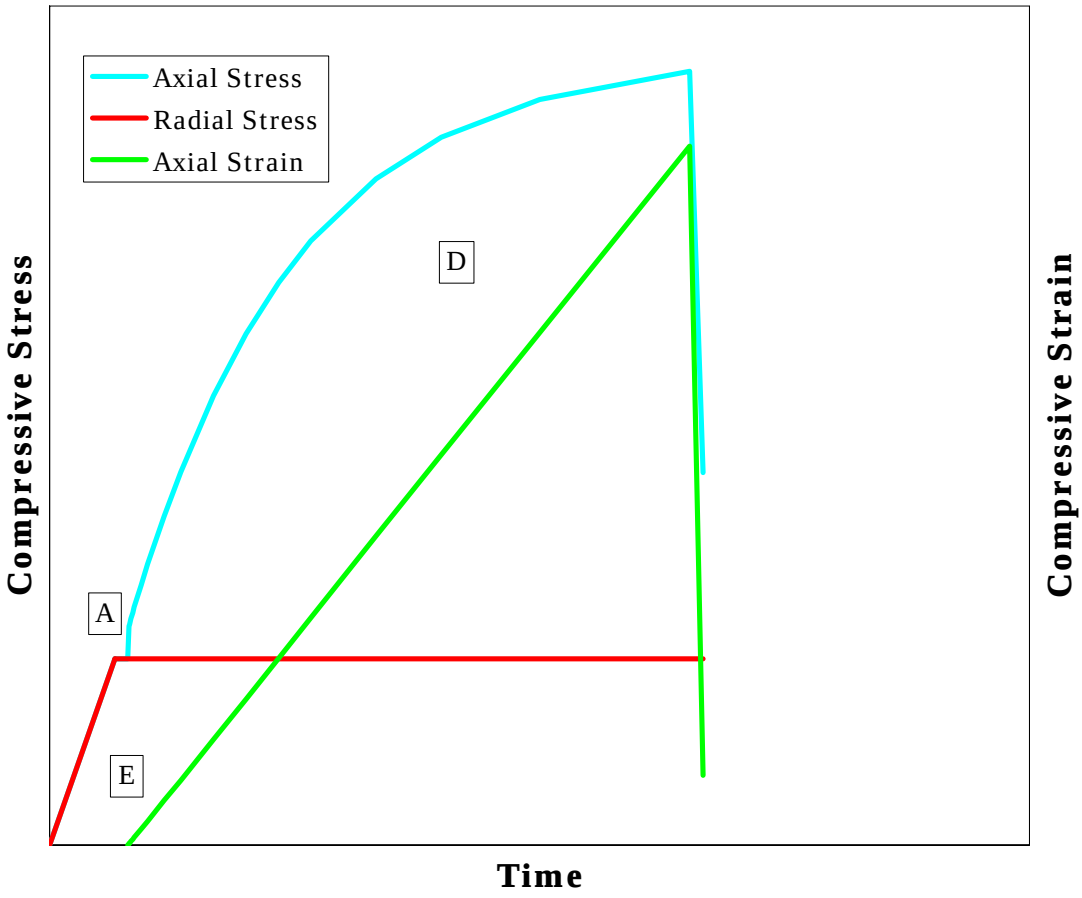

Figure 4-2. Triaxial Compression Under Axial Strain Rate Control.

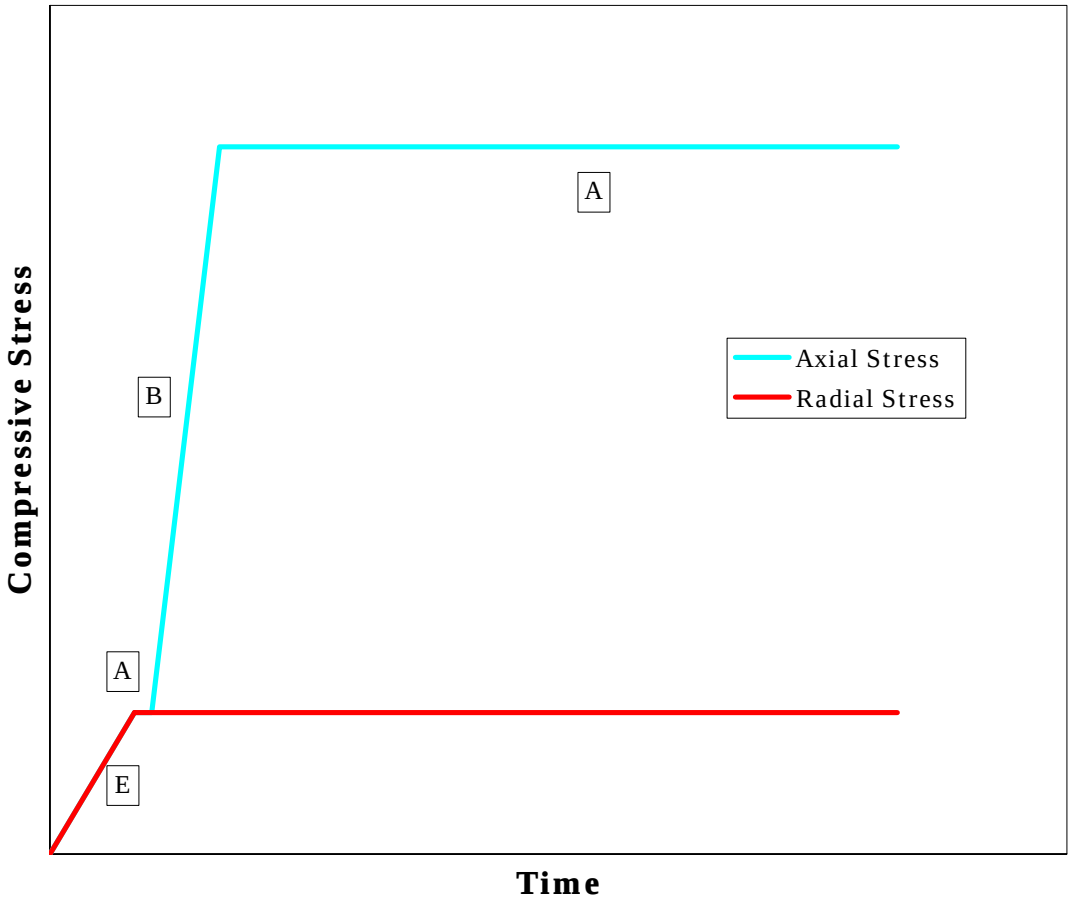

Figure 4-3. Triaxial Compression Creep.

then used to change the control of the axial loading from constant axial stress rate (or constant axial strain rate) to constant axial strain. The axial strain and the confining pressure are then held constant (load path *C*) over an extended period of time. Typically, the axial stress begins to decay (stress relaxation) as inelastic processes dissipate the elastic energy stored in the specimen during loading. A typical load path for a stress relaxation test is shown in Figure 4-4.

4.3.4 Constant Mean Stress

The constant mean stress (CMS) test begins with path *E* by applying a hydrostatic stress ramp to the desired confining pressure. Upon reaching the desired pressure, the specimen may then be subjected to a short application of path *A*, which is a condition of constant hydrostatic compression. The application of path *A* is usually neglected because it typically is of very short duration or the specimen does not exhibit significant deformations. At the conclusion of path *A*, the primary portion of the test begins by following path *E* where the axial stress is increased while the confining pressure is decreased. More specifically, the axial stress is increased at twice the rate of decrease in confining pressure, resulting in a constant mean stress path. Loading continues until the specimen fails or some other limiting condition is encountered. A typical limiting condition is the point where the confining pressure reaches zero. Common compressive test systems are not capable of imposing a tensile radial stress (which would be required to maintain a constant mean stress), so the test is terminated when the confining pressure reaches zero. A typical load path for a constant mean stress test is shown in Figure 4-5.

4.3.5 Uniaxial Strain (Axial Stress Rate or Axial Strain Rate Control)

The uniaxial strain test begins with path *E* by applying a hydrostatic stress ramp to the desired confining pressure. Upon reaching the desired pressure, the specimen may then be subjected to a short application of path *A*, which is a condition of constant hydrostatic compression. The application of path *A* is usually neglected because it typically is of very short duration or the specimen does not exhibit significant deformations. At the conclusion of path *A*, the primary portion of the test begins by following either path *F* where the axial stress is increased at a constant rate or path *G* where the axial strain is increased at a constant rate. In either case, the confining pressure is used to prevent an increase in radial strain. Loading continues until a prescribed axial strain level is imposed or the confining pressure reaches its upper limit. A typical load path for a uniaxial strain test under axial stress rate control is shown in Figure 4-6. A typical load path for a uniaxial strain test under axial strain rate control is shown in Figure 4-7.

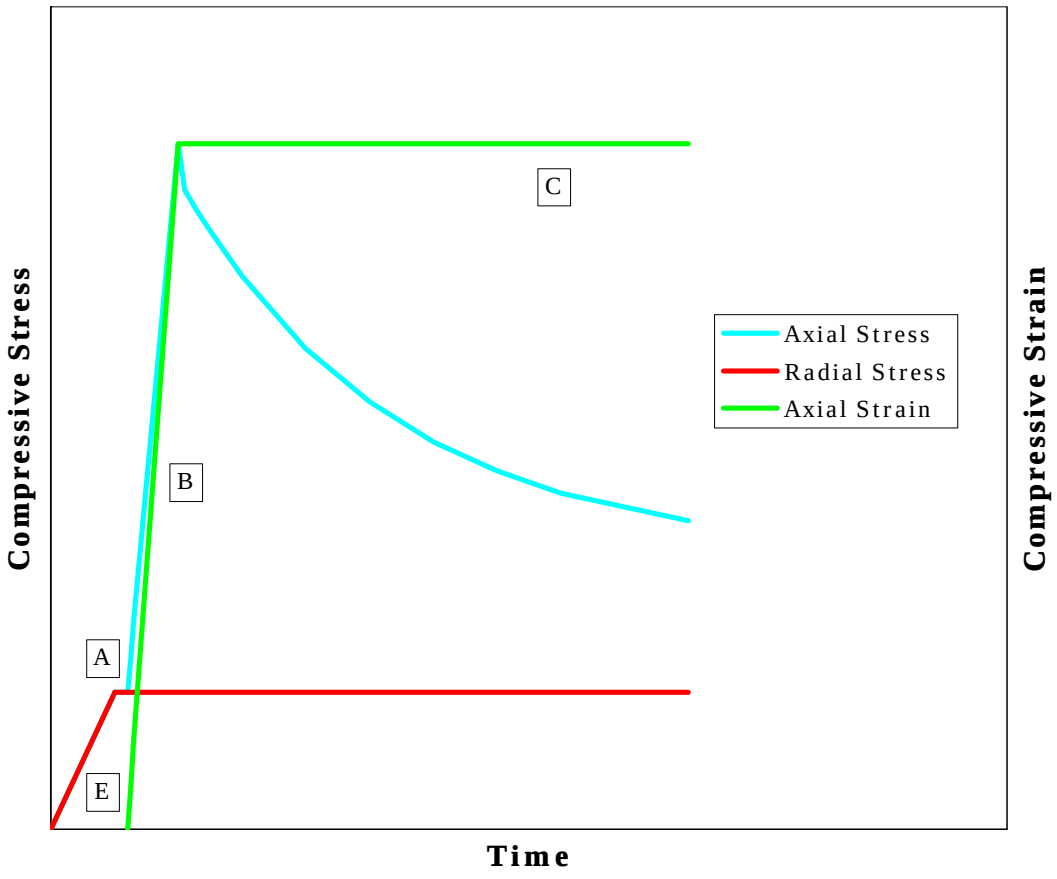

Figure 4-4. Stress Relaxation.

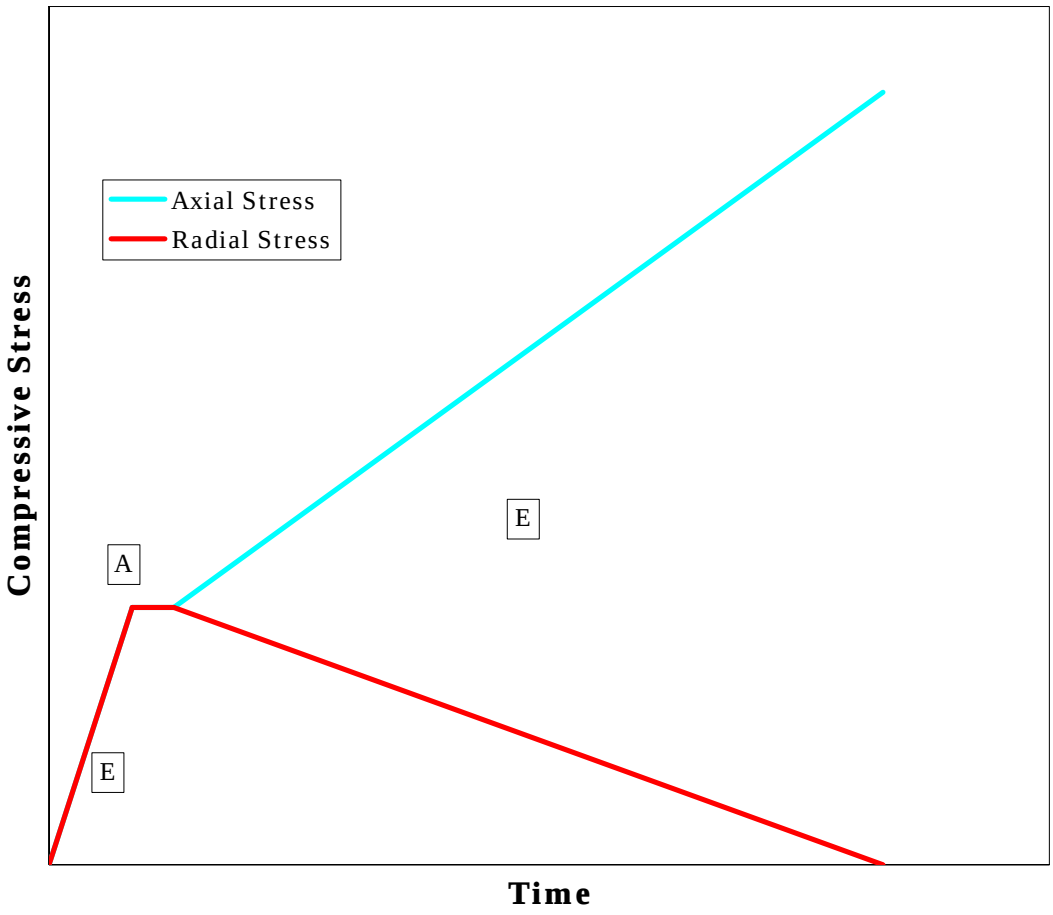

Figure 4-5. Constant Mean Stress.

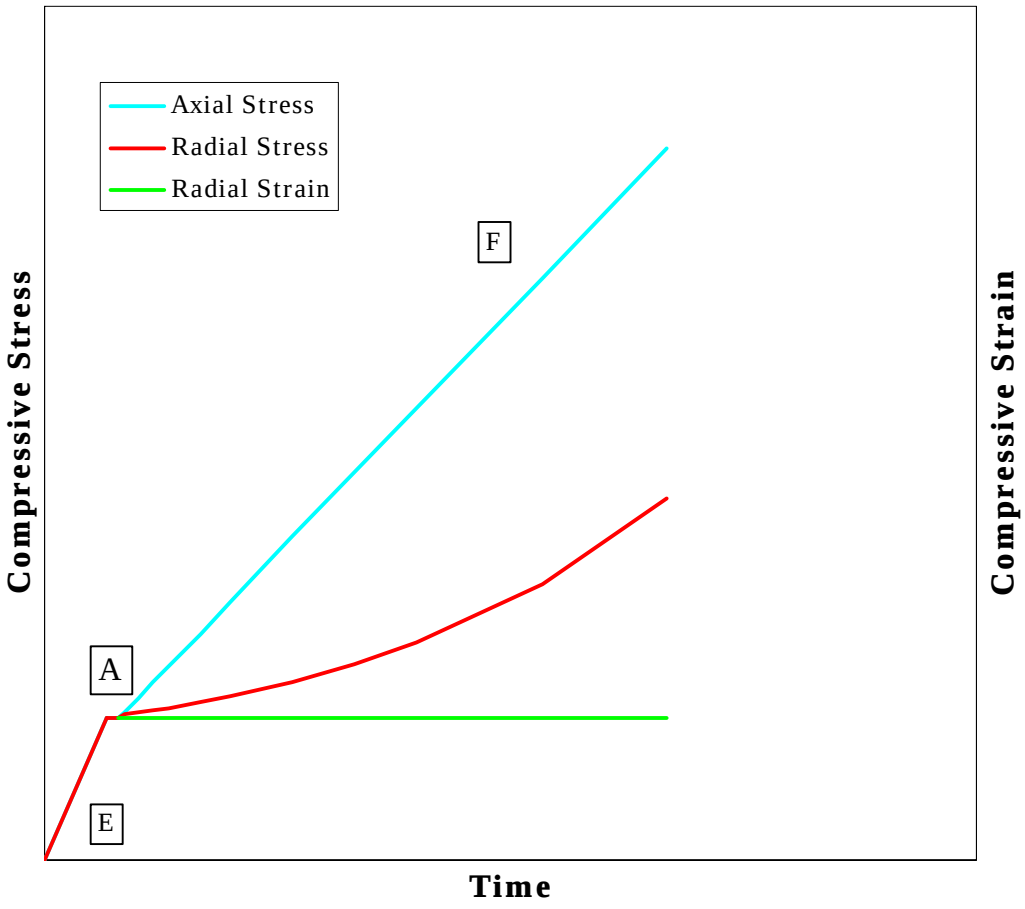

Figure 4-6. Uniaxial Strain Under Axial Stress Rate Control.

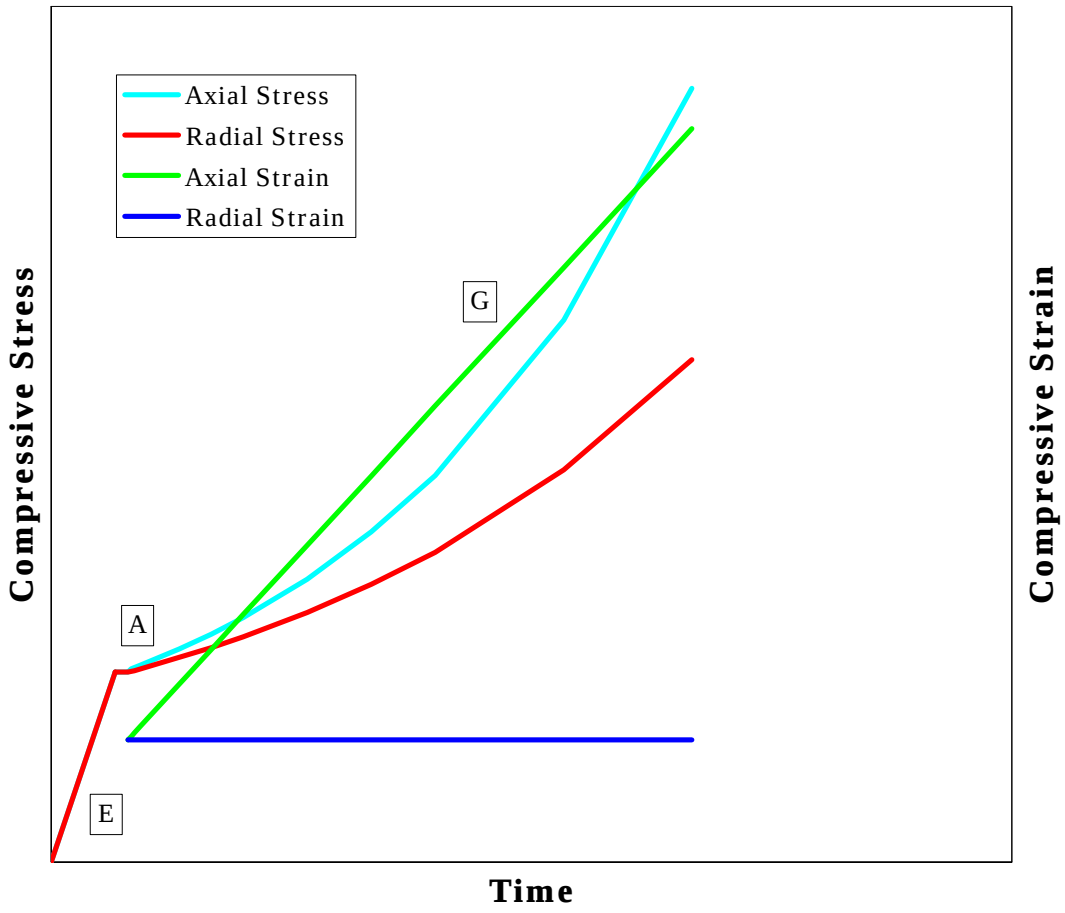

Figure 4-7. Uniaxial Strain Under Axial Strain Rate Control.

5.0 TEST MATRIX DESIGN

5.1 APPROACH

The approach taken in the test matrix design is similar to that described by Senseny and Fossum [1995; 1996] and Fossum [1997]. In these studies, Senseny and Fossum used sensitivity coefficients to show the influence of model parameters in highly nonlinear material models on the test specimen response as a function of load history. The sensitivity coefficients are defined as the derivative of the test specimen response (i.e., stress or strain) with respect to the parameter in question. An efficient test matrix is developed by choosing tests and test conditions in which the sensitivity coefficient of each parameter that needs to be determined is sufficiently large to confidently determine the parameter value.

This approach requires the derivation of sensitivity coefficients for each of the free parameters in the MDCF model for each of the load paths described in Chapter 4.0. The expressions for the sensitivity coefficients are obtained by differentiating the axial strain rate in stress-controlled tests, or the axial stress rate in strain-controlled tests with respect to each parameter, P, and integrating with respect to time. When test conditions resulted in a significant change in dilatant volumetric strain, sensitivity coefficients of dilatant volumetric strain were also calculated. Axial strain sensitivity coefficients are obtained by integrating:

$$\frac{\partial e_a}{\partial P} = \int \frac{\partial \dot{e}^i_{11}}{\partial P} dt \tag{5-1}$$

where ε_a is the axial strain and $\dot{\varepsilon}^i_{11}$ is the axial component of the inelastic strain rate defined by the MDCF constitutive model (Equation 3-1). Similarly, sensitivity coefficients for volumetric strain, ε_v, is calculated by integrating:

$$\frac{\partial e_v}{\partial P} = \int \left(\frac{\partial \dot{e}^i_{11}}{\partial P} + \frac{\partial \dot{e}^i_{22}}{\partial P} + \frac{\partial \dot{e}^i_{33}}{\partial P} \right) dt \tag{5-2}$$

over the duration of the test. For axial strain-rate control, the axial stress sensitivity coefficient is obtained by integrating:

$$\frac{\partial s_a}{\partial P} = \int \frac{\partial \dot{s}_a}{\partial P} dt \tag{5-3}$$

where:

$$\dot{s}_a = E(\dot{e} - \dot{e}^i_{11}) \tag{5-4}$$

and:

$\dot{\varepsilon}$ = applied axial strain rate
ε^i_{11} = resulting inelastic axial strain rate
E = Young's modulus.

Because the inelastic strain rate is a function of the evolutionary variables ς and ω, whose rates are described by Equations 3-10 and 3-22, respectively, each of the integrations results in a set of first-order differential equations. A fifth-order Runga-Kutta method for solving sets of first order differential equations described by Press et al. [1992] was used to integrate the equations. Although it is possible to obtain closed-form derivatives of the inelastic strain rate which are required to evaluate the sensitivity coefficients, because of the complexity of the MDCF model, derivatives were calculated numerically using a first-order forward difference technique [James et al., 1985]. Thus, for a stress-controlled test, the strain sensitivity coefficient for a parameter, P, at time T is calculated as:

$$\left.\frac{\partial e}{\partial P}\right|_T \cong \frac{\int_0^T \partial \dot{e}^i_{11}(P + \Delta P)dt - \int_0^T \partial \dot{e}^i_{11}(P)dt}{\Delta P} \tag{5-5}$$

where ΔP is a very small fraction of the parameter value. Sensitivity coefficients for volumetric strain and for stress were calculated in a similar manner.

The calculated sensitivity coefficients were normalized by multiplying by the parameter value to allow direct comparison between the sensitivity coefficients for different parameters. Although the sensitivity coefficient could be further normalized by dividing by the measured response (i.e. stress or strain), fictitiously high sensitivity coefficients occur when the measured response was equal to or nearly equal to zero.

5.2 SENSITIVITY ANALYSIS

Various mechanisms and parameters of the MDCF model can be isolated by using the appropriate load paths. For example, if an undamaged specimen is loaded with a deviatoric stress state that is less than the damage stress measure as described by Equation 3-19, then only the dislocation creep portion (the first term in Equation 3-1) is active. Depending on the value of the internal variable ς and the applied load, the strain-hardening branch or the

recovery branch of the dislocation creep portion of the model can also be isolated (see Equation 3-6). Applying a hydrostatic stress to a damaged specimen can isolate the healing term (the fourth term of Equation 3-1) because no creep or damage strains can occur without a deviatoric stress state. The shear damage term cannot be completely isolated because the dislocation creep mechanism is also active any time a deviatoric stress is applied. These techniques of parameter and mechanism isolation were used in choosing the tests and test stages for the sensitivity analysis.

The complex load paths of 17 typical laboratory tests were simulated using the MDCF parameters listed in Table 3-1 for both the A-salt and B-salt from the Cavern A and Cavern B sites, respectively. Test simulations were made at the cavern midheight temperatures of 113° F and 122° F for Cavern A and Cavern B, respectively. All of the test simulations assume that the specimen is initially undamaged ($\omega = \omega_0 = 0.0001$) and unhardened ($\varsigma = 0$). Tensile stresses and strains were assumed to be positive for all simulations. A summary of the tests simulated for the sensitivity analysis is given in Table 5-1.

For each simulation, axial stress sensitivity coefficients were calculated for strain-controlled load paths and axial strain sensitivity coefficients were calculated for stress-controlled load paths. For damaging or healing load paths in which the inelastic volumetric strain changed by a significant amount (more than about 0.005), volumetric strain sensitivity coefficients were also calculated. Each test stage was treated independently in the sensitivity analysis (i.e., the sensitivity to a given parameter in an earlier stage does not necessarily mean that the parameter is influential in later stages).

Sensitivity to a parameter was considered significant if its maximum value during the test stage was at least 10 percent of the maximum sensitivity of the most sensitive parameter. Tables 5-2 and 5-3 list the parameters for which the sensitivity coefficients were significant during the various test simulations for A-salt and B-salt, respectively. Each of the test simulations are discussed in more detail below.

5.2.1 Constant Mean Stress/Hydrostatic Compression Test Simulations

Three three-stage constant mean stress (CMS)/hydrostatic compression tests were simulated. In each of these test simulations, the specimen is initially loaded hydrostatically to the given mean stress. Deviatoric stress is applied by increasing the axial stress and decreasing the radial stress at rates which maintain the mean stress. During the second stage, the deviatoric stress is decreased by decreasing the axial stress and increasing the radial stress until a state of hydrostatic stress is obtained. For the third stage of the test, the hydrostatic stress is held constant for 100,000 seconds. The tests are summarized in Table 5-1. Figures 5-1 and 5-2 show the applied stresses and resulting strains, respectively, as functions of time for Test Simulation No. 2 (only a portion of the third stage is shown).

Table 5-1. Summary of Simulated Laboratory Tests (Page 1 of 2)

Simulation No.	Stage No.	Load Path Description
Constant Mean Stress/Hydrostatic Compression Test Simulations		
1	1	Increase stress difference from 0 to 3,000 psi over 400 seconds while maintaining 1,000 psi mean stress.
	2	Decrease stress difference from 3,000 to 0 psi over 400 seconds while maintaining 1,000 psi mean stress.
	3	Hold at 1,000 psi hydrostatic stress for 100,000 seconds.
2	1	Increase stress difference from 0 to 4,500 psi over 560 seconds while maintaining 1,500 psi mean stress.
	2	Decrease stress difference from 4,500 to 0 psi over 560 seconds while maintaining 1,500 psi mean stress.
	3	Hold at 1,500 psi hydrostatic stress for 100,000 seconds.
3	1	Increase stress difference from 0 to 4,650 psi over 580 seconds while maintaining 2,000 psi mean stress.
	2	Decrease stress difference from 4,650 to 0 psi over 580 seconds while maintaining 2,000 psi mean stress.
	3	Hold at 2,000 psi hydrostatic stress for 100,000 seconds.
Creep/Hydrostatic Compression Test Simulations		
4	1	1,000 psi stress difference creep with 2,000 psi confining pressure for 1,000,000 seconds.
	2	1,000 psi stress difference creep with no confining pressure for 1,000,000 seconds.
	3	1,000 psi hydrostatic compression for 1,000,000 seconds.
5	1	2,000 psi stress difference creep with 2,000 psi confining pressure for 1,000,000 seconds.
	2	2,000 psi stress difference creep with no confining pressure for 1,000,000 seconds.
	3	2,000 psi hydrostatic compression for 1,000,000 seconds.
6	1	3,000 psi stress difference creep with 2,000 psi confining pressure for 1,000,000 seconds.
	2	3,000 psi stress difference creep with 350 psi confining pressure for 1,000,000 seconds.
	3	3,350 psi hydrostatic compression for 1,000,000 seconds.
7	1	3,000 psi stress difference creep with 2,000 psi confining pressure for 500,000 seconds.
	2	1,500 psi stress difference creep with 2,000 psi confining pressure for 1,000,000 seconds.
Constant Strain Rate/Relaxation Test Simulations		
8	1	Axial strain rate of 10^{-6} s^{-1} to 0.02 with 200 psi confining pressure.
	2	Relaxation for 30,000 seconds.
9	1	Axial strain rate of 10^{-5} s^{-1} to 0.02 with 200 psi confining pressure.
	2	Relaxation for 30,000 seconds.
10	1	Axial strain rate of 10^{-4} s^{-1} to 0.02 with 200 psi confining pressure.
	2	Relaxation for 30,000 seconds.
11	1	Axial strain rate of 10^{-5} s^{-1} to 0.02 with a confining pressure of 2,000 psi.
	2	Relaxation for 30,000 seconds.

Table 5-1. Summary of Simulated Laboratory Tests (Page 2 of 2)

Simulation No.	Stage No.	Load Path Description
Constant Strain Rate/Uniaxial Strain Compression Test Simulations		
12	1	Axial strain rate of 10^{-4} s^{-1} to 0.03 with confining pressure of 200 psi.
	2	Constant axial strain rate of 10^{-6} s^{-1} to 0.04. Constant radial strain.
13	1	Axial strain rate of 10^{-4} s^{-1} to 0.03 with confining pressure of 200 psi.
	2	Constant axial stress rate of 5 psi/s for 600 s. Constant radial strain.
Confined Compression Test Simulations		
14	1	Constant axial stress rate of 5 psi/s to 4,500 psi and 4,000 psi stress difference for Cavern A and Cavern B, respectively. Confining pressure of 200 psi.
15	1	Constant axial stress rate of 10 psi/s to 4,500 psi and 4,000 psi stress difference for Cavern A and Cavern B, respectively. Confining pressure of 200 psi.
16	1	Constant axial stress rate of 20 psi/s to 4,500 psi and 4,000 psi stress difference for Cavern A and Cavern B, respectively. Confining pressure of 200 psi.
17	1	Constant axial stress rate of 10 psi/s to 4,500 psi and 4,000 psi stress difference for Cavern A and Cavern B, respectively. Confining pressure of 2,000 psi.

Figure 5-3 shows the relative axial strain sensitivity coefficients of the significant parameters during Stage 1 of Test Simulation No. 1 for A-salt. As the deviatoric stress increases, the creep parameters (n_2, β, and α) are the first to become sensitive; as the specimen is damaged, the damage parameters c_5 and c_2 become sensitive. Figure 5-4 shows the relative axial strain sensitivity coefficients of the significant parameters during Stage 2 of Test Simulation No. 1 for A-salt. The sensitivities to the parameters level off quickly as the stress difference is decreased. Because only a very small amount of damage accumulated during Test Simulation No. 1, it is not likely that any of the healing parameters could be obtained from the hydrostatic compression stage. However, as demonstrated by Test Simulations No. 2 and No. 3, as the mean stress is increased the maximum stress difference is also increased resulting in larger amounts of damage and increased sensitivity to the healing parameters k_1 and τ_1. Figure 5-5 shows the sensitivities of the healing parameters during the hydrostatic compression stage of the 2,000 psi CMS test (Test Simulation No. 3) on A-salt.

Tables 5-2 and 5-3 show which parameters were sensitive for the tests on A-salt and B-salt, respectively. The predicted strains for both the A-salt and B-salt are sensitive to the same parameters. The results are also similar for the different mean stresses. However, as the mean stress was increased, the maximum stress difference also increased, resulting in sensitivity to a few more of the damage parameters. Volumetric strain sensitivities were calculated for Test Simulations No. 2 and No. 3. The volumetric and axial strains are sensitive to the same parameters.

5.2.2 Creep/Hydrostatic Compression Test Simulations

Three three-stage and one two-stage creep/hydrostatic compression tests were simulated (Test Simulations No. 4, No. 5, No. 6 and No. 7). The first stage of the three-stage tests was

Table 5-2. Parameters With Significant Influence During Simulated Tests of A-Salt (Page 1 of 2)

Test	Stage	Transient				Steady-State Creep						Shear Damage				Healing				Shear and Tension Damage							Damage and Healing			
		α	β	K_0	δ	A_2	B_1	B_2	n_2	σ_0	q	x_{3s}	x_8	ξ_s^1	ξ_s^2	k_1	τ_0	τ_1	x_4	t_0	c_0	c_2	c_3	c_4	c_5	n_3	x_2	x_6	x_7	p_1
Constant Mean Stress/Hydrostatic Compression Tests																														
1	1	*	*						*													*			*					
	2	*	*						*													*			*					
	3																													
2	1	*	*							*												*		*	*	*				
	2	*	*							*												*		*	*	*				
	3																	*												
3	1	*	*							*												*		*	*	*	*	*		*
	2	*	*							*												*		*	*	*	*	*		*
	3															*		*												
Creep/Hydrostatic Compression Tests																														
4	1		*						*																					
	2								*																					
	3																													
5	1								*																					
	2			*					*	*																				
	3																													
6	1		*	*					*	*	*																			
	2											*		*											*		*			*
	3															*		*												

* Indicates parameter meets significance criterion

Table 5-2. Parameters With Significant Influence During Simulated Tests of A-Salt (Page 2 of 2)

Test	Stage	Transient				Steady-State Creep						Shear Damage				Healing			Shear and Tension Damage								Damage and Healing			
		α	β	K_0	δ	A_2	B_1	B_2	n_2	σ_0	q	x_{3s}	x_8	ξ_s^1	ξ_s^2	k_1	τ_0	τ_1	x_4	t_0	c_0	c_2	c_3	c_4	c_5	n_3	x_2	x_6	x_7	p_1
Creep/Hydrostatic Compression Tests Continued																														
7	1		*	*					*	*	*																			
	2			*	*				*																					
Constant Strain Rate/Relaxation Tests																														
8	1	*	*						*													*			*	*				
	2		*						*																*					
9	1	*	*						*	*	*		*									*			*	*	*			*
	2		*						*	*												*			*					
10	1	*	*						*	*	*		*									*		*	*	*	*			*
	2		*						*													*			*					
11	1	*	*					*	*	*	*											*		*	*		*	*		*
	2	*	*	*					*	*	*					*												*		*
Constant Strain Rate/Uniaxial Compression Tests																														
12	1	*	*						*	*	*		*									*		*	*	*	*			*
	2	*	*						*	*	*							*									*	*		*
13	1	*	*						*	*	*		*									*		*	*	*	*			*
	2	*	*						*	*	*																*	*	*	*
Confined Compression Test																														
14	1	*	*								*											*		*	*	*				*
15	1	*	*							*												*		*	*	*				*
16	1	*	*							*												*		*	*	*				*
17	1	*	*					*	*	*	*														*		*	*		*

* Indicates parameter meets significance criterion

Table 5-3. Parameters With Significant Influence During Simulated Tests of B-Salt (Page 1 of 2)

Test	Stage	Transient				Steady-State Creep						Shear Damage				Healing			Shear and Tension Damage								Damage and Healing			
		α	β	K_0	δ	A_2	B_1	B_2	n_2	σ_0	q	x_{3s}	x_8	ξ_s^1	ξ_s^2	k_1	τ_0	τ_1	x_4	t_0	c_0	c_2	c_3	c_4	c_5	n_3	x_2	x_6	x_7	p_1
Constant Mean Stress/Hydrostatic Compression Tests																														
1	1	*	*						*																					
	2	*	*						*																*					
	3																													
2	1	*	*							*												*		*	*	*				
	2	*	*							*												*		*	*	*				
	3																	*												
3	1	*	*							*												*		*	*	*	*	*		*
	2	*	*							*												*		*	*	*	*	*		*
	3															*		*												
Creep/Hydrostatic Compression Tests																														
4	1	*	*	*					*																					
	2			*					*																					
	3																													
5	1	*	*	*					*	*																				
	2			*					*	*		*		*																
	3																													
6	1	*	*	*					*	*	*																			
	2								*			*		*											*		*			*
	3															*	*	*												

* Indicates parameter meets significance criterion

Table 5-3. Parameters With Significant Influence During Simulated Tests of B-Salt (Page 2 of 2)

Test	Stage	Transient				Steady-State Creep						Shear Damage				Healing			Shear and Tension Damage								Damage and Healing			
		α	β	K_0	δ	A_2	B_1	B_2	n_2	σ_0	q	x_{3s}	x_8	ξ_s^1	ξ_s^2	k_1	τ_0	τ_1	x_4	t_0	c_0	c_2	c_3	c_4	c_5	n_3	x_2	x_6	x_7	p_1
Creep/Hydrostatic Compression Tests Continued																														
7	1	*	*	*					*	*	*																			
	2			*	*				*	*																				
Constant Strain Rate/Relaxation Tests																														
8	1	*	*	*					*	*															*					
	2	*	*	*					*	*	*														*					
9	1	*	*						*	*	*		*									*			*		*			
	2	*	*	*					*	*	*											*			*					
10	1	*	*						*	*	*		*									*			*	*	*			
	2	*	*						*		*														*					
11	1	*	*						*	*	*																			
	2	*	*	*					*	*	*																			
Constant Strain Rate/Uniaxial Compression Tests																														
12	1	*	*						*	*	*		*									*			*	*	*			
	2	*	*	*					*	*	*							*							*		*	*	*	*
13	1	*	*						*	*	*		*									*			*	*	*			
	2	*	*						*	*	*																	*		*
Confined Compression Test																														
14	1	*	*																			*			*	*				
15	1	*	*																			*			*	*				
16	1	*	*																			*			*	*				
17	1	*	*						*	*	*																			

* Indicates parameter meets significance criterion

RSI-621-99-016

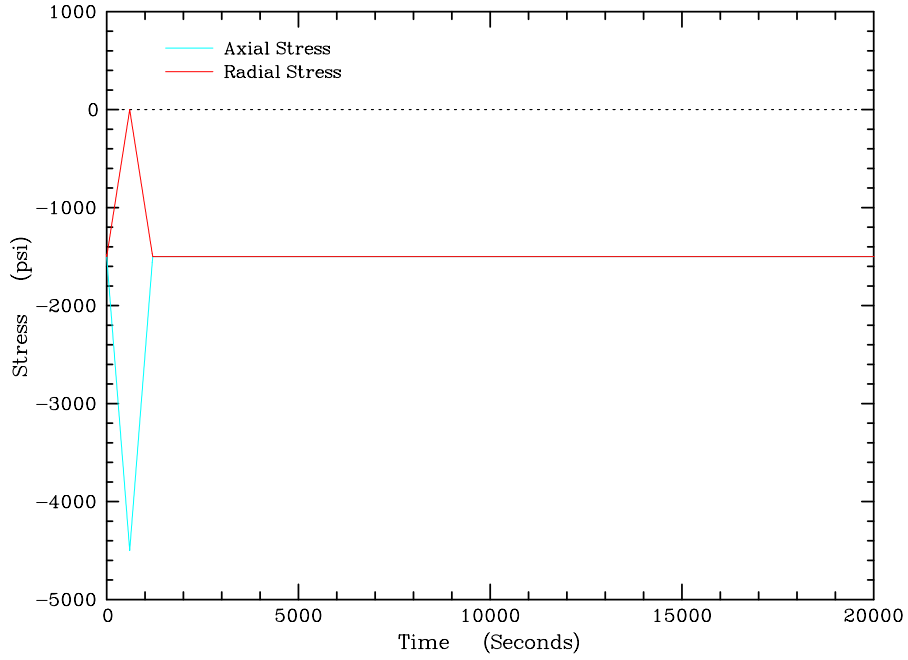

Figure 5-1. Applied Stresses for Test Simulation No. 2 (Constant Mean Stress/Hydrostatic Compression) on A-Salt.

RSI-621-99-017

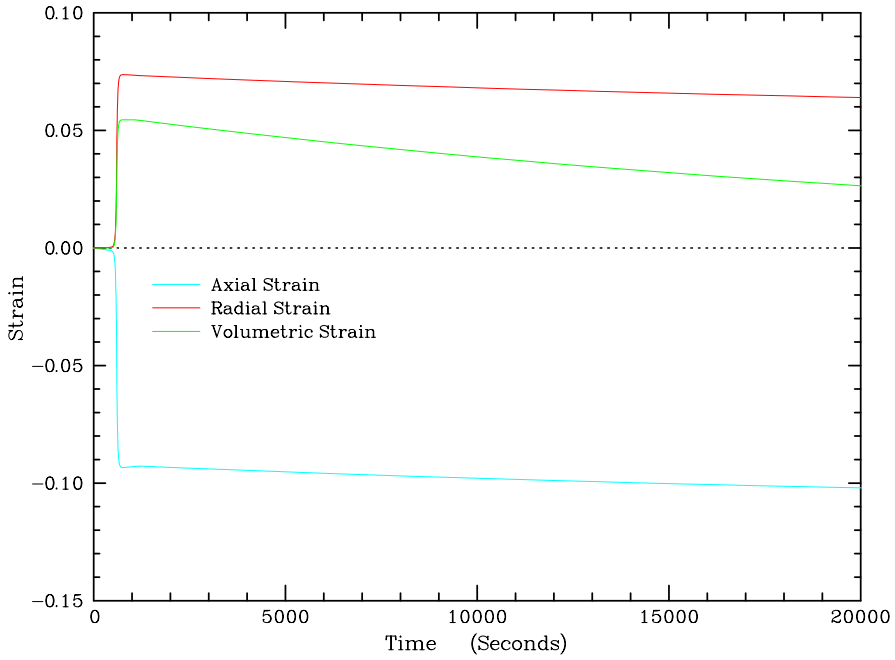

Figure 5-2. Predicted Strains for Test Simulation No. 2 (Constant Mean Stress/Hydrostatic Compression) on A-Salt.

RSI-621-99-018

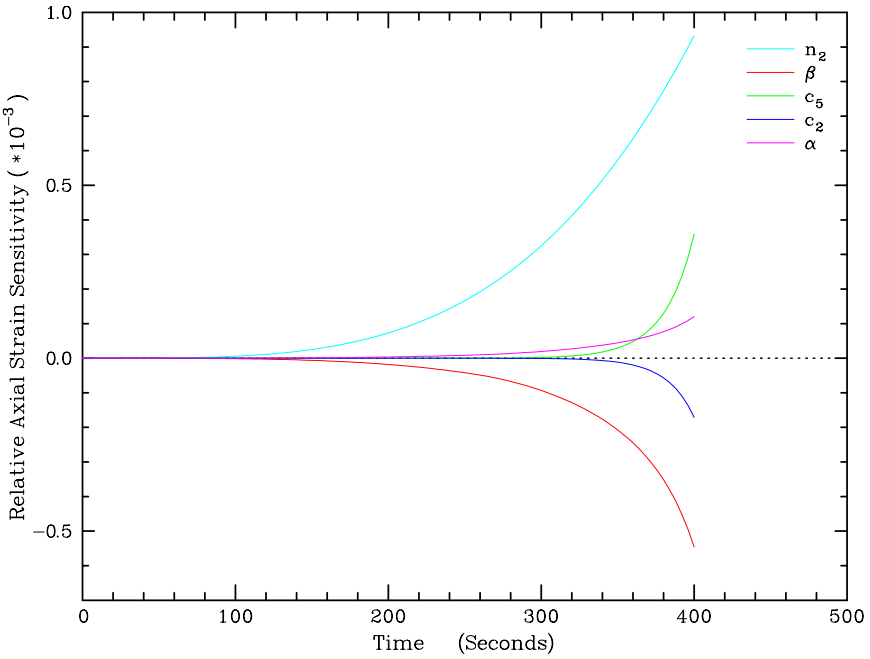

Figure 5-3. Significant Relative Axial Strain Sensitivity Coefficients During Stage 1 of Test Simulation No. 1 (Constant Mean Stress Application of Stress Difference) on A-Salt.

RSI-621-99-019

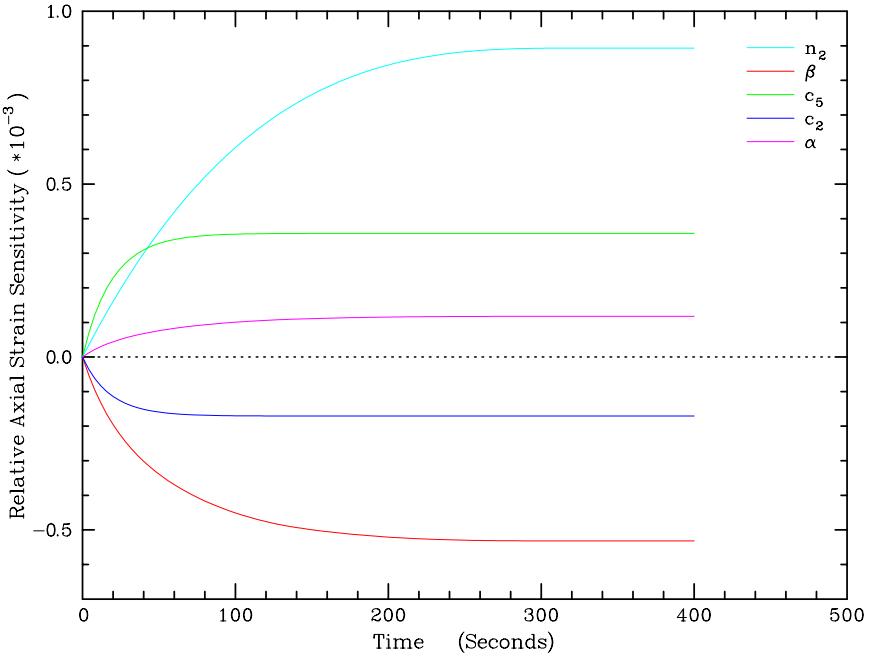

Figure 5-4. Significant Relative Axial Strain Sensitivity Coefficients During Stage 2 of Test Simulation No. 1 (Constant Mean Stress Removal of Stress Difference) on A-Salt.

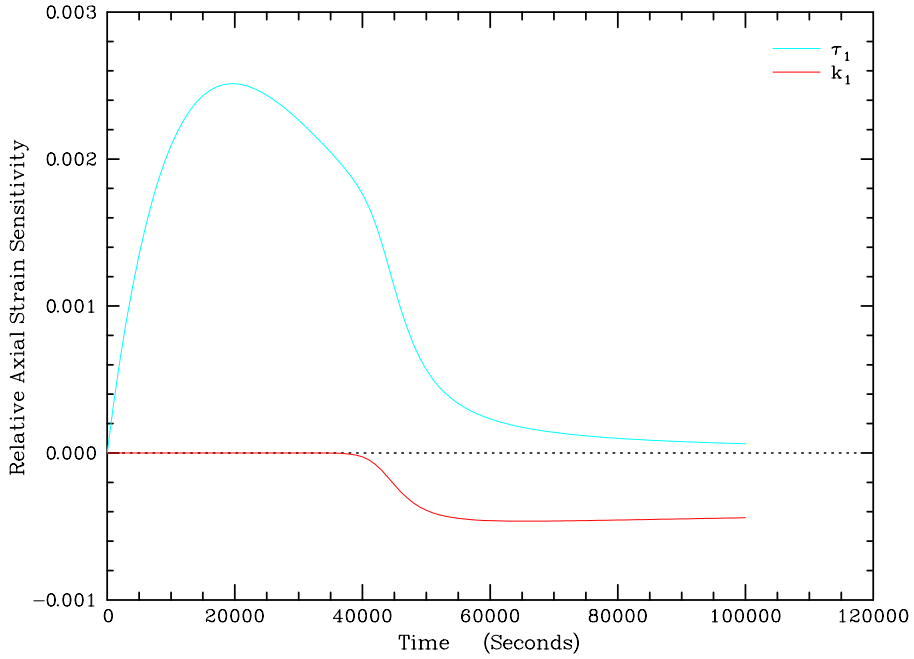

Figure 5-5. Significant Relative Axial Strain Sensitivity Coefficients During Stage 3 of Test Simulation No. 3 (2,000 psi Hydrostatic Compression) on A-Salt.

modeled with stress differences of 1,000, 2,000, and 3,000 psi, respectively, all with a high confining pressure (2,000 psi) to prevent damage from occurring. The purpose of this stage was to isolate the dislocation creep parameters of the MDCF model. The second stages of the three-stage tests were modeled with the same stress difference, but with the confining pressure lowered to initiate damage. For the third stage of the tests, a constant hydrostatic stress was modeled. The purpose of this stage was to isolate the healing parameters of the MDCF model. The length of each stage is 1 million seconds (about 11.5 days). A summary of the tests is shown in Table 5-1.

Figures 5-6 and 5-7 show, respectively, the stresses and strains versus time for Test Simulation No. 6 on B-salt. Figure 5-8 shows the relative axial strain sensitivity coefficients for the significant parameters during the first stage of this test. The confining pressure in this stage is high enough so that very little damage occurs, thus isolating the dislocation creep parameters. The parameter n_2 has the largest sensitivity. This result is also true for the first stage of the other tests, including those on the A-salt. Like the CMS tests, the creep tests with a higher stress difference had more sensitive parameters than those at lower stress differences.

Figure 5-9 shows the relative axial strain sensitivity coefficients for the significant parameters during the second stage of Test Simulation No. 6 on B-salt. The confining pressure in this stage is low enough to initiate damage. Most of the sensitive parameters during this stage are damage parameters. However, this is not true for Test Simulations No. 4 and No. 5.

RSI-621-99-021

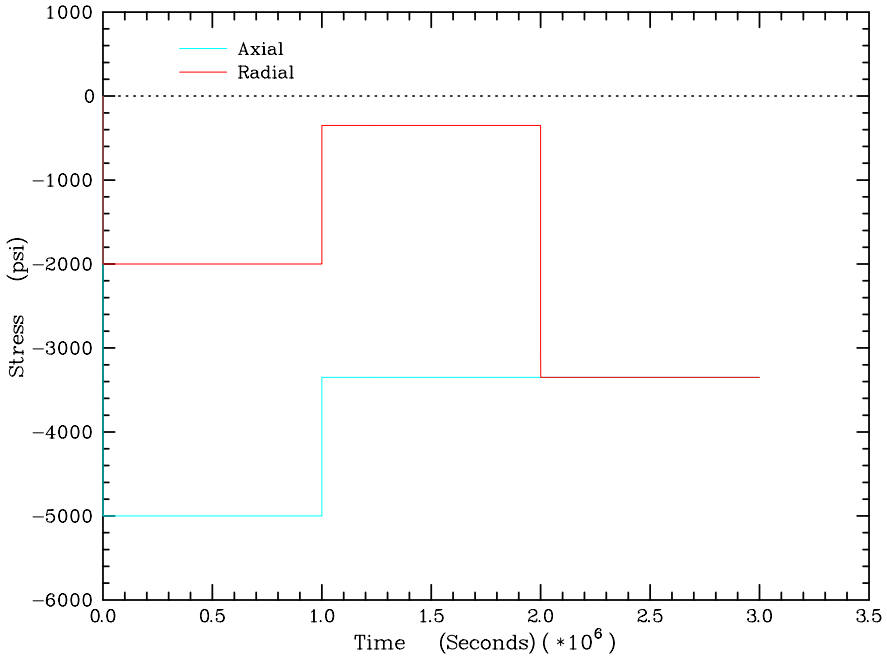

Figure 5-6. Applied Stresses for Test Simulation No. 6 (Three-Stage Creep/Hydrostatic Compression) on B-Salt.

RSI-621-99-022

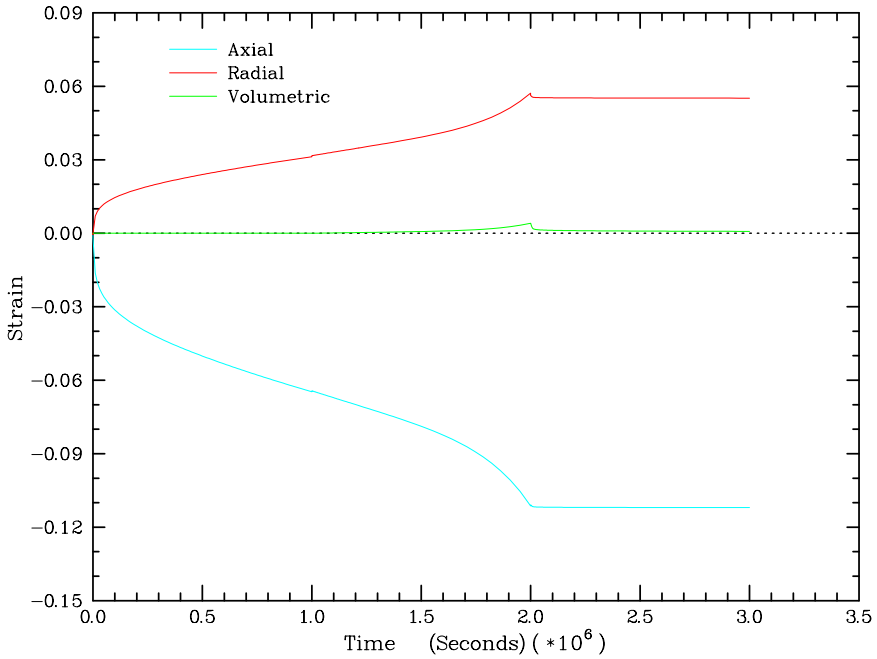

Figure 5-7. Predicted Strains for Test Simulation No. 6 (Three-Stage Creep/Hydrostatic Compression) on B-Salt.

RSI-621-99-023

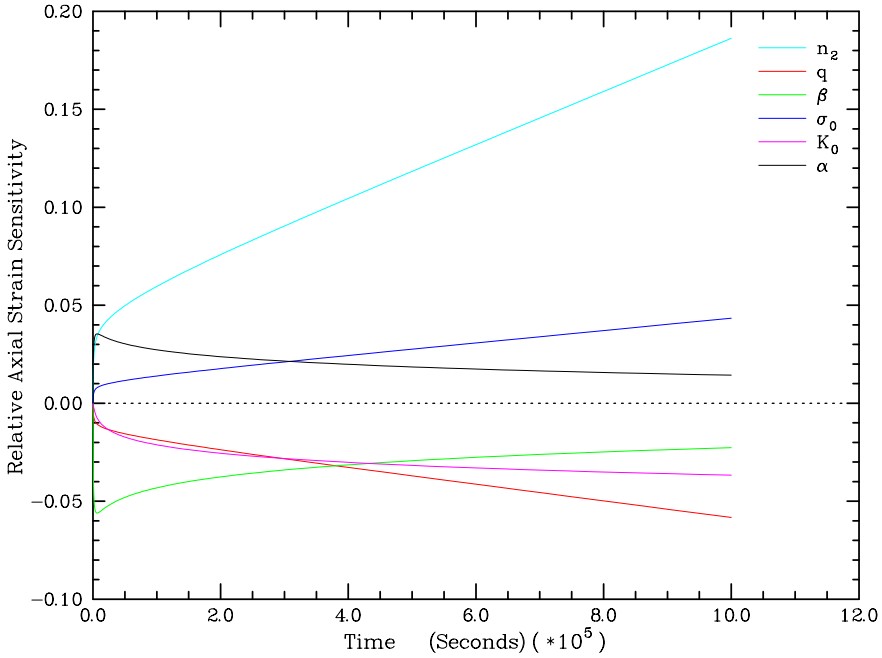

Figure 5-8. Significant Relative Axial Strain Sensitivity Coefficients During Stage 1 of Test Simulation No. 6 (Three-Stage Creep/Hydrostatic Compression) on B-Salt.

RSI-621-99-024

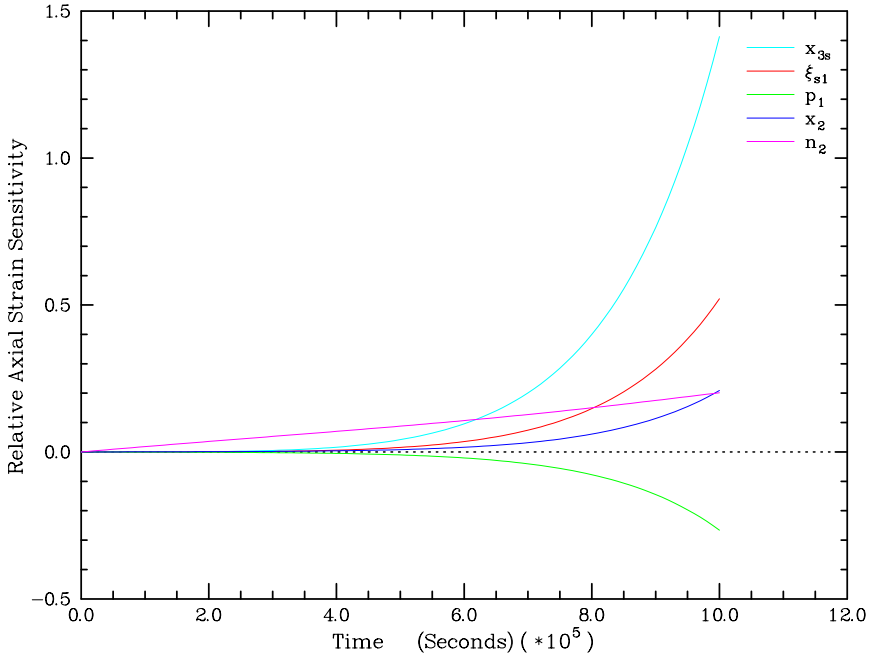

Figure 5-9. Significant Relative Axial Strain Sensitivity Coefficients During Stage 2 of Test Simulation No. 6 (Three-Stage Creep/Hydrostatic Compression) on B-Salt.

In the second stage of Test Simulation No. 4, which had a stress difference of 1,000 psi, no damage was induced in either salt, and thus the dislocation creep parameters are the most sensitive. In Test Simulation No. 5 (2,000 psi stress difference), only the B-salt incurred damage during the second stage.

Little or no measurable dilatant volumetric strain occurred during the second stages of the 1,000 and 2,000 psi stress difference tests (Tests No. 4 and No. 5) for both salts. Thus, only limited healing volumetric strain occurred during the hydrostatic consolidation portions of these tests. Figure 5-10 shows the relative axial strain sensitivity coefficients during the third stage of Test Simulation No. 6 for B-salt. Because this stage is conducted at hydrostatic pressure, the only active mechanism is the healing mechanism.

In the first and third stages of the creep/hydrostatic compression tests, most of the sensitivity coefficients peak in a short period of time, indicating that these stages may be shortened. However, in the second stage of the creep tests, the sensitivities of the damage parameters accelerate with time, suggesting that the duration of this stage should be increased to determine the damage parameters.

A fourth creep test, Test Simulation No. 7, was simulated to demonstrate how the parameter δ might be obtained from testing. The parameter δ influences the transient creep rate during recovery (the lower branch of Equation 3-6). The first creep stage of this test is conducted at a high stress difference (3,000 psi) to increase the value of the internal variable ς. This stage is followed by a low stress difference creep stage (1,500 psi) in which the transient strain limit ε_t^*, (Equation 3-7) is smaller than the value of ς, putting the specimen into recovery. A high confining pressure was used so that no damage was accumulated during the test. Figure 5-11 shows the strain response for B-salt during this test. Because of the strain hardening during the first stage, the specimen exhibits very little straining during the lower stress-difference stage. Figure 5-12 shows the relative axial strain sensitivities of the parameters during the second stage of this test. The relative axial strain sensitivities are small because of the small amount of strain that occurs during the stage. Although increasing the length of the stage will increase the magnitude of the sensitivities, the sensitivity of n_2 is increasing at a much higher rate than the sensitivity of d so the relative influence of d will be reduced as time goes on.

5.2.3 Constant Strain Rate/Relaxation Test Simulations

Four constant strain-rate/relaxation tests were simulated. The first stage of Test Simulations No. 8, 9, and 10 were conducted with axial strain rates of $10^{-6}\,s^{-1}$, $10^{-5}\,s^{-1}$, and $10^{-4}\,s^{-1}$, respectively, all at a confining pressure of 200 psi. The first stage of the fourth test, No. 11, was conducted with an axial strain rate of $10^{-5}\ s^{-1}$ and a confining pressure of 2,000 psi. In each test simulation, the specimen was deformed to an axial strain of 0.02 during the first stage. Then, the axial strain was fixed and the specimen was allowed to relax for 30,000 seconds during the second stage. A summary of the tests is given in Table 5-1.

RSI-621-99-025

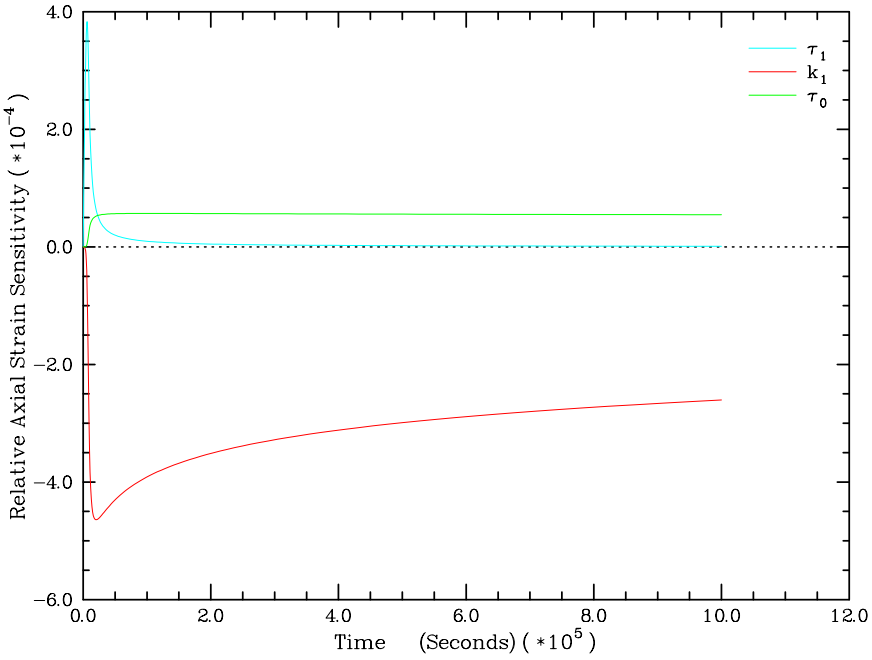

Figure 5-10. Significant Relative Axial Strain Sensitivity Coefficients During Stage 3 of Test Simulation No. 6 (Three-Stage Creep/Hydrostatic Compression) on B-Salt.

RSI-621-99-026

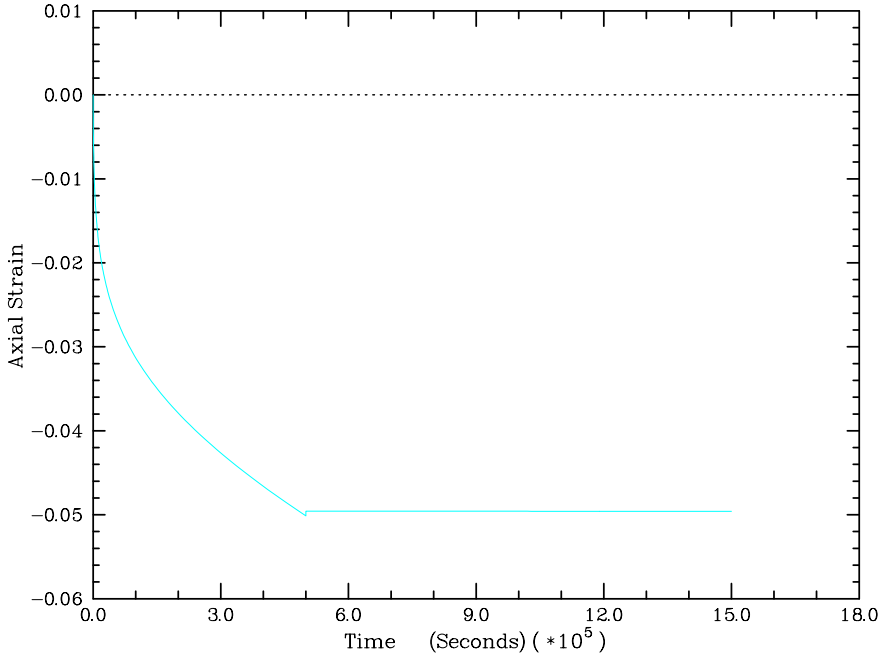

Figure 5-11. Predicted Axial Strain Response for Test Simulation No. 7 (Recovery Creep Test) on B-Salt.

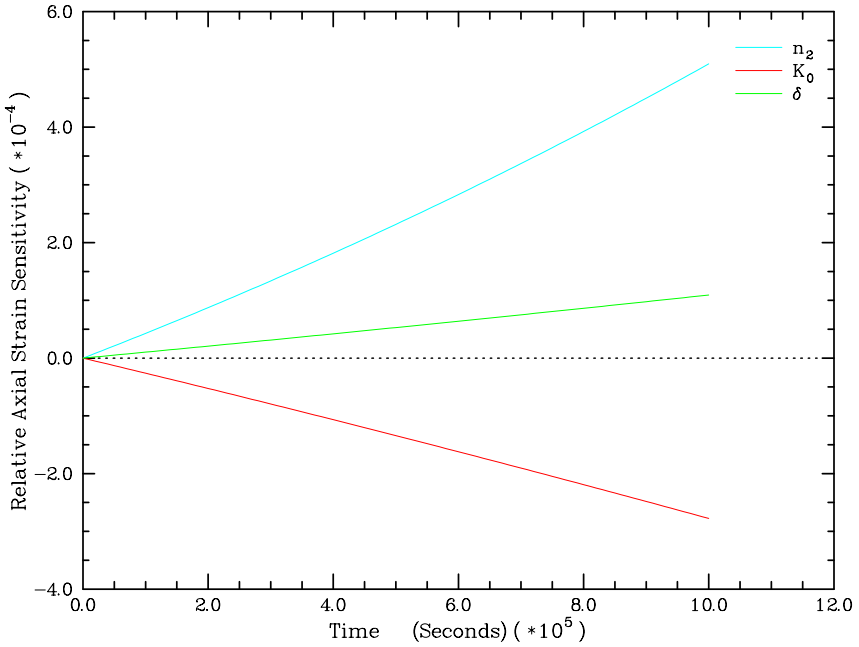

Figure 5-12. Significant Relative Axial Strain Sensitivities During Stage 2 of Test Simulation No. 7 (Recovery Stage) on B-Salt.

Figures 5-13 and 5-14 show, respectively, the stresses and strains versus time for Test Simulation No. 9 on A-salt.

Figure 5-15 shows the relative axial stress sensitivity coefficients of the parameters during the constant strain rate portion of Test Simulation No. 8 on A-salt. As with the constant mean stress tests, the creep parameters during the constant strain rate stage are the first to become sensitive. Then, as the specimen is damaged, the damage parameters become sensitive. The tests with higher axial strain rates have a larger number of parameters that meet the sensitivity criterion when compared to the tests with lower axial strain rates. Test Simulation No. 11 has two more parameters that meet the significance criterion than does Test Simulation No. 9, which has a lower confining pressure but the same axial strain rate.

The volumetric strain predicted during Stage 1 of Test Simulation No. 8 was not large enough to calculate volumetric strain sensitivity coefficients. However, in Test Simulations No. 9 and No. 10, which had larger volumetric strains, the relative volumetric strain sensitivities are significantly different than the relative axial stress sensitivities. The parameters x_8 and $x_{2,}$ which have not been very influential in most previous load paths, have a large influence on volumetric strain during the constant strain rate tests. Figure 5-16 shows the relative volumetric strain sensitivity coefficients for Stage 1 of Test Simulation No. 9 on A-salt.

RSI-621-99-028

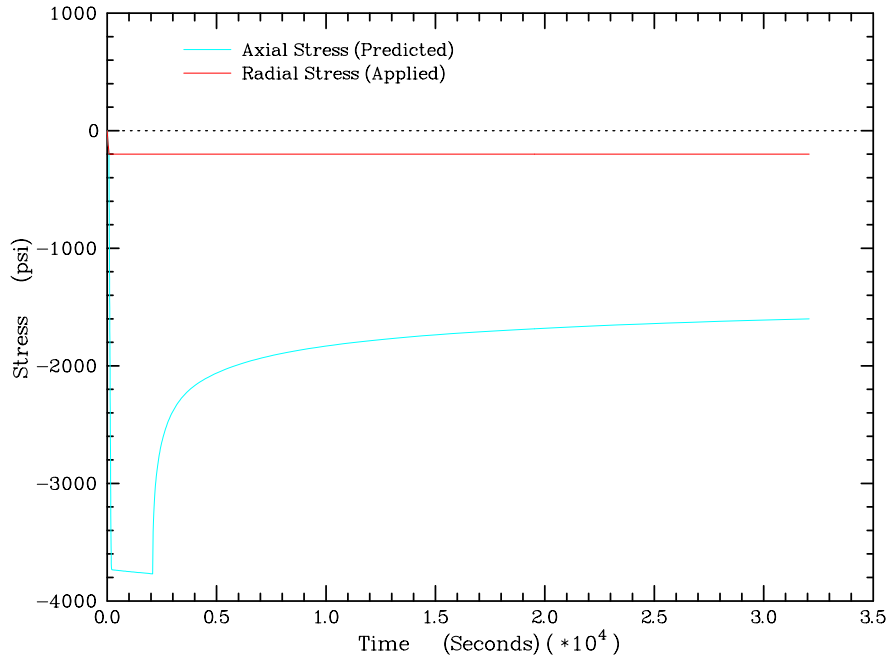

Figure 5-13. Applied and Predicted Stresses for Test Simulation No. 9 (Constant Axial Strain Rate/Relaxation) on A-Salt.

RSI-621-99-029

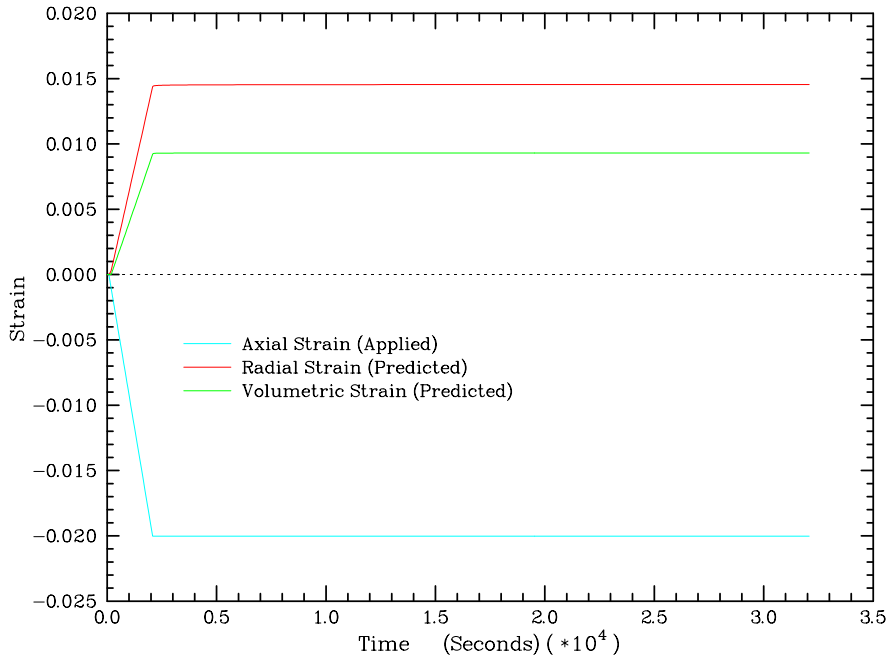

Figure 5-14. Applied and Predicted Strains for Test Simulation No. 9 (Constant Axial Strain Rate/Relaxation) on A-Salt.

RSI-621-99-030

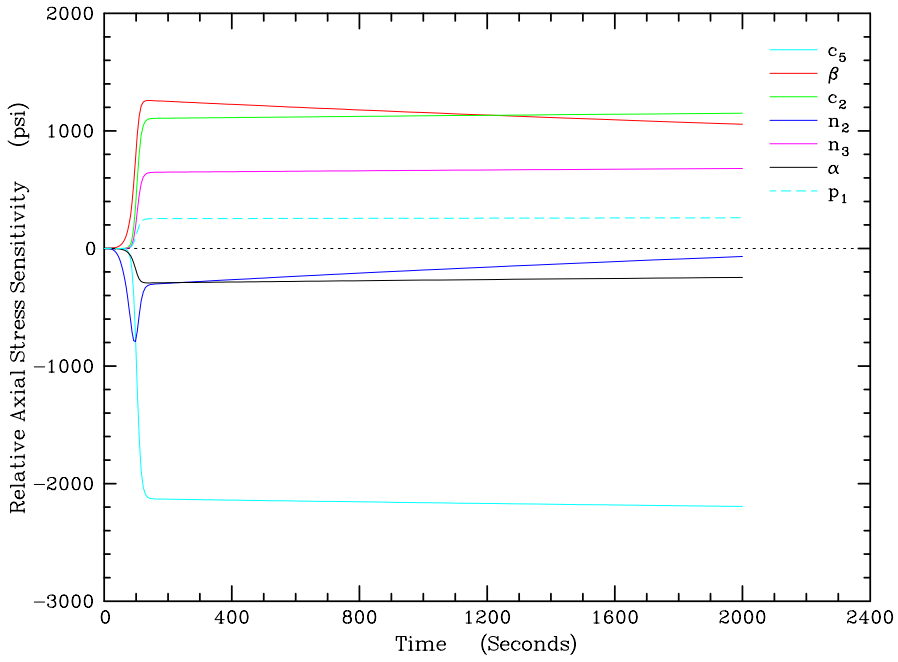

Figure 5-15. Significant Relative Axial Stress Sensitivity Coefficients During Stage 1 (Constant Axial Strain Rate) for Test Simulation No. 8 on A-Salt.

RSI-621-99-031

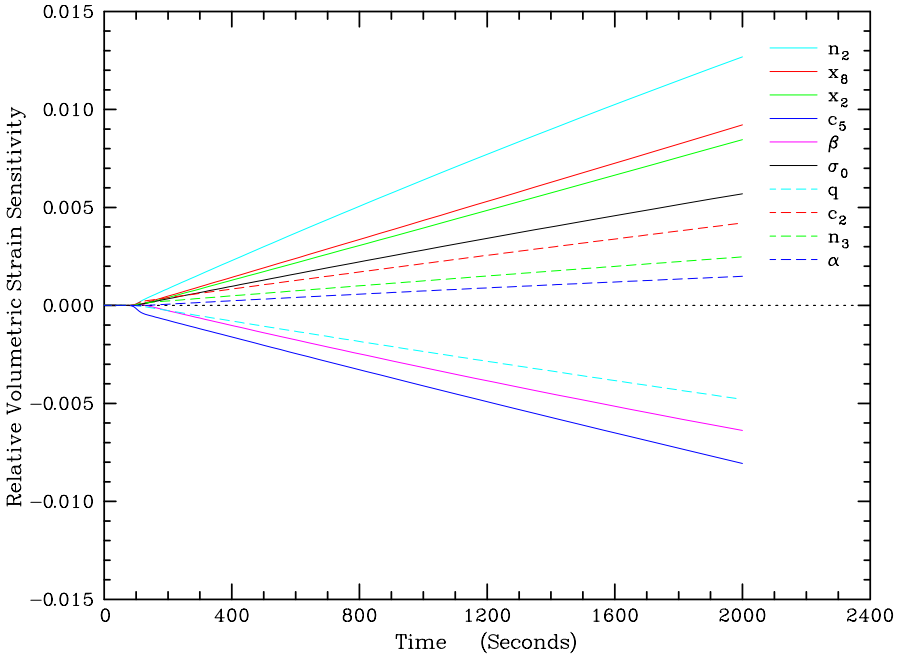

Figure 5-16. Significant Relative Volumetric Strain Sensitivity Coefficients During Stage 1 (Constant Axial Strain Rate) for Test Simulation No. 9 on A-Salt.

Figure 5-17 shows the relative axial stress sensitivity coefficients of the parameters during the relaxation portion of Test Simulation No. 9 on A-salt. The sensitivities to most parameters decreases very quickly. However, the sensitivities to n_2 and b remain high for the duration of the relaxation period. Volumetric strains were not large enough to calculate volumetric strain sensitivities during the relaxation stage for any of the tests.

5.2.4 Uniaxial Strain Test Simulations

Two test simulations were used to evaluate load paths with constant radial strain. The first stage of the two tests was initiated with a confining pressure of 200 psi and a constant axial strain rate of 10^{-4} s^{-1}. Stage 1 loading was completed when the axial strain reached 0.03. In the second stage of the test, the radial strain is fixed. In Test Simulation No. 12, a constant axial strain rate of 10^{-6} s^{-1} is applied during the second stage. In Test Simulation No. 13, an axial stress rate of 5 psi/s is applied during the second stage. The tests are summarized in Table 5-1.

Figures 5-18 and 5-19 show, respectively, the stresses and strains versus time for Test Simulation No. 12 on B-salt. Figure 5-20 shows the relative stress sensitivities for the uniaxial strain compression stage of Test Simulation No. 12 conducted on B-salt. The axial stress is sensitive to a relatively high number of parameters. Most of the sensitivities level off quickly, however the sensitivities to n_2, b, and t_1 continue to change throughout the stage. The results for the second stage of Test No. 13, which had a constant stress rate instead of a constant strain rate, are similar except fewer parameters met the sensitivity criterion. Figure 5-21 shows the relative axial strain sensitivities for the uniaxial strain compression stage of Test Simulation No. 13 conducted on B-salt.

For the uniaxial strain stages, sensitivities with respect to volumetric strain could only be calculated for Test Simulation No. 12 because the volumetric strain did not change significantly during the uniaxial strain stage of Test Simulation No. 13. The volumetric strain for the uniaxial strain portion of Test Simulation No. 12 is sensitive to about the same parameters as the axial stress for the A-salt and the B-salt.

5.2.5 Confined Compression Test Simulations

Four confined compression tests were simulated. Three of the tests have a confining pressure of 200 psi, while the fourth has a confining pressure of 2,000 psi. Stress rates of 5, 10, and 20 psi/s were evaluated. The tests are summarized in Table 5-1.

Figures 5-22 and 5-23 show respectively, the stresses and strains versus time for Test Simulation No. 15 on A-salt. Figure 5-24 shows the relative axial strain sensitivities for test No. 15 on A-salt. The applied axial stress rate had no effect on the sensitivity results. Test Simulation No. 17, which had a high confining pressure, was sensitive to a few more of the

RSI-621-99-032

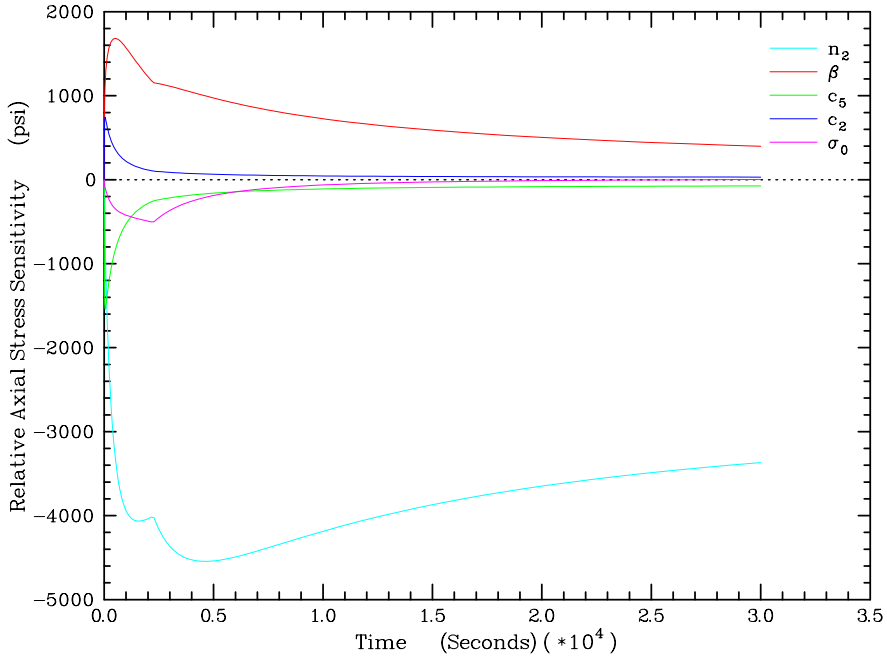

Figure 5-17. Significant Relative Axial Stress Sensitivity Coefficients During Stage 2 (Relaxation) of Test Simulation No. 9 on A-Salt.

RSI-621-99-033

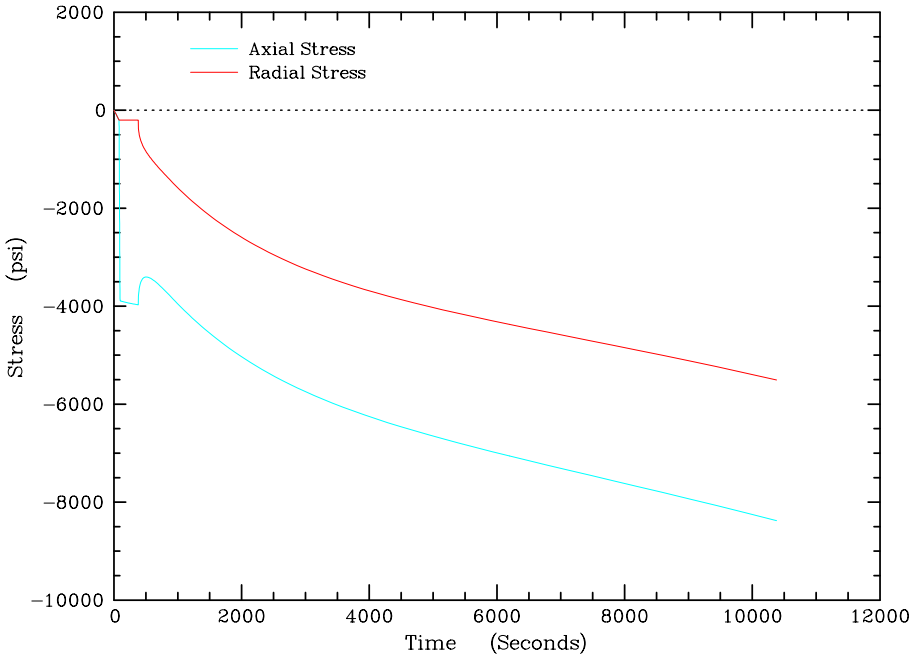

Figure 5-18. Applied and Predicted Stresses for Test Simulation No. 12 (Constant Axial Strain Rate/Uniaxial Compression) on B-Salt.

RSI-621-99-034

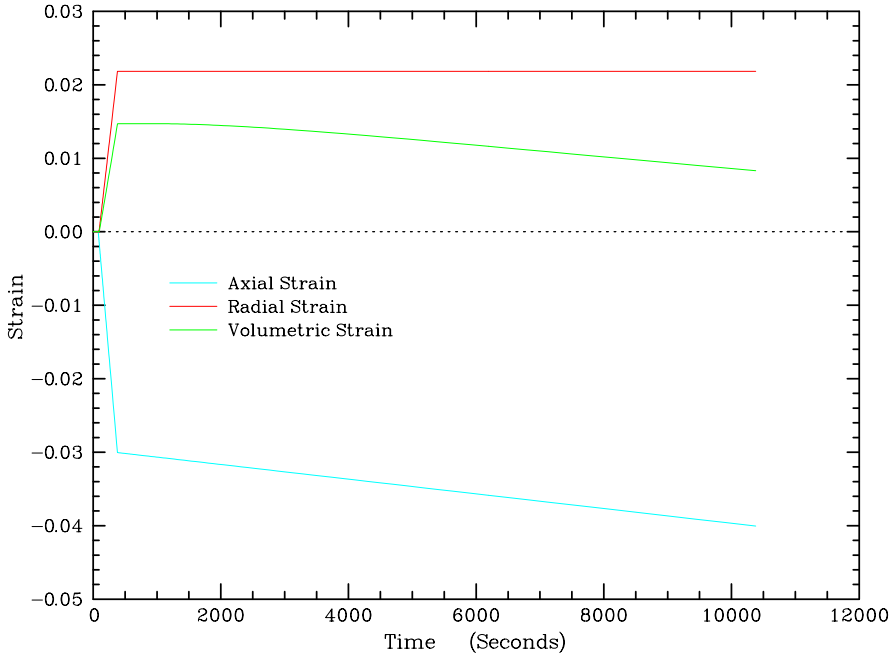

Figure 5-19. Applied and Predicted Strains for Test Simulation No. 12 (Constant Axial Strain Rate/Uniaxial Compression) on B-Salt.

RSI-621-99-035

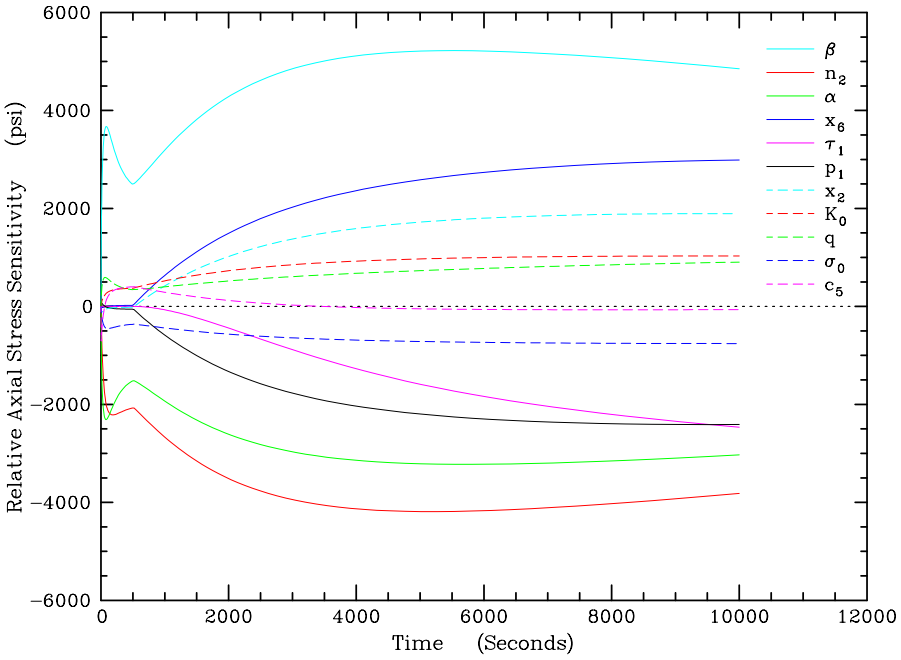

Figure 5-20. Significant Relative Stress Sensitivities for Stage 2 of Test Simulation No. 12 (Uniaxial Compression) on B-Salt.

RSI-621-99-036

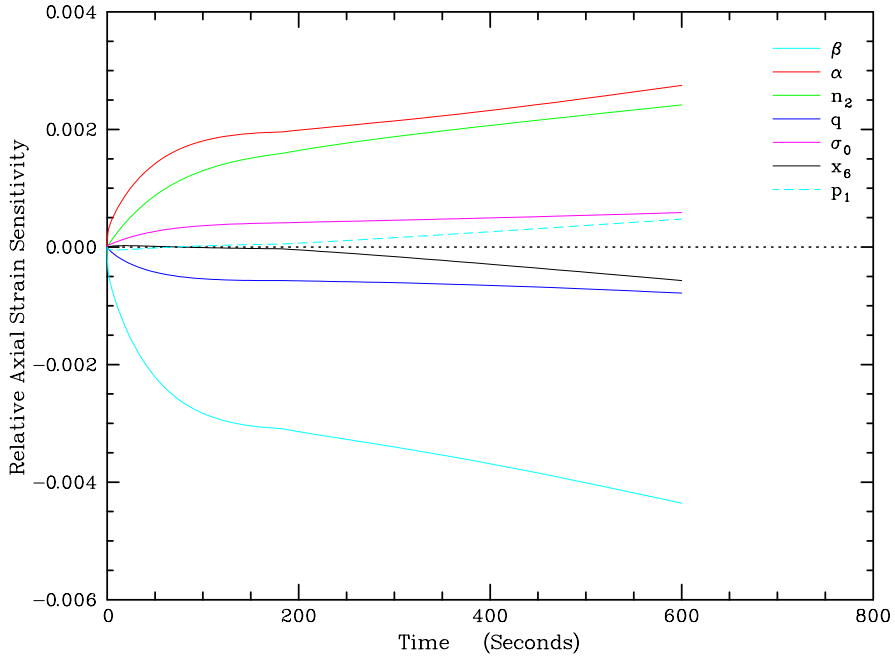

Figure 5-21. Significant Relative Axial Strain Sensitivities for Stage 2 of Test Simulation No. 13 (Uniaxial Compression) on B-Salt.

RSI-621-99-037

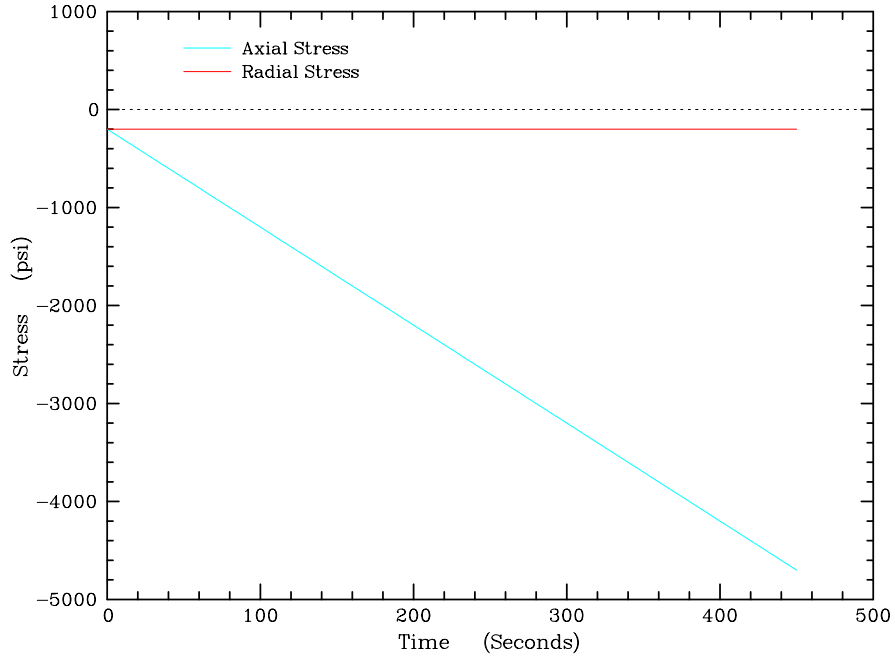

Figure 5-22. Applied Stresses for Test Simulation No. 15 (Confined Compression) on A-Salt.

RSI-621-99-038

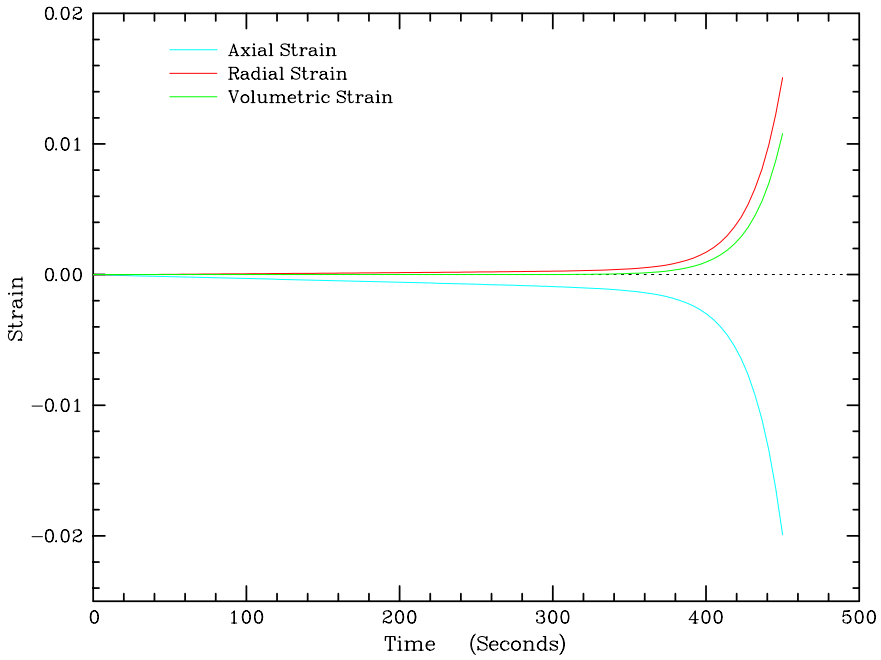

Figure 5-23. Predicted Strains for Test Simulation No. 15 (Confined Compression) on A-Salt.

RSI-621-99-039

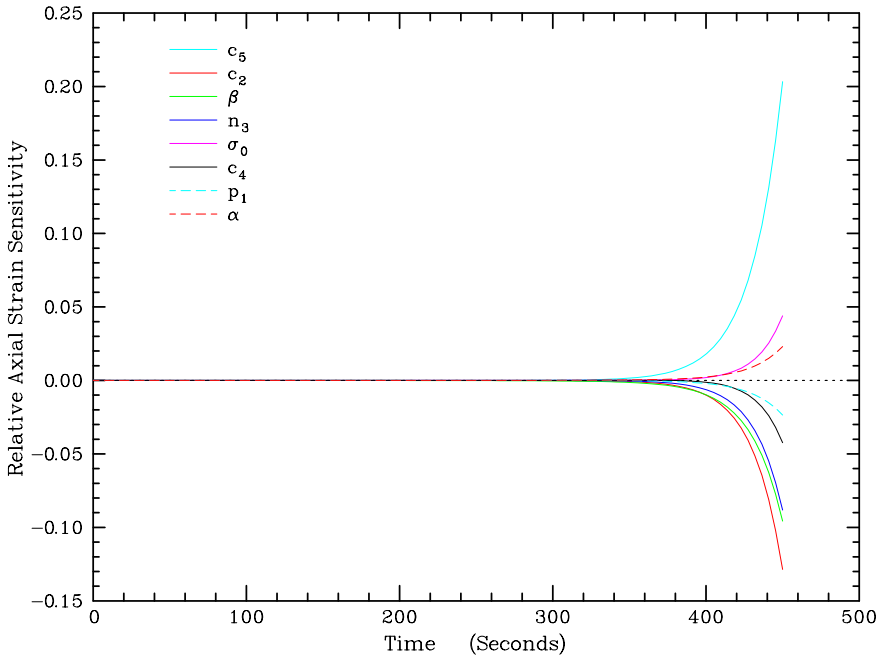

Figure 5-24. Significant Relative Axial Strain Sensitivities for Test Simulation No. 15 (Confined Compression) on A-Salt.

creep parameters when compared to Test Simulations No. 14, No. 15, and No. 16, but not sensitive to the damage parameters since no damage was predicted. The sensitivity results were similar for the volumetric and axial strains.

5.2.6 Discussion of Sensitivity Results

Ideally, it should be possible to find load paths in which the material behavior is dominated by one or only a few of the model parameters. Although this possibility exists, the sensitivity coefficients for some of the parameters are very small for all of the load paths simulated. The parameters with very little or no influence include A_2, B_1, B_2, x_{3s}, ξ_s^1, ξ_s^2, t_0, x_4, t_0, c_0, c_3, and x_7. If the load paths simulated encompass those that will exist around the actual cavern, then determination of these parameters is not necessary because they do not affect the response of the constitutive model.

The sensitivity results were very similar for both salts examined. However, since no testing was performed to determine the damage parameters for these salts, both were assigned the same damage parameters determined for WIPP salt. It is likely that the sensitivity results for salts with significantly different creep and damage characteristics than those examined here may be very different.

It is also likely that some of parameters will be difficult to determine from laboratory test data because of correlation with other variables. Correlation between variables is evident when sensitivity coefficients for two or more variables have similarly shaped curves during a given load path. For example, in Figure 5-8, the relative axial strain sensitivities for α and β are nearly mirror images of each other indicating a very high negative correlation between these variables. This finding agrees with our past experience in determining these variables from laboratory creep data and is also evident amongst the sensitivity coefficients for the damage parameters.

Methods were investigated to numerically determine correlation coefficients between the parameters, but these methods were unsuccessful. Specifically, the asymptotic correlation matrix commonly used in nonlinear regression was calculated. This calculation involves inverting a covariance matrix whose members are cross-products of sensitivity coefficients summed over the data points. However, when one or more of the sensitivity coefficients is zero, this matrix becomes singular and cannot be inverted.

5.3 PROPOSED TEST MATRIX

As outlined in the previous section, the free parameters identified for the modified constitutive model can be estimated from a database constructed of laboratory test results. The results of the sensitivity analysis provide guidance on designing an efficient test matrix

comprised of load paths and boundary conditions attainable in most modern laboratory facilities. This section presents the test matrix developed for the case being addressed in this report.

All the tests will be performed at a single temperature. A single temperature was proposed because the effects of thermal gradients at most sites is expected to be relatively small. In addition, the right-circular cylindrical specimens to be tested will be prepared from core samples that have a nominal diameter of 100 millimeters. A typical length-to-diameter ratio for specimens used in compression tests is between 2.0 and 2.5. Four types of tests are proposed for estimating the free parameters. The following list presents the four tests along with a brief description of each test. As described in Chapter 4.0, each of these tests actually represents a complex load path, but only the primary portion of each test is summarized here.

- Constant Stress Creep Test In a creep test, the principal stresses are the controlled variables and the principal strains are the response variables. The axial stress is maintained at a higher level than the radial stresses ($\sigma_1 > \sigma_2 = \sigma_3$), and the stress state is held constant over a long period of time while the principal strains are monitored.

- Constant Mean Stress Test In a constant mean stress test, the principal stress rates are the controlled variables and the principal strains are the response variables. The axial stress is increased at twice the rate the radial stress is decreased ($\dot{\sigma}_1 = -2\dot{\sigma}_2$) while the principal strains are monitored. This load path applies a deviatoric stress while maintaining a constant mean stress.

- Constant Strain Rate Test In a constant strain rate test, the controlled variables are axial strain rate and confining pressure. The response variables are axial stress and radial strain. The axial stress is increased as required to maintain the specified axial strain rate while the confining pressure is held constant.

- Hydrostatic Compression Test In a hydrostatic compression test, the principal stresses are the controlled variables and the principal strains are the response variables. The axial stress is maintained at the same level as the radial stresses ($\sigma_1 = \sigma_2 = \sigma_3$) and the stress state is held constant over a long period of time while the principal strains are monitored.

The types of tests being proposed were chosen based on two criteria: (1) they had to be conventional tests that most laboratories could perform and (2) they had to incorporate load paths where at least some of the constitutive model parameters displayed high sensitivity coefficients. A summary of the valuable characteristics of each test type is given in Table 5-4.

The remaining task is to fix the number of tests and their test conditions. A test matrix was designed that supplies sufficient data to estimate the free parameters in the constitutive model. The test matrix is shown in Table 5-5 where the stress levels for the individual tests are given

in generic terms; i.e., low stress, medium stress, or high stress. This generic specification approach was used because some of the parameters are stress-dependent and the exact dependency is unknown until site-specific salt is tested. In other words, what constitutes a high stress level for salt from one site may be characterized as a medium stress level for salt from a different site. The problem specifying exact stress levels is addressed within the test matrix by those tests shown in shaded background. These tests are to be performed first using particular stress levels that are considered (from experience) to be well within the low and high stress level regimes. The results of these initial tests can then be examined to establish the particular stress levels for the rest of the matrix. The test durations (especially creep) are based primarily on the degree to which parameter sensitivity changes with time. If the parameter sensitivities are reasonably constant after some period of time, continuation of the test beyond that time would yield little additional useful information.

Table 5-4. Summary of Test Type Characteristics

Test Type	Characteristics
Constant Stress Creep	Provides data for estimating the time-dependent inelastic parameters. Typical test durations may be about 1 month.
Constant Mean Stress	Provides a means for introducing controlled damage in a specimen. Especially good for determining onset of dilation (damage).
Constant Strain Rate	Good strength test. Also used for estimating elastic parameters. Can be used for inducing controlled damage.
Hydrostatic Compression	Used for estimating healing parameters in predamaged specimens. Performed after a known amount of damage has been induced by some other load path.

5.4 ESTIMATED LABORATORY COSTS

The test matrix given in Table 5-5 contains tests that can be performed by most rock mechanic laboratories. This section presents an estimate of the costs a commercial testing laboratory would quote for performing those tests and reporting the results. The estimates are based on our experience within the RESPEC laboratory and our interactions with other, similar laboratory operations. The unit cost estimates for each test represent only those costs associated with performing and reporting the tests; the costs associated with fitting a constitutive model to the data to obtain parameter estimates are estimated separately.

Table 5-5. Proposed Constant Temperature Test Matrix

Test Type	Test No.	Stress Conditions		
		$\Delta\sigma$	σ_3	σ_m
Quasi-static Triaxial Compression	1		Low	
	2		Medium	
	3		High	
	4		Low	
	5		Medium	
	6		High	
Constant Mean Stress Triaxial Compression	7			Low
	8			Medium
	9			High
	10			Low
	11			Medium
	12			High
Constant Stress Triaxial Compression Creep	13	Low	Low	
	14	Low	Medium	
	15	Low	High	
	16	Medium	Low	
	17	Medium	Medium	
	18	Medium	High	
	19	High	Low	
	20	High	Medium	
	21	High	High	
Hydrostatic Triaxial Compression Healing	22-27	Use lithostatic healing pressure.		

(1) The shaded tests are run first to estimate the best stress conditions for the remainder of the test matrix.

(2) The healing tests are performed on those specimens that display dilatancy.

A summary of the laboratory testing costs is given in Table 5-6. A unit cost is given for each test type. The unit costs assume that testable specimens are already available to the laboratory and do not include costs for sample acquisition and preparation. The creep test cost of $4,000 is the total cost for 1 month of testing. This $4,000 cost represents an initial test setup cost of $1,000 and a monthly creep testing charge of $3,000. Thus, if additional months of testing were desired, the unit cost of a creep test would be increased by $3,000 for each additional month of testing. The $3,000 monthly rate is also seen in the unit cost for the healing tests. These tests are likely already in the test frame at the end of the load path segment where a controlled amount of damage was induced, so an initial test setup charge is not required. However, the healing test is essentially the same as a creep test except the stress differences are zero, so the $3,000 monthly rate was applied. In addition to mechanical testing, mineralogic analyses are required to determine the impurity content (ρ) of the salt. The estimated cost of each mineralogic analysis is $300.

Table 5-6. Estimated Laboratory Costs for Determination of MDCF Constitutive Parameters

Test Type	Quantity	Unit Cost	Total Cost
Quasi-static Triaxial Compression	6	$1,500	$9,000
Constant Mean Stress Triaxial Compression	6	$1,500	$9,000
Constant Stress Triaxial Compression Creep	9	$4,000	$36,000
Hydrostatic Triaxial Compression Healing	6	$3,000	$18,000
Mineralogic Analysis	10	$300	$3,000
Total Cost Estimate			**$75,000**

The data generated in Table 5-5 are useful for determination of the constitutive parameters in the model, but they do not necessarily generate two useful material strength properties; namely, the unconfined compressive strength and the indirect tensile strength. These two properties can be easily estimated using the relatively inexpensive laboratory tests known as the unconfined compression test ($600) and the indirect tension test ($100). If six of each test type were performed in addition to the constitutive parameter testing, the additional cost would amount to $4,200 and the total laboratory testing costs would then rise to $79,200.

As was mentioned at the beginning of this section, there is a significant cost associated with the fitting of the laboratory data to obtain good estimates of the constitutive parameters. The

exact fitting procedures can vary depending upon the type of data available, but the general result is that the fitted constitutive parameters represent best estimates of their true values in a least squares sense. This means that a nonlinear regression approach is used to determine the combination of parameter values that produces the least sum-of-squared-error between the measured and predicted levels of the response variable. This approach requires development of a response model representative of the load path over which a particular data set was generated and since multiple load paths are being used, multiple response models must be investigated. In addition, the data sets themselves are often subject to prefitting manipulations to control their size and relative influence. The prefitting manipulations may require sampling of the data sets to reduce the number of data points from thousands to perhaps only a hundred. The data may also require scaling so that one test with numerically larger results does not carry an undue amount of influence within the regression fitting routine. All of these actions generally are carried out in an iterative, or trial-and-error, fashion that consumes a significant amount of personnel time. The time estimate offered here is reduced because most of the response models have already been developed. If a different constitutive model were to be substituted for the one described in this report, additional hours would have to be allocated for producing the new response models. Thus, the time estimate for the data manipulation and fitting is expected to be 100 person-hours. Using a unit cost rate of $100 per hour, the data analysis is expected to cost about $10,000.

The total laboratory-related cost estimate is $89,200, which is the sum of $75,000 for constitutive parameters testing, $4,200 for material strength properties testing, and $10,000 for data analysis and fitting.

6.0 COST ANALYSIS

6.1 SALT CAVERN STORAGE

The major advantage of storing natural gas in salt caverns is the immediate availability during peak demands. The deliverability of natural gas from many existing salt caverns is over 250 million cubic feet (MMscf) per day. In comparison, the average deliverability for storage facilities in depleted gas fields and aquifers is closer to 50 MMscf per day (e.g., Ratigan and Hall [1999]). As a result, storage of natural gas in salt deposits has proven to be economically viable, especially in regions where the end user is near the storage facility and/or high withdrawal rates are needed for peaking services.

It has been demonstrated through use of the MDCF model that under certain conditions, the minimum gas pressure can be lowered in storage caverns in salt for reasonable periods of time without jeopardizing cavern stability. A reduction in the cavern minimum operating pressure results in an increase in the working gas capacity. This increase in deliverable gas comes without an increase in cavern size. The MDCF model can be adopted by all existing and future storage facilities in salt without any modification to the storage facility. Thus, other than the cost for developing the site-specific properties and performing a geomechanical analysis using the MDCF model, no additional operating or capital expenses are associated with the cavern design criterion. Although the cost for performing a geomechanical analysis of a storage cavern will vary depending on the complexity of the site, a reasonable cost estimate will typically range between $25,000 and $75,000. Therefore, including the estimated cost of approximately $89,200 to evaluate the site-specific parameter values, the total expected cost for adopting the MDCF model to determine the minimum design gas pressure ranges between $115,000 and $165,000 per cavern.

Determining the total potential savings to the CNG industry that could be attributed to adopting the MDCF model is a formidable task that depends on future expectations that are unknown, such as the actual cavern service cycles and outcome of the geomechanical analyses using the MDCF model. It is believed that use of the MDCF model will provide a more accurate prediction of the salt. As a result, less conservative estimates for the minimum gas pressure can be determined. A reduction in the minimum gas pressure allowable in salt storage caverns can benefit the CNG storage industry in several ways:

- Increase deliverable gas without an increase in storage requirements
- Increase peaking service
- Reduce capital expenditure

- Lower storage costs
- Reduce storage construction cost.

The cost savings to industry will depend on how much the working gas capacity can be safely increased for each storage cavern and if this increased capacity is utilized. The increase in working gas capacity cannot be determined without performing the appropriate geomechanical analysis. The geomechanical analysis using the MDCF model cannot be performed without first determining the site-specific parameters. Therefore, it follows that some assumptions must be made regarding the expected decrease in the minimum gas pressure so that an assessment of the cost benefit associated with the MDCF model development can be performed.

6.2 ILLUSTRATION OF INCREASED WORKING GAS CAPACITY

As previously mentioned, a lower minimum gas pressure increases the working gas capacity of the storage cavern. As a result, existing caverns can deliver more gas if the design minimum gas pressure is lowered. To illustrate this point, consider the two storage caverns analyzed during the feasibility study for this project [DeVries et al., 1998]. The approximate total gas volume of Cavern A is 10.7 billion cubic feet (Bcf), assuming a design maximum cavern pressure of 1,707 psi at the casing shoe (0.85 psi/ft of depth). The approximate design minimum gas pressure determined using a conventional model (Damage Potential method) is 280 psi (0.14 psi/ft). At a cavern gas pressure of 280 psi, the working gas volume and cushion gas volume remaining in Cavern A are approximately 9.2 Bcf and 1.5 Bcf, respectively. However, if a design minimum gas pressure less than 280 psi was determined, the working gas volume would increase and the cushion gas volume would decrease by the same amount, as shown in Figure 6-1.

Figure 6-2 is similar to Figure 6-1 except it shows working gas and cushion gas volumes as a function of minimum gas pressure for the other cavern analyzed during the feasibility study (Cavern B). The approximate total gas volume of Cavern B is 5.0 Bcf, assuming a design maximum cavern pressure of 3,475 psi at the casing shoe (0.85 psi/ft of depth). Because Cavern B is deeper than Cavern A, the design minimum gas pressure determined using the Damage Potential method is higher than that of Cavern A. The approximate design minimum gas pressure determined for Cavern B is 900 psi (0.22 psi/ft), resulting in working gas and cushion gas volumes of 3.8 Bcf and 1.2 Bcf, respectively.

6.3 ILLUSTRATION OF REDUCED CAPITAL COST

If a geomechanical analysis of Cavern A and Cavern B using the MDCF model indicates that the minimum gas pressure can be reduced, the operators of these caverns will have more flexibility in managing product storage. Depending on the immediate need, the operator may

RSI-621-99-047

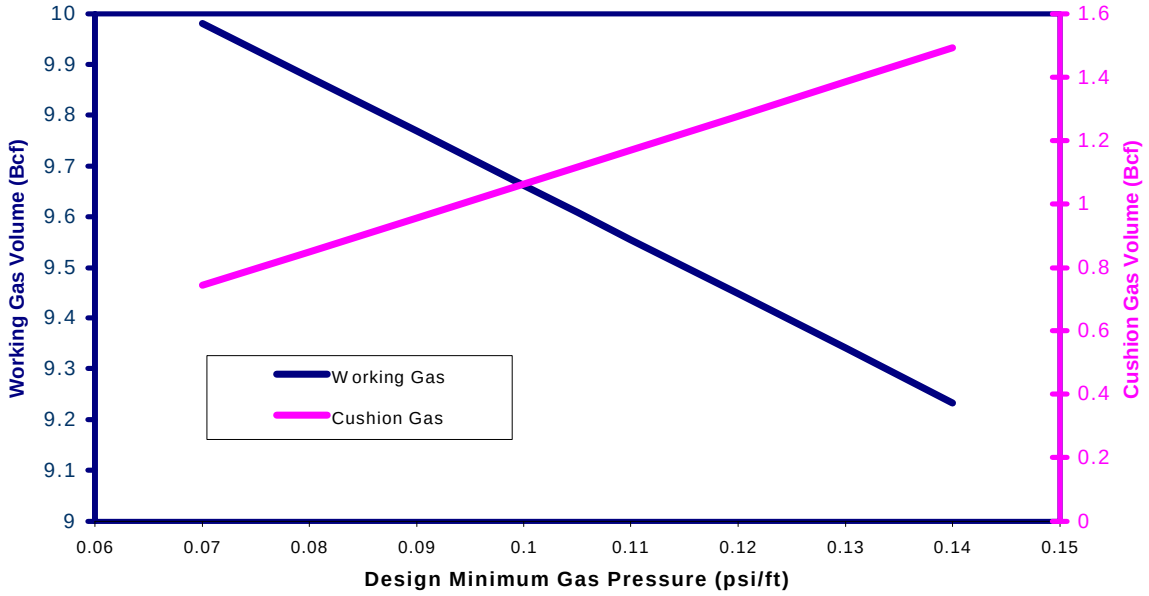

Figure 6-1. Cavern A Working Gas and Cushion Gas Volumes as a Function of Minimum Gas Pressure.

RSI-621-99-048

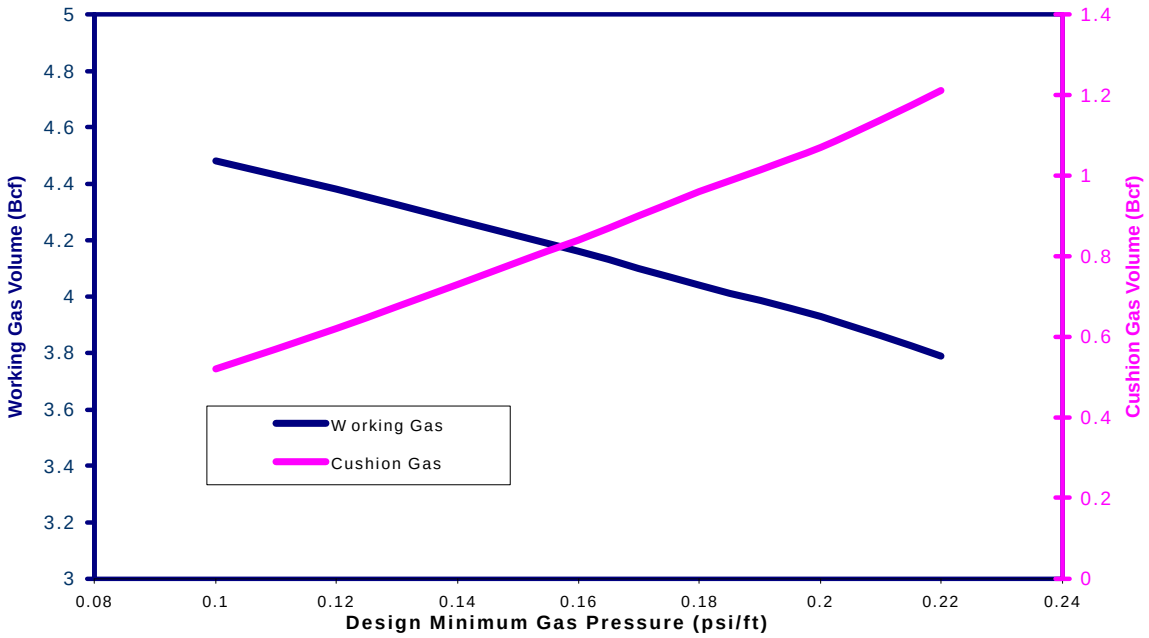

Figure 6-2. Cavern B Working Gas and Cushion Gas Volumes as a Function of Minimum Gas Pressure.

chose to (1) use the increased capacity to sell more or larger contracts or (2) reduce storage inventory but maintain the same working gas volume. In either case, the operator is able to recoup the capital cost associated with the reduction in the volume of cushion gas. Table 6-1 and Table 6-2 illustrate the capital cost savings realized for Cavern A and Cavern B, respectively, for different design minimum gas pressures and gas prices. Based on these tables, it is apparent that only a small reduction in the design minimum gas pressure (approximately 0.01 psi/ft) is necessary to offset the price of adopting the new design criterion.

Table 6-1. Potential Capital Cost Savings for Cavern A

Minimum Gas Pressure (psi/ft)	Minimum Gas Pressure (psi)	Working Gas Volume (Bcf)	Cushion Gas Volume (Bcf)	Reduction in Capital Expense[a] (US dollars)		
				Gas Cost ($/MMBtu)[b]		
				$2.0	$2.50	$3.0
0.14[c]	280	9.23	1.49	-	-	-
0.13	260	9.34	1.38	$198,720	$248,400	$298,080
0.12	240	9.45	1.28	$395,600	$494,500	$593,400
0.11	220	9.56	1.17	$592,480	$740,600	$888,720
0.10	200	9.68	1.06	$789,360	$986,700	$1,184,040
0.09	180	9.77	0.96	$986,240	$1,232,800	$1,479,360
0.08	160	9.88	0.85	$1,181,280	$1,476,600	$1,771,920
0.07	140	9.98	0.74	$1,376,320	$1,720,400	$2,064,480

(a) Capital Expense = (Volume of Cushion Gas) x (Gas Cost).
(b) A thermal factor of 0.92 was used to convert Mscf to MMBtu.
(c) Baseline pressure determined using the Damage Potential method.

6.4 ILLUSTRATION OF REDUCED STORAGE COST

Natural gas storage company customers include producers, pipeline companies, local distribution companies, utilities, and natural gas marketers. Salt cavern storage companies permit customers to contract for storage space, injection, and withdrawal capacities. The storage company usually provides contracts for gas services on a firm, secondary firm, and interruptible basis. The size and number of contracts for a given storage cavern depend upon the physical limitations of available space and injection and withdrawal capacity. Typically, the majority of the storage company s contracts are on a firm basis where the customer pays a premium or demand fee for the availability of the storage space and for injection and withdrawal rights regardless of usage. A secondary firm contract is similar to a firm contract except the fee is generally lower since the storage company has the right to refuse services to

the secondary firm customer if the firm contracts require the available space and deliverability. Interruptible contracts are similar to secondary firm contracts; however, no demand fee is charged. Interruptible clients often receive a discount since variations in demand reduce the reliability of service through constant interruptions caused by imbalances of the pipeline system. Because a majority of the storage company s contracts are to provide firm service, profits depend largely on the volume of storage available rather than gas inventory in storage. It is possible for a storage operator to have contracts that exceed the volume of gas stored or deliverability of the storage facility. This is possible since customers with firm contracts do not typically utilize all of their storage, injection, and withdrawal capacity at all times. As a result, companies offer secondary and interruptible services to increase utilization. In this case, the storage company runs the risk of paying high penalties if the firm or baseload contracts are called and cannot be delivered.

Table 6-2. Potential Capital Cost Savings for Cavern B

Minimum Gas Pressure (psi/ft)	Minimum Gas Pressure (psi)	Working Gas Volume (Bcf)	Cushion Gas Volume (Bcf)	Reduction in Capital Expense[a] (US dollars)		
				Gas Cost ($/MMBtu)[b]		
				$2.0	$2.50	$3.0
0.22[c]	900	3.79	1.21			
0.20	818	3.93	1.07	$257,600	$322,000	$386,400
0.18	736	4.04	0.96	$460,000	$575,000	$690,000
0.16	654	4.16	0.84	$680,800	$851,000	$1,021,200
0.14	572	4.27	0.73	$883,200	$1,104,000	$1,324,800
0.12	490	4.38	0.62	$1,085,600	$1,357,000	$1,628,400
0.10	409	4.48	0.52	$1,269,600	$1,587,000	$1,904,400

(a) Capital Expense = (Volume of Cushion Gas) x (Gas Cost)
(b) A thermal factor of 0.92 was used to convert Mscf to MMBtu.
(c) Baseline pressure determined using the Damage Potential method.

By increasing the working gas volume, storage operators can benefit through the sale of larger or more contracts and/or reduced penalty risk. How much the operator charges for gas storage depends on a number factors, including the type of contract (firm, secondary firm, or interruptible) and length of contract. In addition to capacity charges, deliverability, injection, withdrawal, fuel, and tariff charges are applied to the cost of storage. Conservatively, it can be assumed that only the profit associated with the capacity charge is affected by an increase in the working gas capacity, provided additional capital expenditures are not necessary to handle the increased capacity. Since the increase in working gas capacity comes without an increase

in cavern size, the cost benefit is directly proportional to the percent increase in working gas capacity.

An approximate estimate for the range in the capacity charge for storing natural gas in salt caverns located in the southeastern United States is between $0.07 and $0.15 per MMBtu s per month. Using these values, it is possible to estimate the cost benefit that can be realized for the two caverns identified above (Cavern A and Cavern B). Tables 6-3 and 6-4 illustrate the potential increase in annual revenue realized for Cavern A and Cavern B, respectively, for the working gas volumes computed for various minimum design gas pressures. The increase in annual revenue provided in these tables are given assuming the minimum and maximum storage capacity charges of $0.07 and $0.15 per MMBtu per month. The increased revenue given in Tables 6-3 and 6-4 can be considered a net profit, provided the expense associated with deliverability, injection, and withdrawal are covered by other fees changed by the storage operator. This profit could not be realized without a decrease in storage cost per unit volume obtained by increasing the working gas volume without an increase in cavern size.

6.5 ILLUSTRATION OF LOWER CONSTRUCTION COST

The cost of developing a storage facility in a salt formation varies from a low of about $3 per thousand cubic feet (Mscf) to a high of approximately $25 per thousand cubic feet, depending on the site location. If the design maximum and minimum gas pressures are known before construction of a facility, it is possible to estimate the size of the cavern(s) that are necessary to meet the desired capacity of the facility. If a lower design minimum pressure is determined, it follows that the size of the cavern(s) could potentially be reduced. A reduction in the cavern size would equate to lower construction costs since solution mining, pumping, brine disposal, etc., would be reduced proportionately.

As shown in Figures 6-1 and 6-2, a nearly linear relationship exists between working gas volume and the design minimum gas pressure for the range of pressures plotted. For Cavern A, the working gas volume increases approximately 5.3 MMscf for every 1 psi decrease in the design minimum gas pressure. Similarly, the rate of change in the working gas volume of Cavern B is 1.1 MMscf /psi change in the minimum gas pressure. If a lower design minimum gas pressure had been used to determine the cavern size necessary to achieved the current working gas volume for these caverns, the total cavern volume could be smaller.

Assuming the lower construction cost of $3 per Mscf, every 1 psi decrease in the design minimum gas pressure could reduce the construction cost of Cavern A by $15,900. Similarly, the construction costs of Cavern B could be reduced by $3,300 for each 1 psi decrease in the minimum gas pressure. Based on these figures, it is apparent that only a small reduction in the

design minimum gas pressure (10 psi for Cavern A and 50 psi for Cavern B) is necessary to offset the $115,000 to $165,000 cost of adopting the new design criterion.

Table 6-3. Potential Cost Benefit Resulting From an Increased Capacity in Cavern A

Minimum Gas Pressure (psi/ft)	Minimum Gas Pressure (psi)	Working Gas Volume (Bcf)	Increase in Working Gas Volume (%)[a]	Potential Increase in Annual Revenue[b] (US dollars)	
				Capacity Charge Rate[c] ($/MMBtu/month)	
				$0.07	$0.15
0.14[d]	280	9.233	-	-	-
0.13	260	9.341	1.2	$83,462	$178,848
0.12	240	9.448	2.3	$166,152	$356,040
0.11	220	9.555	3.5	$248,842	$533,232
0.1	200	9.662	4.6	$331,531	$710,424
0.09	180	9.769	5.8	$414,221	$887,616
0.08	160	9.875	7.0	$496,138	$1,063,152
0.07	140	9.981	8.1	$578,054	$1,238,688

(a) Increase in working gas volume from baseline case.
(b) Revenue = (Increase in Working Gas Capacity) x (Capacity Charge Rate).
(c) A thermal factor of 0.92 was used to convert Mscf to MMBtu.
(d) Baseline minimum pressure determined using the Damage Potential method.

The above example illustrates the potential for lowering construction costs associated with solution mining caverns in salt. If a lower design minimum gas pressure were used to determine the required size of a storage facility, the reduced storage and capital costs discussed in the preceding sections could not be realized.

6.6 BENEFIT TO MARKETERS

No cost benefit can be determined for storage operators who wish to take advantage of the opportunities of the prevailing market through short-term storage. Storage companies, like marketing and production companies, can store natural gas at their facility when prices are low and withdraw natural gas when the prices increase. This form of storage is strictly speculative with a high degree of risk since the owner is gambling that the price of natural gas will increase so that it can be sold at a profit. However, the potential benefit from the sale of the cushion gas could be significant, especially during times when gas requests approach or exceed the working gas available.

Table 6-4. Potential Cost Benefit Resulting From an Increased Capacity in Cavern B

Minimum Gas Pressure (psi/ft)	Minimum Gas Pressure (psi)	Working Gas Volume (Bcf)	Increase in Working Gas Volume (%)[a]	Potential Increase in Annual Revenue[b] (US dollars)	
				Capacity Charge Rate[c] ($/MMBtu/month)	
				$0.07	**$0.15**
0.22[d]	900	3.79	-	-	-
0.20	818	3.93	3.7	$108,192	$231,840
0.18	736	4.04	6.6	$193,200	$414,000
0.16	654	4.16	9.8	$285,936	$612,720
0.14	572	4.27	12.7	$370,944	$794,880
0.12	490	4.38	15.6	$455,952	$977,040
0.10	409	4.48	18.2	$533,232	$1,142,640

(a) Increase in working gas volume from baseline case

(b) Revenue = (Increase in Working Gas Capacity) x (Capacity Charge Rate).

(c) A thermal factor of 0.92 was used to convert Mscf to MMBtu.

(d) Baseline minimum pressure determined using the Damage Potential method.

7.0 SUMMARY AND CONCLUSIONS

Simulations of laboratory tests on salt were made to aid in the design of an efficient test matrix for the purpose of determining site-specific parameter values for the MDCF constitutive model. The MDCF model was first examined to determine which of the parameters can be fixed based on theoretical or other considerations and which parameters must be treated as free parameters. Sensitivity coefficients for each of the free model parameters were calculated for each of the test simulations. Based on the results of the sensitivity analysis and laboratory test constraints, an efficient test matrix was determined. Finally, the potential cost benefits associated with the reduction in required cushion gas by using the MDCF model were compared to the additional testing and analysis costs required to evaluate the parameters for the model.

The MDCF model was initially developed to model the extreme conditions expected at nuclear waste repositories in salt. The MDCF constitutive model contains 41 parameters. However, because of the limited range of stress and temperature conditions experienced in the salt surrounding CNG storage caverns, it is not necessary to determine all of the parameters in the MDCF model. Also, several parameters have a theoretical basis or are determined by mineralogy. The parameters that do not need to be evaluated on a site-specific basis for CNG storage caverns can be treated deterministically, and can be assigned typical values. Based on these considerations, 12 of the 41 model parameters were treated as deterministic parameters, reducing the number of free parameters to 29.

Simulations were made of the available laboratory test types using two different parameter sets. The creep properties used are based on laboratory testing of salt from the Cavern A and Cavern B sites. However, because neither salt was tested to determine damage parameters, the damage parameters for both salts were assumed to be the same as those determined for WIPP salt. The sensitivity of the simulated measured response to each free parameter was calculated for each of the test simulations. The sensitivity results were very similar for both salts. However, it is likely that the sensitivity results for salts with significantly different creep and damage characteristics than those examined here may be different.

Ideally, it should be possible to find load paths in which the material behavior is dominated by one or only a few of the model parameters. However, the sensitivity coefficients determined for some of the parameters are very small for all of the load paths simulated. The parameters with very little or no influence include A_2, B_1, B_2, x_{3s}, ξ_s^1, ξ_s^2, t_0, x_4, t_0, c_0, c_3, and x_7. If the load paths simulated encompass those that will exist around the actual cavern, then determination of these parameters is not necessary because they do not significantly affect the response of the constitutive model. It is also likely that some of parameters will be difficult to determine from laboratory test data because of correlation with other variables. Correlation between variables

is evident when sensitivity coefficients for two or more variables have similar trends during a given load path.

The results of the sensitivity analysis were used to provide guidance on designing an efficient test matrix comprised of load paths and boundary conditions attainable in most modern laboratory facilities. The types of tests being proposed were chosen based on two criteria: (1) they had to be conventional tests that most laboratories could perform and (2) they had to incorporate load paths where at least some of the constitutive model parameters displayed high sensitivity coefficients. A total of 37 tests is proposed. A single testing temperature is proposed because the effects of thermal gradients at most sites is expected to be relatively small. Five types of tests are proposed for estimating the parameters in the MDCF model. The proposed test matrix includes:

- Nine Constant Stress Creep Tests - In a creep test, the axial stress is maintained at a higher level than the radial stresses and the stress state is held constant over a long period of time while the principal strains are monitored. Damage can be either suppressed or enhanced depending on the applied stress difference and mean stress. The tests would be performed at three stress differences and three mean stress levels. Creep tests provide data for estimating creep and damage parameters of the MDCF model.
- Six Constant Mean Stress Tests - In a constant mean stress test, deviatoric stress is increased while maintaining a constant mean stress. This test provides a means for introducing controlled damage in a specimen and is especially good for determining the onset of damage.
- Six Constant Strain Rate Tests - In a constant strain rate test, the axial strain is maintained at a specified rate while the confining pressure is held constant. This load path is a good strength test and can be used to induce controlled levels of damage. If unload/reload cycles are included during the test, elastic properties can also be determined.
- Six Hydrostatic Compression Tests - In a hydrostatic compression test, the axial stress is maintained at the same level as the radial stresses and the stress state is held constant over a long period of time while the principal strains are monitored. This load path will be performed at lithostatic pressure on specimens predamaged in the other load paths. This load path completely isolates the healing parameters in the MDCF model.
- Ten Mineralogic Analyses Tests - Mineralogic analysis will be used to determine the impurity content (ρ) of the salt.

In addition, the unconfined compressive strength and the indirect tensile strength can be easily estimated using the relatively inexpensive laboratory tests known as the unconfined compression test and the indirect tension test. Six of each of these tests are recommended to determine these properties.

The total laboratory-related cost estimate is $79,200, which includes $75,000 for the MDCF constitutive parameters testing and $4,200 for material strength properties testing. These costs assume that testable specimens are already available to the laboratory and are based on our experience within the RESPEC laboratory and our interactions with other, similar laboratory operations. The estimated cost for data analysis and fitting of the constitutive parameters is $10,000. The cost of performing a geomechanical analysis of a storage cavern can range between $25,000 and $75,000, depending on the complexity of the site. Thus, the approximate cost for adopting the MDCF model to determine the minimum design gas pressure is expected to be between $115,000 and $165,000.

Determining the total potential savings to the CNG industry that could be attributed to adopting the MDCF model depends on future expectations that are unknown, such as the actual cavern service cycles and outcome of the geomechanical analyses using the MDCF model. It is believed that use of the MDCF model will provide a more accurate prediction of the salt. As a result, less conservative estimates for the minimum gas pressure can be determined. A reduction in the minimum gas pressure allowable in salt storage caverns can benefit the CNG storage industry in several ways:

- Increase deliverable gas without an increase in storage requirements
- Increase peaking service
- Reduce capital expenditure
- Lower storage costs
- Reduce storage construction cost.

The cost savings to industry will depend on how much the working gas capacity can be safely increased for each storage cavern and if this increased capacity is utilized. In this study, cost savings were estimated as the reduced capital expense resulting from a reduction in cushion gas volume, the lower storage costs related to the increase in working gas storage space available for lease, and the lower construction costs of a new facility. Examples of the cost savings are given for Cavern A and Cavern B.

If it is possible to lower the minimum gas pressure of a cavern, the operator is able to recoup the capital cost associated with the reduction in volume of the required cushion gas. Based on the analyses of Cavern A and Cavern B, only a small reduction in the design minimum gas pressure (approximately 0.01 psi/ft at the casing shoe) is necessary to offset the price of adopting the new design criterion.

By increasing the working gas volume, storage operators can also benefit through the sale of larger or more contracts and/or reduced penalty risk. Cost savings estimates for Cavern A and Cavern B, assuming a storage lease rate of $0.07 per MMBtu s per month, suggest annual cost

savings of $83,500 and $163,000, respectively, for a reduction in the design minimum gas pressure of 0.01 psi/ft at the casing shoe.

In estimating the reduction in construction costs for a new facility, cost savings were based on the reduced cavern size required when the MDCF model is used in cavern design. Based on a conservative construction cost of $3 per thousand cubic feet of working gas, it was estimated that every 1 psi decrease in the design minimum gas wellhead pressure could reduce the construction cost of Cavern A by $15,900 and Cavern B by $3,300. Using these estimates, only a small reduction in the design minimum gas pressure (10 psi for Cavern A and 50 psi for Cavern B) is necessary to offset the $115,000 to $165,000 cost of adopting the new design criterion.

8.0 REFERENCES

Chan, K. S., S. R. Bodner, A. F. Fossum, and D. E. Munson, 1992. A Constitutive Model for Inelastic Flow and Damage Evolution in Solids Under Triaxial Compression, *Mechanics of Materials,* Vol. 14, pp. 1-14.

Chan, K. S., S. R. Bodner, D. E. Munson, and A. F. Fossum, 1996a. Inelastic Flow Behavior of Argillaceous Salt, *International Journal of Damage Mechanics*, Vol. 5, No. 3, July, pp. 292-314.

Chan, K. S., D. E. Munson, A. F. Fossum, and S. R. Bodner, 1996b. A Constitutive Model for Representing Coupled Creep, Fracture, and Healing in Rock Salt*, Proceedings, Fourth Conference of The Mechanical Behavior of Salt*, École Polytechnique de Montréal, Mineral Engineering Department, Québec, Canada, June 17 and 18, M. Aubertin and H. R. Hardy Jr. (eds.), Penn State University, Trans Tech Publications, Clausthal, Germany, 1998, pp. 221-234.

DeVries, K. L., J. D. Nieland, and J. L. Ratigan, 1998. *Feasibility Study for Lowering the Minimum Gas Pressure in Solution-Mined Caverns Based on Geomechanical Analyses of Creep-Induced Damage and Healing,* RSI-0969, prepared by RESPEC, Rapid City, SD, for U.S. Department of Energy, Morgantown, WV.

Fossum, A. F. 1997. Parameter Estimation for an Internal Variable Model Using Nonlinear Optimization and Analytical/Numerical Response Sensitivities, *Journal of Engineering Materials and Technology*. Vol. 119, pp. 337-345.

Fossum, A. F., G. D. Callahan, L. L. Van Sambeek, and P. E. Senseny, 1988. *How Should One-Dimensional Laboratory Equations be Cast Into Three-Dimensional Form?,* Proceedings, 29th U.S. Symposium on Rock Mechanics, University of Minnesota, Minneapolis, MN, June 13 15, P. A. Cundall, R. L. Sterling, and A. M. Starfield (eds.), A. A. Balkema, Rotterdam, pp. 35-41.

Hansen, F. D., M. J. Leroch, L. L. Van Sambeek, and M. S. Lin, 1993. Gas Barrier Design for the WIPP, *Proceedings, 34th U.S. Symposium on Rock Mechanics,* University of Wisconsin Madison, Madison, WI, June 27 30, B. C. Haimson (ed.), International Journal of Rock Mechanics and Mining Sciences & Geomechanics Abstracts, Pergamon Press, Vol. 30, No. 7, pp. 1515-1518.

Hardy H. R., 1982. *Theoretical and Laboratory Studies Relative to the Design of Salt Caverns for the Storage of Natural Gas,* American Gas Association, Arlington, VA.

James M. L., G. M. Smith, and J. C. Wolford, 1985. *Applied Numerical Methods for Digital Computation*, 3rd Ed., Harper & Row Publishers, New York, NY.

Kachanov, L. M., 1958. On the Creep Fracture Time, *Izv. Akad. Nauk, USSR, Otdgel. Tekh, Nauk.*, Vol. 8, p. 26.

Law Engineering Testing Company, 1983. *Geothermal Studies of Seven Interior Salt Domes,* ONWI-289, prepared by Law Engineering Testing Company, Columbus, OH, for the Office of Nuclear Waste Isolation, Battelle Memorial Institute, Columbus, OH.

Lin, M. S. and L. L. Van Sambeek, 1992. *Waste Isolation Pilot Plant Alcove Gas Barrier Final Design Report,* SAND92-7307, prepared by Parsons Brinkerhoff Quade & Douglas, Inc., San Francisco, CA, and RE/SPEC Inc., Rapid City, SD, for Sandia National Laboratories.

Munson, D. E., A. F. Fossum, and P. E. Senseny, 1989. *Advances in Resolution of Discrepancies Between Predicted and Measured In Situ WIPP Room Closures,* SAND88-2948, Sandia National Laboratories, Albuquerque, NM.

Press W. H., S. A. Teukolsky, W. T. Vetterling, and B. P. Flannery, 1992. *Numerical Recipes in Fortran The Art of Scientific Computing,* 2nd Edition., Cambridge University Press, New York, NY.

Ratigan, J. L., and O. Hall, 1999. *Commercial Potential of Natural Gas Storage in Lined Rock Caverns (LRC)*, SZUS-0005, prepared by Sofregaz US Inc., Houston, TX, for U.S. Department of Energy, Morgantown, WV.

Ratigan, J. L., L. L. Van Sambeek, K. L. DeVries, and J. D. Nieland, 1991. *The Influence of Seal Design on the Development of the Disturbed Rock Zone in the WIPP Alcove Seal Tests,* RSI-0400, prepared by RE/SPEC Inc., Rapid City, SD, for Sandia National Laboratories, Albuquerque, NM.

Ratigan, J. L., J. D. Nieland, and J. D. Osnes, 1993. Rock Mechanics Aspects of Natural Gas Storage in Domal Salt, presented at the *Solution Mining Research Institute Fall Meeting*, Lafayette, LA, October 25-26.

Senseny, P. E., and A. F. Fossum, 1995. On Testing Requirements for Viscoplastic Constitutive Parameter Estimation, *Journal of Engineering Materials and Technology*, Vol. 117, April, pp. 151 - 154.

Senseny, P. E. and A. F. Fossum, 1996. Testing to Estimate the Munson-Dawson Parameters, *Proceedings, Fourth Conference of The Mechanical Behavior of Salt,* École Polytechnique de Montréal, Mineral Engineering Department, Québec, Canada, June 17 and 18, M. Aubertin and H. R. Hardy Jr. (eds.), Penn State University, Trans Tech Publications, Clausthal, Germany, 1998, pp. 263-276.

Van Sambeek, L. L., D. D. Luo, M. S. Lin, W. Ostrowski, and D. Oyenuga, 1993. *Seal Design Alternatives Study,* SAND92-7340, prepared by Parsons, Brinkerhoff, Quade & Douglas, San Francisco, Ca, and RE/SPEC Inc., Rapid City, SD, for Sandia National Laboratories, Albuquerque, NM.

Advanced Design Criterion to Improve the Working Gas Capacity of Natural Gas Storage Caverns in Salt Deposits

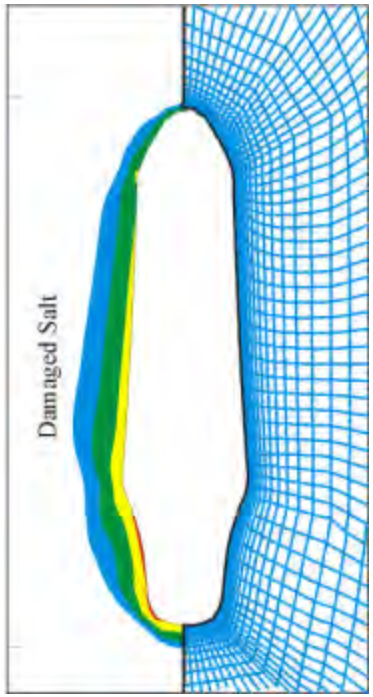

Presented by

John Osnes

Kerry DeVries Kirby Mellegard

Sponsored by

U.S. Department of Energy

National Energy Technology Laboratory

(Contract No. DE-AC26-97FT34350)

RESPEC

An Integrated Consulting and Services Company

Objective of Research

- Develop a new design criterion for the minimum gas pressure allowed in a storage cavern based on an advanced material model for salt
  - Phase I: Assess likelihood that minimum gas pressures can be decreased from values based on current design criterion
  - Phase II: Determine types of testing required to implement new design criterion and evaluate cost
- Working gas capacity ($$$) can be increased if minimum gas pressure can be decreased

RESPEC
An Integrated Consulting and Services Company

Overview of Presentation

- Performance Objectives for Storage Caverns
- Behavior of Salt Around Storage Caverns
- Design Criteria for Minimum Gas Pressure

— Break —

- Development of New Design Criterion
- Development of Optimal Laboratory Test Matrix for Site-Specific Parameters
- Cost-Benefit Analysis of New Design Criterion

— Questions & Discussion —

RESPEC
An Integrated Consulting and Services Company

Performance Objectives for Storage Caverns

- Maintain a stable cavern
  - Avoid spalling of salt
  - Avoid failure of nonsalt units
- Contain gas with no leakage
  - Limit microfracturing of salt
  - Preclude failure of casing seat
  - Avoid hydraulic fracturing between caverns
- Limit rate of cavern closure
- Limit rate of ground subsidence

RESPEC
An Integrated Consulting and Services Company

Primary Factors Affecting Performance

- Site-specific strength and deformation properties of surrounding salt and nonsalt units
- Preexisting in situ state of stress
- Cavern size, shape, and proximity to other caverns
- Operating pressure range in cavern
  - Maximum pressure limited by depth and regulations
  - Minimum pressure determined by satisfying the performance objectives given the site-specific conditions

RESPEC
An Integrated Consulting and Services Company

Behavior of Salt Around Natural Gas Storage Caverns

Kirby Mellegard

RESPEC
An Integrated Consulting and Services Company

Characteristics of Salt

- Salt can be brittle; i.e., it can crack
- Salt can be ductile; i.e., it can flow
- Salt is time-dependent; i.e., it can creep
- Salt has a crystalline microstructure that can be damaged and/or healed

RESPEC
An Integrated Consulting and Services Company

Mechanical Properties

- Elastic Properties
  - Young's Modulus and Poisson's Ratio
- Strength
  - Compressive strength and tensile strength
- Plastic Properties
  - Time-dependent (creep)
  - Stress and temperature dependent
- Microstructural
  - Microfractures (damage)

RESPEC
An Integrated Consulting and Services Company

Modern Laboratory Test System

- Pressure vessel
- Cylindrical specimens
- Computerized operation
- Servocontrol features
  - Axial force
  - Pressure
  - Temperature
- Instrumentation
  - Electronic transducers
  - Loads & displacements

RESPEC
An Integrated Consulting and Services Company

Unconfined Compression Test

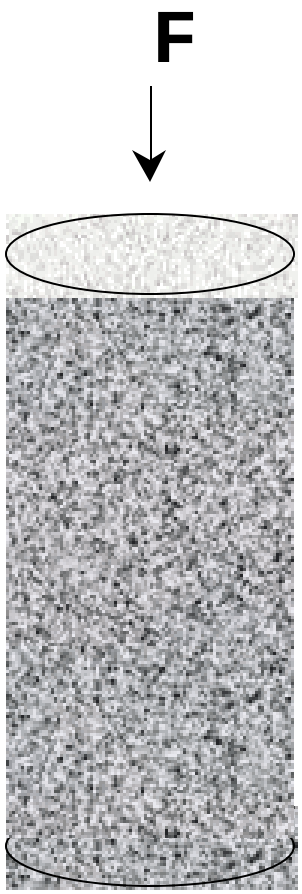

- Increase axial force until specimen failure
- Record maximum force, $\mathbf{F}_{max}$
- Calculate specimen area, $\mathbf{A}_s$
- Calculate unconfined compressive strength

$$C_o = F_{max} / A_s$$

RESPEC
An Integrated Consulting and Services Company

UCC Properties are Site-Specific

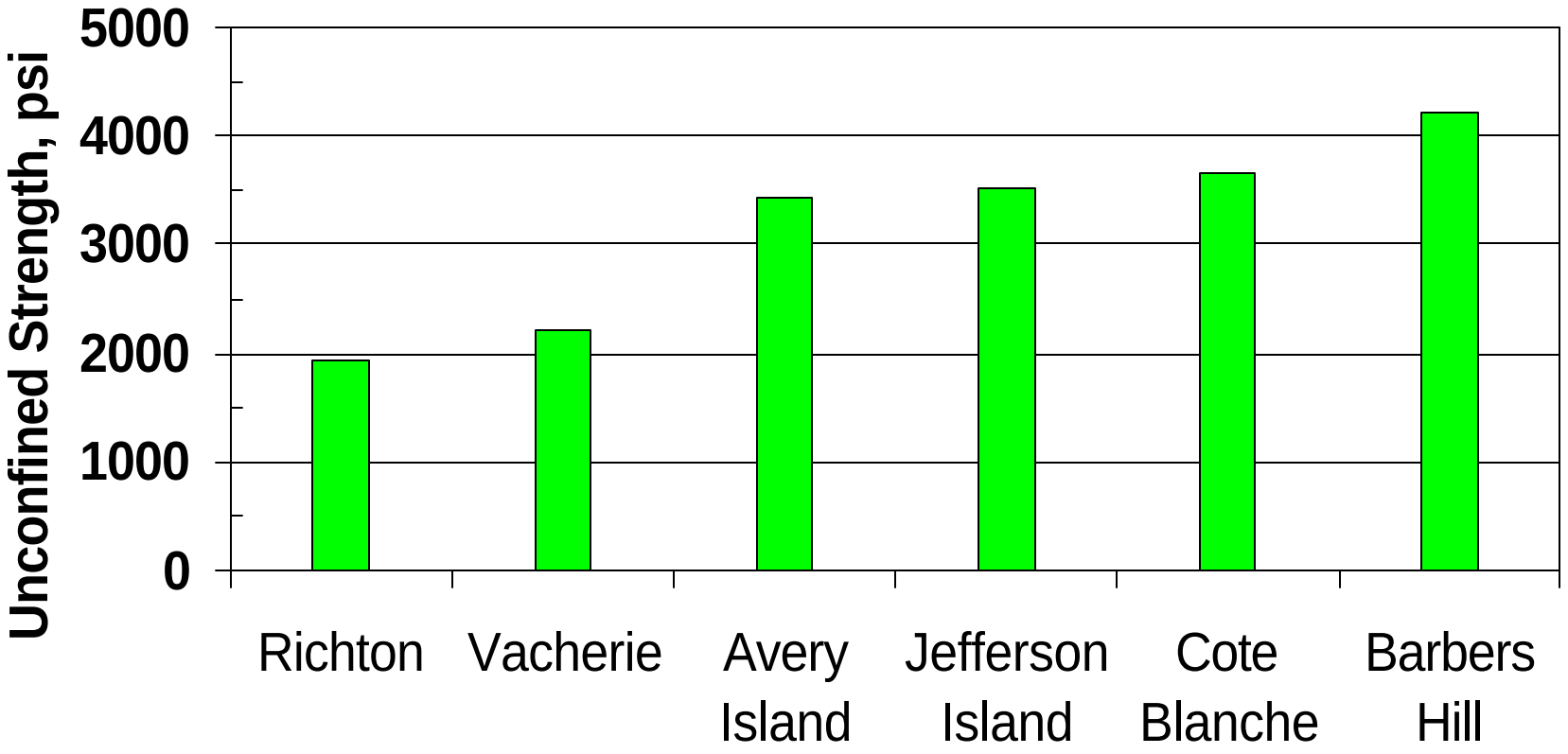

RESPEC
An Integrated Consulting and Services Company

Salt Varies From Site to Site

RESPEC
An Integrated Consulting and Services Company

Triaxial Compression Test

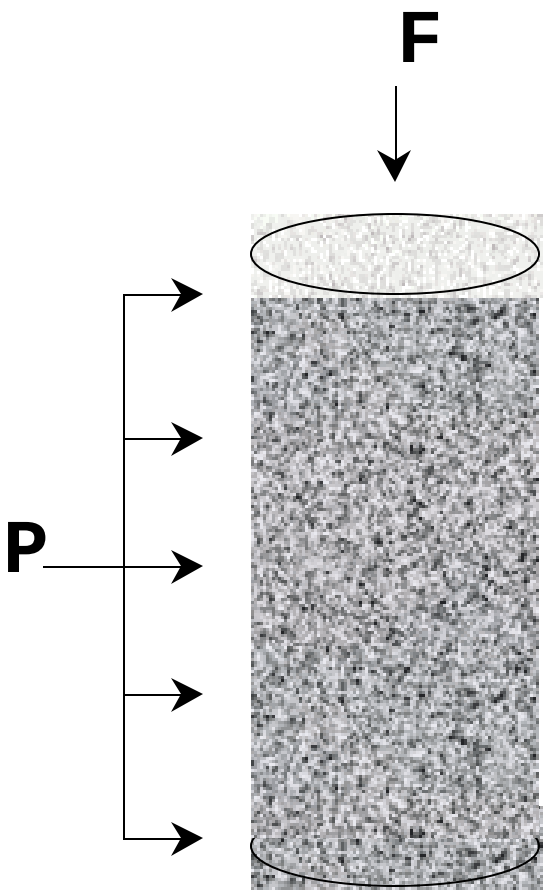

- Quasi-static Test:

  F increases with **P** constant

- Creep Test:

  F and **P** constant, (**F**/A) > **P**

- CMS Test:

  Increase **F** and decrease **P**

  { $\mathbf{s}_m = (\mathbf{F}/A + 2\mathbf{P})/3$ }

RESPEC
An Integrated Consulting and Services Company

Salt Can Flow

- Triaxial test conditions of high confining pressure and elevated temperature
- Pre-test specimen setup between loading platens
- Post-test specimen shows no visible cracking, even though salt has flowed up and around the platens

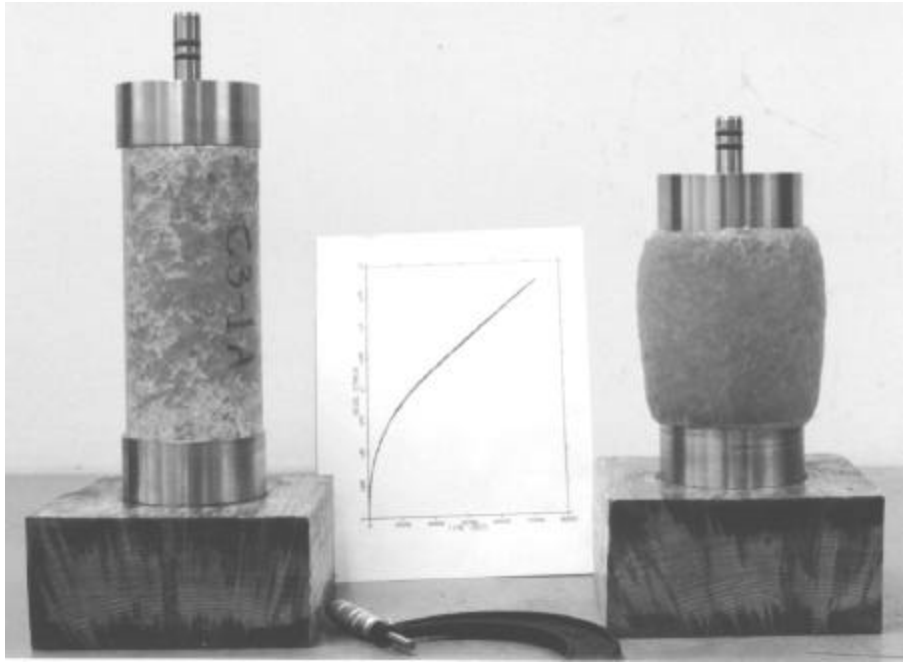

Pre-test **Post-test**

RESPEC
An Integrated Consulting and Services Company

Damage = Volume Increase

Pre-Test **Post-Test**

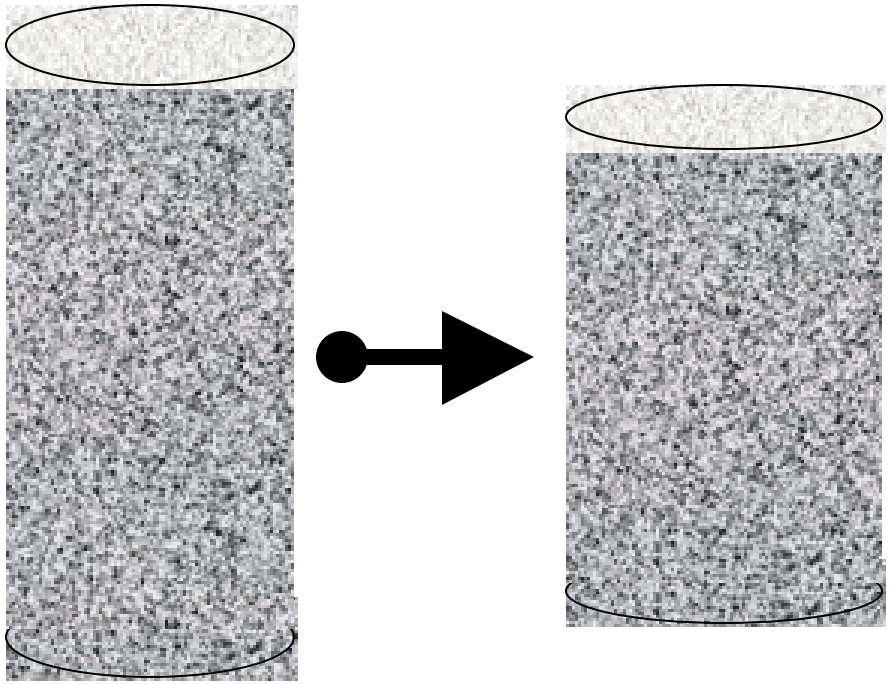

- Isovolumetric
  - Specimen shape changes but the volume remains the same. No microfracturing (damage)
- Dilatant
  - Specimen shape changes and the volume increases. The volume increase is a result of microfracturing (damage)

RESPEC
An Integrated Consulting and Services Company

Three Phases of Creep

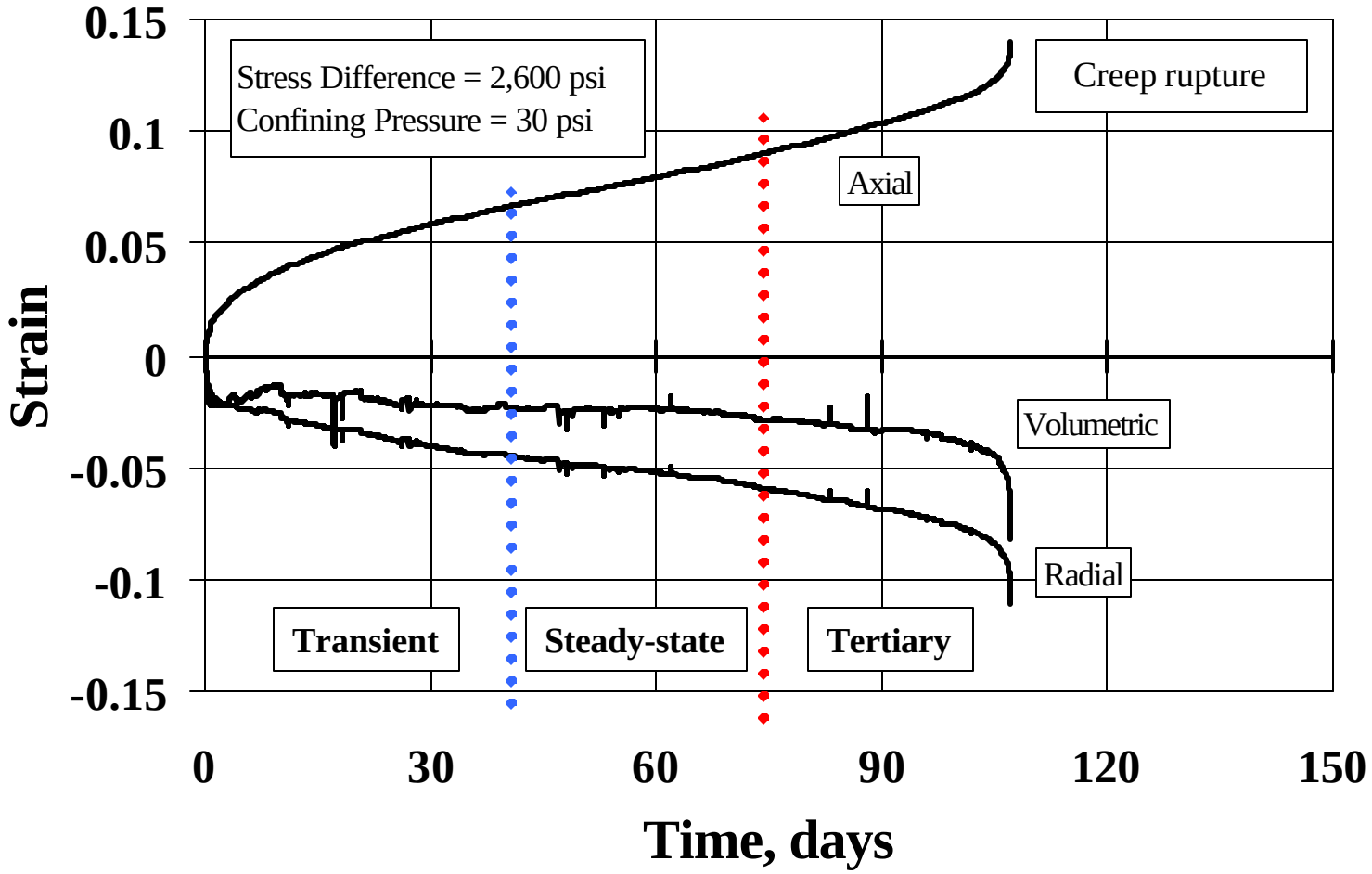

RESPEC
An Integrated Consulting and Services Company

Creep Response is Stress-Dependent

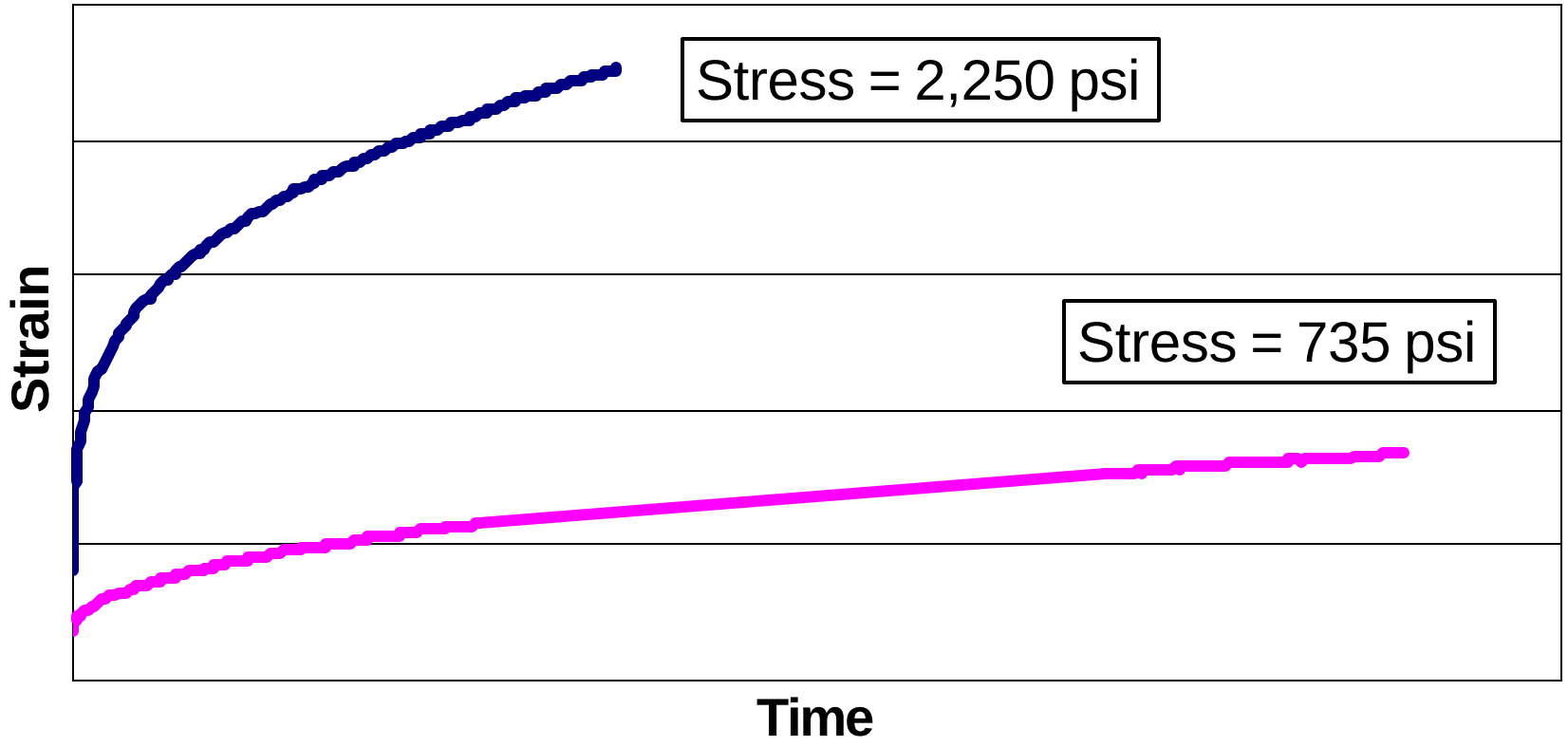

RESPEC
An Integrated Consulting and Services Company

Dilation (Damage) Determination

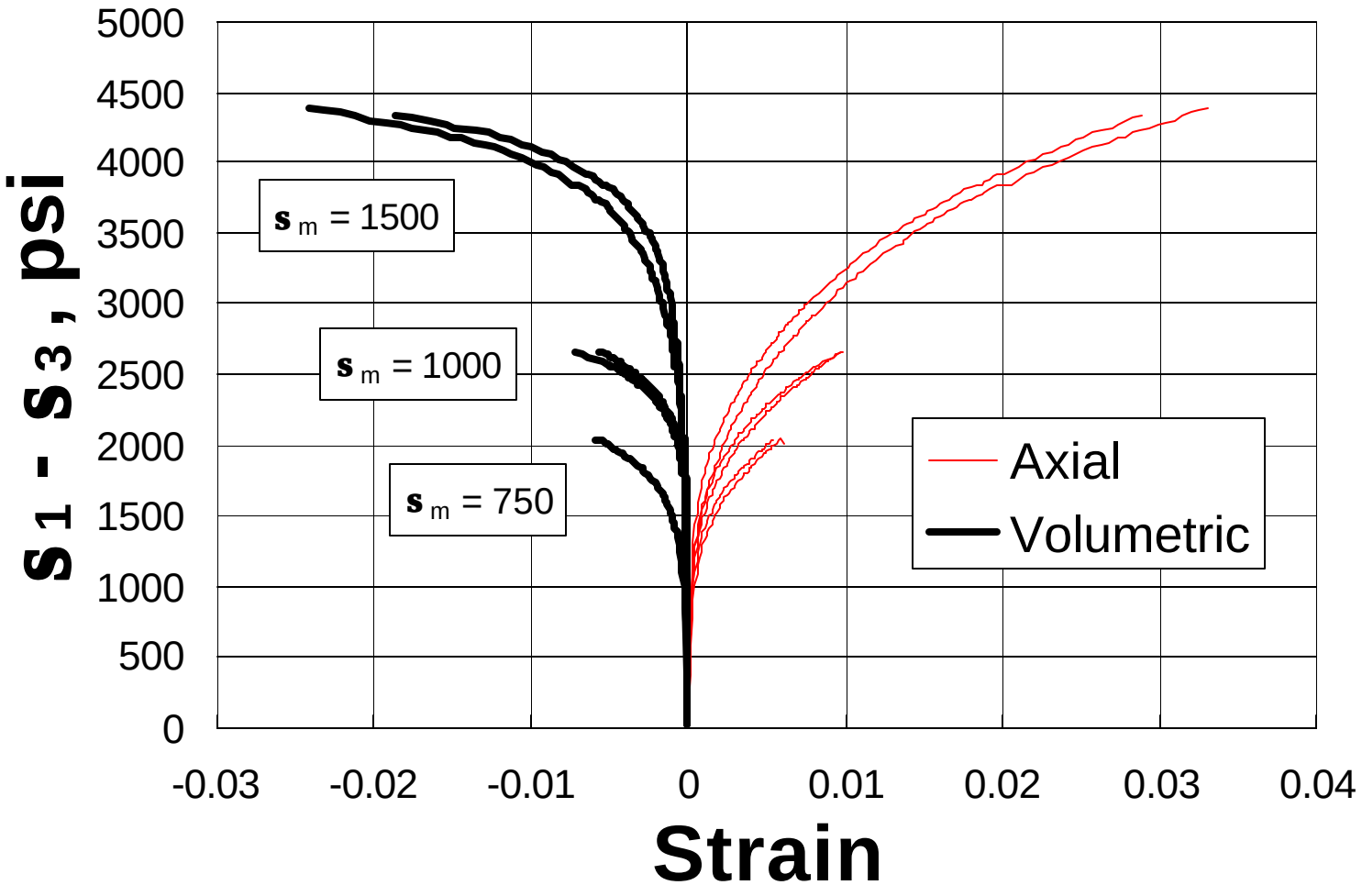

RESPEC
An Integrated Consulting and Services Company

Damage Potential

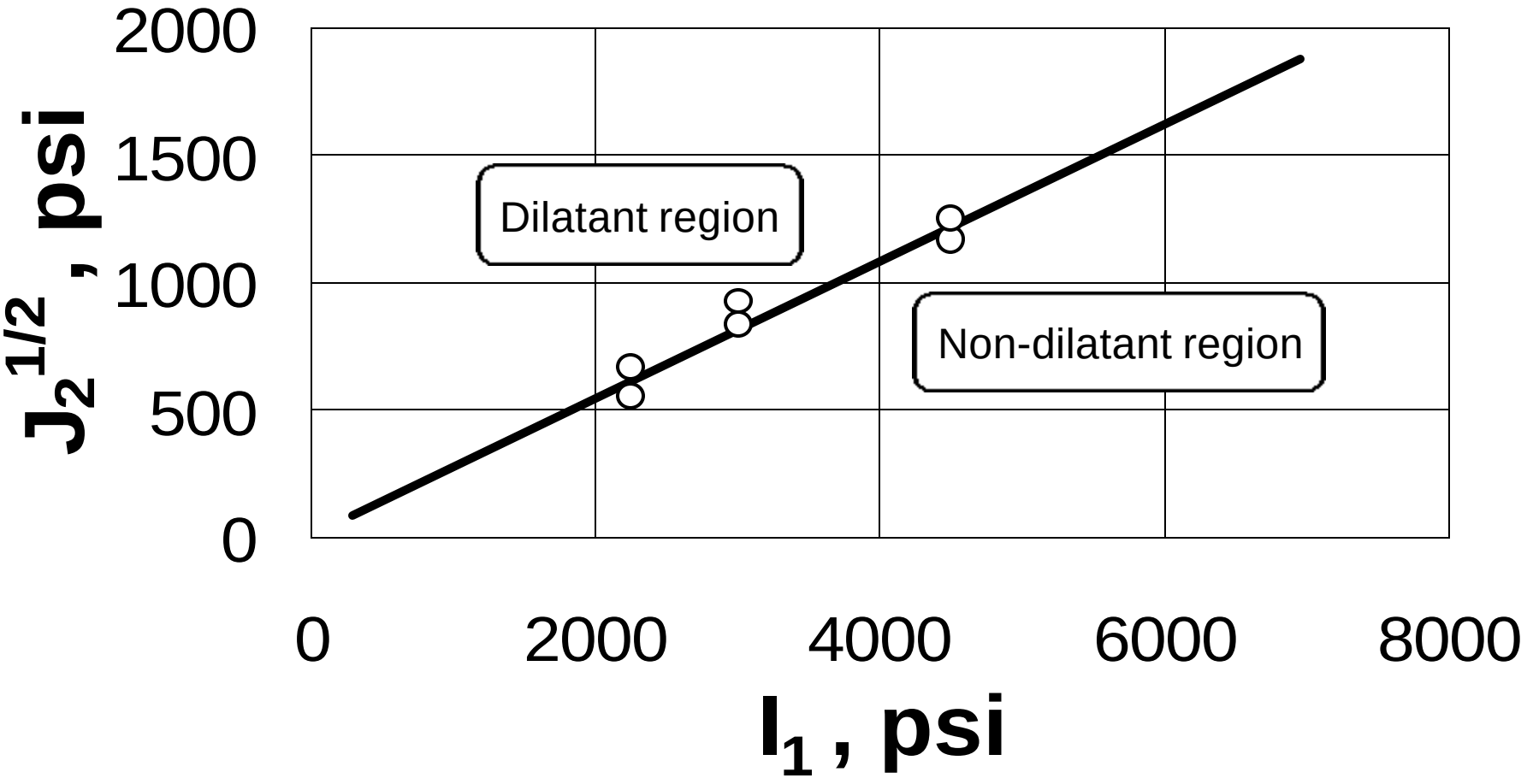

RESPEC
An Integrated Consulting and Services Company

Damage Recovery (Healing)

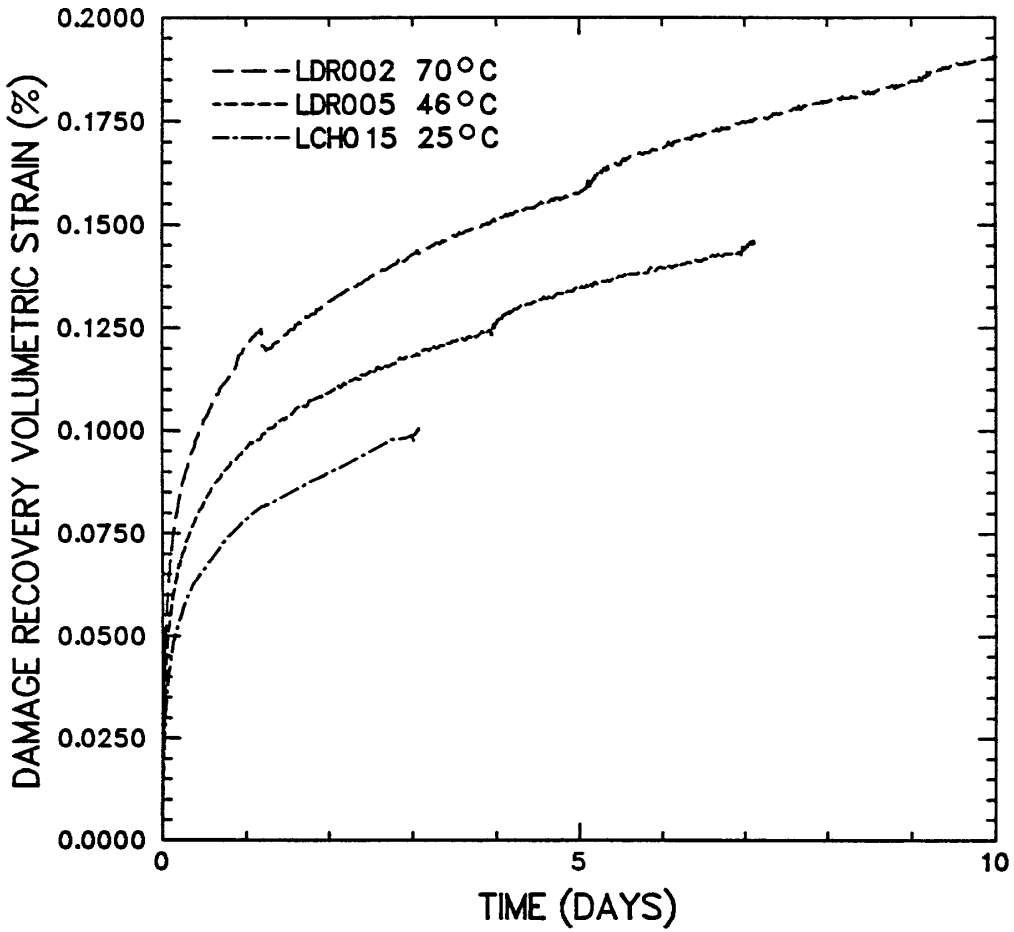

RESPEC
An Integrated Consulting and Services Company

Impacts on Cavern Design/Operation

- Site-specific salt properties
  - If you change locations, the properties of the salt can be significantly different
- Salt response depends on stress & temperature
  - The cavern environment (e.g., depth) and geometry play important roles in cavern integrity
- Salt damage/healing impacts cavern operation
  - Damage/healing induced in the salt is closely linked to the minimum allowable working gas pressure

RESPEC
An Integrated Consulting and Services Company

Design Criteria for Determining the Minimum Gas Pressure in a Salt Cavern

John Osnes

RESPEC
An Integrated Consulting and Services Company

Salt Stresses Near a Storage Cavern

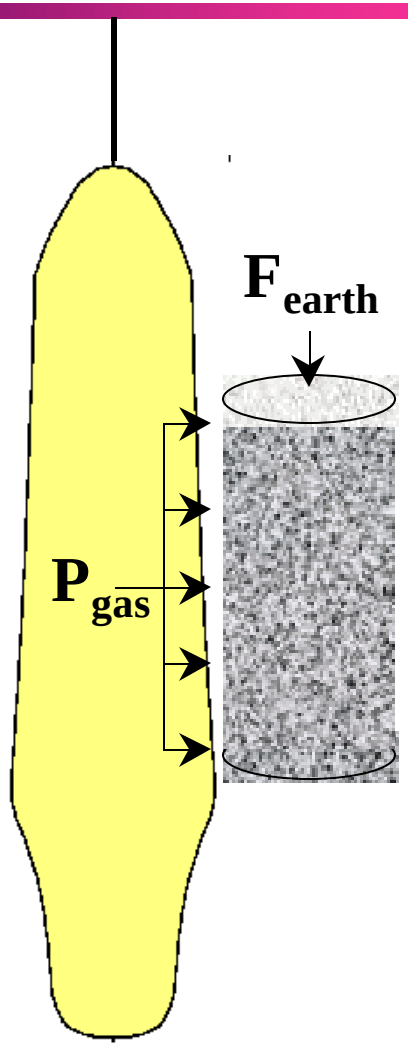

- Overburden stress (F_{earth}) remains fairly constant
- Gas pressure (P_{gas}) varies between maximum and minimum values
- $F_{earth} > P_{gas}$
- Creep causes salt to flow into cavern and cavern to shorten
- Differential load on salt *increases* as P_{gas} *decreases*

RESPEC
An Integrated Consulting and Services Company

Salt Dilation in Creep Tests

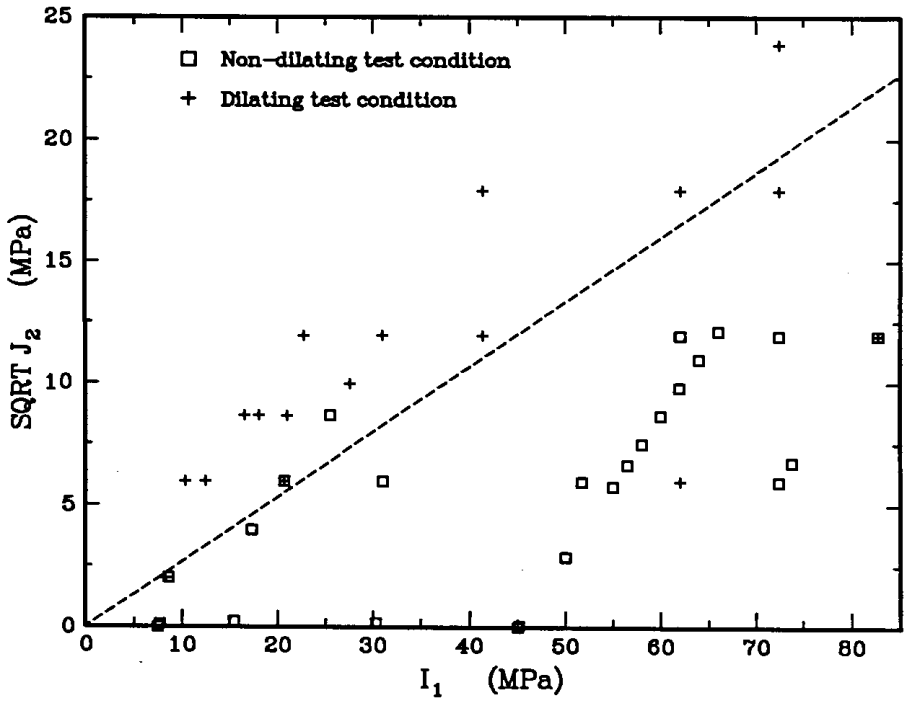

$$\text{Damage Potential} = \frac{\sqrt{J_2}}{I_1}$$

- Large database of Avery Island & WIPP creep tests analyzed by Ratigan et al. [1991]
- Categorized tests by whether salt expanded volumetrically (dilated) during test
- Volumetric expansion (dilation) indicates microfracturing (damage)
- Boundary apparent between dilating and non-dilating stress states (in $J_2^{1/2}$ versus I_1 plot)

RESPEC
An Integrated Consulting and Services Company

Design Based on Damage Potential Criterion

Design Basis

Salt microfracturing (damage) occurs when the *Damage Potential* exceeds a threshold value.

- Determine limiting value of Damage Potential from lab testing (varies for different salts)
- Predict distribution of Damage Potential around cavern as function of minimum gas pressure from numerical modeling
- Determine minimum gas pressure at which Damage Potential around cavern does not exceed limiting value

RESPEC
An Integrated Consulting and Services Company

Limitations of Damage Potential Criterion

- Conservative because does not allow *any* damage (*no* microfracturing)
- Stress-based criterion
  - Only determines whether damaging stress states exist or not
- Amount of damage cannot be quantified
  - Salt can tolerate *limited* damage without adverse effects on performance
- Healing of damage is not evaluated
  - Salt may heal when gas pressure is high

RESPEC
An Integrated Consulting and Services Company

Criterion Based on Advanced Salt Model

- Advanced material models for salt that represent damage and healing under development
- Multimechanism Deformation Coupled Fracture (MDCF) model
  - Developed for Waste Isolation Pilot Plant (WIPP)
  - Extends Munson-Dawson creep model
  - Includes damage accumulation and healing
- Use MDCF model to develop damage-based criterion
  - Allow *limited* damage accumulation at low gas pressures
  - Account for healing of damage at high gas pressures

RESPEC
An Integrated Consulting and Services Company

Development of a New Design Criterion Based on an Advanced Material Model for Salt

Kerry DeVries

RESPEC
An Integrated Consulting and Services Company

Focus of Phase I

- Compare Damage Potential Method to MDCF model prediction
- Establish criterion for damage as the limiting value that assures cavern stability
- Use numerical modeling methods to evaluate cavern performance

RESPEC
An Integrated Consulting and Services Company

MDCF Model

- Predicts transient, steady-state, & tertiary creep
- Predicts damage evolution and healing
  - Damage predicted during transient, steady-state, & tertiary creep
  - Healing a function of stress and level of damage
- Quantifies damage as scalar variables
  - Dilatant volumetric strain
  - Damage variable (ω)

RESPEC
An Integrated Consulting and Services Company

Cavern Design Criterion

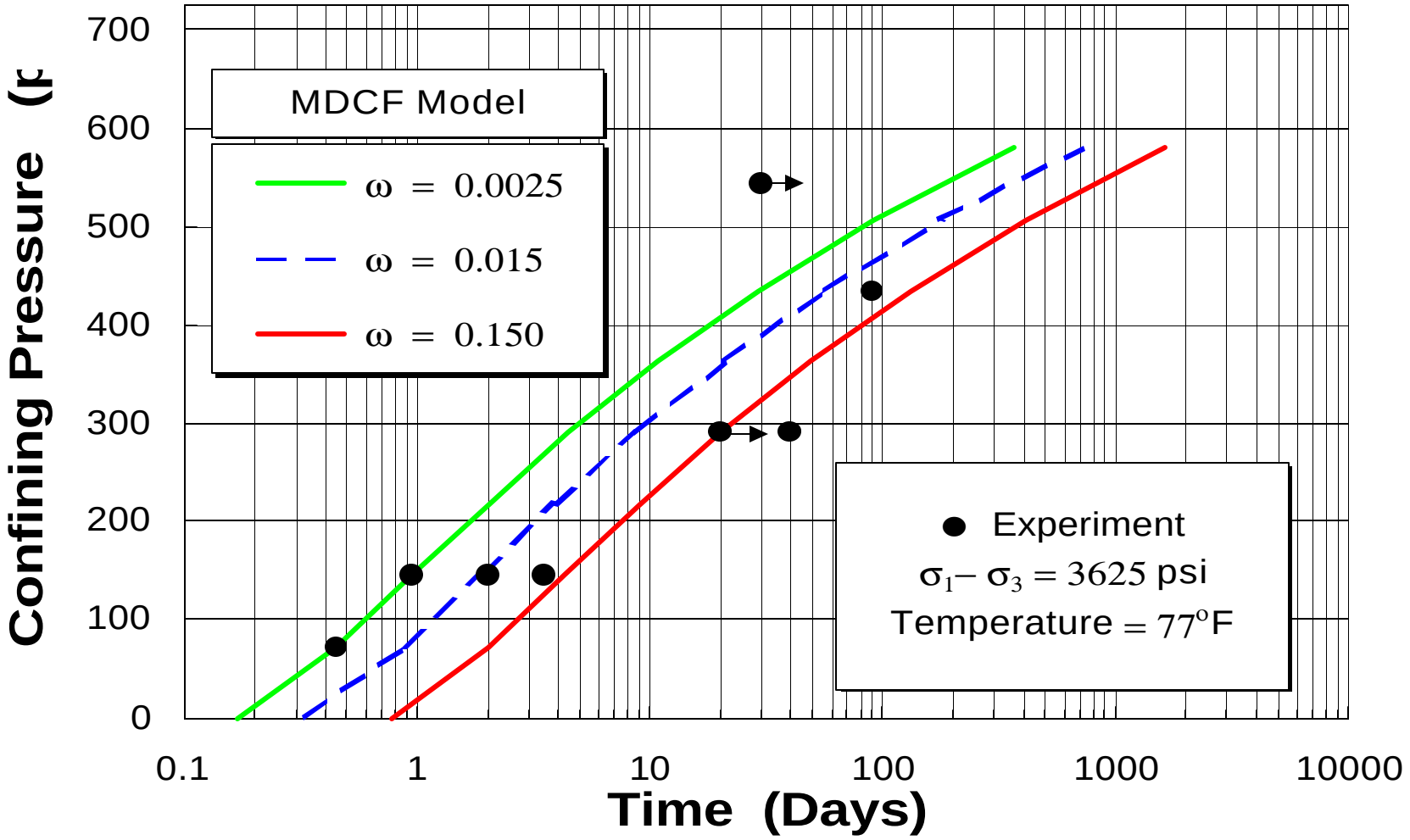

RESPEC
An Integrated Consulting and Services Company

Cavern Stability Analysis

- Technical approach
  - Selected two natural gas storage caverns
  - Predict minimum gas pressures that completely suppress damage
  - Predict damage in salt for typical gas service cycles at pressures that do not completely suppress damage
  - Evaluate accumulation of damage and healing over several natural gas cycles
  - Estimate time at minimum gas pressure before caverns exceed recommended design limit

RESPEC
An Integrated Consulting and Services Company

Dilation Boundaries

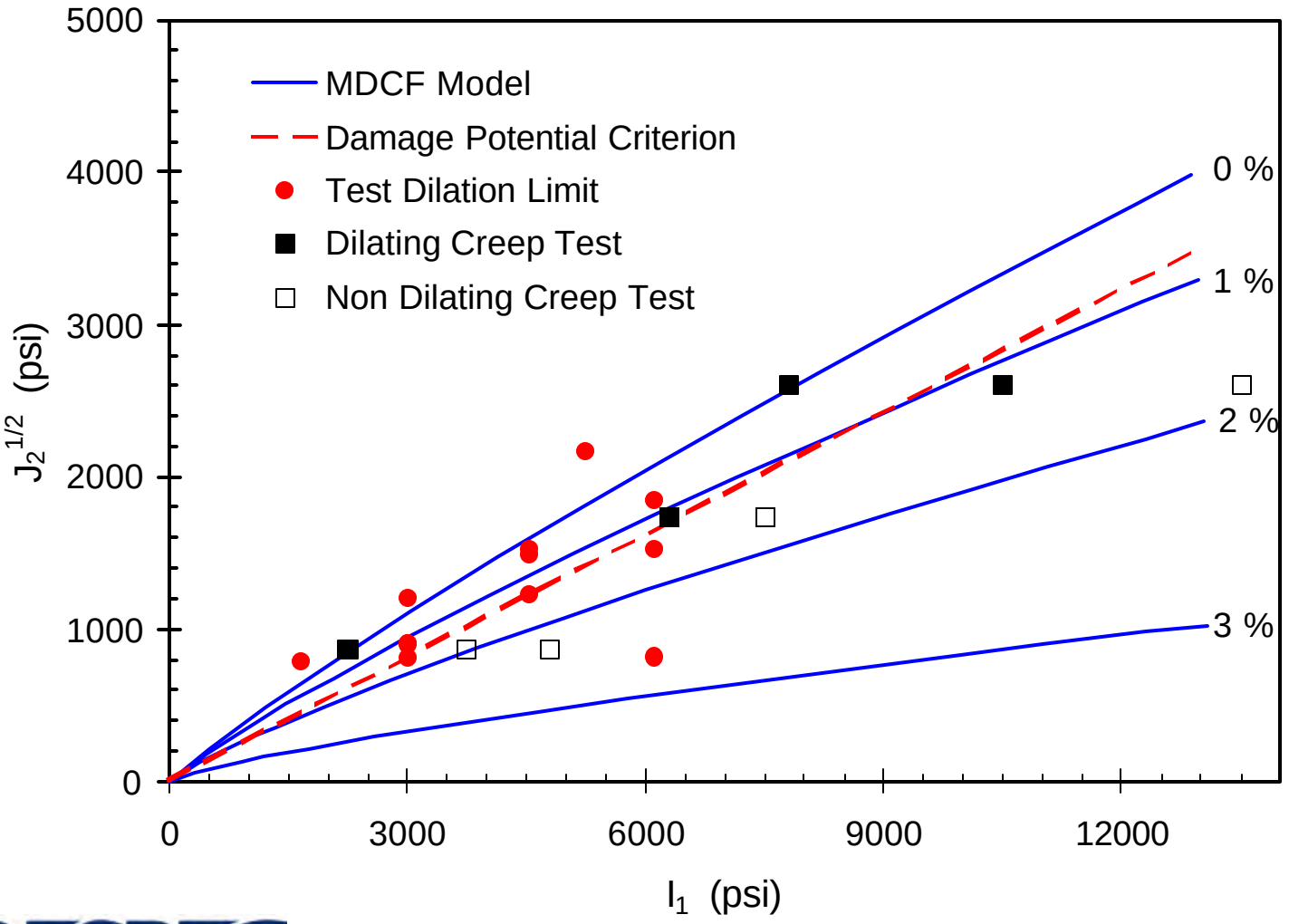

RESPEC
An Integrated Consulting and Services Company

Contours of Dilatant Salt

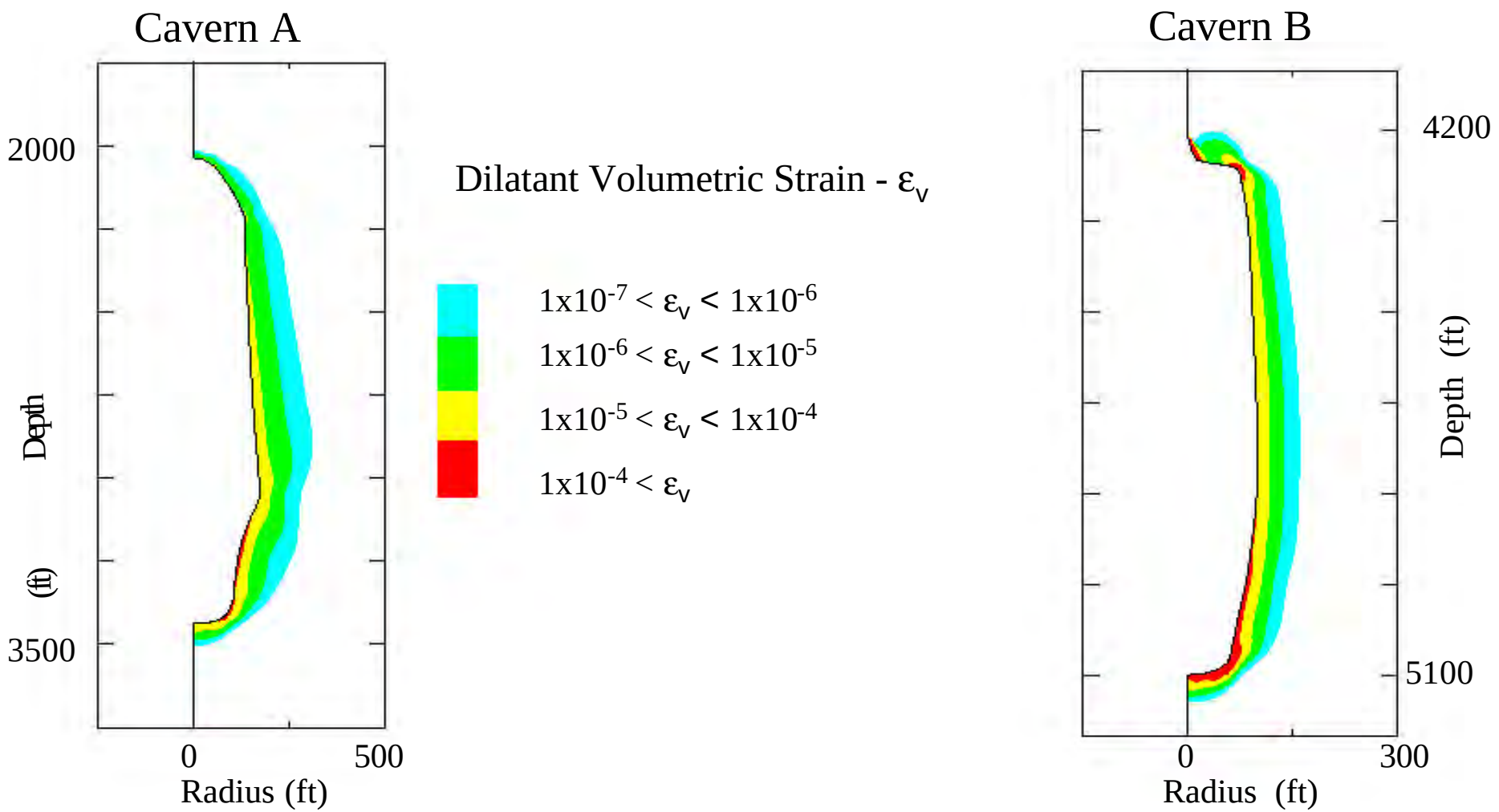

RESPEC
An Integrated Consulting and Services Company

Gas Service Cycle

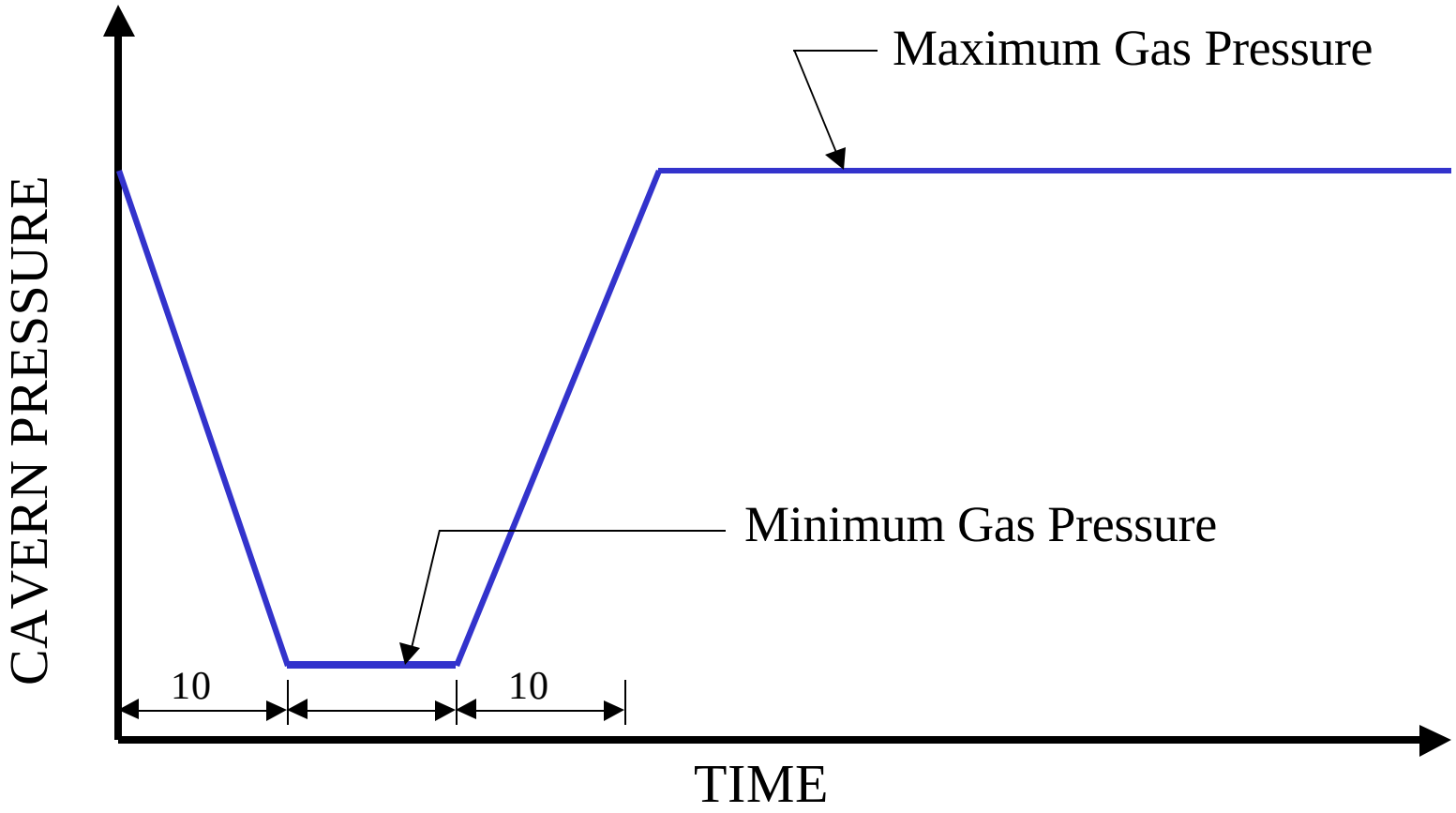

RESPEC
An Integrated Consulting and Services Company

Dilating Salt Around Cavern A

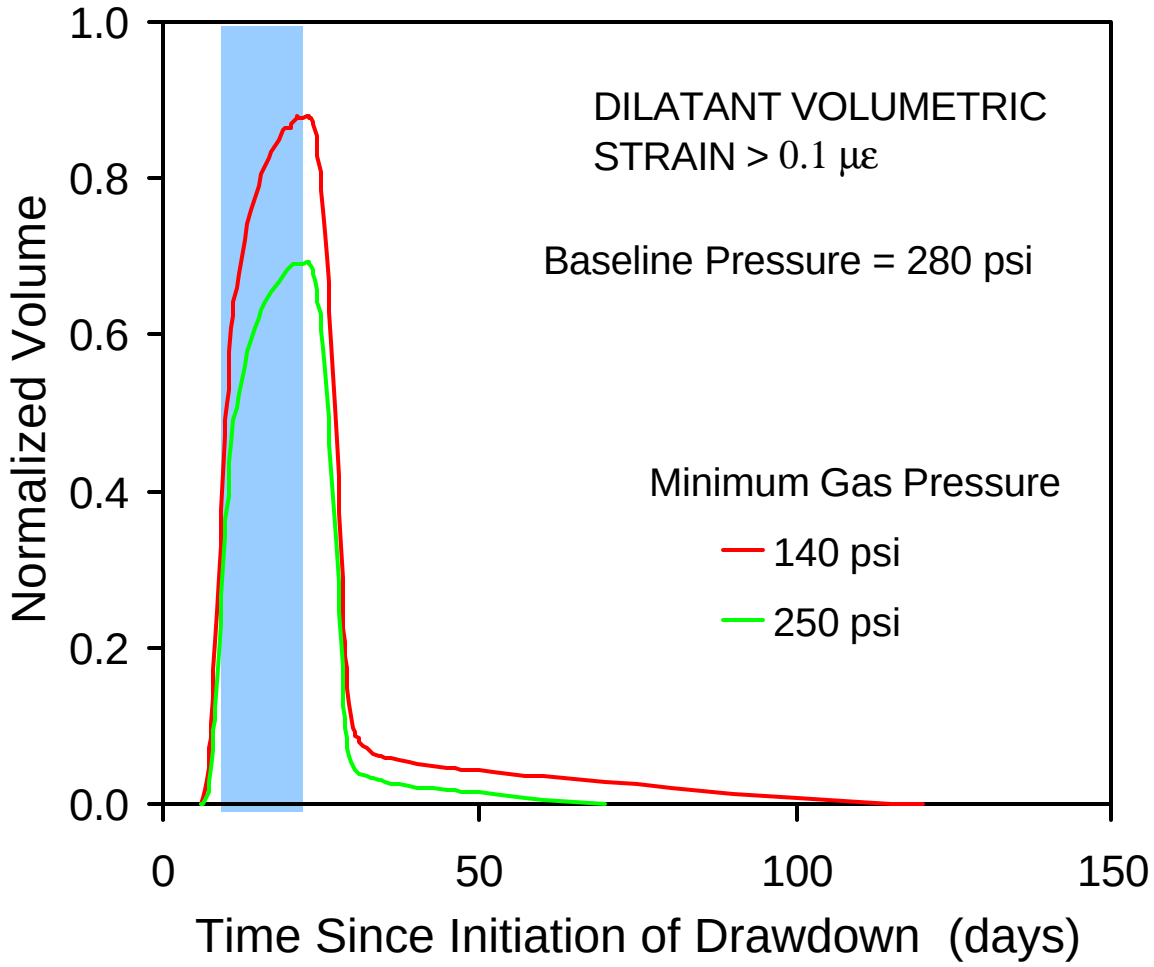

RESPEC
An Integrated Consulting and Services Company

Volume of Dilating Salt

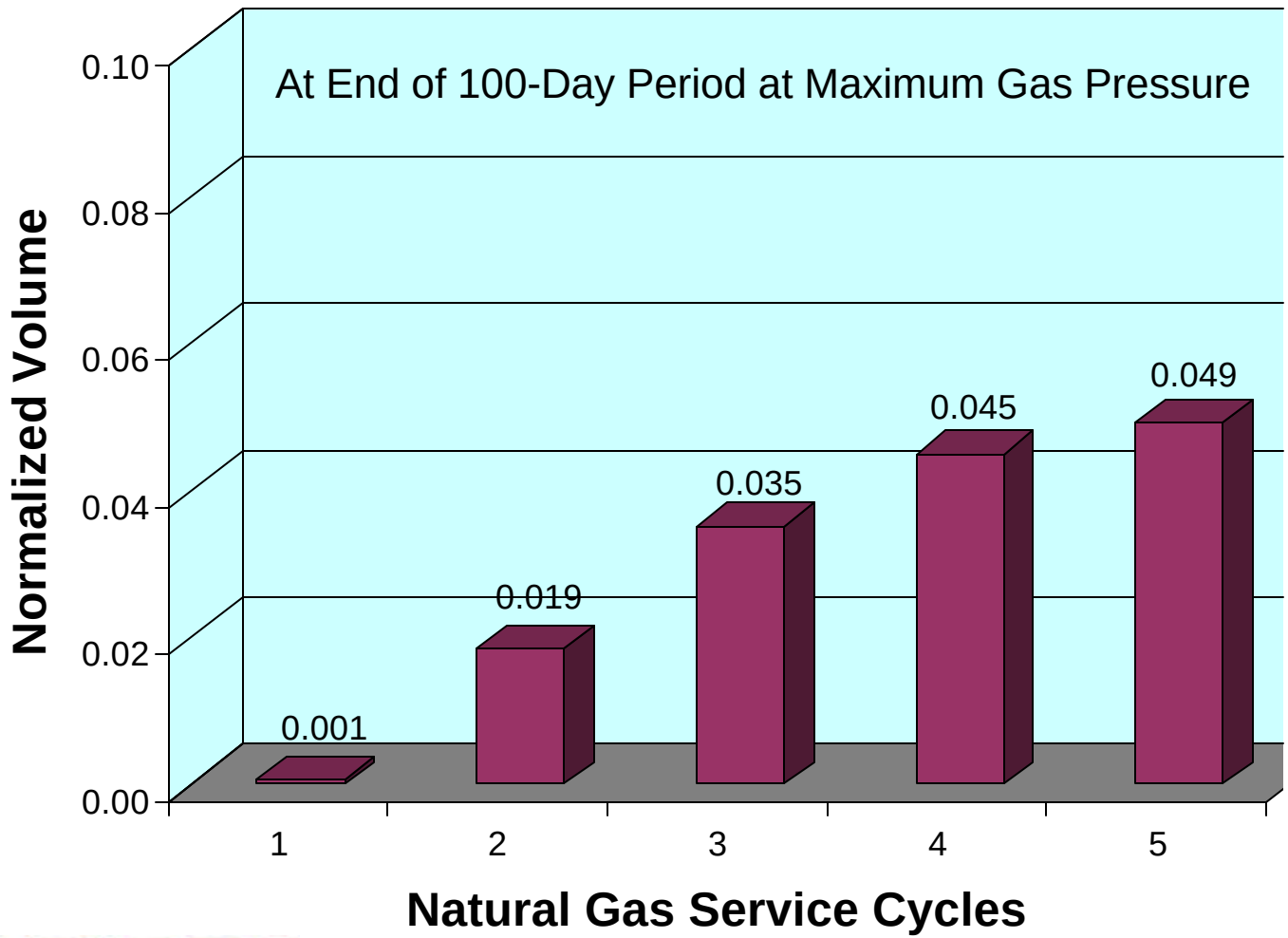

RESPEC
An Integrated Consulting and Services Company

Damage Versus Time - Cavern A

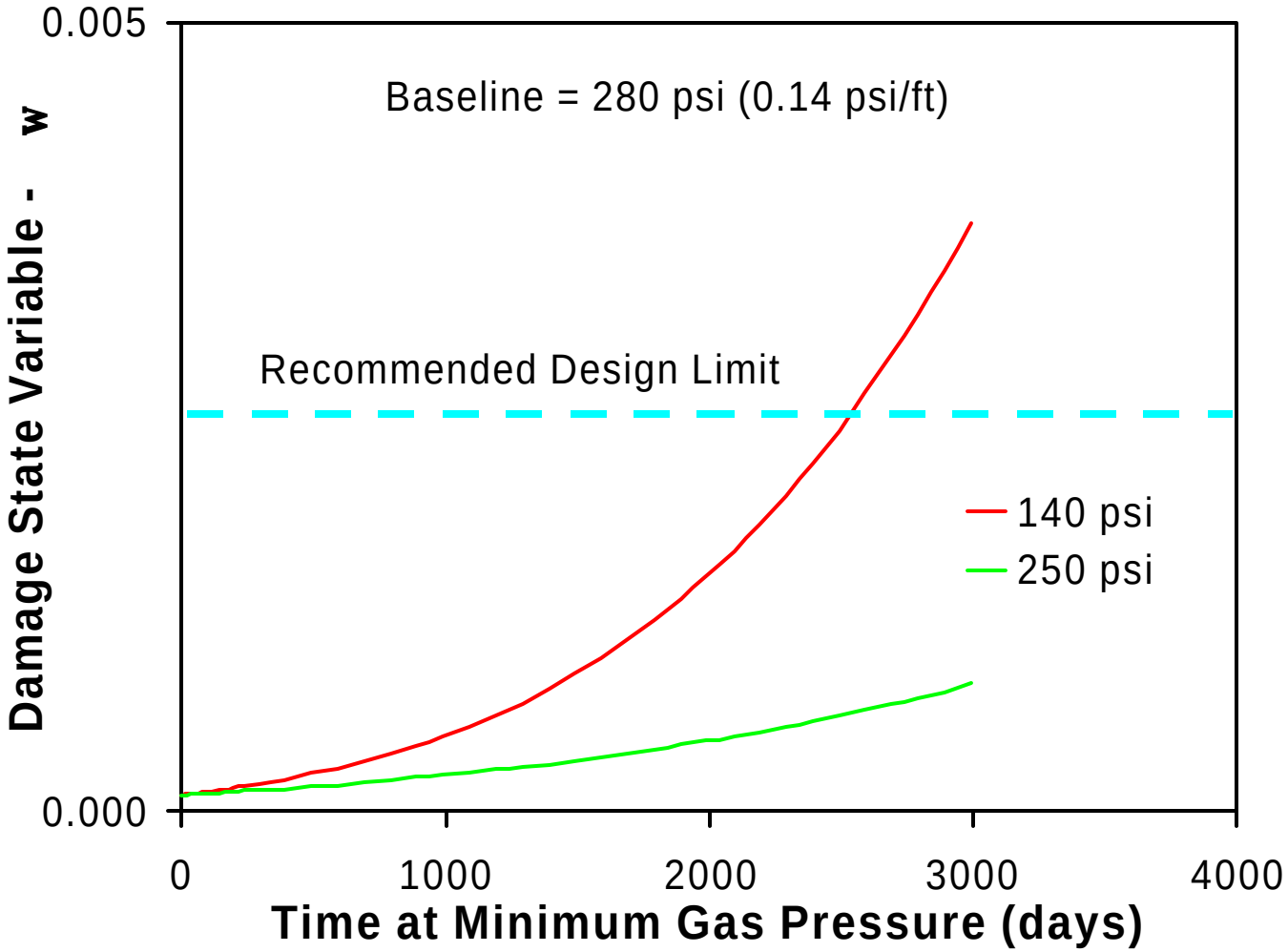

RESPEC
An Integrated Consulting and Services Company

Damage Versus Time - Cavern B

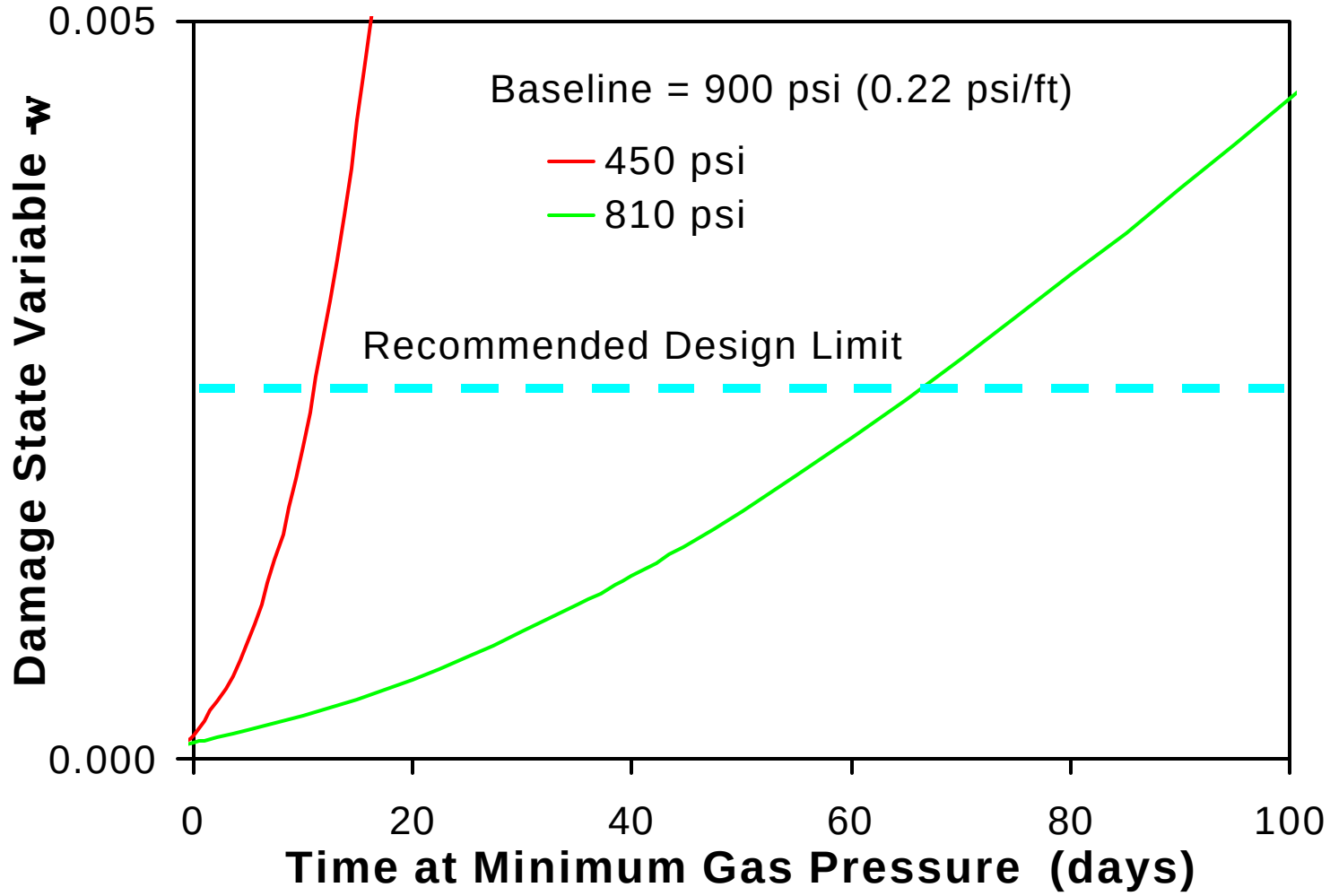

RESPEC
An Integrated Consulting and Services Company

Cavern A versus Cavern B

Why does damage evolve more quickly around Cavern B?

- Salt behavior
  - Cavern B salt creeps faster
  - Dilation boundary for Cavern B more conservative
- Depth
  - Cavern A ~ 2000 feet deep
  - Cavern B ~ 4000 feet deep
- Size and shape
  - Cavern A is three times larger than Cavern B
  - Cavern B has flatter roof

RESPEC
An Integrated Consulting and Services Company

Conclusions

- Geomechanical analysis techniques are available to predict damage around real caverns
- Minimum gas pressure can be lowered without jeopardizing cavern stability
- Healing occurs at maximum gas pressure
- Time at minimum gas pressure should be limited

RESPEC
An Integrated Consulting and Services Company

Development of an Optimal Test Matrix for Determining Material Model Parameters for the New Design Criterion

Kirby Mellegard

RESPEC
An Integrated Consulting and Services Company

Mechanical Properties Needed

- Elastic properties
  - Young's Modulus and Poisson's Ratio
- Strength properties
  - Compressive and tensile strengths
- Plastic properties
  - These are effectively the parameters used in the MDCF material model

RESPEC
An Integrated Consulting and Services Company

MDCF Model Parameters

- The MDCF model parameters are grouped by functional characteristics

Transient creep	6 parameters
Steady state creep	11 parameters
Shear damage	4 parameters
Tension damage	3 parameters
Healing	3 parameters
Shear and tension damage	8 parameters
Damage and healing	6 parameters
TOTAL	**41 parameters**

RESPEC
An Integrated Consulting and Services Company

Reduce MDCF Parameters

- All 41 parameters are needed for nuclear waste repository design
- Range of stress and temperature in caverns allows 12 parameters to be deterministic
- Sensitivity analysis shows 12 parameters do not significantly affect model predictions
- The result is that only 17 parameters need to be determined in the laboratory

RESPEC
An Integrated Consulting and Services Company

Parameter Sensitivity to Load Path

Quasi-static test

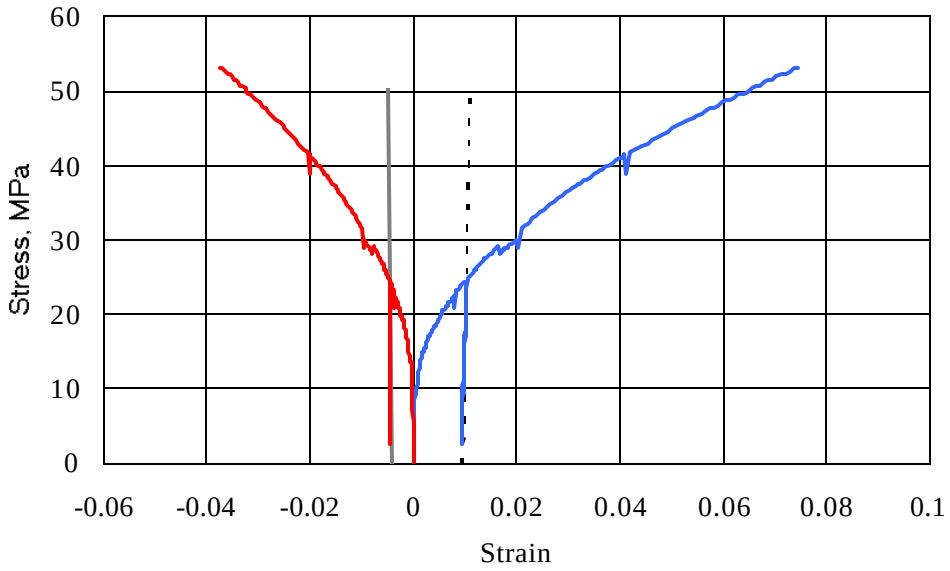

This is a good test for elastic constants

Creep test

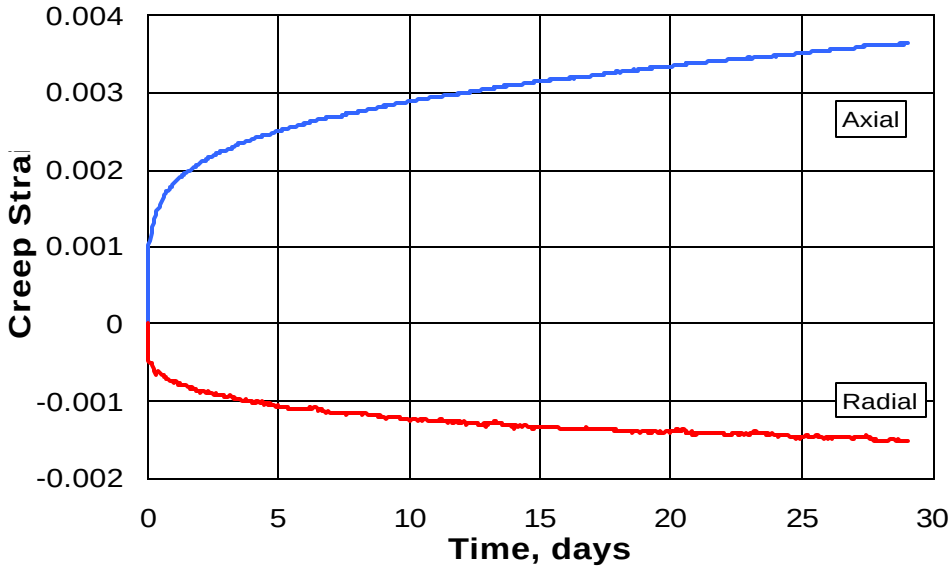

This is a good test for creep parameters

RESPEC
An Integrated Consulting and Services Company

Creep Test Sensitivity Analysis

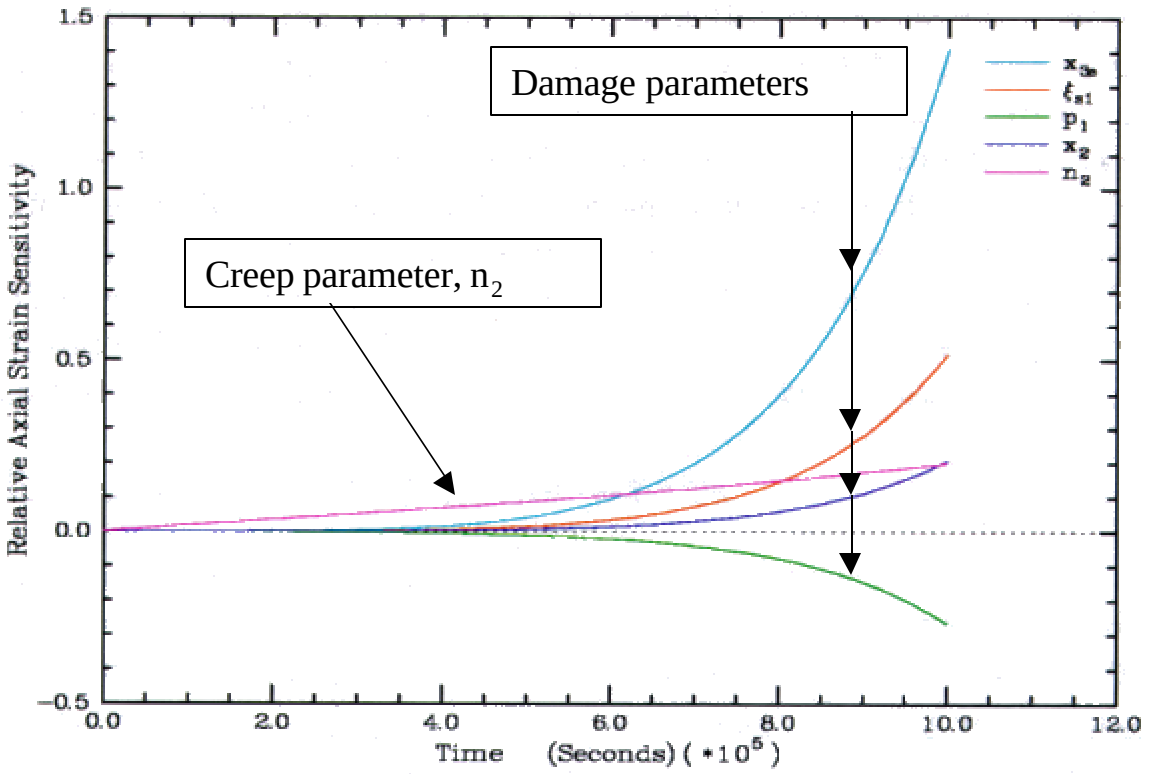

For this high stress difference creep test, the creep parameter n_2 is less important to strain predictions than the four damage parameters because high stress differences can cause damage.

For a low stress difference creep test, the creep parameter n_2 would be more important to strain predictions than the other four damage parameters because damage is less likely at low stress differences.

RESPEC
An Integrated Consulting and Services Company

Load Path Control

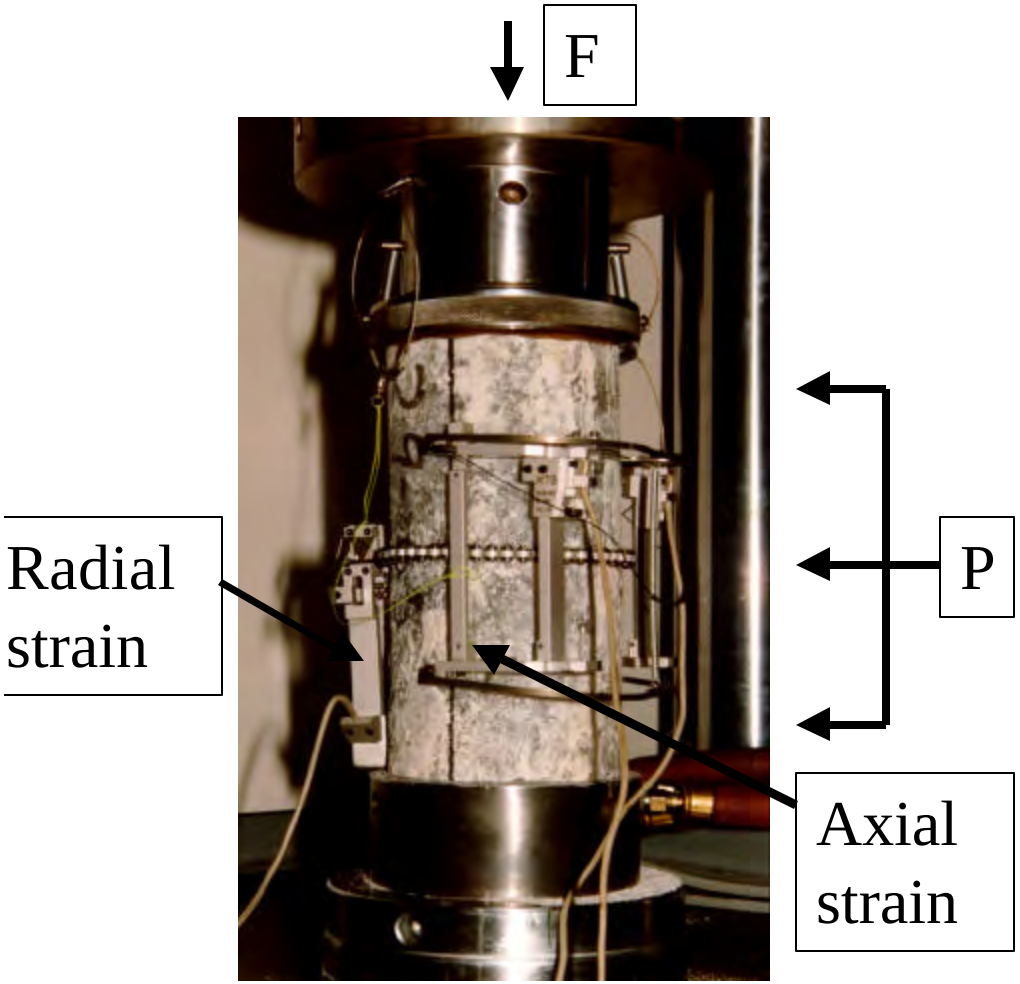

- Four variables
  - Axial stress & strain
  - Radial stress & strain
- Two servocontrol axes
  - Axial direction
  - Radial direction
- Choose two variables to control and the other two are response

RESPEC
An Integrated Consulting and Services Company

Approach to Test Matrix Design

- Identify conventional laboratory tests that are available in most modern laboratories
- Use sensitivity analysis to identify load paths where only one or a few MDCF parameters affect the model predictions
- Establish the nominal test conditions for the tests to be performed

RESPEC
An Integrated Consulting and Services Company

Conventional Laboratory Tests

- Constant Stress Creep Test
  - Inelastic, time-dependent parameters
- Constant Mean Stress Test
  - Onset of dilation damage (microfracturing)
- Constant Strain Rate Test
  - Strength and elastic parameters
- Hydrostatic Compression Test
  - Damage recovery (healing) parameters

RESPEC
An Integrated Consulting and Services Company

Proposed MDCF Test Matrix

Test Type	Test No.	Stress Conditions		
		Ds	**s_3**	**s_m**
Quasi-static Triaxial Compression	1		Lo	
	2		Me	
	3		Hi	
	4		Lo	
	5		Me	
	6		Hi	
Constant Mean Stress Triaxial Compression	7			Lo
	8			Me
	9			Hi
	10			Lo
	11			Me
	12			Hi
Constant Stress Triaxial Compression Creep	13	Lo	Lo	
	14	Lo	Me	
	15	Lo	Hi	
	16	Me	Lo	
	17	Me	Me	
	18	Me	Hi	
	19	Hi	Lo	
	20	Hi	Me	
	21	Hi	Hi	
Hydrostatic Triaxial Compression Healing	22-27	Use lithostatic healing pressure.		

RESPEC
An Integrated Consulting and Services Company

Laboratory Testing Summary

- 27 triaxial compression tests
  - 6 Quasi-static
  - 6 CMS
  - 9 Creep
  - 6 Healing
- 12 strength tests (UCC and tensile)
- 10 mineralogical analyses
- Total cost ≈ $90,000

RESPEC
An Integrated Consulting and Services Company

Cost-Benefit Analysis of New Design Criterion

Kerry DeVries

RESPEC
An Integrated Consulting and Services Company

Benefit of Lower Minimum Gas Pressure

- Increase deliverable gas
- Increase peaking service
- Lower storage costs
- Reduce capital expenditure
- Reduce construction cost

RESPEC
An Integrated Consulting and Services Company

Working Gas Capacity

Cavern A	Cavern B
280 psi vs 140 psi	900 psi vs 450 psi
9.1 Bcf vs 9.9 Bcf	3.8 Bcf vs 4.4 Bcf
8 % Increase	16 % Increase

RESPEC
An Integrated Consulting and Services Company

Increase in Storage Capacity

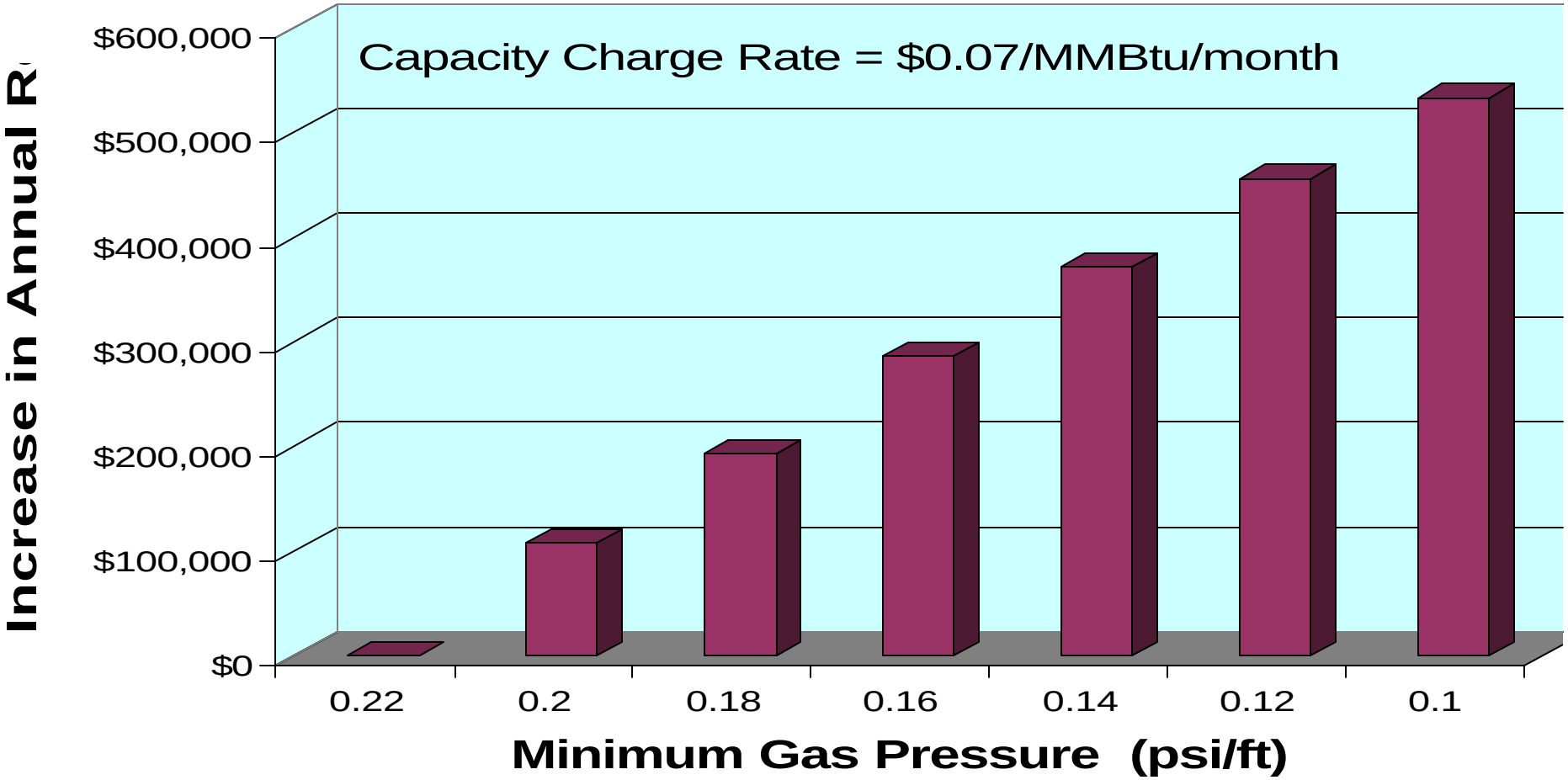

RESPEC
An Integrated Consulting and Services Company

Reduction in Cushion Gas Expense

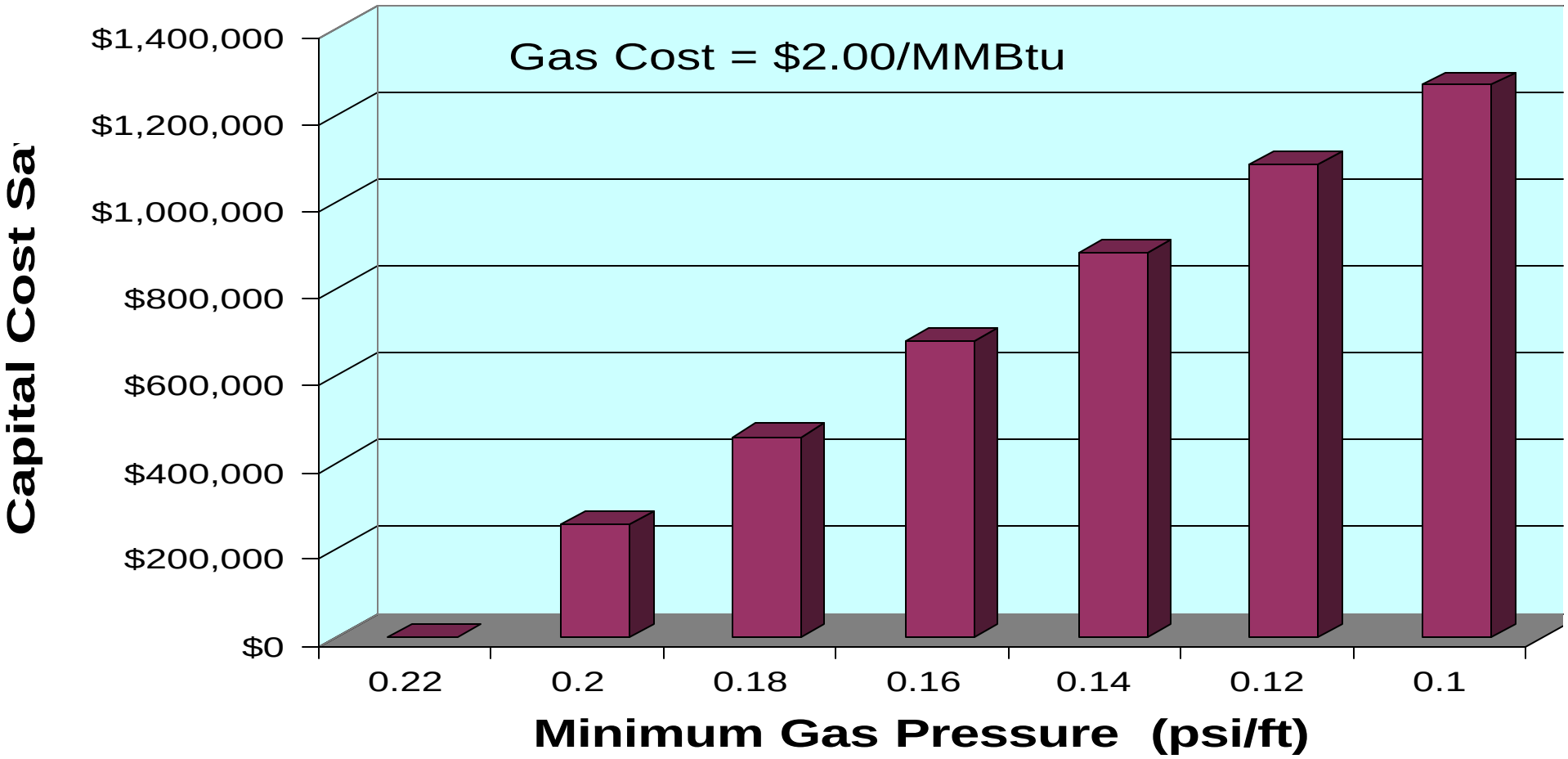

RESPEC
An Integrated Consulting and Services Company

Construction Cost Savings

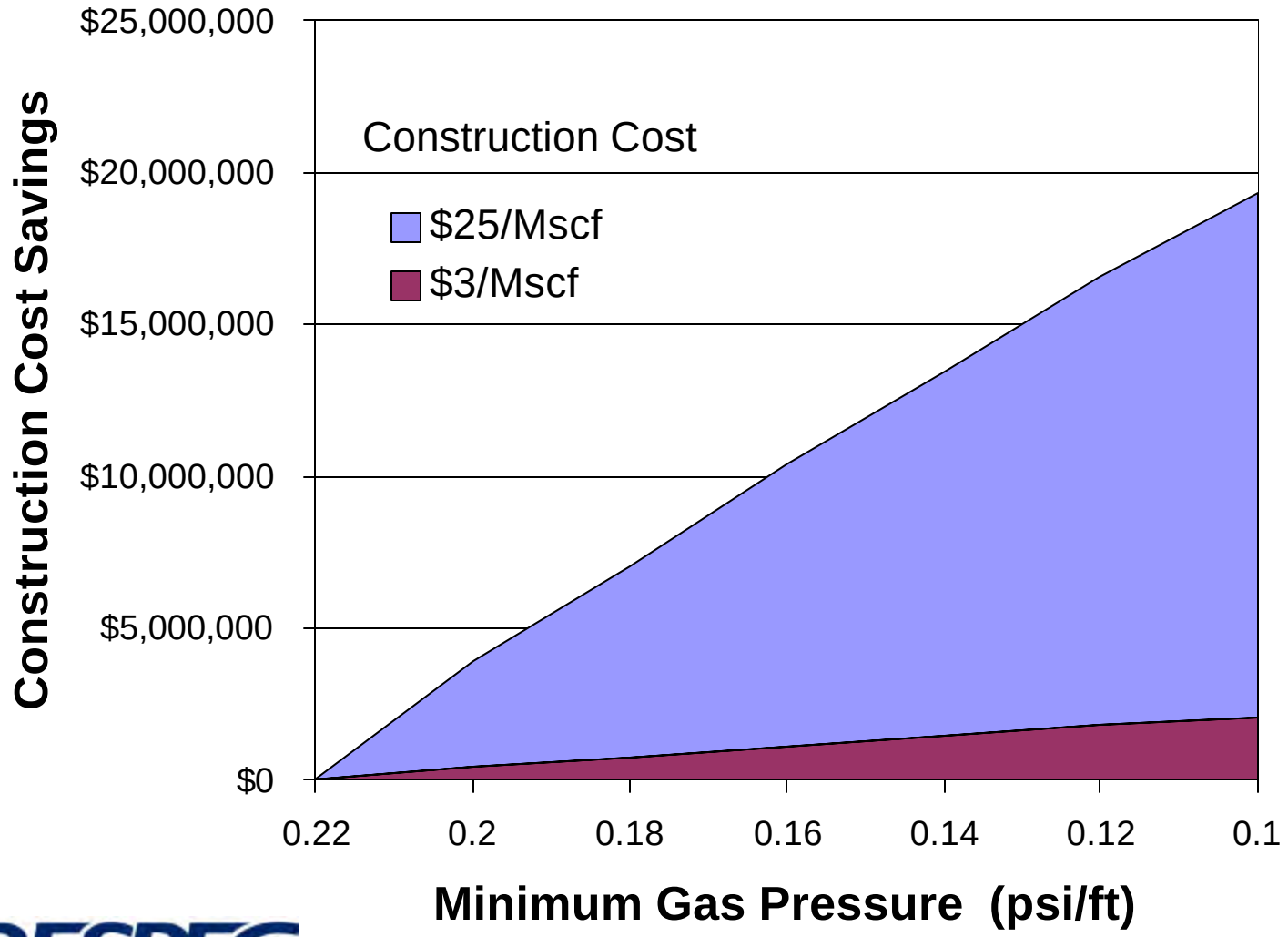

RESPEC
An Integrated Consulting and Services Company

Cost Summary

- Assuming proven technology, estimated cost of adopting new criterion
  - Laboratory testing ≈ $90,000
  - Geomechanical analysis ≈ $75,000
- Decrease in minimum gas pressure required to recover estimated cost in first year
  - Based on reduced cushion gas ≈ 0.02 psi/ft
  - Based on capacity charge ≈ 0.04 psi/ft
  - Based on construction cost ≈ 0.02 psi/ft

RESPEC
An Integrated Consulting and Services Company

Conclusions

- Laboratory testing required
- Geomechanical analyses required
  - Well geometry
  - Temperature profile
  - Gas service pressure history
- Small reduction in minimum gas pressure covers cost of new design concept

RESPEC
An Integrated Consulting and Services Company